A UNITED STATES DEPARTMENT OF COMMERCE PUBLICATION

NBS SPECIAL PUBLICATION 348

The Science of Ceramic Machining and Surface Finishing

U.S. DEPARTMENT OF COMMERCE
National Bureau of Standards

UNITED STATES DEPARTMENT OF COMMERCE • Peter G. Peterson, *Secretary*

The Science of Ceramic Machining and Surface Finishing

Proceedings of a Symposium Sponsored by the American Ceramic Society, the Office of Naval Research, and the National Bureau of Standards, November 2-4, 1970, held at NBS, Gaithersburg, Maryland

Edited by
S. J. Schneider, Jr.
Institute for Materials Research
National Bureau of Standards
Washington, D. C. 20234
and
R. W. Rice
Naval Research Laboratory
Washington, D. C. 20390

Associate Editors

C. F. Bersch, Naval Air Systems Command, Washington, D. C. 20360; A. M. Diness, Office of Naval Research, Arlington, Virginia; and J. B. Wachtman, Jr., Institute for Materials Research, National Bureau of Standards, Washington, D. C. 20234

National Bureau of Standards Special Publication 348

Nat. Bur. Stand (U.S.), Spec. Publ. 348, 431 pages (May 1972)
CODEN: XNBSAV

Issued May 1972

For sale by the Superintendent of Documents, U.S. Government Printing Office, Washington, D.C. 20402—Price $5.25
(Order by SD Catalog No. C13.10:348).

Abstract

This volume presents the proceedings of the Symposium on the Science of Ceramic Machining and Surface Finishing held at the National Bureau of Standards in Gaithersburg, Maryland on November 2–4, 1970. The symposium was jointly sponsored by the Baltimore-Washington Section of the American Ceramic Society, the Office of Naval Research, and the National Bureau of Standards. The purpose of the conference was to survey the developing science of ceramic machining and to stimulate further progress by discussion of current problems and research programs. In addition to a panel discussion, 37 review and original research papers were presented with attention focused on four main areas: (1) Techniques and Mechanisms of Removal and Shaping (2) Surface Treatment (3) Analysis and Characterization of Machining Effects and (4) Mechanical and Other Effects of Finishing. An edited version of the floor discussion following each paper is given.

Key words: Ceramics; ceramic machining; mechanical effects of machining; removal and shaping of ceramics; surface treatment.

Library of Congress Catalog Card Number: 79-611323

Foreword

One way in which the National Bureau of Standards attempts to achieve its goal—to strengthen and advance the nation's science and technology and to facilitate their effective application for public benefit—is by insuring the availability of basic data on the properties of materials. In this effort the Institute for Materials Research holds symposia that provide a forum for discussion of the latest research results, and that focus attention on areas of material science in which basic knowledge is lacking or needs improvement.

The latest of these symposia was on the Science of Ceramic Machining and Surface Finishing. Ceramics have long been used in high temperature and structural applications and yet have not achieved the full measure of reliability demanded by modern technology. Therefore, the entire spectrum of ceramic processing and in particular the ceramic machining segment must be elevated to new scientific levels. In recognition of this need NBS, the Office of Naval Research, and The American Ceramic Society organized this symposium so that the groundwork for a science of ceramic machining could be established.

The National Bureau of Standards is publishing these Proceedings not only to make an important body of knowledge available, but to stimulate further research efforts in the field as well.

Lewis M. Branscomb
Director

Preface

Presented here are the proceedings of the symposium on the Science of Ceramic Machining and Surface Finishing held at the National Bureau of Standards at Gaithersburg, Maryland on November 2–4, 1970. Approximately 190 scientists, engineers, and others versed in ceramic machining attended the three-day meeting. Overall, seven countries, including the USA, were represented.

The machining and finishing process is of fundamental importance to the manufacture of many commercial ceramic products. Ultimate success and reliability often lies with the nature of machining variables. Previously this facet of production was relegated to state-of-art procedures generally derived from knowledge attained in the processing of metals. Of late, however, many in the ceramic sciences have become cognizant that a better understanding of machining and all its ramifications must be gained if ceramics are to realize their full potential. Increased awareness of this is evidenced by the recent report of the Materials Advisory Board on Ceramic Processing (Ad Hoc Committee on Ceramic Processing, J. A. Pask, Chairman, National Academy of Sciences Publication 1576 (1968)). The Panel on Finishing surveyed various techniques, mechanisms, and resultant surface character and put forth recommendations for further study. Significantly this symposium is a perfect adjunct to the work of the Panel.

The symposium had as its stated purpose "To survey the developing science of ceramic machining and to stimulate further progress by discussion of current problems and research." These objectives were met through the presentation of a variety of invited summary papers, supplemented with contributions on original research. Accordingly the scope of the conference broadly encompassed the techniques, analysis, and effects of machining and surface finishing by several basic techniques which include mechanical, energy beam, and chemical methods. The known effects of such operations on ceramic properties, especially mechanical properties, were covered with emphasis being placed on the fundamental nature of these effects. Analysis and characterization of resultant surfaces and subsurfaces are also covered since this information is necessary to an understanding of removal mechanisms and their effects on properties. The symposium fittingly concluded with a panel discussion which effectively focused attention on significant trends and problem areas.

The symposium and the proceedings admittedly are not the last word in the complex subject of machining. It is hoped, however, that the papers published here can lead to a better understanding of material removal mechanisms and resultant surface structures and properties, and thus to an eventual improvement in the technology of ceramic finishing. Furthermore, the symposium can serve as an aid in the development of a true Science of Ceramic Machining and Surface Finishing.

S. J. Schneider, Jr. and R. W. Rice
Editors

Acknowledgment

The editors wish to thank all those who participated in the symposium either as attendees, speakers, session chairmen, or panel members. Special thanks are due the following for their assistance in organizing the meeting and for publication of the proceedings:

R. T. Cook, National Bureau of Standards
B. L. Oberholtzer, National Bureau of Standards
K. M. Smith, Applied Physics Laboratory of Johns Hopkins University.

Contents

V. MECHANICAL AND OTHER EFFECTS OF FINISHING

Session Chairmen

W. H. Rhodes, AVCO Corporation
J. B. Wachtman, Jr., National Bureau of Standards

VI. PANEL DISCUSSION

J. B. Wachtman, Jr., Moderator
F. Ernsberger, P. J. Gielisse, A. H. Heuer, W. H. Rhodes, R. W. Rice
Panel Members

Participants

Samuel J. Acquaviva
Army Materials & Mechanics
Research Center
Watertown, Massachusetts 02172

Jon J. Aho
Bausch & Lomb
635 St. Paul Street
Rochester, New York 14602

Guy H. Allgeyer
Owens-Illinois
1700 North Westwood
Toledo, Ohio 43607

Jan Appelo
D. M. Stewart Manufacturing Co.
Post Office Box 510
Chattanooga, Tennessee 37701

F. Gary Augeri
MIT/Draper Lab
275 Massachusetts Avenue
Cambridge, Massachusetts 02139

Frank P. Bailey
Chemical Research Laboratories
C.S.I.R.O.
Post Office Box 4331
Melbourne, Victoria, Australia

Jimmy D. Bailey
American Lava Corporation
Laurens, South Carolina 29360

Spencer H. Baker
Norton Company
New Bond Street
Worcester, Massachusetts 01606

Norris H. Barbre
Can-Tex Industries
Division of Harsco Corporation
Post Office Box 254
Weatherford, Texas 76086

Y. Baskin
Ferro Corporation
Technical Center
4150 East 56th Street
Cleveland, Ohio 44105

C. H. Bates
Bell Aerospace Company
Post Office Box 1
Buffalo, New York 14240

P. F. Becher
Naval Research Laboratory
Code 6136
Washington, D.C. 20390

Richard Behrens
Dow Corning Corporation
Saginaw Road
Midland, Michigan 48640

L. Berrin
Bell Telephone Laboratories
555 Union Boulevard
Allentown, Pennsylvania 18103

C. Bersch
Naval Air Systems Command
Jefferson Plaza, Room 1000
Arlington, Virginia 22901

R. E. Bickelhaupt
Southern Research Institute
2000 Ninth Avenue South
Birmingham, Alabama 35205

Joe Blaze
McDanel Refractory Porcelain Co.
510 Ninth Avenue
Post Office Box 560
Beaver Falls, Penna. 15010

Sherman D. Brown
University of Illinois
Dept. Ceramic Engineering
Urbana, Illinois 61801

W. R. Brown
Corning Glass Works
Fluidic Products Department
Corning, New York 14830

D. M. Busch
Diamond Research Laboratory
Industrial Division
Post Office Box 916
Johannesburg, South Africa

D. J. Cameron
Atomic Energy of Canada Ltd.
Whiteshell Nuclear Research
Pinawa, Manitoba, Canada

William B. Campbell
The Ohio State University
2041 North College Road
Columbus, Ohio 43210

John J. Capellman
PPG Industries
Creighton, Pennsylvania 15030

R. J. Caveney
Diamond Research Laboratory
Post Office Box 916
Johannesburg, South Africa

David W. Chalkley
Trans-Tech, Inc.
12 Meem Avenue
Gaithersburg, Maryland 20760

Jaime W. Colon
Potter Instrument Co.
Plainview, New York 11803

L. V. Colwell
University of Michigan
2046 East Engineering Bldg.
Ann Arbor, Michigan 48104

Donald G. Cooper
Avco Bay State Abrasives Division
Union Street
Westboro, Massachusetts 01581

Wade Cooper
McDanel Refractory Porcelain Co.
510 Ninth Ave., P. O. Box 560
Beaver Falls, Penna. 15010

Kristofer T. Dahl, 2Lt. USAF
SMAMA (MAQQLC)
McClellan Air Force Base
California 95652

A. U. Daniels
Air Force Machineability
Data Center
3980 Rosslyn Drive
Cincinnati, Ohio 45209

William H. Daniels
Westinghouse Research Lab
Beulah Road
Pittsburgh, Penna. 15235

N. S. Dempster
Embassy of Australia
1601 Massachusetts Avenue, N.W.
Washington, D.C. 20036

Frank V. DiMarcello
Bell Laboratories, Inc.
Mountain Avenue
Murray Hill, New Jersey 07974

A. M. Diness
Office of Naval Research
Room 619, Ballstron #1
Arlington, Virginia 22217

Sam DiVita
U.S. Army Electronics Command
AMSEL-KL-EC
Fort Monmouth, New Jersey 07703

Louis P. Domingues
Trans-Tech, Inc.
12 Meem Avenue
Gaithersburg, Maryland 20760

David J. Donovan
Data Magnetics
355 Maple Avenue
Torrance, California 90503

S. Doroff
Office of Naval Research
Washington, D.C. 20207

James W. Douglass
Perkin-Elmer
Norwalk, Connecticut 06553

Bruce W. Dunnington
The Glennel Corporation
908 Chickadee Lane
West Chester, Pennsylvania 19380

Richard A. Edsall
Trans-Tech, Inc.
12 Meem Avenue
Gaithersburg, Maryland 20760

A. E. Edwards
Material Dynamics
3151 Fostoria Way
San Ramon, California 94583

Shane A. Ellis
Ferroxcube Corporation
Saugerties, New York 12477

J. K. Emery
Accumet Engineering Corp.
25 Broad Street
Hudson, Massachusetts 01749

Fred Ernsberger
PPG Industries
Box 11472
Pittsburgh, Pennsylvania 15238

James W. Evans
Corning Glass Works
Process Research-Sullivan Park
Corning, New York 14830

George Eyerly
D. M. Stewart Manufacturing Co.
Post Office Box 510
Chattanooga, Tennessee 37401

Iain Finnie
University of California
Berkeley, California 94720

Ross Firestone
Case Western Reserve University
White Building
University Circle
Cleveland, Ohio 44118

P. L. Fleischner
National Beryllia
Haskell, New Jersey 07420

R. K. Frazer
Applied Physics Lab
Johns Hopkins University
Scaggsville, Maryland 20910

Nicholas Friedman
Duramic Products, Inc.
426 Commercial Avenue
Palisades Park, New Jersey 07650

Frank S. Gardner
Office of Naval Research
495 Summer Street
Boston, Massachusetts 02210

Erberto Francisco Gentile
Instituto de Energie Atomica
C. P. 11049
S. Paulo, Brazil

Peter J. Geilisse
University of Rhode Island
Kingston, Rhode Island 02881

William F. Gilbert, Jr.
Bell Telephone Laboratories, Inc.
555 Union Boulevard
Allentown, Pennsylvania 18103

A. J. Gitter
Engineered Materials Division
Hi-Purity Materials, Inc.
Box 363, Church Street Station
New York, New York 10008

Harry J. Green, III
IBM-Components Division
Route 52, Bldg. 320–33, D/281
Hopewell Junction, New York 12533

Bernard A. Greene
Griffin Pipe Products Co.
Milledgeville, Georgia 31061

Victor A. Greene
Automated Business Systems
550 Central Avenue
Orange, New Jersey 07051

Irwin G. Greenfield
Mechanical & Aerospace Engr. Dept.
University of Delaware
Newark, Delaware 19711

William T. Greenfield
Corning Glass Works
Fluidic Products Department
Corning, New York 14830

William R. Griffin
Raytheon Company
130 Second Avenue
Waltham, Massachusetts 02154

Nelson Grimm
General Electric Company
24400 Highland Road
Richmond Heights, Ohio 44143

William E. Gurwell
Easton, Yale & Towne, Inc.
26201 Northwestern Highway
Southfield, Michigan 48075

Robert S. Hahn
Heald Division-Cincinnati Milacron
New Bond Street
Worcester, Massachusetts 01606

David M. Haines
INSACO, Inc.
Post Office Box 422
Quakertown, Pennsylvania 18951

Joe N. Harris
Georgia Institute of Technology
High Temperature Materials Div.
Atlanta, Georgia 30332

Pat Hart
Battelle Northwest
Post Office Box 999
Richland, Washington 99352

D. P. H. Hasselman
Lehigh University
Bethlehem, Pennsylvania 18015

Howard Herzig
NASA
Goddard Space Flight Center
Code 284.1
Greenbelt, Maryland 20771

A. H. Heuer
Case Western Reserve University
Cleveland, Ohio 44106

Terrence P. Hobin
British Embassy
3100 Massachusetts Avenue
Washington, D.C. 20008

B. J. Hockey
National Bureau of Standards
Room A359, Building 223
Washington, D.C. 20234

M. W. Hoelscher
RCA Incorporated
New Holland Pike
Lancaster, Pennsylvania 17604

E. Horowitz
Institute for Materials Research
National Bureau of Standards
Washington, D.C. 20234

J. W. Hunt
Duplate Canada Limited
Ceramics Division
First Avenue
Oshawa, Ontario, Canada

Robert H. Insley
Champion Spark Plug Company
20000 Conner Avenue
Detroit, Michigan 48234

Virgil Irick, Jr.
American Lava Corporation
Cherokee Boulevard
Chattanooga, Tennessee 37405

Lonnie F. Ivey
American Standard
Post Office Box A
Paintsville, Kentucky 41240

R. Jackel
Office of Naval Research
Washington, D.C. 20207

Paul J. Jorgensen
Stanford Research Institute
333 Ravenswood Avenue
Menlo Park, California 94025

Paul G. Juenemann
Trans-Tech, Inc.
12 Meem Avenue
Gaithersburg, Maryland 20760

Erwin E. Kipfer
Pfaudler Company
1000 West Avenue
Rochester, New York 14603

Henry P. Kirchner
Ceramic Finishing Company
Post Office Box 498
State College, Pennsylvania 16801

R. J. Kleinwassink
Philips Research Labs
Eindhoven, Netherlands

B. G. Koepke
Honeywell Corporate Research
500 Washington Avenue, S.
Hopkins, Minnesota 55343

J. Koorneef
Philips Research Labs
Eindhoven, Netherlands

William Kovacs
Atomic Energy of Canada Ltd.
Whiteshell Nuclear Research
Pinawa, Manitoba, Canada

Don A. Kubose
Naval Ordnance Laboratory
White Oak, Maryland

Paul L. Kuzmick, Jr.
Paul L. Kuzmick Company
271 Grove Avenue
Verona, New Jersey 07044

Richard Lane
Hamco
1000 Millstead Way
Rochester, New York 14624

Fred F. Lange
Westinghouse R&D
Churchill Boro
Pittsburgh, Pennsylvania 15235

Robert E. Lasson
IMB Corporation
2800 Sand Hill Road
Building 031, Dept. 201
Menlo Park, California 94025

D. W. Lee
Arthur D. Little Inc.
Acorn Park
Cambridge, Massachusetts 02140

Henry C. Leistner
National Bureau of Standards
325 South Broadway
Boulder, Colorado 80302

James D. Lester
U.S. Army Frankford Arsenal
Philadelphia, Pennsylvania 19137

Newton Levy, Jr.
W. R. Grace & Company
Clarksville, Maryland 21029

P. W. Levy
Physics Department
Brookhaven National Laboratory
Upton, New York 11973

Jack Liker
Basic Ceramics Inc.
221 7th Avenue
Hawthorne, New Jersey 07507

Alan Little
Duplate Canada Ltd.
50 St. Clair Avenue, West
Toronto, Ontario, Canada

W. C. Lo
Bell Telephone Laboratories, Inc.
555 Union Boulevard
Allentown, Pennsylvania 18103

William D. Long
Kaman Sciences
1700 Garden of the Gods Road
Colorado Springs, Colorado 80907

Evan C. Luce
Norton Company
1 New Bond Street
Worcester, Massachusetts 01606

Howard L. McCollister
Owens-Illinois Inc.
1700 North Westwood
Toledo, Ohio 43607

J. F. McMahon
13 Sayles Street
Alfred, New York 14802

B. A. MacDonald
Office of Naval Research
Washington, D.C. 20207

William McDonough
Naval Research Laboratory
Washington, D.C. 20390

Karl R. McKinney
Naval Research Laboratory
Washington, D.C. 20390

H. A. McKinstry
Pennsylvania State University
161 Engineering Science Bldg.
University Park, Penna. 16802

I. Machlin
Office of Naval Research
Washington, D.C. 20207

Donald J. MacIntyre
Basic Ceramics Inc.
Box 2090
Hendersonville, N. C. 28739

Frank Magnanelli
Trans-Tech, Inc.
12 Meem Avenue
Gaithersburg, Maryland 20760

Alan Maietta
Paul L. Kuzmick Company
271 Grove Avenue
Verona, New Jersey 07044

Joseph A. Martis
Metallurgy Product Department
General Electric Company
11177 East Eight Mile Road
Detroit, Michigan 48232

John Matsko
Division 5332
Sandia Laboratories
Albuquerque, New Mexico 87115

George Mayer
U.S. Army Research Office
Box CM, Duke Station
Durham, North Carolina 27706

George L. Metzger
James H. Rhodes & Company
1026 West Jackson Boulevard
Chicago, Illinois 60607

H. C. Miller
Super-Cut, Inc.
3418 North Knox
Chicago, Illinois 60641

Herbert R. Moeller
Union Carbide Corporation
Post Office Box 985
Union, New Jersey 07083

J. A. Mueller
The Carborundum Company
Post Office Box 403
Niagara Falls, New York 14302

M. K. Murthy
Ontario Research Foundation
Sheridan Park
Ontario, Canada

Donald R. Ness
Western Gold & Platinum Co.
555 Harbor Boulevard
Belmont, California 94002

M. J. Noone
General Electric Company
Space Sciences Laboratory
Room M-9126, P. O. Box 8555
Philadelphia, Penna. 19101

Theodore Nussbaum
Burroughs
Box 472
Piscataway, New Jersey 09854

Martin J. O'Hara
Battelle Memorial Institute
505 King Avenue
Columbus, Ohio 43201

William J. Otto
Ferroxcube Corporation
Mt. Marian Road
Saugerties, New York 12477

Hayne Palmour, III
North Carolina State University
Department of Engineering Research
Raleigh, North Carolina 27607

W. H. Parker
Kaiser Refractories
Post Office Box 870
Pleasanton, California 94566

William H. Parrish
Material Dynamics
Physics International Company
3151 Fostoria Way
San Ramon, California 94583

Edwin A. Pascoe
General Electric Company
6325 Huntley
Worthington, Ohio 43085

Damon S. Paulley
Coors Porcelain Company
600 9th Street
Golden, Colorado 80401

D. J. Perduyn
N. V. Philips
Eindhoven, Netherlands

H. A. Perry
Naval Ordnance Laboratory
Code 2301
Silver Spring, Maryland 20910

Raymond Pietras
Howmet Corporation
Roy Street
Dover, New Jersey 07801

J. T. A. Pollock
Tyco Laboratories, Inc.
16 Hickory Drive
Waltham, Massachusetts 02154

Kenneth Prince
Norton Company
1 New Bond Street
Worcester, Massachusetts 01606

W. G. Rauch
Office of Naval Research
Washington, D.C. 20207

Robert F. Rea
Champion Spark Plug Company
20000 Conner Avenue
Detroit, Michigan 48234

William H. Rhodes
AVCO Corporation
Lowell Industrial Park
Lowell, Massachusetts 01851

R. Rice
Naval Research Laboratory
Code 6136
Washington, D.C. 20390

John Robertson
American Standard Inc.
834 East Broadway
Louisville, Kentucky 40204

Kenneth S. Rolley
Hamco Division Kayex Corp.
1000 Millstead Way
Rochester, New York 14624

George W. Roust
Lawrence Radiation Laboratory
Post Office Box 808
Livermore, California 94551

W. A. Schmidt
Naval Research Laboratory
Code 5210
4555 Overlook Avenue, S.W.
Washington, D.C. 20390

S. J. Schneider
B214, Materials Building
National Bureau of Standards
Washington, D.C. 20234

Rudolf Sedlacek
Stanford Research Institute
333 Ravenswood Avenue
Menlo Park, California 94025

D. J. Shanefield
Western Electric Company
Post Office Box 900
Princeton, New Jersey 08540

H. Shapiro
Duramic Products Inc.
426 Commercial Avenue
Palisades Park, New Jersey 07650

Earl P. Shapland
Flo-Con Systems, Inc.
Box 355
Fisher, Illinois 61843

Lawrence Sharper
Frankford Arsenal
Philadelphia, Pennsylvania 19137

William A. Shelton
National Lead Co.
4511 Hyde Park Blvd.
Niagara Falls, New York 14305

Charles R. Sherman
The Babcock & Wilcox Company
Lynchburg, Virginia 24505

C. R. Shuff
American Standard, Inc.
Post Office Box A
Paintsville, Kentucky 41240

Melvin W. Shupe
Los Alamos Scientific Lab
Los Alamos, New Mexico 87544

Carl J. Smith
Dow Chemical Company
Rocky Flats Division
Post Office Box 888
Golden, Colorado 80401

K. M. Smith
Applied Physics Laboratory
Johns Hopkins University
Scaggsville, Maryland 20910

Leonard I. Smith
Norton Company
1 New Bond Street
Worcester, Massachusetts 01606

F. X. Sorg
Stackpole Carbon Company
Stackpole Street
St. Marys, Pennsylvania 15857

Joseph Stanislao
Department Chemical Engineering
University of Rhode Island
Kingston, Rhode Island 02881

John M. Stanley
Griffin Pipe Products Co.
Orchard Hill Road
Milledgeville, Georgia 31061

H. Stuart Starrett
Southern Research Institute
2000 Ninth Avenue South
Birmingham, Alabama 35205

R. J. Stokes
Honeywell Corporate Research
500 Washington Avenue, South
Hopkins, Minnesota 55343

H. Nathan Stone
AVCO Bay State Abrasives Div.
Westboro, Massachusetts 01581

R. C. Sundahl
Bell Telephone Laboratories
555 Union Boulevard
Allentown, Pennsylvania 18103

C. J. Swafford
Georgia Tech
Atlanta, Georgia 30332

Jeff Templeton
James H. Rhodes & Company
1026 West Jackson Boulevard
Chicago, Illinois 60607

George R. Thompson
Commonwealth Scientific Corp.
500 Pendleton Street
Alexandria, Virginia 22314

Robert L. Tienken
International Precision Ferrite
141 Ulster Avenue
Saugerties, New York 12477

Ronald J. Tillen
American Optical Corporation
Southbridge, Mass. 01550

James J. Tuzzeo
General Electric Company
6325 Huntley Road
Worthington, Ohio 43085

John E. Tydings
Naval Ordnance Laboratory
White Oak, Maryland

Ray Van Pamel
Arnold Engineering
Post Office Box G
Marengo, Illinois 60152

J. B. Wachtman, Jr.
B308 Materials Building
National Bureau of Standards
Washington, D.C. 20234

Basil E. Walker, Jr.
Naval Research Laboratory
Code 6130
Washington, D.C. 20390

Thomas W. Wallace
Westinghouse
Cheswick, Pennsylvania 15024

Addison Watkins
American Lava Corporation
Cherokee Boulevard
Chattanooga, Tennessee 37405

G. Wells
International Business Machines
Dept. 204, 1701 North St.
Endicott, New York 13760

Warren W. West
E. I. du Pont de Nemours & Co.
Eastern Laboratory
Post Office Box 67
Gibbstown, New Jersey 08027

Rodgers Westlake
Diamonite Products Mfg. Co.
Shreve, Ohio 44676

A. R. C. Westwood
R.I.A.S.
Martin Marietta Corporation
1450 South Rolling Road
Baltimore, Maryland 21227

E. W. White
Pennsylvania State University
161 Engineering Science Bldg.
University Park, Penna. 16802

Sheldon Wiederhorn
Inorganic Materials Division
National Bureau of Standards
Washington, D.C. 20234

James O. Williams
C–E Refractories
Valley Forge, Pennsylvania 19481

William A. Wilson
National Bureau of Standards
325 South Broadway
Boulder, Colorado 80302

Vladimir E. Wolkodoff
Coors Porcelain Company
600 9th Street
Golden, Colorado 80401

David S. Yang
C–B Refractories
2563 West 18th Street
Chicago, Illinois 60608

The Science of Ceramic Machining and Surface Finishing

Welcome

E. Horowitz

Institute for Materials Research National Bureau of Standards Washington, D.C. 20234

Good morning and welcome to the National Bureau of Standards. I can see from the time on the NBS clock, and the program schedule, that this is going to be the shortest welcoming address in the history of our symposium series. This conference is being co-sponsored by the American Ceramic Society (Baltimore-Washington Section), the Office of Naval Research, and the National Bureau of Standards, and NBS is pleased to be both a host and a participant in these proceedings. We at NBS consider meetings of this type to be extremely important because they are a prime mechanism for developing discussion, promoting communication, and for coupling science and technology. This comment is particularly appropriate in view of your chairman's remark that this is the first truly scientific meeting dealing specifically with ceramic machining and surface finishing.

I would like to say to those of you who are here for the first time, and particularly the visitors from the six foreign countries, that we will do all that we can to make this meeting productive, and your visit to NBS enjoyable and informative. Please call upon the NBS staff if there is anything that we can do to be of assistance while you are here. From reading the published schedule it is clear that the sponsors have prepared an extremely interesting and a full program. I think we ought to get on with the business of the symposium and let me wish you a fruitful meeting.

I. INTRODUCTION

Session Chairman

S. J. Schneider, National Bureau of Standards

Science and the Machining and Surface Finishing of Ceramics

R. W. Rice
Naval Research Laboratory
Washington, D. C. 20390

C. F. Bersch
Naval Air Systems Command
Washington, D. C. 20360

A. M. Diness
Office of Naval Research
Arlington, Virginia 22217

Historically, the technology of machining and surface finishing of ceramics has advanced by empirical methods. Further advances appear limited without gaining basic knowledge of the mechanisms of removing or redistributing material from or on ceramic surfaces. Because of the diversity of ceramic behavior, this is a challenging scientific problem. However, meeting this challenge can result not only in improved or new machining and finishing processes, but also in greater understanding of the character of the resultant surface and sub-surface, and hence of the surface-dependent properties.

Key words: Machining; machining costs; methods of machining and finishing; surface-dependent properties; surface finishing.

1. The Prior Status of Ceramic Machining and Surface Finishing

Modern methods of machining and finishing of ceramics have grown empirically from such earlier arts as machining and finishing of glassy bodies, polishing of jewels, and applicable metals technology. The improvement of properties and behavior which depend on machining and finishing has also been empirical, with the possible exception of optical properties. While some characterization of resultant surfaces has been carried out, it has been limited. There has been almost no effort to characterize the subsurface of machined or finished ceramics. Little effort has been directed to understanding the basis of surface generation or alteration processes which control machining and surface finishing operations as well as the character of the resultant surfaces and dependent properties. The materials removal processes responsible for surface generation are complex and arise from the interplay between grinding operations and microstructural features of the workpiece.

Chemistry and physics provide some insight into the mechanisms of chemical and thermal (annealing and flame polishing) finishing. However, little basic understanding of the mechanisms of most other machining and surface finishing methods for ceramics, especially mechanical modes, now exists because they have not had the benefit of fundamental research.

2. The Motivation for Studying Ceramic Machining and Surface Finishing

There are two basic motivations for studying ceramic machining and finishing: intellectual and economic. The intellectual motivation is the quest for knowledge and understanding which stimulates the scientist's endeavors. The economic motivation is to improve the processes in order to achieve lower costs, greater productivity, and improved products. Basic knowledge of (1) the machining and finishing processes, (2) the resultant character of the surface and affected subsurface, and (3) the consequent effect on ceramic properties is needed in order to satisfy both of these motivations.

Intellectual motivation in its broadest sense arises because of the importance and scope of ceramic materials and the wide diversity of kinds of behavior they exhibit. The importance results from ceramics being one of the three major classes of solid (ceramic, metallic, and organic) materials. Thus, lack of knowledge and understanding of them represents a major scientific gap. The scope of ceramic materials in terms of structure, bonding, defects, and resultant properties presents a unique challenge and test of scientific theories. More specifically, machining and finishing are important to ceramists and other scientists whose specialization may be far from this area because of its importance in determining the character of ceramic surface and subsurface regions and thus many important properties. Optical and mechanical properties are obvious ones; magnetic and electrical properties can also be affected. The latter become more important as miniaturization of many parts progresses (with concomitant increases in surface-to-volume ratio).

The economic motivation is very significant because of two factors. The first is the impact of existing machining and finishing practices on the cost of ceramic components. Machining costs are very commonly of the order of 50 percent, and not infrequently in excess of 90 percent, of the total cost. Thus improvements in machining can have a major impact on the cost of parts. The second factor is the increasing demands of technology. Better performance is demanded of existing bodies, especially with respect to mechanical factors such as the level and reliability of strength. In addition, new bodies that are more difficult to machine than conventional ones are being developed to meet new needs. Finally, technology places new and more severe demands on both old and new materials. Finer tolerances, e.g., in finishing of gas bearings for gyroscopes and magnetic recording heads, are obvious examples. However, control of special surface topographies can also be important. These include controlled surface depressions for fluid reservoirs (e.g., for lubrication) or controlled surface roughness (e.g., for friction).

The intellectual and economic motivations are mutually dependent. Obviously, the immediate or ultimate cost of science must come from economic gain. However, further economic gain from machining and finishing ceramics is increasingly dependent on gaining basic understanding, the current lack of which limits applied goals. Substantial gains have been obtained empirically in the past, but cut-and-try techniques are unpredictable and can be excessive in cost when applied to ceramic components fulfilling critical functions.

3. The Challenge

Gaining an understanding of both the processes and effects of machining and finishing of ceramics presents many challenges. The multiple and often interacting parameters of the tool and the work piece in grinding and polishing are complex, with very limited basic understanding from which to start. The situation is compounded by the use of other mechanical

methods such as single point, ultrasonic, and fluid-driven abrasive machining, and by nonmechanical means such as chemical, electrical discharge, laser, etc.

The same range of machining and finishing methods has been applied to metals. However, ceramics present additional challenges. First is the general absence of macroscopic ductility to inhibit fracture inward from the surface. Second is the much broader range of structure and bonding and related intrinsic properties such as hardness, conductivity, and elastic modulus. Third is the broader range of microstructures that must commonly be dealt with. Porosity and second phases more frequently occur in many commonly used ceramic bodies. Further, ceramic bodies, especially in recent years, have been produced with substantially finer grain sizes (e.g., 0.1–1 μm) than are common in most metals.

Because of these greater challenges with ceramics and a lower level of research than in metals, ceramics start from a poorer background of knowledge. For example, it is only now coming to light that during mechanical machining and finishing considerable microplasticity occurs in the surface of crystalline ceramics and possibly some type of deformation occurs in the surface of amorphous materials. However, our knowledge of the details of these important processes is very poor, much more so than in metals.

4. The Rewards

The general rewards expected from the study of ceramic machining and surface finishing are, of course, the scientific understanding and economic gain that result as well as the attainment of improved property levels with higher degrees of reliability and reproducibility. The recognition by, or reminder to, many scientists that complex problems of practical importance in this area can involve stimulating, challenging, and fruitful research is hopefully also to be realized. More specifically, it seems reasonable to predict that an understanding of the mechanisms of removal and the character of the resultant surface can be gained, in part, by one aiding the other. Understanding these, in turn, can increase our knowledge of surface-dependent, e.g., mechanical, properties and hence provide the basis for improving these properties. Any or all of these advances may, in turn, lead to the development of new machining tools, some possibly designed explicitly for ceramics, and to new or broader application of ceramics, especially under demanding mechanical conditions or for electromagnetic components.

Among the specific trends that appear is the use of greater removal rates during grinding of many ceramics, and hence possible increased productivity. It seems clear that improvement or evolution will occur in properties, economics, rates of removal, tool and wheel life, and so on. On a broader scale, there should be a greater choice between mechanical and nonmechanical means of machining and finishing, as well as more choices within these two categories for many materials and their applications. The technology involved in the field of ceramic machining and finishing should mature rapidly if necessity, which often prompts invention, is recognized, and it can draw upon a growing base of sound scientific research and understanding.

This conference and the resulting volume should provide a good basis and a substantial first step for further scientific study and practical improvement of ceramic machining and surface finishing.

NATIONAL BUREAU OF STANDARDS SPECIAL PUB. 348, The Science of Ceramic Machining and Surface Finishing, Proceedings of a Symposium Sponsored by the American Ceramic Society, the Office of Naval Research, and the National Bureau of Standards, held at NBS Nov. 2–4, 1970, Gaithersburg, Md. (Issued May 1972).

II. TECHNIQUES AND MECHANISMS OF REMOVAL AND SHAPING

Session Chairmen

R. W. Rice, Naval Research Laboratory
V. E. Wolkodoff, Coors Porcelain Company
A. H. Heuer, Case Western Reserve University

A. Mechanical Methods

Mechanical Methods of Ceramic Finishing

Peter J. Gielisse and Joseph Stanislao
University of Rhode Island, Kingston, Rhode Island 02881

Mechanical methods of finishing ceramics have been reviewed based on current practice as well as past and present research results. A total systems evaluation involves technical process and economic parameters. State of the Art information indicates a need for scientific evaluation of the basic stock removal process.

Experiments simulating grinding with single point diamond tools have generated quantitative and qualitative data on mechanical, dynamic and thermal aspects of the stock removal process. Generation of the data involved specially designed techniques.

Analysis of the results have been made in terms of mechanical, geometric and material parameters. A mechanical and thermodynamic model is presented.

Key words: Abrasive; ceramics; diamond; fracture; grinding; grinding forces; grinding temperatures; machining; polishing; residual stresses; stock removal; surface analysis; theory of grinding.

1. Introduction

1.1. General

The objective of this presentation is to review the mechanical methods of ceramic finishing present, the state of the art, and explore the knowledge to-date on the theory of ceramic finishing and the effect of the finishing system on the final product.

Mechanical removal or grinding of ceramics has long been an art, the progress of which has almost entirely been based on experience. True scientific knowledge in this area has been meager. This is surprising since a major factor in the manufacture or fabrication of ceramic products is detailed knowledge of the variables and their interrelation in the processing and finishing cycles. Moreover, the critical link between the processed part and the characteristics of the end product is provided by the finishing cycle.

1.2. The Ceramic Finishing System

The two criteria for the selection of a ceramic finishing system are: (a) the economic considerations influenced by stock removal rates, tool life, initial cost, and grinding ratios (ratio of stock removal to wheel wear), and (b) the technical considerations. Economic factors have been and still are of major concern in the finishing cycle. For this reason, and also because they are more easily evaluated, the major emphasis in ceramic finishing studies has been on economics.

However, a better understanding of the technical aspects has lately become very desirable, if not imperative, especially with the many types of present-day high performance ceramics. Fundamental technical know-how in this area is particularly needed for:

- elucidating the basic stock removal process in ceramics, aimed at the development of generally applicable ceramic finishing data,
- understanding the nature of the influence of the finishing cycle on the finished product,
- accelerating improvement in the application and methods of finishing systems,
- guaranteeing reproducibility of each step of the finishing process and end product,
- evaluating the pros and cons of the various available methods of ceramic finishing,
- exploring the possibilities for preventing, minimizing or removing deleterious results,

439-921 O - 72 - 2

- enhancing knowledge of the behavior of or resistance of ceramics to various types of stress systems peculiar to the finishing mode,
- improving the economic factors which will enhance the feasibility of wider application of ceramics in society's technology.

With demands for specific properties in the finished product, it is imperative that all the capabilities, as well as the limitations of finishing techniques, be examined and evaluated. This evaluation can only be achieved when all available scientific and engineering knowledge is applied to establish optimum systems in order to gain the desired reliability in ceramic products.

Of all presently available stock removal processes—chemical, mechanical and other techniques—grinding is the furthest developed and most widely applied in the ceramic industry [1] [1]. Grinding has become a highly effective means of stock removal because of the continual improvements which have been made in controlling the various parameters in this process.

In the choice of abrasive, a diamond abrasive system appears most versatile and, in many cases, except for very soft ceramics, is the only choice. A diamond abrasive system can handle almost all degrees of finishing on practically every type of ceramic material. It is available for finishing in every grinding, cutting, or drilling mode on most sizes and with standard equipment. Its real cost, i.e., cost per finished part, is low. Furthermore, the diamond abrasive system can combine most of the "ideal" requirements in one stock removal system. Silicon carbide can be quite effective when applied in the appropriate mode, but is not generally competitive when stock removal rate has to be optimized. Aluminum oxide is used in finishing "green" ceramics.

Grinding, specifically diamond grinding, is thus recognized as a highly effective means of stock removal in ceramic systems. Present insufficient knowledge and lack of availability of information contribute to an often inadequate set of criteria being used in the selection of a grinding wheel for a specific application [2]. Moreover, this approach of random selection totally ignores the need for a full systems analysis of the complex energy (thermal, mechanical, electrical and chemical) mass interaction in ceramic finishing, to produce a fully characterized end product (workpiece). The choice of mode of application and abrasive does not define the system. A total systems study may in this context be regarded as the ultimate goal. Unfortunately, the behavior of many of the variable parameters as a function of total systems performance is virtually unknown. As an example, it is known that different surface finishes can be obtained under similar sets of conditions on various bodies having different structural and or compositional characteristics. Also, the result of the mass-energy interaction of the finishing cycle may be very desirable in one case but no so in another—particularly when it is realized that recrystallization, melt formation, changes in hardness, polymorphism, embrittlement, chemical solution, micro- and macrocracking, grain growth, residual stresses, formation of high dislocation densities, twining, slip, and the like may occur and change the characteristics of the original body thus influencing its performance.

The mode of material removal in grinding of ceramics affects the strength of the end product [2]. Dry grinding may be less economical, but wet grinding alters strength. One type or size of diamond in a specific wheel matrix may or may not act similarly to another type in a different matrix. Chemistry of the process or environment may influence the results.

In almost all cases, a highly selective, qualitative picture has emerged but no generally applicable quantitative data is available or has been developed. A lack of knowledge about the mechanism of abrasive material removal [3] in these high energy rate transfer processes has placed the selection of grinding parameters on an entirely arbitrary and pragmatic basis.

Figure 1 schematically shows the simplified

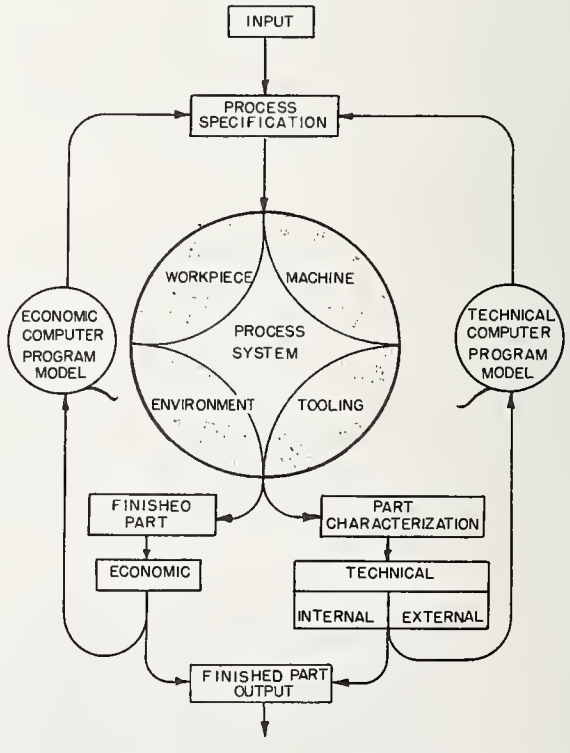

FIGURE 1. *Schematic presentation of a ceramic finishing system.*

[1] Figures in brackets indicate the literature references at the end of this paper.

ceramic finishing cycle, beginning with the needs as expressed in a set of finished piece specifications. The system can, via the economic loop and the technical loop, provide information of importance to the economics or the technical aspects of the process. The significant difference between the two components of the system is that the output provides the economic picture directly, while the technical information is not provided until the part characterization has been performed. It may further be noted that the technical information subdivides into two parts: the internal and external components. The external aspects would include such matters as geometry, finish, tolerances, roughness and waviness; while the internal aspects primarily refer to micro- and/or macrocracking, residual stresses, chemical contamination, alteration of transformation, resolidified or redeposited material, i.e., surface and possibly bulk alterations. A full systems analysis of the ceramic grinding process would produce a technical and economic model, close the cycles and provide for the possibility of entering particular specifications directly into the system to produce a ceramic product, fully characterized, in the economic and technical sense.

With the present state of the art, such a cycle of information cannot be expected to be completed or a complete theory or model of ceramic finishing devised in the very near future. However, it is possible to devise correlations which describe certain facets of the components of the system. Most important of all is the need to start an organized effort in the systems analysis of the ceramic finishing cycle, which should provide information generally available and applicable to random material or application requirements. Some knowledge is available for metallic finishing systems, in cutting as well as grinding, but virtually none has been developed for ceramic systems. It is at present impossible to consult one single source which gives normalized information significant in the determination of the choice of grinding wheel to be used in any one ceramic finishing application.

Any such study should start with the generation of information which will further the understanding of the fundamental and basic aspects of the ceramic finishing process. Such studies cannot escape the need for basic analyses with both single-point diamond tools and multipoint grinding implements (grinding wheels).

Again, a further choice indicates the primary need to be for single-point cutting tool studies since single-point studies unequivocally establish the true nature of many of the phenomena which are part of the ceramic finishing cycle. This can be done without interference from the many uncontrollable factors intrinsic to grinding wheels (variations in hardness, shape, size, concentration, bonding, etc.,) or need for recourse to complex statistical analysis. Statistical analysis is generally required when multipoint cutting tools are used. Such information by itself can, however, never establish the basic physical nature of the stock removal process. The research reported here deals, therefore, with the elements of a qualitative and subsequent quantitative study of the stock removal phenomena in ceramics by means of single-point (diamond) tools of known geometry.

A full systems analysis of a finishing cycle on ceramics is difficult due to several factors which comprise its very nature:

- the multipurposed objective in finishing
- the nature of ceramics
- the nature of the finishing cycle
- the inability to properly characterize ceramic surfaces internally and externally
- the lack of knowledge of a ceramic's reaction to conditions unique to the material removal system
- the still inadequate ways of specifying, in terms of physically recognizable and measurable quantities, the properties of a finished product.

1.3. Nature of Ceramic Finishing

The purpose of stock removal is generally to obtain a simple or complex final shape; to reduce to size and to specific, often highly accurate, dimensions; and to generate desirable surface finishes or properties as well as eliminate undesirable surface or bulk characteristics. It is thus clear that the requirements put on a bulk stock removal process are quite different from that which is called upon to produce a less than one micron finish in a fragile micro circuit substrate. The repeatability needed in the latter operation is not necessarily significant if gross shape features are the only objective. Detailed technical knowledge of the function and interaction of each parameter in a variety of stock removal systems employed is thus required to obtain the desired result.

Ceramics vary widely in characteristics which normally influence the stock removal process: hardness, compressibility, chemical reactivity, brittleness or ductility, elastic impedance, and resistance to thermal or mechanical stresses. The physical nature of ceramics further influences their behavior in stock removal. They can be homogeneous as in single crystals or heterogeneous as in the majority of technical and structural ceramics. Great differences in mode of stock removal may be observed depending on the ceramics grain size, degree and type of porosity, impurity level, presence or absence as well as nature of a secondary amorphous phase, and most important-

ly, the microstructural features which are the result of an often inadequately controlled or understood processing history. Much could be gained if properly characterized ceramics in which only a specific parameter such as grain size were a variable could be made available. This would considerably enhance the possibilities of investigators carrying out their researches on typical ceramic systems rather than on what is often alleged to be the less important, more idealized controllable systems as are, for instance, found in single crystals. This is not to say that work on such systems is not very important in terms of fundamental characterization of the basic principles but transition to the more complex and more generally encountered ceramics should be made and efforts should be expanded to facilitate this work.

Finishing of ceramics, through grinding, is in many ways similar to other commonly applied removal processes such as milling, cutting, and shaping, and has many of the facets of the thoroughly investigated field of finishing metallic materials. Yet there are significant differences. Grinding per se is probably one of the least understood processes. This is due to randomness of physical characteristics such as grit geometry or morphology, friability or hardness of the grain, degree of bonding to the matrix, and the nature and influence of the matrix on the process as well as the concentration and grain size of the abrasive itself. From the point of view of the finishing "tool" no one set of characteristics can be specified as is typical in, e.g., a metal cutting tool. Furthermore, significant interactions are hard to observe or study. Parameters common in metal finishing studies such as rake angle, depth of cut, shear angle, and chip geometry are not fixed but are variable in process which often necessitates the application of statistical analysis. Although notable, knowledge regarding the physical process often goes undetected. This is particularly true with regard to the cutting action of individual grains. The machine process creates further differences between abrasive machining and classical machining. Abrasive finishing is presently done at tool speeds about an order of magnitude higher than in cutting. Depth of cut, of the individual grain, is considerably less. Circular versus linear tool motion, the possibility of "up grinding" or "down grinding," and continuous versus discontinuous tool-workpiece interaction all add additional factors to be considered. Although wheel speeds in grinding are considered high as compared to speeds of cutting tools, present research indicates the desirability of increasing speeds well beyond those presently employed. Further complications arise when the different modes of abrasive machining are considered, each of which is distinctly different from the other in the mechanism whereby material is removed from the workpiece. This topic will be further discussed in section 2 of this paper.

Proper characterization of a generated surface is, as figure 1 shows, a very important part of a full ceramic finishing system. Characterization of the surface of a processed material in a particular application can, in general, be classified into one of three modes, according to chemical, physical, or geometrical parameters (see fig. 2). This is not necessarily synonymous

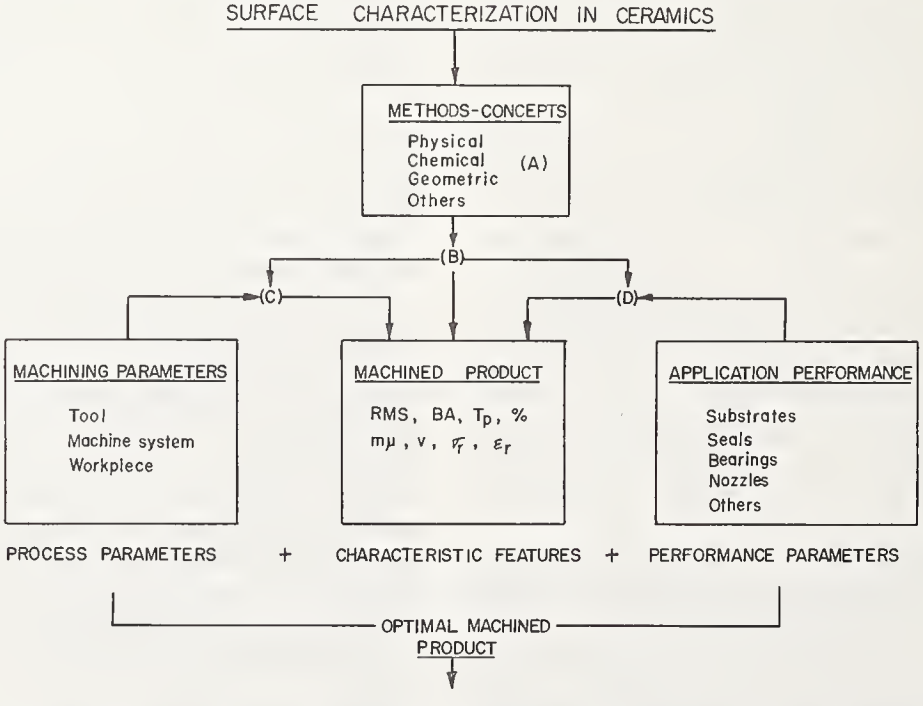

FIGURE 2. *Surface characterization in ceramics.* Schematic of interrelated components.

with a subdivision of the techniques being geometrical, physical, or chemical, i.e., a chemical technique may point toward the nature and extent of physical inhomogenieties in a surface, such as etching reveals dislocations. Discussion of the physical and chemical techniques of surface analysis is beyond the scope of this article. The topic will be extensively discussed in other sections of this conference.

At the moment geometrical characterization of a surface is readily carried out, widely investigated and developed, and generally accepted for comparative purposes. It should be pointed out, however, that the function of a surface is invariably influenced by its chemical and physical parameters. In many, if not most cases, the geometrical constitution of a surface will markedly influence the chemical and physical aspects, as well; a physical property, such as the coefficient of friction, is greatly influenced by the "roughness" of two mating surfaces, the reaction (chemical) between the tool and the workpiece (tool life) in a cutting operation strongly depends on the surface geometry of the tool as it engages the workpiece. Analysis of the functionality of a surface in a particular environment invariably requires geometrical analysis.

It is important to point out here that the development of a surface *test*, which will characterize and guarantee the performance of a surface in a particular application, presupposes that a surface *analysis* has been made. Attempting to obtain surfaces of lower and lower roughness readings of the peak (overall roughness) or averaged (AA or RMS) variety, and equating this with surface improvement, constitutes a positive result only if it has been determined that there is a direct correlation between this measured parameter and the functionality of the surface. At present, it must probably be assumed that, in the majority of cases, a surface test is attempted ahead of the more critical surface analysis. Surface analysis therefore attempts to establish the parameter or parameters most directly connected with the optimum functionality of a surface.

The objectives of a complete surface analysis may be thought of as consisting of four parts—the improvement of the surface function, the influence of every processing step, the guarantee of part reproducibility, and the provision of meaningful criterion on surface conditions.

The first objective is the improvement of the surface function or functionality. The solution of this problem requires the determination of the often missing link between the surface conditions of the processed part and its ultimate performance in the application. At present no standards exist in even the most general of cases. The ultimate solution lies in the close cooperation between the producer and user in determining the critical parameters of the process under identical conditions. Specifications on parts will only have meaning when such specifications are determined under identical test conditions. This is of particular importance when it is realized that the functionality of a surface may critically depend on the processing mode. Standards on a ground surface may have to be altered when such a surface is found to be more economically produced by a turning operation.

The second objective is the determination of the influence of each and every step in the processing on the final functionality of the part. Considerable economic advantage may be obtained if the sequence of operations leading most advantageously to the desired surface can be determined. It might thus be possible to replace particular operations with others, or eliminate them completely. A final polishing or lapping operation could be prevented by judicious choice of the previous grinding parameters (speeds, feeds, hardness of wheel, etc.)

The third objective is the guarantee of part reproducibility. Without the ability to guarantee part reproducibility, uniform part performance will not be possible. Part reproducibility requires the investigation of the influence of the individual process parameters of any one processing mode on the final surface conditions. Again, in the case of a grinding operation the influence of the variation of parameters, such as speed, grain size and hardness of the wheel, and often even the type of grinder, should be known. If such parameters can be or are already being controlled, it suffices to relate their variation to the surface conditions of the single part and thus guarantee reproducibility.

The fourth objective is to provide a meaningful criterion on surface conditions. The importance here lies in the establishment of an objective measurement to replace the often subjective opinions or criteria (reflectivity, appearance, etc.) which easily lead to misunderstanding. An objective measurement eliminates such misunderstandings.

It should be apparent that the task of surface finishing is not a simple one and cannot be carried out without intensive surface analysis. Significant advances have been made during the last decade in determining the functionality of a finished ceramic workpiece. This is primarily true with regard to the influence of surface and subsurface characteristics on mechanical properties.

1.4. Effect of Ceramic Finishing on the Workpiece

Machining operations, such as grinding, lapping and polishing, leave residual surface defects and, as a result, these defects impair the mechanical strength of a ceramic. The nature

of the damage, the physical mechanism by which it is produced, and above all the extent of the depth below the surface of such damage is not very well known. Surface damage (cracks or flaws left in the machined surface) is generally distinguished from subsurface damage (introduced lattice defects). Brittle materials show the development of surface damage more than subsurface damage which appears to dominate in semibrittle ceramics. The two types of damage, however, can occur simultaneously and their relative extent depends on the stock removal mechanism (speeds, feed, wheel or abrasive characteristic) and the nature of the polycrystalline ceramic. Koepke and Stokes [4] have studied the nature and extent of subsurface damage in MgO after grinding with Al_2O_3 and diamond wheels. Their etched Al_2O_3 ground specimen shows a distinct plastically deformed layer, the thickness of which increases with the depth of cut. Slip bands in $(10\bar{1})$ and (101) planes penetrate beneath the plastically deformed layer at high depth of cut and feed rates, as may be seen in figure 3. The extent of the damage is higher in the dry grind than the wet grind mode. Diamond grinding produces a less well defined deformed layer with evidence for formation of screw dislocations below and parallel to the ground surface. No simple relationship was found between the depth of damage and the material removal rate as in the case of Al_2O_3 grinding. Lower limit of depth of damage was found to be about 50 μms or 1.5 times that with an alumina wheel. This seems to clearly indicate a difference between the reaction of Al_2O_3 and diamond particles when interacting with the same workpiece. Diamond tends to deform less, grain penetration is higher and energy absorption and stress concentration is higher for the workpiece in the diamond case. Surface damage showed again a difference in behavior for Al_2O_3 and diamond. Al_2O_3 grinding produced a network of surface cracks normal to the grinding direction. This is due to tensile stresses generated by thermal quenching. Al_2O_3 grinding can be high temperature grinding due to the low thermal conductivity of the grain and possibility of wheel loading. At these high temperatures material removal can be made by plastic flow. The material often becomes burnished. In diamond grinding of MgO crack formation is limited because of cool grinding with unloaded wheels. Gielisse et al. [1] have previously indicated that this should be the case. Section 3 of this paper has worked out this concept further. Whereas the work of Koepke and Stokes indicates a definite influence on surface and subsurface properties as a result of grinding, the nature and extent of the damage depends on the parameters of the grinding mode. Cool grinding with nonloading wheels, containing discrete cutting points of which the penetration depth and stress concentration for any one ceramic can be controlled, appear indicated. Rice [5] has made similar investigations and observed dense layers of dislocations, slip bands and sometimes cracks in MgO, with the extent of the phenomena again depending on machine and material parameters. Fine grain size and high yield stress limits the depth of the altered layer. There also is a direction dependency (anisotropy). Inhibition of motion and surface work hardening were observed. Annealing of the finished specimen can reduce the grinding damage considerably. The effects have been observed in both single and polycrystalline samples. Rice's work also includes investigations on the lower yield strength CaO. X-ray techniques have been used by Cutter and McPherson [6] to examine handlapped or sanded single crystals of hot pressed MgO. Dense layers of dislocations (10^{11} dislocations/cm^2) were observed below the surface. Harrison [7], as well as Evans and Davidge [8], have observed cracks in diamond cut MgO crystals. Ion beam thinning in conjunction with transmission electron microscopy is presently being used to study subsurface structure in polycrystalline ceramics. Hockey [9] has used these techniques to provide direct evidence of plastic deformation occurring as a result of abrading aluminum oxide. Single and polycrystalline specimens of Al_2O_3 show high dislocation densities, basal as well as nonbasal, within the near surface areas when polished with diamond as fine as one quarter of a micron. This may indicate a considerable amount of plastic deformation during abrasive wear. Regions of the highest dislocation densities defined the traces of surface scratches produced by individual abrasive particles. This is shown in figure 4. Rice has used R.F and ion beam sputtering techniques to explore the extent of damage in surface finishing. Figure 5 shows the effect of R.F. sputtering of scribe marks on cleaved MgO crystals. The nature of Hockey's techniques enabled him to

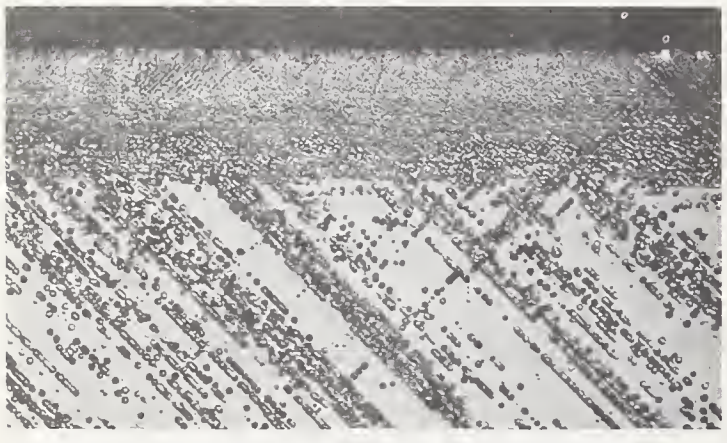

FIGURE 3. *Etch pitted damage layers in magnesium oxide single crystals as a result of grinding magnification app. 95X.* From Koepke and Stokes [4].

FIGURE 4. *Dislocation produced as a result of diamond polishing polycrystalline* Al_2O_3 *magnification 10.000X.* Courtesy B.J. Hockey, National Bureau of Standards, Washington, D.C.

observe the introduction of relatively large compressive residual surface stresses [9].

It is thus rather well established that grinding of ceramics is a mutative process. The question is whether the mutation is detrimental or advantageous and what factors play a major role in their generation or prevention. The formation of regions of high density dislocations as a result of thermal and/or mechanical effects in surface finishing should lead to surface strain or work hardening. This has been observed by Rice [10] to be particularly pronounced in large grain size, low yield strength materials. Fine grain size materials can be weakened due to the more limited degree of workhardening and the higher stresses reached in the finer flaws of these materials. The mutative effect of surface finishing processes can be more easily quantified when expressed in terms of the surface residual stresses resulting from the combined physical processes that cause them; thermal, chemical or mechanical. Plastic deformation due to non-uniform dilation, volume changes as a result of chemical reactions, phase transformations, precipitation, melting and nonuniform plastic deformation due to mechanical working are respective examples of such processes. When considering strength, compressive residual stresses are generally regarded favorable in ceramics. The compressively stressed surfaces prevent the

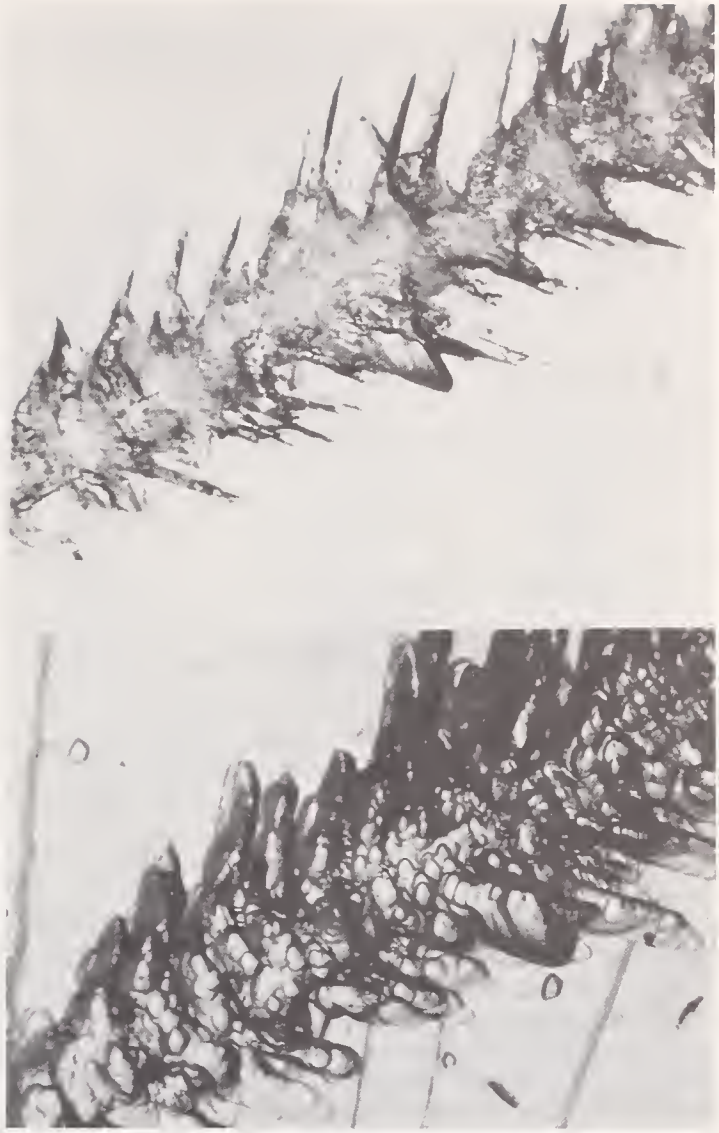

FIGURE 5. *R.F. sputtered scribe marks on cleaved MgO crystals.* Two hours (top) and seven hours (bottom). Courtesy Roy W. Rice, U.S. Naval Research Laboratories, Washington, D.C.

propagation of cracks. Both compressive and tensile stresses must be controlled when a high degree of flatness in thin, low cross-section parts, such as in substrates, is required. Residual stresses due to finishing can lead to failure in thermally cycled ceramics such as in ruby laser applications. Above all, a convenient nondestructive method for determining subsurface residual stresses and stress distribution is needed. No satisfactory method is available as yet. Hara et al., [11], using the x-ray stress measurement technique, have recently shown that grinding induces compressive residual stress (>100 kg/mm^2) in cemented WC which decreases with increasing distance from the surface and finally become tensile. They also measured the lattice distortion and came to the remarkable conclusion that residual stresses can extend beyond the depth zone of lattice distortion. Residual stresses can be reduced by an-

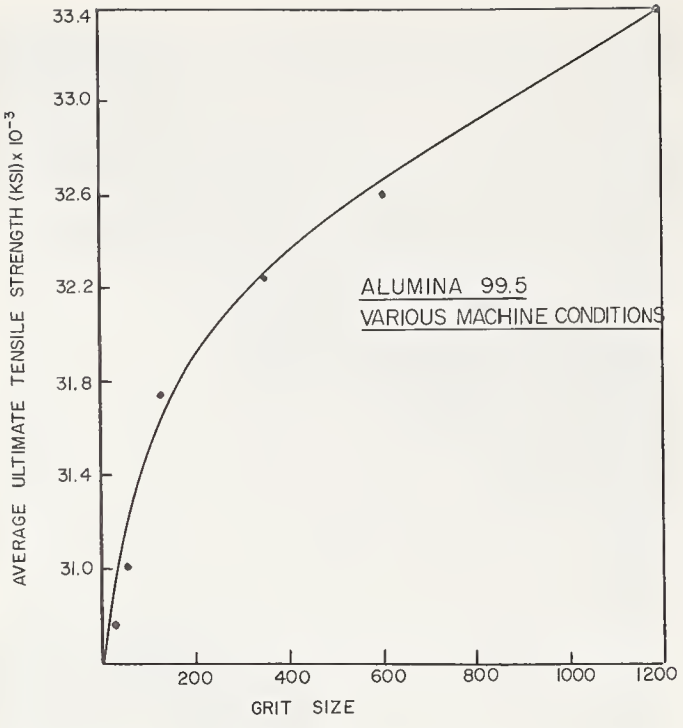

FIGURE 6. *Average tensile strength of 99.5 alumina as a function of diamond grit size.* After data from Sedlacek [12].

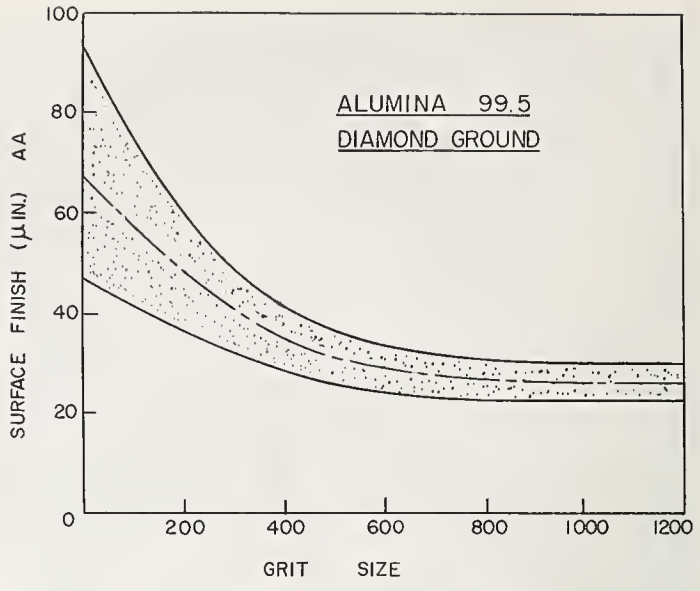

FIGURE 7. *Surface finish as a result of diamond wheel grit size.* After data from Sedlacek [14].

nealing. Annealing reduces dislocation density as conclusively shown by Rice [5] and Hockey [9] in their investigations on MgO and Al_2O_3 respectively. Knowledge of residual stress patterns should enable a more direct quantitative way of studying mutative effects due to subsurface alterations in the workpiece.

Since grinding establishes the surface and subsurface characteristics of the workpiece, the influence of the various system parameters should be examined. The work by Sedlacek [12] has made significant contributions in showing that diamond grit size has a definite and systematic effect on strength. Figure 6 is a plot of average ultimate tensile strength as a function of diamond grit size. Data are from Sedlacek's investigations on 99.5 alumina using the internal grinding mode. The effect is found regardless of previous grinding history. The relationship is systematic and shows a decrease in strength with increase in particle size. Similar results have been reported by McKinney and Herbert [13] on SiC ground AlSiMag 614 (94% pure alumina near zero porosity). A relationship seems to exist between strength and the depth of surface flaws if one assumes that larger grain sizes leave larger surface cracks. This can be further examined in figure 7 which was plotted using data from Sedlacek [14]. It may be observed that larger grit size produced a wider spread in and higher values of surface roughness. The boundary lines were drawn in to accentuate the apparent trend. The data do not, however, indicate whether the effect may be due to subsurface cracking generally observed with larger grit sizes. Laboratory results [15] indicate a considerable increase in grinding temperature with increase in depth of cut (i.e., increase in grit size). What appears very significant is the influence of the matrix of the grinding wheel. A 100 grit resin bonded wheel was found to produce the same surface finish and strength as a 32 grit metal bonded wheel. A larger grit size can cause a much smaller effective scratch when it is allowed to absorb part of the grinding force in a low modulus matrix. Sedlacek [14] further found a considerable effect of the rate of material removal but distinguishes between infeed and table speed both of which determine rate of removal. Heavy infeeds are detrimental to strength. Dry grinding lowers strength presumably due to an increase in thermal upset. In general, the mode of material removal influences the strength of the final product. The extent of this influence is considered by Sedlacek to be less than the effect of environment on the strength of alumina. He holds a stress activated chemical reaction (stress corrosion) between alumina and surface absorbed water responsible for the decreased strength of alumina in a wet environment. Our experiments in O_2, N_2, air and a water mist show a considerable decrease in both tangential and normal forces for a single grain cutting through various types of ceramics in the case of the H_2O mist (see fig. 8). A limited difference is found between the gases. A larger difference is apparent from material to material, pointing towards the importance of microstructure (grain size and composition) of the workpiece itself.

Careful monitoring of the dynamic aspects, i.e., force pattern, will be relevant with regard

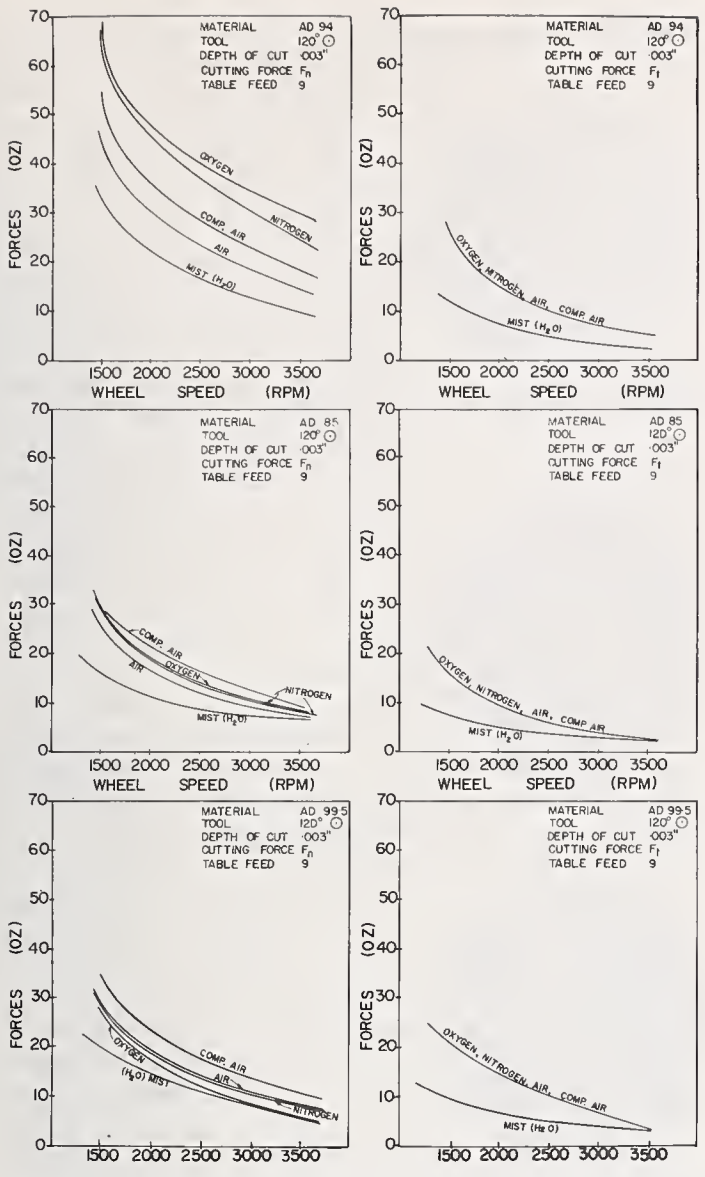

FIGURE 8. *Influence of environment on grinding forces in single point cutting of three types of alumina.*

to the study of subsurface plastic deformation as a result of the stresses imposed by the wheel. These forces depend primarily on the properties of the ceramic as will be shown in another section of this paper. Control of the thermal aspects will influence the extent of the surface damage.

2. Mechanical Finishing Processes

2.1. General

Stock removal by mechanical means can be accomplished in one of two ways: on a microscale where material is removed by abrasive interaction, atom by atom or molecule by molecule, or alternatively on a macroscale in which the dimensions of the resultant particulate matter are orders of magnitude larger than that of the basic molecular constituent (see fig. 9). The former process leads to a perfectly smooth

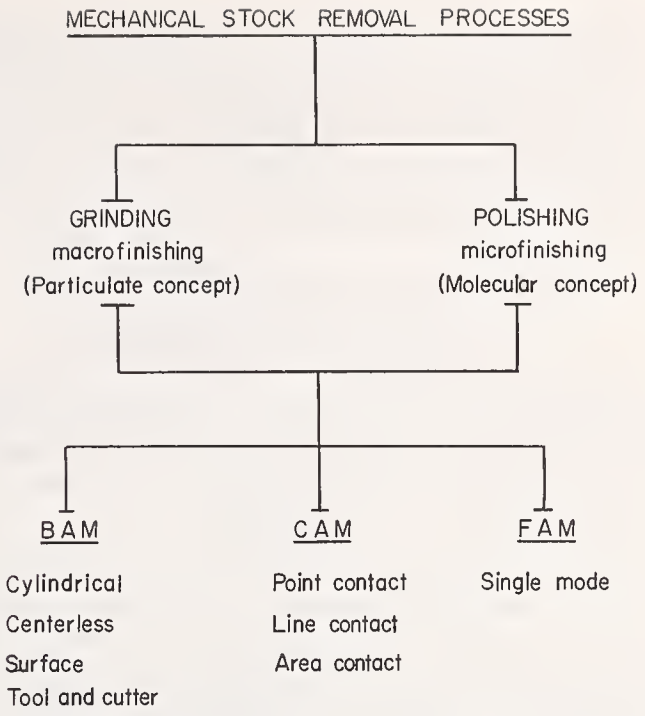

FIGURE 9. *Subdivision of mechanical stock removal processes.*

surface if the process is carried on long enough and a homogeneous material is assumed. In principle, perfectly smooth surfaces could be obtained in macrofinishing if the material were removed by an internal shearing process as a result of total and perfect plastic deformation. Broadly speaking, mechanical stock removal in metals is a process of this type albeit not totally perfect, while stock removal in brittle or semibrittle ceramics is primarily the result of an internal fracturing process. The macrofinishing mode requires penetration of the surface which is accomplished only if sufficient energy is imparted by the system on the workpiece to overcome its yield strength. The concepts of macro- and microfinishing leads to the distinction between the two fundamental types of abrasive mechanical surface finishing—grinding and polishing. Grinding requires penetration of the grit into the workpiece surface and material of macroscopic dimensions is removed. It may be referred to as macrofinishing. In grinding ceramics, as a result of insufficient plastic deformation, penetration of the abrasive produces a crack field extending in front of the abrasive. By multiple interaction the grinding particles are produced. Because of the need for penetration, grinding is a high pressure process.

Polishing does not require penetration, and material of microscopic dimensions is removed. This will be referred to as microfinishing, and it is inherently a low pressure process. Polishing can, of course, be done by other than mechanical processes. Thermal processes in which surface layers are melted have been applied; flame

polishing is an example. Chemical processes such as chemical etching have been successfully used. Combinations of mechanical and chemical action are also possible. Polishing of boron carbide surfaces with alumina or boron carbide itself is an example. Several of these processes will be discussed in detail in other sections.

2.2. Mechanical Methods of Surface Finishing in Ceramics

Virtually all methods of ceramic surface finishing to-date are multipoint abrasive operations, as distinct from single point tool operations. Therefore, only multipoint processes will be discussed.

Both grinding and polishing processes fall into three fundamental categories based on the way in which the abrasive is held: Bonded Abrasive Machining (BAM), Contained Abrasive Machining (CAM), and Free Abrasive Machining (FAM). A diagrammatic presentation of this subdivision is given in figure 9.

a. Bonded Abrasive Machining

Bonded abrasive machining can be equated with standard wheel grinding. The abrasive is fixed in a matrix of a vitreous, metallic or organic nature. By feeding the rotating wheel into the moving workpiece, the abrasive is forced to penetrate it. The individual abrasive grain intermittantly impacts and moves through the workpiece at speeds of thousands of surface feet per minute. Recent research indicates that desirable speeds differ with materials [15]. Low speeds can quickly generate very high forces. Indications are that high speeds are generally beneficial if the resultant high temperatures are not detrimental. Truly high speed processes (>10,000 SFM) in ceramics have not been investigated sufficiently. This is discussed further in section 3 of this paper. The nature of the bond is all-important. The matrix should have mechanical properties which enable the individual grains to effectively penetrate the workpiece without premature breakdown of the grain itself. The mechanical characteristics of the workpiece primarily dictate the choice of matrix properties. Thermal properties must be compatible with the temperatures developed during stock removal. The optimum elasticity of the wheel under any one set of machining parameters is primarily determined by the choice of matrix material but can be further influenced by adjusting abrasive concentration, size, morphology, filler type and content and processing parameters. Generally insufficient attention is being paid to the possibilities of optimizing the process by varying the above parameters. The primary reason for this is lack of fundamental understanding and knowledge in this area. The performance of the abrasive in the BAM process is determined by its abrasion resistance. The physical characteristics which are known to play a major role are: (hot) hardness, strength, morphology, chemical reactivity, frictional and thermal properties. These have recently been reviewed [16] and need not be further reviewed here. The above considerations lead to the inescapable conclusion that for finishing ceramics with present BAM techniques, diamond is the preferred abrasive. Some reports indicate that manufactured diamond may, on ceramics, be preferred over its natural counterpart [1]. Physical characteristics are more important than the abrasive's origin, particularly since natural diamond can be processed to yield closely resembling characteristics. A classification of diamond types on the basis of physical characteristics is important since all types are used in distinctly different finishing operations on ceramics. A brief overview follows. See figure 10.

Low impact strength diamond (LISD) is a relatively friable diamond crystal essentially anhedral, or without prominent crystalline faces. Its large surface area and irregular geometry make possible excellent bonding and retention in the resin matrix in which it is almost exclusively used. Because of its relatively high friability, it will generate new cutting points on materials with a high modulus of resilience (MOR), but would create undue wheel wear on low MOR materials. Its applications in ceramic systems is on very high yield strength aluminas (99.9), Lucalox, or hot pressed polycrystalline alumina. The large number of asperities make for low pressure per contact point and possibilities of effective polishing.

Modified low impact strength diamond (MLISD) is basically a friable-type crystal surrounded by a high-modulus metal shell. It generates new cutting points on high MOR materials, but does so in a controlled manner. Retention of the abrasive and thermal conductivity are both enhanced. The net result is usually a significant increase in grinding efficiency. A nickel coated product is used in wet grinding and a copper coated product in dry grinding of more ductile ceramics such as cemented tungsten carbide.

Medium impact strength diamond (MISD) is a less friable or semifriable diamond in which crystal faces are moderately well-developed. Geometry is decidedly more blocky, generating higher pressures per contact point and thus more efficient penetration. MISD is a tougher diamond than the low impact strength diamond and is primarily used in metal bond systems and is ideally suited for grinding glass and ceramics. On low or high MOR materials it will cause undue wheel wear.

High impact strength diamond (HISD) is a very strong crystal with large, well-developed

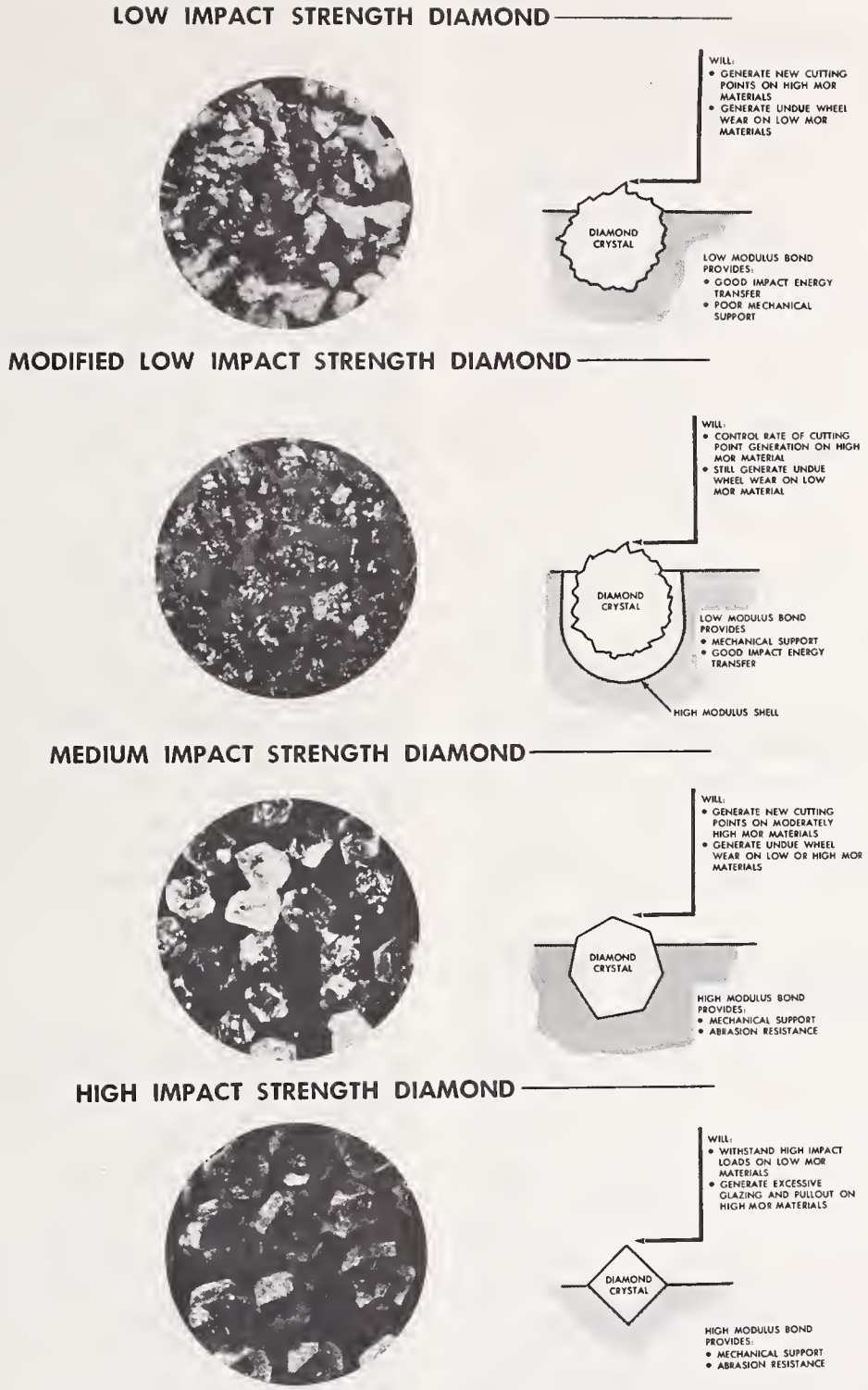

FIGURE 10. *Principal Types of Diamond and Their Major Applications.*

cubic and octahedral crystal faces. It will withstand high impact loads on low MOR materials because of its strength, but alternately (mainly because of its smoothness and relatively low surface area) it will generate excessive glazing on high MOR materials and thus promote pullout from its metal bond. Its application in ceramics is in cutting and slicing of both natural and manufactured products.

Relative grinding performance and efficiency of the various types of diamond are shown in figure 11. Generalized workpiece characterization as a function of the modulus of resilience is given in figure 12. Other abrasives used in BAM processes are SiC and Al_2O_3. Silicon carbide is used in machining "green" ceramic parts. Alumina has the advantage of not introducing materials of different chemical composition. The same operation is often performed with carbide cutting tools in conventional turning or drilling operations. Bisque fired parts could be handled by the same abrasives. Finish-

ing of bisque fired parts is not commonly practiced because of the additional processing step involved in manufacturing the part. In addition to the true matrix type wheels, plated wheels

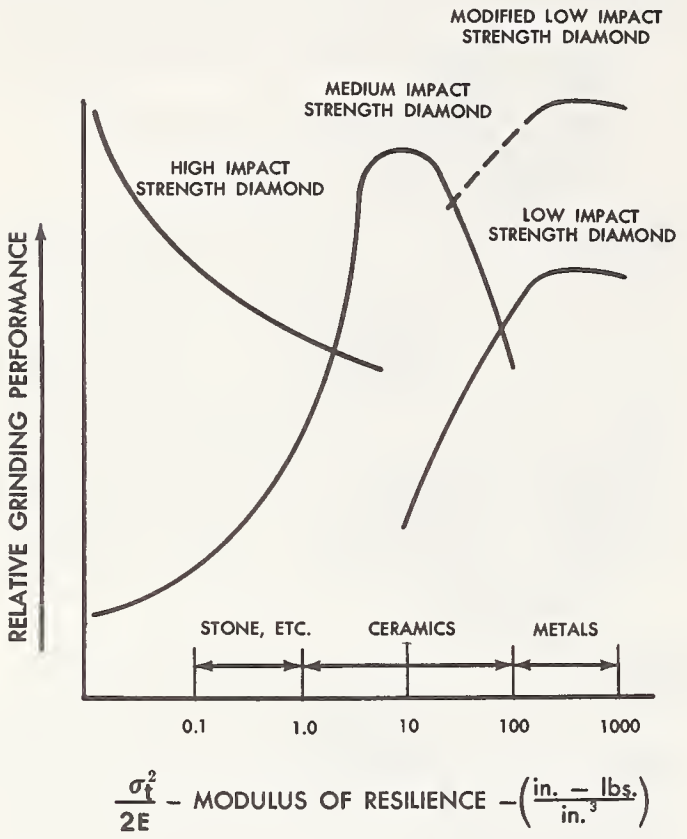

FIGURE 11. *Relative grinding performance of principal diamond types as a function of modulus of resilience.* After data from reference 1.

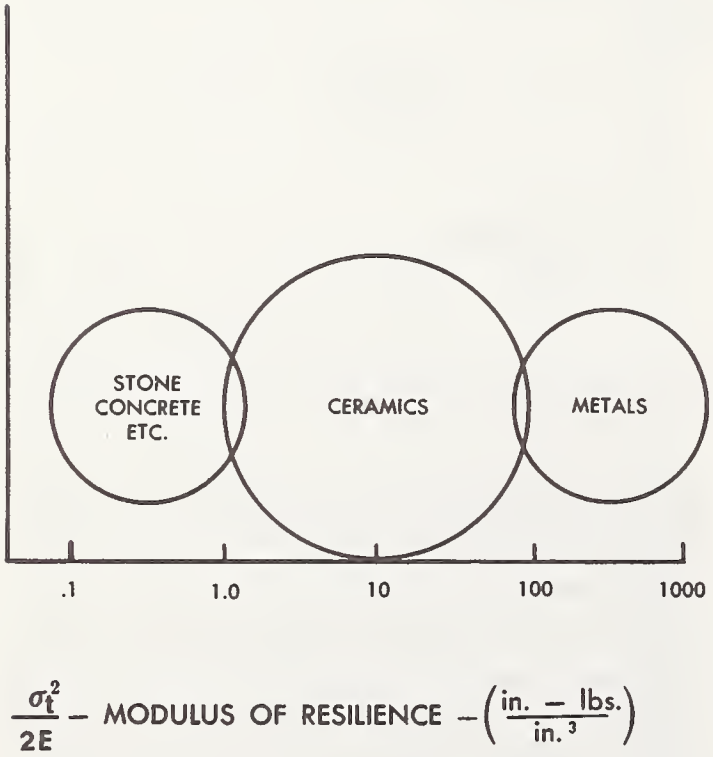

FIGURE 12. *Workpiece characterization [1] as function of the modulus of resilience.*

in which a monolayer of diamond is deposited on a metal base are finding more widespread application. They are particularly useful when complex shapes have to be imparted (form wheels) or when process parameters require it, as in rotary ultrasonic machining.

The bonded abrasive machining method can be applied in a variety of forms depending on the finishing mode and the geometry of the workpiece. Various types of BAM techniques are shown diagrammatically in figure 13. In CYLINDRICAL GRINDING the workpiece periphery of a rigidly supported rotating workpiece held between centers is ground by a wheel revolving at high speeds while the work rotates at much lower speeds of 75—150 surface feet per minute. The wheel is fed into the work, and either workpiece or wheel is traversed. Variants are the universal center type grinder in which tool post and stock holder can be moved around a vertical axis enabling bevels and angles to be ground. Roll grinders are designed to handle large diameter rolls such as those used in the textile, paper and printing industry. In chucking grinders used on short pieces, the work is held in a chuck or collect rather than between centers. Tool post grinders carry the wheel for external or internal work on a tool post or the compound rest of a lathe. The wheel is directly driven from a motor shaft. CENTER-

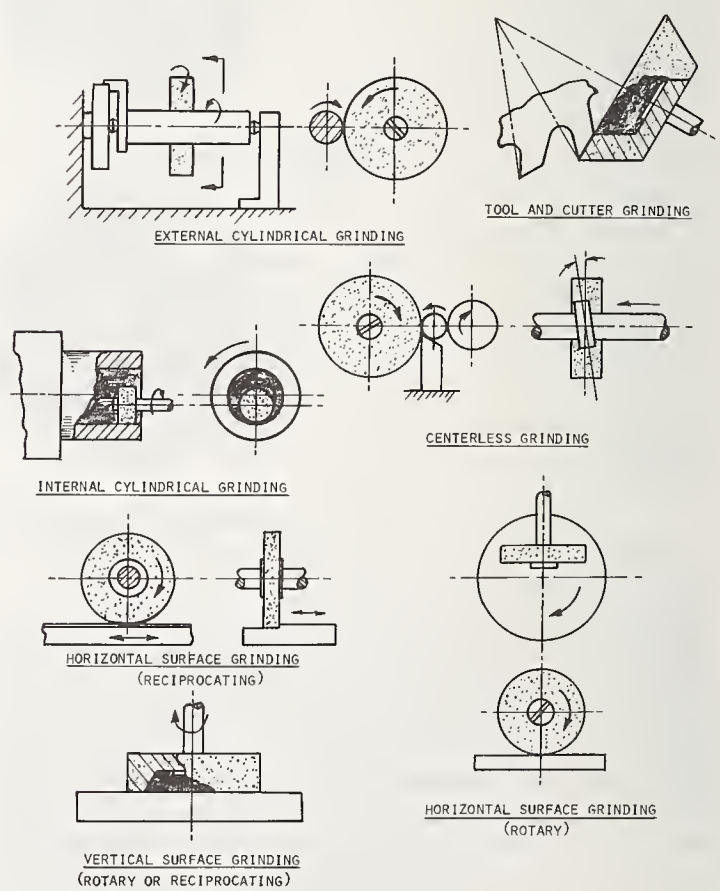

FIGURE 13. *Diagrammatic presentation of the major bonded abrasive machining techniques.*

LESS GRINDING can be done internally and externally by supporting the workpiece on a work rest blade and revolving it between a drive wheel and the grinding wheel mounted on opposite sides of the cylindrical post. Additional pressure rolls and supporting rolls are often used in internal grinding of this type. This regulating wheel is often mounted at an angle to the plane of the grinding wheel to accomplish through feed. These grinders are limited to grinding cylindrical parts and are most commonly used in mass production. INTERNAL GRINDING can be of the chucking or centerless type with relatively small wheels mounted on spindles revolving at high speeds and traversing the workpiece by hydraulic movement of the grinder bed on which the spindle is mounted. The wheel is simultaneously fed into the workpiece. SURFACE GRINDING is used to produce flat surfaces or grind irregular surfaces by means of shaped or formed wheels in form grinding operations. The various types are based on the movement of the wheel into vertical or horizontal spindles while the table holding the workpiece may be reciprocating or rotary. The reciprocating horizontal surface grinder is the all purpose shop and tool room machine, while all other types are more generally applied where many parts need to be produced in a mass production fashion. Vertical spindle rotary table grinding is very common in nonmetallic or ceramic applications. Frequently more than one grinding head is used in vertical spindle, rotary table grinders. Work is held by magnetic, electrostatic or vacuum flat chucks or is cemented or clamped down on the grinder's table. TOOL AND CUTTER GRINDERS are used to sharpen the edges of milling cutters, reamers, drills, etc. They are outfitted to move the workpiece horizontally and vertically. The wheel can move up or down with a 360 degree rotation around a vertical axis. By employing beveled or cup shaped wheels, virtually any tool configuration can be accommodated. NONCONVENTIONAL MECHANICAL TECHNIQUES can take several forms. Abrasive jet machining is the removal of material through the action of a focused stream of fluid generally containing abrasive particles. Ultrasonic abrasive machining cuts material by high frequency repetitive impact between a tool and workpiece with an abrasive slurry in between. Rotary Ultrasonic Machining (RUM) is a relatively new technique with particular promise for the ceramic area. It is, therefore, discussed in somewhat greater detail. In RUM the actions of high speed rotary grinding and reciprocation of the rotating tool at ultrasonic frequencies are combined. Conventional ultrasonic machining does not employ rotary motion and uses an abrasive slurry between a preformed tool and the workpiece. Tapering of the hole, imbedding of abrasive into the workpiece and limitations on stock removal are cited as the disadvantages of this method, which are overcome by simultaneously rotating and ultrasonically vibrating. The RUM technique employs a bonded (plated) diamond abrasive rotating at variable speeds up to 5000 RPM. The application of ultrasonics to the rotating diamond tool assists the grinding by reducing friction between the tool and the workpiece, preventing clogging of the wheel through ultrasonic cleaning action of the coolant and reducing the required grinding pressure. Disadvantages are primarily derived from the limitations of weight of the diamond tool (70 gram maximum) which can be effectively coupled with the present 20 KHz sonic vibrator and coupled horn.

In principle, the method lends itself to drilling, threading, grinding and milling operations. Material limitations are those commonly connected with the use of diamond, although operation on carbides, tungsten, titanium, as well as boron carbide, has so far not been successful. In general, application is limited to hard, brittle, nonmetallic materials such as sapphire, ruby, beryllium oxide, aluminas, glass, ferrites, quartz, zirconium, pyroceram, lucalox and boron composites where chemical interaction with the carbonaceous abrasive does not play a significant role.

No clear advantage has been developed for the use of fluids other than water. The fluid functions as a lubricant, coolant and cleaning agent. Ultrasonics may add to the operation by atomizing the fluids. Dry operation leads to appreciable heat generation resulting in premature tool failure. Fundamental knowledge of his technique is still lacking, probably more so than for any other BAM method. Tool pressures are said to be less than for other grinding operations. Tool loads range from 5—60 lb depending on tool type and operation. A force of 5 lb is considered typical on a 0.040 in core drill. Surface finish data are not available for direct and objective comparison. Finishes of ~32 rms with a 120 grit diamond tool are considered standard.

Material removal rates and optimum machine parameters have not as yet been determined. Where applicable, the method is invariably faster and performs the operation with less chipping, tapering or break-through problems. Figure 14 compares the feed rates in drilling 99 percent alumina employing RUM and with the ultrasonic vibration turned off. As the figure shows, the feed rates drop off as the drilling depth increases for both methods although the average drill rate appears twice as fast with RUM for the conditions of this particular test.

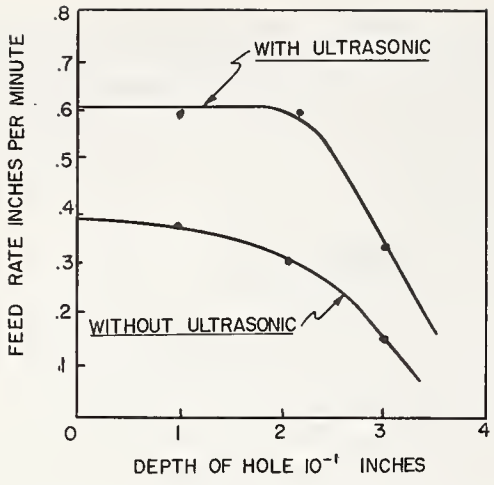

FIGURE 14. *Comparison of performance data in drilling 99 percent alumina with and without ultrasonic assist.* Data generated by the authors.

b. Free Abrasive Machining

Free abrasive machining is different from bonded abrasive machining (standard wheel grinding) or contained abrasive machining (lapping) in that the abrasive is suspended in a vehicle and held between a very hard (R_c 60–62) horizontally rotating alloy steel wheel and the workpiece. In this fashion the abrasive grain is in contant surface contact with the workpiece and is rolled over the wheel surface without being embedded in it. It is an inherently cool machining method with the wheel reaching temperatures around 200° F. The successful operation is predicated on the fact of two favorable hardness ratios: the wheel hardness to abrasive hardness ratio and the abrasive hardness to workpiece hardness ratio. The former is ideally held at a value of 1:1 or 2:1 and primarily governs the degree to which the abrasive is effectively rolling over the surface without embedding. The second ratio is ideally regarded as having a 1.5:1 or higher value and generally determines the degree to which the abrasive can penetrate the workpiece and subsequently remove stock. The term hardness is again used as expressing a combination of static physical characteristics such as a combination of physical hardness and toughness reflecting the degree of inpenetrability of a sharp point. A peculiar situation exists in which on the one hand one desires as "hard" an abrasive as possible to remove stock whereas the "hardness" of the abrasive at the same time has to be limited to a value which prevents embedding in the wheel to facilitate the mechanism of free abrasive machining in the first place.

Silicon carbide is generally used as the abrasive and most generally approaches the above requirements for a wide variety of applications. It is advantageous from an economic point of view. Very little difference in performance, if any, can be detected between different grades of SiC (black or green). Boron carbide is effective on certain very hard materials such as tungsten carbide. The economic disadvantages are offset by the possibility of recycling or recovering the abrasive for further use. Aluminum oxide can be applied on soft materials but with a much reduced stock removal ratio when compared to SiC.

Maintaining the abrasive film is all-important. Several types of vehicles are used such as diesel fuel oil of various viscosities as well as water. The type of vehicle depends on the operation. The abrasive film requirements limit the grain size in an effective abrasive machining operation to approximately 5–10 μ with subsequent limitations on surface finish. With very small grain size the forces required to affect penetration would be high enough to break the grains down by shear or imbed them into the rotating wheel. It is at this point that free abrasive machining merges into a CAM operation in which abrasives of any particle size can be employed.

The effectiveness of the operation is governed primarily by speed, pressure, concentration and size of the abrasive. The rotational speed of the wheel varies with its diameter (3 in—87 rpm, 48 in—63 rpm, 64 in—45 rpm, 84 in—31 rpm) to give an average constant surface speed. Higher speeds would mean higher stock removal rates but speed is limited by the properties of the vehicles (evaporation and decrease in viscosity) and the centrifugal forces which would remove the abrasive prematurely. Pressure increases stock removal rates. Pressures of from 3 to 5 psi are most favorable, the exact value depending on the material ground. This is considerably higher than the pressure in an average contained abrasive machining operation which is generally held at from ½–2 psi but lower than the (dynamic) pressures in bonded abrasive machining. This becomes an important consideration when surface alterations due to pressure or temperature are expected to have an adverse effect on the workpiece. Pressure is required to force the abrasive into the workpiece causing deformation or brittle fracture as a result of the high pressure in the actual contact zone. Subsequent stock removal follows as a result of the rolling or cantilevering action of the abrasive grain. Figure 15 top shows a generalized pressure versus stock removal curve. The sharp drop off after 5 lb/in is primarily due to premature breakdown of the particles at pressures higher than their friability limit. A certain minimum concentration of abrasive is required to estab-

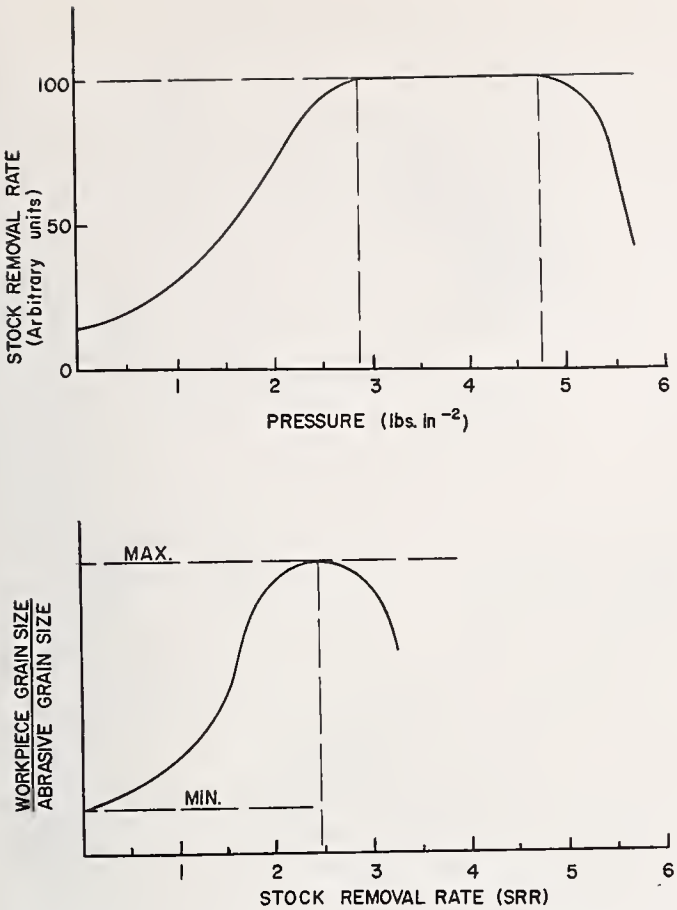

FIGURE 15. *Performance criteria for free abrasive machining.* Stock removal rate versus pressure (top) and WGS/AGS ratio versus stock removal rate (bottom).

lish the abrasive film before any cutting action commences. Stock removal rate than increases rapidly as concentration is increased up to a maximum which in the absence of more detailed information is presently stated as "1 lb of abrasive per gallon of vehicle." Actual optimum concentration should be a function of abrasive particle density, a maximum being reached at the point where free unrestrained rolling is significantly limited by too high a particle density. The size of the abrasive determines the stock removal rates. In general, a larger grain size results in higher rates. This is not so much due to size alone, but primarily in polycrystalline material, to an effective workpiece grain size (WGS) to abrasive grain size (AGS) ratio (see fig. 15 bottom). A small AGS can be considered to be a small single point tool which volumetrically speaking is not as effective in stock removal as the larger grain which is able to remove complete workpiece grains or aggregates rather than only small grain particles. There is yet another reason demonstrated by the abrasive action in this method on composite materials such as cemented tungsten carbide. Material removal does not become appreciable until the AGS is larger than the WC particle spacing. Below this value the abrasive grain becomes to a large extent embedded in the softer (cobalt) matrix. The need for larger particle sizes is probably not entirely governed by this phenomenon but to a certain degree also by the fact that small grain size high MOR materials are harder to grind, requiring larger particle sizes for appreciable removal rates. Because of the randomness of the lay of the abrasive and subsequent abrasive action, the surface of FAM finished workpieces is invariably matte or has a sandblast like appearance. In contained abrasive machining a multidirectional-lay and in bonded abrasive machining a roughly parallel lay are affected. Roughness is directly proportional to size, the larger sizes giving the rougher surfaces, but is inversely proportional to the hardness of the work, the harder surfaces generally giving a lower reading for roughness for any one abrasive size. This is directly related to the extent of penetration of the abrasive particles. Stock removal rate is governed by grain size as previously indicated, but primarily by the workpiece characteristics. Figure 16 shows the variation of this rate as a function of grain size. The materials with the lower strength to modulus ratios (Modulus of Resilience) show the lower rates. In increasing order of favorable grindability and by group only, the following general series is established: Hard refractory elemental and polycrystalline materials (WC, Ti), hard to soft steels, nonferrous materials, plastics, and finally the very brittle or very soft inorganic materials such as glass and ferrite. It may be noted that metallic aluminum is essentially on par with the plastics, that brittle plastics (phenol formaldehyde) perform better than the low modulus plastics, and that the influence of AGS is most noted in the multiphase materials with appreciable difference in physical properties between grain and matrix (Alumina ceramics and WC). Members of the same material type are primarily differentiated on the basis of hardness (see e.g., the steels in figure 16). As may be seen from figure 16, free abrasive machining is not competitive, on a stock removal basis, with bonded abrasive machining, but may be conducted on almost any material with various degrees of efficiency. It is limited to flat surfaces and finds its best application when very large amounts of parts have to be finished without appreciable stock removal requirements, or where conventional grinding and machining are impractical or impossible. An example is on very thin workpieces where magnetic or vacuum distortion could produce warping. Of all FAM applications it is estimated that approximately 30 percent is done on nonmetallic materials. In terms of material ground, in decreasing overall quantities, it primarily handles cold rolled steel, non-ferrous metals, cast iron, stainless steel, ceramics, glass,

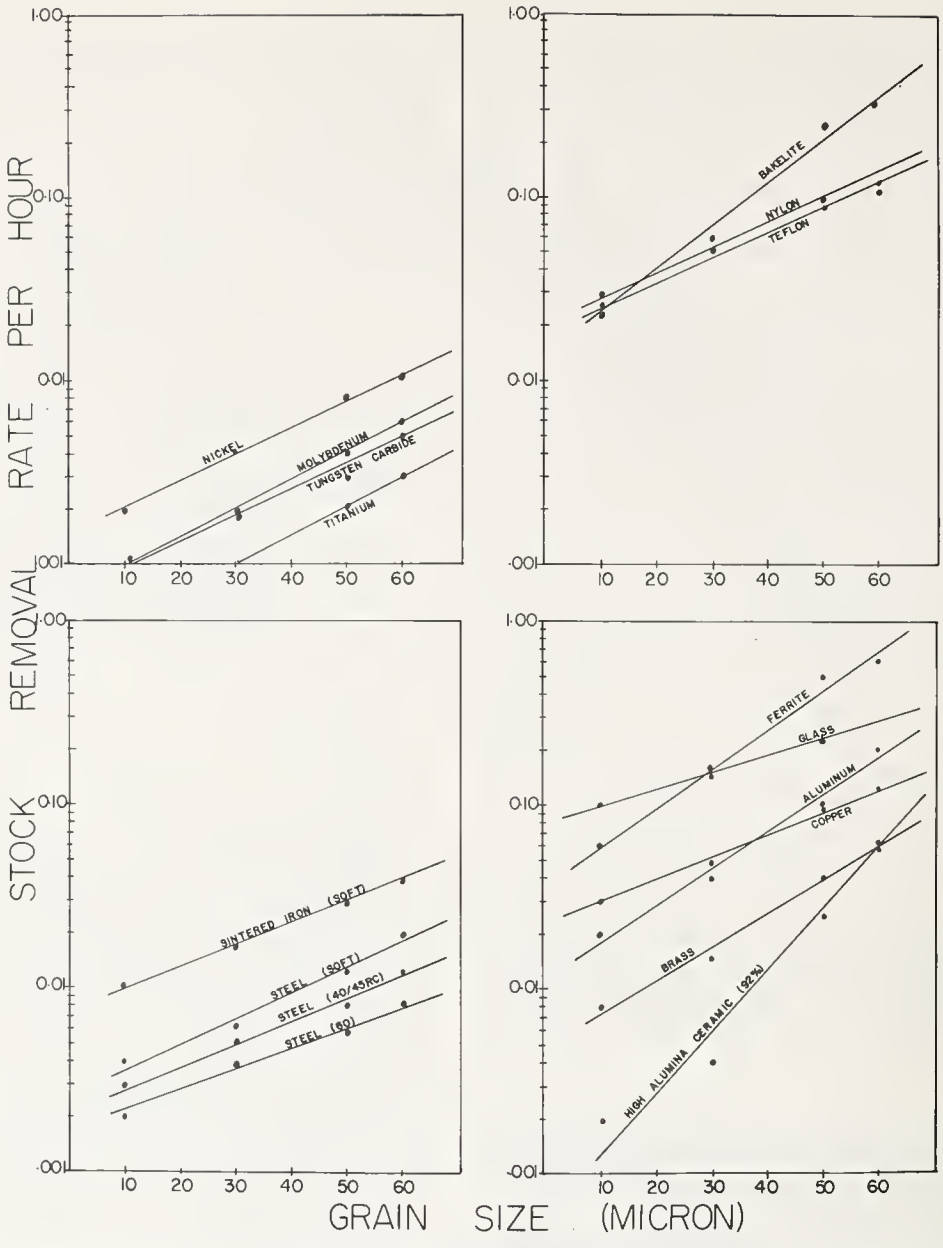

FIGURE 16. *Stock removal rate versus abrasive grain size for various material types ground in the FAM mode.*

quartz, plastics, ferrites and boron carbide. The biggest single research need in this area is for further information on the mechanics of stock removal.

c. Contained Abrasive Machining

This mode of stock removal accomplishes grinding or polishing by holding, or generally containing, an abrasive between tool and workpiece in such a way that the abrasive's movement is neither fully restricted as in BAM or entirely free as in FAM. Limited movement due to the elastic properties of the matrix in the BAM mode is not of the magnitude considered important for the above distinction. CAM is different only in that it combines the features of BAM and FAM. It cannot be directly equated with lapping which merely connotes the use of a flat revolving disk. Lapping per se can be done in several modes. The use of the word lapping to indicate fine (abrasive grinding) finishing is entirely arbitrary with respect to the degree of finish, minimum or maximum. The action between a revolving disk, charged with an abrasive, and a workpiece can be either grinding or polishing. True polishing will ensue only if conditions are such that no penetration of the workpiece occurs and particulate matter of macrodimensions is removed.

The CAM method generally entails the use of an active element to which the abrasive is applied. The abrasive is retained in the element by special vehicles (compounds), a retainer (felt, cloth, wire mesh) or by the mere action of penetration of the abrasive into the active element, usually a combination of the above. The abrasive is retained but not rigidly localized. Application modes may be divided as

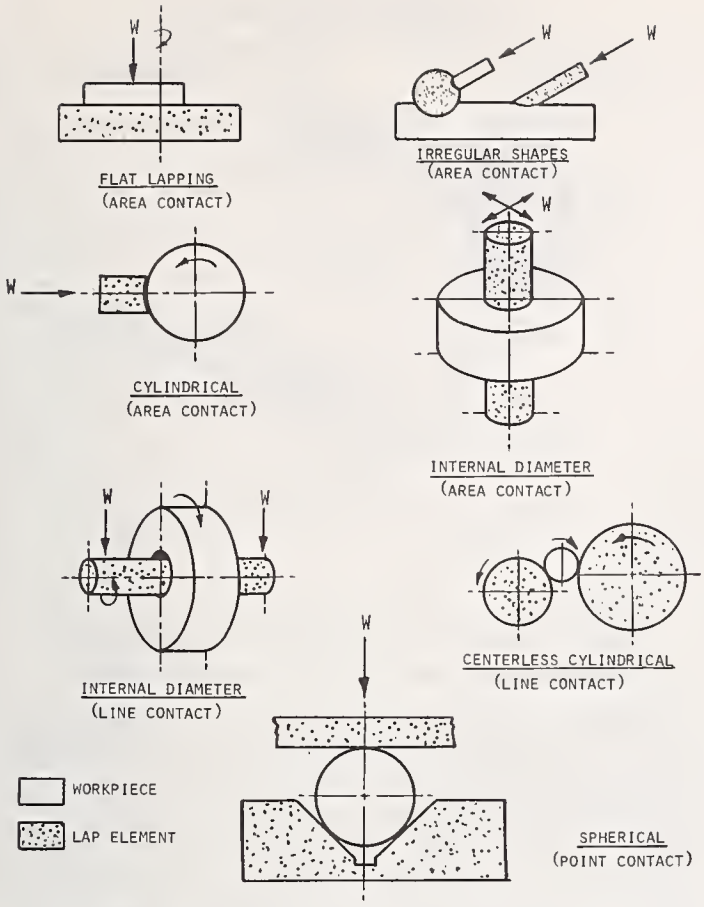

FIGURE 17. *Subdivisions of the application modes in contained abrasive machining (CAM).*

shown in figure 17 into area contact, line contact, and point contact. It is understood that similar operations may be carried out with the principles of BAM. Contained abrasive machining is generally applied when finer finishes are desired. The use of successively smaller grain size abrasive leads to a natural transition from the predominantly grinding action to ultimate polishing. Abrasive requirements are all-important. Ideal conditions are uniform size, shape, strength and purity of the abrasive. Application of CAM to ceramics uses diamond almost exclusively as the abrasive. The active element should be relatively hard. Ceramic or ceramic composite materials may be used successfully. This eliminates the possibility of contamination of the workpiece with material from the active element. CAM is usually practiced in the presence of a coolant-lubricant. Its desirable action is in part dictated by chemical requirements such as possible detrimental effects on the workpiece but is primarily governed by its ability to effectively disperse the abrasive, act as a lubricant and coolant and keep the process residue in suspension.

A diagrammatic overview of mechanical stock removal processes is given in figure 9. The BAM mode offers the highest stock removal rates per part and consequently is the most widely used method in ceramic finishing. Subdivision into types is influenced by the nature of the products produced. Table 1 gives a breakdown of machine usage by type differentiated on the basis of the nature of the operation.[2]

TABLE 1. *Machine usage by type and operation in ceramic finishing*

Type of Operation	Machine usage percent	
	Specialty technical ceramics operations	General ceramics operations
Surface grinding (vertical)	34	10
Cylindrical grinding	20	5
Centerless grinding	10	60
Surface grinding (Horiz.-"Blanchard")	8	
Universal grinding (O.D.–I.D., radius)	7	15
Specialty grinding		10
Jig	4	--
Drilling	16	--
Slicing	1	--

The economic importance of the finishing step in ceramic part processing becomes apparent when it is realized that approximately 75 percent of the direct cost of the part is due to finishing in speciality technical ceramics. The figures are 60 percent up to 90 percent in general ceramics manufacture for large and small parts respectively.

3. Science and Theory of Ceramic Finishing

3.1. General

In grinding, the kinetic energy of an abrasive particle at the periphery of a rotating grinding wheel is transferred to the workpiece and dissipated in a variety of ways: kinetic energy of the chips, difference in energy between the old and the new surface, possible residual energy of the material and the chips due to distortion by the grinding process, and energy required to remove material, and thermal energy. Quantitatively, the last two are the most important.

Analysis of the mechanical stock removal energy requires a knowledge of the forces imparted to the workpiece under the dynamic loading conditions of the grinding system. The conditions under which such forces should be determined must be characteristic of a typical grinding cycle. The grinding conditions to

[2] Figures are a result of a survey conducted in the ceramic industry by the authors.

439-921 O - 72 - 3

which the workpiece is subjected creates material behavior aspects which are not normally found under static loading conditions. The most important aspects are the highly transient localized nature of the loading, the dynamic quality of the rapid or impulsive loading, and the spatial and temporal distributions of the load. Furthermore, the possibility for change of the material properties in the relatively small region to which the high pressure, rapid-rate loading is applied, may influence the level and distribution of the stresses. There are additional factors which set apart the analysis of material behavior under grinding conditions. The material reaction is influenced by its physical properties as well as those of the imparting member (load). As will be seen later, this latter determines to a large extent the efficiency of the grinding process. Secondly, the impulsive loading imparts motion to the material upon which it impacts and each loading cycle is followed by a removal phase. Thirdly, as a result of geometric restrictions, the loadbearing areas at first increase and then decrease providing cyclic pressure dependence in the contact area. Finally, the highly complicated nature of the impact phenomenon takes place at appreciably elevated temperatures.

High temperatures are generated during the contact time (t_c) of load and workpiece. A cooling cycle ensues during time (t_r—t_c) where t_r is the time required for a full revolution of the load. With increasing time, the temperature will continue to rise and eventually, in the absence of forced environmental cooling, attain an equilibrium temperature the exact value of which will be determined by the thermal properties of all system components. Heat will be distributed primarily into the abrasive and wheel, the workpiece, and the grinding residue. This involves conduction convection and radiation mechanisms. Exact determination of the extent of the heat flow into all three major components would be required to draw a complete heat balance on the grinding process. An approach to the solution of this problem is presented in one of the following sections.

Primarily for the reasons outlined above, initial fundamental knowledge on the dynamic and thermal aspects of stock removal in ceramics can only be obtained when data are collected using the most simple experimental simulation, while at the same time retaining all operational aspects of the process. The authors' experimental procedures and the results are presented in this report.

3.2. Experimental Design

Grinding action on ceramics has been simulated using a single point diamond "tool" of varied geometry mounted on the periphery of a

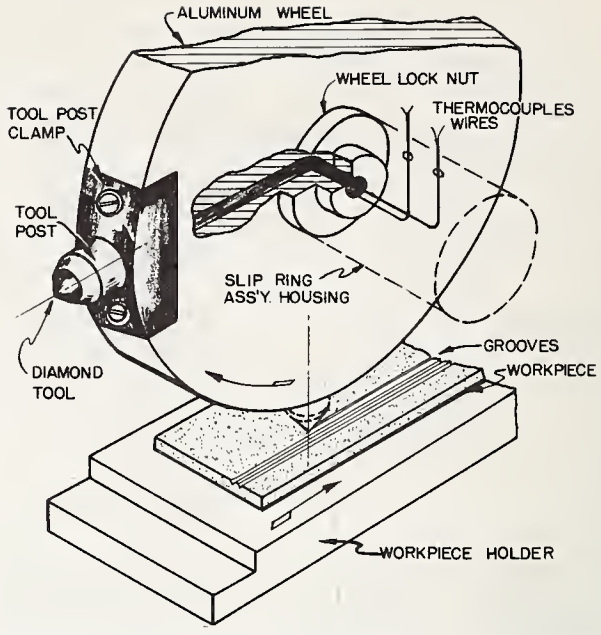

FIGURE 18. *Perspective drawing of single point diamond wheel indicating diamond, thermocouple wires and slipring assembly mount.*

7 in diam. one-half in thick alumina disk. See figure 18. A basic grinding machine was modified to conduct the experiments. A special calibrated strain gauge type dynamometer designed similar to the original concepts by N. H. Cook [17] recorded tangential and normal grinding forces. A plastic housing encased the entire grinding table enabling control of grinding environment. The collection of grinding debris was by a specially designed tray. This is shown in figure 19. The speed of the force recorded (Sanborn Model 321) was sufficient to register the force level at each pass of the diamond through the workpiece. It was thus possible to examine the variation of the force level during each pass. Data indicate that for a perfectly flat surface, the force level remains constant during each pass across the workpiece. The force level in both the normal and the tangential component decreases as a function of the time required to impart the full tool geometry to the workpiece. Even with a perfectly rigid diamond, more than one pass was required to impart the full diamond geometry to the workpiece. Under certain conditions, a continuous grinding action of forty passes was observed. Further details will be discussed in the following section.

The initial temperature measurements during the grinding action were made by means of chromel-alumel thermocouples. One of the thermocouples was mounted against the back of the diamond body while the other thermocouple was mounted as close to the tip of the diamond as possible without interfering with the cutting action. The thermocouple wires were brought through the metal diamond housing, through the groove in the wheel and the shaft and onto a slipring assembly. With a known volume and

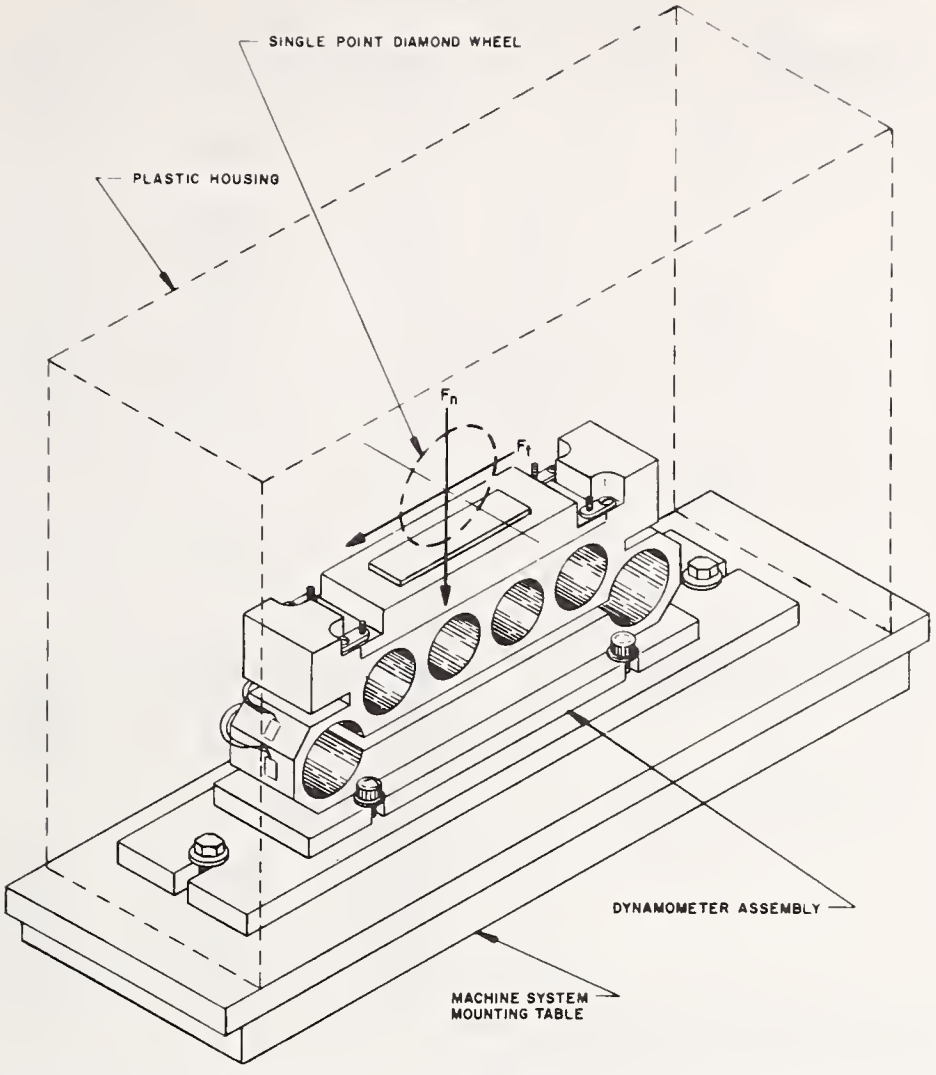

FIGURE 19. *Two dimensional grinding dynamometer designed and used for the studies reported here.*

path length of the diamond, two thermocouples provide the input for heat transfer calculations and possible extrapolation to the actual temperatures at the interface between the diamond and the workpiece. Infrared photography, microscopy, and liquid crystal targets were used to obtain further temperature data.

The workpiece materials initially consisted of four different conventional alumina types: 85, 94, 99.5, 99.9 percent alumina.[3] They were chosen to be distinctly different in terms of mechanical as well as thermal properties. The characteristics of the four workpieces are tabulated in table 2. All workpieces were preground to essential flatness and a finish of 10 microinches so as to ensure a constant depth of cut during table traverse. Except for the 99.9 percent alumina, which had to be stacked, the workpiece dimensions were 7½-in long, 2-in wide and 1-in thick. Materials from other sources but with the same nominal composition were used for comparison experiments.

In single point experiments and for a given downfeed, tool geometry and workpiece material, the only variables in the process are wheel speed and table speed. The experimental approach was such that output data would yield force levels and temperatures as a function of both wheel speed and table feed.

Observations on material behavior were carried out by reflected light microscopy. Use of scanning electron microscopy has been initiated.

3.3. Results and Discussion of Experimental Work

a. Force Measurements

Results of force measurements as described in the previous section are shown in figures 20, 21, and 22 for a 90 degree cone angle diamond cutting the four materials and for a 120 degree diamond in the case of AD 85. Experiments on AD 99.9 have in no case been carried beyond

[3] Source: Coors Porcelain Company, Golden, Colorado 80401.
Certain commercial products and instruments are identified in this paper in order to specify adequately the experimental procedure. In no case does such identification imply recommendation or endorsement by the National Bureau of Standards, nor does it imply that the products or equipment identified are necessarily the best available for the purpose.

TABLE 2. *Mechanical and thermal properties of selected ceramics**

Property	Units	Alumina 85%	94%	99.5%	99.9%
Specific gravity	g/cc	3.42	3.62	3.84	3.96
Compressive strength	psi	240,000	300,000	300,000	650,000
Tensile strength	psi				
70°F		18,000	27,000	--	60,000
2000°F		9,000	10,000	--	--
Modulus of elasticity	psi	33×10^6	41×10^6	52×10^6	56×10^6
Shear modulus	psi	13×10^6	17×10^6	22×10^6	23×10^6
Bulk modulus	psi	20×10^6	24×10^6	30×10^6	33.3×10^6
Poisson's ratio		0.22	0.21	0.21	0.22
Hardness	Rockell 45N	75	78	81	90–91
Color		White	White	Pink	White
Specific heat @ 100°C	Cal/G/ °C	0.22	0.21	0.21	0.21
Thermal conductivity	Cal/CM²/ CM/Sec/ °C				
20°C		0.035	0.043	0.075	0.0744
100°C		0.029	0.035	0.065	.0550
400°C		0.016	0.017	0.028	.0409
800°C		0.010	0.010	0.017	.0310
Thermal coefficient of Expansion	Per °C as noted				
−200 to 25°C		2.3×10^{-6}	3.4×10^{-6}	3.4×10^{-6}	3.6×10^{-6}
25 to 200°C		5.4×10^{-6}	6.3×10^{-6}	6.8×10^{-6}	6.8×10^{-6}
200 to 500°C		6.8×10^{-6}	7.7×10^{-6}	8.0×10^{-6}	8.0×10^{-6}
500 to 800°C		8.3×10^{-6}	8.5×10^{-6}	8.9×10^{-6}	8.9×10^{-6}
800 to 1200°C		9.0×10^{-6}	9.2×10^{-6}	9.7×10^{-6}	9.7×10^{-6}
25 to 1000°C		7.5×10^{-6}	8.0×10^{-6}	8.4×10^{-6}	8.4×10^{-6}

*Compiled after data provided by Coors Porcelain Company, Golden Colorado on their products designated with the nominal alumina percentages as indicated.

speeds of 2000 rpm due to premature failure of the diamond. Initial impact forces are such that physical integrity of the diamond is destroyed. The grinding forces during the material removal phase are, however, well within the capability of the diamond.

The results show that for any table speed, the force level is directly related to the wheel speed. The forces decrease rapidly as the wheel speed increases. The table speed was found to have a considerable influence on the force level which increased as the table speed was increased. Increasing table speed is indicated in the figures by an increase in number from six through fourteen. It should be noted here that the indicated forces are the sums of the forces registered during each pass of the diamond across the ceramic, until the full geometry of the diamond, at a particular downfeed, had been imparted to the workpiece and no further forces could be measured. This is the only way in which a total force for the energy required to remove a given amount of stock from the workpiece, could be successfully obtained. As the amount of material removed per revolution is increased by increasing the depth of cut, the force level is raised. See figure 22.

If the ceramic grinding forces could be viewed as being governed by strictly geometric considerations, an analysis of the force levels would be relatively simple. For an initial model we could assume that the amount of material removed would be dependent on the shape and depth of penetration of the diamond and the machine parameters only, i.e., no densification, plastic deformation or extent of deformation beyond the tool workpiece contact zone. Direct visual observation of cutting grooves reveals that this does not reflect the actual process. The use of a strictly geometric model does, however, assist in understanding some of the force variations as a function of changing grinding conditions. Let the number of revolutions of the wheel per unit time equal V, the depth of cut equal d, the table speed v, and the width of the groove at the surface W_a. The volume removed per unit time, A, will be

$$A = (v\, d\, W_a)/2 \qquad (1)$$

and the volume per revolution of the wheel, A′

$$A' = (v\, d\, W_a)/2V \qquad (2)$$

The exact shape of the removed volume under grinding conditions is complex and its exact

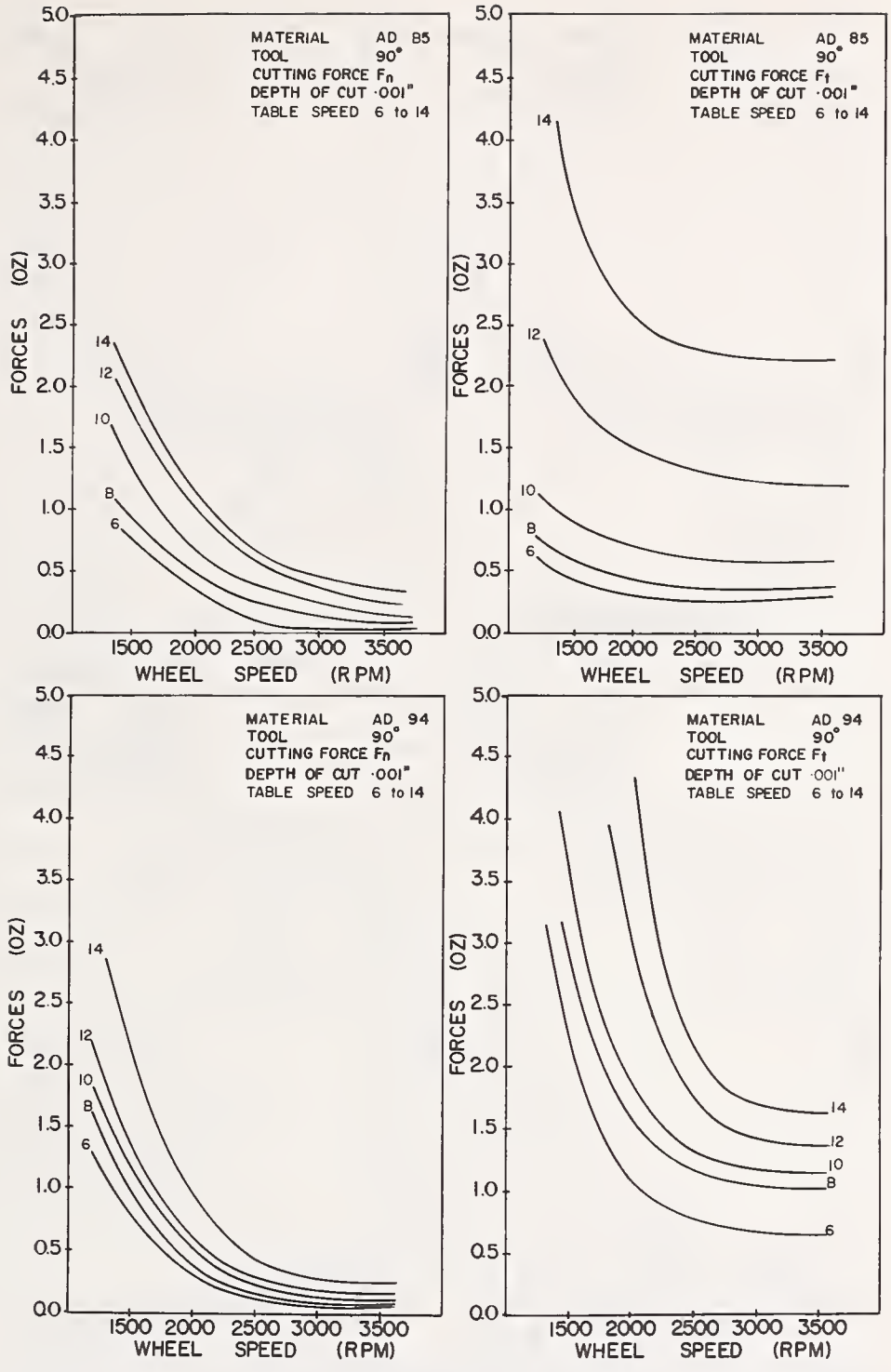

FIGURE 20. *Force versus wheel speed for 85 and 94 percent aluminas, .001 in depth of cut, 90° angle.*

length and area are not easily determined. It has been shown [18], in the case of surface grinding metals, that the length of the grain path L for $v << V$ may be expressed as $L = (Dd)^{1/2}$ where D is the diameter of the grinding wheel. If we assume the force to be proportional to the cross-sectional area of the removed material, then the relative single point force (F) would be

$$F = (v\, d\, W_a)/2V\, L \qquad (3)$$

or using $L = (Dd)^{1/2}$

$$F = (v\, W_a)\,(dD)^{1/2}/2V \qquad (4)$$

For a given diameter of the wheel, the relative single-point force is therefore expected to decrease as the wheel speed (V) increases and to increase as the table speed and depth of cut are increased. This is supported by the data in figures 20 through 22. The increase in force level when the cross sectional area, i.e., W_a, is

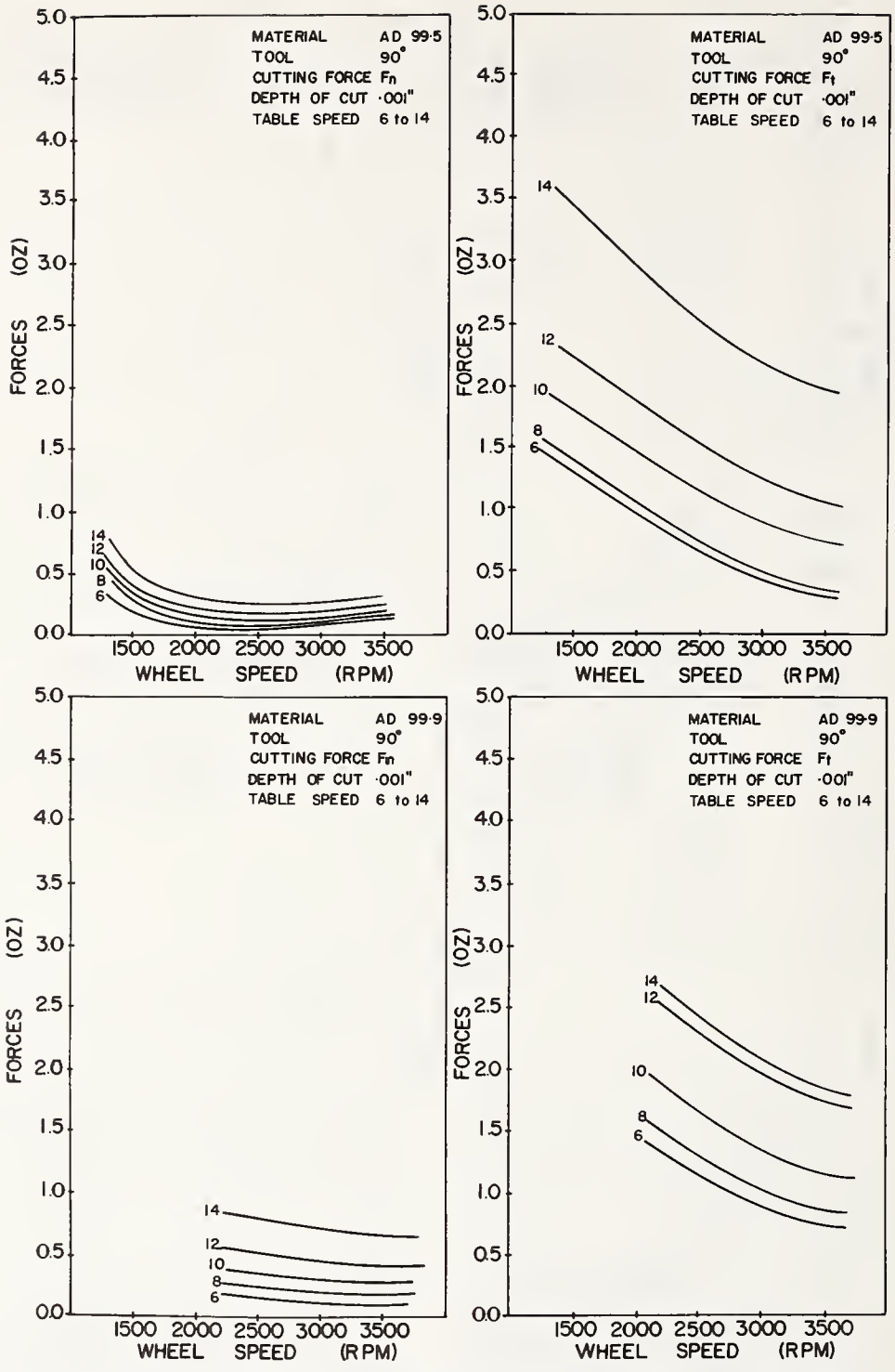

FIGURE 21. *Force versus wheel speed for 99.5 and 99.9 percent alumina, .001 in depth of cut, 90° cone angle.*

increased such as in going from cone angle 90 degrees to 120 degrees, may readily be seen when comparing figures 20 and 21, and 22. Most efficient grinding, in terms of expended cutting force, is, therefore, done at high wheel speeds, low table speed and depth of cut with diamonds of small cross-sectional area. Even the simplified geometric model is further complicated by the fact that feed and wheel speed are not independent variables.

Consider a surface as shown in figure 23, where the relative speeds are such that individual cuts are made per revolution of the wheel. If the table speed is kept constant but the revolutions per minute increased by a factor of two, the result will be as indicated in the center part of figure 23. The amount removed per pass will have increased. The number of revolutions per inch will be V/v. The more revolutions per in, the more material will be removed per unit length. In reality, an increase in table feed (v) not only reduces the number of revolutions per

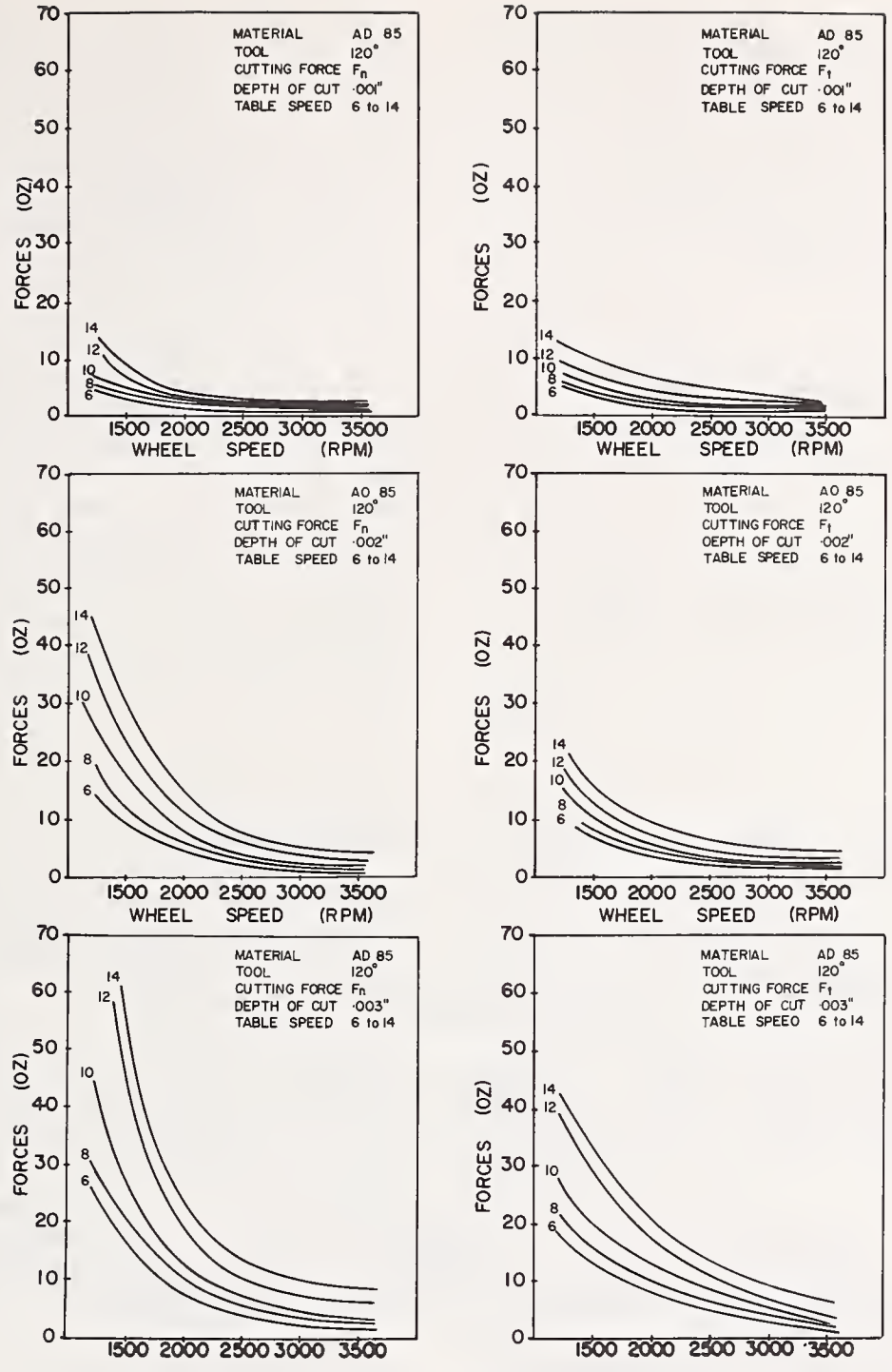

FIGURE 22. *Force versus wheel speed for 85 percent alumina, three depths of cut, 120° cone angle.*

unit length, but also increases the length of the cut path as shown in the lower part of figure 23. There will thus be a table feed at which the number of passes will level off. This tendency is apparent from figure 24 which shows the dependence of the number of passes required to remove a unit volume of stock as a function of the various grinding parameters. This behavior is characteristic of the single-point grinding action only, since in multipoint cutting tools (wheels) the path of one diamond is followed by many others. The action of the single-point as a function of the various grinding parameters thus influences the nature of the generated surface. An increase in depth of cut also increases the length of the cut, which for a given wheel diameter was found to be proportional to $\sqrt{d}$. The total amount of revolutions per inch and hence the amount of material removed per pass is thus proportional to $V/v\sqrt{d}$,

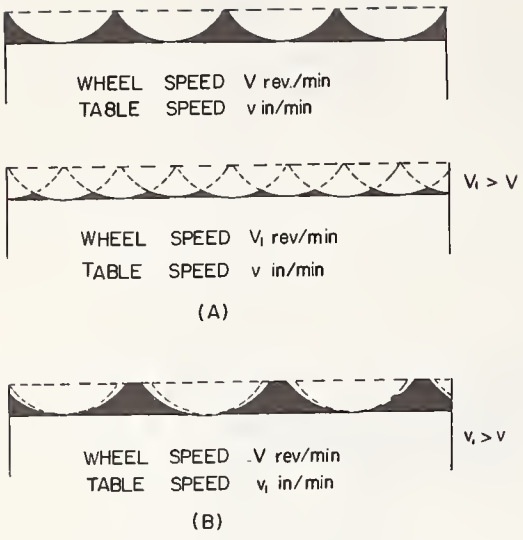

FIGURE 23. *Diagrammatic representation of the amount of material removed per pass as influenced by increase in wheel speed (top two) and increase in table speed (bottom).*

or the number of passes required $N \propto v\sqrt{d}/V$. These findings are borne out by the experimental results as shown in figure 24. Figure 24 may indicate a trend in showing an increased number of passes required, when going from low to high modulus materials. The nature of the fracture phenomena must influence the actual amount of material removed per pass.

Although no two ceramics show identical force patterns, there are several important common features. A sharp increase in force level occurs at low speeds. The speed at which the sharp increase in slope occurs is primarily governed by the type of material and secondarily by factors influencing the total amount of material removed per unit time, namely table speed and depth of cut. For the materials examined here, the inflection point lies at lower speeds the lower their respective (fracture) strengths. Figure 25 shows idealized force-speed plots for two hypothetical materials. Material removal forces are higher for the

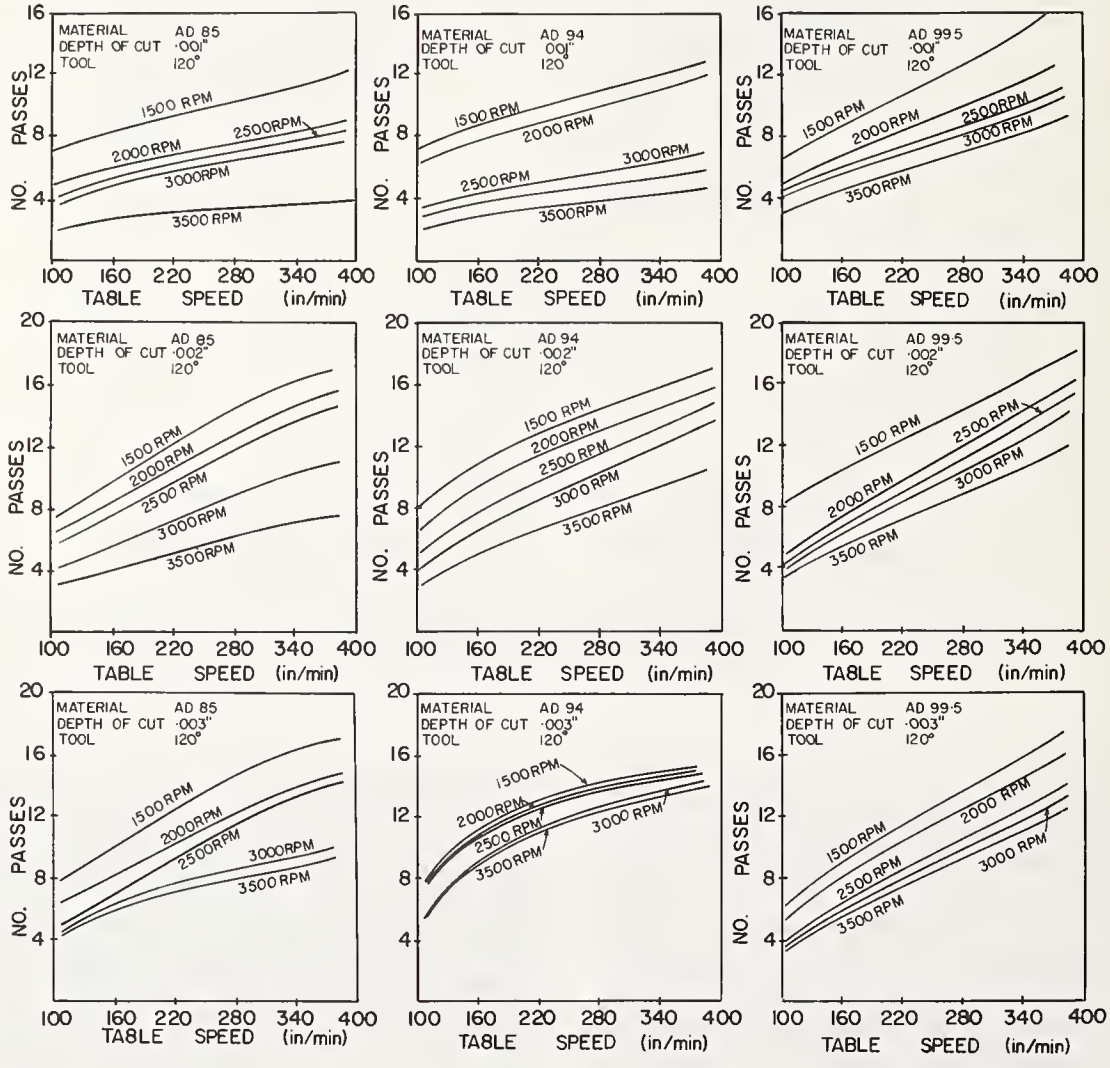

FIGURE 24. *Number of passes required to remove unit volume of stock as a function of table feed for various wheel speeds at three depths of cut.*

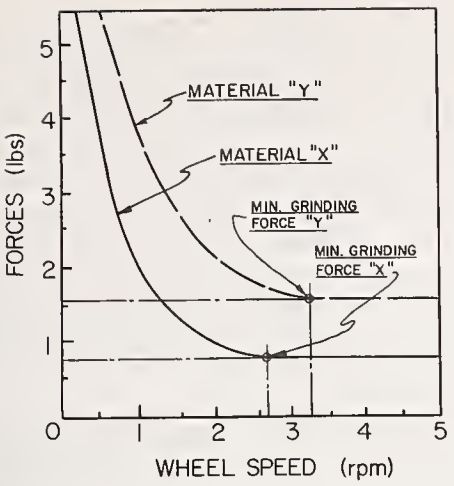

FIGURE 25. *Idealized grinding force versus wheel speed plots for two hypothetical ceramics.*

stronger material although surprisingly little difference was found between the various types of aluminas. A sharper differentiation between materials can be found at lower speeds where the material type more drastically influences the rate of increase. Based on the position of the inflection point, a cutoff speed for lower force grinding can be indicated which differs for each material. As figure 22 indicates, the volume parameters (feed and depth of cut) also shift the inflection point. This is not shown in the idealized curves of figure 25. Tangential and normal forces follow the same trend. The magnitude of the forces as well as the ratio of tangential to normal force is primarily influenced by the geometry of the cutting diamond. The tangential forces are higher than the normal forces for cone angles of 90 degrees or lower whereas the value F_t/F_n moves closer to unity at higher cone angles. Experiments with cone angles greater than 120 degrees were not conducted. The magnitude of the tangential force may be regarded as more directly reflecting the amount of energy required to remove the material. The value of the normal force component is particularly important with regard to the extent of surface or subsurface damage. In actual cutting experiments the diamond is only weakly supported by the fracturing workpiece so that the bulk of the normal force field is concentrated at the small area of direct contact between diamond tip and the newly generated surface of the workpiece. Very high stress fields are thus set up. At sufficiently high pressures the contact area becomes plastic and leads as a result of permanent deformation to residual stresses. The initially high compressive stresses lead on relaxation to substantial tensile strains which may cause subsurface cracking. Recent studies of fracture phenomena in statically and dynamically loaded soda-lime glasses by Peter [19] have shown the development of in-line subsurface cracking ("tiefenriss"). Koepke [4] observed subsurface cracking in severely workhardened surface layers when grinding MgO single crystals with alumina wheels. Finely polished ceramic surfaces often reveal small surface cracks on profilometric traces. Peter [19] further indicated relaxation times for the development of subsurface cracking of the order of days. This phenomena has to our knowledge never been studied in ceramics. It certainly deserves attention particularly in glass-phase bonded ceramics. The extent of subsurface cracks increases as a function of both pressure and velocity of the diamond.

The foregoing discussions provide qualitative insight into the dynamic process of diamond-workpiece interaction, based on geometric considerations. It leaves, however, some very important areas uncovered. The force expressions developed thus far do not take into account the specific differences created by the physical properties of the workpiece. The (linear) dependency of the parameters shown in eq (4) is not borne out by experimental observations. This is in part due to the nature of failure of the ceramic. As may be easily observed, ceramic failure is at least in part effected by side cracking or divergent fracturing which as a result of propagation and interaction ejects flake like particles from the surface. This (mechanical) spalling effect can extend in dimension to up to three or four times the width of the diamond at the workpiece surface. Nature and extend depend on material type. Furthermore, rigidly mounted diamonds fail on grinding high modulus aluminas in spite of tangential and normal stock removal forces of the same order as those on lower modulus materials.

In ceramic grinding the impact phase creates the initial fracturing which is followed by the removal phase for which the energies are determined by the work required to propagate and remove the material which has failed in a brittle or ductile fashion or both. In grinding, the propagation of the initial impact fracturing is aided by the extreme forces which continue to work on it as the wheel revolves. The work to extend the fracture will be larger and the velocity of propagation less for ductile failure. The magnitude, durations and distribution of the forces that are set up will be determined by the way the diamond and the ceramic react on one another. Fracture formation within the material which is intimately associated with its mechanical properties will determine the kind of load imparted to the diamond. The main areas of interest are, therefore, the distribution of forces at the impact interface as a function of time, and the way in which the load distributes itself within both ceramic and diamond.

High velocities or increasing strain-rates generally raise the flow stress of a material so that in a high speed grinding operation on already brittle ceramics, little plastic deformation is expected to precede fracturing.

In high velocity high pressure impact experiments (such as in shock waves) use is made of the one dimensional mass and momentum conservation relationships [20],

$$V = V_0(1-U_p/U_s) \tag{5}$$

and

$$P = P_0+\rho_0 U_p U_s \tag{6}$$

to calculate pressure and specific volume behind the shock front from the experimentally determined shockwave velocity (U_s) and the "particle velocity" or bulk material velocity (U_p) behind the shock front.

A first order approximation of the normal fracture stress occurring in the region of fracture at the moment of impact may be obtained from eq (6). Equating the particle velocity with the wheel velocity at 6000 ft/min (3×10^3 cm/s) and taking the average of alumina density at 4 g/cm^3 and the longitudinal sound speed at 1×10^6 cm/s, the fracture stress computes at 12×10^9 dyne/cm^2 (12 kbar). Eq (6) strictly holds only for infinite bodies which do not sustain shear and both elastic and inelastic processes should be considered. Wear or deterioration of the diamond will occur if the prevailing stress level falls above its yield strength. Accurate data on the strength of diamond is scarce and unsatisfactory. Careful measurements by Hull and Malloy [21] come to the conclusion that, if extraordinary precautions are taken to avoid stress raisers, the failure shear stresses in clear natural diamond will fall around 43,000 psi and a compressive strength of 1.261×10^6 psi is indicated. The latter value should be compared with data from Schwarzkopf and Kieffer [22] which give a compressive strength of 284×10^3 psi. Their transverse rupture strength falls at $42{,}6\times10^3$ psi. Considering the above figures, diamond will fail in compression between 20 and 100 kbar in shear, and will transverse rupture at about 3 kilobars. If fluxural strength is taken as an indication of failure and a value of one sixth the compressive strength is assumed, the failure limit must be set at 13 kbar. It is doubtful that the theoretical (hydrostatic) compressive strength of diamond will be the governing factor in the grinding mode. It may, therefore, be concluded that the stress levels of a rigid diamond impacting on the hardest of the aluminas at speeds of 100 ft/s or up is in the neighborhood of the critical failure stress. Experimental observations indicate premature failure on the ceramic with the highest density and highest sound velocity, namely the 99.9 percent alumina. For any given force, size, shape, and orientation, the rate of loading will influence the stress experienced by the diamond. The degree of support or energy absorption characteristic of the bond will thus largely determine the erosion characteristics of the diamond at impact on any one type of ceramic. These bond characteristics will, for optimal grinding conditions, usually have to be adjusted for each type of ceramic. Single point diamond grinding tests may be a good way to determine the failure strength of diamond under dynamic loading conditions.

The effect which the transient disturbance of the impacting diamond has on the workpiece is largely determined by its physical characteristics. At least the qualitative aspects of the behavior may be analyzed from the point of view of an elastic approximation.

A knowledge of the extent of the damaged area per unit kinetic energy may be obtained from the following simplified model. At impact the kinetic energy per unit area, E_k will be

$$E_k = \frac{mV^2}{2A} \tag{7}$$

where m = diamond mass
A = impacting area
V = velocity of the wheel

Energy consumption will be the product of the energy density and the extent of the damage

$$E_c = \sigma\epsilon S \tag{8}$$

where σ = stress
ϵ = strain
S = depth of damage

At constant stress, the value of the strain at any point into the solid may be expressed as [23],

$$t = \frac{\sigma_1}{E}(1 - e^{-tx}) \tag{9}$$

where $x = \eta/E$, the relaxation time and η characterizes the viscosity of the deformation process and E is the elastic modulus. Substituting eq (9) into eq (8) and equating with eq (7) leads to

$$\frac{\sigma^2}{E}(1 - e^{-tx})\ S = \frac{mV^2}{2A}$$

assuming $\sigma = \sigma_1$, or

$$S = \frac{mV^2}{2A}\frac{E}{\sigma^2}\frac{1}{(1 - e^{-tx})} \tag{10}$$

The extent of the cracking can thus be regarded as a product of a term expressing the level of the impacted energy as determined by systems parameters, and an energy density term reflecting the strength of the material or

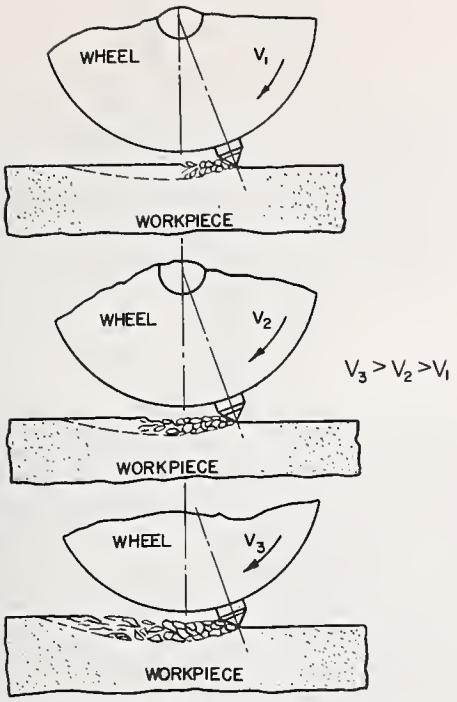

FIGURE 26. *Schematic presentation of the extent of fracturing at impact at increasing wheel speeds for a hypothetical alumina.*

the resistance to failure. The second term combines the deformation impedance and yield strength characteristics of the material into a dynamic damage resistance parameter. The extent of the damage for materials with very small relaxation times will be inversely related to their modulus of resilience (MOR = $\frac{\sigma^2}{2E}$). A minimum stress (σ_0) is required to propagate a crack of length C_0 according to the Griffith theory,

$$\sigma_0^2 = \frac{\gamma E}{C_0}$$

where γ = surface energy of the material. Substitution into eq (10) leads to,

$$S = \frac{mV^2}{2A} \quad \frac{C_0}{\gamma} \quad \frac{1}{(1 - e^{-tx})} \qquad (11)$$

The smaller the initial crack length (grain size) and relaxation time and the larger the surface (fracture) energy of the material, the more limited the extent of the damage at impact becomes. Among the investigated materials these properties are most enhanced in the 99.9 percent alumina. Figure 26 gives a schematic

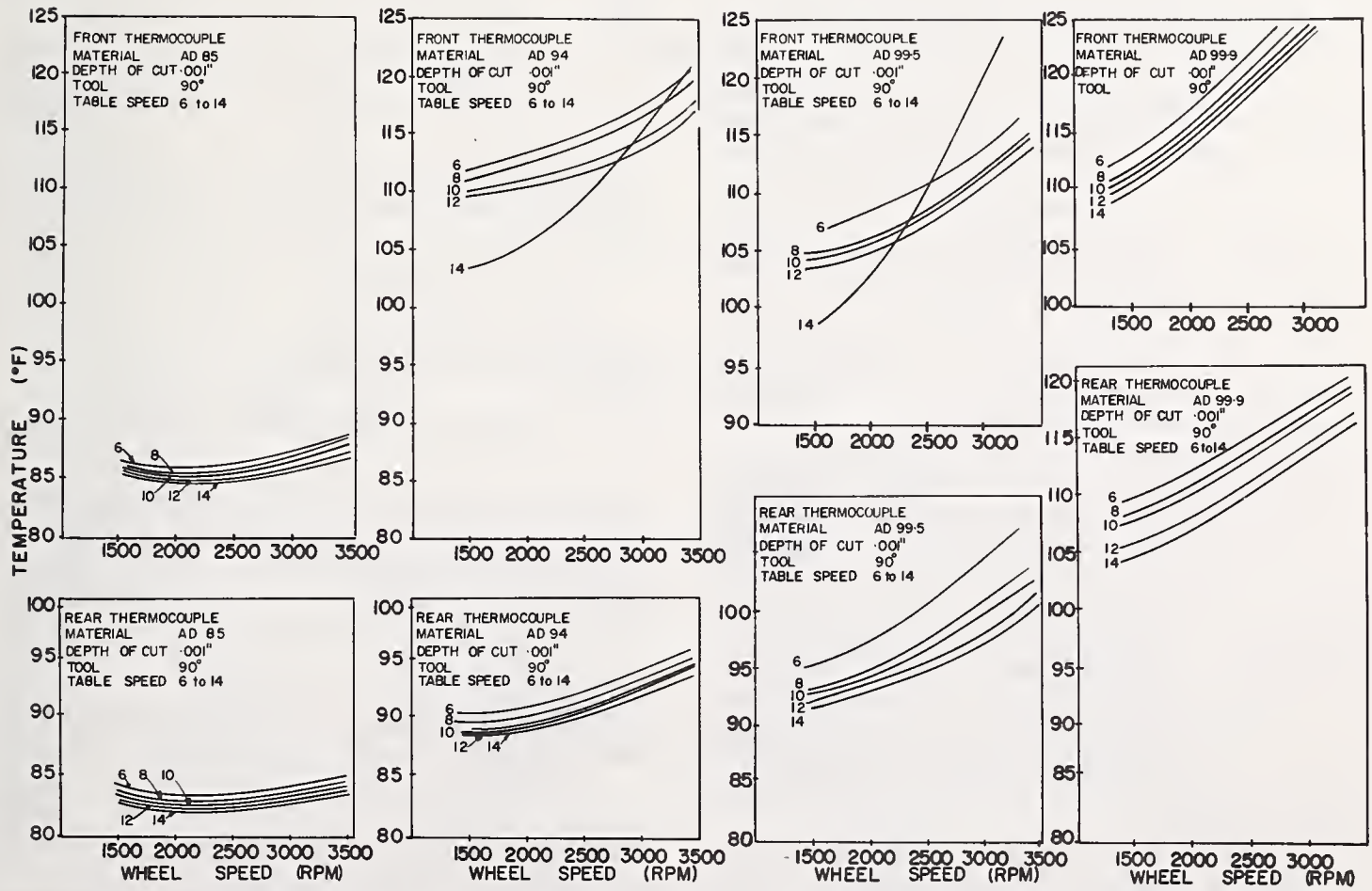

FIGURE 27. *Temperature recorded by tip and back thermocouples for various ceramics as a function of wheel speed, 0.000 in depth of cut, 90° cone angle and several table feeds.*

interpretation of the increase in damage at impact as a function of increasing wheel speed for a hypothetical material. Forces required to remove the entire volume at the lowest speeds (top fig. 26) would be the highest as a result of the need to induce crack propagation during completion of the interaction cycle.

b. Temperature Measurements

Figure 27 shows the results of grinding temperature measurements. The recorded results are the highest temperatures observed during each experiment conducted. They are intended to show the temperature trends as a function of the various grinding parameters. An increase in temperature is obtained with an increase in wheel speed and a decrease of the table speed. The temperature is also greatly influenced by the type of material ground. The highest temperatures were recorded on the 99.9 material. Temperatures increased considerably when depth of cut was increased, with an increase of about 30 degrees per mil in the case of 99.5 percent alumina. The temperature trends can be explained by the thermal model as discussed below. The temperature increases as a function of speed, appear to contradict the inverse relationship shown for the force levels (see fig. 22). The explanation may be found in the fact that the temperatures indicated are those generated during each grinding event for a given set of grinding parameters. As such, the temperatures will be directly related to the number of passes required to remove the total volume from the groove. As may be seen from figure 23, higher speeds required fewer passes and, therefore, a greater amount of heat was dissipated per pass resulting in higher temperatures. The same analogy may be used in evaluating the influence of the table feed. The higher the table feed, the greater the number of passes and subsequently the lower the temperature per cutting event. The temperature, therefore, is directly proportional to the amount of energy expended per unit time.

The grinding temperature generated at the diamond workpiece interface will be dissipated to the wheel, the ceramic, and the chips. A knowledge of heat flow distribution is as much needed as the magnitude of the grinding temperature itself since it determines how and to what extent the various system components will be thermally affected. The nature of the grinding process necessitates an analysis in terms of an intermittent transient (unsteady) heat transfer model. Only the essential concepts can be given here. Further details may be found elsewhere [24].

The general heat conduction equation which governs the temperature distribution and the conduction heat flow in a solid, without internal heat sources,

$$\frac{1}{a}\frac{\delta T}{\delta \theta} = \frac{\delta^2 T}{\delta x^2} \tag{12}$$

where, $a = \kappa/c_p$, κ = thermal conductivity, c_p = specific heat and ρ = density, and T and θ indicate temperature and time respectively, has for the case of a one-dimensional transient heat conduction in a semi-infinite solid a solution according to the following equation

$$\frac{T - T_\infty}{T_0 - T_\infty} = G\ \frac{x}{2\sqrt{a\theta}} \tag{13}$$

where $(T - T_\infty)$ = temperature difference at any one point and $(T_0 - T_\infty)$ = initial potential difference x = distance into the surface. The quantity on the right hand side of the equality is known as the Gaussian error integral. The rate of heat flow at the surface, q, may be obtained from eq (13), by evaluating the temperature gradient at the surface. The total change of internal energy or heat flow, Q, may then be found by integration

$$Q = \int_0^\theta q\,d\theta \tag{14}$$

from which

$$Q = 2\kappa A(T_\infty - T_0)\sqrt{\frac{\theta}{\Pi a}} \tag{15}$$

and

$$q = \frac{Q}{\theta} = \frac{2A}{\sqrt{\Pi}}\left(\frac{\kappa \rho c_p}{\theta}\right)^{1/2}(T_0 - T'_\infty) \tag{16}$$

Setting $T = (T_0 - T_\infty)$, the heat flow into the workpiece material will be

$$q_m = -T\left(\frac{\kappa_m \rho_m C_{pm}}{\theta_w}\right)^{1/2}\frac{2A}{\sqrt{\Pi}} \tag{17}$$

and similarly into the wheel

$$q_w = -T\left(\frac{\kappa_m \rho_m C_{pd}}{\theta_w}\right)^{1/2}\frac{2A}{\sqrt{\Pi}} \tag{18}$$

where subscripts m, d, and w refer to material, diamond, and wheel respectively. Heat exchange to the grinding chips is related to the mass rate of removal (m), the heat capacity (C_{pm}) and the temperature through

$$q_c = mC_{pm}T \tag{19}$$

Mass rate of removal for a 120° diamond cone and table speed V will be,

$$m = d^2 \tan 60 \rho_m V \tag{20}$$

The area of contact is simply given by the half cone area at a particular depth of cut.

Using eqs (17), (18), and (19) and multiplying by the factor

$\frac{\sqrt{\Pi}}{2A\sqrt{T}}\ \theta_w^{1/2}$,

$$F_1 = (\kappa_m \rho_m C_{pm})^{1/2} \tag{21}$$

$$F_2 = (\kappa_d \rho_d C_{pd})^{1/2} \tag{22}$$

$$F_3 = m\, C_{pm}\, \frac{\sqrt{\Pi}}{2A}\, \theta_w^{1/2} \tag{23}$$

The contact time follows from

$$\theta_w = \frac{\Psi}{360}\ \frac{60}{N}$$

where N = revolutions per minute of the wheel and Ψ is the number of degrees of arc over which the diamond is in contact with the workpiece. The value of the latter quantity can be obtained from a rather complex formulation [18]. It varies generally between three and five degrees for 0.001 in and 0.003 in depth of cut. Contact times range subsequently from 1×10^{-3} to 6×10^{-3} seconds. Eqs (21), (22) and (23) afford determination of the heat flow ratios such as

$$\frac{q_m}{q_t} = \frac{F_1}{F_1 + F_2 + F_3} \tag{24}$$

and similarly for $\frac{q_w}{q_t}$ and $\frac{q_c}{q_t}$, where

$$q_t = q_m + q_c + q_w.$$

The results were obtained with the aid of a small computer program and are shown in figure 28. Material differentiation is primarily on the basis of the thermal properties. The largest amount of heat goes into the wheel followed by chips and workpiece material. From a thermal point of view, diamond grinding ceramics is a gentle operation. Cooling of the wheel as a whole, not only at the grinding interface, is bound to result in very low thermal effects on the workpiece. This is particularly true at the more efficient higher wheelspeeds, because of the steep slopes indicated in the upper right hand graph of figure 28.

On account of process limitations the thermocouple mounted on the cone part of the diamond is a finite distance away from the actual grind-

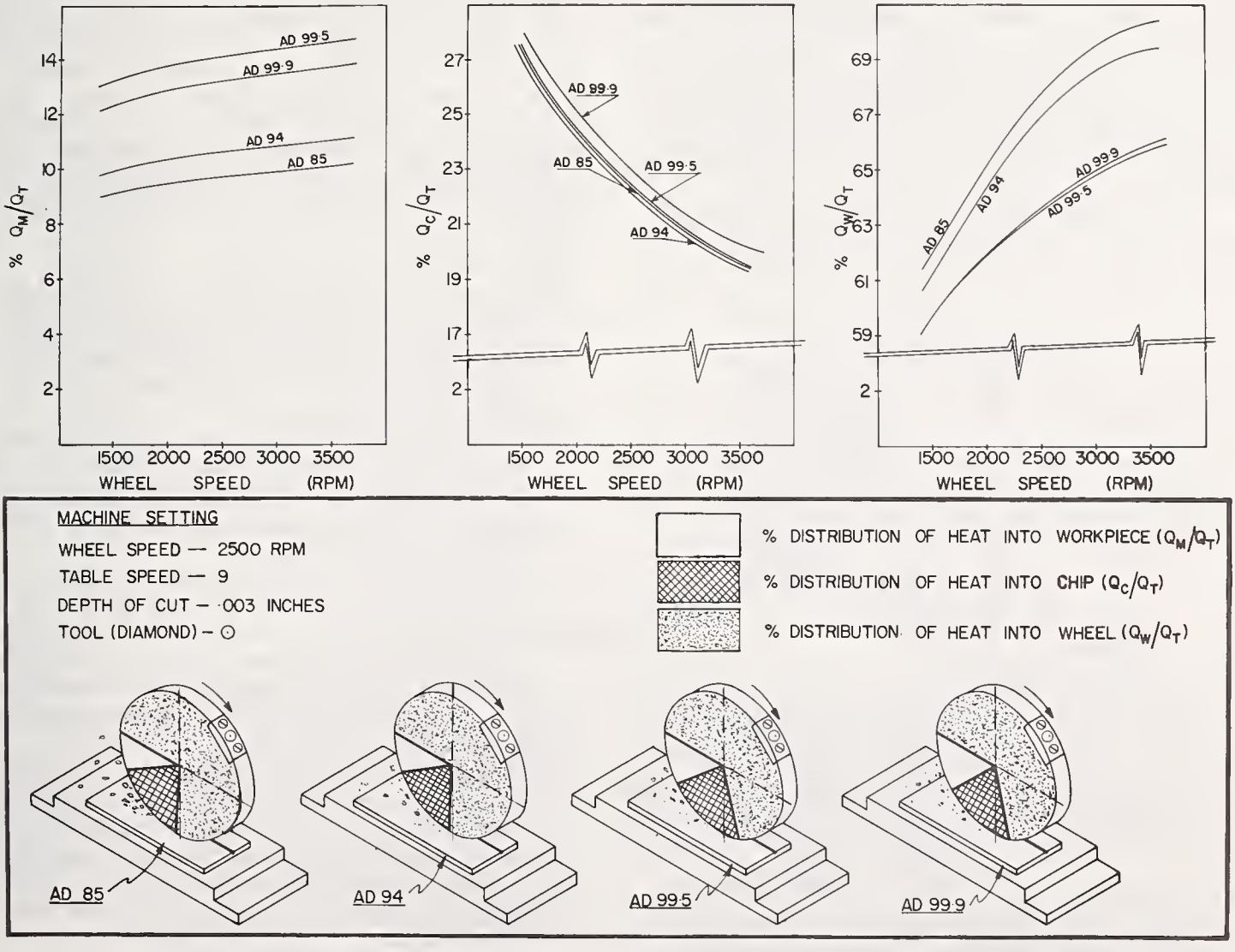

FIGURE 28. *Percentage heat flow into the major components of a ceramic finishing system.*

ing interface. Using a steady state heat conduction model [24] it has been possible to find an expression relating the measured temperature (T_2') to the grinding temperature T_0

$$T_0 = \frac{1.99}{a} T_2' \qquad (25)$$

where "a" varies in value from 0.79 to 0.94 for wheelspeeds of 1500 and 3500 rpm respectively. The model takes care of heat losses by conduction and convection during the time that the wheel revolves in air. As a result the temperature at the single point diamond-ceramic grinding interface on AD 99.9 at 1500 rpm, 0.001 in depth of cut with a cone angle of 90°, is estimated at 275° F. (See also fig. 27).

Attempts at determining the swarf temperature directly by means of a small field of view (0.010 in) infrared microscope have not led to quantitative results. Conversion of the millivolt reading of the infrared instrument is predicated on the field of view being entirely filled with the source to be measured. During grinding the percentage filling of the field of view is a constantly changing function of time. Qualitatively we have been able to determine relative temperature variations in the area of the diamond tip and its surroundings by training the center of the field of view on various X–Y coordinates. The results are shown in figure 29. The highest temperatures (highest numbers) are found directly in front of the moving diamond.

If the temperature of a chip in flight can be determined, the temperature at the point of origin can be calculated. Particulars are given in another communication [24]. Thermally sensitive targets such as surfaces coated with liquid crystals have been used. The thermal mass of the particles is generally too small to create areas of color change large enough to be photographed. Targets which leave a permanent record are presently being investigated. Infrared photography has been applied and works in principle. Calibration of the film colors is hampered by a curious phenomena. It has been observed during grinding tests in different gaseous atmospheres that the color of the "sparks" is different from one environment to another. It is felt, therefore, that the color of the sparks is partially thermal and partially due to gaseous discharge as a result of high electric fields during the rubbing action of the two contacting dielectics. Special filtering will be required to separate the various components.

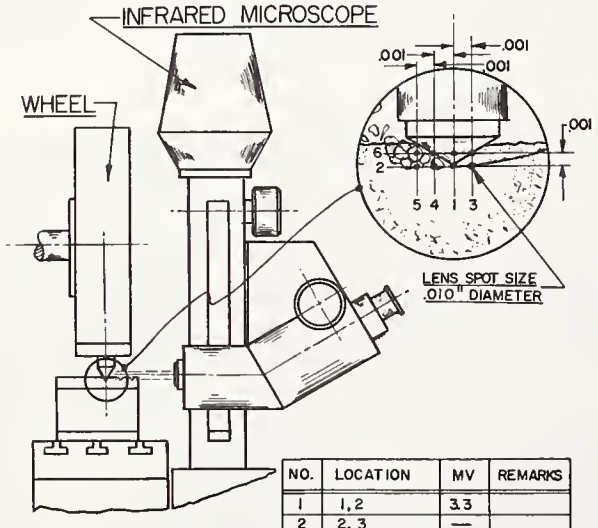

NO.	LOCATION	MV	REMARKS
1	1, 2	3.3	
2	2, 3	—	
3	2, 4	3.2	
4	2, 5	—	
5	6, 1	1.2	
6	6, 3	—	
7	6, 4	2.2	
8	6, 5	2.2	

FIGURE 29. *Relative grinding temperatures in the area surrounding the diamond as obtained by infrared microscopy.*

4. Conclusions

It is apparent that considerable progress has been made in recent years in the science of ceramic finishing. One of the fundamental objectives of this paper was to identify the state of the art in ceramic machining. A total systems approach was undertaken to analyze the mechanics of the process, determine the behavior of the ceramic material during grinding, and identify the thermodynamic and mechanical parameters. An understanding of the machine system, which delivers the motion and energy, is necessary to clarify the overall grinding process.

Some major findings are:

- Mechanical stock removal can be classified into three categories: Bonded Abrasive Machining (BAM), Free Abrasive Matching (FAM), and Contained Abrasive Machining (CAM).
- Cutting forces that are generated between diamond (tool) and material (workpiece) are directly related to the impact energy, rigidity of the system, and physical properties of the workpiece.
- Thermodynamic properties of the interacting materials are very important in the grinding process. A thermodynamic model shows that the greatest percent of the heat is absorbed in the wheel, and the remaining heat flow is distributed between the chips and the workpiece.
- Machine parameters are an important consideration in determining the optimal grinding process. Wheel speed generally had the greatest influence on the process behavior. Table speed has a lesser effect, while depth of cut primarily determines diamond life.
- Studies have indicated that environment

has an effect on the cutting force. A water mist has the largest effect, and reduces cutting forces when compared to grinding in oxygen, nitrogen, air, and compressed air environments.

- In general, high volume of material removed combined with low cutting speeds requires disproportionately large cutting forces and reduces diamond life. With a decrease in depth of cut and an increase in cutting speed, the diamond has a long life time.

In general, continued emphasis should be directed to the mechanics of stock removal in all three modes of abrasive machining. Specifically, in the Free Abrasive Machining (FAM) mode, scientifically justifiable information appears to be totally lacking. Quantitative information on surface and subsurface damage, while grinding, needs to be developed and expressed in terms of measurable and controllable parameters.

One of the most significant indications derived from this research is the necessity for in-process control. In-process feedback control, will emerge as an absolute necessity to repeatably produce finished ceramics with characteristics specified prior to the finishing cycle.

5. References

[1] Gielisse, P.J., Mathewson, W.F., Martis, J.A., and Ratterman, E., Ceramic Finishing with Diamond, Ceramic Industry, Feb., March, April issues (1968).

[2] Sedlacek, R., Processing of Ceramics—Surface Finishing Studies, Final Technical Report, Contract #N00019–67–0494, November (1968).

[3] Gross, G.E., Physical Parameters Affecting Fracture Strength and Fracture Mechanisms in Ceramics, Technical Report, Contract #N00019–68–C–0127, December (1968).

[4] Koepke, B.G., and Stokes, R.J., A Study of Grinding Damage in Magnesium Oxide Single Crystals, Technical Report, Contract #N00014–69–C–0123, July (1969).

[5] Rice, R.W., Machining and surface workhardening of MgO, to be published.

[6] Cutter, I., and McPherson, R., Examination of abraded MgO by x-ray diffraction line broadening, Phil. Mag., 20 (165), 489–94 (1969).

[7] Harrison, W.B., Influence of surface condition on the strength of polycrystalline magnesium oxide, J. Am. Ceram. Soc., 47 (11) 574–79 (1964).

[8] Evans, A.G., and Davidge, R.W., The strength and fracture of fully dense polycrystalline magnesium oxide, Phil. Mag., 20 (164), 373–88 (1969).

[9] Hockey, B.J., Observation of plastic deformation in alumina due to mechanical abrasion, Am. Ceram. Soc. Bull. 49, (4) 498 (1970). idem Plastic Deformation of Aluminum Oxide by Indentation and Abrasion, J. Am. Ceram. Soc., to be published.

[10] Rice, R.W., personal communication.

[11] Hara, A., Megata, M. and Yazu, S., X-ray study of residual stresses in ground cemented carbides, Powder Metallurgy International, 2 (2), 43–47 (1970).

[12] Sedlacek, R., Processing of Ceramics—Surface Finishing Studies, Final Technical Report Contract #N00019–67–C–0494 (1968).

[13] McKinney, K.R., and Herbert, C.M., The Effect of Surface Finishing on Structural—Ceramic Failure, NRL Report 6942, Naval Research Laboratory, Washington, D.C.

[14] Sedlacek, R., Processing of Ceramics—Surface Finishing Studies, Final Technical Report, #N00019–68–C–0388 (1969).

[15] Gielisse, P.J. and Stanislao, J., this paper.

[16] Gielisse, P.J., and Stanislao, J., Abrasion, in Encyclopedia of the Solid State (Marcel Dekker, Inc., New York, New York (1970).

[17] Cook, N.H., Loewen, E.G., and Shaw, M.C., Machine tool dynamometers, American Machinist 98, 125–129 (1954).

[18] See for instance Mathews, S., Thermal Aspects Related to Stock Removal of Ceramic Systems, M.S. Thesis, University of Rhode Island (1970).

[19] Peter, K., Sproedbruch und Mikroplastizitaet von Glas in Eindrucksversuchen, Glastechnische Berichten 37, (7), 333–345 (1964).

[20] Duvall, G.E., and Fowles, G.R., Shockwaves in High Pressure Physics II, R. S. Bradley ed. (Academic Press, New York, New York, 1963).

[21] Hull, E. H., and Malloy, G. T., The strength of diamond, Presentation Annual Meeting American Society of Mechanical Engineers, Chicago, Illinois (1965).

[22] Schwarzkopf, P., and Kieffer, R., Cemented Carbides, p. 236 (MacMillan Book Company, New York, New York, 1960).

[23] Steverding, B., Brittleness and impact resistance, J. Am. Ceram. Soc. 52, (3), 133–136 (1969).

[24] Gielisse, P.J., and Stanislao, J., A Thermal Model for Ceramic Grinding Temperatures, to be published.

Discussion

O'HARA: You mentioned that 70 percent of the heat goes into the workpiece rather than the tool itself; now that's primarily governed by the fact that the tool was a higher thermal conducting material than the workpiece. Is that not true?

GIELISSE: That's correct. As a matter of fact our wheel is essentially our diamond and the large difference in the thermal conductivity and heat transfer processes is, of course, due to the very thing you indicated.

O'HARA: In this case you are using a single crystal. Depending upon the bond, heat transfer conditions may change if you are using an actual wheel having a composite structure.

GIELISSE: That's right, and specifically so when you use a polymer bond.

NATIONAL BUREAU OF STANDARDS SPECIAL PUB. 348, The Science of Ceramic Machining and Surface Finishing, Proceedings of a Symposium Sponsored by the American Ceramic Society, the Office of Naval Research, and the National Bureau of Standards, held at NBS Nov. 2–4, 1970, Gaithersburg, Md. (Issued May 1972).

Direct Observation of Material Removal Process During Grinding of Ceramics by Micro-Flash Technique

Osamu Imanaka, Seiji Fujino, and Shin-ei Mineta [1]

Electrotechnical Laboratory, Tokyo, Japan

In order to make the mechanism of grinding ceramics clear, chip removal processes have been observed during grinding with a specially-built setup which consists of a flash lamp, synchronizer, microscope and motor-driven camera. Duration time of the flash is about 0.8 μs in half-value width, and a storage capacitor in the flash lamp circuit can store an energy of about 10 W·s. By choosing the flashing point, grinding phenomena at different positions on the contact arc can be photographed at certain time intervals.

The experiments were done mainly by using one grain of diamond attached to a disk which was mounted on a shaft of a surface grinding machine. Workpiece materials examined were glass-ceramics and several types of oxide ceramics, e.g., alumina, forsterite, and steatite ceramics. The main results obtained are as follows: Under moderately large depth of cut, the chips generated from ceramics are generally of a fragment type and are distinguished from those of ductile materials. Part of these chips were observed to be removed, of course, directly by the grain, but a considerable part of them were found to splinter out of the workpiece surface in a short time after the grain has passed over. Possible explanations are proposed for those phenomena. The above-mentioned facts suggest that a damaged layer may remain under the ground surface of ceramic materials. It is also demonstrated that chips of continuous type are occasionally observed at high grinding speed and under moderately small depth of cut. The chip formation of this type depends delicately on the materials to be ground.

Key words: Alumina; brittle fracture; chip removal process; forsterite; glass-ceramics; grinding of ceramics; micro-flash technique; observation of chips during grinding; steatite.

1. Introduction

In research into the cutting mechanism of abrasive grains on the grinding wheel, direct observation of chip formation during grinding is thought to be one of the most effective approach to the object. In metal grinding, Schwartz [2] photographed the surface of a grinding wheel at certain intervals during grinding with a specially-built equipment, which consisted of a substandard film camera, a stroboscopic light, suitable synchronization setup, and optical compensation. However, little has been reported concerning the cutting behavior of the abrasive grain during grinding, and the information has been limited to the occurrence on the peripheral surface of the grinding wheel.

The purpose of this study was to observe the chip removal processes directly during grinding and to provide with new insights on the cutting performance of abrasive grains in ceramics grinding. Photographs of grinding chip removal from different materials taken by means of a synchronized flash lamp are presented and discussed.

2. Experimental Setup and Procedure

The experiments were done mainly by using one grain of diamond attached to a aluminum disk of 200 mm diam, which was mounted on a shaft of a surface grinder as shown in figure 1.

The diamond grain used had the shape of a truncated quadrangular pyramid of 90° facing angle. Diamonds were chosen with edges between 20 and 30 μm to simulate flat worn surfaces on actual grinding wheels. Grinding was done by pyramidal face (not by an edge).

Workpiece materials examined are shown in table 1. Before an experiment, the surface of the specimen was finished to a roughness of less than 1 μm maximum height by lapping with silicon carbide abrasives of 2000 mesh grit size.

TABLE 1. *Workpiece materials used*

Workpiece materials	Microhardness, Hv (kg/mm^2)
Steatite ceramics (77% MgO·SiO)	674
Forsterite ceramics (97% 2MgO·SiO)	773
Alumina ceramics (94% Al_2O_3)	1860
Insulator porcelain	651
Glass-ceramics	685
Synthetic sapphire	2130
Bearing steel, SUJ 2 (hardened)	623

[1] Chief, Senior Scientist, Junior Scientist of Fabrication Technology Section, respectively.
[2] Schwartz, K.E., Industrie-Anzeiger 80, 1391 (1958).

439-921 O - 72 - 4

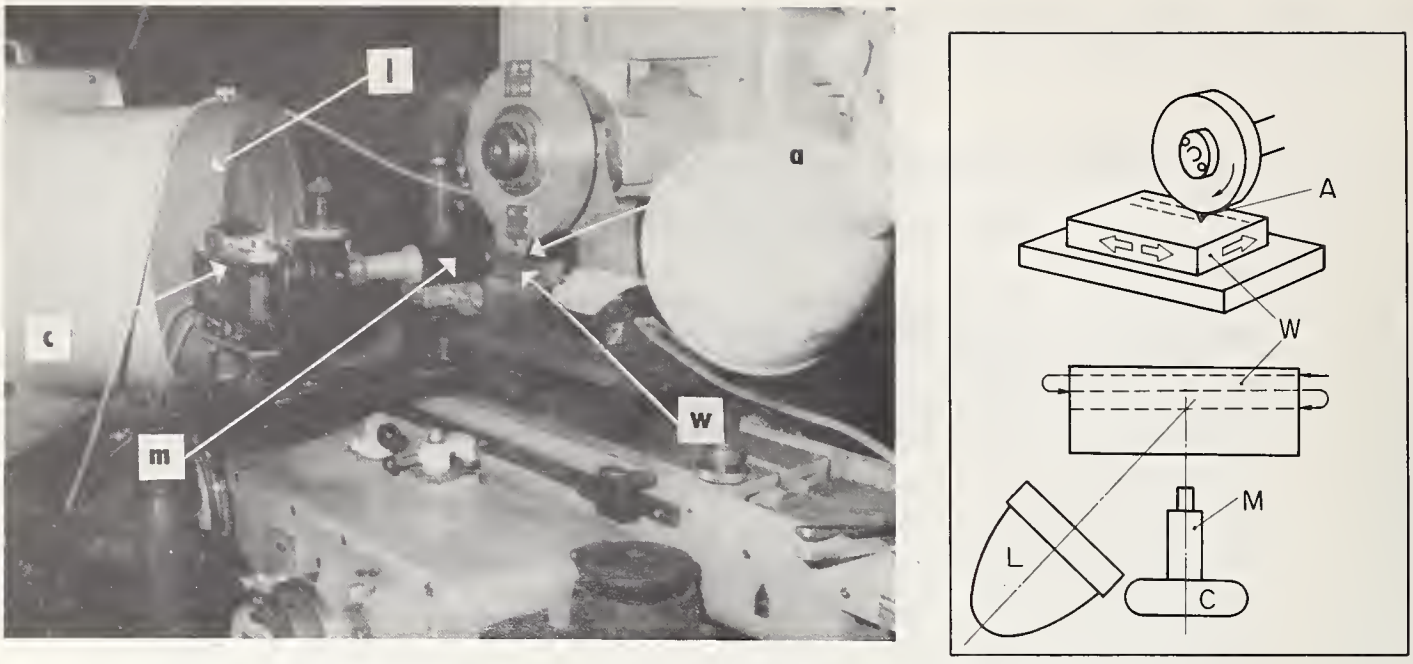

FIGURE 1. *Experimental set-up.* A, abrasive grain; C, camera; L, synchronized flash lamp; M, microscope; W, workpiece.

The grinding speed, U, and the table speed, v, adopted in the experiments were 12.5 to 37.5 m/s and 0.042 to 0.125 m/s, respectively. The depth of cut, g, was chosen to be 3 to 4 μm except the case shown in figure 15. For the convenience of observation, all the experiments were carried out without supplying grinding fluid.

By means of a parabolic reflector and Fresnel lens, the light beam from the flash lamp is converged on the grinding part to be photographed. In order to photograph the chip removal process during the grinding at a specific, chosen position of the grain (refer to fig. 4), a synchronized illumination system shown in figure 2 was adopted. When the shutter of the camera is opened, the flash lamp lights up in agreement with a preset angular position of the disc. Namely, the beam reflecting from the synchronizing mark on the disk comes to the synchronizer, and makes the photocell emit an electric pulse which is amplified and gives the signal to trigger the flash. The synchronization is good to within 0.2 μs at each time.

The light-emitting spark gap of the flash lamp is enclosed by a fused quartz cylinder which is filled by high-pressure argon gas. Input voltage to the flash lamp is 20kV and the built-in storage capacitor can store an energy of about 10 W · s. Restoring charges of the capacitor needs 10 s after the preceding flash has finished.

The duration of a light pulse of the flash was measured at about 0.8 μs in half-value width as shown in figure 3. Provided that an exposure time to the film is equal to 0.8 μs and that the

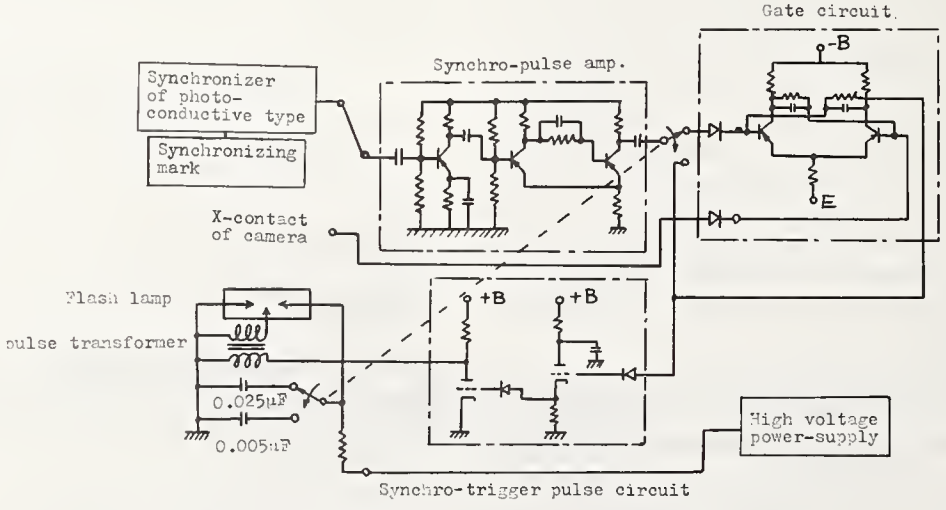

FIGURE 2. *Schematic arrangement of illumination system.*

FIGURE 3. *Oscillogram showing the duration of a light pulse.* Time scale: 1 μs/div.

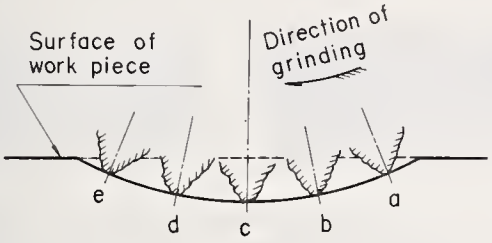

FIGURE 4. *Flashing point.*

grinding speed of the grain is 25 m/s, the movement of the grain is 0.02 mm in the time of exposure. When a blur on the film of 0.2 mm is allowed, photographs can be taken at magnification of 10 diam without the picture's quality being noticeably degraded. A flashing point (fig. 4) can be altered by moving the position of the beam emitter of the synchronizer or by using a time-delay device which presets a pulse-delay between an input pulse and triggering of the flash.

3. Results

A series of photographs taken at different flashing points during grinding forsterite ceramics are shown in figure 5, where the photographs (a), (b), (c), (d), and (e) were recorded at the positions a, b, c, d, and e in figure 4, respectively. On the right side of each photograph, is arranged a schematic sketch of chips. Each photograph was taken approximately 10 s after the preceding one had been done. (The same procedure was used in figs. 6 through 9.) Hence the chips in different photographs are not identical. However, since the wear of the diamond tip can be regarded as negligible during such a sequence photographs (fig. 5), they can be regarded as an accurate composite picture of the chip forming process.

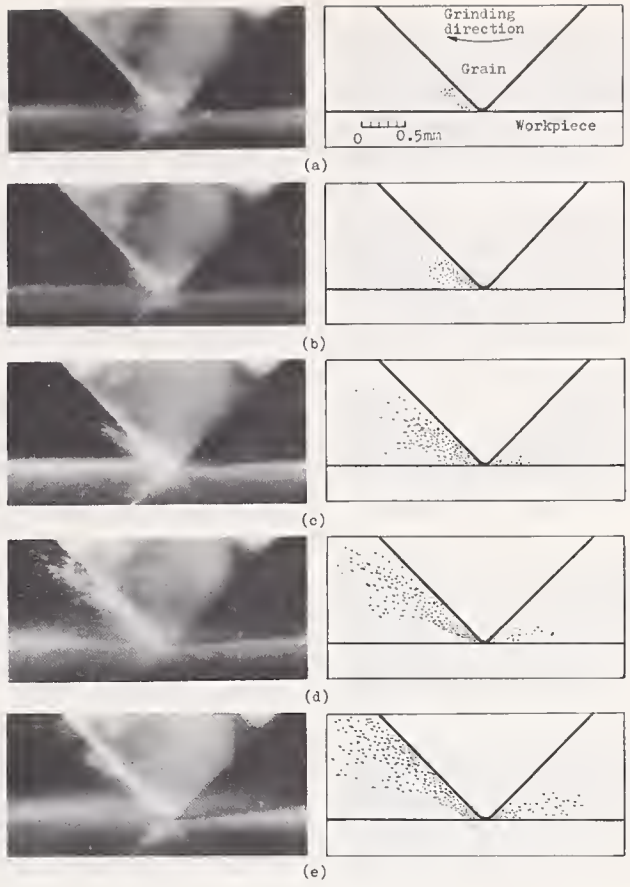

FIGURE 5. *Chips from forsterite ceramics at different grinding stages.* $U=12.5$ m/s, $v=0.042$ m/s.

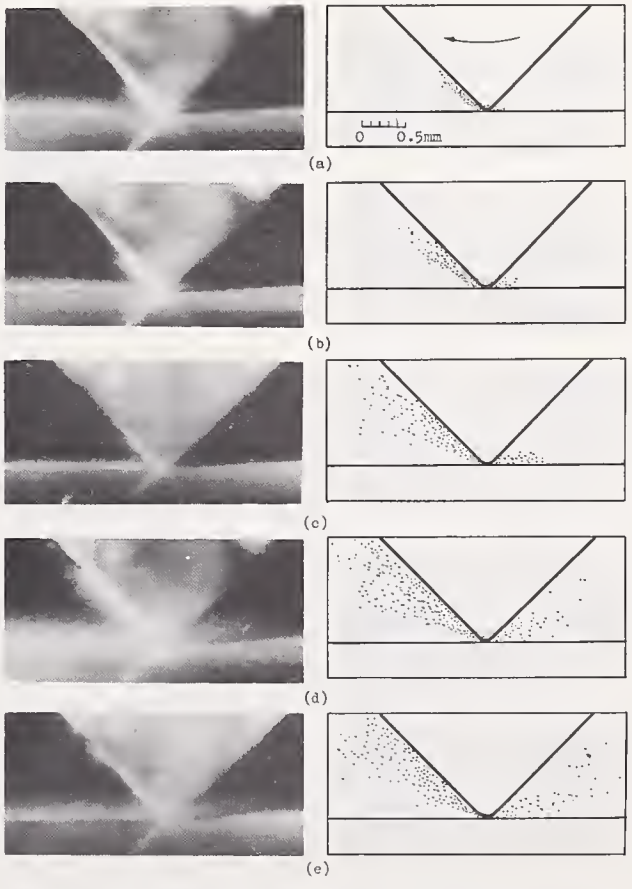

FIGURE 6. *Chips from insulator porcelain at different grinding stages.* $U=12.5$ m/s, $v=0.042$ m/s.

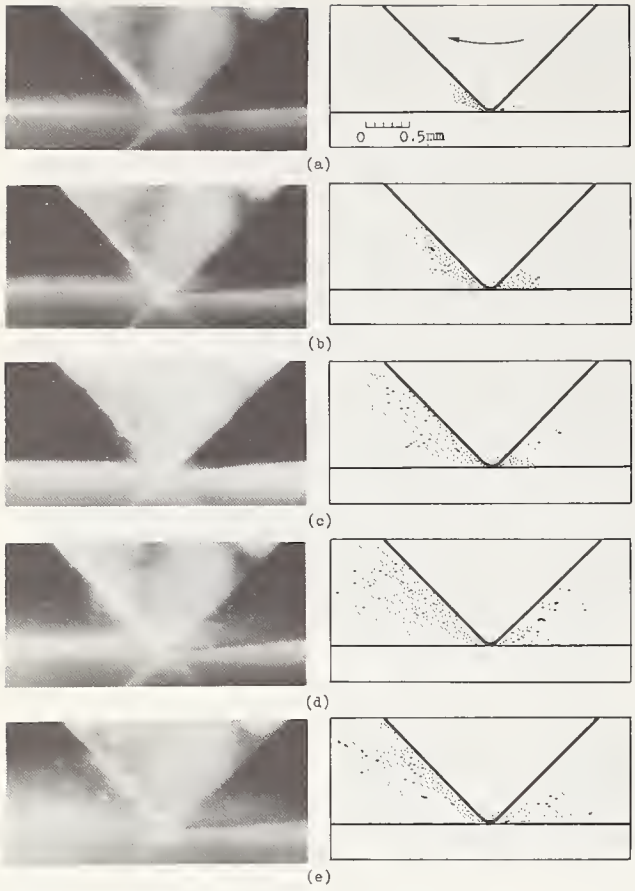

FIGURE 7. *Chips from glass-ceramics at different grinding stages.* $U=12.5$ m/s, $v=0.042$ m/s.

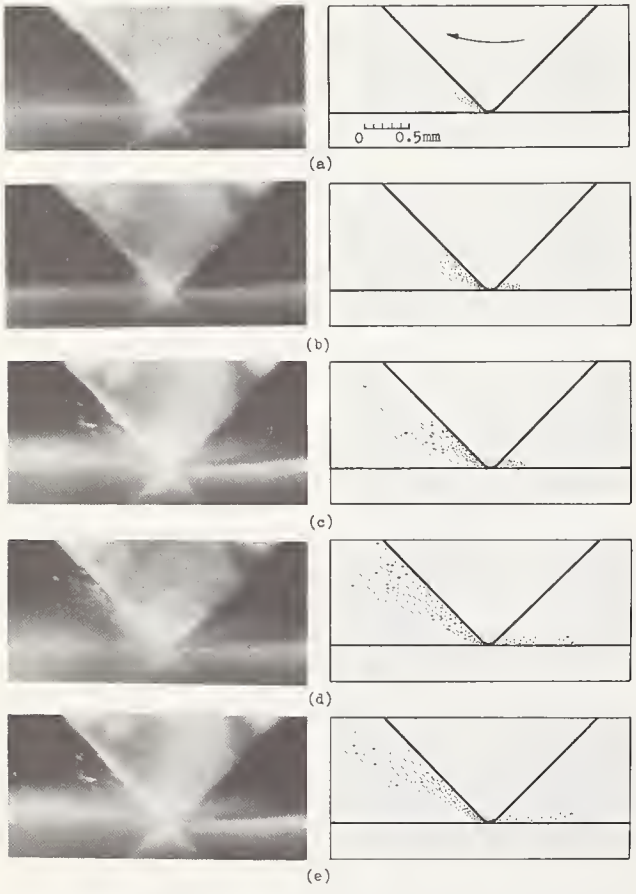

FIGURE 8. *Chips from alumina ceramics at different grinding stages.* $U=12.5$ m/s, $v=0.042$ m/s.

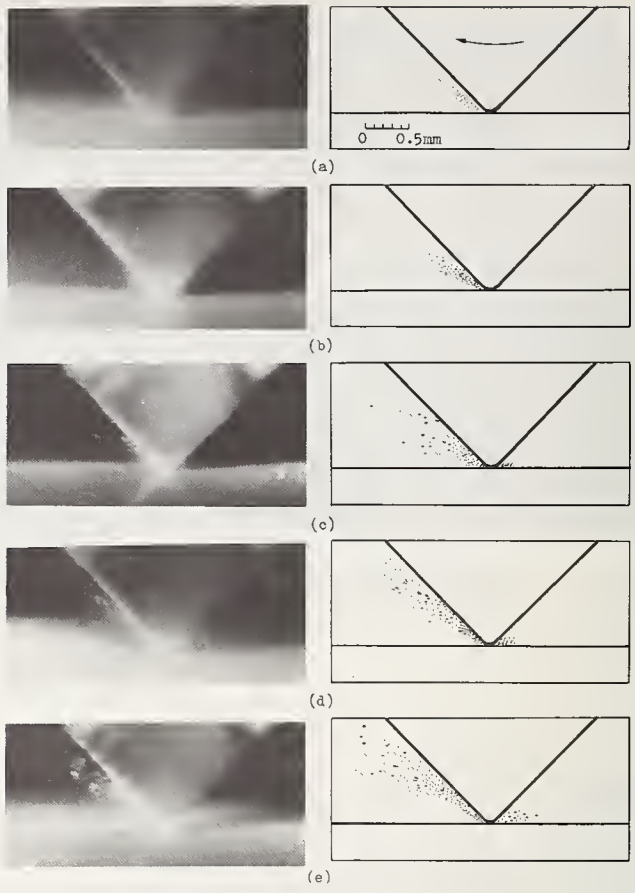

FIGURE 9. *Chips from steatite ceramics at different grinding stages.* $U=12.5$ m/s, $v=0.042$ m/s.

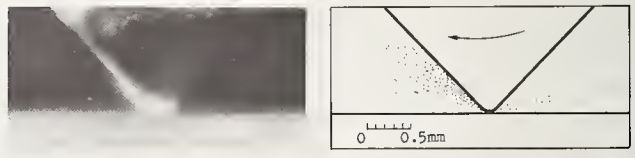

FIGURE 10. *Chips from synthetic sapphire.* Photographed at the position "c" in figure 4. $U=12.5$ m/s, $v=0.042$ m/s.

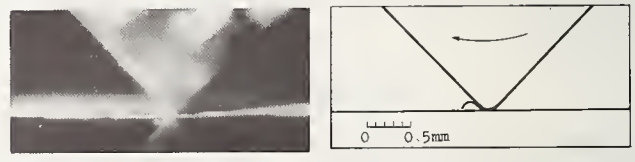

FIGURE 11. *Chip from hardened steel.* Photographed at the position "c" in figure 4. $U=12.5$ m/s, $v=0.042$ m/s.

Figures 6, 7, 8, and 9 show typical chips observed at different stages in the grinding of insulator porcelain, glass-ceramics, alumina and steatite, respectively. From the figures illustrated above, it is clearly seen that the chips from these materials under the grinding conditions examined are commonly of a fragment type. This characteristic is also seen in grinding synthetic sapphire (fig. 10).

In the case of grinding ductile materials, the removed chips have been observed to curl

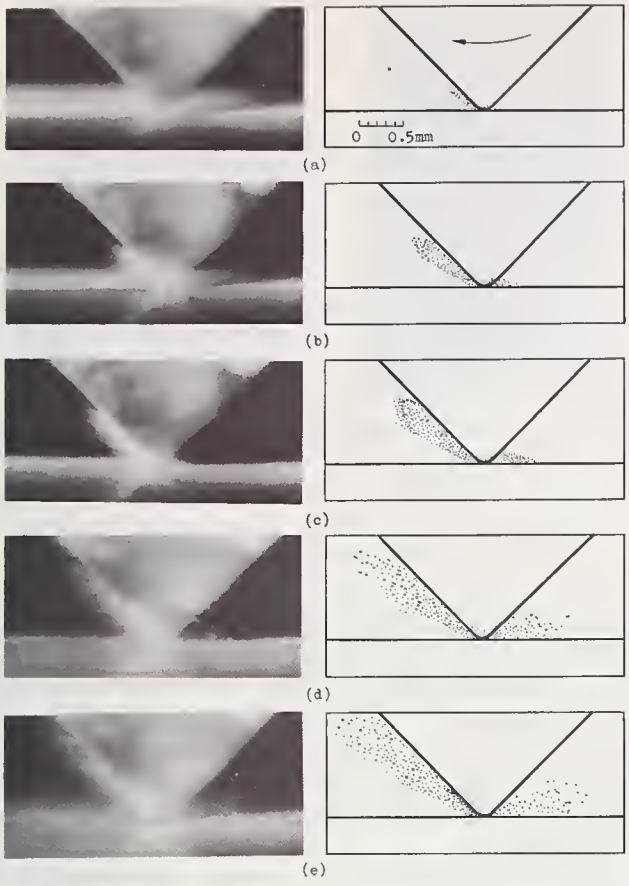

FIGURE 12. *Chips from forsterite ceramics at different grinding stages.* $U=37.5$ m/s, $v=0.125$ m/s.

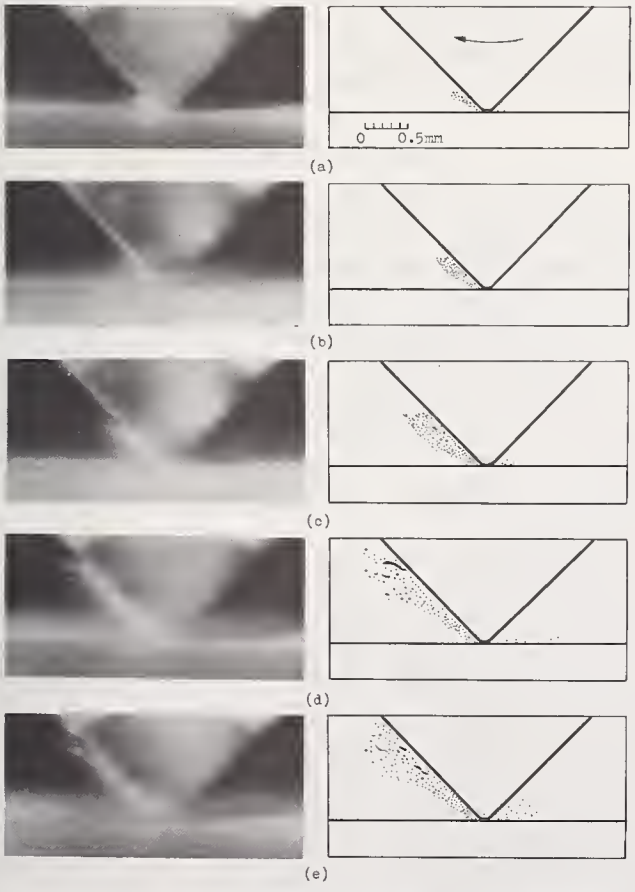

FIGURE 13. *Chips from steatite ceramics at different grinding stages.* $U=37.5$ m/s, $v=0.125$ m/s.

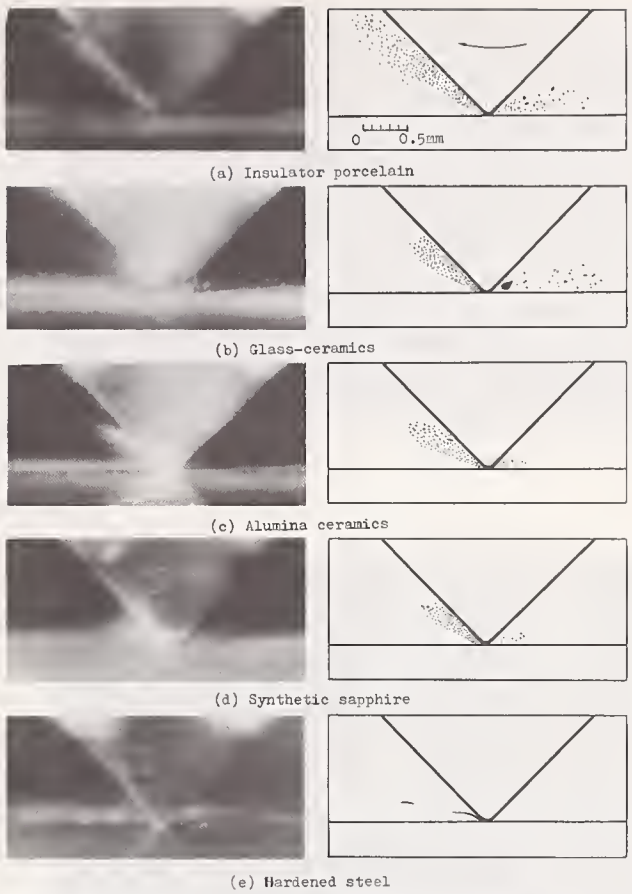

FIGURE 14. *Chips from various materials.* Photographed at the position "c" in figure 4, $U=37.5$ m/s, $v=0.125$ m/s.

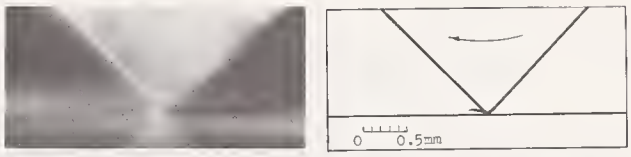

FIGURE 15. *Continuous chip formed in grinding glass-ceramics under small depth of cut.* Photographed at the position "c" in figure 4. $U=37.5$ m/s, $v=0.125$ m/s.

in front of the abrasive grain, which bear some resemblances to the one formed in turing with a bit.[4] The shape of chips varies, of course, according to the shape of abrasive grain tip, but the chips from ductile materials are generally of a "continuous" type.[4] An example of the chip during grinding hardened steel with the diamond model grain is shown in figure 11.

On the other hand, it is seen from figures 5 through 10 that a considerable part of chips are flying off in front of the grain. From the blur of the photographs, their flying velocities are thought to be considerably higher than that of the peripheral speed of the grain. Moreover, part of chips are observed to splinter out of the specimens surface in a short time after the grain has passed over. This phenomenon is pronounced, especially in the grinding of for-

[4] Imanaka, O., Fujino, S., and Mineta, S., Bull. Electrotech. Lab. 32, 907 (1968).

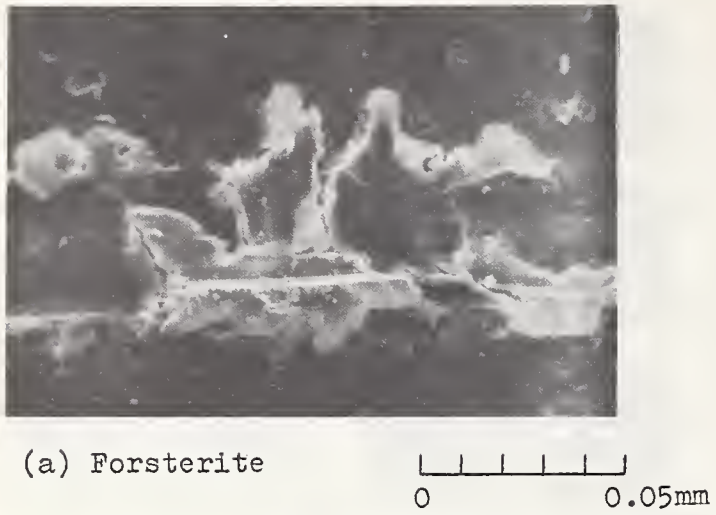

FIGURE 16. *Ground tracks on forsterite and steatite surfaces.* $U=12.5$ m/s, $v=0.042$ m/s.

sterite, insulator porcelain and glass-ceramics. The amount of such chip splintering after passage of the grain is fairly small in the case of steatite.

The chips formed at higher grinding speed are shown in figures 12 through 14. The photographs in figure 14 were taken at the position of "c" in figure 4. General characteristics are almost the same as those seen at lower grinding speed. But the velocities of chips flying out in front of the grain are observed to be much higher than those at lower grinding speed.

In addition, it should be pointed out that, even in grinding brittle materials, a sort of continuous type chips are likely to be formed at high grinding speed and under moderately small depth of cut as seen in photographs (d) and (e) in figure 13. Under the conditions examined, "continuous" chips were apt to be observed in grinding steatite. Another example of this type chip is illustrated in figure 15, where the depth of cut adopted was less than 2 μm.

Fig. 16 shows the ground tracks on the forsterite and steatite surfaces. In grinding forsterite, which is the most brittle ceramic

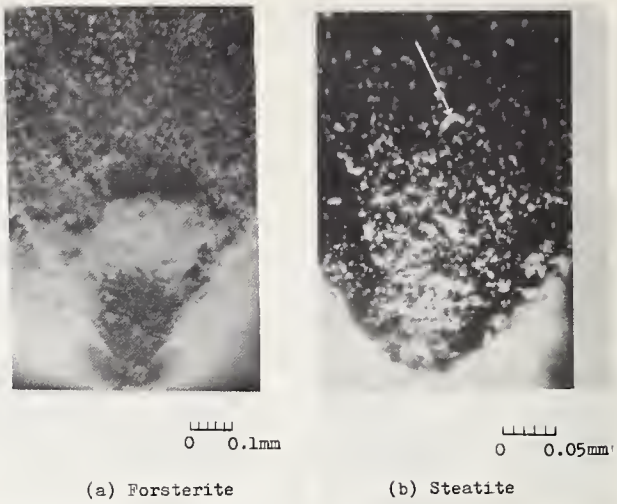

FIGURE 17. *Chips sticking to pyramidal face of grain.* $U=12.5$ m/s, $v=0.042$ m/s.

examined, local fractures in the workpiece surface and deep fissures extending into the workpiece body are clearly seen. Existence of these fissures suggests that a damaged layer may remain under the ground surface. In grinding steatite, though brittle features are observed, the disorder of the cracks is much less than in the above case.

Fig. 17 illustrates the chips sticking to the pyramidal face of the grain. Measurement shows, a number of chips are larger in diameter or thickness than the grain depth of cut. It should also be noticed that figure 17(b) shows a "continuous" type chip (indicated by arrow) similar to those in figure 13(d) or (e).

4. Summary

In order to make the cutting behavior of the abrasive grain in ceramics grinding clear, the chip formation processes have been observed during grinding with a model grain by using the synchronized illumination setup developed.

The main results obtained are as follows: In grinding ceramics under moderately large depth of cut, fragment type chips generally appear, and part of them splinter out of the specimen surface a short time after the grain has passed over.

Considering the fissures on the ground surface which extend into the workpiece body, a model of chip formation process in grinding brittle ceramics may be proposed as shown schematically in figure 18. The sketch illustrates the cracks produced under ground surface, the extent of which depends on the properties of workpiece material and on stresses caused by the abrasive grains. When the load at the contact area of the workpiece and the abrasive grain is suddenly released at the instant that the grain has just passed over, the portion deformed elastically while being loaded will tend to recover its deformation. This portion,

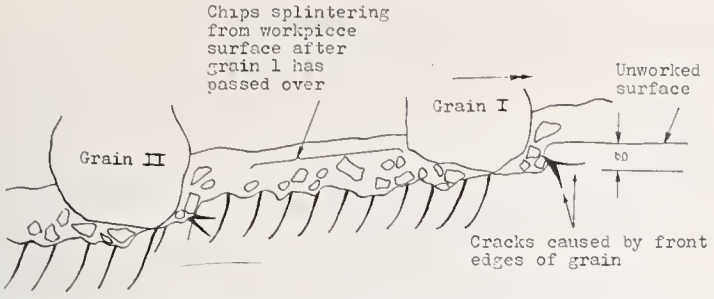

FIGURE 18. *Schematic model of chip formation process in grinding brittle materials.*

being prevented from recovering by tiny fragments of the workpiece material or by air compressed in the cracks, may make the shoulder parts above the cracks splinter off. This is a possible explanation for the splintering of chips along the locus of the grain after its passing.

The type of chips also depends on the properties of workpiece materials and on the grinding conditions. In grinding steatite and glass-ceramics at higher grinding speed and under moderately small depth of cut, chips of "continuous" type are occasionally formed. This phenomenon is thought to be due to the microplasticity of the materials.

Concerning the relationship between the grinding characteristics and the material properties of ceramics, a great deal of further work is required.

NATIONAL BUREAU OF STANDARDS SPECIAL PUB. 348, THE SCIENCE OF CERAMIC MACHINING AND SURFACE FINISHING, Proceedings of a Symposium Sponsored by the American Ceramic Society, the Office of Naval Research, and the National Bureau of Standards, held at NBS Nov. 2–4, 1970, Gaithersburg, Md. (Issued May 1972).

Grinding—A Means of Shaping and Sizing Ceramics

J. A. Mueller

The Carborundum Company

Bonded Abrasives Division, Niagara Falls, New York 14302

The shaping and sizing of ceramic bodies can be done with abrasive grinding wheels. From a grinding wheel point of view, ceramic bodies may be classified into two groups. One group that is harder than 800 Knoop and the other group that is softer than 800 Knoop.

The materials that are harder than 800 Knoop generally require the use of diamond wheels. Diamond wheels have the capability to remove stock, to generate precise geometry, and to produce finishes as fine as those that are measured in light bands.

The selection of the diamond grinding wheel is critical because improper selection can cause excessive grinding costs, poor quality, and low productivity. The selection of the diamond grinding wheel includes not only the selection of the specification of the wheel formulation but also the selection of the geometry of the wheel.

Case histories of finishing and shaping ceramic bodies illustrate the capability of the grinding wheel in these areas. Suggestions for starting speeds, feeds, and wheels together with a list of practical everyday "Rules of Thumb" for efficient grinding are documented.

Key words: Capability; ceramics; grinding wheels; selection; shaping; sizing.

1. Function of Grinding Wheels

The sizing and shaping of ceramics involves practically every known kind of grinding operation. Offhand grinding, surface grinding, both horizontal spindle and vertical spindle, disk grinding, internal grinding, centertype and centerless cylindrical grinding, thread grinding, and cutting off are used in the manufacturing of ceramic bodies. Grinding, therefore, is an essential and important part of the manufacturing process.

It is the object of this article to define the capability of abrasive grinding wheels to shape and size these ceramic bodies.

In a general classification, from a grinding wheel point of view, these ceramics include two types of material. Prefired ceramics together with ceramics softer than 800 Knoop hardness represent one classification and fired ceramics harder than 800 Knoop hardness represent the second classification.

The materials softer than 800 Knoop are often ground with silicon carbide wheels and a satisfactory product can be produced. Traditional grinding practices are used and generally no difficulties are encountered.

The materials in the second classification that are harder than 800 Knoop require the use of diamond wheels and at times present some difficulty in grinding, particularly if good grinding practices are not used. It is to this group of materials that the remainder of the article will be directed.

The function of a grinding wheel includes the following:

(a) Capability to remove stock.
(b) Capability to generate geometry.
(c) Capability to produce fine finishes.

In today's manufacturing many times one grinding wheel is expected to perform all three functions. In a great number of cases it can and does. However, to efficiently perform all three functions with one wheel necessarily demands that a compromise be effected between one or more of the functions.

By documentation of case histories in specific areas of grinding, hopefully an awareness of the capability of the grinding wheel will be developed, and with this awareness, then, practical use can be made of the grinding wheel in everyday operations to produce parts to size, shape, and finish at minimum cost and satisfactory productivity.

2. Selection of Grinding Wheels

2.1. Grinding Wheel Formulation

The selection of the grinding wheel is important and critical if the lowest cost of grinding is to be effected without sacrificing quality of grind or dimensional accuracy. Evidence of this is shown dramatically in table 1. High purity alumina pieces were surface ground on a vertical spindle rotary table grinder. By substituting a coarser 80 grit wheel in place of a finer 100 grit wheel, the cost of grinding was reduced 28 percent. Then by substituting a 50 concentration diamond wheel in place of a 100 concentration diamond wheel, the cost was reduced 61 percent.

Diamond concentration is defined as the number of carats of diamonds per cubic centimeter of wheel. Lower concentration means less diamonds and therefore less cost of wheel.

Table 1 defines and demonstrates a rule of

TABLE 1. *Effect of diamond grit size on the cost of grinding*

Machine	Vertical spindle rotary table grinder		
Material			
Type	96% Alumina		
Size	0.75 cm wide × 15.2 cm long		
Grinding fluid	Water soluble synthetic fluid 1–80 concentration.		
Operating conditions:			
Total area ground	46.5 square cm		
Table speed—r.p.m.	50		
Down feed rate	0.13 mm per minute		
Results:			
Tolerance—flatness	+0.08 mm or −0.08 mm		
Tolerance—squareness	+0.08 mm or −0.08 mm		
Abrasive specification			
Size	45.7 cm × 1.9 cm × 40.6 cm − 1.9 cm face		
Type	2A2T		
Speed	890 rpm.		
Abrasive specification	MD100–P100–M	MD80–P100–M	MD100–N50–M
Abrasive usage—mm	0.020/100 pcs.	0.014/100 pcs.	0.008/100 pcs.
Number of dressings	1—2 per shift	1 per shift	Seldom

diamond grinding that states, "It is advisable to use the coarsest grit size diamond possible that will satisfy the finish and quality of grind requirements." Coarser grit sizes will produce a better finish when larger areas are ground than when smaller areas are ground.

It also defines the rule that it is advisable to use the lowest concentration diamond wheel that will satisfy the quality requirements of the finished product.

Until experience has been generated on a specific grinding operation, it is advisable to use 100 concentration diamond wheels for centerless, surface, and cylindrical grinding. Lower concentrations are adaptable for use in offhand grinding operations and in cutting off.

Included in the selection of the grinding wheel is not only the grit size, hardness, and concentration but also the bond type. Metal bond diamond wheels are generally the choice for ceramic grinding because ceramics possess high abrasion properties and consequently tend to wear other bonds quickly. Resinoid bond can be used particularly for producing fine finishes. Resin bond wheels, however, wear away rapidly and generally are expensive to use. Because of their high wear characteristics, at times resin bond diamond wheels have difficulty in generating dimensional accuracy.

Table 2 compares wheel life and grinding rate as a function of the bond of the wheel.

2.2. Grinding Wheel Geometry

Recent performance data have documented the impact that diamond wheel geometry can have on performance and productivity.

Figure 1 illustrates a diamond wheel with radial slots in it. This wheel compared to a wheel without slots and having a solid face of diamonds differs widely in performance. Table 3 describes this performance. The solid diamond face wheel was able to remove 1.83 mm from an area of 2916 square cm of high purity alumina and then the wheel required dressing. By slotting the wheel with a varying number of slots, the amount of stock that could be removed without dressing ranged as high as 192 percent more. Translated into productivity, this

TABLE 2. *Effect of diamond wheel bond type on grinding performance*

Wheel Bond	Wheel life	Wheel Grinding rate
Metal	Longer	Slower
Vitrified		
Resinoid	Shorter	Faster

FIGURE 1. *Slotted face resinoid bond diamond grinding wheel.*

TABLE 3. *Grinding performance of solid face versus slotted face grinding wheel*

Machine	Vertical spindle rotary table grinder
Wheel size	45.7 cm × 1.9 cm × 40.6 cm–2.5 cm face.
Wheel speed	720 rpm—17.2 m per second
Grinding fluid	Water soluble synthetic fluid 1–80 concentration.
Table speed	33 rpm
Downfeed rate	0.10 mm per min.
Material ground	96% Alumina—4 pieces 30.48 cm diameter × 2.22 cm thick. Total area—2916 sq. cm.
Wheel specification	CMD180–L50–B8

Type of Wheel	Amount of infeed—millimeters before dressing was necessary	Percent increase in length of infeed before dressing was required
Solid Rim	1.83	—
8 slots	2.64	44
16 slots	2.79	53
32 slots	3.35	83
64 slots	4.11	125
128 slots	5.33	192

NOTE: All slots 0.16 cm wide.

means that the solid wheel required three dressings to one dressing with the wheel having 128 slots. Dressing automatically means a loss in productivity because of the time lost in dress and in addition means some loss in total life of the wheel because diamonds are dressed away without producing any useful work. Many times abrasive life is controlled by the amount of dress. Frequent dress produces short life. A softer wheel permitted to wear away somewhat faster often times has outproduced a wheel that wears away more slowly and requires frequent dressing.

After the wheel for grinding has been selected, it remains to define what the wheel can do.

FIGURE 2. *96 percent Alumina disc.* Ground to a reflective surface with a roughness of 0.08 μ.

3. Grinding Wheel Capability

In stock removal capacity, diamond grinding wheels have removed high purity alumina at rates as high as 16.2 cubic cm per minute.

The ability to generate a surface finish of high reflectivity is demonstrated in figures 2 and 3. Figure 2 is a picture of a 15.2 cm diameter flat made from high purity alumina that was ground to a reflective finish such that the scale can be seen reflected in the face of the disc. Figure 3 illustrates the same capability on a much smaller area of grinding.

Both pieces were ground on a vertical spindle rotary table surface grinder using diamond wheels and a water soluble grinding fluid. A 120 grit metal bond diamond wheel rough ground the material to a finish of 0.13–0.15 μ and the finish grind was produced by the 500 grit metal bond segmental wheel shown in figure 4. A surface roughness of 0.05–0.08 μ was generated.

In grinding this material, caution needs to be exercised so that the grinding wheel does not produce an impact shock on the piece. Too great an impact may crack it. In order to avoid this, the part to be ground should be placed as close to the center of the chuck as possible so that the wheel remains on the work piece all during the grinding cycle.

Grinding wheels, therefore, possess the capability of generating surface roughness on ceramic parts to as fine as 0.05 μ. On the other

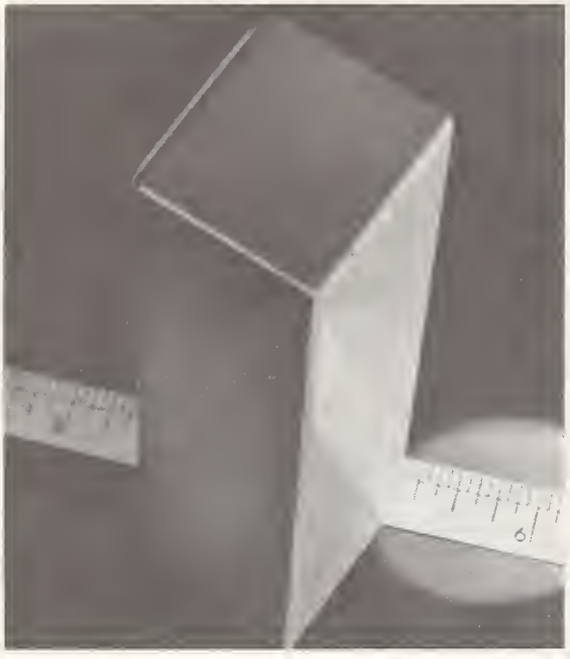

FIGURE 3. *96 percent alumina rectangle ground to a reflective surface with a roughness of 0.08 μ.*

hand, rougher surfaces may be generated with no difficulty.

Table 4 broadly defines the range of surface roughness that can be produced with various grit sizes of diamond grinding wheels. The quality of the material to be ground will change the ability of the grinding wheel to produce a finer finish. Generally finer grained bodies permit finer finishes than coarser grain ceramic bodies.

Manipulation of the operating conditions of the grinder will permit some range of finish that can be generated by the same wheel.

FIGURE 4. *500 Grit metal bond segmental type diamond wheel.*

Table 5 demonstrates the change in surface roughness that was produced by lengthening the time of spark out. This example shows a refinement of finish that appears to be small, yet this change was difficult to achieve because the actual finish is so fine. On parts that have a rougher finish, refinement of finish shows more dramatically the effect of increased spark out time.

Figure 5 shows the body whose finish was

TABLE 4. *Effect of diamond grit size on surface roughness*

Diamond wheel grit size	Finish μ
100	0.38—0.76
320	0.13—0.38
500	0.05—0.13

TABLE 5. *Effect of spark out on surface roughness*

Machine	Vertical spindle rotary table grinder			
Wheel speed	720 rpm—17.2 m per second			
Wheel type	Segmental			
Material ground	High purity alumina			
Grinding fluid	Water soluble synthetic fluid 1—80 concentration			
Table speed	33 rpm			
Abrasive specification				
Type	Segmental—60 segments 0.95 cm × 2.54 cm			
Grading	D500–N100–M			
Diameter	45.7 cm			
Total infeed	Rate of infeed	Spark out	Finish	
mm	*mm/min*	*min*	*μ*	
0.13	0.03	5	0.15—0.20	
0.30	0.03	10	0.15—0.18	
0.30	0.03	15	0.15	Newtonian rings visible

FIGURE 5. *96 Percent alumina ceramic valve disc ground to a finish of 0.15 μ.*

refined by spark out to such a degree that Newtonian bands appeared on the ground surface. The 500 grit metal bond segmental wheel shown in figure 4 was used for this grinding operation.

The third function of a grinding wheel is to generate geometry and dimensional accuracy. Dimensional accuracy capability has been demonstrated by the ability to produce a fine finish. Finishes in this range necessarily mean accurate dimension.

Generation of geometry on the other hand involves shaping of complex forms and shapes that require ability to grind angles, radii, contours, and at the same time blend in contour with angles.

Figure 6 illustrates such a part. This part necessitates the forming of a radius, an angle, or taper, and a blend of the taper and the radius.

Grinding wheels possess the capability of performing work of this kind. This particular form can be generated by using a straight 1A1 grinding wheel or a formed wheel.

If a 1A1 wheel were used it would need to be a small wheel mounted on a mandrel and inserted into a spindle. The entire spindle mount would then need to be swung in a radius equivalent to the radius being formed. The taper would be ground in a conventional manner.

This kind of part can also be ground by using a formed wheel such as shown in figure 7. The advantage of this method over the method using an 1A1 wheel is that substantially higher productivity can be achieved. Formed diamond wheels are becoming widely used and offer an opportunity to grind complex shapes at fast rates of productivity.

Threads can be ground into ceramic bodies using conventional thread grinding practices with a diamond grinding wheel.

Another example of the ability of the grinding wheel to fabricate a complex form is shown in figure 8. This cone was ground with a resinoid bond diamond wheel to a wall thickness of 0.51 mm without cracking or breaking the

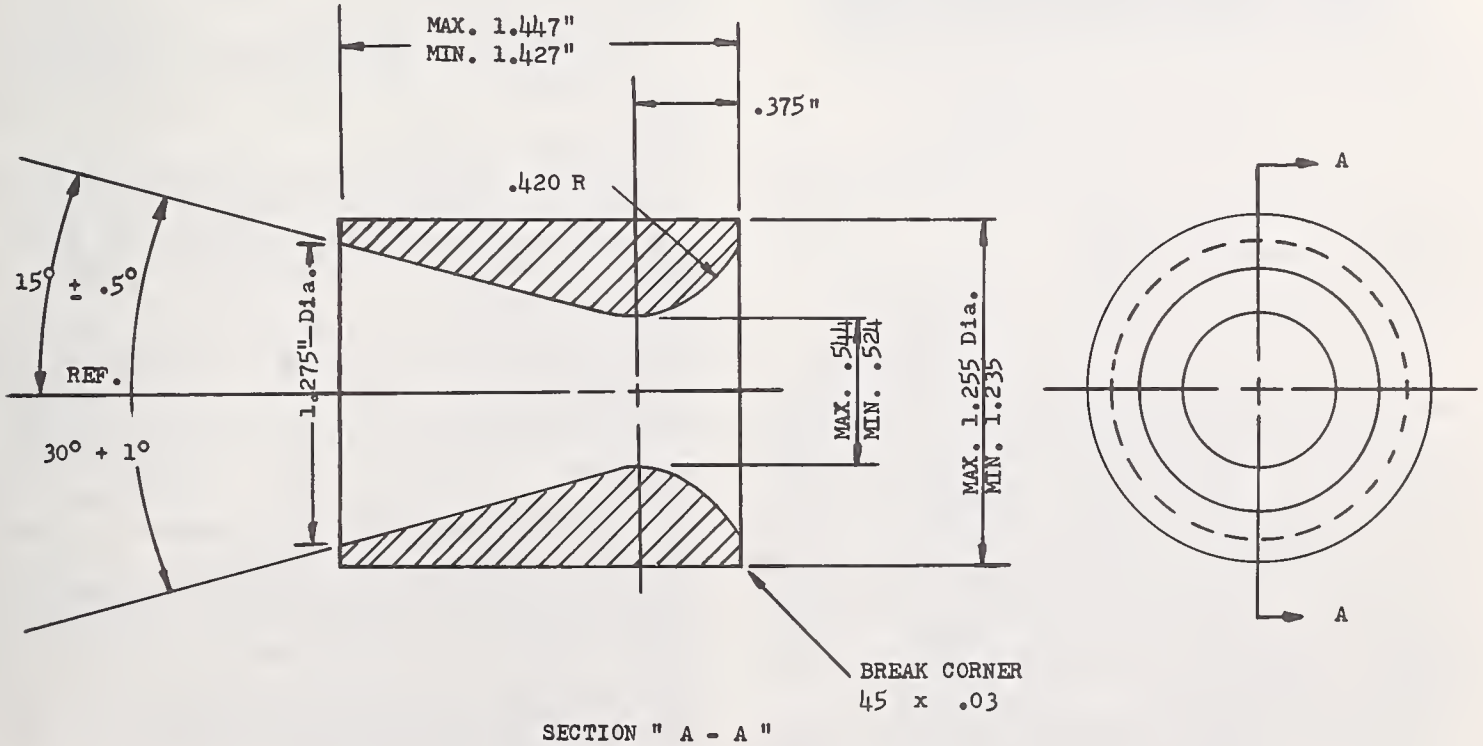

FIGURE 6. *Alumina nozzle insert.*

FIGURE 7. *Metal bond diamond formed grinding wheel.*

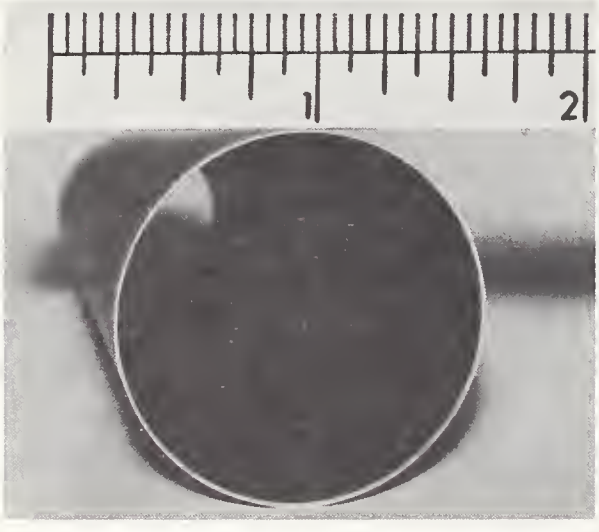

FIGURE 8. *High Purity alumina cone ground to a wall thickness of 0.5 mm.*

cone. Grinding wheels possess the demonstrated capability of being able to grind shapes and forms into ceramic bodies.

4. Grinding Machine Availability

In addition to the grinding wheel that is used, the grinding machine on which the wheel is mounted can play a critical role in the manufacture of ceramic bodies. Because of their inherent characteristics, the grinding of ceramics generally require rigid machines to prevent or minimize wheel vibration and its consequent effect on finish, quality, and even chipping or breakage. Fortunately, machine design has kept pace with the advance in grinding wheel capability.

Figure 9 typifies a machine that can grind a variety of shapes with the use of a grinding wheel. The machine essentially is a center type

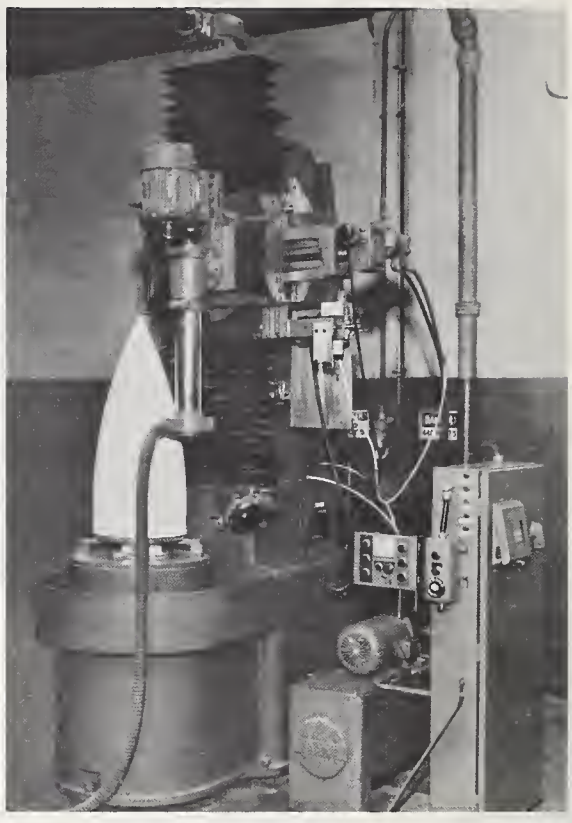

FIGURE 9. *Vertical spindle template grinder using a metal bond diamond grinding wheel.*

cylindrical grinder. The workpiece, which in this illustration is the cone, rotates on its center. The grinding wheel is driven and traverses across the work. The direction of rotation of the wheel and the work are the same so that at the point of contact, the wheel and work direction are opposed. Infeed motion is provided for sizing and provision can also be made for automatic size control.

The path of the grinding wheel is controlled by a template. In general terms, the grinding wheel will be able to follow whatever path the template provides.

A similar operation on a horizontal spindle surface grinder is shown in figure 10.

Machines are available to permit the grinding wheel to grind a multiplicity of shapes in a variety of sizes.

The fabrication of ceramic bodies necessitates many times the use of an abrasive wheel to cut off pieces.

Table 6 illustrates the difference in chipping that was produced by using a segmental type 1A1RSS cut off wheel and a continuous rim type 1A1R cut off wheel. The segmental wheel produced chipping, the continuous rim wheel was able to cut without chipping. This is particularly significant because the continuous rim wheel that was used was 46 grit which was substantially coarser than the segmental wheel and in addition, the continuous rim wheel was 50 concentration compared to 100 concentration for the segmental wheel.

TABLE 6. *Effect of solid rim versus segmental rim cut off wheels on chipping*

Machine	Cut off		
Wheel speed	3080 rpm—57.3 m per s		
Cutting fluid	Tap water		
Material cut	Dense porcelain—Size 5.08 cm × 6.35 cm		
Procedure	Plunge cut full depth.		
Wheel size	35.6 cm × 0.32 cm × 2.54 cm		
Wheel grading	1A1R MD46–N50–M	1A1RSS MD100–N100–M	1A1RSS MD100–L100–M
Time per cut (seconds)	61	135	237
Quality of cut	No chipping	Chipping	Chipping

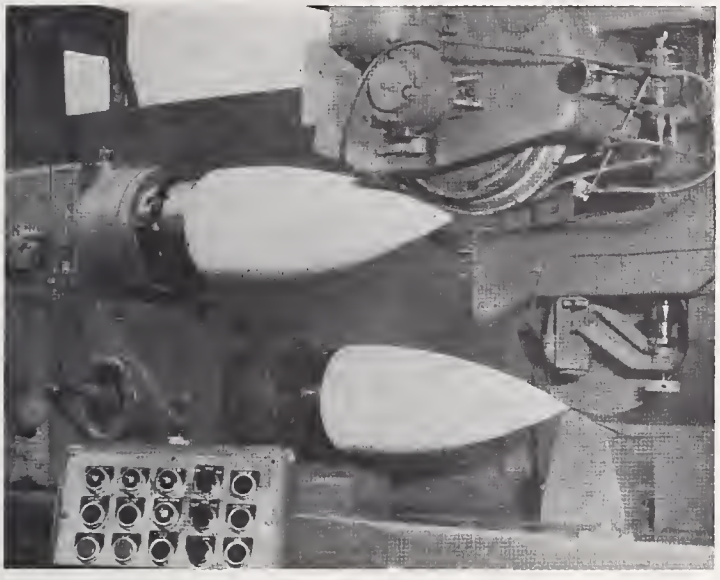

FIGURE 10. *Horizontal spindle template grinder using a formed diamond grinding wheel.*

To provide chip free cuts, it is advisable to use continuous rim cut off wheels in as coarse a grit size as the quality will permit.

The specification of the grinding wheel and the conditions under which that wheel should be used are most difficult to define in a general way. However, to provide a starting point so that experience may be gained, suggestions are offered in table 7 for grinding the hard dense ceramic bodies.

5. Rules of Thumb

In addition to these suggested starting points, and for the same purpose, the following "Rules of Thumb" are listed.

(a) Use the coarsest diamond grit size wheel that can satisfy the finish and quality requirements.

(b) It is advisable to use 100 concentration diamond wheels on any specific job until experience has been gained.

(c) Metal bond diamond wheels produce long life and slow grinding rates.

(d) Resinoid bond diamond wheels produce shorter life and faster grinding rates.

(e) The longer the time of spark out, the finer the finish and the flatter the surface.

(f) For fine finishes, use fine grit wheels.

(g) For coarse finishes, use coarse grit wheels.

(h) For chip free quality cuts use a 1A1R continuous rim cut off wheel.

(i) When grinding large areas, coarser grit diamond wheels may be used to improve performance.

(j) Ceramic grinding uses grinding practices similar to those used in metallic grinding and consequently knowledge of metallic grinding can be transferred for use on ceramic grinding.

6. Summary

(a) Abrasive grinding wheels, including diamond wheels, possess the capability to:
1. Remove stock rapidly.
2. Generate precision geometry.
3. Produce fine finishes.

(b) Machines are available to utilize the capability of the grinding wheel.

(c) The limiting factor in sizing and shaping ceramics is often the composition and geometry of the body itself.

(d) Grinding of ceramic bodies essentially is the same as the grinding of metal. Knowledge of metal grinding, therefore, can be transferred for use in the grinding of ceramics.

TABLE 7. *Starting grinding wheel recommendations for cylindrical and surface grinding*

Grinding wheel specification	Cylindrical grinding	Vertical spindle surface grinding
Grain type	Diamond	Diamond
Grit size		
Roughing	100—150	100—150
Finishing	220—500	220—500
Grade	N	N
Bond preferred	Metal	Metal
Bond to eliminate chipping	Resinoid	Resinoid
Speeds and feeds		
Grinding wheel speed—m per sec.	27.9—33.0	22.9—27.9
Work speed—m per sec.	0.51	—
Table speed—rpm	—	33
Traverse Speed—cm per min.	7.6—15.2	—
Crossfeed—mm	0.25—0.50	—
Infeed—mm	0.01—0.08	—
Infeed Rate—mm per min.	—	0.01—0.25
Grinding fluid	Water soluble	Water soluble

NOTE: These specifications are starting points. They may need refining depending upon the area of contact, the type of material that is ground, and other specific characteristics of the local grinding operation.

Discussion

HEUER: What is "spark out"?

MUELLER: "Spark out" is simply a term for permitting the wheel to grind without any additional in-feed. It is a method of relieving the pressure on the grinding wheel.

PERRY: If the goal is to minimize structural damage to the surface how would you modify your rules of thumb for the selection of grinding parameters?

MUELLER: To minimize surface damage, the following parameters of grinding are suggested:

(a) soft grade vitrified bonded wheels;
(b) slow wheel speed—2000 to 3000 S.F.P.M.;
(c) light infeeds— 0.0002 in to 0.0005 in;
(d) fast table speeds—80 F.P.M. and higher;
(e) sharply dressed grinding wheel with a sharp diamond;
(f) dress grinding wheel before spark out; and
(g) selected straight grinding oils for use as the grinding fluids.

NATIONAL BUREAU OF STANDARDS SPECIAL PUB. 348, THE SCIENCE OF CERAMIC MACHINING AND SURFACE FINISHING, Proceedings of a Symposium Sponsored by the American Ceramic Society, the Office of Naval Research, and the National Bureau of Standards, held at NBS Nov. 2–4, 1970, Gaithersburg, Md. (Issued May 1972).

Aspects of Machining Glass-Ceramic Materials

G. H. Allgeyer

Corporate Research Department, Owens-Illinois, Inc.
Toledo, Ohio 43651

and

L. V. Colwell [1]

Department of Mechanical Engineering, University of Michigan
Ann Arbor, Michigan 48104

The manufacture of optical and mechanical parts from glass-ceramic materials usually requires the removal of unwanted stock resulting from casting, hot forming, or the cutting of blocks from large ingots or blanks. Desired surface finishes at specified dimensions are the usual requirements. Conventional metalworking cutting tools did not produce satisfactory results. Scratching, splintering and brittle fracture were responsible for the material removal action in the sawing, drilling, turning and milling operations attempted. Very rough unsatisfactory surfaces resulted.

The physical and mechanical properties of CER–VIT®[2] material classify it as a brittle, crystalline material in the usual machining state. The best controllable means of material removal was found to be abrasive machining. The high hardness (550 Knoop) and abrasive character of these materials conclusively recommends diamond as the most satisfactory cutting medium. Machinability studies were conducted on CER–VIT® glass-ceramic material using diamond abrasive tooling while adjusting the controllable machining variables. The results and relationships of these techniques as applied to CER–VIT® glass-ceramic are discussed.

Significance of the experimental results are explored with particular emphasis being placed upon the predictable performance of diamond tools and the feasibility of programming of machining variables for utilization of numerically controlled machining processes.

Key words: Abrasive machining; brittle chip formation; brittle fracture; chip accomodation; glass; glass-ceramics; machining and grinding technical ceramics; material removal rate; specific energy; wheel structure.

1. Introduction

Mechanical parts can be machined as readily from glass-ceramics as from metals providing adequate consideration during the planning stage is given to the unique properties of these materials.

The most relevant of these properties is the brittleness in chip formation which manifests itself persistently over the entire range of useful cutting speeds and sizes of cut. Thus the development of quantitative guide lines for planning machining operations on technical ceramics involves the measuring and analysis of several operational factors with emphasis upon identifying the role of brittleness.

Early attempts to use the more conventional turning and milling operations met with failure not because of excessive tool wear but because the brittle chip formation at the sizes of cut peculiar to these operations with conventional cutting tools resulted in substantially unacceptable conditions of surface finish and size control. The search for more productive techniques narrowed rapidly toward abrasive machining with various forms of diamond tools.

The authors do not claim originality for much of the material discussed in this presentation, but they have applied the results of basic research reported in the technical literature from various parts of the world and have succeeded in developing reliable guidelines for planning machining operations on technical ceramics.

The nature of these guidelines and several other important aspects of the problem are discussed under the sections carrying the headings: Theoretical Considerations, Experimental Results and Priorities for Extending Productivity.

2. Theoretical Considerations

The theoretical aspects of the machining of glass ceramics are dominated by the chip formation almost to the exclusion of all others except for fracture stress and surface energy. Tanaka and Ikawa [1] [3] investigated the grinding of relatively hard and strong sintered carbides with both conically and spherically pointed

[1] Mr. Colwell is Professor of Mechanical Engineering at the University of Michigan, and Consultant to Owens-Illinois, Inc.
[2] ® A registered trademark of Owens-Illinois, Inc.
[3] Figures in brackets indicate the literature references at the end of this paper.

439-921 O - 72 - 5

diamonds and found that the normal stresses were not only of the same order of magnitude as the flow stress of the work material, but also that they could be predicted mathematically by the application of the principles of theory of elasticity along with the geometry of the individual diamonds. This has been explored also by Colwell [2] in connection with the physical properties of the tool-work material combination and the changes in tool geometry arising out of tool wear.

These results, as well as related efforts by many other investigators, have established that it is necessary to build up a stress between the tool and work material at least equal to the flow stress in the case of brittle materials like glass.

In the cutting of ductile metals the total energy requirements arise from four sources. Shear-flow energy is dominant by requiring 70 to 90 percent of the total while most of the remainder is needed to overcome friction. The energy required to create new surface is almost negligible by comparison.

Glass by contrast requires no energy for shear flow, which results in the requirements being dominated by that required to create new surface and to overcome friction. As a consequence chip formation and related particle size become of prime importance.

2.1. Chip Formation

Investigators at the Electrotechnical Laboratory in Tokyo, Japan, carried out studies of chip formation at actual grinding conditions with the microflash technique. The results [3] prompted them to characterize the mechanism of chip formation in glass and ceramics as shown in figure 1. It was believed that the chips or glass particles found in the grinding debris come primarily from the shoulders designated by the cross-hatched segments at the right in the figure.

They noted also that:

a. Chips are most frequently larger than the attempted thickness of cut, and that—

b. Chips were found to be formed and leave the surface *after* the grain had passed over the point of origin of the chip, which lead them to suggest that most such chips crack off upon elastic relaxation of the load created by the indenter.

The fact that the chips are brittle fragments, and that they can be larger than the attempted thickness of cut places emphasis upon grain size of the abrasive and especially upon those aspects of the structure of the grinding wheel which determine its ability to accomodate the chips; i.e., chip space.

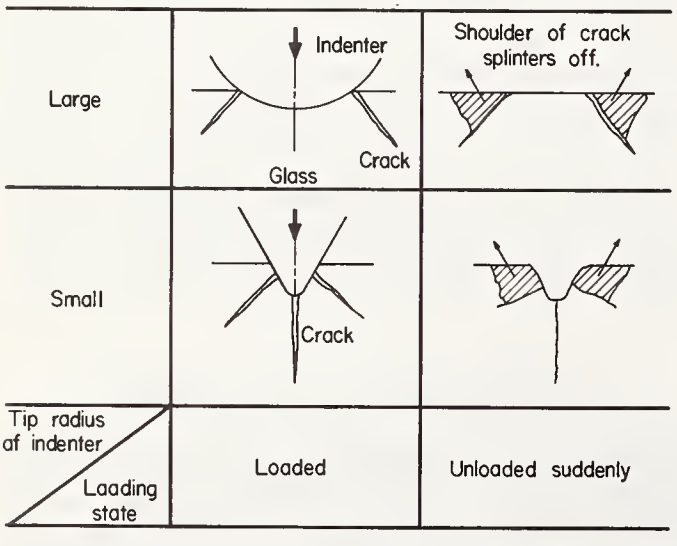

FIGURE 1. *Schematic diagram of splintering of glass scratched by hard indenter (from O. Imanaka, et. al. [3]).*

2.2. Grinding Wheel Structure

Prokhorchik [4] of the U.S.S.R. investigated the structure of diamond grinding with the objective of developing techniques for predicting the capacity of any given wheel for accomodating the chips, since he had found that this was the major limitation on the rate of removal. The experience of the authors of this paper has lead to substantially the same conclusion.

Prokhorchik concerned himself with the model illustrated in figure 2 and tried to relate

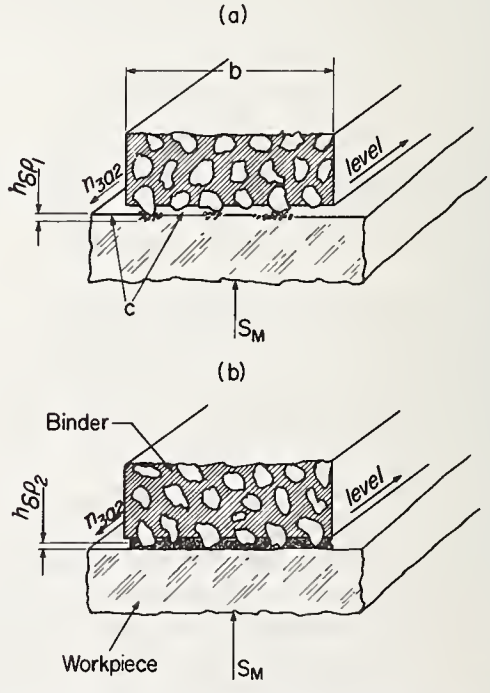

FIGURE 2. (*From Prokhorchik* [4]) *Normal operating conditions will accomodate all of the chips as at* (*a*). Too little projection of the diamonds, too high a concentration of diamonds, or too high a feed rate will overcrowd the available chip space as at (b).

the maximum capacity for chip accomodation to grain size, diamond concentration and the average projection from the sintered metal matrix. This could be accomplished only empirically and was complicated by the fact that the matrix material frequently projects into the grinding surface, especially with fine grained wheels as reported by Tanaka and Ikawa [1].

Despite these difficulties, Prokhorchik was able to establish that the capacity for chip accomodation was the most important deterrent to greater removal rates, and further that such capacity varied directly with diamond grain size and exhibited an optimum in relation to concentration. Experience gained by the authors of this paper strongly support these correlations and point further toward the potentially superior chip accomodation capacity of plating-bonded, single-layer diamond tools compared to the more conventional metal and resinoid matrix-bonded, multi-layer tools.

3. Experimental Results

Against the background of theoretical considerations found in the technical literature, the authors of this paper initiated a research program to develop necessary guide lines for applying basic principles in the machining of CER-VIT® and companion materials in a line of technical ceramics. The prime objective of this effort was not only to meet the usual size and surface finish specifications, but above all to achieve a maximum of productivity while fulfilling these other conditions.

The research program sought initially to find the limits of removal rate and to identify or confirm its determinants. Much of this has been carried out with conventional surface grinding on the periphery of plain circular wheels, but the established principles and guide lines have also been confirmed in other operations which must be performed in machining parts from these materials.

It is always advisable to use the most sophisticated investigative techniques available when searching for new information, but frequently such simple parameters as average spindle power and cutting forces may yield all one needs to know to greatly improve a process. This was the case in surface grinding CER-VIT® glass-ceramic materials.

Figure 3 is a plot of net spindle power as a function of rate of removal at constant wheel surface speed but for ranges of both table speed and depth of cut. The wheel was a single-layer diamond wheel with a grain size of 60/80 grit ($177/250 \times 10^{-6}$m). It will be noted that all of the experimental points for removal rates below about 2.5 cu in per minute (6.83×10^{-7} cu m/s) are closely grouped about a single straight line while those at higher removal rates

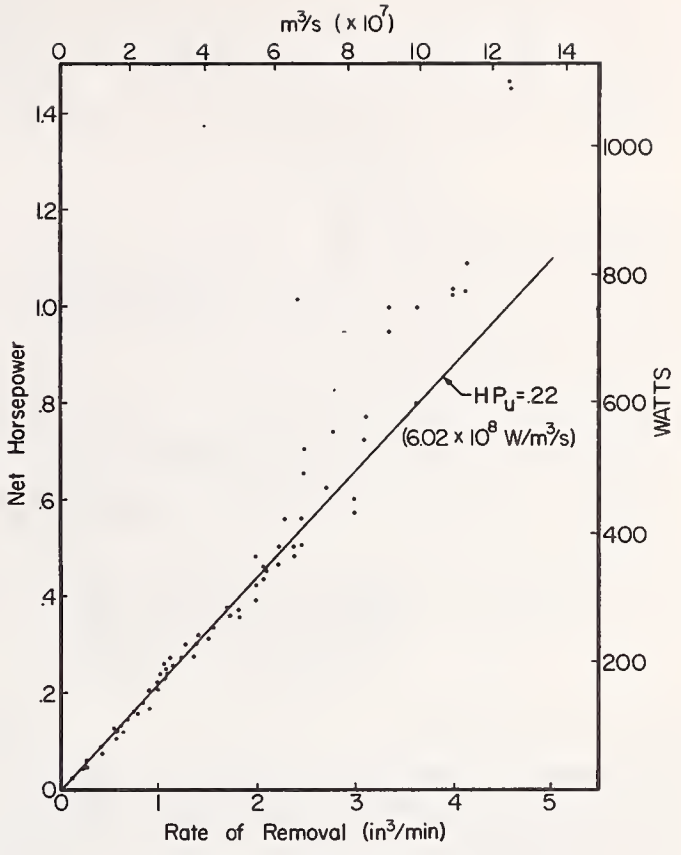

FIGURE 3. *Net spindle power versus rate of removal while surface grinding.* Wheel: 60–80 grit ($177–250 \times 10^{-6}$m) single-layer diamond; Work material CER–VIT® glass-ceramic.

are above the line because of greater friction due to varying degrees of incipient overcrowding of the available chip space in the wheel.

The straight line in figure 3 is labeled HP_u with a numerical value of 0.22. The designation HP_u is commonly used in technical literature on metal cutting and usually is referred to as "Unit Power" (specific energy), since it is obtained by dividing net spindle horse power by the rate of material removal. Consequently the units are Horsepower per cu in per min (the SI unit for specific energy is watts per cubic meter per sec ($W/m^3/s$), and 0.22 hp/in^3/min$=6.02\times10^8$ $W/m^3/s$). If the value of HP_u is multiplied by 33,000 foot pounds per minute (the equivalent of one horsepower), the result is the number of foot pounds of energy required to convert 1 cu in of the work material into chips (The horsepower equivalent of 33,000 ft-lb/min is 746 joules per second (J/s), or 746 watts). Thus it would appear that the energy requirements are not critically sensitive to the variations of surface energy peculiar to the variation of particle size as between light cuts and heavy cuts. On the other hand, the specific energy for fine grained wheels has been found to be as much as two times greater.

The overcrowding tendency indicated by the points above the line in figure 3 is delineated more sharply when the unit power is plotted

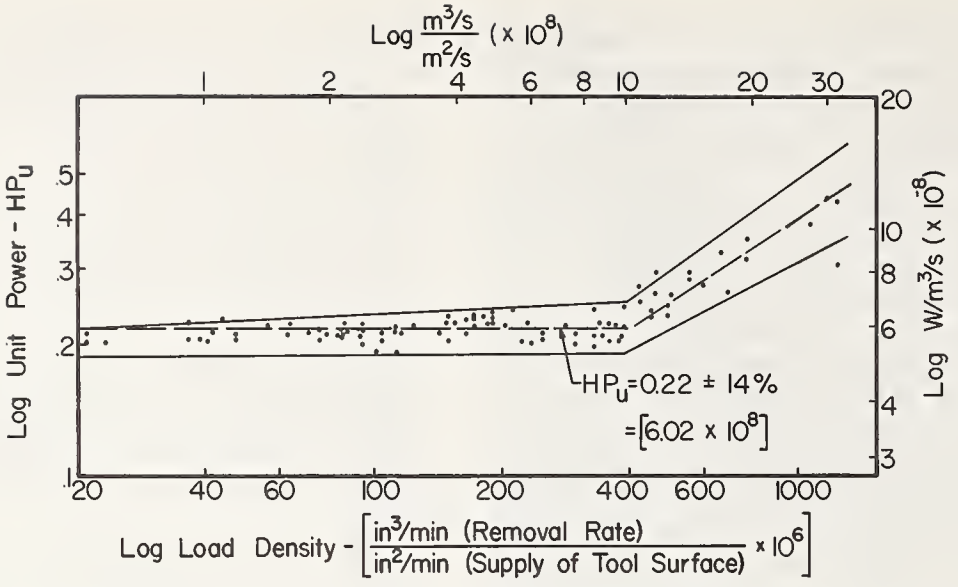

FIGURE 4. *Specific energy requirements normalized against rate of supply of tool surface area for a constant wheel speed and wide ranges of depth of cut and table speed in surface grinding.* Wheel and work material same as in figure 3.

against the degree of utilization of available chip space in the wheel. This has been done on double logarithmic coordinates in figure 4.

The degree of utilization of chip space has been designated as "Load Density" and has been calculated by dividing the removal rate by the area of wheel surface which has passed over the surface being ground in the same period of time. Thus the value of 1000 on the abscissa represents the loading of one thousandth of a cu in of work material over each sq in of wheel surface ($25.4 \times 10^{-6} m^3/m^2$). Similarly the figure 100 represents only one tenth as much loading.

It is to be noted especially that the wheel becomes seriously overloaded or overcrowded at load densities above 400 microinches (1.016×10^{-5}m). Dulling of the wheel will shift the entire band of points upward but will have little effect on the 400 microinch breaking point. Similarly, wheel speed should have little effect, but variations in the effectiveness of coolant application can shift the breaking point substantially.

4. Priorities for Extending Productivity

As mentioned earlier, Prokhorchik established that chip accomodation was a most important limiting factor in achieving greater material removal rates. The authors observed that the size and shape of chips produced by the finer grain sizes of diamond were much more persistent in packing tightly in the available chip space than those produced by the coarser grain sizes. As the "Load Density" increases, friction increases, and the unit power curve rises sharply as shown in figure 4. In figure 5 the data in figure 4 has been plotted in

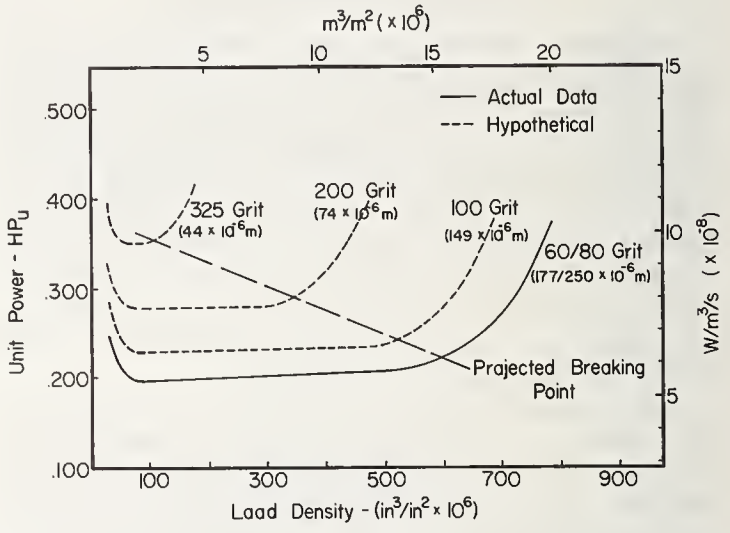

FIGURE 5. *Specific energy requirements versus Load Density projected for a range of diamond grain sizes.*

linear coordinates with an expanded "Unit Power" scale. The sharp rise in unit power at the origin indicates a high amount of frictional energy due to rubbing caused by insufficient depth of cut. The sharp rise to the right indicates the approach of full utilization of available chip space. The solid line was derived from actual test data; the dotted lines are hypothetical projections for finer diamond grains.

As the diamond grain sizes are reduced, an increase in the unit power may be anticipated; while the critical load density may be expected to decline. The slope of the dashed line connecting the others may be relevant to the different characteristics of a particular bond, or the diamond concentration. Large diamond grain sizes, "open" bond, and effective coolant application point the way to higher material removal rates

and greater productivity. Knowing the breaking points of the curves in figure 5 for the diamond tools to be used can point to an optimum choice of variable factors for a particular machining application.

5. Conclusions

The knowledge of predictable tool performance is essential to success in economical metalworking operations. The data resulting from the authors' experimental effort in this instance indicates convincingly that this is equally true in the machining of glass-ceramics. Many machine operations involve the removal of a nonuniform depth of material from the workpiece. This presents a problem in selecting a suitable depth of cut, feed rate and tool surface cutting speed for any individual cut.

All of these elements combine to control the "Load Density" mentioned earlier. Consequently predictable performance of a diamond tool suggests the feasibility of programmed feeds, speeds and depth of cut essential for the application of Numerical and Adaptive Control techniques to the machining of glass-ceramics.

6. References

[1] Tanaka, Yoshinobu, and Ikawa, Naoya, Cutting mechnism of the bronze-bonded diamond Wheel, Annals of the C.I.R.P. XIII pp. 443–440. Ms. 78/3. (1966).

[2] Colwell, L. V., Methods for sensing the rate of tool wear, Preprint of a presentation to the C.I.R.P. in Torino, Italy (1970).

[3] Imanaka, O., Fujino, S., and Mineta, S., Observation of chip removing process in grinding by a microflash technique. Preprint of a presentation by A. Kobayashi to the C.I.R.P., Nottingham (1968).

[4] Prokhorchik, S. M., Productivity of a process for grinding glass using an annular diamond tool, Soviet Journal of Optical Technology, 34, Number 3 (1967).

Discussion

WESTWOOD: What cutting environments did you use?

ALLGEYER: Our environment was primarily one of a circular wheel on a small surface grinder using a commercial coolant material.

RICE: I think Dr. Westwood was asking what sort of coolant material; was it a water soluble one?

ALLGEYER: It was a commercially available water soluble material.

MARTIS: What type of single point cutter was used in obtaining the unsatisfactory results on the glass ceramic material?

ALLGEYER: It was a commercial grade of one of the tungsten carbides.

MARTIS: Was a coolant used?

ALLGEYER: Yes and no. Both cases existed here and I can't tell you now whether this was one with or without coolant. We used a spray mist form of coolant when we did use one.

MARTIS: Is this a big application of single point turning versus centerless grinding in this type of machining?

ALLGEYER: Actually, no. It was more of a curiosity on my part. I had to explore it to see what the aspects of it really were. This type of operation has been done on a production basis in other applications to produce contoured surfaces. Aspheric lens generation, for instance, at one time had been single-point turned.

NATIONAL BUREAU OF STANDARDS SPECIAL PUB. 348, THE SCIENCE OF CERAMIC MACHINING AND SURFACE FINISHING, Proceedings of a Symposium Sponsored by the American Ceramic Society, the Office of Naval Research, and the National Bureau of Standards, held at NBS Nov. 2–4, 1970, Gaithersburg, Md. (Issued May 1972).

The Principles of Grinding

Robert S. Hahn and Richard P. Lindsay [1]

Cincinnati Milacron Corporation, Heald Division,
Worcester, Massachusetts 01606

Three distinct actions are shown to take place in the grinding process, namely rubbing, ploughing, and cutting. A clue to the relative importance of each of these can be obtained by plotting the volumetric rate of stock removal against the wheel-work interface force for unit width (force intensity). Such plots show for some materials a threshold force intensity below which no stock removal occurs. Equations relating the stock removal rate and the interface force intensity are developed and a "material removal parameter" is defined. Similar equations for the wheel wear and a "wheel wear parameter" are also developed. It is found for many materials that the stock removal rate is a linear function of the interface force intensity. However the abrasive removal rate or dimensional wheel wear is found to vary approximately as the square of the interface force intensity. Increasing wheel surface speed is generally found to raise the material removal parameter.

The essential parameters in dressing with single pointed diamonds are introduced and their effect on controlling the sharpness of a grinding wheel is discussed. Semi empirical equations for predicting wheelwear are given in terms of force intensity, wheel hardness and wheel-workpiece conformity. The factors influencing surface finish are described including the dressing lead, the depth of cut of the dresser diamond and the interface force intensity. Thermal damage and surface integrity are discussed. The existance of a threshold force intensity (or feed rate) below which no thermal cracking takes place is shown. Raising the workspeed tends to raise this threshold. Wheel sharpness is also found to be an important variable and means for quantitatively measuring wheel sharpness are given.

Key words: Abrasive wear parameter; grinding; material removal parameter; principles of grinding; surface finish in grinding; surface integrity in ground surfaces; wheel dressing.

1. Introduction

As manufactured components are used more and more in critical areas where reliability is important, a knowledge of the technological factors in the manufacturing process and their effect on the workpiece becomes essential. To achieve greater productivity and lower costs the proper setting of machining and grinding parameters is also very important. In order to accomplish the above it is necessary to develop quantitative relationships between the important variables in the grinding process. Some of these relationships are developed below.

Although the majority of the work to be reported here deals with the grinding of metals, the principles and the approach can be equally well applied to the grinding of ceramic materials, sintered carbides etc. In the grinding of metals Hahn [1][2] has shown that three distinct processes take place between the abrasive grain and the work piece namely (a) rubbing—where the grain rubs on the work causing elastic and/or plastic deformation in the work material with essentially no material removal, (b) ploughing—where the grain causes plastic flow of the work material in the direction of sliding as well as transverse to the direction of sliding, extruded material being thrown up and broken off along the sides of the groove resulting in low rates of stock removal, (c) cutting—where a fracture takes place in the plastically stressed zone just ahead of the rubbing grain causing the formation of a chip and resulting in fairly rapid stock removal rates. These three processes can be observed as shown in figure 21 where the "wheel depth of cut" i.e., the radial advance of the wheel per revolution of the workpiece in cylindrical plunge grinding, is plotted against normal force intensity (normal force per unit width of wheel-work contact). Rubbing takes place in figure 21 up to about 7 N/cm, ploughing up to about 26 N/cm and cutting thereafter. In this case the transition from rubbing to ploughing and from ploughing to cutting is fairly distinct.

Recent grinding studies by Busch [2] on glass, cemented carbides and several steels have also shown evidence of rubbing, ploughing and cutting. Under certain conditions he found continuous chips in grinding glass and other evidence of plastic deformation. The grinding of sintered aluminum oxide and a group of cemented carbides with diamomnd wheels was studied recently by Buttner [3]. He observed a migration of the diamond particles in the resin bond as well as a charring of the bond due to heat. Pahlitzsch [4] investigated the grinding of sintered aluminum oxide and gives

[1] Manager of Research and Senior Research Engineer, respectively.

[2] Figures in brackets indicate the literature references at the end of this paper.

resultant forces and wheel wear. Ida, Arai, and Inomori [5] carried out surface grinding tests on nine ceramic materials, observing grinding forces, surface finish, and microstructure.

2. Material Removal Equations

In studying the grinding process it has been the custom to report results in terms of down feed (on surface grinders) or infeed rate (on cylindrical grinders). Under these conditions the grinding performance is dependent on the rigidity of the machine tool. For example a down feed of 0.05 mm on a very stiff machine will induce a much larger wheel-work contact force than the same downfeed on a more compliant machine and accordingly the grinding performance (surface finish, wheel wear, surface integrity) will differ even though the same wheel and work material are used. Consequently, in order to become independent of the machine tool rigidity it is convenient, in plunge grinding operations to relate the grinding performance to the wheel-work interface contact force instead of downfeed or feed rate.

Consider the grinding configuration shown in figure 1, the cross slide is advancing at a feed rate, $\bar{v}_f$. Simultaneously the work radius is receeding at a rate $\bar{v}_w$, while the wheel is wearing at a rate, $\bar{v}_s$. Obviously, in the steady state:

$$\bar{v}_f = \bar{v}_w + \bar{v}_s \ . \tag{1}$$

During the steady state process, a force is induced between the wheel and the workpiece. The normal force per unit width, F_n', or force intensity is a convenient parameter to use in describing grinding behavior. The metal removal rate per unit width can be written.

$$Z'_w = \pi D_w \bar{v}_w \tag{2}$$

Likewise, the wheel removal rate or wheel wear per unit width is:

$$Z'_s = \pi D_s \bar{v}_s \tag{3}$$

Plotting data for external, internal and rotary surface grinding [6, 7, 8] as shown in figure 2, one notes that a linear relationship exists between the material removal rate and the force intensity, thus:

$$Z'_w = \Lambda_w F_n' \tag{4}$$

where Λ_w is a constant of proportionality [9], having dimensions of "volume of material removed per unit time per unit of wheelwork interface force and called the metal removal parameter."

Using eq (2), eq (4) can be written in the following two ways

$$\bar{v}_w = \frac{\Lambda_w F_n'}{\pi D_w} \tag{5a}$$

$$F_n' = \frac{\pi D_w \bar{v}_w}{\Lambda_w} \tag{5b}$$

The first equation applies to controlled force grinding where the force intensity is prescribed. The second equation applies to feed rate grinding. In practice the wheel wear velocity v_s in eq (1) is usually small compared to v_w so that v_f can be substituted for v_w in eq (5b) giving

$$F_n' = \frac{\pi D_w \bar{v}_f}{\Lambda_w} \tag{5c}$$

Equation (5c) gives the induced force due to a feed rate v_f. It will be seen that the induced force is directly proportional to workpiece diameter and inversely proportional to the Metal Removal Parameter.

Figure 2 is representative of "easy-to-grind" materials such as normal tool steels, AISI 52100, AISI 4150 etc. In these materials a chip is readily formed and material removal is predominately accomplished by the cutting process with little or no rubbing or ploughing. The Metal Removal Rate Z'_w plots as a straight line going through the origin. On the other hand, for "difficult-to-grind" materials where excessive rubbing and ploughing take place the plot of Z'_w vs F_n' often exhibits a non linear behavior and may have an intercept on the force intensity axis as illustrated in figure 3.

Since the slope of the Z'_w versus force intensity curve is Λ_w, Metal Removal Parameters in the range of 0.1 $mm^3\ s^{-1}N^{-1}$ are obtained for these difficult-to-grind alloys, whereas from figure 2, Λ_w was 0.5 to 0.7 $mm^3\ s^{-1}\ N^{-1}$, without any threshold force intensity.

Analogously, one may write the wheel removal rate or volumetric wear rate per unit width as

$$Z'_s = \pi D_s \bar{v}_s \tag{6}$$

From figure 4 it may be seen that a similar relationship exists for wheelwear:

$$Z'_s = \Lambda_s F_n' \tag{7}$$

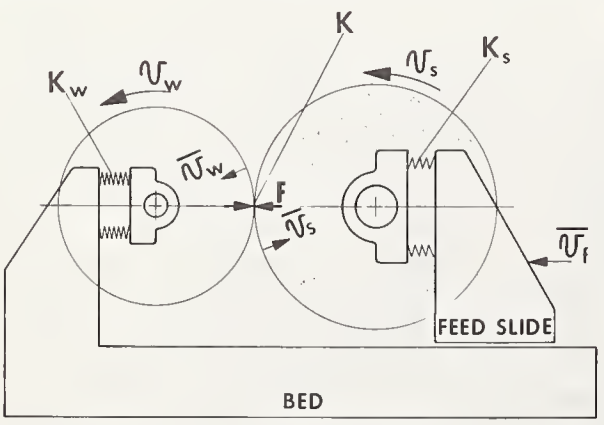

FIGURE 1. *O.D. center type grinder showing system springs and nomenclature.*

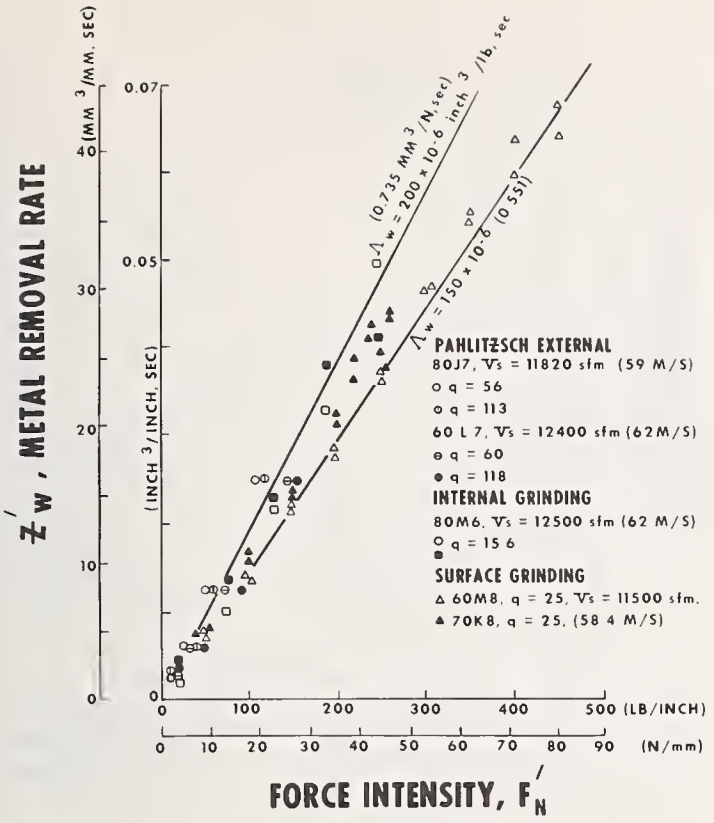

FIGURE 2. *Metal removal rate versus force intensity (after Pahlitzsch [6].)*

External
- Wheel: EK80J7VX and EK60L7VX
- Wheel Speed: 59 m/s and 62 m/s
- q: 56 and 113 and 59 and 118
- Wheel diameter: 28.3 in (720 mm)
- Work diameter: 4.0 in (102 mm)
- Work: RIV RINGS

Internal grinding
- Wheel: XA80M6VFMD2
- Wheel Speed: 63 m/s
- q: 15.6
- Wheel diameter: 3.25 in (82.5 mm)
- Work diameter: 3.75 in (95.2 mm)
- Dressing lead: 0.004 in/rev (0.1 mm/rev)
- Coolant: Water-based soluble
- Work material: AISI 4610, $R_c = 62$ (Roller bearing cup 3920)

Rotary surface grinding:
- Wheel: 32A70K8VBE
- Wheelspeed: 58.4 m/s
- q: 23
- Wheel diameter: 3.25 in (82.5 mm)
- Workpiece: 3 in O.D. × 2 in I.D. (76 mm O.D. × 50.8 mm I.D.)
- Dressing lead: 0.004 in/rev (0.1 mm/rev)
- Coolant: Florex at 110 N/m^2
- Work material: AISI 52100 at Rock C 60

However if the wheelwear rates for the difficult-to-grind materials are plotted, one notes that at high force intensities the Wheel Removal Rate Z'_s is no longer linear with F_n'. Figure 5 illustrates this behavior.

2.1. Factors Affecting Λ_w

Since Λ_w is the "gain" of the material removal process, knowledge of the factors which

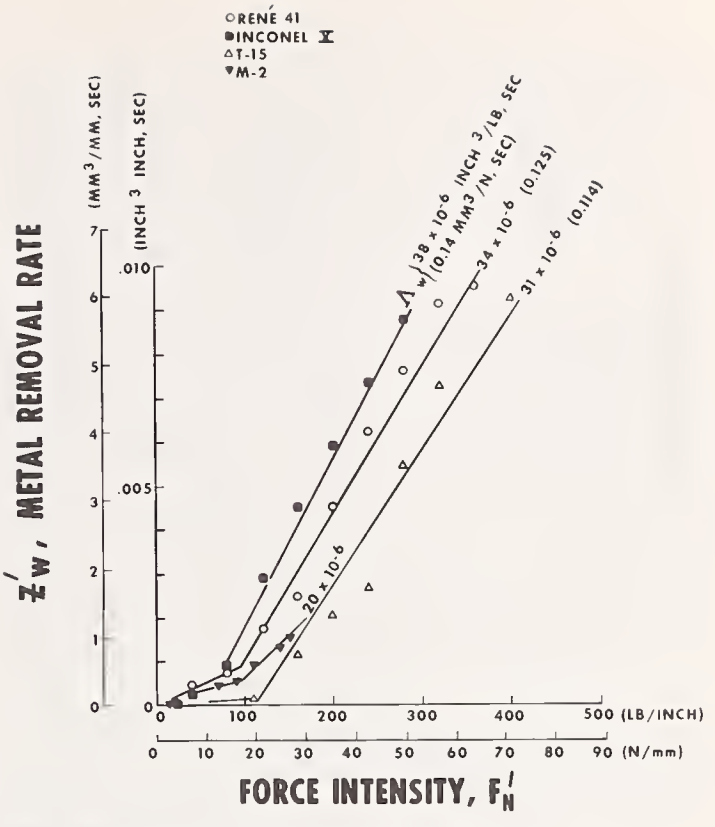

FIGURE 3. *Metal removal rate versus force Intensity.*
- Wheel: 32A70M6VBE
- Wheel speed: 33 m/s
- q: 6.8
- Wheel diameter: 1.73 in (44mm)
- Work diameter: 1.87 in (47.5 mm)
- Work material: M–2; T–15; Rene 41, Inconel X.
- Coolant: Water based soluble
- Internal grinding:

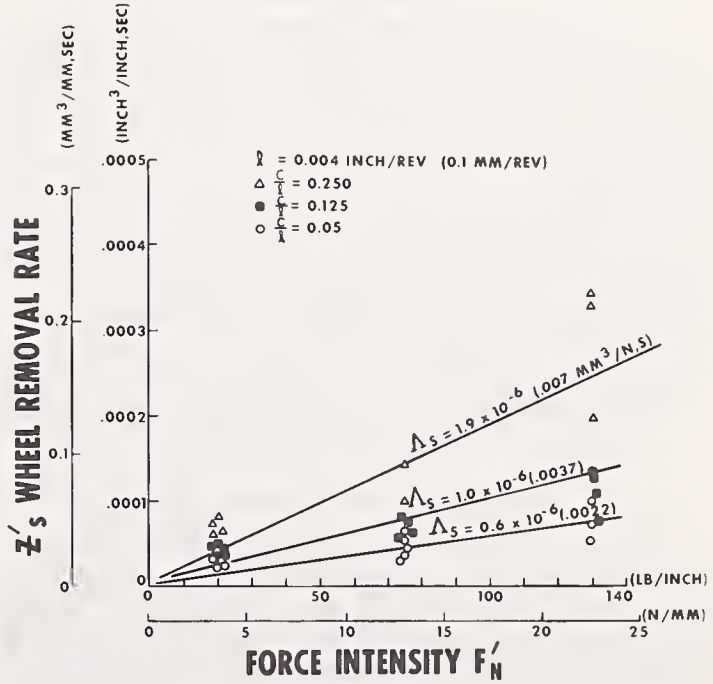

FIGURE 4. *Wheel removal rate versus force intensity.* Test conditions same as internal grinding for figure 2.
Additionally:

Dressing Ratio $\frac{c}{l}$ = 0.25, 0.125, 0.05

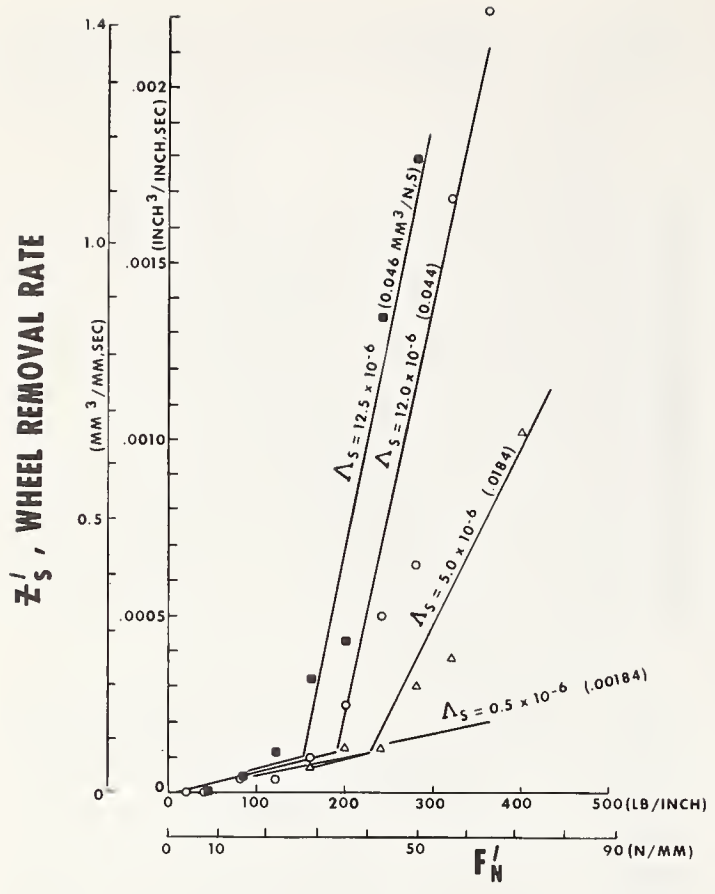

FIGURE 5. *Wheel removal rate versus force intensity.* Test conditions same as figure 3

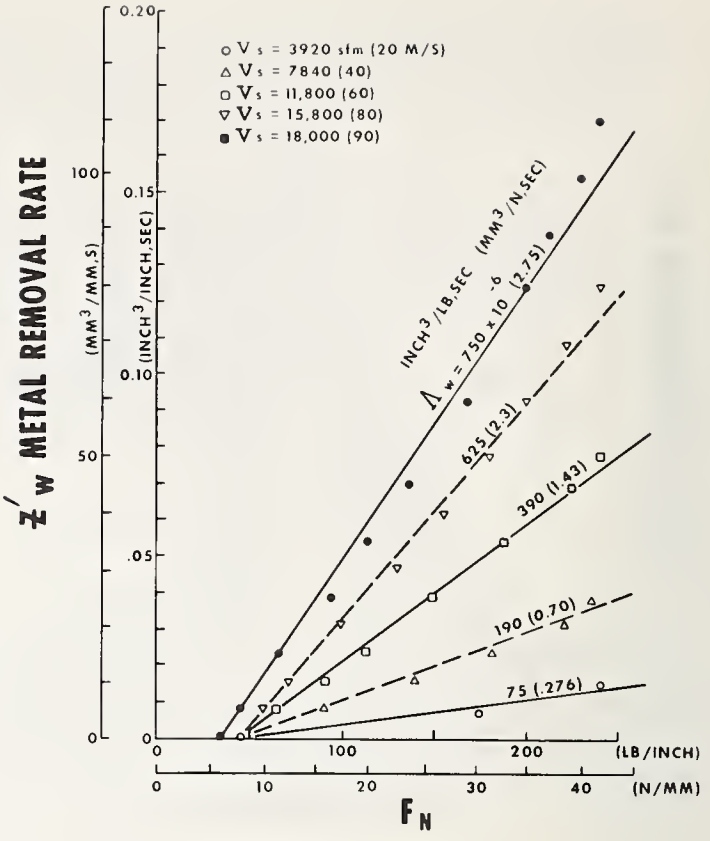

FIGURE 6. *Metal removal rate versus force intensity.*

Wheel:	EK80L7VX
Wheel speed:	3920, 7840, 11,800, 15,000, 18,000 sfm (20, 40, 60, 80, 90 m/s)
q:	60
Wheel diameter:	19.6 in (500 mm)
Work diameter:	1.37 in (35 mm)
Dressing lead:	0.004 in/rev (0.1 mm/rev)
Coolant:	Cutting oil
Work material:	CK45N (AISI 1045) at R_C = 23 (Vickers 250)

External grinding (after Konrad Guhring [10]

increase Λ_w would be important in reducing grinding time and increasing production.

a. Wheel Speed

The effect of wheelspeed upon grinding is fairly well known. Gühring [10] externally-ground relatively soft steel and obtained decreasing force intensities at a given feed rate. Replotting his data against F_n' as in figure 6 and noting Λ_w to be the slope of the Z'_w vs. force intensity curve, one obtains Λ_w values from 0.27 to 2.75 $mm^3\ sec^{-1}\ N^{-1}$ as the wheelspeed is increased from 20 m/s to 90 m/s.

Internal grinding of roller bearing cups, as illustrated in figure 7, also shows increasing Λ_w values for larger wheelspeeds.

If one plots Λ_w versus wheelspeed, as in figure 8, one sees essentially a linear relationship.

b. Area in Contact and Dressing

It has been previously shown [11] that Λ_w depends upon the real stress existing in the contact interface between the wheel and work. Measuring the area of the wear flats existing on the wheel by planimetering a photo micrograph and considering the length of the wheel-work contact, a plot of Λ_w versus normal contact stress (normal force divided by real area of contact) can be obtained as shown in figure 9. Thus to maximize Λ_w, the real area of contact should be made as small as possible. (In figure 9, larger real areas resulted from flats wearing on the grains through extended usage of the wheel without dressing. As the area increases, the real stress falls (at constant normal force) and Λ_w is reduced).

Since dressing with a diamond is a way to sharpen the wheel, one can define the dressing parameters as in figure 10. The depth of diamond penetration while dressing is denoted as c/2 since compensation in the trade is generally referred to diameter. The dress lead is the distance that the diamond moves along the wheel axis per wheel revolution. The fact that dressing can actually machine a "thread" into the wheel is shown in figure 11 which is a trace (Bendix Profilometer) of a ground workpiece. The periodic waves noted most easily in the middle trace correspond to the dressing lead used in dressing the wheel prior to a 3 second plunge grind.

If the diamond point is assumed sharp, the

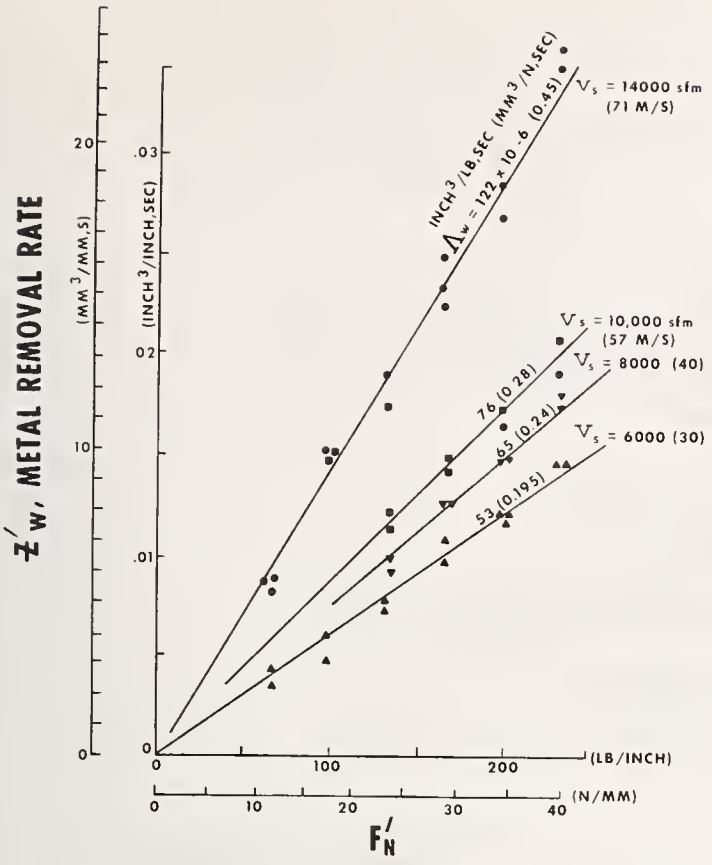

FIGURE 7. *Metal removal rate versus force intensity.*

Wheel:	97A80L6VFMD2
Wheel speed:	6000, 8000, 10,000, 14,000 sfm (30, 40, 50, 70 m/s)
Work speed:	400 sfm (2 m/s)
Wheel diameter:	2.37 in (60.3 mm)
Work diameter:	2.74 in (69.6 mm)
Dressing lead:	0.0035 in/rev (0.09 mm/rev)
Climb work rotation	
Coolant:	Water soluble oil
Work material:	AISI 4620 at R_c = 60 (Roller bearing cup 25520)
Internal grinding	

meaning of c/l, the dressing ratio, can be noted from figure 12. As c/l approaches 1.0 the "thread" on the grains becomes sharp, whereas if c/l approaches zero, the dressed grain appears dull (figure 12 is schematic, but descriptive of what occurs in dressing). Thus increasing the dressing ratio c/l, at constant lead produces a sharper wheel. Internal grinding of roller bearing cups produced the data shown in figure 13. As c/l is increased from 0.05 to 1.0, Λ_w increases from 0.24 to 0.68 mm^3 s^{-1} N^{-1}, a factor of 2.85.

Also, at constant c/l = 1.0, with a lead of 0.1 mm/rev, Λ_w = 0.68 mm^3 s^{-1} N^{-1}, whereas with a lead of 0.025 mm/rev, Λ_w = 0.40 mm s^{-1} N^{-1}, as seen in figure 14.

Thus larger leads and larger c/l values increase Λ_w, as seen in figure 15. Both these actions reduce the real area on the grinding wheel thereby increasing Λ_w by increasing the real stress at the interface.

2.2. Wheelwear

As has been previously suggested, the wheelwear rate, Z'_s versus F_n' curve is nonlinear. Figure 16 shows stock removal and wheelwear measurements for rotary surface grinding of 52100 steel (Rockwell C 60–62) and points out very clearly the increasing wheelwear rate as force intensity is increased.

To better define the wearing action, consider figure 17 which shows schematically the elastic action of the wheel in contacting a workpiece. In production grinding at workspeeds above 100 fpm (0.5 m/s) the wheel depth of cut (advance per revolution of work) is generally small compared to the elastic flattening of the grinding wheel (Youngs modulus for a Vitreous bonded wheel is approximately 1/4 that of steel) and may be neglected in calculating the length of the interference zone between wheel and work. For low workspeeds as in reciprocating surface grinding neglecting the wheel depth of cut may not be permissible.

Neglecting the influence of the wheel depth of cut on the length of contact, the length of elastic contact l_c has been found by Lindsay [12] to be:

$$l_c \left\{ \begin{matrix} \text{inches} \\ \text{meters} \end{matrix} \right\} = \left\{ \begin{matrix} 10^{-3} \\ 1.335 \times 10^{-6} \end{matrix} \right\} \left[\frac{D_s D_w}{D_w \mp D_s} \left(\frac{F_n'}{d^2 \, (1.33\,H + 2.2S - 8)} \right) \right]^{1/3} \quad (8)$$

where (lb and in) or (N and meters) are to be used. The values of H and S are given below.

In plunge grinding the average normal wheel-work contact pressure P is defined as

$$P = \frac{F_n'}{l_c} \quad (9)$$

or

$$P \left\{ \begin{matrix} \text{lb } in^{-2} \\ Nm^{-2} \end{matrix} \right\} = \left\{ \begin{matrix} 1000 \\ 0.75 \times 10^6 \end{matrix} \right\} \left(\frac{D_w \mp D_s}{D_w D_s} \right)^{1/3} d^{2/3} \left(1.33H + 2.2S - 8 \right)^{1/3} \left(F_n' \right)^{2/3} \quad (10)$$

where: $\left(\frac{D_w - D_s}{D_w D_s} \right)^{1/3}$ is used for internal grinding

$\left(\frac{D_w + D_s}{D_w D_s} \right)^{1/3}$ is used for external grinding

$\left(\frac{1}{D_s} \right)^{1/3}$ is used for surface grinding

(1.33H + 2.2S −8) is the percent of bond in the wheel.

It can be found by:

{ Hardness of wheel: H, I, J, K, L, M etc.
"H" factor is : 0, 1, 2, 3, 4, 5 etc. }

and

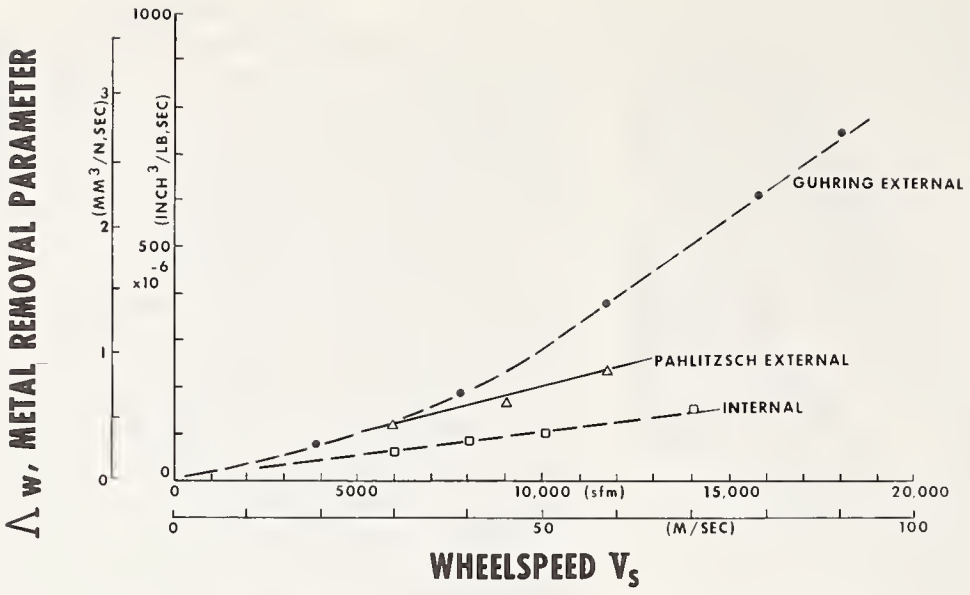

FIGURE 8. *The metal removal parameter versus wheelspeed.*

Test conditions:

Guhring [10] external:	Same as figure 6
Pahlitzsch external [6]	Same as figure 2
Internal:	Same as figure 7

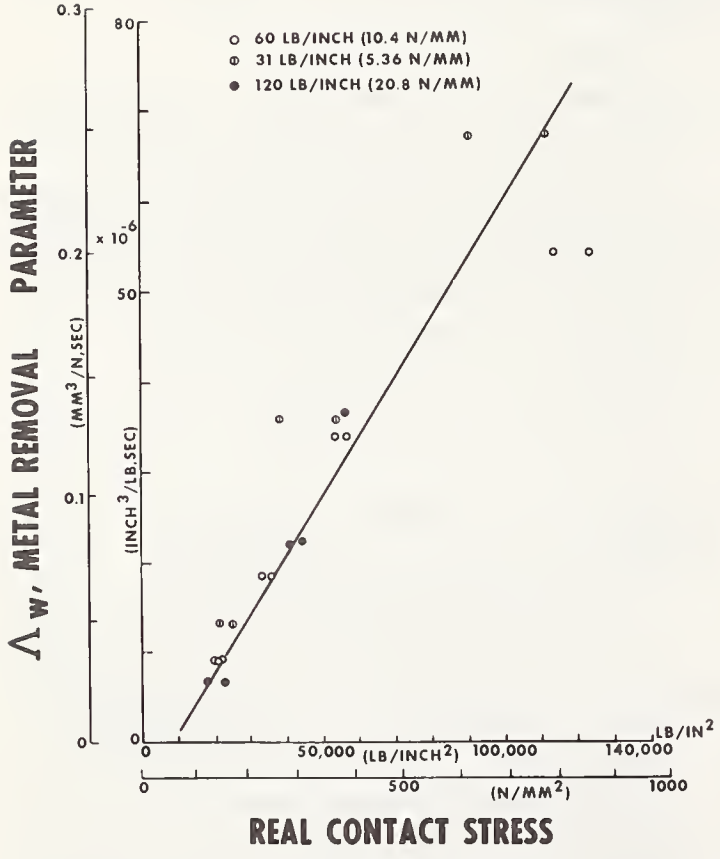

FIGURE 9. *The metal removal parameter versus the real contact stress.*

Wheel:	A60L5V
Wheel speed:	7200 sfm (36 m/s)
q:	6.1
Wheel diameter:	1.87 in (47.5 mm)
Work diameter:	2.50 in (63.5 mm)
Work material:	AIS152100, Rock C60
Coolant:	Texaco soluble D
Climb work rotation	
Dress lead:	0.003 in/rev (0.075 mm/rev)

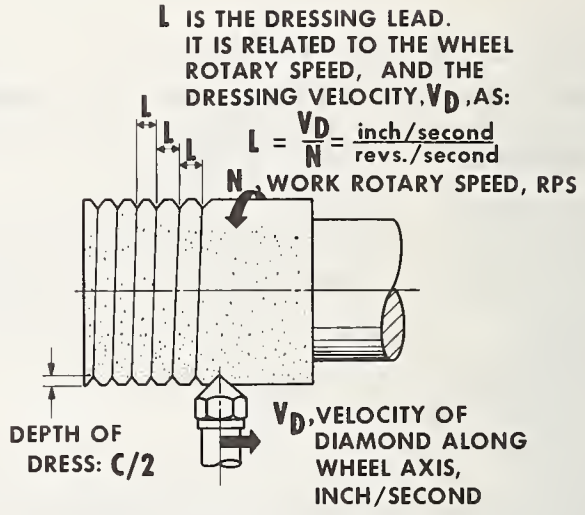

FIGURE 10. *Dressing nomenclature.*

S is the structure number of the wheel:
$S = 4, 6, 8$ etc.
Thus an 80M6 wheel has $H=5$, $S=6$, and so $(1.33H+2.2S-8) = 1.33\times5+2.2\times6-8) = 11.85$

One may plot the pressure P existing for any F_n' and geometry.

If the factor $\frac{Z'_s}{V_s}$ is plotted versus P as in figure 18, an empirical equation for wheelwear may be written as:

$$\frac{Z'_s}{V_s}\left\{\begin{matrix}\text{inch}\\ \text{meter}\end{matrix}\right\} = \left\{\begin{matrix}3.0\times10^{-17}\\ 0.22\times10^{-21}\end{matrix}\right\} P^3 \left\{\begin{matrix}lb\ in^{-2}\\ Nm^{-2}\end{matrix}\right\} \quad (11)$$

Since P is a function of force intensity and since Λ_s is defined as the derivative of Z'_s with

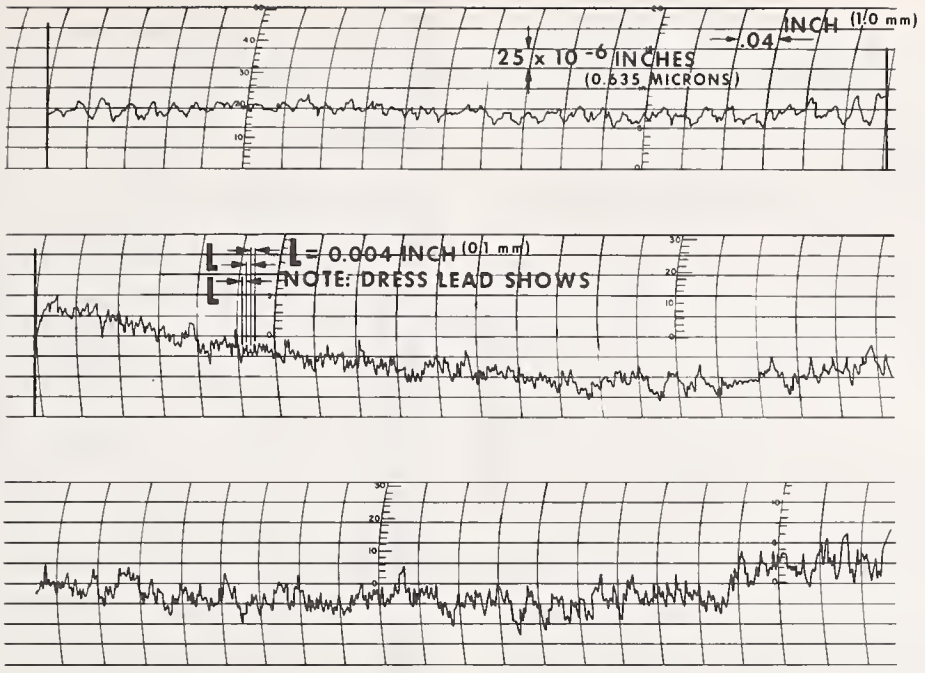

FIGURE 11. *Proficorder traces of some workpieces.*
Test conditions: Same as internal grinding from figure 2.

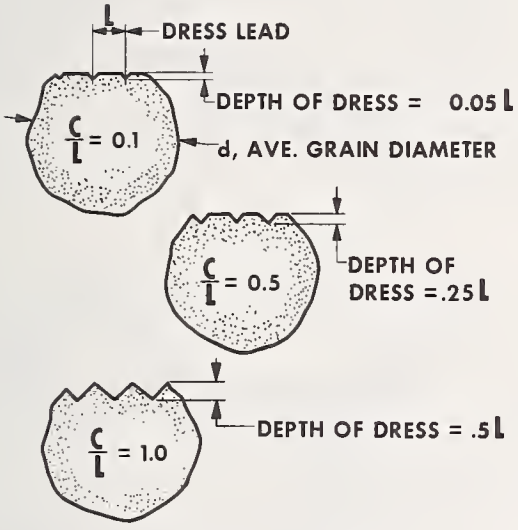

FIGURE 12. *Dressing ratio and its significance.*

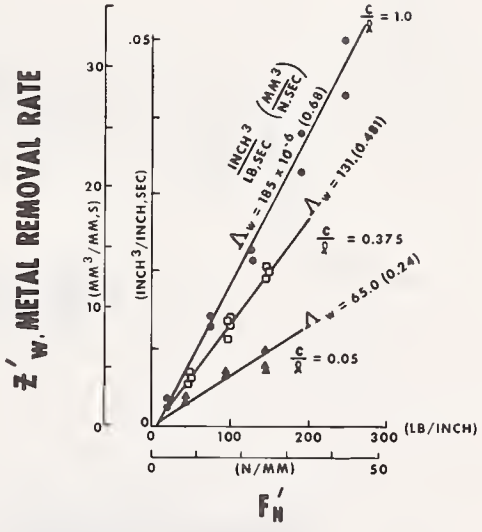

FIGURE 13. *Metal removal rate versus force intensity.*

Test conditions: Same as internal grinding from figure 2.

respect to F_n', one can insert eq (10) into eq (11) and take the derivative to obtain

$$\Lambda_s \left\{ \frac{in^3}{\text{sec. } lb} \atop \frac{m^3}{\text{sec. } N} \right\} = \left\{ 6.0\times10^{-8} \atop 0.186\times10^{-3} \right\} \left(\frac{D_w \mp D_s}{D_w D_s} \right) d^2 \ (1.33H+2.2S-8) \ V_s F_n' \quad (12)$$

From eq (12) it will be seen that the wheel wear parameter Λ_s is linear with force intensity. Using eq (12) the wheel wear eq (7) can now be written as:

$$Z'_s \left\{ \frac{in^2}{\text{sec}} \atop \frac{m^2}{\text{sec}} \right\} = \left\{ 6.0\times10^{-8} \atop 0.186\times10^{-3} \right\} \left(\frac{D_w \mp D_s}{D_w D_s} \right) d^2 \ (1.33H+2.2S-8) \ V_s \ (F_n')^2 \quad (13)$$

It will be seen from eq (13) that the wheel wear rate is a quadratic function of force intensity as was observed experimentally in figure 16.

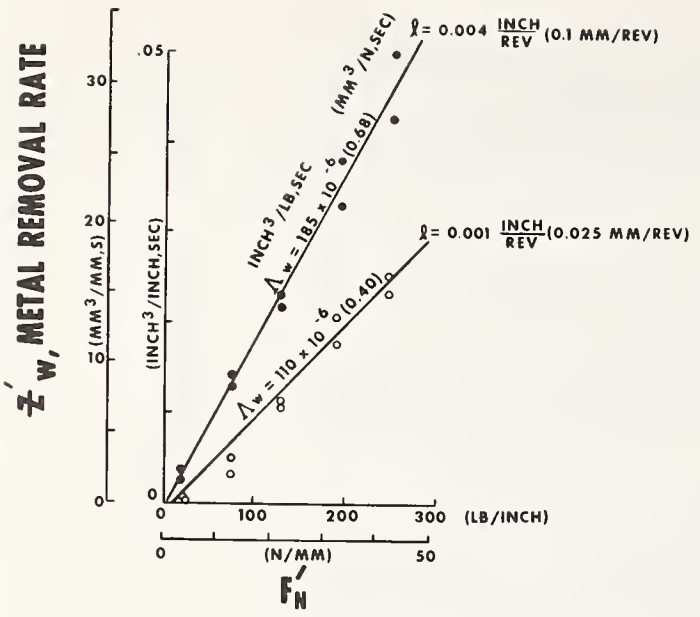

FIGURE 14. *Metal removal rate versus force intensity.*
Test conditions: Same as internal grinding from figure 2.

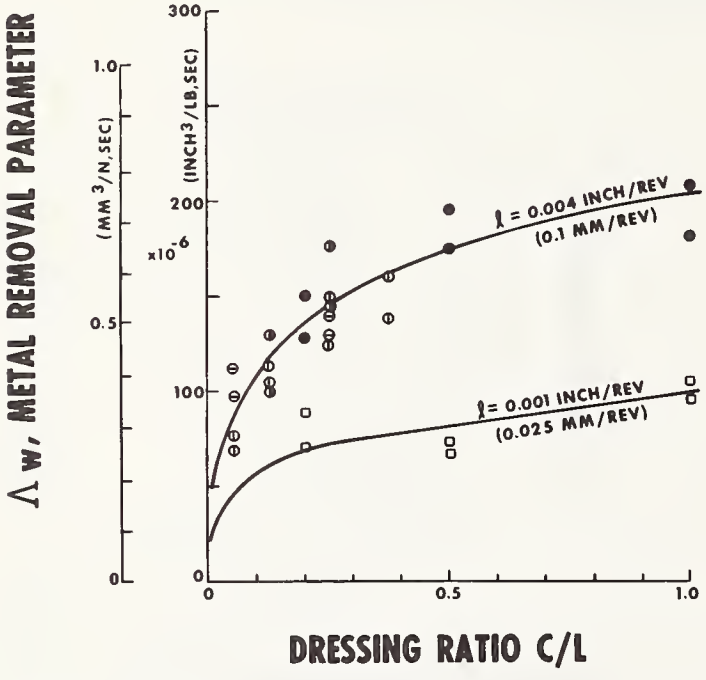

FIGURE 15. *The metal removal parameter versus the dressing ratio.*
Test conditions: Same as internal grinding from figure 2.

3. Surface Finish

External grinding date published by Guhring [10] and plotted in figure 19 indicates that the surface finish is improved by increasing wheelspeed at a given stock removal rate. However, one may obtain the force intensity induced during these grinds and cross-plot the surface finish obtained versus the force intensity as shown in figure 20. This causes the external grinding data of Guhring [10] to fall essentially on one curve.

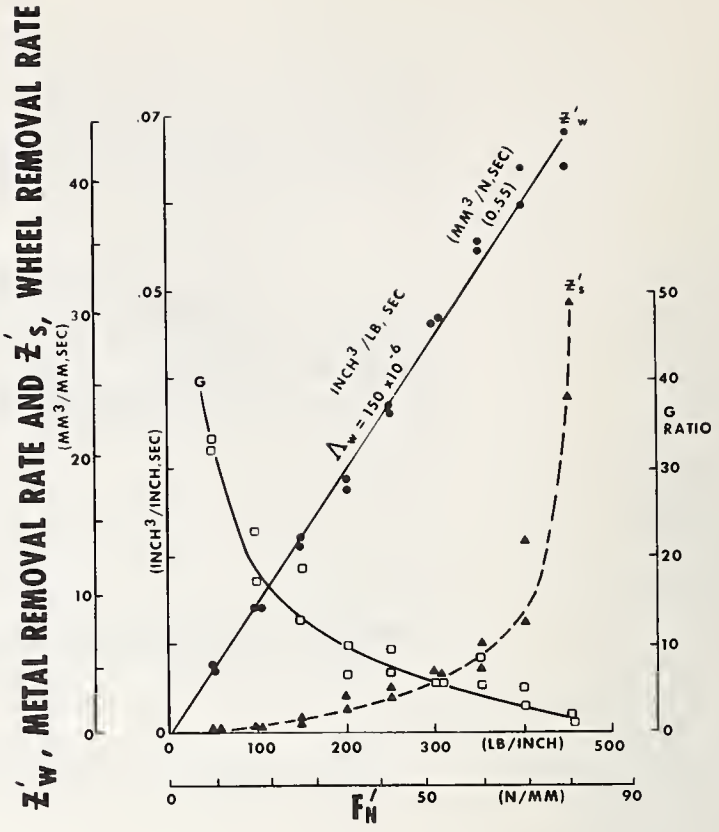

FIGURE 16. *Metal removal rate and wheelwear rate and G ratio versus force intensity.*
Test conditions: Same as rotary surface grinding from figure 2.

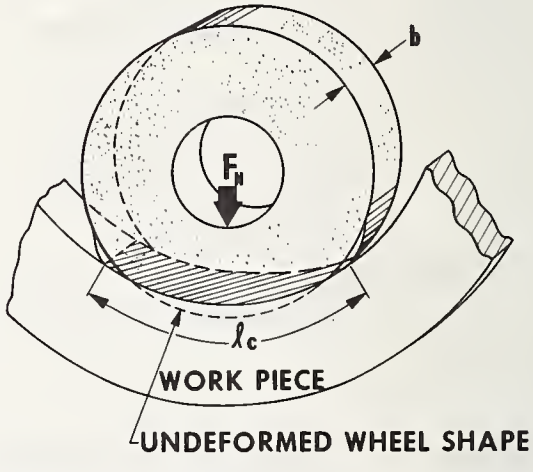

FIGURE 17. *Grinding wheel deformation in an internal workpiece showing nomenclature (schematic).*

Also shown in figure 20 is internal grinding data and the same relationship to force intensity is seen to exist: the surface finish is proportional to $(F_n')^{1/3}$. Moreover it has been experimentally observed that:

$$\text{surface finish} \sim l^{1/2} \left(\frac{c}{l}\right)^{3/10} \left(F_n'\right)^{1/3} \qquad (14)$$

Thus, low dress leads and dressing ratios as well as low force intensities produce low surface finishes (fig 21); wheelspeed only affects the

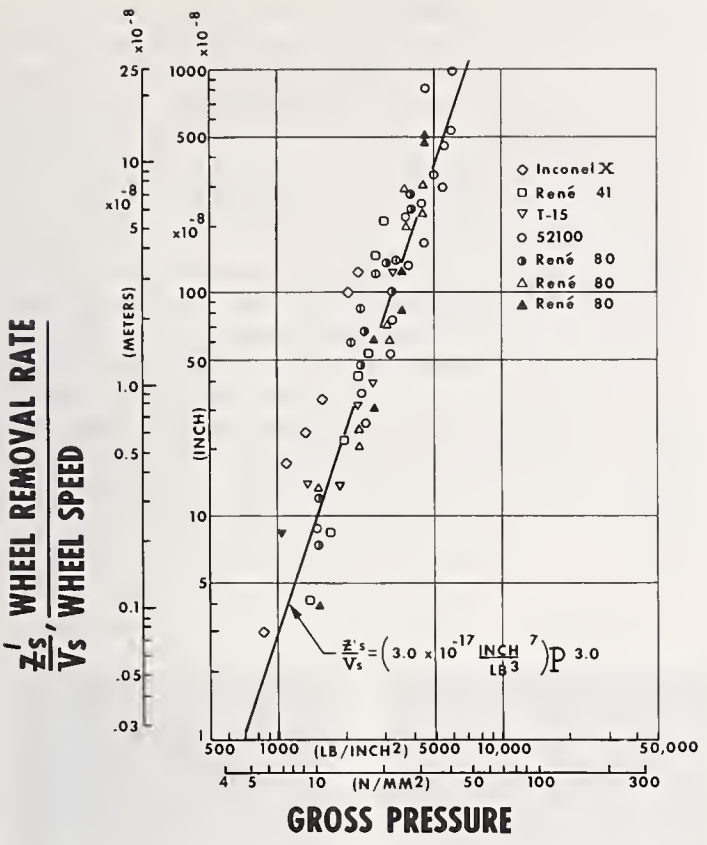

FIGURE 18. *Wheel removal factor versus gross contact pressure.*

Data from:
A. Rotary surface grinding (test conditions: See figure 2)
B. Internal grinding
(Test conditions: See figure 3)
(Test conditions: See figure 2)

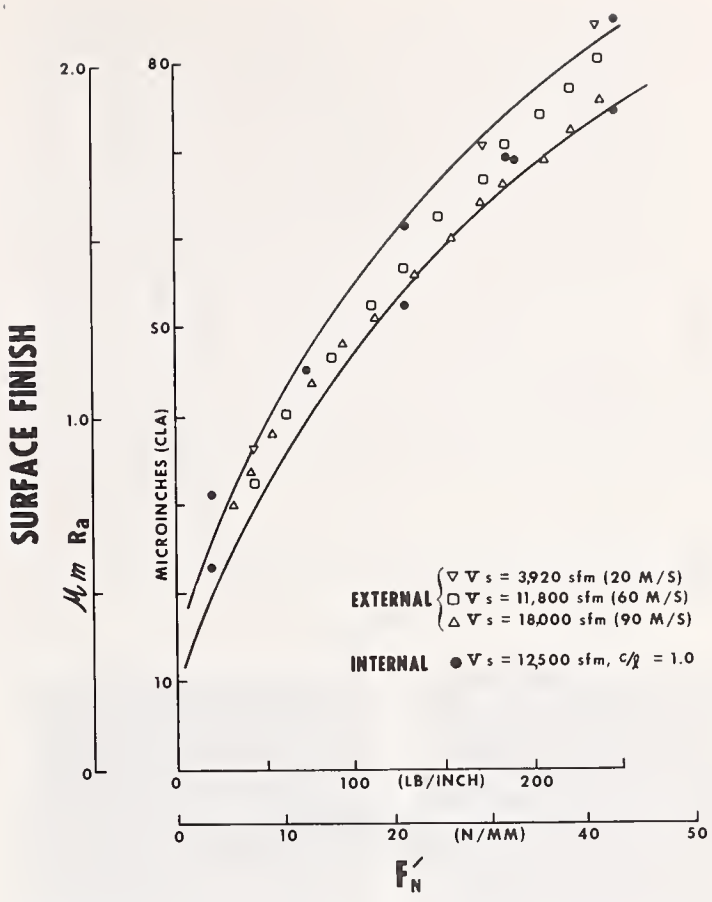

FIGURE 20. *Surface finish versus force intensity.*
Test conditions: External grinding: Same figure 6.
Internal grinding: Same figure 2.

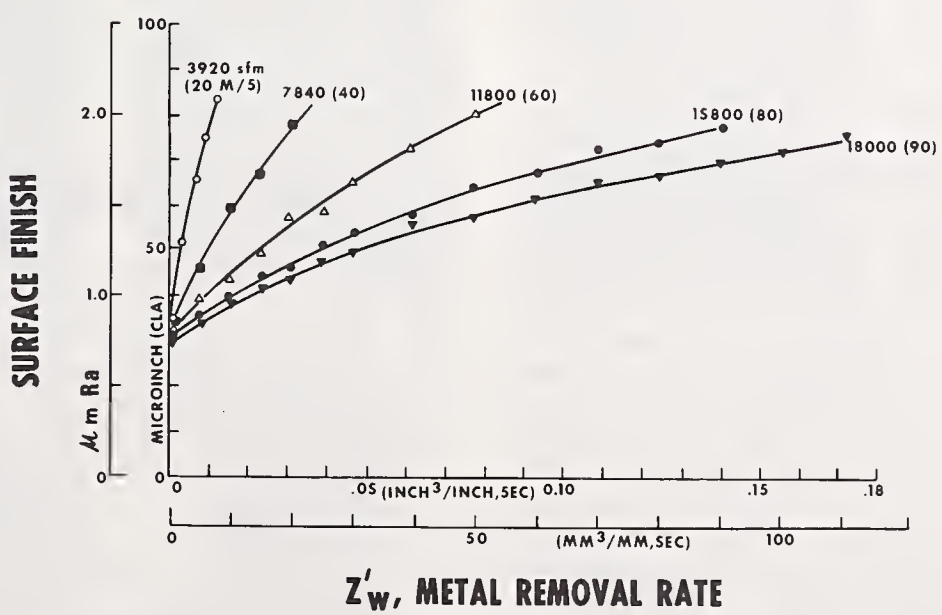

FIGURE 19. *Surface finish versus metal removal rate.*
Test conditions: Same as figure 6.

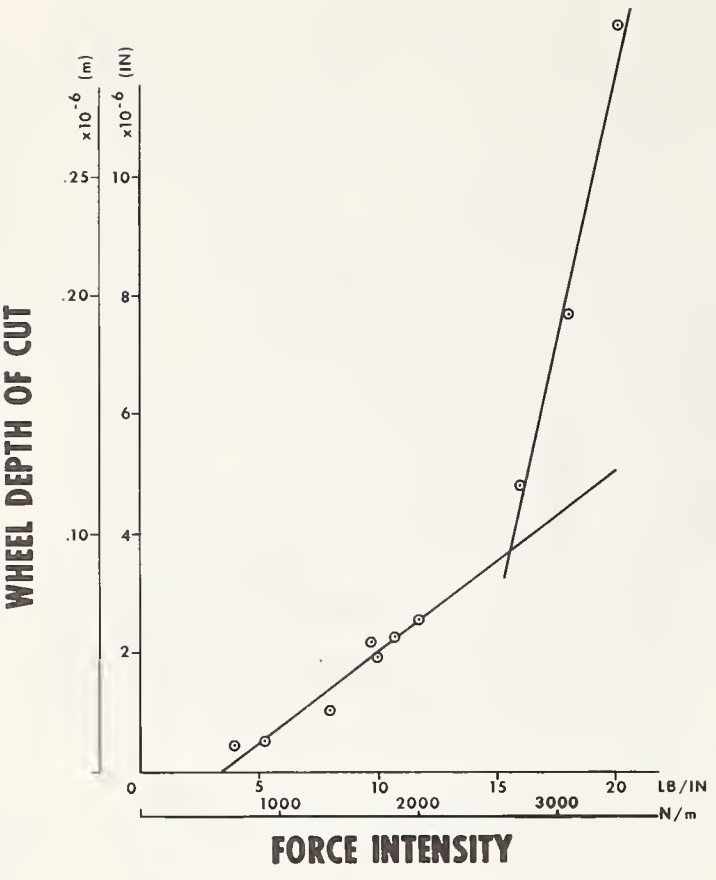

FIGURE 21. *Wheel depth of cut (radial advance per work rev.) versus force intensity.*

Wheel:	38A801L8VBE
Wheelspeed:	566 RPS
Work speed:	23 RPS
Wheel diameter:	0.87 in (22 mm)
Work diameter:	1.50 in (38 mm)
Dress lead:	0.0001 in/rev (2.5 μm/rev)
Conventional work	rotation sense
Coolant:	Flow Rex 100
Work material	AISI 4150 53–55 R_c

finish in so far as it reduces the induced wheel-work force during feed rate grinding.

4. Surface Integrity

Various authors [3, 4, 5, 6, 7, 8, 9] have discussed the stresses present in the surface layer of ground workpieces. Generally to prevent damage in the workpiece the admonitions are to use a "gentle grind" consisting of low wheel speeds, a lubricating rather than a cooling fluid (i.e., oil rather than water), sharp wheels and low down-feed rates. Unfortunately most of the reported data was obtained on reciprocating surface grinders where work speed is generally less than 50 sfm (0.25 m/s). Obviously, the shorter the wheel-work contact time the smaller the heat input to the work. Work speed is a very important parameter in regard to surface integrity and has been nearly completely ignored by most authors. In fact, in most of the test work, the work speed has been at the worst possible value: extremely low.

In order to investigate the surface integrity problem, it is important to recognize that work speed, interface force intensity and wheel sharpness are important variables relating to surface damage. The most elusive variable among these is the wheel sharpness. The wheel sharpness can be defined in terms of the metal removal parameter, Λ_w.

The slope of the Z'_w vs. force intensity curve has already been seen to be the metal removal parameter, Λ_w. It has also been shown [11] that if a grinding wheel is dressed and then used continuously under precision grinding conditions, wear flats will develop on the abrasive grains. If gross wheelwear does not occur, (i.e., the wheelwear is attritious) these flat areas will

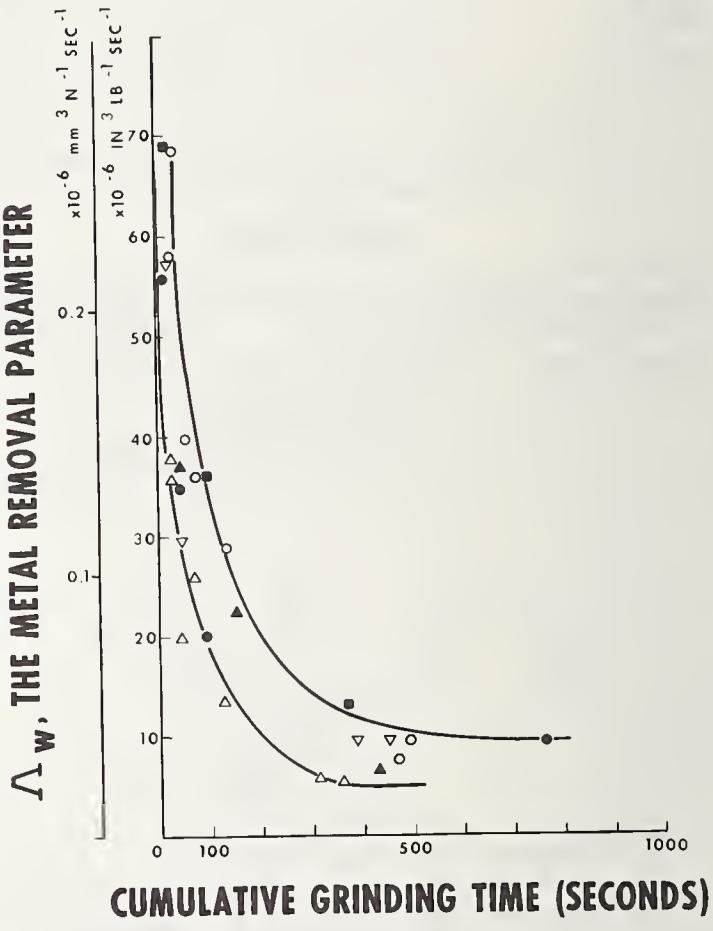

FIGURE 22. *Metal removal parameter versus cumulative grinding time.*

●	60 lb/in (10500. N/m)	Wheel A60L5V
□	30 lb/in (5250 N/m)	Wheel A60L5V
△	120 lb/in (21000 N/m)	Wheel A60L5V
	60 lb/in (10500. N/m)	Wheel 2A90P6
	20 lb/in (3500 N/m)	Wheel 2A90P6
△	100 lb/in (17500 N/m)	Wheel 2A90P6

Wheelspeed:	7600 FPM (38 m/s)
Work speed:	1100 FPM (5.5 m/s)
Wheel diameter:	1.87 in (47.5 mm)
Work diameter:	2.37 in (60.2 mm)
Dress lead:	0.003 in/rev (0.076 mm/rev)
Climb work rotation:	
Coolant:	Flow rex 100
Work material:	AISI 52100 R_c 60
Internal grinding:	

continue to grow to create some stable characteristic real area of contact. If in addition, these tests be performed under conditions where the interface normal grinding force between the wheel and work is held constant, it will be found that the developed grinding rate $\bar{v}_w$ (rate of change of work radius) will diminish with time. Thus the wheel is losing it's ability to remove material through the dulling action. Now since the growth of the real area causes v_w, at some force intensity, to diminish, then the metal removal parameter must be decreasing with time.

Figure 22 shows the relationship of Λ_w with time under controlled-force, precision internal grinding conditions. Λ_w then is an indicator of the sharpness of the wheel as measured by it's ability to remove stock: When Λ_w is large the wheel is acting sharp, when dulling occurs Λ_w diminishes.

Since Λ_w is then a measure of wheel-work grinding capability, we have a quantitative means of describing wheel sharpness. It has been shown that variations in the dressing ratio c/l can affect Λ_w. Thus by dressing a wheel differently, its sharpness can be changed, but as long as Λ_w can be measured, one can determine changes in sharpness due to changes in dressing methods. Wheel sharpness will be seen to be an important parameter in determining the surface integrity of ground surfaces.

Workpiece residual tensile stresses are a function of the amount of heat injected by the grinding process. Various methods are available to determine the magnitude of such stresses including x-ray diffraction and deformation analysis.

Some steels, including AISI–E52100, are susceptible to hydrogen embrittlement when immersed in hot hydrochloric acid. The absorbed

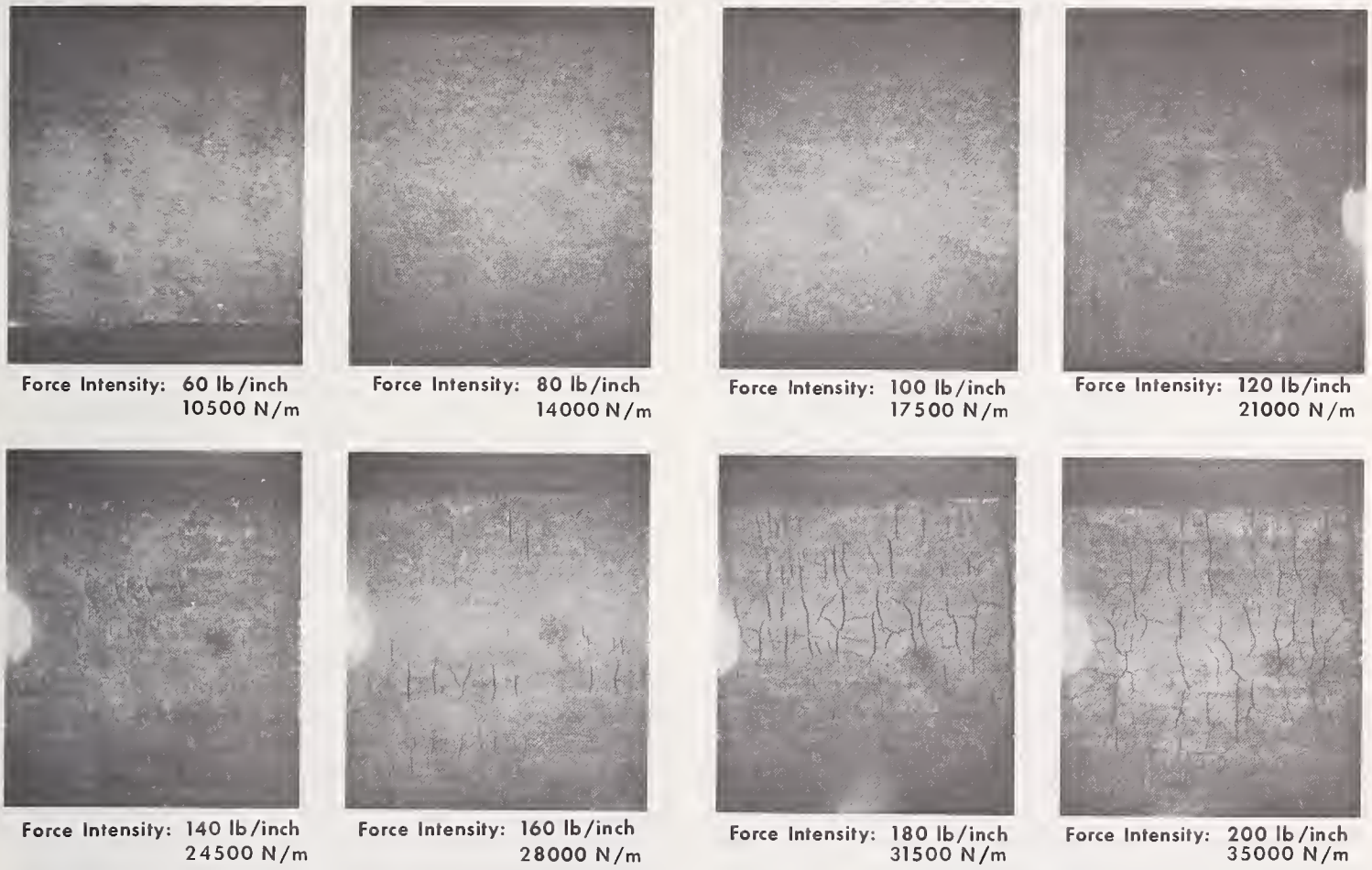

FIGURE 23. *Workpieces ground under various force intensities for constant wheel sharpness.*

Wheel:	97A1001L6VFM
Wheelspeed:	7700 FPM (38.5 m/s)
Work speed:	180 FPM (0.9 m/s)
Wheel diameter:	2.0 in (51 mm)
Work diameter:	2.31 in (59 mm)
Dress lead:	0.004 in/rev (0.10 mm/rev)
Climb work rotation	
Coolant:	Cimperial 20:1, 110 psi (7.7 Kg/cm ^{2})
Work material:	AISI 52100 R_c60
Internal grinding:	
Hydrochloric acid etch after each grind—10 min at 150 °F (65 °C)	

439-921 O - 72 - 6

hydrogen causes the surface layer of the work to become brittle and if residual tensile stresses exist, the brittle layer will crack. Thus cracking of the workpiece after hot hydrochloric acid etch, indicates that the grinding operation had produced tensile stresses.

In order to establish threshold limits for force intensities beyond which thermal damage will occur, grinding tests were made on AISI–E52100 steel rings, at Rockwell C 60.

The test procedure was to increase the interface force at each work speed and to examine the workpiece after hydrochloric acid immersion. A representative run is shown in figure 23 which presents photographs of the ground and etched parts taken at 15× magnification through a microscope. As the force intensity is increased, cracking begins at the edges of the workpiece and spreads across the piece, until, at high force intensities, cross cracking (i.e., parallel to the direction of the grinding grit path) occurs. The limiting force intensity is defined as that which causes the first appearance of cracking.

Figure 24 shows this critical force intensity plotted against work speed for two sharpness values: Λ_w equal to 88 × 10^{-6} in^3/s, lb, (0.323 mm^3N^{-1} s^{-1}) a sharp wheel, and equal to 25 × 10^{-6} in^3/s, lb, (0.0918 $mm^3N^{-1}S^{-1}$), a dull wheel. As workspeed is increased, the tolerable force intensity rises, for each wheel sharpness. The importance of knowing the degree of wheel sharpness, or Λ_w, may be illustrated by a hypothetical grinding operation, using skip dressing (avoidance of dressing for some time). With work speed at 500 sfm, (2.5 m/s) a force intensity of 180 lb/in (31 N/mm) is permissible (see fig. 24) and as long as the wheel remains sharp, thermal tensile stressing of the work will not occur. However if the wheel dulls (as it will with continual usage) so that Λ_w is reduced to say 25 × 10^{-6} in^3/s, lb, (0.0918 mm^3-N^{-1} S^{-1}) the force intensity of 180 lb/in (31 N/mm) is above the permissible level for that Λ_w sharpness value, and the work will have thermally induced tensile stresses. To be conservative and set a force intensity below that permissible for a dulled wheel, here say 120 lb/in, (20.6 N/mm) will cause grinding time to be lost since the penetration rate, v_w, will be slow, even with a sharp wheel.

In view of the above the maximum permissible grinding rate can be achieved by grinding at controlled force intensities while continuously monitoring wheel sharpness [3] thereby maintaining surface integrity.

5. Conclusion

The development of the technology of grinding through the use of material and abrasive removal parameters permits the prediction of grinding performance. The prediction of stock removal rates, or induced force intensities, of surface finish, of local and general wheelwear, and of surface damage effects leads to the ability to rationally design grinding cycles and to improve those grinding operations currently in production. The use of interface force intensity as the independent variable allows the grinding process to be described in terms which are independent of the machine tool rigidity. The use of contact pressure as an independent variable permits the evaluation of wheel wear for any wheelwork geometry or conformity. The development of tabulor data on the material removal and abrasive removal parameters for various work materials and wheels will substantially aid industry in the development of efficient, economic grinding operations.

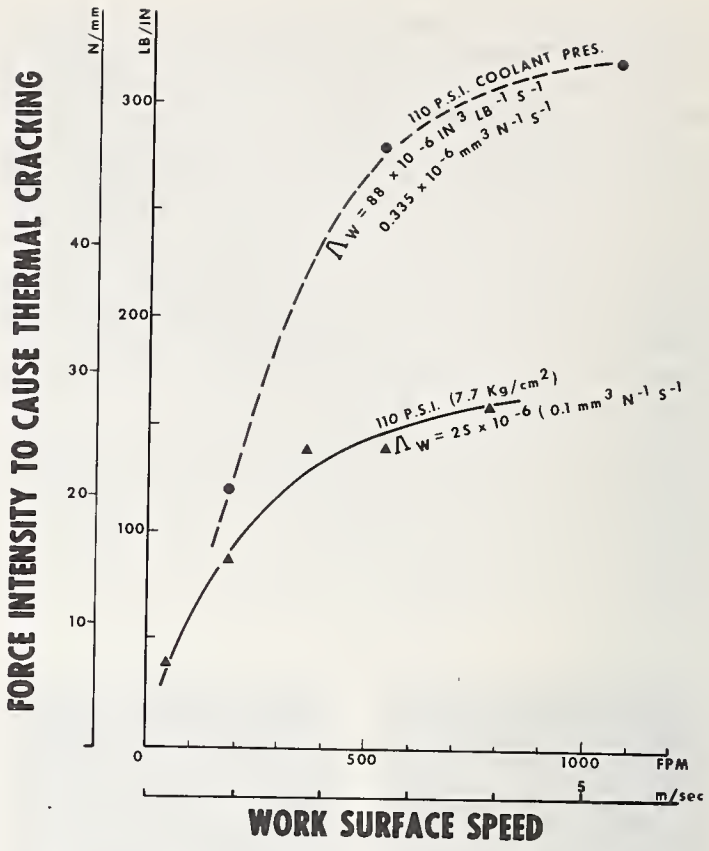

FIGURE 24. *Threshold force intensity to produce thermal cracking.*

Wheel:	97A1001L6VFM
Wheelspeed:	7700 FPM (38.5 m/s)
Workspeed	180 FPM (0.9 m/s)
Wheel diameter:	2.0 in (51 mm)
Work diameter:	2.31 in (59 mm)
Dress lead:	0.004 in/rev (0.10 mm/rev) sharp
	0.0001 in/rev (0.025 mm/rev) dull
Climb work rotation:	
Coolant:	Cimperial 20:1, 110 N/m (7.7 Kg/cm^2)
Work material:	AISI 52100 R_c60
Internal grinding:	

Hydrochloric acid etch after each grind—10 min at 150 °F (65 °C)

[3] Patent App. No. 717853

6. Nomenclature

b	=	Width of grind
D_w	=	Diameter of workpiece
D_s	=	Diameter of wheel
F_N	=	Normal force intensity existing at the interface.
$\bar{v}_w$	=	Radial velocity of the recession of the workpiece surface due to stock removal.
$\bar{v}_s$	=	Radial velocity of the recession of the abrasive wheel due to wheel wear.
$\bar{v}_f$	=	Feed rate of cross slide
V_s	=	Surface speed of grinding wheel
V_w	=	Surface speed of workpiece
q	=	V_s/V_w
Λ_w	=	The Metal Removal Parameter
Λ_s	=	The Wheelwear Removal Parameter
l_c	=	Length of contact measured along the work surface.
l	=	Dress lead: inches of axial motion that the single point diamond moves per wheel revolution.
$\frac{c}{2}$	=	Half-compensation, or radial depth of dress
d	=	Diameter of average grain in the wheel
P	=	Average grinding pressure
F_N	=	Normal force per unit width—(force intensity).
Z_s'	=	Volumetric rate of wheel wear per unit width.
Z_w'	=	Volumetric rate of stock removal per unit width.

7. References

[1] Hahn, R. S., On the Nature of the Grinding Process, Proc. 3rd International MTDR Conference, (University of Birmingham), pp. 129–154, September 1962 (Pergamon Press).

[2] Busch, Dieter M., Ritz und Verschleissuntersuchungen an sproden Werkstoffen mit einzelkornbestuckten Hartstoffwerkzeugen. Doctoral Thesis, Technische Hochschule Hannover, Hannover West Germany (1968).

[3] Buttner, Axel, Das Schleifen Sprodharter Werkstoffe mit Diamant-Topfscheiben unter besonderer berucksichtigung des Tiefschleifens. Doctoral Thesis, Technischen Universitat Hannover, Hannover, West Germany. (1968).

[4] Pahlitzsch, G., Schleifen oxydkeramischer Werkstoffe. Annals of the C.I.R.P. XXXIII, (Pergamon Press, 1966), p. 331–338.

[5] Ida, Arai, Inamori, Grinding Characteristics of Ceramics for Circuit Components with Metal Bonded Diamond Wheels, Annals C.I.R.P. XVII (Pergamon Press, 1969), pp. 259–268.

[6] Pahlitzsch, G., Ing. Thormahlen, C.I.R.P. Arbeitsgruppe G: Gemeinschaftliches Versuchsprogramm (C.I.R.P. Annual Meeting, Geneva, Switzerland); Technischen Universitat, Braunschweig, August (1969).

[7] Lindsay, R. P., Dressing and its effect on grinding performance, Society of Manufacturing Engineers, Paper No. MR69–568, S.M.E., Dearborn, Michigan (1969).

[8] Lindsay, R. P., Hahn, R. S., The effect of parameter variations in precision grinding; Paper No. 70–PROD–1, American Society of Mechanical Engineers (ASME), New York (1970).

[9] Hahn, R. S., Lindsay, R. P., The Influence of Process Variables on Material Removal, Surface Integrity, Surface Finish and Vibration in Grinding, 10th Annual M.T.D.R. Conference, University of Manchester, Great Britain, September (1969).

[10] Guhring, K., Hochleistungsschleifen, Dissertation, T. H., Aachen, Germany, (1967).

[11] Hahn, R. S., Lindsay, R. P., On the Effects of Real Area of Contact and Normal Stress in Grinding, Annals of C.I.R.P., XV, pp. 197–204, Great Britain, (1967).

[12] Lindsay, R. P., Stock Removal Rates in Internal Grinding: A Model of the Process, MSc Thesis, M.I.T., Cambridge Mass. (1966).

[13] Littman, W. E., The influence of grinding on workpiece technology, ASTME paper MR67–593, (1967).

[14] Colwell, L. V., Sinnott, M. T., Tobin, J. C., The determination of residual stresses in hardened ground steel, Trans. ASME, 77, 1955 1099–1105 (1955).

[15] Letner, H. R., Residual grinding stresses in hardened steel, Trans. ASME, 77, 1089–1098 (1955).

[16] Letner, H. R., Influence of grinding fluids upon residual stresses in hardened steel, Trans. ASME, 79, 149–153 (1957).

[17] Halverstadt, R. D., Analysis of residual stress in ground surface of high-temperature alloys, Trans. ASME, 80, 929–939 (1958).

[18] Tarasov, L. P., and Lundberg, C. O., Detection, causes and prevention of injury to ground surfaces, Trans. ASME 36, 389 (1946).

[19] Hahn, R. S., The relation between grinding conditions and thermal damage in the workpiece, Trans. ASME, 78, 807-812 (1956).

Discussion

GIELISSE: I wanted to ask Dr. Hahn why do some of the plots of your metal material removal parameters not go through the origin?

HAHN: Well, mainly because of the rubbing and an inability of the grit to get a fracture going in the surface.

BROWN: When I saw your equation up there I thought to myself in anticipation, well, that's great, this is going to be different for different metals. Then I saw the plot where you plotted Z versus the F for several metals and they all seemed to follow along the same plot. I thought that this was quite amazing. Later you show the bar chart of Λ_w versus various metals and I see that Λ_w does vary. Now I don't know what to use.

HAHN: Well, it does vary with metals. The bar chart was kind of a rough thing. If you take metals that are classified "easy to grind steels", the Λ_w won't be much different. In other words, there is not much difference in Λ_w in 4150 steels. There are small differences, but if you go to different materials like M2 or M50 you can see large differences. There is a tremendous difference in Λ_w in cast iron and M4.

BROWN: So then you'd actually get a difference in slope on the Z versus F chart?

HAHN: Yes.

SMITH, K. M.: Evidently then, you do have a hammering action on these wheels as a high spot comes around. Isn't that true?

HAHN: What do you mean a hammering?

SMITH: In essence hammering means that high spot is hitting ahead of anything else.

HAHN: Well, most of these grinding wheels are trued with a diamond. The surface of a precision grinding wheel runs true within perhaps 5 millioniths of an inch, so there is not much run out of the grinding wheel.

SMITH: Does it stay that way very long?

HAHN: As the wheel wears, the soft areas in the grinding wheel wear more than the little hard knots. For example, like a log of wood with knots in it, the knotty part doesn't wear as fast as the soft adjacent part.

SMITH: In other words, you're setting up strains. As soon as the wheel begins to wear it will hit the soft spots.

HAHN: That is true.

NATIONAL BUREAU OF STANDARDS SPECIAL PUB. 348, THE SCIENCE OF CERAMIC MACHINING AND SURFACE FINISHING, Proceedings of a Symposium Sponsored by the American Ceramic Society, the Office of Naval Research, and the National Bureau of Standards, held at NBS Nov. 2–4, 1970, Gaithersburg, Md. (Issued May 1972).

A Basic Study of the Diamond Grinding of Alumina

D. M. Busch and J. F. Prins

De Beers Diamond Research Laboratory

P. O. Box 916, Johannesburg, South Africa

Experiments were performed using single diamond points to cut Coors AD96 alumina, under conditions simulating the grinding of this material. These studies involved different diamond particles and the forces were recorded during the cutting action.

Parallel to the single diamond experiments, grinding tests were performed on the same ceramic material using the same types of diamonds with which the single point studies were done. The grinding experiments and the single diamond experiments were then compared to get a better understanding of the actual cutting mechanism involved when grinding aluminium oxide.

The wear of the diamond particles and the damage inflicted on the ceramic material were studied with the aid of electron-microscopy. A relationship was found between the forces measured, the deterioration of the bonding material, and the wear of the diamonds.

Special attention was given to diamonds of the MDA–S type, a blocky, sharp edged diamond grit, and diamond spheres. These two types of diamonds were compared in grinding, and showed similar results due to the production of flat areas on the spheres, and the movement and wear of the blocky particles in the bonding material to present flat faces to the workpieces.

The grinding experiments also entailed a study of machine vibrations, especially chatter vibrations and the grinding noise associated with it.

Key words: Abrasion; chatter vibrations; forces in grinding; fracture of alumina grains; grinding noise; grinding of alumina; scratching of glass; single diamond cutting of alumina.

1. Introduction

A perusal of the relevant technical literature on the grinding of ceramic materials reveals considerable variations in the suggested grinding parameters to be used. For example, if a high stock removal rate is required in the surface grinding of ceramics, then the recommended downfeeds vary between 10 μm and 250 μm, depending on the properties of the ceramic material, and grinding parameters, such as table traverse speed, wheel speed, etc. [1, 2, 3, 4, 5].[1] The present study is not an investigation into the optimum grinding conditions for machining a ceramic, but deals more with some of the basic problems encountered during the grinding of such a material.

For the purpose of this investigation, experiments were carried out using single diamond points to cut a high density alumina, (specifically 96% Coors aluminum oxide), under conditions that simulated the grinding of this material. These studies were executed using different types of diamond particles, and the surface damage inflicted on the ceramic material with these diamonds was studied with the aid of electron microscopy. Microscopic investigations were also carried out to study the wear of the diamond particles and the effect on the bonding material in which the diamond is embedded. Parallel to these experiments, actual grinding tests were performed on the same material using wheels containing the same types of grits with which the single point studies were done. These grinding tests and the single grit experiments were then compared in order to obtain a better understanding of the mechanics of the cutting process. In performing the grinding experiments due attention was given to machine vibrations, especially chatter vibrations.

Special attention was given to the De Beers synthetic diamond type MDA–S, a blocky, relatively sharp edged diamond grit, and to diamond spheres [6] shaped from the MDA–S (fig. 1). It was reasoned that the behaviour of these two different types of grit should give an insight into the mechanism by which the ceramic material is removed by the diamond particles; i.e., whether the single diamond particle removes the workpiece material by a cutting process or, by crushing the ceramic grains to smaller sizes, and then scraping these smaller particles from the surface of the material. Thus the mechanism of the removal process should influence the wear of the single diamond grit particle: If the diamond particle removes material mainly by impacting and crushing the ceramic grains, then one would expect less wear of the spherical diamonds because these particles possess the greater compressive strength [7, 8].

[1] Figures in brackets indicate the literature references at the end of this paper.

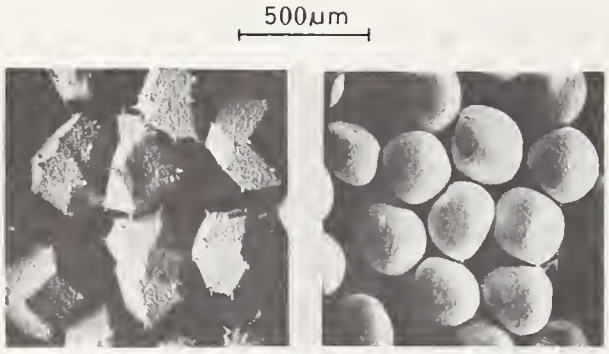

FIGURE 1. *Diamond particles used in grinding and single diamond experiments.*

2. Test Equipment and Conditions

The grinding experiments were executed on a small surface grinding machine with a horizontal spindle, using peripheral diamond wheels. Table 1 is a summary of the applied grinding parameters, the types of grinding wheels and the work-piece specifications.

The scratch tests, which were done in conjunction with the grinding experiments, were executed on the Single Grit Testing Machine which has been described previously. [9]. A single diamond particle was mounted on the periphery of a wheel, such that the effective radius was 63.5 mm. While the wheel rotates at the selected speed, the ceramic material is brought to the correct position within a single revolution, and a cut is then made on the material. During the next revolution the material is removed from the wheel to ensure that only a single cut is made.

When the single diamond is in contact with the ceramic surface the normal and tangential forces associated with the cut are sensed by means of pressure sensitive transistors, the signals from which are displayed on a double beam oscilloscope. Figure 2 is an example of such a recording, in which the time basis is 100 μs. per cm. The average force is estimated by dividing the area under the curve by the total time of cutting. As the force curves follow approximately a Gaussian distribution, the average force is taken to be about 0.4 times the maximum force as indicated in figure 3.

For convenience, all the force values obtained from the scratch tests reported in this paper are given in terms of the maximum forces, F_{max}.

From the cutting time τ (fig. 3) and the known wheel speed, it is possible to calculate the length of cut, L_T, and the maximum depth of cut, h_T. The maximum depth of cut, h_T, or the theoretical depth of cut was taken as equal to the infeed, and force measurements were recorded as a function of this theoretical infeed.

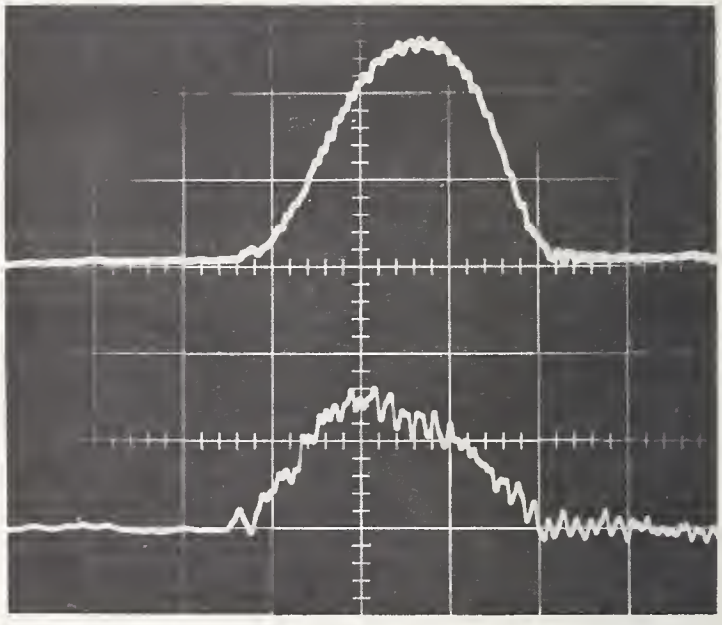

FIGURE 2. *A recording of the normal (top) and tangential (bottom) forces on the single grit machine.* Time scale 100 μs/cm.

TABLE 1. *Test conditions (grinding)*

Machine parameters		Diamond wheels	Workpiece
Surface grinding machine		Wheel type D1A1	Coors alumina AD96
(Horizontal grinding spindle) with 3 hp spindle drive motor		Wheel size 127mm × 4.7mm × 31mm Bond depth 3.1 mm	Specific gravity typical 3.72
Spindle revolution	3600 rpm	Diamond types: De Beers MDA–S–	Minimum 3.67
Wheel speed	24 m/s	(MC) and diamond spheres shaped	Crystal size range: 2–20 μm
Downfeed	50 μm; 125 μm.	from MDA–S	
Crossfeed	1.25 mm. per table reversal	Diamond mesh size 60/80 and 60/70 Diamond concentration:	Modulus of elasticity: 3×10^4 kg-force/mm^2
Table traverse speed	16 m/min	100 (=4.4ct/cm^3)	Compressive strength:
Stock removal rate 1cm^3/min; 2.5^3/min		Bond Bronze 80/20; Resin R-grade	typical 25 °C 210 kg-force/mm^2

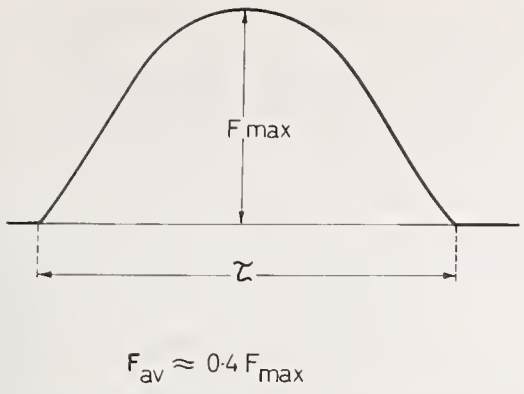

FIGURE 3. *The relationship between the average force and the maximum force on a gaussian force curve.*

The conditions under which the single grit experiments were performed are given in table 2.

In the grinding experiments, forces were measured with a strain gauge wired dynamometer [10]. Displacement and acceleration transducers and a frequency analyzer were also used to determine the chatter vibrations during grinding. The grinding noise was recorded on a tape recorder.

3. Experiments and Results

3.1. Preparation of the Grinding Wheels and Single Diamond Tools

Before the diamond wheels were used in grinding, they were dynamically balanced and then trued while rotating on the spindle of the grinding machine. The latter operation was achieved with the aid of a diamond block (with a diamond concentration of 200) and a silicon carbide block dresser. After trueing, the eccentricity of the wheels was checked using an accurate displacement transducer on the periphery of the wheel [14]. The profiles of the circumferences of the metal bonded wheels after trueing are shown in figure 4.

After the trueing process, the number of

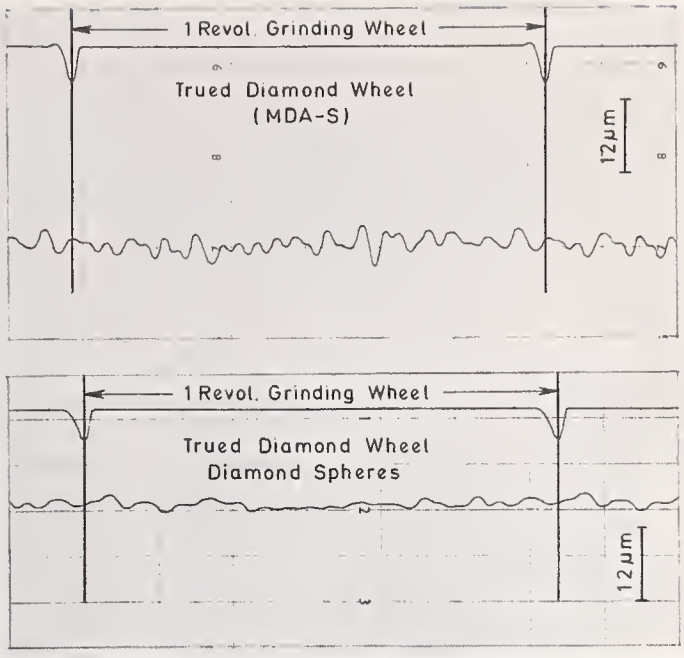

FIGURE 4. *The circumferential waviness of the bronze bonded diamond wheels after trueing.*

diamonds visible in the bond was counted on ten different areas on the wheel circumference [11]. The counting was carried out with the aid of a stereoscopic microscope containing a grid in one of the eyepieces. The average number of diamonds in the square field (2 mm. × 2 mm.) was determined.

In table 3, the average number of diamonds per 2 mm square on the wheel circumference is given for the two different types of diamond wheels after trueing, after a stock removal of 925 cm^3 at a downfeed of 50 μm, and after a further stock removal of 575 cm^3 at a downfeed of 125 μm. From this table it can be seen that the bronze-bonded diamond wheel containing the MDA–S type crystals possessed 20 to 24 percent more diamond particles than the wheel containing the diamond spheres. This percentage difference did not alter appreciably during grinding and, as will be seen later, this

TABLE 2. *Test conditions (single diamonds)*

Machine parameters		Diamond types used		Workpiece
Single grit testing machine		Diamonds mounted in hollow screw heads using resin.		Same as in table 1.
Spindle revolution:	3600 rpm	Screw with diamond then mounted on a		
Wheel Speed	24 m/s	mild steel wheel of diameter 127 mm.		
Downfeed:	Increasing in steps from about 10 μm to about 90 μm.	Diamond types:	De Beers MDA–S and diamond spheres shaped from MDA–S	
No crossfeed:	Table stationary during cutting process.			
		Diamond size:	~220 μm diam.	

TABLE 3. *Number of diamonds per 2 mm × 2 mm field on the bronze bonded diamond wheels*

Time of counting	MDA–S	Diamond spheres	Difference
			percent
After trueing	25	19	24
After a stock removal of 925 cm^3 at 50 μm downfeed	24	19	21
After a further stock removal of 575 cm^3 at 125 μm downfeed	25	20	20

difference in number of diamonds is a necessary prerequisite to explain some of the grinding results.

The single diamond points were mounted in a little cup using resin as the bonding material. The cup was machined to give it a threaded stem which screwed into the periphery of a mild steel wheel. The distance from the centre of the wheel to the diamond tip was kept at 63.5 mm. Figure 5 is a scanning electron micrograph of the cup with the diamond protruding from it. After the diamonds had been mounted, the excess of bonding material surrounding the single diamond was cautiously removed with the aid of a small file and steel tweezers, to allow the diamond to protrude above the surface of the bond. Scanning electron micrographs of a diamond sphere and a blocky MDA–S particle, which are mounted and ready to cut, are shown in figure 6.

3.2. Wear Behaviour of the Bronze-bonded Diamond Wheels, and the Single Diamond Points

A relatively high downfeed was applied during the grinding experiments (50 μm and 125 μm) in order to subject the diamond particles in the grinding wheels and the workpiece materials to high cutting loads. (Stock removal rates were 1 cm^3/min and 2.5 cm^3/min respectively).

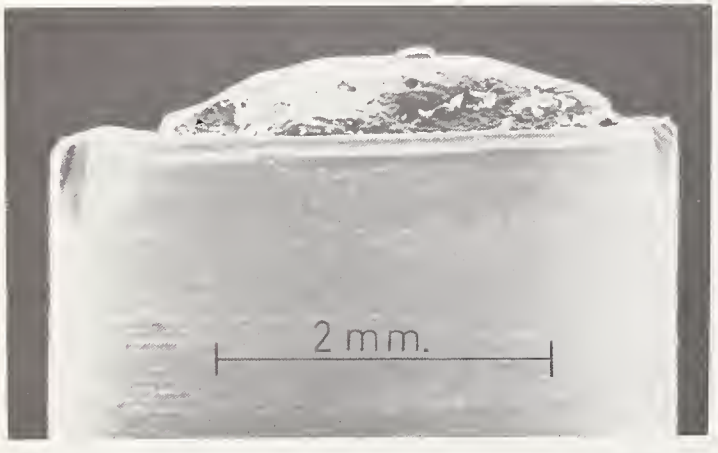

FIGURE 5. *Single diamond tool as seen from the side with the diamond protruding.*

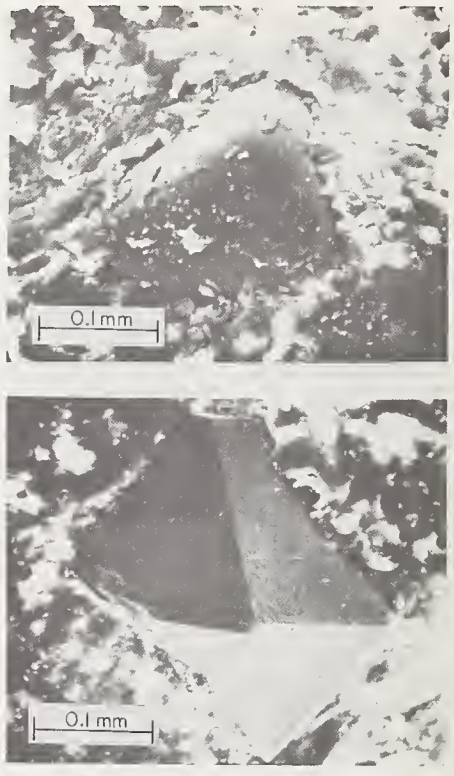

FIGURE 6. *Scanning electronmicrographs of two single diamonds mounted and ready for scratching tests.*

The wheel containing MDA–S diamonds gave G ratios of the order of 17,000 to 20,000 which seemed to be almost independent of the downfeed (50 μm and 125 μm). After a stock removal of 1500 cm^3, a wear of about 40 μm was observed on the grinding wheel.

The grinding wheel containing spherical diamonds gave a grinding ratio of 15,000 which is about 22 percent lower than the G ratio obtained with the wheel containing MDA–S. In view of the difference in the number of diamonds on the periphery of the two types of wheels, which is given in table 3 as approximately 20 percent, the two types of diamond wheels gave very similar grinding ratios when interpreted in terms of diamonds retained in the matrix.

In order to observe the possible wear of diamonds in the grinding wheels specific areas, and diamonds, on the wheels were replicated successively after different amounts of stock

removal, and observed in the scanning electron microscope [15]. The results are shown in figures 7 and 8 for the MDA–S and spherical diamonds respectively.

For comparison, the single diamond tools were also observed in the scanning electron microscope after scratching. The results are shown in figure 9. It has to be remembered that the scratch tests were done without using a coolant on the surface while the actual grinding experiments were done using a coolant.

For both the grinding experiments and the single grit tests, the diamonds quickly developed wear flats. No pronounced break-out of the edges of the diamond particles was observed. Although cracks were observed in some of the diamonds, wear of the diamond particles took place mainly by abrasion. The diamonds that did crack during grinding had already been cracked during the wheel trueing process.

The wear was slightly more pronounced on the spherical diamonds than the blocky ones, due to the fact that the blocky diamonds turned in the bond and thus presented new surfaces towards the workpiece material, (compare figures 7 and 8). The turning of the MDA–S

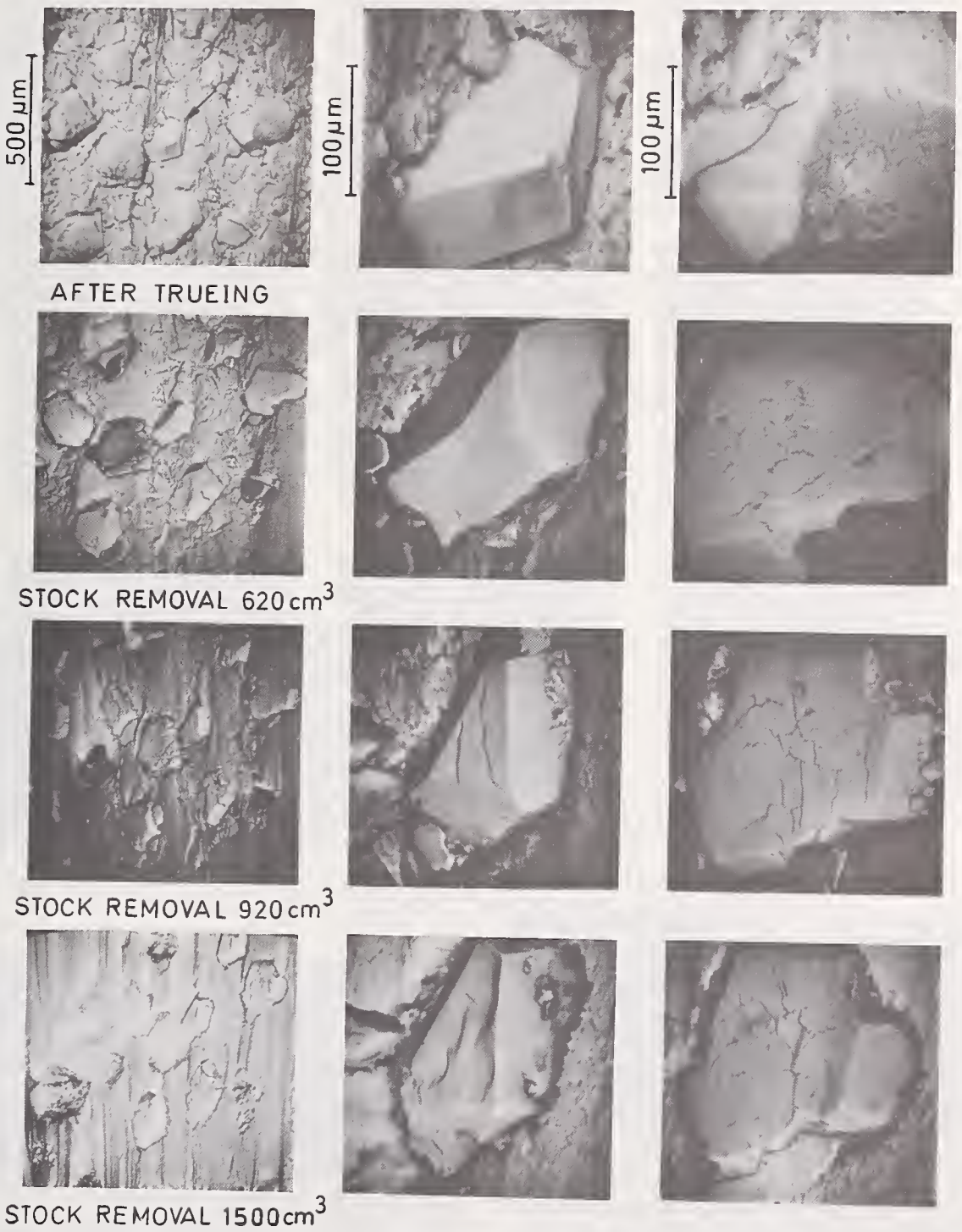

FIGURE 7. *Wear behaviour of the bronze bonded diamond wheel containing manufactured MDA–S diamonds. Workpiece: Coors AD96.*

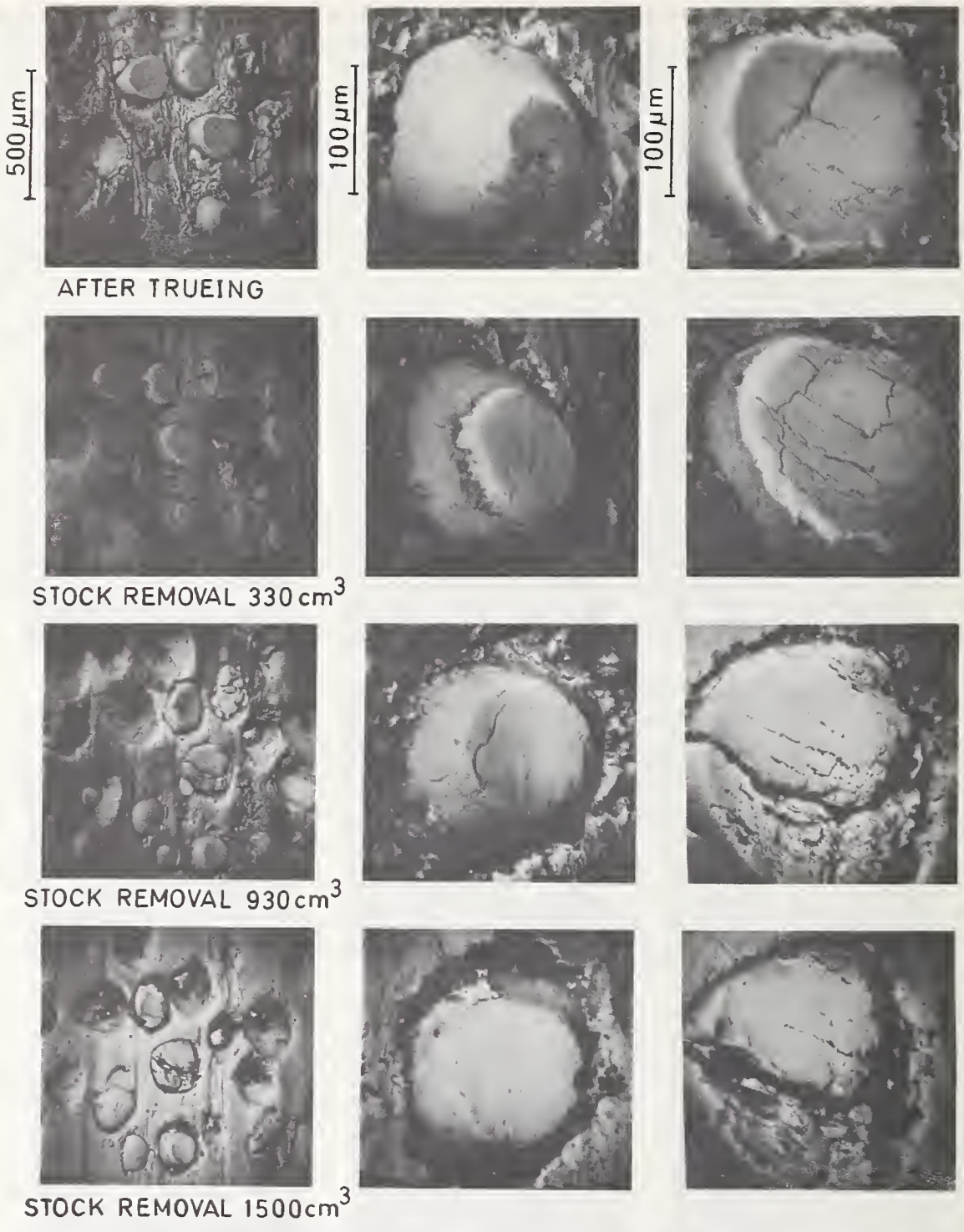

FIGURE 8. *Wear behaviour of the bronze bonded diamond wheel containing diamond spheres (shaped from MDA–S).* Workpiece: Coors AD96.

crystals was even more pronounced in the single grit tools, and in these tools the blocky particles were usually lost before a sufficient number of scratches could be obtained to produce pronounced wear. In contrast, the spherical diamonds stayed in the scratching tools and developed marked wear, with pitting, after a large number of scratches (see fig. 9). This pitting was seldom found on the diamonds in the grinding wheel, and might be due, in the single grit tools, to an absence of coolant on the workpiece surface. The pitting had some effect on the forces measured during cutting (see para. 3.3).

It is further clear from figures 7 and 8 that the first diamond layer on the grinding wheels did not wear away by the time 1500 cm^3 of stock has been removed. This is to be expected because of the low wheel wear (about 40 μm), and because of the grit size of the diamonds (177—250 μm). On the other hand, the wear of the bronze bond was high enough to make redressing unnecessary.

TABLE 4. *Normal and tangential forces when grinding with bronze bonded diamond wheels*

Downfeed	Diamond type	Normal F_n (kg Force)	Tangential F_T (kg-Force)	Difference between the two wheels	
				For F_n	For F_t
125 μm	MDA-S	11.8	1.2	18%	17%
	Spheres	9.7	1.0		
50 μm	MDA-S	5.0	0.46	24%	
	Spheres	3.8	Not measurable		

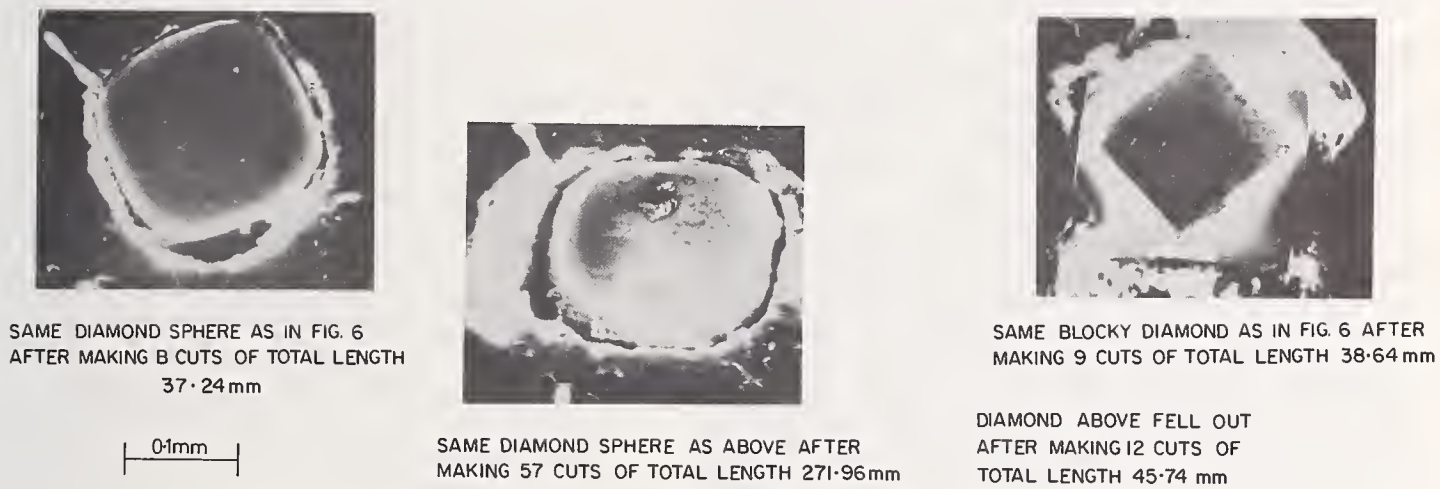

FIGURE 9. *Wear of single diamond tools during scratching of Coors AD96 alumina.*

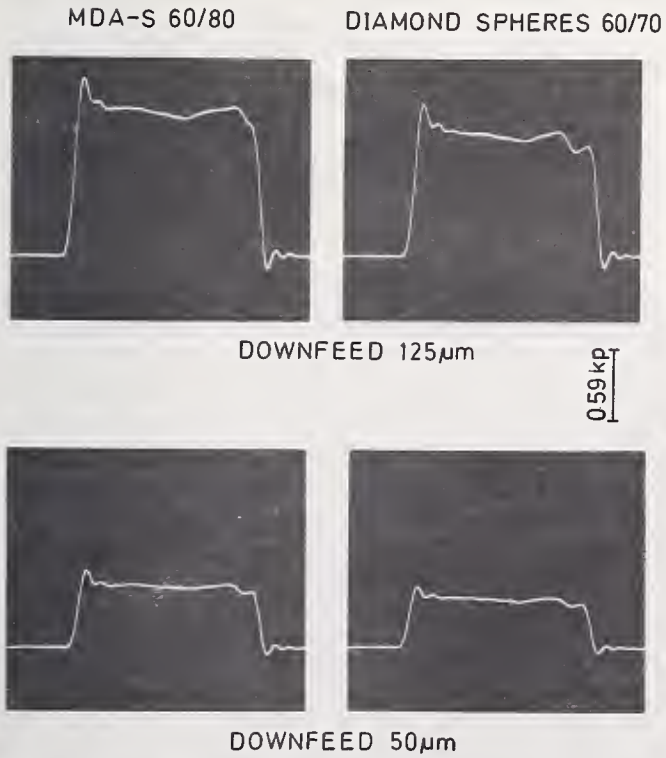

FIGURE 10. *Measurement of the normal forces exterted by the bronze bonded diamond wheels.*

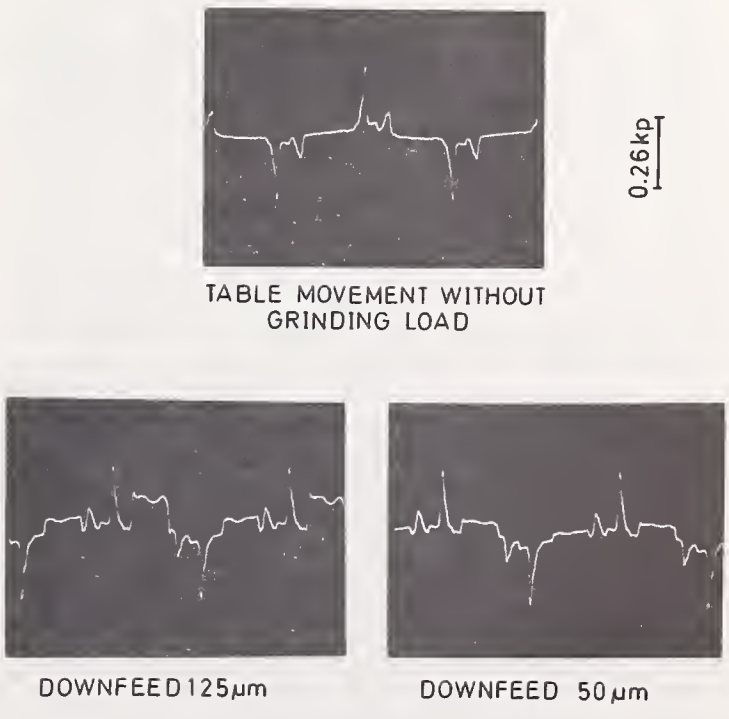

FIGURE 11. *Measurement of the tangential forces exerted by the bronze bonded diamond wheels.*

3.3. The Forces Involved During Grinding and Scratching

The normal and tangential forces for the grinding wheels and the single point tools were measured. For the grinding wheels these forces were measured after a stock removal 1500 cm³.

The normal and tangential forces recorded for the two types of wheels used are shown in figures 10 and 11 respectively [10]. In order to measure the relatively low tangential forces, the sensitivity of the carrier frequency amplifier had to be increased. This caused the influence of the table-reverse on the dynanometer to be recorded with the force recordings. To separate the two signals, an output force was recorded while the table moved without the wheel contacting the workpiece surface (see fig. 11). When the downfeed was changed from 50 μm to 125 μm, the forces increased correspondingly.

The average normal and tangential forces, listed in table 4, show that the forces exerted by the grinding wheel containing MDA–S are 17 to 24 percent greater than those developed by the wheel containing the spheres. This result can again be explained in terms of the different numbers of diamonds in the two wheels as shown in table 3. The magnitude of the forces is small compared to the forces measured when tungsten carbide is ground under similar grinding conditions. Another surprising feature is the ratio of approximately 10:1 measured for the normal forces relative to the tangential forces.

For the single diamond points, the forces were measured as a function of the theoretical depth of cut, h_T. In figure 12 the curves are given for the normal force (F_n), tangential force (F_t) and the ratio of the normal force to the tangential force for the spherical diamond and a blocky MDA–S diamond. These curves are quite constant from one diamond to another of the same type, but are different for the spherical and blocky diamonds. The blocky MDA–S crystals, however, turned in the bond during cutting, causing the force curves and ratio of the forces to be more uncertain than the measurements on spherical diamonds. From the curve of the ratio F_n/F_t for the spherical diamonds it is clear that the ratio of the forces is of the correct magnitude when compared to the force measurements on the diamond grinding wheels. Although the ratio increases with higher infeeds, to values over 20:1, for the single diamond, the increase would not be so marked when higher downfeeds are used with a grinding wheel. If the downfeed with a grinding wheel is 125 μm, not all the diamonds making contact with the ceramic surface will have depths of cut of 125 μm.

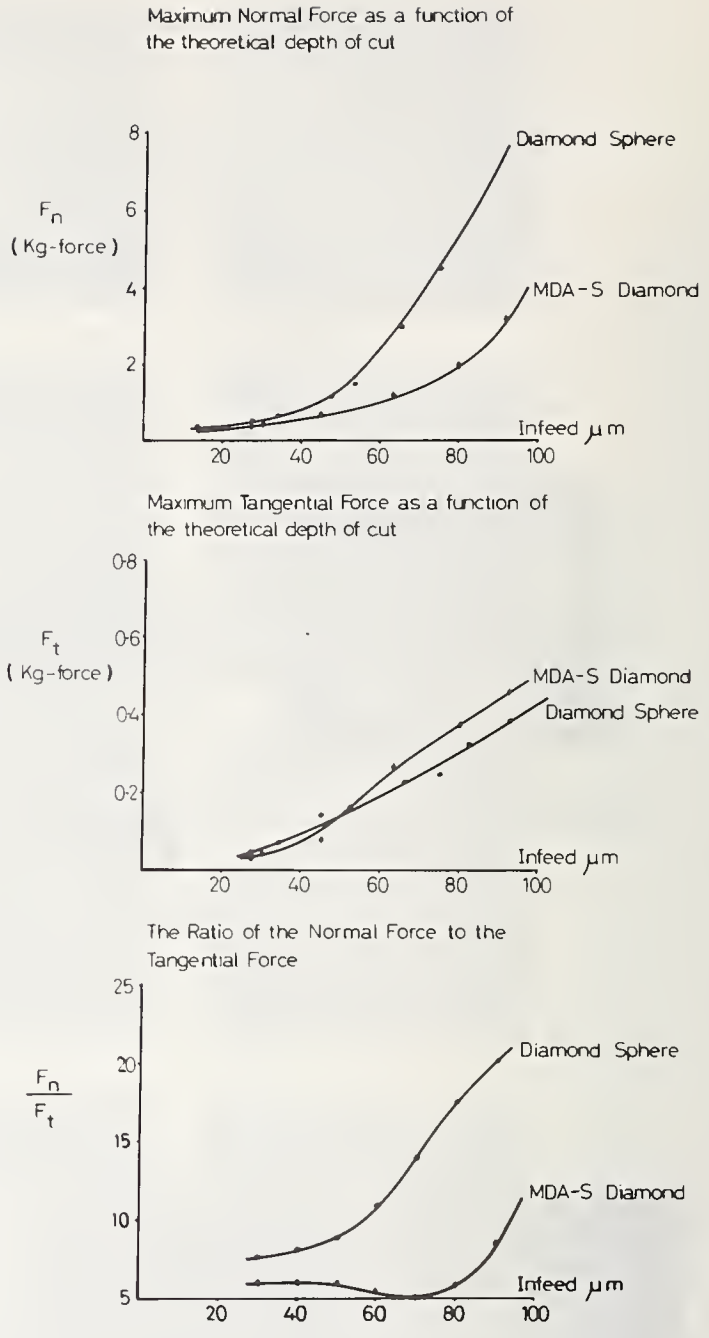

FIGURE 12. *Normal and tangential forces, and their ratio as measured when using single diamonds on Coors AD96 alumina.*

There will be some diamonds with lower infeeds.

The curve for the MDA–S diamond tools is low due to the fact that the diamond turns during cutting. This causes the diamond to be more easily pressed into the bond. The bond is then effectively more elastic, causing the actual depth of cut to be less than the theoretical depth of cut. A lower normal force is thus measured.

If the forces are compared for the fresh spherical diamond surface, shown in figure 6, with the worn pitted spherical diamond surface, shown in figure 9, the results are widely different as shown in figure 13. The normal

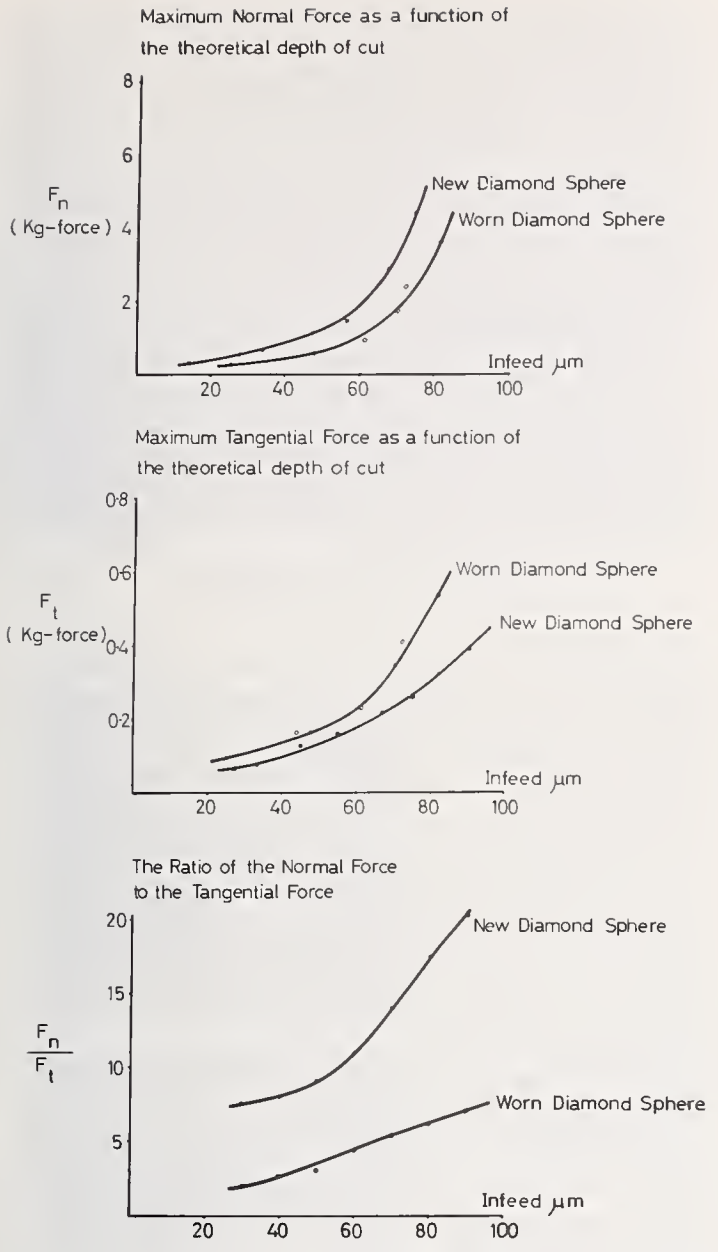

FIGURE 13. *Normal and tangential forces, and their ratio when a freshly mounted diamond is cutting compared to these forces when the same diamond is worn.*

force is lower for the pitted diamond than for the fresh diamond. This is probably due to the fact that the pitted diamond sits very loosely in the bond as can be seen in figure 9, causing the bond to be more "elastic" and having the same result as discussed above. On the other hand the tangential force is higher for the pitted, worn diamond sphere than for the fresh diamond sphere. This result is expected owing to the roughness of the pitted diamond. The ratio between the normal force and the tangential force is thus considerably smaller for the worn, loose diamond than for the freshly mounted diamond.

The last result has some significance on the results found for the grinding wheels. Some diamonds are more worn and have loosened to a greater extent in their bond than others, thus lowering the ratio of the normal force to the tangential force compared to the better bonded, less worn, diamonds. The average ratio of the normal to the tangential force will thus be somewhere between the two ratio curves in figure 13, and a ratio of 10:1 as obtained is thus understandable. For a wheel that is less worn than the wheels used for the force measurements in this study even higher ratios could be expected for high downfeeds.

3.4. Development and Determination of Chatter Vibration When Grinding a Ceramic Material

During the grinding experiments with the bronze-bonded diamond wheels, the wheel profile of each wheel was measured after different amounts of material had been removed. The increase in waviness of the wheels as a function of stock removal could thus be determined and is represented in figure 14.

The waviness increases with the amount of stock removed, and thus, with the time of grinding. From this it follows that even when grinding ceramics, chatter vibrations develop. The origin and development of chatter vibrations have been investigated previously, when diamond wheels were used on cemented tungsten carbide [12,13,14]. Vibrations frequently occur on the machine tool when grinding, and lead to a relative motion between the grinding wheel and the workpiece. These vibrations which cause visible, as well as macroscopically invisible, chatter marks on the ground workpiece surface are called chatter vibrations. Chatter vibrations are responsible for deterioration of the workpiece surface, increased grinding wheel wear, excessive machine tool

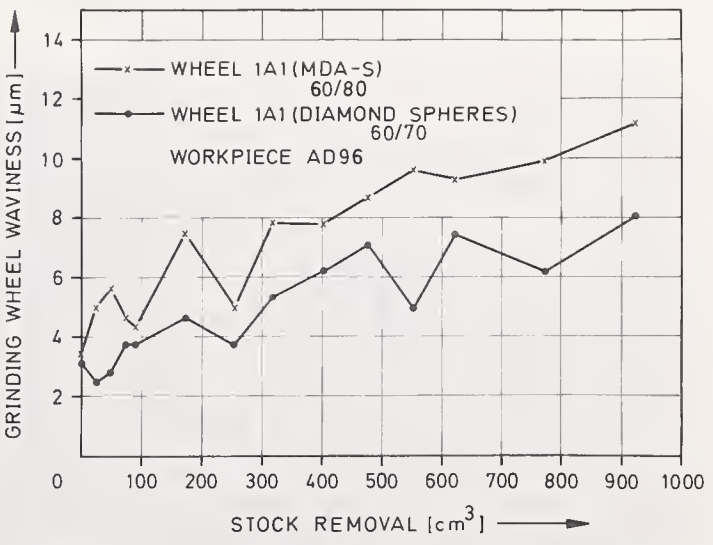

FIGURE 14. *The development of waviness on the circumference of a bronze bonded diamond wheel containing MDA-S—diamonds.*

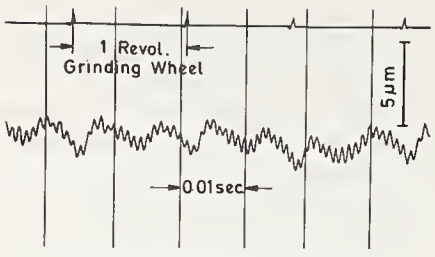

CHATTER VIBRATION AMPLITUDE
DISPLACEMENT

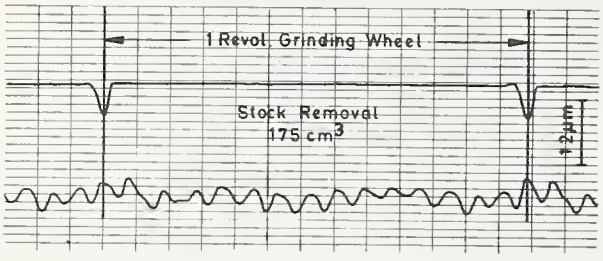

GRINDING WHEEL WAVINESS

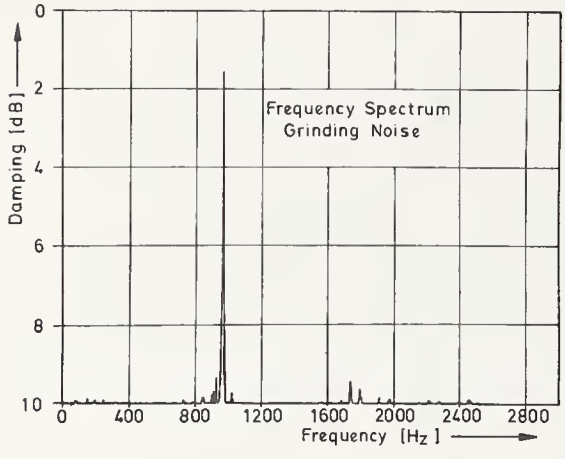

FIGURE 15. *Curves showing the amplitude of chatter vibrations, the waviness of the wheel and the frequency spectrum of the grinding noise when grinding with a resin bonded MDA–S diamond wheel at a downfeed of 50 µm.*

wear and a reduced stock removal rate.

These vibrations were recorded when using a resin bonded wheel containing metal clad MDA-S diamonds of size 60/80 mesh. Figure 15 shows an example of the recorded chatter vibrations, from which the vibration amplitude can be derived, the development of the waviness on the circumference of the wheel, and a frequency spectrum obtained from a recording of the grinding noise.

The amplitude of the chatter vibrations was found to increase with the grinding time. With the development of the chatter vibration amplitude a waviness occurs on the grinding wheel circumference, the depth of which also increases with the grinding times.

From previous investigations [12,14] it was established that the chatter vibrations were caused by a self-excited vibration, the frequency of which depends on the natural frequencies, the rigidity, the damping coefficients and the coupling stiffness of the grinding machine—grinding wheel—workpiece system. Chatter vibrations can also be reinforced by forced vibrations which stem, for example, from imbalances of the grinding wheel or other rotating machine parts, damaged and misaligned bearings, etc.

When comparing chatter vibrations on alumina and cemented tungsten carbide a retarded development of these vibrations was found for the alumina. This slower development of the chatter vibrations is the result of the lower cutting forces necessary to grind alumina.

3.5. Influence of the Grinding Wheels and Single Diamond Tools on the Surface of Coors AD96 Alumina

After grinding and scratching of the alumina, replicas were made of the ground and scratched surfaces and studied in the transmission electron-microscope. The ground surfaces could then be compared with the as-sintered unground surfaces.

In the case of the scratching experiments the preparation of the surface to be scratched presented some difficulties. The ceramic blocks required for mounting on the single grit machine must have the dimensions of 10 mm × 8 mm × 4 mm. In order to obtain these size blocks, the ceramic material had to be sawn and ground to the correct size. The ceramic blocks thus had an as-ground surface and not an as-sintered one. Polishing of the surfaces with a diamond powder did not improve matters at all, because during polishing, the glassy binder material melts and is smeared over the surface rendering a totally different surface than the one seen by the diamond during grinding (see fig. 16). If the polished surface is etched in molten sodium hydroxide to expose

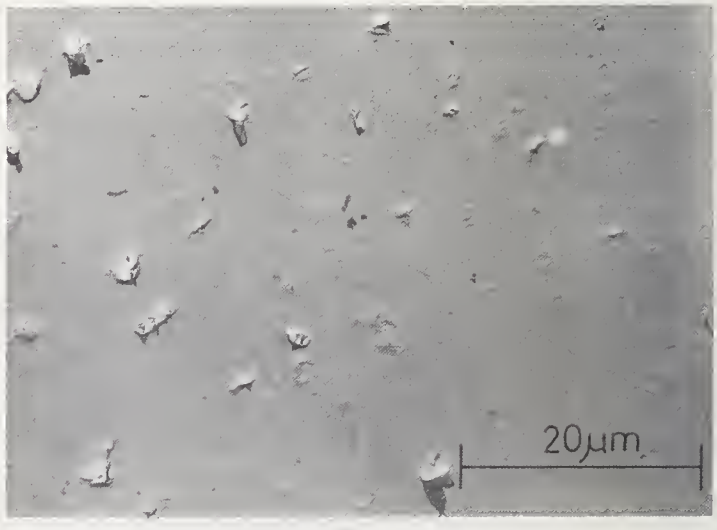

FIGURE 16. *A polished alumina surface.*

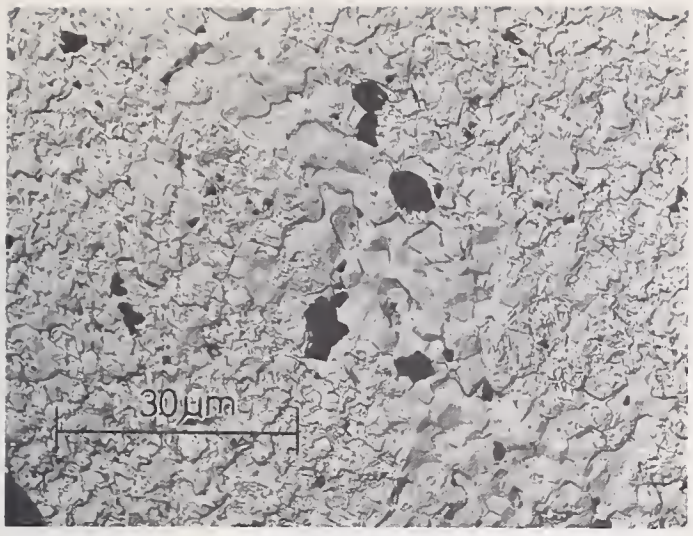

FIGURE 17. *An etched, polished alumina surface which was then scratched.*

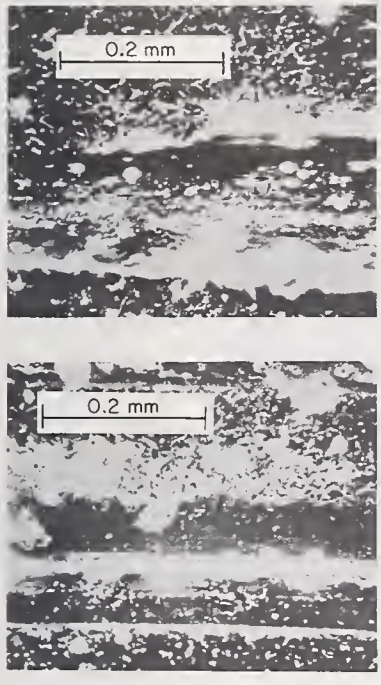

FIGURE 18. *A scanning electronmicrograph of cuts made in alumina.*

the underlying grains, the situation is not improved. Figure 17 shows an etched polished surface on which a single scratch was made. It is clear that the polishing process causes profuse fracture of the surface grains with subsequent reduction in grain size. A scratch on such a material thus only removes the fractured top layer of material and exposes the larger underlying grains (fig. 17). It was thus decided to use an as-ground surface obtained by using a wheel containing DXDA-MC grits of size 140/170 in an R-grade bond and to compare the cuts on these surfaces with the as-ground surface.

Viewing the cuts in the scanning electron microscope before etching reveals that some of the glassy binding material was extruded during cutting and smeared over the surface. This effect was more pronounced for the spherical diamond than for the MDA-S diamond. Figure 18 shows two cuts of theoretical depth about 60 μm, one made with a diamond sphere and the other with a blocky MDA-S particle. More extrusion and smearing of the glassy material is found for the diamond sphere than for the blocky particle, and the cut obtained with the sphere is obviously deeper than the one obtained with the blocky particle. This result is expected when compared with the force measurements.

When replicas of the scratched and etched surfaces are viewed in the electron microscope the difference between the scratched part and the as-ground part is not very pronounced. This is to be expected because the grains in the

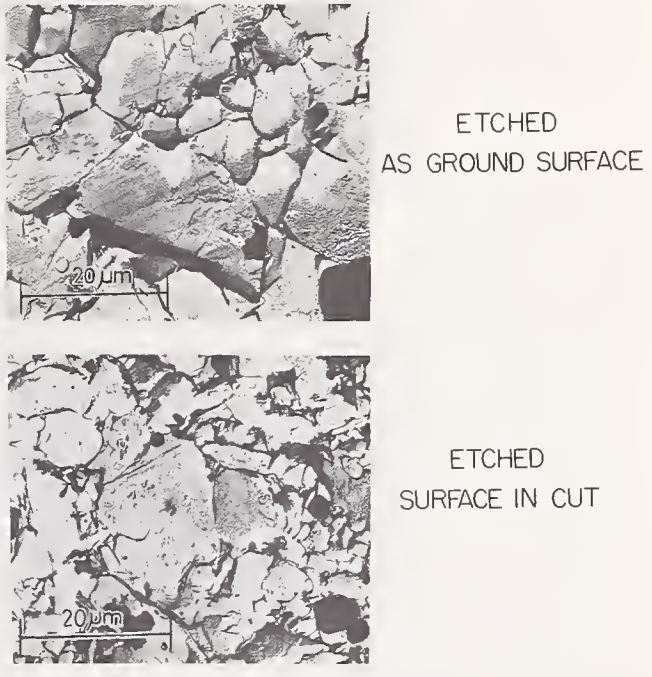

FIGURE 19. *Grains in a cut and on an as-ground surface using a spherical diamond.*

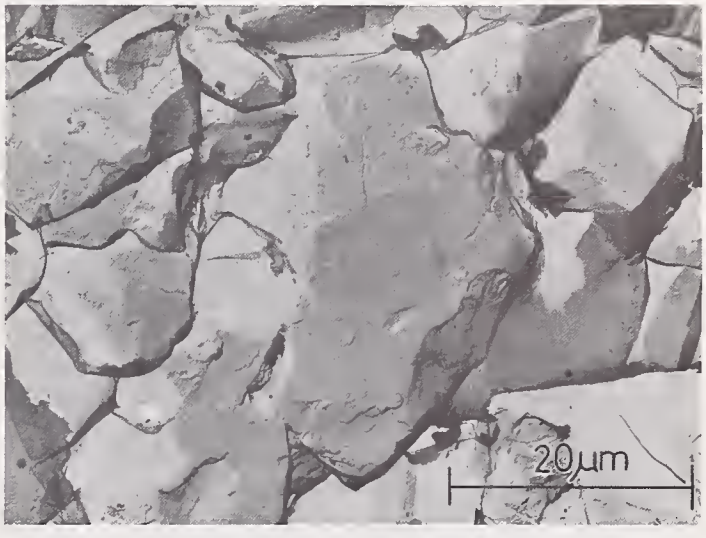

FIGURE 20. *Abrasion marks on aluminium oxide grains.*

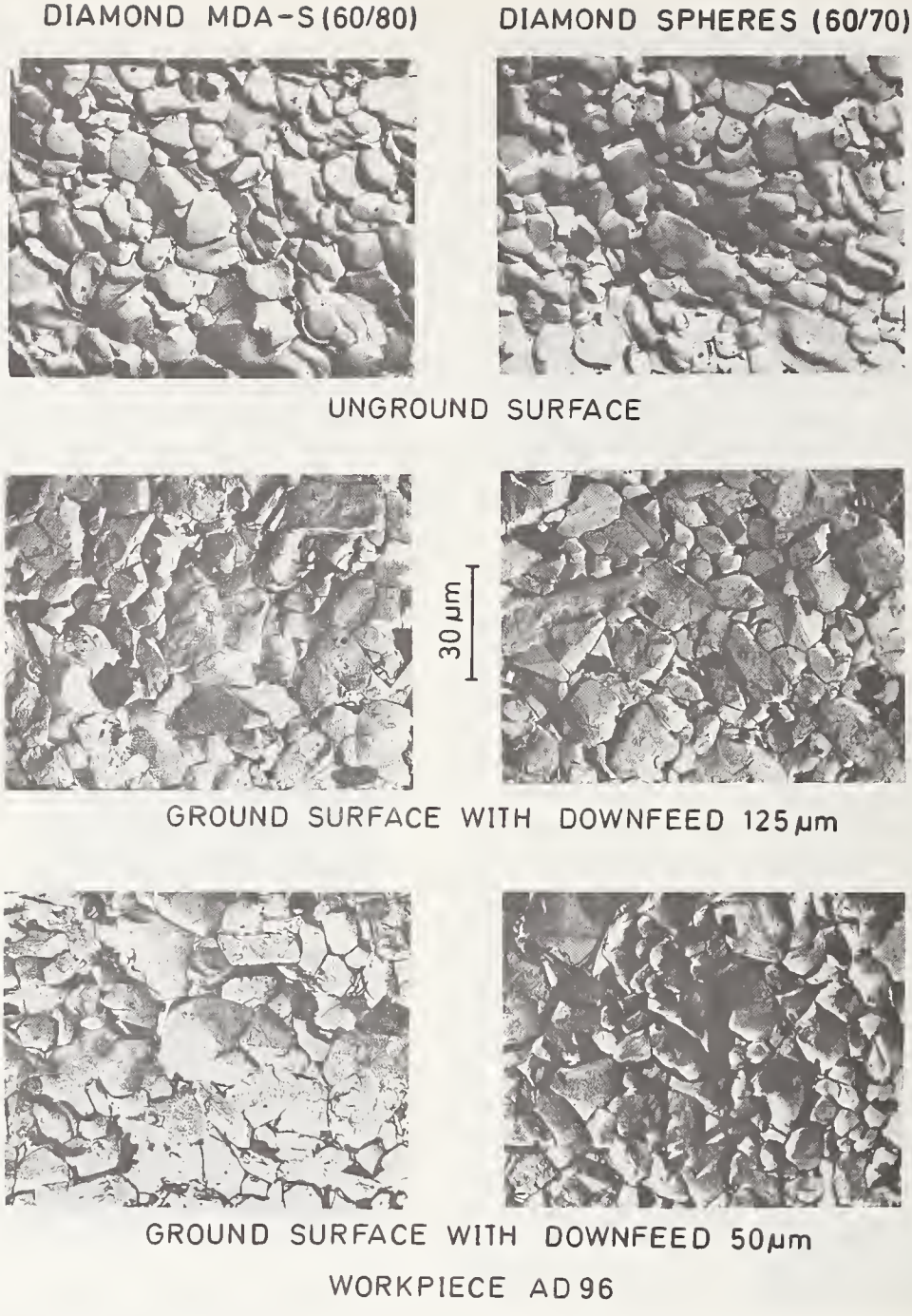

FIGURE 21. *Replica's of etched aluminium oxide surfaces comparing the ground surfaces with the unground surfaces.*

scratch should fracture in the same way as the grains on the as-ground surface. No difference could be found between the surface and scratches on the specimens which were scratched with the blocky diamonds. However, in the scratches made with the spheres, the grains in the scratches are a bit more fractured than the grains on the as-ground surface (see fig. 19). This result is also expected from the force measurements. Abrasion of the aluminum oxide grains can be seen clearly on some of the larger grains. An example is given in figure 20.

A comparison of the ground and etched surfaces produced with the bronze-bonded diamond wheels, and the as-grown surface of the aluminum oxide is given in figure 21. On all the ground surfaces fracture of the grains is evident, but the fractures did not alter appreciably the size distribution of the aluminum oxide grains. Some of the grains have large fractures which nearly cleave them, but these large fractures were not usually accompanied by the break-out of one part of the grain. Most of the exposed fracture surfaces show that small splinters of the ceramic grains were removed. These fracture surfaces are usually confined to the tops of the ceramic grains, and rarely extended further than the depth of a single layer of the grains. On all surfaces abrasion marks could be detected, especially on the larger grains. It is interesting to note that the grains exposed after grinding with a downfeed

of 125 μm, are more closely packed, with the wheel containing diamond spheres, and have a flatter appearance, thus giving a smoother surface.

Both wheels remove material without changing the size distribution of the grains on the ceramic surface to any marked extent, and the surfaces are very similar to the as-grown surface, but do have a slightly better texture. Consequently, these wheels are not suitable for a very fine surface finish, which, according to the polishing experiments mentioned (figs. 16 and 17), should have finer grains than the as-grown grains. Both wheels are, however, suitable for stock removal without inducing too much surface damage.

4. Conclusions

Both the spherical diamonds and the MDA-S diamonds gave comparable grinding results and remove material from the aluminum oxide by fracturing and abrasion. The fracturing occurs as a consequence of the large ratio of the normal forces to the small tangential force, and the extent of fracture should thus be a function of the size of the diamond.

It was also established that the normal force decreases when the bond deteriorates.

The spherical diamonds and the MDA-S diamonds developed wear flats very quickly when used in the grinding and scratching experiments. Some of the MDA-S diamonds especially those with sharp corners protruding, turned in the bond thus presenting a flat surface to the workpiece. Thus within a relatively short time both the spherical diamonds and the MDA-S diamonds present flat areas to the workpiece material. It is thus not surprising to find similar grinding ratios for both types of diamonds.

5. Scratching Tests on Glass Surfaces

The comparative study between sharp-edged blocky diamonds and diamond spheres was derived from a previous study where diamonds were used to scratch glass surfaces. In those experiments it was found that, at high loads, the glass fractured, and, if a sharp-edged diamond was used for cutting, the diamond sometimes also broke at the same time. This was not as frequently observed for spherical diamonds because of their higher compressive strength.

It was then thought that if the grinding of a ceramic material entailed fracturing of the ceramic grains and subsequent removal of these grains then, according to the tests done on glass, the spherical diamonds should wear less than the sharp-edged ones.

The previous tests [7] on scratching glass surfaces were conducted at room temperature, 20° C, and a relative humidity of 65 percent.

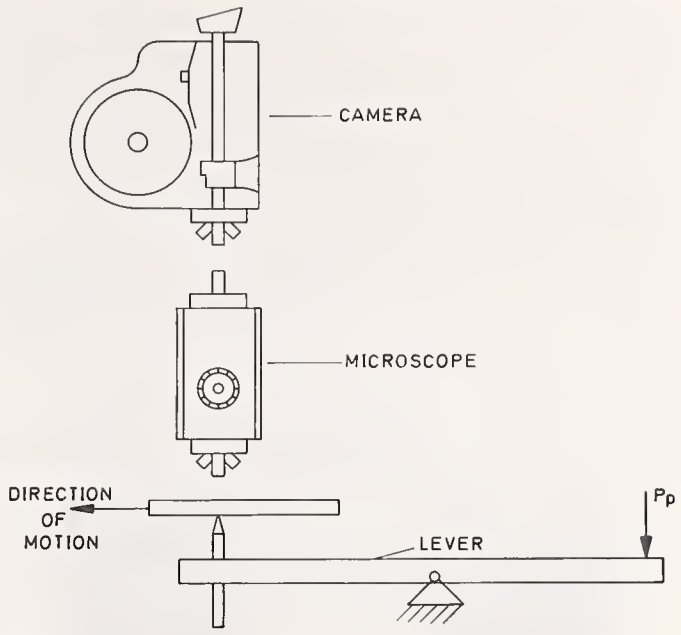

FIGURE 22. *Apparatus used in glass scratching experiments.*

The scratching speeds were 20 μm/s and 40 μm/s respectively. The tests were carried out with a scratch device similar to the Martens—Scratch—Hardness—Tester (fig. 22). The spherical polished tools, which were fastened to a steel lever were pressed against the glass surface with a known force. The movement to produce the scratch was executed by the workpiece. For the observations and photographing of the scratching process an optical microscope and a 16mm—Ariflex camera were used, the latter being attached to the top of the microscope. The sequence occurring during the scratching process on the glass surface was filmed at a speed of 24 frames per second.

The film of scratching rough spectacle glass B260 (Deutsche Spiegelglass A.G. Grünenplan) depict the elastic and plastic behaviour of glass and the development of fractures [16, 17, 18, 19, 20].

For many years these phenomena which occurred on the surface during the polishing of glass could not be explained. It was thought that there was no essential difference between the grinding and polishing process.

The elastic behaviour of the glass, when scratched by the spherical tipped tools, manifests itself in the film by a wave motion on the glass surface which forms behind the tool and which disappears again with increasing distance away from the tool.

At a certain surface pressure of about 350 kp/mm^2 there is an increasing wave motion of the glass, which cannot elastically reform itself when the force with which the tool is pressed against the glass surface is increased. Chipping and glass fractures are thereby not observed so that the plastic behaviour of the

439-921 O - 72 - 7

glass by this process demonstrates itself in microscopic ranges. Figure 23 illustrates the scratch traces produced during the tests using a diamond cone having a spherical tip. Wall-like mounds can be observed at each side of the scratch groove and these consist of plastically displaced material.

It can be seen from figure 24 and from the film recordings that the fractures of the glass material to form the scratch groove take place in front of the tool. It seems possible that at certain places on the scratch groove and at some distance behind the scratching tool, a break formation also could occur because of elastic resiliences of the glass material.

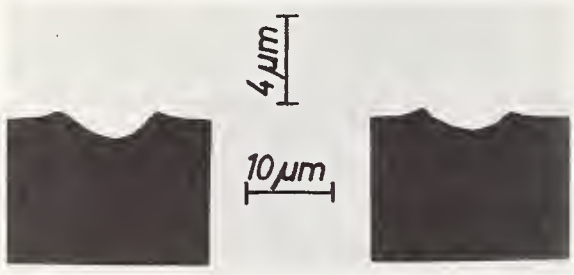

FIGURE 23. *Cross-section of scratches on a glass surface showing plastic deformation (wall-like mounds).*

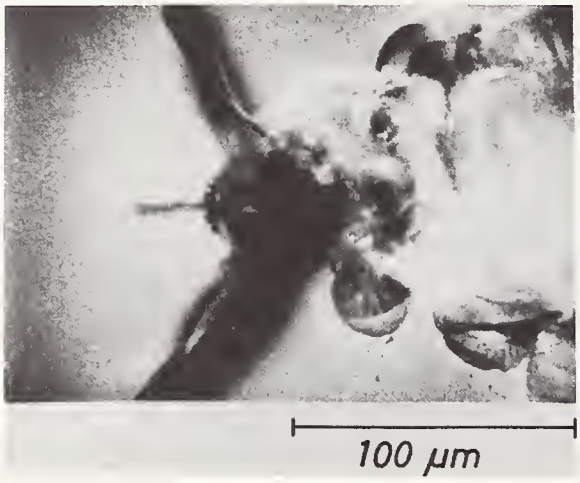

FIGURE 24. *Fracture formation in front of the tool when scratching a glass surface.*

FIGURE 25. *Flow-chip formation of glass when cutting with a diamond tool.*

The plastic behaviour of glass in microscopic ranges can be explicitly proved by figure 25 and by the film recordings of the flow-chip formation of the glass when it is scratched with a sharp and pointed edged diamond tool having a positive rake angle. During these cutting tests a glass chip approximately 8mm long was produced and did not tear off at the cutting point.

The chip surface was approximately 2 µm thick and 7 µm wide.

The grinding process can, in principle, be distinguished from the polishing process on the basis of the evidence of plastic behaviour of glass in microscopic ranges. Glass is rapidly abraded by cracking and breaking out of chips during grinding. The surface layer thereby remains continuously broken up for a thickness of several lengths of light waves. The abrasion of the material is caused by side cracks, and the spreading of these cracks and interaction results in the chip-like pieces of glass peeling off. The polishing process, in contrast to the grinding process, is based on plastic deformation on the glass surface in microscopic ranges which represent a genuine flowing process. The cracks and indentations caused by the grinding process are evened out to a fraction of a wave length.

It is a pleasure to acknowledge the cooperation of the following persons: V. Conradi for manufacturing the grinding wheels, D. R. Harding for help given in running the single grit testing machine, J. Fourie for help on the grinding experiments, J. Eckert who made the replicas for electron microscopy, and J. Grassmann for the force measurements on the grinding wheels.

6. References

[1] Luce, E.C., Why use diamond wheels when maching ceramics?

[2] Ida, I., Arai, Y., Fukuda, M., Inamori, K., and Sugiura, M., Relations between material properties and grinding characteristics when using diamond wheels on ceramics for circuit components, Reprinted from the Review of the Electrical Communication Laboratory. 17, No. 9, (1969).

[3] Primak, L.P., and Shripko, G.F., The contact temperature in the surface grinding of high alumina ceramics, Industrial Diamond Review 30, No. 357, 318–320 (1970).

[4] Sawluk, W., Flachschleifen von Oxydkeramischen Werkstoffen mit Diamand-Topfscheiben, Dr.-Ing. Dissertation, Technische Hochschule Braunschweig (1964).

[5] Gielisse, P.J., Mathewson, W.F., Martis, J.A., and Rattermann, E., Keramikbearbeitung mit

Diamenten, Sonderdruck aus Fachberichte fur Oberflachentechnik 7, Heft 1/2, 3/4, 5/6 (1969).
[6] Fluid Energy Mills, private communication.
[7] Busch, D.M., Ritz-und Verschleiss-untersuchungen an sproden Werkstoffen mit enzelkornbestückten Hartstoffwerkzeugen. Dr.-Ing. Dissertation, Technische Universitat Hannover (1968).
[8] Kobayashi, A., Recent development in diamond wheel grinding.
[9] Prins, J.F., and Harding D.R., An apparatus for testing single diamond particles under simulated working conditions, Diamond Research 1970, A supplement to Industrial Diamond Review (Jan. 1970).
[10] Levitt, C., and Grassmann, J., Diamond Research Laboratory dynamometer uncover grinding force secrets, Industrial Diamond Review 29, No. 347, 401–405 (1969).
[11] Büttner, A., Das Schleifen sprodharter Werkstoffe mit Diamant-Topfscheiben unter besonderer Berücksichtigung des Tiefschleifens, Dr.-Ing. Dissertation Technische Universitat Hannover (1968).
[12] Busch, D.M., Machine vibration and its effect to the diamond wheel. Diamond Information L20., De Beers Industrial Diamond Division.
[13] Busch, D.M., and Büttner, A., Effect of machine vibrations on the grinding result, D.R.L. Report No. 12/70(C).
[14] Busch, D.M., The development of chatter vibrations when grinding with diamond grinding wheels, D.R.L. Report No. 16/70(C).
[15] Eckert, J.D., and Caveney, R.J., A replica technique for conventional and scanning electron microscopy, Journal of Scientific Instruments 3, No. 5, 413–414 (May 1970).
[16] Busch, D.M., Verformen von Glas mit Ritzwerkzeugen, Film B984 des Inst. Wiss. Film, Güttingen (1967).
[17] Busch, D.M., Verformen von Glas mit Ritzwerkzeugen—Mikroelastisches Verhalten—Film E 1328 des Inst. Wiss. Film, Gottingen (1967).
[18] Busch, D.M., Verformen von Glas mit Ritzwerkzeugen—Mikroplastisches Verhalten—Film E 1329 des Inst. Wiss. Film, Gottingen (1969).
[19] Busch, D.M., Verformen von Glas mit Ritzwerkzeugen—Bruch—Und Schollenausbildung—Film E 1330 des Inst. Wiss. Film, Gottingen (1967).
[20] Busch, D.M., Zerspanen von Glas mit Diamantschneidwerkzeug—Spanbildung beim Ritzen—Film E 1331 des Inst. Wiss. Film, Gottingen (1967).

Discussion

WIEDERHORN: I'm curious about two things. One, in the movie there were some waves on the surface that appeared to be damping out. What did you attribute these waves to?

BUSCH: I'm not quite sure yet. It could be an effect of vibrations on the system. That could be possible but it might be something else because we have to expect, let's say, a deformation in front of the tool like a bow wave.

WIEDERHORN: Would you say it was relaxation of a deformation?

BUSCH: You mean elastic deformation? Yes, I would say so, but there are some effects which can't be explained at present.

WIEDERHORN: The other question was, what was the environment? Was it air?

BUCSH: It was in air, 20 °C and humidity 65 percent. No coolant was used.

GREENFIELD: In the last movie sequence, you showed a very large helical chip. Did you make any diffraction patterns of the chip? In other words was this chip at all crystalline?

BUSCH: We could not obtain the chip for examination.

LANGE: It appeared to me that the movie showed that the contact area was much larger, but yet, the crack or cracks only started at one point on the perimeter of the tool. Was there any reason?

BUSCH: The geometry of the tool was always the same. It was a cone with a radius of curvature of about 50 μm.

LANGE: In other words, what we saw was actually the point of the tool cutting the glass and not what appeared to be a spherical contact area.

BUSCH: Sorry, there were two types of tools; spherical tools and in this last movie sequence where chips were produced, it was actually a cutting tool with special angles. In this sequence you saw the point of the tool cutting the glass. In the earlier sequences you saw the projection of the spherical tool through the glass.

GIELISSE: Have any experiments been made on the effect of change on what one refers to as the rake angle cutting point during the generation of the glass chips?

BUSCH: No.

GIELISSE: Do you expect this to behave as you showed in the film as the rake angle grows?

BUSCH: Yes. In these glass investigations a diamond cutting tool was used with a positive rake angle.

NATIONAL BUREAU OF STANDARDS SPECIAL PUB. 348, THE SCIENCE OF CERAMIC MACHINING AND SURFACE FINISHING, Proceedings of a Symposium Sponsored by the American Ceramic Society, the Office of Naval Research, and the National Bureau of Standards, held at NBS Nov. 2–4, 1970, Gaithersburg, Md. (Issued May 1972).

On the Strength of Ceramics as a Function of Microstructure, Grinding Parameters, Surface Finish, and Environmental Conditions

Rudolf Sedlacek, F. A. Halden, and P. J. Jorgensen [1]

Stanford Research Institute, Menlo Park, California 94025

The tensile strength of four aluminas is described in terms of their microstructure and composition. The effect of microstructure on the attainable surface finish is discussed, and the results of profilometric evaluation of ground surfaces are presented. Various postgrind treatments are shown to have differing effects on microstructure. Griffith's flaw theory is applied to aluminas of different grain sizes, and calculated strengths are found to agree with experimental data. The phenomena of delayed fracture and stress corrosion are discussed; the strength of alumina is found to be higher under vacuum than in air and is independent of stress rate.

Key words: Alumina; delayed fracture; grinding of ceramics; microstructure; stress corrosion; vacuum strength.

1. Introduction

Ceramic manufacturing is a complex process consisting of a number of separate steps, each of which can have a pronounced influence on the physical and mechanical properties of the final product. Each individual step requires quality control that cannot always be applied effectively, and, as a result, the properties of ceramics show a certain amount of variation.

Considering the high potential of ceramics for load-bearing applications at elevated temperatures, an understanding of the factors influencing mechanical properties is most desirable. Particularly, the tensile strength of these materials is of interest, because it is relatively low and often shows a disturbing lack of reproducibility. In recent years, new tensile testing methods have been developed which have proved that much of the data scatter found in older literature can be attributed to the use of faulty testing techniques. These new techniques now appear to provide data that can be utilized with much more confidence.

In order to work systematically toward an improvement of strength of ceramics, it is necessary first to gain a better understanding of the factors presently limiting their strength. These factors cannot all be studied simultaneously. Instead, it appears more practical to concentrate on those factors that are most obvious and that can be most easily isolated.

Since the formulation of Griffith's flaw theory, it has been widely accepted that the key to the strength of ceramics lies in the perfection of their surfaces. Whenever a ceramic part has to meet close dimensional tolerances, it is shaped in the final step of the manufacturing process by grinding with bonded diamond. This operation then determines not only the geometry of the piece, but also the quality of the surface finish. Obviously, grinding is an important step in the manufacturing process, and it is surprising how little is known about it.

It has been shown [1] [2] that by changing the grinding conditions, the strength of alumina can be varied about 10 percent, while the attendant surface finish changes by a factor of four. It is also known that, for a given grinding treatment, different alumina ceramics attain different surface finishes. This means that the results of the grinding operation are linked to the microstructural properties of the ceramic materials. This relationship is discussed in the following article. Also discussed are the dependence of the strength of alumina on various post-grind treatments, on stress rate, and on test conditions such as vacuum.

2. Experimental Procedure

2.1 Test Materials

The alumina bodies used in this study were Al–300, Al–600, Al–995 (all manufactured by the Western Gold and Platinum Company, Belmont, California) and AD–995 (product of the Coors Porcelain Company, Golden, Colorado). These materials were chosen in the hope that the correlation of different chemical compositions and microstructures (see fig. 1) with the grinding procedure, surface finish, and various post-grinding treatments would indicate—in terms of strength—the overall problems of diamond finishing of ceramics.

The composition of the four bodies, determined by semiquantitative emission spectrochemical analyses are shown in table 1, and

[1] Senior Research Ceramist, Associate Director Materials Laboratory, Manager Ceramics Group, respectively.

[2] Figures in brackets indicate the literature references at the end of this paper.

TABLE 1. *Emission spectrographic analyses of alumina bodies*

Element	Amount in each body, wt percent			
	AD–995	Al–300	Al–600	Al–995
Al	Principal constituent in each sample			
Si	0.25	1.25	2.	0.4
Mg	0.25	0.02	0.75	0.5
Ca	0.04	0.6	0.3	0.08
Na	<0.02	<0.02	<0.02(?)	----
Cr	0.2	0.001	0.002	----
Fe	0.08	0.07	0.12	0.12
Ga	0.02	0.015	0.01	0.015
Ti	0.01	0.025	0.02	0.025
Zr	0.02	0.006	0.015	0.005
B	<0.01	0.15	<0.01	----
Mn	<0.001	<0.001	0.001	0.001
Pb	<0.002	----	<0.002	----
Cu	0.0005	<0.0005	<0.0005	0.001
Ba	0.002	0.001	0.001	0.002
Ag	less than 0.0005% in each			
Sr	less than 0.005% in each			
V	less than 0.005% in each			

TABLE 2. *Physical properties of the test materials*

Material	Density kg/m^3 × 10^3	Average grain size m × 10^{-6}	Color
Al–300	3.75	32	Bluish white
Al–995	3.80	18	White
AD–995	3.75	13	Pink
Al–600	3.71	10	White

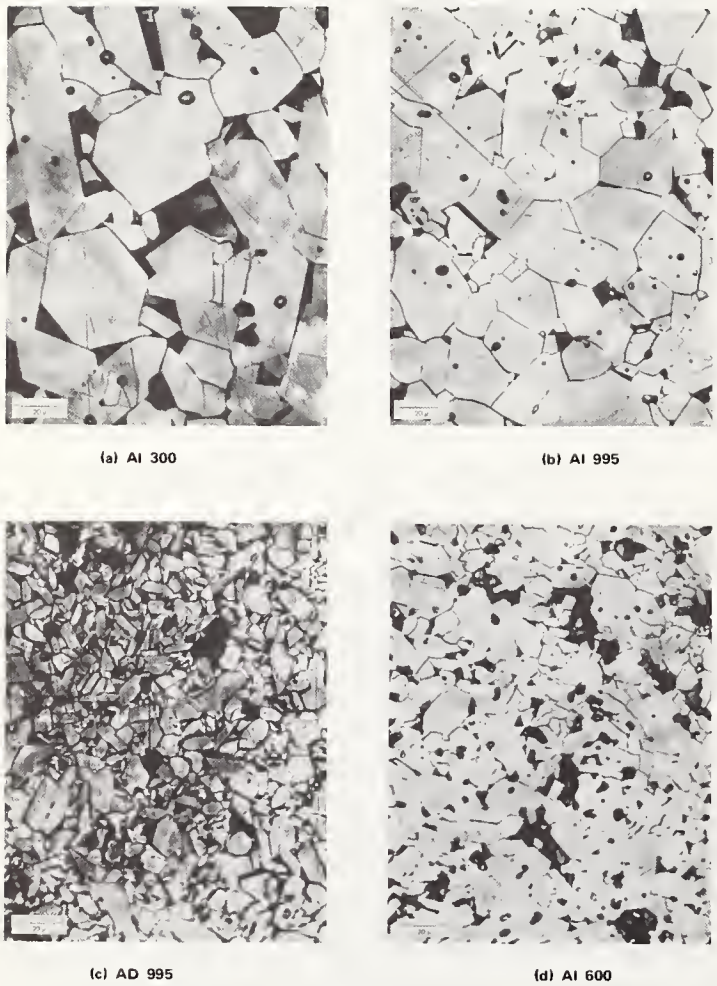

FIGURE 1. *Microstructure of test materials.*

some of the physical properties of the four test materials are presented in table 2. The aluminas designated with the prefix Al were white, although each type was of a slightly different shade of white. The pink color of AD–995 alumina varied considerably from piece to piece, but no correlation between color and strength was observed.

2.2. Grinding Procedure

The general grinding procedures used in the study have been described in detail elsewhere [1], and the grinding variables were held constant during this investigation. The faces and O.D. of all specimens were ground with the 320 grit wheel (D–320–N–100 Ml/16) and the I.D. was ground with the 120 grit wheel (D–120–N100Ml/16). The same grinding conditions were used in both operations:

Surface speed	30 m/s (5700 sfpm)
Infeed	6.4 × 10^{-6} m/pass (0.00025 in./pass)
Table travel	5.1 × 10^{-3} m/s (1 ft/min)
Spark-out	180 s

All specimens, except the Al–600 group, were ground to the same dimensions:

Inside diameter	5.08 × 10^{-2} m (2.000 in)
Wall thickness	2.54 × 10^{-3} m (0.100 in)
Height	7.6 × 10^{-3} m (0.300 in)

The Al–600 blanks were ground to 2.0 × 10^{-3} m (0.080 in) wall thickness, 9.5 × 10^{-3} m

(0.375 in) height, and 5.08×10^{-2} m (2.000 in) internal diameter. After grinding, the specimens were degreased in trichlorethylene vapor, thoroughly washed in detergent, and rinsed with hot water. Finally, they were dried for 1 h in an oven at 150 °C, sized, and stored for testing or for postgrinding treatments.

2.3. Testing Method and Apparatus

The ultimate tensile strength of all specimens was determined by the expanded ring test method developed at Stanford Research Institute. A description of this method can be found in the open literature [2] and will not be repeated here. All specimens were loaded to fracture at the rate of 2.1×10^{6} N/m²s (3000 psi/s).

2.4. Postgrinding Treatments

The purpose of this work was to determine whether or not a particular set of conditions to which alumina ceramics are exposed in storage and/or in testing may be responsible for a decrease in strength or some abnormal trend in test results. In this context, the influence of water on the strength of alumina is of particular interest. There is general agreement among workers in the field of strength properties of ceramics that the presence of water is detrimental to strength. However, opinions vary as to the mechanism by which water affects the strength. Some authors [3,4] believe that hydrates of alumina are formed on long exposure to water, (liquid or vapor). The majority of workers prefer the explanation that in the presence of water a stress-enhanced reaction takes place at the tip of the flaws which results in high localized stresses. The following postgrinding treatments were carried out in an attempt to clarify the part which water plays in influencing the strength of ceramics.

a. Treatment 1

Specimens were heated under a vacuum of 13.3×10^{-4} N/m² (1×10^{-4} torr) and the temperature was increased linearly in 4 hours to 1000 °C where it was held for 1 h. Then the temperature was lowered again linearly for 4 hours, until it reached approximately 300 °C; below this temperature cooling proceeded more slowly. While the specimens were still warm, 50 to 60 °C, the vacuum was broken, and the specimens were removed from the furnace and tested in air as rapidly as possible. The vacuum was expected to decompose alumina hydrates, if present, and drive off physically absorbed water. The short time for which the specimens were exposed to atmosphere during testing should not permit the formation of new hydrates and the absorption of water on the surface may not go to completion.

b. Treatment 2

Vacuum-baked specimens were placed for 2 weeks in desiccators over a saturated solution of potassium carbonate. At the room temperature of 23 °C the relative humidity in the desiccators was 43 percent. This treatment was designed to show whether prolonged exposure to water vapor would cause alumina to revert to the prebakeout conditions.

c. Treatment 3

Vacuum-baked specimens were immersed for 1 week in distilled water. Before testing, the specimens were thoroughly dried with paper towels and left to equilibrate for 1 h under ambient conditions. Only Al–300 and Al–995 aluminas were given this treatment. The objective here was the same as that of treatment 2, except that liquid water was substituted for vapor.

d. Treatment 4

Ground specimens were stored in water for 1 week, then they were dried and left to equilibrate for 1 h under room conditions. The results of exposure to water of as-ground and vacuum-baked specimens were compared.

e. Treatment 5

As-ground specimens were placed—one set at a time—in a closed jar provided with a thermometer and cooled in an ice bath slightly below the dew point. After 15 min below the dew point, the specimens were taken out of the jar, one by one, and tested as rapidly as possible.

f. Treatment 6

As-ground specimens were immersed in distilled water for a few minutes, then they were taken out, the excess water was shaken off, and the specimens were tested while they were still covered with a visible film of water. In treatments 5 and 6 the effect of liquid water on the surface of alumina under stress was appraised.

3. Results and Discussion

3.1. Evaluation of Ground Surfaces

The texture of the ground surfaces was evaluated using a Clevite Surfanalyzer 150 System. All measurements were made with the cutoff width of 7.6×10^{-4} m (0.030 in) and stylus speed of 2.54×10^{-4} m/s (0.01 in/s). The results are presented as roughness (arithmetic average, AA) and profile (defined by Standard B46.1–1962 of the American Standards Association).

Profile traces of the four materials ground identically are shown in figure 2. On these

graphs each vertical division represents 5.08 $\times 10^{-7}$ m (20 μin), and each horizontal division equals 2.54 $\times 10^{-5}$ m (1000 μin). The subscripts under the profile traces show the corresponding AA roughness values. It can be seen that there is little difference between the profile traces and the AA roughness values for the Al–300 and Al–995 aluminas, notwithstanding the sizable difference in grain size (32 $\times 10^{-6}$ m and 18 $\times 10^{-6}$ m, respectively). However, the surface of the AD–995 material is considerably smoother, and Al–600 has the best finish of all. In fact, the Al–600 finish is even slightly better than the finish obtained on Al–995 alumina, when ground with 1200 grit diamond [1]. Since all four materials have the same grinding history, it appears that the surface finish obtained in a given grinding operation is largely controlled by some inherent materials property, e.g., grain size and/or grain boundary strength.

3.2. Strength Measurements

Because of the relative nonuniformity of tensile strength data generally obtained in testing ceramics, any attempt to compare results must include a careful examination of all factors that can influence the strength. Moreover, these factors are usually interdependent, so that it is difficult, if not impossible, to isolate the effect on strength of a single factor. The factors studied in the work described were: microstructure (typified by grain size); to a lesser extent chemical composition of the test materials; and the various postgrinding treatments described in the preceding section. The test results are summarized in table 3. The data lend themselves to comparison of microstructure effects in several ways. The easiest comparison can be made between groups having no postgrinding treatment. From table 3 it is seen that the average tensile strength values (groups A–1, B–1, C–1, and D–1) cover a broad range:

Al–300–19.2 $\times 10^7$N/m^2 (27.8 $\times 10^3$ psi)
Al–995–21.6 $\times 10^7$N/m^2 (31.4 $\times 10^3$ psi)
AD–995–24.3 $\times 10^7$N/m^2 (35.3 $\times 10^3$ psi)
Al–600–27.3 $\times 10^7$N/m^2 (39.6 $\times 10^3$ psi)

The individual group strength values are distinctly different. There is no overlap of standard deviations, and the results of the statistical analyses indicate that these strength values are significantly different on the 1 percent confidence level. The increase in strength is accompanied by a decrease in grain size (see table 2) and improvement of surface finish (fig. 2).

The clear-cut difference between the strengths of the four test materials prompted a cursory comparison of the above experimental results with theoretical strength values derived from Griffith's theory of failure of brittle materials. Griffith's criterion for failure enables one to predict the strength of polycrystalline materials on the basis of known or estimated parameters, i.e., E (Young's modulus), γ (fracture

TABLE 3. *The effect of post-grinding treatments on the tensile strength of alumina*

Group	Material	Treatment	Avg. tensile strength		Std. deviation	
			N/m^2 $\times 10^7$	psi $\times 10^3$	$\pm$N/m^2 $\times 10^6$	$\pm$psi $\times 10^3$
A–1	Al–300	None	19.2	27.8	7.6	1.1
B–1	Al–995	None	21.7	31.4	12.6	1.8
C–1	AD–995	None	24.3	35.3	12.4	1.8
D–1	Al–600	None	27.3	39.6	14.7	2.1
A–2	Al–300	1	20.3	29.4	8.5	1.2
B–2	Al–995	1	23.0	33.4	7.2	1.00
C–2	AD–995	1	23.2	33.6	7.2	1.0
A–3	Al–300	2	20.3	29.5	11.4	1.7
B–3	Al–995	2	22.5	32.7	9.5	1.4
C–3	AD–995	2	23.2	33.6	9.6	1.4
A–4	Al–300	3	19.6	28.4	8.3	1.2
B–4	Al–995	3	22.6	32.8	8.1	1.2
A–5	Al–300	4	19.1	27.7	5.2	0.8
B–5	Al–995	4	21.2	30.8	7.5	1.1
C–5	AD–995	4	23.8	34.5	8.8	1.3
A–6	Al–300	5	17.4	25.2	6.6	1.0
B–6	Al–995	5	17.8	25.8	4.2	0.6
C–6	AD–995	5	22.8	33.0	11.4	1.7
A–7	Al–300	6	14.6	21.2	5.0	0.7
B–7	Al–995	6	17.0	24.6	5.1	0.7
C–7	AD–995	6	19.7	28.5	11.9	1.7

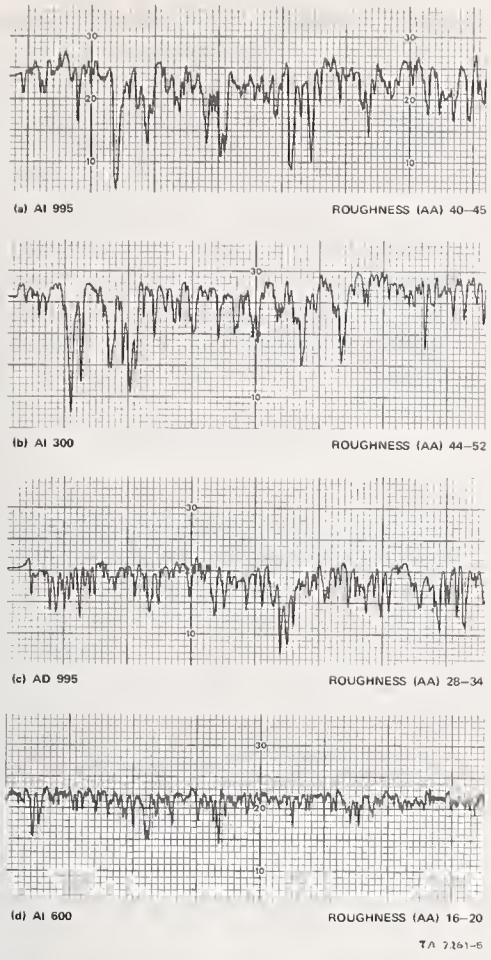

FIGURE 2. *Profile traces of surfaces of various aluminas ground with 120 grit diamond.*

surface energy), and L (maximum length of crack).

The predicted strength, S, is given by the following relationship:

$$S = \left(\frac{2\lambda E}{\pi L}\right)^{1/2} \quad (1)$$

For the sake of expediency the following assumptions were made:

$E = 37.9 \times 10^{10}$ N/m² (55×10^6 psi) for all four materials.

$\gamma = 7.0$ J/m² (see ref [5])

L = twice the average grain size when steady state has been achieved following normal grain growth [6].

Substituting these values into eq (1) for each of the four aluminas, we obtain the comparison of experimental and calculated strength data shown in table 4. The good agreement obtained tends to support the contention that grain size—rather than surface finish—is the important factor controlling strength. If one assumes that in a polycrystalline body the depth and length of a Griffith-type surface flaw is proportional to the grain size, then it is not surprising to find that changing grinding variables over a broad range (see ref [1]) does not change strength in proportion to the observed changes in surface finish. It appears that reasonable grinding conditions do not alter the density and severity of Griffith-type flaws, and consequently strength variations are relatively small. Similarly, harsh grinding conditions (deep infeed) lower strength without impairing noticeably the surface finish because the forces experienced by the work piece in grinding are sufficient to drive existing flaws beyond the one grain size limit.

3.3. Effect of Various Treatments on the Tensile Strength of Alumina

a. The Effect of Treatment 1 on the Strength of Alumina

The maximum temperature of the vacuum bakeout and the firing schedule were fixed arbitrarily, since no information was found in the literature as to the optimum conditions covering all four test materials. The results in table 3 show that the effect of vacuum bakeout on strength varies widely. The strength differences between the heat-treated specimens and those tested as ground can be considered to be the result of the vacuum bakeout on the 1 to 5 percent confidence level.

In Al–300, the bakeout produced a 5.8 percent increase in strength. In Al–995, the increase in strength was 6.4 percent. The effect of the bakeout is reversed for the AD–995 material which has a smaller grain size. In AD–995, the bakeout produced a decrease in

TABLE 4. *Comparison of calculated and experimental strength values for different aluminas*

Material	Strength calculated		Strength experimental	
	N/m² × 10^7	psi × 10^3	N/m² × 10^7	psi × 10^3
Al–300	17.9	26.0	19.2	27.8
Al–995	21.4	31.1	21.7	31.4
AD–995	25.9	37.5	25.2	36.3
Al–600	28.3	41.1	27.3	39.6

strength of 3.4 percent. Fragments of the bakedout specimens were polished and etched, and a new grain count was performed. The bakedout specimens had a significantly larger grain size, particularly the AD–995 alumina, (17.3×10^{-6} m as compared to 11.7×10^{-6} m). In Al–995 no grain growth was observed. An increase in grain size from 32×10^{-6} m to 34×10^{-6} m was observed in Al–300.

b. The Effect of Treatment 2 on the Strength of Alumina

In applying treatment 2 it was reasoned that since the attack of water must start from the surface, test specimens having different surface conditions might react differently to the same atmospheric moisture conditions. Also, if the action of water was essentially chemical in nature, materials having different compositions might show different responses. Both of these premises were found to be wrong. Taking the data from table 3 and comparing groups of specimens given treatment 1 with those that received treatment 2, we find that the differences in strength are either negligible or non-existent. We therefore conclude that exposure to atmospheric moisture under the conditions used in this program does not cause any deterioration of strength.

c. The Effect of Treatment 3 on the Strength of Alumina

After the vacuum bakeout, a group of Al–300 and a group of Al–995 specimens were immersed in distilled water for 1 week. The average tensile strength of these groups was statistically indistinguishable from that of the groups of Al–300 and Al–995 aluminas which were given treatments 1 and 2. Because of the limited number of specimens available, treatment 3 was not extended to the other materials.

d. The Effect of Treatment 4 on the Strength of Alumina

As-ground specimens were also immersed in distilled water for 1 week. Before testing, the specimens were again thoroughly dried as described previously. The Al–300 alumina (group A–5) had a slightly lower strength than groups A–3 and A–4, but the difference is negligible and it is not statistically justifiable to attribute it to treatment 4. The same is true for Al–995, where there is no meaningful difference between group B–5 and groups B–3 and B–4. In the case of AD–995, the difference is again insignificant. The strength of group C–5 is somewhat higher than the strength of other groups in the AD–995 series (C–2, C–3, and C–4) that were given a vacuum bakeout. This observation appears to corroborate the finding that the bakeout under conditions used in the work described is detrimental to the strength of this material.

e. The Effect of Treatment 5 on the Strength of Alumina

The presence of condensed water on the surface of specimens during testing caused a marked lowering of strength of the Al–300 and Al–995 aluminas (groups A–6 and B–6, respectively). The strength of AD–995 alumina (group C–6) did not seem to be affected. The reason for this is not clear, but it is possible that, because of poor control, the temperature of these specimens might have risen above the dew point.

f. The Effect of Treatment 6 on the Strength of Alumina

The strength data for groups A–7, B–7, and C–7 show conclusively that a film of water on the surface of the specimens drastically lowers the strength. An interesting fact is that the extent of strength deterioration grows larger with increasing grain size. Comparison of the strength of groups C–1 and C–7, B–1 and B–7, and A–1 and A–7 shows that the decrease in strength is 19.3 percent in AD–995, 21.7 percent in Al–995, and 24.5 percent in Al–300. The mechanism of the attack by liquid water can possibly be found in the nature of the test method used. It can be visualized that the rubber bulb transmitting the hydrostatic pressure to the specimen forces the liquid into cracks and pores on the inner wall where the water can act as a hydraulic wedge.

3.4. Vacuum Strength of Alumina

To complete the picture of the effect on strength of alumina of various post-grinding treatments—all of which involve moisture—it seems appropriate to consider the opposite situation, i.e., the strength behavior of alumina under vacuum.

It has long been suspected that atmospheric moisture is detrimental to the strength of ceramics, but this phenomenon was not properly recognized until Roberts and Watt observed that alumina specimens failed in static tension after varying lengths of time under load [7]. Pearson observed that delayed fracture can be practically eliminated when the test specimens are given a vacuum bakeout and are tested under vacuum [8].

Sometimes the deleterious effect of the moisture on the strength can assume more subtle aspects and may not be recognized as such. A good example is the effect of stress rate on strength, which has been studied previously at SRI [9]. The results of this study are shown as the S–shaped curve in figure 3 which is a plot of strength of alumina versus stress rate. When the original curve was constructed, the reasons for its existence and shape were explained on a simple mechanistic basis. It was postulated that at high stress rates the propa-

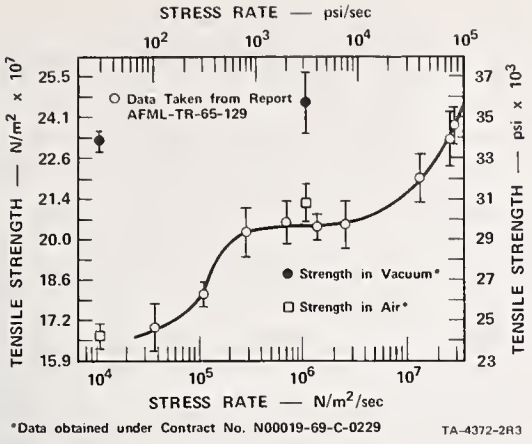

FIGURE 3. *The effect of stress rate and test conditions on the tensile strength of Al–995 alumina.*

gating crack is forced to seek the shortest route even if it entails going across grains which require a higher driving force. On the other hand, at slow stress rates, the crack is allowed to find the path of least resistance, which leads to lower strength values. However, this explanation was never considered very satisfactory and other interpretations were sought. Static fatigue studies of other workers [7, 8] provided the clue, and stress corrosion was considered. Accordingly, the following experiments were performed. Al–995 alumina specimens ground in the conventional way were tested at two stress rates, 2.1×10^4 N/m² s and 2.1×10^6 N/m² s (3×10 psi and 3×10^3 psi/s) first in air, and then under vacuum. The results are shown superimposed on the curve in figure 3 and the comparison of air and vacuum strengths is presented in table 5. The strength values obtained in air (16.8×10^7 and 21.2×10^7 N/m² -24.3×10^3 and 30.8×10^3 psi) agree closely with the old data generated on a different lot of Al–995 alumina [9]. The vacuum strengths are much higher and very similar, i.e., 23.4 and 24.7×10^7 N/m² (33.9×10^3 and 35.8×10^3 psi) and strongly indicate that under vacuum the effect of stress rate on strength is practically nil. The difference (5.3%) between vacuum strengths is small when compared to the difference between air strength values obtained at the two stress rates (21.1%). Even the 5.3 percent difference can be plausibly explained as a finite permeability of rubber separating the pressurized water from the specimen.

In the light of these results the relationship between stress rate and strength becomes quite understandable. It is safe now to presume that there is a stress-activated chemical reaction (stress corrosion) between alumina and water which takes place at the crack tip. The kinetics of this reaction are controlled by the diffusion rate. Therefore, at slow stress rates, there is a sufficient supply of water at the crack tip, stress corrosion takes place, and low strengths result. As the stress rate increases, the rate of water transport begins to fall behind the rate of force application. Stress corrosion at this point becomes diffusion or transport limited, and a plateau in strength versus stress rate is observed. Finally, at higher stress rates, stress corrosion becomes less and less active and the strengths increase.

There is experimental evidence that the water responsible for the lowering of strength of ceramics is physically adsorbed on the surface and can be easily driven off. It was not possible to obtain the same vacuum each time and experiments were carried out in the pressure range of 6.7×10^{-4} N/m² to 2.7×10^{-6} N/m² (5×10^{-5} to 2×10^{-7} torr). The variations in pressure produced no noticeable change in strength. Also the difference in lengths of time for which the specimens were kept under vacuum could not be correlated with strength.

4. Conclusions

Microstructure, typified by grain size, is the most important factor controlling the strength of ceramics. Under reasonably careful grinding conditions, surface flaws of the Griffith type penetrate only one grain depth into the body. The relationship of grain size to strength can be demonstrated by the application of Griffith's failure criterion for brittle materials. The type of surface finish obtained in grinding aluminas is not solely the result of the grinding technique, but is strongly dependent on the grain size of the ceramic. Exposure to water (liquid or vapor) does not impair the strength of alumina since hydrates were not formed. The strong de-

TABLE 5. *Average tensile strength of Al–995 alumina in air and under vacuum*

Conditions	Stress rate		Strength		Coeff. of var., percent
	N/m²s	psi/s	N/m² × 10^7	psi × 10^3	
Air	2.1×10^4	3.0×10	16.8	24.3	2.3
Vacuum	2.1×10^4	3.0×10	23.4	33.9	1.5
Air	2.1×10^6	3.0×10^3	21.2	30.8	3.2
Vacuum	2.1×10^6	3.0×10^3	24.7	35.8	4.4

pendence of the strength of alumina on stress rate is shown to be caused by stress corrosion. The strength of alumina is higher under vacuum than in air and is independent of stress rate.

The work described was sponsored by the Naval Air Systems Command under Contract Nos. NOOO19–68–C–0388 and NOOO19–69–C–0229.

5. References

[1] Sedlacek, R., Halden, F. A., and Jorgensen, P. J., The effect of grinding variables on the strength and surface finish of alumina, these proceedings.
[2] Sedlacek, R., and Halden, F. A., Method of tensile testing of brittle materials, Rev. Sci. Instr. 33, 298–300 (March 1962).
[3] Frish, B., Die Hydratation von α Aluminiumoxid, Ber. Deutsch. Keram. Ges. 42, 149–160 (1965).
[4] Charles, R. J., and Shaw, R. R., Delayed failure of polycrystalline and single-crystal alumina, General Electric Research Laboratory Report No. 62–RL–3081M, (July 1962).
[5] Wiederhorn, S. M., Fracture of sapphire, J. Am. Ceram. Soc. 52 [9], 485–491 (1969).
[6] Hillert, M., On the theory of normal and abnormal grain growth, Acta Metallurgica 13, 227–238 (1965).
[7] Roberts, J. P., and Watt, W., Mechanical properties of sintered alumina, Ceram. glass 10, 53 (1952).
[8] Pearson, S., Delayed fracture of sintered alumina, Proc. Phys. Soc. (London) 69 (ffB), 1293–1296 (1956).
[9] Sedlacek, R., Tensile Strength of Brittle Materials, Technical Report AFML–TR–65–129, (August 1965).

Discussion

FIRESTONE: I notice that you did some experiments where your specimens were immersed in water. You said that there was no significant decrease in strength, and yet when the water condensed on the surface there is.

SEDLACEK: You have misunderstood. When the specimens are immersed in water and tested wet there is a quite pronounced decrease in strength. The decrease follows the grain size; the greater the grain size, the greater the decrease in strength. However, if you immerse the specimens in water after bakeout for instance, and then take them out, wipe them, and leave them at room temperature to equilibrate for about one hour, their strength will be exactly the same as if they had not had any treatment. The same goes for variable humidity as I mentioned.

CAMERON: Would the presence of a film of moisture between the rubber membrane and your specimen act as lubricating layer leading to a more efficient load transfer?

SEDLACEK: I don't think there is a need for any lubrication because the rubber expands linearly with the expansion of the specimen. There is no friction between the two.

WIEDERHORN: About three years ago, we did some experiments on crack propagation in single crystal sapphire using the double cantilever technique.[1] Crack propagation in this case was on the (1012) twin plane. We duplicate your results if crack velocity versus the applied load is plotted.

SEDLACEK: I have seen your data. You plotted the velocity of crack propagation as a function of relative humidity and you ended up with a series of S-shaped curves.

WIEDERHORN: We had S-shaped curves and we believe that we had plateaus in the curves.

SEDLACEK: Do you have an explanation for the plateau?

WIEDERHORN: Yes. When cracks were moving fast enough the rate of crack propagation was controlled by the rate at which the water diffused to the crack tip. Water diffusion in gas is not load sensitive, therefore, the crack velocity was not sensitive to applied load in the plateau region.

WESTWOOD: What was the mechanism?

SEDLACEK: I would say that the reduction of surface energy holds for the case of the specimens being covered with a liquid film. The concept of stress corrosion is more important in this case.

WESTWOOD: May I suggest another possibility involving the Rebinder effect? Consider a crack with water in it. The water "softens" the region ahead of the crack tip, allowing dislocations to be generated and moved more easily. Subcritical crack growth then occurs by the mechanisms discussed by Bob Stokes, Freddy Clarke, and others. In other words, slow crack growth occurs because of the moisture—but not because of corrosion or surface energy reduction phenomean. You should see such effects at slow rates of loading.

HEUER: I think there are other explanations, not involving dislocation phenomena, which allow a slow rate of crack growth in the presence of a film of moisture.

WESTWOOD: Corrosion is one.

SEDLACEK: There is one thing that I would like to add if I can have the last slide back again. The curve, as I said, undergoes inflection. I must emphasize that this curve is typical only for Al 995 alumina. It may not assume exactly the same shape for other aluminas. Presently, we are working with PZT materials and they,

[1] S M. Wiederhorn, Int. J. Fract. Mech., 4, 171 (1968)

for instance, don't show any effect of different stress rates from 5000 to 150,000 psi per second.

WESTWOOD: That is an important point, because one of the things which has come out of our studies of the Rebinder effect is the fact that in ionic solids it is very sensitive to impurities. In fact, one can get adsorption-induced hardening or softening effects depending on the concentration and state of ionization of the impurities. I would imagine that if you could find the right impurity concentration (and chemistry) to give you an environment-sensitive hardening effect, you would not see delayed failure. On the other hand, corrosion or surface energy dependent processes should not be so sensitive to impurity concentration.

HEUER: No, that's not true. Impurities can also affect the surface energy. The point I was making is that you can get slow crack growth by an adsorption mechanism. The difficulty with a conventional Griffith-type approach, involving the reduction of surface energy, is that the effect is too small. On the other hand, it may be that a slow crack growth can take place at subcritical Griffith stresses if adsorption occurs.

RICE: Following along with what Bert Westwood said, you essentially explained the lower value of strength at the lower stress rate as possibly being due to an environmental problem, but it might also be an indication of, for example, a dislocation or a twin type effect since you can expect a lower strength for lower stress rates.

SEDLACEK: Well, as soon as I removed the moisture, I don't get a decrease.

RICE: Your chart showed somewhat lower strengths at lower stress rates.

SEDLACEK: Because the membrane is not completely impermeable.

RICE: Right, but that's one hypothesis, but I'm saying another. Dislocations or twins are important, and these would also cause lower strengths.

RHODES: We have noticed similar effects in hot pressed alumina. I think for the record I would like to ask whether or not your alumina is free of glassy phase.

SEDLACEK: No, it is not. It is nominally 99.5 percent alumina and it has about 0.3 percent silica. So it has a glassy phase.

NATIONAL BUREAU OF STANDARDS SPECIAL PUB. 348, THE SCIENCE OF CERAMIC MACHINING AND SURFACE FINISHING, Proceedings of a Symposium Sponsored by the American Ceramic Society, the Office of Naval Research, and the National Bureau of Standards, held at NBS Nov. 2–4, 1970, Gaithersburg, Md. (Issued May 1972).

Grinding Alumina with Diamond Abrasives

R. J. Caveney and N. W. Thiel

De Beers Diamond Research Laboratory
Johannesburg, South Africa

This paper is the result of a preliminary investigation into the grinding of high density alumina with diamond abrasive grinding wheels.

Following extensive work on the application of diamond for tungsten carbide and steel grinding, the De Beers Diamond Research Laboratory recently embarked on a research programme to study the various aspects of ceramic grinding. In the Diamond Abrasive Technology Centre's Grinding Section, ceramics with three different alumina contents were ground with a variety of diamond types both natural and synthetic to establish what effect changes in wheel speed have when surface grinding these materials. The mode and extent of damage of the ground surfaces of the specimens were investigated using conventional electron microscopy. In addition to these investigations, measurements were made of the quality of the surface finishes that can be obtained under different grinding conditions. Variations in grinding efficiency, machining costs and surface damage are discussed for the three alumina grades tested. The mechanism of wear of the different diamond types was studied and is demonstrated by means of scanning electron micrographs.

Also reported in this paper, are the initial results obtained from tests on cylinders of the same three alumina grades mentioned above. These initial tests were aimed at finding the most suitable combination, from the point of view of wheel life, of wheel and workpiece speeds, and incorporated tests with both natural and synthetic grits.

Key words: Alumina; cylindrical grinding; diamond grinding wheel; electron microscopy; removal mechanism; surface damage; surface finish; surface grinding; wear mechanism.

1. Introduction

Little has been published on the science and technology of grinding ceramics with diamond abrasive wheels. Many articles have, however, demonstrated the feasibility, utility and economy of diamond wheels in this application. It is further known that diamond wheels are used extensively in the ceramics industry. Due to the lack of published data, it is not known whether this use has been optimised using scientific and economic principles. For these reasons, the De Beers Diamond Research Laboratory recently embarked on a research programme to establish the techniques and fundamentals of the diamond grinding of ceramics. The present paper and an associated paper [1][1] report the preliminary results of this study.

The underlying principle on which this work has been based is that the maximum removal rate consistent with surface damage that is not excessive should be employed. In order to evaluate surface damage, it was necessary to undertake an electron microscope study of the workpieces after grinding. This study also enabled an assessment of the mode of material removal to be made. Besides stock removal and surface damage, surface finish or roughness must also be determined and the latter minimised.

As was noted earlier, this work is still in its initial stages. Only three grades of alumina have been studied, namely 85 percent, 94 percent and 96 percent alumina. The material ground was in the form of large blocks. At a later stage it is anticipated that ceramics with alumina contents greater than 99 percent will be studied, and the effect of the grinding parameters on the chipping of small samples will be evaluated.

1.1. General Test Conditions

It is well known that the condition of the surface of a diamond abrasive grinding wheel can have a considerable effect on the results obtained by the wheel. Because of this fact all the wheels used in this test programme were given a conditioning run under the test conditions before the actual tests were started.

A coolant flow rate of 3 litres per min (40 gallons per hour), measured by rotameters, was used throughout the tests. Coolant tanks were replenished with premixed coolant at the start of each test and completely renewed after five tests. Each machine is equipped with a centrifuge to clarify the used coolant and the bowl of the centrifuge, containing the grinding sludge, was cleaned at the end of each test.

Since the tests were initially aimed at achieving a high stock removal rate, no attempt was made to obtain good surface finishes. At the end of each of these stock removal rate tests,

[1] Figures in brackets indicate the literature references at the end of this paper.

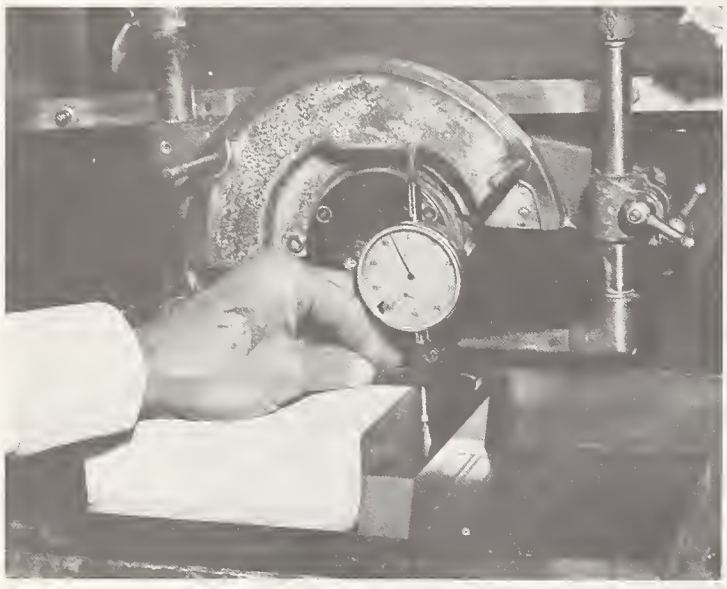

FIGURE 1. *Measurement of specimen block for amount of material removed.*

a spark-out, without downfeed, of two full passes across the specimen was given. A further investigation was carried out at the conclusion of the stock removal programme to determine the surface finish that could be obtained. Measurements of the surface finishes obtained were carried out with Hommel-Tester Type T equipment, the figures quoted being AA or middle roughness values.

The amount of material removed from a specimen during a test was measured, in the case of surface grinding, with a dial depth indicator (see fig. 1) at each corner of the ground block before and after the test, and with micrometers in the case of the cylindrical specimens. In surface grinding the average amount of material removed in one test was 345 cm^3 (21 in^3), while, for cylindrical grinding, the average removal was 800 cm^3 (49 in^3).

After each conditioning run or test, the wheels were placed in a temperature controlled measuring room (held at 20° C ±½ deg) for at least 24 hours before measurements were made. This is the standard procedure used in the Diamond Abrasive Technology Centre's Grinding Section, since it allows the wheel to overcome the effects of centrifugal and thermal expansion.

The amount worn from the wheels during a test was measured on special jigs (see fig. 2 and 3).

The wheel efficiency, *G* ratio, is the ratio of volumes worn from the specimen and the wheel during a test.

$$G = \frac{\text{Volume material removed}}{\text{Volume wheel worn away}}$$

Calculations of cost have been made at a rate of $12.00 per hour for machine, operator and overhead costs, and $25 per cubic centimeter

FIGURE 2. *Special jig for measuring wear of wheels for surface grinding tests.*

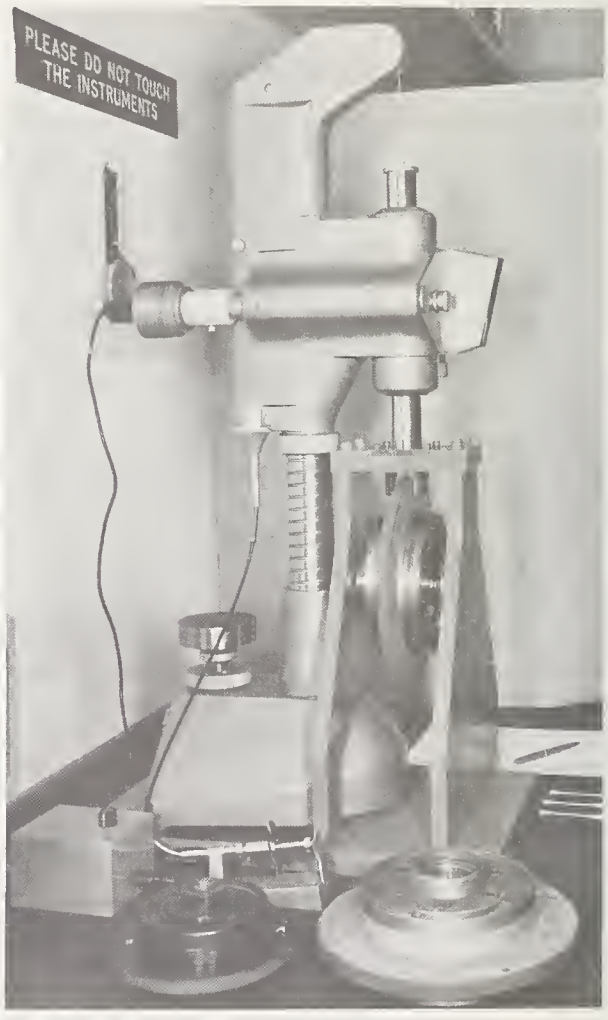

FIGURE 3. *Special jig for measuring wear of wheels for cylindrical grinding tests.*

of grit-bearing bond for 100 concentration wheels.

2. Surface Grinding

2.1. Introduction

This preliminary investigation of the effect of alumina content and wheel speed on grindability, with different diamond and bond types, was conducted on horizontal spindle, reciprocating table surface grinders. This type of grinder had to be used because the Diamond Abrasive Technology Centre (D.A.T.C.) does not, at present, have machines of the vertical spindle, rotary table type, on which the greater proportion of surface grinding of ceramics is done. Further tests on the latter type of machine are planned for the future.

Three different alumina types were ground with ten different wheels. Of the ten, six were metal bond wheels containing three grit types in each of two sizes, while the remaining four wheels contained two different resin bond grits also in two sizes. Initially the machines were set at maximum crossfeed and table speed (1.75 mm (0.070 in) and 20 m/min (65 ft/min) respectively), and the downfeed was increased from 0.025mm (0.001 in) to 0.0625 mm (0.0025 in) per pass. When an attempt was made to use a downfeed of 0.125 mm (0.005 in), the machines stalled and both crossfeed and table speed had to be reduced.

It was found that by reducing the crossfeed and table speed to the D.A.T.C.'s standard values used for tungsten carbide grinding, viz 1.5 mm (0.060 in) and 16 m/min (53 ft/min) respectively, and the 0.125 mm (0.005 in) downfeed, the maximum stock removal rate was achieved. Because of the relatively small surface damaged caused by this heavy downfeed, all subsequent tests, with the exception of surface finish tests, were conducted under these conditions. The wheels were then run at three different peripheral speeds on each ceramic type to ascertain the effect on the grinding efficiency.

The ceramic workpieces, before and after etching, were examined in the electron microscope, and the depth of damage assessed. The modes of diamond wear and wheel wear were studied using optical and scanning electron microscopy.

2.2. Test Conditions

Machine	Two Jones and Shipman 540 Tool Room Surface Grinders with 1.5 kw (2 hp) spindle drive motors.
Wheel type	D1A1
Wheel size	127 × 6.3 × 31.8 mm (5 × ¼ × 1¼ in)
Wheel speeds	3000, 4000, 5000 r.p.m.
Wheel peripheral speeds	19.9, 26.6, 33.3 m/sec (3930, 5240, 6650 ft/min)
Diamond types	De Beers RDAR55N, DXDA–MC (resin bond), DXDA, MDA–S, SND–MB (metal bond)
Diamond mesh sizes	80/100 and 140/170 U.S. mesh.
Diamond concentration	100
Bond depth	3.1 mm (⅛ in)
Downfeed	0.125 mm per pass (0.005 in)
Total downfeed per test	22.5 mm (approx ⅞ in)
Crossfeed	1.5 mm per table reversal (0.060 in)
Table traverse speed	16 m/min (53 ft/min)
Coolant	Water plus Bryto 5 (100:1)
Coolant flow rate	3 l/min (40 gallons per hour)
Specimen types	Coors AD 85, 94, 96
Specimen face size	152.4 × 101.6 mm—155 cms² (6 × 4 in—24 in²)
Sparkout	Two spark out passes, without downfeed at the end of each test.

The initial surface damage tests were carried out with a table traverse speed of 20 m/min (65 ft/min), a crossfeed of 1.75 mm per table reversal (0.070 in) and 4000 rpm wheel speed.

2.3. Test Results

The results of the wheel efficiency tests under the above conditions are given in figures 4, 5 and 6. The results of examinations of the wheels and workpieces are discussed below.

2.4. Discussion

In the ensuing discussion, frequent mention is made of the various grit types.

RDA55N is a metal clad synthetic diamond abrasive designed for use in resin bond wheels. The underlying particle is characterised by its friability and irregular shape. The metal cladding, 55 per cent by weight, results in better retention of the diamond particles in the wheel bond.

DXDA consists of strong, fracture resistent diamond particles which are blocky with a controlled proportion of cubo-octahedra. This grit is used in metal bond wheels. The same grit, after metal cladding, is known as **DXDA–MC** and is used in resin bond wheels.

MDA–S consists of very strong synthetic

439-921 O - 72 - 8

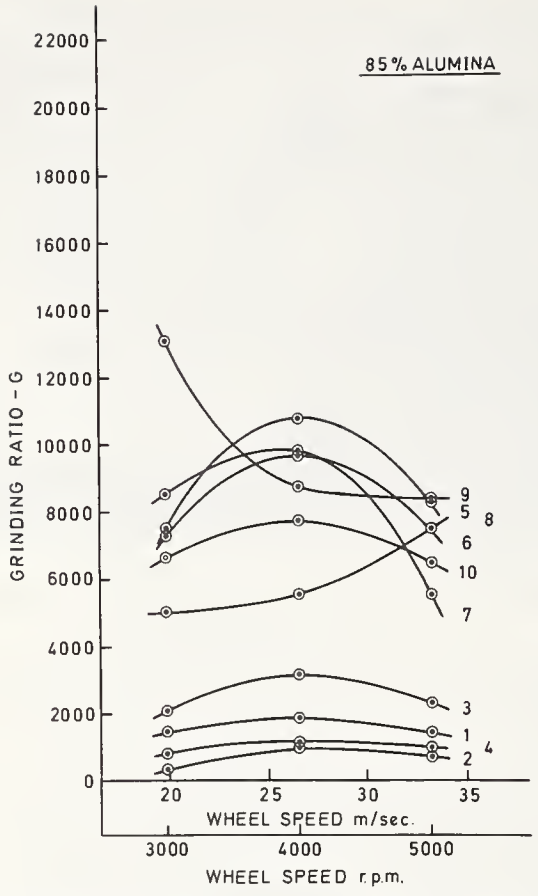

FIGURE 4. *Changes in grinding ratio with wheel speed for 85 percent alumina.* Resin bond wheels: 1. DXDA–MC 80/100, 2. DXDA–MC 140/170, 3. RDA55N 80/100, 4. RDA55N 140/170. Metal bond wheels: 5. MDA–S 80/100, 6. MDA–S 140/170, 7. SND–MB 80/100, 8. SND–MB 140/170, 9. DXDA 80/100, 10. DXDA 140/170.

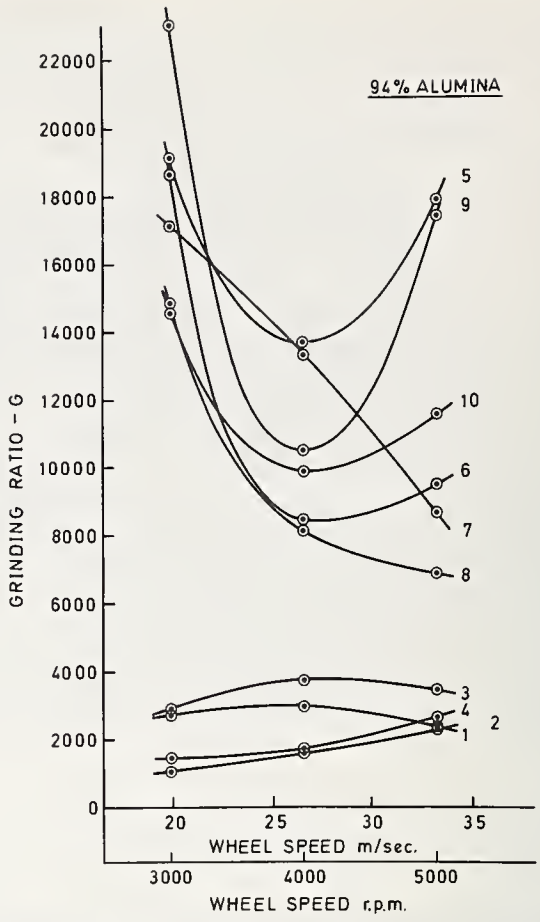

FIGURE 5. *Changes in grinding ratio with speed for 94 percent alumina.* (Curves marked as in fig. 4).

diamond crystals, mainly cubo-octahedra, for use in metal bond wheels.

SND–MB is a natural diamond abrasive designed for use in metal bond wheels. This grit consists of strong, blocky particles which are prepared from larger diamonds using a milling process.

a. Examination of the Workpieces

Two sets of observations were made. The unetched workpieces of all three grades of alumina were studied after grinding tests at 4000 rpm and infeeds of 0.025, 0.0625 and 0.125 mm (0.001, 0.0025 and 0.005 in). Replicas, prepared using a water soluble plastic [2, 3], of the ground surface and the face perpendicular to the ground surface (and parallel to the grinding direction) were studied in a Philips EM200 electron microscope. The second set of observations was made on etched (one minute in boiling NaOH) ground surfaces of the three ceramics after grinding tests at 4000 rpm and 0.125 mm (0.005 in) downfeed.

(1) **Unetched Specimens.** Damage of the grains in the ground surface was noted in almost all cases. The surface structure consisted of fracture surfaces of grains, and freshly exposed grain surfaces, some of which exhibited traces of cracks. The degree of damage varied depending on the wheel with which the material was ground and the grinding parameters. In the case of the 85 percent alumina, some evidence of extrusion of the binder material was noted. This is illustrated in figure 7 for the 85 percent alumina ceramic ground with a resin bond wheel containing the 140/170 RDA55N grit.

Figure 7 also shows the multiple grain fracture characteristic of the surfaces ground with resin bond wheels containing 140/170 RDA55N. This is further illustrated for the 96 percent alumina in figure 8. The same behaviour, but to a lesser degree, was noted for the resin bond wheels containing 80/100 RDA55N and 140/170 DXDA–MC, and the metal bond wheel containing 140/170 SND–MB. These observations are similar to those made on tungsten carbide-cobalt composites after grinding with resin bond wheels [4]. In this case, cobalt is extruded to the free surfaces and the carbide grains are extensively fractured.

The ground surface of the ceramics machined with metal bond wheels containing MDA–S and

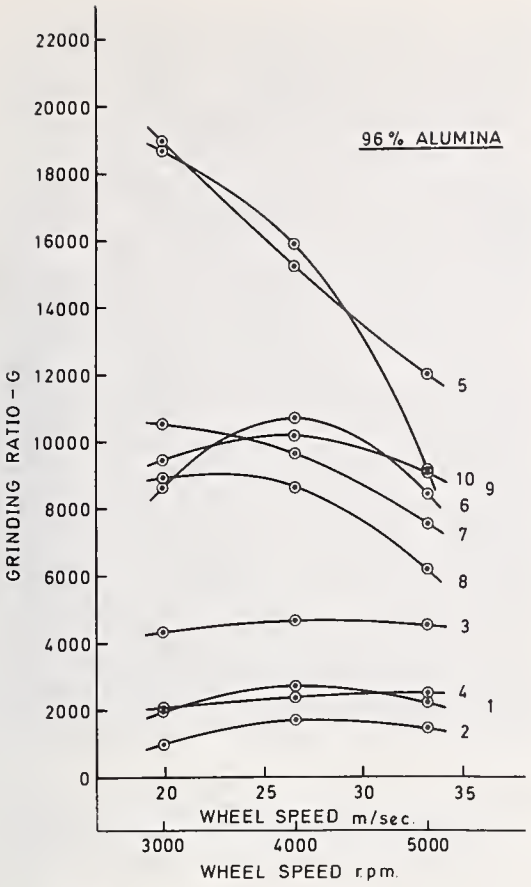

FIGURE 6. *Changes in grinding ratio with wheel speed for 96 percent alumina.* (Curves marked as in fig. 4).

DXDA grits exhibited fairly extensive fracture of the grains (see figure 9). The degree of fracture and extrusion was less than for the ceramics ground with resin bond wheels as described earlier. This behaviour is different from that of tungsten carbide-cobalt composites when grinding with metal bond wheels [4], where extensive cobalt extrusion and minimal fracture of the grains were noted. The differences are most likely due to the different flow characteristics of the binder materials and the different strengths of the tungsten carbide and aluminum oxide grains.

Less grain damage was observed for the ceramics ground with the resin bond wheel containing 80/100 DXDA–MC and the metal bond wheel containing 80/100 SND–MB. This is illustrated in figure 10. Another interesting observation is that there appears, when grinding with these wheels, to be a tendency for the damage to decrease on increasing the severity of the grinding above a critical level.

On studying the face perpendicular to the ground surface, it was noted that the damage was, for the most part, confined to the surface layer of grains. The depth of damage did not increase appreciably on increasing the infeed from 0.0625 mm (0.0025 in) to 0.125 mm (0.005 in); in the latter case, a few grains in the second layer below the surface exhibited

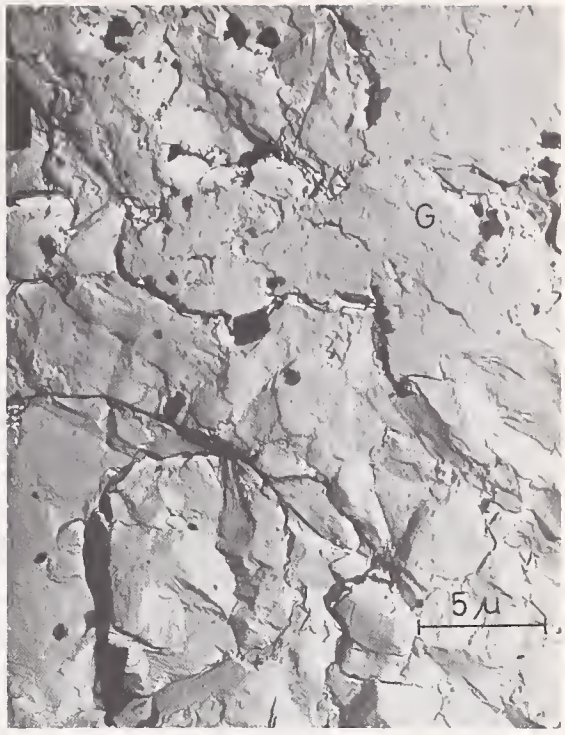

FIGURE 7. *Electron micrograph of a replica of the surface of 85 percent alumina after grinding with a resin bond wheel containing 80/100 RDA55N.* Extruded binder material (*G*) is observed.

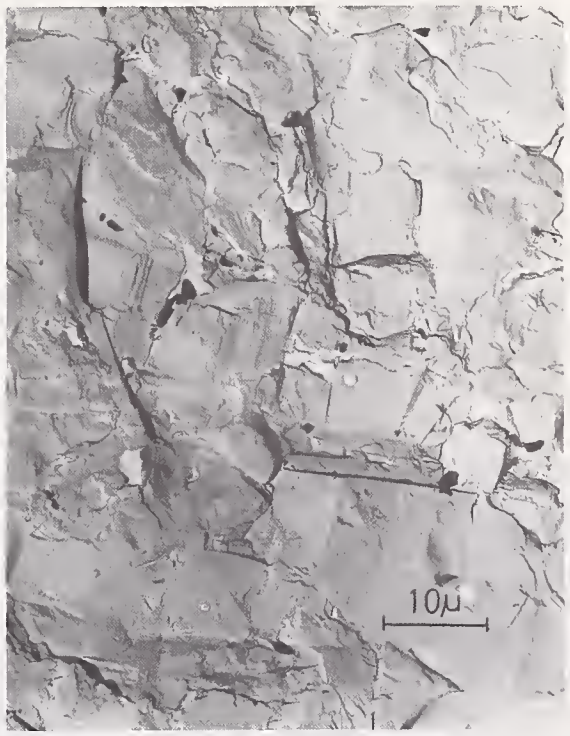

FIGURE 8. *Electron micrograph of a replica of the surface of 96 percent alumina after grinding with a resin bond wheel containing 140/170 RDA55N.*

fracture (see figure 11). Elimination of "spark-out" does not appear to affect the extent or depth of damage.

(2) **Etched Specimens.** It was difficult to assess the damage because of the fact that both the fracture and grain surfaces have a similar

FIGURE 9. *Electron micrograph of a replica of the surface of 96 percent alumina after grinding with a metal bond wheel containing 80/100 MDA–S.*

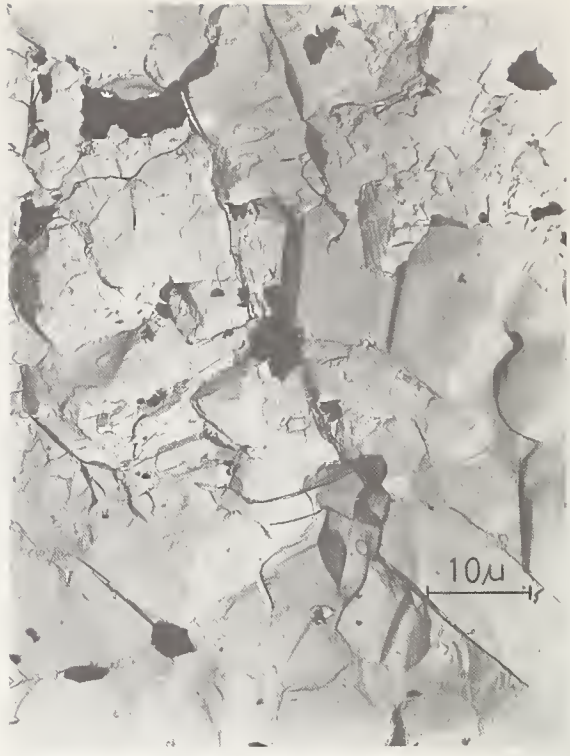

FIGURE 10. *Electron micrograph of a replica of the surface of 96 percent alumina after grinding with a resin bond wheel containing 80/100 DXDA–MC.*

appearance after etching. However, the grain boundaries are more readily observed, and the fracture cracks readily observed as shown in figure 12. The assessment of damage gave the same results as described for the unetched specimens.

b. Study of the Grinding Wheels

The wheels, after grinding the 96 percent alumina at 4000 rpm and 0.125 mm (0.005 in) infeed, were studied by means of optical scanning electron microscopy. A plastic replica technique [3] was used to study the macroscopic specimens in the scanning electron microscope.

The degree of retention of the grit in the bond, and the mode of diamond wear, are summarized in table 1.

For the resin bond wheels, the RDA55N grits are better held in the bond than the DXDA–MC grits. This is particularly noticeable in the 80/100 size range. This effect is caused by the increased roughness of the RDA particles, and hence the coated grit surface, compared to the DXDA particle. The 140/170 grits are better retained in the bond than

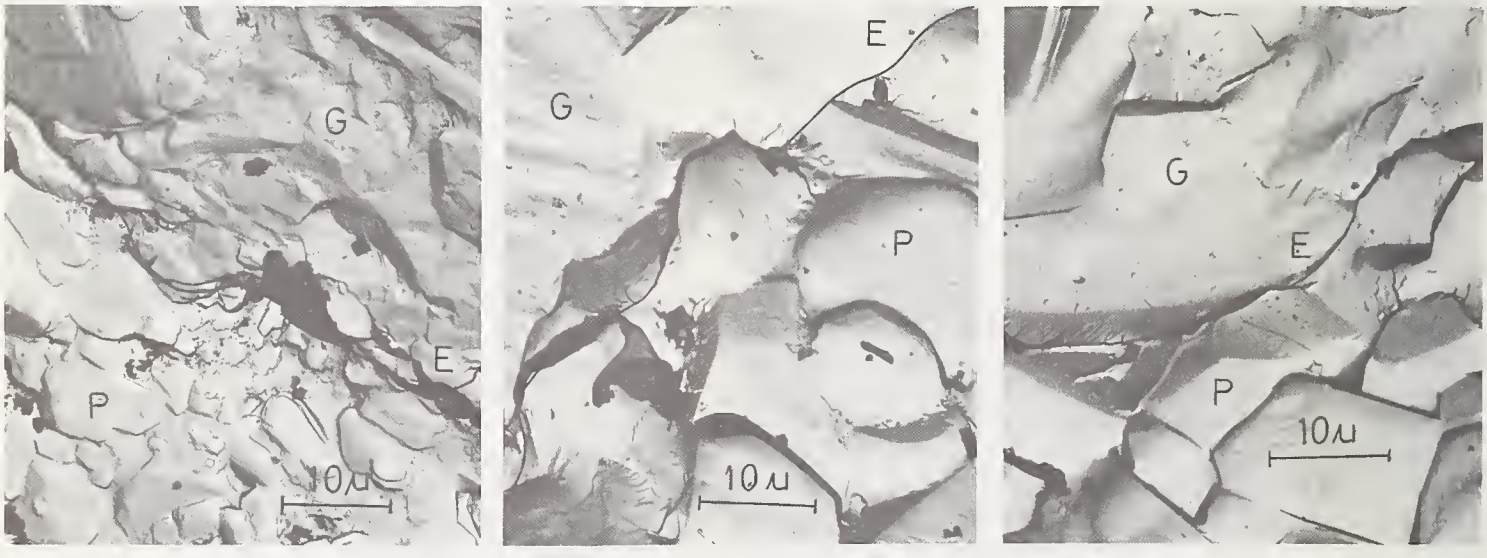

FIGURE 11. *Electron micrographs of replicas showing the ground surfaces (G), the edge (E) and the face perpendicular to the ground surface (P) of (a) 85 percent alumina, (b) 94 percent alumina and (c) 96 percent alumina after grinding with a metal bond wheel containing 80/100 MDA–S (0.125 mm (.005 in) downfeed).*

FIGURE 12. *Electron micrograph of a replica of an etched 96 percent alumina surface after grinding with a metal bond wheel containing 140/170 SND–MB.*

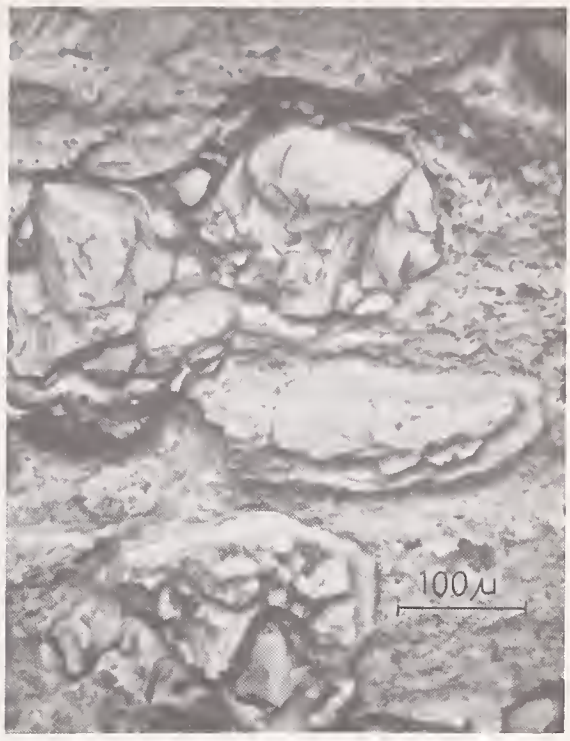

FIGURE 13. *Scanning electron micrograph of a replica of the resin bond wheel containing 80/100 RDA55N.*

the 80/100 grits. The percentage of grits retained in the metal bond wheel is of the order of 80 percent, regardless of size. The SND–MB grit retention is superior to that of the MDA–S and DXDA grits due to the serrated nature of the surface of the SND-MB grit particle. The DXDA grit appears to be held better than MDA–S grit in the 80/100 size, and vice-versa for the 140/170 size.

From table 1 it is apparent that the mode of diamond wear is different for the different types of grit. As observed after grinding tungsten carbide-cobalt composites, the RDA grit particles are extensively fractured (figure 13). The RDA grit is engineered to be of a friable nature and suffers repetitive multiple fracture so that sharp fracture points are continuously presented to the workpiece. The 140/170 DXDA–MC grit in a resin bond wheel has a similar fractured appearance to the RDA grit, except that a significant amount of abrasion wear is present.

TABLE 1. *Summary of wheel observations*

Grit	Size	Bond	Percentage retention in bond	Percentage of grit exhibiting no wear	Percentage exhibiting predominantly abrasion wear	Percentage exhibiting predominantly fracture wear
DXDA–MC	80/100	R	50	12	55	33
DXDA–MC	140/170	R	72	13	32	55
RDA55N	80/100	R	73	Predominantly fracture, small abrasion marks on approximately 60 percent of grit particles.		
RDA55N	140/170	R	81	Very little abrasion observed.		
MDA–S	80/100	M	78	2	55	43
MDA–S	140/170	M	84	12	55	33
SND–MB	80/100	M	86	8	36	56
SND–MB	140/170	M	86	9	36	55
DXDA	80/100	M	82	11	57	32
DXDA	140/170	M	75	4	67	29

FIGURE 14. *Scanning electron micrograph of a replica of the metal bond wheel containing 80/100 DXDA.*

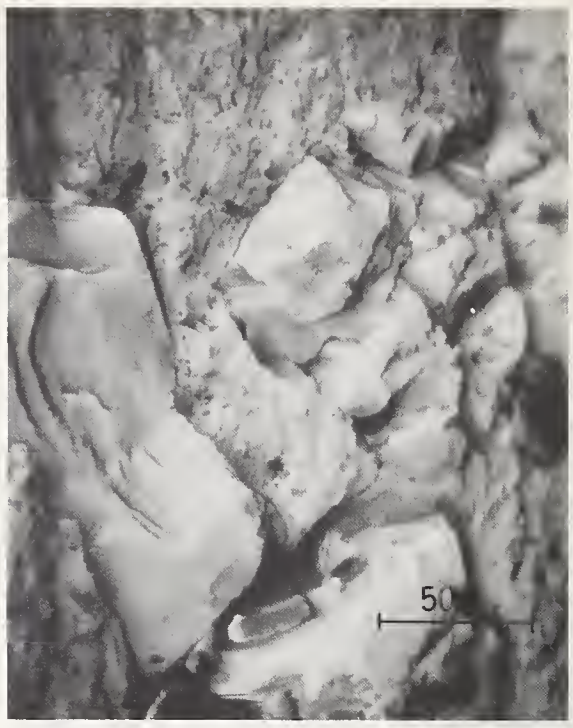

FIGURE 15. *Scanning electron micrograph of a replica of the metal bond wheel containing 140/170 SND–MB.*

Abrasion wear flats are dominant in the MDA–S and DXDA grits in the metal bond wheels (fig. 14). Most of the SND–MB grits in the metal bond wheels have a predominantly fractured appearance; some abrasion wear is, however, present (fig. 15). The behaviour of the SND–MB grits is caused by the fracture centres introduced in the milling process, as opposed to the as-grown strong MDA–S and slightly weaker DXDA grits.

Of the grit particles present in the surface of the 80/100 DXDA–MC wheel, 55 percent exhibit predominantly abrasion wear flats. However, only 50 percent of the grit particles are retained in the bond, and hence the role of abrasion wear is not as dominant as is the case with the MDA–S and DXDA grits in the metal bond wheels (for example: 80/100 MDA–S, 55 percent of diamond grit particles exhibit predominantly abrasion wear flats, but 78 percent of the grit particles are retained in the wheel). In fact the balance between abrasion and fracture of the grit in the 80/100 DXDA–MC resin bond wheel is similar to that of the 80/100 SND–MB metal bond wheel. Grit pull-out, however, starts at an earlier stage in the working history of a grit particle for the DXDA–MC grit than for the SND–MB grit. The balance between the abrasion and fracture modes of diamond wear is dependant on the effective strength of the grit particles and the bond in which the grit is incorporated.

c. Grinding Efficiencies

(1) **85 percent Alumina.** As is shown in figure 4, with the exception of two of the wheels, the highest efficiencies on this ceramic are achieved at a wheel speed of 26.6 m/s (5240 ft/min). The exceptions are the metal bond wheels with 140/170 SND–MB grit, which shows an increase in efficiency as the wheel speed increases, and with 80/100 DXDA, which shows a decrease in efficiency with an increase in wheel speed. At this stage, there can be no definite explanation of why these two grits should behave in this way, but it is thought that a change in mode of grit wear could be the cause of the different behaviour of the SND–MB wheel.

Clearly, the resin bond wheels containing RDA55N and DXDA–MC do not perform as well as the metal bond wheels. It is interesting to note that the weaker resin bond grits (RDA55N) give higher efficiencies at all speeds and in both grit sizes.

With the exception of the anomalous behaviour of the metal bond wheel containing 80/100 DXDA (highest G ratio at 3,000 rpm), the wheel containing 80/100 MDA–S appears to give the best grinding efficiencies.

(2) **94 percent Alumina.** From figure 5 it is immediately apparent that this material grinds in an entirely different way from the 85 percent alumina. With the 94 percent alumina, there are only two wheels that achieve the highest *G* ratio at 26.6 m/s, these being the resin bond 80/100 DXDA–MC and RDA55N wheels. The same grit types in the 140/170 size show an increase in efficiency as the wheel speed increases. On the other hand, the SND-

MB wheels decrease in efficiency as speed increases, the *G* ratio at 33.3 m/s (6550 ft/min) being only 50 percent of that obtained at 19.9 m/s (3930 ft/min) for the 80/100 grit size and 46 percent for the 140/170 grit size.

The other metal bond wheels give their lowest *G* ratios at 26.6 m/s (5240 ft/min). Before any conclusions can be drawn from these trends it is obvious that further tests are necessary at higher and lower speeds.

One other fact that is surprising is that the *G* ratios when grinding 94 percent alumina are generally higher than those obtained on 85 or 96 percent.

(3) **96 Alumina.** It can be seen from figure 6 that 96 percent alumina grinds in a similar manner to 85 percent. The resin bond wheels show a general peak in efficiency at about 27 m/s (5300 ft/min). The *G* ratios at this speed can be correlated with the appearance of the wheel surface i.e., grit pull-out and grit wear mechanisms. The RDA55N wheels have higher efficiencies and higher grit retention than the DXDA–MC wheels. This is shown in table 2.

The SND–MB grit has the best retention in the metal bond wheels. However, grit wear, in this case, is mainly by fracture, and hence more rapid than when abrasion wear is dominant. For this reason, the wheels containing SND-MB have lower grinding efficiencies than those containing MDA–S and DXDA grits when grinding at 26.6 m/s (5240 ft/min). The MDA–S and DXDA grits have the same basic wear pattern, and hence grinding efficiencies are, to a large degree, dependant on grit retention. This is illustrated in table 3 and figure 6.

The patterns of behaviour of the DXDA and 140/170 MDA–S wheels on this material are again similar to those on the 85 percent alumina. Here, however, the 80/100 MDA–S wheels also decrease in efficiency as the speed increases, and the SND–MB wheels behave in a similar way. In fact, the trends of the latter wheels are very similar on 94 and 96 percent alumina.

It should be noted, however, that the diamond grit wear mechanism may change with grinding conditions. This is especially true for the 80/100 DXDA–MC grit in a resin bond wheel and the 80/100 SND–MB grit in a metal bond wheel. Under light grinding conditions, abrasion wear will play a dominant role, but as the conditions become more severe, the balance will swing to fracture wear with a corresponding large decrease in grinding efficiencies.

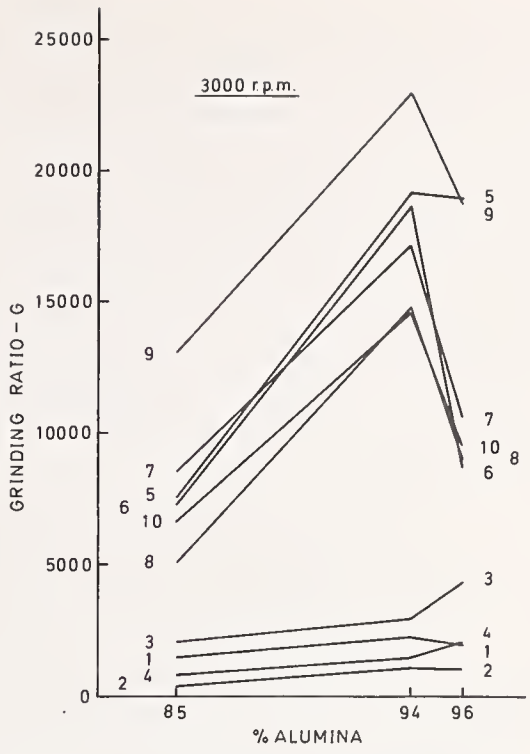

FIGURE 16. *Changes in grinding ratio with alumina content for 3000 rpm.* Resin bond wheels: 1. DXDA–MC 80/100, 2. DXDA–MC 140/170, 3. RDA55N 80/100, 4. RDA55N 140/170. Metal bond wheels: 5. MDA–S 80/100, 6. MDA–S 140/170, 7. SND–MB 80/100, 8. SND–MB 140/170, 9. DXDA 80/100, 10. DXDA 140/170.

It is felt that these concepts apply to all the workpieces and grinding conditions.

(4) **Effect of Alumina Percentage.** The ways in which alumina percentage affects grinding efficiencies for the three wheel speeds used are shown in figures 16, 17 and 18.

At 19.9 m/s (3930 ft/min) all wheels, except the resin bond wheels containing RDA55N grits, achieve their highest efficiencies on 94 percent alumina, with 85 percent being the most difficult to grind in all cases. This grade is also the hardest to grind with the RDA55N

TABLE 2. *Comparison of grinding ratio and grit retention for the resin bond wheels, (96% alumina, 0.125 mm (0.005 in) downfeed and 4000 rpm)*

Grit	Size	Percentage grit retention	Grinding ratio
RDA55N	80/100	73	4660
DXDA–MC	80/100	50	2720
RDA55N	140/170	81	1990
DXDA–MC	140/170	72	1720

TABLE 3. *Comparison of the grinding ratio and grit retention for metal bond wheels containing MDA–S and DXDA (96% alumina, 0.125 mm (0.005 in.) downfeed and 4000 rpm)*

Grit	Size	Percentage grit retention	Grinding ratio
MDA–S	80/100	78	15,260
DXDA	80/100	82	15,920
MDA–S	140/170	84	10,700
DXDA	140/170	75	10,190

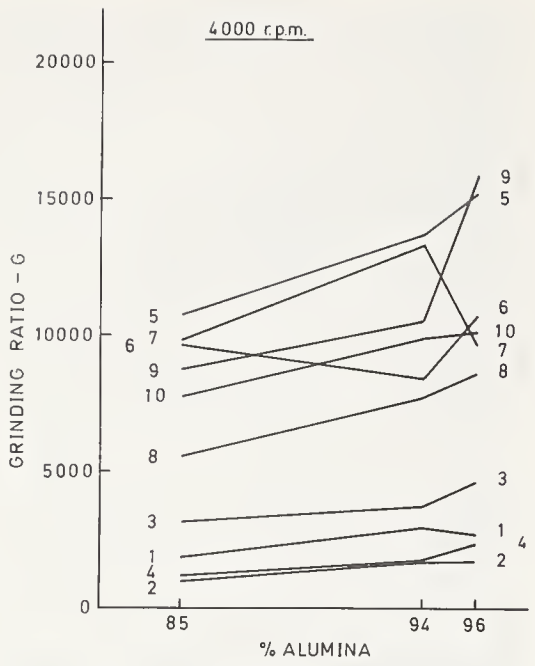

FIGURE 17. *Changes in grinding ratio with alumina content for 4000 rpm* (Curves marked is in fig. 16).

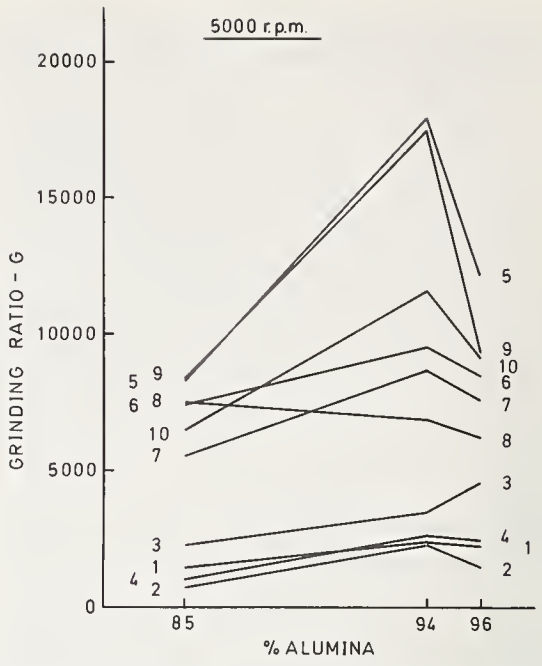

FIGURE 18. *Changes in grinding ratio with alumina content for 5000 rpm* (Curves marked as in fig. 16).

wheels. These latter wheels, however, achieve their highest G ratios on 96 percent alumina.

At 26.6 m/s (5240 ft/min) the pattern changes and this can be related to the appearance of the ground surfaces. With the exception of the surfaces ground with the resin bond wheel containing 80/100 DXDA–MC and the metal bond wheel containing 80/100 SND–MB the damage on the ground surface generally increases with increasing alumina content. The grinding efficiencies also increase. For the 80/100 DXDA–MC resin bond wheel and the 80/100 SND–MB wheel, the amount of damage after grinding the 96 percent alumina was less than that on the 85 percent and 94 percent aluminas. The grinding efficiencies also correspondingly decreased. It appears, therefore, that the efficiency and surface damage are related. This is interpreted as a change of diamond grit wear from a dominant abrasion wear mechanism to a dominant fracture mechanism on increasing the alumina content of the workpiece.

With a wheel speed at 33.3 m/s (6550 ft/min), only the RDA55N 80/100 and 140/170 SND–MB wheels are exceptions to the same trend as found at 19.9 m/s (3930 ft/min) i.e., highest G ratios on 94 percent and lowest on 85 percent alumina. The 140/170 SND–MB wheel exhibits an unusual decrease in efficiency with increase in alumina content.

d. Material Removal Mechanism

The alumina is removed by two basic processes, fracture of the grains and subsequent removal of the fracture pieces, and removal of the individual grains. This is analogous to the removal of material when grinding tungsten carbide-cobalt composites [4]. The balance between these two modes depends upon the nature of the grit surface presented to the workpiece.

When many fracture points are presented to the workpiece, as is the case when grinding with the RDA type grits, then the principal mode of material removal is by grain fracture and removal of the fractured pieces. When the grit has many abrasion wear flats (MDA–S and DXDA in metal bond wheels), then a certain amount of crushing of the grains occurs, and some grains are removed individually. The fracture of the 80/100 DXDA–MC and SND–MB grits appears to favour removal of individual alumina grains. The difference between the behaviour of the two forms of fractured grit, i.e., the RDA type and the DXDA–MC/SND–MB type, can be explained as follows. In the RDA type grit, the fracture is governed by the metal inclusions and other such bulk defects in the diamond particles; hence a large number of very sharp points are presented to the workpiece. For the stronger blocky grits, however, the fracture is controlled by surface energies, i.e., usually takes place along cleavage plains and hence the fracture points are not generally as sharp as those found for the RDA type grits. These "blunter" fracture points have the ability to remove individual grains.

e. Surface Finish

As indicated earlier, two spark-out passes, without downfeed, were given at the end of each test. The surface finishes obtained in this

way for the tests at a wheel speed of 26.6 m/s (5240 ft/min) on 96 percent alumina are given in table 4.

At the conclusion of the *G* ratio tests, the wheels were redressed to get a flat profile and then given the following runs on the material mentioned above and at the same speed:–

5 passes at 0.025 mm (0.001 in) downfeed.
2 passes at 0.01 mm (0.0004 in) downfeed.
2 passes at 0.005 mm (0.0002 in) downfeed.
2 spark-out passes.

The surface finishes obtained in this way are also given in table 4.

It is evident that the surface finishes obtained at the end of the *G* ratio tests are far from good. However, one point shows up clearly. Most of the metal bond wheels used on ceramics at the present time contain natural diamond and it is frequently stated that better surface finishes can only be obtained with resin bond wheels. The figures, however, show that with DXDA in the metal bond, finer finishes can be obtained than with resin bond wheels. This is true even when the finishing technique given above is used.

Although the quoted figures obtained using the above technique are not yet considered good for ceramics, one point must not be overlooked. The Standards of the Alumina Ceramic Manufacturers Association [5] are based on a measuring instrument stylus having a 0.013 mm (0.0005 in) radius. The figures given in table 3 were, however, measured with a stylus having a radius of 0.005 mm (0.0002 in) i.e., smaller than the average grain size of 0.011 mm (0.0004 in) of the 96 percent alumina tested.

f. Grinding Costs

Complaints about the high costs of grinding ceramics are very common but in the light of the results of this preliminary investigation, these complaints are not really justified. It must, however, be borne in mind that the grinding conditions used here are extremely severe, when compared with conditions normally used in the ceramic industry. Despite this fact, the wheel costs are very low, the highest wheel cost throughout this investigation being only 6.8 cents (U.S.) per cubic centimeter of material removed, compared with a wheel cost of 17.6 cents (U.S.) per cubic centimeter of material removed with a good wheel of the same size grinding tungsten carbide at a downfeed of only 0.025 mm (0.001 in). [6]. The lowest wheel cost achieved when grinding alumina in this test series was 0.11 cents (U.S.) per cubic centimeter of material removed.

Table 5 shows some of the costs involved in removing a cubic centimeter of the different aluminas. Included with these figures are costs for grinding tungsten carbide and titanium under the same machine conditions but with a reduced downfeed, [6, 7]. Clearly, as the actual removal rate decreases, time costs increase substantially.

2.5. Conclusions

From this preliminary investigation it is difficult to draw very definite conclusions. However, one can deduce that 94 percent alumina is generally easier to grind than either 85 percent or 96 percent. A wheel peripheral speed of about 26 to 27 m/s (5100 to 5300 ft/min) gives the highest efficiency with most grit and bond types on both 85 percent and 96 percent alumina. Metal bond wheels are more efficient than resin bond wheels at all speeds tested. However, it is possible that resin bond wheels may be better in cases where edge chipping presents a problem. With the three grades of

TABLE 4. *Comparison of surface finishes achieved with different diamond types. (96% alumina, 0.125 mm (0.005 in) downfeed and 4000 rpm)*

Grit	Size	Surface roughness AA μm	
		After testing	After finishing
DXDA–MC	80/100	3.00	1.68
DXDA–MC	140/170	3.38	2.68
RDA55N	80/100	3.35	1.65
RDA55N	140/170	2.75	1.75
MDA–S	80/100	2.62	1.75
MDA–S	140/170	3.42	1.82
SND–MB	80/100	3.68	1.81
SND–MB	140/170	3.80	1.85
DXDA	80/100	2.12	1.47
DXDA	140/170	2.37	1.25

TABLE 5. *Comparison of grinding costs on aluminas, and titanium and tungsten carbide*

Grit	Size	Material ground	*G* ratio	Per cubic centimeter removed			
				Time (min)	Time cost U.S. cents	Wheel cost U.S. cents	Total cost U.S. cents
DXDA–MC	140/170	AD85	368	0.83	16.6	6.8	23.4
RDA55N	80/100	AD96	4660	0.82	16.4	0.54	16.94
SND–MB	80/100	AD94	17170	0.82	16.4	0.15	16.55
MDA–S	80/100	AD94	19160	0.82	16.4	0.13	16.53
DXDA	80/100	AD94	23000	0.82	16.4	0.11	16.51
DXDA–MC	80/100	Titanium [1]	50	5.32	106.4	50.0	156.4
RDA55N	80/100	P20 [2]	142	4.12	82.4	17.6	100.0

[1] Downfeed 0.02 mm (0.0008 in)
[2] Downfeed 0.025 mm (0.001 in)

alumina used, wheel costs are negligible, and where a part is rigid enough, severe conditions can be used without causing undue surface damage.

3. Cylindrical Grinding

3.1. Introduction

Cylindrical components make up a fairly large percentage of all ceramic parts ground. Diameters vary from 3 mm (⅛ in) to 300 mm (12 in) and larger. Despite the fact that so much cylindrical grinding is done, the feeds and speeds recommended by different suppliers vary a great deal. It was therefore considered advisable to look at the effects of these parameters.

In this preliminary evaluation, three different diamond grits were used in metal bond wheels to grind 75 mm (3 in) diameter × 300 mm (12 in) long rolls of three different alumina grades. Two work speeds and two wheel speeds were used to determine which combinations would give the longest wheel life.

3.2. Test Conditions

Machine	Jones and Shipman 1310 Cylindrical Grinder
Wheel type	D1A1
Wheel size	254 × 12.7 mm (10 × 1/2 in)
Wheel speeds	2200 and 2700 rpm
Wheel peripheral speeds	29.2 and 35.9 m/s (5750 and 7070 ft/min)
Diamond types	De Beers DXDA, SND–MB, MDA–S
Diamond mesh size	80/100 U.S. mesh
Diamond concentration	100
Bond depth	3.1 mm (1/8 in)
Infeed	0.025 mm (0.001 in)
Total infeed per test	Approx. 30 mm (1 3/16 in)
Workpiece rotation	145 and 415 rpm
Traverse rate	300 mm/min (12 in/min)
Coolant	Water plus Bryto 5 (100:1)
Coolant flow rate	3 1/min (40 gallons per hour)
Specimen types	Coors AD85, 94, 96.
Specimen size	75 mm O.D. × 300 mm long. (3 in. O.D. × 12 in long)
Sparkout	Two spark out passes, without infeed at the end of each test.

3.3. Test Results

The results of this series of tests are shown in table 6.

3.4. Discussion

a. Grinding Efficiencies

The main purpose of this investigation was to determine which combinations of wheel and work speeds would give the highest *G* ratio and hence the longest wheel life. Considering all three alumina grades together, preliminary tests showed that a low wheel speed with a high work speed, or a high wheel speed with a low work speed are poor combinations. However, tests at low speeds for both wheel and workpiece, and high speeds for both, yielded substantially better results. The *G* ratios obtained with these two combinations are the ones shown in table 6.

Considering the individual alumina types separately, it can be seen that the highest *G* ratio on 85 percent alumina is achieved at high work and wheel speeds. The most suitable grit for this material is DXDA which gives much better results than the other grits tested. On the 94 percent alumina, high work and wheel speeds again yield the best efficiency but here the MDA–S grit is superior. Recalling how, in

Table 6. *Grinding ratios for cylindrical grinding*

Work and wheel speeds		145, 2200 rpm			415, 2700 rpm		
Alumina content		85%	94%	96%	85%	94%	96%
Grit	Size	Grinding ratio			Grinding ratio		
DXDA	80/100	3470	6110	6620	8025	3940	5225
SND–MB	80/100	3130	4860	4125	2470	5020	6150
MDA–S	80/100	4970	7090	2910	4540	7260	3510

surface grinding, the 94 percent alumina appeared to be the "odd man out", with 85 percent and 96 percent being similar, it is surprising to find that the 96 percent alumina gives a higher grinding efficiency at low wheel and work speeds in cylindrical grinding. It should be noted, however, that the G ratios obtained at high work and wheel speeds are not much lower than those obtained at the lower speeds. For this material, DXDA is again the better grit type.

b. Surface Finish

Table 7 shows the surface finish that can be obtained when grinding 96 percent alumina at both combinations of wheel and work speed under discussion. It is interesting to note that the finer surface finishes are obtained when grinding with high wheel and workpiece speeds. This, then, is another reason why the higher speed combinations should be used. Although the SND–MB wheel gives the best finish, the DXDA wheel gives an only slightly rougher surface.

c. Grinding Costs

Once again, as with the surface grinding tests, the wheel costs are extremely low, varying from 0.31 to 1.01 cents (U.S.) per cm^3 material removed. The time costs in this case are fairly constant and are of the order of 12 to 14 cents (U.S.) per cm^3 material removed. When these are compared with a wheel cost of 55.5 cents (U.S.) and a time cost of 16.5 cents (U.S.) per cm^3 of material removed, obtained when grinding tungsten carbide rolls of the same diameter at the same feeds and speeds [8], it is once again obvious that wheel costs in particular are negligible when grinding ceramics of the types tested here.

3.5. Conclusions

The conclusions that can be drawn from this investigation are that a high workpiece speed and wheel speed are generally the most suitable for grinding 85, 94 and 96 percent aluminas. DXDA appears to be the better grit type to use. Wheel costs are so low that they do not influence the total product cost very much.

4. General Conclusions

Although it has been stated several times before, it must be stressed that this is a preliminary investigation. Many of the results obtained have merely been presented as found, with no explanation of the strange behaviour being given. What, it is hoped, has been shown is that, as with other materials, there are variations and exceptions to the general rules and it is advisable to study each particular operation carefully in order to get the best result from diamond abrasive grinding wheels.

5. References

[1] Busch, D.M., and Prins, J.F., A basic study of the diamond grinding of alumina, these Proceedings.

[2] Eckert, J.D., A replica technique for examining crystals and for retracing particles in grinding wheels, Industrial Diamond Review, 28, 75–77, (Feb. 1968).

[3] Eckert, J.D., and Caveney, R.J., A replica technique for conventional and scanning electron microscopy, Journal of Physics E: Scientific Instruments 3, 413–414 (1970).

[4] Caveney, R.J., and Eckert, J.D., Electron microscopic study of grinding workpieces, Proc. Diamond Conf., Reading, Sept. 24–27, 1969.

[5] Standards of the Alumina Ceramic Manufacturers Association for High Alumina Ceramics, 3rd Edition, (1969) published by the Alumina Ceramic Manufacturers Association.

[6] Hughes, F.H., Grinding with diamond abrasives,

Table 7. *Comparison of surface finishes achieved with different wheel and workpiece speeds. (96% alumina)*

Grit	Size	Surface roughness AA μm	
		Low speeds (145, 2200 rpm)	High speeds (415, 2700 rpm)
DXDA	80/100	2.48	2.15
SND–MB	80/100	2.03	1.93
MDA–S	80/100	2.88	2.73

part 2: Tungsten carbide, De Beers Industrial Diamond Division's Diamond Information L23.
[7] Dyer, H.B., Grinding with diamond abrasives, part 1: Steel, De Beers Industrial Diamond Division's Diamond Information L22.
[8] Diamond Abrasive Technology Centre test result.

Discussion

GIELISSE: I noticed an increase in 50 percent of your cost in grinding AD 85 as compared to AD 94.

CAVENEY: I think this was due to a different grit type. Referring to the table of costs (table 5) the *G* ratio was very low for the resin bond wheel used in the cost evaluation of grinding AD 85.

GIELISSE: The reason I asked the question was the danger in this type of comparison.

CAVENEY: Well, what we are pointing out here is the different *G* ratios. This one was particularly low and it did make a big difference in the cost. The others which were comparable, ranging from 5000 up to about 23,000, made very little difference in the cost. I think that high cost was due to a very low grinding efficiency.

DONOVAN: You are convinced that different aluminas grind quite differently?

CAVENEY: Well, from our evidence, yes. You can see from those curves (fig. 4 to 6) that two ceramics exhibited similar behavior, but that one of them had an enormous dip in the *G* ratio with increasing wheel speed.

DONOVAN: What about the resin versus the metal bond on alumina?

CAVENEY: Well, the behavior was more similar in the resin bond case than it was in the metal bond case, I agree with you there. We have to obviously extend this work in the next phase of grinding triple 9 aluminas and also grinding small parts where we can't use these large infeeds.

SMITH, C. J.: Did you do all this work dry?

CAVENEY: This was all done wet. The details are given in the paper.

SMITH, C. J.: My question is, have you ever done anything dry?

CAVENEY: Not as yet. Do you suggest that we do some work dry?

SMITH: No, I was interested in grinding ratio comparison, wet and dry.

CAVENEY: I see.

NATIONAL BUREAU OF STANDARDS SPECIAL PUB. 348, THE SCIENCE OF CERAMIC MACHINING AND SURFACE FINISHING, Proceedings of a Symposium Sponsored by the American Ceramic Society, the Office of Naval Research, and the National Bureau of Standards, held at NBS Nov. 2–4, 1970, Gaithersburg, Md. (Issued May 1972).

Ceramic Substrate and Specimen Fabrication

H. C. Leistner [1] **and W. A. Wilson** [1]

National Bureau of Standards
Boulder, Colorado 80302

Procedures have been developed to fabricate ceramic materials used as substrates for precision, coaxial, thin film resistors. Excellent radio frequency characteristics have been obtained from this procedure in developing radio frequency standards at the National Bureau of Standards at power levels of 10 milliwatts to 100 watts and frequencies from direct current to 4.0 gigahertz. Substrates fabricated for this purpose require precise tolerances and surface finish to insure uniformity of thin films deposited on a ceramic substrate.

In addition, procedures have been developed to fabricate specimens used in determining the dielectric and magnetic properties of ferrites, insulating ceramics, glass, fused silica, and single crystal materials. A variety of shapes are required including spheres, rods, disks and ellipsoids. Precise tolerances are required to obtain qualitative property measurements of the materials involved.

In both procedures, special techniques are used with existing equipment in grinding ultrasonic machining, lapping and polishing to obtain the required end product. This paper deals with both the application of the required products and the methods used to fabricate these products.

Key words: Ceramics; finishing; grinding; specimens; subtrates; ultrasonic machining.

1. Introduction

In recent years the use of ceramic materials has become quite prominent in scientific research and development programs because of their characteristics and adaptability to special applications. A number of applications have evolved at the Boulder Laboratories of the National Bureau of Standards which have required special consideration of available fabricating techniques and equipment to accomplish the desired end product. Most requirements were accomplished through the use of surface and cylindrical grinders and an ultrasonic cavitron machine.

It should be noted that the Instrument Shops Division at the Boulder Laboratories primarily supports research and development type programs and as a consequence, normally fabricates "one of a kind" pieces of equipment or components as opposed to a multiple, production-type operation. The result is that, because of the lack of specialized equipment to perform a specific task, improvision and special tooling is necessary to fabricate the required product. With the increasing use of ceramic materials, even more improvision is required and oftentimes an experimental approach to fabricating techniques is necessary to meet the specifications.

The intent of this paper is to recognize some of the tasks that have been accomplished in fabricating ceramic materials for the support of research and development programs at the Boulder Laboratories. The examples cited are by no means all-inclusive, but are representative of approaches taken to machine and finish ceramic materials with available equipment. The areas covered include radio frequency power measurement, utilizing coaxial, thin-film resistors, and electromagnetic measurements of the dielectric and magnetic properties of materials. These areas are dealt with separately to relate in further detail the approaches taken to accomplish the required objectives.

2. Radio Frequency Power Measurement

To meet the increasing complexity and higher performance characteristics of radio frequency power, developments have been accomplished at NBS to more accurately measure radio frequency quantities. Using the calorimetric principle, Crawford and Hudson [1][2] developed a dual-flow coaxial calorimeter power meter as a reference standard to accurately measure radio frequency power. Quoting Crawford and Hudson, "The measurement of electrical power using this principle depends upon the complete conversion of the electrical energy as delivered by a generator into thermal energy in a resistive load." To extend the measurement range and further improve the radio frequency reference standard, Crawford [2] developed an rf-dc substitution calorimeter incorporating automatic controlled reference dc input power.

An important feature of the calorimeter used to develop these reference standards is the load resistor which transforms the electrical energy into thermal energy. The configuration most suitable to this application is a thin film re-

[1] Instrument Shops Division, National Bureau of Standards Laboratories, Boulder, Colorado 80302.
[2] Figures in brackets indicate the literature reference at the end of this paper.

sistor of either a cylindrical or conical shape, matched to the mounting structure such that the characteristic impedance of the line is equal to the resistance of the load resistor at any point along the length of the load.

The desired thin film resistor was fabricated by depositing a metallic film on a ceramic substrate of the proper configuration. Thin films used for resistors are typically about 4 microinches thick. In providing substrates for these thin film resistors, precise dimensions and smooth surfaces are important to insure uniformity of the film deposited on the substrate. Thin spots in the resistant film cause the film to operate at higher temperatures in the thin area, resulting in short life or complete failure. Any surface defects with sharp edges are disastrous. Consequently, all surfaces must be polished to a finish of 20 microinches or better and scratches more than a few microinches deep are intolerable.

Figure 1 shows the configuration of a more complex substrate fabricated from aluminum oxide. Even though a variety of modifications were used to meet different substrate requirements, this example will serve to illustrate the approach necessary to accomplish this fabrication task. This substrate was ground between centers on a cylindrical grinder, using a resin-bond diamond wheel and oil-free cutting fluid. A male center was ground on the small end of the cone while a brass adapter epoxied to the large end of the cone provided the female center for that end. These provisions were necessary in order to maintain concentricity of the conical and cylindrical portions of the ceramic substrate within a tolerance of ± 0.0002 in (± 5.08 micrometers). The table of the grinder was tilted to the proper angle to grind the conical portion.

The grooves on the large end of the substrate were machined with a surface grinder. A brass adapter was fabricated to match the taper of the cone and waxed to the ceramic substrate. Using this adapter as a holding fixture, the grooves were cut in the aluminum oxide on a surface grinder with a resin-bond diamond wheel.

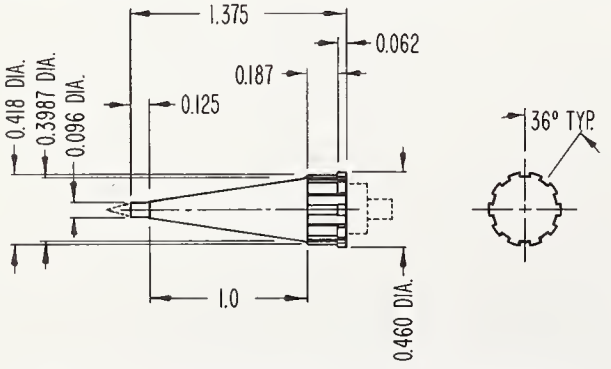

FIGURE 1. *Conical substrate for a load resistor used as the termination of a coaxial transmission line.*

Since the surface of the substrate was relatively coarse after grinding, the cylindrical and conical portions were lapped, using a 4–8 micron grade diamond lapping compound to obtain a 10 to 20 microinch finish surface. With the substrate fabricated to the closest tolerance and finish possible, the load resistor was completed by depositing an alloy of Au, Ni, and Cr 4 microinches thick on the cone portion of the substrate and firing silver on both cylindrical ends of the substrate.

3. Dielectric and Magnetic Properties

For a number of years investigations have been underway at the National Bureau of Standards to measure the dielectric and magnetic properties of materials relative to radio and communications applications. These measurements were made in a variety of ways to establish absolute values and determine the effects of various shapes and orientations of the sample material examined. The purpose of the investigations was to establish reliable values of these parameters for use in circuit design and wave transmission calculations.

Bussey [3] has made a survey of the methods used to measure these parameters, citing the correlation that developed and the conclusions that were resolved after many years of experimental and theoretical investigations.

The electromagnetic measurements of the dielectric and magnetic properties of materials required precise fabrication of sample specimens. Among the specimens examined were small diameter rods, thin disks, spheres and ellipsoids fabricated from a number of materials including ceramic ferrites, alumina, fused silica, and glass.

A variety of sizes of round rods were fabricated from the above materials. A typical example was the fabrication of a rod 0.039 in (0.9906 mm) in diameter and approximately 1–1/4 in (31.75 mm) long. Occasionally diameters of 0.016 in to 0.020 in (0.4064 to 0.508 mm) were required. We did not have a centerless grinder available when this work was done; however, some experimentation revealed that such a rod could be fabricated satisfactorily on a cylindrical grinder. A larger piece of stock material was placed on a chuck and oriented such that the axis of the stock material was parallel with the cross feed of the grinder and the grinding wheel set at a slight angle from the centerline of the stock material (fig. 2). By starting at the unsupported end of the stock material and plunge grinding in one continuous operation, the sample specimen was fabricated within the desired tolerance, but more important, with a uniform diameter throughout its

entire length. The precise diameter required was established by trial operations on an expendable glass rod before starting on the final test piece.

An auxiliary, motorized gear drive was connected to the cross feed of the cylindrical grinder to provide a slow, uniform feed during this plunge grinding operation. The cross feed rate was approximately 0.010 in (0.254 mm) per minute. A metal-bonded, diamond grinding wheel was used to grind the aluminum oxide material.

In contrast with this approach, when attempts were made to plunge grind the specimen from the side in multiple steps with the axis of the grinding wheel parallel to the axis of the stock rod material, control was not precise enough to avoid small steps between each plunge position of the grinding wheel. Since the diameter of the specimen was not consistently uniform, it was not acceptable as a test specimen, and the plunge from the end approach described above was developed.

Small disk specimens were fabricated from aluminum oxide using a conventional surface grinder and a diamond grinding wheel. A typical size was 2 in (50.8 mm) in diameter by 0.100 in (2.54 mm) thick. The tolerance on the thickness was ± 0.0003 in (± 7.62 μm). This fabrication requirement was accomplished by either using a vacuum chuck or attaching the sample material to a base plate with wax and holding the base plate in position with a magnetic chuck. After surface grinding was completed on both sides of the specimen, the final desired tolerances and surface finish were obtained by hand lapping with a diamond lapping compound.

Spheres were fabricated primarily by the tumbling method, using equipment constructed specifically for this purpose. Bond [4] introduced an early tumbling method for making small spheres. The tumbling machine shown in figure 3 consisted of a hollow tube oriented perpendicular to a high speed, rotating, abrasive wheel. The specimen material, initially in the form of a cube, was retained inside the tube and formed into a sphere through operation of the rotating wheel. A further development in tumbling equipment resulted in the air driven machine shown in figure 4. The inside of the abrasive wheel was formed to the desired shape and provided a track for the specimen to follow as it was forced around the inside of the wheel by high velocity air flow.

Using these two tumbling machines, spheres were fabricated from ceramics, ferrites, garnets and silica in a range of sizes from 0.016 in (0.4064 mm) diameter to 0.120 in (3.048 mm) diameter. It was possible to obtain spheres with a roundness tolerance of ± 0.0005 in (± 12.7 μm). The size of the sphere was controlled by time of machine operation and, with

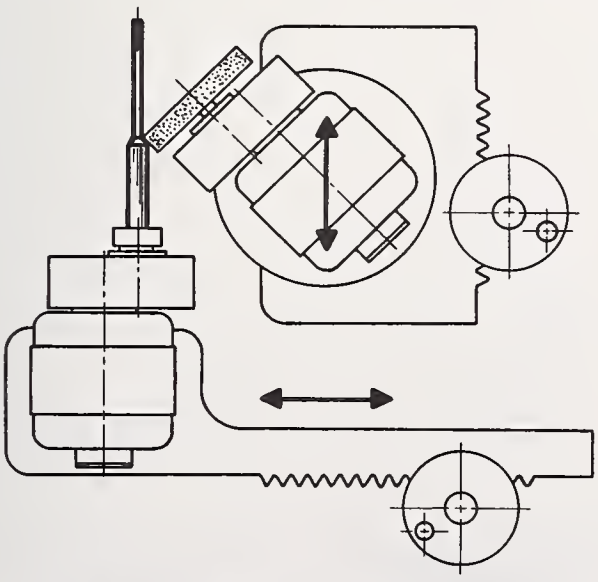

FIGURE 2. *Plunge grinding a cylindrical specimen; arrows show how diameter is set, and direction of grinder travel.*

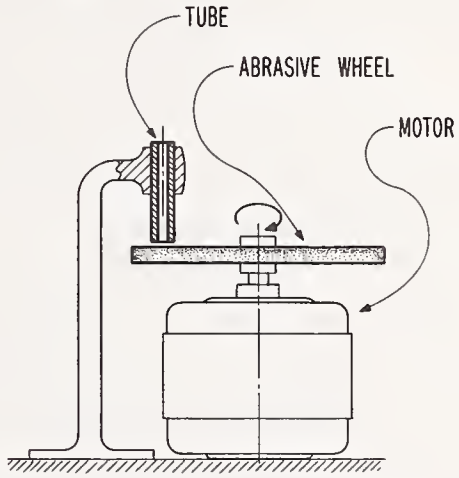

FIGURE 3. *Motor driven tumbling machine with guide tube and rotating abrasive wheel.*

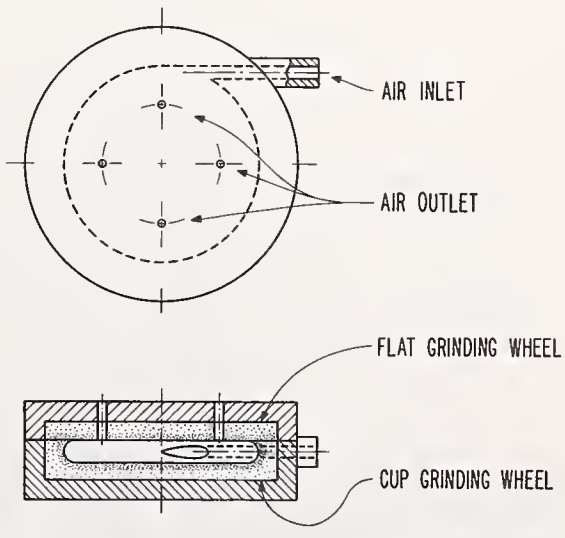

FIGURE 4. *Air driven tumbling machine showing air flow and shape of abrasive wheel.*

some experience, could be held quite close to the desired size. To further control the size and finish of the sphere, a finishing tool was developed as shown in figure 5. This tool consisted of a motor-driven, brass rod with a conical depression on the extended end to receive the spherical specimen. A similar bakelite rod was manually held against the specimen, which provided a means for lapping the specimen to a more precise size and finish. Using this procedure it was possible to control the roundness of the sphere within a tolerance of $\pm$ 0.0001 in ($\pm$2.54 μm).

Ellipsoidal specimens were fabricated by first milling the desired size and shape of lapping plate in either cast iron or brass material. The required elliptical groove was obtained by tilting the milling cutter with relation to the alignment of the stock material. Both oblate and prolate ellipsoid lapping plates were formed as shown schematically in figure 6. The lapping plate was securely attached to the work surface of a conventional milling machine with adhesive wax. The lapping procedure and quantity of material removed was controlled by adjusting the work surface and the spindle of the milling machine. Thus, through the vertical and rotary motion of the milling machine, the specimen material was lapped into the desired shape. With the lapping plates as shown in figure 6, half of the ellipsoid was formed in one setup. The specimen was then reversed 180° and the remaining half of the ellipsoid completed. A variety of sizes were fabricated for use in measuring the spin wave magnetic properties of the specimen materials. A typical example was an oblate ellipsoid 0.080 in (2.032 mm) major diameter by 0.040 in (1.016 mm) minor diameter. Ellipsoidal specimens were fabricated from ferrites and garnets, using lapping compounds appropriate for the material involved.

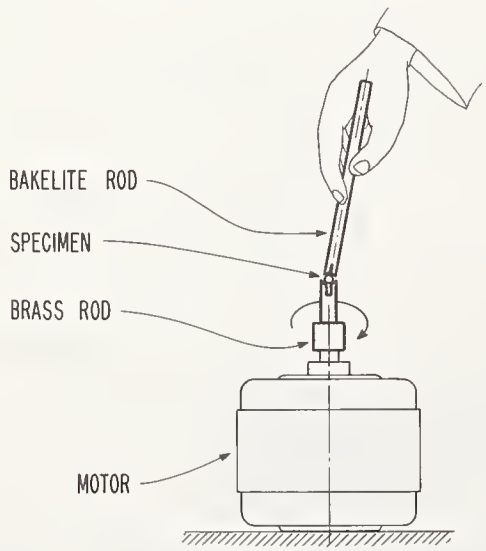

FIGURE 5. *Lapping tool used to finish small diameter sphere specimens.*

4. Cavitron Machining

In citing the above machining approaches, it is evident that other machining capabilities are necessary to meet the many demands required in machining ceramic materials. An ultrasonic cavitron machine is used to machine various sizes and shapes of holes, slots or grooves in ceramic materials. With proper tooling and appropriate fixtures, very good control can be obtained in machining ceramic materials with a cavitron machine. A boron carbide slurry has performed quite well in penetrating silicon carbide, fused quartz and aluminum oxide, as well as other brittle and hard materials.

5. Summary

In summary, the above examples illustrate some of the approaches taken to fabricate ceramic materials for special applications. They further illustrate the variety of fabrication requirements that are necessary to support a research and development organization. As noted in these examples, the basic approach is to use grinding equipment with diamond wheels and diamond lapping compound to provide the desired machining and finishing capability for ceramic materials. In addition, the ultrasonic cavitron machine is used to machine various sizes and shapes of holes, slots or grooves in ceramic materials.

The authors wish to acknowledge M. L. Crawford, P. E. Werner, and H. E. Bussey for

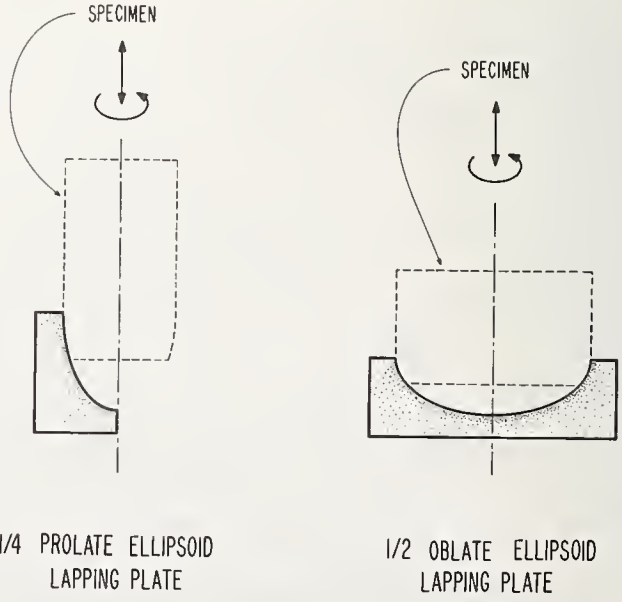

FIGURE 6. *Lapping plates used for forming ellipsoidal specimens.*

the information they supplied in the preparation of this paper.

6. References

[1] Crawford, M. L., and Hudson, P. A., A dual-load flow calorimeter for RF power measurement to 4 GHz, J of Res., Nat. Bur. Standard. (U.S.), 71C (Eng. and Instr.), No. 2, 1–178 (April-June 1967).

[2] Crawford, M. L., A new rf-dc substitution calorimeter with automatically controlled reference power, IEEE Trans., Instrument and Measurement, IM–17, 378–384 (Dec. 1968).

[3] Bussey, H. E., Measurement of rf properties of materials, a survey, Proc. IEEE, 55, 1046–1053 (June 1967).

[4] Bond, W. L., Making small spheres, review of scientific instruments, 22, 344–345 (May 1951).

NATIONAL BUREAU OF STANDARDS SPECIAL PUB. 348, The Science of Ceramic Machining and Surface Finishing, Proceedings of a Symposium Sponsored by the American Ceramic Society, the Office of Naval Research, and the National Bureau of Standards, held at NBS Nov. 2–4, 1970, Gaithersburg, Md. (Issued May 1972).

439-921 O - 72 - 9

On the Shaping of Brittle Solids by Erosion and Ultrasonic Cutting

H. L. Oh, K. P. L. Oh, S. Vaidyanathan and I. Finnie [1]

General Motors Research Laboratories, Warren, Michigan 48090 and University of California, Berkeley, California 94720

In mechanical shaping processes for brittle solids, materials is removed by the propagation and intersection of cracks. To control the resulting surface finish, the extent of cracking is localized by loading the surface in very small regions, usually with small abrasive grains. Thus, in analyzing such processes as erosion and ultrasonic cutting, we have to examine the fracture patterns produced by small hard indenters.

As a starting point, it is shown that fracture loads for indenters subjected to normal force may be predicted from conventional strength tests by using Weibull's statistical treatment of brittle strength. It is then shown that Weibull's procedures may be extended to predict the distribution of fracture location in brittle solids. For the case of a spherical indenter under normal and tangential forces, many cracks may form as the load is increased. It is shown that the location of the outermost of these cracks may be predicted. Estimates may also be made of the depth of cracking and thus the extent of the cracking produced by a single contracting particle may be described.

These results may be applied directly to study the process of erosive shaping. The influence on volume removal of changes in the velocity and size of the impacting particles is predicted and shown to be in accord with experiment. Many other features of the erosion process may be described including a transition to "ductile" behavior in the case of glass when the impacting particles are small enough. The analysis of ultrasonic cutting presents greater difficulty because the distribution in size of the abrasive grains is of great importance. However, predictions may be made for the influence of load, grain size, and material properties on the rate of volume removal and these are shown to be in general accord with experiment.

Key words: Abrasion; brittle-ductile transition; erosion; fracture location; ring-cracking; shaping; size-effect; statistical nature of strength; ultrasonic cutting; Weibull distribution.

1. Introduction

The shaping processes that we shall consider are those in which material is removed from a body by mechanical action to convert it to a useful shape. When one attempts to develop an analysis for such material removal operations, it is often convenient to consider the two extremes of mechanical behavior—the ideally ductile and the ideally brittle. An ideally ductile material undergoes large plastic strains before separation occurs and such materials may be shaped by the displacing or cutting action of a tool. By contrast, in an ideally brittle material only elastic deformation occurs prior to fracture. Thus, in mechanical shaping operations on brittle solids, material will be removed from the surface by the propagation and intersection of cracks ahead of and around the loaded region. The concepts of ideally ductile and ideally brittle behavior while somewhat over-simplified do describe to a close approximation the behavior of many real materials and allow analytical solutions to be obtained.

With the reader's indulgence we will discuss very briefly a few of the historical aspects of the shaping of solids before turning to consider some of the mechanical shaping processes which may be applied to brittle materials.

The classical problem is of course, the shaping of brittle solids since stone was used for tools and weapons and buildings by ancient civilizations. Techniques were developed, during the Stone Age and later, for loading a block of stone and splitting off pieces of a desired shape. The methods may appear primitive but fracture in a brittle solid is hard to control and such techniques could only have been developed after a great deal of careful experiment and experience. Much later in the pre-Columbian Americas the art of shaping brittle solids became very highly developed. The Incas in Peru matched massive stone with incredible perfection over large areas while Aztec craftsmen are said to have been able to produce 100 knife blades of obsidian in an hour. Unfortunately, one cannot find any scientific articles from the Stone Age or even from the Aztec or Incas and what we know about their shaping techniques is largely based on the finished objects and in a few cases on construction sites where work was interrupted and never resumed.

The first technical literature one finds on the shaping of solids is in the 1850's. A number of machine tools appeared in their present form

[1] The authors are respectively, Associate Senior Research Engineer, General Motors Corporation Warren, Michigan 48090; Research Assistant, Post Graduate Research Engineer, Professor of Mechanical Engineering and Chairman of the Division of Mechanical Design, University of California at Berkeley 94720.

between 1840 and 1850. Steel was first produced in large volume in the 1850's and shortly afterwards, technical papers dealt with the cutting of ductile metals began to appear. Based on a study of the early literature [1][2] it appears that analytical studies kept pace with practical developments until about 1900. By that time, the analysis of cutting forces in machining had become almost as well developed as it has today. But then, high speed tool steels were developed, the practical art of metal cutting took an enormous step forward and the analytical aspects appear to have been left behind. Despite the many studies of metal cutting which have been made in recent years, the equations one finds in text books to relate tool geometry, friction coefficient and the angle at which metal is sheared, are essentially those presented by Zvorykin [1] in Czarist Russia in 1893. Unfortunately, the equations are far from adequate for accurate predictions. It may be reassuring to those who are attempting to understand brittle behavior to know that despite the modern equipment which is used to shape ductile metals we are still lacking a basic relation between the material properties and the various geometrical features involved in the cutting process.

Now, in recent years we find the shaping of brittle solids coming back into the picture as designers wish to employ such materials as oxides, carbides, and graphite. A single point cutting tool or a single impact is rarely suitable for machining such materials for it produces large and uncontrolled fractures, perhaps leaving the object in several pieces. To our knowledge it has not been possible to control the age old techniques of "knapping" or flaking brittle solids with sufficient accuracy to make this a precise shaping process. So what is done, is to control the extent of fracture and the resulting surface roughness by loading the brittle solid in very small regions using small hard particles. Various processes are used and differ essentially in the manner by which the particles are brought into contact with the surface. Thus we have:

Erosion in which a stream of particles, usually entrained in a jet of air, strike the surface with a given velocity and direction;
Ultrasonic Cutting in which a vibrating tool forces particles contained in a slurry into the surface being machined;
Abrasion or *Grinding* in which the particles are embedded in a flat sheet or a wheel and are moved across the surface while under a load which tends to push them into the surface;
Lapping in which loose particles are pressed against the surface being machined by another surface, the lap.

The terminology may vary but it is clear that all these processes involve fracture under small hard particles loaded by various combinations of normal and tangential forces. We have listed erosion first and will treat it in detail because it appears to be the easiest of the processes to analyze. In erosion the interaction of a typical impacting particle and the surface may be considered without reference to the particle size distribution. For the other processes the applied load is distributed over all the contacting particles and thus the loads on the individual particles will depend on particle size distribution.

In contemplating an analysis of erosion or one of the other processes, one thinks first, perhaps, of an energy approach in which the volume removal is taken as proportional to the kinetic energy of the impacting particles or to the kinetic energy lost by the impacting particles. This type of approach is often followed in rock drilling studies and enables crude predictions of volume removal to be made. However, the values reported for "energy required per unit volume crushed," i.e., the specific energy, vary greatly for a given type of rock and it seems most unlikely that we could make detailed predictions about the role of particle size, particle velocity, impact angle, etc., on this basis. Crushing studies on brittle solids show that the essential energy requirement, that to produce fresh surface, is a very small and unpredictable fraction of the total energy expended in crushing [2]. So unless fragment size and surface area can be predicted in advance, it would appear to be most unrealistic to use a model based on energy to study the shaping of brittle solids.

In the fields of rock mechanics and coal mining, analyses have been made of the chipping that occurs under an indenting tooth or wedge. The solutions apply only when the included angle of the wedge is small, so that chipping rather than crushing occurs, and do not appear to be applicable to the case of fracture under polyhedral or spherical abrasive grains.

Since volume removal in brittle solids occurs by fracture, we decided to study shaping operations by looking at the cracking that occurs when an idealized abrasive particle of spherical shape loads the surface. This route leads us into a study of the fracture of brittle solids by spherical indenters. Some of this work will now be summarized and then applied to study shaping operations.

2. Fracture Under Spherical Indenters

We consider the case of a sphere pressed against a semi-infinite solid by a static force P

[2] Figures in brackets indicate the literature references at the end of this paper.

or striking the solid with velocity U. For the present we consider only normal loading (perpendicular impact) but will show later that the approach may be extended to combined normal and tangential loads. The elastic solution due to Hertz and Huber is well known (e.g., it has been summarized by Hamilton and Goodman [3]) and shows that the surface stresses, prior to fracture, are compressive within the contact area while outside, on the free surface the radial stress is tensile while the circumferential stress is of equal magnitude but compressive. Below the surface the tensile stress decreases very rapidly. Figure 1 shows the variation of the radial tensile stress on the free surface with radius. It is known [4] that the impact problem is pseudo-static up to very high velocities and hence the maximum load P corresponding to a given impact velocity U may be shown to be

$$P = \frac{4}{3}\left(\frac{5}{4}\right)^{3/5} \pi^{3/5} (\rho_1)^{3/5} U^{6/5} R^2 \div \left[\frac{1-\nu_1^2}{E_1} + \frac{1-\nu_2^2}{E_2}\right]^{2/5}$$

where ρ_1 is the mass density of the sphere and ν and E are the Poisson's ratio and Young's Modulus of the sphere (1) and the surface (2).

Fracture, when it first occurs, appears as a ring on the surface, usually well outside the contact area, and spreads out below the surface to form the frustum of a cone. If loading is continued, the initial crack spreads deeper into the solid and additional concentric ring cracks form at successively greater radii.[3] Eventually, at a high enough load, or velocity, extensive crushing occurs under the indenter. This behavior is illustrated in figure 2 where we have used a relatively large spherical particle for analytical convenience. It is interesting to note that despite the extensive amount of cracking which occurs, the load-deflection relation is estimated quite well by the elastic solution for an uncracked solid. Presumably this is because the stress state under the indenter is primarily compressive and the cracked material is capable of transmitting compressive load. Thus, we base our study of the shaping processes on the type of cracking shown in figure 1 and assume that the Hertz equations may be used to relate deflections to load.

In attempting to predict ring cracking, there is little value in the classical concept that a brittle solid fractures when the tensile stress reaches a certain magnitude. The load required to produce ring cracking in glass shows a great deal of scatter. In addition there is a strong size effect such that if the indenter size is decreased from, say 1 in ($2.54 \times 10^{-2} m$) to 0.01 in ($2.54 \times 10^{-4} m$), there is a threefold increase in the value of σ_a, the stress at the rim of the contact area, computed from the mean fracture load. These observations are not new for about 30 years ago they led Weibull [5] to propound his statistical theory of brittle strength. Basically, Weibull's idea was that flaws are distributed at random in brittle solids. These flaws are, in general, too small to be detectable, and so one cannot relate flaw size to strength as in the familiar "Linear Elastic Fracture Mechan-

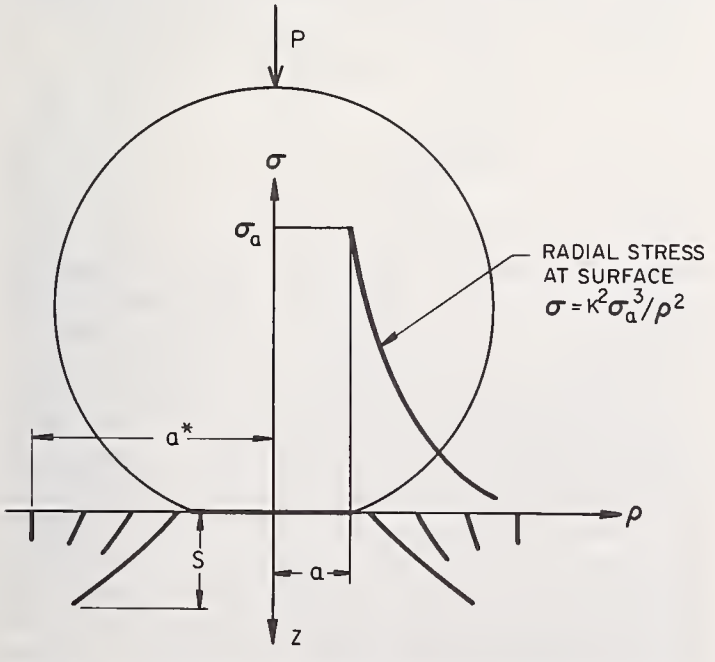

FIGURE 1. *Coordinate system used in study of ring cracking.*

[3] We have observed this type of cracking during tests on glass and by sectioning aluminum oxide specimens after testing.

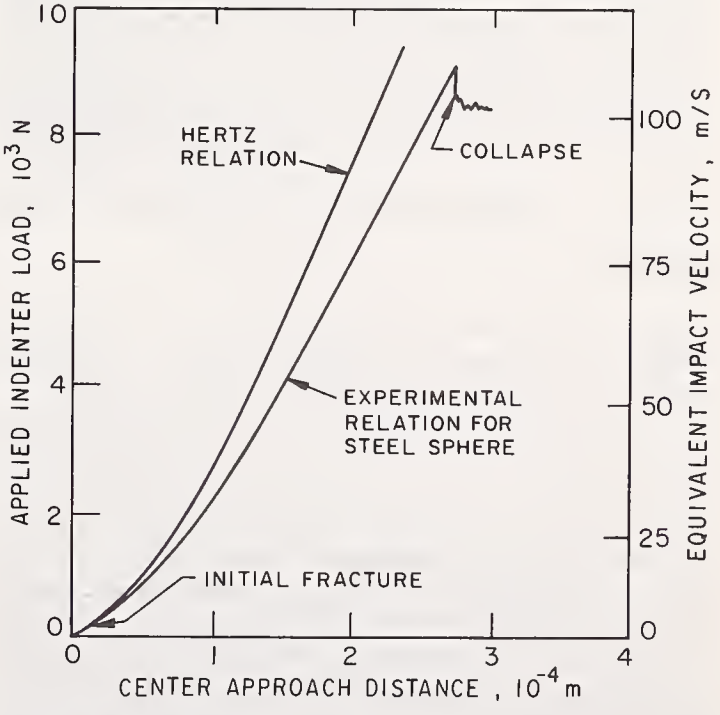

FIGURE 2. *Variation of approach of center of 1/8 in* (3.175×10^{-3}m) *diameter steel ball to undeformed region of glass plate with load.* The impact velocities corresponding to the applied load were calculated for steel sphere from the Hertz equations.

ics" approach. Rather one has to test a large number of specimens and determine the probability of failure for a given stress level and specimen size. As the size of the stressed region decreases the probability of finding a severe flaw decreases and as a consequence the mean stress at failure increases. Strangely enough, although the ring crack was what led Weibull to his statistical treatment of brittle strength, he did not analyze this problem in any detail. Recently two of the present writers [6,7] studied the ring-cracking of glass in some detail and showed that the mean fracture load, the standard deviation of fracture load and the mean location of the initial ring-crack for indenters of various radii could be predicted from bending test data. Here, to illustrate the procedures followed, and to obtain a result which we will use later, we compute the distribution of the stress σ_a at which ring cracking occurs.

Following Weibull [5] we take the probability $F(\sigma)$ that a specimen of volume V fractures under a uniform tensile stress $\leq \sigma$ as

$$F(\sigma) = 0 \qquad \sigma \leq \sigma_u$$

$$= 1 - \exp - V \left(\frac{\sigma - \sigma_u}{\sigma_0}\right)^m \qquad \sigma > \sigma_u$$

where σ_u, σ_0, m, the parameters of the probability distribution, are assumed to be constants for a given material. If these constants are estimated, e.g., from a series of tension tests on specimens of a given size, then this equation may be used to predict the probability of failure at a given stress level for other specimen sizes and loadings.

When the tensile stress, σ, is not uniform but varies over the volume, then the expression $\left(\frac{\sigma - \sigma_u}{\sigma_0}\right)^m$ is integrated over the volume stressed in tension.

$$F(\sigma) = 1 - \exp - \int_V \left(\frac{\sigma - \sigma_u}{\sigma_0}\right)^m dV \qquad \sigma > \sigma_u$$

$$= 0 \qquad \sigma \leq \sigma_u$$

In this form the Weibull distribution may be used, for example, to make predictions about the distribution of bending strength.

Glass is a brittle solid which is convenient for experimental work. However, unlike polycrystalline ceramics in which the strength impairing flaws are distributed throughout the volume, glass inevitably fails due to surface flaws. Thus, if preceding equations are applied to glass, V must be taken as the surface area stressed in tension.

For ball indentation on glass the Weibull distribution may be shown to take the form

$$F(\sigma_a) = 1 - \exp - \left\{ \int_{A_1} \left(\frac{\rho/K - \sigma_u}{\sigma_0}\right)^m 2\pi\rho d\rho + \int_{A_2} \left(\frac{K^2\sigma_a^3/\rho^2 - \sigma_u}{\sigma_0}\right)^m 2\pi\rho d\rho \right\}$$

$$= 1 - \exp - \left\{ \pi (K\sigma_0)^2 \left(\frac{\sigma_a - \sigma_u}{\sigma_0}\right)^{m+2} \sum_{i=o}^{\infty} \left[\frac{3}{m+1} \left(\frac{\sigma_u}{\sigma_a}\right)^i + \frac{m!(3+1)!}{(m+3+i)!} \left(1 - \frac{\sigma_a}{\sigma_u}\right)^{i+1} \right] \right\} \qquad \sigma_a > \sigma_u$$

$$= 0 \qquad \sigma_a \leq \sigma_u$$

where $K = \frac{3\pi R}{2(1-2\nu_1)} \left(\frac{1-\nu_1^2}{E_1} + \frac{1-\nu_2^2}{E_2} \right)$;

and we have expressed the radial tensile stress σ in terms of the maximum tensile stress σ_a and integrated over surface areas which are or have been under tensile stress. From this distribution we may calculate, for example, $\bar{\sigma}_a$ the average value of $\bar{\sigma}_a$ at fracture:

$$\bar{\sigma}_a = \int_0^1 \sigma_a dF(\sigma_a)$$

$$\simeq \sigma_u \left\{ 1 + \Gamma\left(1 + \frac{1}{m+2}\right) \left[\left(\frac{\sigma_u}{\sigma_0}\right)^m \frac{3\pi (K\sigma_u)^2 m!}{(3+m)!} \left(m^2 + 5m + 8\right) \right]^{-\frac{1}{m+2}} \right\}$$

$$\simeq \sigma_u \left\{ 1 + (\text{constant})\, R^{-\frac{2}{m+2}} \right\} \qquad (1)$$

After obtaining the parameters, σ_u, σ_0, m, in this case from bending tests [6], the computation may be carried out and gives the results shown in figure 3. The agreement with experiment is reasonable over a wide range of indenter sizes.

Another quantity which is of interest in shaping operations is the location of the outermost ring crack. The subject of fracture location has seldom been considered in fracture studies and has never formed part of the Weibull theory. However, by extending the Weibull approach and looking at the probability of failure of differential elements which compose the solid, we may derive the distribution of fracture location.

For a given load in ball indentation, if we divide the region under tension into concentric

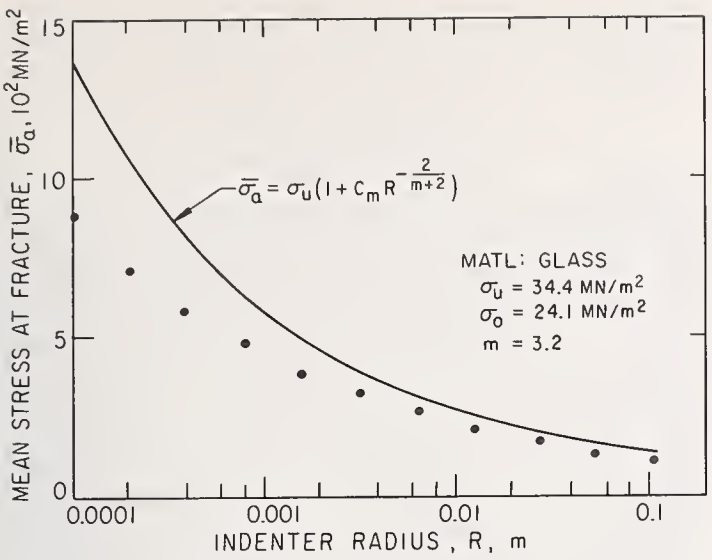

FIGURE 3. *Predicted and experimental values of σ_a as a function of indenter size.*

differential annuli, we can formulate the distribution of the outermost ring crack location as:

$$\text{Prob.}\left[\begin{matrix}\text{outermost ring crack}\\ \text{occurs at a radius a*}\end{matrix}\right]$$

$$= \text{Prob.}\left[\begin{matrix}\text{the annulus at location}\\ \text{a* fails}\end{matrix}\right] \times \text{Prob.}\left[\begin{matrix}\text{all annuli exterior}\\ \text{to this annulus survive}\end{matrix}\right]$$

This formulation has been carried out in detail in a separate paper [7] and it is shown there that aside from elastic constants of the materials, the distribution of the outermost ring crack locations $G(a^*)$ is also a function of Weibull parameters m, σ_u, σ_0, the indenter radius R and the stress level in the solid, σ_a. That is

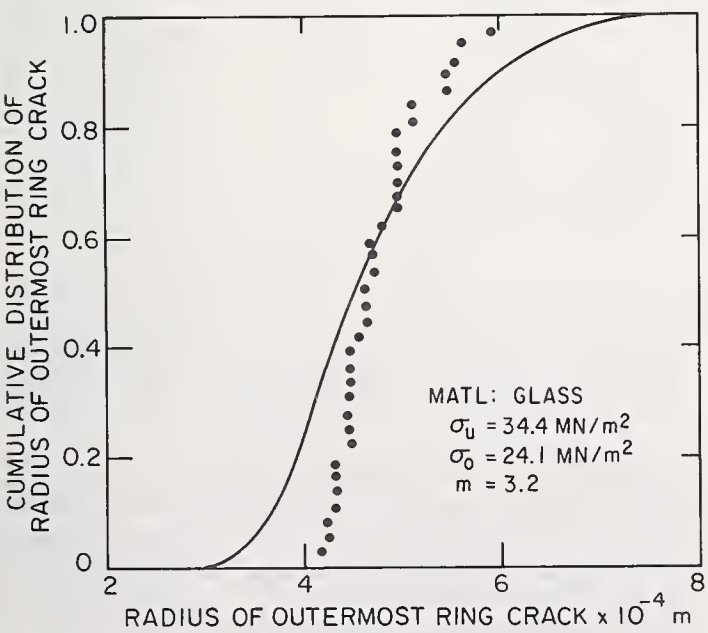

FIGURE 4. *Predicted and experimental values for the cumulative distribution of the outer ring crack when a glass plate is loaded by a 3/32 in.* (2.38 × 10^{-3}m) *radius indenter under a load of 154 lbs (684 N).*

$$G(a^*) = f(\sigma_u, \sigma_0, m, \sigma_a, R).$$

Figure 4 shows the calculated result for $G(a^*)$ when a glass plate, $m=3.2$, $\sigma_u=5000$ psi (34.4 MN/m^2), $\sigma_0=3500$ psi (24.1 MN/m^2), is loaded by a 3/32 in (2.38 × $10^{-3}m$) radius indenter up to a load of 154 lbs (684 N). The agreement between prediction and experiment is quite satisfactory, particularly in view of the complex nature of the multiple type of fracture being considered. Again, knowing $\overline{G(a^*)}$ we may calculate various moments of the distribution. For example, we make use later of (a^{*2}), the average value of $(a^*)^2$, which is:

$$(\overline{a^{*2}}) = \int_0^1 a^{*2}\, dG(a^*) = f_1(\sigma_u, \sigma_0, m, \sigma_a, R) \quad (2)$$

3. Analysis of Erosion

3.1. Spherical Particles Making Perpendicular Impact

We are now in a position to analyze the erosion of brittle solids and consider first the case of perpendicular impact by spherical particles. By examining fracture patterns such as shown in figure 1, and noting that the radius a^* is considerably larger than a, it seems reasonable to take the volume damaged by a single eroding particle V_p as

$$V_p \propto (\overline{a^{*2}})\ S\ F(\sigma_a). \quad (3)$$

where $F(\sigma_a)$ is the probability of the particle ring cracking the surface and S is the depth of the primary ring crack as shown in figure 1. Examination of ring cracks in glass indicates that the depth S of the primary ring crack is proportional to the depth X to which the sphere indent the surface.

From the Hertz equations we find:

$$X \propto R\,\sigma_a^2$$
$$X \propto P^{2/3} R^{-1/3} \propto RU^{4/5} \quad (4)$$

So that $\sigma_a \propto U^{2/5}$ and $V_p \propto RU^{4/5}\ \overline{a^{*2}}\ F(\sigma_a)$. Since $\overline{a^{*2}}$ is a function of m, σ_u, σ_0, R and σ_a, where σ_a in turn depends on U we now have an expression for the volume damaged by each particle which is a function only of R, U and the Weibull parameters (σ_0, σ_u, m). We examine this prediction, which requires numerical computation to evaluate the integral, by varying the Weibull parameter σ_u, holding the other four quantities (σ_0, m, R, U) constant. Effectively σ_u, the stress below which fracture does not occur, may be changed by inducing biaxial compressive stress in the surface. This was done by shrink-fitting steel rings onto glass disks. The predicted and observed values for relative volume removal are shown in figure 5 and agree very well. As another test of our formulation,

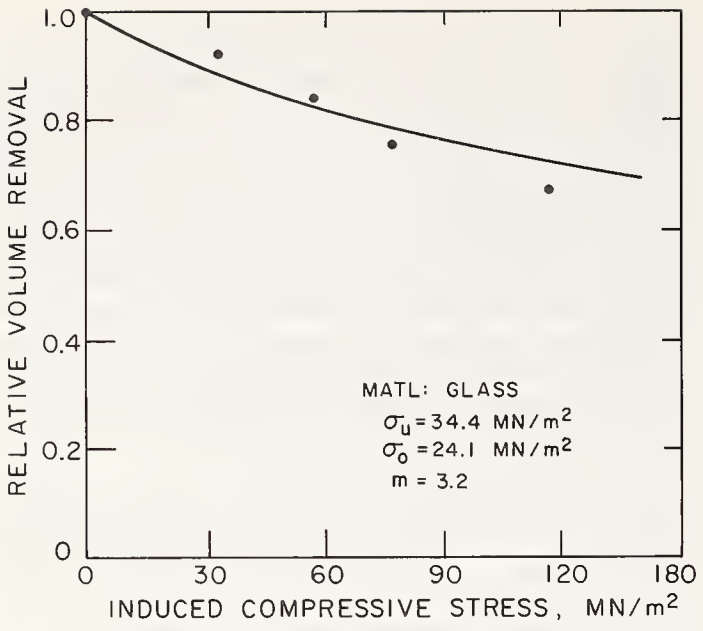

FIGURE 5. *Influence of biaxial compressive stress on erosion of glass by 0.0165 in* (4.19 × 10^{-4}m) *diameter steel shot at a velocity of 270 ft/sec* (*82.29 m/s*) *and perpendicular impact.*

we took erosion data reported by Sheldon and Finnie [8] for three brittle solids which were eroded by spherical steel shot of various sizes at different velocities. The observed volume removal per particle is plotted against $RU^{4/5}$ $(\overline{a^{*2}})$ $F(\sigma_a)$ in figure 6, 7, 8 for glass, magnesia and graphite respectively. For magnesia and graphite $(\overline{a^{*2}})$ was computed by integrating over the volume stressed in tension rather than using area stressed in tension as in the case of glass. If the volume removed per particle is linearly

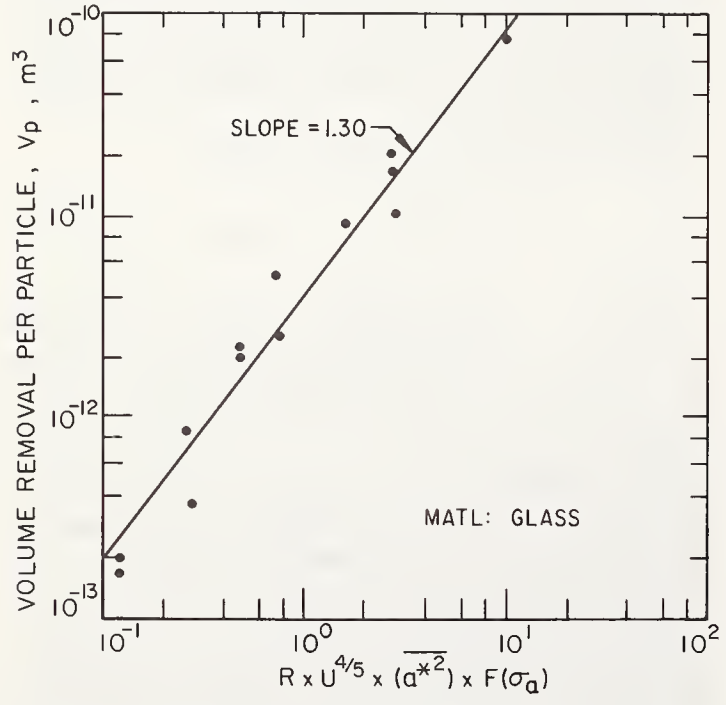

FIGURE 6. *Experimentally observed values of volume removed per particle (for a wide range of velocity and particle size) as a function of the predicted damaged volume.* Material: pyrex glass.

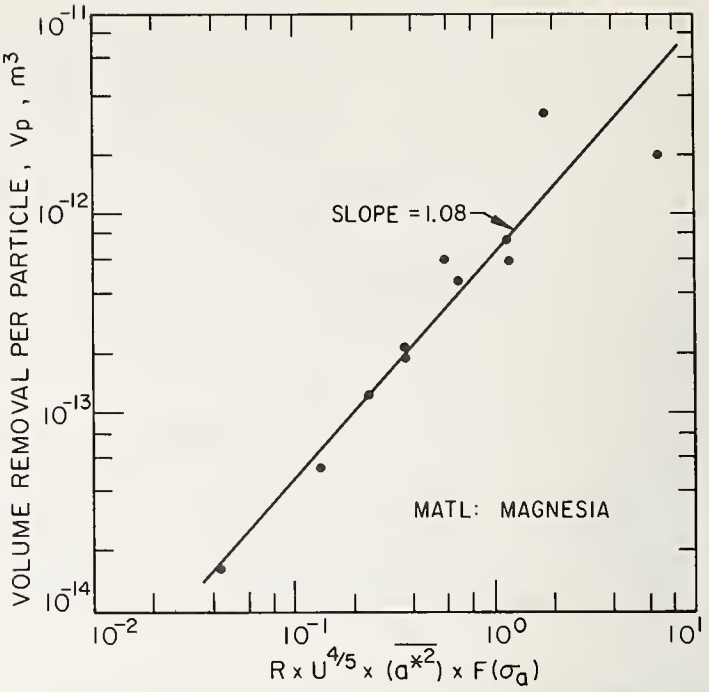

FIGURE 7. *Experimentally observed values of volume removed per particle (for a wide range of velocity and particle size) as a function of the predicted damaged volume.* Material: magnesia.

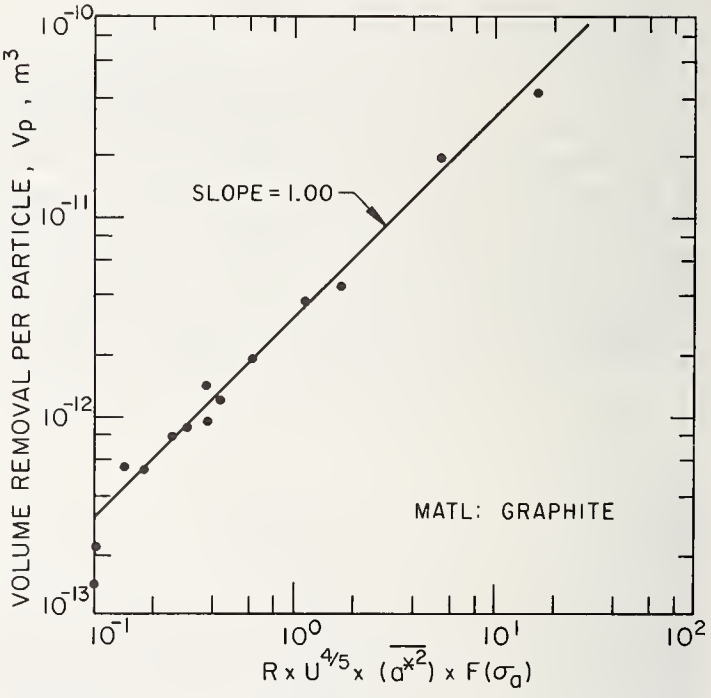

FIGURE 8. *Experimentally observed values of volume removed per particle (for a wide range of velocity and particle size) as a function of the predicted damaged volume.* Material: graphite.

proportional to the predicted volume damaged per particle, we expect the data points to fall on a straight line of slope unity. For magnesia and graphite this relation is indeed observed while for glass the points fall on a straight line of slope 1.3. We speculate that the discrepancy in the case of glass is primarily due to the fact that the strength of glass in dynamic tests (erosion) is higher than in static tests (ring-

cracking experiments). Possibly the use of the Weibull parameters obtained from dynamic tests would improve the prediction for glass.

3.2. Spherical Particles Striking at Oblique Angles

The extension of the preceding formulation to the case of oblique impact presents considerable difficulty. When a sphere is pressed against a surface with horizontal as well as vertical force the ring cracks are distorted and at relatively low values of horizontal force they become "horseshoe" shaped (open in the direction of sliding). The stress distribution prior to fracture is known from the work of Hamilton and Goodman [3]. Since fracture tends to propagate along a principle stress trajectory [9] (of the stress state prior to fracture) it is possible to compute the shape of these "horseshoe" cracks. We have done this and assumed that cracking terminates at a point where the maximum tensile stress prior to fracture equals a value σ_u. On this basis it is possible to predict the distribution of the "outermost" cracks as was done for the ring cracks. Although the ideas are straightforward, the equations are cumbersome and require extensive numerical computation. The results have been given by K. P. L. Oh [10] and we merely report them here. In the present case we take the volume damaged by a single particle as the area bounded by the outermost horseshoe crack multiplied by the depth of cracking computed as before from the vertical component of velocity. The only additional parameter in the analysis is the coefficient of friction between the sphere and the surface for this determines the horizontal force. In figure 9 the predictions are compared with experiment and it is seen that good agreement is obtained at angles near 90° with a coefficient of friction of $\mu = 0.03$. This value for μ is not unreasonable. Typical values for rolling friction coefficient between a ball and plate, including some shear along the contact area, are 0.001 to 0.01. For irregular geometry the quoted values are 0.05 to 0.2 [11]. At lower angles the decreased depth of cracking due to the decreased vertical component of velocity becomes the dominant factor and the choice of friction coefficient is not so important.

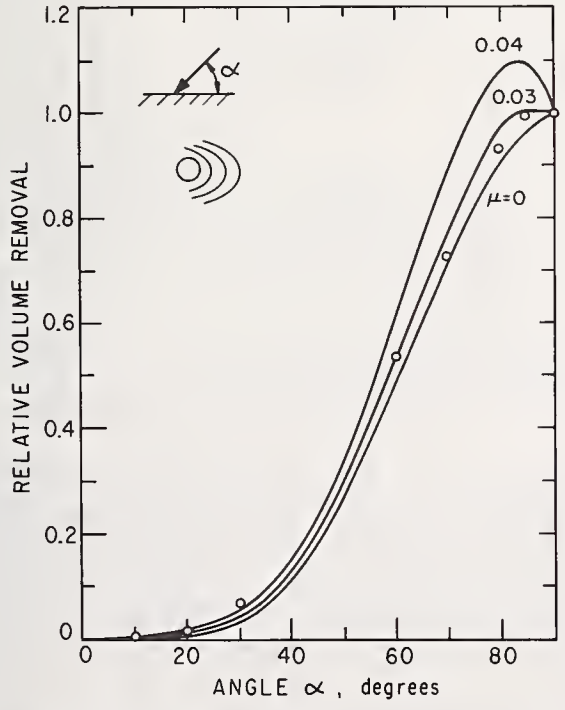

FIGURE 9. *Predicted and observed values of the relative volume removal as a function of angle of impingement for glass eroded by No. 110 steel shot at 200 ft/s* (60.96 m/s). Predictions are made for three values of μ, the coefficient of friction. The inserted sketch shows the contact circle and the horseshoe cracks.

3.3. Angular Abrasive Particles Striking Perpendicular to the Surface

In practice, erosion is often produced by angular abrasive particles rather than spheres. Since a detailed analysis of this probelm, similar to that developed for spheres, does not appear possible at the present time, we present an approximate solution following the approach suggested by Sheldon and Finnie [8] which was later developed by Finnie and H. L. Oh [12].

Surfaces struck by eroding particles typically have the appearance shown in figure 10. There is relatively little damage under the particle which is perhaps due to large hydrostatic compressive stresses at this point. On the surface surrounding the indentation, a fairly extensive region of material is cracked. Based on this observation, we assume that the volume removed by an eroding particle, V_p, is proportional

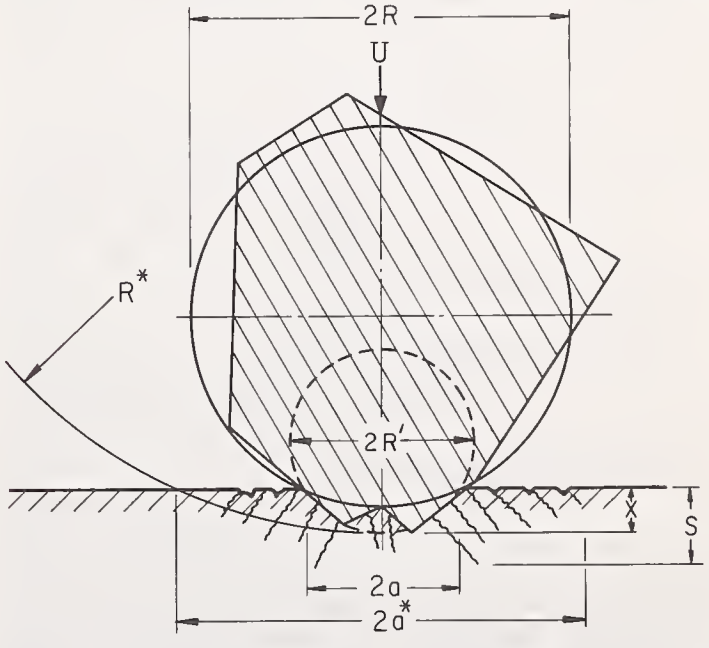

FIGURE 10. *Schematic view of cracking due to particle impact.*

to the damaged volume enclosed in the spherical cap of radius R^* and depth S. That is

$$V_p \propto S^2 R^*$$

In case the particle is not a sphere but irregular in shape, we may invoke two radii: radius R which corresponds to a sphere of equal weight as the particle and radius R' which is effective in producing fracture.

Now, we have to estimate S and R^* and as before, we shall take S as proportional to the depth of indentation X obtained from the Hertz solution. We consider R^* to be the radius of a much larger indenter than the actual particle which on the average produces a ring crack at radius a^*. This assumption is perhaps not too unreasonable because the cracked material is capable of transmitting load. Thus we write

$$S \propto X \propto R^* (\sigma_a^*)^2$$

But from eq(1) we see that approximately

$$\sigma_a^* \propto R^{*-\frac{2}{m+2}}$$

Eliminating σ_{a^*}, we arrive at a relation between R^* and X:

$$R^* \propto X^{\frac{m+2}{m-2}}$$

We relate the depth of indentation to the particle velocity, the particle mass and the radius of curvature R' of the contacting region following the general approach given by Timoshenko [4] to obtain

$$X \propto [R^6/R']^{1/5} U^{4/5}$$

where U is the particle velocity. Finally, volume removed per particle is:

$$V_p \propto S^2 R^* \propto X^2 R^* \propto X^{\frac{3m-2}{m-2}}$$

$$\propto \left[\frac{R^6}{R'}\right]^{1/5\left(\frac{3m-2}{m-2}\right)} U^{4/5\left(\frac{3m-2}{m-2}\right)}$$

We distinguish two cases

spherical particle: $R' = R_1$

$$V_p \propto R^{\frac{3m-2}{m-2}} U^{4/5\left(\frac{3m-2}{m-2}\right)}$$

irregular particle: R'

$$V_p \propto R^{6/5\left(\frac{3m-2}{m-2}\right)} U^{4/5\left(\frac{3m-2}{m-2}\right)}$$

These expressions for the dependence of volume removal on particle size and velocity have been confirmed. In experiments on six brittle solids over a wide range of velocities and particle sizes [13] it was indeed found that the volume removal per particle could be written as

$V_p \propto R^a U^b$ for spherical steel shot

$V_p \propto R^{a'} U^b$ for angular silicon carbide particles

A comparison of the predicted and observed values of a, a' and b is given in figure 11. Except for glass eroded by spherical steel shot the correlation between theory and experiment is good, particularly in view of the number of assumptions involved.

3.4. The Brittle-Ductile Transition

An interesting consequence of the size-effect on strength of brittle solids is that if they are loaded on smaller and smaller regions, the stress required to produce fracture may eventually exceed that required for yield. Thus, we can understand the familiar observation that microhardness or scratch hardness tests on brittle soldis may produce flow rather than fracture. In erosion the response of brittle and ductile solids to changes in the angle of impingement are markedly different, as shown schematically in figure 12. Thus a transition to ductile behavior should be easily detectable.

To estimate the particle size at which ductile behavior should be noticed in erosion testing of nominally brittle solids, we need only the parameters of the Weibull distribution and inden-

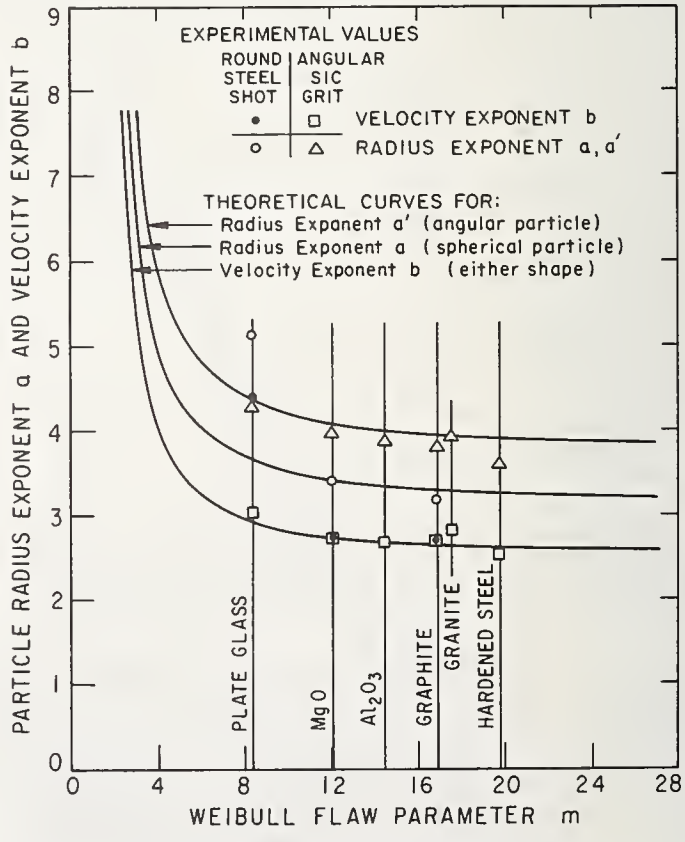

FIGURE 11. *Comparison of theoretical and experimental values of particle velocity and radius exponents as a function of the Weibull flaw parameter* m.

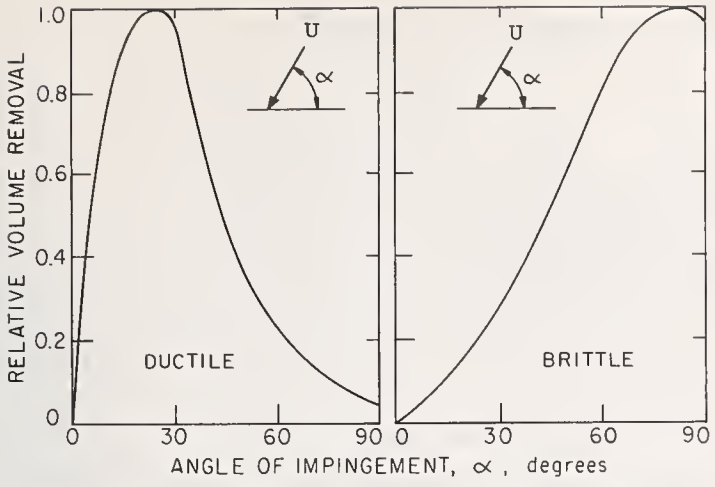

FIGURE 12. *Schematic representation of the erosion behavior of ductile and brittle solids.* The maximum erosion is taken as unity in both cases.

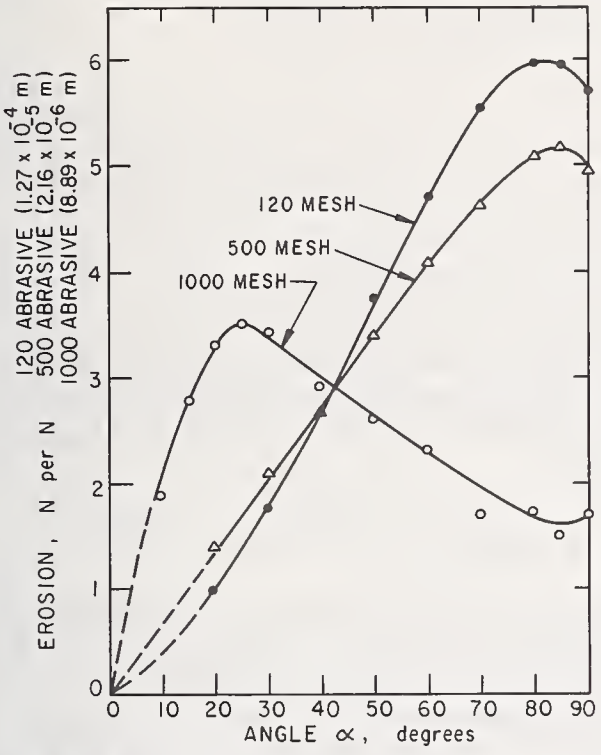

FIGURE 13. *Weight removal per newton of abrasive as a function of particle approach angle α for glass eroded by silicon carbide particles at 500 ft/sec* (152.4 m/s).

tation hardness measurements. For glass, this estimate can be made even more directly from the data shown in figure 3. The mean value of σ_a (the stress at the rim of the contact area) required for fracture is related to the average stress p under the indenter through the Hertz equations as:

$$p = \sigma_a 2/(1-2_V) \sim 4\sigma_a$$

So, for an indenter of radius 10^{-3} in (2.54×10^{-5}m) we would estimate $\sigma_a \simeq 250{,}000$ psi (1,724 MN/m²) and $p \simeq 10^6$ psi (6,895 MN/m²) from figure 3. Values of the flow pressure $p_{(yield)}$ for glass have been given by Marsh [14] and are typically about 800,000 psi (5,516 MN/m²) for ordinary hardness tests and about 2,000,000 psi (13,790 MN/m²) for hardness tests at low temperature where time-dependent effects are absent. The points in figure 3 are of course for static tests and would be somewhat higher if dynamic loading had been used. So direct comparison is impossible but it appears that yield should occur before fracture for particles in the range 10^{-4} in (2.54×10^{-6}m) to 10^{-3} in (2.54×10^{-5}m) in radius. Erosion tests on glass show just such behavior. In figure 13 it is seen that erosion tests on glass with particles 5×10^{-3} in (1.27×10^{-4}m) and 8×10^{-4} in ($2.03 \times 10^{-5}m$) in diameter lead to typically brittle behavior while 3.5×10^{-4} in ($8.89 \times 10^{-6}m$) diameter particles show erosion behavior which is typical of ductile metals. Other aspects of the brittle-ductile transition in erosion have been discussed by Sheldon and Finnie [15].

4. Analysis of Ultrasonic Cutting

In this shaping process a slurry of hard abrasive particles and water separates a vibrating tool from the surface being shaped. Typically the tool vibrates normal to the surface at a frequency of about 25,000 Hz with amplitude of the order of 10^{-3} in ($2.54 \times 10^{-5}m$). Thus the particles are driven into the surface to produce localized fracture. A small average force is applied between the tool and the workpiece to keep them close together during the operation. Much has been written on ultrasonic cutting including three textbooks and several comprehensive reviews with the most complete theories having been given by Shaw [16] and by Russian workers [17]. However, the statistical nature of the strength of the workpiece does not appear to have been considered. As Cook [18] points out "It seems clear that until we understand small-scale fracture of brittle materials, we will not be able to properly analyze this process."

We will now show that the material properties may be incorporated into an analysis of ultrasonic cutting and will base our treatment on the cracked configuration shown in figure 1. Since the boron carbide particles, which are used in our experiments, and in most practical ultrasonic cutting operations, are more nearly spherical than angular we consider only the case of spherical particles in analyzing this process. The formulation of the expression for volume removal is more difficult than erosion for the particle size distribution must be considered. In erosion all particles may participate in removing material but in ultrasonic cutting only the largest particles are active. As shown in figure 14, when the tool descends to its lowest position at a distance c from the workpiece, only those grits whose diameter $\xi > c$ indent and remove material, and then the depth of indentation

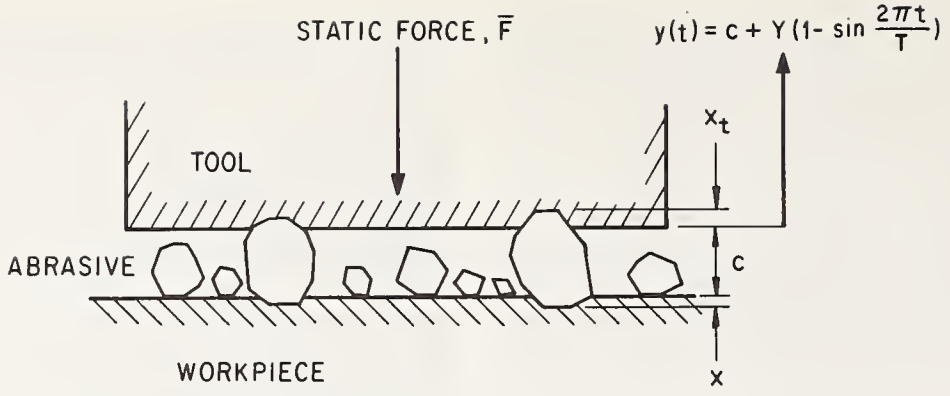

FIGURE 14. *Configuration involved in ultrasonic cutting.*

varies from grit to grit. Because of this aspect of the process, it is no longer appropriate to consider volume removal on a single particle basis as we have done in eq (3). Rather, we should consider the average volume removal

$$\bar{V} \propto \int_c^{\xi_{max}} X \, \overline{a^{*2}} \, F(\sigma_a) \frac{d\Phi(\xi)}{d\xi} \, d\xi \propto I(c) \quad (5)$$

where $\Phi(\xi)$ is the grit size distribution, ξ_{max} denotes the maximum grit diameter, (ξ_{max}, c) denotes the range of the active particle diameter, and $I(c)$ denotes the values of the integral, a function of c.

As indicated by eq (2), $(\overline{a^{2*}})$ is a function of σ_a and R, given values of the Weibull parameters. In turn, σ_a may be expressed in terms of X and R thru eq (4). The quantity $I(c)$ in eq (5) may therefore be evaluated once the range of the active particle diameter is determined and if an independent relation between X and R can be established. This may be obtained through a consideration of the mechanics of the process as outlined below.

We assume that the tool oscillates with amplitude Y and period T at a distance $c + Y(1-\sin 2\pi \frac{t}{T}$ from the work piece with an average force $\bar{F}$ exerted on it as shown in figure 14. By geometery,

$$X + X_t = \xi - c - Y\left(1 - \sin\frac{2\pi t}{T}\right)$$

Also, from the Hertz equations,

$$P(t) \propto X^{3/2} R'^{1/2} \propto X_t^{3/2} R'^{1/2}$$

It follows that

$$X \propto X_t \propto \xi - c - Y\left(1 - \sin\frac{2\pi t}{T}\right)$$

$$P(t) \propto R'^{1/2}\left[\xi - c - Y\left(1 - \sin\frac{2\pi t}{T}\right)\right]^{3/2}$$

When the tool reaches its lowest position c (i.e., $t = T/4$) the depth to which a particle indents the workpiece is

$$X \propto (\xi - c) \quad (6)$$

and the impulse delivered is

$$\int P(t)\, dt \propto R'^{1/2} \int^{T/4} \left[\xi - c - Y\left(1 - \sin\frac{2\pi t}{T}\right)\right]^{3/2} dt$$

$$\frac{T}{2\pi} \sin^{-1}\left(\frac{c + Y - \xi}{Y}\right)$$

$$\propto T\left(\frac{R'}{Y}\right)^{1/2} (\xi - c)^2$$

Since the momentum developed over one cycle $\bar{F}\ T$ must equal the average total impulse delivered by the N particles underneath the tool, we have

$$\bar{F} \propto N\left(\frac{R'}{Y}\right)^{1/2} \int_c^{\xi_{max}} (\xi - c)^2 \frac{d\Phi(\xi)}{d\xi} \, d\xi \quad (7)$$

A form for $\Phi(\xi)$ must now be chosen in order to evaluate the integral. We chose a Beta function because under normal operations, only particles with diameters close to ξ_{max} are active and in the neighborhood of ξ_{max}, the Beta function can describe the actual grit size distribution quite accurately. Thus,

$$\Phi(\xi) = 1 - \left(1 - \frac{\xi}{\xi_{max}}\right)^{\beta+1}.$$

For example, it is seen in figure 15 that by taking $\beta = 2.15$, $\xi_{max} = 39.8$ microns ($39.8 \times 10^{-6} m$) a good description of the 500 mesh boron carbide that we used is obtained in the upper 15 percent range. Employing a Beta function for $\Phi(\xi)$ in eq (7) and carrying out the integration, we have

$$\bar{F} \propto (\beta+1)\frac{\Gamma(\beta+1)\Gamma(3)}{\Gamma(\beta+4)} N (\xi_{max})^2 \left(\frac{R'}{Y}\right)^{1/2}$$

$$\left(1 - \frac{c}{\xi_{max}}\right)^{\beta+3} = K_u \left(\frac{R'}{Y}\right)^{1/2} \left(1 - \frac{c}{\xi_{max}}\right)^{\beta+3}$$

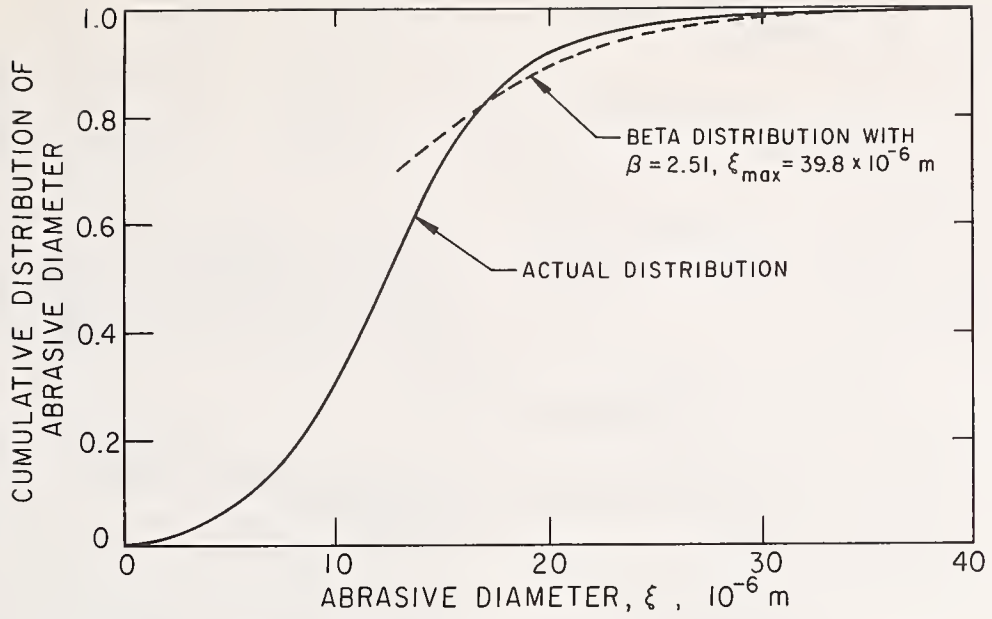

FIGURE 15. *Particle size distribution of the boron carbide used in the experiment.*

where we make use of the fact that $N\ (\xi_{max})^2$ is a constant for constant tool cross-sectional area. The proportionality constant K_u involves β, the cross sectional area of the tool, the slurry concentration and the elastic properties (E,μ) of the tool, grit and workpiece. The value of c may therefore be evaluated for known values of process variables and together with eq. (6) would allow us to estimate I(c) in eq. (5). We have used the following data in our calculations and preliminary experiments:

$Y \simeq 0.001$ in $(2.54 \times 10^{-5}{}_m)$

$\overline{F}$ = 12 oz, 16 oz and 24 oz (3.33 N, 4.45 N and 6.67 N)

Slurry concentration, water/abrasive by weight = 1.5

Tool cross sectional area = 0.08 sq in $(5.16 \times 10^{-5}{}_m{}^2)$

Tool material: mild steel, $E = 30 \times 10^6$ psi $(2.07 \times 10^5\ MN/m^2)$, $\mu = 0.30$

Grit material: Boron carbide 500 mesh, $E = 42 \times 10^6$ psi $(2.89 \times 10^5\ MN/m^2)$, $\mu = 0.25$, size distribution as shown in figure 15

Work piece material: MgO and glass, with properties as reported by Sheldon and Finnie [8].

The results are shown in figures 16 and 17, where we have plotted observed volume removal against I(c) for three values of $\overline{F}$ for glass and magnesia. The data points fall on a straight line of slope unity indicating that predictions are indeed satisfactory. We intend to conduct more experiments in the future to confirm the predictions over a wider range of the variables.

5. Quantitative Prediction of Volume Removal

In our treatment of shaping processes we have taken the volume removed by a single particle as proportional to the cracked volume produced by a single particle contacting a

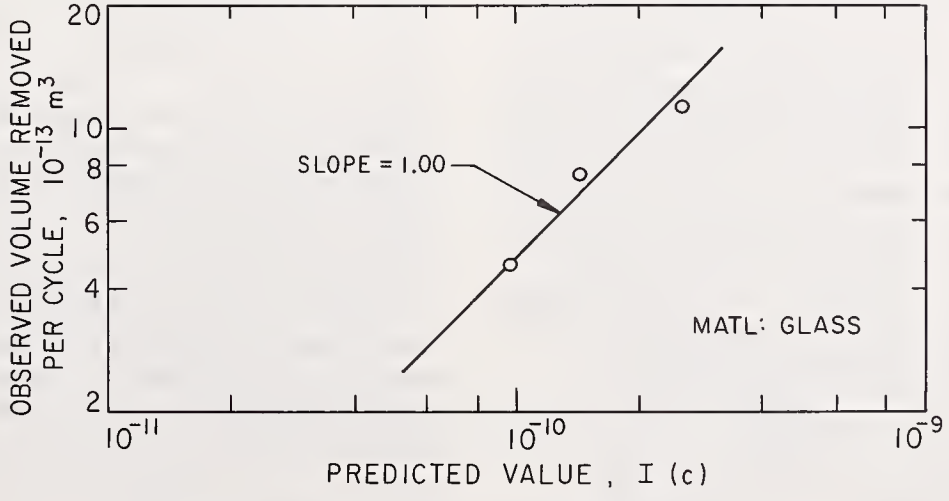

FIGURE 16. *Observed volume removal as a function of predicted value,* I(c), *for ultrasonic cutting of pyrex glass.*

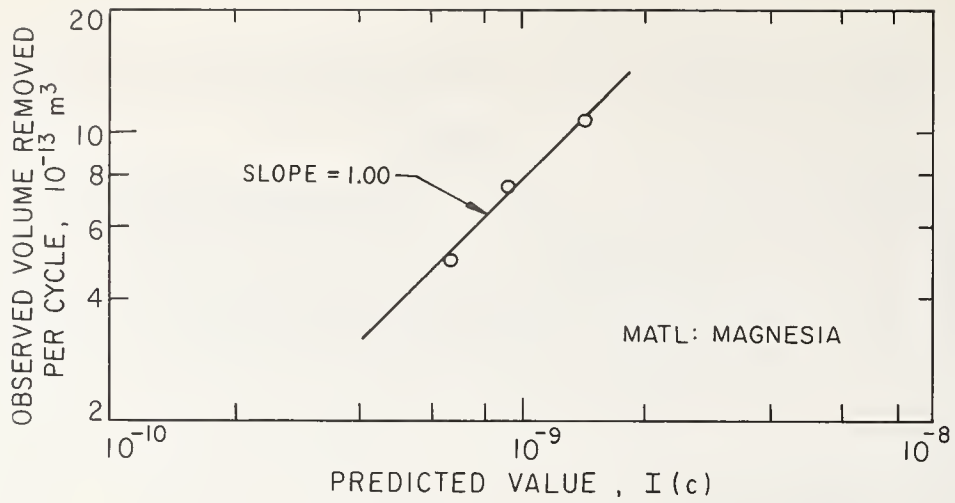

FIGURE 17. *Observed volume removal as a function of predicted value, I(c), for ultrasonic cutting of magnesia.*

smooth surface. Thus at least one test, using the shaping process of interest, must be made on the chosen material before quantitative predictions can be made. We took this approach because the intersection of the fracture patterns from many particles will be a complex process and more work needs to be done on this topic before a complete quantitative treatment of shaping operations is possible. However, it may be of value to outline some preliminary considerations in this regard.

Generally, one would expect that the extent of cracking in any brittle solid would depend only on the stress state in the part prior to fracture on the fracture toughness of the material. This latter quantity could be expressed by an effective surface energy for fracture under plane strain conditions G_{IC} $\frac{\text{in lbs}}{\text{in}^2}$ (mN/m^2) or by the related value of the stress intensity factor K_{IC} lbs/in$^{3/2}$ $(N/m^{3/2})$ where

$$G_{IC} = \frac{K^2_{IC}}{E}(1-\mu^2) \simeq \frac{K_{IC}{}^2}{E}$$

Normally, the elastic modulus does not appear in elastic solutions for the stresses but in the present case, because of the change of contact area with load, we would expect the stress state and hence the crack depth in the solid to depend on the modulus as well as on the load (or velocity) and the radius of the indenter.

In our analysis of shaping by spherical particles we took the depth of cracking as proportional to the depth of indentation. That is:

$$S \sim \frac{P^{2/3}}{R^{1/3}E^{2/3}}$$

where E is a weighted average of the moduli of indenter and surface given by the Hertz equations. A limitation of this expression is that the surface energy for fracture is not included and hence the constant of proportionality must depend on K_{IC} (or G_{Ic}).

By contrast, Barenblatt [19] in discussing the literature on fracture under a cylindrical punch, where the contact area does not change with load, showed that the diameter of the base of the cone crack is proportional to:

$$\left(\frac{P}{K_{IC}}\right)^{2/3} \sim \frac{P^{2/3}}{(G_{IC}E)^{1/3}}$$

Very recently, we have made further studies of the depth, S, of the initial ring crack in glass loaded by spherical indenters. Rather than finding S proportional to the indentation X, i.e., $S \sim P^{2/3}/R^{1/3}$, recent work suggests $S \sim \frac{P^{5/6}}{R1/3}$

Hence from dimensional consideration, we speculate that:

$$S \sim \frac{P^{5/6}}{R^{1/3}G_{IC}E^{1/2}} \sim \frac{P^{5/6}}{R^{1/3}K_{IC}{}^{2/3}E^{1/6}}$$

This new result will not change any of our previous predictions significantly but does suggest that the coefficient of proportionality between the volume $(a^{*2})\ X\ F\ (\sigma_a)$ and the volume removed per particle should involve $1/(G_{IC}{}^{1/3}E^{1/2})$. Representative values of G_{IC} are not easy to obtain for brittle solids. However, from the literature we obtained the following approximate values for the materials we studied

	G_{IC} $\frac{\text{in lb}}{\text{in}^2}$	E $\frac{\text{lb}}{\text{in}^2}$	$(G_{IC}^{-1/3}E^{-1/2})$	$\frac{\textit{Observed Damage Per Particle}}{(a^{*2})\ X\ F\ (\sigma_a)}$
Glass	15×10^{-3}	10×10^{6}	3	9*
Graphite	5×10^{-1}	1×10^{6}	3	7*
MgO	80×10^{-3}	30×10^{6}	1	1

*Relative to MgO as unity

Comparison of the last two columns shows that this method of predicting volume removal is far from precise but may be worth pursuing in future work.

6. Conclusions

We have shown that the Weibull statistical treatment of brittle strength may be used to predict the loads required to produce fracture under small indenters. An extension of the Weibull treatment allows prediction to be made about the location of fracture. In determining the region that is damaged by a single spherical particle we have seen that an important quantity is the outermost ring crack and that this can also be predicted. Essentially, we use statistical considerations to determine the extent of cracking on the surface and empirical experimental observations to determine the depth to which cracks extend below the surface. Improvements in the analysis could perhaps be made by a better understanding of the interaction of cracks and the extent to which they propagate. Recent work in this direction is discussed.

We have attempted to analyze these shaping operations without any consideration of optimizing them, although this has been touched on briefly in previous work [12]. It could be argued that all shaping operations we have discussed are relatively inefficient because they involve loading the material predominantly in compression and brittle solids are much stronger in compression than they are in tension. Bailey and Dean [20] in a study of ice drilling compared the "specific energy" required in various drilling methods. On this basis a man with a pick was 100 times better than present drilling methods. Presumably he looks for a weak spot, inserts the pick and loads the material in tension. While we could shape brittle solids by reflecting compressive elastic pulses from free surfaces as tension waves this process would be extremely difficult to control if precise shaping was desired. Thus, until the flaws inherent in brittle solids can either be eliminated or detected we will have to use shaping operations which are inherently inefficient as material removal processes. Because of the "size-effect" in strength, if smaller particles are used to obtain a finer surface finish, the processes become even more inefficient and eventually with small enough particles some brittle solids will behave in a ductile manner.

7. References

[1] Finnie, I., Review of the metal cutting theories of the past hundred years, Mech. Eng. 78 (1956) 715–721.

[2] Walker, D. R., and Shaw, M. C., A physical explanation of the empirical laws of communition, Mining Eng. 6 (1954) 313–320.

[3] Hamilton, G. M., and Goodman, L. E., The stress field created by a circular sliding contact, J. Appl. Mech. 33 (1966) 371–376.

[4] Timoshenko, S., and Goodier, J. N., Theory of elasticity (McGraw Hill Book Co., New York, N. Y. 1951).

[5] Weibull, W., A statistical theory of the stength of materials, Handl., Stockholm, 1939). No. 151.

[6] Oh, H. L., and Finnie, I., The ring cracking of glass by spherical indenters, J. Mech, Phys. Solids, 15, 401–411 (1967).

[7] Oh, H. L., and Finnie, I., On the location of fracture in brittle solids I—due to static loading, Int. J. of Fracture Mechanics. Sept. 1970) 287–300.

[8] Sheldon, G. L., and Finnie, I., The mechanism of material removal in the erosive cutting of brittle materials, Trans. ASME 88B, 393–400 (1966).

[9] Erdogan, F., and Sih, G. C., On the crack extension in plates under plane loading and transverse shear. Trans. ASME, J. Basic Eng., 519–525 (1963).

[10] Oh, K. P. L., On the Statistical Nature of Brittle Fracture, PhD. thesis in Mechanical Engineering, University of California, Berkeley, (1970).

[11] McClintock, F. A., and Argon, A. S., Mechanical behavior of materials, 665 (Addison Wesley Publishing Co., 1966).

[12] Finnie, I., and Oh, H. L., An analysis of rock drilling by erosion, Proc. 1st. Congress Int Soc. Rock Mechanics 2, 99–104 (1966).

[13] Sheldon, G. L., Erosion of Brittle Materials, PhD. thesis in Mechanical Eng., Univ. of California, Berkeley, (1965).

[14] Marsh, D. M., Plastic flow in glass, Proc. Roy. Soc. (London) 279A, 420–435 (1964).

[15] Sheldon, G. L., and Finnie, I., On the ductile behavior of nominally brittle materials in erosive cutting, Trans. ASME 88B, 387–392 (1966).

[16] Shaw, M. C., Ultrasonic Grinding, Microtecnic, X, No. 6, 257–265 (1956).

[17] Kazantsev, V. F., and Rosenberg, L. D. The mechanism of ultrasonic machining, Ultrasonic, 166 (1965).

[18] Cook, N. H., Manufacturing Analysis, 134 (Addison Wesley Publishing Co., Reading Mass. 1966).

[19] Barenblatt, G. I., Mathematical theory of equilibrium cracks, in advances in applied mechanics H. L. Dryden and T. von Karman, editors (Academic Press 7 1962) 55–129.

[20] Bailey, J. J. and Dean, R. C., Jr., Rock mechanics and the evolution of improved rock cutting methods, in Failure and Breakage of Rock Proc. 8th Symposium on Rock Mechanics AIMME, New York, (1967), 396–409.

Discussion

KIRCHNER: Why do you use the volume theory rather than the surface theory?

FINNIE: For the case of glass we use surface. V would represent an element of surface area. For the case of polycrystalline ceramics we integrate over the volume stressed in tension.

KIRCHNER: How do you justify that?

FINNIE: There is a fair amount of evidence from people who have studied bending tests that the flaws in polycrystalline ceramics are distributed throughout the volume.

RICE: Would a small amount of plastic deformation prior to fracture explain, at least partially, the location of ring cracks outside of of the ball contact area?

FINNIE: For the ball sizes for which we observed the location of fracture, the stress levels are such that we would not expect plastic deformation in the steel ball or in the glass.

NATIONAL BUREAU OF STANDARDS SPECIAL PUB. 348, THE SCIENCE OF CERAMIC MACHINING AND SURFACE FINISHING, Proceedings of a Symposium Sponsored by the American Ceramic Society, the Office of Naval Research, and the National Bureau of Standards, held at NBS Nov. 2–4, 1970, Gaithersburg, Md. (Issued May 1972).

Sonic Machining of Ceramics

William B. Campbell[1]

The Ohio State University
Columbus, Ohio 43210

The effect of 10 kHz sonic vibrations on the shaping and finishing of fired ceramic shapes was investigated to identify optimum machining conditions commensurate with product and surface quality. Sonic motors, developed at The Ohio State University and with outputs up to 15 horsepower, were used to activate the machine tool. Significant improvements in tool wear were observed in impact-tuned systems that produced removal rates greater than 45 cu in per min. Template and profile tooling were successfully used to obtain open cutting surfaces. Over 3000 test cuts provided the data necessary to identify optimal parameters of operation.

Key words: Abrasive; ceramic machining; sonic machining; vibrational machining; wheel machining.

1. Introduction

Among the major methods for obtaining surface finish and complex configurations are mechanical finishing and shaping processes. For ease of application and minimumization of process costs, most ceramic machining processes are confined to green ware; however, many fired products require final finishing or shaping. Vitrified grinding wheels, some floor tile and refractory shapes are among present products requiring final finishing.

A recent program in the Department of Ceramic Engineering at the Ohio State University was concerned with the evaluation and development of machining processes for shaping, and finishing vitrified grinding wheels. Sonic cutting methods were evaluated to establish conditions necessary for optimum machining rates commensurate with product and surface quality. The major parameters defining the cutting conditions were:

1. Wheel speed (surface speed)
2. Feed rate
3. Degree of open surface
4. Uniformity of dimensions
5. Depth of cut
6. Tool shape
7. Tool orientation
8. Power source requirements

Over 3000 test cuts were required to identify conditions which produced open surfaces and uniform dimensions. For comparative purposes, all data were evaluated against a production removal rate of 20 in per min feed, 0.040 in depth and 170 RPM resulting in an average removal rate of 8.8 cu in per min. Sonic cutting produced acceptable product properties and exceeded the current rate of removal in production. Roll crushing cuts and profiles were simulated with a template tool; the depth and degree of open surface surpassed present specifications.

2. Sonic Motors

Energy transfer by mechanical vibrations of a single frequency has been termed sonic power [1][2]. Although these mechanical vibrations are identical in character to acoustic vibrations, no fundamental change occurs when their frequency is raised from the audible to the ultrasonic range. At higher frequencies, processing applications are limited by material capabilities because transducers typically operate with amplitudes inversely proportional to the operating frequency. Inertial forces exceed material property limits because acceleration increases with the square of frequency. In many practical applications where amplitudes of several mils (0.001 in) are necessary, conventional transducer power sources are unsuitable [2].

A new transducer design [3–5], developed at the Ohio State University Sonic Power Laboratory, incorporates lead-zirconium titanate ceramic crystals mounted on a metal "horn" and concentrates the vibrations at the tip. Operation at 10 kHz and 2600 volts is powered by a commercial rotating inductor generator and a step-up transformer. A set of crystals, costing less than fifty dollars [6], are connected electrically in parallel to produce a tip displacement of 0.0035 in with a measured delivered power of 10 kw (15 hp) in the P–11 motor and a delivered power of 500 watts (approximately one-half hp) in the P–7 motor. The measured efficiency of each motor exceeds 90 percent, the former approaching 97 percent.

Two prototype sonic motors, figures 1 and 2, illustrate the range of size and ratings currently available. The one-half hp motor has about one cubic inch of active piezoelectric ma-

[1] Associate Professor, Department of Ceramic Engineering.
[2] Figures in brackets indicate the literature references at the end of this paper.

terial which activates the half wave horn to dynamic conditions shown in figure 3. With its steel resonator and force-concentrating unit, the P–7 motor weighs about three pounds. The larger motor, P–11, has a piezoelectric volume of five and one-third cubic inches, operates with a full wave dynamics shown in figure 4, and has a total weight of 22 lbs.

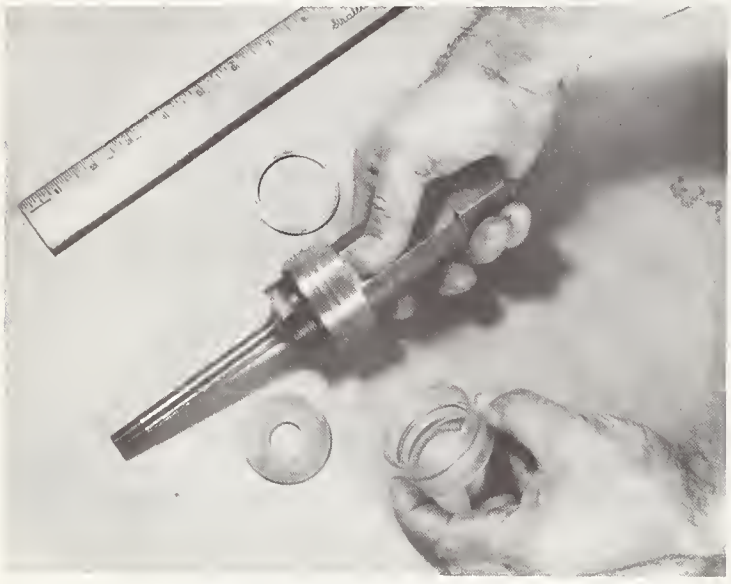

FIGURE 1. *One-half horsepower sonic motor of one-half wavelength stepped-horn design.*

FIGURE 2. *Fifteen horsepower sonic motor with catanoidal full wave horn design.*

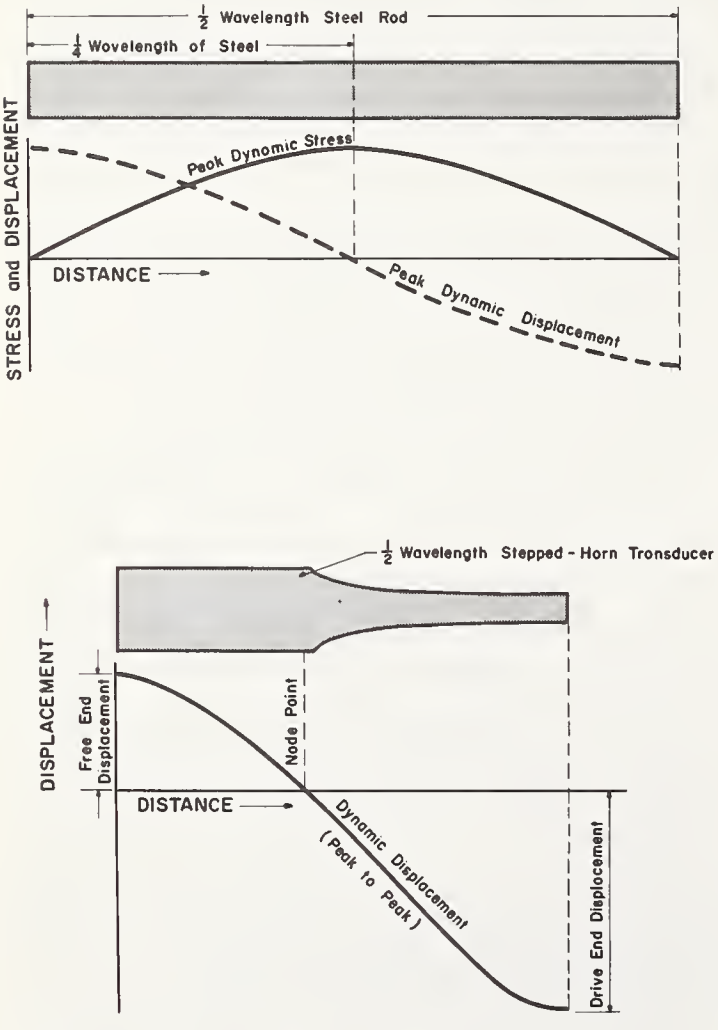

FIGURE 3. *Dynamic operating conditions in half wave horn transducer.*

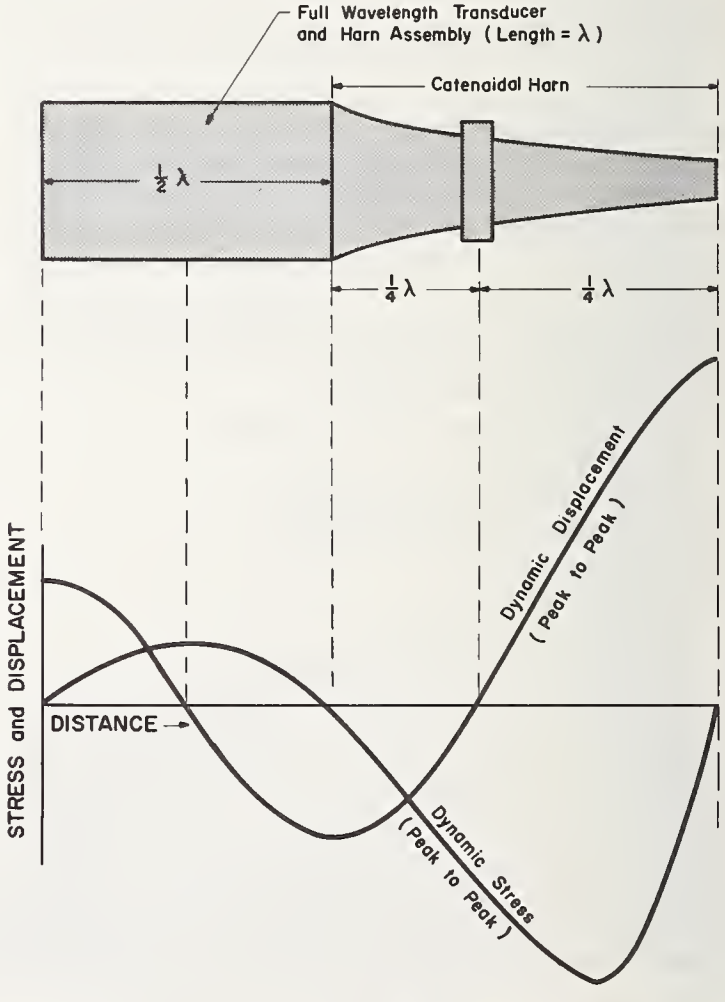

FIGURE 4. *Dynamic operating conditions in full wave horn transducer.*

3. Machining Criteria

For most abrasive products the term *grade* is used to define "the tenacity with which the bonding material clings to the abrasive grains in times of stress, and keeps them from breaking out[7]". This characteristic has been related to a microstructural model by Kingery and co-workers [8]. The similarity of our specimens to the constraints of their model permits a direct analysis of machining forces.

Assuming the case of a particle having one residual bond, figure 5, fracture will occur when the fracture strength of the bond is reached.

$$\sigma_{\max} = \frac{Mc}{I} \tag{1}$$

where M = force movement
C = distance to outer fiber
I = moment of inertia

and

$$\sigma_{\max} = \frac{2RF}{\pi h^3/4} \tag{2}$$

The force for fracture is

$$F = (\sigma_f)\ \frac{\pi h^2}{8(R/h)} \tag{3}$$

Since the load on one grain is inversely proportional to the number of grains in the work areas, the critical force at the machining interface is

$$F' = (\sigma_f)\frac{\pi}{8}\ \frac{h^3}{R^3}\ R^2/kV_aR^2 \tag{4}$$

$$F' = G\sigma_f/k \tag{5}$$

where k is a geometrical constant dependent on wheel size, tip shape and work area, and

$$G = \pi h^3/8R^3V_a \tag{6}$$

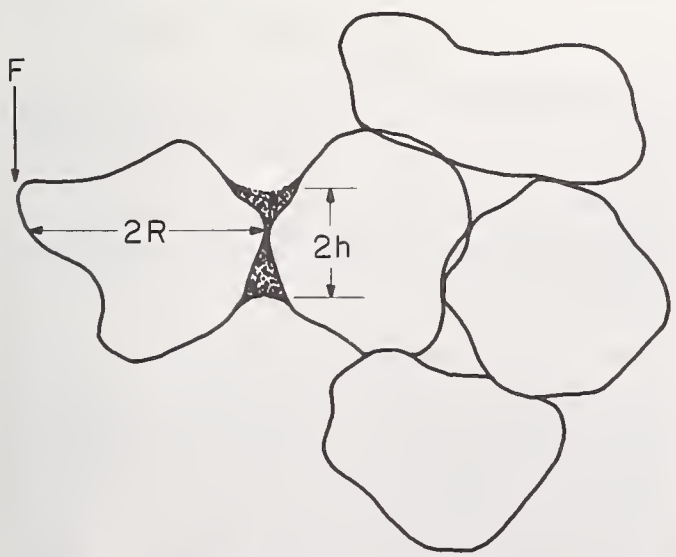

FIGURE 5. *Applied force F braking a single particle from a wheel.* [8]

is the analytical grade factor. Thus, the inherent bond fracture strength is more controlling than the amount of bond present since V_a is constant.

Extending this relationship to examine elastic behavior, the critical force becomes

$$F'' = (E_b\epsilon\epsilon_b)G/K \tag{7}$$

If the critical value of ϵ_b is exceeded, fracture occurs in the bond and the rate of fracture, or grain removal, will depend upon the rate of tip movement or work area. Brittle bond fracture will occur only when the elastic limit is exceeded; however, the application of vibrations to the tool increases the applied stress. Thus, the effective work area may be increased. Moore and Kibbey [9] reported high rates of ceramic tool wear for conditions of high amplitude and frequency. Their tests were qualitative but indicated the direction of vibration and high frequencies to be most detrimental on ceramic wear rates.

The only factor in eq (7) that is dependent on system kinetics is the geometrical constant, k. This constant will have different values for differing kinetic conditions because it is related to work area, which is related to feed and speed. As the work increases, the force per grain decreases until it is not sufficient to remove each grain; at this point tool wear increases and material removal decreases. With impressed vibrations the response is similar except that the higher stress level (vibrational energy proportional to the cube of frequency) extends the wear and removal units. Thus, an optimum feed and speed for sonic machining is to be anticipated.

4. Conventional Machining Rates

The cutting rate reported as representative of current production operations was calculated to be *8.8 cubic in per min.* This value is the weighted average between the peripheral rate of 15.2 in^3/min and the spindle rate of 2.55 in^3/min. The weighted average is equal to the value obtained by weight loss measurements and subsequent volume calculations based on density. For actual cutting tests, the removal rate was determined by weight loss and time measurements, as well as by measurements of dimensional changes. A comparison of these independent volume values indicated a two per cent maximum deviation.

5. Tool Shapes and Orientations

Three tool shapes were evaluated for cutting performance at different orientations. The tool shape and optimum orientation are shown in figures 6, 7 and 8. Tools were shaped from standard carbide tips, No. TNG–334, Grade B–106, Ultramet Corporation, Urbana, Ohio. The

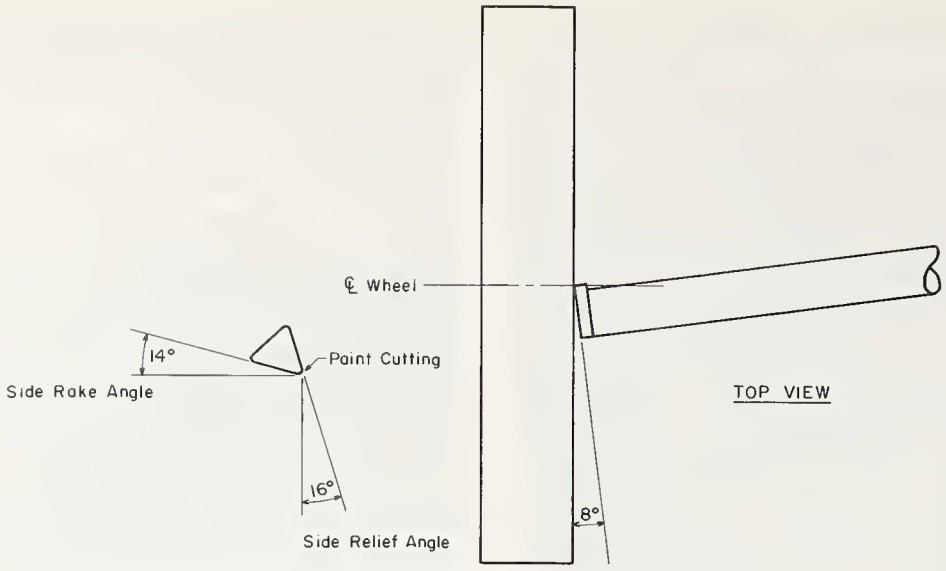

FIGURE 6. *Optimum orientation for tip 1.*

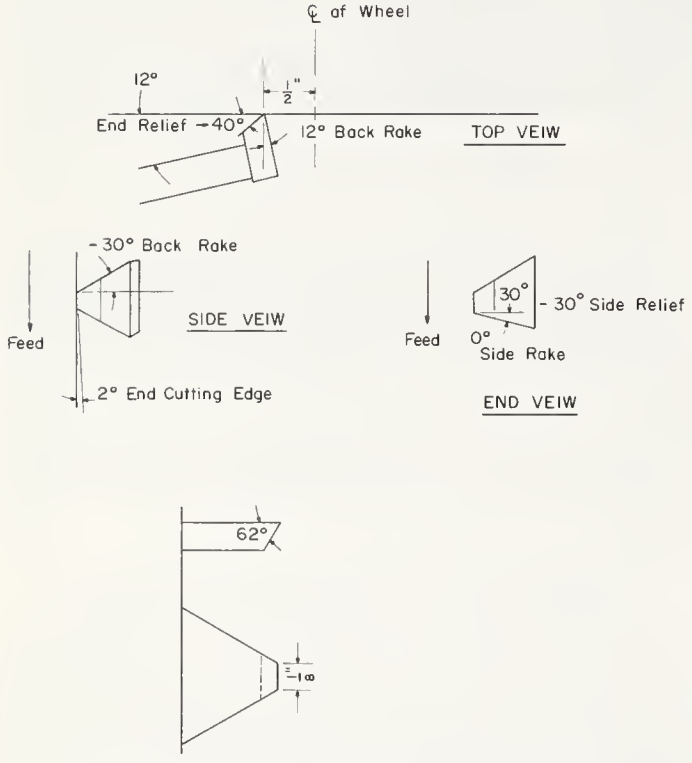

FIGURE 7. *Optimum orientation for tip 2.*

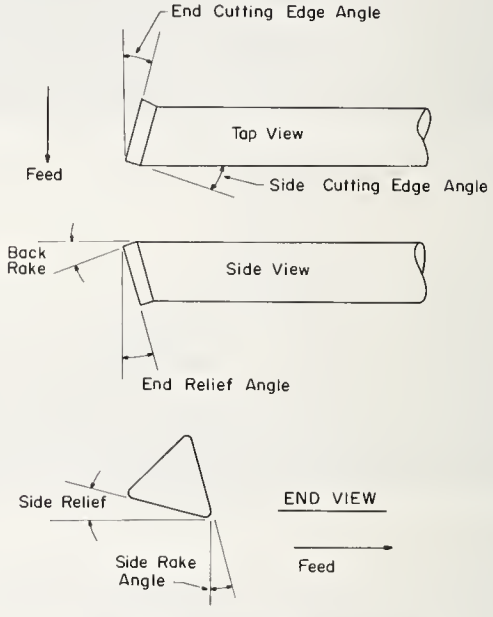

FIGURE 8. *Optimum orientation for tip 3.*

tips were brazed to the mounting cap or bar prior to installation on the motor. The carbide tips were satisfactory for the purposes of this study; however, it is anticipated that further improvements in both material and shape remain for future investigations.

The following nomenclature and tool orientations were utilized in this study.

Rake angle: The wedge angle of the tool at the point of workpiece contact.

Relief angle: The angle between the tool surface and the unmachined surface which prevents contact (usually less than 10 degrees).

Cutting edge angle: The angle describing the distance that the nose trails the leading edge.

Nose radius: Radius at the cutting tip.

The principal tool orientations are illustrated in figure 9.

6. Optimum Speed

The effect of wheel speed was determined over the range 150 to 400 RPM for each combination of tool shape, power source, machining orientation and wheel grade. In all cases, the optimum removal rate was achieved at speeds shown below for six inch wheels. Above these speeds, tool wear was excessive and

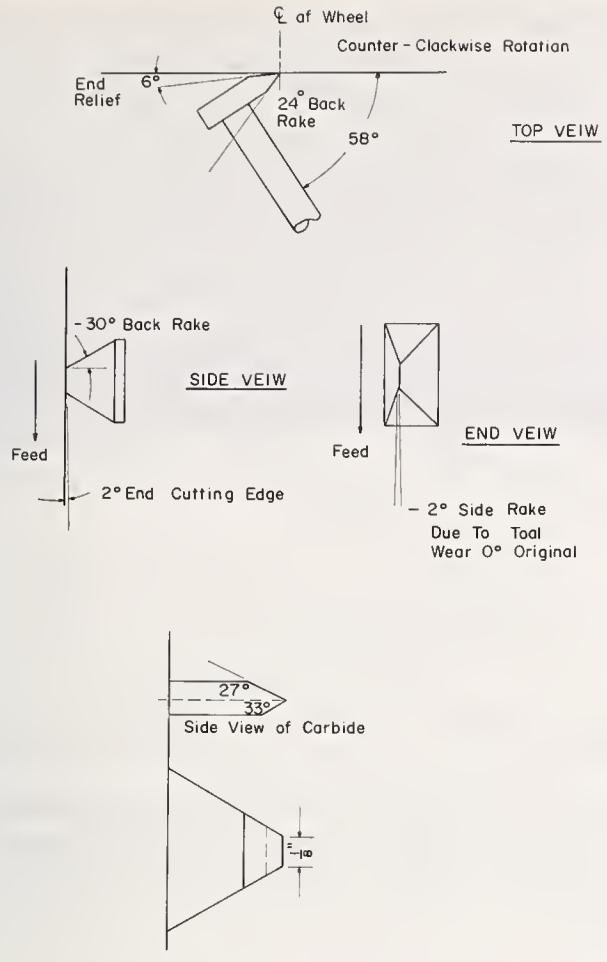

FIGURE 9. *Principal tool orientations.*

Motor	RPM	SFPM
P–7	200	50–310
P–11	300	80–475

removal rates slowly decreased; below these speeds the rate of removal was not maximum. Actual cutting speeds were controlled within 5 rpm.

7. Sonic Machining Rates

Sonic motors were mounted on a #2 Cincinnati Cutter and Tool Grinder driven by a variable-speed motor. A power drive for tool feeding was installed to obtain constant head velocities. The arrangement for the P–7 motor is shown in figure 10 and detailed in figure 11. The crystal and electrode end of the motor were contained in the box shown at the left of each photograph. The motor was attached to the box at the vibration-free node ring. The carbide cutting tip is shown at the motor tip. These positions were used for side cutting where the tip moved vertically down the wheel.

Figure 12 shows the mounting for the P–11 motor and the impact tool mount. Supported at the node ring, the P–11 utilized an extension to contact the impact tool mount. As shown, the

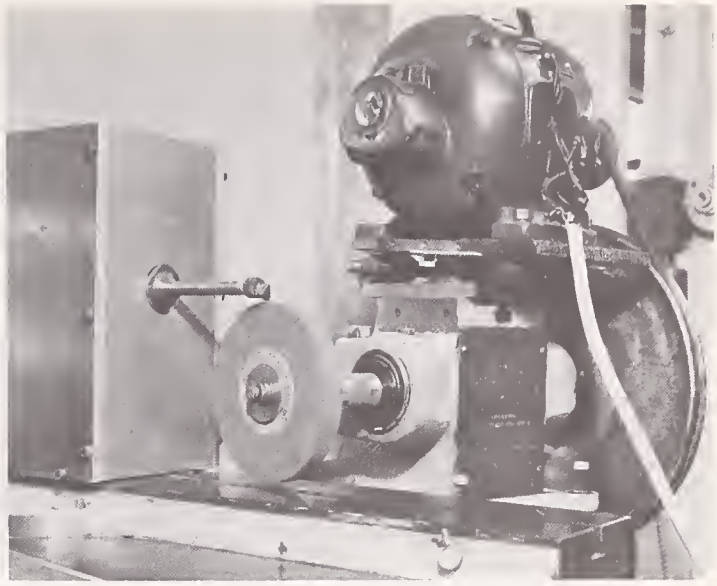

FIGURE 10. *P–7 sonic motor and tool mounted in position.*

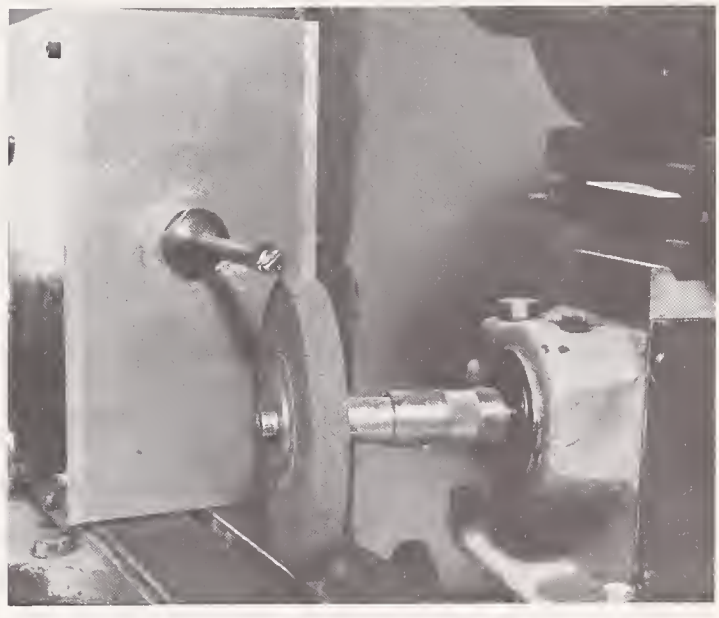

FIGURE 11. *Detail view of P–7 tool and wheel for peripherial cutting.*

template tool and orientation for groove cutting are apparent.

The basic differences between the two cutting arrangements are the horsepower ratings of each motor and the use of an impact reed mount. The P–11 is rated at 15 hp, whereas the P–7 is approximately 1 hp. The impact tool mount permits the cutting tool to obtain the optimum translation frequency for machining the workpiece; whereas, the rigid mount maintains the frequency of the motor at the tool-workpiece interface. The impact mount serves to self-tune the tool to the frequency required by the changing conditions of the workpiece in side cutting. By comparison, the impact tool mount resulted in a substantial reduction (100%) of tool wear. Neither the higher power

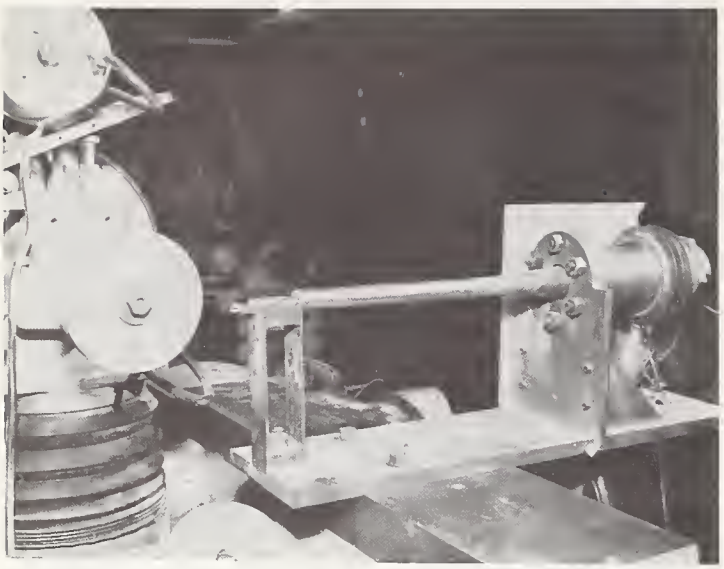

FIGURE 12. *P–11 sonic motor with half wave extention and impact tool mount.*

motor nor the type of tool mount affected the rate of removal. These observations are to be expected in the machining of brittle materials.

Peripheral cutting rates were less than side cutting rates and decreased with increased depths. It is speculated that the geometry of the tool contact at the periphery is responsible. The important factor is the elapsed time to cut the periphery and sides. The time is similar for each operation because of the wheel dimensions. The data are shown in figure 13.

The rates for side cutting with both motors are shown in figure 14. It should be noted that the volume is directly proportional to the depth of cut; thus, indicating that sufficient energy was available at all tested depths. The feed rate maximized at 36 in per min and remained constant at higher rates. For 0.040 in depth, the maximum removal rate was above 25 cu in per min, or about three times present rates. At the maximum cutting depth, 0.080 in, 48 cubic in per min were removed at a feed 36 in per min.

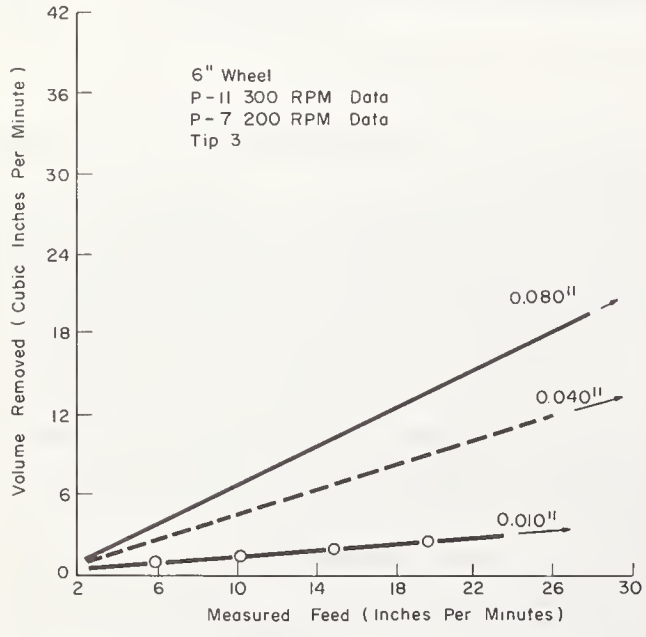

FIGURE 13. *Peripherial cutting rates (A80–V).*

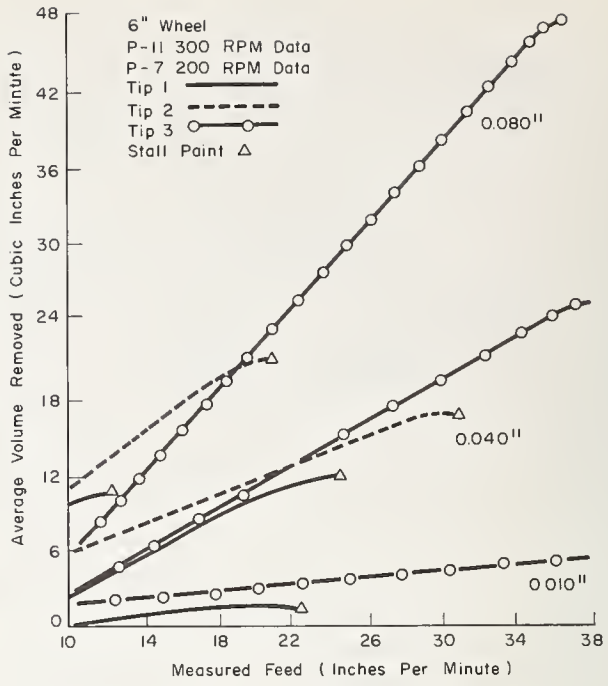

FIGURE 14. *Side cutting rates (A80–V).*

8. Template Cutting

The simulation of roll crushing profiles was accomplished by the template tool shown in figure 15. The tool was handfed at a slow rate and typical results are shown in figure 16. The surface was very open and the detail exceptional.

Thanks are extended to Mr. Hudson Jayne and Mr. Robert Meads for their technical assistance in all phases of the experimental program. The cooperation of the personnel of the Sonic Power Laboratory, Ohio State University, was most helpful.

FIGURE 15. *Template cutting tools, new and 3 hours wear.*

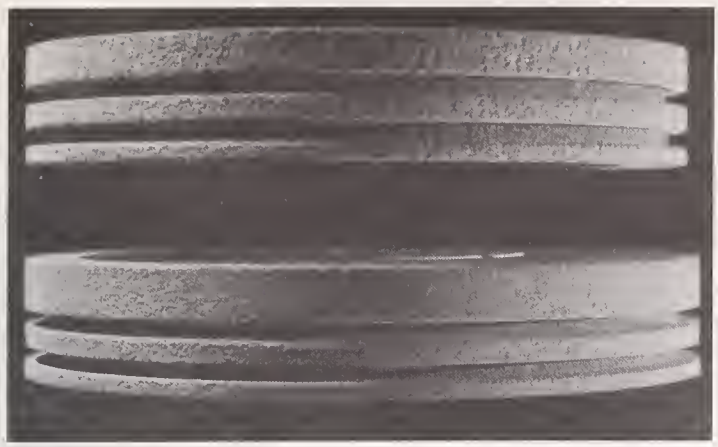

FIGURE 16. *Simulated roll crush cut using template tool.*

9. References

[1] McMaster, R. C., Sonic power—university research with an industrial payoff, news in Eng., College of Engineering, The Ohio State University, Columbus, Ohio, July, 1967.
[2] Houck, F., Vibration as an asset in design engineering, 66–MD–18, Am. Soc. Mech. Eng., (1966).
[3] McMaster, R. C., U.S. Patent 3,368,085.
[4] Libby, C. C., U.S. Patent 3,368,086.
[5] Minchenko, H. M., U.S. Patent 3,396,285.
[6] Delong, R. B., Sonic riveting, news in Eng., May 1968 (College of Engineering, The Ohio State University, Columbus, Ohio).
[7] Lewis, K. B., Grinding wheel, Grinding Wheel Institute Cleveland, Ohio (1959).
[8] Kingery, W. D., Sidhwa, A. P., and Waugh, A., Structure and properties of vitrified bonded abrasives, Bull. Am. Cer. Soc., 42, 5, (1963).
[9] Moore, H. D., and Kibbey, D. R., Development of Accelerated Testing Procedures for Ceramic Cutting Tools, E. E. S. Report 169 (The Ohio State University, Columbus, Ohio) 1962.

Discussion

BATES: During the erosion machining of these ceramics, was it a dry or a wet medium?

CAMPBELL: All of this work was dry.

BATES: I've been doing similar work on cavitation erosion of ceramic materials using a similar device as yours. This is a magnetostrictive device, however, and I think that the use of a wet media would introduce cavitation erosion and increase the overall erosion rate.

NATIONAL BUREAU OF STANDARDS SPECIAL PUB. 348, THE SCIENCE OF CERAMIC MACHINING AND SURFACE FINISHING, Proceedings of a Symposium Sponsored by the American Ceramic Society, the Office of Naval Research, and the National Bureau of Standards, held at NBS Nov. 2–4, 1970, Gaithersburg, Md. (Issued May 1972).

Environment-Sensitive Machining Behavior of Nonmetals

A. R. C. Westwood and R. M. Latanision

Research Institute for Advanced Studies

Martin Marietta Corporation, Baltimore, Maryland 21227

Liquid environments can influence the efficiency of machining nonmetallic solids in a variety of ways, e.g., by serving as lubricants, coolants, or particle dispersants. More importantly, however, certain environments can markedly increase or decrease the hardness of the nearsurface regions of such solids, and thereby exert a profound influence both on the rate of material removal and on tool life. Because of its technological potential, the characteristics and possible mechanisms of this latter phenomenon—the Rebinder effect—receive primary consideration in this paper.

For crystalline ceramics, Rebinder effects in machining arise because of the influence of the environment on nearsurface dislocation behavior. Effects resulting from adsorption-induced changes in the surface free energy of the solid are of minor importance. Rebinder effects can also occur in noncrystalline solids, however, and recent observations on such effects in various glasses are described. The possibility that these effects are caused by a stress-plus-chemisorption-induced redistribution of sodium ions in the near-surface region is discussed.

The importance of considering the total cutting system, environment-solid-tool, in any account of environment-sensitive machining is stressed, for environments which facilitate material removal when one type of tool is used can be detrimental to the effectiveness of another tool with a different cutting action.

Key words: Adsorption; ceramics; drilling; environmental effects; fracture; glasses; machining; mechanical behavior.

1. Introduction

Liquid environments can significantly influence the rate of material removal from ceramic or glassy solids by an abrasive tool. Sometimes the cause of their effects is relatively straightforward, for example, when they serve as coolants, lubricants, or dispersants. However, as Rebinder has pointed out [1][1], certain environments can act literally as "cutting liquids", because they interact with the solid in such a manner as to facilitate its mechanical destruction. Such effects can be quite spectacular, figure 1 [2]. Yet, despite the potential technological value of this phenomenon—the Rebinder effect—a survey of the literature reveals that, apart from their application to rock drilling in the U.S.S.R. [1] and to a limited extent in the U.S.A. [3, 4], the fundamental parameters underlying the environment-facilitated machining of ceramic and vitreous materials have yet to be studied in a sufficiently systematic manner to allow predictability or optimization of cutting rates for any practical engineering material.

This situation makes the preparation of any review of the "scientific aspects" of the influence of environments on machining on the one hand relatively simple . . . because there is little to review, and on the other rather difficult . . . because the few investigations undertaken to date have barely scratched the surface of this field of study, and it is likely that many important factors have yet to be considered and evaluated. Thus, only a limited amount of information exists upon which can be constructed any mechanistic understanding of the phenomena involved.

Recognizing this situation, the authors have recently initiated a study of the influence of simple organic liquids on the flow, fracture and machining (primarily drilling) behavior of such model solids as MgO and CaF_2 monocrystals and a conventional soda-lime glass. This paper will be primarily concerned with a discussion of the results and implications of this work. It should be appreciated that at this stage in the development of the field, much of what is said in regard to mechanisms should be considered current opinion—not established fact. Progress in understanding has been made, and some general concepts can be stated with reasonable certainty. For example, it has become apparent that adsorption-induced reductions in surface free energy are of limited consequence, while adsorption-induced changes in the flow behavior of the near-surface regions of the solid are of considerable importance. However, it has also become evident that the details of the mechanisms involved are sufficiently complex that it will be some time before the specific behavior of any particular cutting system (environment-solid-tool) can be predicted.

[1] Figures in brackets indicate the literature references at the end of this paper.

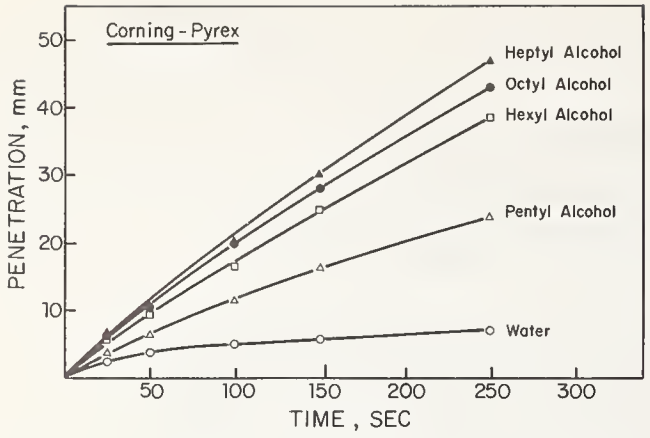

FIGURE 1. *Illustrating the significant differences in rate of bit penetration that can be produced by changing drilling environment.* The material is Corning "Pyrex". Diamond-studded bit. Load 450g. [2].

2. Environment-Sensitive Machining of Crystalline Ceramics

2.1. Mechanisms

The rate of penetration of a bit at constant thrust into a ceramic body depends on (i) the type of bit, and (ii) the hardness of the solid. Some bits are designed to cut most efficiently through solids which exhibit a significant amount of plasticity, and their operation primarily involves ploughing and shearing of the material. Such bits include twist and spade drills. Other bits are designed for use with more brittle solids, and their effectiveness appears to depend on how easy it is to initiate and propagate a brittle crack through the material. Such tools include diamond-studded bits, two-cone rock microbits [3], and those tools which remove material via repeated impacting.

Now, since the hardness of ceramic solids can be significantly affected by the adsorption of surface active species [5–7], the observation of adsorption-sensitive drilling or machining behavior in these materials is to be expected. Presuming, then, that such effects on machining behavior probably are a consequence of the effects of environments on hardness, the first step towards understanding the mechanisms of environment-sensitive machining behavior must be a clarification of the mechanisms underlying the adsorption-sensitive hardness of nonmetallic solids.

The first example of the latter effect was noted by Rebinder in 1928 [7], and in the intervening period several possible explanations have been proposed for this phenomenon. (For reviews see [8, 9]). The most widely known hypothesis is that due to Rebinder himself, who suggested that the decreases in microhardness usually observed are caused by adsorption-induced reductions in the surface free energy of the solid. This suggestion is based in part on the premise that most of the energy involved in creating a hardness impression in a brittle material is utilized in creating new surface area. There are several reasons why this hypothesis is questionable. First, in reality, only a small fraction of the energy utilized in the removal of material is required to generate new surface area, typically less than 1 percent [10]. Most of the energy is absorbed in plastic flow and heat generation processes. Second, adsorption-induced increases in hardness also have been observed, both in crystalline solids such as CaF_2 [11], and in soda-lime glass [12]. Such effects are thermodynamically unlikely on the basis of the reduction in surface free energy hypothesis [13]. Finally, it has been shown that environments which produce significant influences on drilling behavior have no significant effect on the energy to propagate cleavage cracks in MgO [14], or "super-critical" cracks [2] in a soda-lime glass [12].

In view of the limitations of the Rebinder hypothesis, therefore, attention is now being focused on the fact that in crystalline solids which exhibit some degree of plasticity, the deformation processes which lead to fracture and removal of material usually involve the generation and motion of dislocations in the near-surface layers of the solid. Thus a feasible basis for the occurrence of Rebinder effects is that they are related to adsorption-induced changes in the ease with which dislocations are either able to (i) move and interact so as to initiate cracks, or (ii) be generated at and move around in the vicinity of crack tips, and so influence propagatability. Also, in recent years a better understanding of the factors involved in chemisorption on ionic solids, and in determining the mobility of dislocations within these materials has become available, and these advances in knowledge have now been incorporated by Westwood, Goldheim and Lye (WGL) [11, 15, 16] into an alternate mechanism for Rebinder effects in crystalline ceramics. This model assumes (i) that the mobility of dislocations in ionic crystals is controlled predominantly by interactions with such point defects as vacancies and impurity atoms, etc., [17–19], and (ii) that chemisorption on such materials involves—at least in part—electron transfer between nearsurface point and line defects and the adsorbate [20, 21].

The suggestion is, essentially, that adsorption-induced changes in the electronic state of nearsurface point defects and dislocations—whether caused by direct interactions with the adsorbate or as a result of band bending effects—introduce variations in their mutual inter-

[2] However, preliminary data from studies of the slow growth of "stable" cracks in glass suggest that this process may be influenced by adsorption-dependent flow processes [2].

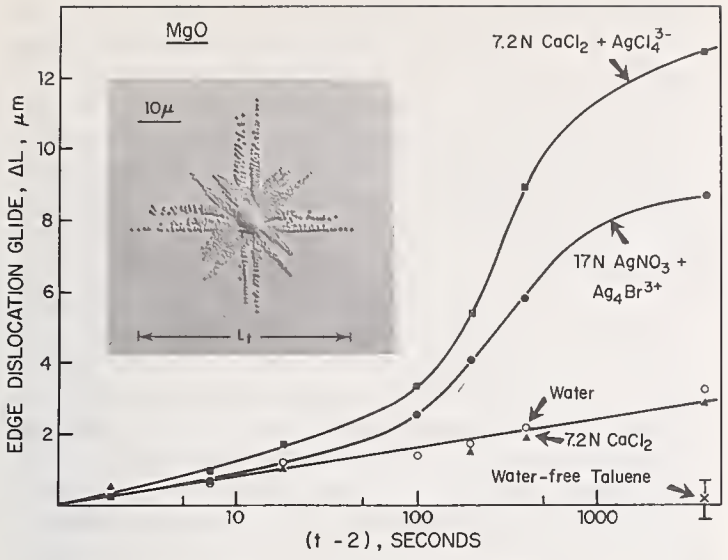

FIGURE 2. *Variation of* ΔL *with log (indentation time,* t, *minus 2 s) for freshly cleaved Norton MgO crystals exposed to toluene or various aqueous environments.* Indenter load = 10g. Room temperature. Insert shows typical distribution of dislocation etch pits around indenter impression. [15]

actions. Such variations are then manifested as environmentally-induced changes in dislocation mobility, and hence in microhardness, i.e., as Rebinder effects.

The validity of this hypothesis has been examined by studying the effects of adsorbed ions, complex-ions, and organic molecules on the room temperature mobility of nearsurface dislocation halfloops introduced by a diamond indenter into freshly cleaved surfaces of MgO [15, 16] and CaF_2 [11]. The principal experimental variables were time of indentation and composition of the environment, and the parameter measured was ΔL, where ($\Delta L = L_t - L_2$); L_t being the extent of edge dislocation glide occurring during an indentation time t, and L_2 that during a two second indentation, this being the minimum practical time for reproducible results. In effect, the larger the value of ΔL after a given time of loading, the softer the crystal. Values of L_t and L_2 were determined by optical measurements of the distribution of edge-dislocation etch pits surrounding the indentations (e.g., see the insert to fig. 2).

Figure 2 illustrates the variation of ΔL with indentation time for MgO exposed to several environments. When the surface was exposed to water-free toluene, no significant dislocation motion occurred following that produced within the initial two seconds of loading. When the crystal was exposed to moist air, water or an aqueous salt solution, dislocation creep [3] occurred, the edge dislocations moving some 3μ in 4000s. However, exposure to environments

[3] This is the "anomalous indentation creep" observed at room temperature when MgO, Al_2O_3 or TiC, etc., are indented in a laboratory atmosphere, and shown by Westbrook and Jorgensen [22] to be associated with the presence of adsorbed water.

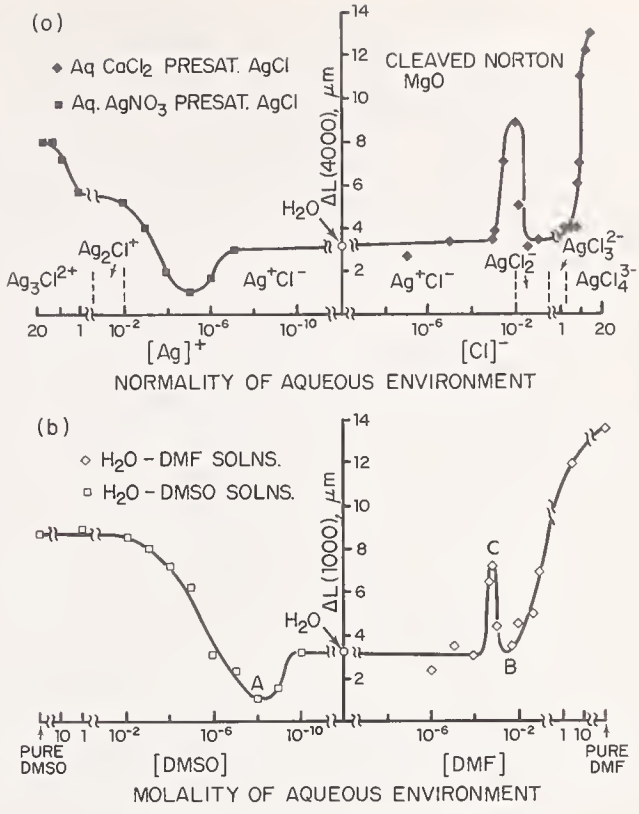

FIGURE 3. (*a*) *Variation of* ΔL (*4000 sec*) *with normality of aqueous solutions of either* $CaCl_2$ *or* $AgNO_3$ *presaturated with* AgCl *for Norton MgO.* The predominant complex species present in these solutions are indicated. (b) Variation of ΔL (1000 sec) with molality of aqueous solutions of DMSO or DMF. Compare with (a). Note similarity in form of curves. [16]

containing highly-charged complexes resulted in significant increases in mobility. For a 7.2N solution of $CaCl_2$ presaturated with AgCl, the latter being present predominantly in the form of $AgCl_4^{3-}$ complex ions, edge dislocations propagated some 13μ in 4000 s. For a 17N $AgNO_3$ solution containing Ag_4Br^{3+} complex ions, dislocation loops propagated some 9μ in the same period of time. The actual variation of the extent of near-surface dislocation creep in some fixed time t, $\Delta L(t)$, with charge on the predominant complex species in the environment is quite complicated, as is evident from figure 3(a).

Experiments [16] in organic liquid environments revealed that dimethyl formamide (DMF) or dimethyl sulphoxide (DMSO) molecules absorbed on {100} MgO surfaces exert the same influence on the mobility of near surface edge dislocations as do negatively or positively charged silver chlorocomplexes, respectively. This correlation may be seen by comparing figures 3(a) and (b). It appears from these data that DMF molecules act as electron-donor adsorbates with a respect to (impure) MgO, as $AgCl_4^{-3}$ complexes would be expected to do, while DSMO molecules act as elec-

FIGURE 4. *Variation of* ΔL *(1000 sec) with composition of DMSO–DMF environment at room temperature for two types of MgO.* Data points are omitted to improve clarity. Curve I is for "as received" Norton MgO crystals. Curve II is for hydrogen-treated Norton MgO. Note shift in position of minimum A with state of ionization of impurities in MgO [16].

tron-acceptor adsorbates, as would Ag_3Cl^{2+} complexes.

The characteristic double minimum in the relationship between ΔL and environment can also be produced in water-free DMSO-DMF environments, figure 4, Curve I, and—as would be expected on the basis of the WGL model—the exact locations of the minima at A and B depend on the concentration and state of ionization of the impurities present in the material [16]. In figure 4, for example, Curve I is for "as received" Norton MgO containing, among other impurities, ~150 ppm of iron predominantly as Fe^{3+}. Curve II, on the other hand, is from otherwise similar crystals which have been heat-treated in hydrogen at 1650° for 24 h. prior to indenting to reduce trivalent impurity cations to the divalent state.

Another alternative mechanism for Rebinder effects has been suggested by Westbrook and Hanneman [23], and this model is based on the premise that the coefficient of friction between an indenter and a crystal may be significantly altered by the presence of adsorbed species. Such an effect could lead to variations in the complex distribution of stresses around the indenter, and so to a dependence of dislocation mobility—and hence microhardness—on environment. However, studies [11] of the relaxation behavior of near-surface dislocations in CaF_2 have revealed that active environments influence dislocation mobility even in the absence of stresses imposed by a loaded indenter. Moreover, for any particular environment, a correlation exists between the extent of dislocation motion induced by a loaded indenter and the amount of relaxation which occurs after the indenter is removed. It appears, therefore, that indenter-lubrication effects are not fundamental to the occurrence of Rebinder phenomena [11].

Rebinder effects can also occur in crystalline semiconductor materials and in glasses. For the former types of solid, it is well known that chemisorption can lead to significant variations in surface charge and charge carrier density [20], and also that variations in bulk carrier concentration can lead to variations in hardness (dislocation mobility) [24]. Thus, Rebinder effects in such materials may be a consequence either of electron transfer directly between the adsorbate and localized energy levels associated with dislocation cores, or of the chemisorption-induced bending of energy bands in the vicinity of the surface which leads to changes in the population of the core states of dislocations [8]. However, it is not yet known whether dislocation-like defects play any significant role in determining the flow behavior of glasses, and current opinion is that this is unlikely. Thus, a mechanism not dependent upon the mobility of dislocations must be sought to explain the existence of Rebinder effects in this class of solids, and some possibilities will be considered in 3.1.

2.2. Observations on the Environment-Sensitive Drilling Behavior of Ceramics

The experimental observations reported in 2.1 demonstrate clearly that active environments can markedly influence the mobility of nearsurface dislocations in ceramic monocrystals. The next logical step, therefore, is to determine the relationship between such effects and the occurrence of environment-sensitive machining behavior. With this in mind, Westwood and Goldheim recently undertook a study of the adsorption-sensitive drilling behavior of MgO and CaF_2 monocrystals [25].

a. Monocrystal Drilling Studies

These experiments utilized a precision drill (30 rps) fitted with either a freshly sharpened carbide spade bit (2mm diam.) or with a diamond-studded, hemispherical-headed bit (3mm diam.). These two types of bit were selected because their differences in cutting action might

be expected to lead to differences in response to environmental changes. Carbide spade bits of the type used in this work function more effectively when the solid exhibits some sensible degree of plasticity. The diamond-studded bits used, on the other hand, perform better in harder and more brittle solids. Conceptually, therefore, one might expect that an environment which softens the test piece would facilitate its drilling with a spade bit, but be detrimental to drilling efficiency when a diamond bit is used.

The experimental procedure was as follows: A freshly cleaved crystal was immersed in the test environment and the bit lowered gently onto its surface. A load was then applied to the drill shaft by means of a lever system and the drill started. Holes were drilled normal to the freshly cleaved surface of the specimen, and the depth of penetration, D, under some fixed load monitored as a function of time by an LVDT-recorder system.

Some results from drilling experiments with *carbide spade bits* are presented in figures 5 and 6. Note first that certain DMSO-DMF solutions which soften (increase ΔL) and facilitate drilling in MgO with respect to its behavior in water, e.g., 50 v/o DMF in DMSO, figure 5, harden and make drilling more difficult in CaF_2, figure 6. It follows that the variations in drilling efficiency shown in figures 5(b) and 6(b) are not related to differences in coolant properties of the solution environments. On the other hand, a comparison of the data in figures 5(a) and 5(b), and in 6(a) and 6(b), reveals that $\Delta L(1000)$ and the depth of penetration in 600 sec., D(600), vary in an essentially identical manner with composition of the environment surrounding the crystal. It is apparent, therefore, that, when a carbide spade bit is used, the efficiency of the drilling process in both MgO and CaF_2 is related directly to the mobility of near-surface dislocations in these materials. A similar correlation between drilling efficiency and dislocation mobility has also been noted when dilute aqueous solutions of $AlCl_3$ ($\sim$ 0.1 w/o) are used with MgO [25]. Such solutions have for some time been recog-

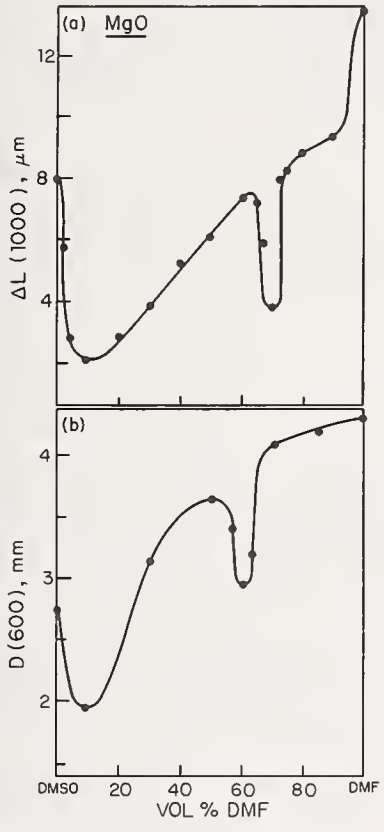

FIGURE 5. *Influence of DMF–DMSO environments on (a) extent of edge dislocation motion produced during indentation period between 2 and 1000 s around indentation in freshly cleaved {100} MgO surface [16] and (b) depth of penetration of a carbide spade bit in 600 s, D(600), in [100] direction into similar crystal.* Room temp. [25]. Note similarity in variation of ΔL (1000) and D(600) with environmental composition.

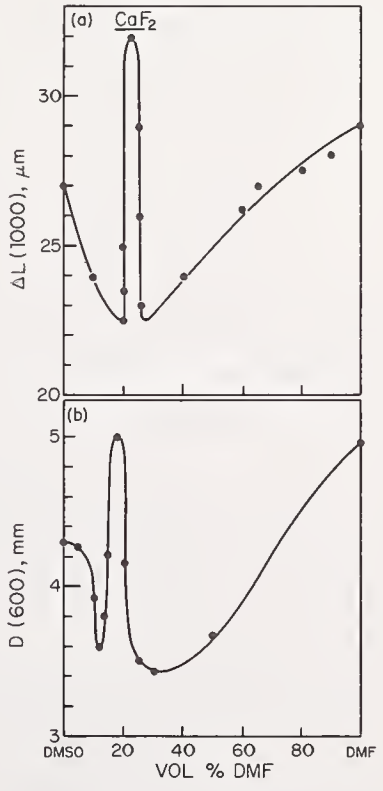

FIGURE 6. *Data similar to that in fig. 5, but for* CaF_2. This material cleaves on {111} planes and was drilled in a direction perpendicular to this plane [25]. Dislocation mobility data from ref. [11].

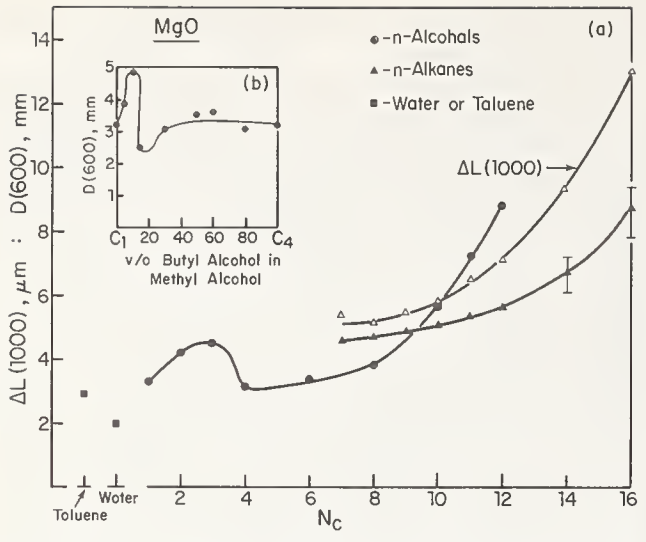

FIGURE 7. *(a) Influence of various environments on* D(600) *in* MgO, *and of n-alkane environments on* ΔL *(1000). N_C* is the number of carbon atoms in the molecule [2, 25]—(b). Effect of binary alcohol solutions on D(600). Note that solutions of butyl alcohol in methyl alcohol can reproduce the maximum in D(600) occurring in propyl alcohol (N_C=3). [2].

nized by Rebinder [1] as hardness reducers for drilling quartz and granite.

The influence of n-alkane environments on the drilling and near-surface dislocation behavior of MgO and CaF_2 monocrystals has also been studied [25], and it has been found that both $\Delta L(1000)$ and D(600) increase regularly with chain length for the series from n-heptane (number of carbon atoms, N_C, = 7) to n-hexadecane (N_C = 16), figure 7. In n-alcohol environments, however, a maximum in D(600) occurs at N_C = 3, figure 7 [2]. Such an effect is reminiscent of an effect noted previously in toluene-dodecane solutions (fig. 8, Ref. [25]) and, on the basis of the earlier work, it implies that alcohol environments act as electron donor adsorbates with respect to MgO surfaces. Also of especial interest is the observation that by mixing together alcohols of $N_C = x$ and $N_C = y$ (in this case $x < y < 5$), it is possible to reproduce the characteristic variation of D(600) for alcohols having values of N_C between x and y, figure 7(b). The generality of this phenomenon will become evident from other results to be presented below, and a possible interpretation is suggested in 3.3.

In experiments conducted using *diamond-studded bits*, the efficiency of drilling was assessed not in terms of penetration after a given time, $D(t)$, but in terms of the average rate of drilling during the period 150–250 sec, this being designated D(200). It was possible to use this more meaningful parameter because the rate of drilling with diamond bits was relatively constant after the first 100 sec. As mentioned earlier, diamond bits drill relatively hard and brittle materials more effectively than they do softer and more ductile solids (an attempt to drill brass or aluminum with a diamond bit will provide proof of this). Thus. one might expect the observed tendency for drilling efficiency to increase with N_C for alkane and alcohol environments having $N_C > 5$ when spade bits are used (figure 7) to be reversed when diamond bits are used. Furthermore, one might expect that, for the diamond-studded bits, the alcohols would be superior cutting environments to the alkanes when N_C is < 10, and inferior when $N_C > 10$. These predictions are borne out by the results shown in figure 8. Note that the maximum in D(600) for alcohol environments having $1 < N_C < 4$, figure 7, is reflected as a minimum in D(200) in the data of figure 8. Note also the reversal in relative cutting efficiencies of toluene and water for the spade bits and diamond-studded bits, cf. figures 7 and 8.

b. Other Observations on Ceramic Monocrystals

To examine the possibility that hardness-reducing environments influence crack initiation in notch-sensitive solids, comparative scratch tests were performed on freshly cleaved {100} MgO surfaces exposed to air (i.e., adsorbed water) and surface active n-hexadecane [23]. A Kentron microhardness machine was used, with a 20g load on the indenter, and a traverse rate of ~ 0.03 cm/sec. The results are shown in figure 9. Cracks were not formed in surfaces exposed to air, figure 9(a), except where the track crossed a cleavage step. Under hexadecane, however, cracking was prolific, figure 9(b), fracture occurring on both {110} planes intersecting the surface and {100} planes below the surface. Thus, under conditions in which material is removed via ploughing, it is clear that "softening" environments facilitate crack initiation in MgO.

c. Drilling of Polycrystalline MgO

Figure 10 presents some results from drilling experiments on polycrystalline MgO (Kodak

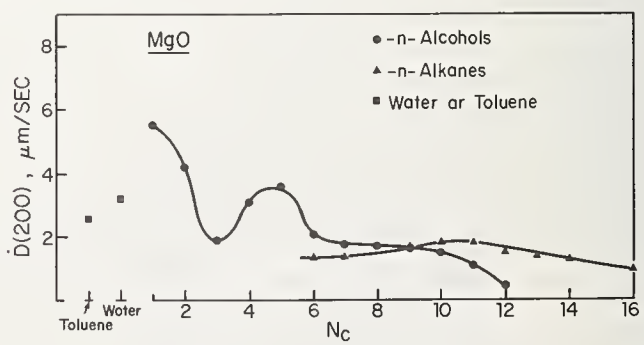

FIGURE 8. *Influence of environmental composition on rate of drilling after 200 sec, D(200), with a diamond-studded bit in MgO.* Note that the characteristic variation in D(200) for the n-alcohol and n-alkane environments is the converse of that obtained when spade bits are used; cf. these data with those in figure 7. [2].

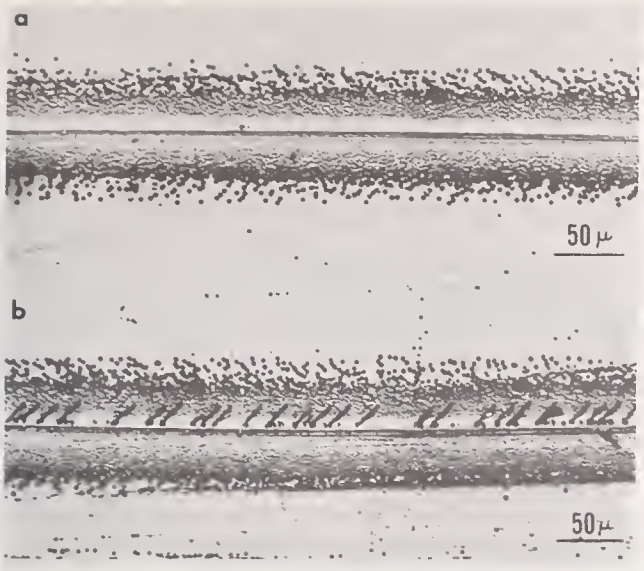

FIGURE 9. *Indenter tracks in freshly cleaved MgO surfaces produced (a) in air (i.e., with adsorbed water present), and (b) under surface-active n-hexadecane.* Loan on indenter was 20g, and it was moved from left to right. Room temperature. Note prolific cracking induced by softening hexadecane environment. [25].

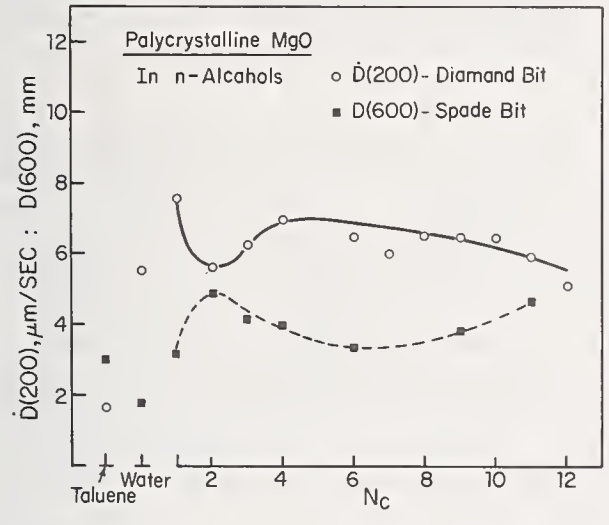

FIGURE 10. *Influence of n-alcohol environments and type of bits on efficiency of drilling polycrystalline MgO.* Note opposite influences of environment for the two bits. [2].

IRTRAN) in n-alcohol environments [2]. These data demonstrate again the necessity of considering the total cutting system, environment —solid—tool, in any discussion of environment-sensitive machining behavior. Clearly, environments which facilitate cutting with a spade bit tend to reduce the effectiveness of a diamond-studded bit.

2.3. Comments on the Environment-Sensitive Drilling of Ceramics

A liquid environment might influence drilling efficiency in several ways, for example, (i) as a consequence of its lubricant or coolant action, reducing bit wear, (ii) by decreasing the surface free energy of the solid, or (iii) by changing the flow and/or fracture characteristics of the solid. Certainly, cooling effects introduced by liquid environments are beneficial to cutting. It has been noted, for example, that drilling MgO with a spade bit in air is very inefficient. In these experiments the bit became blunt within 15 s after very limited penetration. In surface-inactive toluene, on the other hand, the drill penetrated three times further before blunting occurred [25]. However, neither the coolant nor the lubricating action of environments are considered of primary importance in controlling environment-sensitive machining behavior because (i) certain environments which facilitate drilling in MgO, say 50 v/o DMF in DMSO, make drilling more difficult in CaF_2 (cf figs. 5 and 6), (ii) additions of an alkane to toluene improve drill penetration in MgO but reduce it in CaF_2 (compare figs. 6(a) and 8(b) in Ref. [25]); and (iii) Selim, et al. [26] have demonstrated that the addition of certain organic compounds to water which facilitate the cutting of quartzite actually increase the coefficient of friction in drilling. As mentioned in 2.1, there are also valid reasons to reject the view that variations in drilling behavior are related to adsorption-induced reductions in the surface free energy of the solid.

It does appear, however, that the results of several investigations [1–3, 25–6] are consistent with the view that Rebinder-type effects in drilling are associated with adsorption-induced variations in the flow and flow-dependent fracture characteristics of nonmetallic solids. In particular, we consider that the correlation between drilling efficiency and near-surface dislocation mobility demonstrated by the data for carbide spade bits in figures 5 and 6 does represent a real and important relationship between these two properties. A possible explanation for this correlation is that for a tool which removes material primarily by ploughing and shearing, any environment which facilitates dislocation motion in the nearsurface region of a notch-brittle solid will effectively facilitate crack initiation, and hence material removal. Conversely, for a tool which operates primarily as a consequence of repeated high energy impacts and brittle crack propagation, a softening environment will be detrimental to cutting, causing crack blunting and reduced propagatability.

Robinson's observations on the environment-sensitive drilling behavior of Indiana limestone [3] may also be interpreted in this manner. He found that 2 percent solutions of sodium adipate increase slightly (+5%) the compressive yield stress of this limestone with respect to its value in water, whereas solutions

of sodium azelate reduce this stress (−19%). In comparative drilling tests using a microdrag bit—which causes failure to occur predominantly by *plastic* shearing processes—he found that sodium azelate solutions increased the rate of drilling by ~ 70 percent with respect to that in a pure water environment, while sodium adipate solutions reduced it by about 28 percent. However, the use of a two-cone rock microbit, which is considered to cause rock removal primarily by *brittle* failure processes, resulted in smaller but opposite influences on drilling behavior.

Unfortunately, very little work of a mechanistic nature has been conducted on the environment-sensitive machining behavior of polycrystalline ceramics, despite its potential practical value. Thus, at this time, it is only possible to speculate on some of the possible modifying influences of internal surfaces.

It is known, of course, that grain boundaries can serve as relatively "soft" sources, so that many of the dislocations involved in plastic flow in polycrystalline solids are likely to be produced at sites remote from the free surface. In this case, environments are less likely to exert a significant influence on deformation behavior. Also, by acting as stable obstacles to dislocation motion, grain boundaries are known to play an important role in crack initiation processes in ceramic solids. Whether the process of crack nucleation at grain boundaries is or is not affected by environmental conditions will depend on a number of factors, including, for example, the influence of non-equilibrium concentrations of point defects and impurities at or near the boundaries [30] on local adsorption behavior. Such segregation could affect the local relaxation or concentration of stresses by dislocations.

Other possible effects could arise from the known anisotropy of adsorption on different crystallographic surfaces—in this case, different grains [31]. It has been shown that this phenomenon is responsible for the apparent anisotropy in microhardness when nonmetallic crystals are tested in a moist atmosphere; the effect disappears when the tests are conducted on dry, clean crystal surfaces [9, 31]. Nevertheless, such an anisotropy of adsorption could conceivably cause one particular grain to be hardened, while its neighbor is softened.

In short, the as yet unknown influences of such factors could significantly hinder the rapid transfer of understanding gained from monocrystal studies to an interpretation of the behavior of polycrystalline ceramics. It is evident that mechanistically oriented studies of the environment-sensitive machining behavior of polycrystalline ceramics of various compositions, purities and grain sizes are urgently required.

3. Environment-Sensitive Machining of Glasses

3.1. Mechanisms

Explanations for the environment-sensitive fracture behavior of oxide-type glasses usually fall into one of two categories (i) those dependent upon adsorption-induced reductions in surface free energy [7, 32], and (ii) those which assume the presence of water to be critical, and of which the stress-enhanced corrosion mechanism of Charles and Hillig [33] is perhaps most widely accepted. For explanations in category (ii), the role of testing media other than water is usually considered to be simply that of screening the highly reactive water molecules from the glass surface [34–6].

However, there is ample evidence that, under conditions where fracture is induced by abrasion or grinding, certain organic environments are considerably *more* active than water [37–8]. For such examples of environment-sensitive fracture behavior it would certainly appear that explanations dependent upon the dominant presence and corrosive influence of water could not be valid. However, it does not follow that such effects must therefore be caused by adsorption-induced reductions in surface free energy, because it is well known that flow can occur in certain glasses at room temperature [39–42]. Thus, an alternative possibility is that certain examples of the environment-sensitive fracture behavior of glass may be a consequence of adsorption-induced variations in the flow and flow-dependent fracture properties of the near-surface regions of this solid [12].

As mentioned earlier, current opinion does not favor the view that dislocations, or dislocation-like defects, are involved in flow processes in glass. Indeed, very little appears to be known about the actual mechanisms of flow, or of flow-sensitive fracture, in this class of solids. Of course, this means that any mechanism proposed for the environment-sensitive flow and/or fracture behavior of glasses must of necessity be speculative in nature. Recently, however, the authors [12] have considered the relative merits of a model based on the fact that stress [43] and potential [21, 44] gradients can cause redistribution of the sodium ions in the near-surface layers of a glass. Recognizing further that the flow of sodium ions towards an electrode causes an increase in volume of the glass there [45], then a feasible consequence of any stress-plus-chemisorption-induced flow of sodium *towards* the surface of a glass specimen should be some relaxation of any tensile stresses created there [46], and by virtue of the increased concentration of sodium ions, a decrease in the hardness of this region. Then, depending on the mode of action of the

cutting tool, such a change could either facilitate or hinder machining. Presumably any environment which interacts to produce a positive surface charge on the glass should tend to induce sodium ions to diffuse *away* from the surface. Such movement should then result in the opposite influences on drilling efficiency, dependent upon the tool.

The possible relevance of this mechanism, and of the surface energy reduction and stress-enhanced corrosion models, to the environment-sensitive machining behavior of several glasses is under current investigation [2]. Some of the results obtained so far will now be described.

3.2 Observations on the Environment-Sensitive Drilling Behavior of Oxide-Type Glasses

This work has been concerned with the influence of water, toluene, the n-alkanes, n-alcohols, and methyl esters on the drilling behavior of various glasses, and, to date, most of the experiments have been conducted on a conventional soda-lime glass containing ~ 13 percent Na_2O and 9 percent CaO. With one exception, all of the data to be discussed were obtained using the hemispherical-headed, diamond-studded bits and experimental procedures described in 2.2.a.

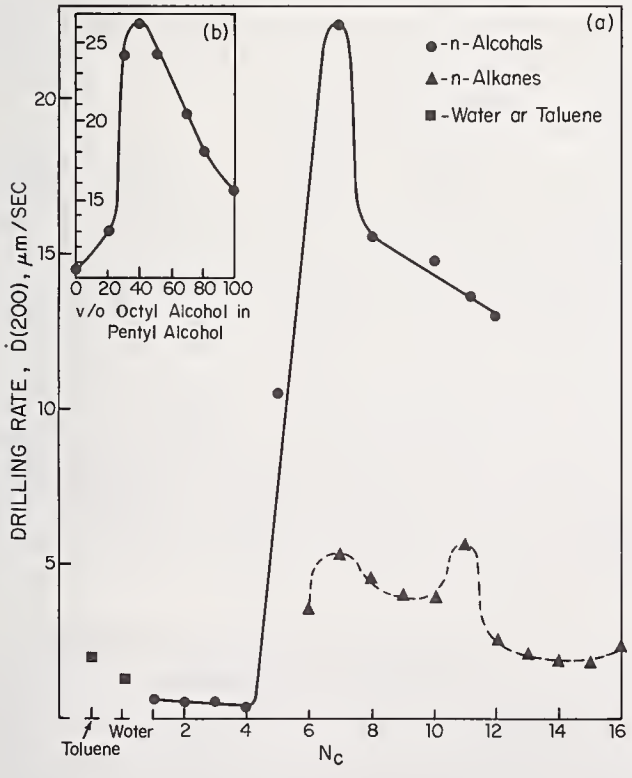

FIGURE 11. *Variation in D(200) with environmental composition for a soda-lime glass at room temperature.* Diamond-studded bits. Note that solutions of octyl alcohol (N_C=8) in pentyl alcohol (N_C=5) can reproduce the peak in drilling efficiency which occurs in heptyl alcohol (N_C=7). [12].

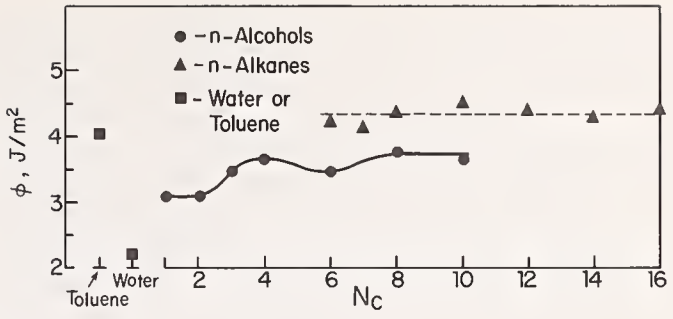

FIGURE 12. *Variation in fracture energy, φ, of a soda-lime glass at 25 °C with environmental composition.* φ determined by double cantilever technique. [12].

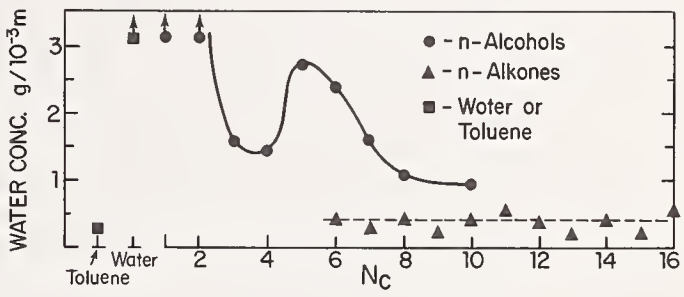

FIGURE 13. *Water content of environments used to produce data shown in figures 11, 12, 14–17* [12]. The Karl Fischer technique was used in these measurements.

The variation of D(200) with test environment for the soda lime glass is shown in figure 11. For this material, water and toluene are relatively poor drilling environments, all of the alkanes being superior. Note particularly that n-alcohols having $N_C > 5$ are extremely effective drilling environments, and that D(200) for glass in heptyl alcohol is some twenty times greater than that for water. Again it was observed that, by mixing two n-alcohols of different chain length, it is possible to reproduce the drilling characteristics of the n-alcohols of intermediate chain length in the homologous series, figure 11(b).

To examine the relevance of the reduction in surface energy hypothesis to these results, experiments have been conducted to determine the energy, ϕ, required to propagate pre-existing cracks in this glass as a function of the same test environments. The double-cantilever technique was used [47–9], and the data from these tests, as well as the water content of the environments (determined by the Karl Fischer technique) are presented in figures 12 and 13. The values of ϕ obtained for this soda-lime glass in water, $2.2 \pm 0.3 J/m^2$, and in the n-alkane series from $N_C = 6$ to $N_C = 16$, 4.2 ± 0.4-J/m^2, figure 12, are essentially identical to those found by other workers for similar en-

439-921 O - 72 - 11

vironments [50–1]. Note particularly, however. that ϕ does not vary significantly with N_C for the alkane environments. For the n-alcohols, values of ϕ intermediate between that for water and those for the alkanes were obtained, and consideration of the data in figures 12 and 13 suggests that these values reflect the higher concentration of water present in the alcohols. The value of ϕ determined for this glass in relatively waterfree toluene was $\sim 4.0 J/m^2$.

Now, if the data in figures 11–13 are compared, it becomes clear that no sensible relationship exists between drilling efficiency and either the fracture energy of the glass in these testing environments, or the water content of the environment. If, on the other hand, the drilling behavior of this glass is indeed related to adsorption-induced variations in its near-surface flow characteristics, then one should be able to demonstrate that its hardness. H, also is environment-sensitive. This possibility was examined using a single fulcrum (tungsten carbide) pendulum sclerometer [10]. The relative magnitude of H is evaluated with this instrument from measurements of the damping behavior of the loaded, oscillating pendulum. When a hard and brittle solid is tested, relatively little energy is absorbed in near-surface flow or fracture processes, and so the rate of pendulum damping is small. For a softer and more ductile solid, however, relatively more energy is absorbed by such processes, and so the rate of damping is greater. In this work, the relationship between H and pendulum damping behavior derived by Rebinder (see Ref. [10] was used to estimate the relative values of H, and the results are presented in figure 14.

Significant variations in the magnitude of H occur with N_C. particularly for the n-alcohol environments, and it is evident that this soda-lime glass is markedly harder in heptyl alcohol (N_C=7) than in any of the other alcohols or alkanes tested. Note that the variation in H with environment is not related to the water

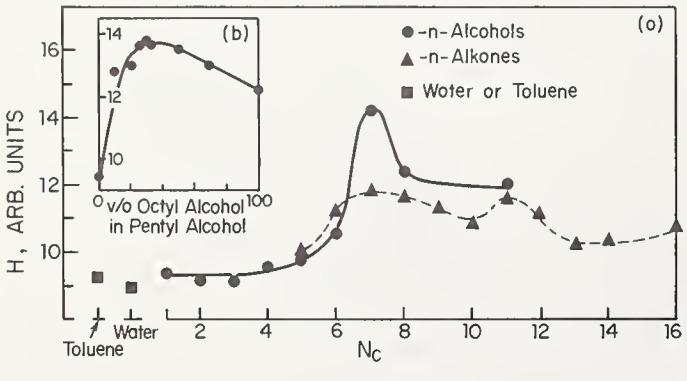

FIGURE 14. *Influence of various environments on the pendulum hardness,* H, *of a soda-lime glass at 25 °C.* Note that variation in H with N_C is similar to that of D(200) in figure 11. Compare also figures 11(b) and 14 (b). [12].

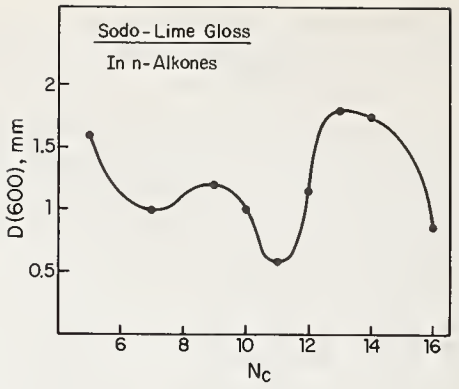

FIGURE 15. *Influence of n-alkane environments on drilling behavior of a soda-lime glass using carbide spade bits at 25 °C.* Note opposite variation with N_C to that obtained with diamond-studded bits, fig. 11. [2].

content of the environment, cf. figures 13 and 14, but is identical in form to the variation in D(200), figure 11. Thus, environments which harden glass (relative to some standard value, e.g., its hardness in surface-inactive toluene) facilitate its drilling by diamond-studded bits. Based on experience, therefore, such environments should be deterimental to the drilling of glass by carbide spade bits, a prediction verified by the data shown in figure 15.

Data from tests conducted in solutions of octyl alcohol in pentyl alcohol are also included in figure 14. Note particularly the existence of a maximum in H for such solutions, the value of H_{max} being similar to the value of H for an heptyl alcohol environment.

Only a limited amount of work has been conducted on other glasses [4], and some of the data obtained are shown in figures 16 and 17 [2]. It can be seen from figure 16 that the drilling efficiency of each of these materials is greatest in heptyl alcohol, though the peak is least pronounced for fused silica. For n-alkane environments, on the other hand, the data indicate that the principal peak in drilling efficiency occurs in undecane, N_C=11, figure 17. A similar peak occurs when soda-lime glass is drilled in the methyl ester homologous series of environments. In this case, octyl acetate is the most effective cutting medium [2].

3.3 Comments on the Environment-Sensitive Drilling of Glasses

Consideration of the data presented in figures 11 and 15–17 leads the authors to conclude that the efficiency of drilling various oxide-type glasses in alcohol or alkane environments is in no way related to the water content of these environments. Nor is it likely that the energy

[4] CER–VIT (Registered trademark, Owens-Illinois, Inc.) is a polycrystalline glass ceramic material, produced by controlled crystallization and used in the manufacturer of telescope lenses [52].

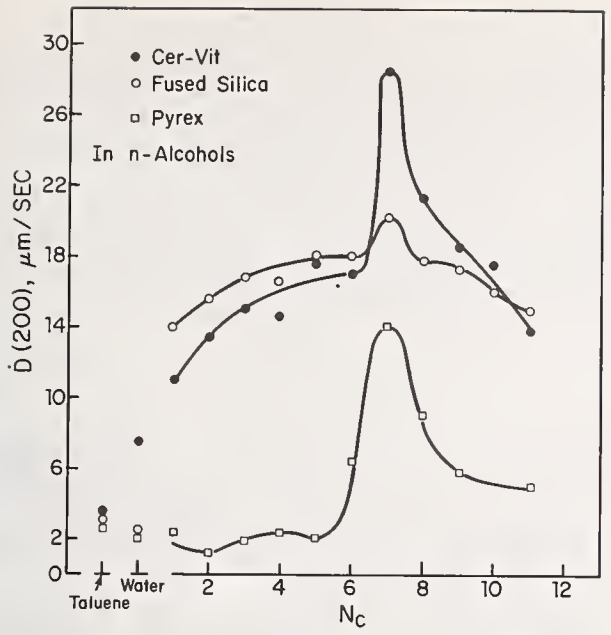

FIGURE 16. *Effects of n-alcohol environments on the efficiency of drilling Pyrex, fused silica, and the glass ceramic material Cer–vit at 25 °C. Diamond-studded bits.* [2]. Note characteristic peak at N_C=7 also found with soda-lime glass, cf, fig. 11 [12].

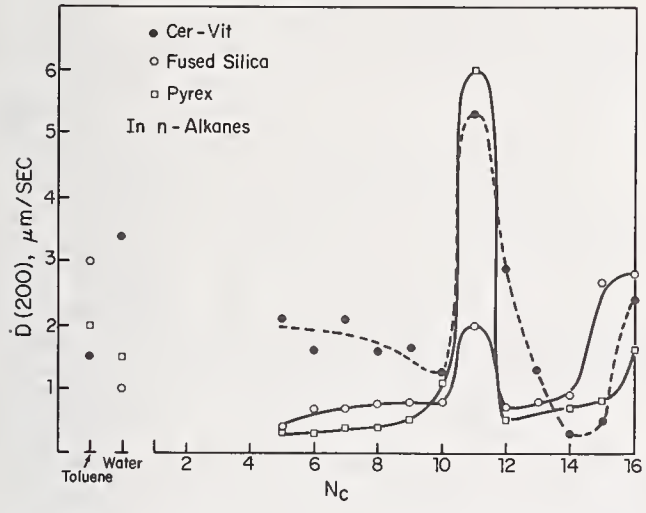

FIGURE *17. Effects of n-alkane environments on efficiency of drilling Pyrex, fused silica, and Cer-vit with diamond-studded bits at 25 °C.* Load 300g. Note characteristic peak at N_C=11 also found with soda-lime glass, cf. fig. 11. [2].

to propagate cracks in a brittle manner (i.e., the surface energy) is an important factor in the drilling process. It appears, therefore, that neither of the two mechanisms customarily relied upon to explain the environment-sensitive fracture behavior of glass is relevant to the results described in 3.2, and so other possibilities, including the flow-dependent mechanism, must be considered.

It is of interest, then, to determine whether any of the more obvious environmental variables might be the factor determining the magnitude of D(200). Possibilities include the dielectric constant (ξ) [53,54], dipole moment (p), interfacial energy (γ_{s1}), heat of adsorption (Q_A), or wetting (Q_W) [39], viscosity (η), or coefficient of friction (μ_F). Considerations of elementary theory or previous work reveal, however, that for the alcohols or alkanes none of these parameters varies with N_C in such a manner that one might reasonably expect a maximum in D(200) at any particular value of N_C such as is evident in the data presented. For example, as N_C increases, γ_{S1}, ϵ and μ_F decrease monotonically, Q_A and η increase monotonically, and p does not vary significantly. The further possibility that variations in D(200) are related to differences in the effectiveness of these environments as coolants can probably be eliminated in view of (i) the correlation between the data from pendulum sclerometer and drilling experiments, cf. figures 11 and 14, and figures 11(b) and 14(b)—thermal dissipation effects are unlikely to be important in the former case, and (ii) the influence of mixed alcohols on D(200), figure 11(b)—it is difficult to see how mixing two "inferior" cutting environments produces a "superior" one if coolant action is the factor determining drilling efficiency.

It remains, therefore, to consider further the hypothesis that the observed variations in D(200) are a consequence of environmentally-induced variations in nearsurface deformation behavior. This possibility appears reasonable because: (i) previous work has established that adsorbed species *can* influence the anelastic behavior of glass when tested in bending [55], (ii) the observed variations in D(200) are reminiscent of the environment-sensitive variations in drilling behavior of MgO which, as shown earlier, have a demonstrable relationship with adsorption-induced changes in near surface flow and fracture behavior, and (iii) the hardness of a solid is a nearsurface or bulk property rather than a true surface property—yet figure 14 shows that this property, as manifested by pendulum sclerometer measurements, can be significantly influenced by the test environment.

The problem then resolves into determining the mechanism by means of which the hardness (i.e., flow or stress-relaxing behavior) of the near-surface regions of a glass can be influenced by an environment such that drilling behavior is significantly affected, but ϕ is not. Now it may be assumed that ϕ for soda-lime glasses is relatively insensitive to sodium ion concentration, since the values of ϕ for fused silica and a soda-lime glass containing 14 percent Na_2O are essentially identical at 77°K, namely $\sim 4.5 \pm 0.2 J/m^2$ [49]. On the other hand, soda-lime glass is considerably softer than fused silica (typically by about 40%).

Thus if, for some reason, the concentration or distribution of sodium ions in the glass surface becomes different from that in the bulk, the hardness of the surface regions also will be different. It is also known that the capacity of the alcohols and alkanes to act as electron donors varies with molecular chain length [56], thus the surface charge resulting from their chemisorption will vary—in some as yet unpredictable manner—with N_C. Then, if the surface charge influences the local sodium ion concentration, as postulated by Volkenstein [21] and others, H also will vary with N_C, and so will drilling efficiency.

The observation that binary solutions of alcohols or alkanes produce drilling efficiencies equivalent to those of pure, intermediate alcohols or alkanes appears to be consistent with this hypothesis in that such environments might be expected to produce, via adsorption, surface charges intermediate between those of the two participating species, the specific charge depending on the relative surface concentrations of these species.

4. Conclusion

In our view, the potentially most important application of the Rebinder effect is facilitation of the machining of hard ceramics, glasses, and minerals, and the intent of this paper has been to demonstrate that, for such nonmetallic solids, an important correlation exists between the influence of an active environment on near surface flow behavior and on ease of drilling. Although the specific mechanisms involved remain poorly understood, it appears that many experimental observations can be interpreted conceptually in terms of the influence of adsorbed species on the distribution or state of ionization of point defects and impurity ions, and hence on near-surface dislocation or flow behavior. These are, however, complex phenomena, and much sophisticated research will be required before it will be possible to predictably formulate a cutting environment capable of, for example, increasing the conventional material removal rates of a specific solid by, say, ten fold. The need for further studies on polycrystalline ceramics is especially urgent, since very little information is available on their behavior. It has also become clear that one must always think in terms of the total cutting system, environment-solid-tool, in order to appreciate the nature of environment-sensitive machining behavior. Given sufficient effort, however, it should be possible for Rebinder effects to finally assume their rightful place as a *conventional* approach to machining nonmetals in time for the golden anniversary of their discovery.

The sponsorship of the U. S. Office of Naval Research. (currently under Contract NOOO14–70–C–0330, NR–032–524) during both the preparation of this review and the performance of much of the work described, is much appreciated. It is also a pleasure to acknowledge the capable and enthusiastic assistance of R. D. Huntington in the recent RIAS studies of environmental effects in machining.

5. References

[1] Rebinder, P. A., Schreiner, L. A., and Zhigach, K. F., Hardness Reducers in Rock Drilling (C.S.I.R.O., Melbourne, Australia, 1948).

[2] Westwood, A. R. C., Huntington, R. D., and Latanision, R. M., RIAS, Baltimore, Md., unpublished work (1970).

[3] Robinson, L. H., Effect of hardness reducers on failure characteristics of rock, Soc. Petrol. Eng. J., 294–300 (Sept. 1967).

[4] Boozer, G. D., Hiller, K. H., and Serdengecti, S., Effect of pore fluids on the deformation behavior of rock subject to triaxial compression (Fifth Symp. on Rock Mechanics, U. of Minnesota, May 1962).

[5] Rebinder, P. A., Effect of surface energy changes on cohesion, hardness, and other properties of crystals, Proc. Sixth Physics Conf., p. 29 (State Press, Moscow, USSR, 1928).

[6] Engelhardt, W. von, Versuche zur Verinderung der Bohrarbeit in Harten Quarzgesteinen, Oel und Kohle, 39, 707–709 (1943).

[7] Engelmann, W. H., Terichow, O., and Selim, A. A., Zeta potential and pendulum sclerometer studies of granite in a solution environment, RI 7048, USBM, 16pp (1967).

[8] Westwood, A. R. C., Effects of adsorption on hardness and the mobility of near-surface dislocations in nonmetals, Adv. in Materials Res., vol. 2, Microplasticity, pp. 365–382 (Interscience Publishers, Inc., New York, 1968).

[9] Westbrook, J. H., Surface effects on the mechanical properties of non-metals, Surfaces and Interfaces, vol. II, Physical and Mechanical Properties, pp. 95–138 (Syracuse University Press, Syracuse, N. Y., 1968).

[10] Kuznetsov, V. D., Surface Energy of Solids, pp. 45 and 74–110, (Trans. H.M.S.O., London, 1957).

[11] Westwood, A. R. C., and Goldheim, D. L., Occurrence and mechanism of Rebinder effects in CaF_2, J. Appl. Phys. 39. No. 7, 3401–3405 (1968).

[12] Westwood, A. R. C., Parr, G. H., and Latanision, R. M., Adsorption-sensitive mechanical and machining behavior of a soda-lime glass (Proc. Third Intl. Conf. Physics of Noncrystalline Solids, Sheffield, U. K., Sept. 1970) to be published.

[13] Rebinder, P. A., Institute for Physical Chemistry, Academy of Sciences, Moscow; private communication, (January 1969).

[14] Shockey, D. A., and Groves, G. W., Origin of water-induced toughening in MgO crystals, J. Am. Ceram. Soc. 52, No. 2, 82–85 (1969).

[15] Westwood, A. R. C., Goldheim, D. L., and Lye, R. G., Rebinder effects in MgO, Phil. Mag. 16, No. 141, 505–519 (1967).

[16] Westwood, A. R. C., Goldheim, D. L., and Lye, R. G., Further observations on Rebinder effects in MgO, ibid, 17, No. 149, 951–959 (1968).

[17] Johnston, W. G., Effect of impurities on the flow stress of LiF crystals, J. Appl. Phys. 33, No. 6, 2050–2058 (1962).
[18] Pratt, P. L., Chang, R., and Newey, C. H., Effect of divalent metal impurity distribution, quenching rate and annealing temperature on flow stress of ionic crystals, Appl. Phys. Letters 3, No. 5, 83–85 (1963).
[19] Pratt, P. L., Harrison, R. L., and Newey, C. H., Dislocation mobility in ionic crystals, Disc. Faraday Soc., No. 38, 211–217 (1964).
[20] Volkenstein, F. F., Electronic Theory of Catalysis on Semiconductors (Pergamon Press, Oxford, U. K., 1963).
[21] Volkenstein, F. F., Electronic processes at the surface of a semiconductor during adsorption, Sov. Phys. Uspekhi 9, No. 5, 743-751 (1967).
[22] Westbrook, J. H., and Jorgensen, P. J., Indentation creep of solids, Trans. AIME 223, No. 2, 425–428 (1965).
[23] Hanneman, R. E., and Westbrook, J. H., Effects of adsorption on the indentation deformation of nonmetallic solids, Phil. Mag. 18, No. 151, 73–88 (1968).
[24] Seltzer, M. S., Influence of charged defects on mechanical properties of PbS, J. Appl. Phys. 37, No. 13, 4780–4784 (1966).
[25] Westwood, A. R. C., and Goldheim, D. L., Environmental control of drilling in MgO and CaF_2 monocrystals, J. Am. Ceram. Soc. 53, No. 3, 142–147 (1970).
[26] Selim, A. A., Schulz, C. W., and Strebig, K. C., Effect of additives on impregnated diamond performance, Soc. Petrol, Eng. J., Preprint No. 2387 (January 1969).
[27] Clarke, F. J. P., and Sambell, R. A. J., Microcracks and their relation to flow and fracture in single crystals of MgO, Phil. Mag. 5, No. 49, 697–707 (1960).
[28] Clarke, F. J. P., Sambell, R. J., and Tattersall, H. G., Mechanisms of microcrack growth in MgO, ibid, 7, No. 75, 393–413 (1962).
[29] Stokes, R. J., Johnston, T. L., and Li, C. H., Effect of slip distribution on the fracture behavior of MgO single crystals, ibid, 6, No. 61, 9–24 (1961).
[30] Aust, K. T., Mechanical effects at grain boundaries, Surfaces and Interfaces, vol. II, Physical and Mechanical Properties, pp. 235–269 (Syracuse University Press, Syracuse, N. Y., 1968).
[31] Westbrook, J. H., and Jorgensen, P. J., Effects of adsorbed water on indentation hardness anisotrophy in crystals, Antisotropy in Single Crystal Refractory Compounds, vol. 2, pp. 353–360 (Plenum Press, Inc., New York, 1968).
[32] Orowan, E., The fatigue of glass under stress, Nature 154, 341 (1944).
[33] Charles, R. J., and Hillig, W. B., The kinetics of glass failure by stress corrosion, pp. 511–527, Symp. on Mechanical Strength of Glass and Ways of Improving It (Union Scientifique du Verre, Charleroi, Belgium, (1962).
[34] Moorthy, V. K., and Tooley, F. V., Effect of certain organic liquids on strength of glass, J. Am. Ceram. Soc. 39, No. 6, 215–217 (1956).
[35] Culf, C. J., Fracture of glass under various liquids and gases, J. Soc. Glass Tech. 41, 157–167T (1957).
[36] Mould, R. E., Strength and static fatigue of abraded glass under controlled ambient conditions; IV–Effect of surrounding medium, J. Am. Ceram. Soc. 44, No. 10, 481–491 (1961).
[37] Engelhardt, W. von, Schleiffesstigkeit und Grenzflachenenergie fester Stoffe, Naturwiss 33, No. 7, 195–203 (1946).
[38] Ramsauer, R., Uber den Einflub von Flüsigkeiten auf die mechanische oberflachenvergroberung von Glas, Glastechnische Berichte 24, No. 10, 239–247 (1951).
[39] Weyl, W. A., Surface structure and surface properties of crystals and glasses, J. Am. Ceram. Soc. 32, No. 11, 367–374 (1949).
[40] Marsh, D. M., Plastic flow in glass, Proc. Roy. Soc. A279, 420–435 (1964).
[41] Dick, E., Neue Versuche Zur Mikroplastizat von Glas, Glastechnische Berichte 43, No. 1, 16–21 (1970).
[42] Lange, F. F., Non elastic deformation during fracture of glass, Tech. Rept. No. 3 on Contract NOOO14–68–C–0323, NR–032–507. Westinghouse Elec. Co., R. & D. Center, Pittsburgh, Pa. (1970).
[43] Weber, R., and Goldstein, M., Stress-induced migration and partial molar volume of sodium ions in glass, J. Chem. Phys. 41, No. 9, 2898–2901 (1964).
[44] Weyl, W. A., The rheology of inorganic glasses, Rheology, vol. 3, pp. 299–340 (Academic Press, New York, 1960).
[45] G. Quinke, Ann. d. Physik 10, 160, 374, 512 (1880). See Weyl, Ref. [44], p. 339.
[46] Westwood, A. R. C., Latanision, R. M., and Lye, R. G., Adsorption-sensitive anelastic effects in glass, Phys. Stat. Solidi, (a) 3, K17 (1970).
[47] Gilman, J.J., Direct measurements of the surface energies of crystals, J. Appl. Phys. 31, No. 12, 2208–2218 (1969).
[48] Weiderhorn, S. M., Fracture surface energy of soda-lime glass, Mat. Sci. Res., vol. 3, pp. 503–528 (Plenum Press, New York, 1966).
[49] Weiderhorn, S. M., Fracture surface energy of glass, J. Am. Ceram. Soc. 52, No. 2, 99–105 (1969).
[50] Linger, K. R., and Holloway, D. G., The fracture energy of glass, Phil. Mag. 18, No. 156, 1269–1280 (1968).
[51] Weiderhorn, S. M., and Johnson, H., Failure of glass under biaxial loading, N.B.S. Rept. No. 10145 on Contract NAonr–7–70, NR–032–517.
[52] Stewart, D. R., and Davis, W. L., Evaluation of a large glass-ceramic mirror blank, Appl. Optics 9, No. 4, 938–941 (1970).
[53] Berdennikov, W. P., Measurement of surface tension of solids, Zhur Fiz. Khim. 5, No. 2–3, 358–371 (1934).
[54] Cox, S. M., Glass strength and ion mobility, Phys. and Chem. of Glasses 10, No. 6, 226–239 (1969).
[55] Aslanova, M. S., and Rebinder, P. A., Effects of adsorption on elasticity and creep of glass fibers, Dokl. Akad. Nauk 156, No. 2, 299–302 (1954).
[56] Ingold, C. K., Structure and Mechanism in Organic Chemistry (Cornell Univ. Press, Ithaca, N. Y., 1953).

Discussion

DINESS: What was the concentration of sodium ion in the fused silica?

WESTWOOD: I don't know. It must be quite low, however.

DINESS: Do you think that your rationalization can account for this effect in such a low concentration of sodium?

WESTWOOD: That is a good question, Art,

and I can't give you a straightforward answer. All commercial glasses have some sodium present, however, and our calculations indicate that increases in sodium ion concentration of only $\sim$ 10 ppm in a surface layer $\sim$ 0.1 μm thick are sufficient to relax quite large tensile stresses* and hence, presumably, to influence the crack initiation step.

DINESS: One further point, have you looked at any non-oxidic glasses?

WESTWOOD: No.

WIEDERHORN: Regarding the sodium concentration in fused silica, I believe the range to be of the order of 10 parts per million and less. You could also get rather large hydroxyl concentrations. I don't know how this would affect your results.

WESTWOOD: Yes, that's a good point. In fact, while one might expect a negative surface charge to attract sodium ions to the surface, a positive surface charge probably would attract hydroxyl ions instead. The presence of either species in the surface layers is likely to lead to some reduction in hardness.

WIEDERHORN: Let me ask you another question regarding hardness. Did you try the conventional pyramidal type of indenter?

WESTWOOD: Yes, but it proved very difficult to find the indentations made under the test environment with indenter loads of only 1—10 g after the environment was removed. Accordingly, our hardness determinations were made with the pendulum device.

RICE: Just briefly, you have addressed yourself mainly to glasses and ionically bonded materials. Do you expect somewhat similar effects in the hard materials such as carbides, borides, and nitrides which are more often characterized by covalent bonding? In these materials lattice friction is probably much more important.

WESTWOOD: Yes, there is considerable evidence for Rebinder effects in solids which have some degree of covalent bonding**. One has to be careful when talking about carbides though because they have a significant amount of metallic bonding. However, Jack Westbrook has shown such effects in TiC. One further point: Rebinder effects are sensitive to both light and imposed potentials—two other variables that may prove exploitable in technology.

HEUER: I'd like to ask, since there is a lot of interest in the machining of alumina, whether you intend to do any work on alumina.

WESTWOOD: Yes, we plan to.

KIRCHNER: When your report came out about a year ago, we became interested in the effect of these media on the strength of alumina. We, however, found essentially no effect on the strength. Now, do you have any comments on the relationship of this and the role of microplasticity in the failure of alumina?

WESTWOOD: Was this polycrystalline alumina?

KIRCHNER: Yes.

WESTWOOD: And you measured tensile strength?

KIRCHNER: Well, we measured flexure strength.

WESTWOOD: Of course, when one is dealing with polycrystalline solids, there are a lot of new factors involved in the problem. Imagine that we had many, many grains throughout the solid, but only the surface layer was affected by the adsorbing species. Imagine also that the actual mechanical properties were dominated by the presence of voids, cracks, and other sort of defects within the solid. In this case, one would not expect to see any effect of environment on the tensile strength. On the other hand, if one were to study, say, the bending fatigue behavior of such a solid, in which case the deformation process is initiated and concentrated near the surface, then this property may well be dominated by the environment, and one might expect to see effects. Machining is, of course, a near-surface dominated process—that's why it is possible to see such spectacular effects.

*(Westwood, A. R. C., Latanision, R. M., and Lye, R. G., Phys. Stat. Solidi (a) 3, K17 (1970).

**(For a review of such effects see Westwood, A. R. C., in "Microplasticity", Interscience Publishers, New York, pp. 365–82 (1968).

NATIONAL BUREAU OF STANDARDS SPECIAL PUB. 348, THE SCIENCE OF CERAMIC MACHINING AND SURFACE FINISHING, Proceedings of a Symposium Sponsored by the American Ceramic Society, the Office of Naval Research, and the National Bureau of Standards, held at NBS Nov. 2–4, 1970, Gaithersburg, Md. (Issued May 1972).

B. Nonmechanical Methods

Shaping or Figuring Ceramic Surfaces by Ion-Beam Bombardment*

Paul W. Levy

Brookhaven National Laboratory, Upton, New York 11973

The shaping or figuring of glass and ceramic surfaces by ion-beam erosion is a relatively new technique. All operations are carried out in a vacuum. Usually the optic is bombarded by a collimated beam of rare gas ions whose energy is between 1–100 keV. Selected areas can be eroded by electrostatically deflecting the beam or, less conveniently, by moving the optic. The erosion area can be controlled by focusing the beam with electrostatic or magnetic lenses. The basis of the erosion process is the physical phenomenon known as sputtering. This occurs when the incident ions scatter elastically with atoms near the surface of the target and some of the displaced atoms, after participating in one or more collisions, acquire sufficient velocity to escape from the solid. Other dislodged atoms become interstitials and, together with vacancies created in the recoil process, create a radiation-damaged layer just below the eroding surface, whose thickness is roughly the range of the bombarding ions. For ceramic materials typical erosion rates are on the order of angstroms/μamp/cm^2/min and increase with increasing angle of incidence. Ion-beam currents up to 100 μamp/cm^2 are practical. Under these conditions the material struck by the beam may reach temperatures between 300 and 700 °C. The maximum lattice disruption occurs at a depth of one incident ion range from the original surface, just as the eroding surface reaches this point. Additional bombardment does not increase the damage beyond this maximum. Furthermore, the damage is minimized by using bombardment conditions which maximize the temperature in the target. It is not known if there are any radiation damage effects which reduce the usefulness of ion-beam figured optics. At the moment, it would appear that ion-beam figuring is a practical technique for "touching up" conventional optics and, more importantly, for fabricating non-spherical or non-axially symmetrical optics. Also, the ion-beam erosion process is particularly amenable to computer control.

Key words: Figuring; ion-beams; optical surfaces; polishing; radiation damage; sputtering.

1. Introduction

For approximately two hundred years ceramic surfaces, particularly glasses, have been shaped and polished by methods employing abrasive substances. During the last decade or two a number of new shaping or figuring techniques have been introduced. One of the most interesting, and promising from a technological point of view, is "ion-beam sputtering" or "ion-beam erosion." Very briefly, this process is based on the physical phenomenon known as "sputtering," which occurs when metal, ceramic, or even plastic surfaces are bombarded by energetic ions and, incidentally, even electrons. When a fast moving ion enters the surface of a solid the interaction is sufficiently violent to eject one or more atoms from their normal positions in the crystal or glass lattice. Some of these atoms will be scattered towards the surface and will escape from the solid. Other atoms will penetrate into the solid to produce "radiation damage effects." Still other atoms will make one or more collisions and eventually come to rest in a normal lattice position. As the bombardment continues the surface is gradually eroded and a layer of disrupted or radiation-damaged material develops just below the slowly eroding surface.

The literature on ion-beam erosion or sputtering is, with very few exceptions, confined to papers which deal with the physics of this process. However, it is closely related to radiation damage processes, and a considerable amount of useful information can be obtained from publications on this subject. A good example in this category is the book by Carter and Colligan [1].[1] In fact, this book contains background information on almost every subject discussed in this article. A useful compendium of papers on sputtering physics is contained in the "Proceedings of an International Conference on Atomic Collisions and Penetration Studies with Energetic (keV) Ion-Beams" [2]. The most comprehensive source of information relating directly to ion-beam figuring, which appears to be available at this time, is a Kollsman Instrument Company Report, "Ion-Beam Optical Figuring" [3]. More than a few publications could be listed which describe the application of electron- and ion-beam bombardment to cleaning, deoxidizing, degassing, etc., of metal and non-metal surfaces for a variety

*Supported in part by Advanced Research Projects Agency (ARPA) Contract with Kollsman Instrument Corp. and in part by the U.S. Atomic Energy Commission.

[1]Figures in brackets indicate the literature references at the end of the paper.

of purposes. There are indications in a large fraction of these papers that sputtering, i.e., bombardment-induced erosion, is the process actually producing the observed effects. Since they have only peripheral applicability, they have not been included. Apparently there are only two papers [4, 5] which are concerned directly with the application of ion-beam bombardment to the figuring of optics.

The next section will contain a description of the basic elements in an ion-beam figuring system. The following section will describe the basic physical processes occuring during sputtering. This will include some practical information on the rate of material removal as a function of ion energy, angle of incidence, etc. During this discussion, it will become apparent that the material immediately below the eroded surface is in a radiation-damaged condition. Consequently, a separate section will be devoted to radiation damage considerations. This will lead to some conclusions, or recommendations, for figuring pieces in a way that minimizes radiation damage effects. Finally, the last section will be a brief discussion on the practical applications of the ion-beam figuring technique.

2. The Basic Ion-Beam Figuring Process

The basic elements that are contained in a typical ion-beam figuring arrangement are shown schematically in figure 1. First, all operations are performed in a vacuum chamber. The piece to be worked or figured is securely fastened to a holding device which is usually mounted on the center line of the ion beam. The bombarding ions are first ionized and then accelerated by an electrostatic accelerator. The

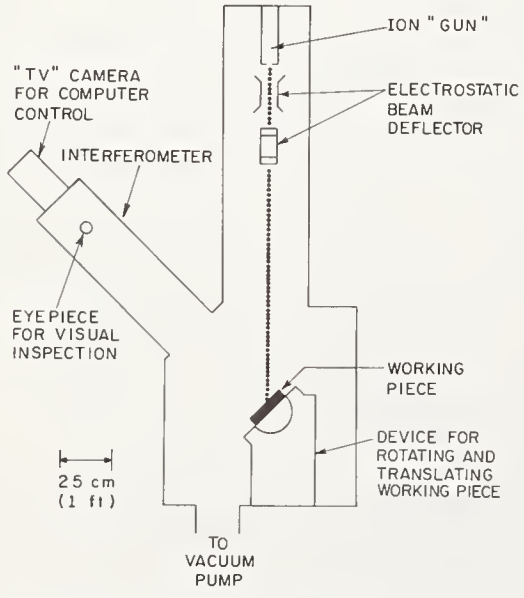

FIGURE 1. *The basic elements in an ion-beam figuring system.*

position of the beam on the working piece is usually controlled by electrostatic and/or magnetic lenses. The surface configuration changes occuring during bombardment can be determined with an interferometer by removing the piece from the chamber at desired intervals or monitoring during irradiation. Some additional information on each of these basic elements of the system is described below.

Typically, ion-beams are produced by low energy electrostatic accelerators. For figuring purposes the energy is usually in the range of 1 to 100 keV. The accelerator contains sections for producing the ions by ionizing rare gas atoms, accelerating them to the desired velocity or energy, and focusing them into a relatively narrow beam which can be focused on the surface of the target. Almost always, the bombarding beam consists of rare gas ions since they possess several advantages over other atoms or molecules. Rare gases are chemically inert and do not react with the working piece or exposed parts of the vacuum chamber. Also, they consist of monoatomic atoms which can be singly ionized without producing a troublesome number of doubly ionized atoms. Furthermore, they are convenient to handle and, with the exception of helium, are relatively easy to pump.

Two methods are commonly employed to fix the position where material is removed from the surface of the working piece. The first method employs a beam maintained in a fixed position with the piece moved in a controlled fashion by the holding device. Alternatively, the piece is held in a fixed position and the beam directed to the point on the surface where material is to be removed. Actually, for both methods it is desirable that the apparatus include a device for directing, or steering, the ion beam. Either electrostatic or magnetic deflecting arrangements can be used. Electrostatic deflection is the simpler but magnetic deflection may provide more precise control.

If the ion-beam is maintained in a fixed position and erosion control obtained by moving the working piece, the holding device must include several important features. First, it must be able to control precisely the position of the piece or, alternatively, it must be capable of rotating the piece about a precisely controlled axis. Furthermore, it is essential that vibrations be reduced to an absolute minimum and it is highly desirable to be able to control these movements from outside of the sputtering chamber.

Clearly, it is advantageous to follow the progress of the figuring during bombardment. There are a number of different interferometer arrangements that can be used for this purpose. The fringe patterns appearing in an interferometer can be observed visually, or with a "television camera" and displayed on a televi-

sion monitor, and they can be recorded photographically.

Since it is possible to follow the progress of the figuring during bombardment, it is desirable to be able to control where the erosion is taking place. As mentioned above, this can be accomplished by maintaining the beam in a fixed position and mechanically moving the piece about. However, it would appear that there are distinct advantages in keeping the piece fixed and controlling the erosion process by electrostatically or magnetically deflecting the beam. This arrangement reduces the complexity but does not eliminate the mechanical target-moving apparatus. It is apparent that video fringe registration and electrical control of the erosion process are features which can be combined in a closed-loop computer controlled figuring system. In fact, a study completed in 1968 indicates that a completely automatic computer control system is feasible [3]. Also, systems combining manual and computer control would appear to be particularly desirable. It would appear, at least to the writer, that one of the major difficulties which will be encountered in an automatic system is the distortion of the surface occurring at the erosion point due to heat deposited by the ion-beam. This distortion disappears as soon as the beam is removed, and, in principle, it should be possible to include a time-dependent correction for the distortion in the computer control program.

Inasmuch as the ion source continuously emits atoms, the system must be continually pumped. For efficient erosion the vacuum requirements are not great. The pressure must be maintained at a level where collisions between the residual gas atoms and the ions in the beam are negligible.

One additional feature, not included in figure 1, should be described. This is the device for preventing charge build-up on the target piece. During bombardment the piece becomes positively charged, first because the rare gas ions are positively charged, and secondly because of electron emission from the surface during bombardment. This positive charge build-up can be prevented by including an electron gun in the chamber which continuously directs negatively charged electrons on the target.

3. The Basic Atomic Sputtering Process

3.1. Interactions Involving Energetic Ions and Solids

Almost all of the physical processes which occur when energetic ions interact with a solid are illustrated in figure 2. The energy of the incident ion will be quite high as it enters the target. It will interact with the atoms in the

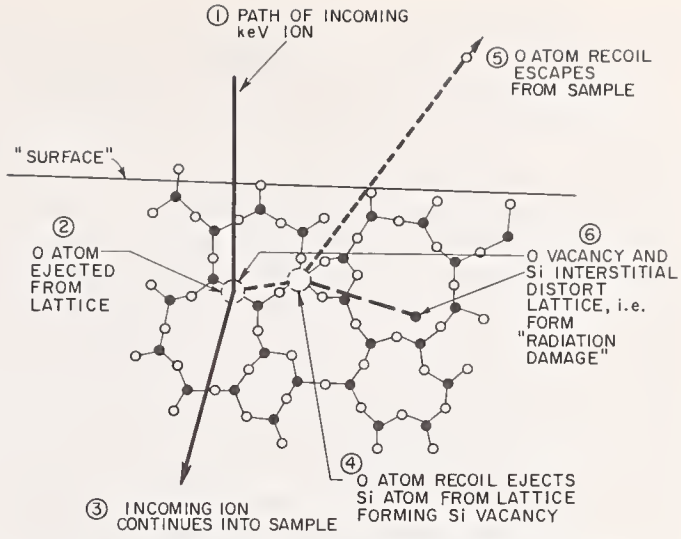

FIGURE 2. *The collision processes occurring during a typical sputtering event.*

solid in two distinct ways. First, both the incident particle and the stationary atoms may be considered as hard "billiard balls" that collide or scatter elastically. Each collision will reduce the energy or velocity of the incident particle and it will gradually slow down. The slowing down rate depends on the energy and mass of the incident particle and the mass of the atoms in the solid. This particular process is characterized by the term, "nuclear stopping power." If the stopping power is large, the incident ion quickly loses energy. Conversely, if the nuclear stopping power is low, the ion will lose energy slowly and penetrate relatively deeply into the solid. A second important energy loss mechanism results from the fact that the incident ion is charged and usually remains charged until its velocity is quite small. Specifically, there is an electrostatic interaction between the charged ion and the electrons and shielded nuclear charge of the atoms in the solid which causes the incident ion to lose energy. This second energy loss mechanism is characterized by the term, "electronic stopping power." Actually, the electronic stopping power is roughly proportional to the velocity of the ion or, i.e., to the square root of its energy.

If, in an elastic collision, sufficient energy is transferred to a lattice atom, it will be ejected from its normal position. The exact energy that must be imparted to any atom to cause this to occur depends on several factors. These include: the strength of the binding forces acting on the lattice atoms, the masses of the atoms involved, the geometrical arrangement of the surrounding atoms, etc. Very roughly, an average of 25 eV must be imparted to a typical glass atom to cause it to be ejected from the lattice.

All of the collision processes violently excite the atoms along the trajectory of the incident ion and the trajectory of any displaced atoms.

This local excitation can be viewed as a rapid and large increase in temperature and is often referred to as a "thermal spike." The energy in a typical thermal spike is dissipated in nanoseconds or even shorter times. Some of the properties associated with thermal spikes will be discussed in more detail below.

The slowing down processes described above limit the distance that an energetic incident ion can penetrate into a solid. All particles having a specific energy E will penetrate very nearly the same distance into the solid. However, the trajectory followed by one ion will differ from that of all other ions. Intuitively, one can readily understand that the sequence of scattering events will differ for each particle. The average distance penetrated by a beam of ions, incident normal to the surface and having a specific well-defined energy E, is defined as the range. The statistical variation in penetration depth, about the range, is called the "straggle." More precisely, the straggle is defined as the mean square variation in the penetration distance and is usually on the order of 1 to 5 percent of the range. Both of these concepts are suggested, but not precisely described, in figure 3.

3.2. Conventional Range and Energy Relations

A very large fraction of the experimental and theoretical papers that deal with the basic sputtering process make use of the so-called dimensionless range and energy relations:

$$\rho = R\left\{4\pi\, a^2\, N\, M_1 \frac{M_2}{(M_1 + M_2)^2}\right\}$$

$$\epsilon = E\left\{\frac{a}{Z_1 Z_2 e^2} \frac{M_2}{M_1 + M_2}\right\} .$$

In these expressions:

R = Range, ρ = dimensionless "range"
E = Energy, ϵ = dimensionless "energy"
N = number of atoms per unit volume
M_1 = mass of the bombarding ion
Z_1 = atomic number of the bombarding ion
M_2 = mass of the atoms in the target
Z_2 = atomic number of the atoms in the target

$$a = \frac{0.885\, a_0}{(Z_1^{2/3} + Z_2^{2/3})^{1/2}}, \quad \text{where}$$

$a_0 = 0.529 \times 10^{-8}$ cm, i.e., the Bohr radius.

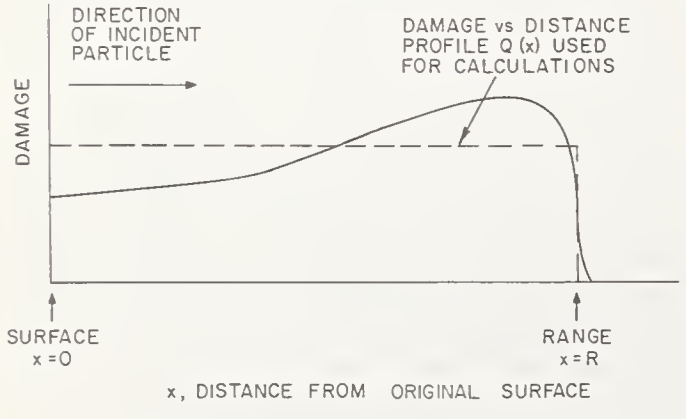

FIGURE 3. *A typical damage versus penetration distance profile determined experimentally and the damage versus depth profile used in the calculations in the text.*

The first of these is the range (ρ for range) relation and the second the energy (ϵ for energy) relation. These two relations contain a surprising amount of information and in particular indicate how the range depends on the energy, mass, and atomic number of the incident particle and the mass and atomic number of the atoms in the target solid. Although these two relations are useful, one does not have to understand them in detail to obtain a good grasp of the basic sputtering process described in the next section.

3.3. The Basic Sputtering Process

The basic physical processes producing sputtering are illustrated in figure 2. In this diagram the first interaction occurs when the incident particle makes a glancing collision with an oxygen atom quite near the surface. In turn, this oxygen recoil makes an additional collision with a nearby silicon atom and passes out of the surface, i.e., it escapes from the solid. Although there are relatively few individual events in this particular sequence, it demonstrates one of the most important features of the sputtering process, namely the multiple collision sequence or cascade. Single-event sputtering collisions can occur, especially if the incident ion enters the surface at a glancing angle. However, theoretical treatments on sputtering indicate that multiple collision processes account for a very large fraction of the escaping atoms. It should be apparent that the efficiency of the sputtering process will be least for normally incident ions and should increase as the angle of incidence is increased. This is demonstrated by numerous measurements. In order that a recoiling atom escape from this solid, it must possess two properties. First, it must have a velocity component away from the surface. Second, it must have sufficient energy to overcome both the nuclear and electronic energy losses that it will suffer in traversing the solid and, in some materials, it must have sufficient additional energy to overcome surface binding forces. The surface binding forces are between 1 and 100 eV and can usually be neglected. For most practical sputtering situations the incident ion energy is 20 keV or more and thus the surface binding effects are completely negligible. The disrupted lattice which remains after a typical sputtering cascade, often re-

ferred to as radiation damage, cannot be ignored. Some comments will be made about it immediately; however, detailed radiation damage considerations are contained in the next main section.

3.4. Sputtering-Produced Lattice Distortion

The sputtering process, outlined above and illustrated in figure 2, obviously produces considerable lattice distortion. Actually, a large number of distinctly different processes, all involving the movement of atoms, contribute to this distortion. Only the more important of these will be described. First, as is indicated in figure 2, the incident ion can penetrate into the lattice and come to rest in an interstitial position. If it happens to locate in a sufficiently large empty volume, typically found in glass lattices, it will not distort the surrounding lattice appreciably. If it comes to rest in a tightly packed region it can produce appreciable distortion. These comments apply equally well to any lattice atoms which have been ejected from their normal positions during the sputtering cascade and do not escape through the surface. In fact, since the number of lattice atoms ejected by an incident ion is usually much greater than one (1), there will be many more lattice-atom interstitials than incident-ion interstitials. The other principal contribution to the lattice distortion arises from the vacancies, i.e., the empty lattice sites which remain after atoms have been ejected from their normal positions. Incidentally, vacancies created during one sputtering event have a high probability for capturing mobile atoms from later events. It is easy to understand that interstitials have a tendency to expand the radiation damage part of the lattice. Surprisingly, under certain circumstances the introduction of vacancies also has a tendency to expand the lattice. Perhaps the easiest way to explain this is to point out that the removal of an atom also removes the binding forces holding together the atoms on either side.

3.5. Sputtering Yield and Sputtering Efficiency

It is essential for anyone interested in the sputtering process or ion-beam erosion to differentiate clearly between two commonly used definitions. These are the sputtering yield and the sputtering efficiency which are defined by the following expressions:

$$\text{Sputtering Yield} = \frac{\text{number of sputtered atoms}}{\text{number of incoming ions}}.$$

$$\text{Sputtering Efficiency} = \frac{\text{energy of the sputtered atoms}}{\text{energy imparted by incoming ions}}.$$

Note that the sputtering yield refers to the number of sputtered atoms produced by each entering ion, whereas the sputtering efficiency is defined in terms of energy. More specifically, to determine the sputtering efficiency one must determine, or add up, the energy of all of the atoms which escape from the target and compare it to the total energy of the incident ions. The sputtering yield is the more common expression and will be used throughout the remainder of this paper. However, both of these quantities are functions of numerous parameters, e.g., incident ion energy, mass, atomic number, angle of incidence, and, in particular, the mass and the atomic number of the atoms in the target piece. For practical purposes it is convenient to use a quantity called the erosion rate, which is usually expressed in angstrom (Å), of material removed per square cm per unit beam current per unit time. Typical sputtering yield values for fused silica, as a function of incident ion energy, are shown in figures 4 and 5. This illustrates three important features: first, the sputtering yield increases as the mass of the incident particle increases; second, the yield vs. energy curve has a distinct maximum; and third, the maximum yield increases to higher energies with increasing incident particle mass. The data given in this figure is for the incident ions striking the surface perpendicularly, i.e., for zero angle of incidence. Above it was implied that the sputtering yield should increase as the angle of incidence is increased. This is clearly demonstrated by figure 6 which shows how the erosion

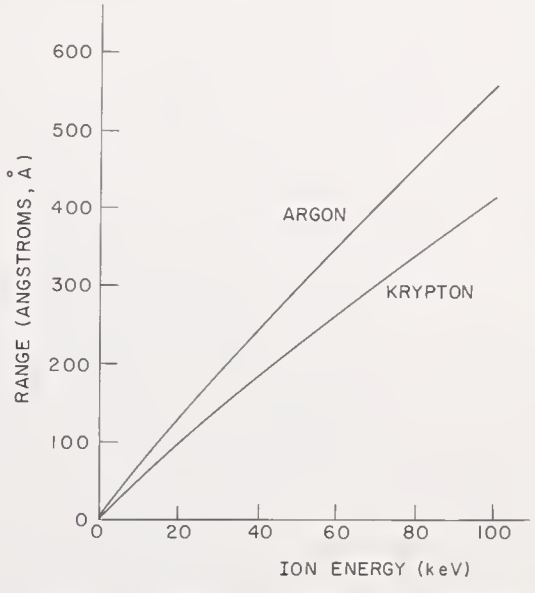

FIGURE 4. *Range of argon and krypton ions in fused silica.*

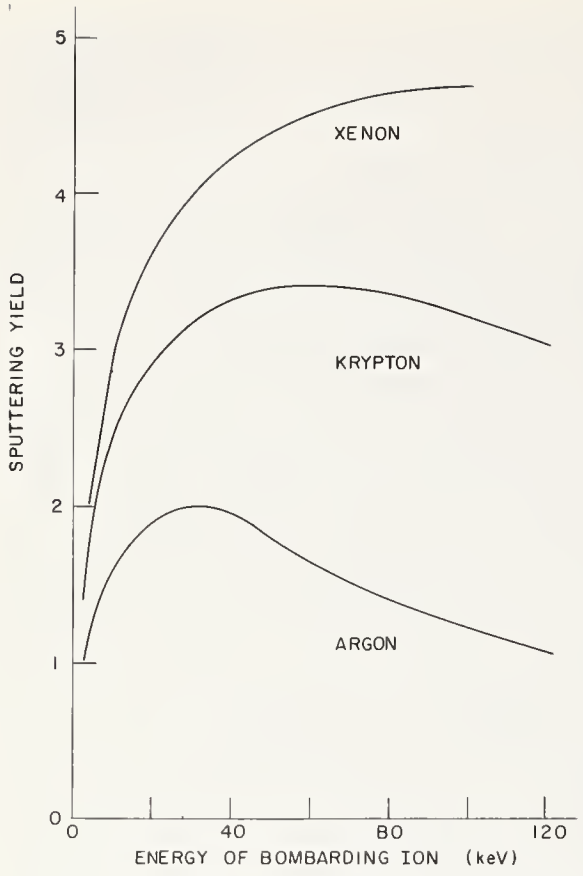

FIGURE 5. *Typical sputtering yield versus incident ion energy curves for fused silica.*

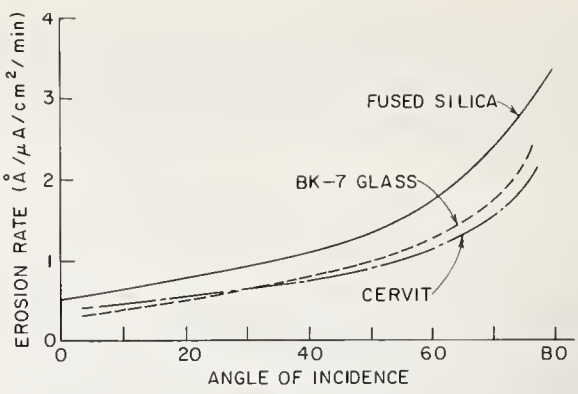

FIGURE 6. *Typical sputtering yield versus ion-beam angle of incidence curves.*

rate varies with angle of incidence for three common lens materials. The yield versus angle of incidence curves also depend on the mass and energy of the incident ion.

3.6. Target-Area Temperature During Bombardment

During bombardment numerous sputtering cascades are taking place, and the volume immediately below the area struck by the beam can attain surprisingly high temperatures. This is readily understood by pointing out that the sputtering process converts the incident ion energy into the motion of atoms in the target and to electronic excitation. In reality, both of these energy-transfer processes can be regarded as increasing the local energy temperature. As mentioned above, the rapid increase and decrease in temperature associated with a single cascade event is often called a thermal spike. When a given area is under bombardment and each incident ion produces an individual spike, the net result is a large temperature increase directly below the surface. The actual temperature will depend on numerous parameters, e.g., beam size and energy, thermal conductivity of the target piece, and the temperature of the holding arrangement which might act as a heat sink. Consider just one example, the maximum temperature attained by a typical glass or fused silica optic under continuous bombardment. A 100-microamp beam of 100 keV ions will impart 10 watts to the surface. If the beam strikes an area of one square centimeter the following approximate temperatures occur at the center of the beam and at various points near the surface. On the surface the temperature is 700 °C, 1 mm below the surface it is 400 °C, and 6 mm below the surface it is 150 °C. Incidentally, these values apply to a piece approximately 10 cm in diameter and 1 cm thick. As soon as the beam is "shut off" the temperatures drop very rapidly. In fact, when the surface temperature is approximately 300 °C during bombardment it will drop to between 50 and 100 °C within one-tenth of a second after the bombardment is terminated. These considerations indicate that it is possible to erode an optic without raising its temperature excessively at any point by the simple expedient of moving the eroding beam back and forth on the surface. However, as will be demonstrated in the next section, radiation damage effects can be minimized by figuring the piece under conditions which maximize the temperature near the surface.

3.7. Channeling and "Amorphous Sputtering"

One of the more interesting radiation effects discovered during the last decade is the phenomenon known as channeling. It is now known that the concept of the penetration depth or range introduced above can be applied precisely only to glassy or amorphous substances. More specifically, it needs to be modified when applied to most crystalline materials. When crystalline substances are bombarded by particles which are accurately aligned along certain crystallographic directions, it is found that a large fraction of the incident particles penetrate into the crystal considerably beyond the range defined above. In fact, the particles may penetrate to a depth of 10, 20, or even 30 times

greater than the "range." The reason for this is now well understood. The atoms in many crystals are aligned in a way that produces well defined channels. Once an energetic particle enters such a channel with its velocity vector closely aligned with the channel axis, it can proceed in an almost uninhibited fashion. As long as the particle is traversing a part of the crystal which is free of defects there is nothing in its path to restrict its progress. Furthermore, even if the velocity vector does not correspond precisely to the axis of the channel, the particle is assisted along the channel by various "focusing effects." Inasmuch as such channels do not exist in glassy or amorphous materials, channeling effects are not observed in these substances.

It is reasonable to expect that channeling effects will play a role in the ion-beam figuring of crystalline materials. It might be expected that they would be particularly important in radiation damage considerations. However, in this paper all comments on channeling are confined to this subsection. In crystalline materials it is convenient to define a range which does not include channeling effects. Unfortunately, the range defined in this way is usually referred to as the amorphous range. Also, the parameters associated with the sputtering process, e.g., the sputtering yield or the sputtering efficiency, are defined in a way which obviates (actually it ignores) all channeling effects. These parameters are said to apply to the "amorphous" materials. Thus, in the literature one sees references to the sputtering parameters for amorphous Al_2O_3, a substance which, as far as the writer can determine, does not exist in a glassy or amorphous form.

4. Radiation Damage in Ion-Beam Figured Materials

4.1. The Necessity for Radiation Damage Considerations

The description of the sputtering process, contained in the previous section, indicates that the material just below the surface of the target is in a "radiation-damaged" condition. This region contains vacancies and interstitials which will, almost certainly, distort the lattice. It may contain numerous color centers or, i.e., may have become colored. The glass technologists would say that it has been browned by the bombardment. Intuitively one might expect that the damaged or distorted lattice would be unstable in one or more respects. A sufficiently large change in dimension occurring after an optic had been figured by ion-beam erosion would render the piece useless. Consider another example: for certain applications the index of refraction of the material at its surface must be stable, e.g., for dielectric coating or thin-film applications. Thus, even if the material were dimensionally stable, a change in dielectric constant would be intolerable. Radiation-induced changes in the density, index of refraction, and the dimensions of quartz and fused silica samples have been extensively studied [6]. These and other radiation effects usually observed in ceramic materials have been discussed previously [7]. However, and this point must be made explicitly clear, with only one or two exceptions, all of the available radiation effects information on glasses and other ceramic materials has been obtained from materials bombarded in a reactor or with gamma rays or x rays. Perhaps the most pertinent work is a study of ion-bombardment induced changes in the index of refraction of fused silica [8]. However, it is difficult to apply this work to practical figuring applications. There are studies on the release of trapped ions implanted during bombardment, the diffusion of implanted ions, etc., that provide useful information but only peripheral to the considerations described above.

4.2. Nature of the Radiation-Damaged Material

The process leading to the formation of vacancies and interstitials along the trajectory of the bombarding ion and recoil atoms has been amply described. However, the distribution of vacancies and interstitials along the trajectory of the incoming ion varies considerably. This is shown in figure 3 where $Q(x)$ is the number of displaced atoms along the trajectory a distance x from the surface from the target. It is difficult to approximate the true $Q(x)$ function analytically, and consequently the approximations shown in this figure will be used throughout the remainder of this paper. Specifically, it will be assumed that $Q(x)$ is a constant for all values of x less than the range R and is O for values of x greater than r. Note that $Q(x)$ describes the number of displaced atoms produced by each individual incident ion. Inasmuch as more than one bombarding ion may contribute to the damage at any specific point x, where $x<R$, the damage may be greater than $Q(x)$. The quantity $D(x,t)$ will be used to describe the damage at point x, at time t, after the bombardment has commenced. If the bombardment has proceeded for a considerable time and the concentration of vacancies and interstitials has reached an appreciable level, the vacancies and interstitials produced late in the bombardment have increased probability for combining with their opposite or "antipodal" defects and the rate of damage formation will be decreased. In other words, if the bombarded material contains an appreci-

able concentration of vacancies and interstitials, any vacancies or interstitials produced in subsequent events can re-enter or rejoin the normal lattice. Thus the damage produced by each incident ion will diminish as the bombardment progresses. This phenomenon is sometimes called "radiation annealing." However, in the considerations that follow it will be assumed that the induced damage is linearly proportional to the number of incident ions. The annealing of radiation damage by radiation-produced processes should not be confused with the removal of damage by the thermal processes which will be discussed in a later section.

The sputtering process includes an appreciable number of ionization events. That is, electrons are excited to an extent that they escape from bound atoms and peregrinate, or wander about, the target material. Also, the "missing charges" or (electronic) holes are mobile. When electrons or holes are trapped by certain entities such as vacancies, impurities, or more complex defects, color centers are formed. As mentioned above, this is referred to as coloring or browning. For many practical purposes, e.g., in reflecting optics, the coloring is unimportant. Scientifically this coloring can be quite useful. When defects such as oxygen atom vacancies are converted into color centers by charge trapping, the color-center concentration can be used as a measure of the damage concentration. This technique has been described in a previous paper [9] and, as will be described below, provides information directly applicable to radiation-damage considerations in ion-beam figured fused silica.

4.3. The Measurement of Radiation Damage in Figured Optics

Radiation damage can be characterized by color-center measurements under some circumstances. However, a really good indicator for measuring radiation damage in ion-beam eroded materials does not exist. Furthermore, a method might be devised which would apply to one damage characteristic but not another. For example, an interferometer measurement might indicate that a figured piece does not contain a detrimental amount of damage. However, an entirely unsatisfactory amount of damage may be present when assessed by another method. For example, a piece which is acceptable in most respects may be unacceptable when evaluated in terms of its resistance to attack by water vapor. This discussion has been included to emphasize the point that it is not possible to conclude that radiation damage in figured optics can be ignored on the basis of one or two types of tests.

4.4. Kinetics of Radiation Damage Formation

The discussion on the kinetics of radiation damage formation during ion-beam figuring, contained in this section, will be based on the assumption that neither radiation annealing nor thermal annealing processes are important. This is equivalent to restricting the derivations to the case in which the ion-beam currents are low enough to prevent the target from being heated more than a negligible amount. Also, it is assumed that the total or integrated flux is low enough to prevent extensive overlap of individual damage regions. In practice this latter condition is hard to realize. However, by adopting it the calculations can be very greatly simplified without eliminating any important features of the description of the damage formation process.

4.4.1. Definitions

The following parameters will be used in the derivation of the equations describing the rate of radiation damage formation in a target being eroded by ion-beam bombardment.

t = time, $t=0$ corresponds to the start of the erosion bombardment

x = distance or depth measured from the coordinate of the surface prior to bombardment, i.e., the surface is at $x=0$ when $t=0$.

$x_s(t)$ = position of the surface at time t, $x_s(t)=0$ at $t=0$.

R = range or penetration depth of the incident ion.

$Q(x)$ = number of defects (per unit length) introduced along the trajectory of each incident particle. It will be assumed that $Q(x)$ is constant, or more specifically:
$Q(x)=Q$, if $x_s \leq x \leq x_s+R$, *and*
$Q(x)=0$, if $x>x_s+R$.

$D(x,t)$ = concentration of defects at time t and point x. If the eroding surface has passed the point x, i.e., if $x<x_s$, $D(x,t)$ has no meaning.

I = flux (number of ions per unit time, per unit area) of bombarding particles striking the target.

S = surface erosion rate. Specifically S is the depth of material removed, per unit area, by one incident ion. Also, S is assumed to be constant, i.e., independent of the amount of prior bombardment.

4.4.2. The Basic Erosion Rate Equation

The rate at which the target surface erodes during sputtering can be described by a surprisingly simple expression. First, it is assumed that the incident ion flux is uniformly distrib-

uted over the target area and that the beam current is constant. In a time period Δt, the total number of ions striking a unit surface area is $I\Delta t$, and this number of ions will, using the definitions given above, cause the surface to erode a distance $\Delta x = SI\Delta t$. If the total bombardment time is t, the surface will move a distance $x_s(t)$ given by

$$x_s(t) = \int_0^t dx = \int_0^t SIdt = SIt \cdot$$

It will become apparent that the simple equation

$$x_s(t) = SIt$$

is very useful.

4.4.3. Damage Formation at a Depth Greater than the Incident Ion Range

The description of the rate of radiation damage formation at a point x_i below the surface of the target will be divided into two parts. First, in this section the damage formation will be described for a point x_1 which lies farther from the original surface than the maximum penetration depth or range of the incident ions. Second, the damage formation will be described for a point which lies between the original target surface and the maximum penetration depth. Note particularly that the position or coordinate of a particular point in the target is always measured with respect to the position of the target surface before bombardment. In other words, the surface of the target is receding during erosion but distances are always reckoned from the surface coordinate at irradiation time $t = 0$. The geometry of the situation to be considered first is illustrated in figure 7. At the time when the irradiation is started, the incident ions will penetrate a distance R, and there will not be any radiation damage formation at x_1 until the surface has eroded to the extent that the ions will penetrate to this point. Thus, the surface must erode a distance $x_1 - R$ before damage is formed at x_1. The total amount of damage at the point x as a function of time is illustrated in figure 8. A time $t = (x_1 - R)/IS$ will elapse before the surface has moved sufficiently to permit the penetrating ions to reach a depth, measured from the moving surface, equal to the range R. Once the ions penetrate to the depth x_1, the damage will increase with time. Inasmuch as it was assumed that the damage produced by each incident ion is the same at every point along its trajectory (see fig. 3), the damage at a point x_1 will be proportional to the total number of ions passing this point, and, if the current is constant, the damage will increase linearly with time. The time required for the surface to erode from its original position to a depth x is simply x/IS. Clearly, the maximum damage at the depth x_1 occurs just as this point is reached by the eroding surface. Also, it is meaningless to talk about the damage concentration at any point after it has been eroded away. Thus, the damage at the point x_1 as a function of time $D(x,t)$ is given by the following expression:

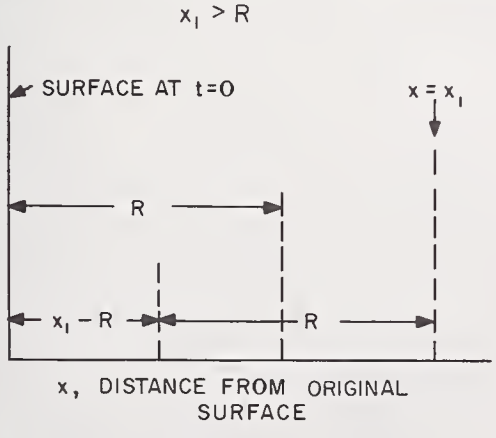

FIGURE 7. *Spatial relations for determining the rate of damage formation at a point which lies at a distance* x_1, *measured from the original surface, greater than the range of bombarding ions.*

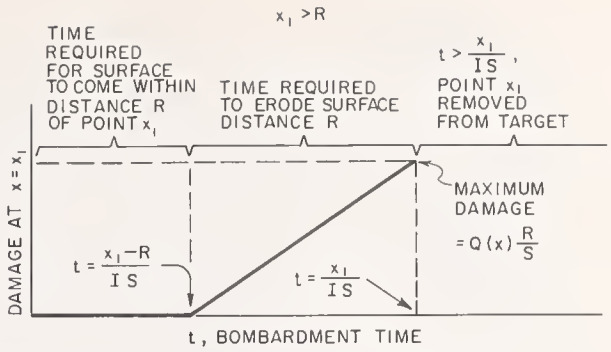

FIGURE 8. *Damage formation at the point* x_1, *described in the previous figure, versus bombardment time.*

$$D(x_1,t) = I\int_{\frac{x_1-R}{IS}}^{t} Q(x)\,dt = IQ(x)\left[t - \frac{x_1-R}{IS}\right]$$

$$\text{when } \frac{x_1-R}{IS} < t \leq \frac{x_1}{IS}$$

$$D(x,t) = 0, \text{ when } t \leq \frac{x_1-R}{IS} \text{ or } t > \frac{x_1}{IS} \cdot$$

The maximum damage which occurs during sputtering occurs when $t = x_1/(IS)$, or

$$D_{max}(x,t) = Q(x)\frac{S}{R} \cdot$$

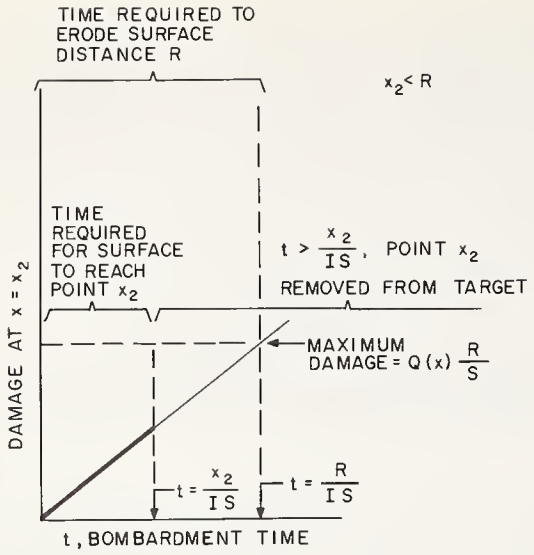

FIGURE 9. *Damage formation versus bombardment time at a point* x_2 *which is between the original surface and a depth equal to the range of the bombarding ions.*

Note that D_{max} does not contain the time t or the ion current I; thus this simple computation leads to the following important generalization. Namely, the total amount of radiation damage introduced into a target during sputtering has a maximum value, given by $Q(x)R/S$, and this quantity is independent of the ion current or bombardment rate.

4.4.4. Damage at a Depth Less than the Range

Consider next the rate of damage formation at a point x_2 which lies between the original surface and the maximum penetration depth of the bombarding ions. This situation is illustrated in figure 9. Inasmuch as the point x_2 lies within the range of the bombarding particles, the damage will begin to accumulate as soon as the bombardment has commenced and will accumulate for a time $t = x_2/IS$, when the surface reaches the point x_2. Thus in this case the damage $D(x_2,t)$ is given by the expression

$$D(x_2,t) = \int_0^t IQ(x)dt = IQ(x)t,\ 0 < t \leq \frac{x_2}{IS}\ .$$

Again, it is meaningless to discuss the damage at the point x_2 after this point has been removed by the erosion process. In this case the damage is always less than the maximum obtainable.

4.4.5. Spatial Distribution of the Radiation Damage

Consider next the distribution of radiation damage below the surface at various times during the bombardment. The damage distributions are illustrated in figures 10 and 11. The

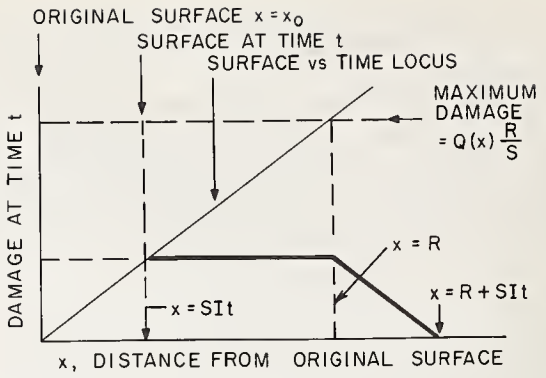

FIGURE 10. *Damage versus depth distribution for a time* $t < R/(IS)$ *after the bombardment has commenced.*

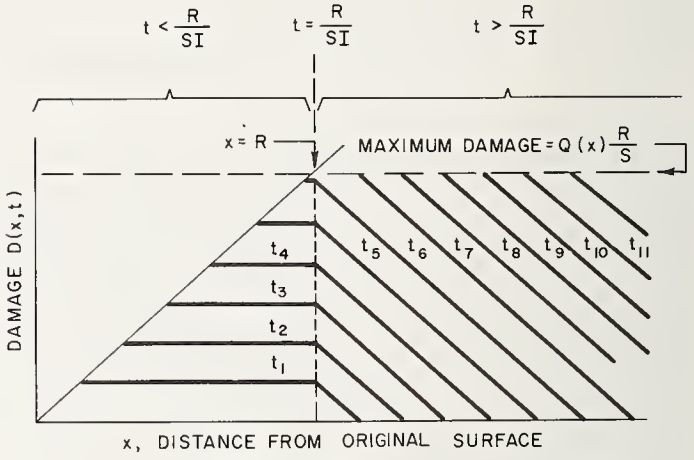

FIGURE 11. *Damage versus depth distributions for a sequence of times* $t_1, t_2, \ldots t_n$ *after the bombardment has commenced.*

line from the origin to the intersection of the maximum defect line and the line parallel to the defect axis at $x = R$ is the locus of the eroding surface during bombardment. The heavy lines, indicating the damage level, were computed from the $D(x,t)$ expressions by inserting the appropriate values of t_1, t_2, etc. These considerations lead to the following important generalizations. First, as stated above, when the material removed by ion-beam erosion reaches a depth equal to the range of the bombarding ions, the radiation damage is a maximum. Secondly, the distribution of damage with respect to the surface of the figured material will remain unaltered by additional figuring. Incidentally, one can readily show that these conclusions are valid for any reasonably smooth $Q(x)$ curve, and more specifically they are valid for the observed $Q(x)$ curve shown in figure 3.

It is important to reiterate that the radiation damage formation kinetics described in this section are subject to at least one important limitation. Namely, it was assumed that all annealing effects were negligible. Annealing effects are described in the next subsection and, it will be seen, they can be appreciable.

4.5. Radiation Damage Annealing

4.5.1. Measurement of Ion-Bombardment-Induced Radiation Damage and Annealing

As explained above, very few, if any, measurements of ion-beam bombardment-induced radiation damage have been made which are directly applicable to figuring considerations. Furthermore, very few studies have been made which provide information about the annealing of ion-beam-induced damage that can be applied to figured optics. Specifically, the dimensional stability of an ion-beam-eroded surface has not been thoroughly investigated. Consequently, the discussion on annealing which follows is based entirely on annealing studies made on reactor-irradiated glasses and especially fused silica. In fact, this treatment can be regarded as an extrapolation of information on the annealing of reactor-radiation-induced damage to the ion-beam bombardment case.

4.5.2. Annealing of Reactor-Induced Damage in Fused Silica

Studies on the annealing of the reactor-induced radiation damage in fused silica will be described very briefly since most of this material has been described elsewhere [7,9]. During reactor bombardment both oxygen and silicon atoms are ejected from their normal lattice positions and both vacancies and interstitials are formed. In this respect, ion-beam-induced and reactor-induced radiation damage are very similar. Part of the oxygen vacancies which are produced during the original bombardment will, at the same time, be converted into color centers by trapping electrons. The remaining oxygen vacancies can be converted into color centers by exposing the sample to a source of purely ionizing radiation at a later time. Thus, the concentration of oxygen vacancies can be determined by making optical absorption measurements on these color centers.

If, after a sample has been irradiated, it is heated at a temperature above the irradiation temperature some or all of the color centers will disappear. The reduction in color-center concentration is attributable to two factors. First, some of the oxygen vacancies are "annealed out" by capturing peregrinating oxygen atoms. Clearly for each vacancy destroyed in this manner one color center will be destroyed. However, consider the following complication. At certain temperatures the heat treatment will cause thermal untrapping of electrons from vacancies. In this case the vacancies remain in the material but they do not contribute to the color-center absorption. However, the remaining vacancies can be reconverted to color centers by exposing the sample to ionizing radiation after each heat treatment. Usually this conversion would be carried out at room temperature.

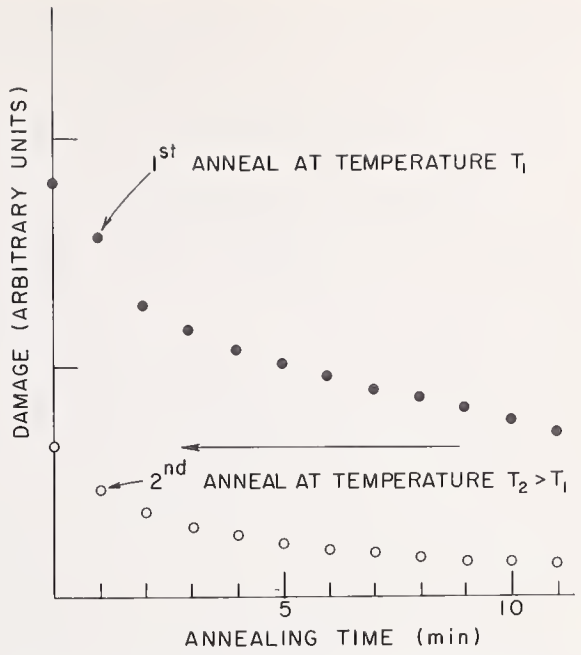

FIGURE 12. *Typical damage versus annealing time data for two different temperatures.*

A typical and somewhat idealized radiation damage annealing measurement is illustrated in figure 12. This might apply to the following sequence. The sample is irradiated in a reactor at 70°C. Subsequently at room temperature it is exposed to ionizing radiation and the oxygen vacancy concentration determined from optical absorption measurements. Next, the sample is annealed at temperature T_1, greater than 70°C, returned to room temperature, exposed to ion-

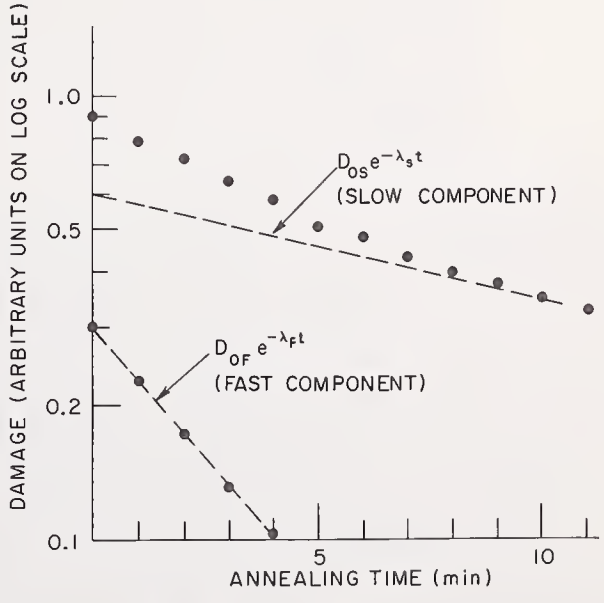

FIGURE 13. *The damage versus annealing time data, shown in the previous figure, plotted on a semilog paper.* This illustrates that the annealing occurring at a fixed temperature can be approximated by two decreasing exponential functions representing a fast and a slow annealing component.

izing radiation. and the optical absorption measured again. Thus the radiation damage or, more specifically, the oxygen vacancy concentration has been determined after irradiation and after the initial anneal. These damage measurements correspond to the uppermost two points in figure 12. The remaining points on this curve are obtained by repeated anneals at temperature T_1. Next, the annealing temperature is raised to a value T_2 greater than T_1 and repeated anneals carried out at the higher temperature. In this way the lower curve in figure 12 is obtained. These annealing curves can be approximated by decaying exponential expressions. Thus when the data points on figure 12 are replotted on semilog paper, it is seen that each of the curves can be divided into two components. This is illustrated in figure 13. Obviously it is appropriate to refer to these as the "fast" and "slow" components. In other words, the radiation damage annealing occurring at temperature T_1 can be approximated by the following expression:

$D(t)$ = (Initial Damage) — (Fast Component) — (Slow Component)

or $D(t) = D_0 - D_{of}e^{-\lambda_f t} - D_{os}e^{-\lambda_s t}$

where

$D(t)$ = damage remaining after total annealing time t.

D_o = initial damage concentration.

D_{of} = that part of the damage which anneals rapidly at a given annealing temperature.

λ_f = fast annealing component decay constant.

D_{os} = that part of the damage which anneals slowly at a given annealing temperature.

λ_s = slow annealing component decay constant.

This separation into components can be demonstrated analytically if it is assumed that the activation energy for annealing is not constant but can be expressed as a temperature-dependent function. This demonstration is too long to present here. In addition, it should be mentioned that radiation damage annealing studies employing both chemical and physical measurements provide empirical evidence for the existence of fast and slow components.

An additional useful annealing characteristic can be described with the aid of figure 13. Both the magnitude and the slope of the fast-decaying component of the T_2 curve increases as the temperature difference $T_2 - T_1$ becomes larger. The intensity of the slow T_2 component also decreases; however, its slope changes very slightly.

The results of a careful study of the annealing of reactor-induced radiation damage in fused silica are shown in figure 14 [7, 9]. When this material is irradiated in a reactor or with sufficiently high energy gamma rays, the absorption band, i.e., the color center, at 5.82 eV increases as the dose increases. Additional studies employing optical and ESR techniques provide evidence indicating that this band should be attributed to an electron trapped on an oxygen atom vacancy [10]. It is a good example of the type of defect described above which can be observed when it has trapped a charge but cannot be detected when it is uncharged. Furthermore, since it is associated with a fundamental defect, namely a vacancy, it should be a good "indicator" of the extent of the damage in fused silica. The data in figure 14 were obtained by repeating the procedure described above until all of the radiation-induced change in absorption had been "annealed out."

Several useful comments can be made about the results in figure 14. First, note that all the radiation-induced defects are removed by heating slightly above 700°C. This provides illustrative material for a point made previously. Namely, this particular set of data may not be a true indicator for all of the radiation damage which could be present in this sample. For example, it is known that fused silica contains radiation-induced absorption bands in the vacuum ultraviolet. These were not studied during these measurements and could possibly be attributed to still other radiation-induced defects. Thus, if the sample had to be heated above 700°C to remove all of the vacuum ultraviolet bands, one would have to conclude that they were better radiation damage indicators. Second, note that the damage decreases slowly from the irradiation temperature to approxi-

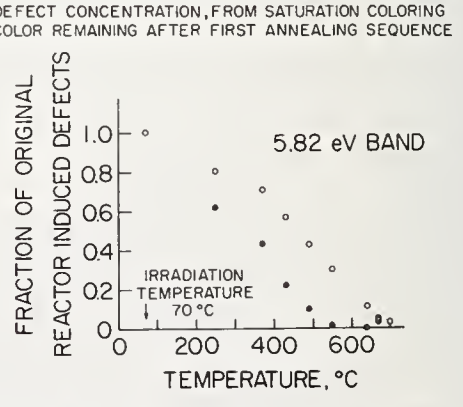

FIGURE 14. *The annealing of reactor-radiation-induced defects in fused silica. The defects removed by each increase in annealing temperature corresponds to the fast component described in the previous figure.* The 5.82 eV band has been attributed to a color center formed when an electron is captured by an oxygen vacancy.

mately 700°C. Thus, to remove all of the damage it is necessary to heat the piece above this temperature. However, it is entirely possible that a reliable optic can be achieved by annealing at a considerably lower temperature. Third, note that all of the coloring is removed by heating at 550°C but approximately 1/3 of the radiation-induced defects remain at this temperature. Thus, in this case the removal of the radiation-induced browning does not indicate that the sample is free of defects. It does show that the coloring can be eliminated at a temperature considerably below the defect annealing temperature.

4.5.3. Figuring Conditions for Minimizing Radiation Damage

Some practical conclusions about the figuring conditions that will produce optics containing a minimum amount of radiation damage result from the considerations given above.

First, it is apparent that the damage will be minimized if, during bombardment, the temperature of the working piece is allowed to become as high as possible. To attain a high temperature one would maximize the beam current and adjust the impact area size to attain the maximum desirable temperature for as long as possible. Also, the beam should be moved across the working pieces as slowly as possible. From the damage removal viewpoint, it is clearly better to make a few passes at high current density than many passes at low current density.

Second, consider the situation requiring that a large amount of material must be removed from a few areas and very little or none at all from other areas. After the required material has been removed from a given area the radiation damage immediately below the surface will be a maximum. In contrast, other areas which have been eroded very little or not at all will contain little or no damage. Thus, in the worst possible case, this non-uniform distribution of damage may be conducive to subsequent surface distortion. This situation might be alleviated by covering the entire surface with a uniform damage distribution. This could be achieved by first figuring the surface to the desired configuration and then removing a layer one range thick from the entire surface. Alternatively, it might be possible to remove most of the required material at high-beam energy and then, as the actual surface approaches the desired configuration, reduce the beam energy so that the damaged layer becomes very thin or approaches zero.

Third, it is entirely possible that radiation damage introduced during the figuring process could be removed by subsequently heat-treating the entire piece. This approach might be useful for removing the radiation-induced coloring. Often this can be removed by heating to a relatively low temperature.

4.6. Future Radiation Damage Studies

As indicated in the introduction to this section, there is very little, if any, reliable information on radiation damage effects in figured optics. In particular there is very little information on the annealing of damage. Obviously, if the figuring process produces a negligible amount of damage it will be unnecessary to study the annealing characteristics in detail. However, before ion-beam figuring can become an accepted technique it must be demonstrated that the figured optic possesses long-term dimensional stability. Furthermore, it must be demonstrated that ion-beam erosion does not produce any unanticipated effects. To give just one example in this latter category, consider the possibility that the eroded surface is considerably more susceptible to chemical attack than the normal surface.

These few comments on future work have been included to make it explicitly clear that additional research on ion-beam erosion is required before one can regard this as a practical technique for figuring optics.

5. Applications of Ion-Beam Figuring

It is appropriate to conclude this paper with a very brief discussion on applications of ion-beam figuring. To begin, inasmuch as it is possible to follow the progress of the figuring during ion-beam erosion, this immediately suggests several unique applications. First, this would appear to be a particularly promising alternative to "hand finishing" or for "touching up" optics which had been shaped close to their final configurations by conventional polishing techniques. Second, it can be used to produce aspherical or nonspherical surfaces from spherical surfaces if the amount of material to be removed is not too great. Figure 15, which was published previously [11], is a paraboloid formed by ion-beam erosion from a spherical surface which had previously been prepared by conventional polishing. Third are optics containing non-axially symmetric configurations. For example, figure 16 shows grooves cut into an originally flat surface. Actually. this picture was obtained as part of a series of erosion rate measurements [3] ; however, it clearly illustrates non-symmetric figuring. A large number of interesting possibilities become apparent when partial or complete on-line computer control is combined with the ion-beam figuring process. In principle, it would appear that this arrangement makes it possible to obtain almost any non-spherical and non-axially symmetric surface configuration. In fact, it

FIGURE 15. *The fringe pattern, observed with an interferometer, from a paraboloid produced by ion-beam figuring.* From Ref. [11].

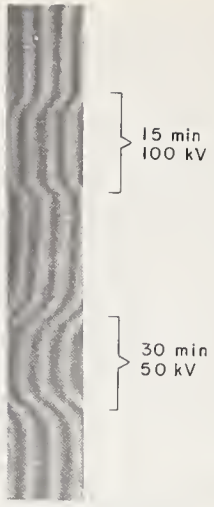

FIGURE 16. *The fringe pattern, observed with an interferometer, from BK–7 glass after it had been subjected to ion-beam erosion using different bombardment conditions.*

would appear to be particularly well suited for the production of Schmidt plates and similarly shaped pieces. Finally, one "far out" application must be mentioned. Ion-beam figuring would appear to be a particularly good technique for correcting astronomical reflectors on satellites or on the surface of the moon.

6. References

[1] Carter, G., and Colligon, J. S. Ion Bombardment of Solids (Heinemann, London, 1968).

[2] Proceedings of an international conference on atomic collisions and penetration studies with energetic (keV) ion beams, Can. J. Phys. 46, 449 (1968).

[3] Ion beam optical figuring. Kollsman Instrument Corp. Tech. Rpt., Contract No. F33615–68–C–1146 (1968).

[4] Meinel, A. B., Bashkin, S., and Loomis, D. A. Controlled figuring of optical surfaces by energetic ionic beams, App. Optics 4, 1674 (1965).

[5] Schroeder, J. B., Bashkin, S., and Nestor, J. F. Ionic polishing of optical surfaces, App. Optics 5, 1031 (1966).

[6] Primak, W., and Bohmann, M. Radiation Damage In Ceramics, Progress in Ceramic Science, Vol. 2, p. 104, Ed. J. E. Burke (Pergamon, London, 1962).

[7] Levy, P.W., Physical properties of irradiated ceramic materials, nuclear science and technology for ceramists, Nat. Bur. Stand. (U.S.), Misc. Publ. 285, 21 pages (1967).

[8] Hines, R. L., and Arndt, R. Radiation effects of bombardment of quartz and vitreous silica by 7.5–keV to 59–keV positive ions, Phys. Rev. 119, 623 (1960).

[9] Levy, P.W., Use of color centers for detection and measurement of defects, the chemical and physical effects of high-energy radiation on inorganic substances, p. 3 (Amer. Soc. for Testing and Materials, Philadelphia, 1964).

[10] Lell, E., Kreidl, N. J., and Hensler, J. R. Radiation effects in quartz, silica, and glasses, Progress in Ceramic Science, Vol. 4, p. 1, Ed. J. E. Burke (Pergamon, London, 1966).

[11] Narodny, L., and Tarasevich, M., Parabolid figured by ion bombardment, App. Optics 6, 2010 (1967).

Discussion

WIEDERHORN: As a practical consideration, what rate of thinning do you get on material such as alumina, glass, etc.?

LEVY: 100 angstroms per minute is quite feasable.

GIELISSE: You stressed the point that the expression for the maximum concentration of defects contains neither the time or ion beam current. Does not the range which does occur in the expression, depend upon the level of ion beam current?

LEVY: No, the range depends only on the energy, not on the current density.

K. SMITH: This application, doesn't it pro-

duce strain on the surface due to the differential of the temperature?

LEVY: Yes, it does. In fact, the principal practical problem that seems to occur is the distortion of the surface during bombardment due to thermal effects.

K. SMITH: Does that have a weakening effect on whatever you are trying to make?

LEVY: I doubt it. I can visualize certain materials which seem to be somewhat more susceptible to crazing and things like that. But any material can be bombarded at a rate high enough to melt the surface.

HEUER: We have used a similar technique to make electron microscope foils. By taking stereo pairs, the radiation damage can be seen as very small defects and they are indeed confined to the top and bottom of the foil and not anywhere in the interior bulk.

NATIONAL BUREAU OF STANDARDS SPECIAL PUB. 348, THE SCIENCE OF CERAMIC MACHINING AND SURFACE FINISHING, Proceedings of a Symposium Sponsored by the American Ceramic Society, the Office of Naval Research, and the National Bureau of Standards, held at NBS Nov. 2–4, 1970, Gaithersburg, Md. (Issued May 1972).

The Effect of Sputtering on Surface Topography and Strength of Ceramics

R. W. Rice

Chemistry Division, Naval Research Laboratory
Washington, D.C. 20390

The topography developed as a result of R.F. sputtering on a variety of ceramic surfaces is described showing that surface cracks, scratches, pits, etc., are fairly rapidly rounded out. Generally, this occurs without differential grain boundary sputtering. However, some bodies develop a rough finish due to nonuniform microstructural removal. Limited trials with ion beam sputtering show it also rounds cracks, etc., but does not develop a rough finish on bodies that will with R.F. sputtering.

Because of the rounding of stress concentrating features and generally similar effects on single and polycrystalline bodies, sputtering was investigated as a substitute for flame polishing, but with much wider applicability. Flame polished strengths were not obtained. However, some materials (e.g., $MgAl_2O_4$) do show greater improvements in strengths than others (e.g., Al_2O_4) as a result of sputtering. These differences will be discussed and results compared with other methods of surface finish.

Both the detailed nature of the sputtered surface as well as enhancement of grain boundaries and other microstructural features under certain conditions indicate that sputtering may also be useful as an etching technique.

Key words: Carbides; glass, ion beam sputtering; nitrides; oxides; RF sputtering; strength; surface finish; twins.

1. Introduction

Obtaining nearly perfect surfaces by flame polishing or chemical polishing is very valuable in the study of mechanical properties of ceramics. However, the applicability of these techniques is limited. High melting points, or reactivity, prevent flame polishing of many materials. On the other hand, the large, often columnar, grains that result from melting the surface of polycrystalline bodies generally preclude the use of flame polishing polycrystalline bodies (e.g., Al_2O_3) which can be flame polished in single crystal form. Further, flame polishing generally works well only for round rods. Techniques of chemical or electropolishing (of conductive ceramics) for producing good surfaces are known for only a few materials. Preferential attacks on certain crystal surfaces and at grain boundaries also limit the application of these.

Etching to reveal grain boundaries subboundaries, dislocations, and twins in ceramics is also important in studying their mechanical behavior. While chemical etches have been developed so that a substantial number of ceramics can be suitably etched, improvements are still needed.

Sputtering [1] which is the process of removing material from a surface by bombardment of the surface with ions, appeared to be a way to obtain near perfect surfaces on many ceramics. The achievement of such surfaces was suggested by both the fact that (a) removal is normally atom-by-atom, and (b) sputtering has been very successful in thinning a wide variety of ceramic materials for electron microscopy [6, 7] which require specimens of such thinness that little variation in thickness can be tolerated. It was also felt that etching, which tends to be contrary to obtaining near perfect surfaces, might be obtained by varying sputtering conditions (e.g., bombarding ion energy), especially on certain materials (e.g., those with two phases). A search of the literature indicated other examples of obtaining good surfaces [1, 7–9] and some examples of etching [1, 7, 8, 10–12] by sputtering. However, these past studies have generally not studied the effect of prior surface finish on the resulting sputtered topography, and none have considered what effect sputtering has on mechanical properties. The latter is important not only because sputtering may affect surface sensitive strengths, but also because sputtering is being considered as a means of machining and finishing ceramics [14–16].

This paper presents results of a study of sputtering of ceramics. The initial emphasis was on determining whether or not strengths achieved by flame or chemical polishing could be achieved by sputtering. When it was found that such high strengths were generally not obtained, the emphasis was on determining what strength changes did result from sputtering. This has also resulted in considerable information on the type of topography developed. While it has not been possible to study etching in detail, some examples of it are also reported.

[1] Several reviews of the sputtering process are available. Some of these are tabulated in references [1–5]. (Figures in brackets indicate literature references at the end of this paper.)

TABLE 1. *Materials studied* [1]

ZrO_2, unstabilized crystals	Skull melting		W. & C. Spicer Ltd. St. Marys Winchcomb Glouchestershire England
ZrO_2, CaO stabilized (9 W/O) crystals			
ZrO_2, Y_2O_3 stabilized (14.5 W/O) crystals			
ZrO_2, Partially stablized (2.9% CaO)	Sintered	Zircoa C	Zircoa Corporation Solon, Ohio
ZrO_2, MgO stablized	Sintered	Zircoa 1027	

[1] Other materials studied have been listed in table 1 of ref. [17].

2. Experimental Technique

2.1. Specimen Preparation

A variety of samples were used as listed in table 1 and reference [17]. Grinding, gas polishing, and flame polishing of specimens were as discussed elsewhere [17–19]. Mechanical polishing was done by standard methods.

2.2. Sputtering

Samples were sputtered by both radio frequency (RF) and Ion Beam (IB) sputtering [2]. RF sputtering uses ions generated in a glow discharge which are accelerated to the sample (target) by the potential difference between the target electrodes. The simplest type of arrangement and the one used here is sketched in figure 1; however, several other variations exist [2–5]. RF rather than dc potentials, are used to prevent possible charge buildup on nonconducting samples. Since glow discharges depend on the pressure, voltage, and electrode separation, the variation of ion energies is limited. Also, ion incident on the target is essentially normal. IB sputtering uses an ion gun to generate and accelerate ions (fig. 1). Since the latter is completely independent of the target, the ion energies and angle of incidence are quite variable. Specimens are usually rotated to maintain uniformity. Although charge buildup is generally not a problem with IB sputtering despite its dc nature, there are techniques of neutralizing the beam, if necessary.

RF sputtering [3] was done with a commercial unit (manufactured by Materials Research Corporation, Orangeburg, N.Y.), using electrodes approximately 5 cm in diameter (2 in).

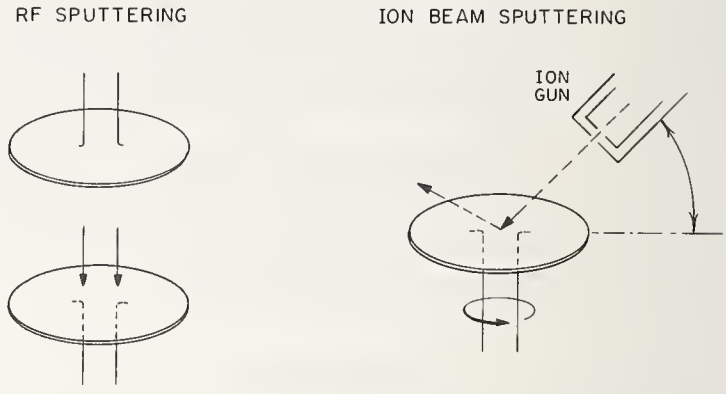

FIGURE 1. *Schematic representation of RF and ion beam sputtering.*

Chamber pressures were typically a few μm, with potential differences of about 2500–3000V (at 13.56 MHz). Because considerable heating (e.g., to of the order of 1000°C) could occur with some specimens, especially at power levels of 0.4–0.5 KW, most sputtering was at 0.1–0.3 KW. Sputtering times were normally about 50 hours in steps of 2 to 6 hrs.

Because the specimen holder is mounted in an inverted position, it was necessary to hold the specimens to the holder. This was done with wires, as shown in figure 2.

IB [4] sputtering was done with a commercial unit (manufactured by ALBA, Paris, France) normally used for thinning specimens for electron microscopy. The unneutralized argon beam was typically accelerated at 6 kV and struck the specimen holder at an angle of 15–20 from the horizontal (the thickness of specimens and the specimen holder-ion gun geometry did not allow lower angles of incidence.). The aluminum or stainless steel specimen holders were rotated at about 15 rpm. In order to avoid possible loss of specimens due to rotation, specimens were held down by wires near each end. Five specimens were mounted, separated by 1–3 mm, on the approximately 3 cm diameter holder. Because of the beam diameter, sputtering was greatest in the central half of the holder. Sputtering times were typically 50–80

[2] It should be noted that sputtering here refers to the removal of surface material from a bulk specimen, not the deposition of the removed material. Sputtering has come into wide usage, especially in electronics, as a technique whereby the atoms removed from one surface are deposited on another surface similar to vacuum deposition. Such sputter deposition is not concerned with the surface left on the material from which the atoms are removed (the "target"). Confusion sometimes results, since sputter deposition is often referred to only as sputtering and the removal (sputtering) process as sputter etching which should not be confused with grain boundary, etc., etching discussed in the introduction.

[3] RF sputtering was done by Drs. G. Sigel and W. Anderson of the Solid State Division of the U.S. Naval Research Laboratory.

[4] IB sputtering was done by Dr. B. Hockey of the Institute for Materials Research, National Bureau of Standards.

FIGURE 2. *RF sputtering holder.* Note ceramic bars held in place by wires.

hours. A few preliminary 2-hour trials were also made with a neutralized beam unit [5].

In order to sputter as many specimens as possible, and to avoid possible differential sputtering on different surfaces of round single crystals, flat bars were used. Initially these were about 2.5 × 5 mm in cross section, but most specimens were about 1.8 × 3.8 mm. The bar edges were rounded in order to obtain some sputtering of the edges.

2.3. Specimen Evaluation

Surfaces were examined by optical and replica electron microscopy. It should be noted that most optical photos were made using Nomarski interference contrast to emphasize surface topography, and hence should not be taken as representative indication of the roughness of the surface.

Ambient mechanical strengths were measured in three-point bending using an Instron test machine with a head travel speed of 0.127 mm/min. Most specimens were tested on a span 1.27 cm and a few were tested on a span of 0.89 cm.

3. Experimental Results

3.1. RF Sputtering Topography of Single Crystals

RF sputtering of single crystals of oxide ceramics generally developed a topography best described as a series of shallow rounded depressions. The depth of these averaged about 1 μm, but the number, size and extent of these depended primarily on the prior surface finish. Thus, for example, they completely covered the surface of ground specimens as shown in figures 3 and 4, with a remnant pattern of grinding stria generally being retained (fig. 3). Progressively finer mechanical finishing prior to sputtering reduced the density of these depressions. Even with a relatively poor polish, most of the depressions are separated as shown in figure 5. This figure also shows that each pit left in the mechanically finished surfaces becomes a rounded depression on sputtering, and that considerable rounding occurs within two hours of sputtering. Electron micrographs (fig. 6) show more clearly the extent of rounding features with extended sputtering. While some smaller depressions normally occur inside of larger ones during sputtering, this became particularly pronounced (fig. 7) when significant specimen heating occurred.

This development of depressions is generally true for various orientations of Al_2O_3, spinel (Al_2O_3–rich), zirconia (CaO or Y_2O_3 stabilized), TiO_2, and MgO crystals. Electron microscopy showed that a variety of precipitates were re-

FIGURE 3. *RF sputtering of ground surfaces.* Ruby ground in vertical direction. Note remnants of grinding streaks. Note also the apparent imperfection revealed by sputtering (approximately rectangular object near top of photo).

[5] Tests run by Dr. H. Garvin of Hughes Research Laboratory, Malibu, Calif.

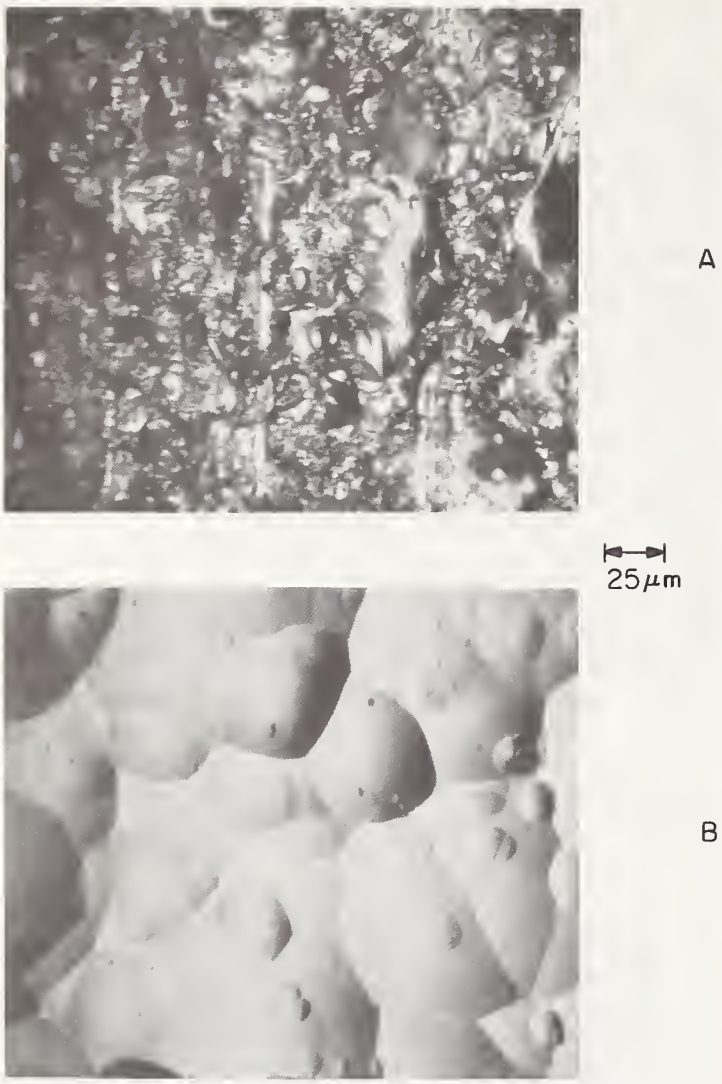

FIGURE 4. *RF sputtering of ground spinel crystal.* (A) as diamond ground (grinding direction vertical) (B) similar area of same specimen sputtered approximately 54 hours.

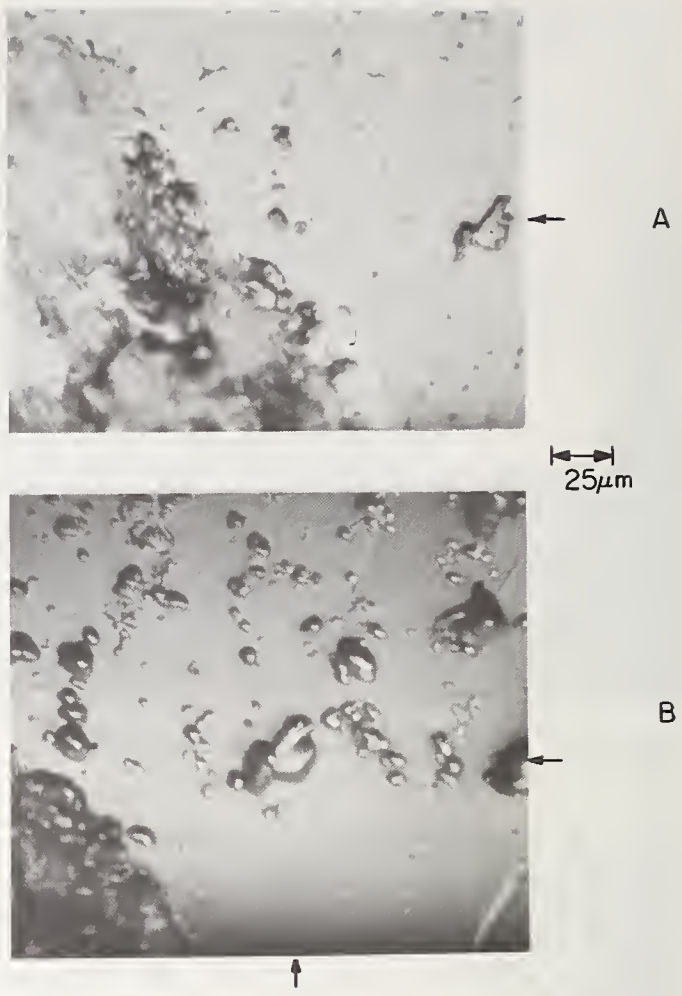

FIGURE 5. *RF sputtering of ruby.* (A) Specimen as polished with 1 micron diamond paste. (B) Most of the same area sputtered 2 hours. Note correspondence of pits and their rounding with sputtering (portion of scribe mark and arrows to same largest pit index photos).

vealed in the stabilized ZrO_2 crystals by sputtering, corroborating optical indications of their presence. Unstabilized ZrO_2 crystals tended to develop a pattern that was apparently modified by differential surface energies giving a partially faceted appearance. Some TiO_2 crystals, and to a lesser extent MgO, also tended to do this some. Figure 8 shows that sputtering did occur part way down the sides of the beveled bars. While the Nomarski contrast exaggerates the edge irregularity, many sections of the edges were somewhat irregular. Particles of debris, apparently accumulated from material removed from the surface, were often found in the grooves formed between specimens by their beveled edges. Some of this appeared to be bonded to the specimen.

Flame polished sapphire generally did not develop depressions until after several hours of sputtering. Some depressions did develop fairly early in areas where the flow of a wave of melt had been interrupted [19] and similar areas of expected stress concentrations. When more depressions began to occur with continued sputtering, it was most commonly as clusters in such areas where densities of 10^{6}–10^{7} per sq. cm. were reached in contrast to 10^{4}–10^{5} away from the areas. Gas polished specimens [18] developed, even fewer depressions, and they were generally random, not occurring in clusters.

Besides rapid rounding out of damage from scribing Al_2O_3 and $MgAl_2O_4$, some features were often found associated with the scribe marks. As shown in figure 9, features which appear to be twins emanate from the tips of many lateral cracks along scribe marks. Though these twins could be seen by careful examination prior to sputtering, limited sputtering (e.g., 2 hrs) appeared to bring them out more clearly. Some could also be seen along a few deeper grinding marks where surrounding areas were clear enough to distinguish them. These were typically 20 μm long and varied from 2 to 10μm apart. Some unusual features also developed around some of the larger lateral

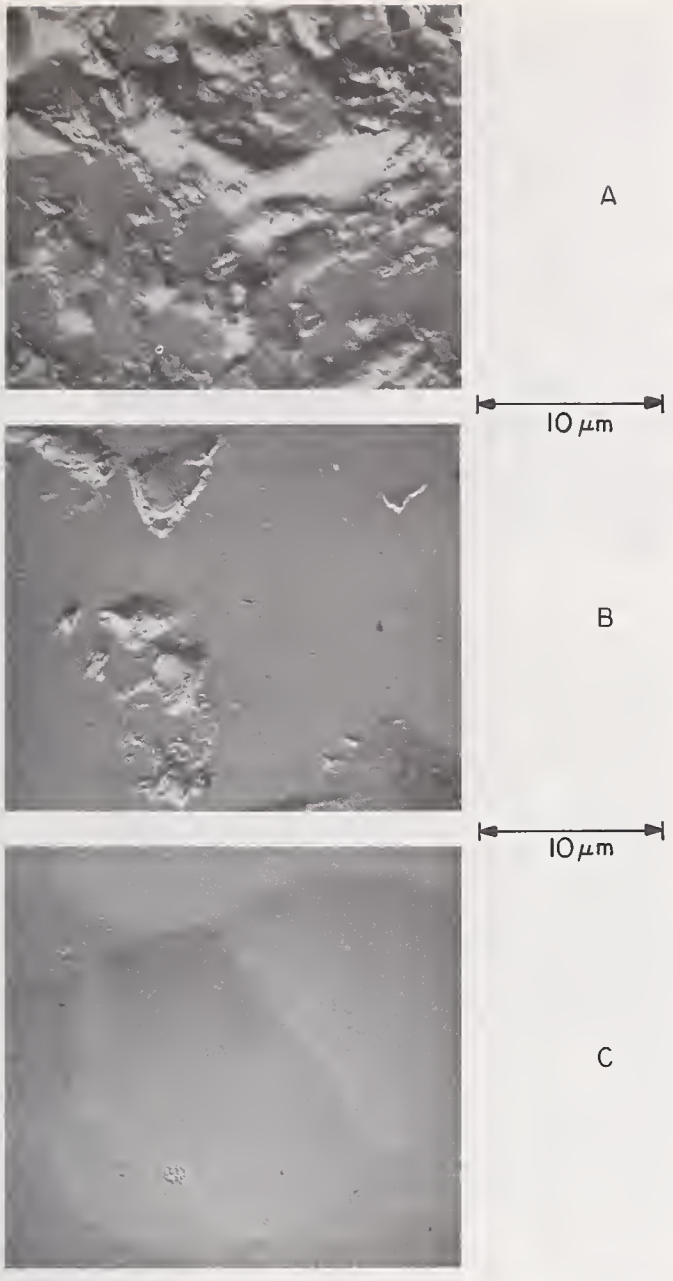

FIGURE 6. *Electron micrographs of crystal surfaces.* (A) As ground. (B) Polished (3 micron B_4C). (C) Sputtered surface subsequent to polishing.

cracks as shown in Fig. 10A. Figure 10B shows that lateral cracks emanating from scribe marks on $MgAl_2O_4$ often ended in a depression, indicating that limited sputtering was "etching" preferentially at or near the tips of these cracks.

A variety of sporatic features was observed that appear to be due to impurities and defects in the crystals. A few more regular objects such as the rectangular feature near the top of figure 3 were observed. These are believed to be voids. A variety of circular to very irregular and very sharp to very diffuse objects were observed that are believed due to impurities.

3.2. RF Sputtered Topography of Glass

Sputtering of soda lime glass generally developed shallow crescent-shaped depressions,

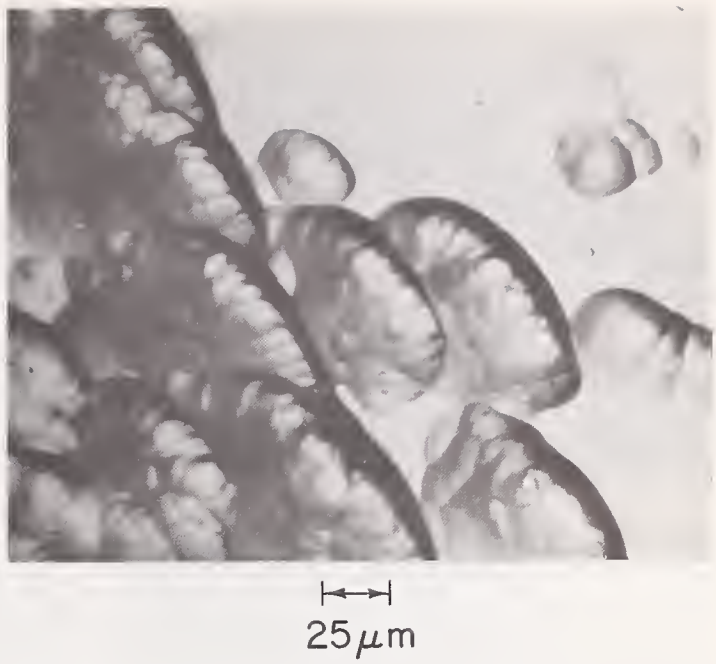

FIGURE 7. *Typical lengthening of major depressions and development of many smaller depressions within larger ones in RF sputtered samples that got hot during sputtering.* This suggests that depressions may be due to dislocations, which move or multiply due to heating.

FIGURE 8. *RF sputtering of specimen edge.* Top of photograph is looking down the edge of an Al_2O_3 rich $MgAl_2O_4$ crystal specimen. The edge was rounded prior to polishing, then the specimen was sputtered approximately 54 hours.

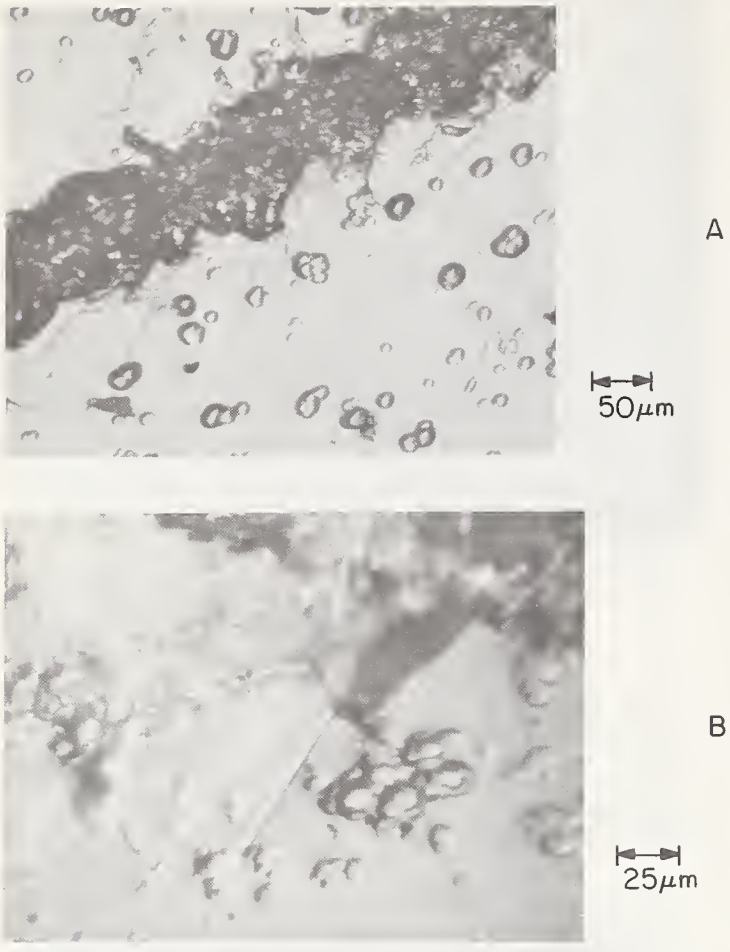

FIGURE 9. *Possible RF sputtering of twins along scribe marks on ruby.* (A) Specimen polished with 1 micron diamond paste, then sputtered—surrounding areas sputtered 5 hours, scribe mark sputtered 2 hours. (B) A similar ruby with background sputtered 5 hours, and scribe mark sputtered 2 hours. Note that apparent twins generally emanate from the tips of lateral concoidal cracks.

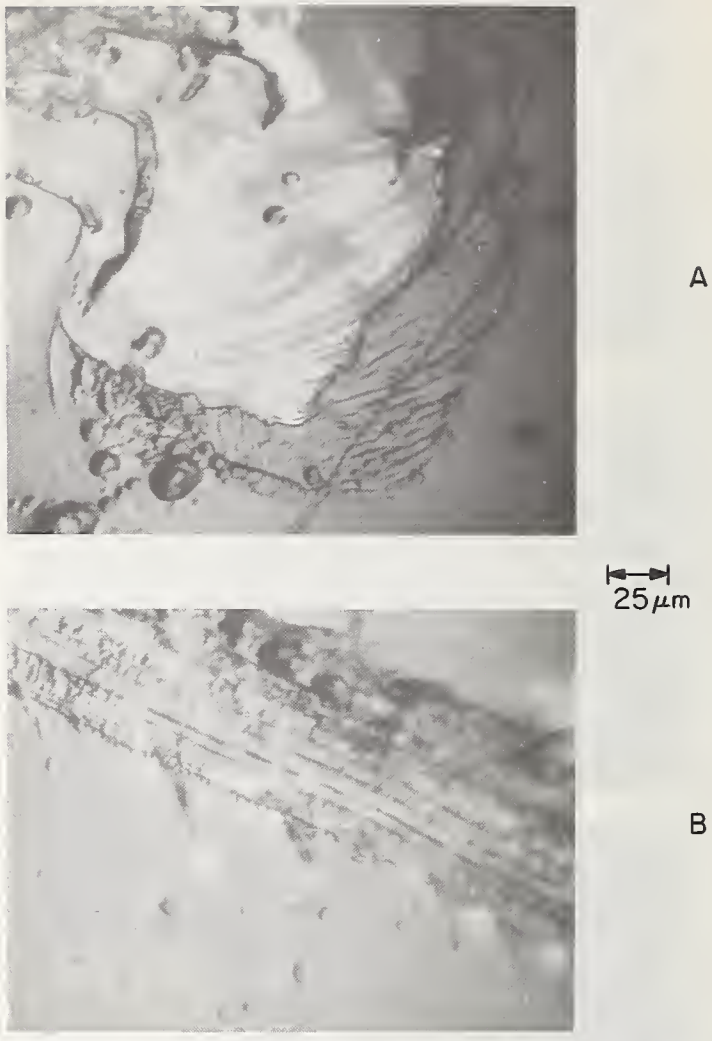

FIGURE 10. *RF sputtering of cracks in ruby and spinel crystals.* (A) Features sometimes developing around tips of large cracks on the side of a scribe mark on ruby. (B) Apparent cracks seen along scribe marks on some Al_2O_3-rich $MgAl_2O_4$ crystal (approx. 3 MgO: 3.5 Al_2O_3). Note there always appears to be a round sputtered depression at or near the tip of these cracks. Background polished and sputtered 5 hours, scribe marks sputtered 2 hours in both cases.

as shown in figure 11. These followed the general trend found for depressions in oxide crystals. That is, their density was clearly increased by abrasion. For example, completely covering a glass section with scratch marks by hand sanding produced a crescent density comparable to the density of depressions on ground crystals. In partially abraded areas, these crescents tended to start from scratch marks and spread out to cover intervening polished areas. All specimens, including previously flame polished ones, tended to develop a craze-type pattern, as shown in figure 12 after several hours of sputtering. Crescents tended to form near these "craze lines" and spread into intervening areas not already covered with them, e.g., on areas of mechanically polished and especially on flame polished specimens.

Small dots, which were apparently hillocks, averaging about 0.2μm in diameter were observed in densities of 10^{4}–10^{5} per cm^{2} over many areas by electron microscopy. Much larger and less dense dark spots, sometimes surrounded by several smaller satellite spots were often seen optically, usually associated with the craze pattern as shown in figure 12B. On specimens sputtered at higher power (0.3–0.5 KW), cracks (fig. 12) were often associated with the craze pattern and these spots, which appear to be pores. Longer sputtering (e.g., after several hours) generally developed a terrace-type topography (fig. 12B).

3.3. RF Sputtering Topography of Polycrystals

In general, polycrystalline specimens developed the same general pattern of depressions, but with two important differences. The first of which is related to grain size. As seen in figure 13, sputtering of dense fine grain (approximately 3 μm) hot pressed Al_2O_3 with a ground surface results in a high density of very fine

FIGURE 11. *RF sputtered soda lime glass.* The specimen was sputtered 2 hrs. before this electromicrograph was made.

depressions (e.g., compare with figs. 2–5). On the other hand, a large grain (approximately 60 μm Lucalox) specimen developed depressions comparable with those on single crystals as shown in figure 14. The decreasing size of depressions with decreasing grain size appears to be due to the fact that pits left from mechanical finishing which are a major source of depressions usually decrease in size with decreasing grain size. The density of depressions on the Lucalox was also quite high due to a high density of pits left from semi-polishing. Subsequent thermal etching (by annealing) of the Al_2O_3 showed that the depressions have no definite association with grains or grain boundaries as shown in figure 14C.

Annealing of dense hot pressed Al_2O_3 bodies prior to sputtering clearly reveals grain boundaries, which are then completely obscured by long sputtering as shown in figure 15. A high density of depressions also develops on such annealed surfaces, but at a much slower rate than on a machined one.

The second difference between single and polycrystals appears to be related to the presence of grain boundaries or varying crystal orientation in certain bodies. Thus, for example, commercial ZrO_2 stabilized with CaO or MgO initially had grain boundaries enhanced as shown in figure 16, but these then became obscured with further sputtering. Figure 16 also shows that previous pits (and voids) in the

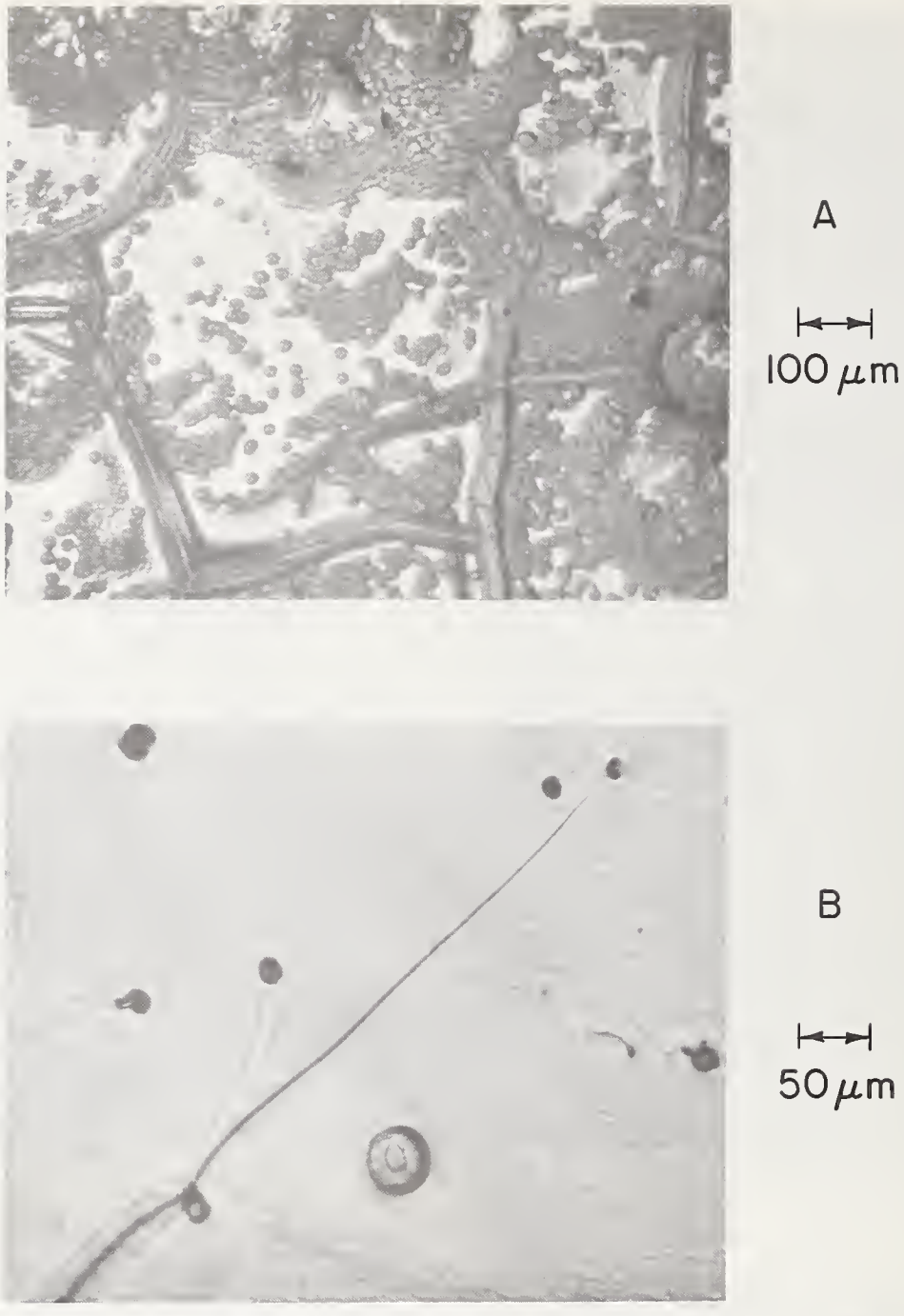

FIGURE 12. *Craze pattern and cracks on RF sputtered soda lime glass.*

specimen result in depressions on sputtering, and that polishing results in fewer depressions as with oxide crystals.

In contrast to this, dense hot pressed MgO specimens, progressively developed a rougher topography. In the most extreme case, this appeared to be due mostly to a very different sputtering rate of grain boundary material (fig. 17A), while in the other case, this appeared to be due partially to differential removal from boundaries and to differential removal from different crystal surfaces. SiC showed a somewhat similar trend (fig. 17B), with a rougher topography forming a network around patches of normally appearing sputtered areas. This network appears to start at the grain boundaries, and widen with increased sputtering. Observations of fracture surfaces normal to the edge of the SiC sputtered surface showed that, while fairly well rounded, the grain boundary areas were lower than the center of the grains.

Trials with a medium grain commercial sintered Al_2O_3 (Alsimag 614), and dense hot pressed $MgAl_2O_4$, Si_3N_4, and B_4C, all indicated that they behaved similar to that of the dense alumina of corresponding grain sizes discussed above. In B_4C, clusters of pores within grains (observed on fracture surfaces) were also revealed by sputtering.

3.4. Ion-Beam Sputtering Topography

Most specimens sputtered with the unneutralized ion beam developed topography very

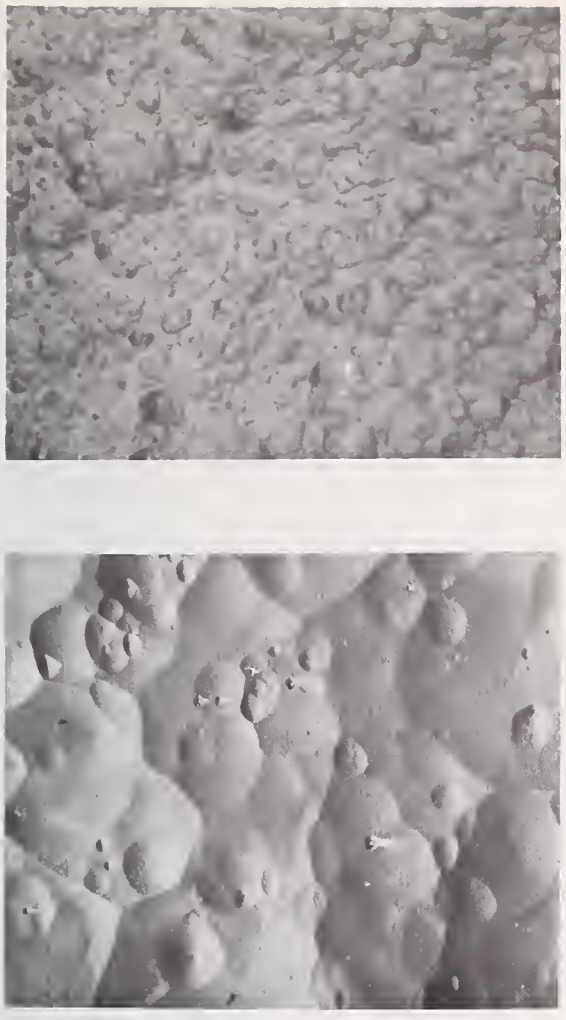

FIGURE 13. *RF sputtering of dense fine grain (3μm) Al_2O_3.* Specimen hot pressed from Linde A powder, then air annealed at 1315 °C, then sputtered approximately 54 hours. (A) Optical photo. (B) Electron micrograph.

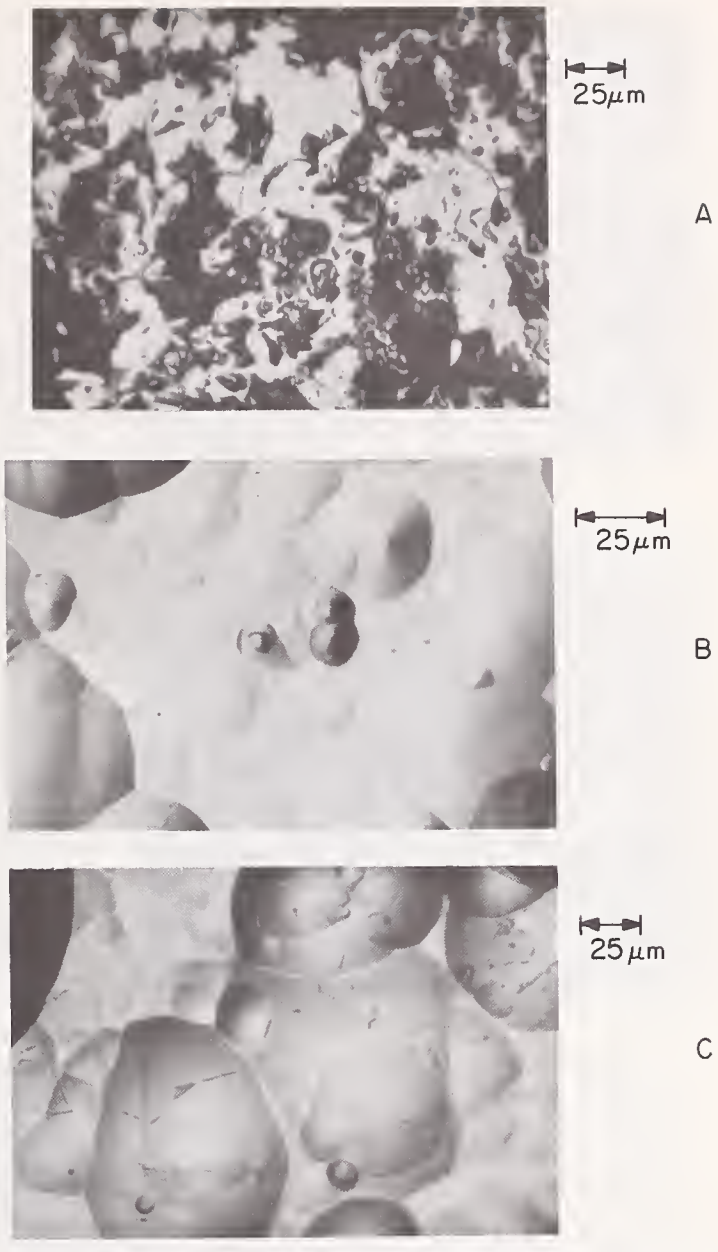

FIGURE 14. *RF sputtering and annealing of Lucalox.* (A) Surface as semi-polished (with Linde C). (B) Similar surface sputtered approximately 30 hours. Note faint lines (especially on right) suggestive of grain boundaries, which are more pronounced in this photo than average. (C) Similar specimen annealed in air one hour at approximately 1300 °C to reveal grain boundaries. This shows that sputtering depressions are not related to grains or grain boundaries.

similar to that obtained with RF sputtering; i.e., a series of depressions rapidly developed. Their density and surface coverage generally decreases with finer finish, and their size generally decreases with decreasing grain size as with RF sputtering. The main difference in these depressions was a tendency for an elongated and apparently shallower nature. Length to width ratios varied from just over one to as high as three to four (figs. 18, 19). As with RF sputtering, remnants of grinding striations remained, and a few grain boundaries were revealed (figs. 18A, 19).

The main differences that were observed between RF and IB sputtering were with glass and polycrystalline MgO and SiC. IB sputtering did not result in the crescents observed in RF sputtering. Instead, the glass developed what appeared to be hillocks very similar to depressions in other materials such as Al_2O_3 and $MgAl_2O_4$. The density and surface coverage of these again decreased with finer finishing. However, as shown in figure 20, rounded trenches were observed between some of the hillocks like features, and the latter generally had several dots on them (fig. 20A). The polycrystalline MgO, which had developed fairly to extremely rough topography in RF sputtering, responded more like other materials in IB sputtering. (There was, however, some preferential grain removal as shown in fig. 21.) Polycrystalline SiC developed a surface topography quite similar to other materials in contrast to RF sputtering.

Sample trials with a neutralized ion beam sputtering device indicated the same general trends in initial 2-hr runs.

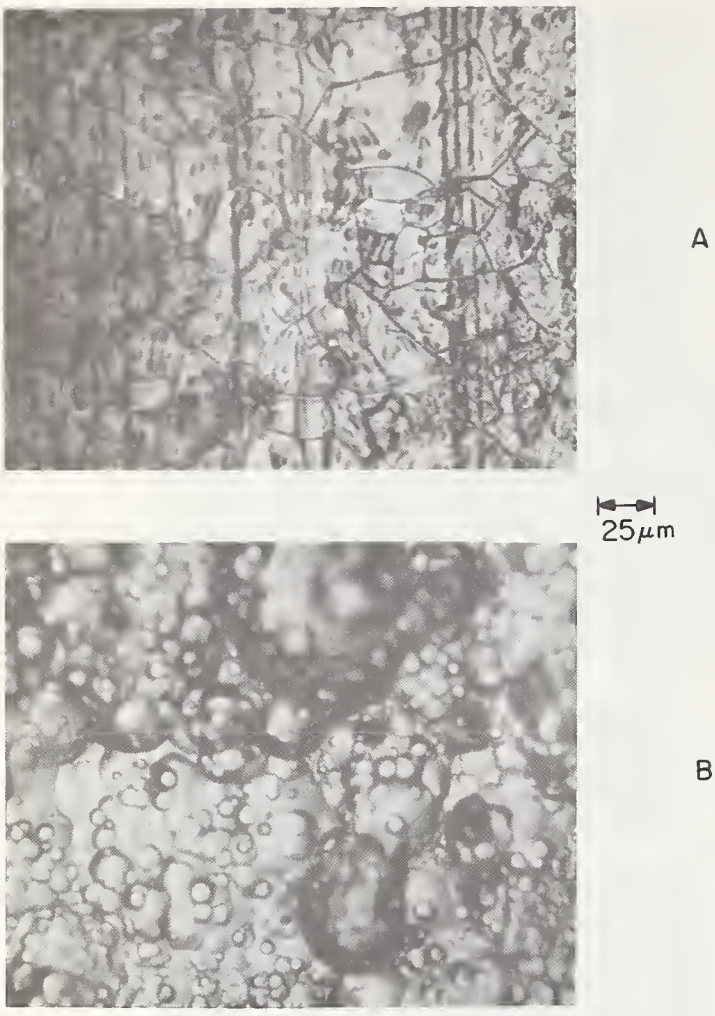

FIGURE 15. *RF sputtering of annealed Al_2O_3.* Linde A Al_2O_3 powder hot pressed to near theoretical density, diamond ground, then annealed in air at 1790 °C. (A) As annealed surface showing rounding of (vertical) grinding marks and thermal etching of grain boundaries. (B) Similar area of same annealed surface after approximately 54 hours of sputtering.

3.5. Sputtering Rate and Behavior

Initial sputtering was done at 0.4–0.5 KW; however, most was done at 0.1–0.3 KW since sample heating was more frequent and excessive at the higher power. This varied from run to run and from sample to sample, apparently due to varying thermal contact with the holder. Some specimens glowed a dull red, indicating temperatures of the order of 1000°C were reached. This glow was clearly not luminescence since it slowly built up during initial sputtering and diminished fairly slowly when sputtering was stopped. Some specimens also luminesced, e.g., MgO crystals gave a light green color, and different spinel specimens gave different degrees of a light green color. During most of the initial runs at higher powers, ZrO_2 specimens turned black in many areas, some of which were on the side and back as well as the front. The depth and distribution of these areas was very consistent with reduction due to excessive heating because of poor and inhomogeneous thermal contact. TiO_2 crystals also darkened substantially during RF sputtering.

While measurements on sputtering rates were not a primary goal, some estimate of these can be made from micrometer measurements (at the ends of bars) before and after sputtering. In RF sputtering, the overall sputtering rates averaged slightly over 1 μm/hr, or about 200Å min. This is in good agreement with literature values for Al_2O_3 which constituted the greatest single portion of the samples. There was a fair amount of variation. For example, glass measurements indicated a rate about twice the average. Also, there was a trend for a higher (e.g., 10–20%) sputtering rate over the outer regions of the sample holder. In general,

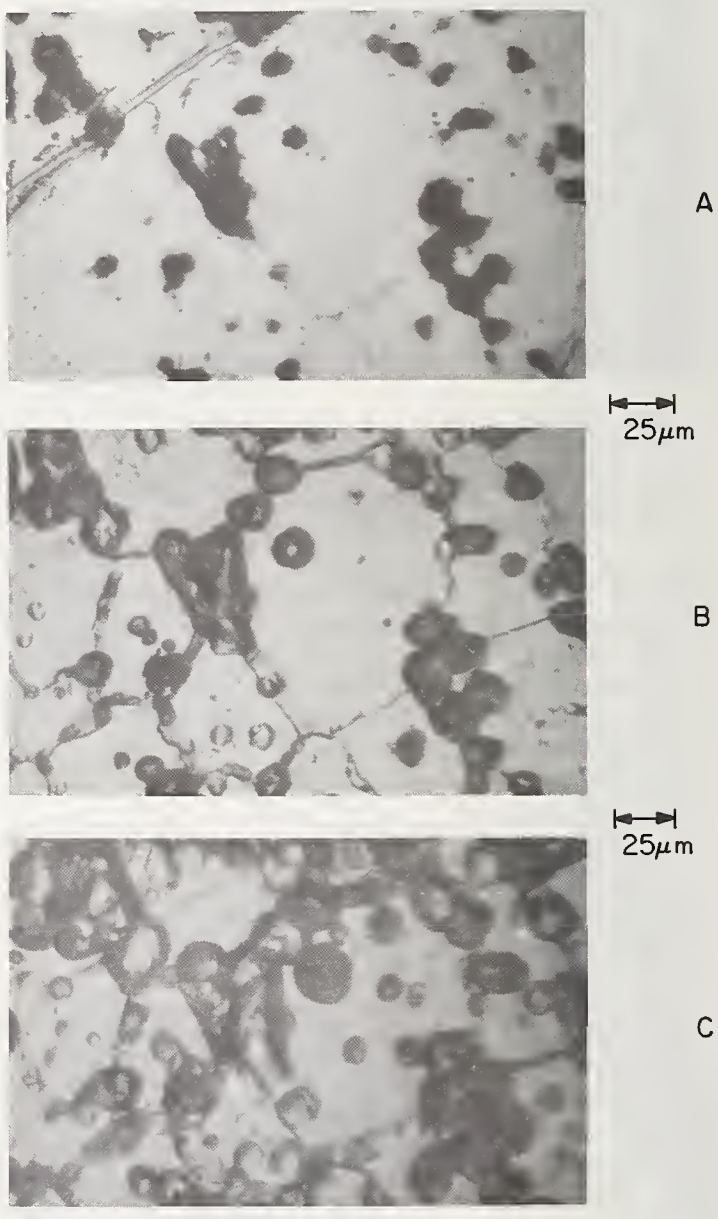

FIGURE 16. *RF sputtering of CaO stabilized ZrO_2 (Zircoa C).* (A) Specimen as polished with 3 micron B_4C. (B) Same area sputtered 2 hours. (C) Same area sputtered 5 hours. Note diamond scribe marker across upper left corner in all photos.

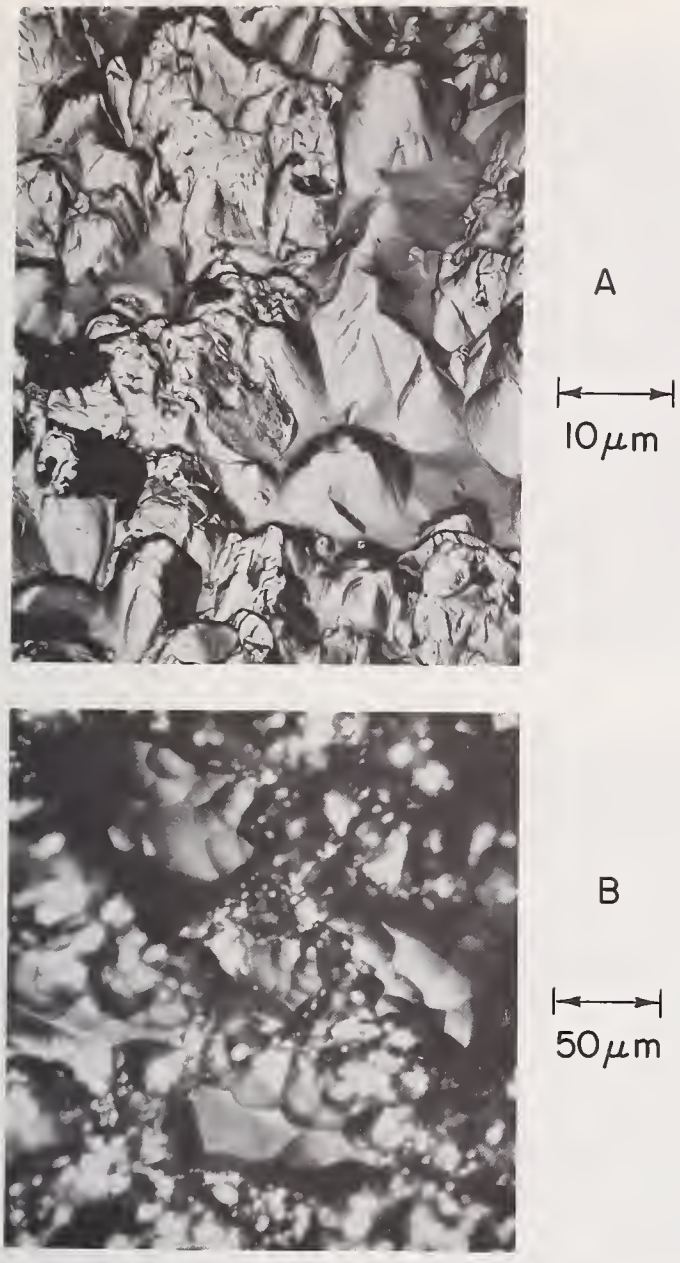

FIGURE 17. *Examples of rough topography on certain RF sputtered polycrystalline samples (A) MgO (B) SiC.*

20 to over 100 μm were removed from samples. Cutting power from 0.4–0.5 KW to 0.2–0.3 KW did not appear to make significant changes in sputtering rates.

Sputtering rates estimated for IB sputtering from measurements on the ends of samples were about a fifth that of RF sputtering, i.e., about 0.2 μm/hr. However, these are definitely low since the amount of sputtering clearly diminished toward the outer edges of the sample holder as would be expected. Differences in sputtered topography between the center and ends of the specimens indicated that the differences in sputtering rate were of the order of two, which would be in approximate agreement with a maximum expected rate of the order of 0.5 μm/hr. Thus actual total removal over much of the sample was estimated at 10–30 μm.

3.6. Strength and Fracture of Sputtered Specimens

The strength tests of RF and IB sputtered glass and oxide crystals are summarized in table 2 along with comparative data for other finishes. These clearly show that, in general, flame polished strengths are not achieved. The levels of strengths achieved are typically about the same as achieved by mechanical polishing. However, this level of strength was generally achieved regardless of prior finish. Thus, for example, samples such as spinel, sapphire, and glass ground perpendicular to the tensile axis were clearly increased in strength. There was also an indication that ground specimens tended to give higher strengths after sputtering than did polished specimens. This is indicated, for example, by the spinel in table 2, and in individual specimens of sapphire and glass.

There are two other possible trends indicated by these tests. First, the limited IB sputtering results indicate that it makes more improvement in strength than does RF sputtering. This is indicated particularly by the averages of ruby and glass, where maximum values achieved by IB sputtering of these materials (with ground surfaces) were about 2 to 3 times the level achieved by mechanical polishing. Second, TiO_2, ZrO_2, and $MgAl_2O_4$ indicate possible increases in strength over mechanically polished levels with either sputtering technique. While the scatter of the ZrO_2 crystal data makes results uncertain, part of this may be due to the fact that specimens from two different crystals of unknown orientation were used. The sputtered specimen from one crystal was twice as strong as the polished specimen. Much smaller differences were observed in the other crystals. The spinel data of table 2 suggests that some crystals were weakened. However, direct comparison of polished and sputtered tests (cut parallel to the boule axis) on the same bar showed the sputtered specimens average 10–20 percent stronger. This is due to the fact that these specimens from that particular boule had lower than average strengths.

Annealing of sputtered rubies in air at 1300°C did not improve strengths. In fact, this may have decreased them some. though the scatter makes this uncertain. Strengths of sapphire that was flame-or gas-polished prior to sputtering averaged over 100,000 psi ($7 \times 10^8 N/m^2$).

Tests were made on several polycrystalline Al_2O_3 and $MgAl_2O_3$ samples, as well as a few polycrystalline ZrO_2, B_4C, SiC, and Si_3N_4 samples. Strengths of a variety of sputtered (IB and RF) Al_2O_3 bodies were clearly not significantly better than achieved by mechanical polishing. Limited trials with commercial ZrO_2 showed the same results. Limited tests with

TABLE 2.

Strength of RF and IB sputtered glass and single crystals (strengths in 1000 psi (and in $10^7 N/M^2$))

Material	Orientation [1]	Specimens prior to sputtering: As-ground surfaces, Parallel	Specimens prior to sputtering: As-ground surfaces, Perpendicular	Specimens prior to sputtering: As-polished surfaces	Specimens after sputtering: RF	No. of tests	Specimens after sputtering: IB	No. of tests
Soda lime glass		14±1 (10)	10±1 (7)	17±3 (12)	14±6 (10)	14	21±8 (14)	6
$MgAl_2O_4$	∥		21±1 (14)		44±12 (30)	7		
$MgAl_2O_4$	∥	34±2 (23)		37±9 (26)	28±8 (19)	5	38±15 (26)	4
$MgAl_2O_4$	⊥	34±5 (23)	20±1 (14)	39±11 (27)	46±6 (32)	11	40±4 (28)	3
Sapphire	∥	48±9 (33)	25±7 (17)	53±15 (37)	58±8 (40)	3	52±3 (36)	4
Ruby	⊥	62±21 (43)			70±12 (48)	15	100±34 (69)	2
ZrO_2 (Y_2O_3-stabilized)				28±7 (19)	32±1 (22)	4		
TiO_2	⊥	13±1 (9)	11±1 (8)	22±7 (15)	33±3 (23)	2		

[1] ∥ means the tensile axis was parallel with the boule axis; and ⊥ that the tensile axis was perpendicular to the boule axis.

B_4C, SiC, and Si_3N_4 indicated no change with RF sputtering, but possible improvements with IB sputtering with B_4C giving somewhat clearer results (e.g., a possible 20% increase). Fine grain spinel bodies indicated improvements in strength of the order of 25–50 percent due to RF sputtering, while large grain bodies of dense spinel showed no definite change.

Fracture origins were located in many specimens, especially in glass and single crystals. Many origins were from the edges with these being more common in higher strength specimens, especially in glass and spinel crystals. Edges of some RF specimens had debris attached at or near the origin.

4. Discussion

4.1. Surface Topography

Depressions similar to those observed in this study have been reported by Dugdale and Ford [10] on Al_2O_3 and (fused) SiO_2. These were attributed to porosity in the Al_2O_3, but were noted as an "interesting but unexplained phenomenon" in SiO_2. This work, e.g., on ZrO_2, shows that pores can be sources of these depressions, but they are more frequently caused by pits left from mechanical finishing which is the likely source in SiO_2. However, the appearance of depressions on certain areas of flame polished specimens, and generally on annealed specimens, as well as within existing depressions, suggests other sources. All of these observations are consistent with dislocations also being sources of pits. This was corroborated by etching studies of flame polished specimens which showed a high density of dislocations in the same type of areas in which many depressions developed [19]. The multiplicity of smaller depressions within larger ones when samples were heated during RF sputtering may then be due to migration or generation of dislocations.

The apparent enhancement of features that are believed to be twins is reasonable since sputtering rates are dependent on crystal orientation. Thus a twin will have a different orientation and hence different sputtering rate on many intersecting planes. Besides apparently etching twins and dislocations, some grain boundaries (e.g., in ZrO_2) were also etched by RF sputtering for shorter periods (e.g., 2 hr). Pores and impurity areas also appear to be etched. The extremely irregular topography of the polycrystalline MgO also is probably due to impurities, since the author observes variable concentrations of Ca and Si at grain boundaries in this material. The less extreme MgO sputtered topography may be due in part to this also. However, differential sputtering rates between different crystal surfaces may be more important.

While the origins of the features on sputtered glass are uncertain, they are suggestive. The association of crescent-shaped depressions with abrasion suggests that they may be flaws. The "craze-type" patterns may also represent more extended flaws but these may well have developed due to heating during RF sputtering. Clearly, the black spots and the fine hillocks suggest different degrees of inhomogeneity in glass, with the latter possibly being related to phase segregation.

These examples of etching indicate sputtering can be a useful etch technique. However, it should be noted that once a surface feature is

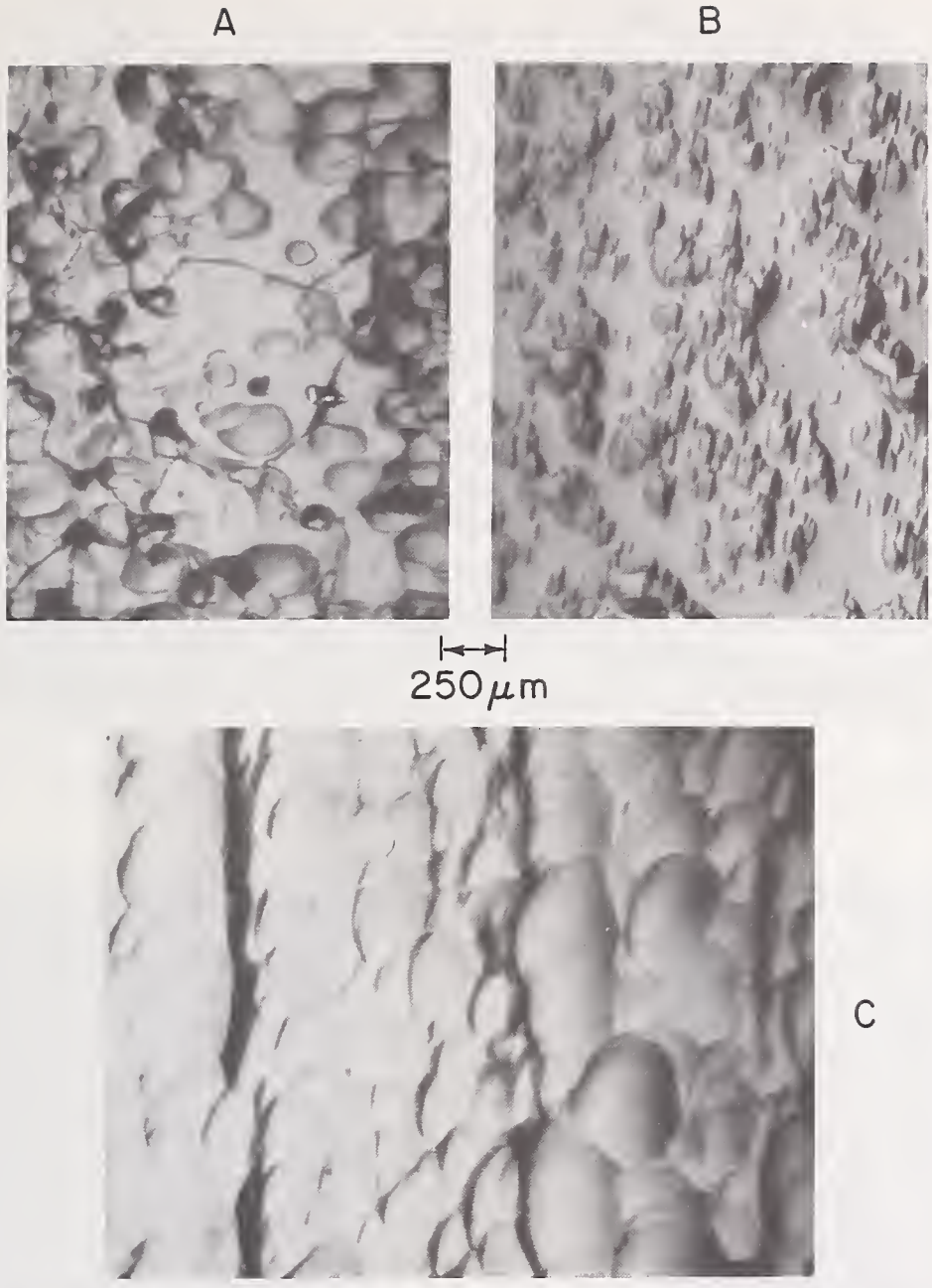

FIGURE 18. *Typical ion beam sputtered surfaces.* All specimens sputtered about 50 hours. (A) Polycrystalline ZrO_2, partially stabilized with CaO previously mechanically polished. Note evidence of a grain boundary which was not too common. (B) Sapphire, previously mechanically polished. (C) Ruby previously ground in the vertical direction.

developed it will continue to be preserved even after its original cause is gone. Thus etching by sputtering tends to give an integrated effect, that is, showing features from various previous levels on the same surface. This can be useful, but might also be misleading. It is clear that etching is best with a fairly high angle (e.g., normal) incidence. IB sputtering should also be feasible in this orientation, and hence should be as useful, or more so (due to acceleration control) than RF sputtering.

On the other hand, while RF sputtering does a very similar job on many materials, IB sputtering produces flatter surfaces on some materials. Heating during RF sputtering was also a problem. This could be reduced, especially in a system in which the specimens rested on a flat surface rather being inverted, so gravity would pull them onto the electrode rather than away from it. However, electron bombardment during RF sputtering means there will always be greater heating there than in IB sputtering. Thus, except for greater sputtering rates, RF sputtering is less versatile than IB sputtering.

Recently, Schmidt et al. [20] have shown that IB sputtering can be very useful in more clearly revealing magnetic domains and providing more accurate magnetic measurements in

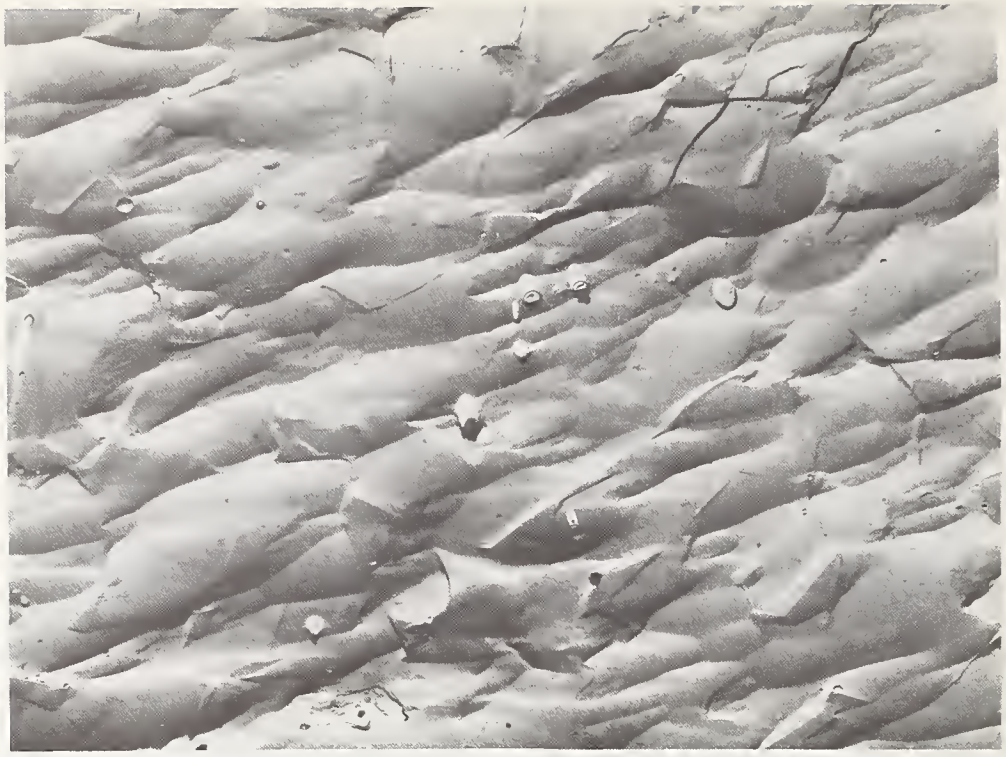

FIGURE 19. *Ion beam sputtering of a medium grain (about 10–20 m) commercial Al_2O_3 (Alsimag 614).* Electron micrograph showing elongation of depressions, exposed pores, and some traces of grain boundaries.

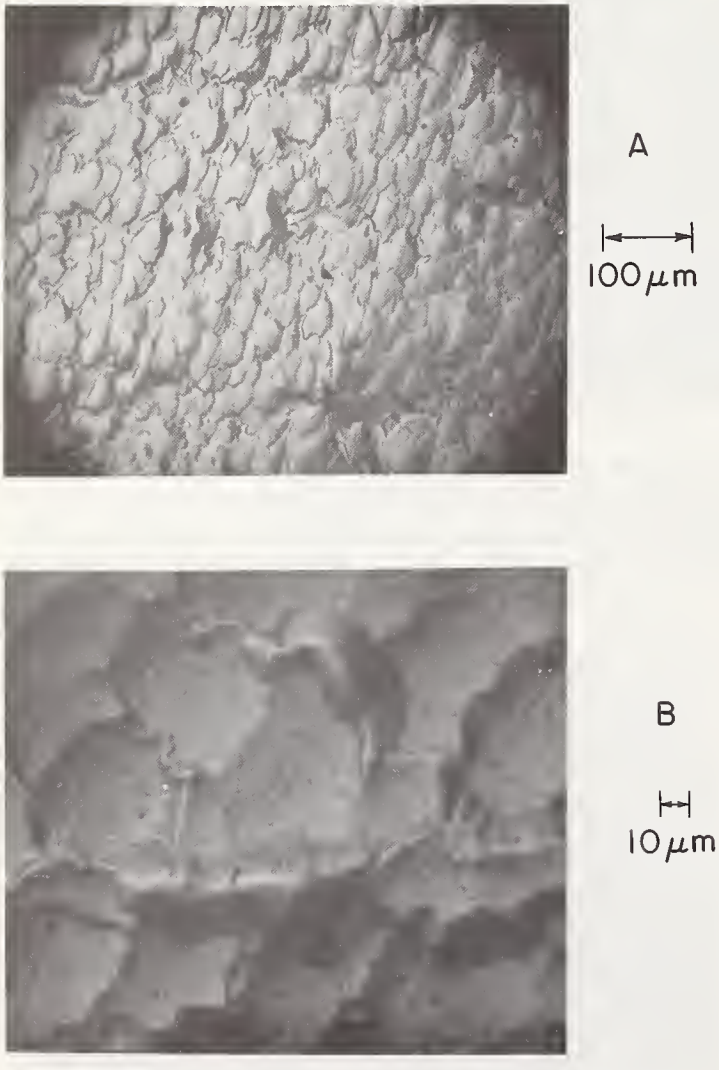

FIGURE 20. *Ion beam sputtered soda lime glass.*

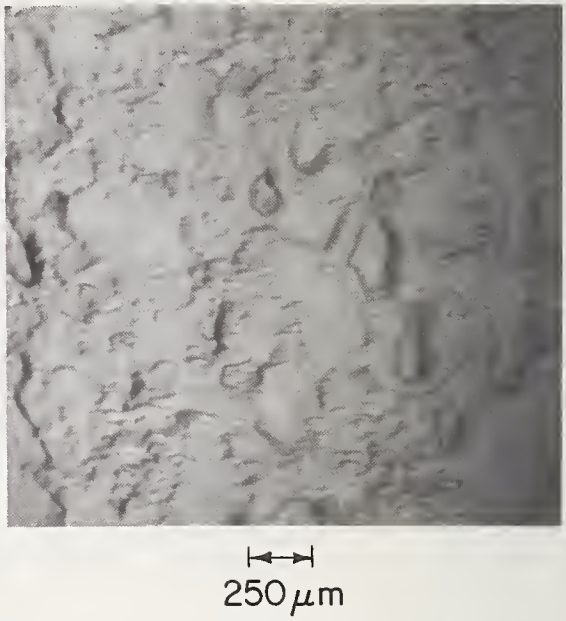

FIGURE 21. *Ion beam sputtered polycrystalline MgO.*

thin films (by removing mechanical damage and related strains). One would also expect that the use of reactive gases during sputtering might be very beneficial for etching purposes. Reiswig's [21] work showing excellent etching of grain structure in graphitic materials, possible deformation twins in graphite, and of the interface and grain structure in Au-Ag diffusion couples by sputtering with hydrogen is very suggestive of what might be done. Thus sput-

tering to reveal microstructure and related features appears to be quite promising.

4.2. Strength of Sputtered Specimens

The rapid rounding of surface pits and scratches is clearly consistent with the fact that substantially weaker specimens are strengthened by sputtering. However, most sputtered specimens did not exhibit strength substantially greater than mechanically polished specimens. While complete explanations cannot be given for this or for some of the indicated trends, some factors can be identified and others suggested.

Since many specimens, especially the higher strength ones, failed from the edges and sides, edge effects appear to have been a limiting factor. This is reasonable in view of the somewhat irregular nature of the edges, especially on RF sputtered specimens. The fact that surfaces were not flat also means that some strength will be lost; however, this effect should be relatively small.

The general tendency for previously ground specimens to give higher sputtered strengths than previously polished specimens is also reasonable. Since specimens tend to be more sensitive to a few isolated stress concentrations than to many, the high density of depressions on previously ground surfaces and edges would favor higher strengths. The possibility that sputtering may remove surface imperfections from ground surfaces, but leave some work hardened material on ground specimen which might strengthen them must also be considered.

The observation of twins in sputtered sapphire and ruby bars and the fact that they generally showed no increase in strength is consistent with other results [19] indicating that twins can severely limit strength in these materials. The heating in RF sputtering may aid the growth of twins left from machining. The absence of such heating in IB sputtering may have resulted in 1 ruby section free of twins and hence with higher strength. Such twinning effects would also explain that lack of improvement of polycrystalline Al_2O_3 on sputtering.

The increase in the strength of the rutile crystals may be due, at least in part, to heating. Strengths approaching those obtained by sputtering have been observed by the authors as a result of annealing similar specimens. The darkening indicating reduction (and heating) may also be a factor. This may also be a factor in the possible increases in strength in the ZrO_2 crystals. However, the fact that little or or no reduction was apparent in many areas of strengths similar to reduced areas indicates that reduction effects are at best small in ZrO_2. Heating of the spinel crystals could cause precipitation of Al_2O_3, which would be expected to strengthen them some at the expected temperatures [22]. However, the fact that nearly as high values were obtained in IB sputtering where heating is not a problem indicates this cannot be the major effect. It would also not explain the increase observed in the fine grain polycrystalline spinel since this material was essentially stoichiometric. Heating to cause some annealing of these samples may have been a factor there. These bodies do show substantial increases in strength on annealing, but only at much higher temperatures.

The strength of RF sputtered glass appears to have been limited by the cracks that often developed. Heating was probably a major factor in this since these cracks were not observed on IB sputtered specimens. The latter clearly tended to have their strength increased; however, the irregular surface was probably a major factor in limiting these increases.

There is a possible trend in most of these increases. Recent work by the author (to be published) indicates that the strength of MgO and Al_2O_3 are more frequently controlled by microplasticity than by flaws, while flaw mechanisms appear to be controlling in $MgAl_2O_4$, ZrO_2, B_4C, SiC, and Si_3N_4. These latter materials, along with glass would then be expected to be more sensitive to surface finish than MgO and Al_2O_3. The data does indicate such a trend for ZrO_2 crystals and single and polycrystalline spinel, and for glass. The poorer quality of most of the polycrystalline ZrO_2, SiC and Si_3N_4 samples are probably factors in their showing little effect.

5. Summary and Conclusions

Both radio frequency (RF) and ion beam (IB) sputtering of a number of ceramics have been investigated. RF sputtering normally produces a series of symmetrical depressions in the surface. Pits left from mechanical finishing and subsequently rounded (rapidly) by sputtering are a major cause of these depressions. While these depressions are generally not associated with grain boundaries, they do decrease in size with decreasing grain size since pits left from mechanical finishing normally decrease in size with decreasing grain size. Ground surfaces develop a high density of pits and surfaces of finer finishes progressively fewer depressions. However, the development of depressions inside of others, on surfaces without pits, and their change due to heating during sputtering all suggest that dislocations may be another source of these depressions. These depressions are typically about 1 micron deep, so sputtered surfaces are normally not too rough. However, some polycrystalline materials can develop a very rough topography, apparently due mostly to impurities, but differential

sputtering between different plans may also be a factor (e.g., in MgO). Soda lime glass develops crescent-shaped depressions that may originate from flaws.

Besides the apparent etching of flaws and dislocations noted above, several other examples of etching (e.g., of impure areas, pores, twins, and some grain boundaries) were observed. These were generally clearest after limited (e.g., 1-3 hrs RF sputtering). Besides normal ion incidence, the lower accelerating potential used in RF sputtering may also have been favorable to such etching. Such etching tends to be cumulative since once a feature develops it tends to be preserved even after its original cause is gone. Longer sputtering normally rounded such features sufficiently to make them less distinct, or to obliterate them.

Ion beam sputtering at low angles of incidence generally developed similar topography. However, depressions were less symmetrical, and somewhat shallower. There was less evidence of etching, and much more regular surfaces were obtained on those polycrystalline bodies that gave rough surfaces in RF sputtering. IB sputtering at high angles of incidence may also be very useful for etching. Use of reactive gases may also be very beneficial.

Either type of sputtering clearly improved strengths of weaker samples (e.g., those ground perpendicular to the tensile axis). Generally, strengths comparable to those achieved by mechanical polishing were achieved by sputtering any mechanically finished body. Annealing (e.g., 1300 °C) after sputtering did not increase strengths and may have decreased them some. Limited trials showed no obvious degradation of the strengths of flame or gas-polished specimens.

Results do suggest that some materials (e.g., glass, $MgAl_2O_4$ and possibly ZrO_2) can have their strengths increased by sputtering. Sapphire might also be strengthened, but this may depend on the absence of twins or easily activated twin sources. However, this will generally require improvement of edges separating specimens so debris does not accumulate on the sides. Ion beam sputtering appears to be favorable to producing better edges. Study of round rods, or of plates tested biaxially near their center would be good for further study.

The higher rates (e.g., about 1 μm/hr) of RF sputtering were favorable to it. However, IB sputtering otherwise appears more desirable. At low angles of beam incidence on the specimen, smoother topography is obtained, along with better edge finish. Heating and attendant problems (reduction of material and possible expansion of twins and dislocations) are much less. Further, since lower accelerating potentials and at least near normal incidence are obtainable, in IB sputtering, it should be useful for etching.

The author is extremely grateful to Drs. Sigel, Anderson, Hockey, and Garvin for sputtering specimens. The aid of C. Herbert, J. Breen, and S. Slawson in preparing specimens and of J. Robinson for electron microscopy is gratefully acknowledged as are the initial discussions of the sputtering process with Dr. G. Wehner.

6. References

[1] Bebrisch, R., Festkorperzerstaubung durch ionenbeschuss, Ergebnisse der Exaton Naturwissenchaften 35, 295 (1964).

[2] Weston, G. F., Cold Cathode Glow Discharge Tubes, ILIFFE Books, Ltd., London, 1968.

[3] Wehner, G. K., Sputtering, Sciences and Technology, 32 (1968).

[4] Wehner, G. K., and Anderson, G. S., The nature of physical sputtering, to be published in handbook of thin film technology, McGraw-Hill.

[5] Davidse, P. D., Theory and practice of RF sputtering, Symposium on the Deposition of Thin Films by Sputtering, University of Rochester, Rochester, New York, 1966.

[6] Tighe, N. J., Microstructure of fine-grain ceramics, Ultrafine-Grain Ceramics, Edited by U. Burke, Reed, N., Weise, N., 109–33, (Syracuse Univ. Press., Syracuse, New York, 1970).

[7] Paulas, M. and Reverchon, F., Study of the Parameters of the Ionic Bombardment of ferritesapplication of the thinning at almost grazing Incidence of Porous materials, International Symposium on Ionic Bombardment Theory and Application, 324–35, (Gordon and Breach, New York, 1962).

[8] Trillat, J. J., Ionic bombardment, a new method for the study of surfaces, *ibid.*, 13–51.

[9] Navez, M., Sella, C., Shaperot, D., Electron microscope study of the effects of ionic bombardment of glass, *ibid.*, 339–53.

[10] Dugdale, R.A., and Ford, S.D., The etching of alumina and fused silica by sputtering, Trans. Brit. Ceramic Society 65, 165 (1966).

[11] Keig, G. A., and Haines, H. R., The Cathodic etching of plutonium ceramics, Trans. Brit. Ceramic Society 62, 363 (1963).

[12] Bierlein, T. K., Newkirk, H. W., Jr., and Mastel, B., Etching of refractories and cermets by ion bombardment, J. Am. Ceram. Soc. 41 (6) 196 (1958).

[13] Tarpenian, A., Electrochemical and ion bombardment etching of pyrolytic graphite, *ibid.*, 532.

[14] Beecham, D., Sputter machining of piezoelectric transducers, J. Appl. Phys. 40, 4357 (1969).

[15] Schroeder, J. B., Bashkin, S., and Nester, J. F., Ionic Polishing of Optical Surfaces, Applied Optics 5, 1031 (1966).

[16] Levy, P. W., Shaping or Figuring Ceramic Surfaces of Ion Beam Bombardment, these proceedings.

[17] Rice, R. W., The Effect of Grinding Direction on Strength of Ceramics, these proceedings.

[18] Rice, R. W., Becher, P. F., and Schmidt, W. A., The strength of gas polished sapphire, these proceedings.
[19] Becher, P. F., and Rice, R. W., Flame polishing of flat oxide bars, these proceedings.
[20] Schmidt, P. H., Spencer, E. G., and Walters, E. M., Ion milling of magnetic oxide platelets for the removal of surface and near-surface imperfections and defects, J. Appl. Phys. 41, 4740 (1970).
[21] Reswig, R. D., The use of hydrogen in cathodic vacuum etching, Microstructures, 15 (1970).

Discussion

SCHNEIDER: Was there any evidence of chemical change or did you investigate this?

RICE: No, we haven't had a chance to look at this on these materials. I don't think there is much evidence for change but this is an area that would be good to try and check in more detailed studies.

WHITE: I was wondering, have you checked for any possible evidence of argon implanted in the damaged layer?

RICE: Pardon?

WHITE: What is the gas?

RICE: It's argon. The acceleration potential of the RF sputtering is of the order of 2 kilovolts and about 6 kilovolts in the ion beam sputtering.

WHITE: We have found argon in very surprising situations.

RICE: Argon stuffed in the surface would probably provide a compressive layer which would increase the strength. I feel that this probably is not a major factor. For example, annealing after sputtering did possibly decrease some strengths a little, but there were no clear changes of significance. Other factors such as twinning in sapphire may be more important variables.

PERRY: Did you notice any difference in statistical scatter in the strengths of the glass?

RICE: Yes, I mentioned that particularly in the case of glass we get some specimens that are maybe three, even four times stronger than we would get by mechanically finishing. That is, you tend to have strength say from about the mediam of that found for normal mechanically polished glass to substantially greater strengths. This suggests that there is indeed a potential for improving the strength of glass, considerably higher than that achieved by mechanical finishing.

GREEN: Did you observe an increase of strength of the glass while removing 1 to 4 mils of sputtering?

RICE: Yes.

LANGE: In chemical polishing, the topography depends on the rate of the polishing. Did you find any change in topograph by rate of sputtering?

RICE: Really we haven't been able to investigate a significant difference in rate.

HEUER: If you have any dirt in your system, you can get a very interesting but unwanted topography. This is probably the most important factor in obtaining uneven topography.

RICE: This can be a factor since sputtering is essentially an integrating or accumulative process. However, I clearly observed that the major factor in the uneven topography was the prior surface finish and whether the specimen was polycrystalline or not. The type of sputtering and the sputtering parameters also appear to affect this.

UNIDENTIFIED: How wide were the ion traps that you originally showed in some of your examples?

RICE: You mean the scribe mark? Oh, I don't recall, probably something like 25 microns or so. It was done with just a hand held diamond scriber. The scale was on the figure, but I don't recall explicitly the dimensions of the scribe mark.

NATIONAL BUREAU OF STANDARDS SPECIAL PUB. 348, THE SCIENCE OF CERAMIC MACHINING AND SURFACE FINISHING, Proceedings of a Symposium Sponsored by the American Ceramic Society, the Office of Naval Research, and the National Bureau of Standards, held at NBS Nov. 2–4, 1970, Gaithersburg, Md. (Issued May 1972).

Computer Controlled Ionic Polishing of Optical Surfaces

James W. Douglass [1]

Perkin-Elmer Corporation, 77 Danbury Road
So. Wilton, Connecticut 06897

Results of the development of an ionic polishing investigation are described. During this investigation many controlled polishing experiments were performed. The results of two of these experiments are presented. In the first of these, a 0.203 m diameter optical flat of fused silica was polished to a diffraction limited surface quality of 95A (9.5 nm) rms. The second experiment described was the conversion of a 0.203 m diameter Cervit sphere into an f/5 paraboloid of diffraction limited quality by using analytical expressions to generate the removal distribution. The ionic polishing process was computer controlled for this experiment. The temporal stability and optical scatter performance of ionically polished surfaces has been determined to be as good as or better than conventional surfaces.

Key words: Computer controlled process; ion beam technology; ionic polishing; optical fabrication; optical scatter; sputtering.

1. Introduction

The limitations of modern optical systems stem in many instances from the inordinately long time required to produce the surface figures necessary for their high performance. Furthermore, the recognized benefit of larger aperture systems makes the fabrication of even the conventional surfaces more difficult.

For some time, Perkin-Elmer has been directing considerable effort toward developing optical fabrication processes whose goal is to fabricate optical components in an automatic or semiautomatic fashion, and which require high speed numerical analysis and control. A goal of these programs is to eliminate much of the "art" that has always been an important requirement in conventional optical fabrication and to replace it with techniques based on sound technology.

The discovery by Meinel, Bashkin, and Loomis [1][2] of the University of Arizona that an ion beam can polish optical glass, indicated the possibility that a controllable polishing technique might be developed. Perkin-Elmer entered into an exclusive agreement with the University of Arizona to explore this technique. As a result, efforts have been underway in our Process Development Laboratory to develop a controlled polishing or figuring process based on the use of ion beams. Some very early results were published [2, 3], but since that time our results have been essentially unpublished. This article discusses some of our developments since that time. The approach will be to emphasize the results without going deeply into the historical development or the extensive theories which describe the phenomena contained within the ionic polishing process.

[1] Physicist, Group Leader Advanced Processes.
[2] Figures in brackets indicate the literature references at the end of this paper.

2. Technical Discussion

2.1. Definition of Ion Polishing

Ionic polishing is the controlled removal of surface material from optical elements by sputtering with an ion beam.

This definition does not limit the type of material to be polished or the characteristics, such as mass, energy, and charge of the ion employed. The implicit point is that the process must be very accurately controlled.

2.2. Relationship Between Ionic Polishing and Sputtering

An atomic displacement occurs when an energetic particle strikes an atom or ion in a solid and transfers sufficient energy to break the chemical bond and force the atom to move away from its original site. This is called a knock-on collision. If the knock-on occurs near the surface, the displaced atom may leave the solid completely. Dislodging molecules in this fashion is the process of sputtering. Sputtering of dielectrics is generally produced with neutral plasmas created by radio frequency fields so that the alternate bombardment by oppositely charged particles precludes the buildup of a net charge on the dielectric. The significance of the discovery by Meinel, et al. is that ion beams may be used instead of neutral plasmas to produce sputtering, and thus makes available techniques for the control of the process far beyond that possible for plasmas. Controlled sputtering by ion beams is referred to as ionic polishing. Any net charge which may accumulate on the surface of the dielectric does not produce fields strong enough to produce any undesirable effects resulting from surface charge accumulation.

2.3. Brief Description of the Research and Development Effort

A prototype ionic polishing laboratory was set up with a Texas Nuclear linear accelerator (30 — 300 KeV) with an RF ion source. The beam obtained from this accelerator was magnetically analyzed and focussed onto the surface of the test specimen in a sample chamber. This beam was electrostatically deflected in a rectangualr pattern, so as to produce rectangular areas of polishing in order to simplify determinations of sputtered volume. In this way, a parametric study was conducted to determine the sputter yield, i.e., the ratio of the number of sputtered atoms to the number of incident ions, for various optical materials as a function of the species of incident ion, its mass, charge state, energy, and angle of incidence to the test sample. This investigation was principally limited to the following optical materials: fused silica, BK–7, ULE, and Cervit. The ions were primarily those of the noble gases, although some experiments were performed with H^+, HH^+, and HHH^+.

These experiments were conducted on one-inch diameter samples, and sputtered volume measurements were performed interferometrically. A typical interferogram of such a sample is shown in figure 1. Experiments were performed on polished and ground surfaces. The results of this investigation indicated sputter yields in the range of 1 — 3 and that these values strongly depend on the species of ion, but are only weakly dependent on the ion energy. The sputter yield varies approximately as the inverse cosine of the angle of incidence in the range of 0 to 60°. Ground surfaces may be polished, but long polishing times are required for beam currents on the order of 100μA. Consequently, all subsequent work has been on polished surfaces.

FIGURE 1. *Interferogram showing uniform removal in a rectangular pattern.*

2.4. Description of the Ionic Polishing and Data Handling Systems

The current ionic polishing system is shown in figure 2. The performance of this system differs from the earlier prototype in that the ion beam is rapidly raster scanned over the test sample. The effective velocity of the beam spot is controlled by controlling the beam spot dwell

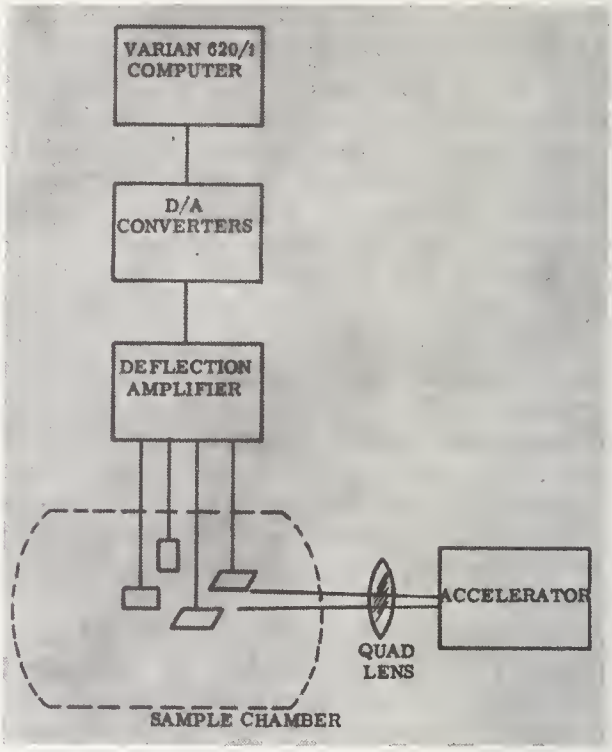

FIGURE 2. *Block diagram of ionic polishing system.*

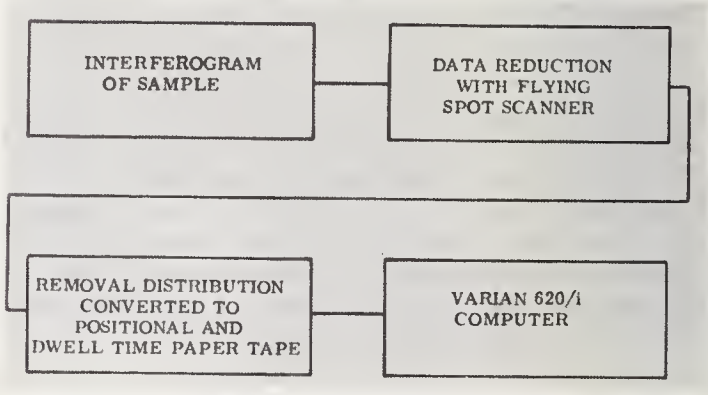

FIGURE 3. *Block diagram of data handling system.*

time at discrete locations on the piece separated by intervals which are small compared with the beam spot diameter. The positional and dwell time controls are effected by an on-line Varian 620/i computer. Provided the beam spot diameter is small compared with the dimensions of the highest spatial frequency of interest on the sample, one may linearly relate the dwell time at any location to the desired removal at that location and thus produce controlled figuring. In practice, the computer core is stored with coordinate and dwell time information. The computer cycles through this data as described, as long as is required to figure the sample. Both rectangular and polar coordinate systems are used to match the geometry of the removal distributions on the sample.

The data handling system is shown in figure 3. Due to extensive use of computers, a great deal of special data processing is possible; i.e., deconvolution of data and coordinate transformations, as well as the generation of removal distributions, based on purely analytical expressions.

3. Experimental Results

3.1. Figuring Experiments on Optical Flats

Many experiments have been performed whose goal was to polish optical flats to a high degree of perfection. The results of one such figuring experiment are shown in figure 4. This experiment was designed to figure a 0.203 m diameter fused silica flat whose peak-to-peak and RMS departures are 1100Å. (110 nm) and 180Å (18 nm) respectively. The final surface is of diffraction limited quality with peak-to-peak and RMS departures of 700Å (70 nm) and 95Å (9.5 nm) respectively. This experiment was performed with a 120 μA ion beam of 150 KeV Ar^+. The removal profile was determined from the initial interferogram.

3.2. Figuring Experiments on Spheres

Experiments have also been performed on non flat samples, i.e., spheres and aspheres. One particularly notable experiment was the automatic conversion of a spherical surface into a paraboloid. In this experiment a 0.203 m diameter sample of Cervit was ground and polished into a sphere with a radius of curvature of 2.03 m. A removal distribution was generated analytically which represented the minimum volume conversion into an f/5 paraboloidal surface. This removal distribution is shown graphically in figure 5. This figure was made by time exposing an x-y plot of the removal distribution with an oscilloscope as it was output by the Varian computer. The degree of exposure at each location is a measure of the dwell time at that location. Figure 6 shows the

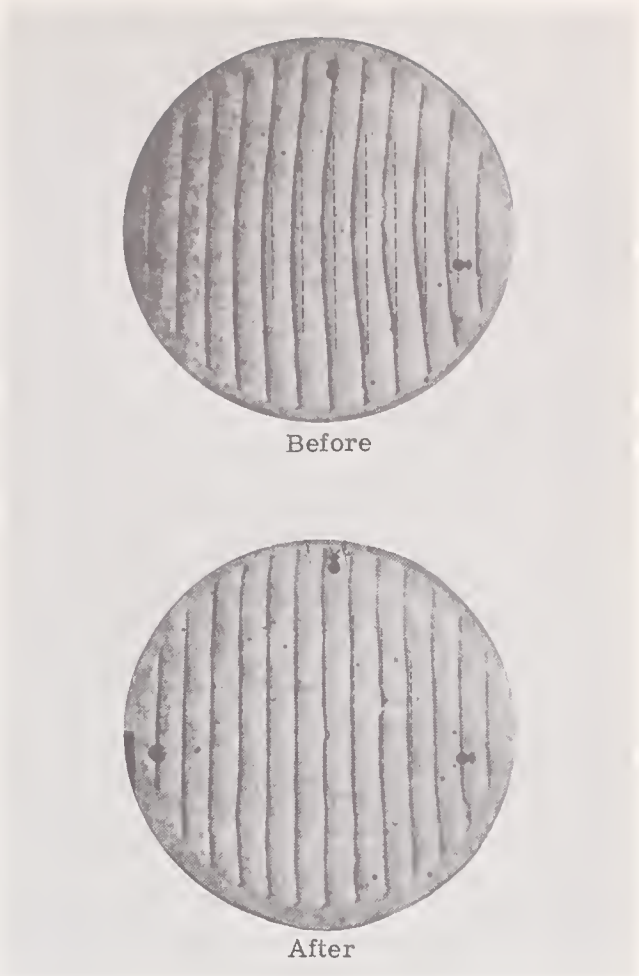

FIGURE 4. *Before and after interferograms of a 0.203 m Diameter.* Fused silica optical flat figured by ionic polishing to a final surface figure of 95A (9.5 nm) RMS.

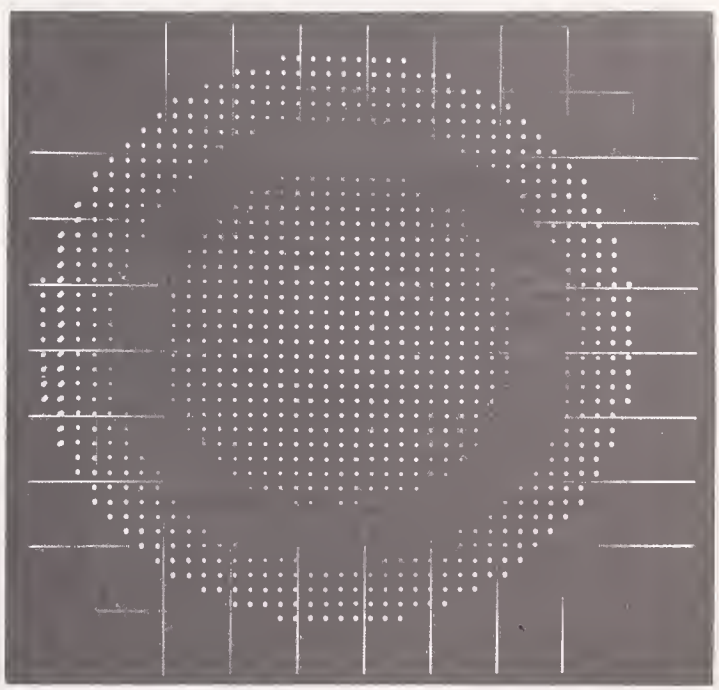

FIGURE 5. *Time exposure of positional and dwell time data used to convert a cervit sphere into a diffraction limited f/5 paraboloid.*

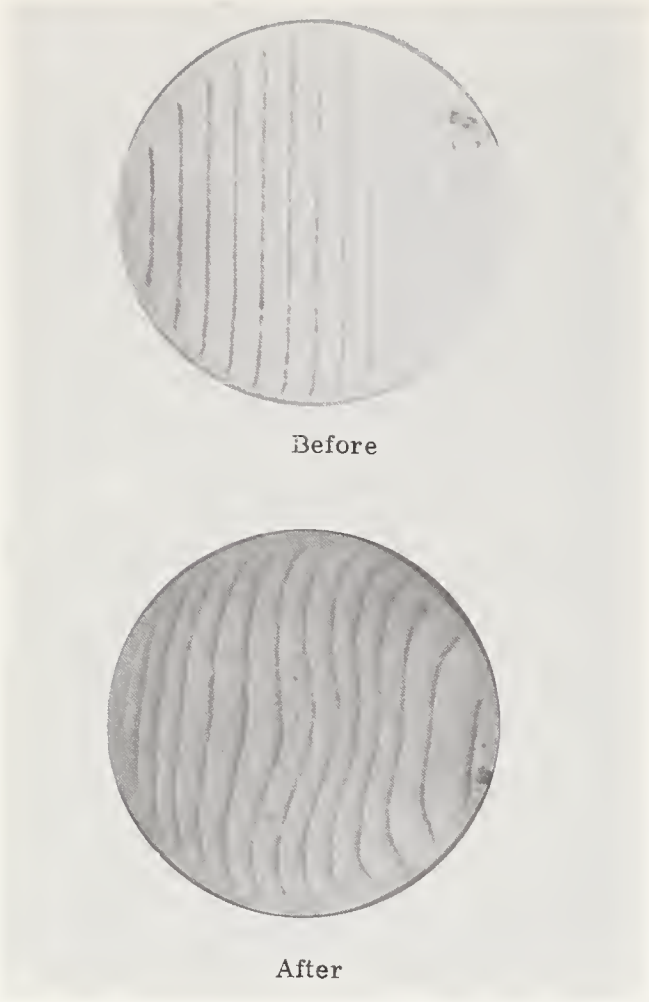

FIGURE 6. *Before and after interferograms of a cervit sphere converted to a paraboloid.* Computer generation and control of ionic polishing system data was used. Interferograms were taken in a spherical wavefront interferometer.

interferograms of this sample before and after figuring. These interferograms were made in a spherical wavefront multiple beam interferometer [4]. Consequently, the initial sphere shows straight and equally spaced fringes while the paraboloid exhibits the characteristic "hole and roll" interferogram. The final paraboloid is also of diffraction limited quality having a maximum departure of 600Å (60 nm) from the desired paraboloid. This amount of departure corresponds roughly to 130Å (13 nm) RMS. This experiment was performed with a 30 KeV Ar^+ ion beam and required approximately 18 hours to perform.

3.3. Stability of Ionically Polished Surfaces

Subsequent interferometric measurements of the optical flat of Section 3.1 over a 12 month period show that this ionically polished surface is as stable as conventionally polished surfaces in that no change in the shape of the surface was detected. The values of the surface stress induced by the implantation of the ions have been determined for ULE and Cervit when irradiated with 30 KeV Ar^+. These measurements indicate stress levels too low to cause any significant strains in modern optical components and are generally no larger than the bulk stresses commonly found in optical materials.

3.4. Surface Cosmetic Finish of Ionically Polished Surfaces

Optical scatter measurements have been performed on ionically polished surfaces. These measurements indicate that these surfaces are at least as good as conventionally polished surfaces, and in some cases better. These measurements indicate an RMS surface roughness in the range of 10Å — 50Å (1nm — 5 nm). Recent unpublished work at Perkin-Elmer indicates that ion beam polishing may be used to improve the surface smoothness of sapphire laser optics.

4. Summary and Conclusions

Ionic Polishing has been applied to figure optical elements with automatic control by a computer. In this way, optical flats and image forming elements have been produced which are of diffraction limited quality. The stability and optical performance of these surfaces is as good, or better than, the initial surface.

Ionic Polishing has been shown to be a useful process for the production of conventional optical components. Since the process is capable of producing any arbitrary surface, it is expected that a new generation of optical systems may result due to the manufacturing capabilities which were not available with conventional polishing techniques.

5. References

[1] Meinel, A. B., Bashkin, S., and Loomis, D. A., Appl. Opt. 4, 1674 (1965).

[2] Schroeder, J. B., Bashkin, S., and Nester, J. F., Appl. Opt. 5, 1031 (1966).

[3] Schroeder, J. B., and Dieselman, H. D., J. Appl. Phys. 40, 2559 (1969).

[4] Polster, H. D., Appl. Opt. 8, 522 (1969).

NATIONAL BUREAU OF STANDARDS SPECIAL PUB. 348, THE SCIENCE OF CERAMIC MACHINING AND SURFACE FINISHING, Proceedings of a Symposium Sponsored by the American Ceramic Society, the Office of Naval Research, and the National Bureau of Standards, held at NBS Nov. 2–4, 1970, Gaithersburg, Md. (Issued May 1972).

Arc, Laser, and Electron Beam Machining of Ceramics

R. W. Rice

U. S. Naval Research Laboratory
Washington, D.C. 20390

The various types of arc, laser, and electron beam machining, the considerations that are required in their operations, and some of the applications for which they have been tried or used, are briefly reviewed. The most general consideration is whether thermal shock and stress cracking will be a problem. The environmental and material parameters, which vary substantially with the types of these different machining processes, can also be quite important. Meeting the requirements of all these considerations does limit the versatility and applicability of these techniques. Nevertheless, they deserve consideration for a variety of applications.

Key words: Arc machining; cutting; drilling; electron beam machining; laser machining; shaping; thermal shock control.

1. Introduction

Speakers who have been actively investigating arc, laser, or electron beam machining of ceramics were not able to attend this conference. Since these technologies offer a number of opportunities for machining ceramics, and since the author has had some experience with these technologies, it was felt worthwhile to review these techniques. This review is not meant as a detailed analysis of these techniques, nor an exhaustive compilation of their applications. Rather, it is a brief introduction to these techniques and a summary of some of the trials or uses made of them.

2. Types of Arc, Laser, and Electron Beam Machining

Much of the scope of arc, laser, and electron beam machining, shown in table 1, can be recognized from the fact that these techniques can be used for welding. From metals technology, it is clear that welding techniques are easily converted to cutting techniques, which is one of the major applications of these techniques. It has a major advantage over abrasive cutting of hard materials in that it does not depend on hardness. High melting (or vaporization) temperatures, which are usually associated with high hardness, will limit the rate of such cutting; but generally not near as much as in abrasive cutting. Cutting by these techniques also has the advantage of being nearly as versatile as a jig saw on wood. While the tolerances of such cutting usually restrict it to rough or general shaping, it nonetheless has considerable potential for many hard materials. Oxidation-assisted cutting of some nonoxides with an impinging oxygen stream as done with metals (e.g., Ti) may also have some promise. Drilling is of course a special case of cutting.

The vaporization and fracture behavior of many ceramics have important effects on these machining operations. Many ceramics undergo considerable vaporization near their melting point, and many vaporize without any melting. This can increase the tolerances of such machining since the irregular layer of solidified melt is reduced or eliminated. For example, running an electron beam over SiC which does not melt leaves a groove very similar to that achieved with an air-driven abrasive stream. This is important in drilling fine holes since there is little or no melt to close the hole. Vaporization generally absorbs substantially more energy than melting, and so takes more power or may reduce the thickness that can be handled, but this does not appear to be a major limitation for many applications in view of powers available for some of these techniques.

Minimizing or preventing fracture from ther-

TABLE 1. *Types of arc, laser, and electron beam ceramic machining*

Processes involving:	
Complete penetration:	Incomplete penetration:
1. Cutting	1. Cut and fracture
2. Shaping, by cutting pieces out	2. Score for later fracturing
3. Drilling—complete holes	3. Drilling—incomplete holes
	4. Shaping—vary surface topography by melting or vaporizing areas

mal shock is a major consideration in these techniques, which is discussed below. However, it should be noted that in some cases thermal shock fracture can be utilized to advantage. Also, these techniques may be used to score materials for subsequent fracture along the scored lines.

3. Considerations in Arc, Laser, and Electron Beam Machining

A number of factors must be evaluated for each of the different techniques and their variations. The most general and important is fracture due to thermal shock. This will decrease in importance as the thermal shock resistance of materials considered increases, and as the size of the part to be machined decreases. Thus it may be possible to machine fairly large pieces of SiO_2 and possibly Si_3N_4, while smaller pieces of Si_3N_4 and SiC can probably be machined without any precautions against thermal shock. In some cases, e.g., rough cutting, some cracking along the edges may be tolerable. However, in many cases, thermal shock will be a problem to contend with. This can generally be solved by supplemental heating, as used in welding of ceramics [1][1]. The procedure is to simply provide additional heating in the region of cutting or drilling (or welding) so that the net thermal gradient is below that which will cause fracture. Supplementary heating of 1000 °C ± 300 °C is often adequate.

A variety of considerations pertinent to each of the three techniques is listed in table 2. Lasers can of course be used in essentially any atmosphere. Arcs are limited in vacuum, but can operate in a variety of atmospheres, though penetration is dependent on the atmosphere (e.g., greater penetration in He than A). The conventional and glow discharge electron beams are limited to vacuum, as listed. Electron beams that are generated by conventional vacuum electron guns, but ejected into the air (about 1.8 cm working distance) remove the vacuum restriction from the part, but at the expense of capital cost (by a factor of two or more). Material coupling is most limited with arc techniques, since a conductor is required. However, heating can make many oxides conductive. With lasers, the primary question is the absorptivity, which depends on wavelength. Since CO_2 lasers offer the greatest power and efficiency, absorptivity at their wavelength (10.6 μm) is of greatest importance. Materials with metallic-like reflection (e.g., TaC, TiN, etc.,) will generally have poor absorbance until some heating has occurred. Thus, starting may be slow unless the supplementary heating (if used to prevent thermal shock) changes this enough. Limited oxidation, or other coatings of the area of the beam will start in (or follow) can make important differences. Electron beam coupling is the most general. However, if a material is not a conductor, charge can build up and deflect the beam away. This has not been a problem in welding where supplementary heating is used. The elimination of the problem with supplementary heating apparently results for either enhanced conductivity or enhanced electron emission (with the supplementary heater winding collecting the emitted electrons), or both. While the relative roles of melting and vaporization depend most on the material, they also vary a fair amount with the atmosphere and amount of surface superheating. Arcs are usually used in an atmosphere (generally inert) and heat a considerable depth, so melting is favored. (Note this is true of both the work piece and electrode. To avoid the melting limitations of W, other electrodes such as C, or TaC, can be used.) Electron beam penetration favors melting, but when used in vacuum, this will enhance vaporization. Recent work indicates that laser radiation has limited penetration,

[1] Figures in brackets indicate the literature references at the end of this paper.

TABLE 2. *Arc, laser, and electron beam machining considerations*

A. Technique	Arc	Laser	Electron beam		
B. Mode	Conventional, other—e.g. plasma	Continuous, pulse	Conventional electron gun	Glow discharge	Air ejected beam
C. Operational: Considerations					
1. Atmosphere	Various, but affects penetration	Any	Medium vacuum (10^{-4} -10^{-5} torr)	Low vacuum (0.1 torr)	Any
2. Material coupling parameters	Conductivity	Absorptivity (vs λ and temp)	Electron discharge		
3. Material removal	Favors melting	Favors vaporization	Favors melting		
4. Cut width	Wide	Generally fine	Fine		

which leads to greater surface heating and resultant vaporization than electron beams [2].

Another consideration is the cut width. This is generally widest with arcs, and finest for electron beams, with lasers intermediate, and often substantially finer than arc. In all cases, there will be a substantial bevel on the front edge (or conical entry to holes) and some taper to the edge or hole wall.

4. Applications of Arc, Laser, and Electron Beam Machining

Almost no effort has been made to utilize arc machining. However, one firm apparently tried arc drilling of small Al_2O_3 parts (heated to provide conductivity) with some degree of success.

Many laboratories have probably used a laser to "drill" one or more holes in glass parts out of curiosity or for some special laboratory need, as in the author's laboratory. Several have also probably drilled holes in more refractory materials (e.g., 1 mm × 10 mm holes in ruby [3]). The most extensive application of laser machining is the scoring of Al_2O_3 electronic substrate materials for subsequent fracturing to size [4]. There may be some adverse effects on substrate strength in comparison to mechanically cut [5] ones, but this system is currently used in industry.

Electron beams from glow discharges have been used to drill 0.006 in (0.152 mm) holes in diamond, and to "machine" a spiral groove in 0.5 in (1.27 cm) diameter fused SiO_2 rod [6]. The latter grooving resulted from vaporization and melt flow from the spiral path of the beam. These were apparently done without supplementary heating. Schumacher [7] et al., have demonstrated that pieces of rock over 15 cm thick and several cm in cross section can be split by penetrating 5 cm into them with an air ejected electron beam operating at 9 KW with 150 KV.

5. Summary and Conclusions

Arc, laser, and electron beam methods of machining ceramics offer considerable versatility in cutting, drilling, and shaping ceramics. Some of this versatility is compromised by problems of thermal shock fracturing and the heating techniques often needed to minimize this, as well as by the tolerances and edges achieved. Nonetheless, these processes offer considerable opportunity, especially for applications where the minimization of thermal shock problems are not needed, or are not a significant encumberance. They should, therefore, be considered because of the speed, cost, or size advantages they can offer.

6. References

[1] Rice, R. W., Welding of Ceramics, U.S. Naval Research Laboratory Report 7085, July (1970).

[2] Pahlitzsch, G., and Visser, A., Materials Removal Processes in Laser and Electron Beam Machining, p. 335–57, in Electron and Ion Beam Science and Technology, R. A. Bakish, ed., (The Electrochemical Society, New York, 1968).

[3] Bernal, E. G., and Ready, J. F., Lasers in High Temperature Research, in Proceedings of the 3rd Int. Symposium on High Temperature Technology (Butterworths, 113, London, 1967).

[4] Lumley, R. M. Controlled separation of brittle materials using a laser, Am. Ceram. Soc. Bull. 48(9), 850–54, (1969).

[5] Lo, W. C., Edge effect on the modulus of rupture of ceramic substrates, this proceedings.

[6] Parisi, A. J., Electron-Beam Power Ready to Topple Cost Barrier, Product Eng., pp. 22–24, Nov. 18, (1969).

[7] Schumacher, B. W., Electron Beam Cutting of Rocks and Concrete, p. 447, in Electron and Ion Beam Science and Technology, R. A. Bakish ed., (The Electrochemical Soc., New York, 1968).

NATIONAL BUREAU OF STANDARDS SPECIAL PUB. 348, The Science of Ceramic Machining and Surface Finishing, Proceedings of a Symposium Sponsored by the American Ceramic Society, the Office of Naval Research, and the National Bureau of Standards, held at NBS Nov. 2–4, 1970, Gaithersburg, Md. (Issued May 1972).

The Techniques and Mechanisms of Chemical, Electrochemical, and Electrical Discharge Machining of Ceramic Materials

D. William Lee and George Feick

Arthur D. Little, Inc., Cambridge, Massachusetts 02140

Electrochemical Machining (ECM), Electrical Discharge Machining (EDM), and Chemical Machining (CHM) techniques have not been extensively used as a material removal process for ceramics. The fact that these processes are not dependent upon the hardness of the workpiece should make them attractive for the shaping of ceramics. However, ECM and EDM techniques are limited to material with reasonably good electrical conductivity while CHM may be limited by the availability of effective etchants and the nature of the ceramic itself.

The theory and techniques of chemical, electrochemical and electrical discharge processes will be reviewed. The variables and important parameters of the material removal processes will be discussed, including etchants and mask techniques for chemical milling; current-voltage characteristics, dielectric fluids, electrode materials, etc., for EDM; electrolytes, gap effects, current density, etc., for ECM. The available information and experiences developed on metals and alloys will be used to examine the applications and limitations of these processes to ceramic materials. Where possible the effects of the material removal process on the surface condition, microstructure, and subsequent material properties will be pointed out. Finally, comments will be made on the technical and economic feasibility of ECM, EDM, and CHM processes for the shaping, cutting, and finishing of crystalline ceramics.

Key words: Ceramic materials; chemical machining (CHM); electrical discharge machining (EDM); electrochemical machining (ECM); intermetallic compounds.

1. Introduction

Although electrochemical machining, electrical discharge machining and chemical machining have not been extensively used as material removal processes on ceramic materials, these nonconventional machining processes are potentially attractive for three reasons: First, the processes are not dependent upon the hardness of the workpiece, secondly, little or no mechanical stress is introduced into the workpiece, and thirdly, there is the possibility that these processes could machine configurations and with tolerances not possible with grinding or chip-making processes.

Basically, one would like to know if these nonconventional processes as related to ceramic materials are technically feasible, economically competitive, and finally, what effect the material removal process has on the properties of the machined ceramic body. It is not proposed that this review will provide the answer to these questions, since it is immediately apparent that there is too little information from which to base any firm decisions. Rather, an attempt will be made to describe the process of electrochemical machining, chemical machining, and electrical discharge machining in a general way and to point out previous experience which may shed some light on technical problems and the effects of the machining process on the properties of the material. The analysis of the economic competitiveness of these processes can at best be only qualitative. This review focuses very heavily on the material removal process for crystallized materials and the ways in which these processes have been utilized. Machining and finishing of glass will only be touched on as it is pertinent to the overall machine process.

The practical application of these processes has in many cases been substantial. ECM has been used as a special production method for the past ten years particularly in broaching, trepanning, hole drilling, and contouring of hard tough alloys. CHM has been available for commercial production for thin complex metal parts, engraving and weight reduction of aircraft parts for 15 years. EDM is a well established process for producing holes and cavities in tough materials, superalloys, refractory metals and cemented tungsten carbides since the mid '50's.

In table 1 some of the parameters of these processes are compared. ECM is a low voltage-high current process requiring greater power than other processes. Both ECM and EDM are close contact operations with gap distances of a few thousandths of an inch, resulting in close tolerances. In table 2 a comparison is made of the effects on machined part. The high power consumption of the ECM process is reflected in the high metal removal rate which is comparable to more conventional milling. All processes can produce good surface finish. Surface damage is of particular concern with EDM, while the damage incurred by ECM and CHM can be controlled by proper procedures.

These processes are relatively proven production techniques for metal while for ceramics

TABLE 1. *Physical parameters*

	ECM	CHM	EDM
Potential (volts)	10	—	45
Current (amps)	10,000 DC	—	60 Pulsed DC
Power (watts)	100,000	—	2,700
Gap (meterx10^2)	0.0203	—	0.0254
Medium	Liquid electrolyte	Liquid chemical	Liquid dielectric

TABLE 2. *Effects on machined part*

	Electrochemical	Chemical	Electric discharge	Conventional milling
	(ECM)	(CHM)	(EDM)	(**)
Removal rates m^3/sec (x10^8)	264	0.42	133	111
Dimensional control m (x10^2)	0.0051	0.0051	.0051	0.0051
Surface finish m (x10^6)	10–250	50–250	25–1200	50–500
Depth of possible damage m (x10^2)	0.005	0.005	0.0125	0.0025

**Stagger tooth milling of 4340 steel.

no commercial or production processes are used with the exception of EDM of cemented carbides. Since ECM and EDM are applicable to materials with relatively high electrical conductivity, these techniques are limited by and large to intermetallic compounds of the carbides, borides, nitrides, silicides, etc., and these materials do not contribute any significant commercial dollar volume. Chemical milling, although more generally applicable, is not widely used, principally because of the slow material removal rate and the difficulties of masking.

Chemical etching and polishing of semiconductors are not covered in this review. References [39] and [40] provide a good discussion of the etchant and procedure for II-VI and III-V semiconductor material.

2. Electric Discharge Machining

2.1. Description of the Process

The process was first developed as a practical method of metal working by Lazarenko and others in Russia during the second world war. Since that time it has come into widespread use for difficult and specialized machining operations. It is used especially for shaping hardened steels and high alloys which are difficult to work by conventional methods, and for special operations such as fine drilling and forming complex shapes. The metallurgical applications of EDM have been extensively reviewed [1, 2, 3, 4][1], and will not be considered here. Its applications to ceramic materials have been

[1] Figures in brackets indicate the literature references at the end of this paper.

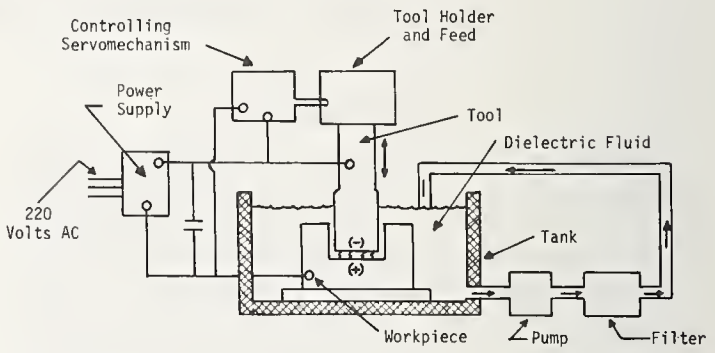

FIGURE 1. *Schematic of a Typical EDM Unit.*

relatively few and are limited to simple shapes such as bending test specimens.

In electric discharge machining (EDM) a series of electric sparks are produced between the workpiece (usually the anode) and a shaped tool which is separated from the work by a thin layer of flowing dielectric liquid (fig. 1). The work (and also the tool) are melted and vaporized by the intense local heating and the resulting erosion product or swarf appears as a dispersion of fine metal particles which are carried away by the flowing dielectric. As the erosion proceeds, the spark gap is kept constant by a servomechanism which advances the tool in response to changes in the gap voltage.

A number of phenomenological descriptions have been proposed for the material removal process. Some mechanisms rely extensively on thermal evaporation, others site shock waves produced by cavitation of the collapsing vapor bubble. Most evidence, however, points to a thermochemical approach. A narrow channel of the dielectric is ionized and the spark discharge occurs as an electron avalanche toward the

anode. The liquid dielectric confines the discharge to a very narrow channel and maintains a very high current density. The avalanche heats the anode causing some evaporation and melting. As the impact area increases and current density falls, the amount of material removed by evaporation reduces and the melting increases as a result of thermal lag. The high temperature gradient results in substantial thermally induced stresses in the subsurface areas. The collapse of the dielectric vapor bubble probably accounts for ejecting some molten material from the crater.

2.2. Effect of Process Variables

The choice of power supply is a major factor in the success of the EDM process. There are three types of spark generators. The particular choice is usually a compromise in speed, accuracy, finish, tool wear, damage reliability and cost. Rotary generators provide long pulses that erode more like an arc and allow large powers to be applied and result in high removal rates. Rotary generators are being replaced by transistor-switched generators. The latter maintain the high cutting rate of the rotary generator while yielding much lower tool wear. For ceramic applications the resistance-capacitance (*R-C*) circuit is most generally applicable (fig. 2). This is a form of relaxation oscillator in which a capacitor is charged through a resistance from a dc power supply. The working gap is connected in parallel with the condenser. When the condenser voltage (Vd) becomes sufficiently high the gap breaks down, and the energy stored in the condenser is released to the spark.

The capacitor C is recharged and the cycle is repeated. The time constant *RC* must be such that the gap voltage does not become so large that arcing occurs. Machining speed is partially a function of spark energy and repetition rate. If the discharge voltage is small compared to the charging voltage, the repetition rate will be high but the energy will be low.

This is a simple and low cost circuit which is at the same time rugged and reliable. In general, *R-C* circuits operate best at relatively high frequency and low machining rates which are the conditions required for ceramics.

The cavity in the work exceeds the size of the tool by an amount corresponding to the width of the spark gap. This is known as overcut and depends both on spark energy and voltage. Low voltage, low energy sparks give minimum overcut.

The use of a liquid dielectric is essential in the EDM process. The liquid not only carries away the swarf but confines the spark energy to a small area. In air or gas the spark energy is spread over a wider area, and little erosion

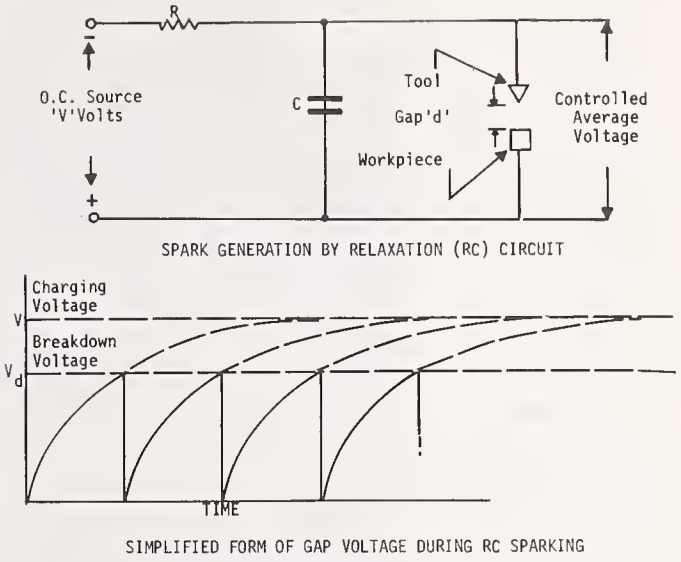

FIGURE 2. *Simplified form of gap voltage during RC sparking.*

takes place. Hydrocarbon liquids such as kerosene or transformer oil are the most commonly used dielectrics, and have the advantage of preventing rust and corrosion. Water and aqueous solutions of polyglycols have been found [1] to give improved machining rates and less tool wear, but they have not yet come into general use.

The erosion rate of both the work and tool depend not only on the spark characteristics and on the dielectric liquid but also on the properties of the materials from which they are made. In general, materials of high melting point and high thermal conductivity are least eroded and therefore most suitable for tool materials (table 3). Tungsten, graphite, copper and brass have been recommended. Since pure tungsten is difficult to machine, a tungsten-silver composite is sometimes used. For ordinary shop work, brass, copper and cast iron are preferred because of their availability and easy machinability. A low-melting alloy of tin and zinc is sometimes used for complex tools be-

TABLE 3. *EDM erosion rates*
(Relative to Copper at 1.0)

Lead	7.0
Zinc	4.5
Aluminum	1.3
Brass	1.1
Copper	1.0
Iron	0.45
Molybdenum	0.39
Tantalum	0.30
Tungsten carbide	0.22
Tungsten	0.19

cause it can be readily cast to shape and is reusable.

Samsonov and Mukha [5, 6] have studied the behavior of many electrode materials and have correlated their results on the basis of electronic structure. Since the electronic structure also correlates with melting point and thermal conductivity, their work leads to the same general conclusions as the melting-point correlation [1].

2.3. Applications to Ceramics

a. Advantages and Limitations of E.D.M. for Ceramics

With minor exceptions (see 2.3.c. below) the EDM process can be applied only to electrically conductive materials. There is no well defined limit of conductance to which spark machining is limited. Increasing the resistivity of the work, however, is equivalent to putting a resistance in series with the spark gap, which limits the current and absorbs energy which would otherwise be available to the spark. Walson et al., [4a] report cutting germanium crystals having a resistance of 31 ohm cm with low spark energies of 10^{-3} to 10^{-4} joule. It is probable that resistivities much greater than this would seriously limit the cutting process. For instance, it has taken 10 hr to cut 1 in (2.5cm) boule of 300 ohm cm silicon. This requirement eliminates the bulk of the conventional ceramic and vitreous materials and limits the application to conductive intermetallic compounds such as the borides, carbides, nitrides and silicides. Examples which will be discussed in further detail include zirconium carbide and nitride, chromium carbide, molybdenum silicide and cemented carbide cutting tools.

A major advantage of the EDM process is that the removal of material is not influenced by the hardness of the work. The removal rate is affected by the melting and boiling point of the work material, and very refractory materials such as ZrC and ZrB_2 are appreciably slower cutting than less refractory substances. We find that removal rates of $10^{-4}-10^{-5}$ in ^{3}/min ($10^{-7}-10^{-8}$ m^3/s) about the optimum. The energy available from the spark, however, is enough to erode any known material including graphite and tungsten compounds.

A second advantage is that the tool does not contact the work and therefore exerts no force on it. This is particularly valuable in the cutting of very brittle materials such as molybdenum silicide. The dielectric fluid exerts some pressure on the work, especially if it is pumped through a hollow tool. This hydrostatic pressure is appreciable only for large pieces, however, and is not ordinarily a factor in shaping ceramics.

The major drawback to the application of EDM to ceramic-type materials lies in the nature of the surface produced by the process. This surface consists of a layer of resolidified melt whose topography consists of small overlapping craters left by the spark together with solidified drops and splashes of liquid. There is also a region of heat-shocked but unmelted material. In the case of brittle materials, both these surface zones contain an abundance of flaws and microcracks which seriously impair the strength of the machined piece (fig. 3).

The extent of the cracking of the surface of large grained polycrystalline $MoSi_2$ depends on the spark energy. Energies above 10^{-3}J produced severely rough and extremely cracked surfaces. We have found that slower cuts at lower spark energies are required for preparation of rough crystals of borides, carbides and silicides.

The nature of the spark-eroded surface is shown in figure 4, which is a scanning electron micrograph of a surface of zone-melted molybdenum disilicide ($MoSi_2$) which was cut off with a 0.015 in (0.035cm) copper wire tool on a "Servomet" machine made by Metals Research Ltd., of Cambridge, England. This machine employs an R–C circuit and the surface

Table 4.

Material	Spark energy (Joules)	Depth of damage (Meters × 10^{-6})	Tool
Copper	5×10^{-3}	1100	Rotating wheel
	5×10^{-6}	300	Rotating wheel
	5×10^{-6}	80	Wire
Fe-3.2%Si	0.6	150	Wheel
	5×10^{-6}	<2	Wire
Tungsten	5×10^{-6}	<10	Wheel
CO/WC	3.6×10^{-2}	200 (Hardness)	?
CO/WC	3.6×10^{-2}	10–50 (Cracks)	?

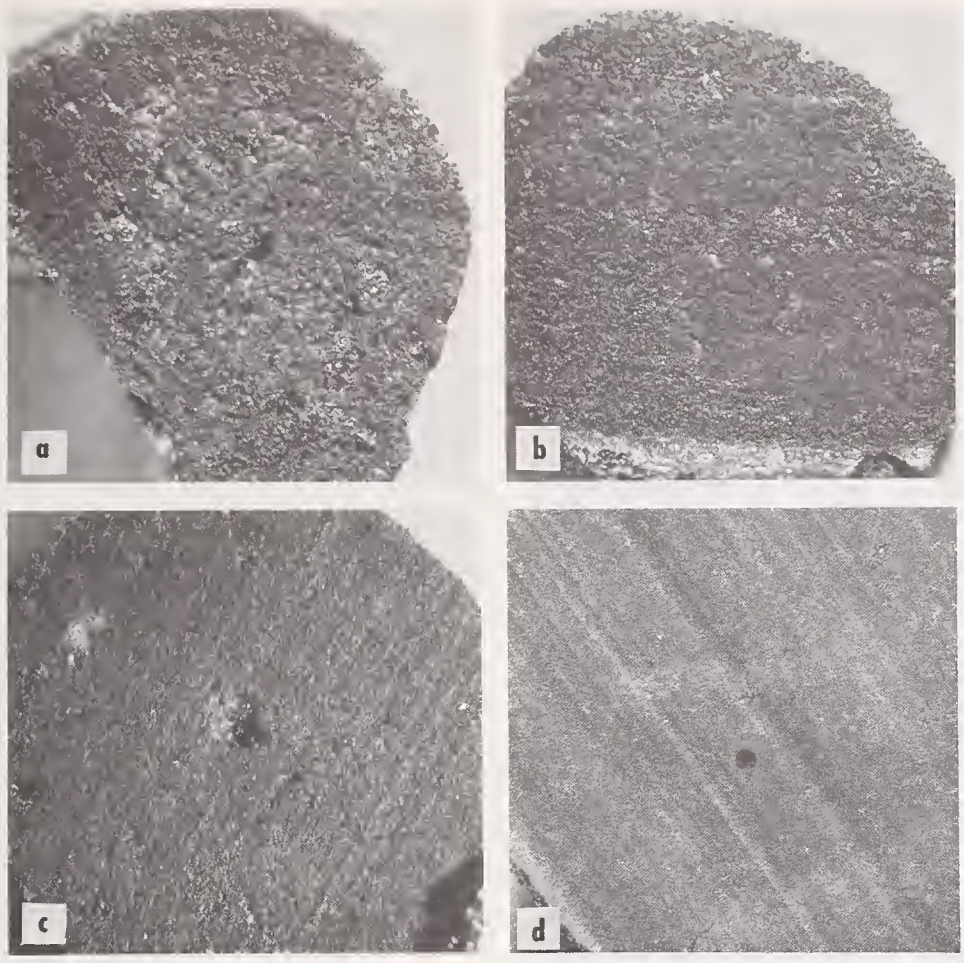

FIGURE 3. *Macrostructure of $MoSi_2$ cut with EDM*
(a) 1.5×10^{-1}J
(b) 2.5×10^{-2}J
(c) 6.5×10^{-3}J
(d) 1.3×10^{-3}J

shown represents a moderately heavy cut (225 v, 1μf, 108 ohms). The surface shows the pitting caused by the sparks together with droplets of resolidified material. The diameter of the piece was 0.235 in (6mm) and the time for cutoff was 14 min. The overcut was about 0.0025 in (0.06mm).

As the energy of the spark discharge is increased, the depth of the damaged layer becomes greater (table 4). This fact limits the spark energies and thus the cutting rates for ceramics to relatively low values as compared to those used for ductile metals.

Spark damage to germanium crystals was studied by Walson et al., [4a]. At spark energies less than about 10^{-4} joules, no surface or subsurface damage could be detected by polishing and etching. Above 10^{-3} joules, however, cracks and dislocations were abundant.

b. Refractory Intermetallic Compounds

Lanin et al., [8] studied the bending strength of ZrC specimens cut by the EDM process, some of which were subsequently lapped with boron carbide powder (fig. 5). They found that the EDM cut surfaces were extensively cracked, especially at higher machining rates (corresponding to greater spark energies), and therefore very weak. Removal of about 50μM of the damaged material from the surface by lapping increased the bending strength by as much as 50 percent in some cases.

Similar results were obtained with ZrN by Yanchur et al., [9] who found that the bending strength of spark-cut single crystals could be improved by about 30 percent by lapping with boron nitride. Even higher strength was exhibited by polycrystalline samples with undisturbed surfaces made by pressing and sintering.

In our laboratories we have utilized EDM techniques for many years to cut and shape single crystals of carbides and diboride (ZrC and ZrB_2). Specimens for deformation studies were rough cut using a tinned copper wire and spark energies of $10^{-3}-10^{-4}J$. In order to remove possible surface damage, specimens were chemically polished to remove up to 25 microns of the surface before testing.

c. Cemented Carbides

Artamonov et al., [10] report that surface damage to cemented chromium carbide was caused by loss of bonding metal from between

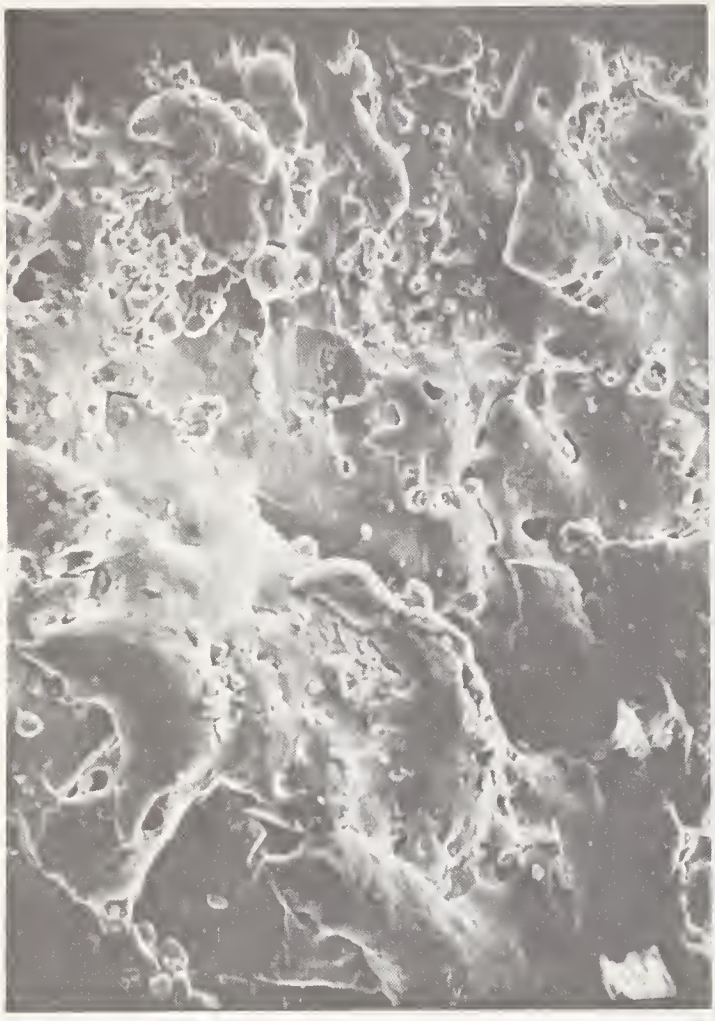

FIGURE 4. *Scanning Electron Micrograph of Surface of $MoSi_2$ after EDM Cutting at 225 Volts, 108 Ohms, 1μF. 625X.*

the carbide grains. Mechanical weakening can be minimized by using short, low-energy pulses with water as the dielectric.

The EDM process has been of some interest for sharpening and shaping cemented carbide cutting tools. Matsuyama and Fukatsu [11] report that in some cases, the electrically sharpened tools containing WC and TiC will give better life than those sharpened by diamond grinding. They attribute the improved life to a new intermetallic phase, detectable by X-ray diffraction, which may be a solid solution of WC, TiC and TiO. Spark energies of 10^{-3} to $10^{-2}J$ are sufficient to form the new phase, however, if the spark energy is too high the heat-affected layers become extensively cracked, and tool life is adversely affected. Based on hardness measurements, the authors report effect of the order of 200μ below the surface. (See table 4.)

The surface layers on electrically machined straight WC–Co were examined by Filimonenko et al., [12] who find that the original hexagonal WC phase is changed to a mixture of W_2C and a face-centered cubic modification of WC. The relative amount of the phases varied inversely with the spark energy and the specific surface reaction depends on the cobalt content.

d. Nonconducting Ceramics

It is usually considered that non-conducting ceramics are not amenable to the EDM process. Saito et al. [13], however, report that the surface of alumina and similar materials may be etched by covering the surface with a thin layer of electrolyte (e.g., NaOH, HCl or HF) in a container of the same liquid in which an inert electrode is immersed. Electrical discharges are generated at the edge of a second

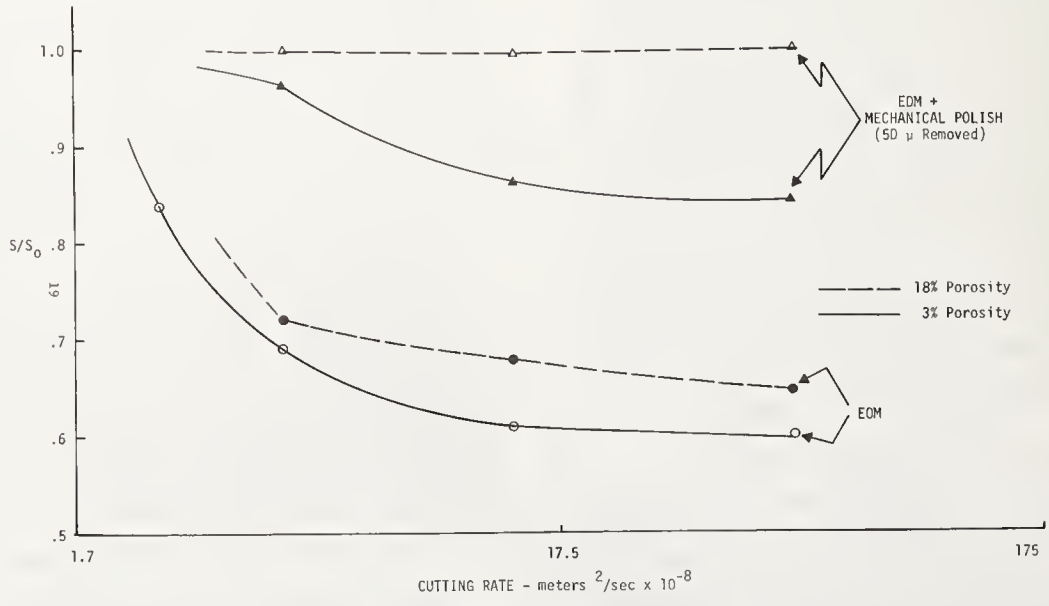

FIGURE 5. *Cutting rate—meters²/sec × 10^{-8}*

electrode which is in contact with the wet ceramic surface and is moved about to give a uniform effect. However, since the rate is slow and the material removal is limited to the edges of the inert electrode, it is doubtful if the process can be utilized as a significant material removal process other than to prepare ceramic samples for microscopic examination.

3. Electrochemical Machining

3.1. Description and Scope of the Process

Controlled electrolytic removal of the metal was first practiced as a method of preparing polished surfaces by Jacquet in 1935, although ECM was first proposed by a Russian, W. Gusseff in a 1929 patent. It was not until about 1950 that any general use was made of the technique.

In the electrochemical machining (ECM) process, the tool and the work are separated by a thin layer of flowing electrolytes—such as an aqueous solution of sodium chloride, nitrate or chlorate—while a heavy DC current is passed between the two (fig. 6). The workpiece is made the anode and the tool is the cathode. Metal is dissolved electrolytically at the anode and is usually precipitated as a hydroxide sludge in the electrolyte by hydroxyl ions generated at the cathode. The electrolyte may be recirculated after filtering to remove this sludge. ECM has come into extensive use in the metalworking industries for the formation of complex shapes of difficult metals such as one piece, high alloy turbine blades, small holes and fragile parts. The process parameters and metalworking applications have been the subject of extensive recent reviews [1, 14, 15, 16, 17, 18, 19].

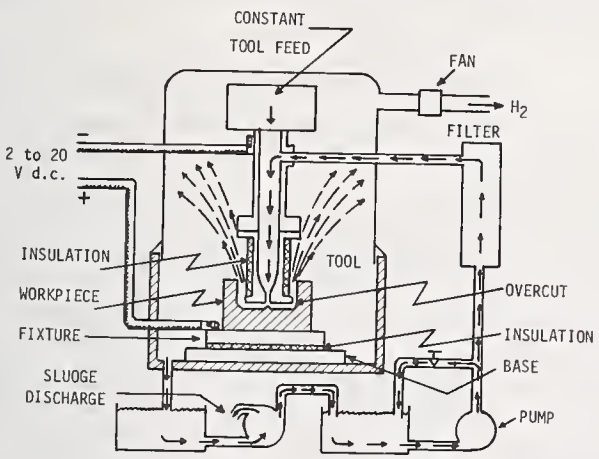

FIGURE 6. *Schematic Diagram of Electrochemical machine.*

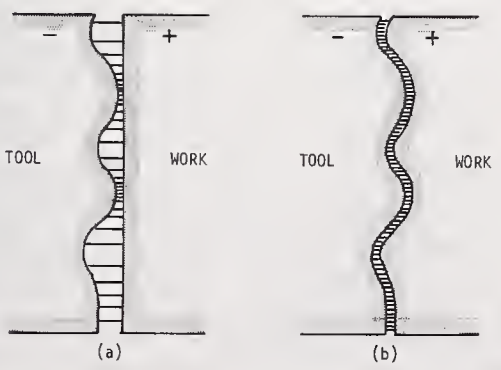

FIGURE 7. *Electrochemical machining.*

Essentially ECM involves passing current through an electrolyte in the gap between the workpiece and a suitably shaped tool (fig. 7). In electropolishing the asperities on the surface have the effect of concentrating the current to the workpiece at these points so they are preferentially removed—in ECM the tool concentrates the current on these parts of the workpiece from which preferential removal of material is required, i.e., the shape of the workpiece then becomes complementary to that of the tool as the process proceeds. The maximum amount of material removed depends on the current flowing and theoretically is given by Faradays law. In practice, rates are usually 75–100 percent of theoretical.

The gap between the workpiece and tool depends on the material removal rate and how the tool is advanced. Control of the working gap is important also in its effect on the flow of the electrolyte. Adequate flow is necessary to prevent overheating and boiling as a result of joule heating since overheating changes the conductivity of the electrolyte. Depending on the application gaps vary from 0.005 − 0.030 in (0.0127 − 0.076 cm). Small gaps give more accurate shapes but large pressures are required to give adequate electrolyte flow.

Although the main function of the electrolyte is to provide ions to carry current in the cell, the electrolyte must be capable of dissolving the workpiece and avoid the formation of insoluble products that may passivate the surface.

The ECM process has many points of similarity to EDM but there are also some differences of importance to the machining of ceramics and other brittle materials. Like EDM, the use of ECM requires that the work be electrically conductive, and it is not affected by the hardness of the work. The tool does not normally contact the work, and the process is therefore well suited to the fabrication of brittle materials.

Specific types of material removal processes applicable to ECM include turning, trepanning, drilling and milling (fig. 8). By feeding a shaped tool into a rotating workpiece, sequential turned parts can be made. Only small tools are required for even large pieces and thin sections can be made since there are no distortions. Milling of tungsten carbide tools can be done without an abrasive using an aluminum

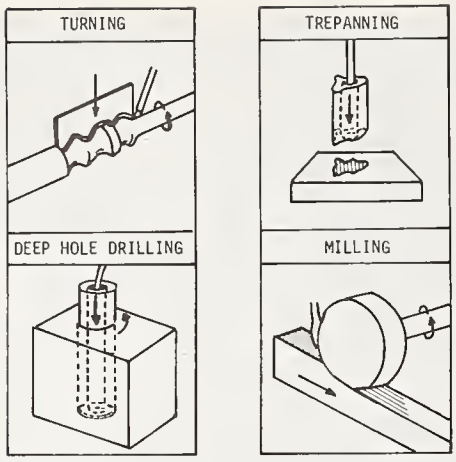

FIGURE 8. *Applications of Electrochemical machining.*

wheel and sodium nitrite. In drilling the tool is a tube with insulated sides and the electrolyte is forced down the center. Although overcutting is minimized by insulating the tool down to the tip, some enlargement is always found. ECM drilling is particularly useful for producing deep small holes, i.e., 0.035 inch diameter × 12–24 in long (0.089 cm by 30–60 cm).

Unlike EDM, however, no melting of the work takes place, and no stress or damage is introduced into the machined surface. In many cases a very smooth or polished surface is obtained. A wide choice of electrolytes is available, and the electrolyte must be chosen to produce the desired surface on the material being worked. Some factors influencing the choice of electrolytes are discussed by Hoare, et al., [20], and by Boden and Evans [21].

3.2. Electrochemical Grinding

Although ECM has not been extensively used for cemented carbides, a related process—electrochemical grinding or ECG—has been extensively used for shaping and sharpening carbide tools [1, 15, 25, 26]. In this process the tool is a metal-bonded diamond wheel which rotates against the work and is fed with an electrolyte instead of a conventional coolant (fig. 9). Current is fed to the wheel through a slip-ring and passes through the electrolyte and the work, the latter being the anode. Metallic contact is prevented by the diamonds projecting from the wheel surface. Most of the stock is removed electrolytically with only a minor fraction being removed by mechanical grinding. As a result, the consumption of diamond is reduced, the rate of cutting is increased and the surface finish is improved. The ECG process is said to reduce grinding costs by 25–40 percent and to reduce diamond consumption by 90 percent [15].

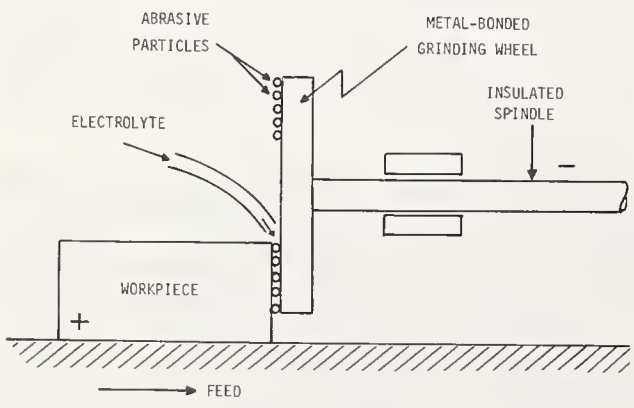

FIGURE 9. *Electrolytic grinding.*

The main function of the abrasive grain is to provide insulation between the anode and cathode and to determine the gap. The particles also continually remove any passive layer that might form. Wheels for electrolytic grinding differ from conventional wheels in the concentration and size of the abrasive particles and in the method of manufacture. Since relatively low metal removal rates are required and because of the mechanical action of the wheel, the electrolytes are generally chosen to avoid corrosion of the machine. Solutions of sodium nitrate, sodium nitrite, sodium phosphate, etc., are common for cemented carbides. Phosphate dissolves the cobalt binder phase and should be avoided. Sodium silicate tends to give better results for WC/Co materials. Current densities are of the order of 100–800 amp/sq in (16–150 amp/cm^2) at 5–20v.

3.3. Application to Ceramics

Up to the present time ECM processes appear to have seen little application to refractory materials.

Cook and his coworkers [22] attempted to increase the material removal rates by using high pressure aqueous electrolytes and molten salt electrolytes. A number of electrolytes were investigated (fig. 10) and the effect of fused NaOH was significant. The material removal rates for several electrolytes are given in table 5. The use of high pressure and fused salts to get higher current densities without boiling of the electrolyte results in substantially increased removal rates.

Lee and Haggerty reported on electrochemical machining of ZrC [23] and ZrB_2 [24]. In these cases the process was used to obtain thin sections for electron transmission microscopy. Single crystals were oriented by X-ray back reflection and the goniometer was transferred to an EDM setup and sections 0.010 in (0.0254cm) thick were cut. The sections were then electrochemically thinned. The apparatus was a typical laboratory electropolishing setup (fig. 11). The electrolyte was four parts methyl alcohol to one part perchloric acid at −35 °C. The situation was more akin to electropolishing in that thin flat specimens were required and

TABLE 5. *Cemented tungsten carbides* [22]

Condition	Current densities	Material removal rate
	(Amps/m²×10⁻³)	*(m/sec ×10⁻⁶)*
NaoH (20%)	465	2.54
Electrolytic grinding	930	6.35
Pressurized tool and electrolyte	1450	33.5
	2930	41.5
Fused salt (NaoH) – 900° C	1800	28.5

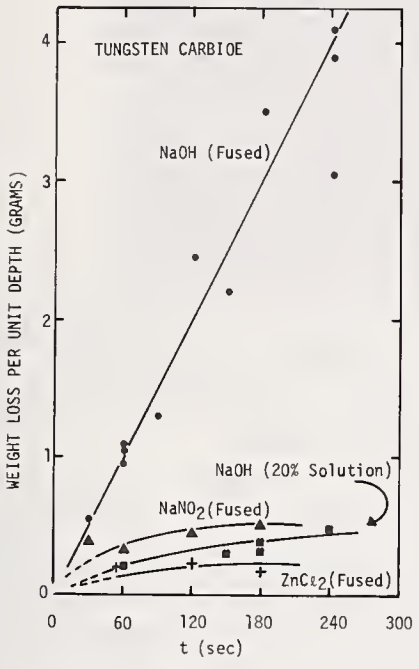

FIGURE 10. *Material removal rates for tungsten carbide in various eletrolytes* [22].

the working gap was very large. Sections were of the order of 500–1000 Å thick.

The problem of possible damage to the section was considered. Etching and X-ray topography were used to show that the dislocations in as grown crystals were largely in low angle boundaries and that the area between the cell boundaries were essentially free of dislocations (fig. 12). The misorientation calculated for the X-ray image was of the order of 0.01 degree and therefore a dislocation spacing of ~1.6 microns. Examination of the ECM prepared sections in electron transmission revealed few dislocations and those that were observed were in row with spacing of approximately 1 micron (fig. 13). Another example is the Burger vector determinations made on ZrB_2 (fig. 14).

We have found the thinning technique to be applicable to the carbides and diborides of hafnium, tantalum, zirconium and titanium as well as $MoSi_2$.

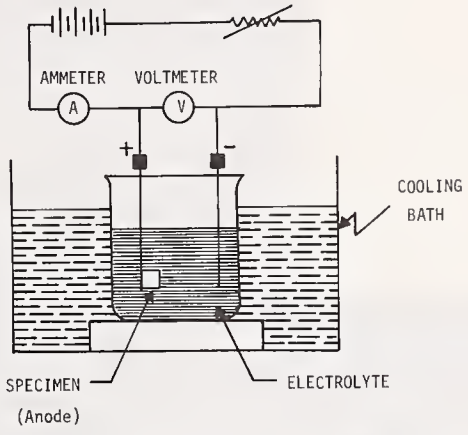

FIGURE 11. *Cell for electrolytic polishing* [15].

4. Chemical Machining

4.1. Description of the Process

Chemical machining (CHM) is a term recently applied in the metalworking industry to the removal of material by simple etching processes, without the use of an electric current (fig. 15). The process shares most of the characteristics of ECM with the additional caution that some etches may cause hydrogen embrittlement on sensitive materials. Much of the art involved in CHM lies in the application of the masking material or resist which blocks the action of the etch from selected areas. Three general methods are in common use. In the "cut and peel" method a thick layer of masking lacquer is applied to the entire metal surface and allowed to dry. The areas to be etched are then cut out and peeled off, thus exposing the metal. This method is adapted to the production of large parts with simple patterns such as aircraft wing sections. Because the masking agent can be heavily applied, it is capable of withstanding deep and severe etches. Stepped work can be made by removing portions of the resist between etching periods.

The second method of masking involves the use of a photoresist, which is coated on the surface and allowed to dry. The areas to be protected are exposed to actinic light through

FIGURE 12. *(a) Single crystal of ZrC etched on a (100) plane in 1:1 boiling H_2SO^4 to show both individual dislocations and dislocation of sub-boundaries, 9X.*
(b) X-ray image of same area as in (a) showing the boundaries to be of a tilt character, 5X.

FIGURE 13. *A row of dislocations which form a low angle boundary in an undeformed ZrC single crystal.*

a suitable mask, which renders the resin insoluble in a developing solvent. The image is then developed by washing off the unexposed areas with the solvent. The remaining image may be baked to increase its chemical resistance and the part is then exposed to the etching liquid. The photoresists are generally not able to withstand severe etching conditions and they are mainly used for fine work and complex parts.

The third method of applying the masking agent is by way of the silk screen method. This method is adapted to moderately severe etches and moderately complex patterns, but the accuracy is not as great as may be obtained by the photographic method.

The etches applicable to various metals and a general review of the process are given by Springborn [1].

For many years simple etching processes using wax resists and hydrofluoric acid etches have been used for the decoration of glassware and polishing of TV face plates. Similar methods have been used for frosting electric light bulbs, although etched surfaces are now being replaced by sprayed coatings. The production of complex and precise parts of vitreous materials, however, became practical only after the development of the photosensitive glasses.

4.2. Photosensitive Glass

Photosensitive glasses and processes for chemical machining were described by Stookey [27, 28, 29] of the Corning Glass Works in 1953 and following years. These glasses contain a metallic photosensitizing agent (such as Cu, Ag or Au) which will precipitate as fine particles when the glass is exposed to light and moderately heated. When the exposed glass is further heated to a temperature below the softening point, these metalic particles serve as nuclei for the growth of a crystalline silicate phase, which eventually results in substantially complete devitrification of the exposed areas. The areas which have not been exposed to light remain in the vitreous form. If the heat-treated glass article is now exposed to hydrofluoric acid, it is found that the exposed and

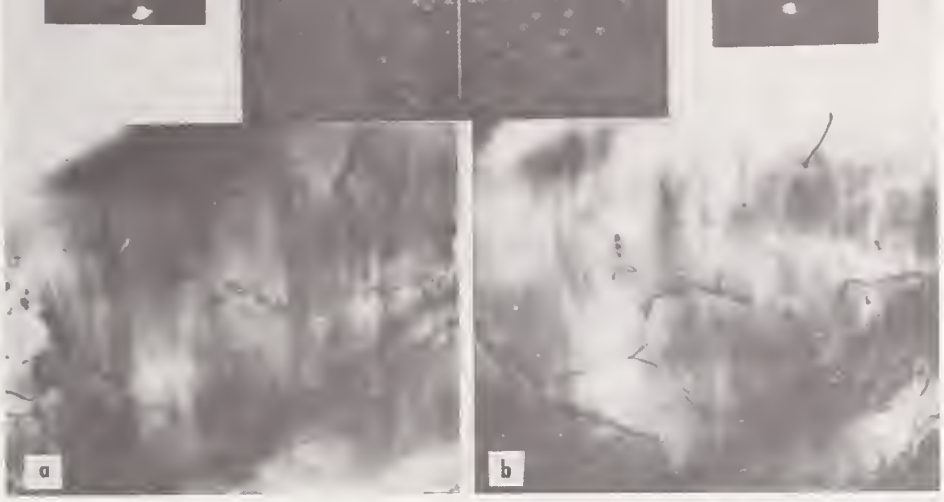

FIGURE 14. *Dark field transmission electron photomicrographs of ZrB_2.* (a) is taken with the (0110) plane diffracting. Magnification app. 17,500X.

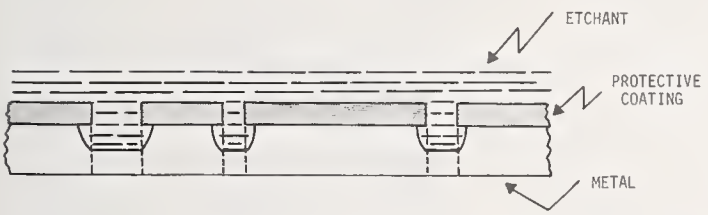

FIGURE 15. *Chemical milling.*

devitrified areas are much more rapidly attacked than the unexposed areas. In this way, complex patterns, perforated parts and shaped electrical insulators can be mass produced. After the parts are etched they can be converted into a glass-ceramic (i.e., devitrified) by further exposure to light followed by heat treatment.

4.3. Application to Ceramics

The application of CHM techniques to ceramic materials has been restricted by the lack of suitable etching agents. Politis and Ohtani [30] give a list of suitable etches for a number of ceramic materials to be used in preparing samples for microscopic examination. Alford et al., [32] give the rate of attack of 85 percent phosphoric acid at 425 °C on the 0001 face of sapphire crystals as 0.00025 in (0.00625 mm) per min. Molten K_3AlF_6 at 1000 °C attacks the 1120 surfaces at the rate of 0.0015 in (0.0375 mm) per min.

Tighe reports the use of hot orthophosphoric acid to chemically thin single crystal sapphire at rates of ~1 micron per min. The material removal rate is sensitive to crystal orientation and temperature.

These low rates indicate that the methods are suitable mainly for surface preparation, rather than true shaping operations. A more serious problem is that of finding suitable resists for these conditions.

In reviewing the available literature on the chemical machining of aluminum oxide, it is quite apparent that the material removal rate and the effects of the machining on mechanical properties are dependent on several factors, such as, the type of etchant used, the processing conditions of the machining operation, and finally the compositional variations on the types of alumina investigated. The variables in chemical machining of aluminum oxide has not been systematically studied. However, there is enough information in the literature to indicate that there are major variations in the material removal process that can have a profound effect on the physical properties of the machined body. The work of Kirchner and his coworkers on compositions containing 94–96 percent aluminum is perhaps a unique application of CHM. Starting with a two-phase structure in which both the alumina and intergranular phases are co-continuous, the action of the etchant, in this case, hydrofluoric acid, was a highly preferential attack on the intergranular phases leaving a matrix of high alumina with

TABLE 6. *Chemical polishing of high alumina materials*

Al_2O_3	Etchant	Temperature	Rate		Initial effect on strength
			m/sec $\times 10^8$	in /min$\times 10^{-5}$	
94–96% Al_2O_3 (ρ=3.86 gm/cc)	H_3Po_4	320° C	—	—	Decrease
0.25 SiO_2, 0.25 MgO (ρ=3.87)	H_3Po_4	320° C	1.6	4.1	Decrease
		280° C	0.3	0.8	Decrease
(0.5 MgO) ρ=3.98	H_3Po_4	320° C	>0.01	—	N C
(0.5 MgO) ρ=3.98	H_2So_4	280° C	>0.01	—	N C
94–96% Al_2O_3 (ρ=3.86)	H_2So_4	250° C	0.1	0.2	Increase
(0.5 MgO) ρ=3.98	$Na_2B_4O_7$	800° C	0.8	0.2	Increase
		850° C	2.0	5.1	Increase
		900° C	3.0	7.6	Increase
94–96% Al_2O_3 (ρ=3.86)	$Na_2B_4O_7$	850° C	2.0	5.1	Increase
94–96% Al_2O_3 (ρ=3.86)	$KHSo_4$	650° C	—	—	Decrease

high pore volume. In this condition the high alumina ceramic can be drilled, turned, and otherwise machined. After shaping is complete the pieces can be refired to restore most of the original strength.

In a more general context there have been a number of observations on the chemical polishing or machining of high Al_2O_3 materials (table 6). This data illustrates the variables that can affect the process, particularly the composition of the materials and etchant used.

In general, phosphoric acid is detrimental to the strength of polycrystalline Al_2O_3, while for single crystals Kirchner reported strengths after polishing in 85 percent orthophosphoric acid to be slightly greater than those of the as received controls [34].

On the other hand, CHM of Al_2O_3 in fused sodium borate has resulted in some substantial increase in the strength of several polycrystalline materials [31, 32] as well as single crystals [34, 35].

The effects that CHM may produce on the machined properties of Al_2O_3 material will depend on the dissolution process, i.e., the particular effect the etchant has in producing flaws or change the geometry of existing flaws. Preferential attack of grain boundaries or of impurities or producing etch pits may create new flaws [35].

In figure 16 the changes in flaw geometry which might take place are shown [38]. The flaw may be rounded or blunted (c) in which case we might expect the strength to improve as a result of the material removal process. The existing flaw may be extended or sharpened by preferential attack at the tip as in (a) and the strength would be expected to be lowered. In case (b) the rounding of the crack may be offset by the increase in length and no effect on the strength would be expected due to the corrosion or dissolution process. Thus, one may find a rationale for strength increases, decreases and no change as a result of CHM.

In the Charles-Hillig theory, flaw sharpening is due to preferential attack at the crack tip

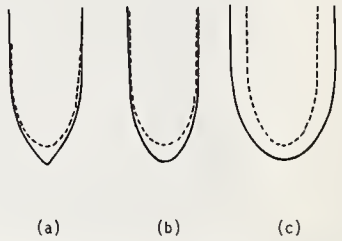

FIGURE 16. *Hypothetical changes in flaw geometry due to corrosion or dissolution.*
(a) Flaw sharpening.
(b) Flaw growth such that the rounding of the tip by stress corrosion balances the lengthening of the flaw.
(c) Simple rounding by corrosion or dissolution (Joffe effect). [38]

through a stress corrosion mechanism. In CHM there is no imposed stress, however, we have found that internal stresses of a thermal nature are sufficient in some cases to provide that necessary for enhanced corrosion.

For instance, polycrystalline $MoSi_2$ undergoes catastrophic failure in O_2 or air at temperatures of 400–500 °C—well below the temperature of significant oxidation—with no external stress applied. Single crystals are not effected. Under similar conditions, however, with external stress, single crystals exhibited static fatigue in the same manner as polycrystalline materials (fig. 17). These results are consistent with the concept of crack sharpening due to stress corrosion according to the Charles-Hillig theory.

We could postulate that depending on the dissolution action of the etchant in producing new surface flaws or altering existing ones, the strength of chemically milled Al_2O_3 may increase, decrease or remain constant (fig. 18).

As far as subsurface damage is concerned, such as introduction of dislocations, the evi-

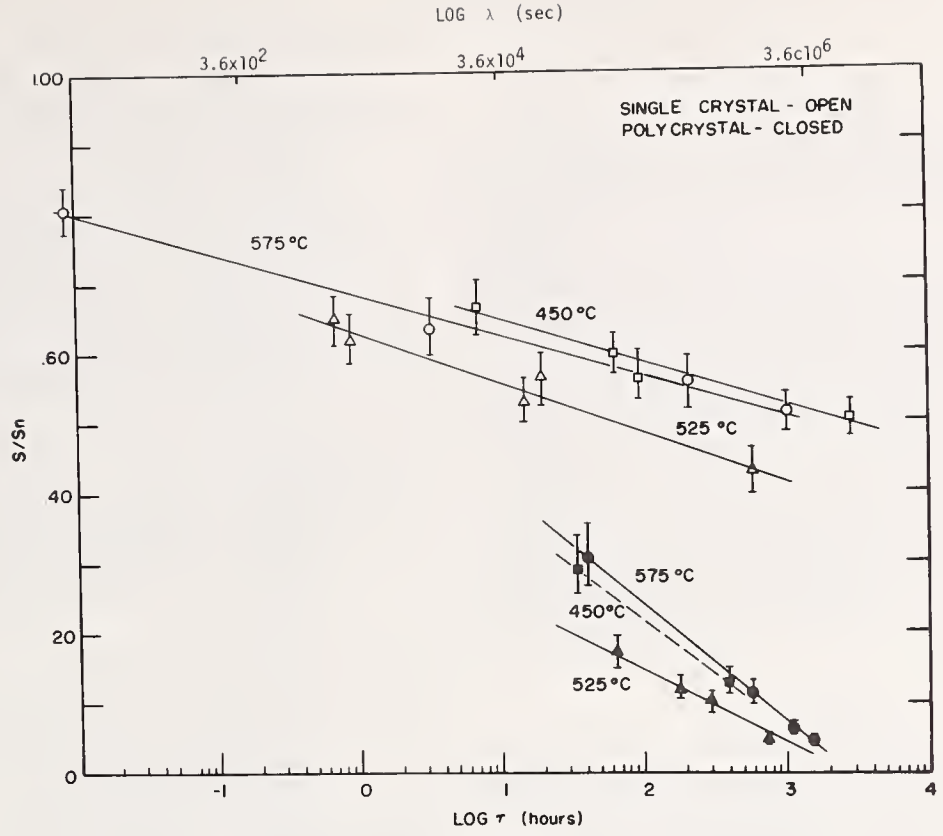

FIGURE 17. *Delayed failure experiments for single crystal, polycrystal and $MoSi_2$.*

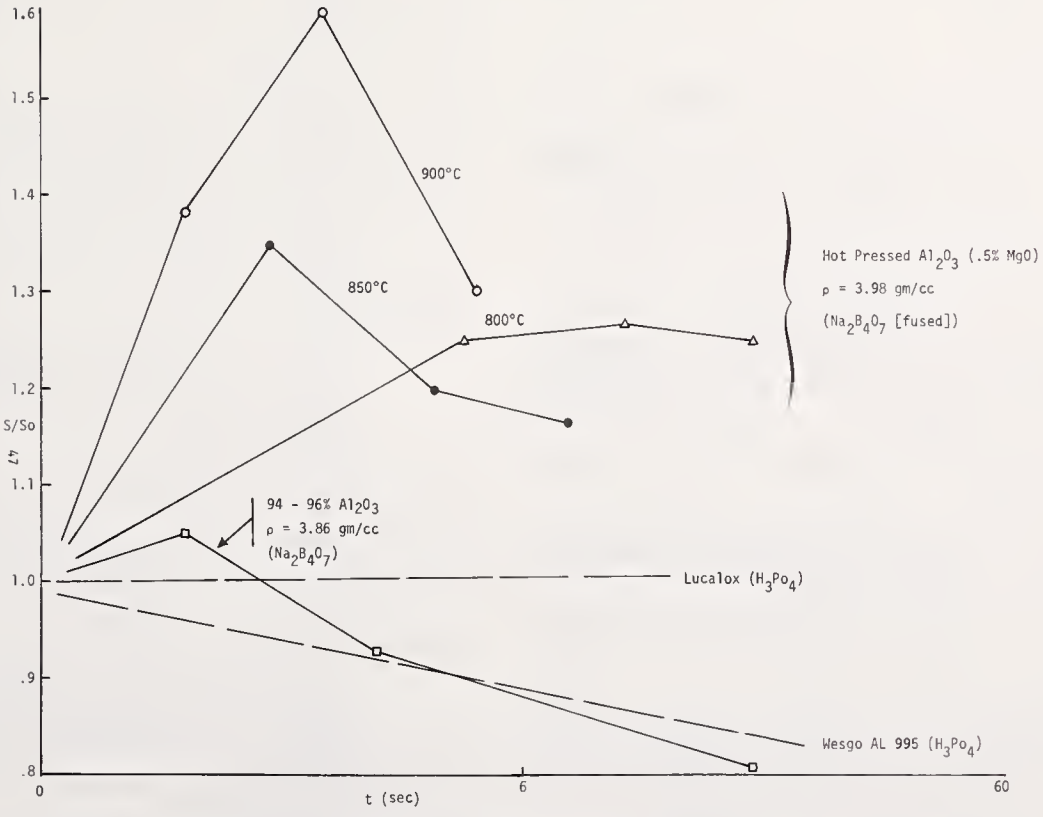

FIGURE 18. *Effect of chemical machining on the transfer rupture strength of polycrystalline alumina oxide.*

dence is that no effects have been observed by Tighe [39] in Al_2O_3 or by Lee and Haggerty in ZrC or ZrB_2.

5. Summary

The process of EDM, ECM, and CHM are attractive techniques for material removal for ceramics; however, little use has been made of these processes. Some part of this is due to the fact that two of the processes are limited to material of relatively good conductivity and to the low material removal ratio of CHM.

It appears that these techniques will continue to be used as a method of preparing special shapes of materials in the laboratory.

In those areas where it has been applied, little information is available on the nature of the prepared surfaces and the extent of any damage. Perhaps a less impirical base would be helpful to choosing machine condition to obtain a desired surface condition and limited but well defined damage.

6. References

[1] Springborn, R. K., Ed., Nontraditional machining process, (American Society of Tool and Mfg. Engineers, Dearborn, Michigan, 1967).

[2] Whiteman, A. R. C., and Leadbetter, R., Electrical discharge machining covering the period 1960 to 1967 (Atomic Energy Research Establishment, Harwell, Berkshire, 1968), (Also available from National Technical Information Service, Springfield, Va. 22151; Accession No. N68-28165).

[3] Krabacher, E. T., Mod. mach. shop 41, (8), 130–137 (1969).

[4] Bucklow, I. A., and Cole, M., Metallurgical Reviews 14, (135), 103–18 (June 1969).

[4a] Walson, R. P., Haworth, W. L., and Birnbaum, H. K., Spark Erosion cutting of Germanium, ONR Technical Report (July 1, 1970).

[5] Samsonov, G. V., and Mukha, I. M., Poroshkovaya Metallurgiya, 7 (67), 81–87 (July 1968).

[6] Ibid, 8 (68) 84–90 (Aug. 1968).

[7] Lee, D. W. et al., Investigation of the Mechanical Properties of Transition Metal Borides and Carbides, Final Report to U. S. Atomic Energy Commission under contract No. AT(30-1)-3411 (14 October 1967).

[8] Lanin, A. G., Fedotov, M. A., and Glagolev, V. V., Poroshkovaya Metallurgiya 5 (65), 97–101, (May 1968).

[9] Yanchur, V. P., Andrievtkii, R. A., Spivak, I. I., and Fedotov, M. A., Neorganicheskie Materials 5 (No. 6), 1012–17 (June 1969).

[10] Artamonov, A., Ya., Lemeshko, A. M., and Murzin, L. M., Poroshkovaya, Metallurgiya 9, 95–100, (Sept. 1969).

[11] Matsumaya, Y., and Fukatsu, T., in Powder Metallurgy, Leszynski, W., ed., 683–700, (Interscience Publishers Inc., N. Y., 1961).

[12] Filimonenko, V. N., Gurland, J., and Richman, M. H., Metallography 2, 125–36 (1969).

[13] Saito, S., Katagiri, M., and Hasegawa, S., J. Ceram. Assoc. Japan 70, (6), 195–9 (1962).

[14] Olofson, C. T., Gurklis, J. A., and Boulger, F. W., in Machining and Grinding of Ultrahigh-Strength Steels and Stainless Steel Alloys, Report on Contract No. DA-01-021-AMC-11651(Z), NASA-SP-5084.

[15] DeBarr, A. E., and Oliver, D. A., editors, Electrochemical Machining (Elsevier, N. Y., 1968).

[16] Throop, J. W., A Mathematical analysis of Electrochemical Machining Phenomena, Paper No. WES7-09 presented to ASM-ASTME 1967 Western Metal and Tool Conference, Los Angeles, (March 13–17, 1967).

[17] Bellows, G., ECM Machinability Data and Ratings, Paper No. WES7-10, presented to ASM-ASTME 1967 Western Metal and Tool Conference, Los Angeles, (March 13–17, 1967).

[18] Hopenfeld, J., and Cole, R. R., Electrochemical Machining-Prediction and Correlation of Process Variables, Paper No. 66-Prod 5 presented to ASME Production Engineering Conference, Detroit, (April 18–22, 1966).

[19] Weingartner, C. J., Electrochemical Machining During Eight Years of Operation, Paper 680659 presented to SAE Aeronautic and Space Engineering and Manufacturing Meeting, Los Angeles, (October 7–11, 1968).

[20] Hoare, J. P., LaBoda, M. A., McMillan, J. L., and Wallace, A. J., J. Electrochem. Soc. 116, 199–203 (1969).

[21] Boden, P. J., and Evans, J. M., Nature 222, 377–8 (1969).

[22] Cook, N. H. Loutrel, S. P., and Meslink, M. C., Increasing Electrochemical Machining Rates, MIT Final report on contract DA-19-066-AMC-268(W), AD659, 004.

[23] Lee, D. W., and Haggerty, J. S., Jour. Am. Ceram. Soc. 52, 642–7 (1969).

[24] Leombruno, W. J., Haggerty, J. S., and O'Brien, J. L., Matl. Res. Bull. 3, 361 (1968).

[25] Benz, H. G., Abrasive Eng. 15, 41–42 (1969).

[26] Marten, K. H., and Heck, K., Werkstatt u Betrieb 101, 615–20 (1968), in German.

[27] Stookey, S. D., Ind. Eng. Chem. 45, 115–8 (1953).

[28] Stookey, S. D., U. S. Patent 2,684,911, July 27, 1954.

[29] Corning Glass Works, British Patent 752,243, July 11, 1956.

[30] Politis, C., and Ohtani, S., Praktische Metallographie 4, (8), 401–16 (1967).

[31] Gruszka, R. F., Mistler, R. E., and Runk, R. B., Ceramic Bull. 49 (6), 575–9 (1970).

[32] King, A. G., Materials Science Research, Vol. 3, edited by W. W. Kreegel and H. Palmaur III, Plenum Press, New York, (1963).

[33] Bortz, S. A. *Ibid.*

[34] Alford, W. J., Bauer, W. H., and Motolka, R. W., Perfection of Single Crystal Alumina Grown in R. F. Plasmas and by Other Techniques, School of Cermaics, Rutgers, the State University, New Brunswick, N. J., June 14, 1966, AFCRL-66-524.

[35] Richel, P. A., Infield, J. M., and Kirchner, H. P., Ceramic Bull. 47, 702–6, (1968).

[36] Kirchner, H. P., Gruner, R. M., and Walter, R. E., J. App. Phys. 40, 3445, (1969).

[37] Malliner, F. D., and Proctor, B. A., Proc. Brit. Cer. Soc. 6, 9, 1966.

[38] Hullig, W. R., and Charles, R. F., in High Strength Materials Surfaces, Stress-Dependent Surface Reaction and Strength, V. F. Zackay, ed. John Wiley and Sons, New York 1965).

[39] Streilow, W. H., J. of Appl. Phys. 40 (7), 2928–2932, (1969).

[40] Gatos, H. C., and Levine, M. C., in Progress in Semiconductors, Vol. 9, Edited by A. F. Gabron and R. E. Burgess, Temple Press, London, (1965).

Discussion

RICE: Would you expect a higher removal rate and possibly less complex surfaces in the machining of materials such as silicon carbides which normally vaporize without melting?

LEE: Yes. I would expect that you would still get some thermal shock in the material. Thermal shock seems to be the major factor causing the poor surface and/or the cracking. I did not find any references to silicon carbide but it would seem to me that silicon carbide is a commercially available refractory material that could be cut and machined quite easily by EDM type techniques.

LASSON: Pertaining to the photosensitive glass that you mentioned, do you know what dimensional tolerance range you would be able to hold? Also, do you get any tapering when you do the etching?

LEE: The tolerance is ± 10 percent. Yes, you do get a 2° taper.

MARTIS: A word of caution concerning EDM and its effect on the removal of cobalt on a wide variety of tungsten carbides. They propagate brittle fracture. This is a major cause of failure.

LEE: Yes, the work done at Brown I believe showed there were extensive areas of cracking of the material, although they didn't make any physical measurements afterwards.

MARTIS: We found you have to remove that particular layer using conventional diamond abrasives.

LEE: That would correlate with the Russian work where they did have to remove at least 15 microns of the material before the strength of the material was restored.

NATIONAL BUREAU OF STANDARDS SPECIAL PUB. 348, THE SCIENCE OF CERAMIC MACHINING AND SURFACE FINISHING, Proceedings of a Symposium Sponsored by the American Ceramic Society, the Office of Naval Research, and the National Bureau of Standards, held at NBS Nov. 2–4, 1970, Gaithersburg, Md. (Issued May 1972).

III. TECHNIQUES AND MECHANISMS OF SURFACE FINISHING

Session Chairman
P. J. Gielisse, University of Rhode Island

Improvements in the Surface Finish of Ceramics by Flame Polishing and Annealing Techniques

M. J. Noone
General Electric Company, Philadelphia, Pennsylvania 19101

A. H. Heuer
Case Western Reserve University, Cleveland, Ohio 44106

Improvements in the surface perfection (i.e. "smoothness") of ceramics can be achieved by thermal treatments at temperatures where material transport may be induced at the surface. Such treatments include annealing in controlled environments, where surface diffusion, vapor transport mechanisms, etc., may be active, and flame polishing, where a thin layer at the surface of the material is melted, allowed to flow freely, and then resolidified.

The effects of these treatments on the surface of single crystals of α–Al_2O_3 are reviewed in this paper. The most sensitive assessment of the degree to which surface perfection is attained is the measurement of the strength of the treated crystals; for this reason, strength data are used extensively to characterize the thermal treatments described. In the case of flame polishing, it found that a sufficient degree of surface perfection can be attained so that the strength is no longer limited by surface defects (the usual experience with ceramics) but by defects within the material. The technological significance of high strength Al_2O_3 filaments for reinforcement of metals and the unfortunate deterioration of the surface in these applications is briefly described.

Key words: α–Al_2O_3; annealing; flame-polishing; reinforcements; ruby; sapphire; strength; surface perfection.

1. Introduction

Improvements in the surface finish of single-crystal specimens of $\alpha - Al_2O_3$ can be achieved by thermal treatments at temperatures up to and including the melting point. Two regimes of temperature are considered separately in this paper: (a) annealing at temperatures up to 1800 °C; and, (b) flame polishing in a steep temperature gradient which includes melting of a thin layer of material at the surface. Improvements in the surface perfection or smoothness arise by movement and redistribution of material at the surface; in the former case (a) by surface diffusion and/or by evaporation and subsequent recondensation, and in the latter case (b) by rapid material transport in a liquid film. The improvement in the surface perfection which arises from any particular treatment can best be measured by determining the changes in strength that are produced in the material, since the strength of single-crystal brittle materials is determined almost entirely by the condition of their surfaces. Flame polishing in particular produces striking changes in strength, since it completely melts all pre-existing surface damage and leads to a "liquid smooth" surface.

Although this paper is devoted exclusively to single crystal $\alpha - Al_2O_3$ (sapphire) and/or Al_2O_3:Cr (ruby), the techniques and mechanisms discussed are applicable to a wide range of ceramic crystals. In the case of brittle ceramic polycrystals however, thermal treatments generally do not produce such profound changes in strength as are found for single crystals; microstructural features absent in single crystals—grain boundaries, second phases, and voids—may limit the surface perfection achievable. Furthermore, such "defects" may be preferentially etched or otherwise accentuated by thermal treatments,[1] thus leading to a degradation of strength. The low strength of brittle single crystals is a result of an abundance of surface defects microcracks and notches—which are introduced during the cutting and grinding operations used to shape a specimen from a bulk crystal. Since such materials are unable to undergo appreciable plastic deforma-

[1] Since the strength of polycrystalline ceramics invariably decreases with increasing grain size, thermal treatments which induce appreciable grain growth will also lead to a loss in strength.

tion at room temperature, stress concentrations arise at the tips of these cracks (or notches) when the crystals are stressed and result in low strengths. The flaw theory of brittle fracture advanced by Griffith [1][2] completely accounts for this phenomenon. (Griffith was able to show that high strengths could be attained in brittle materials (glass fibers) by careful preparation of flaw-free surfaces.)

The existance of a surface perfection/strength relationship in bulk $\alpha-Al_2O_3$ crystals was demonstrated most spectacularly by Morley and Proctor [2], who measured strengths in excess of 7 GN/m^2 (10^6 psi) in carefully flame-polished rods. The strength of these rods was similar to that of α–Al_2O_3 whisker crystals [3] which were considered to have highly perfect internal as well as surface structures. However, the surfaces of $\alpha-Al_2O_3$ whiskers are not atomically smooth; on the contrary, Mehan and Feingold [4] reported growth steps and other surface protruberances to be common features. Marsh [5] showed that a step on a crystal surface could cause a stress concentration of the same magnitude as that around a crack of similar dimensions, which accounts for the fact that, even with whiskers, the measured strength, although often high, rarely approaches the theoretical estimates of the strength. (For alumina, the theoretical strength is of the order of $\frac{E}{15}$ [6]).

Although annealing can also increase the strength of ground sapphire, the strength increases achieved are not as dramatic as for flame polishing; presumably, the degree of surface perfection achieved is greater for the latter process. Nevertheless, annealing may have some technological importance, inasmuch as flame polishing appears to be restricted to simple shapes.

In view of the fact that there appears to be unfamiliarity with the techniques of flame polishing, the nature and experimental details of the process are discussed at some length in this paper (sections 2 and 3). By way of contrast, the literature on annealing is reviewed only briefly, with major emphasis on the degree of strength improvements that have been reported (section 4).

2. Previous Work on Flame Polishing

The earliest reported exploitation of flame-polishing on sapphire was in 1952 by Popov [7] and by Barnes and McCandless [8] who independently developed the process to improve the surface smoothness of crystals for use as thread guides in the processing of textile fibers. Flame polishing was found to be superior to chemical and mechanical polishing for this purpose and has been in general use for many years as a means to reduce friction in thread guides and to improve the surface appearance of simple cylindrical shapes.

Barnes and McCandless [8] described a process for flame polishing sapphire and ruby rods which produced scratch-free, glossy, and wear-resistant surfaces suitable for low friction applications. They melted the surface of a rotating rod using a flame which traversed the length of the rod, and left a resolidified smoothed surface in its wake. Only rods less than 5mm diameter could be successfully polished without fracturing and the best quality surface was achieved on rods in which the c-axis made an angle $<65°$ with the rod axis (growth direction). Flame-polished $\alpha-Al_2O_3$ rods had an average tensile strength of 0.7 GN/m^2 compared to 0.46 GN/m^2 for the as-grown material.

Popov was also the first to report plastic bending of sapphire rods and developed an apparatus for bending flame-polished rods to form curved textile guides [7]. Although the conditions were not well defined in his work ("temperature near to the melting point") a relationship was noted between resistance to bending and the crystallographic orientation in the plane of bending, with almost a factor of two difference in the bending force required between different orientations. The rods had "slip-plane traces" on their surfaces after bending [7] and no doubt also contained extensive deformation twins. The strength of the flame polished rods was not determined during Popov's work.

Popov used as-grown Verneuil sapphire rods, 4—4.5mm in diameter, and polished these by rotating them in an oxy-hydrogen flame at 110–115 rpm in a vertical plane: the polishing was performed within a muffle furnace, which allowed preheating of the rods and slow cooling after polishing. The flame gases were metered separately and mixed roughly in the ratio $1O_2$:$2H_2$ by volume; they were fed through a burner orifice approximately 4 mm in diameter at a distance of 75—80 mm from the rod. The rotating rod was withdrawn downwards through the flame at a rate of 20—25 mm/min. by an automatic screw mechanism. Popov recommended that the polishing operation be repeated at least twice on each rod and that for uniform polishing, it was essential that the rod be concentric with the furnace and for the rotation rate, withdrawal rate, and gas flows to be maintained constant during the operation. No optimum conditions could be established and each polishing unit had to be set up individually, by qualitative assessment of the polished surface in reflected light microscopy at low magnification.

The surface features observed on these rods

[2] Figures in brackets indicate the literature references at the end of this paper.

were similar to results obtained by the present authors using "over-polishing" conditions (section 3.1 below). Although Popov states that ideally only a "thin" layer of material was melted, it is likely that he had to fuse up to 0.5 mm depth of material to accommodate irregularities in diameter and the slightly elliptical nature of the cross section of the as-grown rods. A pronounced ripple was evident on the surface of the rods and many entrapped bubbles were found, together with parabolic markings which probably represent a tendency for the development of crystal facets (see section 3.1); the ripples and thermal etching effects were found to vary with, and relate to, the crystallographic orientation of the rod. Popov also made the observation that contamination of the surface by refractory dust (from abrasion of furnace bricks, etc.) during polishing would result in fusion of particles into the surface, rendering the rod unserviceable as a textile guide. As will be shown later, the presence of contaminants or even coarse Al_2O_3 particles fused into the surface severely limits the strength that can be achieved in flame-polished rods.

Sapphire and ruby rods are available in flame-polished form from a number of commercial suppliers; however, the extent of the polish is generally limited to the point where the material surface is improved aesthetically by appearing glass-smooth on a macro-scale (underpolished in the context of the rods described in this paper). These materials have been used for studies of the mechanical behavior of α–Al_2O_3 (e.g., ref. 9) and the fracture stress is generally only modestly higher than centerless ground rods. A significant advance in the state of the art of flame polishing was made by Morley and Proctor [2] who showed in 1962 that the technique could be used to produce surfaces on sapphire rods with such a high degree of perfection that the strength of the resulting crystals was not limited by the surface condition but by internal defects. Carefully polished rods were bent to over 2 percent elastic strain, and for the first time, stresses in excess of 7 GN/m² were measured in bulk ceramic crystals [2] Proctor, in discussing these results, [10] compared them with results from fused silica and silicate-glass rods with highly perfect surfaces prepared with similar care, and concluded that a strength/size relationship was not valid in sapphire or glasses; a strength/surface-condition relationship dominated the mechanical behavior. Further work by Mallinder and Proctor [11] showed that internal defects, inclusions, bubbles, etc., became significant in limiting the strength of rods when the surface was highly perfect and that the highest strengths were attained in rods with a high degree of both surface and internal perfection.

Mallinder and Proctor described the flame-polishing of centerless-ground sapphire rods 3/4, 1, or 2–1/4 mm diameter and 6–8 cm long [11, 12]. These rods were machined from boules grown by the Verneuil technique and were obtained from several sources (Linde Co. USA, Salford Electrical Co., England, and Hrand Djévahirdjian SA, Switzerland): the crystallographic orientation was random with the c-axis generally making an angle of about 60° with the rod axis. The rods were cleaned for 10 min in an ultrasonic bath containing an aqueous solution of a wetting agent, rinsed in distilled water, and allowed to drain dry. Polishing was accomplished by rotating the rods at about 200 rpm while an oxygen/coal-gas flame traversed along with their length at a rate of about 20 mm/min; the flame size and temperature were varied by adjusting the gas pressure. The rod rotation speed, traversing rate, and jet-to-rod distance were chosen arbitrarily and then held essentially constant during the polishing studies, so that the degree of polishing and quality of the resultant surface was controlled by carefully regulating the flow of gases to the burner jet.

The quality of the polished surface was assessed using incident-light microscopy at high magnification. Optimum flame conditions produced a clear glassy transparent surface, although a faint spiral marking corresponding to the pitch of the flame traverse (pitch = 0.1 mm under the conditions used) was observed. Using a cooler flame, all traces of grinding marks in the surface were not removed; with a more intense flame, a cloudy surface appearance resulted from the generation of voids within the resolidified layer. Over-polished crystals were found to have low strength, similar to that of poorly-polished material, so that precise control of the flame conditions was necessary to ensure high strengths.

By examining a necked area which formed when the flame was extinguished during polishing with an intense flame, Mallinder and Proctor [11] deduced that a "neck" of molten material existed throughout the polishing process and traveled along the rod with the flame. In well-polished rods, the molten neck resolidified epitaxially from the inner core outwards, the surface thus reflecting the structure of the underlying crystal. With an excessive depth of liquid, solidification also began at the outer surface and proceeded inwards; the change in volume as the entrapped liquid subsequently solidified led to the formation of the subsurface voids. Careful examination of the crystallographic orientation of polished rods by optical microscopy and x-ray techniques showed that the resolidified surface crystallized with identical structure to the underlying crystal and that subgrain boundaries at the crystal surface persisted after polishing.

Well-polished rods were carefully selected for freedom from internal defects—bubbles and inclusions, which were rendered visible during the polishing operation by the intense light generated at the molten surface—and were tested in bending with a gauge length of 3 mm or 6 mm selected from the most defect-free portion of the rod. Extreme care was taken to prevent any mechanical contact with the rods after polishing. Only the extreme ends were handled and the bending load was applied through epoxy sleeves cast onto the ends of the rods and then fixed into an elegant testing device, which applied a pure bending moment to the rod without offering any other constraints [11]. This test arrangement was operated in a manner which allowed the rods to be broken while immersed in a small bath of glycerine to reduce the degree of shattering and confine the fragments after fracture. By patient examination of the fragments and careful matching of fracture faces, it was possible to positively identify and locate the sources of fracture initiation. In well-polished rods, the origin of fracture could invariably be traced to internal (growth) defects. Curiously, Mallinder and Proctor [11] state that although dirt on the rod surface gave cloudiness and complex patterns when fused into the surface during polishing, this did not appear to affect the strength. (This is contrary to the experience of the present authors, who found that prepolish cleaning reduced the scatter in strength and increased the average strength of the rods by eliminating many potential flaws ("dirt").)

No relationship between strength and crystallographic orientation was found in the above work. However, an important practical observation was that the perfect surfaces achieved by careful flame polishing were extremely sensitive to damage by mechanical abrasion. The strength of the rods was reduced by a factor of between 2 and 14 by merely allowing the rods to roll under their own weight over a surface sprinkled with 90 mesh silicon carbide grains. Proctor noted that the sapphire rods were markedly less susceptible to abrasive damage than similar high strength silicate glass or fused silica rods and it was suggested that the dependence of strength on crystallographic orientation found in sapphire by other investigators might have been a reflection of the dependence of *susceptibility to damage* on orientation [10].

An interesting recent development in high-strength alumina single crystals is the continuous sapphire rods and filaments produced by pulling crystals of uniform cross-section directly from the melt [13, 14] these have surfaces sufficiently perfect to permit tensile stresses of about 3 GN/m^2 to be attained before fracture. Nevertheless, flame polishing techniques were found to improve the strength of these filaments (section 3.4.d) and tensile strengths up to 3.5 GN/m^2 have recently been reported in an effort to polish the filaments for commercial exploitation of the process [15].

Flame-polishing techniques have thus been used to produce alumina specimens whose surface perfection is such that the fracture stress is no longer limited by surface features but by internal defects within the crystals. It now appears that continuous high strength filaments will soon be available with strength close to the high levels previously found only in laboratory specimens and with good uniformity (small scatter). The greatest potential for exploitation of these filaments is as a reinforcement in a metal matrix at high temperatures. Unfortunately, most useful matrices are chemically incompatible with the filaments and the surface perfection may be degraded during composite fabrication and subsequent use. Preservation of the highly perfect flame-polished surface has proven to be a difficult technical feat in such matrices [16]. and useful exploitation of these high strength filaments depends on the extent to which these highly perfect surfaces can be retained.

3. Experimental

3.1. Flame Polishing

The aim of the work described in this section was to explore the possibility of producing high strength α–Al_2O_3 rods on a routine reproducible basis by a simple flame-polishing process. The work of Mallinder and Proctor [12] was used as a guide in establishing the initial polishing technique.

Single crystal α–Al_2O_3 rods were obtained for use in these polishing studies in various forms. Centerless-ground rods, 0.5 mm and 0.25 mm diameter sapphire and 0.5 mm diameter ruby (0.5 w/o Cr_2O_3 nominal doping level) machined from Verneuil-grown boules, were obtained from ("Linde") Union Carbide Corp., Crystal Products Division, Union, N.J.; 0.5 mm diameter commercially flame polished sapphire and ruby rods were obtained from the same source. In addition, 0.5 mm diameter centerless-ground sapphire and 0.5 mm diameter commercially flame polished sapphire rods were obtained from Insaco Inc., Quakertown, Pa. A small quantity of 0.5 mm diameter centerless ground sapphire rods machined from boules grown by the Czochralski technique was kindly provided by the Union Carbide Corp. for comparison with the Verneuil material. Finally, continuous filaments of melt-drawn sapphire, 0.5 mm and 0.25 mm diameter produced by Tyco Inc., Waltham, Mass., were included in the studies.

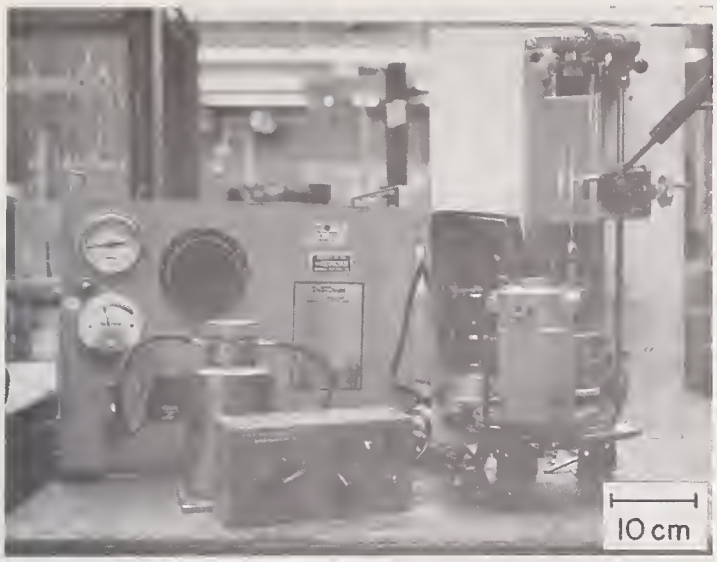

FIGURE 1. *Apparatus used for flame-polishing the surface of α Al_2O_3 rods.*

A flame-polishing rig, shown in figure 1, was constructed which consisted of a small "hobby" lathe ("Unimat-SL", Model DB–200, American Edelstaal Inc., N.Y.) arranged so that a sapphire rod, when held in a pin-vice in the lathe chuck, was rotated with its long axis vertical. The lathe drive was modified to provide continuously variable rotation speeds from 0 to ≈600 rpm; the synchronously driven tool holder moved up and down in a vertical plane at traversing speeds related to the chuck rotation. The tool holder carried an oxygen/hydrogen microtorch, which was used with a range of fine burner jets cut from hypodermic needles, as shown in figure 2.

This rig was operated under a wide range of conditions so that the effects of each variable could be assessed and a suitable set of operating conditions chosen. The rods to be polished were usually 10–12 cm long and 0.5 mm diameter, but rods up to 25 cm long and 3 mm diameter have been successfully polished in this same rig.

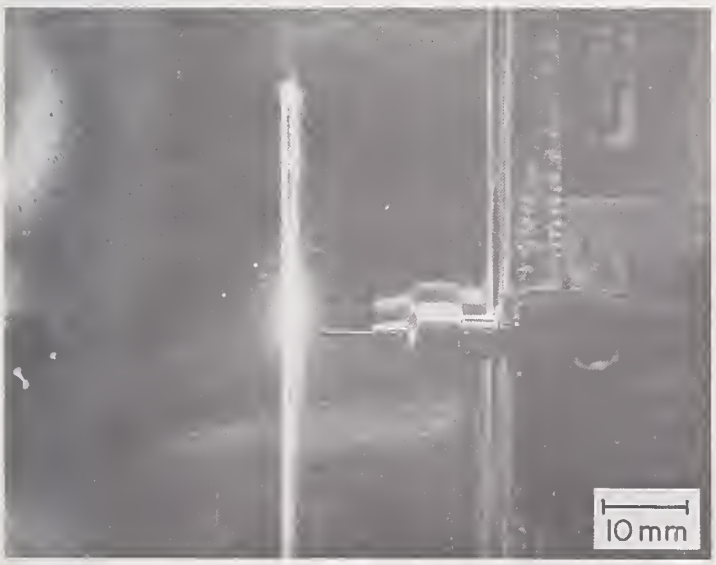

FIGURE 2. *Detailed view of the burner jet and the impingement of the flame (barely visible) on the rod during polishing.* The apparent double-image of the rod is a reflection from the metallic heat shield behind the rod.)

a. Flame Temperature

The gas supply to the flame consisted of a stoichiometric mixture of hydrogen and oxygen generated by electrolysis of water in a small generator adjacent to the lathe ("Water Welder (R)", Henes Manufacturing Company, Phoenix, Arizona); the two gases were never separated and were delivered directly to the burner in one line. The combustion temperature was about 3300 °C, but could be varied by the deliberate introduction of vapors into the gas stream. Initially, a hot flame, with the gases dried by a $CaCl_2$ tower, was used; however, it was found that a greater degree of control could be obtained by using a cooler flame (about 2500 °C) produced by bubbling the gas stream through methyl alcohol. The flame was also rendered more visible by this procedure and had a clearly defined "inner cone" which facilitated positioning the flame with respect to the rod. No difference in appearance of the rods or in their strength was detected between rods polished in the dry flame or in the slightly reducing "alcohol" flame.

b. Flame Size

The size of the flame was determined by the size of the hypodermic needle jet and by the gas pressure; the addition of alcohol vapor increased the size of any given flame. The gas generator had a sensitive pressure gauge which was used to maintain a constant supply pressure of 5kN/m² (controlled by a Variac applying voltage to the electrolytic cell). A range of jet sizes from No. 16 to 27 (1.05—0.19 mm bore) was used during the work. The larger jets provided a flame which was too large to be conveniently accommodated in the space available, and provided too large an excess of thermal energy compared with that required to flame polish a slender rod: flames from the smaller jets were only capable of heating a small volume of the rod with a steep temperature gradient on either side of the hot spot. A No. 23 jet (0.32 mm bore) was found to provide a flame ≈12 mm long × 1 mm diameter, inner cone 2.5 mm long, which was suitable for polishing the 0.5 mm diameter rods. The flame was large enough to envelop the rod, and produced an apparently molten length of about 0.5 mm of the surface. A steep temperature gradient existed above and below the molten zone.

c. Temperature of the Rod Surface

The temperature at the surface of the rods was determined by the distance of the burner jet from the rod and by the rate of movement of the flame over the rod. The distance from the rod was the most critical parameter in the production of well-polished rods and was controlled by the drive screw of the lathe toolpost on which the burner jet was mounted. The position of this screw could be read to ± 0.05 mm and noticeable differences in surface appearance could be detected with changes of 0.2 mm in the rod-to-jet distance.

The rod surface temperature and/or the volume of molten material changed appreciably with changes in the rate of movement of the rod through the flame. For this reason, the rod-to-jet distance necessary to produce a good polish was adjusted to suit the speed of rotation of the rod; larger distances were needed for slower speeds (or smaller diameter rods) and vice versa.

Attempts to measure the temperature at the rod surface by optical pyrometry and to use this as a means of control were unsuccessful. It was soon realized that the simplest, practical means of assessing the optimum temperature and the quality of the polished surface was by visual observation of the rod during polishing through dark-glass "welders" goggles.

d. Lathe Spindle Rotation Speed and Flame Traversing Speed

The speed of rotation of the lathe spindle was initially varied from about 6 to 600 rpm using Variac-controlled motors and a range of pulleys and belts. The lathe chuck was aligned such that a 10—12 cm long rod rotated within 0.05 mm out-of-true about its long axis. Longer rods had to be supported at both ends to ensure stability of rotation and satisfactory polishing. The rate of traverse of the flame was directly linked via pulleys to the lathe spindle and initially was 25 mm of travel per 1000 revolutions of the rod. While it was realized that a high output rate would be desirable for ultimate exploitation of the polishing process, it was thought in the early experiments that better quality surfaces would be produced at a low polishing rate. Initial work was done on rods revolving at 1–200 rpm with automatic traversing which produced a prohibitively low rate af about 0.5 mm/min of polished rod. The spindle speed was progressively increased up to 600 rpm, and the traversing mechanism modified to produce 16 mm/min of polished rod.

The predominant surface feature visible following this polishing procedure was a pronounced helical ripple, coincident with the path traversed by the flame across the surface of the rod. This feature was recognized in earlier work on flame-polished sapphire but was not found to prohibit the achievement of high strength. Barnes and McCandless [8] used a multiple jet burner to produce a broad flame which heated a substantial length of rod and effectively removed the surface ripple; this expedient was not used in the current work. Nevertheless, it was considered desirable to reduce the effect as far as practicable and the traversing pulleys were changed to reduce the pitch of the helix to 0.013 mm. Reduction of the pitch of the helix also reduced the depth of the furrows between the spiral traces and was therefore expected to increase the strength of the rods. The rate of production of polished rod was thus reduced to 8 mm/min (about half of the rods produced in this work were polished at this rate and half at 16 mm/min); experience has indicated, however, that if necessary, higher polishing-rates (over 25 mm/min using higher spindle speeds) are practicable.

e. "Optimum" Polishing Conditions

Good quality polished surfaces were obtained from a wide range of polishing conditions so that the concept of an optimum set of conditions was not appropriate to the process [17]. It was evident that a balance had to be established between the amount of heat supplied to the rod and the various sources of heat expenditure such that an optimum amount of molten Al_2O_3 was maintained at the surface. The depth of the molten pool during polishing was not known with certainty but was estimated to be about 0.05 mm. The importance of heat conduction through the rod was demonstrated by the fact that it was found necessary to start polishing at a short distance ($\approx$2 mm) below the top of the rod so that heat was conducted away from the molten zone equally in both directions. When starting from the top of the rod, a flame that would normally produce a polished surface would melt the whole cross-section of the rod and form a progressively larger droplet as the flame traveled downward, because of heat conduction away from the flame in only one direction.

f. Summary of Conditions Used for Flame Polishing of Rods and the Operating Procedure

The following conditions were adopted for the production of the majority of the polished rods used in this work as a result of the experience described above.

(i) Gas pressure 5kN/m^2 with methyl alcohol vapor addition.

(ii) Jet size 0.32 mm bore (hypodermic Jet No. 23).

(iii) Jet-to-rod distance about 6 mm: the

exact position being determined by visual observation of the rod surface.

(iv) Rod rotation speed 600 rpm; flame traversing rate 0.013 or 0.026 mm per revolution.

The molten Al_2O_3 formed a collar round the rod about 0.5 mm wide by about 0.05 mm deep under these conditions. In operation, conditions (i), (ii), and (iv) were established, the flame was then brought to impinge on the rod 2 mm from the top, the traverse mechanism engaged, and the jet-to-rod distance adjusted to produce the desired degree of polish.

3.2. General Observations on the Polishing Process and Comparison of the Results Obtained on Different Rod Materials

During polishing, the rod acted as a light-pipe for the intense illumination generated by the molten Al_2O_3 and light scattering reflections were produced at any discontinuity within the rod or at its surface; "flaws" were thus readily visible. Examinations of rods during polishing was therefore the most sensitive means of assessing surface perfection and freedom from gross flaws, both internally and at the surface. It was found that if too much Al_2O_3 was melted during the polishing process, coarse ripples and "necking" of the rod occurred—in the extreme, the rod would resemble a string of beads. There was therefore a tendency to err on the side of under-polishing especially for the 0.25 mm diameter specimens, to avoid loss of the rod by complete melting of the cross section. In fact it was not possible to "overpolish" these small rods; (i.e., produce sub-surface voids), as is possible for larger diameter rods, which would tolerate greater depths of molten material without failure.

Examination of the rods from the initial polishing work showed evidence of "foreign" particles in the surface which often corresponded to the edge of fracture faces in rods subjected to strength tests. An ultrasonic cleaning procedure (following Mallinder and Proctor) was subsequently used prior to polishing; a detergent solution, a water rinse, and finally an alcohol rinse was used and a marked improvement in the surface appearance and in the strength of the polished rods was observed. The "foreign" particles had obviously originated in dust and loose grinding debris present on the surface of the as-received ground rods.

Both centerless-ground and commercially flame-polished rods were used in the initial work, and it was found that it was easier to judge the correct polishing condition when using a centerless-ground rod than when using a previously polished one. It was thus more difficult to produce a high-quality polish on previously commercially-polished rods. Also, some debris appeared to be sealed into the surface in the commercial polishing operation and was not easily removed in further polishing. Experience showed that the best quality polish, and hence the highest strength rods, was attained by arranging that the amount of liquid material was sufficient to melt through all pre-existing surface irregularities in a single pass of the flame; multiple polishing rarely improved the strength of the rods unless they were greatly under-polished on the earlier polishing attempt.

Many rods were found to contain internal flaws (bubbles, inclusions, etc.,) which could not be removed by polishing. These internal flaws were suspected as sources for fracture initiation in the rods [11] and therefore the position of the flaws (rendered visible by the illumination of the flame during polishing) was mapped out for several rods which were subsequently broken in bending. Reassembly of the broken fragments showed that in most cases the fracture faces corresponded to the previously located and "mapped" internal flaws.

When polishing the few Czochralski-grown rods included in the studies, it was immediately obvious that it was a much better quality Al_2O_3 material—no internal defects could be detected during polishing. Unfortunately, because of the scarcity of this material at the time, the polishing was performed somewhat cautiously to avoid loss of material or void formation by overpolishing. The measured strength of these rods (Section 3.4.e) was not especially high, despite the high internal perfection, and further examination showed that their surfaces had been slightly underpolished so that all traces of machining damage had not been removed.

When polishing the Tyco c-axis sapphire filaments, it was found to be relatively easy to improve on the as-grown surface (and hence on the strength). However, it was not possible to achieve strengths as high as those measured in other material because the Tyco material tested contained many internal voids [13], some of which appeared to intersect the filament surface. In some samples, there was also a ripple in the surface due presumably to a growth instability. It was therefore easy to melt and reform a more perfect surface but the internal structure, containing many defects, was unchanged. In subsequent testing, only a relatively moderate but nevertheless significant increase in the average strength of the filaments was measured. As a result of this work, a flame polishing process has been studied by Tyco as part of the efforts to improve these filaments with considerable success [15] and may soon become part of the normal production process.

Interesting and highly significant differences in behavior were observed between sapphire and ruby during flame polishing, which were

not completely understood at the time. In sapphire and ruby obtained from the same source and grown by identical techniques (except for chromium addition in ruby) [18], there were significantly less internal defects in the ruby crystals. Also, because of the difference in optical properties, the thermal gradient on either side of the flame was more evident with ruby, so that correct positioning of the flame and observation of the molten zone was greatly facilitated. In practical terms, this meant that high quality polished ruby rods could be produced by unpracticed personnel after only a few minutes instruction, whereas to produce a good polish on sapphire material required considerably more experience. Therefore, a significantly higher average strength was invariably found in polished ruby compared with polished sapphire; even if the surfaces were similar, the scatter in strength was usually less for ruby because of the reduction in internal defects.

Study of ruby was initiated because of reports that the high temperature creep resistance was higher in ruby than in sapphire [9, 19] and because of the possible differences in compatibility behavior between the two materials and Cr-containing metallic alloys. Apart from the differences in strength arising from internal defects referred to above, no significant difference in the mechanical behavior between flame-polished ruby and sapphire were found. Furthermore, there was no detectable difference in behavior in compatibility studies. Electron-probe analysis indicated that the surface layer of the ruby rods was in fact depleted in Cr to a depth which corresponded closely to the depth of molten liquid during polishing. It appears therefore that the surfaces of flame polished "ruby" rods may differ only slightly from those of sapphire rods.

Over a three-year period of studies with ruby rods, it was observed that the red color associated with the chromium doping could vary noticeably from one rod to another, even within a given batch. All the material had a nominal doping level of 0.05 w/o Cr_2O_3 but the color could vary from a pale pink to quite a deep red. No systematic difference in behavior which could be related to this variation was detectable either in the polishing procedure or in the resulting mechanical property measurements.

3.3. Surface Features of α–Al_2O_3 Rods with Varying Degrees of Flame Polish

Figure 3 shows the surface of a centerless-ground sapphire rod and illustrates the amount of surface roughness which has to be melted and recrystallized during flame polishing. It can be seen that damage fragments have typical dimensions of 0.025 mm in the direction of the surface as well as in depth. Figure 4 shows the

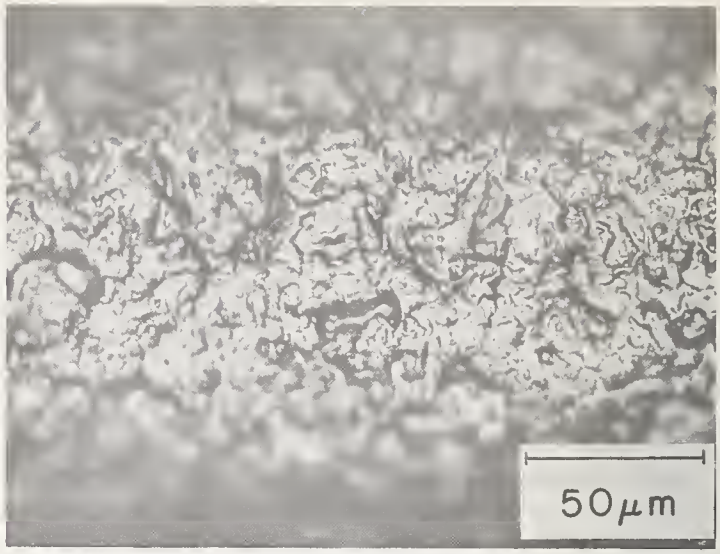

FIGURE 3. *The surface of a centerless-ground sapphire rod.*

surface of a centerless-ground rod after one pass of the flame under grossly "under-polished" conditions. The remnants of the grinding damage, although smoothed and rounded, are still evident and only slight increases in strength occur at this stage. The right-hand end of the crystal in figure 5 has been given a second pass of the flame and is well polished; the surface at the left where the flame had been rapidly removed, contains many bubbles which seem to remain in the molten Al_2O_3 collar and are swept down the rod by the liquid.

The surfaces of typical commercially flame-polished rods "as-received" are shown in figure 6. A large amount of grinding damage and remnants of "dust" particles are still evident but some improvements in strength would be expected over that of a ground surface and was indeed found. No pronounced ripple is vis-

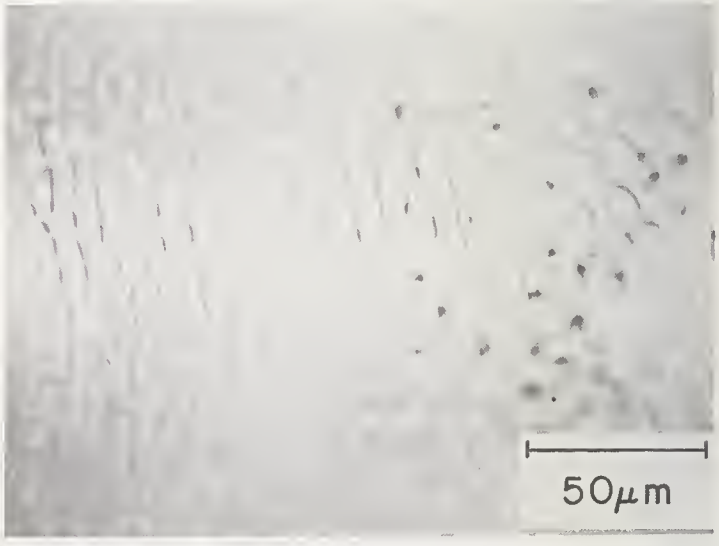

FIGURE 4. *The surface of a centerless-ground sapphire rod after one pass of a flame under grossly "under-polished" conditions.*

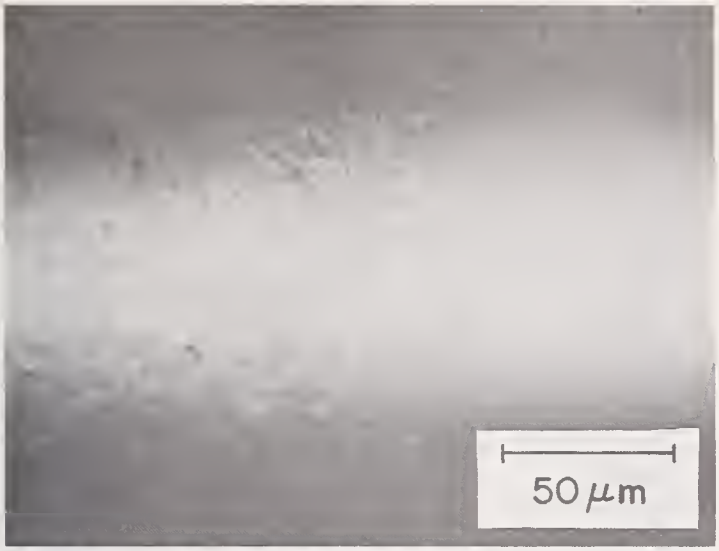

FIGURE 5. *The surface of a rod similar to figure 4 but after the right hand end of the rod had been given a second pass of the flame under ideal polishing conditions.* The left hand end of the rod is where the flame was removed and contained bubbles apparently swept down the rod by the pool of liquid.

ible on the commercially-polished rods, which indicates that only a small amount of Al_2O_3 was liquid during polishing (using a relatively large flame [8]) which appears to have been insufficient to produce uniformly polished rods.

The surface of a typical rod flame-polished in the present work under conditions described earlier is shown in figure 7. The helical ripple is the only visible feature on such a surface. The varying width of the pitch of the helical path is caused by slight changes in friction and slipping in the pulley-driven flame-traversing mechanism.

Other features which have been seen on the surface of apparently well-polished rods are believed to be related to the crystallographic orientation of the underlying material. For example, distinct lines parallel to the rod axis occasionally form and disturb the normal helical ripple; Mallinder and Proctor [17], and Popov [7] observed similar disturbances suggesting development of crystal facets. This behavior was occasionally pronounced on Tyco sapphire filaments, which often had a rounded approximately triangular or even hexagonal cross-section which could be accentuated by polishing. A tendency toward the development of a noncircular cross-section was noted also for many Verneuil-grown rods. The surfaces of a few rods were replicated by standard techniques so that surface features could be studied at high magnification in an electron microscope. One of these rods clearly illustrate the development of crystal features (fig. 8). These were not common features on polished rods and they probably arose due to an over-polishing condition, perhaps also with some thermal etching.

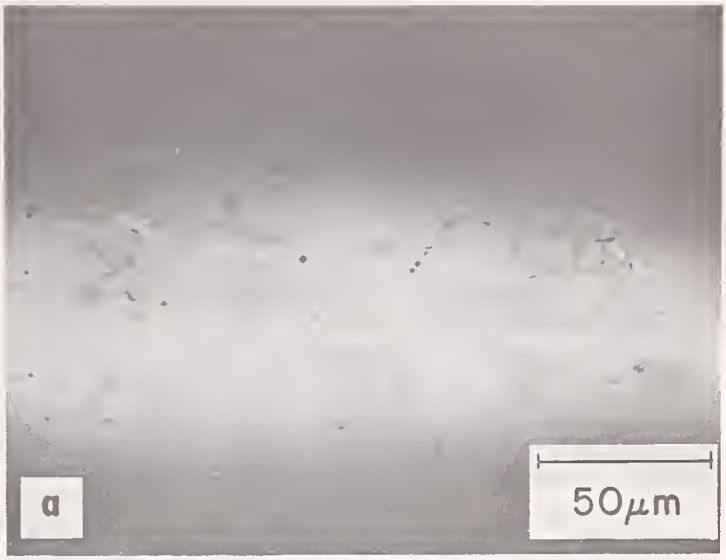

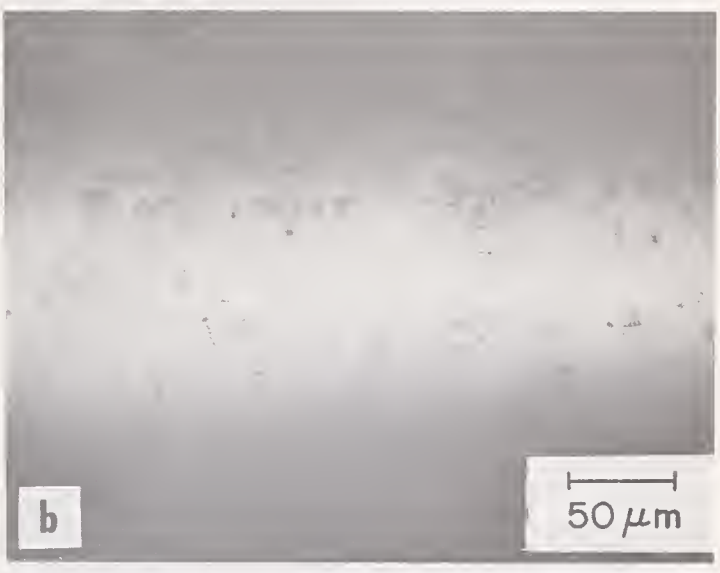

FIGURE 6. (a) & (b) *The surfaces of typical commercially flame polished sapphire rods showing remnants of grinding damage and surface contamination.*

FIGURE 7. *The surface of a sapphire rod flame-polished under ideal conditions in this work.*

Figure 8(a) shows hexagonal outlines of basal planes normal to the emergency of the c-axis from the surface of the rod, while figure 8(b) is from the surface of the same rod at a position roughly 90° around the circumference and shows an edge-on view of the intersection of basal planes with the surface. The bend strength of this particular rod was 4 GN/m², but it is not known whether any of these features were present in the regions of maximum stress during the test.

3.4. Results of Strength Measurement on Flame-Polished α–Al_2O_3 Rods

a. Bend Test Procedure and Fixtures

The degree of improvement in surface smoothness of the flame polished rods was assessed by measuring the strength of polished rods in bending and in tension. Since it was a major object of this work to develop simple routine procedures to produce and evaluate rods, a simple bend test was used to measure their strength. Selection of the test specimen and crystallographic orientation of rods was essentially random (except for a few tests already mentioned in which the position of internal flaws seen during polishing was noted so as to relate them to fracture origins). Rough handling and contact between rods was avoided after polishing but normal handling to transfer rods to the test machine, etc., including occasional deliberate contact of the gauge section with steel tweezers, did not cause noticeable deterioration in the surface or catastrophic reduction in the measured strength at room temperature.

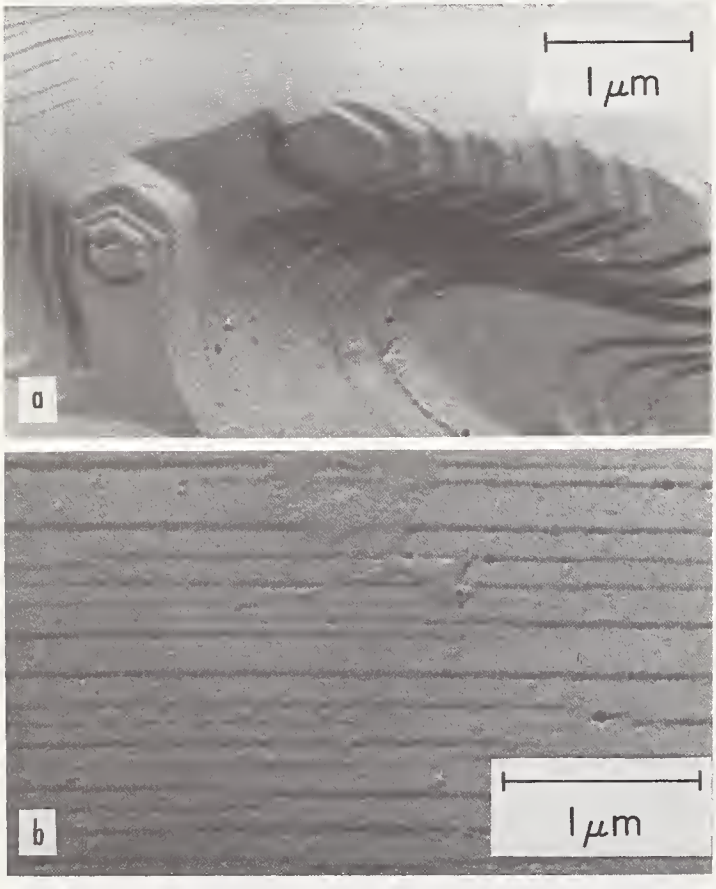

FIGURE 8. *Features on the surface of a sapphire rod following flame-polishing.* (a) shows outlines of a faceted basal plane at the emergence of the c-axis from the surface of the rod and (b) the edges of similar features (i.e., intersection of basal planes with the rod surface) at a position on the same surface approximately 90° around the rod circumference.

It is well known that three-point bend tests should be avoided for ceramic materials, since only a single point on a rod specimen is subjected to the maximum stress. The strength of a ceramic is usually governed by discrete isolated flaws, which are unlikely to occur at the point of maximum stress unless there are many closely spaced flaws. In the case of flame-polished crystals with only a few well isolated flaws, it was expected that a three point bending test would give a wide range of results, with some very high values. This behavior was indeed found in such tests (12.5 mm span and steel knife edges used) of sapphire rods, where strength over 9 GN/m² was measured. The elastic deflection was very large in these tests and the validity of the simple elastic equations used to calculate stress may be in doubt [20]. With high-quality flame polished ruby, a strength of about 9 GN/m² could be measured frequently. This was clearly an unrealistic estimate of the useful strength of these rods.

Testing in four point bending was therefore adopted for routine assessment of the quality of the surfaces produced in this work. All results quoted were obtained on a test fixture with 25.5 mm outer span and 12.5 mm inner span (i.e., a line on the rod surface 12.5 mm long was subjected to maximum stress) with 3 mm diameter steel outer "knife edges" and 0.25 mm radius inner "knife edges". The fixture was carefully and precisely aligned to ensure that each of the rigid center knife edges made contact with the rod at the same time. A small box and plastic screens surrounded the fixture in order to collect the broken fragments. Small pieces of tissue paper were often draped over the free ends of the rods to prevent excessive fragmentation, which was usually caused by impact of pieces of the rod against the fixture following the initial fracture. The test fixture was mounted between the crosshead and a compression load cell of an Instron testing machine, testing being accomplished by moving the crosshead at a rate of 0.5 mm/min.

Large elastic deflections were imparted to the high strength rods before fracture, so that several minutes elapsed before failure in each test. The possibility of error arising from nonlinear behavior at large deflections was considered in calculating the strength of the rods us-

ing only simple elastic bending theory, but it appeared that such errors, even with the strongest rods, were less than 10 percent and meant that the calculated strength was in fact less than the true maximum stress in the rods at fracture [20]. The test fixture is shown in figure 9 with a flame-polished sapphire rod in position under a load corresponding to an outer-fiber stress of 3.5 GN/m². (The camera angle was slightly off center in figure 9 to show the arrangement of the knife edges.) Figure 10 shows a flame-polished ruby rod under test when the outer-fiber stress was 4.4 GN/m², the average strength for all the flame-polished Verneuil-grown material (sapphire and ruby combined). Light reflection from the surface ripples can be seen on the rod in figure 10, particularly at the left hand side; the unpolished ends of the rods are also evident in figures 9 and 10.

b. Results: Verneuil Material

The results of room temperature bend tests on Verneuil-grown sapphire and ruby and having different surface conditions, as described in section 3.1, are summarized in figure 11. No difference in behavior could be detected between sapphire materials obtained from different suppliers and therefore no such distinction is drawn in figure 11. It can be seen that, for any given surface condition, the scatter in the data is approximately the same, i.e., the strongest rod is 2 to 3 times as strong as the weakest rod in each set of data. However, the average strength of the rods changes significantly with changes in the surface smoothness; the average strength of the flame-polished rods being 10 times that of the rods with centerless-ground

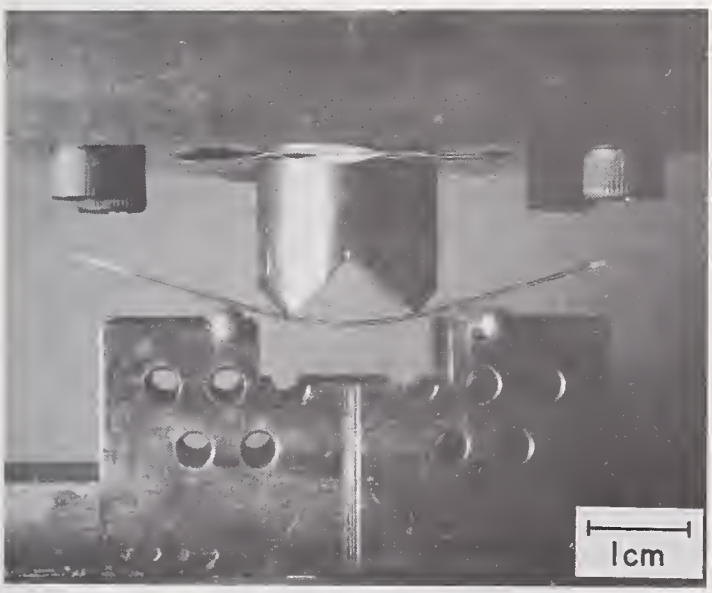

FIGURE 9. *A flame-polished sapphire rod undergoing a bend test at room temperature in the steel test fixture.* The outer fiber stress in the rod at this time was 3.5 GN/m².

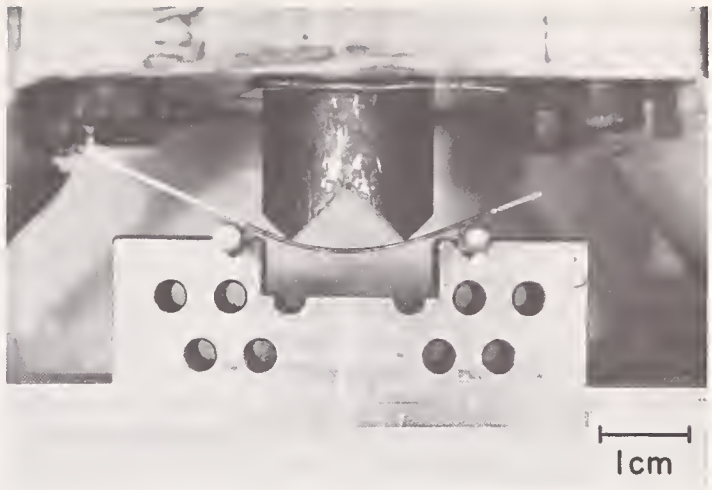

FIGURE 10. *A flame-polished ruby rod undergoing a bend test at room temperature showing the elastic deflection in a rod at a calculated outer fiber stress of 4.4 GN/m², which corresponds to the average strength of flame polished Verneuil material (both ruby and sapphire) produced in this work.*

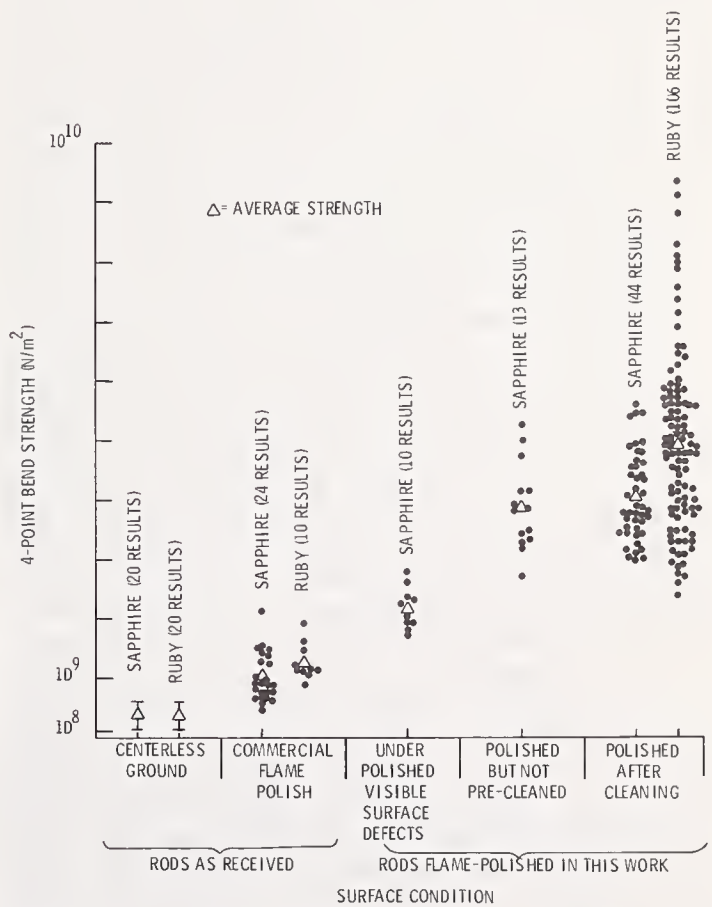

FIGURE 11. *Summary of data obtained in room temperature bend tests on α-Al_2O_3 crystals (ruby and sapphire material) grown by the Verneuil technique and having various surface conditions.*

surfaces. Therefore, although flame polishing does not change one of the disturbing features of ceramic crystals, namely the wide scatter in strength results from any given material and surface condition, it does appear to provide a

means to almost guarantee a minimum strength which is determined by the internal perfection of the crystal. In other words, flame polishing provides a means of attaining stress levels corresponding to the intrinsic strength of the bulk crystal.

As was mentioned earlier, a detailed examination of fracture faces to determine the origin of fracture (surface or internal) was not made; however, the indications obtained from rods in which the position of observable defects was noted during polishing showed a close correspondence with fracture fragments after testing. These observations support the earlier conclusions of Mallinder and Proctor [11] concerning fracture origins in well-polished rods.

It is significant that strengths of the order of 7 GN/m² reported by Mallinder and Proctor [11] were not achieved in 4-point bend testing of sapphire rods in this work. This was initially attributed to the possibility of handling damage and the relatively crude testing technique used in the present work. However, since it was subsequently found that high strengths could frequently be attained in ruby single crystals polished, handled, and tested in the same manner as for sapphire, it was clear that a careful choice of test section was needed to attain freedom from internal flaws for the sapphire specimens. The relative freedom from internal flaws in the as-received ruby rods resulted in more perfect test sections being obtained, even with random rod selection.

It must be emphasized that the "random" selection of rods referred to above does not mean that all the polished rods were acceptable for testing. Experience showed that gross flaws near the surface of the rods could be easily picked out during polishing and these rods were then set aside for other studies. From the strength data obtained (figure 11), it is clear that this visual selection could readily remove all defects corresponding to strengths below about 2.5 GN/m².

Casual handling of rods, including contact with steel, did not catastrophically affect their strength at room temperature but contact with materials of equal or greater hardness (other rods or silicon carbide abrasive) did markedly reduce the strength. Even casual handling, however, could seriously affect the strength of the rods which were heated at 1000 °C for 1 hr in air before testing. Presumably salts, dust, or other contamination stuck to the surface during handling, and then fused or otherwise interacted with the surface during the heat treatment, thus reducing the strength. Rods protected from contamination could be given similar heat treatments without loss in strength. Similar observations were made by Proctor [10] on sapphire rods and also on high strength glass surfaces; the latter were particularly susceptible to damage by even the slightest contact or contamination of the surface.

c. Results: Czochralski Material

The crystallographic orientation of the few Czochralski-grown sapphire rods was similar to the Verneuil rods used previously. Unfortunately, as mentioned earlier, these rods were slightly under polished but the freedom from internal defects was obvious during polishing.

Two rods were long enough for testing in the bending fixture and had strength of 2.98 and 2.93 GN/m². Smaller fragments of these rods were then tested in 3 point bending with a 12.5 mm span and strengths of 8.16, 4.00, and 3.75 GN/m² were measured. It would be interesting to study this material further, particularly in tensile tests, because its high internal perfection should permit the achievement of extremely high strengths, possibly as high as the best Al_2O_3 whiskers.

d. Results: Tyco Sapphire Material

The bend strength of 0.5 mm diameter Tyco sapphire rods (cut from essentially continuous filament) was determined on 2 batches of material obtained at different times. Batch 1 was from the early production material (1968) and the strength was low but reasonably uniform. This material contained many internal voids, some of which appeared to have faceted surfaces and many were close to, or exposed at, the rod surface; a typical rod is shown in figure 12. Batch 2 was specially selected from production material about 12 months later (1969) and had a higher average strength than batch 1, but also had a very large scatter in strength. This material also had a high void content, but the distribution was different than batch 1, the voids being mostly in a zone just below the surface but away from the core of the rod.

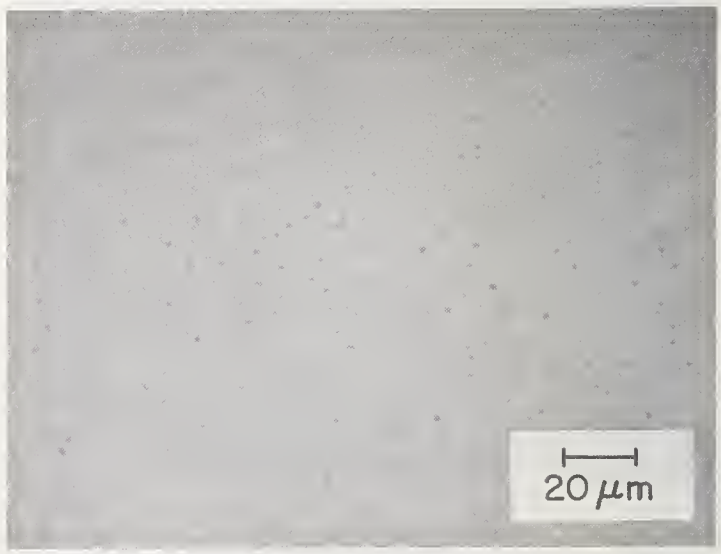

FIGURE 12. *The surface of a typical Tyco sapphire filament (batch 1) in the as-grown condition.*

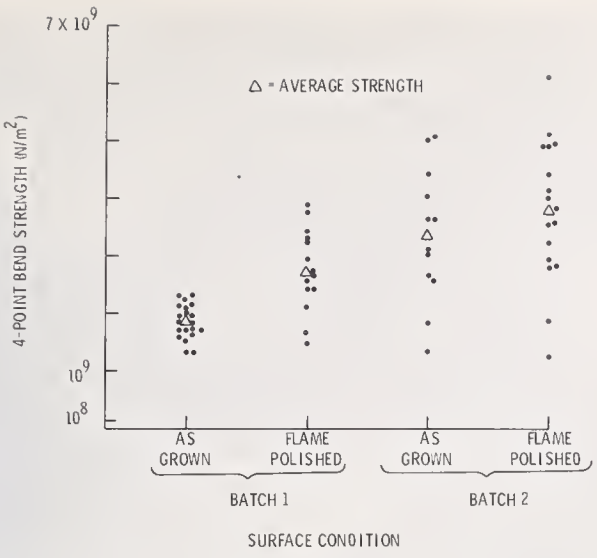

FIGURE 13. *Room temperature bend strength of Tyco sapphire filaments from 2 different batches, with both as-grown and flame-polished surfaces.*

Flame-polishing improved the average strength of both batches of rods, but also increased the scatter in the strength data (fig. 13). A few large flaws in batch 1 were not completely eliminated by polishing but otherwise the surfaces of the Tyco rods appeared to be identical to those obtained on the centerless-ground rods (fig. 7). However, because of voids immediately beneath the polished zone, the lowest strength measured in all 4 sets of data was similar (about 1.3 GN/m²). The highest strengths measured in batch 1 compares favorably with the average strength of the flame-polished Verneuil sapphire rods (fig. 11), and was presumably determined on a relatively void-free length of rod (detailed examination of the void distribution was not made). Also, the highest strength in batch 2 is comparable with a good flame-polished ruby rod and is indicative of freedom from serious flaws, at least in a small volume of the rod. It is noteworthy that a strength of 5 GN/m² was measured on a rod in the as-grown condition, again indicating the potential for the achievement of high strength in these filaments if growth flaws can be avoided.

Because of the large scatter in the bend data and the many internal flaws in the Tyco rods, no tensile testing of flame-polished Tyco filaments was performed. With the material as described above, it was expected that flame-polishing would have an insignificant effect on the tensile strength, since tensile failure is dominated by internal flaws (Sec. 3.4.f). However, recently produced Tyco filaments are much improved in internal perfection and it has been shown that for such crystals, flame-polishing can significantly improve the tensile strength [15].

e. Elevated Temperature Bend Testing of Flame-Polished Rods: Verneuil and Tyco Material

Plastic deformation in Al_2O_3 single crystals at elevated temperatures has been known and studied in both sapphire and ruby for several years [9, 21]. Basal slip has been observed above 900 °C [9] and rhombohedral slip about 1200 °C [22], in suitably oriented specimens, and deformation twinning, both basal and rhombohedral, has been observed over a wide range of temperatures [21, 23]. Wachtman and Maxwell found that creep deformation by basal slip could be induced in commercially flame polished sapphire and ruby rods at temperatures above 900° under low tensile stresses (< 50 MN/m²) [9]. There was no apparent difference between the creep yield stress for flame polished or unpolished rods [9] but since the fracture stress at room temperature was low for both types of rod, the quality of the commercial flame polish was evidently poor. Since high-quality flame-polished surfaces resulted in large increases in the fracture stress at room temperature in the present work, it was of interest to determine the mechanical properties at elevated temperature.

The bend strength of flame-polished ruby rods and of as-grown Tyco filament (both 0.5 mm diameter) was therefore determined using a test fixture identical in geometry to that used for the room-temperature tests but with sintered alumina knife edges and superalloy supporting fixtures. The fixture was surrounded by a Nichrome-wound split-tube furnace capable of operation up to 1100 °C in air. Tests were conducted at temperatures from 900 to 1100 °C (measured by a thermocouple fixed between the center knife edges of the fixture) in an atmosphere of argon/air (an argon flow was maintained through the furnace in an effort to reduce oxidation damage to the metallic parts of the rig). The crystallographic orientation of the ruby rods was random (c-axis in each case was about 60° to rod axis) and the Tyco rods had the c-axis parallel to their length.

The results of the elevated temperature testing are shown in table 1; the room temperature strength quoted for each set of data is the average strength of 10 rods from the same batch as that used for the elevated temperature tests. The onset of plastic deformation was observed in the ruby rods at 1000 and 1100 °C as non-linearity in the stress strain curve. One ruby rod fractured at 1000 °C without evidence for deformation, no doubt because of unfavorable orientation of the slip direction in this crystal. All the Tyco filaments were completely elastic up to fracture, and no evidence for plastic deformation could be detected in the fragments. This was expected because of the unfavorable orientation of the basal planes in these filaments and the previously reported ob-

TABLE 1. *Bend strength of flame-polished ruby rods (Verneuil) and as-grown Tyco sapphire filaments (both 0.5 mm diameter) tested in an air/argon atmosphere at various temperatures*

Temperature °C	Bend strength (GN/m^2)			
	Flame polished ruby	Plastic* deformation	As-grown Tyco sapphire	Plastic* deformation
20	4.13	0	3.31	0
900	2.07	0	1.43	0
900	2.07	0	1.12	0
1000	1.54	+	1.27	0
1000	1.49	0	0.76	0
1100	1.12	+	0.85	0
1100	0.79	+	0.55	0

*+ = slip and/or deformation twins observed
0 = no slip or twinning observed
} optical examination at 100 X in polarized light

servations of rhombohedral slip only at 1200 °C [22]. Two of the ruby rods were plastically deformed under essentially constant load (one at 1000 °C and 1.5 × GN/m^2, the other at 1100 °C and 1 GN/m^2) ; there was a slight load reduction as deformation proceeded until a permanent deformation of several per cent was induced into the rods. The load was then removed and the bent but unbroken rods were recovered from the furnace and examined for evidence of basal slip and deformation twinning.

The data in table 1 shows that the fracture (or yield) stress for the flame-polished rods is at least an order of magnitude greater than that measured on rods with imperfect surfaces [9] ; the strength ratio between perfect and imperfect surfaces is greater even at high temperature than at room temperature. The high stresses withstood by these rods before and during deformation suggests that dislocations necessary for plastic deformation are nucleated at the surface, presumably at flaws or stress concentrations. Therefore, the same mechanism which is responsible for the high fracture stresses in the rods at room temperature (namely the freedom from surface defects) is also responsible for the high yield stress for plastic deformation at high temperatures. The strength/ temperature relationship for the ruby rods is greater than that found for sapphire whiskers with highly perfect (thermally etched) surfaces [3], but not as great as found for rods with imperfect surfaces [24, 26]. Within the scatter in data, the strength/temperature relationship is the same for the Tyco sapphire as for the ruby; the strength at any given temperature is lower for the Tyco material, in proportion to the lower room temperature strength of these rods as compared to the ruby crystals.

f. Tensile Strength Measurements on Flame-Polished Sapphire Rods: Verneuil Material

A cursory examination of fracture surfaces suggested that fracture frequently originated at internal flaws, as was found by Mallinder and Proctor [11, 12]. The maximum stress in a bend test is only at the surface of the rod, and the bend strength of flame-polished rods may not be a realistic indication of the strength of the rods measured in tension, where the entire cross-section is uniformly stressed. Severe internal defects close to the center of the rod would be relatively ineffective flaws in a bend test. Since many potential applications for these rods would require them to carry a direct tensile load, tensile tests were performed on several rods as discussed below.

The apparatus used for tensile testing of short sapphire rods is shown in figure 14. An Instron machine with carefully aligned rigid cell-couplings (developed for whisker testing [27]) was laid horizontally and rods were cemented to carefully aligned rigid anvils with an epoxy resin. (Epon resin 815 (Shell) and Versamid 140 polyimide resin (General Mills) 50/50 by weight were used and cured at 90 °C in about 1 hr under an ultra-violet lamp.) The horizontal arrangement greatly facilitated alignment of the specimen and enabled this alignment to be maintained during curing of the cement. An attempt was made to use as large a gauge length as possible but it was also necessary to have an adequate length (~25mm) immersed in the epoxy in order to prevent 'pull-out' from the grip.

The results obtained using this arrangement

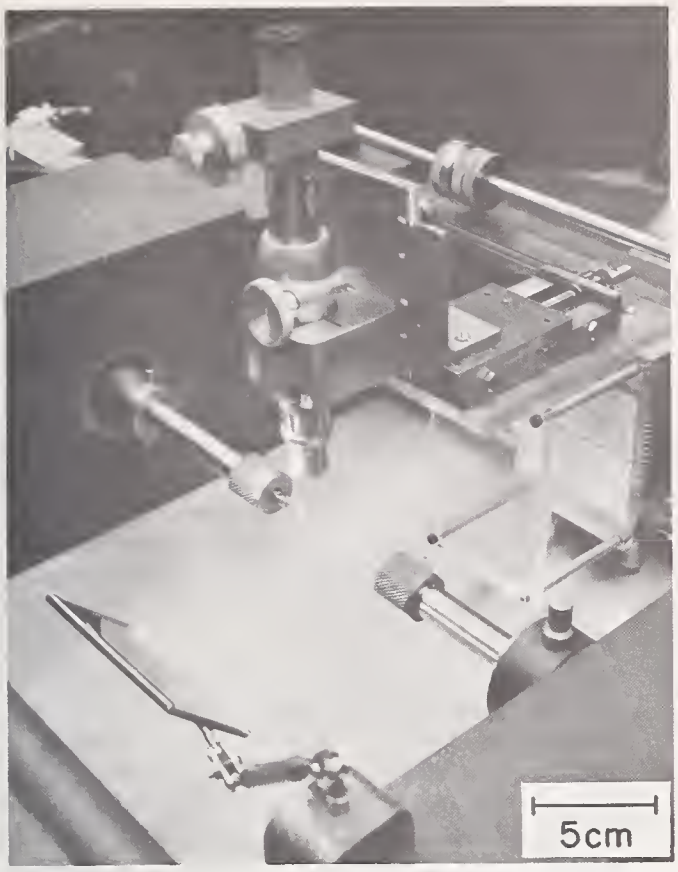

FIGURE 14. *Apparatus used for tensile testing of flame-polished rods 0.5 mm diameter and up to 10 cm long.*

are shown in table 2. It is evident that the rods indeed possess high tensile strength, but examination of fracture surfaces showed that internal defects were limiting that strength. All test results are included in table 2, although good alignment was not achieved in every case; this presumably caused some low strengths to be recorded because high bending forces are developed in this situation [28]. With the exception of tests numbers 4 and 7, in which fracture occurred at visible surface irregularities, all fractures initiated internally. The rods used in these tests were taken from the same batch of sapphire rods used to obtain the bend strength data in figure 2, in which strengths between 2.12 and 5.51 GN/m² were measured. It is significant that the average strength measured in tension was only 65 percent of the average strength measured in bending. These data gave further support to the contention that the strength of the flame-polished material is limited by internal defects and not by the surface perfection.

TABLE 2. *Tensile strength of flame-polished sapphire rods*

Test	Gauge length (mm)	Strength GN/m²	Alignment
1	26	2.85	Good
2	6	> 2.2 (pull-out)	Good
3	15	2.15	Good
4	25	1.93	Good
5	23	3.66	Good
6	5	2.35	Good
7	28	1.89	Good
8	8	1.78	Poor
9	20	2.50	Poor
10	18	3.52	Good
11	10	>3.50 (pull-out)	Good
12	4	3.02	Good
13	30	2.37	Poor
14	10	3.18	Good

The strength measured in test no. 5, table 2, is probably the highest strength yet recorded in tension in a ceramic crystal of this size (23 mm gauge length, 0.5 mm diameter, breaking load 76Kg). This strength, and indeed the average tensile strength, compares favorably with the tensile strength of sapphire whisker crystals of much smaller diameter and length [29]. Furthermore, higher tensile strength has recently been reported in flame-polished Tyco sapphire filaments [15] of smaller diameter (0.25 mm) than those used in this work.

Tensile strength measurements were also made on centerless-ground and commercially-polished sapphire rods of similar dimensions to those used above. The centerless-ground rods had an average strength of 0.21 GN/m² (with a range 0.08 and 0.32 GN/m² for 9 results) and the commercially polished rods had an average strength of 0.36 GN/m² (a range of between 0.26 and 0.45 GN/m² for 4 results). The average tensile strength of the centerless-ground rods was 50 percent of that measured in 4 point bending on similar rods, and that of the commercially polished material was 35 percent of the strength measured in bending (fig. 11).

The tensile strength described above was performed in the early phases of the work before ruby rods were being used. Because of the greater internal perfection of this material it is thought that flame-polished ruby rods would have higher tensile strength than sapphire but this has not yet been determined.

3.5. Further Comments

The ability by flame-polishing to produce highly perfect surfaces on ceramic crystals has been known for several years and yet has received little attention. For example, only recently have such studies been directed toward exploiting the high strength of such crystals in structural applications. Furthermore, it is surprising that the technique has not been more widely used in research studies of the mechanical behavior of Al_2O_3 and other ceramic crystals. It is again emphasized that, with reasonable care, the production of high strength rods is a simple technique—certainly easier and more straightforward than most mechanical polishing procedures which never achieve comparable results.

On the other hand, a drawback for widespread industrial application of the flame-polishing process is that it is best suited to simple rod or cylinders of small diameter, although it has been claimed that the process is applicable to slabs and other shapes [8]. With larger diameter specimens, there is a severe thermal gradient throughout the cross-section of the specimen during polishing, causing high internal strains, which in turn can produce fracture. For diameters above about 3 mm, a large flame with a smaller inner hot zone is desirable, so that the whole cross-section and an appreciable length (say 3 to 5 diameters) of the rod on each side of the hot zone is heated, thus avoiding severe thermal stress. One solution is to flame-polish large diameter (e.g., 5 mm) rods within a muffle furnace.

Attempts have also been made to polish a flat surface on 10 mm diameter × 1.5 mm thick discs of single crystal Al_2O_3 using the smaller flames used for rods. High thermal gradients were inevitable; thermal strains caused visible basal deformation twins to form before surface melting had occurred and spread rapidly across the disc at the point of impingment of the flame. By preheating similar discs to 1200–1500 °C during polishing, it was possible to achieve some surface improvement but the technique has not yet been perfected.

4. The Effect of Annealing

Klassen-Neklyudova [30] first demonstrated that the strength of machined sapphire specimens could be increased by annealing at elevated temperatures. Since that time, similar results have been obtained by Tomilevski [31], Charles and Shaw [25], Davies [32], and by Heuer and Roberts [26], all of whom employed Verneuil-grown crystals. This phenomena will first be summarized and then discussed in detail:

1. There is a threshhold annealing temperature below which strength increases cannot be observed. Since the strength increase results primarily from a reduction in severity of surface damage [26], this threshhold temperature undoubtedly coincides with the onset of gross material transport, either by surface diffusion or by evaporation-condensation. (It is implicitly assumed in this paper that room temperature fracture in sapphire is a purely brittle process and does not involve plastic deformation in any critical or important sense.)
2. The magnitude of the strength increase is a function of the annealing temperature, the annealing atmosphere. and the crystallographic orientation. (The as-machined strength also varies with orientation, due to hardness and wear anisotropy affecting the severity of the surface damage imparted during machining of the specimens. [25]
3. Annealing affects the temperature dependence of the strength between room temperature and 1000 °C. The temperature dependence is anomalous in sapphire, in that a strength minimum is observed between 300 and 600 °C in as-ground specimens (as first reported by Jackman and Roberts [24]) but occurs at ~800 °C in annealed samples [25, 26, 32]. Inasmuch as the explanation for this anomalous temperature dependence is still controversial, it will not be discussed any further here.
4. Although annealing can lead to substantial strength increases, strengths do not approach those obtained for flame-polished specimens with near-perfect surfaces. On the other hand, annealing is a simpler process than flame-polishing and is much more suitable for complex-shaped parts.

In general, results of the several investigators who have studied the effects of annealing in sapphire are in reasonable, although not perfect, agreement. For example, Klassen-Neklyudova [30] reported 30 percent increase in the strength of 90 ° sapphire (c-axis normal to the rod axis) following annealing for 5 hours at 1000 °C, while 0° specimens, which were about twice as strong as the 90° specimens as-machined, showed little, if any, strength increase following this treatment. Tomilevskii [31] reported a 30-40 percent strength increase for 0° and 90° samples annealed at 1300 °C, while Charles and Shaw found a similar strength increase after 1200 °C; furthermore, 0° rods were about 1.8 times as strong as 60° rods but 0° rods did not increase their strength after this annealing. On the other hand, Davies [32][3] found a strength increase of ~250 percent at 1200 °C for 30° rods, while Heuer and Roberts [26], using 45° rods, obtained ~30 percent strength increase for annealing temperatures of 1325–1525 °C but little strengthening at 1250 °C. These latter workers, however, employed annealing temperatures up to 1800 °C, and found the strength increases to be greater as the annealing temperature increased. Since Heuer and Roberts also studied the effects of surface finish [machined versus mechanical polishing] and annealing ambient, their results will be presented in more detail.

Figures 15 and 16 [taken from ref. 26] show the effects of annealing temperature and atmos-

[3] Davies employed tensile testing, all other workers [24–26, 30, 31] employed the bend test.

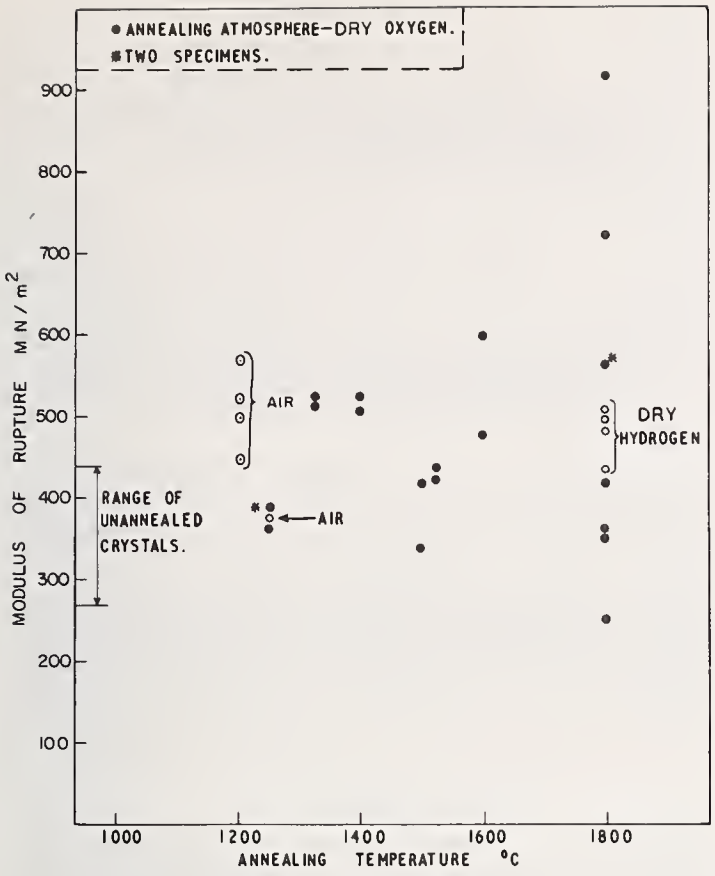

FIGURE 15. *Dependence of the room-temperature modulus of rupture of machined corundum crystals on annealing temperature.* The atmosphere for the annealing was dried oxygen except where otherwise stated, 24 hours were used for all temperatures but 1250 °C, where the annealing time was 6 hours.

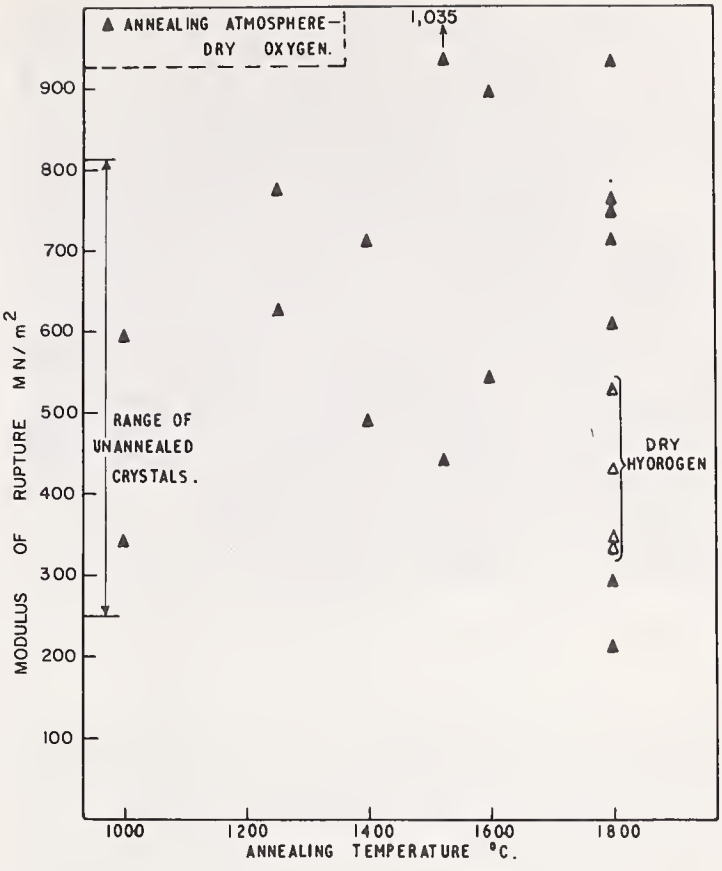

FIGURE 16. *Dependence of the room-temperature modulus of rupture of mechanically polished corundum crystals on annealing temperature.* The atmosphere during annealing was dried oxygen except where otherwise stated; 24 hours were used for all temperatures but 1250 °C, where the annealing time was 6 hours.

phere on the room temperature strength of machined and mechanically-polished sapphire respectively. With machined specimens (fig. 15), quite high strengths were achieved, and the maximum strength obtained increased with increased annealing temperature. Annealing in hydrogen at 1800 °C did not produce as much strengthening as annealing in oxygen at the same temperature. Much greater scatter was observed with mechanically-polished and annealed crystals (fig. 16) but strengthening could certainly be achieved on occasion. (Although the mechanically-polished specimens before annealing also showed greater scatter, the room temperature strengths had usually been less than 0.6 GN/m² [26].) Heuer and Roberts also determined the temperature dependence of strength of a group of machined and mechanically-polished crystals annealed together at 1800 °C for 24 hours in dry oxygen.

[4] Heuer and Roberts [26] also investigated the influence of premachining (i.e., boule) annealing (at ~ 1800 °C) and found it *not* to have any effect on the strength of either machined or mechanically-polished samples. This is an important piece of information relevant to item 1 above, i.e., the strength increase achieved during annealing results from a reduction in the surface damage introduced during preparation of samples from the larger boules. However, Besson [33] has found annealed sapphire windows to be less susceptible to failure in high pressure equipment than unannealed windows, and has ascribed this to a reduction of *internal* strains, rather than to reduction in damage introduced during preparation of the windows.

For machined specimens, strengthening was observed at all temperatures below 1200 °C, for mechanically-polished crystals, strength increases at liquid nitrogen and room temperature were realized but both the maximum strength and the scatter of strength seemed to decrease with increase in testing temperature.

Annealing increased the strength of machined crystals more than it did those with mechanically-polished surfaces. For example, strengths at −196 °C were about the same for the two types of specimens after annealing, whereas before annealing, the mechanically-polished crystals were stronger.

Heuer and Roberts concluded that the main strengthening effect of annealing was to modify surface damage, as shown in figures 17 and 18. Although the detail observed on machined specimens after annealing was difficult to interpret, changes in gross surface roughness were obvious and were confirmed using a Talysurf machine (fig. 19). Decrease in surface roughness was first detected following annealing at 1400 °C, and the surface became significantly more smooth as the annealing temperature was increased; subgrain boundaries could be seen after annealing at temperatures

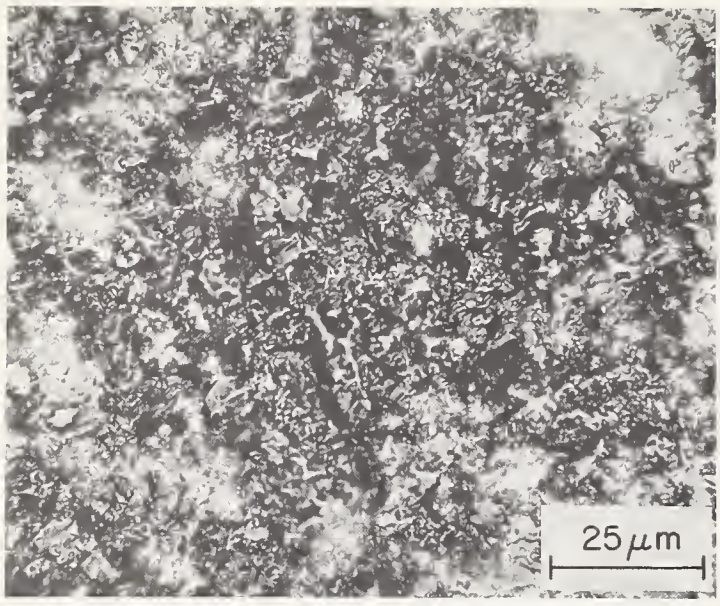

FIGURE 17. *Surface of machined specimen as received (reflected light, normal incidence).*

of 1600 °C and above. This "threshold temperature" for surface improvement is consistent with measurements of surface diffusion kinetics (by grain boundary grooving) in alumina single crystals, which yield very low values ($<10^{-13}$ M^2/sec.) for D_s, the surface diffusion coefficient below 1400 °C [34]; also, LEED measurements, show structural transformations on (0001) surfaces of alumina to occur above 1250 °C in vacuum [35].

The annealing in hydrogen (1800 °C) was more effective in decreasing the gross surface roughness than was annealing in oxygen. Furthermore, machined specimens as-received were initially translucent, and annealing had the effect of increasing the light transmission. The

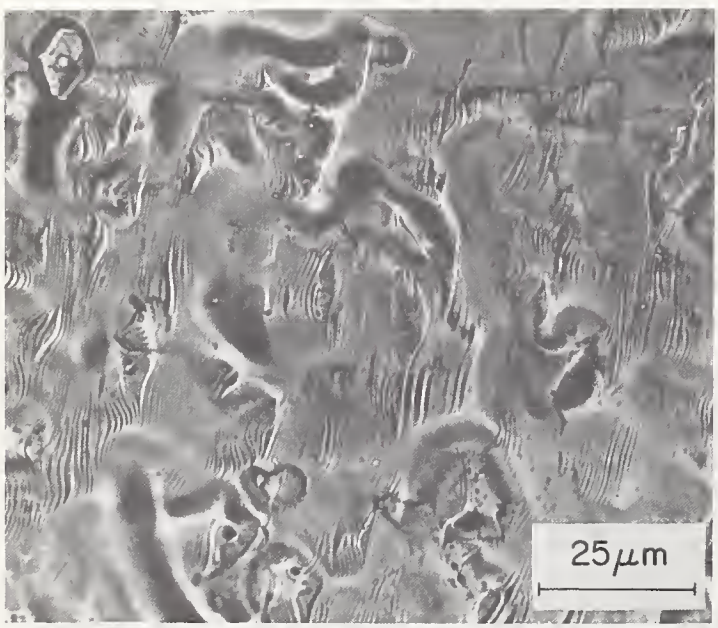

FIGURE 18. *Surface of machined specimen after 24 hour annealing in dry oxygen at 1800 °C (reflected light, normal incidence).*

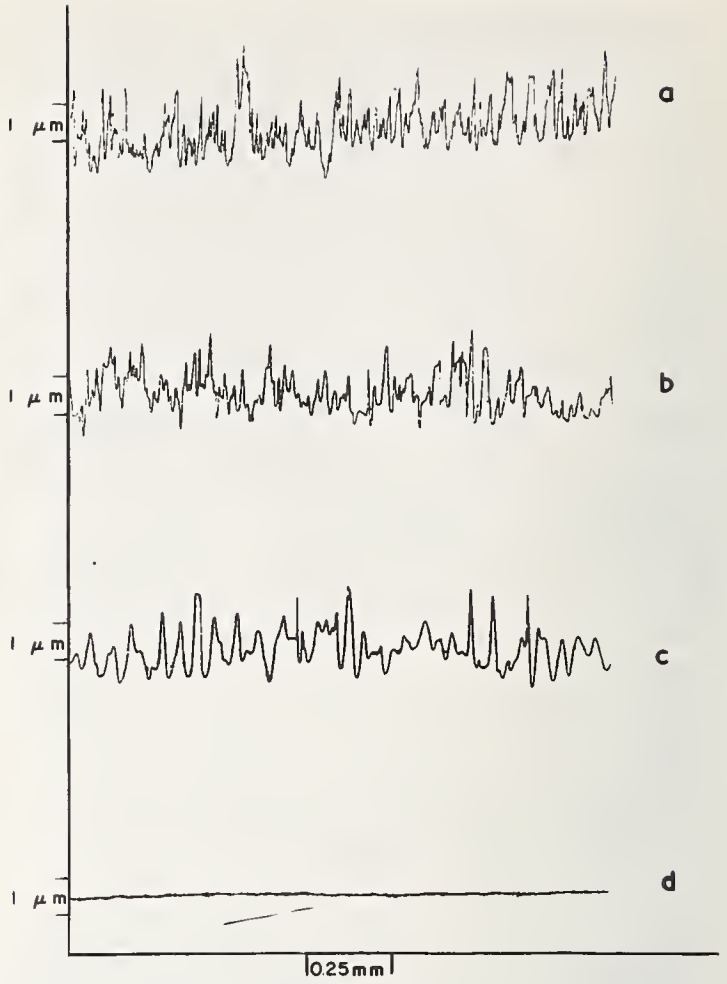

FIGURE 19. *Profiles of surface roughness as determined by a Talysurf machine.*

a. Machined specimen, as received.
b. Machined specimen annealed for 24 hours at 1800 °C in oxygen.
c. Machined specimen annealed for 24 hours at 1800 °C in hydrogen.
d. Mechanically-polished specimen.

specimens annealed in hydrogen (1800 °C), thus, became almost transparent. In view of these results, the weakening effect of hydrogen annealing is not understood, but may be associated with the chemical etching known to occur when alumina is heated in hydrogen above 1300 °C [36].

The changes that occur on mechanically-polished sapphire surfaces after annealing have been discussed extensively by Heuer and Roberts in a separate publication [37].

It may be concluded that air or oxygen annealing is an effective means of strengthening machined alumina single crystals.

5. Conclusions

Both flame-polishing and annealing can be used to improve the surface finish of alumina single crystals, and thereby improve the strength. Flame-polishing in particular is a process using relatively simple techniques and

equipment (available in most laboratories) for routinely producing highly perfect surfaces. The strengths of such crystals with their near-perfect surfaces is generally limited by flaws in the interior of the material and not at the surface—the general case for ceramic materials. It is thus possible to obtain specimens for measurement of the "intrinsic" mechanical properties of the bulk crystals.

Annealing, while yielding much more modest strength increases, may be more suitable for structural parts of complex shape.

The authors express their thanks to A. P. Levitt of the Army Materials and Mechanics Research Center, and to R. A. Schmidt of the Naval Air Systems Command, whose support of research projects enabled much of the work described in this paper to be accomplished. They are also grateful to Dr. D. J. Barbour of Univ. of Essex (England), for providing them with a translation of reference 30.

6. References

[1] Griffith, A. A., (i) Phil. Trans. Roy. Soc. A221, 163–198, 1920 and (ii) 1st Inter. Cong. Appl. Mech., Delft, 55–63, (1924).

[2] Morley, J. G., and Proctor, B. A., Strengths of sapphire crystals, Nature, 196, 1082, (1962).

[3] Brenner, S. S., Mechanical behavior of sapphire whiskers at elevated temperatures, J. Appl. Phys. 33, 33–39, (1962).

[4] Mehan, R. L., and Feingold, E., Room and elevated temperature strength of α-Al_2O_3 whiskers and their structural characteristics, J. Matls. 2, (2), 239–270, (1967).

[5] Marsh, D. M., Stress concentrations at steps on crystal surfaces and their role in fracture, in Fracture of Solids, eds. Drucker, D. C. and Gilman, J. J., 119–142, (1963).

[6] Wiederhorn, S. H., Fracture of ceramics, pp. 217–241, in Mechanical and thermal properties of ceramics, edited by Wachtman, J. B., Jr., Nat. Bur. Stand. (U.S.), Spec. Publ. 303, 268 pages (1970).

[7] Popov, S. K., The growth and uses of gem-grade corundum crystals, in Growth of Crystals, Vol. 2, Shubnikov, A. V. and Sheftal, N. N., eds., 2nd Conf Crystal Growth, Institute of Crystallography, Academy of Sciences, USSR, Translated from Russian by Consultants Bureau Inc., N.Y., pp. 103–152, (1959).

[8] Barnes, M. H., and McCandless, E. L., Flame-glossing of rod shaped single crystals of corundum, (Union Carbide and Carbon Corp.) U. S. Patent 2,608,031, (1952).

[9] Wachtman, J. B. Jr., and Maxwell, L. H., Plastic deformation of ceramic-oxide single crystal: II, J. Am. Ceram. Soc., 40, (11) 377–385, (1957).

[10] Proctor, B. A., The occurrence of specific stress raisers in high strength brittle solids, in Physical Basis of Yield and Fracture, ed. A. C. Strickland, pp. 218–224 (Conference Series 161, Institute of Physics and Physical Society, London, 1966).

[11] Mallinder, F. P., and Proctor, B. A., The Strengths of Flame-Polished Sapphire Crystals, Phil. Mag 13, (121), 197–208, (1966).

[12] Mallinder, F. P., and Proctor, B. A., Preparation of high strength sapphire crystals, Proc. Brit. Ceram. Soc., No. 6, 9–16, (1966).

[13] LaBelle, H. E., Jr., and Mlavsky, A. I., Growth
(a) of sapphire filaments from the melt, Nature, 216, 574–575, (1967).
(b) Tyco, Inc., Special Products Division, Waltham, Mass., Bulletin No. 102, (1968).

[14] Mlavsky, A. I., and LaBelle, H. E., Jr., Growth of continuous whiskers from the melt, in Whisker Technology, Levitt, A. P., ed., pp. 121–133 (John Wiley and Sons, Inc., 1970).

[15] Hurley, G. F., and Pollock, J. T. A., Tyco, Inc.,
(a) Progress Report to XVIIth Refractory Composites Working Group Meeting, Williamsburg, Va., June 1970.
(b) Pollock, J. T. A., Continuous Flame-Polishing of Sapphire Filament, p. this proceedings.

[16] Noone, M. J., Feingold, E., and Sutton, W. H., The Importance of coatings and the preparation of Al_2O_3 filament metal-matrix composites, ASTM, STP No. 452, pp. 58–89, (1969).

[17] Mallinder, F. P., and Proctor, B. A., (Rolls Royce Company, England), Private Communications, (1967).

[18] Keig, G. A., (Union Carbide Corporation), Private Communication, (1968).

[19] Chang, R., Creep of Al_2O_3 single crystals, J. Appl. Phys. 31, 484–487, (1960).

[20] Vrooman, D. L., and Ritter, J. E., Non-linear behavior of thin beams in four-point bending, Amer. Ceramic Soc. Bull. 49, 789–792, (1970).

[21] Heuer, A. H., Plastic deformation in polycrystalline alumina, Proc. Brit. Ceram. Soc. 15, 173–184, (1970).

[22] Bayer, P. D., and Cooper, R. E., A new slip system in sapphire, J. Mater. Sci. 2, 301–302, (1967).

[23] Heuer, A. H., Deformation twinning in corundum, Phil. Mag. 13, (122), 379–393, (1966).

[24] Jackman, E. A., and Roberts, J. P., The Strength of single crystal and polycrystalline corundum, Phil. Mag., Ser. 7, 46, 809–811, (1955).

[25] Charles, R. J., and Shaw, R. R., Delayed failure of polycrystalline and single-crystal alumina, Report No. 62–RL–3081M, General Electric Company, Research Laboratory, Schenectady, N.Y., (1962).

[26] Heuer, A. H., and Roberts, J. P., The influence of annealing on the strength of corundum crystals, Proc. Brit. Ceram. Soc. 6, 17–27, (1966).

[27] Mehan, R. L., Testing Fine Filaments and Whiskers, in Ceramic Fibers and Fibrous Composite Materials by H. W. Rauch, Sr., W. H. Sutton, and L. R. McCreight, pp. 27–48, (Academic Press Inc., New York, N.Y., 1968).

[28] Roberts, J. P., and Watt, W., Selected Government Research Reports (British), Vol. 10 "Ceramics and glass", pp. 31–50, (1952).

[29] Mehan, R. L., and Hertzog, J. A., Mechanical properties of whiskers, in Whisker Technology, Levitt, A. P., ed., pp. 157–195, (John Wiley & Sons, Inc., 1970).

[30] Klassen-Neklyudova, M. V., The mechanical properties of corundum crystals, J. Tech. Phys. (USSR) 12, 519–551 (1942).

[31] Tomilevskii, G. E., Effects of heat treating synthetic corundum crystals at 1300 °C on mechanical properties, Trudy Inst. Krist. Akad., Nauk USSR, 8, 341–354 (1953).

[32] Davies, L. M., The effect of heat treatment on the tensile strength of sapphire, Proc. Brit. Ceram. Soc. 6, 29–35, (1966).

[33] Besson, J. M., Private Communication, Lab. de Phys. de Solid. de la Fac. des Sci. de Paris, France, Equipe de Rech. CNRS, 1970.

[34] Robertson, W. M., and Ekstrom, F. E., Impurity effects in surface diffusion on aluminum oxide in Kinetics of Reactions in Ionic Systems, Vol. 4, Materials Science Research, Gray, T. J. and Frechette, V. D., eds., (Plenum Press, Inc., New York, N.Y., 1970).
[35] French, T. M., and Somorjai, G. A., Composition and surface structure of the (0001) face of α-Alumina by low-energy electron diffraction, J. Phys. Chem. 74, 2489–2495, (1970).
[36] Mercier, J., Dopant transfer in heteroepitaxial Si layers on sapphire substrates, J. Electrochem. Soc. 117, 812–814, (1970).
[37] Heuer, A. H. and Roberts, J. P., Thermal etching of single-crystal corundum, Trans. Brit. Ceram. Soc. 65, 219–232, (1966).

Discussion

GIELISSE: You have promised us a few brief comments on the difference between flame polishing sapphire and ruby.

NOONE: For instance, we found that in our lab scale tests the ruby material which we used was much easier to polish than sapphire. A technician, after only 10 minutes of instruction, could produce a million psi by flame polishing of ruby material; with sapphire this was not the case. We always found much less internal defects in the ruby material than was present in the sapphire. Differences between sapphire and ruby were expected in compatibility studies with metals but on closer examination by electron probe techniques, it turned out that the surface of a flame polished ruby rod was depleted of chromium. Chromium apparently evaporated from the liquid zone during the flame-polishing process so that the "ruby" rod was actually identical to sapphire within maybe 2 mils of the surface. Overall, in the ~ 300 results that I discussed (fig. 11) the average strength of the best batch of ruby was around 790,000 psi. This illustrates, I think, more than anything else the gross effect of internal defects on the strength of these materials.

WIEDERHORN: I am interested in the strength decrease at elevated temperatures for flame polished rods. I noticed that there was no mention made of the temperature region between room temperature and 900 °C.

NOONE: That's right. We haven's yet covered the whole temperature range with flame-polished material unfortunately. We tested at room temperature and above 900° where we expected to see the onset of basal slip which was critical for the proposed applications of these rods as reinforcement at high temperatures.

K. SMITH: I think that you perhaps were forming a suboxide in your hydrogen furnace. Were you getting a fully oxidized alumina?

NOONE: What do you think Arthur? I call on my coauthor to answer.

HEUER: If one goes by the color of the alumina. there is no evidence of reduction.

WACHTMAN: Do you know or care to speculate what the state of stress is in your flame polished rods? Do you expect to have a compressive or tensile stress?

NOONE: We certainly do not know in detail. I don't expect to have a high stress, but the surface must be in tension since it solidifies and cools over an already solid and relatively cold core.

WACHTMAN: One would think that the point at which you could no longer relieve stress would be reached not far below the melting temperature. At this point the surface might still be hotter than the interior and you would have some tension.

NOONE: I suspect you could probably relieve stresses all the way down to about 1200 °C in these small diameter rods. We haven't done the kind of experiments which John Pollock will describe a little later in which he split the rod down a center axis and looked for resultant curvature. We've looked at a lot of rods under polarized light and seen evidence of growth or machine induced strain which appears to be removed by polishing. I think the correct answer is that we don't really know what's going on inside.

LANGE: What are your thoughts either about dislocation motion or twinning prior to fracture, or at fracture in plain polished specimens?

NOONE: At room temperature I see no evidence for plastic flow or deformation twinning in the rods.

LANGE: So fracture more than likely was not nucleated by either dislocations or twinning.

NOONE: Fracture at room temperature we think is nucleated by the internal defects, predominantly bubbles.

NATIONAL BUREAU OF STANDARDS SPECIAL PUB. 348, THE SCIENCE OF CERAMIC MACHINING AND SURFACE FINISHING, Proceedings of a Symposium Sponsored by the American Ceramic Society, the Office of Naval Research, and the National Bureau of Standards, held at NBS Nov. 2–4, 1970, Gaithersburg, Md. (Issued May 1972).

Healing of Surface Cracks in Ceramics

F. F. Lange

Westinghouse Research Laboratories, Pittsburgh, Pennsylvania 15235

Grinding, cutting, thermal shocking, impacting and rough handling all introduce surface cracks that degrade the strength of ceramics. Within the last year, it has been shown that, once introduced, these cracks can be eliminated by either resintering the damaged ceramic component for the case of oxides or oxidizing the component for the case of materials such as SiC.

Results of crack healing experiments, performed on Al_2O_3, ZnO and SiC will be reviewed. The technical implications of these results will be discussed as related to abrasive machining.

Key words: Abrasive machining; ceramics; crack healing; sintering; surface damage.

1. Introduction

Shaping of most ceramic materials into engineering components requiring strict tolerances are currently carried out by what can be most suitably described as abrasive machining. This process involves the surface removal of one brittle material by another, harder, brittle material. Surface removal by abrasive machining leaves a damaged surface which, for many cases, impairs the usefulness of the machined ceramic component. Although the nature of the damage can be described by many property measurements, e.g., residual strain, dislocation, density, electrical conductivity, etc., its appearance can best be described as a surface containing numerous microcracks and notches. These flaws can be directly observed using both optical and electron microscopy. Indirect observations of these flaws can be made using both an oil dye penetrant and strength measurements.

Elimination of this damaged surface can be carried out by several techniques: (1) chemical polishing; (2) surface stressing; (3) lapping (polishing); and (4) heat treatment. Chemical polishing has been found successful for removing surface damage from some single crystals, [1][1] polycrystals, [1] and glasses [2]. Surface stressing (chemical strengthening, glazing, etc.) alters the damaged surface to a surface that supports a compressive residual stress, thus strengthening the material. [3, 4] Lapping is an abrasive machining technique that removes the severely damaged surface and leaves a less damaged surface. Heat treatment, the last of the techniques listed above, is the subject of this review.

Prior to 1970, several investigators [5, 6] reported that the strength of several ceramics could be increased by a heat treatment. One of these heat treating techniques was flame polishing. [7] In this report, it was suggested that surface damage (e.g., microcracks) could be eliminated by heat treatment. During the past year, it was shown [8, 9, 10] that deep surface cracks can be eliminated from several polycrystalline ceramic materials. The object of this paper is to review these recent results and to suggest a simple technique for removing surface damage left by abrasive machining.

2. Healing of Deep Surface Cracks

A large density of surface cracks can be conveniently introduced into ceramic specimens by thermal shocking them from an appropriate quenching temperature into water. Cracks introduced in this manner usually transverse the tensile stress zone formed by the thermal gradients [11] and, therefore, their depth is approximately 1/4 of the specimen width. Both the pattern and depth of these surface cracks can be revealed by an oil dye penetrant. The crack pattern appeared similar to that which appears on a crazed glaze. These deep cracks drastically decrease the material's strength.

This thermal shocking technique was used to introduce deep surface cracks in specimens of ZnO[1] (1/8 by 1/8 by 1 1/2 in), [8] Al_2O_3[2] (1/8 by 1/4 by 2 in) [10] and SiC[2] (1/4 by 1/4 by 2 in) [9] which were quenched from 400 °C, 400 °C and 600 °C, respectively into water at room temperature. Different sets of specimens were heated at 1100 °C for the ZnO, 1700 °C for the Al_2O_3 and 1400 °C for the SiC; each different set was heated for a different period. The first two temperatures were chosen because powders of the respective materials can be sintered at these temperatures. [12] The temperature for SiC was chosen because it was known that an oxide surface layer rapidly forms at 1400 °C. [13] All ambients were air (the ZnO specimens were contained in covered ZrO_2 boats).

After cooling, the flexural strength of each specimen was determined by four point loading. Flexural strengths were also determined

[1] Figures in brackets indicate the literature references at the end of this paper.

[2] Hot-pressed ZnO, Lucalox Al_2O_3 (General Electric Company) and 80 percent dense Crystar SiC (Norton Company).

TABLE 1. *Flexural strengths of 'as-cut' and thermal shocked specimens*

Material	Strength 'as-cut'	Strength thermal shocked
	psi (MN/m^2)	*psi* (MN/m^2)
ZnO	9600±12% (66.2)	3900±12% (26.9)
Al_2O_3	35,800±3% (246.8)	12,800± 7% (88.3)
SiC	19,000±7% (131.0)	9000±11% (62.0)

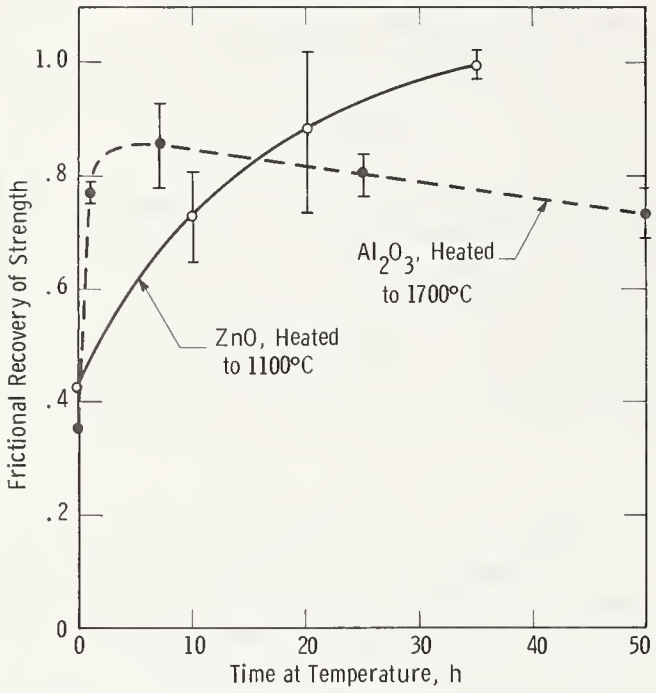

FIGURE 1. *Fractional recovery of initial flexural strength of both thermal shocked ZnO specimens heated to 1100 °C and thermal shocked Al_2O_3 specimens heated to 1700 °C.* (Normalized to as-cut strength (no thermal shock, no heat treatment).

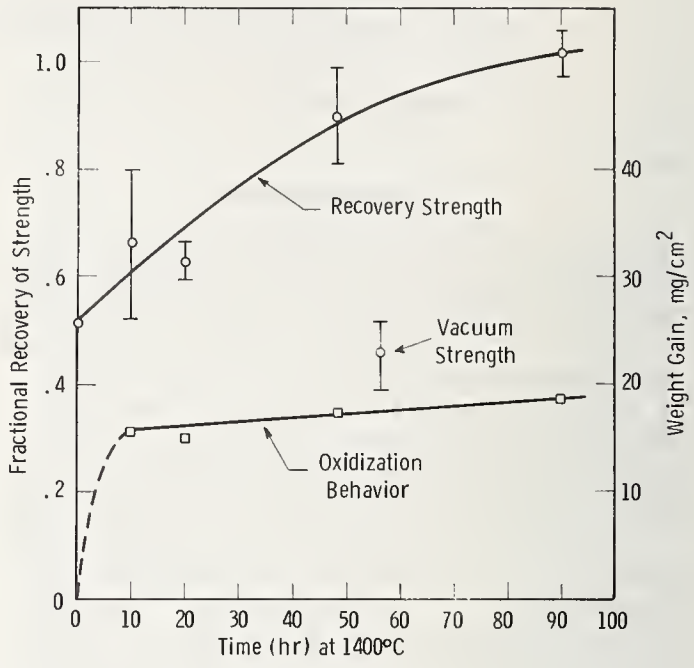

FIGURE 2. *Static oxidation behavior and strength* recovery of 80 percent dense, thermal shocked SiC specimens heated to 1400 °C.* *(Normalized to as-cut strength)

for both "as-cut" specimens (no thermal shock, no heat treatment) and thermal shocked specimens (no heat treatment). These are summarized in table 1. One set of SiC specimens was also heated in vacuum to 1400 °C for 56 hours. The oxidation rate for the SiC material was obtained from weight measurements before and after the specimens were heated. Average grain size measurements were made for all sets of ZnO and Al_2O_3 specimens.

Figure 1 summarizes the normalized flexural strengths of the thermally shocked, reheated oxide specimens. Figure 2 shows both the flexural strengths and weight gain (oxidation rate) of the thermally shocked, reheated SiC specimens. Table 2 lists the grain size measurements.

Both figures 1 and 2 show that all three materials regained all (or a significant portion for Al_2O_3) of their strength after a particular heat treatment. These data suggested that the deep surface cracks were eliminated. For both of the oxides, this was confirmed by an oil dye penetrant, i.e., surface cracks that could clearly be seen after thermal shock could no longer be observed after a certain period of heat treatment. By comparing the data represented in figure 1 with the grain size measurements presented in table 2, it can be seen that complete recovery in strength occurred for the ZnO despite considerable grain growth, whereas grain growth due to prolonged heating affected the Al_2O_3 strength recovery. This latter result has been discussed by Lange and Radford [10].

For the SiC, the surface cracks could still be seen (several surfaces were polished prior to thermal shock) under an oxide surface layer. Fracture surface observations revealed some traces of an oxide surface layer for SiC specimens heated for short periods. This suggested that the oxide filled and healed the deep cracks. This fact was confirmed by the low strength found for the specimens heated in vacuum. Lange [9] has shown that such an oxide bond has little affect on the strength recovery of hot-pressed, high strength SiC.

These data and observations clearly show that surface cracks can be either eliminated (for the case of the oxides) or made inopera-

TABLE 2. *Grain size* of heated oxide specimens*

Time at temperature	Al_2O_3(1700 °C)	ZnO(1100 °C)
hr		
0	43 μm	6 μm
7	44	--
10	--	10
20	--	11
25	52	--
35	--	14
50	54	--

*In micrometers, determined by linear analysis and multiplied by 1.5.

tive (for the case of SiC). Qualitative oil dye penetrant experiments show that heat treatment can eliminate surface cracks in polycrystalline MgO. Evans and Davidge [14] have recently shown that crack-like surface flaws on reaction-sintered Si_3N_4 can be made inoperative by the formation of an oxide surface layer. For certain conditions, they have shown that this results in a strengthening effect. Thus, this author believes that crack healing by heat treatment is a phenomenon general to most ceramics.

3. Heat Treatment of Abrasively Machined Surfaces

Since deep surface cracks can be healed, microcracks introduced by abrasive machining should also heal with heat treatment. To test this hypothesis for the materials reported above, viz., ZnO, Al_2O_3 and SiC, two sets of specimens of each of these three materials were diamond cut; one set was heated for the respective maximum period and temperature reported above. Four point flexural strengths were then determined for each set of specimens. The results are shown in table 3.

These results show that for both ZnO and SiC, a strengthening was observed. The reason for the decrease in strength for the Al_2O_3 is most likely the increased grain size. This has been discussed elsewhere. [10]

Using scanning electron microscopy, both as-cut and heat treated Al_2O_3 surfaces were examined. Representative SEM micrographs are shown in figure 3. Figure 3(a) shows the rough 'as-cut' surface. The arrows on this micrograph show microcracks, grain-pullouts and

TABLE 3. *Strength change for diamond cut specimens after heat treatment*

Material	Heat treatment	Percent average strength change*
ZnO	35h, 1100 °C	+17
Al_2O_3	50h, 1700 °C	−18
SiC	110h, 1400 °C	+10

*Table 1. Contains diamond cut strengths before heat treatment.

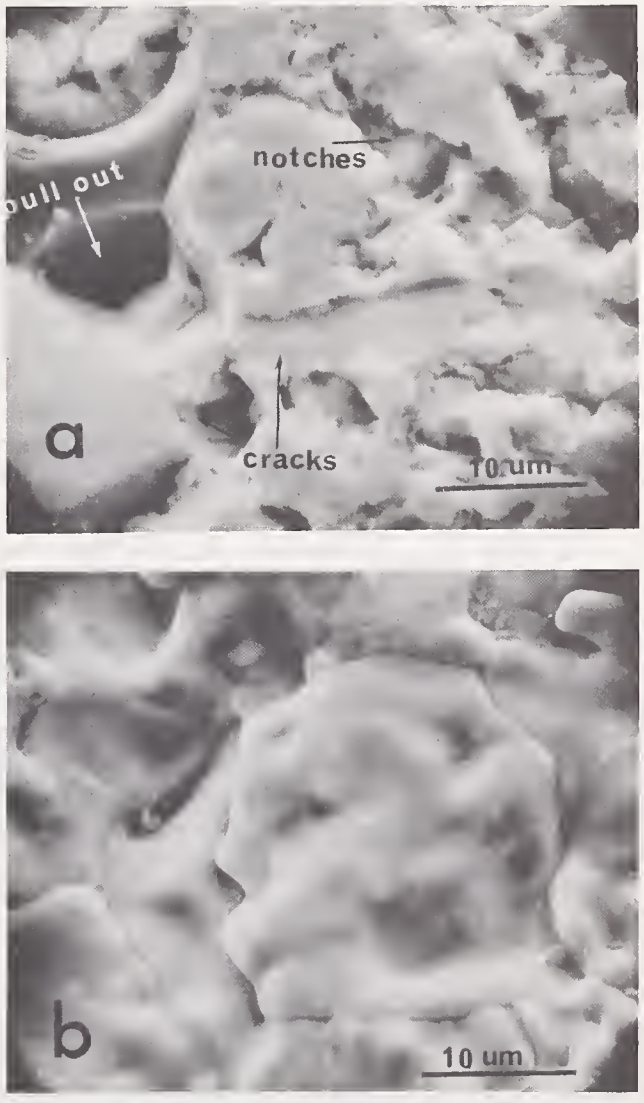

FIGURE 3. *Scanning electron micrographs showing diamond cut surface of Al_2O_3 prior to heat treatment (a) and after heat treatment (b).* Heat treatment was 50h at 1700 °C.

sharp notches. The heat treated surface, shown in figure 3(b), is much smoother, i.e., no transgranular microcracks were observed and all edges and notches were rounded relative to the 'as-cut' surface. Thermal etching appears to have occurred, thus revealing most grain boundaries.

These qualitative experiments and observations show that heat treatment can improve the quality of an abrasively machined surface. It has also been shown here that the temperature and time required of this heat treatment can be chosen as either that required to sinter powders of the oxide or that necessary to form a coherent oxide film for the case of non-oxides. For strength requirements, factors such as grain growth must also be considered. As it was pointed out in the introduction, heat treatment is not the only way of changing degraded surface properties, but it does represent a simple technique for approaching this problem.

The author would like to acknowledge the helpful discussions with both T. K. Gupta and R. C. Radford, both of whom participated in the original work. Support by the Office of Naval Research, Contract NOOO14–68–0323, NR 032–507 was appreciated.

4. References

[1] Stokes, R. J. and Li, C. H., Dislocations and the tensile strength of magnesium oxide, J. Am. Ceram. Soc. 46, 423–34 (1963).

[2] Hillig, W. B. and Charles, R. J., Surfaces, stress-dependent surface reactions and strength, p. 683 in High-Strength Materials, Ed. by V. F. Zackay, Wiley & Sons, New York (1965).

[3] Stookey, S. D., Strengthening glass and glass-ceramics by built-in surface compression, ibid, pp. 669–81.

[4] Kirchner, H. P., Gruver, R. M., and Walker, R. E., Strengthening sapphire by compressive surface layers, J. Appl. Phys. 40, 3445–52 (1969).

[5] Heuer, A. H. and Roberts, J. P., Influence of annealing on strength of corandum crystals, Proc. Brit. Ceram. Soc. 6, 17–27 (1966).

[6] Kirchner, H. P., Graver, R. M., Platts, D. R., Richel, P. A., and Walker, R. E., Chemical strengthening of ceramic materials, Summary Report, Contract NOOO19–68–C–0142, Naval Air Systems (1969).

[7] Mallinder, F. P. and Proctor, B. A., Preparation of high-strength sapphire crystals, Proc. Brit. Ceram. Soc. 6, 9–16 (1966).

[8] Lange, F. F. and Gupta, T. K., Crack heating by heat treatment, J. Am. Ceram. Soc. 53, 54 (1970).

[9] Lange, F. F., Healing of surface cracks in SiC by oxidation, ibid, pp. 290.

[10] Lange, F. F. and Radford, K. C., Healing of surface cracks in polycrystalline Al_2O_3, ibid. pp. 420–21.

[11] Davidge, R. W. and Tappin, G., Thermal shock and fracture in ceramics, Trans. Brit. Ceram. Soc. 66, 405–22 (1967).

[12] Gupta, T. K. and Coble, R. L., Sintering of ZnO:I, J. Am. Ceram. Soc. 51, 521–25 (1968).

[13] Lange, F. F., (unpublished).

[14] Evans, A. G. and Davidge, R. W., The strength and oxidation of reaction-sintered silicon nitride, J. Mat. Sc. 5, 314–25 (1970).

Discussion

RICE: Two questions: First, do you feel the small increase indicated in silicon carbide was real? If so, do you feel this might possibly be due to the fact that SiO_2 is formed in the cracks? This might be a way of putting a compressive stress on the surface layer.

LANGE: Could be. Whether or not it's real, I really don't know. As discussed in the paper, SiO_2 did form within the cracks. I also have tried to heal deep surface cracks in hot-pressed SiC. It was impossible to strengthen this thermally shocked material. Apparently the silica bond was not strong enough relative to the degraded strength of the thermally shocked, high-density silicon carbide.

HOCKEY: I'd just like to add that I've looked at cracks associated with hardness indentations in single crystal aluminum oxide in both the unannealed and annealed state by transmission electron microscopy. In the unannealed case, the cracks always tended to propagate during the thinning of the specimen. In the annealed case, for example at 1000 °C for one hour, I often found dislocations associated with the cracks created during indentation. These cracks remained arrested during thinning.

NATIONAL BUREAU OF STANDARDS SPECIAL PUB. 348, THE SCIENCE OF CERAMIC MACHINING AND SURFACE FINISHING, Proceedings of a Symposium Sponsored by the American Ceramic Society, the Office of Naval Research, and the National Bureau of Standards, held at NBS Nov. 2–4, 1970, Gaithersburg, Md. (Issued May 1972).

Flame Polishing of Flat Oxide Bars

P. F. Becher and R. W. Rice

U. S. Naval Research Laboratory, Washington, D.C. 20390

Some of the problems and limitations of flame polishing flat bars are discussed. Results are presented for single crystal, α–Al_2O_3, as well as for more limited trials of $MgAl_2O_3$, TiO_2 and soda lime glass. The wide variability of strength is partially related to variations in surface, but twinning also appears to be important in sapphire and TiO_2. Preliminary results on twin sources and their effect on strength of sapphire are discussed.

Key words: Flame polishing; glass; rutile; sapphire; spinel; strength; surface characterization; twinning.

1. Introduction

High bend strengths have previously been achieved by flame polishing materials such as Al_2O_3 [1–4][1] and SiO_2 [1]. However, these studies have typically been conducted on round specimens. This paper presents results of an initial study of flame polishing of flat single crystal bars of α–Al_2O_3, $MgAl_2O_4$, TiO_2 and glass. These tests show more clearly the problems of flame polishing flat bars and the advantages of using round bars. Flat bars have some advantages in revealing microstructure and fracture mechanisms, and some reasons for the differences in the flame polishes achieved with these and initial results on fracture mechanisms are presented.

2. Experimental Techniques

Single crystal bend bars of α–Al_2O_3, both undoped and Cr-doped, having $\{10\bar{1}0\}$[2] and/or $\{11\bar{2}3\}$ tension surfaces with the tension axes within 20° of $<11\bar{2}0>$ and 20° of $<42\bar{6}1>$ (normal to $(20\bar{2}5)$), respectively, were flame polished. In addition, bars of $MgAl_2O_3$ and TiO_2 single crystals and of soda lime glass were also cursorily investigated. The flame polishing utilizing an oxy-hydrogen torch consisted of two techniques related to the amount of melt formed. The first, "pool," method required a slow increase in temperature by moving the torch back and forth over the length of the bar until melting was initiated at the edges. Then the torch was brought to close proximity to the surface to form a definite melt pool, which was then "pushed" along the surface.

The second "clearing" technique involved prolonged heating of the bars to obtain a general clearing over the entire surface. A thin layer of melt was apparently formed but was barely, if at all, evident to the unaided eye. The "clearing" polish gave much smoother finishes, generally free of surface artifacts. Prior to flame polishing, the α–Al_2O_3 crystal tension surfaces were prepared by diamond grinding parallel to or perpendicular to the tensile axis, mechanically polishing (1 μm diamond paste) or gas polishing [5, 6]. The other ceramic specimens had as air-polished and/or ground surfaces. The flame polished specimens ($\sim$1.8×3.6 mm in cross section) were subsequently tested in 3 point bending at room temperature over 1.27 cm. spans in an Instron test frame employing a cross speed of 2.1×10^{-2} mm/s. In addition, specimens were examined optically before and after testing, and in some instances, hot prosphoric acid was utilized to delineate the microstructure (especially in the case of the α–Al_2O_3 bars). The sapphire samples were oriented with standard laue back reflection x-ray techniques together with the use of indexing tables [7]. Similar methods were used for the analysis of twins.

3. Results and Discussion

3.1 Flame Polishing of α–Al_2O_3

The room temperature strength of the flame polished sapphire and ruby bars having various prior surface finishes are shown in table 1, together with data for these bars prior to flame polishing. In general, flame polish strengths are greater than machined surfaces (all of which have comparable strengths except for those ground across the tensile axis). The improvements obtained by flame polishing, however, are less than expected from previous studies [1–4]; this is particularly evident in the results with the "pool" technique. The best overall strengths are obviously obtained using the "clearing" method which was most successfully applied to ground surfaces rather than mechanically or gas polished ones.

Cursory flame polishing trials by the authors, using circular rods, demonstrated that greater strengths were achieved in rods versus flat bars

[1] Figures in brackets indicate the literature references at the end of this paper.

[2] Indices of planes and directions based on $c/a = 2.73 : 1$ for α-Al_2O_3.

TABLE 1. *Room temperature strengths of α-Al_2O_3 single crystal bars*
[Modulus of Rupture, 10^3psi ($10^7 N/m^2$)]

Surface finish	Sapphire orientation				Ruby orientation	
	$[10\bar{1}0]^1 \approx <11\bar{2}0>^2$		$[11\bar{2}3]^1 \approx <42\bar{6}1>^2$		$[11\bar{2}3]^1 \approx <42\bar{6}1>^2$	
	Ave. M. R. Range		Ave. M. R. Range		Ave. M. R. Range	
I. Mechanical finishing						
A. As-ground						
1. T. A.[3]	$\frac{25 \pm 7}{14-36}$	(17)	$\frac{24 \pm 6}{14-35}$	(16)		
2. T. A.[3]	$\frac{53 \pm 2}{35-73}$	(37)	$\frac{55 \pm 6}{49-66}$	(38)	$\frac{69 \pm 3}{62-78}$	(48)
B. Mechanically polished	$\frac{59 \pm 4}{42-72}$	(40)				
II. Flame polishing						
A. "Pool" technique						
1. Ground $\perp$ T. A.[3]	$\frac{33 \pm 8}{20-77}$	(23)				
2. Ground $\parallel$ T. A.[3]	$\frac{63 \pm 7}{41-83}$	(43)	$\frac{50 \pm 14}{34-73}$	(34)	$\frac{55 \pm 9}{42-80}$	(38)
3. Mechanically polished	$\frac{47 \pm 8}{33-67}$	(33)				
4. Gas polished	$\frac{71 \pm 10}{57-87}$	(49)				
B. "Clearing" technique						
1. Ground $\parallel$ T. A.[3]	$\frac{109 \pm 9}{92-150}$	(75)	$\frac{140 \pm 7}{135-145}$	(97)	$\frac{126 \pm 21}{97-156}$	(87)
2. Mechanically polished	$\frac{160 \pm 90}{92-232}$	(110)				
3. Gas polished	$\frac{109 \pm 20}{89-140}$	(75)				

[1] Orientation of tension surface.
[2] Orientation of tensile axis.
[3] Tensile axis.

(compare values in table 1 with references [1–4]. Although a difference in the crystal stock characteristics might explain the lower strength values for the bars (as compared to rods), gas polishing of identical flat bars resulted in greatly improved strengths [6] as compared to flame polished flat bars. This indicates that the flame polishing process itself, and not the initial bulk material, limited strengths. A qualitative understanding of the effects of flame polishing can be obtained by observing its effects (microstructural and strengthening) on these specimens. Some of these are more evident in flat bars than in circular rods.

a. "Pool" Technique

Three types of surface features characterized the finishes obtained by the "pool" technique of flame polishing. First of these were surface "waves," of the order of 0.5 cm. in length, which resulted from non-uniform motion of the flame tip to avoid excessive melting. Secondly, surface doming was observed which occurred when a uniform but extensive melt was formed. This thicker melt yielded cross sections having curved polished surfaces as a result of liquid surface tension (fig. 1a). Surface facets generally formed in the region where the melt was deepest, which was usually in the center of the domed region or near "wave" crest. This crystallographic faceting was attributed to solid state diffusion brought about by the slow cooling which results from the melt thickness and slower torch motion in the pool method.

Specimens having "wave"-type surfaces tended to have somewhat higher strengths than the

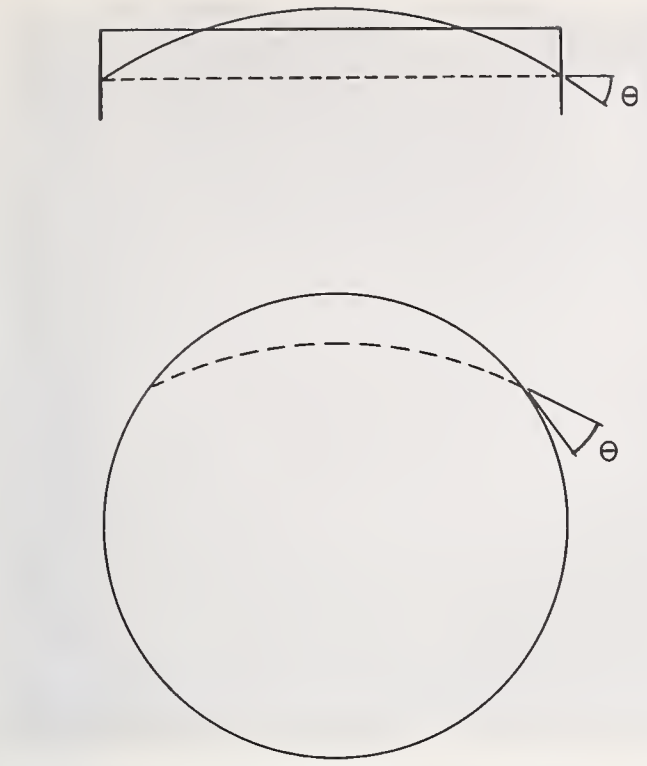

FIGURE 1. *Effect of specimen shape on melt configuration during flame polishing by the pool technique.* Curvature in the surface is a result of liquid surface tension during melting. The greater the amount, and hence extent, of the melt at any one time, the greater the degree of doming. Flame polishing of flat surfaces accentuates this doming as shown in (a), while circular cross sections tend to mask the effect (b) where the surface before and after polishing was approximately coincident as depicted here. In these two cases, the maximum depth of the melt (dotted line) and resultant contact angles are illustrated as being equal.

other types produced by the "pool" technique. In part, this resulted from the discontinuous nature of these surface crests and the increased likelihood of the maximum stress in three point bending to be located away from these regions which are likely to behave similar to domed surfaces.

The domed surfaces and their associated thicker melts were more likely to be subject to subsurface bubble formation as a result of solidification from the melt surface rather than the underlying solid surface. As discussed by Mallinder and Proctor [1, 2], bubbles or voids act as a source of weakness; however, bubbles were not generally observed in the present specimens and few fractures originated at or near bubbles. Thus, bubbles did not appear to be a primary cause of the low strengths obtained in these specimens. The domed surface contour and surface faceting would be expected to lead to stress concentrations; however, their radii of curvature was such that they did not generally appear to explain the low strengths observed. In addition, these surface features were not continuous along the bar samples, and failure often took place in sections devoid of them. Furthermore, gas polishing [6, 8] was utilized to remove surface irregularities from a limited number of these flame polished ("pool" method) bars, yet the strength of these bars was unaltered.

Twins were observed in these specimens, suggesting another source of structural weakness. During cooling of these bars, surfaces are subjected to considerable thermal stresses as a result of heating one surface. Twins have previously been reported to be introduced in α–Al_2O_3 during rapid heating and cooling [9, 10], and flame polishing-induced stresses apparently served to initiate twins especially at regions of stress concentration, i.e., bar edges and surface facets (fig. 2). As noted in figure 3, faceted regions are particularly active twin sources. Both basal and rhombohedral twins were detected using optical and x-ray analysis. Furthermore, there was evidence for slip at basal twin tips (fig. 4) induced by flame polishing. The population of these twins (basal and rhombohedral) was higher in ruby specimens than sapphire bars, consistent with the observations of Levengood [11]. The results of his study at room temperature indicated that the stresses necessary to initiate twins decreased with chromium additions. However, the present results suggested that intersecting twin systems were a more significant influence on strength than twin populations, as seen by the similar strengths of ruby and sapphire flame polished bars. Although twin-twin and twin-subboundary intersections previously reported to result in crack initiation [12–14] were not explicity associated with fracture origins in the present study, cracks were often associated with twins (figure 5), and twins were noted at fracture surfaces. The fact that similar low strengths occurred when nonparallel twins were observed in fracture regions devoid of any surface irregularities, further suggested that twins were a definite factor. Also in support of this, the previously mentioned flame polished bars that were gas polished but had unaltered strengths were found to contain intersecting twins.

b. "Clearing" Techniques

The finest quality (i.e., flattest and most featureless) surfaces were produced by the "clearing" techniques and with moderate effort. Seldom were comparable surfaces achieved with optimum operation of the "pool" method. This was attributed to the much smaller quantity of melt produced, which rapidly solidified, inhibiting surface doming and facet formation. The fact that a melt did form, even though difficult to detect, is seen in that clearing

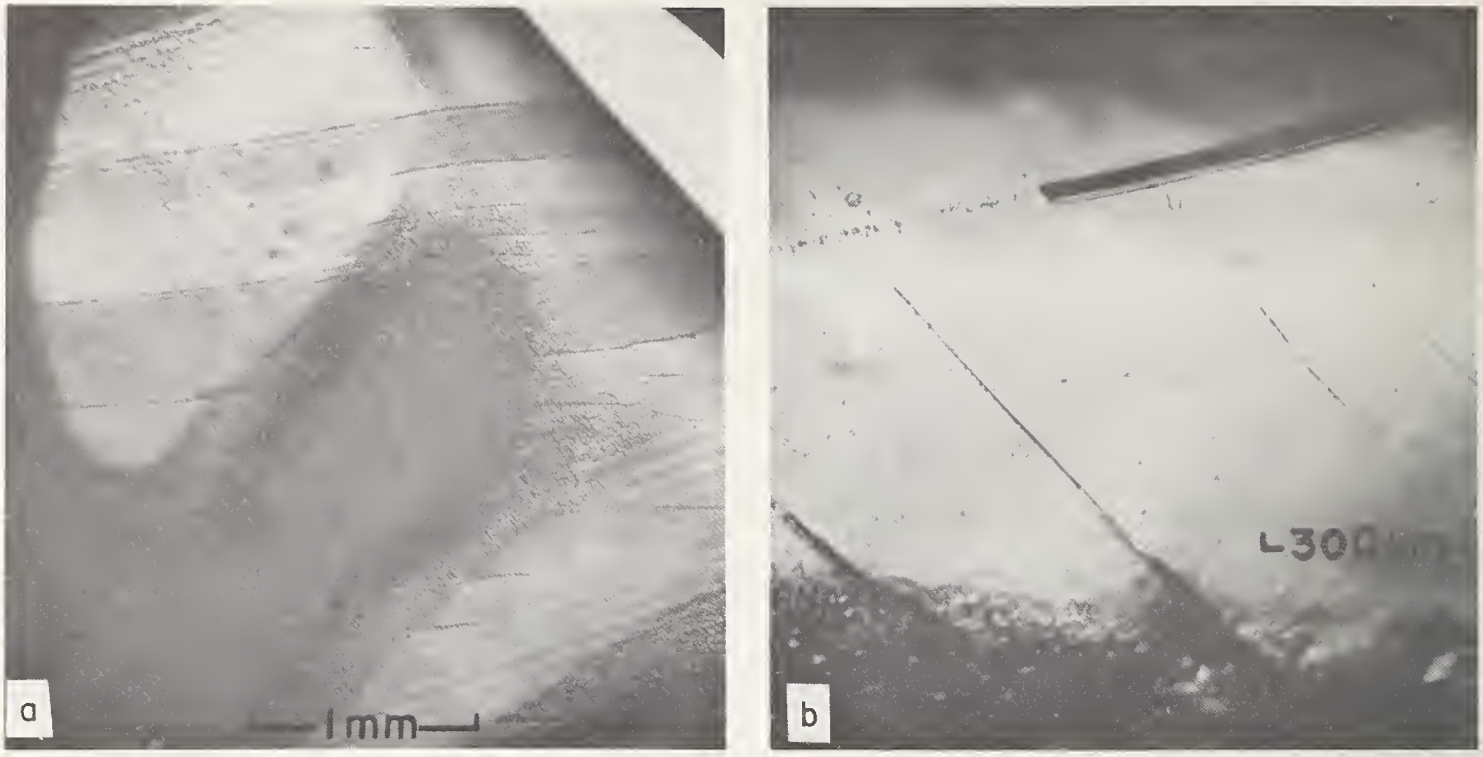

FIGURE 2. *Twinning in α–Al_2O_3 as a result of flame polishing.*
a. As flame polished surface exhibiting wave crests (dark, faceted areas) and linear surface features paralleling the interference fringe bands. Polarized transmitted light.
b. Chemical etching of surfaces similar to (a) delineates intersecting twins which correspond to linear structures in (a). Interference phase contrast, reflected light.

FIGURE 3. *Twin source on flame polished surface.* At slightly higher magnification, it is seen that heavily faceted surface regions serve as an origin of tapered twins occurring on parallel planes. Transmitted light.

FIGURE 4. *Evidence of slip preceding basal twinning in ruby.* Etching of flame polished surface with hot phosphoric acid reveals etch pits in twin interface and a dense row of dislocation etch pits in advance of twin path. These are suggestive of basal twinning involving dislocation glide processes on the basal plane. Interference phase contrast, reflected light.

FIGURE 5. *Fractures associated with flame polishing twins.* Cracks are observed in twin regions or along twin boundaries after testing and the crack at the twin tip above extends to the fracture origin. Chemically etched; interference phase contrast, transmitted light.

"against the grain" of grinding striations could not be accomplished. It was evident that the grinding stria halted the flow of the thin melt layer and good results were achieved only when the melt was allowed to flow along the grinding grooves. In bars ground perpendicular to their lengths, this resulted in problems of melt overlap, partial polishing, and increased thermal stresses. Further problems were encountered with mechanically or gas polished surfaces where the lack of difference of clarity or contrast of the surfaces resulted in poor control of this technique. This lead to formation of thick melts and related problems; however, when properly applied, clearing of mechanically polished surface yielded the highest strength of any flame polished bar (230,000 psi, 155×10^7 N/m^2).

The high quality finishes of the cleared surfaces were consistent with the improvements in strengths of these as compared to the previous "pool" polished bars (table 1). In addition, the cleared bars were generally free of twins and when twins were observed, they occurred only on parallel planes (fig. 6). This observation further indicated that formation of intersecting twins was a factor in the low strengths of the pool polished bars.

3.2. Flame Polishing Other Oxides

a. $MgAl_2O_3$

Several attempts were made to flame polish Al_2O_3-rich spinel single crystal bars, primarily by the pool technique. Here again, the resultant strengths were widely scattered (table 2). Cracks from thermal stress, facetting and subsurface bubbles (which were more frequently associated with surface doming in these bars than in α–Al_2O_3) were also major factors in the low strengths. Nevertheless, the strengths of the flame polished bars were substantially improved over those of as-ground or mechanically polished samples. However, the higher strengths associated with the best finishes appeared to be low as compared to the improvements obtained with α–Al_2O_3. Precipitation of excess Al_2O_3, which has been shown to substantially reduce the strength of spinel [17, 18], may be an important factor in these bars. This was suggested by the cloudy nature of the more domed specimen surfaces of the lower strength bars. Subsequent bars that were annealed and slowly cooled prior to or after flame polishing exhibited even lower strengths (table 2), further indicating that precipitation was a factor in the flame polished strengths. Hence, partial precipitation may have been limiting strengths, so that greater improvements might be obtained in stoichiometric spinel.

TABLE 2. *Strengths of various ceramic oxides* [*Modulus of Rupture, 10³psi (10⁷N/m²)*]

Material	As-ground	Mechanically polished	Flame polished
$MgAl_2O_4$ (Single crystal)	34±2 (23)	—	42±6 [1] (29) 7–122 [2] 85±23 [3] (59) 60–122 26±6 [4] (18) 19–35 38±13 [5] (26) 28–47
TiO_2 (Single crystal)	13±1 (9)	—	2.7± (1.9) 1.7–4.4
Soda lime glass	14±1 (10)	17±3 (11)	15±2 (10) 12–18

[1] All spinel specimens
[2] Range of values.
[3] Spinel specimens devoid of bubbles, cracks, or other obvious defects.
[4] Spinel which was air annealed at $T \geq 1100$ °C prior to flame polishing.
[5] Flame polished spinel with subsequent air anneal, $T \geq 1100$ °C.

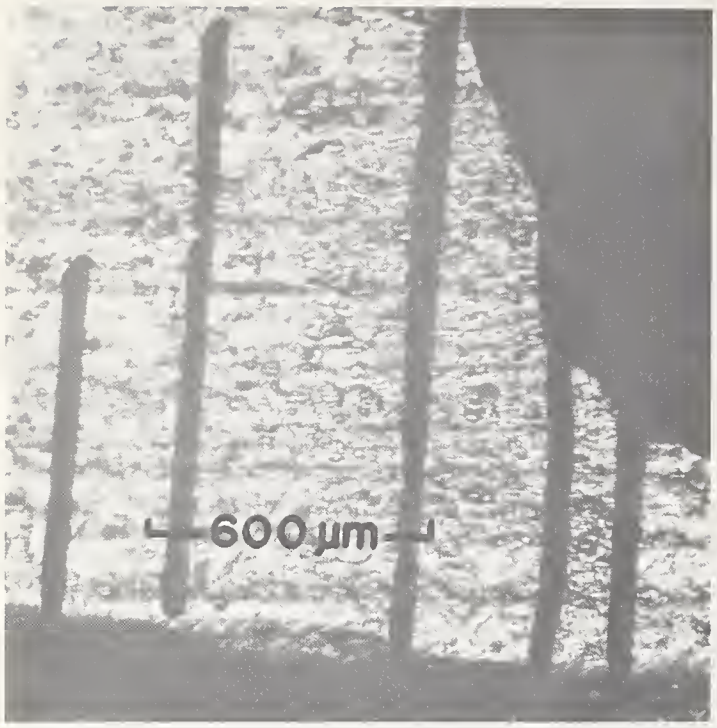

FIGURE 6. *Parallel twins in high strength, flame polished sapphire bar.* These twins, accentuated by etching, are observed to be approximately perpendicular to the twin axis. The two twins at far right intersect fracture surface in region of fracture origin. Interference phase contrast, reflected light.

b. TiO_2

Flame polishing of a limited number of ground rutile bars was attempted, essentially by the pool technique. In comparison to similar as-ground samples, the flame polished strengths were quite low (table 2). In polishing TiO_2, the melt was more difficult to control, resulting in part to a tendency for the melt to skip along the surface. This yielded surfaces having a mixture of wave, dome, clear, and unpolished surface regions. The air-annealed (yellow) TiO_2 specimens also became a dark blue or black, indicating that considerable reduction had occurred during flame polishing. In addition, most specimens cracked, some to the extent that testing was meaningless. During examination of fractured test specimens intersecting, narrow bands, whose optical behavior and etch structure was indicative of twinning, were often found to be associated with fracture origins (fig. 7). These results indicate that TiO_2 was not a likely candidate for further attempts at flame polishing and suggested that flame polishing induced twins which were a source of fracture initiation.

c. Soda Lime Glass

For cursory comparison, a few ground soda lime glass bars were flame polished primarily using the clearing technique. The strengths of these were only slightly higher than those

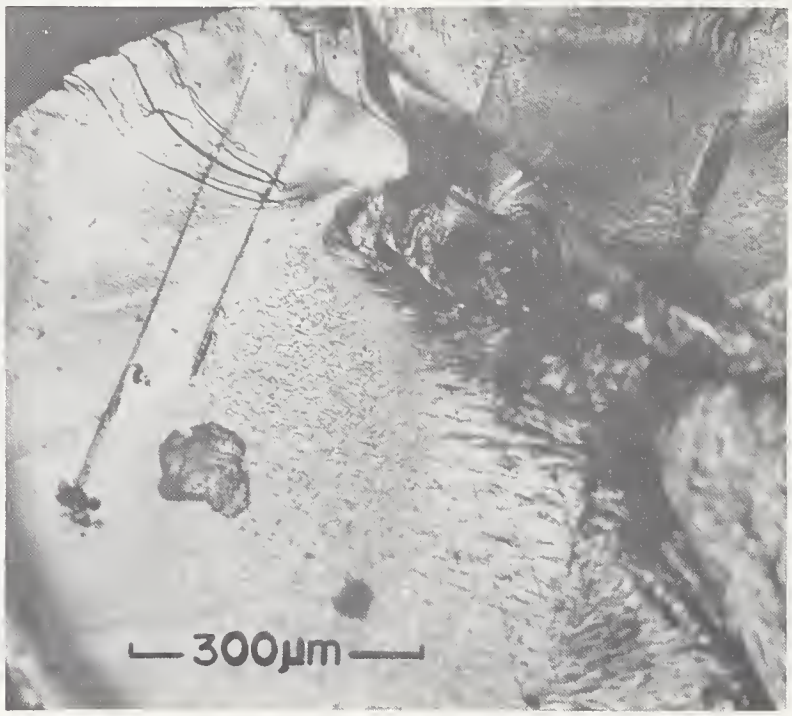

FIGURE 7. *Fracture surface of flame polished TiO_2 crystal.* Fracture origin (to left of center, upper edge) is associated with linear configurations suggestive of twins. Note further that these twin features occur on intersecting planes. Chemical etch (fuming H_3SO_4), interference phase contrast, reflected light.

obtained with mechanical polishing, table 2. It was noted that the flame polished surfaces frequently contained bubbles which generally were sites of fracture initiation. Improvements in flame polishing strengths were seen to be dependent on the quality of previous surface finishing. Smoother prior surfaces might have eliminated bubbles which apparently resulted from gases trapped in grinding stria and cracks.

3.3. Applications of α–Al_2O_3

Briefly, the two flame polishing techniques employed with the flat sapphire bars resulted in significant strength variations. The detection of intersecting twins solely on samples prepared by the pool technique indicates that twinning as well as surface irregularities played an important role in the lower strengths. As compared to flat bars, circular rods polished by the pool method would not be expected to be subjected to such pronounced doming. Although the surface tension would still tend to draw the liquid up, the radius of curvature of the rod would substantially reduce the effect in comparison to flat surfaces (fig. 1). The ability to rotate circular rods (and the melt) is also felt to be influential in maintaining a more uniform shape and this would also be conducive to forming thin melt layers, thus further minimizing the problems associated with thick melts. In this respect, it was previously found that the best quality finishes on circular rods was achieved with thin melt layers [15]. Further, flame polishing was undertaken in that study in a furnace designed to maintain the rod at a fixed elevated temperature prior to and after passing the rod through the torch flame [15]. This feature, as well as control of withdrawal rates, apparently substantially reduced axial thermal stress and eliminated fracture or cracking problems. The rotation of the rods during polishing would also greatly reduce cross sectional (or radical) stresses which were a factor in the polishing of flat bars which are polished on one surface only. The polishing controls for circular rods generally eliminate "wave crest" features found in flat bars; however, under poor polishing conditions, the circular rods exhibited similar structures [15]. Surface features resembling twins were also produced in circular rods, but were avoided by better control afforded by the polishing process [15]. These twins did not appear to occur on intersecting planes consistent with the lack of stress concentration regions (i.e., edges and also facets) in circular rods. The curved surface also reduces the probability of faceting or other surface irregularities being favorably situated for a favorable twin orientation.

It is worthwhile to briefly consider application of these flame polishing techniques to flat surfaces as disks and plates. While the clearing technique of flame polishing is definitely preferred and is applicable to narrow flat surfaces, it would be difficult to apply on large surfaces because of the requirement for more uniform surface heating in comparison to the pool technique. Use of a multiple flame torch or torches with flame dimensions (i.e., width of hot portion of flame) comparable to surface dimensions, might reduce this problem. In addition, initiation of polishing at the center of the surface and traversing out (e.g., in a spiral path) may also reduce thermal stresses in large pieces in comparison to starting from the outer portion or linear motion of the flame along the surface. However, control of the clearing technique is easier on a ground surface but does not work well when the flame motion traverses across grinding stria, thus making spiral-type paths difficult.

The pool technique could be applied, but besides the associated surface finish problems, overlapping of the melt could cause difficulties. This problem would be accentuated by larger radii of torch travel, as the previous melt would have sufficient time to solidify, but might be compensated by increasing rotation speeds with increasing radii of travel. Thermal stressing would also become a greater problem as the piece size increases, but as in circular rods, may be substantially relaxed by supplemental heating. Similar techniques have also been applied during welding of ceramics with success and indicate that maintaining the workpiece at 1000°–1500 °C was necessary to prevent stresses induced during the process [16]. In this regard, the success of supplementary heating will be limited by the problems of eliminating thick melts and surface faceting. Thus, while this work gives some guides to flame polishing flat objects, it is regarded as a difficult task, usually with limited benefits.

4. Summary and Conclusions

The findings illustrate that flame polishing can yield improved strengths of flat surfaces, particularly those with narrow, rectangular cross sections. However, it has been shown that extreme care must be taken to avoid surface irregularities (facets, etc.) and other defects (bubbles and cracks). By employing a technique which forms only a thin melt layer, intersecting twin formation and/or faceting can be avoided in α–Al_2O_3 and strengths are substantially improved over conventionally machined bars. Less perfect flame polish finishes are usually obtained when thick melts are formed resulting in little or even negative improvement of strengthening.

The utility of flame polishing flat bar-shaped samples is not so much in achieving strength improvements; much greater strengths are usually achieved in flame polished round rods [1–4] and gas polished flat bars [6]. The above technique does, however, present some advantages in studying fracture and twin behavior (especially in α–Al_2O_3 and TiO_2). It also illustrates that flame polishing is not necessarily a simple process of melting out surface flaws. Recent work by Hockey [19], showing that many twins and dislocations are introduced in the surface of Al_2O_3 by mechanical machining, indicates that flame polishing is also melting out these defects. Hence, the high strengths achieved by flame polishing are not unequivocal evidence for a flaw mechanism of failure. Further, this work shows that during and after flame polishing twins and dislocations can be reintroduced, depending on specimen and polishing parameters. Results, while not conclusive, clearly suggest that twinning may be an important factor in the room temperature strength of sapphire, as can precipitation in Al_2O_3–rich $MgAl_2O_4$.

5. References

[1] Mallinder, F. P., and Proctor, B. A., The strengths of flame polished sapphire crystals, Phil. Mg. 13, 197 (1966).

[2] Mallinder, F. P., and Proctor, B. A., Preparation of high-strength sapphire crystals, Proc. Brit. Ceram. Soc. 6, 9 (1966).

[3] Kirchner, H. P., Gruver, R. M., Platts, D. R., Rishel, P. A. and Walker, R. E., Chemical strengthening of ceramic materials, summary report, Contract N00019–68–C–0142, Ceramic Finishing Company (1969).

[4] Noone, M. J., and Heuer, A. H., Improvements in surface finish of ceramics by flame polishing and annealing techniques, this volume.

[5] Witter, D. E., and Palmour III, H., PIMAX tables for alpha alumina, Engineering School Bulletin 84, North Carolina State University (1967).

[6] Rice, R. W., Becher, P. F., and Schmidt, W. A., The strength of gas polished sapphire and rutile, this volume.

[7] Rice, R. W., The effect of sputtering on surface topography and strength of ceramics, this volume.

[8] Schmidt, W. A., and Davey, J. E., Preparation of smooth, crystalline, damage-free, sapphire surfaces by gaseous etching, this volume.

[9] Barber, D. J., and Tighe, N. J., Electron microscopy and diffraction of synthetic corundum crystals. I. pure aluminum oxide grown by the verneuil process, Phil. Mag. 11, 495 (1965).

[10] Klassen-Neklyudova, M. V., Mechanical twinning of crystals, Consultants Bureau, New York (1964).

[11] Levengood, W. C., Quantitative Aspects of Twinning Deformation on Sapphire and Ruby Single Crystals, pp. 93–97 in Crystal Growth, H. S. Peiser (editor), Pergamon Press, New York (1967).

[12] a. Heuer, A. H., and Roberts, J. P., The influence of annealing on the strength of corundum crystals, Proc. Brit. Ceram. Soc. 6, 17 (1966).
b. Heuer, A. H., Deformation twinning in corumdum, Phil. Mag. 13, 379 (1966).

[13] Parikh, N. M., Fracture mechanisms in polycrystalline nonmetallic materials, Final Report, DA–19–066–AMC–288(x), IIT Research Institute (1966).

[14] Becher, P. F., and Palmour III, H., High-temperature deformation of alumina double bicrystals, J. Am. Ceram. Soc. 53, 119 (1970).

[15] Popov, S. K., The growth and uses of gem-grade corundum crystals, Part II. The use of corundum in making artificial fibers, pp. 135–152 in Growth of Crystals, Vol. 2, A. V. Shubnikov and N. M. Sheftal (editors), Consultants Bureau, New York (1959).

[16] Rice, R. W., Welding of Ceramics, NRL Report 7085, U. S. Naval Research Laboratory, Washington, D.C. (1970).

[17] Grabmaier, J. G., and Falckenberg, H. R., Strength of flame-fusion-grown magnesium-aluminum spinel, J. Am. Ceram. Soc. 52, 648 (1969).

[18] Rice, R. W., Press forging and recrystallization of ceramic crystals, submitted for publication.

[19] a. Hockey, B. J., Observation of plastic deformation in alumina due to mechanical abrasion, Am. Ceram. Soc. Bull. 49, 498 (1970).
b. Hockey, B. J., Observations on mechanically abraded aluminum oxide crystals by transmission electron microscopy, this volume.

Discussion

HEUER: You were saying that during flame polishing of sapphire, twins were formed. These were interacting with or intersecting other twins and formed small cracks. Was it these cracks that gave rise to the fracture at low stresses?

BECHER: Yes, flame polishing (especially when thick melts occurred) frequently resulted in the formation of twins. Cracks were observed at some twin-twin interactions and some fracture origins were closely associated with intersecting twins or the associated cracks, but the correlation of twinning and specific fracture origins was not always clear. However, it was clear that the strengths were always low (comparable to as-ground samples) when nonparallel twins were produced during flame polishing. When only parallel twins were formed during polishing, both low and high strengths could be obtained. The possibility of twin-sub-structure interactions yielding cracks could account for the lower strengths, and evidence of this type of interaction was observed. The presence of dislocations which appeared to emanate from tips of basal twin tips, somewhat complicates the picture of twinning in fracture. Thus, although the exact mechanism(s) of failure are not fully resolved, twinning is clearly important. This is shown by gas polishing which greatly improves the sur-

face finish of sapphire and in the absence of twins, substantially increases its strength. However, gas polishing of flame polished bars containing nonparallel twins results in strengths comparable to as-flame polished values.

NOONE: I'm not sure that I understand the terminology that you are using. In fact, it appears to me that you are not flame polishing. I am particularly confused with this idea of "clearing." Isn't that nothing more than what we describe as annealing?

BECHER: No, this isn't an anneal. I should have brought out that a very thin melt is formed using the clearing technique. This is most obvious when one tries to use this method in a direction normal to the grain of the grinding striations. In this case, the flow of the melt is impeded and good polishes are difficult to obtain.

NOONE: The strength certainly doesn't reflect the kind of values which are accepted for flame-polished materials. Strengths about 100,000 psi, for instance are normal values which can be achieved by merely annealing.

BECHER: This work in essence points out that flame polishing of flat surfaces is much more difficult. One is not able to control the process nearly as well as in the case of a circular cross sectioned rod.

WHITE: The fissures which you call twins look very much like the compositionally induced twinning which we see as the cause of similar effect?

BECHER: Well, I can answer it this way. These are definitely rhombohedral and basal twins that were induced during flame polishing.

WHITE: Is there a compositional difference in this twinning?

BECHER: From the matrix? I haven't looked at it, but I don't believe so.

H. J. GREEN: Were the bars polished on all four sides?

BECHER: No. We just flame polished the top side. You get a little flame polishing on the edges, however.

K. SMITH: What were the dimensions of those bars?

RICE: About 70 mils thick and 150 mils wide. In addition I just wanted to amplify a little bit on Mike Noone's previous question about why we didn't see higher strengths for flame polished flat bars. One of the things we discussed in more detail in the paper is the fact that when you are flame polishing a flat bar you are only flame polishing one side. Even if you flame polish all sides, it still is normally one side at a time. This generates thermal stresses essentially in three dimensions. When you flame polish a round bar, the thermal stresses are primarily along the length of the bar. The remaining ones are radial. I think it's important to bring this out because these things do play a role in causing lower strengths.

HEUER: One difficulty is that you are comparing three point strengths with Mike Noone's four point tests. When Noone uses three point testing he obtains 1.3 million psi reproducibly. I think that you should use four point testing in your work as this has become almost standard in many laboratories.

RICE: I think that four point bending has a number of advantages and three point bending also has its advantages. I feel that three point bending is adequate or superior for most of the tests we make, but it depends a lot on what you are looking for, neither should be used exclusively for all purposes. The fact that Noone made three point bend tests does give us one very definite basis for comparison. However, the comparison also depends on the volume of stressed materials to near the fracture stress. Thus, in our three point bending of flat bars, we are stressing a volume approaching that stressed in Noone's four point bending of round bars. Generally, I have found results from three point bending in good agreement with others testing the same or similar bodies.

K. SMITH: Have you ever flame polished both sides?

BECHER: No, we haven't done that.

NATIONAL BUREAU OF STANDARDS SPECIAL PUB. 348, THE SCIENCE OF CERAMIC MACHINING AND SURFACE FINISHING, Proceedings of a Symposium Sponsored by the American Ceramic Society, the Office of Naval Research, and the National Bureau of Standards, held at NBS Nov. 2–4, 1970, Gaithersburg, Md. (Issued May 1972).

439-921 O - 72 - 17

Continuous Flame Polishing of Sapphire Filament

J. T. A. Pollock*

Tyco Laboratories, Inc., Bear Hill
Waltham, Massachusetts 02154

Continuous flame polishing of nominal 2.5×10^{-4} m diameter single crystal sapphire filament oriented with the c-direction parallel to the filament axis has resulted in considerable enhancement of the tensile fracture strength. Optimum increases of approximately 1.1×10^{9} N/m^2 (1.6×10^{5} psi) have been obtained on flame polishing many lengths of filament exhibiting as-grown tensile strength of $2.2 - 2.8 \times 10^{9}$ N/m^2 ($3.2 - 4.0 \times 10^{5}$ psi). Flame polishing was carried out in a continuous manner at 6.3×10^{-4} m/sec using an oxygen/hydrogen flame. Data are presented which suggest that that the enhancement is not entirely dependent on the production of a more perfect Al_2O_3 surface. Increases in strength of approximately 5.5×10^{8} N/m^2 (8×10^{4} psi) are reported for filament which has passed through flames not sufficiently hot for surface melting to occur. Maximum strength enhancement is obtained when the oxygen/hydrogen flame temperature is such that an axial molten zone two to three times the filament diameter is produced at the filament surface. When the flame temperature is too high, the geometric integrity of the filament is lost and an apparent fall in tensile strength from the peak value is observed.

Metallographic evidence is presented indicating that the molten zone has a radial depth of less than 6.5×10^{-6} m. Scanning electron microscopy and related surface analysis studies are reported which confirm that optimum polishing results in a smoother filament surface. Experiments to determine the state of stress in the filament before and after polishing are described.

The relative contributions to the reported tensile strength enhancement of thermal strain relieving, thermally activated atomic diffusion leading to blunting of possible fracture sources and the creation of a more perfect Al_2O_3 surface are discussed.

Key words: Characterization; continuous flame polishing; sapphire filament; strength enhancements.

1. Introduction

It is a well attested fact that the mechanical behavior of brittle materials is greatly influenced by surface imperfections and also to a varying extent by their state of internal strain. Mere handling of freshly formed glass results in a severe degradation of the mechanical strength[1].[1] Thus, in order to obtain meaningful values of the strength of glasses, it has been necessary to devise special handling and measuring techniques [2]. The realization that glass could exhibit high strengths has encouraged studies of the high strength properties of other brittle materials. Sapphire, a high melting point oxide with high modulus and hardness values [4.65×10^{11} N/m^2 ($67.5\ 10^{6}$ psi) and 1.93×10^{11} N/m^2 (2.8×10^{6} psi), respectively] has received increasing attention in recent years with a view to its use in composite materials, where its thermodynamic compatibility with many metals at high temperatures would be advantageous.

Sapphire whiskers (4 to 100×10^{-6} m diameter) were investigated by Brenner [3] and found to have strengths in tension in excess of 6.9×10^{9} N/m^2 (10^{6} psi). The strength values obtained were inversely related to the whisker diameter, indicating that surface area and/or volume was playing a role in determining the sapphire strength. Reported strength to bulk sapphire is considerably lower than those for whiskers, bend strength values generally being less than 6.9×10^{8} N/m^2 (10^{5} psi) [4, 5].

The knowledge that surface condition can play an important role in determining the strength of brittle materials has led to the development of techniques for improving the surface condition of bulk sapphire. Morley and Proctor [6] and Mallinder and Proctor [7] reported that considerable strength enhancement was obtained on flame polishing sapphire rods in the diameter range 0.75 to 2.75×10^{-3} m. Selected samples, free from internal flaws, exhibited strength in pure bending approaching 7.0×10^{9} N/m^2 (10^{6} psi), and demonstrated that the strength of bulk sapphire could approach that measured in whiskers. Noone and his co-workers [8] repeated this work at a later date and reported similar increases in strength.

The flame polishing technique used by both groups was simplification of the method devised by Popov [9] who spent a large part of his scientific life investigating methods for producing useable sapphire parts from verneuil boules. His rather complex methods included heating a centerless ground 5×10^{-3} m diameter sapphire rod, in a muffle furnace while held in a rotating holder. An oxygen-hydrogen flame

*Present address: Australian Atomic Energy Commission Research Establishmen, New South Wales, Australia.

[1] Figures in brackets indicate the literature references at the end of this paper.

is inclined and focussed at the sapphire rod. A molten surface bead is produced and the rod is withdrawn while rotating, thus allowing the molten bead to circularly traverse the entire surface area. The rods were then bent at elevated temperatures for use as guides and no strength data were reported. Proctor and his co-workers [6, 7] and Noone, et al., [8] discarded the muffle furnace, probably because they used smaller rod diameters. The former used a coal gas-oxygen flame and the latter an oxygen-hydrogen flame with a methyl alcohol vapor addition. Further details of the results of these investigations will be included in the discussion of the present work.

Recently, long lengths of high strength, single crystal sapphire filament have been produced by a melt-growth technique [10]. The as-grown tensile strength measured for 2.54×10^{-4} m diameter lengths of this material is in the range $2 - 2.75 \times 10^{9}$ N/m^2 ($3 - 4 \times 10^{5}$ psi). Although substantial for a material in this form, these values fall somewhat short of the data reported for whiskers and flame-polished rods. The aim of this study was to flame polish lengths of this sapphire filament in an attempt to raise its strength.

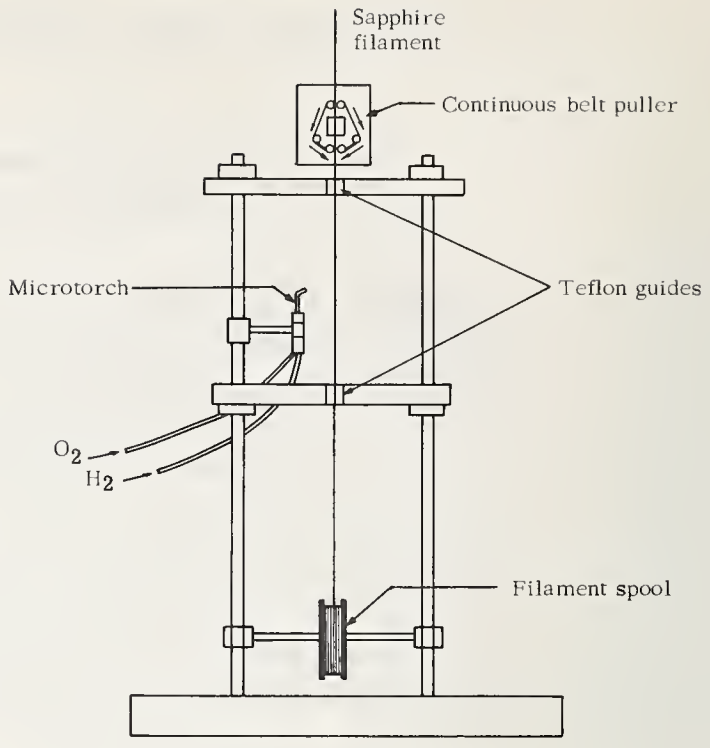

FIGURE 1. *Schematic diagram of apparatus used to flame polish sapphire filament.*

2. Experimental Procedure

2.1. Flame Polishing Technique

C-axis sapphire filament nominally 2.54×10^{-4} m diameter was available in long lengths and was chosen for flame polishing. The problems associated with flame polishing material of this geometry are radically different from those found in polishing larger diameter, short length rods. The rods have a rigidity which enables them to be accurately aligned and a substantial thermal mass in comparison to the filament. Also, the sapphire filament is in long lengths and ideally the technique devised should be one which would allow flame polishing in a continuous fashion. With the latter criterion in mind, the simple setup shown schematically in figure 1 was used.

A coiled length of filament, previously coated with paraffin or starch to prevent self rubbing degradation is supported on a circular rod at the bottom of the apparatus. The filament is fed through two Teflon bearings, which ensure a degree of rigidity, and then through a small pulley belt at the top. An oxygen-hydrogen microtorch is positioned with the nozzle tip (orifice size $\sim 7.5 \times 10^{-4}$m) about 3×10^{-2}m from the filament. Gas flow to the torch is controlled by two separate flow meters. The speed at which the filament can move is continuously variable and all the data reported here are for treatment carried out at 6.3×10^{-4}m/s. The filament is not rotated in any way while being treated. No attempt was made to remove the paraffin or starch coating prior to flame polishing. It was simply allowed to burn off in the cooler part of the flame.

Flame polishing is carried out in the following manner. The belt puller is set in motion and the flame started with only hydrogen (about 4×10^{-6} m^3/s) flowing into the microtorch. Throughout the procedure the hydrogen flow rate is held constant and the flame temperature increased by allowing increasing flow of oxygen into the mixing chamber of the torch. The oxygen/hydrogen flow ratios used, i.e., flame temperatures, vary depending on the filament diameter, but are generally in the range 2.75 to 1.5. Flow readings are taken from meters calibrated in standard cubic feet per hour (scfh) of air and values reported here represent conversions from this scale. They are not particularly accurate since allowance has not been made for viscosity differences. This is especially true of the hydrogen values. Since, however, visual recognition of the optimum flame condition was achieved and changed with variation in filament diameter, it was not considered worthwhile making the readings more accurate. They do, in fact, represent a qualitative measure of the flame temperature within each experiment and are useful as such.

Forty to fifty centimeters of filament were treated at each flame temperature. The general flame/filament area was observed continuously using a stereomicroscope capable of magnification up to 40X. Usually the flame temperature

was increased until necking-down of the filament, the result of excessive surface melting, was observed. The range of the gas flow ratios used to treat the filament depended on the diameter of each length, which varied between 2.2 to 2.6 $\times 10^{-4}$ m. The larger the filament diameter, the hotter the flame needed to produce optimum flame-polishing conditions.

The beginning and end of each length of filament, treated at a given flame temperature, was marked with a wax pencil, and the length carefully broken off as it cleared the puller belt. These lengths were very carefully handled and placed on foam rubber pads prior to layups into tensile samples.

The tensile fracture stress of 2.5 $\times 10^{-2}$ m gauge length samples was determined at a strain rate of 8.3 $\times 10^{-5}$ sec^{-1}. Three of four samples were tested to fracture from each piece of treated filament and an untreated standard length. Additional samples of the filament were carefully set aside and used for metallographic examinations with a view to determining structural changes occurring as a result of flame polishing.

Six flame polishing runs were carried out and characterized in the above fashion, and will be used as the basis for this paper.

2.2. Characterization

a. Internal and Surface Structure

The filament was examined for possible changes in internal structure using transmitted light optical microscopy. Samples were immersed in oil of refractive index close to sapphire ($n_D^{25°C}$ = 1.760) and studied at magnification up to 750X. The primary aim of these investigations was to determine the depth of the molten zone during flame polishing.

Changes in surface roughness as a result of flame polishing were detected by surface analysis using a Bendix profilimeter. The method employed a chisel point probe capable of detecting surface roughness as fine as 2.5 $\times 10^{-9}$ m. While it is realized that the device does not absolutely profile the discontinuities detected in a manner which would permit quantitative conclusions about changes in surface microcracks, it was felt that a qualitative measure of variation in the surface condition could be obtained and would be evidence for changes in surface features affecting the strength. Five samples taken from flame polishing series VI, were used. These samples, over a 5 $\times 10^{-2}$ m long, were tabbed at one end in the form of a flag. Each sample was placed in a groove on a Teflon block and tested at 2.094 radian (120°) intervals along a 3.18 $\times 10^{-2}$ m length using a 7.6 $\times 10^{-3}$ m length using a 7.6 $\times 10^{-3}$ m cutoff.

The filament surface was also studied at various stages of treatment using Scanning Electron Microscopy (SEM). A thin layer of gold-platinum alloy was first vapor deposited to prevent charge buildup.

The single crystallinity of the filament, before and after polishing, was confirmed by obtaining x-ray precession patterns. Filtered Mo$K\alpha$ radiation, a precessing angle of 30°, and a crystal to film distance of 6 $\times 10^{-2}$ m were employed.

b. Residual Stress

Since the filament is produced by a melt-growth process [10] with its concomittant solid-liquid interface temperature profile, the thought was considered that the as-grown filament might be in a state of residual stress similar to that exhibited by tempered glass [11], i.e., a compressively stressed outer shell containing an inner core in mild tension. This stress pattern is advantageous since fracture in tension, which in a brittle material is generally nucleated at the surface, requires that the residual surface compressive force be first overcome. It is possible that the flame-polishing process causes a more extreme stress pattern and thus contributes to the strength enhancement observed.

Petrographic examination of sections taken perpendicular to the growth axis i.e., the optic axis <0001> was difficult, due to problems in sample preparation arising from the hardness and small size of the filament. Samples 3.5 $\times 10^{-5}$ m thick were prepared and examined for evidence of radial stress patterns under polarized light in both conoscopic and orthoscopic conditions.

Another method of determining the filament stress condition was considered. Samples 7.5 $\times 10^{-2}$ m long were cemented lengthwise to glass slides and polished to half their thickness, using silicon carbide papers and diamond paste. On dissolving the cement, the samples were then examined using a stereomicroscope for evidence of curvature, which would indicate the presence of a nonsymmetric stressed state containing longitudinal compression and tension components.

3. Results

3.1. Tensile Fracture Strength and Relationship to Flame Temperature

Average tensile fracture stress and hydrogen/oxygen ratios are listed in table 1, for six flame-polishing experiments. The as-grown strength of the material varied between 2.2 to 2.80 $\times 10^9$ N/m^2 (3.2 to 4.0 $\times 10^5$ psi). With the exception of series I and V, a maximum in tensile strength was measured with increasing flame temperature. This maximum strength varied but always represented an increase of

TABLE 1. *Average tensile fracture stress and H_2/O_2 flame ratios for flame polishing experiments*

Sample N°	Average fracture stress × 10^{11}, N/m^2	H_2/O_2 Ratio	Sample N°	Average fracture stress × 10^{11}, N/m^2	H_2/O_2 Ratio
I –1	2.19	2.5	IV–1	2.64	No flame
2	2.76	2.3	2	2.79	2.21
3	2.90	2.1	3	3.10	2.14
4	2.95	2.04	4	3.27	2.12
5	3.05	2.0	5	3.34	2.09
6	3.35	1.95	6	3.64	2.04
7	2.24	No flame	7	3.25	1.99
II –1	2.73	1.85	V –1	2.64	No flame
2	1.94	1.78	2	2.46	2.4
3	2.64	1.82	3	2.80	2.19
4	2.91	1.90	4	3.08	2.1
5	3.22	1.94	5	3.19	1.99
6	2.98	2.08	6	3.41	1.91
7	2.64	2.12			
8	2.38	No flame	VI–1	2.54	No flame
			2	2.14	2.4
III–1	2.80	No flame	3	2.29	2.2
2	3.14	2.17	4	2.61	2.06
3	3.43	2.10	5	2.88	1.94
4	3.80	2.01	6	3.20	1.85
5	3.65	1.95	7	3.65	1.75
			8	3.28	1.68

0.9 to 1.2 × 10^9 N/m^2 (1.3 to 1.7 × 10^5 psi) over the strength exhibited by the standard filament. A decrease in strength was observed for filament treated in cool flames during runs I, V, and VI. This is thought to be a general occurrence and absent from runs II, III and IV because the filament was not treated in suitably cool flames.

The data given in table 1 for each flame-polishing run all follow the same trend and the variation in tensile strength with flame temperature may be represented by the curve drawn in figure 2. During each run, the filament-flame area was observed using a steromicroscopic and variations in the state of the filament as it passed through the flame could be observed. These observations have been used to divide the curve in figure 2 into four sections as shown.

For flame temperatures in range A, little change was observed in the filament as it passed through the flame. The paraffin or starch coating was easily removed and none was retained on the filament surface.

Ts the flame temperature was increased, small localized areas of intense light, perhaps

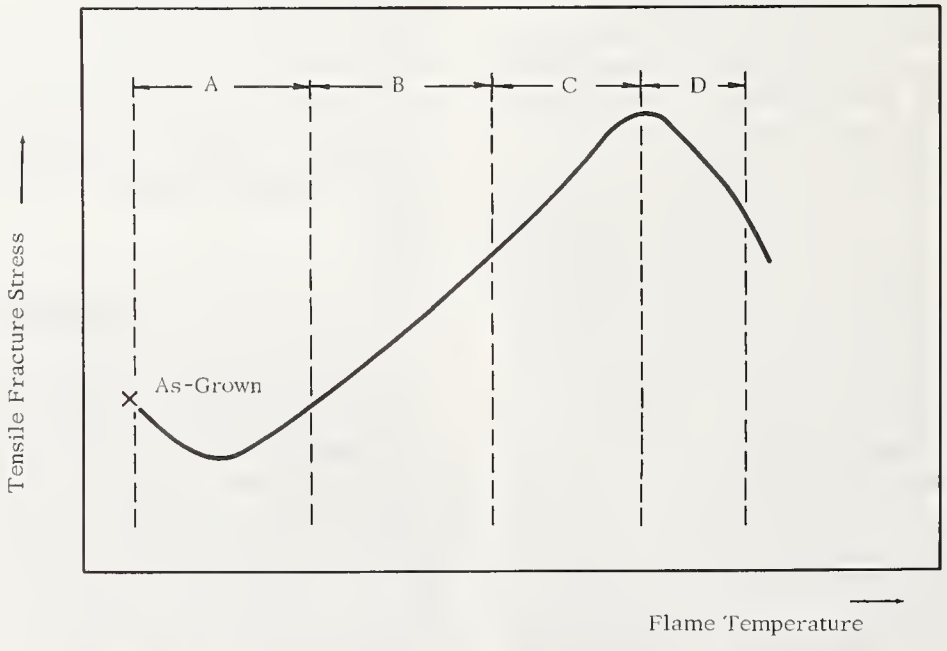

FIGURE 2. *Idealized plot of tensile fracture stress versus flame temperature.*

refracted from microscopic imperfections, could be observed to disappear within the flame. This was not a general phenomenon and occurred infrequently, even in those lengths in which it was noted. An increase in tensile fracture stress over that exhibited by the standard sample was always measured. This was often as much as 5.5×10^8 N/m^2 (8×10^4 psi).

At slightly higher flame temperatures (range C), a flickering white intense zone was observed. This marked the beginning of surface melting of the sapphire filament. When first observed, the zone is unstable and often fades away, reappearing a few seconds later. Also, it tends to move vertically up and down the filament within the flame. As the flame temperature is further increased, the overall length of the zone increases and it becomes essentially stable, remaining fixed in the flame with respect to the moving filament. A photograph of a stable zone is shown in figure 3. Some distortion due to thermal currents is present and makes photographic recording difficult. Optimum polishing conditions and maximum strength enhancements are obtained when the zone is 6.2 to 8.8×10^{-4} m long, i.e., roughly two to three times the filament diameter.

At higher flame temperatures, the filament begins to neck-down and, if this is severe, it assumes an hourglass appearance. A fall in tensile fracture stress from the optimum value is measured. Initially at least, this is not due to a weakening in the filament through the introduction of defects but rather to local reductions in cross-sectional area which are not measured with a micrometer in diameter determinations after testing to fracture.

The above observations of the filament surface conditions are made with respect to the hottest zone in the flame, of which there are two. The flame width at the filament is about 3×10^{-2} m long and the two hot zones are observed at the periphery of the flame. This indicates that the flame is oxygen deficient and maximum temperatures are reached where a supply of ambient oxygen is available. The hottest zone is always at the top, where the filament leaves the flame, and the two zones tend to extend inwards as the hydrogen/oxygen ratio decreases.

FIGURE 3. *Optimum flame polishing conditions showing the stable molten sheath at the filament surface.*

3.2. Condition of Flame Polished Sapphire Filament

a. Depth of Molten Zone During Flame Polishing

Visual observation while flame polishing has indicated that, under optimum polishing conditions, the molten zone has a length in the range 6.2 to 8.8×10^{-4} m. Optical observations were carried out in order to obtain a measure of the radial depth of this molten zone. Photomicro-

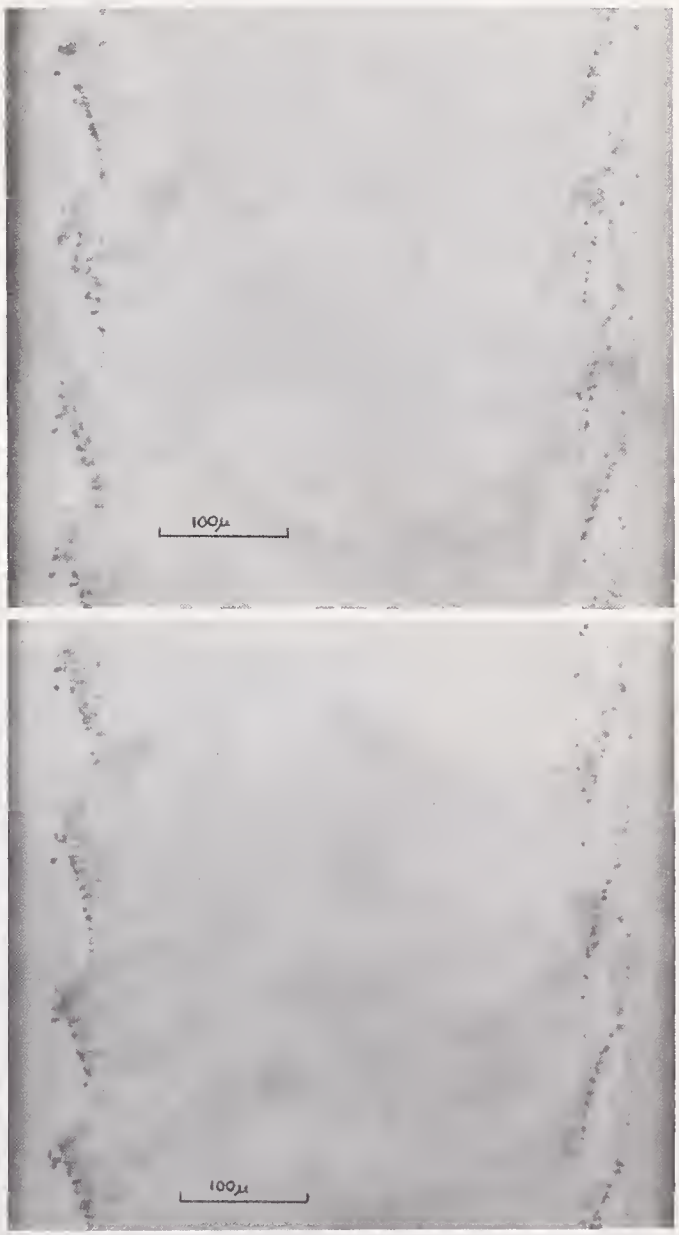

FIGURE 4. *Photomicrographs of as-grown and optimum polished filament.* Mid-plane section. (a) as-grown (b) optimum flame polished

graphs are displayed in figure 4 and are typical of those obtained for standard and optimum polished filament. The microvoids present, formed when the material is grown, are the result of the difference in density between molten and solid sapphire. While the actual void distribution varies somewhat between the lengths treated, the characteristic void-free outer shell is always present. The thickness of this shell varies from less than 6.5×10^{-6} m to as much as 2.5×10^{-5} m. If the molten zone during flame polishing was deeper than these thicknesses, a detectable reorganization of the void layers effected might be expected. Detailed examination of the void distribution before and after flame polishing reveals no evidence that any changes in void distribution have occurred. Further evidence for the depth of the zone being less than about 6.5×10^{-6} m is obtained when filament which has been marginally overpolished (range D in fig. 2) is examined. A photomicrograph is shown in figure 5. Evidently, the radial temperature distribution around the filament is asymmetric and excessive surface melting and loss of geometric integrity has occurred for one side. However, the start of the necking-down has not reduced the cross-sectional area by more than 2×10^{-5} m and the molten zone has not penetrated the void layers. When severe necking-down in a hotter flame is obtained and the filament assumes an hourglass shape, the void distribution is effected and resolidification results in additional voids which are considerably larger. Examples of these microvoids are observed in figure 6. Defects of this type would be expected to weaken the filament.

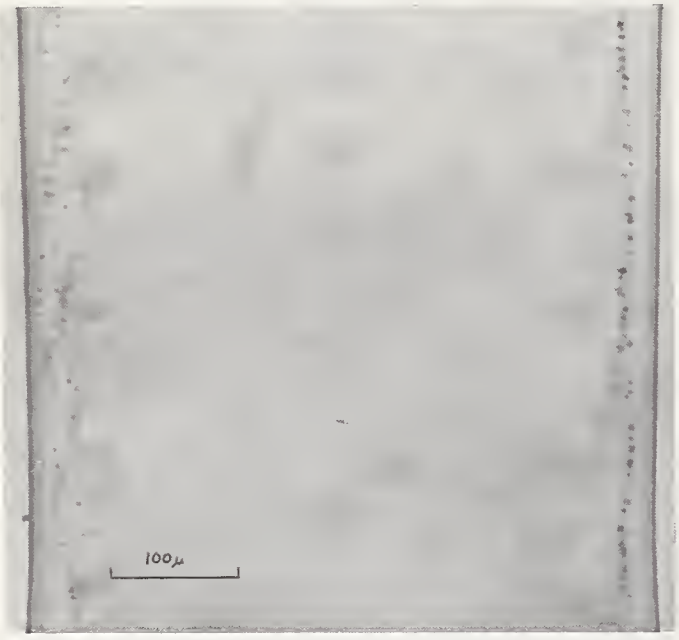

FIGURE 5. *Photomicrograph of slightly overpolished filament showing that the necked-down region has not penetrated the void layers.* Mid-plane section.

b. Surface Roughness

The average and high roughness values obtained by surface profilimeter analysis are plotted versus tensile fracture stress in figure 7. It is immediately apparent that despite some scatter, particularly at the low strength end, a marked trend associating high strength with small values of surface roughness is obtained. The average surface roughness for a sample exhibiting tensile strength close to 3.8×10^9 N/M^2 was 2.5×10^{-8} m as compared with 6.25×10^{-8} m for the standard material with a tensile strength of 2.55×10^9 N/m^2.

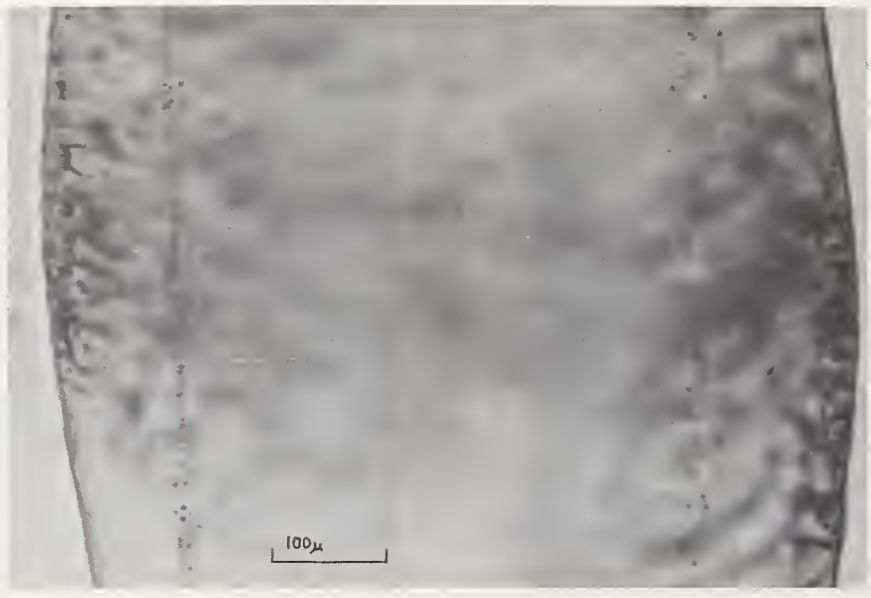

FIGURE 6. *Photomicrograph showing overpolished filament and macroscopic voids associated with solidification occurring both from the center outwards and the surface inwards.* Mid-plane section.

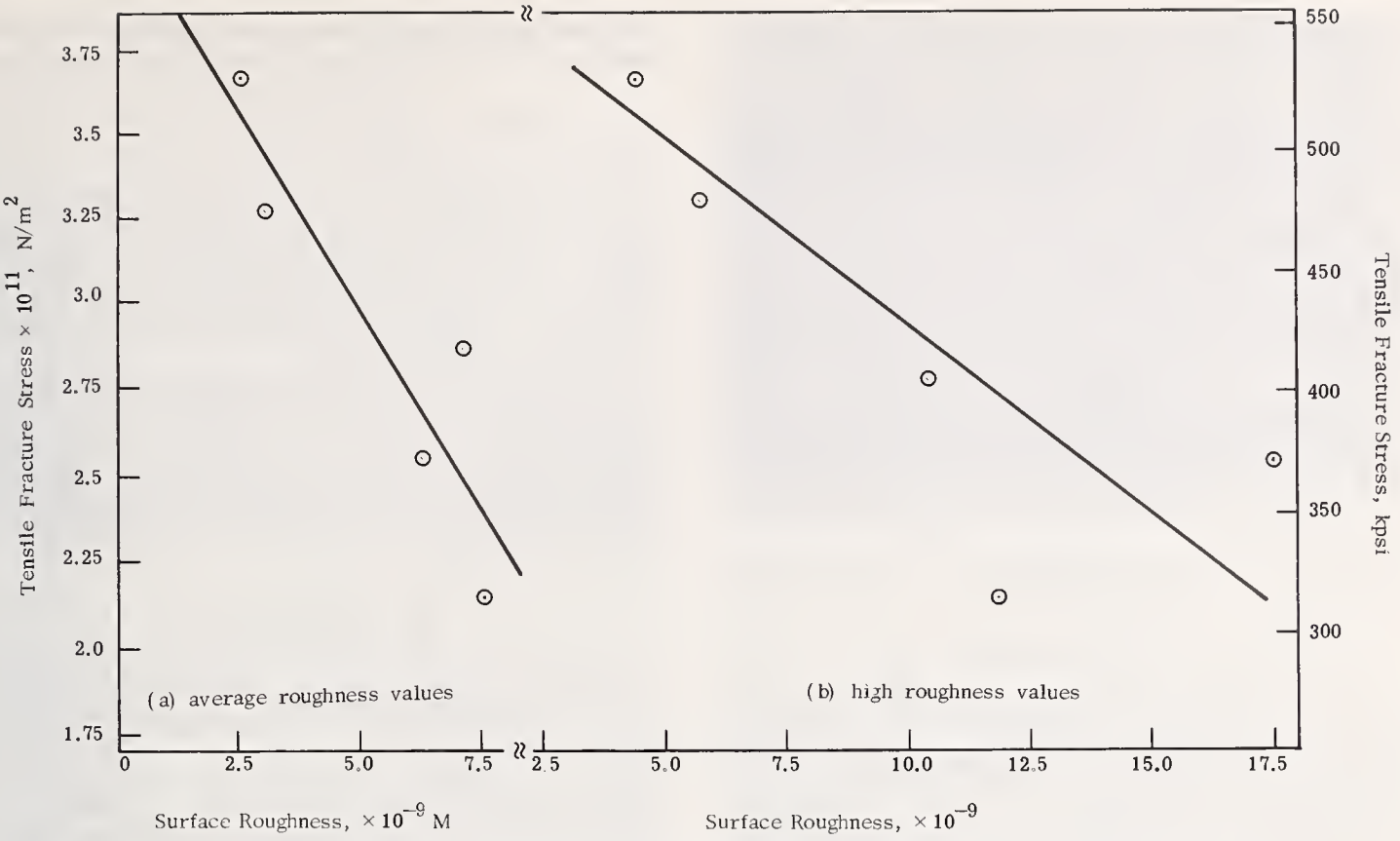

FIGURE 7. *Surface roughness versus tensile fracture stress for flame polished filament from Series VI.*

SEM photomicrographs showing the filament surface at three stages (as-grown, underpolished, and optimum polished) are displayed in figure 8 through 10. Samples in the as-grown condition showed evidence of surface waviness as shown in figure 8. This rippling which is at 0.762 radians (43°) to the growth plane of the filament could be interpreted as microfacetting on the {1013} rhomohedral planes. The central area where the striations are not obtained represents a change in curvature of the filament toward a larger radius and indicates that the material is not perfectly circular.

Figure 9 shows a micrograph of an underpolished surface. The relief shown is not found over the entire surface to the extent of the waviness exhibited by the as-grown material but is typical of surface roughness observed in underpolished samples. The nonuniformity of the surface is considered to be the result of the flickering nature of the molten zone during underpolishing. The surface of the optimum polished material is shown in figure 10. At magnifications up to 5000X, this surface is essentially smooth and shows no signs of rippling.

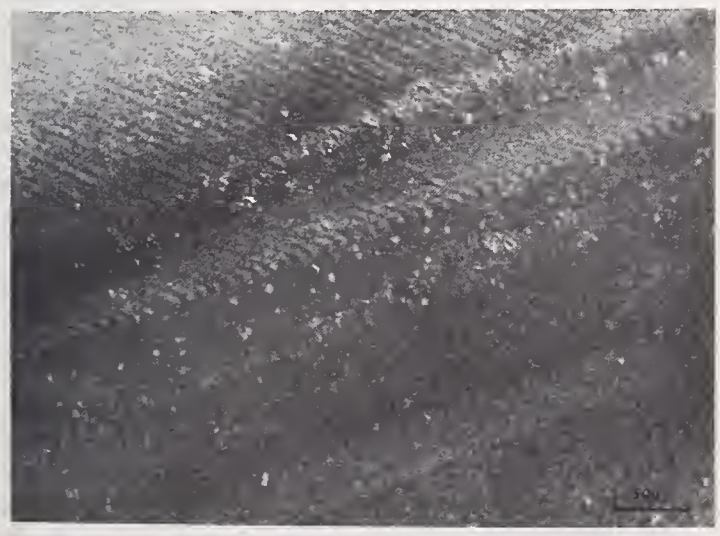

FIGURE 8. *SEM of as-grown sapphire filament surface.*

FIGURE 9. *SEM of underpolished sapphire filament surface.*

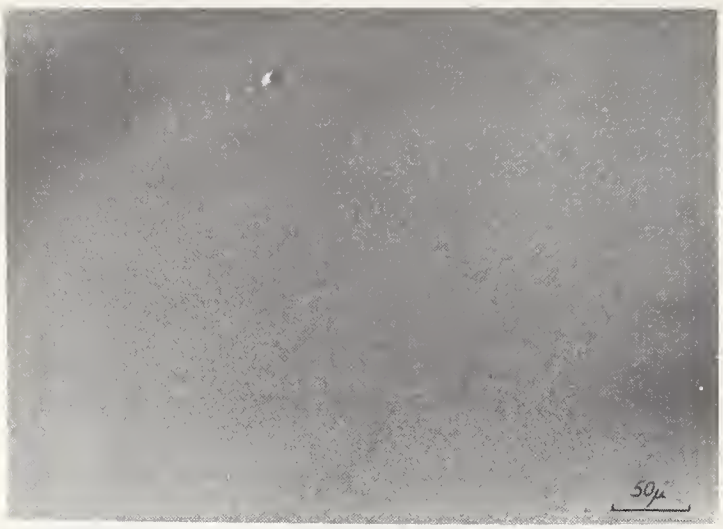

FIGURE 10. *SEM of perfectly flame polished sapphire filament surface.*

c. Residual Stress

Petrographic examinations revealed no evidence of radial stress patterns under polarized light. It is appreciated that the Youngs' modulus exhibited by sapphire makes the detection of elastic strain difficult.

Samples were examined for evidence of bending after polishing in a manner expected to produce a nonsymmetric stress distribution if a radial stress pattern were present.

The curvature to be expected for a given surface stress may be calculated as outlined below [12].

$$\text{Curvature in a uniform member} = \frac{M}{E \cdot I} \qquad (1)$$

where M is the bending moment, E is Youngs' modulus and I is the moment of intertia of the member.

Also:

$$\sigma_f = -\frac{M \cdot y}{I} \qquad (2)$$

where σ_f is the longitudinal stress, y is the distance of the neutral plane from the plane of maximum stress and M and I are as above.

Equations (1) and (2) may be combined and lead to:

$$\text{Filament Curvature} = -\frac{\sigma_f}{E \cdot y} \qquad (3)$$

Consider a stress of 7×10^8 N/M^2 (10^5 psi) and assume that the neutral plane is midway in the polished section (i.e., parallel to and 6.25×10^{-5} m from the polished surface). Thus,

$$\text{Filament Curvature} = -\frac{7 \times 10^8}{4.65 \times 10^{11} \times 6.25 \times 10^{-5}} = -24.1 \text{ m}^{-1}$$

The radius of curvature, ρ, is given by the reciprocal of the filament curvature. Therefore,

$$\rho = -\frac{1}{24.1} = -4.2 \times 10^{-2} \text{ m}$$

This represents a considerable degree of bending. Although the calculation is not rigorous, it may be considered to given an approximate measure of the curvatures expected and has been verified by measurements on highly stressed ribbons [13].

Examination of filament in the as-grown and polished conditions prepared as outlined above, revealed no noticeable curvature and suggest, on the basis of the above calculation, that the components of any tempered stress distribution are much less than 7×10^{10} N/m^2 (10^5 psi).

4. Discussion

Proctor, et al., [6, 7] obtained strength values in pure bending in the range 4.8 to 6.9×10^9 N/m^2 ($7.0 - 10.0 \times 10^5$ psi), which were the highest reported for sapphire in a form other than small ($<10^{-5}$ m diameter) whiskers. Similarly, Noone, et al., [8] obtained values in four-point bending close to 5.5×10^9 N/m^2 (8×10^5 psi). The main disadvantage in comparing these values with those of the present work is that bend tests on cylindrical samples only place a small fraction of the sample surface (a line in the case of four point or pure bending) under maximum stress, unlike tensile testing where the entire gauge volume is stressed uniformly. However, Noone, et al., [8] repeated their measurements in tension testing using similarly flame polished 5.0×10^{-4} m diameter Al_2O_3 rods with an average gauge length of 1.53×10^{-2} m. They obtained an average tensile strength value (14 samples) of 2.6×10^9 N/m^2 (3.77×10^5 psi). The ratio of strength in bending to strength in tension (2.1) for the data reported by Noone, et al., [8] is very close to the value (2.12) for similar measurements in cast iron [14] where the extent of plastic deformation prior to fracture was very small. This factor when applied to the results of Proctor, et al., [6, 7] produces strength in tension values of 2.3×10^9 N/m^2 (3.25×10^5 psi) for samples with a test length of 6×10^{-3} m. Careful selection of more perfect smaller gauge length samples (3×10^{-3} m long) was required to produce bend strength values in the region of 6.9×10^{11} N/m^2 (10^6 psi). The correction factor (2.1) reduces this value to near 3.3×10^{11} N/m^2 (4.75×10^5 psi) for tension testing. In comparison, the maximum tensile fracture stress values obtained during the present investigation, in excess of 3.5×10^{11} N/m^2 (5×10^5 psi) using 2.5×10^{-2} m gauge lengths, can be considered encouraging. It should also be noted

that the material used in the present work was not subjected to any selection process at any point during the investigation.

The optimum flame-polishing conditions produced surfaces which contained none of the helical rippling reported by the two previous investigations [6, 7, 8]. This is the result not only of the nonrotation of the filament during treatment, but also indicative of less severe surface melting taking place. Noone, et al., report that the 5×10^{-5} m long molten collar produced at the rod surface was about 2.5 to 5.0 $\times$ 10^{-5} m deep, suggesting a quite radical change in state of a considerable volume fraction of a 5×10^{-4} m diameter rod (approximately 20%). By contrast, the optical microscopy evidence presented here indicates that the molten zone is less than 10^{-5} m, thick which means that about 10 vol percent of the filament is melted during optimum flame polishing. Thus, viscosity and surface tension enable the geometric integrity of the filament to be maintained and improved, as evidenced by the SEM photomicrographs.

Flame polishing and any other thermal treatment may be expected to change the surface and/or internal characteristics of sapphire filament. As suggested earlier, some consideration has been given to the thesis that a major role in strength enhancement arises through either strain relieving or in the creation of a stressed state akin to that present in tempered glass. The results of the petrography examinations and curvature experiments suggest that the role played by strain is small compared with the changes in strength measured. Therefore, it may be reasonable to consider the strength versus flame polishing characteristics of the filament, as summarized in figure 2, in terms of fracture initiating microcracks present in the material.

Griffith analysis gives the fracture stress in the presence of a crack as:

$$\sigma_f = \sqrt{\frac{\gamma \cdot E}{2c} \cdot \frac{\rho}{a}}$$

where σ_f is the fracture stress, γ is the surface energy, 2c is the internal crack length (c is the surface crack depth), ρ is the crack tip radius, and a is the interatomic spacing. Evidently the stress concentrating effect of the crack is greatly dependent on the value of c/ρ. Thus, the sharper the crack profile the greater its stress concentration effect and the lower the fracture stress observed.

As the filament passes through cool flames, range A in figure 2, these microcracks may widen, due to thermal expansion, causing the depth or length to increase in an irreversible fashion. A small decrease in tensile fracture stress is measured as the result of the increase in crack length.

During optimum and near optimum flame polishing conditions, a substantial increase in strength (1.1×10^{11} N/m^2 (1.6×10^5 psi)) over that exhibited by the as-grown material is observed. The structural evidence presented here is conclusive that this maximum enhancement in strength is coincident with the attainment of a more perfect surface. Indeed, the profilimeter data in figure 7 suggests a simple correlation between decreasing surface roughness and increasing tensile fracture stress. However, a considerable strength enhancement of about 5.5×10^8 N/m^2 (8.0×10^4 psi) is observed for treatment in flames which are too cool for surface melting to occur (range B). This may be attributed to thermally activated diffusion leading to crack blunting, since an improvement in the surface quality has been noted. Any such process will result in a reduction in surface energy and it is not improbable that they will occur at elevated temperatures. Heuer and Roberts [5] and Kirchner et al., [15] reported that strength increases were measured on annealing single crystal and polycrystal aluminia, respectively. Lange and Radford [16] showed that the strength of polycrystalline Al_2O_3, weakened by the introduction of cracks through thermal quenching, was rapidly recovered on annealing at 1700 °C. While in these relatively weak materials the surface of the samples was of primary importance, it is not unreasonable to suspect that similar mechanisms will be operating within the bulk. Thus, it is highly possible that the thermal environment during flame polishing contributes to the strength enhancement by means other than the removal of surface flaws, through remelting.

These considerations suggest that the creation of the molten high temperature surface zone, which does not destroy the geometric integrity of the filament, may also be the creation of an efficient thermal environment for diffusion controlled blunting of internal microcracks. This hypothesis could be confirmed by concrete evidence that fracture origin is internal, before and after flame polishing. Some evidence is available to support this theory. Filament tensile samples fracturing at high loads [i.e., greater than 2.1×10^9 N/m^2 (3×10^5 psi)] generally shatter, at least in the immediate break vicinity. LaBelle and Hurley [17] reported that preliminary examination of the fracture surfaces pointed to internal fracture origin at high fracture loads in tension. This work has been extended, using as-grown samples embedded in epoxy to reduce shattering and loss of the primary fracture surfaces. SEM examination of six fracture surfaces points to internal nucleation in all cases. Details of the investigation will be reported at a later date [18]. Thus, in the sapphire filament used in the present

work [as-grown strength $> 2.1 \times 10^9$ N/m^2 (3×10^5 psi)], there is evidence to support the supposition that fracture origin is internal, perhaps associated with the microscopic spherical voids. While there is conclusive proof that optimum flame polishing results in the creation of a more perfect surface, there is also reason to believe that thermal healing of internal microcracks may be the primary cause for the enhancement in tensile fracture stress observed.

Over-polishing results in a fall in strength, due at first to the reduced cross-sectional area, and then, as the flame temperature increases, to the formation of resolidification voids. These voids are indicative of solidification proceeding, both from the central core outwards and from the resolidified shell inwards. Unlike the 10^{-6} m spherical voids present in the as-grown material, these voids have non-symmetric shapes and higher stress concentrating factors.

5. Summary

Continuous flame polishing of nominal 2.5 $\times 10^{-4}$ m diameter sapphire filament enables strength enhancement of about 1.1×10^9 N/m^2 (1.6×10^5 psi) over values exhibited by as-grown material. Maximum tensile strengths obtained, 3.8×10^9 N/m^2 (5.5×10^5 psi), are the highest reported for sapphire in a form other than small diameter whiskers. These strengths are obtained after polishing in oxygen-hydrogen flames which produce a stable molten zone 8×10^{-4} m long by $\sim 10^{-5}$ m deep at the filament surface. The geometric integrity of the material is completely maintained and surface examination by SEM shows that a highly smooth surface is created. Nevertheless, evidence concerning the internal nature of fracture in the as-grown material suggests that thermal healing of microcracks may be playing a more important role in the strength enhancement process than the creation of a more perfect surface.

The author wishes to thank Mr. John Bailey who carried out much of the flame polishing and mechanical testing, and Drs. G. F. Hurley and F. H. Cocks for valuable discussions of many aspects of the work.

This work was supported by the Air Force Materials Laboratory, Nonmetallic Materials Division, Wright Patterson Air Force Base, Ohio, under Contract No. F33615–69–C–1369.

6. References

[1] Proctor, B. A., Fracture of glass, Appl. Mat. Research 3, 28–34 (1964).
[2] Morley, J. G., Andrews, P. A., and Whitney, I., Strength of fused silica, Phys. Chem. Glasses 5, 1–10 (1964).
[3] Brenner, S. S., Mechanical behavior of sapphire whiskers at high temperatures, J. Appl. Phys. 33, 33–39 (1962).
[4] Wachtman, J. B., and Maxwell, L. H., Plastic deformation of ceramic oxide single crystals, J. Amer. Cer Soc. 37, 291–299 (1954).
[5] Heuer, A. H., and Roberts, J. P., The influence of amealing on the strength of corundum crystals, Proc. Brit. Ceram. Soc., 6, 17–27 (1966).
[6] Morley, J. G., and Proctor, B. A., Strength of sapphire crystals, Nature 196, 1082 (1962).
[7] Mallinder, F. C. and Proctor, B. A., Strengths of flame polished sapphire crystals, Phil. Mag. 13, 197–208 (1966).
[8] Noone, M. J., and Sutton, W. H., Investigation of bonding in oxide-fiber (whisker) reinforced metals, National Technical Information Service (NTIS) AD 664–176.
[9] Popov, D., The growth and uses of gem grade corundum crystals, Book, Growth of Crystals, Ed. A. V. Shubnikov and N. N. Sheftal, Volume II, (Chapman and Hall, London, 1962).
[10] LaBelle, H. E., and Mlavsky, A. I., Growth of sapphire filaments from the melt, Nature 216, 574–575 (1967).
[11] Kingery, W. D., Introduction to Ceramics, 639–641 (John Wiley & Sons, Inc., New York, 1960).
[12] Crandall, S. H., and Dahl, N. C., An introduction to the mechanics of solids, 288–294 (McGraw-Hill Book Co., Inc., New York 1959).
[13] Hurley, G. F., to be published.
[14] Rozner, A. G., Comparison of tensile strength measured in tension and bending, Trans. A. I. M. E. 233, 1646–1647 (1965).
[15] Kirchner, H. P., Gruver, R. M., Platts, D. R., Richel, P. A., and Walker, R. E., Chemical Strengthening of Ceramic Materials, Summary Report, Contract NOOO19–68–C–0142, Naval Air Systems (1969).
[16] Lange, F. F., and Radford, K. C., Healing of surface cracks in polycrystaline Al_2O_3, J. Amer. Cer. Soc. 53, 420–421 (1970).
[17] LaBelle, H., and Hurley, G. F., Strength and fracture of long single crystal sapphire filaments, Sampe Journal, 6 17–23 (1970).
[18] Pollock, J. T. A., and Hurley, G. F., to be published.

Discussion

MATSKO: Did the unidirectional heating of the filament present any problem?

POLLOCK: Yes, in the paper there is some evidence presented which indicates that there is some asymmetry of the actual temperature distribution.

NOONE: Didn't you find that some of the strain that you measured was due to the fact that you were melting more Al_2O_3 on one side of your filament therefore producing this complex stress state? You are adding another variable by melting more on one side than the other.

POLLOCK: As I said, there is some asym-

metry. I don't think it's particularly important. No evidence of strain in the crystals could be detected, before or after treatment.

GIELISSE: Did you mention the cross section size of the filament?

POLLOCK: I didn't. It was 10 mils in diameter.

NATIONAL BUREAU OF STANDARDS SPECIAL PUB. 348, THE SCIENCE OF CERAMIC MACHINING AND SURFACE FINISHING, Proceedings of a Symposium Sponsored by the American Ceramic Society, the Office of Naval Research, and the National Bureau of Standards, held at NBS Nov. 2–4, 1970, Gaithersburg, Md. (Issued May 1972).

Preparation of Smooth Crystalline, Damage Free, Sapphire Surfaces by Gaseous Etching

W. A. Schmidt and John E. Davey

Naval Research Laboratory, Washington, D.C. 20390

Sapphire has a combination of properties such as, relative chemical inertness, exceedingly high resistivity, optical transparency and crystalline structure that suggest its use as a substrate material for various semiconductor devices. Its successful use for silicon vapor phase epitaxy substrates indicates that similar results might be possible with other semiconductors. Previous epitaxial studies have shown that surface crystalline disorder and topographic imperfections inhibit epitaxial growth; therefore highly polished well ordered sapphire surfaces were needed. Mechanical polishing alone is insufficient as it results in cold flow and work damage.

Initial experiments in removing surface damage were performed with hot phosphoric acid and with hydroxide etches. Undesirable preferential etching was observed for both processes and the processes did not seem amenable to the routine production of high quality surfaces. Two other surface treatments for which successful results have recently been reported were investigated.

The first was a hydrogen firing technique in which the substrates were heated in hydrogen in a Mo wound resistance furnace at 1500 °C. The second was a simple laboratory process in which the sample is heated by means of RF heating of a carbon susceptor to 1350 °C in an atmosphere of helium and fluorotrichloromethane (Freon–11). Commercial reagents were used throughout and a fused quartz tube was used for the reaction chamber for the second technique.

Reflection electron diffraction (RED) was used to determine the surface crystalline order, and electron microscopy (EM), using high resolution replication techniques, was used to examine the topography structure of the surfaces. A number of different substrates from various industrial sources, with different surface topographies and different orientations were used.

Hydrogen firing at 1500 °C results in an etch rate of 0.1 10^{-6} m/min. Firing for times up to 45 min did not produce consistent surfaces on the 0°, 60° or 90° orientations. While hydrogen firing did produce high quality well ordered crystallograph surfaces by RED, their topographic condition was poor. Resolvable surface structures could be detected on some with standard optical microscopy (200x, dark field) and for all high resolution EM measurements. The final surface finish quality was related to the quality of the prefired surface, indicating that complete damage removal was not accomplished.

Freon firing at 1350 °C resulted in an etch rate of $1.5.10^{-5}$ m/min. This technique consistently produced well ordered, high quality, surfaces for the 60° and 90° oriented surfaces. EM viewed 60° and 90° freon fired surfaces had no resolvable surface structure after a 5 min etch and were well ordered crystallographically as measured by RED. The same etch produced strongly etched surfaces on 0° oriented material.

Key words: Crystalline sapphire surfaces; fluorinated-hydrocarbon etch; fluorotrichloromethane; freon etching; hydrogen annealing; sapphire; sapphire substrates; sapphire surface preparation.

1. Introduction

Sapphire has a combination of properties which make it a desirable material for use as a semiconductor substrate. [1–2][1] It is resistant to attack by most of the materials used in present semiconductor processing and etching technologies. It is crystalline, transparent, insulating and it has a relatively high thermal conductivity. Table 1 is the table presented by Mueller detailing the particular advantages for its use with silicon technology. [1] Since the transparent window of a sapphire substrate (typically 0.5 mm thick) extends from the near UV to about 62,000 A, optical methods can be used for examining the band gap, and many other electronic transitions within the lattice

[1] Figures in brackets indicate the literature references at the end of this paper.

Table 1. *Advantages of the silicon-on-sapphire technique*

	Electrical advantages
1.	Excellent isolation ($p > 10^{11}$ ohm-cm).
2.	Good high frequency performance (loss tan $<10^{-1}$ at 800 MHz).
3.	Extremely low capacitance devices and circuits.
4.	No possibility of "4-layered latch-up".
5.	No allowance necessary for space-charge spread.
6.	Considerably greater resistance to transient radiation.
	Mechanical advantages
7.	Ability to withstand regular Si processing, temperature of diffusion, chemical etches, etc.
8.	High strength, especially at high temperatures.
9.	Good heat conductivity (50x glass).
10.	Smoothness, no voids.
11.	Very high packing density (10^5 complementary devices per sq. in).
12.	For many circuits, fewer processing steps are required.

of the semiconductor film, by irradiating through the substrate.

The successful use of sapphire as a substrate for Si, Ge and GaAs [1–7] vapor phase epitaxy by various authors indicates that it may be a useful substrate for vacuum deposition of these and other semiconducting materials.

In previous work by the authors on the vacuum deposition of GaAs on GaAs and GaAs on quartz, sapphire, and GaP [8–9] it has been shown that surface crystalline disorder and topographic imperfections inhibit epitaxial growth; highly polished well ordered sapphire surfaces were needed.

Mechanically polished sapphire is an improvement over a completely amorphous material such as fused quartz, however, it is not adequate for use as an epitaxial substrate. The surface of a mechanically polished sapphire sample is essentially amorphous due to work damage and cold flow.

In an attempt to restore the mechanically polished surface to the same crystalline order as the bulk material, various chemical etchants were employed. The initial experiments were performed with hot phosphoric acid and with hydroxide etches. Undesirable preferential etching was observed with both processes, and their complexity was such that the incorporation of these etches as routine steps in normal wafer processing was difficult.

Two articles by Manasevit [10–11] on the gaseous etching of sapphire with sulfur fluorides and fluorinated hydrocarbons and Allison's [2] account of hydrogen etching indicated that the desired surface quality was obtainable. To evaluate these processes the Manasevit procedure was used with fluorotrichloromethane $CFCl_3$ as the freon etchant and samples were hydrogen fired at 1500 °C as described in the Allison article.

2. Experimental Methods

The two forms of gaseous etching investigated, required similar apparatus. The sample was held on an inert support in a high temperature gas flow of the etchant gas.

The high temperature hydrogen etching was performed in a commercially available resistance heated furnace. The hydrogen furnace was tubular in design with a refractory tube which contained the hydrogen atmosphere and the molybdenum resistance heating elements. The sample carrier was coated with alumina to prevent reaction with the samples. Fifteen minute preheat and cool down periods in the cooler end sections were required to prevent thermal shock to the furnace walls and to the sample holder.

Samples were hydrogen etched at two temperatures in this furnace at 1500 °C the temperature used by Allison, [3] and at the maximum temperature of the furnace, 1700 °C.

The He freon apparatus is shown in figure 1. A quartz reaction tube was used to contain the etchant and carrier gasses around the heated samples. Samples were heated to 1350° with R.F. using a spectographic grade ultra pure carbon rod as the sample holder and R.F. susceptor. The hot zone of the carbon rod was held separate from the quartz tube walls by quartz spacer rings and rods, which were attached to the susceptor ends outside of the hot zone. A prefired alumina plate was used to support the samples to eliminate contamination from the carbon. The cold trap on the down stream side of the tube was used to trap reaction products which clogged the vent jet in early runs. Temperature measurements were made with an optical pyrometer looking indirectly through a front surface mirror onto either the edge of the sample or the alumina plate under it. No temperature correction was made for the presence of either the mirror or the quartz tube in the optical path. The design of the gas feed apparatus was dictated by the choice of the type of freon. Freon 11, fluorotrichloromethane, is a liquid at room temperature with a vapor pressure approaching 1 atmosphere. Bubbling a low flow of He gas through a three inch column of freon 11 was sufficient to transport freon vapors into the low pressure system. Initial experiments indicated that passing the entire He flow through the bubbler produced too rich a mixture for reasonable control of etch rate. The total flow rate of the He is determined by the need to maintain a low pressure of He in the main tube with a vent jet size not likely to clog with reaction products. A low He flow was bubbled through the freon 11 and the mixture was returned to the feed line at the outlet of the mainline flowmeter. The mass flow of the freon was measured by weighing the freon container before and after a few test runs to establish the mass flow rate of freon associated with a specific flow of He in the bubbler line.

The flow conditions used were:

Helium	410 ml/min
Helium in freon bubbler	70 ml/min
Freon	0.135 gm/min

All of the samples were examined for their surface quality before and after each etching treatment. The determination of surface quality was made with three types of equipment. Optical microscopes were used to cover the range from 1x to 500x magnification with both brightfield and darkfield illumination. An optical interference microscope was used to measure surface planarity. A JEM–6 electron microscope was used to examine surfaces under high magnification (10^4x). Standard carbon film

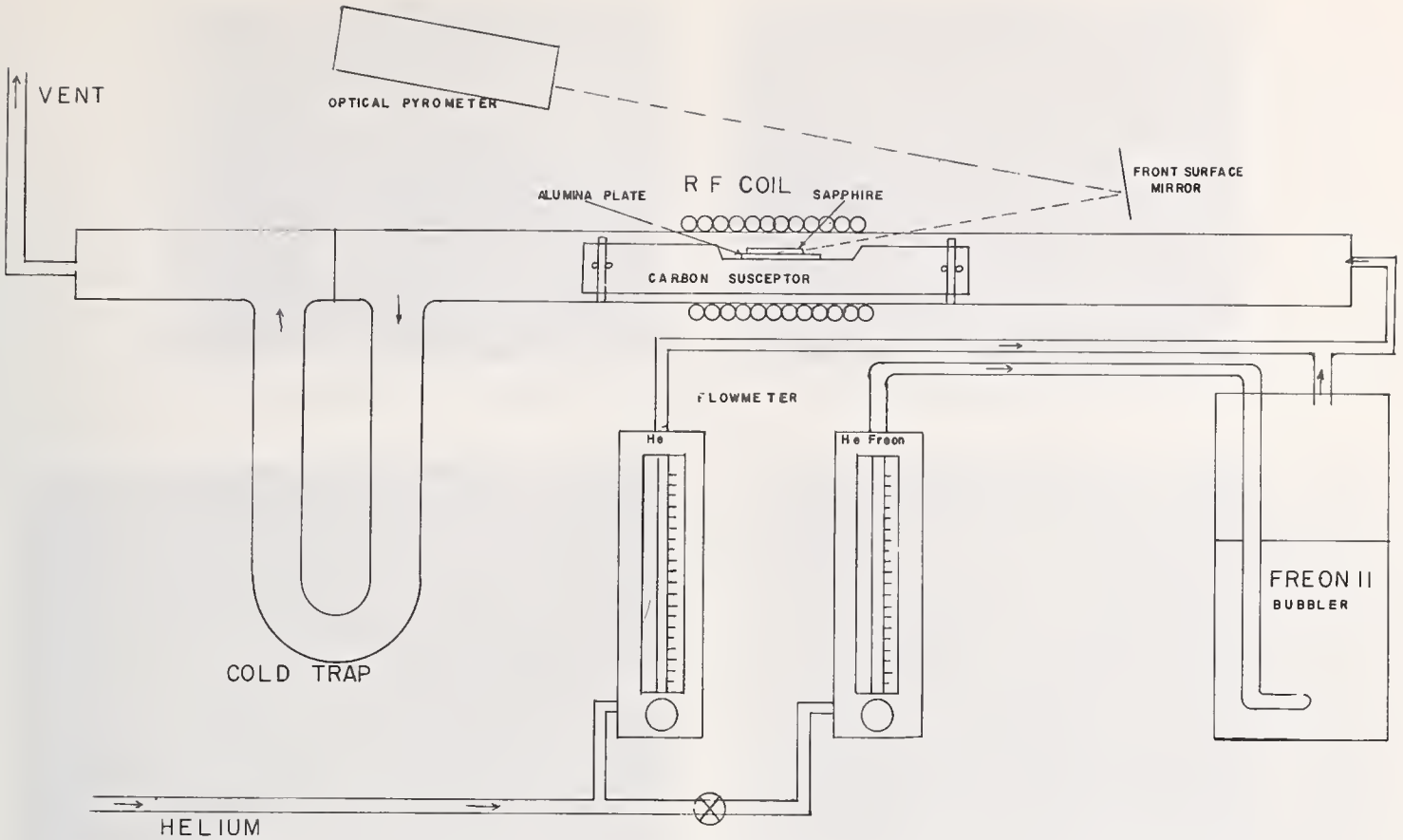

FIGURE 1. *He-freon etching apparatus.*

techniques were used to make the surface replicas. Reflection electron diffraction and x-ray diffraction analysis were used to determine the crystalline order of the surfaces.

The sapphire used was obtained from two sources. Sapphire windows and Czracholski pulled boules of single crystal sapphire were obtained from the Union Carbide Co. The boules were cut and polished in the NRL optical shop. "Substrate" grade blanks similar to those used commercially for silicon vapor phase epitaxy were obtained from the Adolph Meller Co. The surfaces of the samples were quite different, but consistent within a group. (fig. 2) Note distance between marks is 1 μm. Sapphire which was cut and polished at NRL (fig. 2A) using a 1/4 μm diamond final polish had extensive scratches detectable with even a 200x optical microscope. Substrate grade material (fig. 2B) was also heavily scratched. Generally the window grade material had a lower scratch density than the mechanically polished or the substrate grade material. Only a few scratches were seen with the electron microscope on the 60° and 90° (fig. 2D) "window" grade surfaces, while the 0° surfaces were not as high quality (fig. 2C). The crystalline order of the "substrate" grade samples, however was far superior to the other grades of samples (fig. 3). The "substrate" grade samples were ordered as observed by the RED pattern. The other surfaces were completely amorphous. All of the samples used, from all sources, displayed single crystal patterns under x-ray analysis.

3. Experimental Results

3.1. Hydrogen Etching

Hydrogen etching of 60° and 90° samples produced inconsistent surfaces. All of the samples etched in hydrogen had excellent crystallographic quality (fig. 4). The surface topography of these samples (fig. 5) was not consistent. Some samples had scratch free surfaces as examined under the electron microscope, while other retained residual scratches (fig. 5B) and still others had extensive striations (fig. 5A). Entire surfaces were densely covered with striations over 1 μm long.

After 45 minutes of hydrogen etching at 1500°C residual scratches and striations were found in some of the samples. With the etch rate of 10^{-7} meters/minute, the same as Allison, [4] this corresponds to a removal of $4.5.10^{-6}$ meters, and while the samples had numerous scratches prior to etch none were this deep. It was assumed that the scratches remaining after hydrogen etching were the result of work damage. The origin of the striations is at this point unclear. They were found on the etched "substrate" grade material more frequently than on the other grades. With hy-

439-921 O - 72 - 18

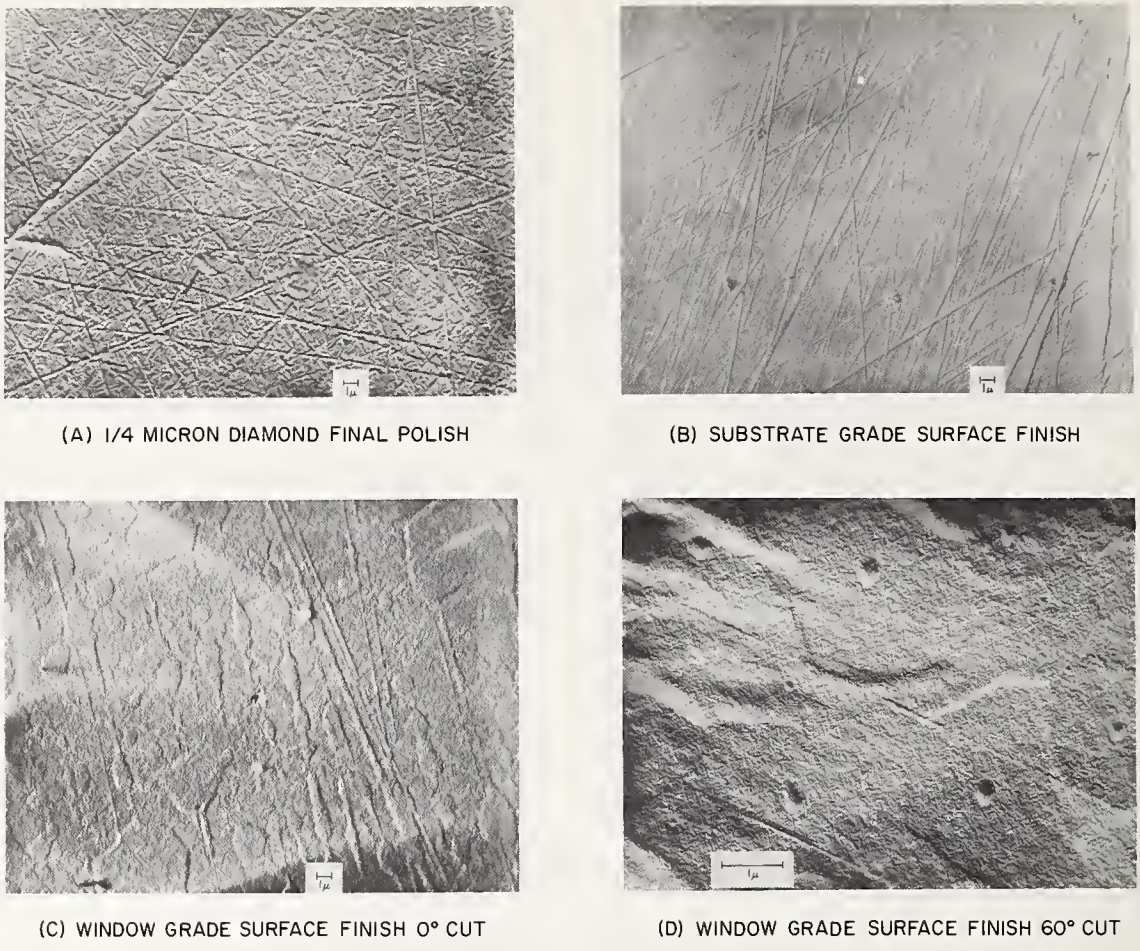

(A) 1/4 MICRON DIAMOND FINAL POLISH

(B) SUBSTRATE GRADE SURFACE FINISH

(C) WINDOW GRADE SURFACE FINISH 0° CUT

(D) WINDOW GRADE SURFACE FINISH 60° CUT

FIGURE 2. *Sample surfaces before gaseous etching by electron microscope examination.*

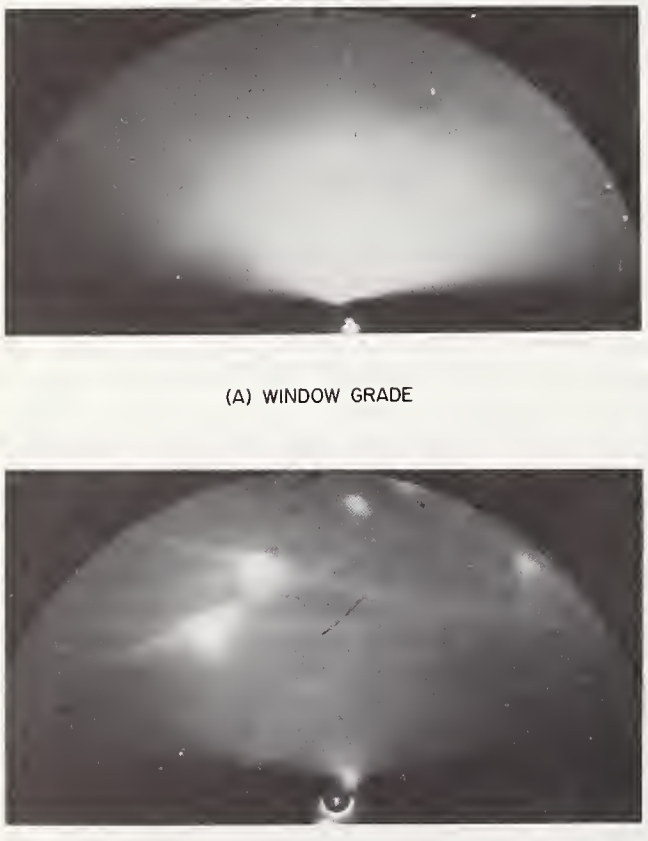

(A) WINDOW GRADE

(B) SUBSTRATE GRADE

FIGURE 3. *Reflection electron diffraction of sample surfaces before gaseous etcthing.*

drogen etching as with other methods of surface preparation the basal plane or 0° surfaces were preferentially etched.

3.2. Freon Etching

With the exception of the 0° surfaces all of the Helium-freon etched surfaces were scratch free and single crystal. (fig. 6). In this figure surfaces etched the standard 5 min as well as a surface etched for an extended time (15 min) are shown. No residual scratches or discrete structures were visible at this magnification other than artifacts of the replication process. The etch rate was typically $7.5.10^{-6}$ m/min. In a typical 5 min etch run 37.5 10^{-6} meters of material was removed from a surface, effectively removing all work damaged material. This etch rate was varied by changing the level of the freon content in the gas. Higher etch rates resulted in heavy etching of the edge of the samples, however, and were not used for that reason. The 0° surface for both He and He-freon were preferentially etched (fig. 7) with the resulting etch structure from freon (A) resembling those found by Manasevit[2] who used chlorotrifluoromethane as the etchant gas. All of our electron microscope data was taken at magnifications about one order of magnitude greater than those of Manasevit, however, there was no indication of the extensive

(A) WINDOW GRADE (B) SUBSTRATE GRADE

FIGURE 4. *Reflection electron diffraction of hydrogen etched surfaces.*

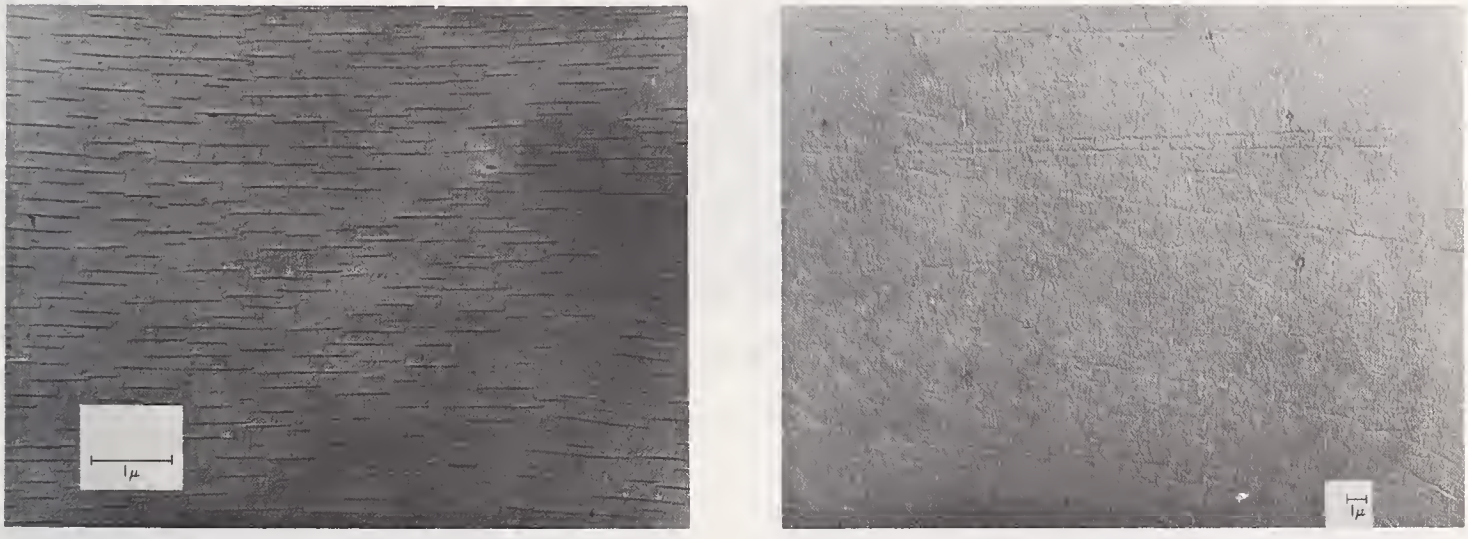

(A) STRIATIONS (B) RESIDUAL SCRATCHES

FIGURE 5. *Typical surfaces after hydrogen etching.*

etch pit formation seen by him except on the basal plane where our etch structures were still about one order of magnitude smaller than his. It is assumed that this difference is a result of etchant chemistry, which is one factor obviously different in the two experiments. The hydrogen annealed 0° surface is typical of other workers results. A common complaint with the use of fluorinated hydro carbon etchants is that the surfaces that result are non planar or have dimpled surfaces. This effect was not observed by the authors.

4. Conclusions

The use of freons as vapor high temperature etchants for sapphire has been established previously, but here the use of one, fluorotrichloromethane, has been shown to be useful in a simple apparatus for producing high quality scratch free ordered, single crystal surfaces. The process has been shown to be more reliable than the hydrogen anneal used by industry, which produces questionable surfaces, containing dense striations and residual scratches. Table 2 summarizes the results found.

TABLE 2. *Summary of results*

Hydrogen etching	
1500° — 1700° C Each Rate 10^{-7} meter/min.	15–45 min.
Results in	ordered crystalline surfaces extensive striations residual scratches 0° surface, preferentially etched
He-Freon etching	
1350° C Etch Rate	5 min. $7.5.10^{-6}$ meter/min.
Results	Ordered-crystalline high Quality Scratch Free Surfaces 0° Surface, Preferentially Etched

Further work is being pursued to incorporate this process into a standard vacuum evaporation process. The corrosive reaction products prevent direct inclusion, and a further insitu cleaning process (thermal bake, H_2 Fire low temp) must be used to compensate for the contamination during transfer through atmospheric ambient.

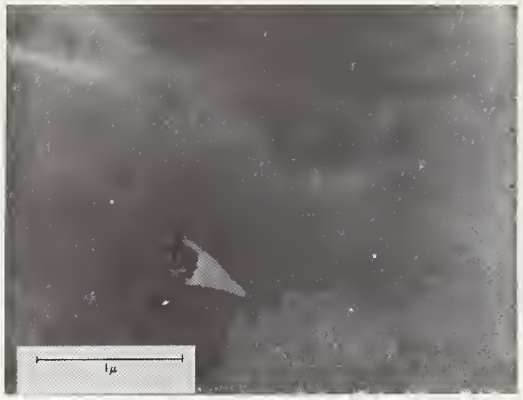

(A) 5 MINUTE STANDARD ETCH
60° AND 90° SURFACES

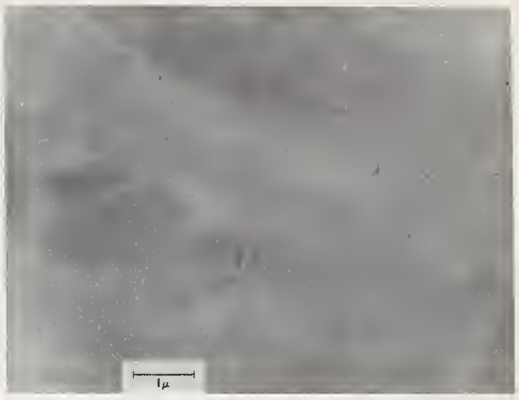

(B) 15 MINUTE EXTENDED TIME ETCH
60° SURFACE

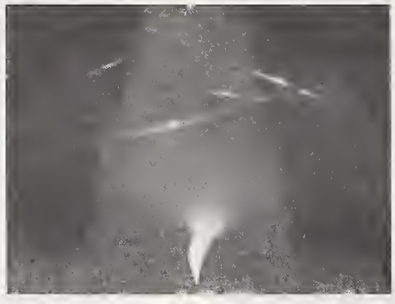

(C) REFLECTION ELECTRON DIFFRACTION
ANALYSIS OF TYPICAL SURFACE

FIGURE 6. *Helium-freon etched surfaces.*

(A) BY HE FREON

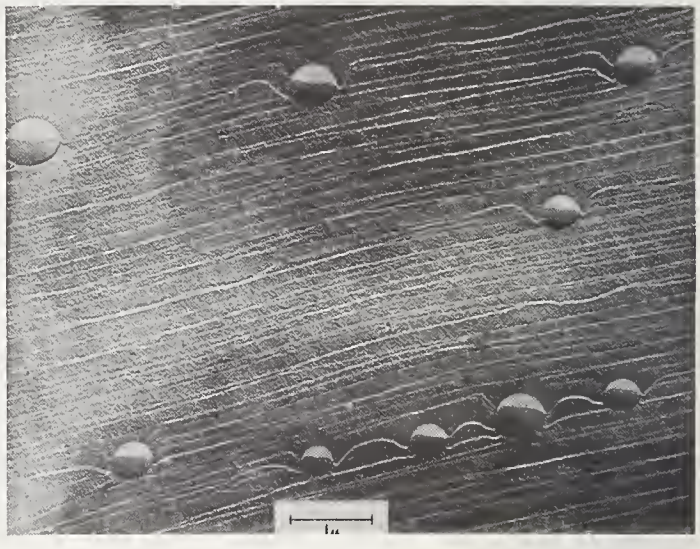

(B) BY HYDROGEN

FIGURE 7. *Preferential etch of 0° cut material.*

5. References

[1] Mueller, C. W., Thin-film devices on dielectric substrates J. of Vacuum Science and Technology 7, 147 (1970).

[2] Allison, J. W., Dumin, D. J., Heiman, F. P., Mueller, C. W., and Robinson, P. H., Thin film silicon: Preparation, properties and device app. Proc. IEEE, 57, 1490 (Sept. 1969).

[3] Manasevit, H. M., Thorsen, D.C., Heteroepitaxial GaAs on aluminum oxide I. early growth studies, Metallurgical Transactions, 1, 623 (Mar 70).

[4] Manasevit, H. M., Single crystal gallium arsenide on insulating substrates, Appl. Phys. Ltrs. 12, 156 (15 Feb. 1968).

[5] Manasevit, H. M., Simpson, W. I., Single-crystal silicon on a sapphire substrate, JAP, 35, #4 1349 (1964).

[6] Manasevit, H. M., Nolder, R., Cadaff, J., et al.,

Heteroepitaxial silicon-aluminum oxide interface, Pare I Trans. Met. Soc. of AIME 233, 540 (Mar 65).
Part II, Trans. Met. Soc. AIME 233, 549 (Mar 65).
Part III, Trans. Met. Soc. AIME 242, 465 (Mar 68).
[7] Zanowich, R. J., Morritz, F. L., Heteroepitaxial deposits of Ge and GaAs/Ge on sapphire and beryllium, J. Electrochem. Soc. 114, #6 146C (Jun 67).
[8] Schmidt, W. A., Davey, J. E., Zn Doping of GaAs Films Using Coevaporation of the Elements, Naval Research Laboratory Report #7100, (April 1970).
[9] Davey, J. E., and Pankey, T., Epitaxial GaAs films Deposited by vacuum evaporation, J. Appl. Phys. 39, #4, 1941, (March 1968).
[10] Manasevit, H. M., Morritz, F. L., Gas phase etching of sapphire with sulfar fluorides, J. Electrochem. Soc. 114, #2 (Feb. 1967).
[11] Manasevit, H. M., Gas phase etching of sapphire III fluorinated hydrocarbons, J. Electrochem. Soc. 115, #4 (April 1968).

Discussion

HEUER: Do you know how those substrate grade samples were prepared?

SCHMIDT: No. The only answer I got in a query of that sort was that it was proprietary information and they weren't willing to give it out. My feeling is that it's probably mechanically polished with quick hydrogen anneal. Clearly the scratches would indicate most of the work damaged material was removed. There is high crystalline order. I would expect a quick hydrogen anneal was performed after mechanical polishing.

HEUER: What were the hexagonal features shown on as-received material?

SCHMIDT: The hexagonal patterns are found on 0° material and are etch pit structures. Both the as-delivered and etched surfaces had these patterns.

NATIONAL BUREAU OF STANDARDS SPECIAL PUB. 348, THE SCIENCE OF CERAMIC MACHINING AND SURFACE FINISHING, Proceedings of a Symposium Sponsored by the American Ceramic Society, the Office of Naval Research, and the National Bureau of Standards, held at NBS Nov. 2–4, 1970, Gaithersburg, Md. (Issued May 1972).

The Strength of Gas Polished Sapphire and Rutile

R. W. Rice, P. F. Becher, and W. A. Schmidt

U.S. Naval Research Laboratory, Washington, D.C. 20390

Surface polishing of α-Al_2O_3 using a helium-freon gas mixture at elevated temperatures is shown to yield bend strengths comparable to flame polished sapphire. However, the gas polishing process proved to be more versatile as evidenced by the success with flat bar surfaces. Further, the process can be readily applied to some other materials as demonstrated by the substantial improvements in the strength of TiO_2 after gas polishing. Limited attempts at polishing other ceramic materials are also discussed, as well as observations on strength variations and fracture behavior.

Key words: Chemical polishing; rutile; sapphire; spinel; strength; twinning.

1. Introduction

Further development by Schmidt and Davey [1][1] of a chemical polishing technique for sapphire utilizing hot, flowing, helium-freon gas mixtures showed that very good surfaces were obtained relatively easily. The high quality of the surfaces produced suggested that high strengths could be achieved by such polishing. Further, it was felt that this polishing technique might also be applicable to some other ceramic materials. This paper presents results of the initial investigation of the strengths of gas polishing ceramics, especially oxides (e.g., Al_2O_3, and TiO_2 crystals). Some observations on fracture are also made.

2. Experimental Technique

The materials used have been previously described [2–4], as has the data on orientations and test techniques. During the gas polishing process, the test bars were placed in graphite fixtures which supported the ends of the samples and prevented contact between sample surfaces. After polishing, sample handling was minimized and any handling and storage was undertaken in a manner to prevent damage to the surface. During the course of polishing and mechanical testing (3 point flexure), it was found that a strip of thin transparent pressure-sensitive tape placed on the compressive surfaces aided in handling and helped retain fracture sections of high strength specimens for later examination.

3 Results and Discussion

3.1. α–Al_2O_3

Sapphire bars up to about 4 cm in length could be polished in the present apparatus. These longer bars were found to polish best on surfaces nearest the gas exit end of the susceptor, indicating that some initial preheating of the gas would be beneficial. In order to minimize any finishing gradients, most bars were polished for 10 minutes in one orientation, then polished again for the same period after being turned 180°. Results show a trend for a more uniform, but generally a less flat, surface resulted if bars were gas polished in the as-ground rather than a mechanically polished condition. During the polishing schedule it was observed that greater amounts of removal gave somewhat smoother surfaces. The resultant surfaces were very glossy and free of any sharp surface discontinuities. Except for some slight rounding of the edges, removal was very uniform on all surfaces, indicating little effect of crystallographic orientation. Chemical etching failed to reveal any inhomogenity of surface texture and pit densities were generally in the order of $10^5/cm^2$. An exception occurred when only a slight amount of material was removed from the surface of the bars; then etch pit densities were generally much higher in residual grinding or polishing stria.

Although not studied in detail, observations on bars that were not extensively polished, at least over part of their length, indicated that removal of less than 0.1 mm. of the as-ground or mechanically polished surface generally resulted in low strengths (of the order of those achieved by conventional finishes). A more detailed characterization of similar sapphire surfaces polished in the same apparatus is given elsewhere [1] and is thus not further discussed here.

Bend test results, listed in table 1, indicate that quite high strengths can be obtained, generally being more reliable than those obtained by flame polishing similar flat bars [4]. In subsequent examination, fracture origins were located on about half of these specimens, being detected somewhat more frequently on lower strength bars. It was found that about 50–60 per cent of the fractures originated from the edges, but no clear trend in strength or other parameters was noted. Fracture mirror

[1]Figures in brackets indicate the literature references at the end of this paper.

dimensions were observed to be generally consistent with other fracture data obtained in a broader study of ceramics (to be published later). Initial optical examination indicated that most samples do not contain twins. The few samples observed to have twins were of average or lower strengths.

Trial gas polishing of dense, high purity, sintered Al_2O_3 bodies having either fine or large grain sizes produced very dull surface finishes. The gas polishing was observed to preferentially remove material at and adjacent to the grain boundaries; however, no sharp local radii of curvature at boundaries were detected. Strengths of such polycrystalline specimens were unaltered from those obtained by either grinding (parallel to the tensile axis) or mechanical polishing.

3.2. TiO_2

Both as-grown (blue) and air annealed (yellow) bars were gas polished after which each type exhibited a yellow color indicating that reduction was not occurring as found in flame polishing [4]. In addition, material was removed from rutile single crystals at a much higher rate than from Al_2O_3 subjected to the same polishing conditions. Some of those TiO^2 specimens developed extremely glossy surfaces, while others developed a frosted appearance over part or all of their surfaces, indicating that polishing was very sensitive to gas flows and temperature conditions (or possible contamination from other materials in the same run). Again, as with the sapphire, removal appeared to be quite uniform from all surfaces.

As shown in Table 1, those bars having very glossy surfaces had strengths from a few to several-fold times those obtained with conventional mechanical finishes. On the other hand, those with even small frosted patches on the side of the bars had strengths comparable to those obtained by conventional machining techniques. Fracture origins were located on all eight specimens, with four being from the tensile surface and four from the edges, yielding no obvious trend with strength or surface condition. Fracture mirrors were usually observed and were found to be consistent with data from other tests. Optical observation of the highest strength specimen showed several twins with intersecting cracks and/or other twins along one edge of the specimen near the fracture. Subsequent chemical etching in fuming sulfuric acid (300–330°C) revealed a dense mosaic of intersecting twins and associated cracks adjacent to the fracture surface around the fracture origin. Since these appeared or became visible very near the fracture origin, interaction of mechanical twins may be limiting strengths. The twins originally observed along the edge of this sample lay in a region of the tensile surface subjected to much reduced stress ($70-100 \times 10^3$ psi, $49-69 \times 10^7$ N/m^2) suggesting that twinning might be important in lower strength rutile samples. This would be enhanced by regions of stress concentration such as the edges of the bar (as noted above) and surface or internal defects.

3.3. Other Materials

A trial polish of a MgO crystal resulted in a badly decomposed crystal which could be crumbled into a white powder. Further work with this material was therefore not attempted.

Unstabilized and CaO-stabilized ZrO_2 crystals which were in positions adjacent to the MgO crystal during the same polishing run were an opaque white through a substantial portion of the bars. The resultant samples were very weak and one was found to be deliquescent. Any success with gas polishing of ZrO_2 was felt to require extensive change in the technique which was not attempted.

Al_2O_3-rich spinel crystals from a separate gas polishing run had a thin white surface coating. Sample strengths of these were lower than those normally obtained by grinding or mechanical polishing. However, a spinel bar obtained in another run (which included the MgO and ZrO_2 samples) developed a fairly glossy finish over part of the surface. The

TABLE 1. *Room temperature bend strengths of sapphire and rutile single crystals*

Material	Average strength as machined				Average strength as gas polished		
	Finish	10^3 psi	10^7N/m^2	Range	10^3 psi	10^7N/m	Tests
Sapphire	Ground	48±9	33	111–495	231±36	159	11
	Mechanically Polished	53±15	37	140–362	207±25	143	9
Rutile	Ground	13±1	9	43–156	[1]78±30	54	4
	Mechanically Polished	22±7	15	15–20	[2]18±1	12	4

[1]Rutile crystals having glossy finishes after gas polishing.
[2]Rutile crystals with frosted finishes after gas polishing.

strength obtained in this region of the bar was comparable to those of mechanically polished specimens. However, the strength achieved may have been limited by precipitation of Al_2O_3 during the cooling from the polishing temperature (~1350 °C). Therefore, gas polishing of spinel crystals, especially stoichiometric ones, is considered to be promising with further development.

Specimens of polycrystalline spinel were also included in both of the previous gas polishing runs. These developed mat or frosted surface finishes, and strengths were in the same range as those obtained by grinding, possibly being on the low side.

Finally, gas polishing of polycrystalline B_4C and SiC was also attempted. These samples were coated over a greater portion of their surfaces with a fairly thick, black deposit; and, in general, there appeared to be little, if any, polishing action. The strengths of both the B_4C and SiC were of the order of one-third to one-half that of as-ground samples. Thus, polishing of these materials does not appear to be promising.

4. Summary and Conclusion

Very excellent quality finishes can be obtained on sapphire by gas polishing which is not detectably influenced by crystallographic orientation. These sapphire bars exhibit much improved strengths, having bend strengths averaging over 2×10^5 psi ($1.4 \times 10^9 N/m^2$), with 5×10^5 psi ($3.4 \times 10^9 N/m^2$) being achieved in these initial attempts. Also the strengthening effected by gas polishing can be achieved much more reliably than can be obtained by flame polishing. In addition, some rutile crystals developed very smooth surface finishes and exhibit fairly high strengths. The present results further suggest that development of this technique may also be fruitful with spinel and possibly for other ceramics. Gas polishing of a variety of polycrystalline ceramic specimens yielded mat or frosted finishes and gave no clear strength increases or even decreases in strength. Thus, although apparently limited to single crystals, the polishing technique has proven to be a very versatile and useful procedure for obtaining good surfaces and substantial increases in strength in sapphire and rutile. Twinning may be limiting further increases in strength of rutile.

Note added in proof: Recently, using only czochralski grown sapphire, average flexure strengths of $8 \pm 0.3 \times 10^5$ psi ($\sim 5.5 \times 10^9 N/m^2$) with maximum strengths of 1.2×10^6 psi ($\sim 8.3 \times 10^9 N/m^2$) have been obtained. Also, average bend strengths of $2.1 \pm 0.25 \times 10^5$ psi ($\sim 1.5 \times 10^9$ N/m^2) have been obtained for rutile while strengths up to 1.5×10^5 psi ($\sim 1.1 \times 10^9 N/m^2$) for stoichiometric spinel crystals were achieved. Fine etch pits also can occur during polishing, especially with rutile, which can either limit strength directly or may act as twin sources.

5. References

[1] Schmidt, W. A., and Davey, J. E., Preparation of smooth, crystalline, damage-free, sapphire surfaces by gaseous etching. This volume.

[2] Rice, R. W., The effect of sputtering on surface topography and strength of ceramics. This volume.

[3] Rice, R. W., Effect of grinding direction on the strength of ceramics. This volume.

[4] Becher, P. F., and Rice, R. W., Flame polishing of flat oxide bars. This volume.

Discussion

RICE: One other piece of data. We tried this experiment on alumina rich spinel and there is some possible improvement in strengths. As a suggestion, I think if you have stoichiometric spinel, gas polishing may give you high strength also.

NATIONAL BUREAU OF STANDARDS SPECIAL PUB. 348, THE SCIENCE OF CERAMIC MACHINING AND SURFACE FINISHING, Proceedings of a Symposium Sponsored by the American Ceramic Society, the Office of Naval Research, and the National Bureau of Standards, held at NBS Nov. 2–4, 1970, Gaithersburg, Md. (Issued May 1972).

IV. SURFACE AND SUBSURFACE ANALYSIS AND CHARACTERIZATION

Session Chairman

W. H. Rhodes, AVCO Corporation

Analysis and Characterization of Ceramic Surfaces for Electronic Applications

R. C. Sundahl and L. Berrin

Bell Telephone Laboratories, Inc., Allentown, Pennsylvania 18103

The criteria which are used to evaluate the surfaces of ceramic substrates for use in the electronics industry must be related to the specific application of the surface. This article emphasizes one such application—the use of a ceramic surface as a support for complex thin film conductor patterns which serve to interconnect silicon integrated circuit chips. Those ceramic surface parameters which are found to be critical to this application are (1) topographical properties, (2) chemical properties and (3) crystallographic properties.

These properties are characterized using such tools and techniques as optical, transmission electron and scanning electron microscopy, profilometry, electron microprobe analysis, ion microprobe analysis, Auger electron spectroscopy and electron diffraction. Special emphasis is placed on the relationship between the results of such analyses and the performance of the surface as part of the SIC interconnect system.

Key words: Aluminum oxide; Auger electron spectroscopy; crystallographic texture; ion microprobe; scanning electron microscopy; substrates; surface defects; surface segregation; thin film adhesion; thin film circuit imperfections.

1. Introduction

The analysis and characterization of surfaces resulting from ceramic forming, machining, and finishing methods are necessary to obtain a fundamental understanding of the effects of such operations on surface properties. It is through this understanding that ceramic surfaces can be improved so as to meet the rigid requirements of the new technologies. In the electronics industry the use of a ceramic surface as a substrate for a thin film circuit imposes certain demands on the properties of that surface [1–5][1]. Thin film properties are particularly sensitive to a wide variety of physical and chemical properties of the substrate surface, hence a wide variety of techniques have been developed to evaluate these substrate properties. In the discussion of more familiar techniques, such as the optical microscope and stylus instrument, the article emphasizes problems associated with the interpretation of observations on ceramic substrates. Several techniques somewhat less familiar in their application to ceramic surfaces are also discussed.

[1] Figures in brackets indicate the literature references at the end of the paper.

Before describing techniques for the analysis of ceramic substrate surface properties it would be instructive to first discuss in brief the ceramic surface as part of a thin film circuit. Figure 1 shows a typical silicon integrated circuit package, a 1,024 bit IGFET (insulated gate field effect transistor) memory used in the Electronic Switching System[6]. A high density alumina substrate, about 80 mm × 30 mm × 1 mm thick, provides support for the Ti-Pd-Au thin film conductor pattern. This thin film circuit, fabricated from a vapor deposited metallization by photolithographic methods, provides the electrical and mechanical interconnections between the forty beam lead integrated circuits. The circuit also provides access to and from the outside world through the leads which are thermocompression bonded at the edge of the substrate.

The adhesion of the metal interconnect film and the integrity of the finely detailed interconnect pattern are critically influenced by the ceramic surface properties. Other factors important in determining compatibility of the ceramic with the integrated circuit assembly are resistance to chemical and thermal degradation during processing, high electrical resistance, appropriate dielectric constant and

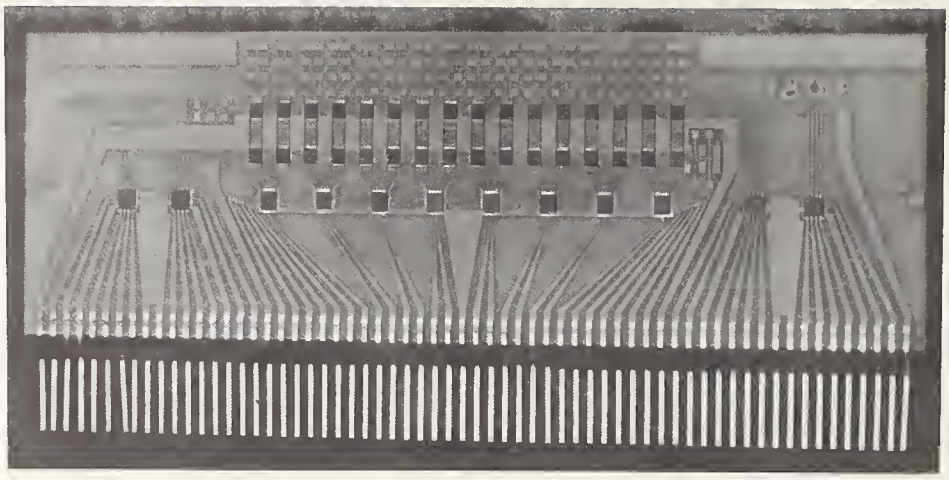

FIGURE 1. *An alumina substrate, approximately 3cm × 8cm, supports the thin film interconnect circuit for a 1024 bit memory.* The 32 chips in the top center of the circuit are 32 bit memory chips, each with 26 leads, 50 μm wide and on 100 μm centers [6].

sufficient mechanical strength to withstand bonding operations and handling.

The techniques for analyzing and characterizing the ceramic surface can be divided into three general categories of surface properties:

(1) **Surface topography**—the techniques used to ascertain the surface roughness and its effect upon the delineation of fine metal lines on the surface. Also included are the number, size distribution and identity of discrete surface defects. These defects have been found to have a critical effect on thin film circuit pattern integrity.

(2) **Surface chemistry**—techniques used for a direct analysis of the chemical composition of the ceramic surface, which, in general, differs from the bulk ceramic. The surface chemistry of a substrate has been found to have an important influence on circuit characteristics such as film adhesion, aging stability of thin film resistors and leakage currents across the substrate surface.

(3) **Surface crystallography**—techniques discussed here include methods of characterizing crystallographic texture; that is, the preferred orientation of the individual crystallites. Also covered are methods for studying the crystal structure on the surface, which in general differs from the bulk structure, and the mechanical damage introduced into the surface by machining operations. There is not a great deal of information available on the surface crystallography of ceramics, probably because it has been felt in the past that these properties are not important to substrate performance.

The techniques described here are discussed in relation to their use for a particular problem, the characterization of substrate surfaces for thin film interconnect circuits. However, many of these techniques have potential usefulness in a wide variety of problems associated with ceramic surfaces.

2. Surface Topography

One of the most common techniques used to characterize surface topography is the stylus trace. The technique provides a rapid method of evaluating surface roughness for routine work and the results can be characterized by a single parameter, the AA or arithmetic average. However, one is often frustrated in his attempt to relate the results of a stylus trace to the performance of the ceramic surface in a thin film circuit package. It has been found that a more detailed assessment of surface topography is necessary to enable one to predict substrate surface performance. This has been recognized by White et al., [7] in an earlier paper, in which they describe the use of computer processed scanning electron microscope images and rastered stylus traces. These techniques are still limited to relatively small areas, as measurements are time consuming.

We have combined rather conventional optical examination techniques, under a *low power microscope*, with a statistical analysis of the observations. This analysis provides information about the number and size distribution of discrete defects in the substrate surface, as well as the effect of these defects on thin film interconnect patterns. More detailed information about the defects and other features of the ceramic surface have been provided by *scanning electron microscope* (SEM) and *transmission electron microscope* (TEM) observations.

2.1. The Stylus Trace

The operation of this instrument is simple in concept. A diamond stylus with a tip which has a radius of curvature typically 2.5 μm, is

brought into contact with the sample surface under a load of less than 500 Kg/cm^2. As the stylus is moved across the surface, the vertical motion of the stylus is converted into an electrical signal by a displacement transducer, the signal amplified, and then displayed on a strip chart recorder. Amplification, the ratio of recorder pen motion to stylus motion, varies from 1,000 to 50,000. The highest gain corresponds to a sensitivity of about 50Å vertical displacement of the stylus. Horizontal displacement of the stylus is directly related to motion of the chart paper and amplification of the horizontal scale is typically 100, or 10 to 500 times less than the verical scale. This accentuation of the vertical motion of the stylus should be kept in mind when examining stylus profiles. Deviations in the surface of only a few degrees slope appear as very sharp peaks when viewed on the stylus trace.

Typical recorder traces of an alumina substrate surface are shown in figure 2. This sample was prepared by an isostatic pressing process[8] and sintered to 99 percent of its theoretical density. It is instructive to study these traces and determine their usefulness. Figure 2A, an as-fired surface, shows the typical small modulations in the profile and peaks and valleys of approximately equal size. After grinding (fig. 2B) the peaks and the undulations are obviously removed. The valleys in the profile probably represent regions of grain pullout. Careful polishing with diamond paste essentially eliminates pullouts (fig. 2C). This last profile, with a ten-fold increase in vertical magnification, shows only an occasional pit, about 0.3 μm diameter, on the surface.

The stylus trace can be characterized by several parameters; namely, (1) an average peak-to-valley distance, (2) the maximum peak-to-valley distance, (3) the average half-height widths of the peaks, and (4) the average number of peaks per unit length. Although a single parameter provides only a very limited description of surface topography, it is quite common to characterize surface roughness by the arithmetic average (AA). The AA is determined electronically from the transducer output by summing peak areas above and below a zero reference point, the center line, and dividing by the stylus trace distance.

The stylus trace does provide a convenient method for monitoring ceramic surface preparation processes, for changes in ceramic prop-

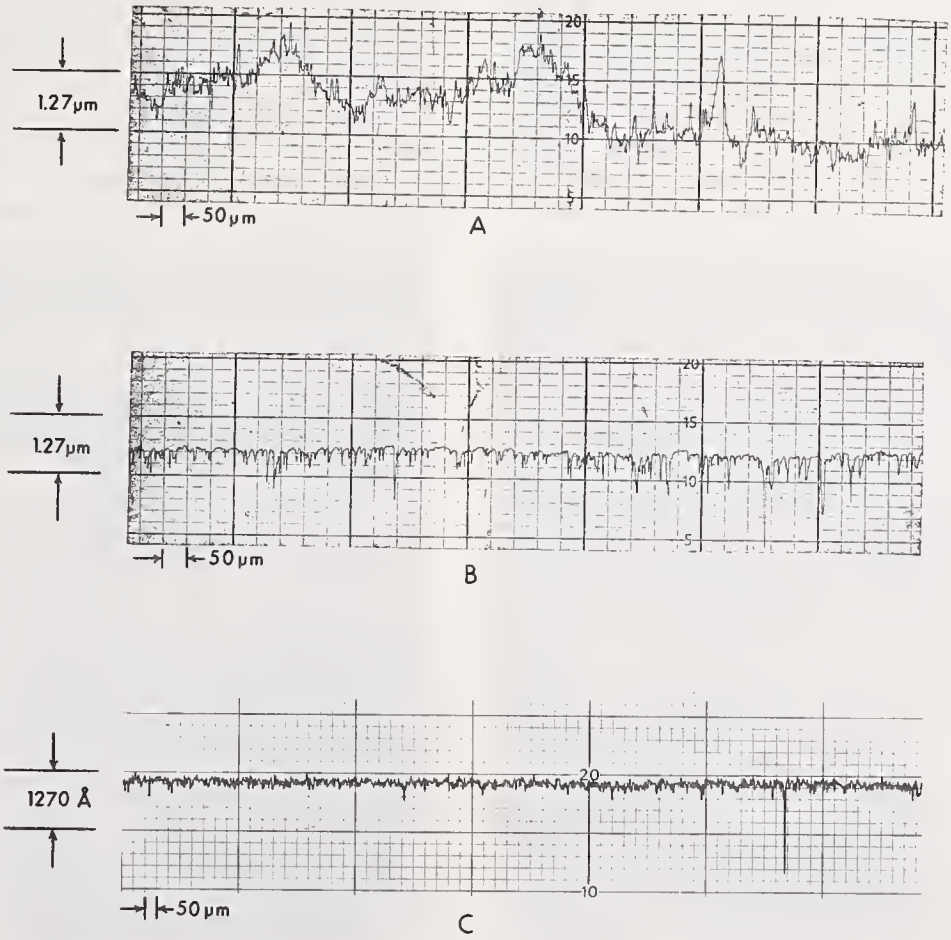

FIGURE 2. *Surface stylus traces of alumina substrate surfaces in three stages of finishing; (A) As-fired, AA = 0.27 μm (10.5 μin) (B) Ground with a 400 grit diamond button wheel, AA = 0.11 μm (4.5 μin), (C) lapped with a diamond polishing compound, AA < 0.005 μm (0.2 μin).*

erties or process steps will generally be reflected by corresponding changes in the appearance of the stylus trace and the AA value. However, it is difficult to characterize surface topography quantitatively with a stylus trace. First, the common use of the AA value alone has some serious drawbacks. Two surfaces with widely differing stylus traces may have identical AA values [5, 9]. Also, low AA or other average values may underweight the effects of a few large surface defects (see fig. 2C) which may have a critical effect on thin film conductor or capacitor pattern yield. Finally, the stylus instrument provides a sample of only a very small area of the surface and without a great amount of effort a few large defects on a single substrate surface would go undetected

2.2. The Optical Microscope

Optical microscopy techniques are well documented in the literature. An example of one such technique is described by Lo [10] in another paper presented at this Symposium. Our concern in this discussion is with the effect of surface defects on the integrity of thin film interconnect circuits [11]. A circuit, such as seen in figure 1, may contain several meters of 50 μm lines on 100 μm centers. Surface defects affect the photolithographic fabrication process so as to cause opens in conductor lines or shorts between adjacent lines. Observations on the effect of various defect types were made by use of fine line test patterns which simulate the worst case conditions encountered in an interconnect circuit.

The test pattern used consists of 15 m of 50 μm conductor lines spaced on 100 μm centers. This pattern is generated on a 20 cm^2 area of substrate using standard thin film (0.1 μm Ti and 1.5 μm Au) and photolithographic techniques. These patterns are examined in detail under a binocular microscope at 60X, using both reflected and transmitted lighting. Examples of surface defects and their effect on the test pattern are seen in figure 3. A surface pit in figure 3A has resulted in a complete open in a conductor line. A burr or protrusion, as seen under low angle reflected lighting conditions in figure 3B, has led to a short between several adjacent lines. This latter defect can easily be detected with the unaided eye, using an intense light source with a low angle of incidence. Observations recorded during such an examination include (1) the number of various defect types and (2) the number, size and types of imperfections produced in the conductor lines by these defects.

There are two implications of this approach which are important to this discussion. First, the ceramic surface can now be characterized by a parameter directly related to its performance, rather than some parameter only vaguely related to use, such as surface roughness. The parameter chosen here is fine line imperfection frequency $f(\lambda,d)$. Here, f is a function both of the width d of the conductor lines of the test pattern (50 μm in this example) and of the criterion used to define a conductor line imperfection. The criterion used here is any short between adjacent lines or any line which is more than 1/3 open ($\lambda = 1/3$).

The second implication is that this quantitative parameter can be used to predict performance of the ceramic surface in a given thin interconnect circuit. If one assumes, reasonably, that substrate surface defects are randomly distributed over the substrate, then

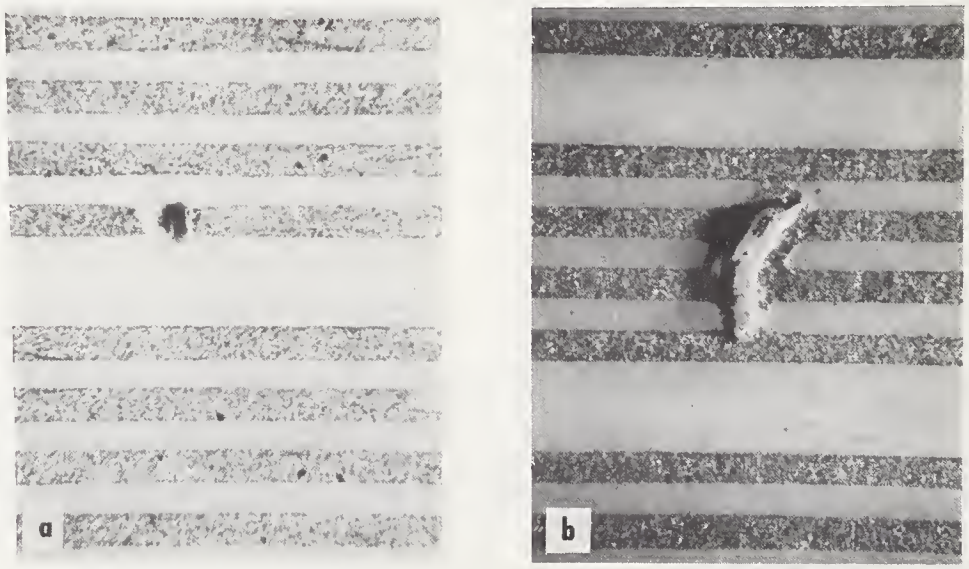

FIGURE 3. *Optical micrographs of alumina surfaces with a conductor line test pattern present.* (A) A surface void, resulting in a complete open in a conductor line, (B) a burr protruding from the surface, resulting in shorts between adjacent lines. Low angle incident lighting.

the probability that a length of line L will have no line imperfection is [11]

$$Y = e^{-Lf}$$

This is, of course, identical to the production yield of a thin film interconnect circuit with conductor line length L, fabricated on a substrate with a characteristic f value. This statistical treatment can be extended to permit estimates of the effects of changes in λ and d on yields [11].

One positive consequence of this approach is the presence of a reference grid on the surface. It has been our experience that visual observations are much more accurate if the test pattern, which acts as a reference grid, is present. The grid also provides a convenient reference to estimate surface defect sizes. The method unfortunately is very tedious, especially in cases where there are only a few defects in a 100 cm^2 area. However, attempts to automate these measurements with the aid of an image analyzer thus far have not met with success, mainly because of the complexity of the analysis and the required contrast and resolution. Therefore, despite the large amount of effort required to obtain statistically significant data and the systematic human error associated with such a technique, we have found this statistical method of characterizing ceramic surfaces to be a most useful approach.

2.3. The Scanning Electron Microscope (SEM)

Although the SEM was introduced into general use only recently, it has rapidly become a standard tool for surface characterization. The SEM is particularly useful for providing more detailed information about the nature of the ceramic surface because of the unique characteristics of the instrument. These characteristics include (a) high resolution—about 500Å is nominal, (b) unusually high depth of field—about 300 times that of the optical microscope and (c) little or no sample preparation. The details of the operation of the SEM has been covered earlier in this Symposium [7].

Figures 4, 5 and 6 illustrate the application of the SEM to the characterization of surface defects [11]. These observations allow one to determine the source of substrate defects and to modify process variables so as to minimize their occurrence. A common surface defect is seen in figure 4. At the lower magnification we see a ground ceramic surface with a surface pit present. In this case the pit had no effect on the conductor pattern. At the higher magnification the microstructure inside the pit is revealed in greater detail. The smooth, equiaxed grain structure is typical of an as-fired surface and suggests that the pit was formed during or, more probably, before the sintering step. Electron microprobe analysis of this defect re-

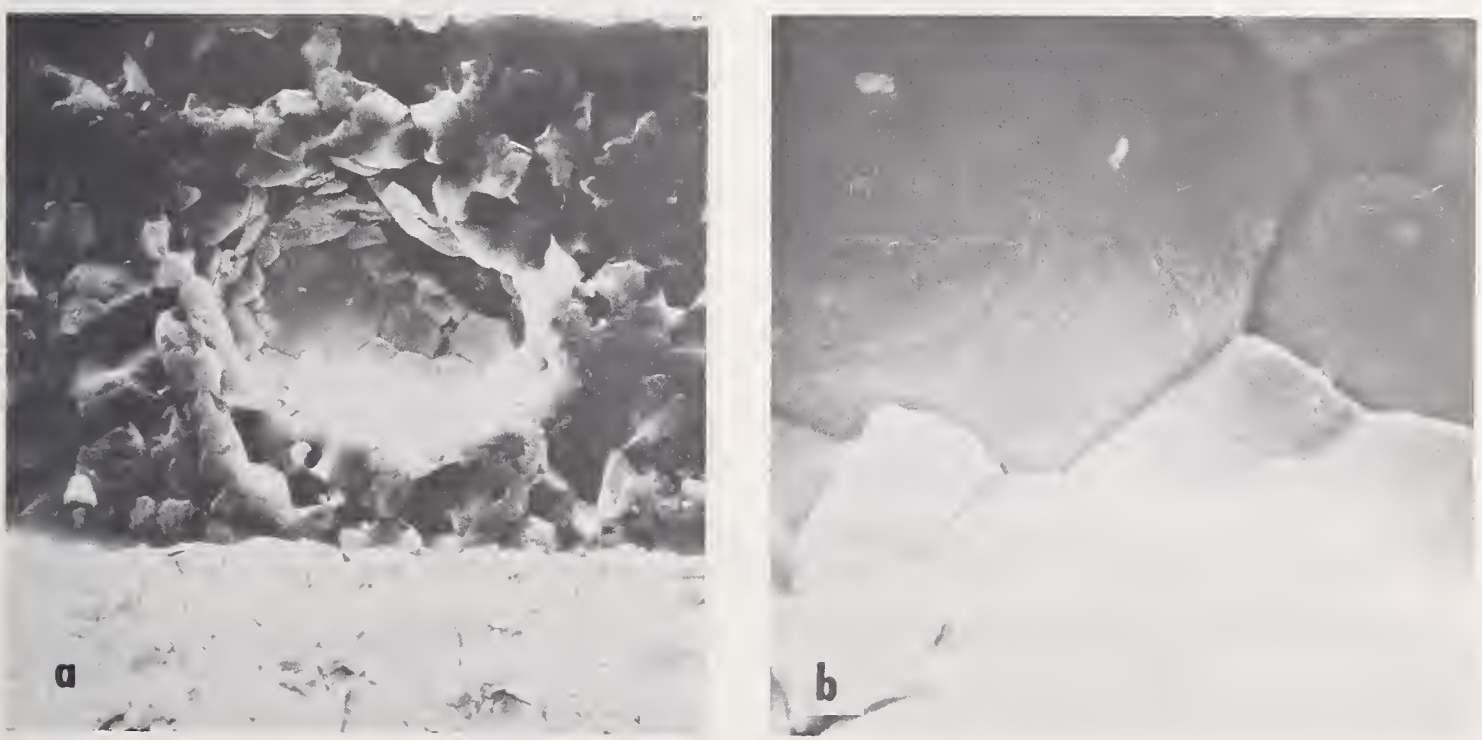

FIGURE 4. *SEM pictures of surface void observed on a ground and annealed isostatic pressed substrate with a fine line test pattern present.* The smooth equiaxed grain structure within the void indicates formation prior to or during sintering. (A) 1000X (B) 5000X.

FIGURE 5. *SEM pictures of surface void of a polished (unannealed) isostatic pressed substrate with test pattern present.* The platelet structure within the void indicates the presence of foreign contamination. (A) 1000X. (B) 5000X.

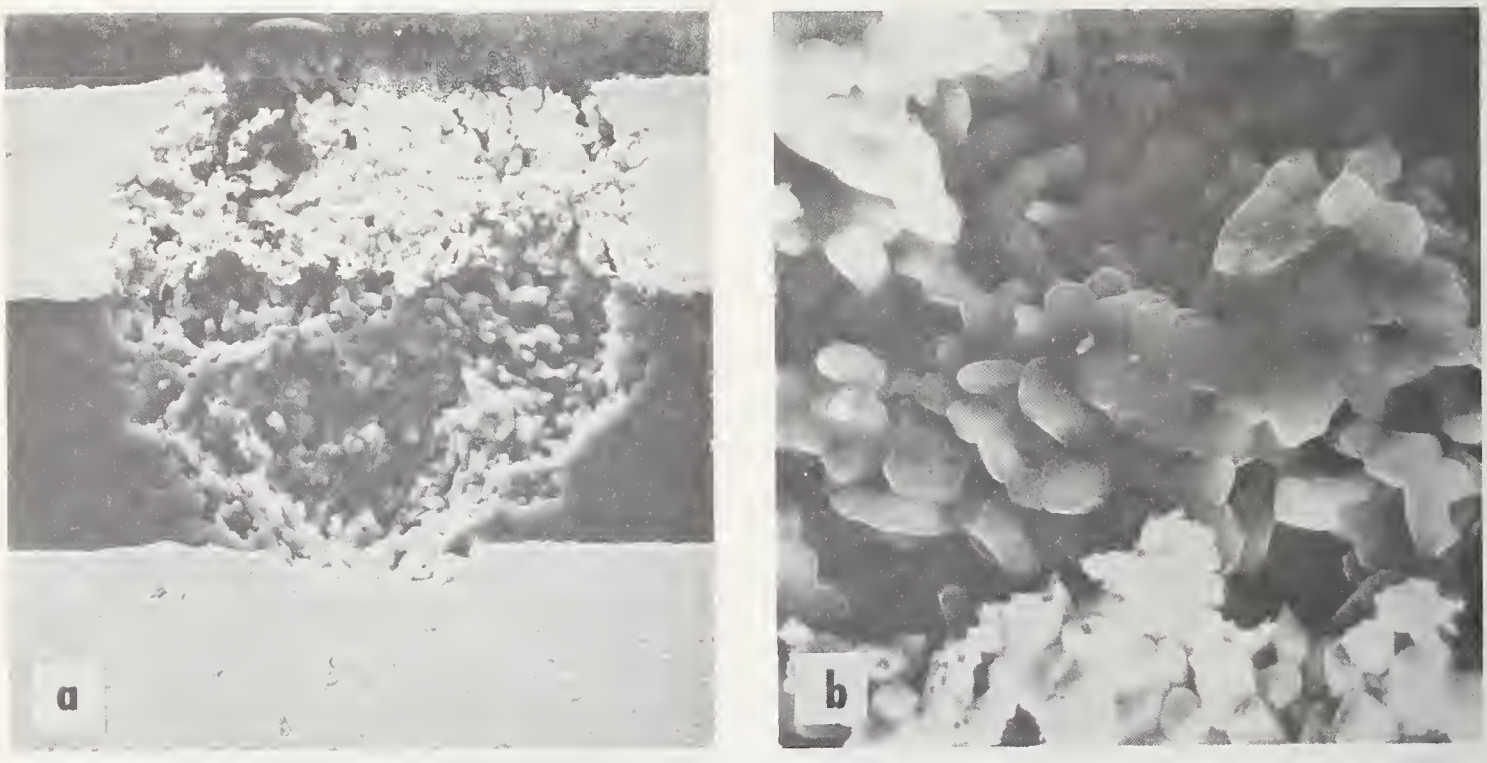

FIGURE 6. *SEM pictures of a large white spot observed on a polished and annealed isostatic pressed substrate.* The fine grain structure indicates that only partial sintering occurred in this region. (A) 500X. (B) 2000X.

vealed no significant contaminants in this type defect.

A second and less common type of surface defect, seen in figure 5, exhibits an anomalous morphology inside the pit. This growth of acicular platelets is indicative of a local contaminant. This conclusion was substantiated when an electron microprobe examination revealed a high concentration of calcium within the void. It would appear then that this type of defect is somehow associated with contaminants in the raw material.

A very common defect observed in high density alumina ceramics is an isolated low density

region. Figure 6 shows the catastrophic effect of this defect upon a 50 μm wide test line. It is seen that this region is actually made up of very small individual grains only partially sintered together. It is suggested that this phenomenon is the result of hard agglomerates existing in the raw material which retain their integrity during the ceramic forming and sintering operations. The defect type exhibited no measurable contamination when examined in the electron microprobe.

There are some problems associated with the use of the SEM for the examination of ceramic surfaces and these warrant a brief review. On insulating samples the electron beam charges the surface negatively. If this charge is not dissipated the picture is distorted and local bright spots appear. This problem is easily overcome through the use of a thin conductive coating, a few hundred angstroms of carbon will do, on the surface of the insulator. One must be careful, however, to completely cover the area to be examined. An examination of figure 4 reveals that an area inside the pit was shadowed during vacuum evaporation of carbon onto the sample, resulting in local charging and bright spots.

A second area of difficulty is the interpretation of SEM images. The contrast effects are quite complex. In the standard secondary emission mode of operation contrast results from variation in secondary emission yield over the sample surface. As discussed in detail by White [7], the yield increases as the angle of incidence of the beam with the surface decreases, giving a topographical contribution to the image. However, secondary yield also varies in a complex manner with surface composition, which in turn may vary from sample to sample or even over the surface of a presumably homogeneous sample. These effects are not completely understood and can lead to confusion.

One attractive feature of the SEM is its versatility. There are several other modes of operation [12] available on most commercial instruments, in addition to the secondary emission mode. These include the "backscatter" mode, in which only the elastically scattered electrons are detected. A combination of information from the backscatter and secondary modes can resolve some ambiguities in interpretation of contrast effects. An inclusion of information from the sample current image may lead to further understanding of the nature of the surface. The SEM can also be used to study cathodoluminescence and some instruments are equipped with dispersive or nondispersive x-ray detectors, converting the instrument into an electron microprobe.

2.4. The Transmission Electron Microscope (TEM) [13–15]

Again, the principles and uses of the TEM are well-documented in the literature. The purpose here is to briefly describe techniques we have found useful in studies of ceramic surface topography.

When a high degree of resolution is sought and the surface to be observed is not overly rough, replica TEM techniques provide micrographs superior to those obtained from the SEM. Thus the method is useful for polished and as-fired surfaces, but is difficult to employ for the examination of ground surfaces or surface defects.

The sample preparation for the TEM is certainly more complex than for the SEM. Two methods that are useful for replicating a surface are the one-step plastic technique and the two-step plastic-carbon replica technique (see fig. 7). The one-step method is relatively simple. The replica is formed by placing on the ceramic surface a dilute solution of collodian or Formvar and allowing the solvent to evaporate. The film is removed from the surface by stripping it off with adhesive tape or floating it off under water. A replica prepared in this manner is a negative reproduction of the original surface. This technique is not applicable to very rough surfaces as the replica is quite fragile. Also, the plastic tends to decompose during long exposure to the electron beam. The two-step process utilizes a thicker first replica which then acts as a substrate for a thin carbon replica. A positive

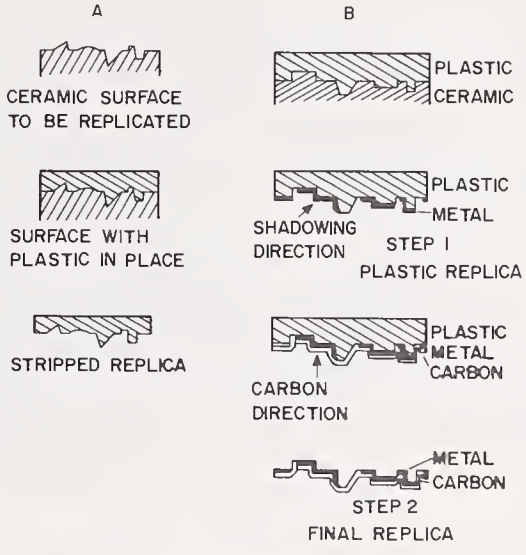

FIGURE 7. *Two common techniques for fabrication of transmission electron microscope replicas of ceramic surfaces.* (A) One-step plastic replica, (B) Two-step plastic-carbon replica with heavy metal shadowing.

439-921 O - 72 - 19

replica results from this procedure. The two-step process is useful for rougher surfaces and the carbon is quite stable in the electron beam.

Figure 8 shows the result of a one-step replication of the surface of a commercially available tape cast substrate. This method appears entirely satisfactory for such application as fine detail is revealed. Some artifacts are evident in the micrograph, some of which are due to tearouts during the film stripping.

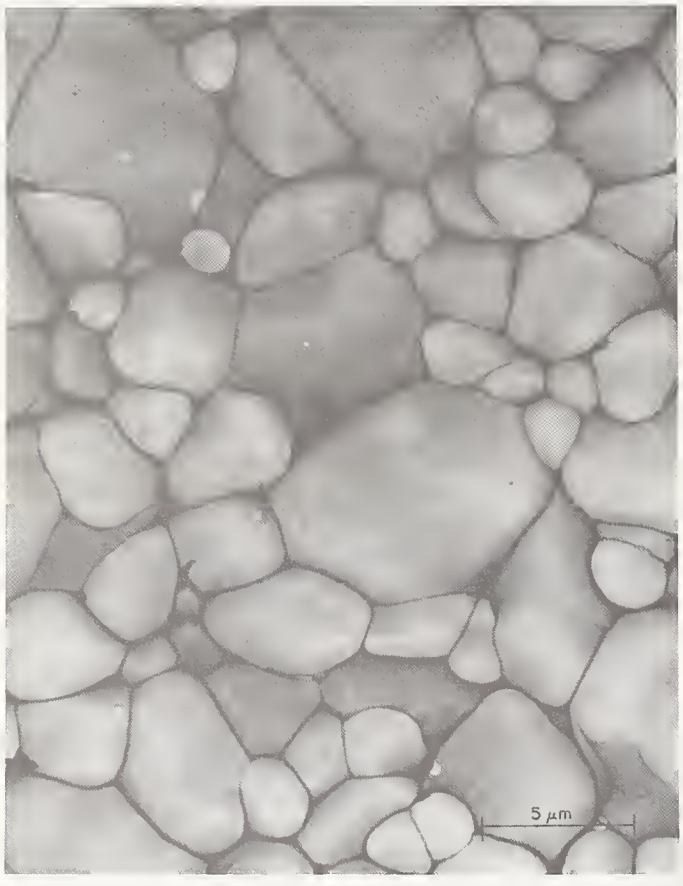

FIGURE 8. *Transmission electron micrograph of an as-fired aluminum oxide surface replicated with plastic (8600X).*

In the TEM electron absorption is not very different for the small differences in specimen thickness and very little difference in contrast results from thickness effects. Contrast in the TEM arises primarily by differential scattering from different parts of the sample. Since the relative degree of scattering is governed primarily by differences in the mass density of a specimen, the most useful method for enhancing contrast is the shadowing technique. This method consists of increasing the density on certain sides of the specimen by oblique vacuum coating with a heavy metal, so that the beam is scattered readily as it passes through those portions of the specimen. It is essential to know the shadow angle so as to obtain quantitative information; i.e., height and depth measurements, of the surface topography.

3. Surface Chemistry

In the past it has been the general practice to determine the effect of the chemical properties of the ceramic substrate surface through some operational measurement of substrate performance, such as adhesion measurements, aging experiments or environmental tests. The role of chemistry has then been inferred indirectly from the results of the experiment and, in some cases, knowledge of the bulk chemical composition of the substrate. Recently, however, there has been a proliferation of new analytical techniques which provide direct information about the chemistry of the surface. These include the electron beam and ion beam methods, such as *electron microprobe analysis*, *Auger electron spectroscopy*, *photoelectron spectroscopy* and *ion microprobe analysis*. These tools can be combined with the more indirect methods of analysis, such as infrared spectroscopy, ellipsometry, contact angle measurements, gas adsorption measurements and the above mentioned performance tests to provide a more complete picture of ceramic surface chemistry.

3.1. The Electron Microprobe [16–18]

The electron microprobe is, of course, not a new method of chemical analysis. In fact, in a strict sense, it is not a method of surface analysis at all. However, a description of the principles behind electron microprobe analysis provide a basis for discussing other beam techniques.

A schematic of the electron microprobe is seen in figure 9. The optics are similar to that of the SEM; the electron beam is rastered across the sample and a display is formed coincidently on a cathode ray tube. In this case, though, the information is the intensity of emission of a particular x-ray line. This instrument may also be used as a crude SEM, just as the SEM can be used as a crude electron microscope. The basic difference in the two instruments is the lower resolution in the electron microprobe. The electron microprobe is limited to about 1 μm beam spot rather than a nominal 100Å for the SEM. This is compatible with the inherently lower resolution of x-ray emission mode of operation.

Figure 10 illustrates the complex processes which occur when a high energy electron beam interacts with a sample surface. Application of the microprobe to studies of ceramic surfaces requires that the investigator keep in mind several considerations illustrated by figure 10:

(1) The incident beam penetrates several microns into the surface, losing energy through the generation of heat and secondary electrons. This heat may cause decomposition of the sample if it is a

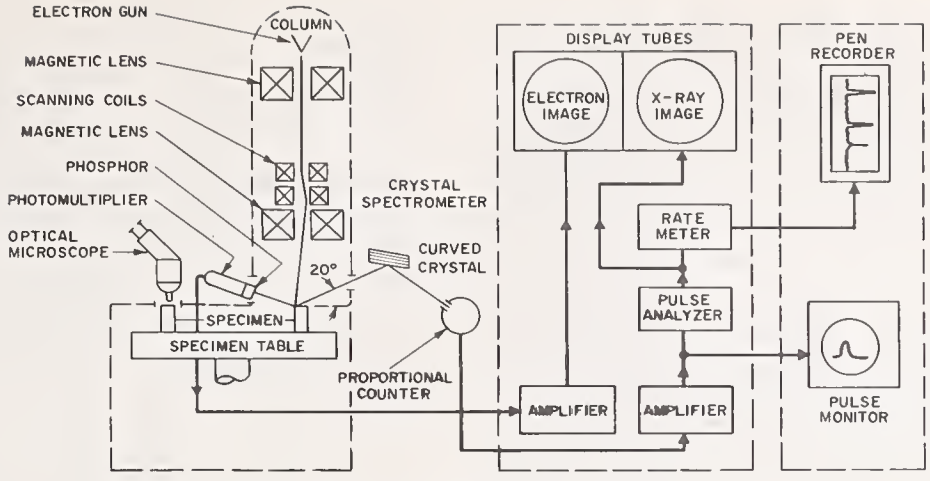

FIGURE 9. *Schematic diagram of the electron microprobe.*

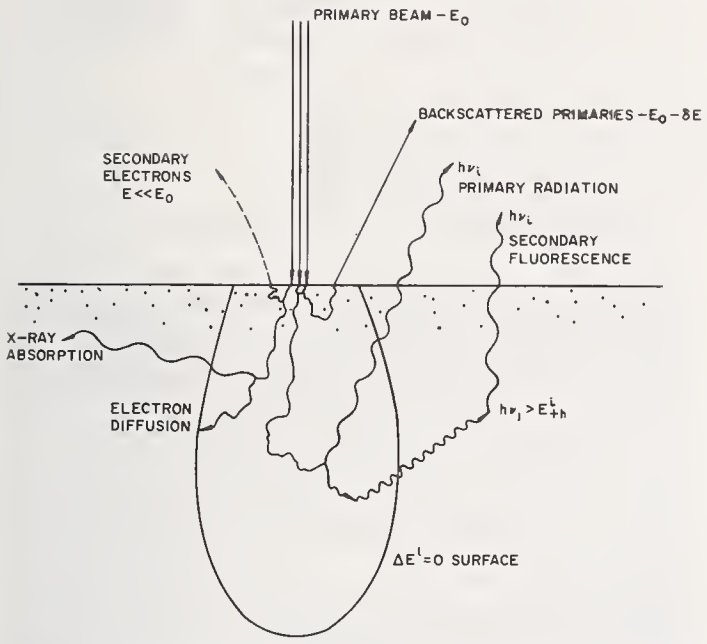

FIGURE 10. *Schematic diagram of electron loss and x-ray emission processes in the electron microprobe.* Primary excitation occurs in a region in which the diffusing electrons maintain an energy E greater than the threshold energy E^i_{th} ($\triangle E^i > 0$).

poor thermal conductor. Radiation damage due to the incident beam may also modify the sample. The generation of secondary electrons results in the surface charging of a ceramic insulator. This again can be eliminated by the use of a thin conductive coating. Finally, penetration of the beam means that x-rays are generated from a depth of several thousand angstroms rather than from the surface alone.

(2) Diffusion of primary electrons in the sample and the generation of secondary x-rays results in loss of lateral resolution, which is on the order of 2 μm.

(3) The complexity of the various processes makes it difficult to obtain a quantitative interpretation of the data. This problem is exaggerated for the lighter elements as absorption corrections introduce the most error. However, there are available elaborate iterative computer programs which do provide quantitative data from the microprobe measurements [19].

(4) The measurements of the light elements are also limited by low signal yield, absorption by the conductive coating and low sensitivity of the detectors to long wavelength x-rays.

Applications of the electron microprobe to the study of ceramic surfaces has thus far been limited to the semiquantitative analysis of inclusions and other macroscopic forms of contamination [18], to interdiffusion at metal-ceramic interfaces [16] and to the segregation of impurities at grain boundaries [17]. The results of grain boundary segregation analyses have some implications relative to the ceramic surface, as one would expect that impurities that segregate at internal surfaces; e.g., grain boundaries, might also segregate on as-fired or annealed surfaces.

3.2. Auger Electron Spectroscopy (AES) [20–26]

The technique of Auger electron spectroscopy (AES) is a new addition to the catalog of tools available for the analysis of surfaces. The instrument is in many ways similar to the electron microprobe. In both instruments an incident beam of electrons is used to excite the atoms and the surface chemistry is characterized in terms of the decay products of these excited atoms. The main difference is that the decay products detected by AES are electrons, not photons. In other words, AES is an electrons in, electrons out technique where the electron microprobe is an electrons in, photons out instrument.

The characteristics of the AES of primary interest for the study of ceramic surfaces are:

(1) The instrument has a high selectivity for the surface atoms. For electrons with an energy of 500 eV, a typical energy of an Auger electron, one expects a mean escape depth of a few atom layers.
(2) AES is able to detect less than 0.01 monolayer of contaminant on the surface.
(3) Below 1000 eV virtually all relaxations are associated with Auger emission, thus the relatively high sensitivity of AES to the presence of light elements.

Applications of AES have been reported in metallurgy (interdiffusion of thin films, grain boundary segregation, surface diffusion), solid state technology (photoemission from semiconductors, contamination on silicon wafers, segregation of impurities at surfaces), catalysis (chemisorption on platinum), and solid state and molecular physics (surface band structure, molecular spectra). Unfortunately, very little work has been done on the characterization of ceramic surfaces with AES. This is undoubtedly due, in part, to the newness of the technique. However, there are some fundamental limitations which may have impeded its application. These problem areas will be discussed after a brief description of the Auger process itself and some of the instrumentation used for its detection.

The Auger process of electron ejection is a relaxation process complementary to x-ray emission. Figure 11A shows an excitation process, the same as for x-ray emission, in which an incident electron ejects an electron from a lower energy shell. The electron beam characteristics are typically 3 keV and 100 μa. X-ray emission (fig. 11B) is seen to result from the relaxation of an excited atom, in this case magnesium, through an electron transition and the simultaneous emission of a photon. In figure 11C the same excitation and decay process is seen, but this time accompanied by the ejection of an Auger electron. To conserve energy, the ejected electron in this case has a kinetic energy of $K-L_2-L'_2$, where L'_2 is the L_2 level perturbed by the double ionization of the Mg atom. This perturbation results in some uncertainty as to the theoretical position of the lines, and in most cases these positions have been determined experimentally [21, 22].

The case of a solid and, in particular, an insulator is complicated by the broadening of energy levels into bands. In MgO, for example, Mg^{++} has no M electrons and consequently no LMM transition would be expected for a purely ionic compound. However, transitions are observed, and it is uncertain as to the origin of the electrons which decay into the lower energy level and the origin of the Auger electrons. These transitions have been explained alternatively in terms of a deviation from ionicity or crossover transitions from the $O^=$ band, as shown in figure 11D.

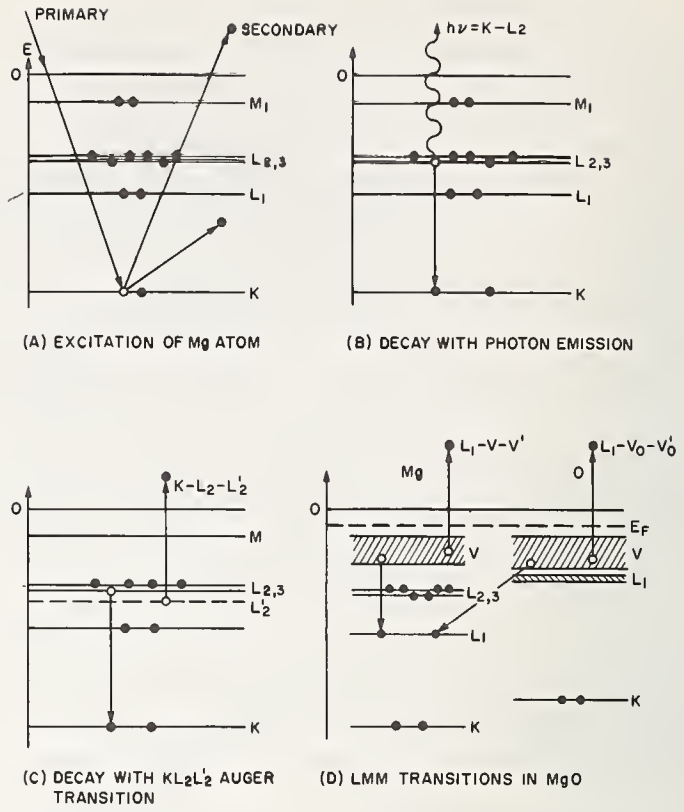

FIGURE 11. *A comparison of Auger and x-ray emission processes for Mg, MgO.* (A) The excitation of the atom with an incident electron is common to both techniques. (B) Relaxation of excited atom via x-ray emission. (C) Relaxation accompanied by Auger ejection of an electron—a KL_2L_2' transition. (D) Auger transitions in MgO.

The major problem associated with the detection of Auger electrons is the low signal-to-background ratio. The incident electron beam produces a large number of secondary and inelastic electrons over all energies below the incident beam energy. The Auger electrons make up a very small fraction of this total signal and herein lies the problem, the detection of the weak Auger signals in a high background. A standard analog technique for solving such a problem is to examine the differential of the secondary electron distribution. The slowly varying background signal has a first derivative near zero, whereas the small, sharp Auger peaks have a significant first derivative. In this manner an increase in signal-to-background ratio of several magnitudes is gained [20].

Figure 12 shows an Auger electron spectrum of MgO. The first derivative of the energy distribution is plotted as a function of electron energy. Note that the appearance of the major Mg LVV transition is quite similar to the differential of a gaussian peak. The MgO spectrum consists of the low energy Mg LVV transitions, depicted in figure 11D, as well as the high en-

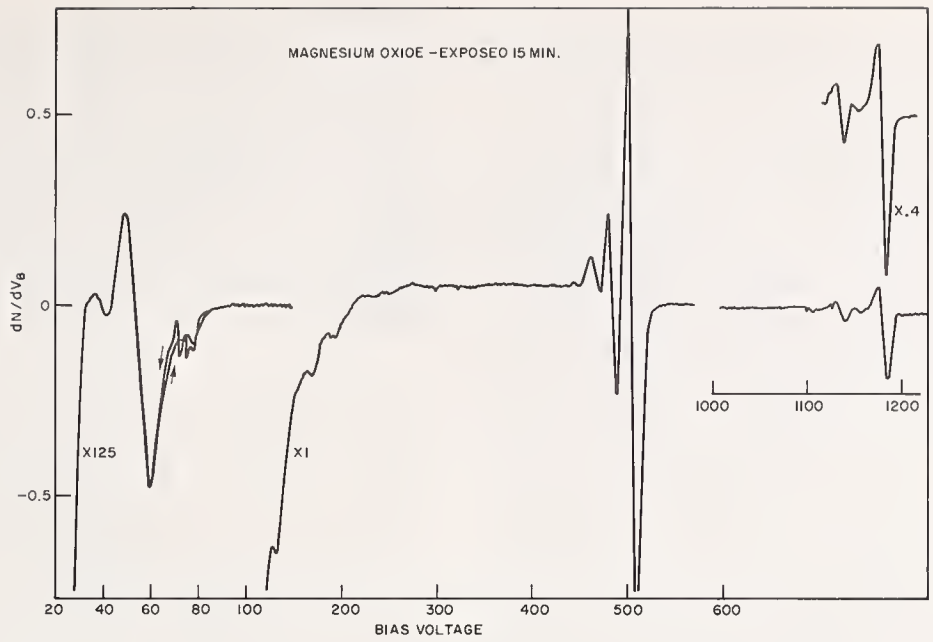

FIGURE 12. *An Auger spectrum of MgO.* The low energy Mg LVV transitions are by far the most intense. A series of weak transitions are observed between 100 V and 300 V which have not been identified. The oxygen and magnesium KLL transitions differ in intensity by an order of magnitude as Auger yield drops off above 1000 V.

ergy oxygen and magnesium KLL transitions. It is to be noted that, despite the similarity of the KLL transitions for the two components, the Mg transition is significantly lower in peak-to-peak amplitude. This reduction in intensity for higher energy transitions occurs because (1) it is more difficult to excite the K level of Mg than O with the 3 kV beam and (2) above 1000 eV some of the excited states decay via photon emission.

Figure 13 is a schematic of a retarding field analyzer used to perform AES measurements [25, 26]. The sample, situated at the center of the spectrometer, is exposed to an incident beam of electrons, in this case supplied by a modified cathode ray tube electron gun. The electron optics of the spectrometer are constructed from a series of nested spherical grids, situated in front of the electron collector. A bias voltage V_B applied to the grid structure allows only secondary electrons from the sample with an energy greater than eV_B to be collected. Thus this instrument provides a collector current i_c which is the integral of the secondary electron energy distribution above eV_B. In order to obtain a plot such as shown in figure 12 a second derivative, d^2i_c/dV_B^2, is needed. This double differentiation of i_c is performed electronically using ac modulation and detection techniques [25]. Briefly, the bias voltage V_B is modulated with a small ac signal, resulting in a corresponding ac component in i_c. The first harmonic of i_c (at frequency ω_0) is proportional to di_c/dV_B and the second harmonic ($2\omega_0$) to d^2i_c/dV_B^2. The detector system is then tuned to the $2\omega_0$ component of i_c and the output plotted vs. the sweep voltage V_B on the x-y recorder. Figure 12 is a direct result of such a measurement. It is then the combination of the retarding field analyzer, with its wide acceptance angle, the concept of measuring the derivative of the secondary electron energy distribution, and the use of modern ac signal processing techniques which have made AES a practical tool.

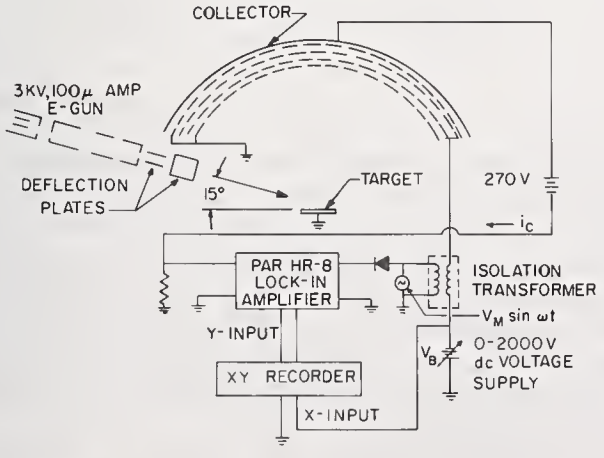

FIGURE 13. *Schematic diagram of the retarding field analyzer.*

As with other electron beam techniques there are some problems associated with the application of AES to the study of ceramic surfaces. These problems are categorized as follows:

(1) **Surface charging of insulators.** This problem is analogous to that described

previously for the SEM and electron microprobe. The problem is more critical here since the charge cannot be dissipated with a thin conductive coating. For, if one used a 500Å carbon coating here, the only component that would be detected is carbon. In general, for energies greater than 200 *eV*, the effect of a positive surface charge is to displace the spectrum uniformly toward a lower voltage. The extent of this voltage shift can usually be estimated if one has a strong peak of carbon or oxygen, for example, to act as fiducial marks on the spectrum. The spectrum at low energies (< 100 *eV*) is more strongly affected by sample charging. In general this lower energy region of the spectrum should be avoided since complications, such as illustrated in figure 11D, make interpretation of low voltage Auger spectra ambiguous.

(2) **Surface contamination.** In certain applications the impurities picked up during machining, firing steps or cleaning operations may play an important role in determining the performance at a ceramic surface. However, contamination from the ambient is usually only a nuisance. In this case it is best to prepare the surface in situ in an ultrahigh vacuum system. The sample can be cleaned in the vacuum station by ion beam etching or by the electron beam itself (electron desorption) but great care is needed so that the "interesting" contaminants are not removed with the "nuisance" contaminants.

(3) **Quantitative analysis.** The processes involved in an AES study of ceramic surfaces are not as well understood as for the electron microprobe. One is generally limited to empirical calibration methods through the use of standards to obtain quantitative information [21, 22]. Experiments of this nature have demonstrated a linear relationship between the peak-to-peak amplitude of the Auger signal and surface concentration for less than one monolayer coverage. Most work in this area to this date has been in the form of semiquantitative correlations between the measured signal amplitude and some macroscopic property, such as ceramic performance.

The next series of figures illustrate the application of AES to one problem associated with ceramic surfaces. Alumina substrates were prepared by grinding the surface with a 400 grit diamond wheel followed by an anneal at 1500 °C for 30 minutes in air. The substrates then went through a cleaning treatment commonly used prior to metallization and then were immediately placed in the spectrometer. Figure 14 shows evidence of the contaminants left behind by the organic cleaning solvents and the ambient. The surface is obviously masked by a carbonaceous residue. A low oxygen peak is detected and there is some evidence of calcium present.

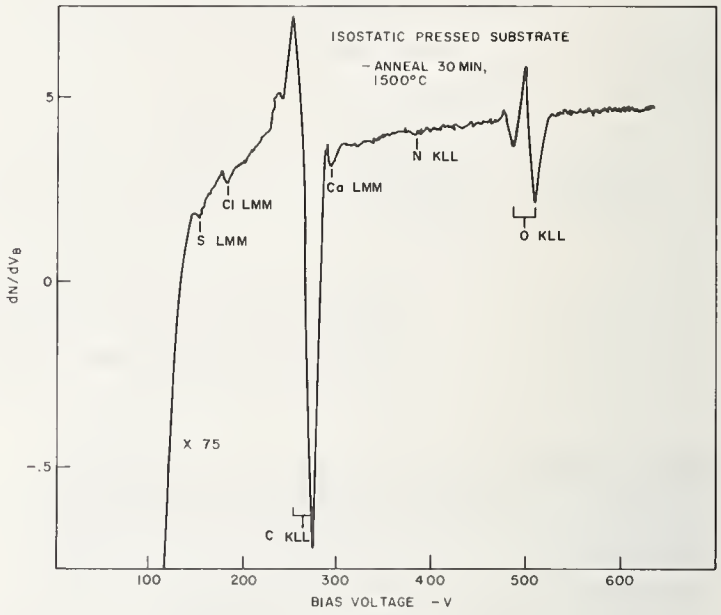

FIGURE 14. *Spectrum of isostatic pressed substrate surface after a 30 min anneal in air at 1500 °C.* Sample area not previously exposed to electron beam. A weak calcium peak is observed on this surface, besides contamination peaks associated with S, Cl, C and N.

After the substrate surface is cleaned with the electron beam the Auger spectra shown in figure 15 was revealed. The increase in the oxygen and calcium signal is evident, as well as the corresponding decrease in the carbon signal. There are also charging effects at low voltages. A careful analysis of the low voltage spectrum reveals a modified Al spectrum with a weak Si peak superimposed on it. Although a bulk chemical analysis of the substrate shows that about 650 ppm Mg is present, there is no indication of any Mg from Auger emission. By measuring the Mg signal from MgO (fig. 12) a rough estimate of the sensitivity of the instrument to Mg segregation is provided. It is estimated then that there is less than 10 percent Mg present on the alumina substrate surface. This is not too surprising as MgO may volatilize from the substrate surface during the annealing procedure.

The presence of a Ca signal on annealed substrates led to some interesting results regarding impurity segregation at the ceramic surface. An Auger spectrum of an as-ground

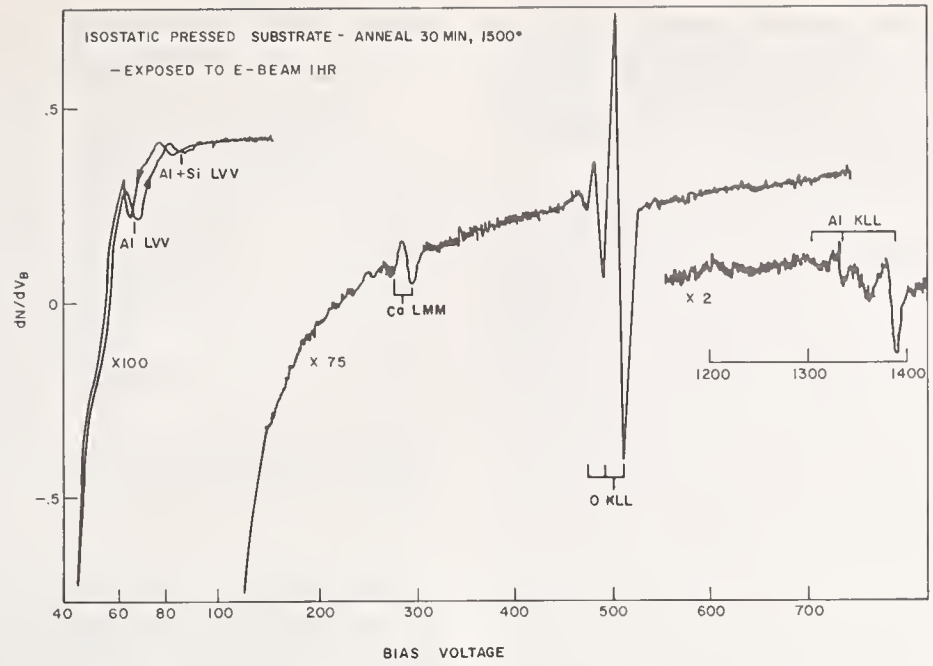

FIGURE 15. *Spectrum of same sample as Figure 14 after a one hour exposure to the electron beam.*

sample (not annealed) showed no evidence of calcium. Annealing the substrate for longer times at 1500 °C brought out the calcium peak. Figure 16 clearly shows the evidence of this segregation of Ca on the alumina surface.

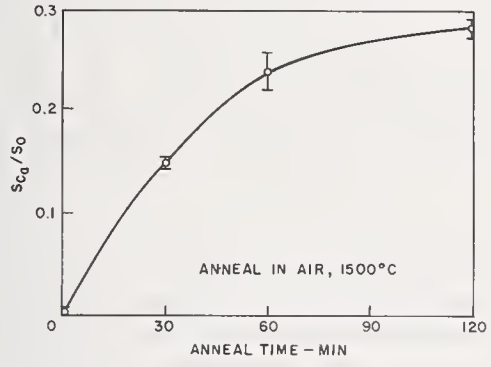

FIGURE 16. *Normalized AES signal amplitude for the Ca* $L_3M_{23}M_{23}$ *peak on the isostatic substrates vs. annealing time in air at 1500 °C.*

3.3. Photoelectron Spectroscopy [27–29]

The technique of photoelectron spectroscopy is similar in many respects to Auger spectroscopy. It differs in that it is a photons in, electrons out method, as shown in figure 17. The excitation source is an intense beam of x-rays (usually an aluminum or magnesium target) and the emitted photoelectrons (or Auger electrons) are analyzed with an elaborate, high resolution electron spectrometer. The attractive feature is that the energy of a photoelectron is directly related to one energy level. The instrumentation has been developed to exploit

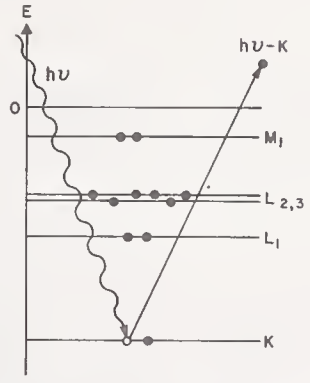

FIGURE 17. *Emission of a photoelectron from an Mg atom.*

the inherently high resolution of this technique. Finally, since there is no incident electron beam, there is little sample charging and a considerable reduction in secondary electron emission and background noise.

The sensitivity of this technique is generally not as high as Auger spectroscopy since the cross section for x-ray excitation is low. The spatial resolution in photoelectron spectroscopy does not compare favorably with either Auger spectroscopy or the electron microprobe. The sample area exposed to the x-ray beam is about 1 cm^2. Finally, the surface selectivity is not as good as AES. Photoelectron energies normally are on the order of thousands, rather than hundreds, of electron volts and correspondingly, average escape depths are about 100Å.

This high resolution spectrometer can also be used to study Auger transitions using both x-ray and e-beam excitation modes. An exam-

ple of a photoelectron Auger spectrum for the Mg KLL transition [27] is seen in figure 18. A higher resolution is obtained (five transitions resolved) than by corresponding AES methods.

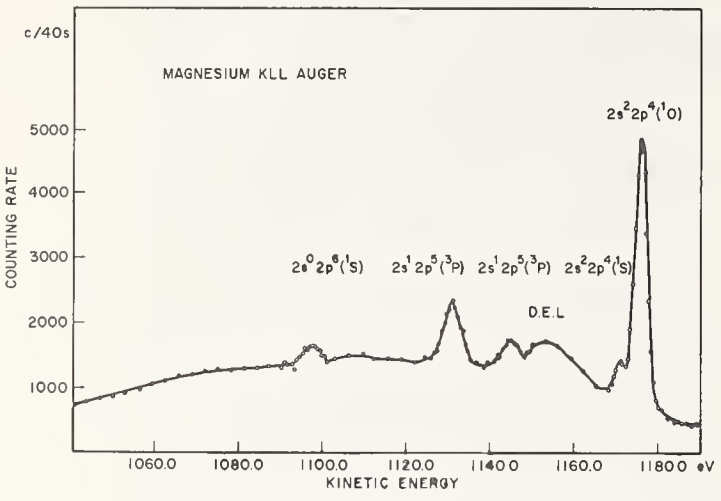

FIGURE 18. *The Mg KLL Auger spectrum measured on a high resolution electron spectrometer* [27]. Five of the predicted six peaks are detected. The sixth peak, at 1183 V, is too weak to be detected.

The high resolution of photoelectron spectroscopy has resulted in its application to a large number of problems associated with chemical bonding, especially with organic molecules. Experiments have also provided information about the band structure of metals, alloys and compounds. Although no literature is reported on its application to ceramic surfaces, the technique does provide a unique method by which detailed information about the chemical structure near the surface can be obtained. There is, therefore, every reason to believe that this technique will find application to problems related to ceramic surfaces.

3.4. The Ion Microprobe [30, 31]

A potentially very powerful tool for surface characterization is the ion microprobe. This instrument uses an incident beam of ions to sputter material from the surface. The sputtered ions are analyzed with a mass spectrometer. One version of the instrument is shown in figure 19. An intense 2 μm diameter beam of ions can be rastered across the surface supplying a two dimensional display of the output, similar to the electron microprobe and SEM. Other versions [30] use a stationary ion beam about 200 μm in diameter. Etching rates on the order of 5Å/s or higher are available.

The sensitivity of the ion microprobe is unparalleled. It is determined by the beam current and mass spectrometer design. Sensitivities of parts per billion are claimed for a monolayer of sample. The surface selectivity is, by definition, confined to the first layer of atoms.

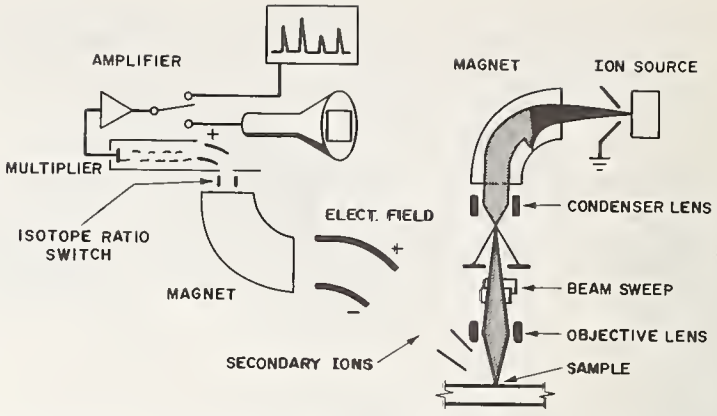

FIGURE 19. *Schematic diagram of the ion microprobe.*

In addition to the high selectivity, it is a unique method for determining a composition profile as the ion beam etching proceeds. A problem, however, is that ions are contributed by the sides, as well as the mottom of the etch pit and this tends to smear out the composition profile. The apertured detector can be adjusted to only accept ions from the bottom of the pit but this has an associated problem of beam stability. Another method is to etch by rastering the beam across the surface. This eliminates the problem but results in a very slow etch rate. An additional feature of the ion microprobe is its ability to perform an isotopic analysis, enabling one to quickly and accurately determine diffusion profiles.

Under carefully controlled conditions, the ion microprobe can provide accurate quantitative information from ppb up to the mole fraction range of concentrations. Figure 20 shows the results of an investigation [32] in which the bulk composition of a sample of moon rock was accurately characterized over a wide range of concentrations of its constituents. The ion microprobe with its obvious potential for the study of ceramic systems has found limited use to date because of the complexity and associated high cost of the instrumentation.

The techniques described above provide direct information about the chemical composition of the surface. There are also a series of methods that will not be discussed, but the reader should nevertheless be made aware. These methods provide indirect information about the surface chemistry and include infrared spectroscopy, ellipsometry, contact angle measurements, and gas adsorption and desorption measurements. Although the data obtained cannot be directly associated with specific surface components, these techniques are often convenient to perform and in many instances are more sensitive to subtle changes in the surface chemistry than are the beam techniques.

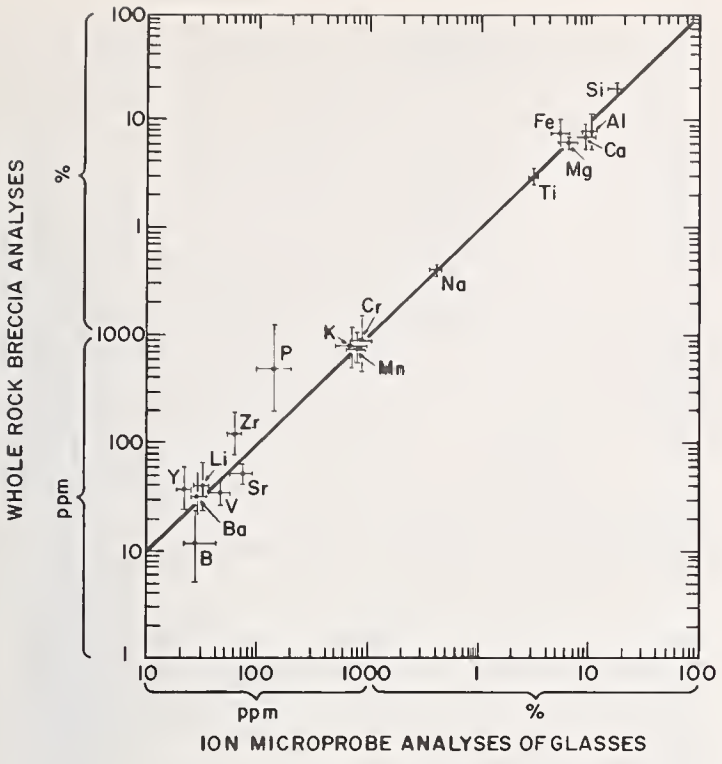

FIGURE 20. *Ion microprobe analyses of lunar material vs. standard chemical analyses of the same components, as performed in several laboratories using the optimum technique for each component* [*32*].

4. Crystallography of Ceramic Surfaces

In this section three techniques will be considered that are used to characterize the crystallography of ceramic surfaces. These techniques are *low energy electron diffraction* (LEED), *reflection high energy electron diffraction* (RHEED or RED), and *x-ray texture analysis*.

In many cases the crystallographic structure of the surface is identical to the bulk. Exceptions, however, can be of some importance, particularly in the field of electronic ceramics. Studies on single crystal surfaces have shown the surface crystallography to be reconstructed within the first few monolayers. This surface structure has been shown to be sensitive to the presence of impurities and surface treatment. Machining operations have been shown to introduce microscopic changes in the crystallography at the surface, increasing the dislocation density and associated residual strains.

On a macroscopic scale, polycrystalline ceramics in some cases exhibit crystallographic texture, or preferred orientation of the individual grains. Examples of texture in bulk ceramics include hot pressed materials, ferrites sludge pressed in a magnetic field and the pressing of acicular particles. There is recent evidence that such effects are also associated with the surface of tape cost substrates. Such texture effects may be of importance for any application of an anisotropic material, such as alumina, when a second rank tensor property; e.g., dielectric constant or thermal expansion coefficient, is critical.

4.1. Low Energy Electron Diffraction (LEED) [33–35]

The first low energy electron diffraction experiments were performed by Davisson and Germer [36] in 1927, demonstrating the wave nature of electrons. Only recently, however, has the technique become a useful tool for the study of crystal surface phenomena. The instrumentation is similar to the AES spectrometer (fig. 13). In fact, the AES spectrometer is a derivative of the LEED apparatus. In LEED a normal incident beam of slow electrons (5–500 eV) interacts strongly with the surface and yields a reflection diffraction pattern, which is displayed on the phosphor-coated electron collector.

There are several consequences of the low energies involved.

(a) The resultant low penetration depth of electrons means that only the first few atom layers contribute to the diffraction pattern. The pattern then is truly representative of the surface.

(b) By satisfying the Laue conditions for diffraction one always obtains a two dimensional diffraction pattern for any orientation of a single crystal. Thus, no pattern is obtained for a polycrystal, limiting LEED to the study of single crystal surfaces.

(c) Quantitative diffraction theory is inadequate to predict the atom arrangements from the diffraction pattern. Usually LEED is used to detect changes in the symmetry of the surface crystal structure.

(d) This technique is very sensitive to surface contamination and, as such, experiments require an ultrahigh vacuum system.

LEED has been successfully used to study structures of insulating crystal surfaces. Chang [37] and Charig and Skinner [38] studied the surface structure of the basal and prismatic planes of sapphire and the epitaxial growth of silicon on these surfaces.

4.2. Reflection High Energy Electron Diffraction (RHEED) [35,39–42]

This technique is applicable to a polycrystalline as well as single crystal surfaces. There is little literature reported for ceramic materials but RHEED has potential utility despite some experimental difficulties. The experimental arrangement is shown in figure 21. A high energy e-beam (10 keV to 100 keV) impinges on the sample surface at a low angle of incidence. Alignment of the e-beam is critical and the familiar problem of surface charging exists. To neutralize the surface charge, the sample can

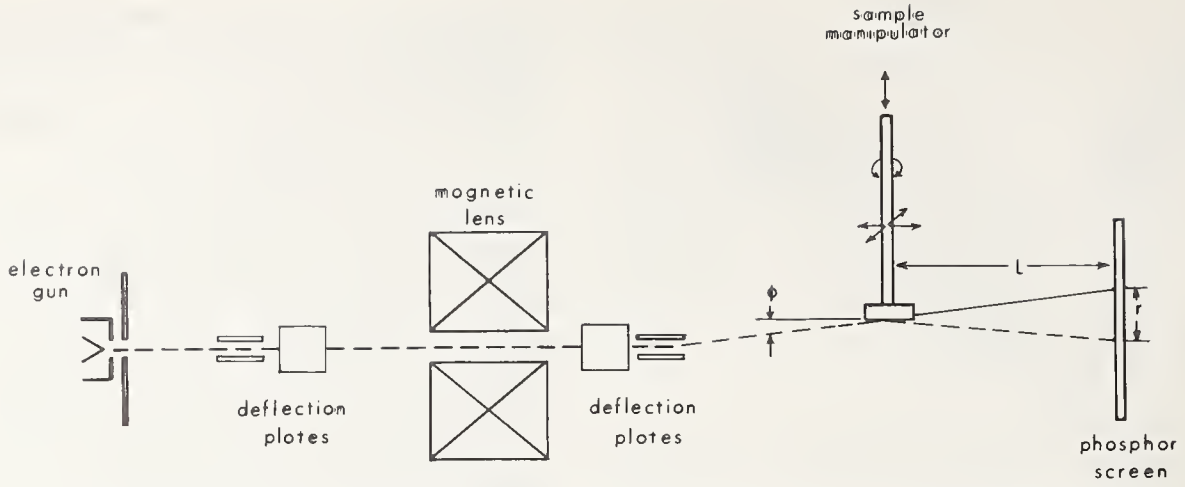

FIGURE 21. *Schematic diagram of reflection high energy electron diffraction system.*

be flooded with a low energy electron beam. As with LEED, the RHEED method is sensitive to the first few atom layers, is affected by surface contamination and it is best to conduct RHEED experiments in an ultrahigh vacuum system ($P < 10^{-9}$ torr).

A consequence of the low angle of incidence is the high sensitivity of the diffraction pattern to surface topography. Two extreme examples are illustrated in figure 22. The diffraction pattern of an atomically flat surface (fig. 22) consists of a series of vertical streaks, a consequence of the low penetration depth of the beam into the surface (about 10Å) and refraction. Diffraction from a rough single crystal surface (fig. 22B) resembles a transmission diffraction geometry more than a reflection geometry. This change in microscopic geometry leads to the familiar spot diffraction pattern. In most cases the geometry is a combination of the two situations. In the case of a rough polycrystalline surface the spot pattern degenerates into Debye rings (fig. 22C). The sharp rings with uniform intensities about their circumference are indicative of a structure made up of randomly oriented, highly perfect crystallites.

A major advantage of RHEED then is the sensitivity to surface structure, topography and orientation, combined with the applicability to polycrystalline surfaces. These positive aspects of the technique are balanced by some negative aspects. Sample preparation is difficult. The diffraction pattern tends to overweight those components which protrude from the surface. Finally, the experiment geometry and dynamical diffraction effects complicate any attempt at quantitative interpretation of intensity data.

There are available in the literature examples of the application of RHEED to a wide variety of problems. The most common use of this technique is the identification of phases present on a surface or in a thin film. Using

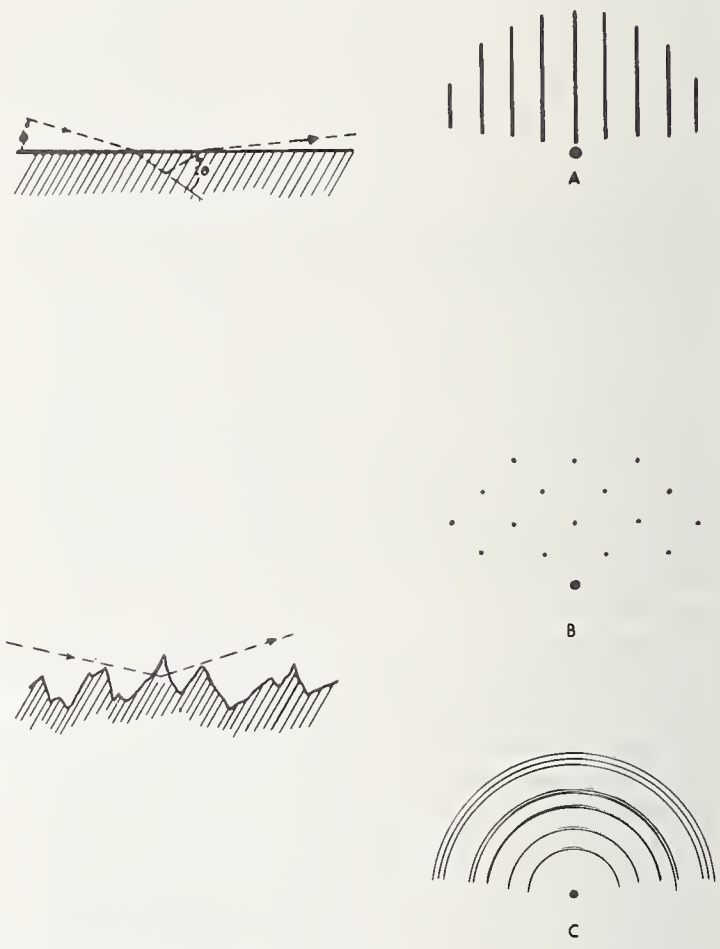

FIGURE 22. *Diffraction of high energy electrons from a surface.* (A) Diffraction from an atomically smooth single crystal surface produces a rod diffraction pattern. (B) Diffraction from a rough single crystal surface produces a spot pattern. (C) A ring pattern from a rough polycrystalline surface.

techniques analogous to the classical x-ray methods of phase identification, the Debye pattern can be indexed according to the d-spacings and line intensities and the results compared to tabulated data. The technique is limited by lack of resolution, accuracy of the d-spacing meas-

urements (usually ~ 1%) and difficulties in interpreting line intensities. Line intensity measurements have been applied quantitatively to studies of phase transformations and chemical reactions occurring at a surface. The literature is replete with examples of the use of RHEED in studies of corrosion reactions. A detailed study of the profile of the diffraction lines provides semiquantitative information about such phenomena as mechanical damage to the surface [43], residual stresses in thin films and surface crystallographic textures. Mechanical damage and residual stress cause the profiles to broaden and preferred orientation causes the Debye rings to break up into arcs.

The extreme limit of mechanical damage would be an amorphous layer. Such a layer is found to be present on metallic surfaces after polishing and a considerable effort has been devoted to the characterization of this so-called Beilby layer [44]. As one might expect, the diffraction pattern of an amorphous film represents the extreme limit of line broadening—only a diffuse electron diffraction pattern is observed. The diffuse diffraction pattern provides a unique opportunity for quantitative interpretation of intensity data, for dynamical effects are no longer important. One example of a quantitative treatment is the work of Drobek [45] in which he analyzed the structure of amorphous thin films of SiO_2 deposited by various techniques on silicon wafers. Two of the diffraction patterns obtained by Drobek are seen in figure 23. A diffuse pattern, characteristic of an amorphous material, was observed for the surface of the 2000Å film (fig. 23A). However, upon etching down closer to the silicon surface, evidence of some crystallization was detected (fig. 23B). It was found that this crystallization propagated upward toward the surface during long periods of aging at room temperature. Quantitative treatment of the intensity data revealed correlations between film structure, deposition techniques, aging behavior and electrical properties.

4.3. X-ray Texture Analysis [46–48]

Measurements of crystallographic texture, or preferred orientation, of polycrystalline metallic materials has evolved to the state of a standardized technique, in many cases automated, and the techniques are described in detail in many texts on x-ray diffraction. As was stated in the last section, the RHEED pattern from a polycrystalline surface is sensitive to the presence of preferred orientation and, indeed, if the phenomenon in question is significant only very close to the surface, RHEED is the best technique for the study of texture. However, the results from such a study are difficult to interpret quantitatively and, in most cases, the standard x-ray methods are superior.

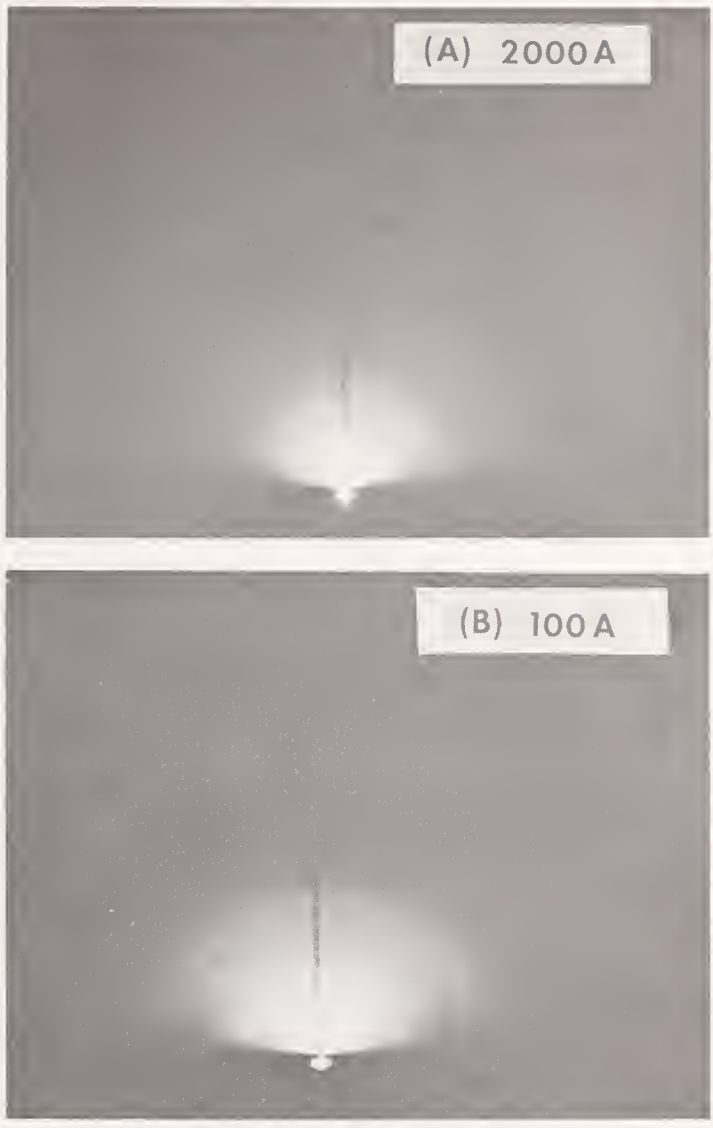

FIGURE 23. *RHEED diffraction patterns of 2000A thermal SiO_2 film grown on Si.* (A) Surface of film, (B) all but 50A of the film stripped by etching [45].

To understand the principles of x-ray texture analysis it is important to understand the standard form for presentation of texture data, the pole figure (fig. 24A). The "pole" referred to in the term "pole figure" is the normal to a particular crystallographic plane of the structure under study. The orientation of a particular crystallite can be defined in terms of the angles that a particular pole P (say the (00.1) pole of a hexagonal crystal) makes with the reference axes of the ceramic surface (fig. 24B). The polar plot in figure 24A is then a plot of the orientation of pole P. A plot of the orientations of the (00.1) poles for each crystallite would provide statistical information about the extent of preferred orientation in the polycrystalline ceramic. Such a probability plot is a pole figure. If the pole figure exhibits uniaxial symmetry about its center, the texture is termed a "fiber texture."

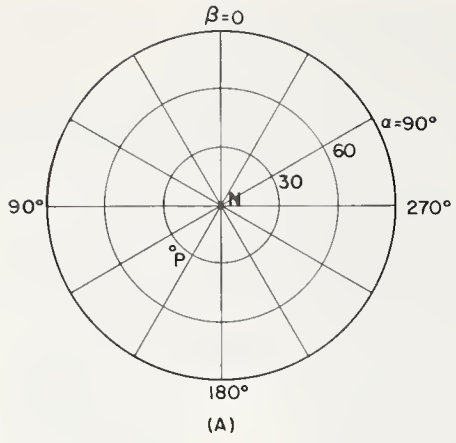

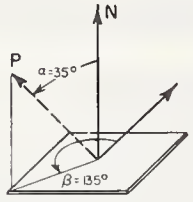

FIGURE 24. *The orientation distribution of the individual crystallites which make up a polycrystalline sample is plotted on a polar coordinate diagram (A), the pole figure.* The reference axes of the pole figure are the normal N and the axes perpendicular to N at $\beta = 0$. In this case N is chosen as the normal to the sample surface and the $\beta = 0$ axis is an arbitrary direction in the plane of the sample. The vector P is a normal to a chosen set of planes for a particular crystallite in the sample.

Detailed information about the orientation distribution is obtained from x-ray reflection intensity measurements, for a given reflection, performed on an x-ray diffractometer equipped with a pole figure goniometer. The goniometer allows orientation of the flat sample into positions corresponding to α, $\beta \neq 0$ (fig. 25). In the case of a fiber texture, the most important information is at $\alpha = \beta = 0$ and so a quantitative investigation of the fiber component of the texture can be performed with a simple diffractometer arrangement. Both types of experiments have been performed recently on different types of tape cast substrates [49,50]. The results of the pole figure measurements [50] indicated that many tape cast alumina substrates have a very strong basal fiber texture (i.e., the (00.6) x-ray reflection was much stronger than found for a randomly oriented sample). Measurements [49] of intensity ratios I(00.6/I(11.3) substantiated these results and also demonstrated that the texture is a surface-associated phenomenon. Measurements for ground samples showed significant decreases in

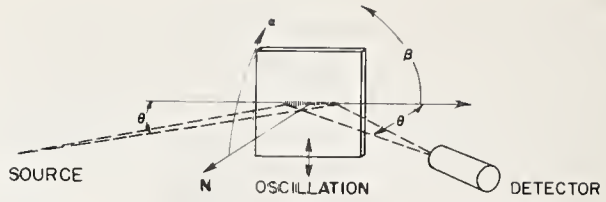

FIGURE 25. *The geometry of experimental arrangement for an x-ray texture study is identical to that for the standard x-ray diffractometer arrangement, with the additional feature of a sample goniometer which allows extra degrees of rotational freedom.* Oscillation of the sample permits an increase in the number of crystallites examined.

basal texture. This texture behavior has also been correlated with optical and dielectric constant observations [50].

A careful consideration of these observations leads to several conclusions about the crystallography of ceramic surfaces. First, the apparent association of preferred orientation with the surface, the lack of orientation in the "green" tapes [49] and the rotational symmetry of the texture about the surface normal suggest that it is the presence of the surface itself which has caused the texture in sintered tape cast alumina substrates. One might suspect that small crystallites which happen to be oriented so as to expose the low surface energy close-packed (00.1) surface will grow during the grain growth stage of sintering at the expense of other grains with higher surface energies. This hypothesis leads to several other conclusions. Since surface energy is generally quite sensitive to surface impurity level, one might expect that the wide variation in observed textures [49, 50] from supplies to supplier is associated with surface impurity variations. If this is indeed the case, the problems associated with correlating some performance measure (i.e., thin film adhesion, mechanical strength) with some material parameter (i.e., grain size, bulk chemistry, texture) are even more difficult, for it is certain that the latter parameters are interrelated in a very complex manner. As an example, one might suspect that texture would have an influence on mechanical strength, for the internal stresses present in a sintered body which are due to the anisotropic thermal expansion coefficient would be relaxed if the grains were oriented. However, mechanical properties of ceramics are most certainly also related to grain size, surface chemistry and surface topography and it is difficult to imagine how one might conduct a controlled experiment in this situation.

5. Conclusion

This paper has described a wide variety of experimental techniques which are useful for

characterizing ceramic surface properties. The techniques were discussed in terms of their application to substrates used in thin film integrated circuits. However, these techniques do have a more general application whenever ceramic surface performance depends in a critical manner on the topographical, chemical or crystallographic features of the surface.

The techniques used for characterizing surface topography are well known. However, it is sometimes difficult to predict surface performance from the results of such experiments. One such approach to the problem, in which the surface topography is characterized directly in terms of a performance test, was described.

The problem associated with the characterization of surface chemistry is the converse problem. The usual approach has been to characterize surface chemistry in terms of some indirect measurement. However, there are now available several newer analytical techniques which provide direct information about the chemical composition of the surface. The most promising of these techniques are Auger electron spectroscopy and ion microprobe analysis.

There is little information available on either the crystallography of ceramic surfaces or subsequent effects on surface performance. This is probably because, in most cases, surface crystallographic effects are masked by more important parameters. There are many special situations where crystallographic features do play an important role and this area of surface characterization should be considered in more detail in the future.

The authors wish to thank E. J. Sedora, who carried out a considerable amount of the experimental work described here; J. Colby, for his comments on the use of the electron microprobe, SEM, and ion microprobe; Y. Nakada, who provided us with the unpublished results of measurements of substrate textures; and J. Drobek for his RHEED results and comments on the RHEED technique.

6. References

[1] Schwartz, B., Microelectronic Packaging, pp. 12–25 in Electronic Ceramics, Amer. Ceram. Soc. Spec. Publ. No. 3, Columbus, Ohio, (1969).

[2] Rigterink, M. D., Present quality of ceramic electrical insulators, pp. 27–33 in Electronic Ceramics, Amer. Ceram. Soc. Spec. Publ. No. 3, Columbus, Ohio, (1969).

[3] Thomas, D. G., Ceramics and glasses—some uses in the communications industry, in Proc. Conf. on Electronic Phenomena in Ceramics, Gainsville, Florida, Nov., 1969 (to be published by Plenum Press, New York, N. Y., 1971).

[4] Berry, R. W., Hall, P. M., and Harris, M. T., Thin Film Technology, Ch. 9 (Van Nostrand, Princeton, N. J., 1968).

[5] Brown, Richard, Thin film substrates, in Handbook of Thin Film Technology, Ed. L. I. Maissel and R. Clang, Ch. 6 (McGraw-Hill Book Co., Inc., New York, N. Y., 1970).

[6] Striny, K. M., and Weingrod, I., Mechanical engineering aspects of a prototype multichip semiconductor store, 1970 WESCON, Los Angeles, Aug., 1970, 16/1.

[7] White, E. W., McKinstry, H. A., and Diness, A., Quantitative surface finish characterization by CESEMI, this proceedings.

[8] Berrin, L., and Kim, Y. S., Preparation of alumina substrates by an isostatic pressing process, Presented at the 72nd Annual Meeting of the Amer. Ceramic Soc., Philadelphia, Pa., May (1970).

[9] Schwartz, N., and Brown, R., A stylus method for evaluating the thickness of thin films and substrate surface roughness, p. 836 in Trans. 8th Nat. Vacuum Symposium, New York, 1961, (Pergamon Press, New York, N. Y., 1962).

[10] Lo, W. C., Ceramic surface texture by reflective replica technique, this proceedings.

[11] Sundahl, R. C., Berrin, L., and Sedora, E. D., Effects of alumina substrate surface defects on thin film interconnect patterns, Presented at the 72nd Annual Meeting of the Amer. Ceramic Soc., Philadelphia, May, (1970).

[12] Thornton, P. R., Scanning Electron Microscopy, (Chapman and Hall, London, 1968).

[13] Hall. C. E., Introduction to Electron Microscopy (McGraw-Hill Book Co., New York, N. Y., 1966).

[14] Heidenreich, R. D., Fundamentals of Transmission Electron Microscopy (Interscience Publ., New York, N. Y., 1964).

[15] Thomas, G., and Bell, W. L., Transmission diffraction electron microscopy, in Techniques of Metals Research, Vol. 2B, Ed. R. F. Bunshah (Interscience Publ., New York, N. Y., 1971).

[16] The Electron Microprobe, Ed. T. D. McKinley, K. F. H. Heinrich, and D. B. Wittry (Wiley, New York, N. Y., 1966).

[17] Gray, T. J., and Zope, J. K., Electron microbeam probe techniques for studying grain boundaries in polycrystalline ceramics, pp. 301–311, Materials Science Research, Vol. 3, Ed. W. W. Kriegel and H. Palmour III (Plenum Press, New York, N. Y., 1966).

[18] Ruddleson, S. N., Applications of the electron probe microanalyser to ceramics, Tran. Brit. Ceram. Soc. 66, 587 (1967).

[19] Colby, J. W., Quantitative microprobe analysis of thin insulating films, p. 287 in Advances in X-ray Analysis, Vol. 11 (Plenum Press, New York, N. Y., 1968).

[20] Harris, L. A., Analysis of materials by electron-excited Auger electrons, J. Appl. Phys. 59, 1419 (1968).

[21] Taylor, N. J., The technique of Auger electron spectroscopy in surface analysis, in Techniques in Metals Research, Vol. 7, Ed. R. F. Bunshah (Interscience Publ., New York, N. Y., 1971).

[22] Chang, C. C., Auger electron spectroscopy, in Modern Methods of Surface Analysis, Eds. P. Mark and J. D. Levine (to be published by North-Holland Publ. Co., Amsterdam Neth., 1971).

[23] Palmberg, P. W., and Rhodin, T. N., Auger electron spectroscopy of fcc metal surfaces, J. Appl. Phys. 39, 2425 (1968).

[24] Weber, R. E., and Johnson, A. L., Determination of surface structures using LEED and energy anaylsis of scattered electrons, J. Appl. Phys. 40, 314 (1968).

[25] Weber, R. E., and Peria, W. T., Use of LEED apparatus for the detection and identification of surface contaminants, J. Appl. Phys. 38, 4355 (1967).

[26] Palmberg, P. W., Auger electron spectroscopy in LEED systems, pp. 29.01–11 in The Structure and Chemistry of Solid Surfaces, Ed. G. A. Somerjai (J. Wiley and Sons, Inc., New York, N. Y., 1969).
[27] Siegbahn, K., Nordling C., et al., ESCA (Almquist and Wiksalls AB, Upsalla, Sweden, 1967).
[28] Siegbahn, K., Nordling, C., et al., ESCA Applied to Free Molecules (North-Holland, Amsterdam, Neth., 1970).
[29] Hercules, D. M., Anal. Chem. 42, 20 (1970).
[30] Soucha, A. J., Analysis of surfaces utilizing sputter ion source instruments, in Modern Methods of Surface Analysis, Eds. P. Mark and J. D. Levine (to be published by North-Holland, Amsterdam, Neth., 1971).
[31] Anderson, C. A., Analytical methods for the ion microprobe mass spectrometer, Intl. J. Mass Spectrom. Ion Phys. 2, 61 (1969).
[32] Anderson, C. A., Hinthrone, J. R., and Fredriksson, K., Ion microprobe analysis of lunar material from Apollo 11, pp. 159–67 in Proc. Apollo 11 Lunar Science Conf., Vol. 1, Ed. A. A. Levinson (Pergamon Press, New York, N. Y., 1970).
[33] Bauer, E., Low energy electron diffraction (LEED), pp. 559–639 in Techniques in Metals Research, Vol. 2, part 2, Ed. R. F. Bunshah (Interscience Publ., New York, N. Y., 1969).
[34] Lander, J. J., Low energy electron diffraction and surface structural chemistry, pp. 26–116 in Progress in Solid State Chemistry, Vol. 2, Ed. H. Reiss (Pergamon Press, New York, N. Y., 1965).
[35] Estrup, P., Surface studies by electron diffraction, in Modern Methods of Surface Analysis, Ed. P. Mark and J. D. Levine, to be publ. by North-Holland, Amsterdam, Neth., (1971).
[36] Davisson, C. J., and Germer, L. H., Phys. Rev. 30, 705 (1927).
[37] Chang, C. C., LEED studies of thin film silicon overgrowths on α-alumina, pp. 77.1–14 in The Structure and Chemistry of Solid Surfaces, Ed. G. Somerjai (J. Wiley and Sons, Inc., New York, N. Y., (1969).
[38] Charig, J. M., and Skinner, D. K., The (0001) surface of α-alumina-LEED observations, pp. 34.1–20 in The Structure and Chemistry of Solid Surfaces, Ed. G. Somerjai (J. Wiley and Sons, Inc., New York, N. Y., 1969).
[39] Pinsker, Z. G., Electron Diffraction (Butterworth, London, England, 1953).
[40] Vainshtein, B. K., Structure Analysis by Electron Diffraction (Pergamon Press, New York, N. Y., 1964).
[41] Marcus, R. B., The characterization of solid thin films by electron microscopy and diffraction, Measurement Techniques for Thin Films, Eds. B. Schwartz and N. Schwartz (The Electrochemical Society, Inc., New York, N. Y., 1967).
[42] Bauer, E., Reflection electron diffraction (RED), pp. 501–557 in Techniques of Metals Research, Vol. 2, Pt. 2 (J. Wiley and Sons, Inc., New York, N. Y., 1969).
[43] Schmidt, W. A., and Davey, J. E., Preparation of smooth, crystalline, damage-free, sapphire surfaces by gaseous etching, this proceedings.
[44] Bowden, F. F., and Tabor, T., p. 145 in Symposium on Properties of Metallic Surfaces (Inst. of Metals, London, 1952).
[45] Drobek, J., Electron diffraction study of phase transformations in grown and deposited SiO_2 films, private communication, to be published.
[46] Cullity, B. D., Elements of X-ray Diffraction (Addison-Wesley, Reading, Mass., 1959).
[47] Taylor, A., X-ray Metallography (J. Wiley and Sons, Inc., New York, N. Y., 1961).
[48] Barrett, C. S., and Massalski, T. B., Structure of Metals, 3rd Ed. (McGraw-Hill Book Co., New York, N. Y., 1966).
[49] Y. Nakada, private communication, to be published.
[50] DiMarcello, F. V., Key, P. L., and Williams, J. C., Preferred orientation in Al_2O_3 substrates for thin film circuits, Presented at the Fall Meeting of the Electronics Division, Amer. Ceramic Soc., San Francisco, Oct., (1970).

Discussion

H. J. GREEN: Are there any special requirements for the operation of the ion microprobe?

SUNDAHL: Usually, it is operated under a vacuum of 10^{-5} to 10^{-6} mm Hg. Initially carbon contamination occurs until the first monolayer is sputtered away.

WIEDERHORN: What is the resolution in the ion microprobe?

SUNDAHL: It depends on the instrument used. Some instruments have a beam diameter of about 300 microns. The instrument discussed here has a beam diameter of about 2 microns. Between 2 microns and 300 microns resolution can be obtained depending upon how it is focused. The resolution normal to the surface depends on the beam current and instrument sensitivity. Resolutions approaching one monolayer are claimed by some designers.

WIEDERHORN: How much do they cost?

SUNDAHL: Well, one instrument I think is selling for one quarter of a million dollars. It's not one you go out and buy everyday. I would suspect that there aren't too many organizations that are going to buy it. I would also presume that it will be possible to perform such experiments on instruments for a $1,000 a day.

RHODES: I'd like to ask one question with regards to the electron spectroscopy. You mentioned something about studies of segregation of impurities at grain boundaries. Could you elaborate on that at all and say a little bit about the geometric resolution limits of the instrument?

SUNDAHL: The lateral resolution is poor with a beam diameter of about a millimeter. The way you perform a segregation study on the grain boundary is to look at a fractured surface. That surface represents the segregation at the grain boundary since you only are looking at the first few monolayers. A great deal of study is being done on steels, correlating segregation, embrittlement, and mechanical properties. However, there has, up to this point at least, been little done on ceramics. We hope to do some measurements in the near future.

HEUER: I was interested in your application of Auger spectroscopy to detect Ca segregation during annealing of alumina substrates. Wasn't there Ca segregation during firing? Was the Ca an accidental impurity in the starting powder?

SUNDAHL: The segregation does occur during the original firing. As the sample was annealed the calcium apparently diffused along the grain boundaries up to the surface and then diffused across the surface. It tends to segregate on the surface in this manner. The calcium impurity level in the fired substrate was 640 ppm CaO by weight. The SiO_2 level was at 900 ppm and MgO at 1000 ppm. The other impurities were almost nil. The CaO impurity level is greater than the solubility limit and is the major source of the surface layer of Ca, although measurements on annealed sapphire lead us to suspect that a small fraction of the contamination could originate from the furnace.

RICE: I've seen the same sort of thing in so-called reagent grade magnesium oxide that has been hot pressed. If you anneal it, you'll find the small quantities of silica and other impurities coming out. In certain materials you get, for example, anisotropic crystal structures formed on the surface. There definitely is preferential migration to surfaces of certain materials.

SUNDAHL: That is right. This is also true for many semiconductors. In the study of highly pure metals experiments have been performed which quantitatively characterized this behavior.

MATSKO: Are these Auger spectrometers commercially available?

SUNDAHL: They are commercially available. There are two companies who make Auger spectrometers. One is PEI, Physical Electronics Industries in Edina, Minnesota, and one is Varian Associates in Palo Alto, California. The particular instrument I showed is not the ideal instrument to use. There is a better instrument now available which has a cylindrical analyzer. In fact, there was some work done on the anlyzer right here at NBS. The cylindrical analyzer is a much more sensitive instrument and much easier to use. We built this one ourselves. There are some people, at Sandia in Albuquerque, New Mexico, who have done quite a bit of work in this area. R. L. Park is one such person.

NATIONAL BUREAU OF STANDARDS SPECIAL PUB. 348, THE SCIENCE OF CERAMIC MACHINING AND SURFACE FINISHING, Proceedings of a Symposium Sponsored by the American Ceramic Society, the Office of Naval Research, and the National Bureau of Standards, held at NBS Nov. 2–4, 1970, Gaithersburg, Md. (Issued May 1972).

Surface Characteristics of Ceramic Substrates for Hybrid and Microwave Electronic Circuits

Jackson K. Emery [1]

Accumet Engineering Corporation, Hudson, Massachusetts 07149

Several methods currently used for finishing ceramic substrates in ready-for-deposition state are discussed, including firing, glazing, burnishing, grinding, lapping, and polishing. Each method tends to exhibit a different and typical combination of surface characteristics, such as variations in thickness, parallelism, camber, waviness, roughness, and localized defects; each of these in turn may influence the deposition process, performance, and reliability. Analysis of some typical surface details, particularly roughness and waviness, as significant surface factors capable of affecting process or function, is presented with comments on instrumentation and measurement procedures.

Significant differences exist in the use of terms relating to substrate surfaces and their characteristics; a need is indicated for more particularized use of such terms, and for recognition of uniform definitions. Clarification of terminology may facilitate improved communications and measurements, which in turn may correlate with current and future requirements in circuit production. Several existing applicable standards are referenced, and definitions of terms are suggested. A number of choices of surface characteristics are presented which may be related with process controls and function, but no recommendations for particular values of surface details are intended.

Key words: Camber; ceramic; fired, flatness; ground; lapped; microwave; polished; roughness; substrate; surface; thick film; thin film; waviness.

1. A Case for Better Substrates

Microwave and hybrid circuit utilization promises rapid growth up to a forty-fold increase in ten years [1][2] due to predicted expansion of applications and technological breakthroughs. To the extent that the common ceramic substrate will remain a factor in this growth, a close reexamination of its functional surface characteristics may be warranted. In fact, it is increasingly recognized that the surface quality of substrates is critically related to circuit performance and reliability [2].

If we examine this rapid growth closely we may see the beginnings of a subtechnology in substrate surface characteristics and control. Such an emergence could become important to the designer, processor, and user of hybrid and microwave circuits, and can be expected to involve disciplines usually outside the normal bounds of electronics, to include materials finishing, microsurface analysis, and dimensional metrology.

Many circuit designs, including vast numbers of both hybrid and microwave circuits, have been reliably applied on ceramic substrates having the normal surface characteristics of as-fired or glazed material. Until recently no economically acceptable alternatives were available. Now, however, we can observe increasing instances of circuits having unusually stringent requirements, as in fineness and uniformity of line or using low allowable percent spread in circuit component performance resulting in narrower tolerances being sought. At the same time, low-cost production capabilities are becoming available for improving substrate surface quality, and better measuring equipment and procedures can be readily acquired. When the several surface parameters are regarded critically in terms of new low tolerances and corresponding functional results, the challenge of exact surface quality in terms of its individual components, their selected emphases and cost trade-offs becomes increasingly complex. In this paper distinctions are proposed between the various characteristics of substrate surface quality, and their terminology, control and measurement are discussed.

2. Standards and Terminology

In reading the literature on substrates one may conclude that some inconsistencies and omissions exist in describing concepts and in understanding and in definitions of terms. To encourage uniformity, attention may be directed to applicable existing standards, which include:

MIL–I–10A, 1962
MIL–S–55620 (EL), 1969
ACMA, Standards for High Alumina Ceramics, 1969
ANSI–B46.1, Texture, 1962
ANSI–B87.1, Decimal Inch
Various commercial standards by ceramic makers, processors, and users.

[1] President, Accumet Engineering Corp.
[2] Figures in brackets indicate the literature references at the end of this paper.

439-921 O - 72 - 20

Some evidence may be noted regarding a need for improved and more detailed standards and terminology for better understanding. A number of definitions of terms are listed at the end of this paper including several less familiar terms for possible consideration.

One important exception to standards adherence appears to be justified in the choice of the most effective symbol denoting microinches. Although ANSI Standard B87, Decimal Inch, 1967, recommends discontinuation of the familiar term μin in favor of the term mk, the use of mk in the publications and communications of the electronic industry is virtually nonexistent at this time. In this paper the term μin will be used to avoid misunderstanding.

3. Units of Measurement

Although *SI* (metric) units are now officially specified for the National Bureau of Standards (NBS) publications, "customary" units (inches) are currently used almost exclusively for designation of lengths, widths, diameters, thicknesses, feature locations, and other details of substrates in most current catalogs, brochures, and drawings issued by substrate manufacturers, processors, or users in the United States of America. Even in brochures of importers substrate dimensions are published in inches for size, thickness, camber, glazed thickness, and finish; various strengths and thermal conductivities are usually shown in "customary" units, not in *SI* units. One major producer states, "All dimensions are in inches." The ACMA standard gives "customary" units in their table 1, but also gives "metric" units in table 2.

In view of the almost nonexistent usage of SI units in this context, they will not be used in this presentation to avoid confusion and difficulty.

4. Dimensions

The dimensions affecting surface features of substrates are principally thickness, parallelism, and localized defects of various kinds. Various standard dimensions are offered by substrate manufacturer, chiefly for length, width, diameter, and thickness in a variety of decimal and fractional inch sizes. The variety of sizes and the frequent use of special sizes having odd dimensions reduces the occurrences of like dimensions to the point that very few of the many sizes are available for immediate delivery. The beginning of a less expensive and immediately available substrate market may depend on standardization of sizes in suitable steps, but in a limited number of varieties; possibility such sizes could be selected from existing lists, but bear an interrelationship based on a preferred number series, or other appropriate guideline. By standardization through reduced variety of sizes gains in ecomomy and availability may justify increased attention to evaluation and improvement in substrate surface characteristics.

5. Tolerances

Substrate surface quality relates to tolerances of thickness, parallelism, flatness, camber, and texture (roughness and waviness). Some of these are included in the definitions at the end of this paper. Tolerances are not uniformly standard, but for principle dimensions of length and width (not precisely surface-related) the major manufacturers specify plus or minus 1 percent, although some users may specify plus or minus 0.5 percent, or plus 0 minus 0.5 percent. Four Thickness tolerances are fairly common: plus or minus 0.001 in, plus or minus 0.002 in, plus or minus 0.003 in and plus or minus 0.004 in for thicknesses 0.010 in, 0.020 in, 0.025 in and 0.050 in. Lapped or polished substrates may have thickness tolerances of 0.0005 in to 0.0002 in or less. Camber tolerances appear to vary widely according to tradition or application for many thousands of an inch per inch to extreme cases of 0.0001 in per inch. Flatness tolerances may be specified separately from camber for critical applications. Parallelism tolerance, when required, is usually less than thickness tolerance. Waviness tolerance is almost never defined or expressed; although waviness may be critical functionally in some applications, it is usually ignored. Roughness tolerance is most frequently expressed as a single value representing the allowable high limit, particularly for very fine fired, glazed, or polished substrates in the order of 10 μin or less. However, a growing utilization of a roughness tolerance concept having a high and low limit appears in hybrid circuit substrates where the variation in printed components such as resistors must be extremely small; typically, such roughness tolerance may be 24 μin AA plus or minus 1.5 μin AA, particularly for precision lapped substrates.

6. Surface Structure and Porosity

Surface quality is dependent on both density and uniformity of the substrate. Nonuniformity in ceramics, such as shown in figure 1, may penetrate deeply and may often run the entire substrate thickness. Some porosity, however fine, random or discontinuous, is inherent in most ceramic structures and can be a cause of holes, pits, pocks, blisters, and blebs (see MIL–S–55620–EL). Isolated pores may occur just under the surface or be intersected by the

FIGURE 1. *Non-homogenous structure in 1 in × 2 in substrate of 99.5 percent alumina; lighter areas show about 1 μin roughness, while darker areas are 6 to 12 μin, pattern is full thickness of 0.0B5 substrate.*

finished plane of a fine polished substrate. Exposing such pores results in inherent structural voids, often mistakingly thought to be "pullouts" resulting from improper grinding or other surface treatment; "pullouts" can be correctly identified only when they exhibit evidence of "tears" or "comet-tails." Surface discontinuities can more or less unfavorably influence the superimposed circuit, depending on the circuit location or vulnerability and the pore dimension. When porosity is poor it not only may effect function and reliability, but can cause deceptively high roughness measurements [3]. Even in fine quality 99.5 percent alumina individual pores commonly measure from 0.0001 in to 0.0005 in width and can be occasionally much larger and closely clustered.

According to MIL–1–10A, porosity shall be determined with dye penetration in accordance with ASTM publication D–116–44; this test may be most useful for inter-connecting porosity. However, since porosity is frequently discontinuous, the importance of isolated pores may not be easily determined by the ASTM test. In such cases substrate surfaces should be visually examined in accordance with MIL–S–55620 (EL).

Remarkable details of fine grade as-fired Alumina (99.5%) may be observed at high magnification by use of a scanning electron microscope; figures 2 and 3 show large differences in grain size, and spaces between grains

FIGURE 2. *As-fired 99.5 percent alumina, scanning electron microscope, (SEM), 1000x.*

FIGURE 3. *As-fired 99.5 percent alumina, scanning electron microscope. 10,000x.*

which may suggest significant subsurface porosity; also of possible interest is the improvement shown at similar magnifications after precision polishing to 2 μin AA, as shown in figures 4 and 5.

7. Flatness

It is widely recognized that controlled flatness of a substrate, along with controlled surface finish is a significant factor in circuit performance and reliability [2]. Flatness error may be considered to include waviness, but can refer to only one side of a substrate at a time. Flatness is not strictly equivalent to camber, since the flatness errors of both sides become components of camber along with variations of thickness, parallelism, and local defects.

Flatness correction, especially through precision lapping and polishing, offers a direct and economical means for eliminating waviness and minimizing camber in precision circuit work. Substrates finished by a lapping operation make possible a rapid and inexpensive flatness well within a most rigorous requirement, without the necessity of either substantial stock removal or prior grinding.

8. Waviness

The familiar succession random ripples, irregularities, and undulations across a surface is called waviness; the usual spacing from crest to crest is considerably greater than that of the spacing of the roughness crests, but less than the surface width. Waviness in one component of texture, according to ANSI B 46.1, and is generally characteristic and attributable to the surface forming process. Inherent in both glazed and as-fired ceramic, waviness may be regular as may occur in surfaces produced with a rigid grinding wheel, or may be extremely random in both vertical heights and horizontal spacings characteristic of firing processes. Actual height variations due to waviness can be measured by sliding a substrate across a small flat anvil with a spherically tipped spindle lightly touching the upper surface. Waviness can also be determined on a conventional stylus type instrument (see figure 6) with a strip chart added. Another measurement

FIGURE 5. *Precision polished substrate from same lot of 99.5 percent alumina as in fig. 2 and 3, 10,000x, showing fine line scratches from diamond polishing, most principal lines less than 0.00001 in wide, open pocks from inherent pores show intact wall detail, no "comet-tails" (SEM).*

FIGURE 4. *Precision polished substrate from same lot of 99.5 percent alumina as in fig. 2 and 3. 1000x, showing open pocks (SEM).*

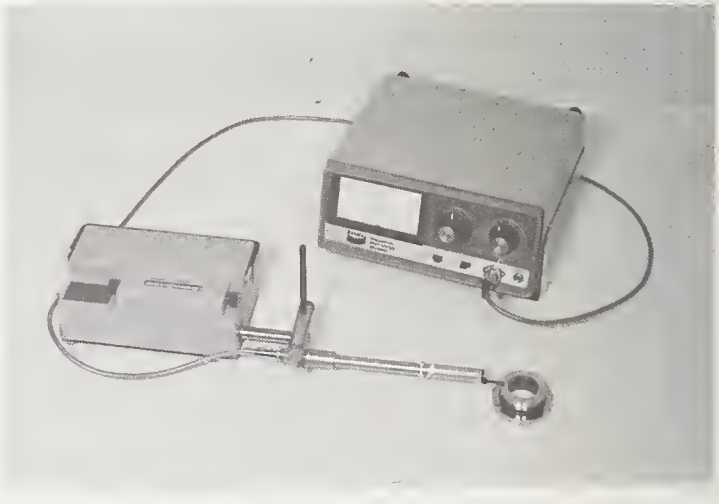

FIGURE 6. *Standard stylus type roughness measuring instrument (Courtesy Industrial Metrology Div., Bendix, Ann Arbor, Mich.)*

method for both waviness and flatness utilizes a Moiré pattern which can yield a direct visual profile of the entire substrate area through a range of variations from 0.010 in to 0.0001 in or less (see figures 7 and 8).

9. Camber

As commonly defined, camber is a three-dimensional concept and is a composite dimension encompassing the combined profiles of both surfaces of a substrate, including variations of flatness, waviness, thickness, parallelism, local raised zones (burrs, blebs, ridges) and other defects. Generally accepted by a go/no go "slot gage" inspection, a substrate which is just under the high limit of the thickness tolerance will be rejected for negligible camber, while substantial camber near the low thickness limit will be accepted. An alternative method for measuring camber uses a simple dial indicator gage and measures camber as the maximum indicator difference between measurement of substrate height with convex side up and a measurement with convex side down. Camber of substrate 0.040 in or less in thickness can also be measured as the indicator gage movement when the substrate is placed on the anvil with convex side up and then sprung down into contact with the anvil. Camber components may be assessed visually and numerically even on dull finished substrates, produced by any manufacturing method including firing, grinding, matte-lapping, or polishing, by observing the Moiré band pattern formed on a fine-line grid (see figures 7 and 8). Polished substrate flatness can also be measured by observing light interference fringes on an optical flat

FIGURE 7. *Drawing of typical Moiré line pattern on a 1000-line grid formed by a 2 in × 2 in as-fired substrate showing combined flatness and waviness of about 0.004 in.* (Each line corresponds to a contour interval of about 0.0005 in.)

FIGURE 8. *Drawing of typical Moiré line pattern on a 1000-line grid formed by a 2 in × 2 in precision polished substrate showing absence of waviness and overall flatness of about 0.0002 in.*

where the manner of reading is identical to that of the Moiré band, except the fringe unit of curvature is about 0.00001 in (one-half the wave length of visible light).

10. Thickness and Parallelism

Thickness variations from substrate to substrate are undesirable particularly when screening because of the effect on screen clearance or contact and consequent effect on the pattern. Some screening departments find advantageous a narrow control of thickness to as little as 0.001 in total variation, provided camber and waviness are also minimized.

Parallelism is usually regarded as simply variation of thickness across a particular substrate. When parallelism error is in the form of a wedge it may cause screening problems. Both parallelism and thickness variations between substrates can cause problems in automated processing. For measurement of thickness and parallelism the instrument contacts should have only a small bearing on the substrate, for example from 0.08 in to 0.125 in to avoid measuring local defects or camber.

11. Roughness

Roughness measurement has been extensively analyzed for several decades and has given rise to authoritative standards. Roughness is described in several ceramic references as microinches CLA. However, the term in μin AA conforms to ANSI Standard B 46.1. Actually CLA (centerline average) and AA (arithmetic average) are essentially equal. Too frequently we still see the term RMS (root mean square average) which was discontinued as a roughness

standard in 1955 in favor of AA; RMS values are about 10 percent greater than AA values.

The standard method of B 46.1 for evaluation of roughness is the diamond stylus tracing technique, as illustrated in figure 6. In this method a polished diamond stylus tip, preferably having a 0.0001 in radius, is made to traverse the specimen in a straight line under a light load (1 gram), thus generating a signal which is proportional to the roughness or texture of the specimen. The accuracy of the result is dependent upon reasonable care and calibration of the electronics and the stylus of the instrument; under reasonably controlled conditions agreement between instruments and operators should be within 20 percent variation, and with care and accurate calibration can be within 10 percent or less. The standard roughness value is read as an amplified signal from either a meter or a strip chart in units of μin AA, according to ANSI B 46.1. It may be of interest, especially to those who apply very fine circuit conductors and components that the true peak-to-valley height on the substrate is from 4 to 5 times greater than the AA value. It has been observed [2] that surfaces having very different real profiles may produce similar AA roughness readings; this problem can be safely neglected only when surface textures produced by similar finishing processes are compared with correct instrumentation. Roughness measurements by air probes usually include a waviness component [4] which may be misleading. Light-section microscopes can be useful by measuring individual scratches or flaws, but are less useful for characteristic roughness especially when AA values are low. An interference microscope will show visually as a topographic fringe pattern the true peak-to-valley height of roughness detail, across a small area, preferably for finishes of 20 μin or less; usually the field is very small, typically from about 0.08 in (60x) to 0.01 in (480x). Ordinary band patterns from light interference or from fineline grids will disclose flatness but not roughness detail.

Standard roughness readings are usually traced at selected locations, as within the four quadrants of the ceramic, to establish the variation of the roughness. It should be remembered that stylus techniques merely permit sampling of the surface as very narrow traces, which is usually very rapid, consistent, and adequate.

12. As-Fired Substrate Surfaces

Surfaces of as-fired substrates may be slightly more dense than the interior by as much as 0.5 percent [2]. These surfaces will exhibit at low oblique viewing a medium gloss and rippled appearance, causing reflected images of straight lines to be wavy. Ordinarily the roughness of 99.5 percent ceramics will be relatively fine, perhaps 10 mk AA or less, while that of 96 percent or 94 percent Alumina will be coarser perhaps 20 mk AA or more. In as-fired substrates, camber is usually present, often to a degree discernible visually and over a relatively broad range, usually being greater on thin or large sized boards. Surface defects inherent with the production process, such as burrs, pits, pocks, and fins or ridges, either occur in profusion or be negligible, according to the quality of the process. Tape-process substrates frequently show low corners or raised zones which can result in thickness variations across the substrate up to 0.002 in or more.

13. Glazed Substrate Surfaces

Glazed substrates have surface characteristics very similar to those of as-fired substrates, except for the very thin smooth glassy surface produced by refiring, often in the order of 1 μin AA roughness. Glazed surfaces show a tendency for a raised zone near the edges. Glazing is usually on one side only. Defects of waviness, flatness, camber, and variations of thickness are similar to those of as-fired ceramics.

14. Burnished (Tumbled) Substrate Surfaces

Substrates having sufficient as-fired defects to render them unsuited for coating are sometimes burnished by various tumbling or vibratory processes, utilizing balls, stones, sand, or abrasive grains. Following an extended cycle of many hours, or days, the substrates exhibit slightly rounded corners or edges, smoothed chips, and reduced burrs. Little change of waviness occurs, although a narrow spread in roughness may be possible [5]. Generally camber (or flatness) and variations in thickness are not altered by the process. Burnishing tends to concentrate on sharp aspects while it changes the broad surface very little. Removal of burrs by burnishing may improve handling and metallization quality.

15. Ground Substrate Surfaces

Grinding a substrate by use of a rigid abrasive wheel removes the irregular surface layers and the characteristic ripple of the as-fired condition. Camber may be improved by precision grinding, or it may be made worse by altering stress balance by incorrect techniques. Ground finishes may contain relatively deep and obscure scratches from a raised grain on the grinding wheel or they may show surface voids as grain pullouts due to improper grinding conditions. Very fine diamond wheels correctly ap-

plied can produce finishes of fair uniformity to 8 μin or less.

16. Lapped Substrate Surfaces

Lapping as a finishing process for ceramic substrates consists of moving a tool or lap against the substrate in the presence of fine abrasive grains either as a rigid layer impregnated into the lap as a thin slurry. Typically the lap material is softer than the work material, and the grains are harder. The pressure between the lap and the substrate is controlled from about 0.5 to 10 psi to suit the conditions. As-fired substrates should be lapped directly without grinding. A proper choice of lapping conditions can rapidly and economically convert irregular ridges, waves, peaks and valleys into a wavefree uniform surface with minimized camber, little stock removal, and reduced variation of thickness. A number of options exist for control of thickness and parallelism. Surface roughness can be narrowly limited at a desired level from 50 to less than 1 μin AA across one surface, or from substrate to substrate. Preferences vary from finishing both sides 2 μin AA maximum, to 30 plus or minus 2 μin AA on one side only.

Four different typical standard grades for lapped hybrid substrates are as follows:

Grade 1. Front only: no waves, reduced camber, controlled finish

Grade 2. Both sides: no waves, reduced camber, controlled finish

Grade 3. Both sides; reduced camber, controlled finish;
Front only: no waves; back only: waves 50 percent removed: Narrow variation for thickness

Grade 4. Both sides: no waves, reduced camber, controlled finish: Narrow variation for thickness and parallelism.

Lapping can be effective for correction or control of surface characteristics on almost any substrate material, purity, shape, size, or thickness from 0.075 in or more to 0.005 in or less. Most substrates can be successfully production lapped in ordinary or unusual configurations with holes, recesses or scored grids. Flatness of lapped ceramics may be typically 0.0002 in; the flatness departure from a perfect plane can be determined by noting band curvature in the Moiré pattern formed against a fine-lined grid, as in figure 8. A visual indication of the change in surface character from as-fired to precision lapped or polished may be noted by comparing details observed in a scanning electron microscope at medium to high magnification, as shown in figures 2, 3, 4, and 5. Note the complete absense of the tears or "comet-tails" characteristic of "pullout."

Possible advantages for use of lapped substrates for hybrid circuits include improved handling and screening, extended screen life, reduction of rejects, minimized resistor trimming, increased capacitor yield and easier assembly.

17. Polished Substrate Surfaces

Precision polishing is an exactly controlled process and may be defined simply as an extremely refined lapping technique, utilizing the finest lap materials and abrasives, which often are especially compounded diamond powders. Polished substrates which exhibit a bright reflective appearance but with poor flatness, camber, and varying smoothness, have limited value. Precision polished substrates are characterized by superior optical grade flatness, no "pullout", negligible camber, and low roughness at a selected level from 10 to 1 μin, held to a narrow spread across the entire surface and from piece to piece and from lot to lot. The finest polishes are made in 99.5 percent alumina, but lower purity and lower density materials can also be polished when required. Surface flatness of most precision polished ceramics can be controlled to less than 0.0001 in; such flatness levels are easily evaluated by observing light interference fringes on an optical flat where a regular pattern will be seen similar to that of figure 9.

18. Thick Film Substrate Surfaces

Fabricators have experienced some disappointments in achieving narrow tolerances for printed resistors [6]. It seems clear that a ma-

FIGURE 9. *Unretouched Polaroid photo of polished 2 in × 2 in alumina substrate showing light interference fringes for an overall flatness error less than 0.00005 in (Note each line here corresponds to a contour interval of half the wavelength of light, or about 0.000012 in.)*

jor improvement in the spread of such resistor values depends not only through control of process variables but through minimizing of substrate variables, especially those of camber, flatness, and roughness [6]. Flatness [1] can be critical in automated thick film printing, especially with fine mesh screen, very narrow lines (0.002 in or less) and up to five or more sequentially printed layers [7]. Some processors have already reported up to 30 percent increase in yield by printing resistors on uniformly lapped substrates.

19. Thin Film Substrate Surfaces

Thin film circuits, which may employ 94 percent to 99.5 percent purity substrates, are subject to failure [8] or poor performance in the event of local overheating due to excessively weak spots in the film, or open circuits and inconsistent resistivity due to discontinuities in the film; such defects can arise from burrs, pits, or local undulations typical of asfired ceramics. Since precision lapped or polished substrates are virtually free from these defects, many substrates for thin film circuits are now lapped.

20. Microwave Substrate Surfaces

Most users of lapped alumina substrates for microwave applications request precision polishing in the very low roughness range from about 10 to 1 μin, chiefly below 5 μin, although the practical limit may currently be about 0.3 μin AA. At this time the above range of polished surface quality is manufactured routinely in production lots primarily in 99.5 percent purity only. Most frequently both sides are specified for the identical finish; alternatively, one side (sometimes called "front") will require typically a 2 μin finish while the opposite side ("back") will require in one case a 10 μin finish, while in another case a 30 μin finish, and in still another case the as-fired finish is retained. Microwave substrates are often specified with low flatness (0.0001 in to 0.0005 in), low camber (0.0002 in to 0.001 in), and zero waviness.

Comparable surface quality, with certain specific limitations, may be applicable to materials other than alumina, including beryllia, ferrite, and others. For example, most beryllia can be polished to 3 μin or less only under very favorable conditions and with relative difficulty, while high quality ferrite can be polished to 1 μin and to optical flatness of 0.000001 in to 0.000010 in.

21. Conclusions

Adequate recognition of the complexity and importance of substrate surface quality requires that distinctions be made between the several separate but interrelated surface characteristics. Proper specification of significant substrate surface characteristics, their dimensions and tolerances, may be enhanced by correlation of functional effects of each surface detail. Attractive economics can be effected through cost tradeoffs based on functionally determined specifications from the most stringent to the most relaxed levels. Additional economics may be possible indirectly through increased implementation of and familiarity with improved measuring methods, new finishing techniques, updated standards, and exact terminology.

22. Definitions

The following list of terms excludes those covered elsewhere in this paper or in applicable references such as the Standard MIL–S–55620 (EL).

Centerline: a line parallel to the general direction of the surface profile such that the sums of those areas between it and those parts of the profile on either side are equal.

Lay: direction of a predominant surface pattern, usually designated not numerically but by orientation, as longitudinal, transverse, diagonal, curved, or random.

Matte dullness of a surface; absence of reflectivity. (Note: a matte surface may have extremely low roughness.)

Polish: reflectivity of a surface.

Profile: an intersection, disclosing detailed texture of a surface, between the surface and a perpendicular plane oriented in a partcular direction.

Roughness: a rating of the profile deviations as an arithmetic average (AA), measured in microinches normal to the centerline.

Texture: the repetive or random deviations from the nominal surface which form the pattern of the surface, consisting of roughness, waviness, lay, and flaws.

Waviness: the more widely-spaced irregularities or undulations of surface texture, the spacing of which is greater than that of individual roughness peaks but less than the surface width.
(Note: roughness may be considered to be superimposed on waviness.)

Also see ANSI Standard B 46.1, Surface Texture.

23. References

[1] Hybrid Microelectronics Review, July, 1970, Matthew F. Romano, Editor.

[2] Szekely, George S., Alumina substrates reliability criteria, a user viewpoint, Nepcon West, Feb. 11, 1969.

[3] Lenz, Robert G., GMC research laboratories, private correspondence, May 11, (1970).

[4] Pifer, B., and Collis, W. P., Special Report No. 476, American Machinist, August 10, 1959 (Surface Finish Measurement).

[5] Indars, G., I. G. Engineering Co. private communication, July, (1970).

[6] Van Hise, Jon A., Process variables in thick film resistor fabrication, Solid State Technology, July, 1970.

[7] Sweet, Alvan F., Insulation forum, Insulation/Circuits, March, (1970).

[8] Groves, H. T., and Keister, F. Z., Know your thin film materials, Electronic Design 19, Sept. 12, (1968).

NATIONAL BUREAU OF STANDARDS SPECIAL PUB. 348, The Science of Ceramic Machining and Surface Finishing, Proceedings of a Symposium Sponsored by the American Ceramic Society, the Office of Naval Research, and the National Bureau of Standards, held at NBS Nov. 2–4, 1970, Gaithersburg, Md. (Issued May 1972).

Ceramic Surface Texture by Reflective Replica Technique

Wing C. Lo

Bell Telephone Laboratories, Inc., Allentown, Pennsylvania 18103

Surface texture is a parameter of general concern in the study of thin film metallizing adherence on ceramic substrates. It refers to the geometrical character of the surface irregularities recurring many times across the ceramic surface tending to form a pattern. In this context, surface texture is determined by the size, shape, arrangement and distribution of the surface constituents.

This note presents a convenient method by which the surface texture of ceramic substrates can be visually assessed and recorded photographically using a simple metallographic microscope.

Examples in applying this technique for distinguishing and differentiating surface textures of different types of ceramic substrates are given. Use of the technique for identifying surface defects is also shown.

The simplicity of the method should warrant its use for monitoring the physical surface quality of ceramic substrates.

Key words: Alumina substrates; surface replica; surface texture.

1. Introduction

Surface texture refers to the geometrical character of the surface irregularities recurring many times across the ceramic surface tending to form a pattern.[1] It is determined by the size, shape, arrangement and distribution of the surface constituents. Surface texture here does not refer to the crystallographic orientation of a material.

The surface texture of ceramic substrates used in thin film applications is a parameter of general interest. Theoretically, the breaking load of a metal lead bonded to a thin film metallized substrate or the electrical properties of the thin film on the substrate can be influenced by the surface texture.[2] Thus, the uniformity and homogeneity of the surface texture of substrates is one of the requisites for maintaining the quality in a finished product. The need for assessing the surface texture is apparent.

One aspect of the surface texture that warrants consideration in thin film applications is the area of the surface accessible to and actually covered by the thin film material. This physical quality of the surface cannot be assessed numerically in terms of a root-mean-square value, a peak-to-valley value or the commonly used center-line-average (c.l.a.) value obtained with a mechanical profile tracer. The fact that c.l.a. values are not functionally dependent on or related to the real surface area has already been pointed out by J. E. Marian.[3] A qualitative, and possibly quantitative evaluation, of this physical quality can be easily achieved by visual observations with the aid of an optical microscope or a scanning electron microscope. (SEM).

However, with an ordinary metallographic optical microscope, one cannot view the surface of the ceramic directly. This is because of the small amount of light reflected from the textured surface. It is even more difficult to record the observed image photographically. The object of this note is to present a convenient technique by which these difficulties may be overcome. This is the reflective metallographic replica technique which has been in use by metallographers for some time.

The advantages of this method are its simplicity and general availability of the equipment required. One does not have to have tedious preparations of the sample before it can be studied. In the case of the SEM, it is necessary to coat the ceramic surface with a conductive film before the surface can be viewed. The limitation in the depth of focus or penetrating power attainable with optical microscope objectives is not always a disadvantage in this application. With the optical microscope one can estimate the depth of surface defects by focusing the top and bottom planes of the defect and measuring the difference in these levels. This estimation of depth is more difficult with the SEM. To assess the homogeneity of the surface texture one would like to view a large enough area of the sample at a glance. This can be accomplished at a magnification of about 200X. At this magnification the field of view is several orders of magnitude greater than the basic pattern of the surface texture. It is high enough to reveal the geometrical features that are of interest. With the SEM, useful magnifications starts at about 500X. Of course, when the asperities on the surface are in the neighborhood of 1 μm or less, then one has to resort to the use of the SEM which has substantially better resolution ($\sim$100Å).

[1] Reason, R. E., The Measurement of Surface Texture, (Cleaver-Hume Press Ltd., Great Britain, 1960).
[2] A paper on the subject is in preparation by the author.
[3] Symposium on Properties of Surfaces, ASTM Special Publication No. 340.

2. Description of Method

The material used in this technique comes from a kit marketed by Struers Scientific Instruments, Copenhagen, Denmark, under the trade name "Transcopy Reflective Metallographic Replica". It can be purchased through W. J. Hacker & Co., Inc., West Caldwell, New Jersey 07006.

The kit consists of a bottle of Transcopy liquid and a box of Transcopy-replicas. The Transcopy-replica is essentially a bright aluminum sheet coated with a green colored plastic film on one side.

The procedure for preparing a Transcopy-replica specimen is shown in figure 1. The first step is to place a small drop of the Transcopy liquid on the surface of the cleaned ceramic sample (fig. 1a). A small piece of the Transcopy replica is immediately placed over the liquid with the green plastic side facing the sample surface (fig. 1b). Hold the replica against the surface with uniform pressure [4] for approximately two minutes. Place a double sided adhesive tape on the back side of the replica (fig. 1c). Attach a glass slide onto the adhesive tape (fig. 1d). Turn the assembly over and remove the ceramic sample (fig. 1e). The mounted replica (fig. 1f) is ready for viewing under the metallographic microscope. The green color of the film serves as a filter for viewing.

From experience better replicas have been obtained with ceramic samples by substituting the Transcopy liquid with a similar replicating solution marketed by Ladd Research Industries, Inc., Burlington, Vermont.

It should be noted that the replica is not useful for low magnifications (below 100X) as the influence from the reflective aluminum layer will become too great with the increased depth of focus.

3. Results

The inadequacy of cla values for describing the surface texture of ceramics is illustrated in figure 2. The c.l.a. values cannot relay the difference between a ground and as-fired surface. Figure 3 demonstrates the vastly different surface textures of 99.5 percent alumina ceramics from different suppliers that meet the same 25 μin (0.64μm) min c.l.a. requirement.

At low magnifications (150X to 200X) the limitations of the usefulness of the scanning electron microscope is illustrated in figure 4. The texture of the two substrates can be easily differentiated visually from the photographs obtained by the replica technique. Their difference is less apparent when one compares the images recorded by the scanning electron microscope.

[4] A pressure of 80 g/mm^2 is adequate.

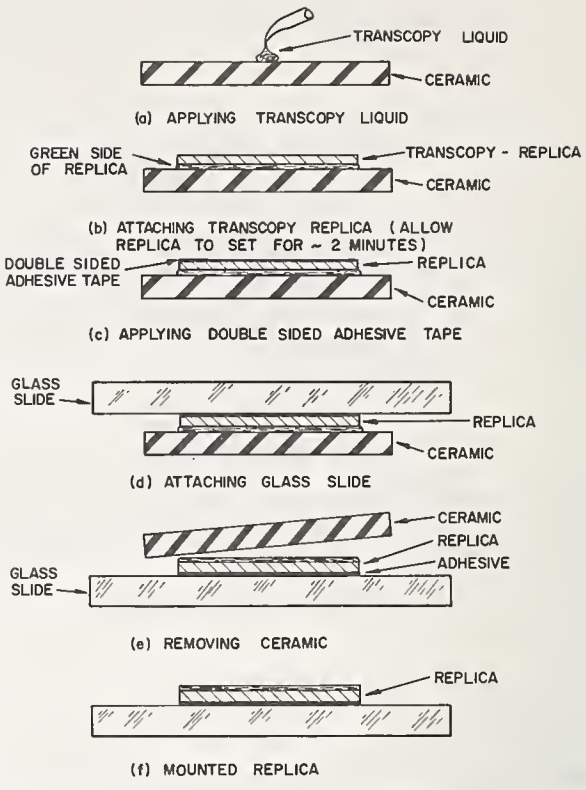

FIGURE 1. *Procedure for preparing a transcopy replica specimen.*

Use of the replica technique in revealing vast differences in surface textures of ceramic which one may get from suppliers is shown in figures 5 through 7. The difference in surface textures of ceramics may be due to differences in body composition and/or in manufacturing methods. Figure 5 compares the surface textures of 99.5 percent alumina ceramics reported to have the same body composition by the supplier but made by different processes, viz., the dry-pressed process and the tape-cast process. Figure 6 illustrates the difference in surface texture of 99.5 percent alumina substrates of the same body designation, made by the tape-cast process but from different lots shipped by the supplier. Figure 7 shows the textures of a dry-pressed 94 percent alumina ceramics in different shipments from the same supplier. According to the supplier, the difference here is due to a change in the finishing operations of the ceramics from grinding to lapping.

Changes in surface texture can also be brought about by post-manufacturing processes. Figure 8 shows the change in surface texture of a 99.5 percent alumina ceramic by refiring it to cone 31. The change in a 94 percent alumina ceramic surface texture effected by an acid etchant (HF and HNO_3 solutions) is shown in figure 9.

Applications of the replica technique in identifying surface defects and damages are shown in figures 10 and 11. Figure 10a is a replication of the surface defect that results in a

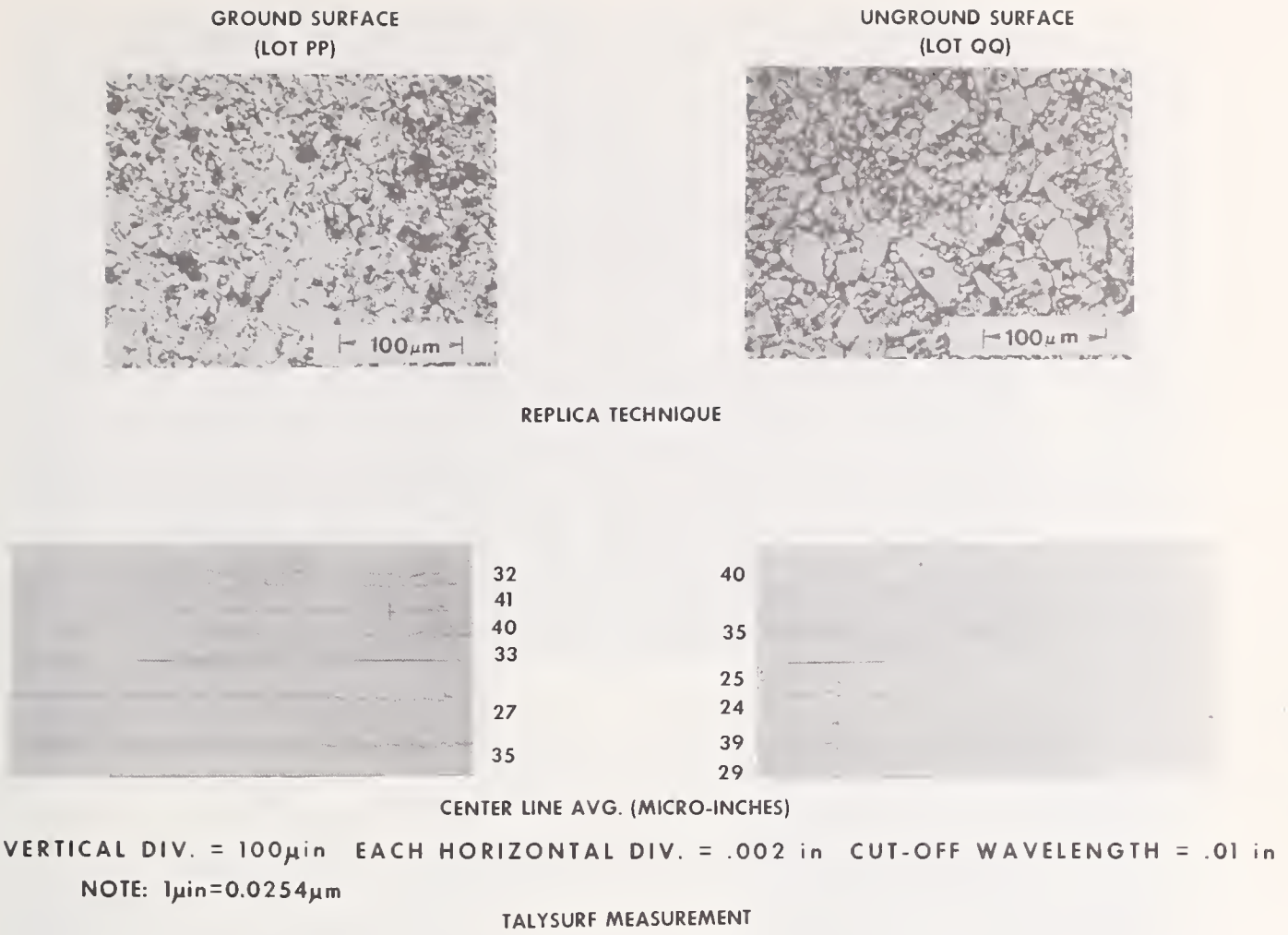

FIGURE 2. *Surface texture of ceramics by replica technique vs center line average values.*

white area on a substrate when inspected with illumination from its back side. This defect is a pit on the back side of the substrate directly below the location of the white area. When illuminated from the back side, the location of this defect on the viewer side of the substrate will look white due to greater amount of light that can get through to the viewer at this location. The presence of relatively large grains in the pit suggests the presence of impurities which caused exaggerated grain growth or the formation of new phases. This could establish the basis for further investigation for remedial actions by the manufacturer. Figure 10b is the replica of a fissure on the substrate surface which shows up as an area that retains fluorescent penetrants. The fissure is possibly caused by impurities imbedded in the surface. Figure 11 shows pull-outs and streaks of distorted material from grinding operations. The same grinding process produces more pits or pullouts on the 94 percent than on the 99.5 percent alumina ceramics.

4. Conclusions

Although the surface texture of ceramic substrates used in thin film applications may not be the only parameter that governs the desired properties of the finished product, it is a variable that should be controlled.

The replica technique offers a simple and practical aid for ceramic suppliers to monitor their manufacturing processes and for users to check on the uniformity in the quality of the parts they receive.

The author wishes to thank Messrs. J. E. Clark, W. B. Grupen, F. L. Howland and P. I. Slick for their encouragement and comments.

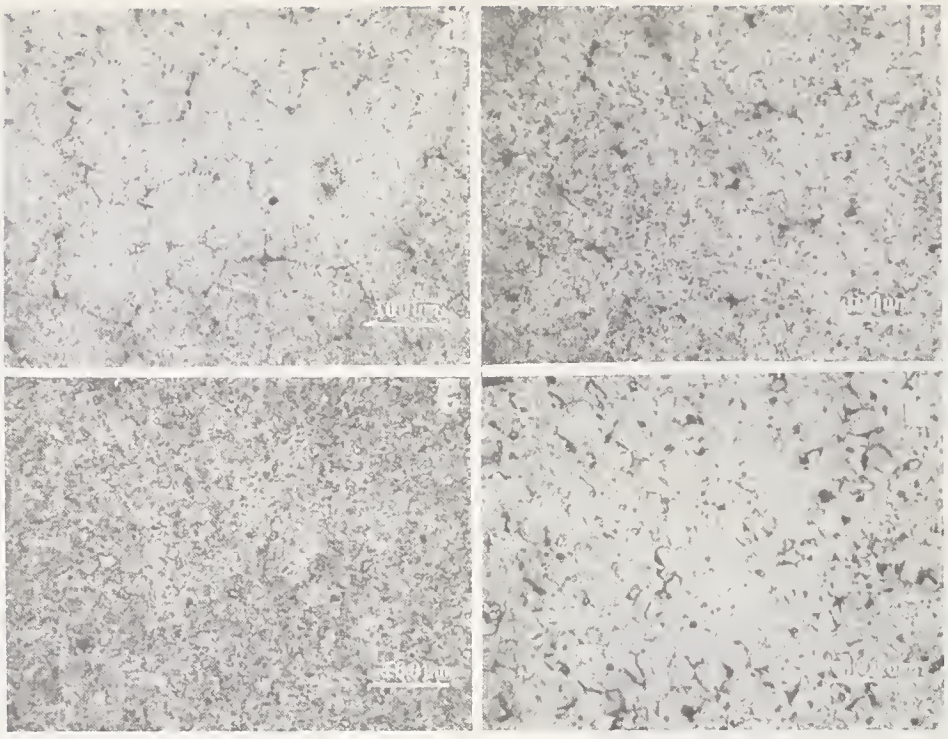

a CERAMIC BODY A ; SURFACE AS-FIRED
b CERAMIC BODY A ; SURFACE TUMBLED
c CERAMIC BODY A ; SURFACE LAPPED
d CERAMIC BODY B ; SURFACE GROUND

FIGURE 3. *Surface textures of 99.5 percent alumina ceramics meeting 25 μin (0.64 mm) CLA finish.*

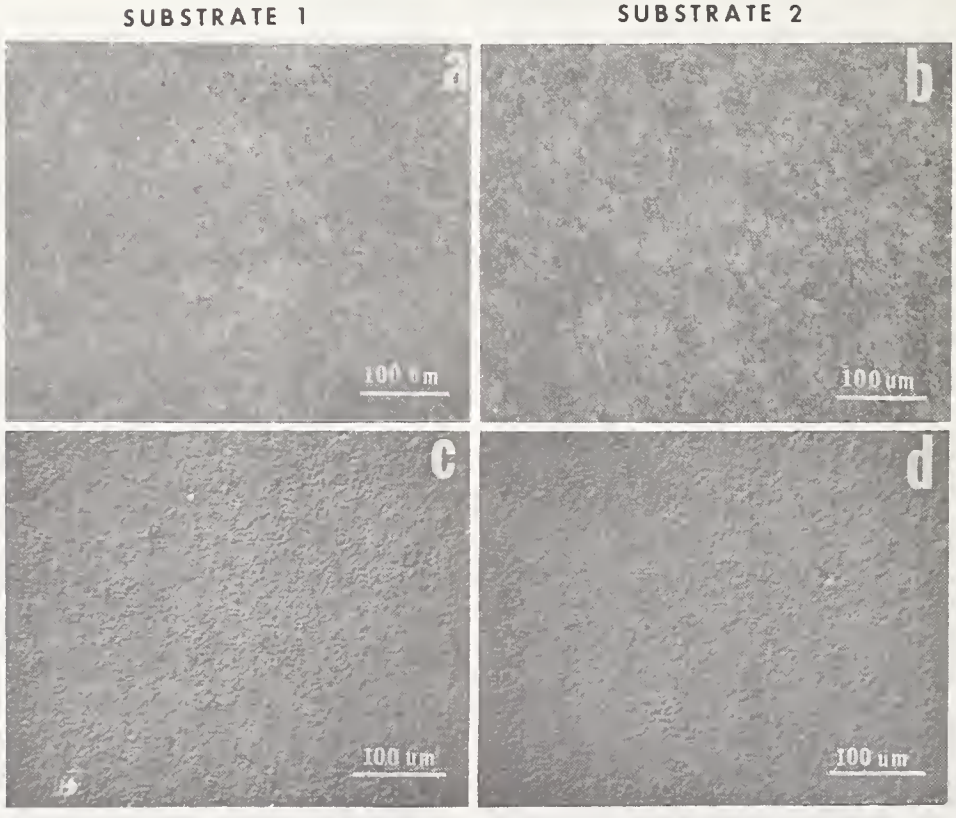

a,b OPTICAL MICROSCOPE USING REPLICA TECHNIQUE

c,d ELECTRON SCANNING MICROSCOPE

FIGURE 4. *Comparison of low magnification micrographs of surface textures taken with optical microscope using replica technique and with electron scanning microscope.*

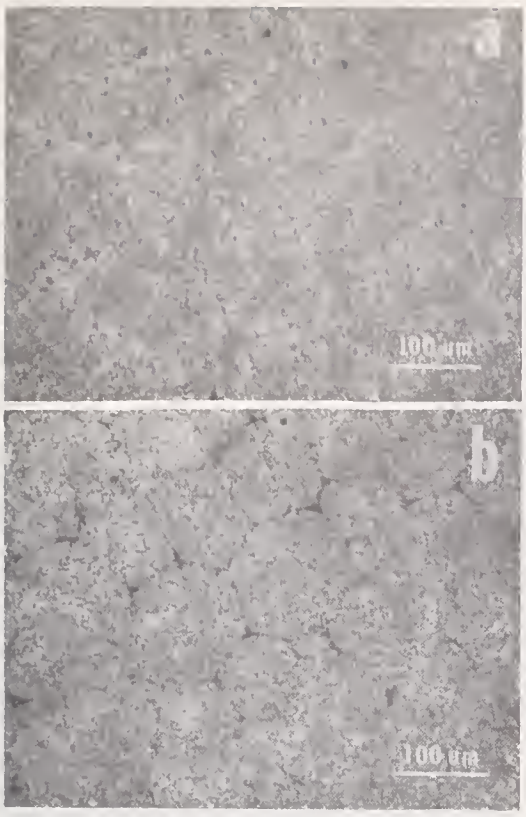

a TAPE-CAST
b DRY-PRESSED

FIGURE 5. *Surface textures of tape-cast and dry-pressed 99.5 percent alumina substrates.*

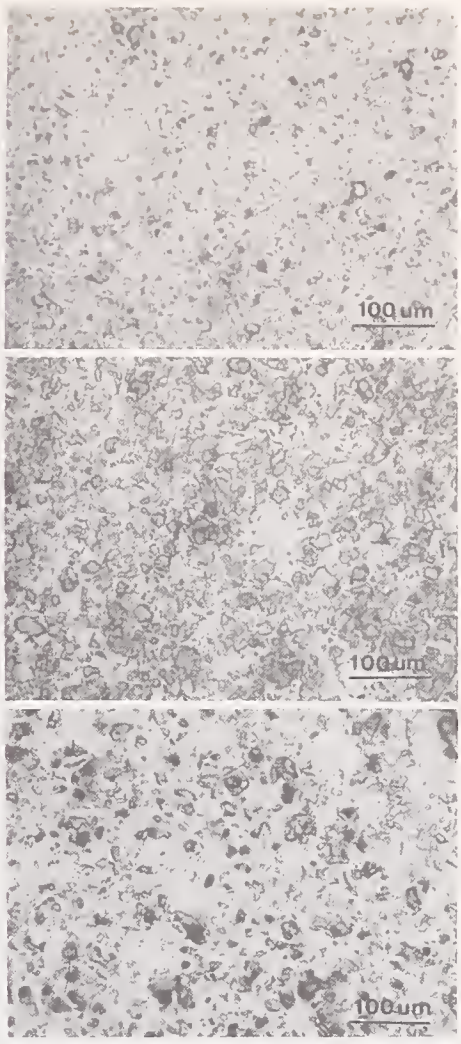

FIGURE 7. *Surface textures of ground dry-pressed 94 percent alumina ceramics from different lots shipped by same supplier.*

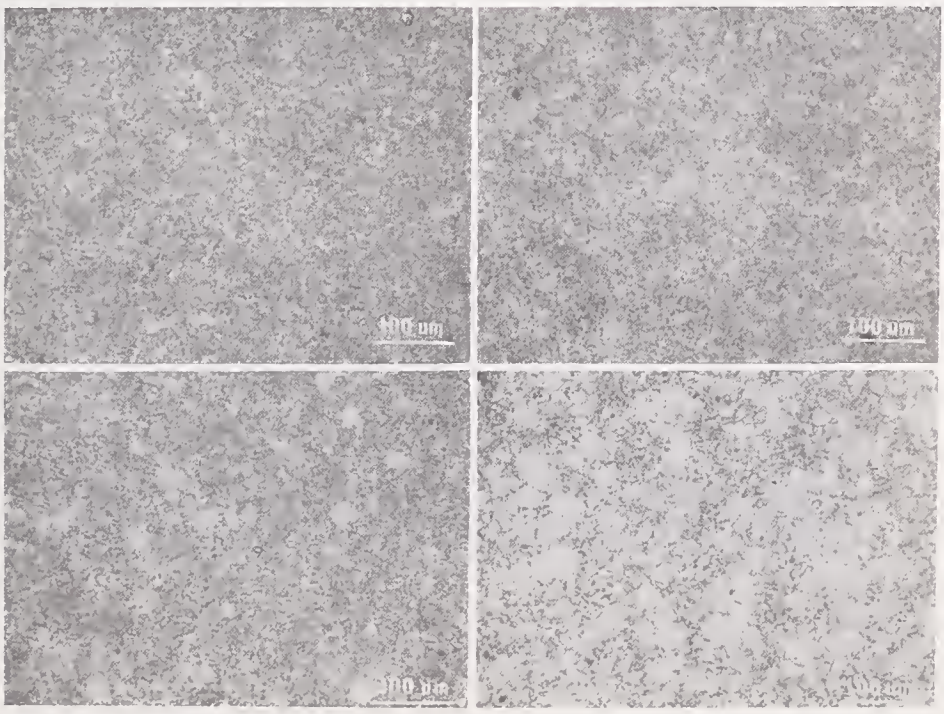

FIGURE 6. *Surface textures of tape-cast 99.5 percent alumina substrates from different lots shipped by same supplier.*

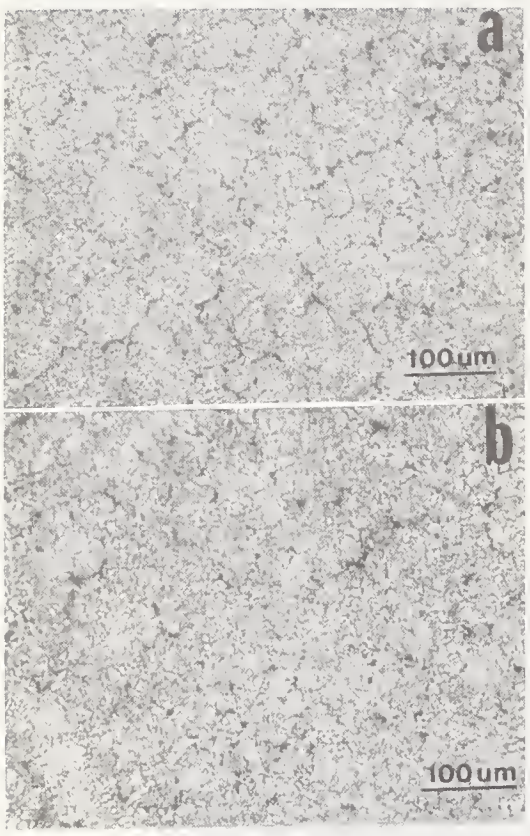

a AS-FIRED

b REFIRED

FIGURE 8. *Change in surface texture of 99.5 percent alumina ceramics by refiring.*

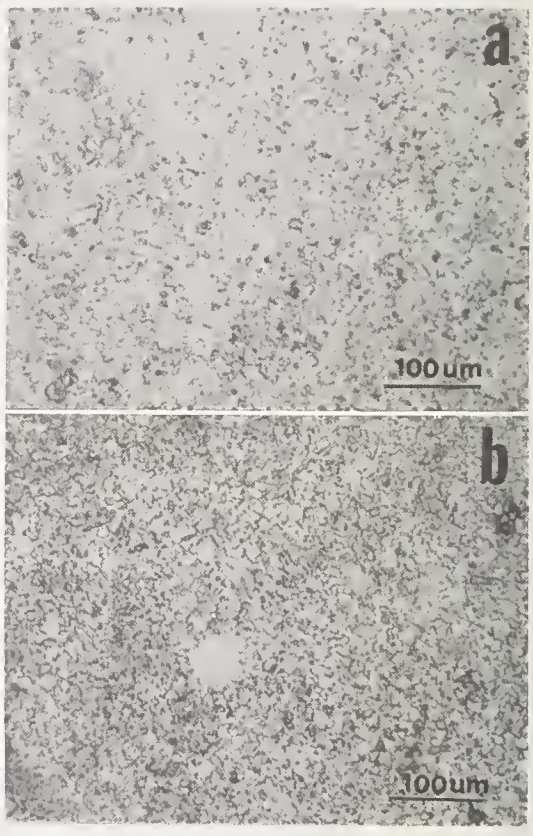

a AS-RECEIVED

b ACID ETCHED

FIGURE 9. *Change in surface texture of 94 percent alumina ceramics by acid etching.*

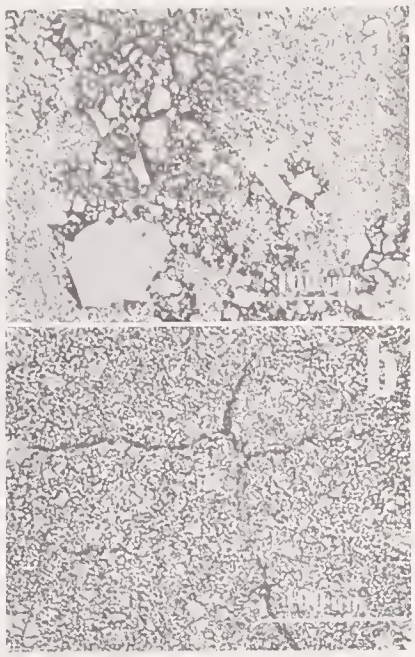

a PIT
b CRACK

FIGURE 10. *Defects on ceramic substrate surfaces.*

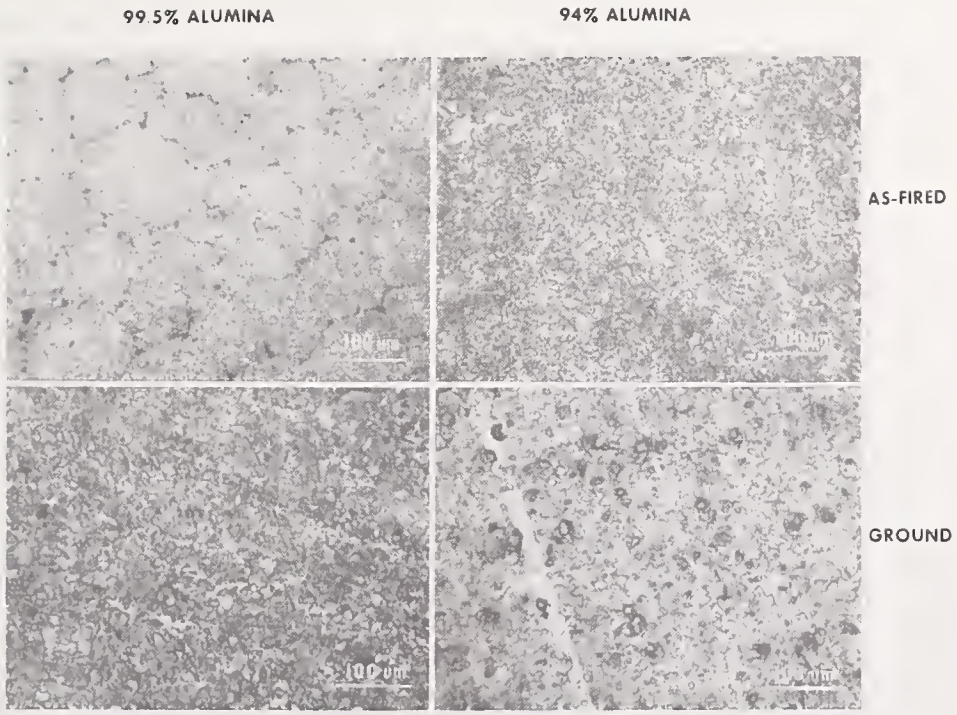

FIGURE 11. *Grinding damages on 99.5 percent and 94 percent alumina ceramic surfaces.*

NATIONAL BUREAU OF STANDARDS SPECIAL PUB. 348, The Science of Ceramic Machining and Surface Finishing, Proceedings of a Symposium Sponsored by the American Ceramic Society, the Office of Naval Research, and the National Bureau of Standards, held at NBS Nov. 2–4, 1970, Gaithersburg, Md. (Issued May 1972).

Quantitative Surface Finish Characterization by CESEMI

E. W. White and H. A. McKinstry

Materials Research Laboratory, Pennsylvania State University, University Park, Pennsylvania 16802

and

A. Diness

Office of Naval Research, Metallurgy Program Arlington, Virginia 22217

A feasibility for quantitative characterization of surface finishes based on the computer evaluation of scanning electron microscope images (CESEMI) has been established. Measurement of the number, size, shape and orientation of isointensity (or selected intensity interval) regions constitute the basic analysis. Brightness in SEM images varies as a function of the steepness of slope of the surface at a given point. In their analysis, the characteristics of grooves, pits, ridges, etc., can be studied separately. Detailed interpretation of the results are not attempted in this preliminary study.

A feasibility for recording and analyzing profilometer rasters has also been demonstrated. Such recordings are, in essence, true three dimensional images of surface topography insofar as the profilometer stylus faithfully follows the surface morphology. Analysis of these profilometer recordings by the basic CESEMI computer programs yield direct descriptions of the topography. The SEM image and profilometer "image" analyses appear to be complementary techniques. One obvious advantage of the SEM image analysis is that it is a no-contact technique hence, there are no problems introduced by stylus damage.

Key words: Ceramic Materials; CESEMI (Computer evaluation of scanning electron microscope images); digital magnetic tape recordings; profilometer; profilometer rasters; quantitative characterization; scanning electron microscope; surface finish analysis; surface morphology; surface roughness; surface topography; three dimensional images.

1. Introduction

Quantitative characterization of surface finish parameters should be useful in evaluation of the mechanisms of material removal by various finishing processes as well as in assessing the relation of final surface finish characteristics to property.

The analysis of ceramic surface finish is the problem of describing quantitatively the important morphological characteristics of the surface topography which result from a particular finishing process such as grinding, burnishing, sputtering, polishing, etc. Parameters of interest include: surface roughness; microfracture characteristics; size, shape and depth of pits, etc. Also of importance are the orientation of elongate features such as scratches, grooves, ridges and fractures.

It is proposed that much of this information might be gleaned from computer analysis of scanning electron microscope images. As a complementary approach, the analysis of rastered profilometer traces (successive line traces over a given area) may be used to get a reading of the complete three-dimensional surface topography.

Instrumentation and computer programs developed for our research on particulate characterization appear to be directly applicable to studies of ceramic surface finish. This paper is intended as a feasibility study to set forth possible approaches and how they might be implemented. To achieve this goal the basis for image formation in the SEM will be reviewed. Results from the analysis of five representative finishes will be discussed. The results from a trial profilometer reading are also presented.

2. Description of SEM Image Forming Process

The SEM employs a finely focused (100–200Å diameter) beam of high energy electrons (5 keV → 30 keV) to dislodge low energy (1–50 eV) electrons from the specimen surface. A highly sensitive electron scintillation detector monitors the currents (10^{-13} → 10^{-9} amps) of the emitted secondary electrons. The detector signal is used to moderate the brightness of a cathode ray tube (C.R.T.) as both the electron beam on the specimen inside the SEM and the C.R.T. spot are rastered synchronously. This results in the generation of an image of the specimen surface viewed on the C.R.T.

The SEM gives quite high resolution (200Å) images of the specimen surface at a depth of field some 300 times greater than for normal

439-921 O - 72 - 21

light microscopy at a given value of magnification. Upon hitting the specimen surface the electron beam penetrates to a considerable depth (up to several microns depending on the keV and specimen composition). Throughout the entire volume of beam penetration, low energy secondary electrons are generated but only those generated within 10–50Å of a surface can escape and become part of the image signal.

Figure 1 shows schematically the sort of intensity of secondary electron emission to be expected from a surface consisting of familiar geometric configurations. From examination of figure 1 it follows that:

(a) deep holes and cracks yield essentially no secondary electron signal.

(b) the steeper the slope of a surface, the higher will be the secondary electron emission.

(c) sharp ridges resulting from the intersection of two steep slopes will yield the highest signal. Any obtuse angle of intersection (peak or ridge) will yield brighter emission than either of the intersecting surfaces.

(d) notches or grooves resulting from the acute angle of intersection of two surfaces will yield intensities lower than from a surface which is normal to the beam.

Not all the emitted secondaries may be collected by the detector. The fraction detected depends upon (1) the degree of collimation or angular selectivity of the detector and (2) reabsorption of the secondaries by prominent features on the specimen surface. These losses introduce shadow effects in the image as illustrated in figure 2 for an extreme case. Most observed images exhibit shadow effects somewhere between these two extremes.

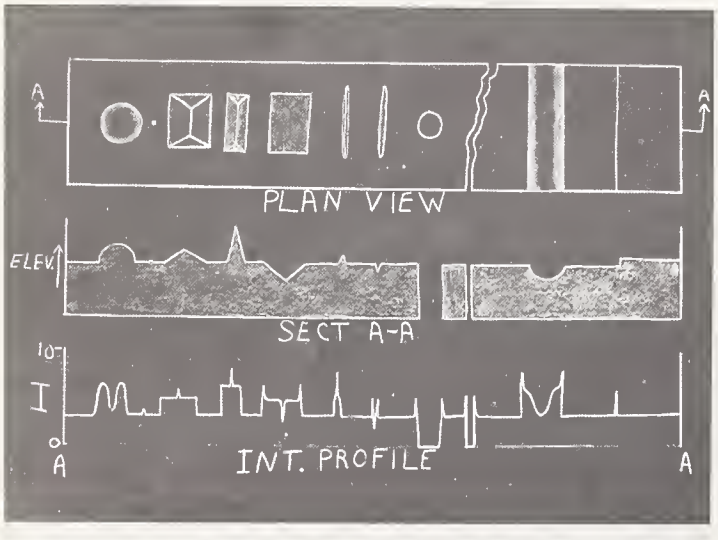

FIGURE 1. *Idealized secondary electron image from selected geometric features.*

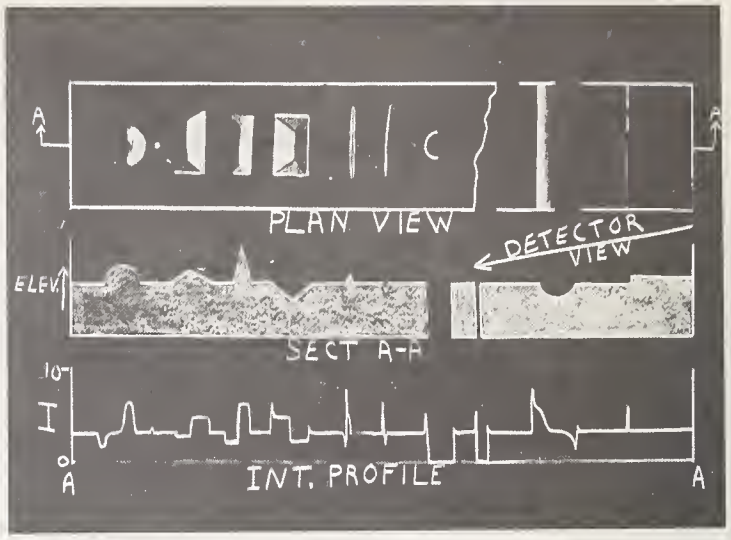

FIGURE 2. *Idealized secondary electron images with exaggerated shadow effect from selected geometric features.*

3. SEM Instrumentation

The SEM and related recording instrumentation used in our study are shown schematically in figure 3. The x-ray channels are not used in this study but could have been. All SEM images were recorded at 300X magnification. Intensities were measured on a gray scale of 2000. There were 250 raster lines with 250 sample points per line giving sample grid of 62,500 data points. The detector was optimized to suppress shadow effects, thus, image bright-

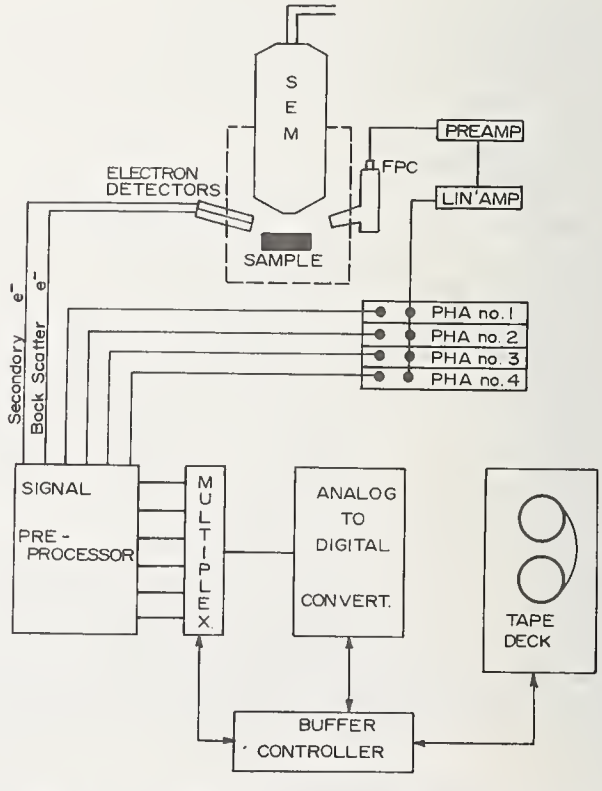

FIGURE 3. *Schematic block diagram for the SEM and instrumentation for digital magnetic tape recording.*

ness for this study closely follows the model shown in figure 1.

Additional details of the instrumentation and the basic computer programs have been published previously [1, 2, 3, 4][1].

4. Profilometer Recordings of Surface Topography

The SEM images give the impression of a three dimensional picture but since the intensities are a complex function of several parameters, the actual surface topography is not measured. A novel technique was developed to obtain the surface topology directly. Within the range of its intended use (resolution etc.,) the signal output from a profilometer is a direct function of the surface height. Thus, by arranging the profilometer to raster the sample surface, a three dimensional representation of the surface is obtained. The recording system and computer programs developed for the measurement of SEM images are suitable for handling this profilometer input. Multiple contours thus made give a topographical map of the material's surface. Our test runs are rather crude in that a makeshift "raster" was utilized, however, they serve to establish the general feasibility.

5. Computer Analysis

The basic computer programs calculate the characteristic features contained above (or below) a selected intensity level in the image. Each continguous field is recognized regardless of its shape complexity. Basic parameters calculated for each such field are its area and perimeter. An ellipse is fitted to the perimeter of each field and its characteristics are calculated including the lengths of major and minor axes and the orientation of the major axis. (Although the axial orientation is used in the program it is not a part of the output generated in this study). From these basic parameters other characteristics such as aspect ratio, ratio of the measured perimeter to ellipse perimeter and etc., are calculated as desired.

6. Results

Five specimens from 48 samples provided by R. J. Stokes of Honeywell and Roy Rice of NRL were chosen to represent a variety of surface finishes, materials and finishing techniques. Secondary electron images were recorded photographically and simultaneously on digital magnetic tape. In all cases the secondary electron detector was set to minimize shadow effects.

In addition to the conventional SEM image, a y-axis modulation photograph was obtained. These displays tend to emphasize topographic features. Unfortunately there is an electronic distortion in these particular images so that corresponding features on the two photos do not register exactly in the verticle direction.

Computer generated binary area and perimeter maps are illustrated in figures 4 and 5. These are photographic reductions of several pages of computer print. Due to the higher density of printed characters per line than the carriage spacing in the print, these representations have a rectangular distortion. Although they are not actually used in the computer analysis, such printouts serve to illustrate certain functions of the programs.

Figures 4 through 8 show the images on which computations have been performed. All results are in the basic program units and not true dimensions. One data point corresponds to 1.33μm or an area of 1.77 $^1\mu m^2$.

The frequency distribution of the contiguous area sizes at two different levels are plotted in figures 9 and 10 suggesting the kind of additional information that can be obtained from the computer analysis. The SEM pictures which show small features have a similar distribution for both peaks and pits. The materials with a smoother appearance have a broad size distribution as one might expect.

The profilometer trace analysis shown in figure 11, indicates the kind of result that one would expect. The contour was drawn at one level and shows the nearly random pattern that should result from a surface of novaculite (crypto-crystalline quartz) ground flat on a grinding wheel using a 600 mesh silicon carbide abrasive.

This work is part of a program being sponsored by the Office of Naval Research, Metallurgy Division under Contract N00014–67–A–0385–0007.

Most of the samples used in the study were supplied by Roy Rice of the Naval Research Laboratory and R. J. Stokes of Honeywell. Profilometer instrumentation was made available by the department of Industrial Engineering and Professor A. B. Draper and Mr. J. M. Samuels, Jr., of that department have assisted by way of several useful discussions.

Other personnel collaborating in this program include: Dr. G. G. Johnson, Jr., Dr. H. Görz, Mr. and Mrs. J. Lebiedzik, Miss K. Mayberry and Mr. R. Hoover.

7. References

[1] McMillan, R. E., Johnson, G. G., Jr., and White, E. W., Computer Processing of Binary Maps of SEM Images. Proceedings of the 2nd Annual

[1] Figures in brackets indicate the literature references at the end of this paper.

Scanning Electron Microscope Symposium, IITRI, pp 439–444 (1969).
[2] White, E. W., Gōrz, H., Johnson, G. G. Jr., and McMillan, R. E., Particle Size Distributions of Particulate Aluminas from Computer Processed SEM Images. Scanning Electron Microscopy/1970. Proceedings of the 3rd Annual Scanning Electron Microscope Symposium, IITRI, pp 57–64, Chicago, Illinois (1970).
[3] Matson, W. H., McKinstry, H. A., Johnson, G. G., Jr., White, E. W., and McMillan, R. E., Computer Processing of SEM Images by Contour Analysis. (in press—Pattern Recognition).
[4] White, E. W., Mayberry, K., and Johnson, G. G., Jr., Computer Analysis of Multi-channel SEM and X-ray Images from Fine Particles. Technical Report No. 3, Office of Naval Research, Metallurgy Program, Contract No. N00014-67-A-0385-0007, December 1970.

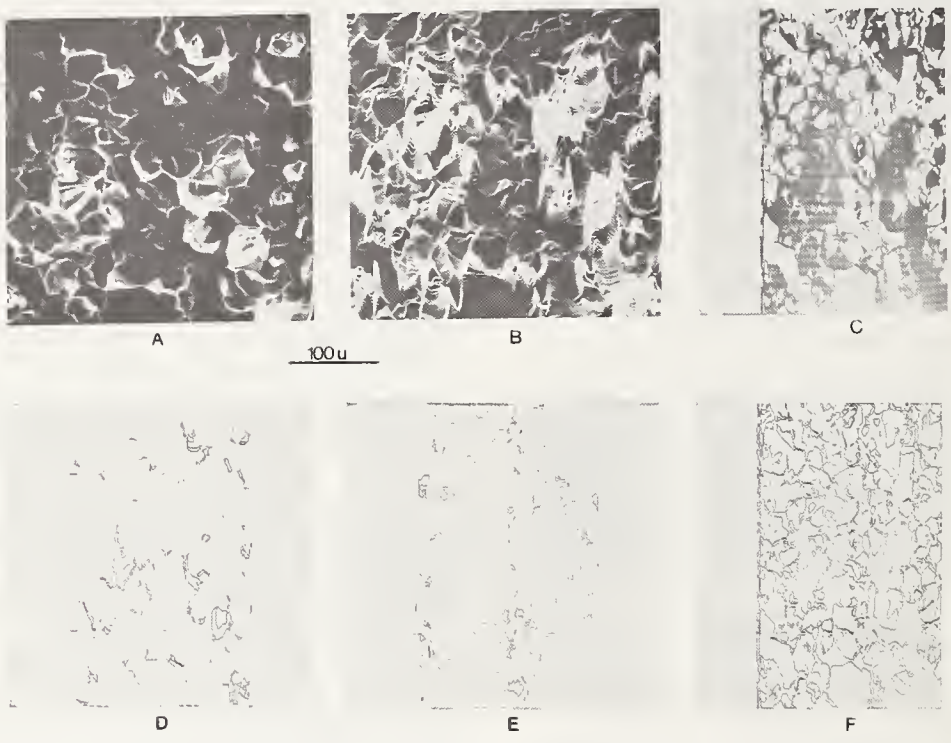

FIGURE 4. *Lucalox gas polished to AA finish of 3.2μm.* Sample supplied by R. Rice.

A. Secondary electron images with detector conditions set to minimize shadowing effects. Regions of steepest slope have greatest brightness.
B. Y-axis modulation of same area as A. An instrumental distortion has elongated this image toward the top so that the registration is not accurate with respect to A.
C. Computer generated binary map at the fifty per cent level. All data points whose intensity is greater than the average value are indicated by a black dot.
D. Computer generated perimeter at the 95% level. The computer printer introduces an elongation in the top-bottom direction. The bright areas in A can be matched to their corresponding configurations.
E. Computer generated perimeter map at the 50% level.
F. Computer generated perimeter map at the 10% level (inverted).

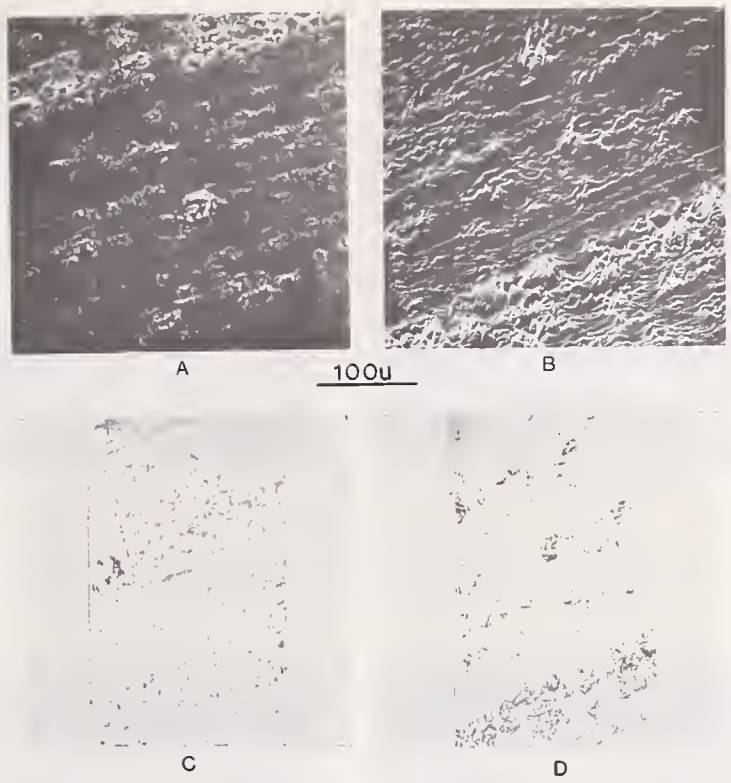

FIGURE 5. *Silicon face (100) ground by an alumina wheel to an AA finish of 0.25μm.* Sample supplied by R. J. Stokes.
A. Secondary electron image showing oriented surface features.
B. Y-axis modulation of same area as A.
C. Computer generated binary map at 10% level (inverted).
D. Computer generated binary map at 95% level.

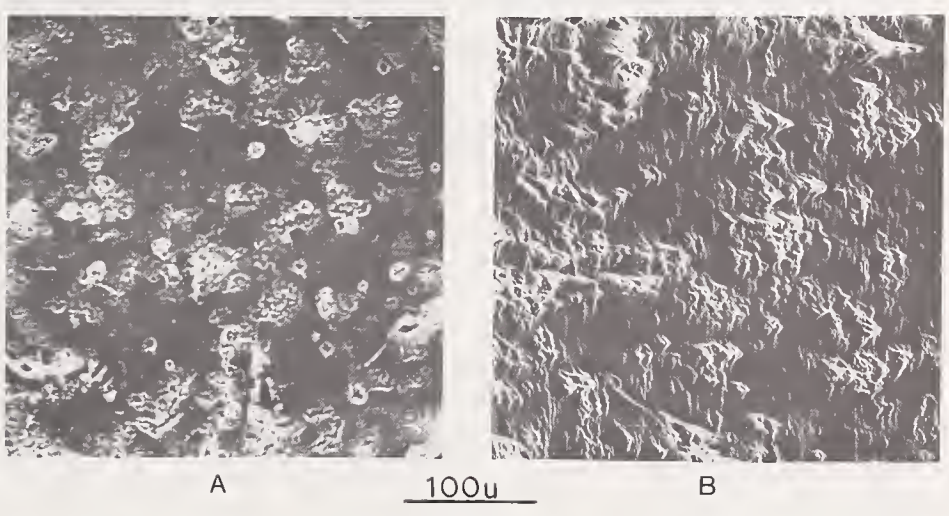

FIGURE 6. *Alumina, diamond polished to an AA finish of 0.32μm.* The sample was obtained from R. Rice.

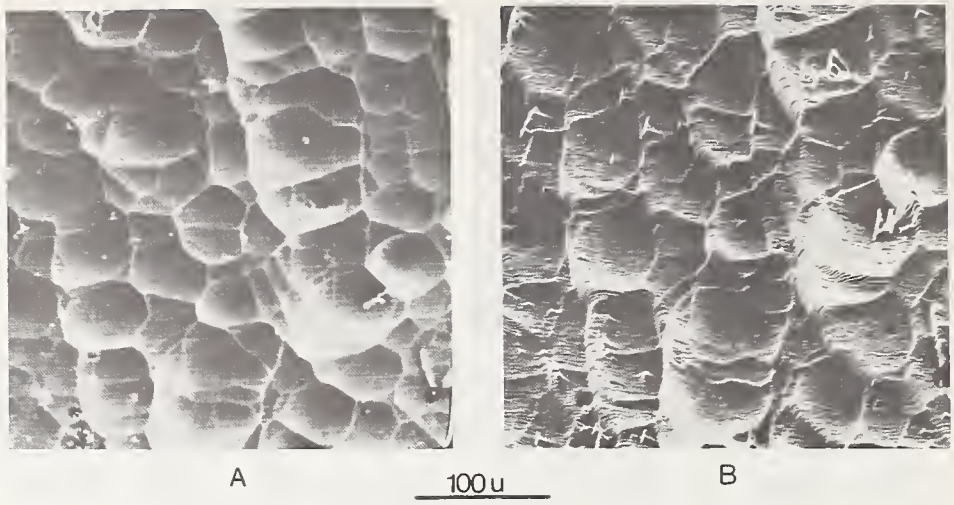

FIGURE 7. *Sapphire surface after R.F. sputtering.* The AA finish is 2.0μm.

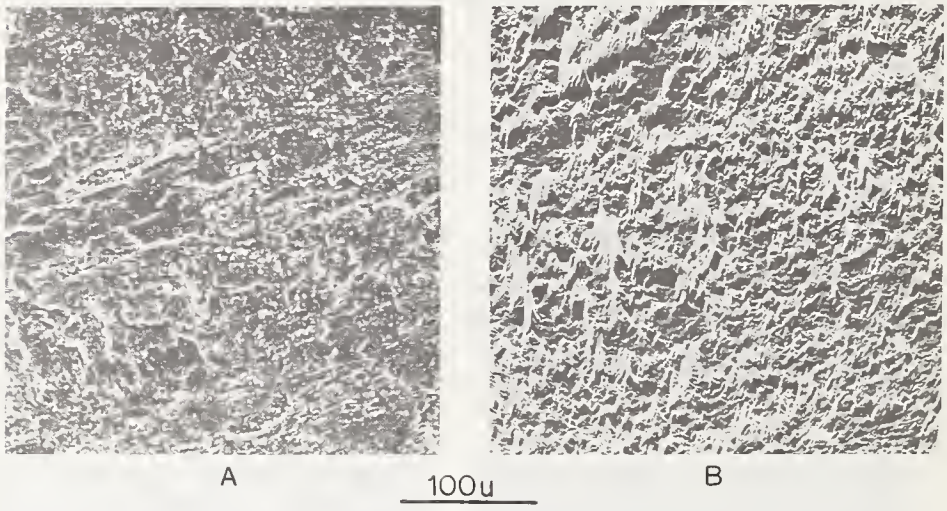

FIGURE 8. *Magnesia surface ground by a diamond wheel to an AA surface finish of 1.1 μm.* Sample obtained from R. J. Stokes.

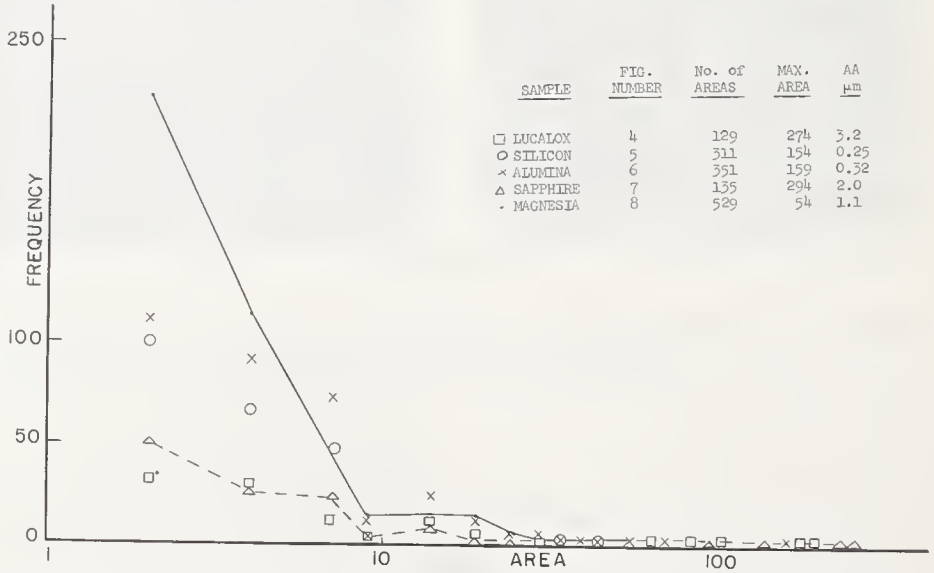

FIGURE 9. *Frequency Distribution of Contiguous Areas at the 95% level.*

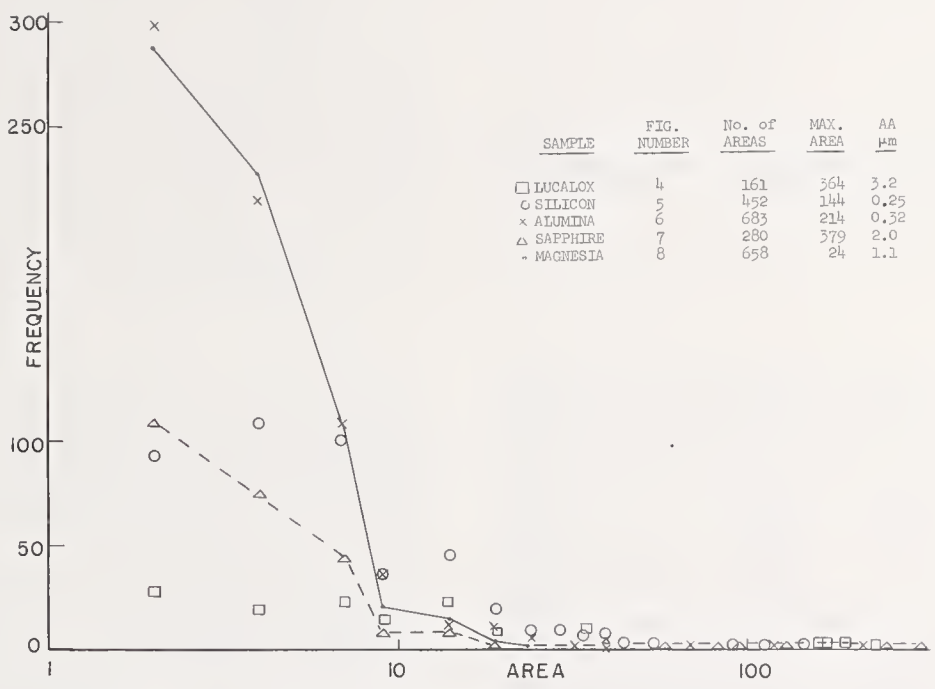

FIGURE 10. *Frequency Distribution of Contiguous Areas at the 10% level.*

FIGURE 11. *Profilometer image of Novaculite surface.* The rastered profilometer image contoured at a 50 percent level by computer processing. Multiple contouring would give a topographic map of the surface.

NATIONAL BUREAU OF STANDARDS SPECIAL PUB. 348, THE SCIENCE OF CERAMIC MACHINING AND SURFACE FINISHING, Proceedings of a Symposium Sponsored by the American Ceramic Society, the Office of Naval Research, and the National Bureau of Standards, held at NBS Nov. 2–4, 1970, Gaithersburg, Md. (Issued May 1972).

An Assessment of Surface and Subsurface Damage Introduced in Ceramics by Semifinish Grinding Operations

B. G. Koepke

Honeywell Corporate Research Center, Hopkins, Minnesota 55343

The nature and extent of grinding damage introduced by surface grinding a number of ceramics having widely varying mechanical properties has been studied. Surface damage has been characterized by optical and electron microscopy and subsurface damage has been observed using etch pit techniques. Grinding damage was found to depend strongly on wheel type and rate of material removal as well as on the mechanical behavior and microstructure of the workpiece. The results indicate that grinding damage is mainly composed of mixtures of three types depending on the mechanism of material removal.

When material is removed efficiently from low impact resistance ceramics (e.g., magnesium oxide and ferrite) the surfaces are generated by brittle fracture and are composed of regions of transgranular and intergranular fracture. When grinding is inefficient; i.e., when the grinding wheel loads up, material is removed by plastic flow. The resultant surfaces on deformable ceramics (e.g., magnesium oxide, ferrite, and silicon) are smooth and burnished, but may contain thermal cracks due to the heat generated. In this instance subsurface damage consists of a discrete, highly deformed layer containing cracks in most cases.

When material is removed efficiently from high impact resistance, nondeformable ceramics (e.g., alumina and boron carbide) material is removed by plastic flow and by transgranular and intergranular fracture. The presence of extensive plastically flowed regions on the ground surfaces of extremely hard ceramics is surprising and points out the extremes of stress and temperature existing under the wheel-workpiece interface during a grinding pass.

Key words: Ceramics; etch pits; fracture; grinding damage; plastic deformation; surface condition; surface grinding.

1. Introduction

Ceramics are finding increased use in modern technology because of their wide range of physical properties. Optimization of the physical properties is generally attained by close control of primary fabrication variables. For many applications extremely close dimensional tolerances are called for. Precise ceramic machining is therefore usually performed as a secondary fabrication operation on material in the as-fired (fully hardened) condition.

To date the most common ceramic machining techniques are those that use abrasives of one form or another for grinding, lapping and polishing operations. Although abrasive machining techniques are highly developed they are quite operator dependent and surprisingly little is known about either the nature of as-machined surfaces or the material removal phenomena leading to the finished surface [1][1]. Even less is known about the condition of the material immediately beneath the finished surface. These points are of concern because it is known that many physical properties of ceramics, particularly mechanical properties, are highly structure sensitive and the successful operation of a precision ceramic device might ultimately depend on its surface condition [2].

Abrasive machining generally involves a sequence of steps; namely, rough grinding (hogging) in which the workpiece is cut to shape, semifinish grinding in which the final shape is obtained, and finally finish grinding, lapping and polishing in which the desired surface finish and tolerances are obtained. From the standpoint of surface integrity, a successful machining operation is one in which the damage introduced during a given step is completely removed by the following step. The most likely place for the introduction of persistent damage is during the rough and semifinish grinding operations. In many instances this damage is not satisfactorily removed by the later machining steps. For this reason it is felt that an understanding of the nature and extent of the damage introduced in ceramics by semifinish grinding is essential if optimum workpiece quality is to be achieved.

This paper presents an assessment of the state of ceramic materials subjected to semifinish grinding. It will compare the damage resulting from semifinish surface grinding operations on different ceramics having widely varying mechanical response to the high stresses imposed by the machining operation. The paper will distinguish between the surface condition, referred to as surface damage, and the subsurface damage. The various types of grinding damage encountered will be discussed in terms of the properties of the workpiece, the characteristics of the grinding system and the tool-workpiece interaction.

[1] Figures in brackets indicate the literature references at the end of this paper.

2. Choice of Materials

The materials used for this study were chosen primarily on the basis of their mechanical behavior. Ceramics may be divided according to three categories of mechanical behavior; namely, completely brittle, semibrittle and ductile [3, 4]. In completely brittle ceramics dislocations cannot move and plastic shear by slip is not possible even at stresses approaching theoretical strength. In semibrittle ceramics dislocations are mobile but slip is restricted to a limited number of slip planes. In ductile ceramics dislocations are extremely flexible and cross slip over many planes results in complete plasticity.

The categories of mechanical behavior of the ceramics used in this investigation are shown in table 1. As table 1 indicates, the mechanical behavior of these materials depends on temperature with a trend towards increased deformability at higher temperature. Differences in mechanical behavior can be expressed by the number of independent slip systems operating at different temperatures. According to the von Mises criterion a crystal needs five independent slip systems to undergo a general change in shape. Note in table 1 that this condition only prevails in magnesium oxide, spinel and silicon at high temperatures. Alumina does not achieve the necessary number of independent slip systems. To the author's knowledge the slip systems in boron carbide have not been determined. However, since the material has a hexagonal crystal structure, its mechanical behavior is presumably similar to alumina.

3. Experimental Procedure

3.1. Materials

Samples of the ceramic materials indicated in table 1 were obtained in both single crystal and polycrystalline form from various sources as indicated in table 2. These materials are listed according to their hardness and it should be noted that a hardness differential is observed even among different samples of the same materials; e.g., polycrystalline alumina.

Prior to machining studies, samples were prepared having approximate dimensions 1/2 in x 1/4 in x 1/8 in. In the case of single crystals of magnesium oxide these could be prepared by cleavage. Silicon single crystals and polycrystalline samples were all prepared by me-

TABLE 1. *Mechanical behavior of ceramics used for this study*

Material	Temperature	Number of independent slip systems	Mechanical behavior	Reference
Magnesium oxide (single crystal and polycrystalline)	R.T.	2	Semibrittle	3, 6
	>1500 °C	5	ductile	3, 5
Ferrite [mechanical properties assumed similar to spinel ($MgAl_2O_4$]	R.T.	5	Semibrittle or brittle	6, 20
	>1600 °C	5	Semibrittle	
Silicon (single crystal)	R.T.	5	Brittle	7
	>650 °C	5	Semibrittle	
Alumina (single crystal and polycrystalline)	R.T.	2	Brittle	3, 8
	>900 °C	2	Semibrittle	
Boron carbide (polycrystalline)	>1400 °C	?	Brittle	9

TABLE 2. *Grain sizes and hardnesses of ceramics used for this study*

Material	Supplier	Grain size (μm)	Hardness (Knoop)
MgO single crystal	Norton	--	336
Sintered MgO	IITRI	18	411
Hot pressed NiZn ferrite	Honeywell	3	670
Si single crystal	Mallinckrodt	--	950
Sintered (Lucalox) Al_2O_3	General Electric	38	1800
Hot pressed Al_2O_3	AVCO	2	2000
Cold pressed and sintered (AD999) Al_2O_3	Coors	2	2100
Hot pressed B_4C	AVCO	8	2800

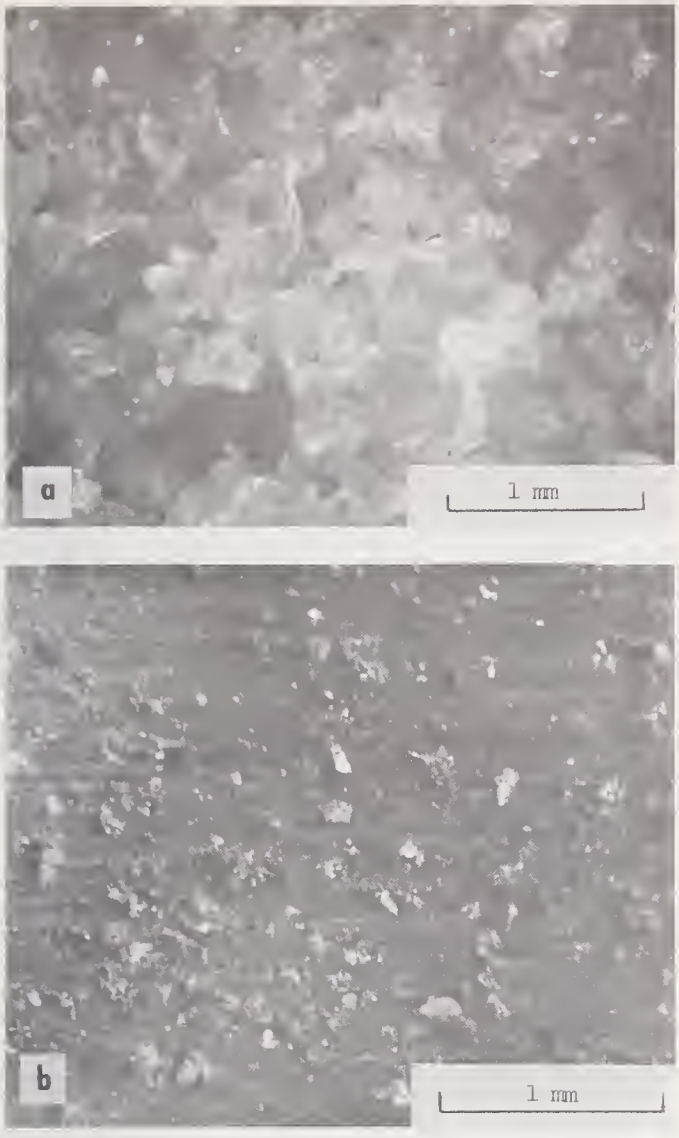

FIGURE 1. *Photomicrographs of the cutting faces of (a) a 46 grit vitrified bond alumina wheel and (b) a 100 grit, resinoid bond diamond wheel.*

chanical sawing and polishing to shape. The magnesium oxide crystals were annealed 1 hour at 1200 °C in air in order to pin all existing dislocations and to place the material in a uniform starting condition with respect to mechanical behavior [10].

3.2. Grinding Parameters

Samples were ground on a DoAll Model D618–7 high speed precision surface grinder. All grinding experiments were performed in the down (climb) grinding mode with the cutting face of the wheel moving in the same direction as the workpiece. Up grinding was not studied since some materials shattered. This problem was particularly severe with magnesium oxide crystals.

The wheel type is an important parameter in any grinding operation. Two wheels have been used in these studies; a 46 grit vitrified bond alumina wheel (Norton type AA–46–H8V40) and a 100 grit resinoid bond man made diamond wheel (DoAll type D1A1–MD100N100-B1/4B3). The alumina wheel is 17.8 cm in diameter and 12.7 mm wide and the diamond wheel is 15.2 cm in diameter and 3.18 mm wide. The wheels have significantly different structures as shown in figure 1. The structure of the alumina wheel is relatively open and many voids exist in the cutting surface. The cutting face on the diamond wheel, on the other hand, is relatively closed and consists of diamond abrasive points protruding from a continuous matrix.

Ground ceramic surfaces were characterized as a function of the machining parameters, wheel depth of cut (d) and workpiece feed rate (V). The spindle speed was fixed at 3540 rpm. Grinding was carried out both dry and wet using water containing water soluble oil in the ratio of 80:1 as a coolant.

The alumina wheel was dressed before each surface was ground. The diamond wheel, on the other hand, was dressed only at the beginning of the program. It was observed that this wheel did not readily load up during grinding. When grinding debris did appear on the wheel it was removed by wiping with a rag moistened in methanol.

Magnesium oxide, ferrite, and silicon were ground with both the alumina and diamond wheels. The harder ceramics were only machined with the diamond wheel.

The rate of material removal is a convenient parameter describing the severity of the grinding operation and is defined as the product (dVb) where b is the width of the area ground during each pass. Feed rates ranged from 0.042 to 4.2 cm/s (1 to 100 in/min) and depths of cut ranged from 12.7 to 508μm (0.0005 to 0.020 in). Typical rates of material removal employed with each wheel are listed below.

Wheel	b(mm)	d(μm)	V(cm/sec)	Rate of Material Removal (cm^3/sec)
46 grit alumina	12.7	25.4	0.042	1.36×10^{-4} — low
		25.4	0.42	1.36×10^{-3} — moderate
		50.8	4.2	2.72×10^{-2} — high
100 grit diamond	3.18	25.4	0.042	0.34×10^{-4} — low
		25.4	0.42	3.4×10^{-4} — moderate
		50.8	4.2	6.8×10^{-3} — high

4. Grinding Damage in Semibrittle Ceramics

4.1. Magnesium Oxide Single Crystals

As might be expected single crystal semibrittle ceramics undergo plastic deformation during grinding. However, it is found that the extent of deformation depends on the ability of the material to respond to the change in shape imposed by the grinding wheel. For this reason, it is necessary to distinguish between magnesium oxide crystals most favorably oriented for shear; i.e., those ground on {100} planes in <100> directions (see figure 2a) and other orientations less favorably oriented for shear (see figure 2b). Further distinctions will be made between subsurface and surface damage.

a. [100] Surfaces Ground in <100> Directions

Previously published results [11] have shown that the nature and extent of grinding damage in magnesium oxide crystals ground on {100} surfaces in <100> directions is a strong function of both wheel type and rate of material removal. Coolant was also noted to have an effect at high rates of material removal.

Subsurface damage was studied on {100} planes cleaved transverse to the ground surface and etched to reveal dislocations. Surface damage was characterized using conventional optical and replica electron microscopy techniques. The results are summarized below.

(a) Subsurface Damage. In all cases it was found that surface grinding resulted in the formation of a discrete, highly deformed layer immediately adjacent to the ground surface that could be observed as a dense band of dislocation etch pits. Examples of subsurface grinding damage in crystals ground wet at low rates of material removal on {100} surfaces in <100> directions with the alumina and diamond wheels are shown in figure 3. The uneveness of the damage layer in the crystal ground with the diamond wheel is attributed to the uneven nature of the impact of the protruding abrasive points on the cutting surface

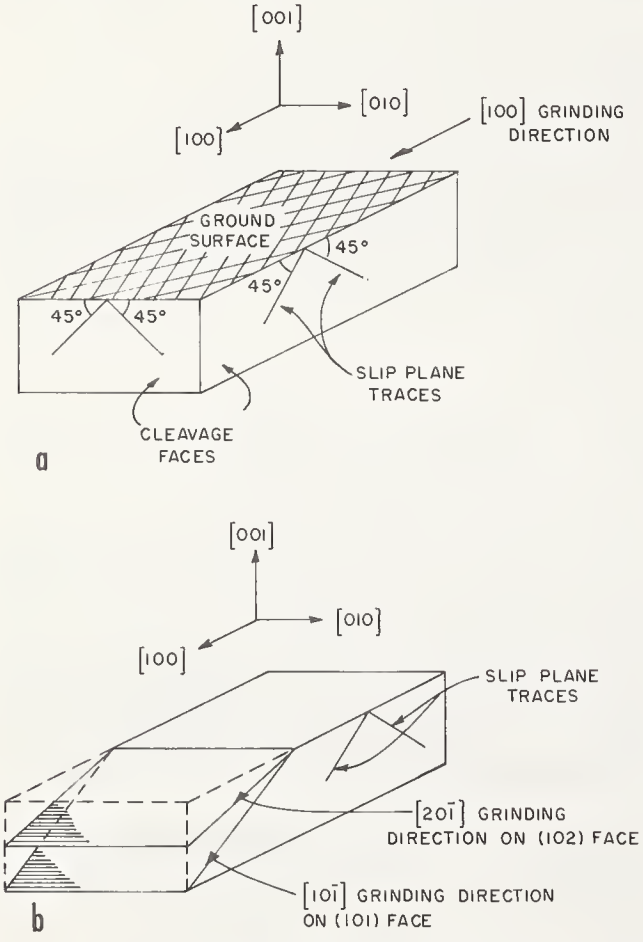

FIGURE 2. *Schematics showing the orientations in which magnesium oxide crystals were ground.* (a) {100} <100> orientation {100} cleavage faces and {110} slip planes favorably oriented for shear are indicated. (b) {110} <110> and {120} <120> orientations.

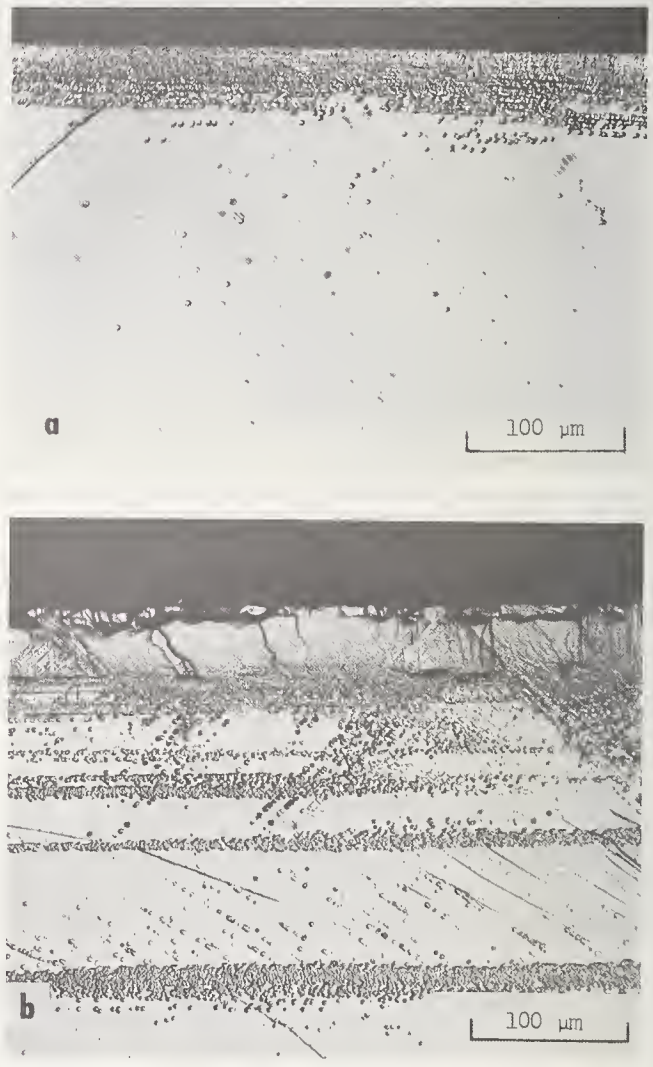

FIGURE 3. *Photomicrographs showing subsurface grinding damage on etched {100} cleavage faces of magnesium oxide crystals ground wet on {100} surfaces in <100> directions.* (a) 46 grit alumina wheel, $d = 25.4\mu m$, $V = 0.055$ cm/s. (b) 100 grit diamond wheel, $d = 25.4\mu m$, V = 0.042 cm/s.

of the diamond wheel. Cracks extending into the subsurface deformed layer were never observed in crystals ground in the {100} <100> orientation with either wheel.

The depth of the damage layer increased with material removal rate when the alumina wheel was used. Measurements of the average depth of the layer in crystals ground wet with the alumina wheel ranged from about 30μm at low rates of material removal to 100μm at high rates of material removal. In crystals ground dry with the alumina wheel the depth of damage ranged from about 30μm at low rates of material removal to 240μm at high rates of material removal. When the diamond wheel was used, the depth of damage remained relatively independent of grinding condition also converging to 30μm at low rates of material removal.

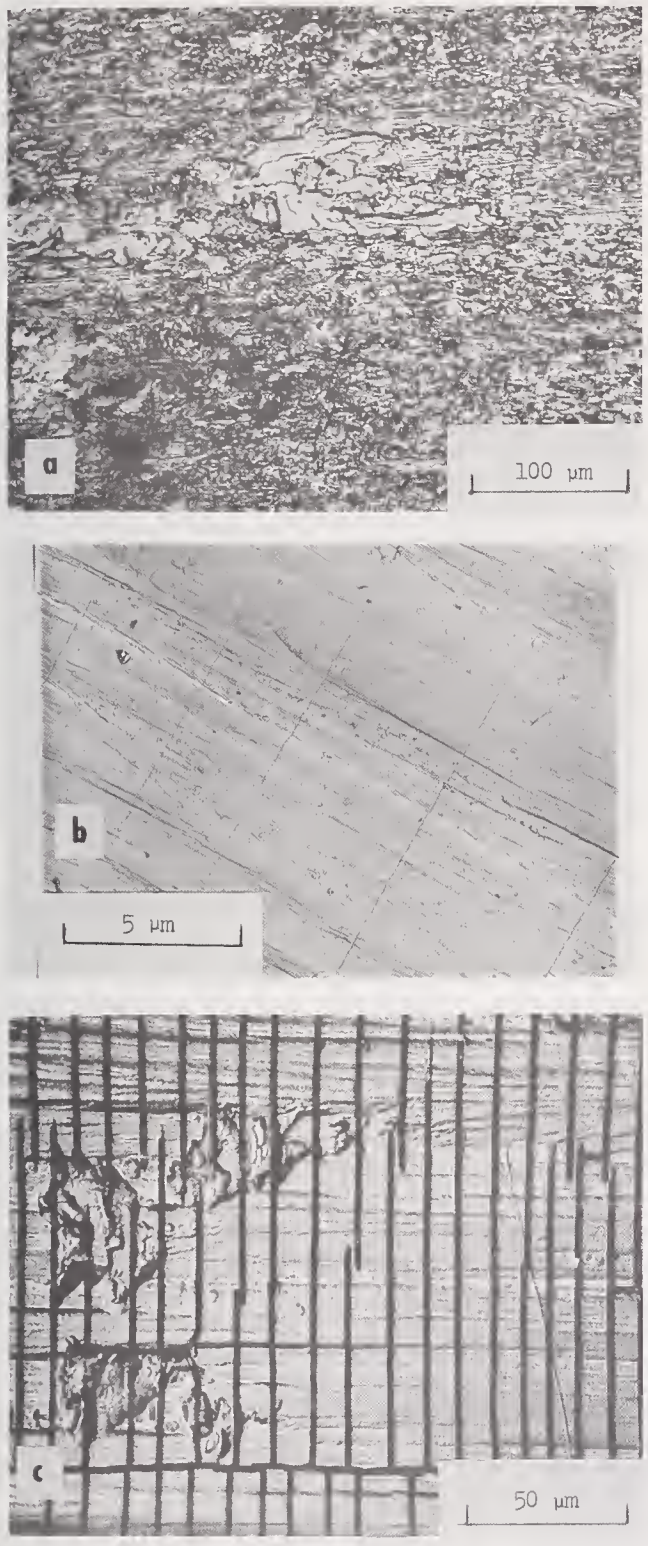

FIGURE 4. *Photomicrographs of {100} surfaces of magnesium oxide crystals ground wet in a <100> direction with a 46 grit alumina wheel at a low and high rate of material removal.* (a) Unetched, d = 25.4μm, V = 0.021 cm/s. (b) Unetched, d = 254μm, V = 0.34 cm/s. *(c)* etched, d = 254μm, V = 0.34 cm/s.

(b) Surface Damage. Crystals ground wet with the alumina wheel exhibited two surface characteristics depending on the rate of material removal. At low rates, (d = 25.4μm, V = 0.042 cm/sec), material was removed by brittle fracture resulting in a rough cleavage faceted surface (fig. 4a). When the rate exceeded that at which swarf could be expelled by the wheel, the voids in the open alumina wheel (fig. 1) loaded up. This prevented fresh cutting points on the wheel from impacting the surface of the workpiece. The frictional component of the grinding forces and the temperature at the surface increased to the point where material was removed by plastic flow. The resulting surface became extremely smooth and burnished as shown in the electron micrograph in figure 4b. This type of surface was observed at even the lowest rates of material removal when crystals were ground without coolant using the alumina wheel.

The regular array of fine cracks present on the surface, shown in figure 4b, resulted from thermal stresses set up when the hot, as-ground surface was quenched following passage of the wheel. Etching enhanced the appearance of the cracks as shown in figure 4c. The thermal cracks were quite shallow and were never found to extend into the subsurface damage layer. The shallow depth of thermal cracking is a strong indication of the steepness of the stress and temperature gradients existing under the wheel-workpiece interface during grinding.

The diamond wheel did not load up wet or dry, at any rate of material removal. Grinding with the diamond wheel always resulted in the typically rough surface shown in figure 5. The white areas on the micrograph are {100} cleavage facets lying parallel to the ground surface.

b. {100} Surface Ground in Other Directions

The effect of crystal orientation on the nature and extent of grinding damage in magnesium oxide crystals is being examined to help relate single crystal observations to machined polycrystalline ceramics. Also, as mentioned earlier, changing the orientation of single crystals leads to configurations less favorably or-

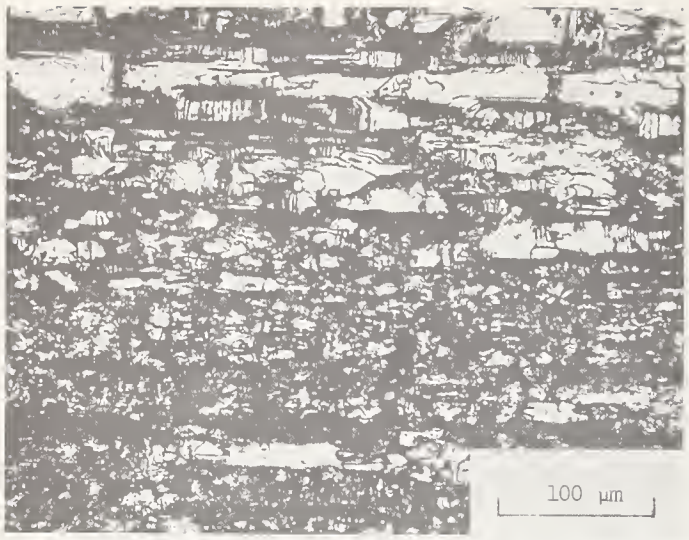

FIGURE 5. *Photomicrograph of the as-ground {100} surface of a magnesium oxide crystal ground wet with a 100 grit diamdond wheel in a <100> direction.* (d = 12.7μm, V = 0.42 cm/s).

ienting for plastic flow. In this series of experiments {100} crystal surfaces (i.e., the same surface as in section 4.1.a) were ground in <110> and <120> directions. In this case, all grinding was carried out wet. Again, the results with both alumina and diamond wheels were compared; however, grinding with the alumina wheel caused the specimens to shatter at all but the lowest rates of material removal.

(a) Subsurface Damage. The subsurface damage in crystals ground on {100} surfaces in directions other than <100> was essentially the same both in nature and extent to that observed on {100} surfaces ground in <100> directions. That is to say a discrete plastically deformed surface layer extending approximately 30 microns beneath the surface was

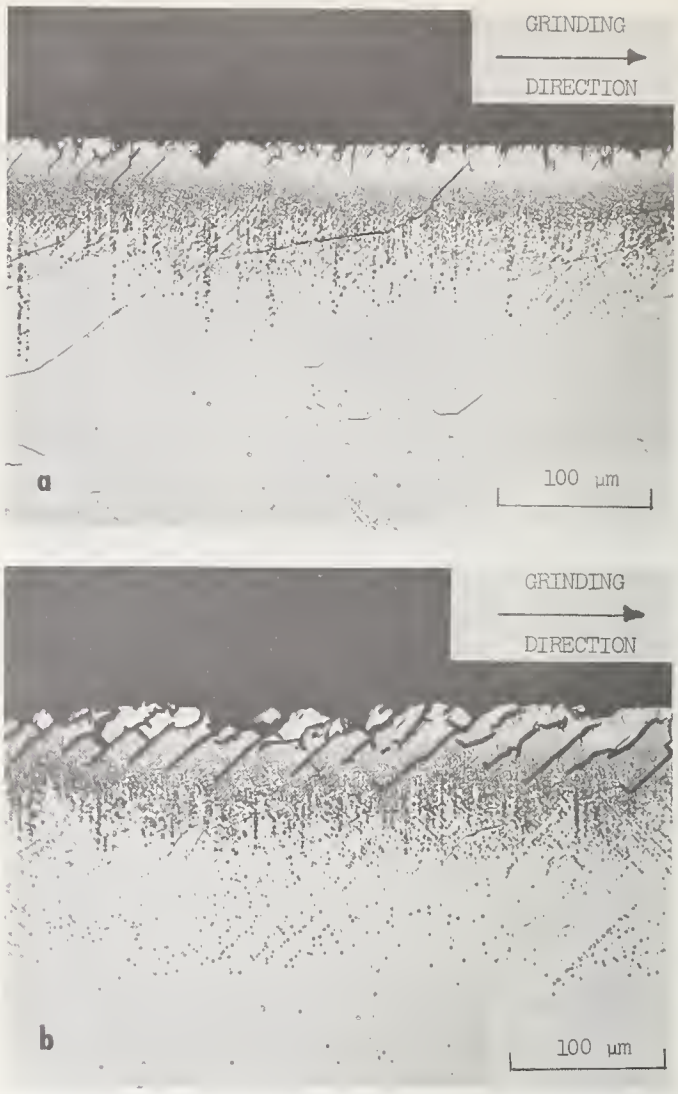

FIGURE 7. *Etched {100} cleavage faces showing subsurface grinding damage in magnesium oxide crystals ground wet on [110] surfaces in <110> directions.* (d = 25.4μm, V = 0.042 cm/s). (a) 46 grit alumina wheel, (b) 100 grit diamond wheel.

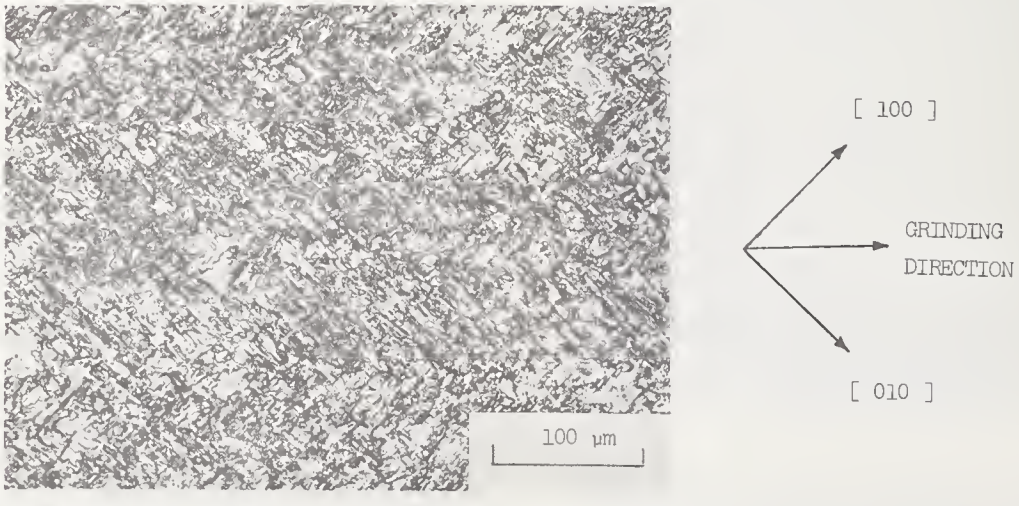

FIGURE 6. *As-ground {100} surface of a magnesium oxide crystal ground wet at a low rate of material removal in a <110> direction with a 46 grit alumina wheel* (d = 25.4μm, V = .042 cm/sec).

observed with the alumina wheel at low rates of material removal and with the diamond wheel at all rates of material removal. The depth of damage of crystals ground with the diamond wheel appeared to be relatively insensitive to both rate of material removal and to the direction of grinding.

(b) Surface Damage. The surfaces of these crystals ground with the alumina wheel at low rates of material removal were generally rough and contained large amounts of cleavage fracture. A typical example of a crystal ground on a $\bar{a}$ {100} surface in a <110> direction is shown in figure 6. It is interesting to note the strong {100} fracture morphology on the surface.

At intermediate and high rates of material removal with the alumina wheel crystals machined in both <110> and <120> directions shattered. Nevertheless examination of the ground areas of the shattered remnants always showed them to be burnished. Thus, for these orientations, as soon as the alumina wheel loaded and the grinding frictional forces increased, the crystals were not able to respond to the necessary change in shape by plastic deformation. Instead they shattered.

It is interesting to note that the transition to shattering was more dependent on the feed rate than on the depth of cut. This is evident from the observations listed below, where it can be seen that a five-fold increase in material removal rate (proportional to dV) resulted in shattering when it was achieved by increasing the feed rate but not when it was achieved by increasing the depth of cut.

Wheel	$d(\mu m)$	$V(cm/sec)$	$dV(cm^2/sec)$	*Grinding direction*	*Crystal shattered*
Alumina	25.4	0.042	1.07×10^{-4}	<110>	No
				<120>	No
Alumina	25.4	0.21	5.33×10^{-4}	<110>	Yes
				<120>	Yes
Alumina	127.0	0.042	5.33×10^{-4}	<110>	No
				<120>	No

c. {110} Surfaces Ground in <110> Directions and {120} Surfaces Ground in <120> Direction

The next step in this study of the effects of orientation on grinding damage in magnesium oxide crystals involved a change to different crystal faces. Specifically grinding was performed on the {110} and {120} planes in <110> and <120> directions respectively. Again, all grinding was carried out wet. Specimens with these surfaces were carefully prepared beforehand by grinding, polishing and annealing.

As figure 2b shows, {100} cleavage surfaces exist perpendicular to the ground surface and parallel to the grinding direction for both orientations. After grinding, specimens were cleaved on this plane and etched to determine the nature of the subsurface damage.

In agreement with the experience of section 4.1.b crystals could be successfully ground with the alumina wheel only at the lowest rates of material removal (d = 25.4μm, V = 0.042 cm/sc). On the other hand, the diamond wheel could be used at all rates of material removal without shattering the crystals.

(a) Subsurface Damage. The subsurface deformation in these crystals was quite similar in nature and extent to crystals ground in other orientations. Again, a discrete, heavily deformed layer existed under the ground surface. Typically, this layer was uniform in crystals ground with the alumina wheel and uneven in crystals ground with the diamond wheel.

The most striking difference from previous observations, however, was the extent of subsurface cracking. Damage layers in crystals ground on {100} and {110} surfaces were routinely found to contain extensive arrays of subsurface cracks. This is shown for crystals ground at a low rate of material removal in the {110} <110> orientation with the alumina and diamond wheels in figure 7. The cracks lie predominantly along {100} traces in both micrographs and extend to the bottom of the damaged layer in the crystal ground with the diamond wheel. Also note the tendency for the cracks in samples ground on {110} faces with the diamond wheel to slant preferentially in the direction that the wheel travels over the surface. Presumably this is due to the nature of the stress state at the wheel-workpiece interface.

Crystals ground on {120} faces also exhibited extensive subsurface cracking. The slip and crack geometry with respect to the ground surface in these crystals was more complicated as evident in figure 8.

It is an interesting point that the damage layers in crystals ground in the {110} <110> and {120} <120> orientations with the dia-

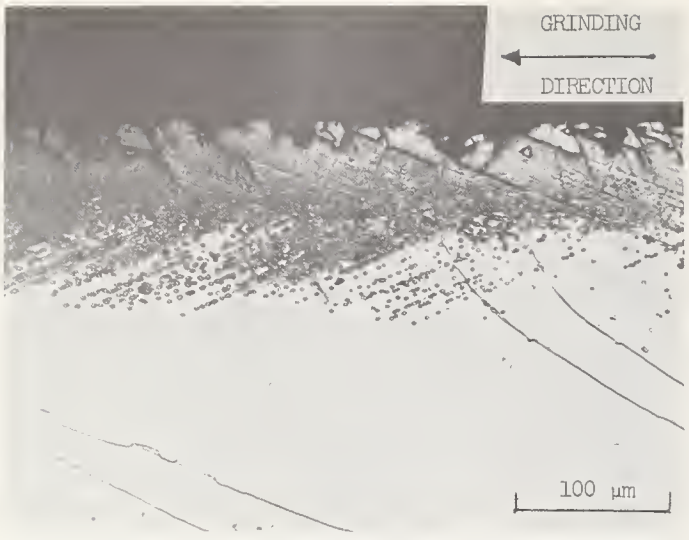

FIGURE 8. *Etched {100} cleavage face showing subsurface grinding damage in a magnesium oxide crystal ground wet on a {120} surface in a <120> direction with a 100 grit diamond wheel.* (d = 25.4μm, V = 4.2 cm/s).

mond wheel using heavy cuts (50.8 and 254μm) contained considerably fewer and shallower cracks than samples given 25.4μm cuts.

(b) Surface Damage. {110} and {120} surfaces ground with the alumina wheel at low rates of material removal were rough and produced by multiple cleavage faceting. At higher rates the specimens shattered, but the surfaces of the fragments indicated that burnishing had occurred prior to shattering.

{110} and {120} surfaces ground with the diamond wheel were typically rough and similar to that shown in figure 4 with the exception that {100} cleavage faces parallel to the ground surface were, of course, not observed.

4.2. Magnesium Oxide and Ferrite Polycrystals

The effects of material removal rate and wheel type on the nature of the surfaces of polycrystalline semibrittle ceramics ground using coolant have been examined for magnesium oxide and hot pressed Ni-Zn ferrite (see table 1). As expected from the results described above on magnesium oxide crystals, the alumina wheel could only be used successfully at low rates of material removal (d = 25.4μm, V = 0.042 cm/sec). At higher rates of material removal the samples shattered. These materials, on the other hand, could be ground quite successfully at all rates of material removal with the diamond wheel.

a. Subsurface Damage

No measurements or observations have yet been made of the subsurface damage introduced by grinding these polycrystalline materials. The depth of the subsurface damage in polycrystalline magnesium oxide machined with a diamond saw has been studied by Evans and Davidge [12] who noted that the maximum depth of flaw (cracks or grain pullouts) penetration depended on grain size. The depth of damage was observed not to exceed two grain diameters in material having grain sizes less than about 100μm and did not exceed one grain diameter in larger grain size material. Whether the machining was carried out wet or dry was not brought out in the paper.

b. Surface Damage

Examination of the ground surfaces of fragments from shattered specimens of polycrystalline magnesium oxide and ferrite ground wet with the alumina wheel indicated that extensive burnishing and thermal cracking had occurred in every case. This observation agrees qualitatively with those made on single crystals.

The as-ground surfaces of magnesium oxide polycrystals ground wet at a number of material removal rates with the diamond wheel showed little or no evidence of plastic flow or burnishing in agreement with the observations made on magnesium oxide single crystals. The major features of as-ground surfaces of semibrittle ceramics ground wet with a diamond wheel are illustrated in figure 9 which is an electron micrograph of a replica of the ground surface of a magnesium oxide polycrystal. Three types of surface feature are evident in figure 9, exposed grain boundaries, exposed grain boundary porosity, and brittle transgranular fracture. The top and bottom grains at the left side of the figure exhibit brittle transgranular fracture while the rest of the figure is composed of exposed grain boundaries resulting from grain pullout. An interesting feature of this micrograph is the slip lines in the grains exposed by the grinding operation. The presence of slip lines indicates the regions

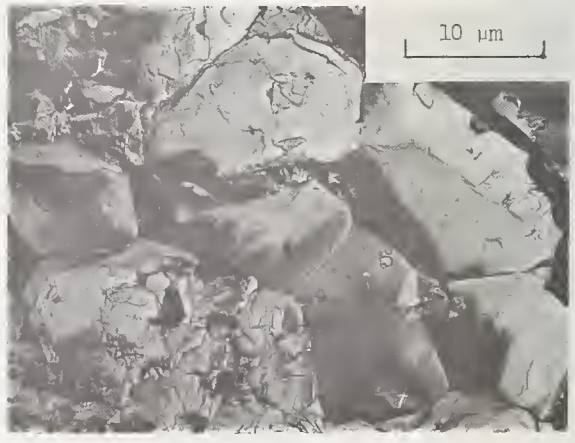

FIGURE 9. *Electron micrograph of a replica of the surface of polycrystalline magnesium oxide ground 50.8μm in successive 12.7μm cuts wet with a 100 grit diamond wheel.*

immediately adjacent to the machined surface of a semibrittle ceramic are plastically deformed. Similar features were observed on replicas of ground ferrite surfaces.

With regard to the effect of the severity of the machining treatment on the nature of ground surfaces of magnesium oxide and ferrite polycrystals, it was observed that an increased rate of material removal resulted in more grain pullout. Grain size can also affect the amount of pullout. In their observations on diamond sawed magnesium oxide polycrystals, Evans and Davide [12] observed that large grain samples exhibited less pullout than small grain material.

5. Grinding Damage in Brittle Ceramics

5.1. Silicon Single Crystals

In these experiments silicon crystals were ground on {111} faces in <110> directions with the 46 grit alumina and 100 grit diamond wheels at various rates of material removal. All grinding was carried out wet.

a. Subsurface Damage

In order to assess the nature and extent of grinding damage beneath the ground surface of silicon crystals an attempt was made to detect subsurface deformation by the etch pit technique. Following grinding, the crystals were cleaved on the {111} plane intersecting the {111} ground surface along a line lying parallel to the grinding direction. The cleavage faces were then etched using the Dash etch [13] and examined for evidence of dislocation etch pits. A number of attempts failed to reveal any dislocation etch pits that could positively be identified with the ground surface and it was concluded that the deformation, if any, produced by surface grinding either does not extend to measurable depths beneath the ground surface or cannot be detected on {111} cleavage faces by the etch pit technique. Stickler and Booker [14] have shown conclusively by transmission electron microscopy that discrete dislocation arrays can be introduced as far as 14μm below the {111} surface of silicon crystals by abrading with No. 240 SiC paper. These arrays are associated with individual cracks and cannot be detected by etch pit techniques because of their close (100Å) spacing. Thus, it appears likely that there is a subsurface damage layer in silicon, but its extent is considerably less than observed in magnesium oxide crystals.

b. Surface Damage

Silicon crystals ground wet with the alumina and diamond wheels exhibited quite different

FIGURE 10. *Photomicrographs of {111} surfaces of silicon single crystals ground in <110> directions wet with a 46 grit alumina wheel at two rates of material removal.* (a) $d = 25.4\mu m$, $V = 0.042$ cm/s (b) $d = 25.4\mu m$, $V = 0.42$ cm/s.

surfaces. {111} surfaces ground with the alumina wheel were burnished as shown in figure 10. The light regions on the micrographs are islands of burnished material. Comparison of the two micrographs in figure 10 shows that increasing the rate of material removal results in an increase in burnished area, as expected. Grinding with the diamond wheel at all rates of material removal resulted in rough surfaces produced by brittle, cleavage or conchoidal fracture. Burnishing was not observed.

5.2. Alumina Polycrystals

In these experiments three kinds of polycrystalline alumina (see table 2) have been ground with the 100 grit diamond wheel. (Naturally, grinding with an alumina wheel was impossible.) Grinding was carried out both wet and dry. The ground surfaces were characterized by optical microscopy and by replica electron microscopy.

439-921 O - 72 - 22

a. Subsurface Damage

No attempt was made to characterize the depth of damage in polycrystalline alumina during this study. Hockey [15], however, has examined single and polycrystalline alumina mechanically polished through 0.25μm diamond by transmission electron microscopy and has noted that the damage extended less than 3μm below the polished surface. Furthermore, the damage consisted of a shallow, highly deformed surface layer containing dense arrays of dislocation half-loops associated with scratches left by the abrasive particles.

b. Surface Damage

A most surprising feature of polycrystalline alumina surfaces ground with a diamond wheel was that they routinely contained regions of burnished material. Figures 11, 12, and 13 show optical and electron micrographs of the surfaces of Lucalox, AVCO, and Coors alumina respectively ground dry using a 25.4μm cut at a feed rate of 0.42 cm/sec.

The light areas on the optical micrographs are burnished regions that correspond to the regions on the electron micrographs containing closely spaced parallel grooves. This has been observed by others [16, 17] and appears to be a common feature of alumina surfaces ground with a diamond wheel.

The dark areas on the optical micrographs correspond to regions in which material has been removed by brittle transgranular or intergranular fracture (pullout). These regions are self-evident on the electron micrographs. There appears to be more extensive burnishing in the AVCO and Coors aluminas than in Lucalox. This could be related to the small grain size (2μm) of these materials as compared with the Lucalox (38μm).

The surfaces of alumina samples ground wet contained features identical to those ground dry (i.e., burnishing, transgranular and intergranular fracture). It was generally noted, however, that the amount of burnishing decreased when a coolant was used.

5.3. Boron Carbide Polycrystals

a. Subsurface Damage

No attempt was made to characterize the depth of damage in polycrystalline boron carbide.

b. Surface Damage

Optical and electron micrographs of the surface of polycrystalline boron carbide ground dry with the diamond wheel (d = 25.4μm, V = 0.42 cm/sec) are shown in figure 14. The optical micrograph indicates that the major features of the ground surface are similar to

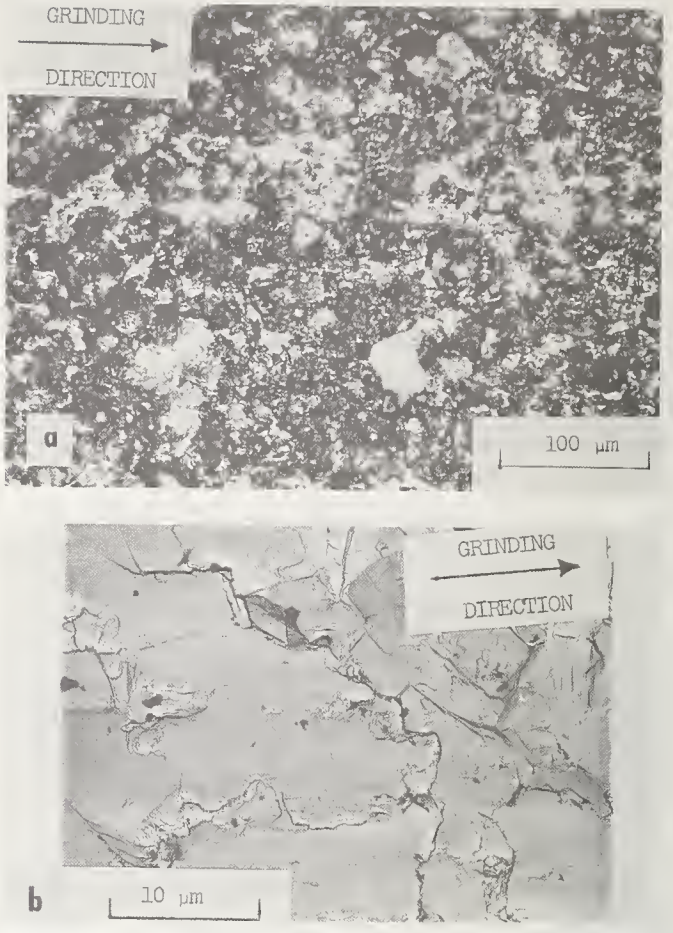

FIGURE 11. *Optical and electron micrographs of the surface of G.E. sintered (Lucalox) alumina ground dry with a 100 grit diamond wheel (d = 25.4μm, V = 0.42 cm/sec).* Grain size 38μm.

those exhibited by polycrystalline alumina; namely, light burnished areas and dark areas where material has been removed by brittle fracture. The electron micrograph, however, illustrates some notable differences. Large portions of the fracture surfaces in areas that are not burnished are conchoidal in appearance and have no size relationship to the grain size of the material. In fact, the surface closely resembles that of Pyrex glass ground with a similar wheel [16]. Material appears to have been removed as flakes lying parallel to the ground surface. Although portions of the surface show slight indications of grain boundaries (see arrow in figure 14) clear cut evidence of grain pull-out has not been observed.

Again, it was noted that boron carbide surfaces ground both dry and wet contained identical features, but that those ground with a coolant contained fewer and smaller regions of burnished material.

6. Discussion of Results

Results of this assessment of surface damage introduced during surface grinding on various ceramic materials are summarized in tables 3,

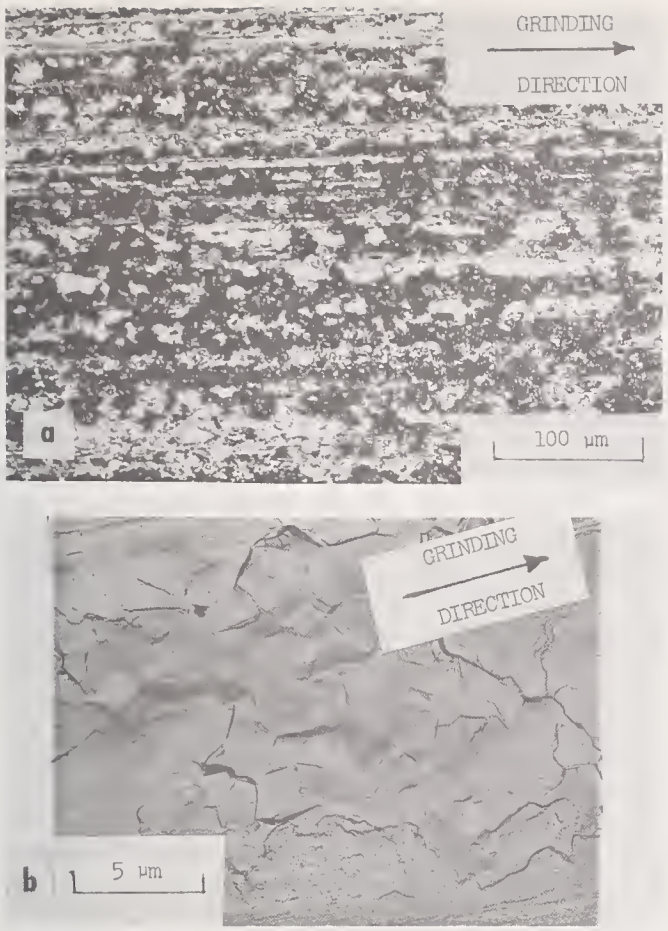

FIGURE 12. *Optical and electron micrographs of the surface of AVCO hot pressed alumina ground dry with a 100 grit diamond wheel* (d = 25.4μm, V = 0.42 cm/s). Grain size 2μm.

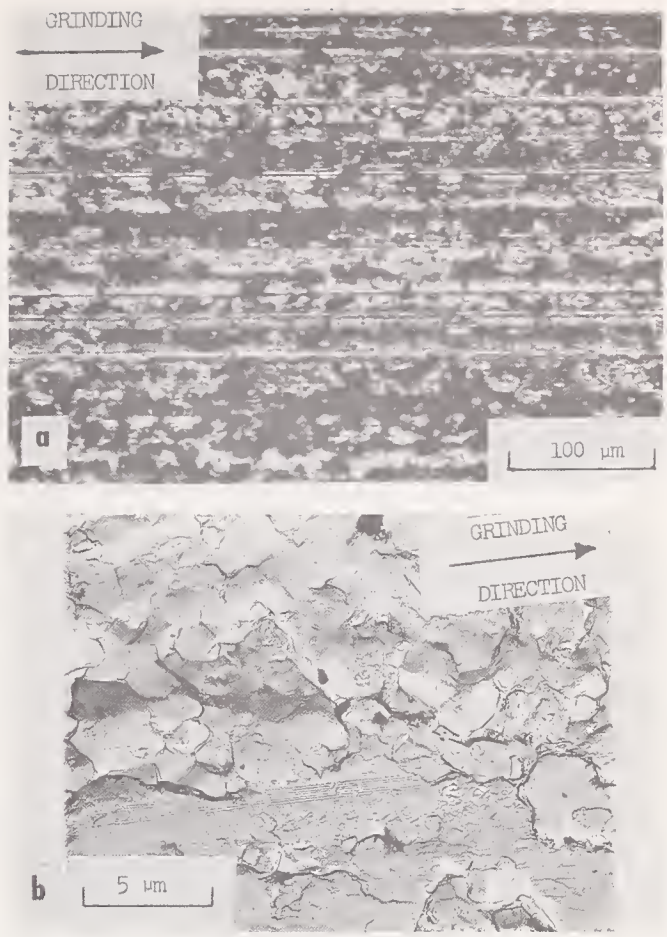

FIGURE 13. *Optical and electron micrographs of the surface of Coors AD999 cold pressed and sintered alumina ground dry with a 100 grit diamond wheel.* (d = 25.4μm, V = 0.42 cm/s). Grain size 2μm.

TABLE 3. *Summary of observations made on ground magnesium oxide crystals*

Orientation	Wheel	Rate of material removal	a. Nature of ground surface b. Mechanism of material removal	Nature of subsurface damage
(100) <100>	Alumina	Low	a. Rough	Discrete plastically deformed layer.
			b. Brittle fracture	No subsurface cracks.
		Moderate	a. Smooth and burnished. Thermal cracking.	Discrete plastically deformed layer.
			b. Plastic flow	No subsurface cracks.
	Diamond	All	a. Rough	Uneven plastically deformed layer.
			b. Brittle fracture	No subsurface cracks.
(100) <110> (100) <120>	Alumina	Low	a. Rough	Discrete plastically deformed layer.
			b. Brittle fracture	No subsurface cracks.
		Moderate	Workpiece shattered	
	Diamond	All	a. Rough	Uneven plastically deformed layer.
			b. Brittle fracture	No subsurface cracks.
(110) <110> (120) <120>	Alumina	Low	a. Rough	Uneven plastically deformed layer.
			b. Brittle fracture	Subsurface cracks.
		Moderate	Workpiece shattered	
	Diamond	All	a. Rough	Uneven plastically deformed layer.
			b. Brittle fracture	Subsurface cracks.

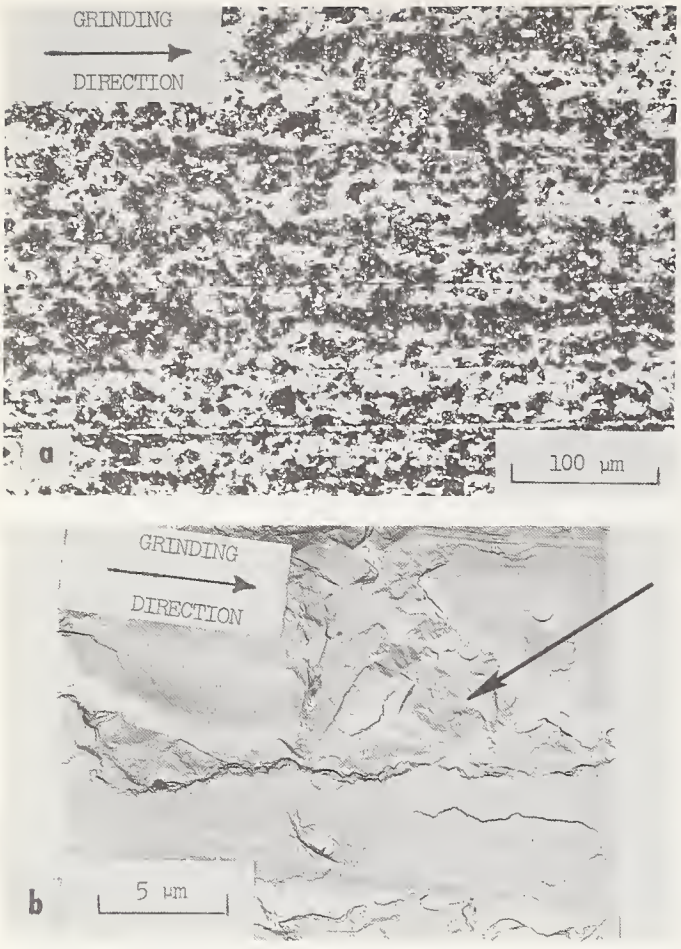

FIGURE 14. *Optical and electron micrographs of the surface of AVCO hot pressed boron carbide ground dry with a 100 grit diamond wheel.* (d = 25.4μm, V = 0.42 cm/s). Grain size 2μm.

4 and 5 for magnesia single crystals, silicon single crystals and polycrystalline ceramics respectively. It can be appreciated that a great variety of surface conditions can be generated varying from smooth burnished surfaces to rough fractured surfaces. The process of material removal responsible for these surfaces is complex. It is a consequence of the interplay between factors relating to the grinding operation itself, such as wheel type and rate of material removal, and to the microstructure and mechanical properties of the workpiece.

It has been pointed out [11] that the stress fields under a grinding wheel can be considered to be of two types; short range and long range. The short range stresses act at the wheel-workpiece interface and arise from the direct interaction of the cutting points with the material. Long range stresses arise from the fact that the workpiece is essentially being forced between the grinding wheel and the bed of the machine. Long range stresses are at a minimum when the wheel is removing material efficiently, but if the grinding wheel should become loaded and operate inefficiently, the long range stresses increase. They must then be relaxed in some manner by deformation of the specimen or the grinding system, if not the workpiece or tool will shatter. Relief of long range stresses by plastic deformation of the specimen is rarely observed in ceramics since they are not easily deformed at low temperatures. It is for this reason that many of the specimens in this study shattered when machined with the alumina wheel at moderate removal rates.

At this stage it is not possible to make any quantitative statements concerning the relative magnitudes of the short and long range stresses. Efforts are, however, being made to monitor them. In discussing the origins of surface damage in machined ceramics it is best for the moment to consider each material separately.

6.1. Magnesium Oxide Single Crystals

Magnesium oxide is an example of a semi-brittle ceramic which shows limited room temperature and extensive high temperature plasticity. Grinding magnesium oxide with an alumina wheel leads to interesting observations at moderate and high removal rates. Under these conditions, the alumina wheel loads up and fresh cutting points are prevented from impacting the workpiece, the frictional forces and therefore, the temperature at the interface increases. Because magnesium oxide is completely plastic at high temperatures (table 1) material removal occurs entirely by plastic flow leaving a completely burnished surface. Thermal quenching after the machining operation is responsible for the fine cracking also observed on the surfaces (see figure 4).

TABLE 4. *Summary of observations made on ground silicon crystals*

Orientation	Wheel	Rate of material removal	a. Nature of ground surface b. Mechanism of material removal	Nature of subsurface damage
(111) <110>	Alumina	All	a. Mixed. Burnished regions and regions containing brittle fracture. b. Plastic flow and brittle fracture.	Not detectable by etch pit techniques.
		Moderate	Workpiece shattered.	
	Diamond	All	a. Rough. b. Brittle fracture.	

TABLE 5. *Summary of observations made on ground polycrystalline ceramics*

Material	Wheel	Rate of material removal	a. Nature of ground surface b. Mechanism of material removal
Magnesium Oxide	Alumina	Low	a. Rough. Some burnished areas. b. Grain pullout, transgranular fracture, and plastic flow.
		Moderate	Sample shattered.
	Diamond	All	a. Rough. b. Grain pullout and transgranular fracture.
Ferrite	Alumina	Low	a. Heavily burnished, some rough areas. b. Plastic flow, grain pullout and transgranular fracture.
		Moderate	Sample shattered.
	Diamond	All	a. Rough. b. Grain pullout and transgranular fracture.
Lucalox sintered alumina	Diamond	All	a. Rough. Some burnishing. b. Grain pullout, transgranular fracture, and plastic flow.
AVCO hot pressed alumina	Diamond	All	a. Rough. Some burnished areas. b. Grain pullout, transgranular fracture, and plastic flow.
Coors AD999 cold pressed and sintered alumina	Diamond	All	a. Rough. Some burnished areas. b. Grain pullout, transgranular fracture, and plastic flow.
AVCO hot pressed boron carbide	Diamond	All	a. Rough. Some burnished areas. b. Conchoidal fracture and plastic flow.

Magnesium oxide crystals oriented for machining over {100} surfaces in <100> directions provide a rare opportunity for a ceramic to relieve long range grinding stresses by plastic deformation (section 4.1.a). It has been pointed out that for this orientation the crystal is ideally oriented and can achieve the necessary change in shape by shear over {110} <110> slip systems. It is significant that as soon as the orientation is shifted slightly away from this ideal orientation the necessary shape change cannot be accomplished by shear and the crystals shatter as soon as the wheel loads up and burnishing commences (sections 4.1.b and 4.1.c).

When material is being removed efficiently, as is the case with the alumina wheel wet at low removal rates and the diamond wheel wet or dry at all removal rates, the machined surface is generated by the initiation and propagation of {100} cleavage cracks due to the impact of the cutting points. This is attributed to the low impact resistance of magnesium oxide. For {100} machined surfaces, cleavage leads to flaking off of material and cracks do not penetrate the surface (section 4.1.a); for {110} and {120} machined surfaces however cleavage planes are inclined to the surface and subsurface cracking is produced (sections 4.1.b and 4.1.c).

The effect of the grinding fluid is difficult to assess from these limited observations. Clearly, the fluid prevented burnishing in crystals ground with the alumina wheel in the {100} <100> orientation at low rates of material removal by acting to enhance the removal of swarf thereby preventing wheel load up. On the other hand, material was efficiently removed by brittle fracture with the diamond wheel at all rates of material removal whether a fluid was used or not. In this case, the fluid apparently did not play a role. There is no doubt that the environment can affect the fracture strength and grinding efficiency of many materials (see Westwood, this volume) but from our results it does not appear that water containing soluble oil has that effect on magnesium oxide.

A study of the effects of different fluids on the grinding characteristics of magnesium oxide is currently underway in our laboratory.

6.2. Silicon Single Crystals

Silicon is an example of a material which is brittle at room temperature but can deform on five independent slip systems at high temperatures. Correspondingly, when silicon crystals are ground with the alumina wheel, the surfaces are partially burnished (see figure 10) due to high temperature flow. The extent of burnishing increases with the rate of material removal until eventually the crystals shatter. Shattering occurs because silicon cannot relieve long range stresses by plastic flow. Normally, the long range stresses must be relieved in some other manner. The rough patches of conchoidal fracture in figure 10 indicate that material is being removed in a brittle manner by

impact in addition to burnishing. It is presumed that by this semiefficient method, the long range stresses are relaxed.

Machining silicon with the diamond wheel results in a rough surface generated entirely by impact fracture. Again this is attributed to be low impact resistance of this material in single crystal form.

6.3. Polycrystalline Magnesium Oxide and Ferrite

For reasons indicated in section 6.1. polycrystalline magnesium oxide cannot undergo plastic deformation to relax long range stresses and thus as soon as the alumina wheel loads up and burnishing starts, the specimens shatter.

With efficient machining conditions, i.e., with the diamond wheel, workpiece integrity is maintained. The machined surfaces of polycrystalline magnesia and ferrite are rough and contain predominantly intergranular fracture (section 4.2.). This is attributed to the low impact resistance of these materials.

Subsurface cracking was observed in magnesium oxide crystals ground in all but the "ideal" {100} <100> orientation and is an expected feature of machined polycrystalline semibrittle ceramics. This has been found to be the case in polycrystalline magnesium oxide by Evans and Davidge [12].

The presence of subsurface dislocations also appears to be a general occurrence in semibrittle ceramics. Evidence of a subsurface deformed layer in machined polycrystalline ferrite has, in fact, recently been noted [2, 21].

6.4. Polycrystalline Alumina

Alumina is an example of a brittle ceramic which does not have the necessary slip systems to become completely plastic at high temperatures.

The surprising feature of the polycrystalline aluminas studied here is that burnishing is observed as well as transgranular and intergranular fracture on surfaces machined with the diamond wheel. (Semibrittle ceramics do not show burnishing when machined with the diamond wheel.) These observations are attributed to the fact that alumina has a higher impact resistance than magnesia. Consequently, efficient material removal does not occur by fracture alone, there is in addition localized plastic flow due to the high stresses existing under the diamond cutting points.

Alumina can be deformed at room temperature by abrasive particles [15] and diamond hardness indenters [18] so the presence of limited plastic flow is not surprising. What is surprising, however, is that large regions are deformed. Possibly the extra degree of freedom afforded by the free surface allows gross deformation even if less than five independent slip systems are operating. Furthermore, the localized grinding temperatures are expected to be high thereby enhancing the deformation process. Gielisse and Stanislao [19] have, in fact, noted white hot illumination to accompany the impact of a diamond particle on a grinding wheel with an alumina surface.

More fracture and pullout was observed in the larger grain size Lucalox than in smaller grain size AVCO and Coors material. This presumably reflects the decrease in impact resistance with increase in grain size in alumina. Note that this is opposite to observations on magnesium oxide cut with a diamond saw [12] which indicate the amount of pullout to decrease with increasing grain size.

The effects of wheel dressing on the nature of ceramic surfaces ground with the diamond wheel was not examined in this study. Since dressing increases the density of sharp edges on the abrasive particles in the cutting face of the wheel, the incidence of brittle fracture would no doubt be enhanced. This would decrease the amount of burnishing observed. The use of a grinding fluid did decrease the incidence of burnishing in brittle ceramics ground with the diamond wheel. Whether this effect is due to surface flushing, interface cooling, or other factors is not known.

6.5. Boron Carbide

Boron carbide surfaces are also extensively burnished by diamond machining (see figure 14) again indicating a high impact resistance and tendency to flow under the high short range stresses imposed by the diamond points. Relaxation of long range stresses occurs by the removal of flakes of material by brittle fracture. It is significant that the fracture surfaces of these flakes in this material are conchoidal and bear no clear relationship to the grain structure. This is further indication of the high intergranular strength and resistance to impact of this material. The effect of a coolant on the nature of the ground surface of boron carbide is identical to that observed in the experiments on alumina.

Alumina and boron carbide surfaces ground with the diamond wheel contained patches of burnished material and patches where material had been removed by brittle fracture. This observation allows one to speculate on the sequence of events occurring at the wheel workpiece interface during a grinding pass. Two possibilities exist. On the one hand, material may be initially removed efficiently by brittle fracture and then patches on the surface load up periodically with grinding debris which burnish. On the other hand, during grinding

burnishing could be occurring over the whole wheel workpiece interface as a result of the high short range stresses set up due to the combined effect of debris in the wheel and high mechanical strength of the workpiece. Burnishing is only a surface effect. To relieve long range stresses larger amounts of material must be removed. This happens when portions of the burnished surface flake off. This process is enhanced by the large temperature and stress gradients existing in the workpiece during grinding. When a patch of burnished material flakes off a patch where material has been removed by brittle fracture remains thus accounting for the observations made in this study on ground brittle ceramics. These flakes are quite large in comparison with the theoretical chip size further indicating they are a result of the long range stress fields in the workpiece. No doubt judicious dressing procedures and light machine settings could decrease or eliminate the burnishing observed in this study if necessary. It is not clear, at the present time, however, if the presence of burnished patches on the machined surface of a brittle ceramic is detrimental.

7. Conclusions

On the basis of the work reported here there appears to be three broad categories of behavior during ceramic machining.

First, there is the burnishing behavior observed on soft, plastically deformable ceramics ground with a loaded wheel, exemplified by {100} magnesia single crystals. Under these conditions the surface of semibrittle ceramics is generated entirely by plastic flow (although there are fine surface cracks due to thermal quenching).

Second, there is the brittle fracture surface observed on brittle (or semibrittle) ceramics of low impact resistance, exemplified by single and polycrystalline magnesia and ferrite ground with a diamond wheel. Under these conditions the surface of these materials is generated entirely by brittle transgranular and intergranular fracture.

Third, there is the mixed, burnished and fractured surface observed on brittle ceramics of high impact resistance ground with a diamond wheel exemplified by polycrystalline alumina and boron carbide. In these materials the extremely high local short range stresses remove material by plastic flow while the long range stresses are relaxed by brittle intergranular or conchoidal fracture.

Further research is concentrating on substantiation of the ideas expressed here, with emphasis on direct measurement of the stresses and temperatures involved and better characterization of the ground surfaces produced.

The author is indebted to Dr. R. J. Stokes for invaluable discussions and to D. Woodward for able experimental assistance during the course of this research. The continued interest of Dr. C. H. Li, Director, Honeywell Corporate Research Center, and Dr. A. Diness, Office of Naval Research, is gratefully acknowledged. This work was supported by the Office of Naval Research.

8. References

[1] Ceramic processing, pp. 134–173 (Publication 1576, National Academy of Science, Washington, D.C., 1968).

[2] Stokes, R. J., p. , these Proceedings.

[3] Stokes, R. J., Mechanical behavior of polycrystalline ceramics, Ceramic Microstructures, Ed. R. M. Fulrath and J. A. Pask, pp. 379–405, (John Wiley and Sons, Inc., New York, New York, 1968).

[4] Stokes, R. J., Fracture of ceramics, Fund. Phen. Mat. Sci. 4, 151–175 (1967).

[5] Day, R. B., and Stokes, R. J., Grain boundaries and the mechanical behavior of magnesium oxide, Mat. Sci. Res. 3, 355–386 (1966).

[6] Choi, D. M., and Palmour III, H., Fractographic evidence of multiple slip in deformed hot-pressed spinel, Mat. Sci. Res. 3, 473–482 (1966).

[7] Pearson, G. L., Read, W. T. and Feldmann, W. L., Deformation and fracture of small silicon crystals, Acta Met. 5, 181–191 (1957).

[8] Wachtman, J. B., Jr., and Maxwell, L. H., Plastic deformation of ceramic-oxide single crystals: II, J. Amer. Ceram. Soc. 40, 377–385 (1957).

[9] Fitzgerald, L. M., The hardness at high temperature of some refractory carbides and borides, J. Less-Common Metals 5, 356–364 (1963).

[10] Stokes, R. J., Thermal mechanical history and the strength of magnesium oxide single crystals: I, Mechanical tests, J. Amer. Ceram. Soc. 48, 60–67 (1965).

[11] Koepke, B. G., and Stokes, R. J., A study of grinding damage in magnesium oxide single crystals, Journ. Mat. Sci. 5, 240–247 (1970).

[12] Evans, A. G., and Davidge, R. W., The strength and fracture of fully dense polycrystalline magnesium oxide, Phil. Mag. 20, 373–388 (1969).

[13] Dash, W. C., Dislocations in Si and Ge crystals, Prop. of Elemental and Compound Semi-conductors, Metallurgical Society Conf. Vol. 5, p. 195 (Interscience Publishers Inc., New York, 1960).

[14] Stickler, R., and Booker, G. R., Surface damage on abraded silicon specimens, Phil. Mag. 8, 859–876 (1963).

[15] Hockey, B. J., p. , these Proceedings.

[16] Sedlacek, R., Processing Ceramics-Surface Finishing Studies, Final Technical Report under Contract No. N00019–67–C–0494, Stanford Research Institute, Nov. 1969.

[17] Ida, I., Arai, Y., and Inamori, K., Grinding characteristics of ceramics for circuit components with a metal bonded diamond wheel, presented at the 1968 General Meeting of C.I.R.P. at Birmingham, Great Britain.

[18] Hurley, G. F., Observation of plastic deformation in sapphire base ceramics, Met. Trans. 1, 2029–2031 (1970).

[19] Gielisse, P. J., and Stanislao, J., Material re-

moval phenomena in ceramics, Final Technical Report under Contract No. N00019–69–C–0131, Univ. of Rhode Island, Dec. (1969).
[20] Newey, C.W.A., and Radford, K. C., Plastic deformation of magnesium aluminate single crystals, Anisotropy in Single Crystal refractory compounds, Vol. 2, Ed. F. Vahldiek and S. Mersol, pp. 321–338 (Plenum Press, New York, New York 1968).
[21] Knowles, D., The effect of surface grinding upon the permeability of manganese-zinc ferrites, J. Phys. D: Appl. Phys. 3, 1346–1351 (1970).

Discussion

MILLER: Why did you select a 100 mesh wheel? Were you deliberately trying to establish certain stresses?

KOEPKE: We used a 100 grit wheel to produce surfaces representative of rough or semi-finish grinding operations.

UNIDENTIFIED: You emphasized, or pointed out at least, the effect of plastic flow. There can be a tremendous difference between conventional and climb grinding in that respect. Which one did you use?

KOEPKE: In all cases we used climb grinding, i.e., the cutting face of the wheel was moving in the same direction as the workpiece. For this reason the chips could not be examined. Since up-grinding resulted in shattering of the workpiece in many cases, we felt the compressive stresses set up during climb grinding would aid in preventing workpiece fracture. This, in fact, turned out to be the case.

UNIDENTIFIED: How much or to what extent can one attribute shattering to chip crowding?

KOEPKE: When a grinding wheel loads up the grinding forces rise very rapidly. In our experiments shattering almost always occurred under a loaded wheel. The 100 grit diamond wheel did not readily load up. As a result, unreasonably high rates of material removal were needed to shatter a workpiece with this wheel.

NATIONAL BUREAU OF STANDARDS SPECIAL PUB. 348, THE SCIENCE OF CERAMIC MACHINING AND SURFACE FINISHING, Proceedings of a Symposium Sponsored by the American Ceramic Society, the Office of Naval Research, and the National Bureau of Standards, held at NBS Nov. 2–4, 1970, Gaithersburg, Md. (Issued May 1972).

Observations on Mechanically Abraded Aluminum Oxide Crystals by Transmission Electron Microscopy

Bernard J. Hockey

National Bureau of Standards, Washington, D.C. 20234

Use of the argon ion-bombardment thinning technique has made possible the examination of the near surface regions of mechanically abraded aluminum oxide by transmission eletron microscopy. Observations on diamond-polished (0.25μm). alumina-polished (0.3μm), and diamond-ground specimens have shown that subsurface damage as well as surface damage is typically produced.

Specifically, mechanical polishing introduces relatively high densities of dislocations to a depth of approximately 1μm from the original surface. The dislocations are generally in the form of half-loops and are clearly associated with surface scratches produced by individual abrasive particles.

The magnitude of residual surface stresses and the irregular surface topography produced by grinding necessitated the removal of at least 2–4μm from the original surfaces. At this depth, both the nature and extent of subsurface damage in polycrystals varied from grain-to-grain. Most grains contained either tangled dislocation arrays or microtwins (either basal and rhombohedral). A number of grains, however, were found to be completely free of damage and may correspond to regions below fracture surfaces which are apparent in observations of ground surfaces by scanning electron microscopy.

Key words: Abrasion; aluminum oxide; dislocations; ion-bombardment; microtwins; scanning electron microscopy; subsurface damage; transmission electron microscopy.

1. Introduction

Despite the extensive use of mechanical abrasion in the fabrication and surface finishing of ceramic materials, there have been few studies on the exact nature and extent of damage produced. Such studies are of considerable value, not only because the residual damage can be related to the basic mechanisms involved during abrasion, but because of the dependence of mechanical behavior on surface perfection.

Abrasive damage is generally classified into two types; (1) surface damage, consisting of cracks and flaws (scratches, notches, "pull-outs", etc.) and (2) subsurface damage, consisting of lattice defects, such as dislocations and microtwins. Because most ceramics can be classified as either "semi-brittle" or "completely-brittle", surface-type damage is commonly produced to an extent which depends upon the particular material and abrasive action employed. Subsurface damage, on the other hand, is generally thought to occur in "semi-brittle" materials for which plastic deformation is known to occur at normal ambient temperatures. The existence of extensive subsurface damage in these materials as a result of abrasion has been well demonstrated by observations on MgO [1, 2][1]. In contrast, previous studies on scratched [3, 4], fully abraded [5], or "wear" surfaces [6, 7] of aluminum oxide, which is considered "completely-brittle", have produced only limited evidence suggesting at most the generation of isolated dislocations or microtwins during abrasion. The results obtained in these studies, while informative, were based exclusively on optical examination of as-abraded or etched abraded surfaces.

For this reason, transmission electron microscopy has been employed in the present study to show directly the full nature and extent of subsurface damage produced in aluminum oxide by abrasion. Three surface finishing treatments were used in the preparation of specimens. These were: (a) grinding with a resin-bonded wheel (325 diamond grit), (b) diamond polishing (0.25 μm diamond grit), and (c) alumina polishing (0.30 μm alumina powder). Examination of the near surface regions by transmission electron microscopy was made possible by using ion bombardment [8] to produce the required thinned sections. This technique was previously used to thin aluminum oxide crystals in a controlled manner so that the regions surrounding and underlying hardness indentations could be examined by transmission electron microscopy [9].

2. Experimental Procedure

The bulk of the observations were made on high purity, large-grained polycrystalline aluminum oxide, which had been obtained commercially in the form of 1/8 in diameter rods. Mechanically polished specimens 50–75 μm thick, which were suitable for subsequent thinning and examination in the electron microscope, were readily prepared by sectioning the rods into disks, grinding the surfaces flat, and then polishing both surfaces of the disks using

[1] Figures in brackets indicate the literature reference at the end of this paper.

progressively finer diamond compounds. For diamond-polished specimens, the final surface preparation consisted of polishing with 1/4 μm diamond, while alumina-polished specimens were additionally polished with 0.3 μm alumina powder. Thin disks with one ground surface were prepared by grinding one side of the cut disks with a 325 diamond grit resin-bounded wheel and diamond polishing the opposite surface, as above, until the final thicknesses of the disks were 50–75 μm.

Observations on the damage produced by diamond-polishing (0.25 μm) single crystal specimens with (0001) surface orientations were also made. These specimens were prepared from slices cut from Verneuil-grown boules and were mechanically polished in the same manner as the polycrystalline specimens. In certain cases, the (0001) sections were chemically polished using the hot phosphoric acid treatment described by Tighe [10] and then lightly abraded again using 0.25 μm diamond.

Examination of the damage associated with the different types of surface finish required thinned sections containing the original surface or regions at various depths below the surface. This was accomplished by using argon ion bombardment [8], which has been previously demonstrated as a suitable thinning technique for a number of ceramic materials [9, 11–13] and is now in general use. It is particularly well suited for surface studies on these materials since the thinning rate from each surface of the specimen can be controlled independently and the removal of material from one surface does not alter the opposite surface.

3. Results

3.1. Residual Surface Stresses

Some indication of the nature and strength of the residual surface stresses introduced by mechanical polishing was found during the preparation of thinned specimens by ion bombardment. Unlike specimens used in other studies, which had been chemically polished, annealed, or thinned simultaneously from both surfaces, these specimens spontaneously developed radial cracks when the thickness of the central area was reduced to approximately 1 μm. Fortunately, the cracks were generally arrested within the thicker surrounding regions. After further thinning until a central hole appeared, it was found that the thin, electron-transparent regions surrounding the hole were curled or bent with the original mechanically polished surface always convex. This final configuration resulted because the thinned regions originally bowed-out in the direction which made the abraded surface concave. It is thus apparent that mechanical polishing with either fine diamond or alumina abrasives leaves relatively large surface stresses which are compressive in nature. The extent to which cracks were produced and the thinned regions curled indicated larger stresses were produced by diamond polishing. Grinding introduced still larger residual surface stresses. The magnitude of these stresses necessitated the removal of at least 2 μm from the ground surface during the early stages of the final thinning process in order to produce whole electron microscope specimens.

As a consequence of the direction of curling in polished specimens, some material was unavoidably removed from the original surfaces during the later stages of thinning. It was only within relatively thick regions, where observations with 100 kV electrons were difficult, that regions containing the original surface or immediately below could be examined. In addition, the curling of the thinned regions severely restricted analysis of observed features.

3.2. Subsurface Damage Produced by 0.25 μm Diamond Abrasive

Observations (including selected area diffraction) in regions of diamond-polished specimens which contained the original surface served only to confirm the existence of intense lattice strains. Within these regions there was even difficulty in distinguishing the individual grains in the polycrystalline material. Removal of approximately 2000Å resulted in marked improvement in diffraction contrast. Observations from these regions clearly showed that relatively high densities of dislocations are produced in aluminum oxide by diamond polishing. As seen in figure 1, the majority of dislocations are confined to narrow, randomly oriented,

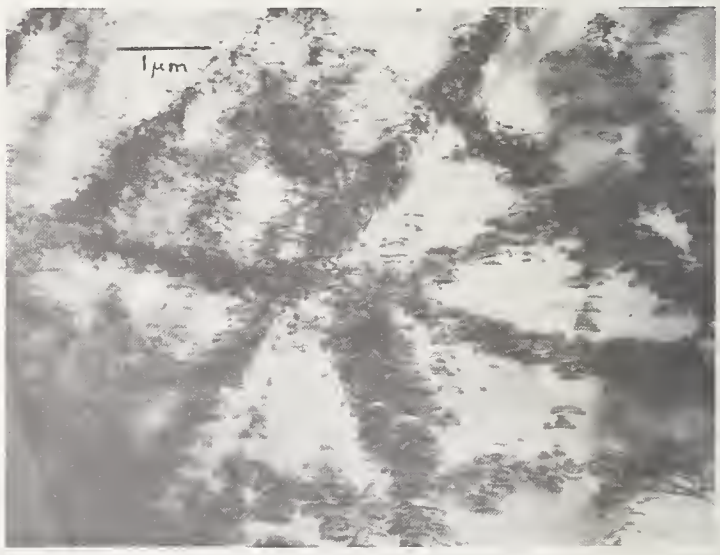

FIGURE 1. *Dislocations produced in polycrystalline aluminum oxide by mechanical polishing with 0.25 μm diamond abrasive.*

linear regions, while the connecting areas contain a relatively low density of dislocations. These regions of high dislocation density obviously define the traces of surface scratches produced by the individual abrasive particles. As a result, the local dislocation density depended upon the size and number of scratches. Certain areas contained such high densities of dislocations that the individual dislocations were difficult to resolve. Differences in the extent of damage associated with the same scratch in different grains and also between two scratches of different orientation within the same grain were also noted. This was due, in part, to the fact that the majority of dislocations generated appeared to be basal half-loops, as seen in figure 1. This result is consistent with previous bulk deformation studies [14, 15, 16], which have established that slip occurs more easily on the <1120> (0001) systems in sapphire, while the nucleation of half-loops from the surface is consistent with the mode of deformation. There were, nevertheless, large numbers of dislocations, which due to their particular configurations within the foils, appeared to lie on nonbasal slip planes. The fact that nonbasal dislocations are also generated was confirmed by observations made on diamond-polished single crystal specimens with (0001) surface orientations. In figure 2, the dislocations associated with a scratch on basal plane surface not only appear to lie on an inclined set of parallel planes, but were found to remain in contrast for all three 3030 type reflections unlike basal dislocations. Observations on basal plane sections also showed that high densities of basal dislocations can be generated. In every case, however, basal dislocations were only found associated with scratches that were larger than those typically produced by 0.25 μm diamond abrasives, as seen in figure 3.

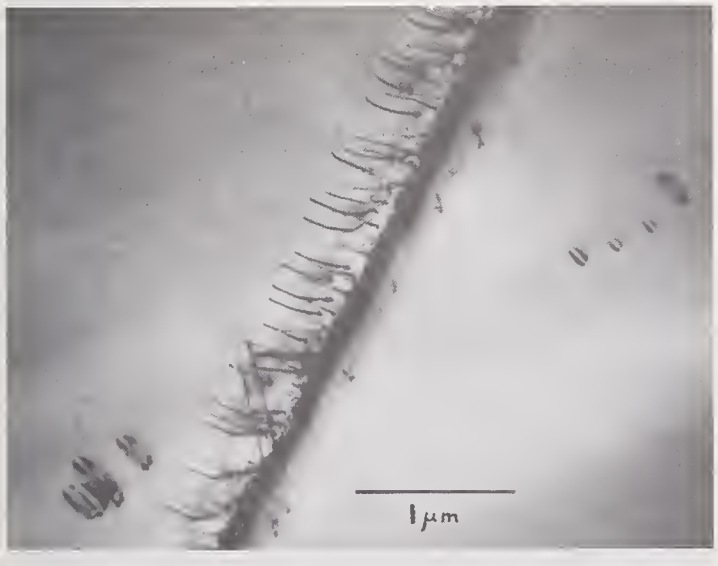

FIGURE 2. *Nonbasal dislocations associated with a single scratch on the (0001) basal plane surface of sapphire.* Scratch and associated damage are typical of that produced by polishing with 0.25 μm diamond.

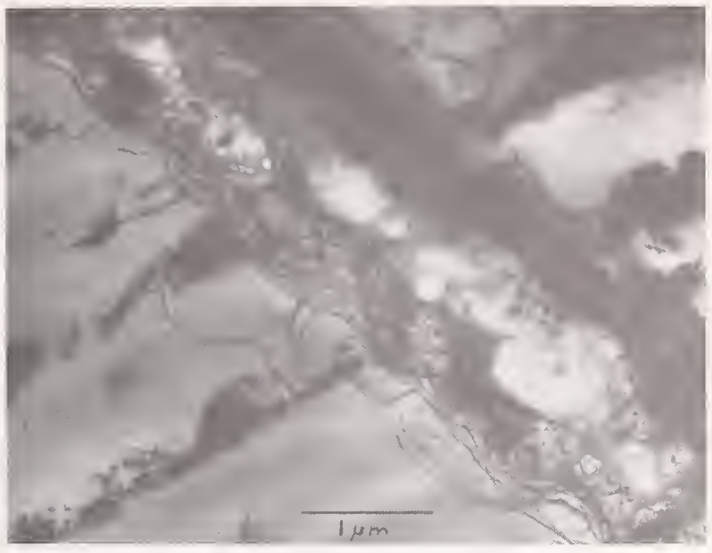

FIGURE 3. *Basal dislocations associated with a relatively deep scratch on the (0001) basal plane surface of sapphire.*

No attempt was made to precisely measure the depth to which subsurface damage extended in these specimens. It was found, however, that removal of about 1 μm from the surface eliminated nearly all traces of subsurface damage produced by 0.25 μm diamond polishing.

3.3. Subsurface Damage Produced by 0.3 Micron Alumina Abrasive

Observations made in regions of alumina-polished specimens which contained the original surface were quite similar to those made on diamond-polished specimens. The presence of severe lattice strains again made it impossible to distinguish individual defects. As before, removal of approximately 2000Å from the original surface resulted in a marked improvement in diffraction contrast. Observations in these regions clearly showed that the extent of damage produced by alumina polishing was much less than that by polishing with diamond of a similar particle size. At this depth below the original surface, it was estimated that nearly half of the grains examined were either dislocation-free or contained only a relatively low density of individual dislocations.

In the remaining regions, the extent of subsurface damage varied locally. Certain areas were found to contain such large numbers of scratches and associated dislocations that they appeared quite similar to areas found in diamond polished specimens, figure 1. These regions, however, were generally located near pores in which the abrasive grit may have ac-

cumulated during polishing. Other areas were found which contained relatively few scratch traces and associated dislocations, as seen in figure 4. The reason for the uneven distribution of surface scratches and therefore subsurface damage in these specimens is considered to be due to either a wide variation in alumina particle size or contamination of the abrasive. It is not considered likely that subsurface damage produced during prior diamond polishing was still present, since more than 25 μm was always removed by polishing with alumina powder during the preparation of the specimens.

In addition to a variation in the extent of damage in various regions of alumina-polished specimens, there was also a variation in the density of dislocations retained within individual grains. Quite often dislocations in one grain were accumulated near the grain boundary, with no dislocations present within the adjacent grains as seen in figure 5. This feature was not apparent in diamond polished specimens and may be associated with the "relief polishing" produced when alumina is polished with alumina powder.

3.4. Subsurface Damage Produced by Grinding With a Diamond Resin-Bonded Wheel

As discussed previously, the extremely irregular surface topography of ground polycrystalline specimens, due in part to a high incidence of fracture, figure 6, together with the existence of large residual stresses, made it impossible to prepare electron microscope specimens that contained regions of the original surface or close to it. For these specimens, it

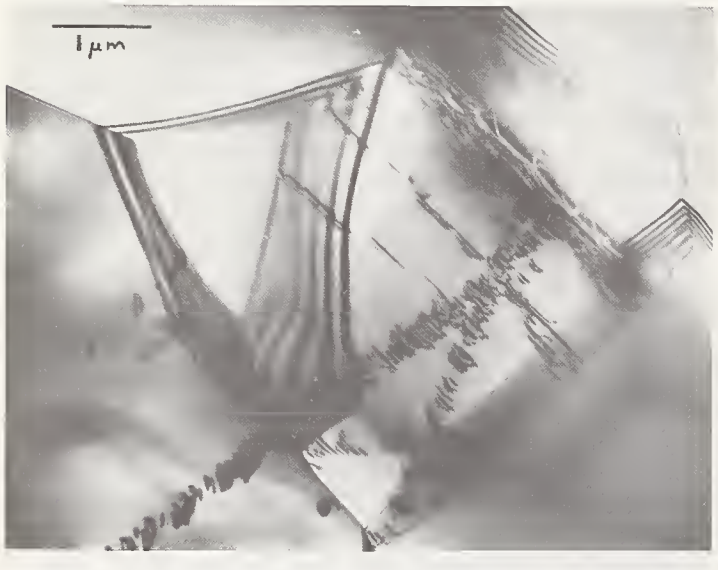

FIGURE 4. *Subsurface damage produced within the near surface regions of polycrystalline aluminum oxide by mechanical polishing with 0.3 μm alumina powder.*

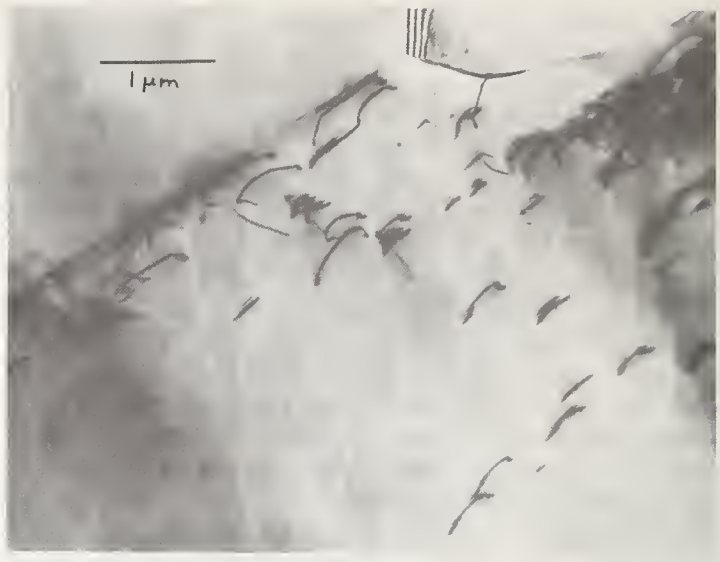

FIGURE 5. *Irregular distribution of dislocations introduced in polycrystalline aluminum oxide by mechanical polishing with 0.3 μm alumina powder.*

was necessary to remove at least 2 μm from the ground surface. The polycrystalline material used, however, contained few grains whose linear dimensions did not exceed 10 μm, so that the observations were made on the original surface grains.

Examination of these foils revealed an irregular distribution of subsurface damage which varied in both nature and extent from grain to grain. A number of grains were found to be dislocation free and apparently corresponded to regions below the obvious fracture surfaces seen in figure 6. It is also possible that due to the highly anisotropic nature of plastic deformation in aluminum oxide, certain grains were unsuitably oriented for plastic flow even to a depth of 2 μm. The majority of grains examined within these specimens were, however, found to have suffered plastic deformation by

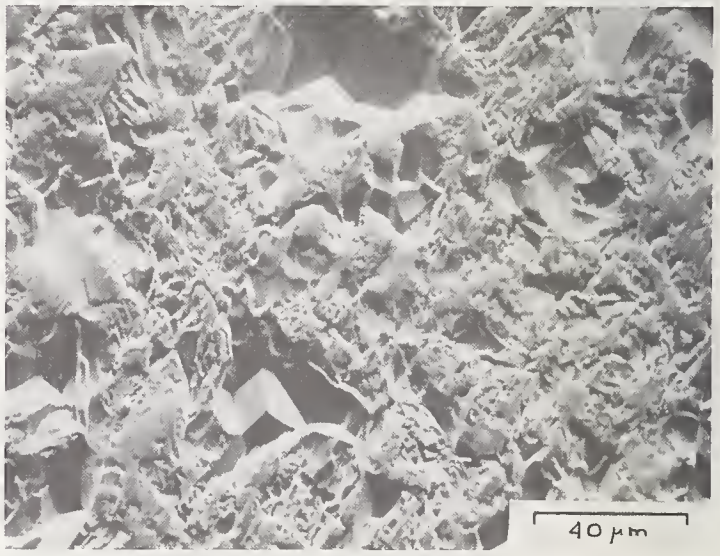

FIGURE 6. *Scanning electron micrograph of diamond-ground surface of polycrystalline aluminum oxide.*

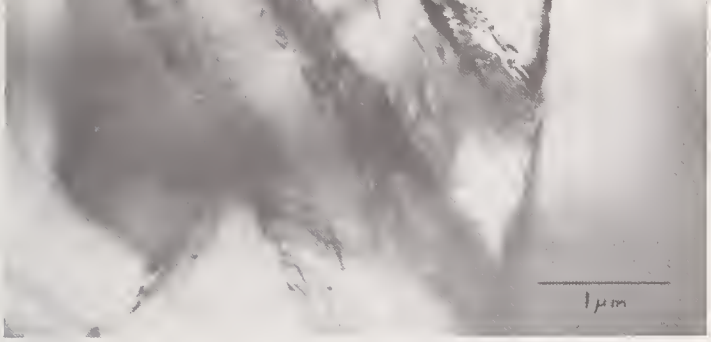

FIGURE 7. *Tangled dislocation arrays produced in polycrystalline aluminum oxide by diamond-grinding.*

either slip or twinning. The relatively high density of dislocations in the form of tangled arrays, shown in figure 7, illustrates the extent of damage retained within grains in which slip had occured. Of the two modes of deformational twinning which are known to occur in aluminum oxide, basal twinning [16, 17] was by far the more prevalent. An example of a grain containing thin basal microtwins, which were identified by selected area diffraction, is shown in figure 8. The presence of both dislocations lying in the boundaries of basal twins and those apparently generated by the internal stresses associated with these twins has been previously documented [9].

Despite the fact that rhombohedral twinning [18] occurs more readily than basal twinning in bulk deformation tests [19, 20], very few rhombohedral microtwins, such as the one seen

FIGURE 8. *Basal microtwins produced within surface grain of polycrystalline aluminum oxide by diamond-grinding.*

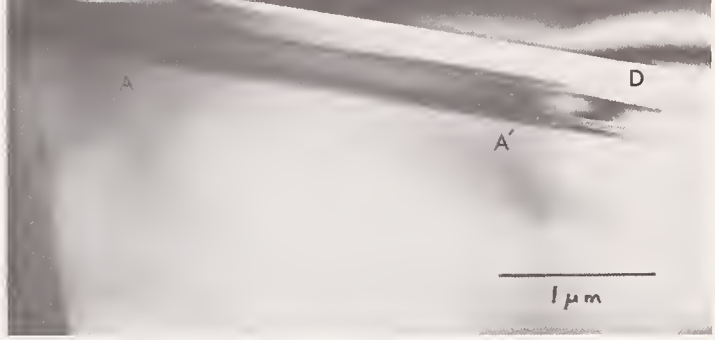

FIGURE 9. *Rhombohedral twin, A–A′, produced in polycrystalline aluminum oxide by diamond-grinding.* Twin appears associated with grain boundary parting along B-C-D.

in figure 9, were found. Figure 9 also illustrates a particularly interesting phenomenon found within these foils, namely the association of plastic deformation with grain boundary parting. In the example shown, the rhombohedral twin A–A′, appears unmistakenly associated with grain boundary fracture along B–C–D. Although the sequence of events cannot be directly determined from observations such as this, it would appear more reasonable to assume that grain boundary parting occured due to the development of large internal stresses at the twin-grain boundary intersection which could not be relieved by slip or twinning within the adjacent grain. Accordingly, plastic deformation even though limited to the immediate surface regions, may be responsible for the nucleation of penetrating cracks which more directly limit the strength. Heuer [18] has previously reported that twin-twin intersections may have been responsible for the nucleation of failure producing cracks in sapphire tested at various temperatures.

4. Discussion

Unlike previous studies, the present observations by transmission electron microscopy have shown that the abrasion of aluminum oxide does lead to considerable subsurface damage in the form of dislocations and microtwins as well as surface type damage. Although this damage has been found to be confined to only the immediate surface regions (approximately 1 μm for surfaces mechanically polished with 0.25 μm diamond) the results indicate that plastic deformation does play an important role in the removal of material by abrasion. Furthermore, the presence of such high densities of lattice

defects near the surface can be expected to significantly alter the subsequent mechanical behavior of abraded bodies. At high temperatures, where bulk plastic deformation has been observed in this material, the surface regions of abraded crystals can either act as ready sources of dislocations and twins, as work-hardened layers, or as both. At present, there is no data on the dynamic behavior of dislocations in aluminum oxide at low or intermediate temperatures (<0.5 Tm) and it is difficult to ascertain the role of subsurface damage at these temperatures. It has been shown, however, that chemical [5, 21] and flame-polishing [21–23], sputtering [24], and prior annealing [25, 26] do lead to substantial strengthening at all temperatures. Each of these treatments results in either the removal of subsurface damage or the relaxation of the internal stresses associated with the high densities of defects as well as the elimination of surface cracks and general improvement in surface topography. Aluminum oxide has also been shown to display environmental effects, such as static fatigue [27, 28], and there is little doubt that the high densities of lattice defects produced by abrasion contribute significantly due to stress corrosion.

The fact that subsurface damage is produced in this material in which bulk plastic deformation has not been observed below 900 °C is considered to be a consequence of the nature and magnitude of the stresses developed under the individual abrasive particles. As is the case of static indentation, the load is applied locally and the stress fields developed contain large hydrostatic components. Under these conditions, the extremely large shear stresses required for dislocation generation can be developed since full relation of the load cannot occur by fracture. Surface heating is not considered to be significant in light abrasive actions, such as polishing, but most certainly plays an important role in cutting and grinding operations. The fact that penetrating arrays of dislocations and microtwins, typical of bulk deformation, are found in the near-surface regions of ground specimens but not in polished specimens is considered to be due in part to the difference in surface heating produced by the two operations.

5. References

[1] Cutter, I., and McPherson, R., Examination of abraded MgO by x-ray diffraction line broadening, Phil. Mag. 20, 489–494 (1969).

[2] Koepke, B. G., and Stokes, R. J., A study of grinding damage in magnesium oxide single crystals, Office of Naval Research Technical Report HR—69—283: 5—26, July 1969.

[3] Palmour, H., Kriegel, W. W., and DuPlessis, J. J., Microbrittleness anisotropy in thermally etched sapphire, pp. 313–328 in The Mechanical Properties of Engineering Ceramics (Interscience Publishers, Inc., New York, 1961).

[4] Levengood, W. C., Quantitative aspects of twinning deformation in sapphire and ruby single crystals, pp. 93–97 in Crystal Growth, Proceedings of an International Conference on Crystal Growth, Boston, 1966 (Pergamon Press, Inc., New York, 1967).

[5] King, A. G., Chemical polish and strength of alumina, pp. 529–538 in Materials Science Research, Vol. 3 (Plenum Press, Inc., New York, 1966).

[6] Steijn, R. P., On the wear of sapphire, J. Appl. Phys. 32, 1951–1958 (1961).

[7] Duwell, E. J., and Butzke, H. C., Microscopial observations of wear surfaces of sapphire, J. Appl. Phys. 35, 3385–3390 (1964).

[8] Paulus, M., and Reverchon, F., Dispositif de bombardment ionic pour preparations micrographics, J. Phys. Rad. 22, 103 A–107 A (1961).

[9] Hockey, B. J., Plastic deformation of aluminum oxide by identation. J. Amer. Ceram. Soc. 54, 223–231 (1971).

[10] Tighe, N. J., Jet thinning device for preparation of Al_2O_3 electron microscope specimens, Rev. Sci. Instr. 35, 520–521 (1964).

[11] Tighe, N. J., and Hyman, A., Transmission electron microscopy of alumina ceramics, pp. 121–136 in Anisotropy in Single-Crystal Refractory Compounds (Plenum Press, Inc., New York, 1968).

[12] Tighe, N. J., Microstructure of fine-grain ceramics, pp. 109–133 in Ultrafine-Grain Ceramics (Syracuse Univ. Press, Syracuse, New York, 1970).

[13] Tighe, N. J., and Hockey, B. J., Ion thinning of electron microscope specimens; pp. 375–380 in Record of the 10th Symposium on Electron, Ion, and Laser Beam Technology (San Francisco Press, San Francisco, California, 1969).

[14] Wachtman, J. B., and Maxwell, L. H., Plastic deformation of ceramic-oxide single crystals, J. Am. Ceram. Soc. 37, 291–299 (1954). Plastic deformation of ceramic-oxide single crystals, II, J. Am. Ceram. Soc. 40, 377–385 (1957).

[15] Kronberg, M. L., Dynamical flow properties of single crystals of sapphire, I, J. Am. Ceram. Soc. 45, 274–279 (1962).

[16] Kronberg, M. L., Plastic deformation of single crystals of sapphire: basal slip and twinning, Acta. Met. 5, 507–524 (1957).

[17] Veit, K., Artificial deformation and transpositions in sapphire, Neues Jahrb. Min., Beil-Bd., 45, 121–148 (1921).

[18] Heuer, A. H., Deformation twinning in corundum, Phil. Mag. 13, 379–393 (1966).

[19] Stofel, E., and Conrad, H., Fracture and twinning in sapphire (alpha–Al_2O_3 Crystals), Trans. AIME, 227, 1053–1060 (1963).

[20] Conrad, H., Janowski, K., and Stofel, E., Additional observations on twinning in sapphire (alpha–Al_2O_3 crystals) during compression, Trans. AIME 233, 255–256 (1965).

[21] Mallinder, F. P., and Proctor, B. A., Preparation of high-strength sapphire crystals, Proc. Brit. Ceram. Soc. 6, 9–16 (1966).

[22] Morley, J. G., and Proctor, B. A., Strengths of sapphire crystals, Nature 196, 1082 (1962).

[23] Mallinder, F. P., and Proctor, B. A., The strengths of flame-polished sapphire crystals, Phil. Mag. 13, 197–207 (1966).

[24] Rice, R., private communication.

[25] Heuer, A. J., and Roberts, J. P., The influence of

annealing on the strength of corundum crystals, Proc. Brit. Ceram. Soc. 6, 17–27 (1966).
[26] Davies, L. M., The effect of heat treatment on the tensile strength of sapphire, Proc. Brit. Ceram. Soc. 6, 29–35 (1966).
[27] Charles, R. J., and Shaw, R. R., Delayed Failure of Polycrystalline and Single-Crystal Alumina, General Electric Co. Report 62–RL–3081M (1962).
[28] Charles, R. J., Static fatigue: delayed fracture; pp. 467–519 in Studies of the Brittle Behavior of Ceramic Materials, Aeronautical Systems Div. Report No. ASD–TR–61–628, Pt. II, (1963).

Discussion

HEUER: Do you think that microhardness anisotropy in Al_2O_3, which gives rise to relief polishing when using Al_2O_3 abrasives on Al_2O_3, was responsible for the heterogenity you observed in damage due to the abrasives.

HOCKEY: I mentioned this possibility in the paper. In alumina powder polished polycrystalline specimens, there were areas in which grains containing dislocations were surrounded by defect-free grains. This was never observed in diamond-polished specimens, which do not exhibit relief-polishing.

CAVENEY: What are your estimates of the depth of damage in the grinding experiments and what are the grinding conditions?

HOCKEY: With regard to the grinding conditions, all I can say is that each specimen examined was ground in the same manner using a 325 diamond grit resin-bonded wheel. Also, no attempt was made to measure the depth of subsurface damage, although this is certainly possible using the techniques described. My rough estimate of the minimum depth to which damage extended would be 10–15 μm. The fact that large numbers of twins are produced by grinding and are undoubtedly the most far reaching defects indicates the extent of damage will be highly anisotropic.

NATIONAL BUREAU OF STANDARDS SPECIAL PUB. 348, THE SCIENCE OF CERAMIC MACHINING AND SURFACE FINISHING, Proceedings of a Symposium Sponsored by the American Ceramic Society, the Office of Naval Research, and the National Bureau of Standards, held at NBS Nov. 2–4, 1970, Gaithersburg, Md. (Issued May 1972).

Acoustic Emission Monitoring of Surface-Damaged Ceramic Materials

L. R. Bunnell, J. C. Crowe, and P. E. Hart

Battelle Memorial Institute, Pacific Northwest Laboratories
Richland, Washington 99352

The acoustic emission response of Lucalox, fused silica, single crystal alumina, Pyroceram, and soda-lime-silica glass to surface damage is reported. Low temperature annealing at 200 °C reduces the response levels; annealing at 400 °C removes all of the induced acoustic activity.

Key words: Acoustic emission; glass; Lucalox; Pyroceram; surface damage.

1. Introduction

Elastic waves produced in a solid by energy released as the material deforms or fractures are termed acoustic emissions. These waves can be detected by a high-sensitivity ultrasonic sensor and, after suitable signal conditioning, can be used as an indication of crack growth or flaw formation. The technique has been applied to metals with considerable success, both for flaw detection in pressure vessels [1][1] and for weld monitoring. [2] It has also recently been applied to crack growth detection in ceramics. [3]

Intuitively, ceramics surface damaged at room temperature should be in a condition of high surface energy and should contain defects which are unstable at elevated temperatures. In order to evaluate the utility of acoustic emission monitoring for surface damage in ceramics, a series of polycrystalline ceramics and glasses were tested for changes in acoustic emission levels upon immersion in hot water following surface damaging and low temperature annealing.

Samples of polycrystalline Al_2O_3[2] (10 and 30 micron grain size), single crystal Al_2O_3, fused SiO_2,[3] glass-ceramic[4] and soda-lime-silica (window) glass were treated as described below:

- The specimens, which were all disc-like, approximately 6 cm² area × 2 mm thick, were annealed[5] to remove damage introduced by sample shaping (usually by diamond-sawing).
- Samples were damaged on one face by wet grinding on Di-Met brass wheels charged with 9 μm (Damage #1) or 63 μm (Damage #2) diamonds.
- Samples at Damage Level #2 were heated in air to either 200 °C or 400 °C, held at temperature for six hours, and furnace cooled.
- A PZT (lead zirconate-titanate) sensor with a primary response at 600 KHz was bonded to each sample on an undamaged edge. The transducer was connected to the monitoring system which recorded count rate and total counts.
- The sample was immersed in water at 90 °C, and emissions occurring within four minutes were recorded.

Figure 1 shows results (total recorded emissions versus time) for the soda-lime-silica glass. The annealed sample produced no emissions, while the two damaged samples both produced emissions. The specimens receiving the severest damage (as supposed from the abrasive size) produced the most emissions. Some decrease in emissions was associated with the 200 °C anneal, while emission output dropped to 0 after the 400 °C anneal.

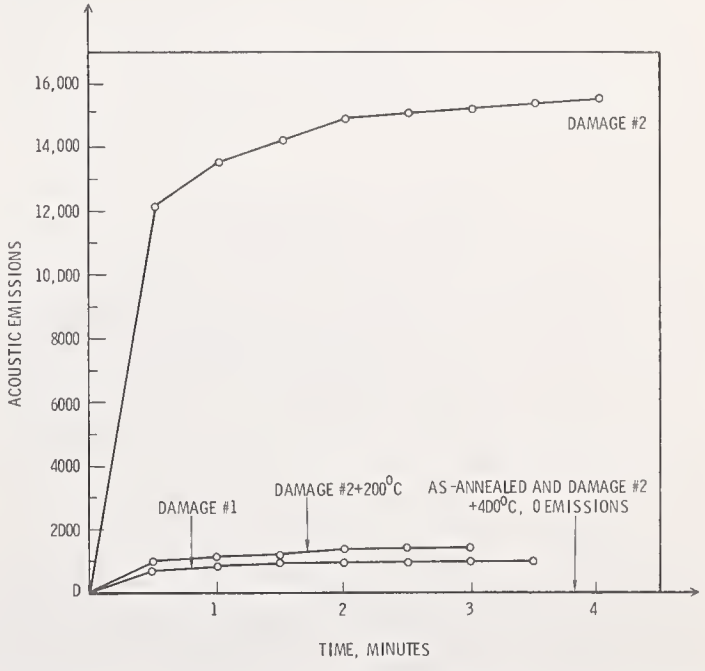

FIGURE 1. *Acoustic emission response (total) versus time for a soda-lime-silica glass given the indicated treatments.*

[1] Figures in brackets indicate the literature references at the end of this paper.
[2] Lucalox, General Electric Co.
[3] General Electric transparent fused SiO_2.
[4] Corning Glass Co.
[5] Annealing temperatures: Lucalox 1500 °C, SiO_2 1050 °C, Pyroceram 800 °C, Glass 500 °C.

439-921 O - 72 - 23

These same trends were followed by all of the other materials, although results did not always coincide with the supposed severity of damage as in figure 1. For instance, in both Lucalox samples, the sample damaged with 9 μm diamonds produced more emissions than that damaged with 63 μm diamonds.

The paucity of data precludes a detailed analysis of the results; however, the experiment shows that effects of surface damage can be detected by acoustic emission monitoring. Measurements on annealed samples showed that emission resulting from surface damage can be altered by heat treatment at lower temperatures than would normally be imagined to cause any annealing effects. The nature of the emission sources, their interaction with water, and the effect of low-temperature heat treatments is not understood.

The results indicate that acoustic emission monitoring is extremely sensitive to surface damage effects in ceramics. While sensitivity does not per se guarantee utility, it is hoped that further experiments will reveal the nature of the events being detected and thereby give a greater insight into the effect of surface finishing on ceramic materials.

2. References

[1] Hutton, P. H., Integrity Surveillance of Pressure Systems by Means of Acoustic Emission, BNWL–SA–2194, October 1969. Published in the Proceedings of the First International Conference on Pressure Vessel Technology Part II by the American Society of Mech Eng.

[2] Jolly, W. D., Acoustic emission exposes cracks during welding process, published by the Welding Journal Vol 48, p 21–29, January 1969.

[3] Romrell, D. M., and Bunnell, L. R., Monitoring of Crack Growth in Ceramics by Acoustic Emission, BNWL–SA–3064, published in Materials Evaluation, December 1970.

NATIONAL BUREAU OF STANDARDS SPECIAL PUB. 348, The Science of Ceramic Machining and Surface Finishing, Proceedings of a Symposium Sponsored by the American Ceramic Society, the Office of Naval Research, and the National Bureau of Standards, held at NBS Nov. 2–4, 1970, Gaithersburg, Md. (Issued May 1972).

V. MECHANICAL AND OTHER EFFECTS OF FINISHING

Session Chairmen

W. H. Rhodes, AVCO Corporation

J. B. Wachtman, Jr., National Bureau of Standards

Effects of Surface Finishing on Mechanical and Other Physical Properties of Ceramics

Robert J. Stokes [1]

Honeywell Research Center, Hopkins, Minnesota 55343

This paper reviews the effects of mechanical finishing operations on the physical properties of ceramics. Ceramic machining results in a defective surface containing cracks, dislocations, point defects and residual stresses. The relative significance of these defects depends on the physical property of interest. The mechanical properties of single crystals are sensitive to dislocations (semibrittle) and surface cracks (brittle); the mechanical properties of polycrystals are sensitive to surface cracks; the electrical properties of semiconductors are sensitive to surface trapping sites; magnetic, piezoelectric and optical properties are particularly sensitive to residual stresses. To optimize physical properties these defects must be eliminated by mechanical lapping, chemical etching or thermal annealing.

Key words: Ceramics; cracks; dislocations; electrical properties; electro-optical; ferrite; machining; magnetic properties; mechanical properties; optical properties; residual stress.

1. Introduction

There is no doubt that ceramics are finding increased application because of their unique physical properties. Until comparatively recently it has been sufficient to fabricate ceramics of special shapes by direct methods such as slip casting or sintering techniques. However, modern technology emphasizes speed, density and accuracy and this in turn demands ceramic materials with precise control over composition and topography. In the past ten years, homogeneous and uniform compositions have been attained through advances in primary fabrication techniques, and dimensional tolerances have been attained through advances in secondary fabrication techniques, namely machining, grinding and lapping.

Another modern trend in the application of ceramics involves the fabrication of components with smaller and smaller dimensions. The result of this trend is to increase the surface to volume ratio to the point where the properties of surface material are of overriding significance. Thus it becomes of extreme importance to consider the effects of surface finishing on the critical physical properties for which ceramics may be chosen.

The purpose of this paper is to consider how surface finishing operations affect the different physical properties of ceramics. In order to do this it will be necessary to review briefly first the features which are associated with a machined ceramic surface. The consequences of these features on the various physical properties will then be considered, using direct experimental illustrations where available.

2. Features of the Mechanically Finished Surface

A number of other papers in this volume and elsewhere consider the nature of grinding damage in considerable detail and we do not propose to elaborate here. The major features associated with a finished surface are listed in table 1 according to their origin. As Koepke [1][1] has pointed out, the surface topography generated by machining operations depends on the abrasive wheel being used, the machining parameter and most important of all, the mechanical properties of the material being machined. Accordingly the surface features depend on whether material is being removed by brittle fracture or plastic flow and on the interior structure of the ceramic.

[1] Manager, Metallurgy Department.
[1] Figures in brackets indicate the literature references at the end of this paper.

2.1 Features Generated by Brittle Fracture

First we consider those features generated when the machining conditions are such that material is removed by the propagation of brittle fracture. The fracture mode may be transgranular (i.e.,—cleavage or conchoidal) or intergranular depending on the material. When the fracture propagates essentially parallel to the finished surface the result is a general surface roughness determined by the faceting of the fracture surface. The scale of this roughness is obviously related to the microstructure and has dimensions approximately $d/2$, where d is the grain size.

When the fracture propagates essentially perpendicular to the finished surface, fine transgranular or intergranular surface cracks are left in the surface. Figure 1 illustrates transgranular surface flaws introduced into a magnesium oxide single crystal by a surface grinding operation. These flaws have a depth of 150 μm.

The dimensions of surface cracks are determined by material properties and microstructure and by the severity of the machining operation. In polycrystalline ceramics the surface cracks typically run until they intercept a grain boundary and thus have dimensions approximately equal to d, the grain size. Direct measurements by Evans and Davidge [2] indicate that diamond sawing polycrystalline magnesium oxide produces intergranular surface cracks with depth approximately one or two grain diameters for small grain size (less than 100 μm) material and less than one grain diameter for larger grain size material. Rice [3] has pointed out that the depths of surface cracks may be related to the distribution and amount of porosity. In porous material a surface crack is likely to intercept and be arrested by pores thus reducing its dimension.

Another surface feature associated with brittle crack propagation is "grain pull-out," which is experienced in final lapping and polishing stages. If earlier rough machining stages have caused intergranular cracks to propagate one or two grains beneath the surface, the grains may not actually separate from the material until a later stage of the surface finishing operation giving rise to the undesirable "grain pull-out" craters illustrated in figure 2.

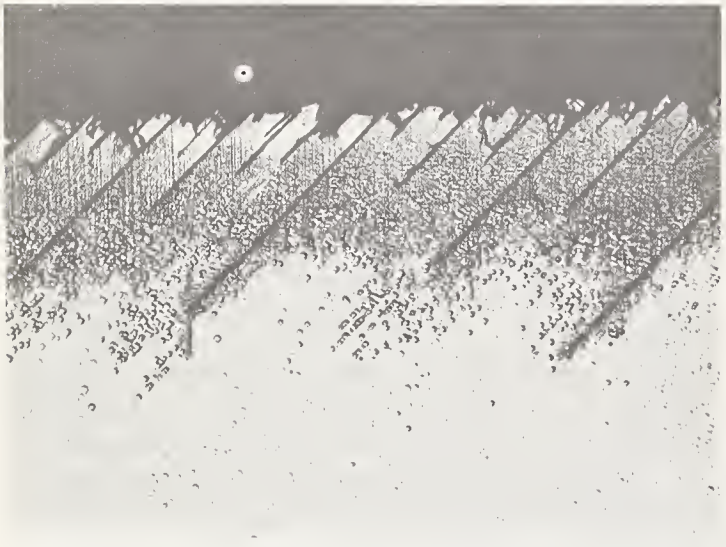

FIGURE 1. *Cleavage cracks introduced into the surface of a magnesium oxide single crystal by a semi-rough grinding operation.* Note layer of etch pits corresponding to dislocations also in surface layer (X250).

2.2. Features Generated by Plastic Flow

Second we consider features due to plastic flow. These may consist of either the dislocations and point defects generated immediately beneath the finished surface or those surface topographical features associated with the removal of material by plastic flow.

One of the consequences of abrasive machining operations is the generation of a defective layer immediately beneath the finished surface. The depth of penetration depends on the mechanical strength of the material and the nature of the abrasion. The cross section through the magnesium oxide crystal in figure 1 illustrates the fact that in this soft semi-brittle material a semi-rough finishing operation generates a layer of extensive plastic deformation approximately 100 μm deep as revealed by the etch pits. The depth of this layer for different machining conditions has been studied by Koepke and Stokes [4].

In harder materials the plastically deformed

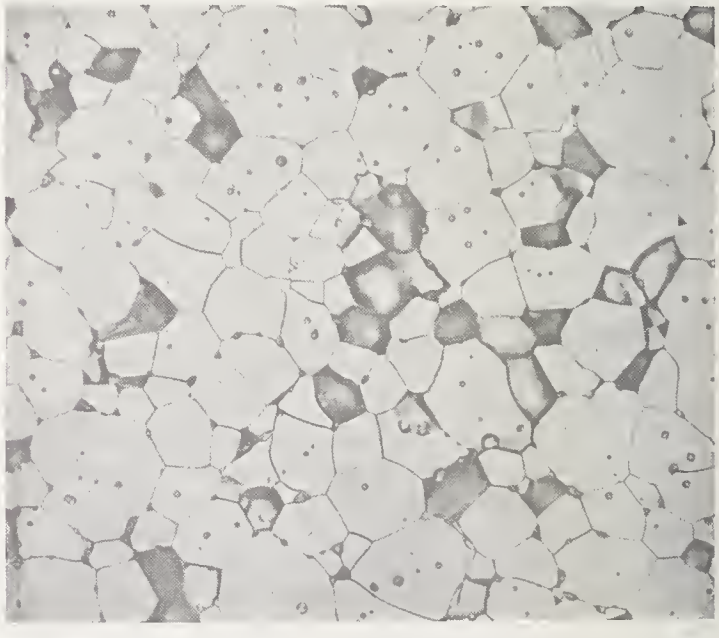

FIGURE 2. *Polished surface of $Ni_{0.36}$ $Zn_{0.64}$ ferrite illustrating surface roughness due to grain pull-out, grain boundary porosity, and intragranular porosity.* Surface etched to reveal grain boundaries (X440).

layer is not so deep. For example, in silicon, hand polishing with silicon carbide under pressure forces dislocations 20 μm beneath the surface [5], whereas polishing alumina with diamond particles injects dislocations only 2–3 μm deep [6]. In polycrystalline materials the depth of penetration varies with the orientation of the individual grains.

Under certain machining conditions [1] the plasticity of the ceramic material may be sufficient for the finished surface to be generated entirely by plastic flow. The surface topography is then smooth and burnished. In some materials the extensive plastic flow at the wheel workpiece interface can result in excessive heating and the subsequent thermal quenching gives rise to fine surface cracks as described elsewhere [4].

The steep temperature, pressure and plastic flow gradients at the wheel workpiece interface can cause phase transformation or recrystallization with preferred grain orientation in the finished surface layers [7].

One of the most significant consequences of irreversible changes occurring in finished surface layers is the generation of residual stress. When the surface layer responds plastically to the stresses under the machining tool then it experiences a residual compressive surface stress which must be balanced by the tensile stresses in the interior. It is important to note that the average magnitude of the internal tensile stress depends on the volume of material available. As the specimen shrinks in size and the finished surface to volume ratio increases, the internal tensile stress increases.

2.3. Features Generated by Exposure of Internal Structure

Another set of features indirectly associated with finishing operations arises from the cross sectioning of a sintered block to expose its internal structure. The surface topography generated by final lapping and polishing operations should be perfectly flat and smooth. However, this is rarely the case in polycrystalline ceramics. There are regions where grains have separated from the surface; these may be due to "grain pull-out" as described earlier or, if due to the relief of internal stresses remaining from fabrication, "grain pop-out." There are other regions where pores are intercepted by the grinding plane as illustrated in figure 2.

The overall surface topography is related to the microstructure, i.e.,—grain size, pore size and distribution.

2.4. Summary

The principal features associated with a finished surface are reviewed in table 1. There

TABLE 1. *Features of the mechanically finished surface*

Surface features	Origin
1. Features generated by brittle fracture	
a. General surface roughness	Transgranular and intergranular fracture approximately parallel to finished surface.
b. Surface cracking	Transgranular and intergranular fracture approximately perpendicular to finished surface.
c. Grain pull-out	Intergranular rupture of isolated surface grains.
2. Features generated by plastic flow	
a. Surface dislocations	Short range and long range stresses imposed by the grinding wheel.
b. General surface burnishing	Plastic flow and heat generated at the wheel workpiece interface.
c. Crystalline reorientation	Plastic flow at the wheel workpiece interface.
d. Phase transformations	Temperature gradients at the wheel workpiece interface.
e. Residual stresses	Plastic flow and chemical gradients.
3. Features generated by exposure of interior structure	
a. Pores	Within grains or along grain boundaries.
b. Grain boundaries	
c. Grain pop-out	Relief of internal stresses.

are surface topographical features such as surface roughness, grain pull-out and pores and subsurface features such as cracks, dislocations, point-defects and residual stress. The relative extent of these features depends on the nature of the finishing operation and the quality and properties of the material. Which feature is of primary concern depends on the physical property being used.

To identify the sensitivity of physical properties to certain features of the surface condition it is necessary to consider the results of simple, definitive experiments. We will now do this where possible for mechanical, magnetic, electrical and optical properties of ceramics.

3. Effects of Surface Finishing on the Mechanical Properties of Ceramics

Much has already been written on the effects of surface condition on the mechanical properties of ceramics. We shall only present a brief review here. It will be found that dislocations and cracks represent the most critical features of the surface condition. For our purpose it will be convenient to subdivide ceramics into those which can undergo limited plastic deformation (so-called semibrittle ceramics) and those which cannot (brittle ceramics) [8]. A further distinction will be made between the behavior of single crystal and polycrystalline material.

3.1. Semibrittle Ceramics—Single Crystals

The distinguishing feature of semibrittle ceramics is that while they can deform plastically they are none the less extremely notch sensitive. In this instance there is a large difference in mechanical response of single crystals depending on whether they are perfect or contain surface defects (dislocation loops) or contain surface cracks.

Crystals which are perfect (i.e.,—whiskers or in some instances, notably MgO, bulk crystals which have been chemically polished to remove all surface dislocations) deform elastically up to stress levels approaching their theoretical cohesive strength. However if a single dislocation loop is injected into such a crystal by the slightest mechanical abrasion then the high strength is lost and the crystal deforms plastically at its yield stress (see table 2). This probably represents the most striking demonstration of the sensitivity of a ceramic material to its surface condition, and illustrates the significance of the presence of fresh surface dislocations [9].

If mechanical abrasion of a semibrittle ceramic crystal results in surface cracks, the cracks are extended under stress until they achieve critical dimensions for brittle fracture. The mechanism of crack extension has not been completely resolved, however it definitely involves plastic flow [10, 11]. The important point about this mechanical behavior is that the fracture strength is approximately equal to the yield strength, and is not determined by the original depth of the crack.

Sensitivity to surface cracks depends strongly on temperature and deformation strain rate. Semibrittle crystals containing surface cracks have been found to remain notch sensitive and brittle within 50 °C of the melting point when deformed under impact [12].

In view of these mechanical responses to surface condition it is reasonable to conclude that semibrittle single crystals will always be weak

TABLE 2. *Effect of surface condition in the strength of magnesium oxide*

Single crystals	Strength		Mechanical behavior
	(MN/m^2)	(*KPSI*)	
Chemically polished	1,105	160	Elastic
Mechanically abraded	35	5	Plastic
Bi-crystals			
Chemically polished	760	110	Elastic
Mechanically abraded	40	6	Brittle
Polycrystals			
(i) Hot pressed-as received (5–30μm)			
Chemically polished	195	28	Brittle
Mechanically abraded	130	19	Brittle
(ii) Hot pressed-annealed (75 μm)			
Chemically polished	130	19	Brittle
Mechanically abraded	100	15	Brittle
(iii) Sintered (10–20 μm)			
Chemically polished	100	15	Brittle
Mechanically abraded	100	15	Brittle

TABLE 3. *Effect of surface condition on the tensile strength of alumina single crystals*

Surface condition	Fracture strength (MN/m^2)	($Kpsi$)	*Percent Theoretical*
Perfect (whiskers)	15,900	2,300	61
Flame polished	7,350	1,100	29
Chemically polished (borax)	6,860	1,000	26
Mechanically polished (annealed in O_2)	1,040	150	4
Mechanically polished (centerless ground)	590	90	2
As machined	440	60	2

and brittle following mechanical finishing. The only way in which this situation can be modified is by chemical polishing to completely eliminate the surface defects introducing by the machining operation.

3.2. Brittle Ceramics—Single Crystals

The distinguishing feature of brittle ceramics is that they cannot deform plastically at low temperatures. Thus whether surface dislocations are introduced or not by a finishing operation makes no difference to the mechanical response of these crystals. What does matter is whether surface cracks are introduced. There is then a large difference in mechanical fracture strength depending on surface finish as indicated in table 3.

In the as-machined condition alumina single crystals deform elastically up to their fracture stress of 440 MN/m^2. Presumably the surface cracks introduced by machining act as Griffith cracks and propagate catastrophically at this stress level. Applying the Griffith relationship

$$\sigma_f = \left(\frac{E\gamma}{c} \right)^{1/2} \qquad (1)$$

where σ_f is the fracture stress (440 MN/m^2)
E is the elastic modulus (3×10^5 MN/m^2)
γ is the fracture surface energy ($\sim 10 J/m^2$), and
c is the surface crack depth
gives a value for c of approximately 10 μm, which is reasonable.

Any process which reduces the dimensions of the surface cracks or eliminates them raises the fracture stress as illustrated by the different surface treatments in table 3.

3.3. Semibrittle Ceramics—Polycrystals

The sensitivity of semibrittle crystals to surface condition extends also to single crystals containing a grain boundary, i.e.,—simple, bicrystals. This can be seen in table 2. Again a chemically polished bicrystal free from surface dislocations behaves elastically up to very high stress levels whereas the defective bicrystal fractures at a stress corresponding to the single crystal yield strength. The onset of slip from surface dislocations in a bicrystal results in internal crack nucleation because the plastic strain discontinuity cannot be accomodated across the grain boundary [8].

Attempts have been made to extend this contrast between chemically polished and defective surfaces to more typical polycrystalline material. The degree of success depends on the microstructure of the material as indicated in table 2. Fully dense hot pressed material does show a significant drop in strength when surface dislocations are introduced. In other less dense materials internal defects mask any sensitivity to this kind of surface condition.

The strength of machined polycrystalline material is dominated more by surface cracking. Accepting the idea that the depth of surface cracks is related to the grain size, then the fracture strength should vary with the grain size, d, according to a modified Griffith relationship in which the crack depth, c, is replaced by the grain size and

$$\sigma_f = K_1 d^{-1/2} \qquad (2)$$

where K, is a constant dependent on the material microstructure. When the grain size and thus the surface crack depth is small, the applied stress exceeds the stress to initiate slip before fracture occurs; slip initiates and extends cracks at stress levels below the Griffith stress. The fracture then follows the Petch relationship

$$\sigma_f = \sigma_i + K_2 d^{-1/2} \qquad (3)$$

where σ_i, is the stress to initiate slip. For a machined polycrystalline ceramic this gives rise to the two stage fracture strength—grain size relationship first noted by Carniglia [13].

When semibrittle polycrystalline ceramics are chemically polished to remove surface cracks then fracture will always be initiated by slip and the strength—grain size relationship follow equation (3). This has been demonstrated by Evans and Davidge [2] in their experimental work on the effects of surface finishing on the fracture strength of polycrystalline magnesium oxide. A replot of their data is included in figure 3.

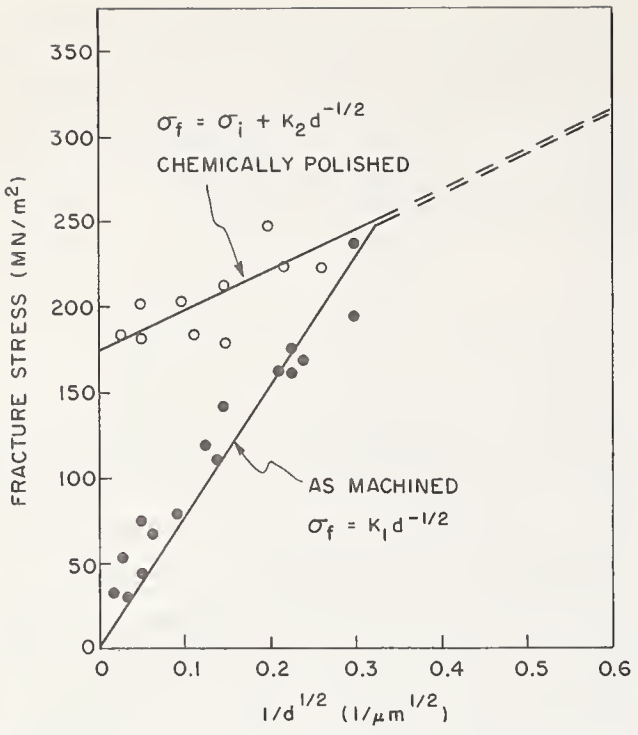

FIGURE 3. *Fracture strength of polycrystalline magnesium oxide as a function of grain size and surface condition.* (After Evans and Davidge-Ref. 2).

Other treatments designed to remove the surface cracks introduced during machining likewise enhance the fracture strength at a given grain size. Harrison [14] showed that fracture strength increased progressively as the machined surface was first lapped with finer and finer polishing grits, then annealed and finally chemically polished to give the best crack free, stress relieved specimen condition.

3.4. Brittle Ceramics—Polycrystals

If there is any connection between flaw size and grain size, the fracture strength of polycrystalline brittle ceramics should follow the modified Griffith relationship of equation (2). However, Carniglia [13] has shown that a two stage relationship fits the available data better, and has suggested that fracture is initiated by plastic flow at small grain sizes. Unfortunately, the extrapolated value for σ_i of 300 MN/m² is far below the tensile strength of single crystals (see table 3) and there is no data on chemically polished crack free material to support the hypothesis. In short, the experimental studies on the effects of surface condition on polycrystalline alumina are neither as comprehensive nor as definitive as those on polycrystalline magnesia.

Thermal and chemical treatments of machined alumina have been found to enhance the fracture strength a small amount [15]. While the improvements are significant as indicated by table 4, they are not as spectacular as in magnesia.

TABLE 4. *Effect of surface treatment on the bend strength of polycrystalline alumina*

Surface condition	Fracture strength	
	MN/m²	*Kpsi*
Chemically polished (borax)	540	78.5
Mechanically polished (annealed in air)	470	68.1
Plasma flame polished	440	63.5
Mechanically finished (ground)	440	64.0

3.5. Summary

The effects of surface finishing on the mechanical properties may be accounted for in terms of surface dislocations, surface cracks and residual stresses. Which feature is the most significant depends on whether the materials are brittle or semibrittle. The magnitude of the effect depends on the microstructure, i.e.,—grain size and porosity. Minimization of surface damage by mechanical, thermal or chemical means generally results in an increase in strength.

4. Effects of Surface Finishing on the Magnetic Properties of Ceramics

This subject has not been discussed so extensively in the literature as has mechanical properties. The reason for this is that residual stress represents the most critical feature of the surface condition and it is not until specimen dimensions become very small that the residual stress becomes large enough to exert a measurable influence. As indicated in the introduction the use of small components represents a fairly recent development in the technical application of ceramics and thus the deterioration in magnetic response is only just becoming a problem receiving attention.

4.1. Effects of Stress on Magnetic Properties

The effect of stress on the magnetic behavior of materials is well recognized [16]. The magnitude and sense of the changes induced depend on the magnetostriction coefficient. When the magnetostriction coefficient is positive then the application of a tensile stress permits easier domain vector rotation. This enhances the intensity of magnetization and thus the permeability for a given field. The remanence is also increased resulting in a squarer B-H loop. When the magnetostriction coefficient is negative the application of a tensile stress makes the B-H loop flatter. For a compressive stress these effects are reversed.

The effects of stress on the magnetic properties of certain ferrites have been studied in detail and the results are in agreement with the general statements made above [17, 18, 19]. The fractional change in permeability $^{d\mu}/_{\mu}$ due

to an applied stress (σ) has been estimated to be [17];

$$d\mu/\mu = \frac{9}{40}\frac{\lambda \sigma \mu}{\pi I^2} \qquad (4)$$

where λ is the magnetostriction coefficient and I is the intensity of magnetization.

4.2. Effects on Machining on Magnetic Properties

If the effects induced by ceramic machining are due to residual stresses left by the machining operation then there should be certain consequences. First, it should be possible to remove the effects by etching away the highly stressed surface which the internal material is supporting, second it should be possible to minimize the effects by a stress relief heat treatment, and third the magnitude of the effects should be dependent on the surface to volume ratio. Each of these consequences has been demonstrated at one time or another on a variety of ceramic magnetic materials, namely garnets, Ni-Co, Ni-Zn, Mg-Zn and Mn-Mg ferrites [17, 18, 19].

Figure 4 shows the effect of machining and annealing on the shape of the B-H loop for a toroid cut from the $Ni_{0.36}$ $Zn_{0.64}$ ferrite shown in figure 1. The machined (lapped and polished) material has a flatter loop than the annealed material due to a decrease in permeability, remanence and magnetic saturation. This particular ferrite has a negative magnetostriction coefficient and the changes are consistent with the existence of residual tensile stresses.

This observation is significant since tensile stresses exist in the interior of the finished ceramic to balance the compressive stresses left in the surface. Thus the effects of surface finishing or magnetic properties are primarily due to changes induced in the *volume* of the material. Such changes will be larger as the

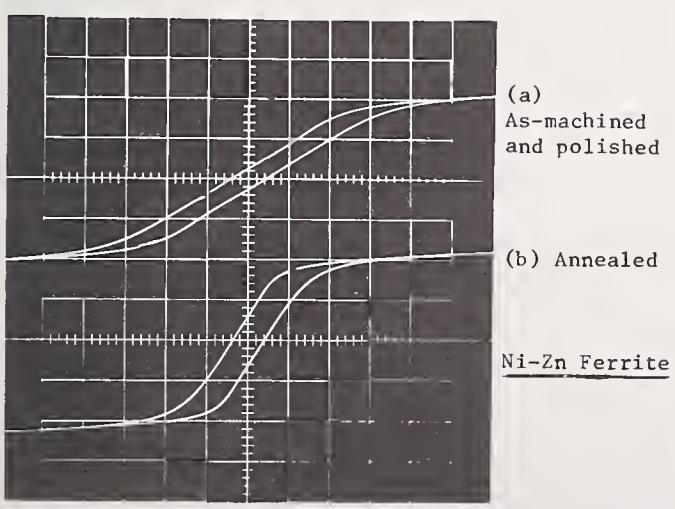

FIGURE 4. *B–H loop for* $Ni_{0.36}$ $Zn_{0.64}$ *ferrite toroid.*
(a) As-machined and polished
(b) Annealed

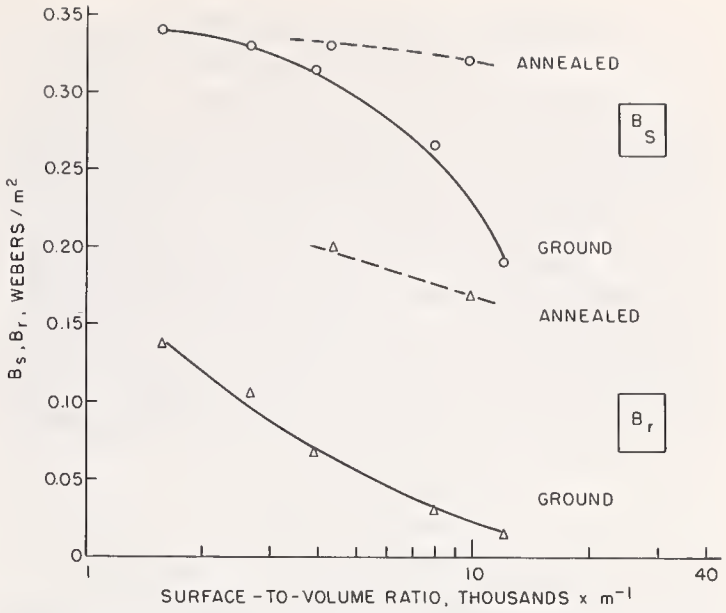

FIGURE 5. *Variation of* B_r and B_s *with specimen size for* $Ni_{0.36}$ $Zn_{0.64}$ *ferrite in the as-machined and annealed conditions.*

volume available to balance the surface stress decreases, as illustrated for remanence (B_r) and magnetic saturation (B_s) in figure 5 for the same NiZn ferrite. Note that annealing causes B_r and B_s to undergo greater recovery as the toroid becomes thinner and the surface to volume ratio iscreases. The fact that annealing does not completely restore these magnetic properties to their true bulk value indicates there is some irreversible surface damage which cannot be removed, this is probably to be associated with surface cracking.

For many applications of magnetic ceramics surface cracking and surface roughness are of great significance. In high frequency multiple gap magnetic recording heads for example, gap alignment and gap definition are extremely important if the flux density is to remain uniform over the total width of the head. The C and I sections of the heads must be lapped flat before bonding and the edge definition must be retained during final shaping of the head. Dimensional tolerances of 0.1 μm are essential and the occurrence of grain pull-out or the incidence of porosity in the gap region are generally unacceptable.

5. Effects of Surface Finishing on the Electrical Properties of Ceramics

Ceramics offer a wide variety of electrical properties. Depending on their composition and crystal structure they may be either semiconductors, dielectrics, insulators or piezoelectrics. Effects of surface condition on the electrical properties have not been studied directly, nevertheless they are extremely important.

5.1. Effects of Surface Finishing on Semiconductor Properties

In order to indicate how surface condition might affect the electrical properties of ceramic semiconductors we have to draw on observations made on the elemental semiconductors, Ge and Si. The drastic effects of mechanical surface damage, produced by sawing and lapping was one of the earliest effects recognized in germanium and silicon transistor research. Indeed, various chemical etchants have been developed specifically to remove mechanically damaged material and this is an important aspect of silicon technology [20].

The most critical features of the machined surface are the surface defects, i.e.,—dislocations, vacancies and cracks. Their primary effect is to provide trapping sites for the positive and negative charge carriers, resulting in their recombination and annihilation. Once annihilated the charge carriers can no longer contribute to the establishment of a current or potential difference essential in a device operation.

The effectiveness of trapping sites as recombination centers may be measured in terms of the surface recombination velocity, i.e.,—the recombination rate per unit surface area. A sensitive method for determining the surface recombination velocity is the measurement of the photoelectromagnetic (PEM) voltage generated when a surface is illuminated while inserted in a magnetic field. The lower the surface recombination velocity the greater the density and separation of the positive and negative charge carriers and thus the higher the PEM voltage.

Figure 6 illustrates the normalized value of the PEM voltage (V_x) in germanium as a function of the material removed by etching. It can be seen that different surface finishing operations cause damage of varying depth with the sand blast treatment being the worst, it damages a layer 32 μm deep.

Surface recombination velocity is a critical parameter in the detectivity (D*) of semiconductor radiation detectors depicted in figure 7. Detailed analysis [21] shows that.

$$D^* \propto f_1 (\mu, \gamma, n) \; f_2 (S_1, S_2) \qquad (5)$$

where f_1 is a complicated function of charge carrier mobility (μ), lifetime (γ) and concentration (n) and f_2 is a function of the front (i.e.,—the illuminated) and back surface recombination velocity (S).

In the photoconductive mode, an electric field (E) is applied during radiation (there is no magnetic field, i.e.,—B = O) and the detector current must be maximized. In this instance both the front (S_1) and the back (S_2) recombination velocities should tend to zero. Thus the whole surface must be chemically etched to eliminate mechanical damage.

In the photoelectric-magnetic (PEM) mode, on the other hand, a magnetic field (B) is applied during radiation (there is no electric field, i.e.,—E = O) and the detector PEM voltage must be optimized. In this instance the charge carriers generated at the front surface drift down the concentration gradient towards the back surface. As they drift they separate to establish the PEM voltage. Charge carriers reflected at the back surface will be deflected by the magnetic field in the opposite sense, generating a voltage tending to cancel out the PEM voltage. Thus to maximize the PEM voltage reflection must be avoided at the back surface by the generation of a charge carrier sink there. To achieve this, recombination (S_2) is deliberately increased by abrading the back surface. This is surely a rare instance where sur-

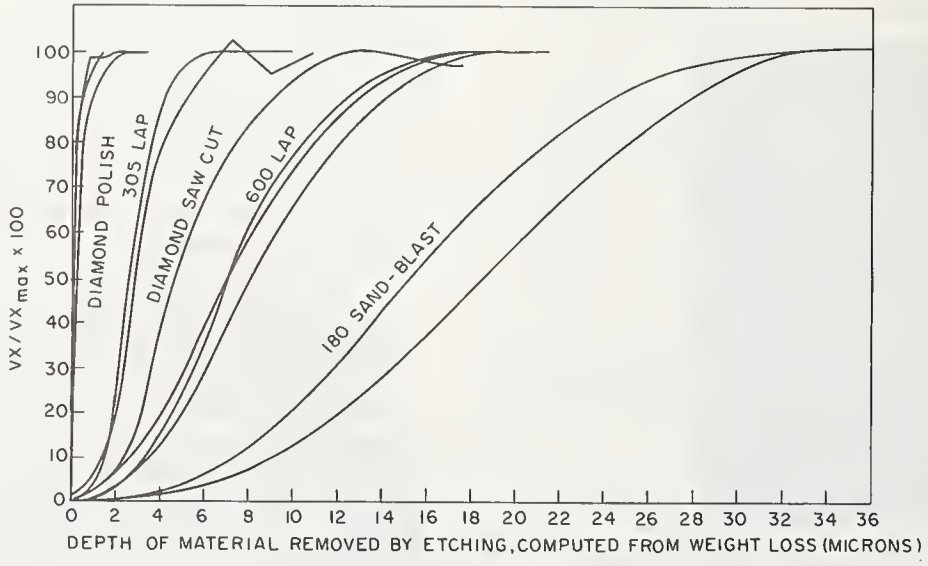

FIGURE 6. *Effect of surface condition on the PEM voltage of germanium.* (After Buck and McKim-Ref. 20).

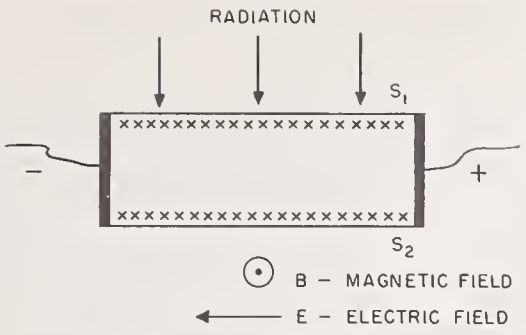

FIGURE 7. *Diagrammatic representation of radiation detectors.* (Photoconductive mode B=0, Photoelectromagnetic mode E=0).

face damage is used to enhance the performance of a device!

We are not aware of comparable studies on the effects of surface finishing on the electrical properties of oxide semiconducting ceramics. However, the introduction of dislocations and point defects by machining will certainly generate a variety of trapping sites in the surface causing effects similar to those noted above.

5.2. Effects of Surface Finishing on Other Electrical Properties

The most prominent problems associated with surface finish on dielectrics and insulators are due to surface cracking. The absorption of conducting materials on the rough surfaces can result in premature electrical breakdown. It is for this reason that most insulating ceramics are glazed to avoid the build up of contamination [22].

In the case of piezoelectric ceramics it is to be expected that the major effects of surface condition will be those associated with residual stresses in much the same manner as described for magnetic materials. The magnitude of the effect will depend on the piezoelectric coefficient. Residual stresses have been shown to affect the temperature at which the ferroelectric phase transition takes place in barium titanate and quartz [23]. Obviously, annealing treatments must be developed for reproducible behavior in piezoelectric devices, whether used for voltage generation or ultrasonic drivers.

6. Effects of Surface Finishing on the Optical Properties of Ceramics

Ceramics find many applications by virtue of their unique optical properties in lasers, light modulators and electro-optic devices. Surface finishing is an important aspect in the fabrication of such devices. There are obvious effects of surface roughness on reflectivity and emissivity although these have not been studied systematically [22]. Residual stresses also have obvious effects on the local refractive index. Precision optical materials must be carefully annealed to relieve residual stresses.

Recent developments of fully dense hot pressed lead zirconate—lead titanate (PZT) ferroelectric ceramics offer unique possibilities for light beam addressable data storage applications [24]. Internal stresses induced by the application of local electric fields cause light to be reflected at internal grain boundaries and modulate the intensity of transmitted light. Any residual stresses from mechanical finishing operations must therefore be minimized or even eliminated by annealing for successful operation of such devices.

7. Summary

As ceramics find new applications requiring precise shape and surface finish it has become necessary to understand the consequences of surface finishing operations on the physical properties being exploited. Ceramic machining results in a defective surface containing cracks, dislocations, point defects and residual stresses. The significance of these defects depends on the particular physical property of interest. Mechanical properties are particularly sensitive to surface cracking; electrical properties are particularly sensitive to surface dislocations and point defects; magnetic, piezoelectric and optical properties are particularly sensitive to residual stress. Special precautions or treatments are necessary to avoid or eliminate surface defects. The finished component may need to be machined, lapped and polished in a precise sequence; the finished surface may need to be chemically etched; or the finished component may need a thermal stress relief anneal to overcome the deleterious consequences of ceramic machining. While this subject has in the past received a general qualitative appreciation of the need to improve surface condition in the application of ceramics, it lacks detailed fundamental studies on the precise magnitude, nature and extent of the changes in physical properties.

The author has benefited immeasurably from discussion with Drs. J. R. Kench, B. G. Koepke, and P. W. Kruse. In particular, the results and analysis of the effect of surface condition on magnetic behavior in figures 4 and 5 are due to Dr. J. R. Kench; the studies of the surface features associated with ceramic machining are due to Dr. B. G. Koepke; and the information on radiation detectors is due to Dr. P. W. Kruse.

8. References

[1] Koepke, B. G., these Proceedings.
[2] Evans, A. G., and Davidge, R. W., Philosophical Magazine 20, 373–388 (1969).
[3] Rice, R. W., Paper presented at 72nd Annual Meeting, American Ceramic Society, Philadelphia, May 1970.
[4] Koepke, B. G., and Stokes, R. J., Journal Materials Science 5, 240–247 (1970).
[5] Stickler, R., and Booker, G. R., Philosophical Magazine 8, 859–875 (1963).
[6] Hockey, B. J., these Proceedings.
[7] Cutter, I., and McPherson, R., Philosophical Magazine 20, 489–94 (1969).
[8] Stokes, R. J., Fundamental phenomena in the materials sciences, Vol. 4, pp. 151–175, (Plenum Press, Inc., New York, N. Y., 1967).
[9] Stokes, R. J., Trans. Am. Inst. Min. Metall. Engrs. 224, 1227–1237 (1962).
[10] Stokes, R. J., and Li, C. H., Fracture of Solids, pp. 289–313, (John Wiley and Sons, Inc., New York, N. Y., 1963).
[11] Clarke, F.J.P.C., Sambell, R.A.J., and Tattersall, H.G., Philosophical Magazine 7, pp. 393–413 (1962).
[12] Johnston, T.L., Stokes, R.J., and Li, C.H., Philosophical Magazine 4, 1316–24 (1959).
[13] Carniglia, S.C., Journal Am. Ceram. Soc. 48, 580–83 (1965).
[14] Harrison, W.B., Journal Am. Ceram. Soc. 47, pp. 574–79 (1964).
[15] Gruszka, R.F., Mistler, R.E., and Runk, R.B., Bulletin Amer. Ceram. Soc. 49, 575–79 (1970).
[16] Bozorth, R.M., Ferromagnetism, p. 620, (D. Van Nostrand Co., Inc., New York, N.Y. 1963).
[17] Ratheneau, G.W. and Fast, J.F., Physica, 21, pp. 964–70 (1955).
[18] Stern, E. and Temme, D., I.E.E.E. Transactions on Microwave Theory and Techniques 13, pp. 873–4 (1965).
[19] Knowles, J.E., Brit Journal Physics, D: Appl. Phys., 3, 1346–51 (1970).
[20] Buck, T.M., and McKim, F.S., Journal Electrochem. Soc. 103, 593–97 (1956).
[21] Kruse, P.W., McGlauchlin, L.D., and McQuistan, R.B., Elements of Infrared Technology, pp. 324–345 (John Wiley and Sons, Inc., New York, N.Y., 1962).
[22] Kingery, W.D., Introduction To Ceramics, p. 524, p. 647, (John Wiley and Sons, Inc., New York, N.Y., 1960).
[23] Bogardus, E.H. and Roy, R., Journal Am. Ceram. Soc., 48, 205–7 (1965).
[23] Land, C.E., Sandia Laboratories Report, SC–R–67–1219, (October 1967).

Discussion

RICE: One brief comment, twinning can cause some of the same surface sensitive effects that slip can and therefore this should also be considered in defining whether a material is totally brittle or semibrittle.

NATIONAL BUREAU OF STANDARDS SPECIAL PUB. 348, THE SCIENCE OF CERAMIC MACHINING AND SURFACE FINISHING, Proceedings of a Symposium Sponsored by the American Ceramic Society, the Office of Naval Research, and the National Bureau of Standards, held at NBS Nov. 2–4, 1970, Gaithersburg, Md. (Issued May 1972).

Strength Effects Resulting from Simple Surface Treatments

H. P. Kirchner, R. M. Gruver, and R. E. Walker

Ceramic Finishing Company, State College, Pennsylvania 16801

In well made polycrystalline alumina ceramics subjected to external loads, fracture originates, in almost every case, at surface flaws rather than at volume flaws. This susceptibility to surface flaw failure has been reliably established in experiments in which compressive surface layers were used to obtain substantial improvements in strength. Knowing that the failures occur at surface flaws, the artificial introduction of surface flaws can be used to obtain an understanding of the ways in which surface flaws affect the strength. Additional information can be gained by using simple treatments to change these artificial surface flaws and by observing the effect of these treatments on the strength.

In the present investigation artificial flaws were introduced by single point tools, abrading, thermal shock, and abrasive machining. The flaws were treated by refiring, chemical and flame polishing, chemical etching, glazing and prolonged storage in various environments.

The changes in the flaws were characterized by microscopy and to a limited extent by profilometry. Both flexural and tensile strengths were measured. The effects of the treatments are discussed in terms of changes in the average strength and variations in the distributions of the individual strengths.

Key words: Abrasive machining; alumina ceramic; chemical polishing; crack healing; delayed fracture; glazing; humidity; refiring; strength; surface flaws; surface treatments; thermal shock.

1. Introduction

Present evidence indicates that there are several classes of flaws that affect the strength of polycrystalline ceramics. These include discontinuities in the elastic properties, chemical flaws and residual stresses. The experiments described in this investigation deal primarily with the first type, discontinuities in the elastic properties, and especially those flaws in which the discontinuity consists of missing material as in the case of surface roughness or cracks. The effects of the other classes of flaws were investigated to a limited extent in delayed fracture and annealing experiments.

In well made polycrystalline alumina ceramics subjected to external loads, fracture originates, in most every case, at surface flaws rather than at volume flaws. This susceptibility to surface flaw failure has been reliably established in experiments in which compressive surface layers were used to obtain substantial improvements in strength. Knowing that the failures occur at surface flaws, the artificial introduction of surface flaws can be used to obtain an understanding of the ways in which surface flaws affect the strength. Additional information can be gained by using simple treatments to change these artificial surface flaws and by determining the effect of these treatments on the strength.

It is usually accepted that the as-fired surfaces of ceramics have the best integrity, in the sense of absence of gross flaws. Therefore, only limited improvement in strength should be expected to result from polishing to improve the smoothness. For example, the specimens with an average flexural strength of 51,500 psi (36.2×10^6 kg/m^2) in the as-fired condition were polished. From 0.0001 to 0.0003 in of material was removed. The amount of material removed was minimized in order to retain as much as possible of the high integrity skin. The average flexural strength of the polished material was 56,100 psi (39.5×10^6 kg/m^2), an improvement of nine percent.

In the present investigation, artificial flaws were introduced into the as-fired surfaces by scoring with single point tools, abrading, thermal shock, and abrasive machining. The flaws were treated by refiring, chemical and flame polishing, chemical etching, glazing, prolonged storage in various environments, and so forth.

The changes in the flaws were characterized by microscopy and to a limited extent by profilometry. The effects of the treatments are discussed in terms of changes in the average flexural strength and variations in the distributions of the individual strengths.

The principal material used in this investigation was a 96 percent alumina body [1], extruded to form rods that ranged from 0.125 to 0.198 in in diameter. The average grain size was about 5 micrometers.

2. Strength Effects Resulting from Simple Surface Treatments

2.1. Humidity, Refiring, and Storage

Humidity is well known to decrease the strength of alumina ceramics if it is present in

[1] ALSIMAG #614, American Lava Corporation.

testing environment. The average flexural strength of the 96 percent alumina decreases from 48,400 psi (34.0×10^6 kg/m^2) when tested in 18 percent relative humidity to 41,700 psi (29.3×10^6 kg/m^2) when tested under water. This difference represents a decrease of about 14 percent. Clearly, it is advisable to make comparative measurements under controlled humidity conditions or at least at the same relative humidity.

Distribution curves for the flexural strengths under four different humidity conditions are shown in figure 1. The shapes of the distribution curves are quite alike, but the curves for 84 percent relative humidity and testing under water do have somewhat greater scatter than the curves for 18 percent and 32 percent relative humidity.

Storage under humid conditions seems to have little or no effect on the flexural strength. For example, soaking in water for 67 hours, followed by testing in the laboratory atmosphere, gave results similar to those expected for as received controls.

When specimens were stored in the laboratory for 300 days, a decrease in strength was observed. This decrease is attributed to the difference in humidity when the specimens were originally tested (about 10%) and when they were tested after storage (about 45%).

Humidity reduces the observed strength of polycrystalline alumina. If similar material is loaded almost to the fracture stress in an environment containing water, the material will fracture within a short time. However, if water is not present the material will withstand the load for very long periods of time, if not forever. This phenomenon involving water is called static fatigue or delayed fracture.

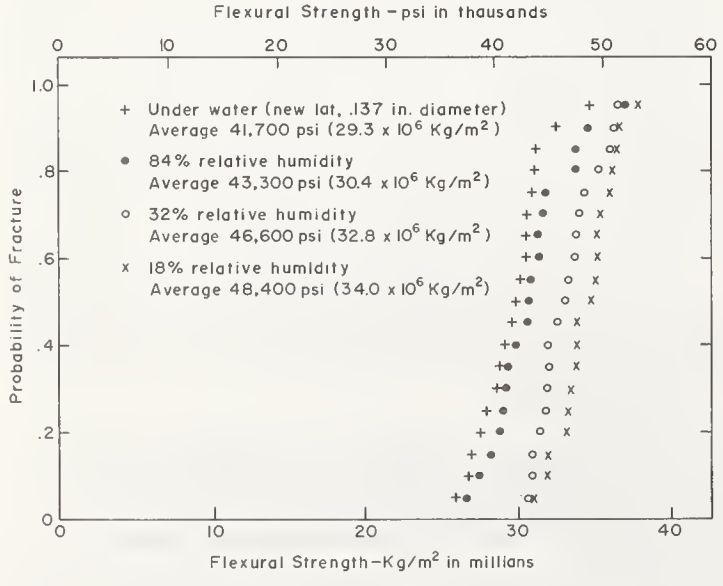

FIGURE 1. *Distribution curves for 96 percent alumina at various relative humidities.*

The effect of immersion in water on delayed fracture performance is shown in figure 2 in which this performance is compared with that of similar material tested in a laboratory atmosphere. The observed strength at short time is similar to that expected from figure 1, but after 10,000 seconds the strength difference narrows only to about 2,000 psi (1.4×10^6 kg/m^2). Based upon these results, it is evident that the delayed fracture curves for increasing humidity will consist of a family of curves between the two curves in figure 2 (and other curves at higher stresses and lower humidities).

Refired may have several effects on the surface of alumina ceramics. Thermal etching may lead to new stress concentrators. Surface flaws may be healed. In addition, annealing may cause reduction of both large scale and localized residual stresses. When 96 percent alumina rods are refired, the average flexural strength increases. These results are presented in figure 3.

If more than one type of surface flaw contributes to the observed failures and if refiring fails to affect at least one of these types of flaws, then one would expect some of the weak-

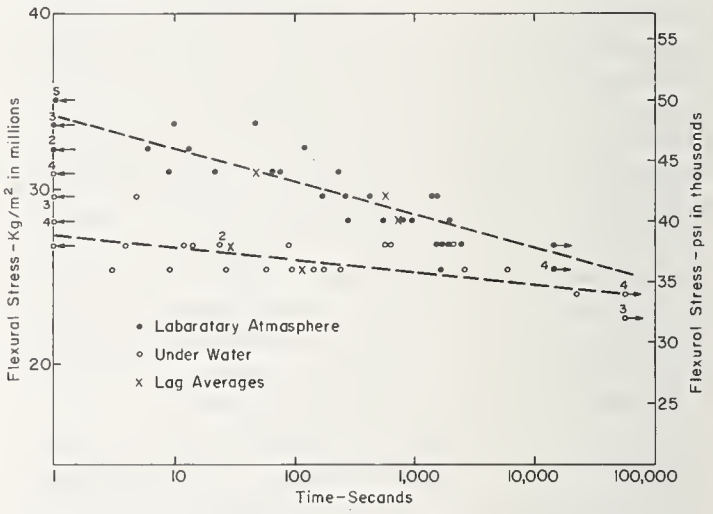

FIGURE 2. *Delayed fracture of 96 percent alumina.*

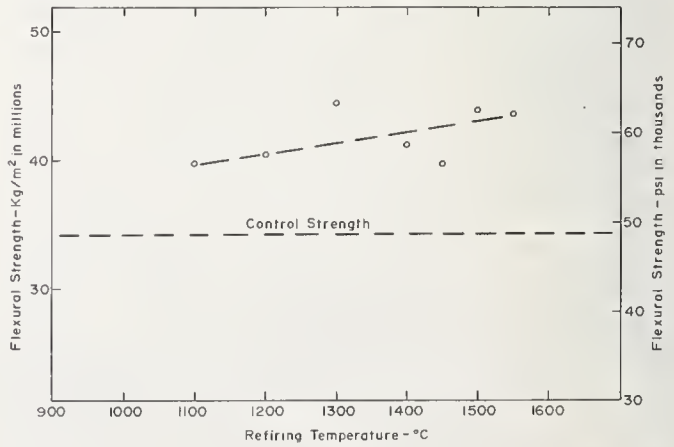

FIGURE 3. *Flexural strength of 96 percent alumina rods refired to various temperatures.*

est specimens to remain weak after refiring. In that case, the scatter of the strengths will increase. Distribution curves for 96 percent alumina rods before and after refiring at 1500 °C for one hour are given in figure 4. The scatter of the refired strengths is much greater than the scatter of the as received strengths. Some of the weakest specimens do remain weak after refiring.

Refined specimens were tested before and after storage for 300 days. The distribution curves are presented in figure 5. Again the small decrease in average flexural strength is attributed to the difference in the humidities when the specimens were tested. The distributions of the strengths remain the same and there seems to be no definite tendency to revert to the less scattered distribution characteristic of the specimen before refiring.

2.2. Flaws Caused by Abrasion

The average strength and the distribution of the individual strength values can be varied by abrasion or proof testing, or by combinations of these treatments. Abrasion, by milling the samples in abrasive grain causes randomly oriented scratches. These scratches decrease the average strength and make the strength distributions more uniform. Apparently, abrasion by fine grain size abrasives introduces small flaws into the surface of the samples. The flexural strengths of the stronger specimens in the group are reduced more than those of the weaker specimens. The flaws introduced into the surfaces of the weaker specimens are not very severe relative to those already present so that the weaker specimens are weakened only slightly if at all.

Proof testing removes the weaker specimens from the distribution. This raises the average strength of the remaining specimens and decreases the scatter of the individual strength values. If specimens are proof tested at a relatively high stress, the remaining specimens will not fail at stresses substantially lower than the proof test level because those with severe surface or volume flaws were removed from the distribution. Subsequently, the specimens can be abraded to reduce the strength of all of the specimens below the stress at which they were proof tested. In this condition none of the specimens will exhibit volume flaw failure.

96 percent alumina in the "as received" condition was proof tested at 45,000 psi ($31.6 \times 10^6 kg/m^2$) removing about 50 percent of the specimens from the distribution and then abraded to reduce the strength of the remaining specimens below the proof test level. The abrasion process. Ten minutes in 240-mesh B_4C, was more severe than expected causing a substantial reduction in strength. Even so, a much more uniform strength distribution with a standard deviation of 1700 psi (1.2×10^6 kg/m^2) and coefficient of variation of 4.2 percent, was obtained. The distribution curve is presented in figure 6 where it is compared with the results for "as received" and "as received"

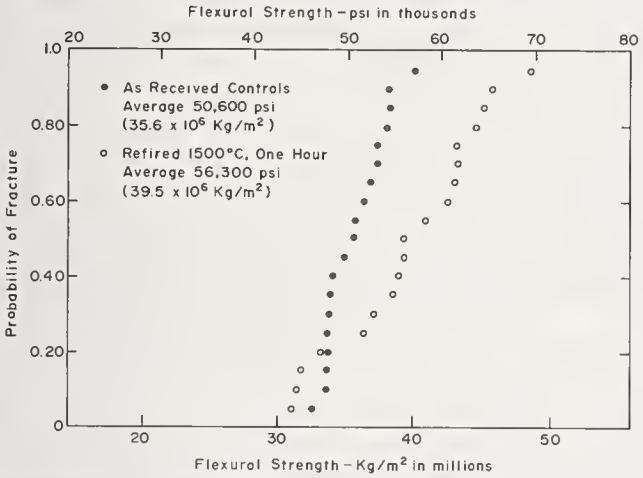

FIGURE 4. *Distribution of flexural strengths of 96 percent alumina before and after refiring at 1500 °C for one hour.*

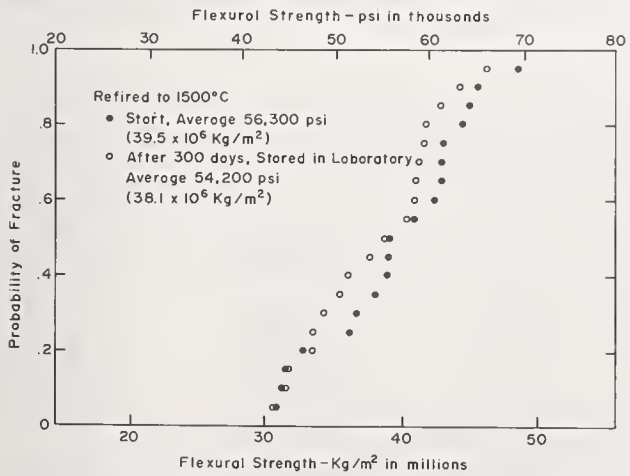

FIGURE 5. *Distribution of flexural strengths of refired 96 percent alumina before and after storage for 300 days.*

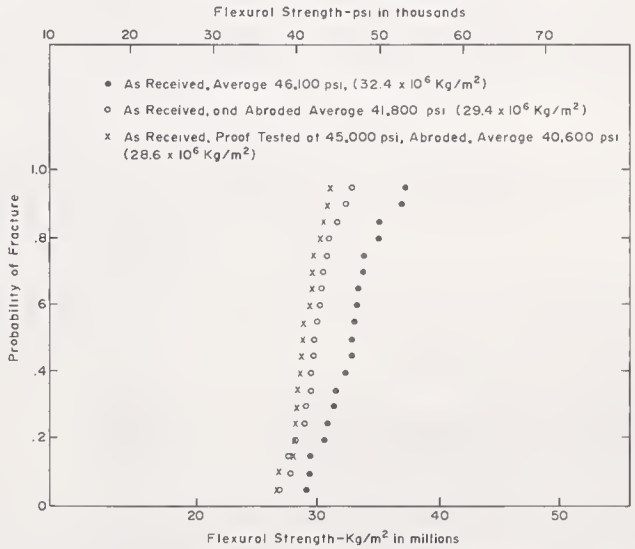

FIGURE 6. *Flexural strength of 96 percent alumina in as received and abraded condition.*

and abraded specimens. The proof testing and abrading reduces the scatter almost in half. The abrasion treatment by itself is quite effective in reducing the scattering of the flexural strength data and resulted in a standard deviation of 2200 psi ($1.55 \times 10^6 kg/m^2$).

Similar reductions in scatter have been observed as a result of abrasion followed by tensile strength measurement.

Flaws were also introduced by abrading the specimens with coated abrasives. After several exploratory treatments, two treatments were selected for further investigation. One of these treatments consisted of using 220-mesh SiC abrasive paper to abrade the surface of the specimen while it rotated in a lathe. A fixed load was applied by hanging a weight on the paper. In the other case, 100-mesh SiC abrasive paper was used and only the center of the rod in a strip one inch wide was abraded. The scratches caused by these abrasion treatments are perpendicular to the stresses. The results of these experiments are presented in table 1. Abrasion with the 220-mesh SiC causes only a slight reduction in the strength compared with the "as received" material. This decrease in strength is more than regained by refiring. The abraded material that was refired is slightly stronger than the refired controls. On the other hand material that is refired and then abraded is weak like the as received and abraded rods. Since the gross surface roughness is unlikely to be much affected by refiring, it is evident that the flaws that affect the strength and that are introduced by abrasion are microscopic in character and are healed by refiring. Glazing of the abraded material further increases the strength to 76,500 psi ($53.8 \times 10^6 kg/m^2$). This glaze has a lower expansion coefficient than the alumina and is in compression after firing. Because of the large difference in elastic modulus between the glaze and the alumina body, the gross roughness in the alumina surface as a result of abrasion still constitutes flaws with large associated stress concentrations. However, the high strengths observed after glazing indicate that these are not critical flaws. Apparently, the flaws that weaken the samples after abrasion are very small and are healed by refiring and subsequently protected by the glaze.

Abrasion by the 100-mesh SiC caused very severe gouging of the surface. The flexural strength decreased 12,400 psi (8.7×10^6 kg/m^2) to 30,000 psi (21.1×10^6 kg/m^2). However, the strength was regained on refiring and increased substantially when the abraded specimens were glazed.

Other specimens were abraded and the delayed fracture performance under water was determined. These results are presented in figure 7. This curve is very similar to that of the unabraded specimens. Therefore, the available evidence does not show any substantial effect of abrasion on delayed fracture.

2.3. Flaws Made Using Single Point Tools

Two methods were used to make surface flaws using single point tools. The first method involved making a single scratch on the alum-

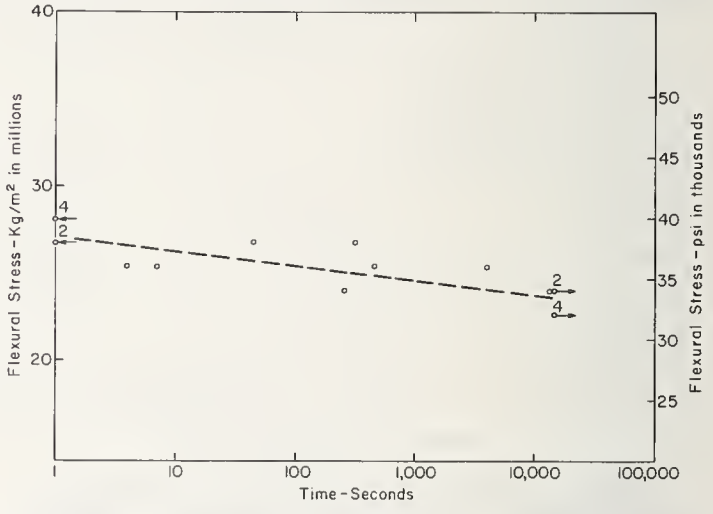

FIGURE 7. *Delayed fracture of 96 percent alumina, abraded by 240-mesh silicon carbide for 10 minutes and tested under water.*

TABLE 1. *Flexural strength of abraded alumina rods treated by refiring and glazing*

Treatment	Refiring conditions		Average flexural strength		
	Temp. °C	Time hours	No. specimens	psi	kg/m² ×10⁻⁶
As received	- - - -	- -	5	42,400	29.8
Abraded, 220 mesh SiC	- - -	- -	5	40,000	28.2
Refired	1500	1	5	50,200	35.3
Abraded, 220 mesh SiC, refired	1500	1	5	51,600	36.3
Refired, abraded, 220 mesh SiC	1500	1	5	41,100	28.9
Abraded, 200 mesh SiC, glazed	1500	1	5	76,500	53.8
Abraded, 100 mesh SiC	- - -	- -	5	30,000	21.1
Refired	1500	1	5	52,300	36.8
Abraded, 100 mesh SiC, refired	1500	1	5	51,600	36.4
Abraded, 100 mesh SiC, glazed	1500	1	5	72,100	50.7

TABLE 2. *Flexural strength [a] 96 per cent alumina rods with axial or circumferential scratches (Rods 0.125 in diameter)*

Load on diamond point	Axial scratch			Circumferential scratch		
	Scratch width	Average flexural strength		Scratch width	Average flexural strength	
grams	*μm*	*psi*	*kg/m²-6 ×10*	*um*	*psi*	*kg/m²-6 ×10*
110	20	48,800	34.3	20	42,400	29.8
220	25	50,800	35.7	30	25,700	18.1
420	30	47,500	33.4	35	24,500	17.2
720	30	45,000	31.6	35	20,700	14.5
220	--	[b]59,400	41.7(b)	--	62,900(b)	44.1(b)

[a] 50 per cent relative humidity
[b] After refiring at 1500 °C for one hr.

ina rod using a diamond point (75° coned wheel dresser, 1/4 carat) subjected to various loads. These rods were scratched in axial and circumferential directions. The flexural strengths of specimens scratched by the diamond point subjected to various loads, were measured. In both cases, the scratches were located in the region of maximum tensile stress during testing. The widths of the scratches and the flexural strengths are given in table 2. The flexural strengths are plotted against applied load in figure 8. The circumferential scratches reduce the flexural strengths much more than the axial scratches. Although the widths of the circumferential scratches at a given load seem slightly greater than the width of the axial scratches, the difference does not seem sufficient to explain the difference in strength.

Specimens scratched under a load of 220 grams were refired at 1500 °C for one hour. As a result of refiring, the average flexural strengths were higher than the strengths before scratching, indicating that the critical flaws associated with these scratches were healed by refiring.

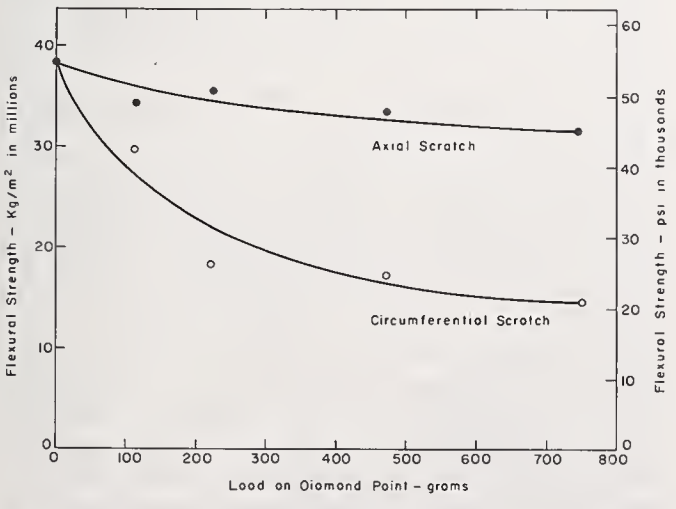

FIGURE 8. *Flexural strength of 96 percent alumina rods vs. load on diamond point.*

The second method involved scoring the alumina rods with a diamond tool while they were held in a lathe. The specimens were scored to various depths. In this case the cuts were several times as wide as they were deep so that the cut itself was not expected to have a large stress concentration factor but smaller cracks resulting from surface damage during the scoring may have serious stress concentrations. Four grooves were cut in the test section of each sample. The grooves were approximately one-eighth inch apart. The flexural strengths were measured and are presented in figure 9 for various depths of cuts. The samples always broke at one or the other of the outermost grooves. Using these results, a depth of cut of 0.002 in was chosen and scored specimens were treated by refiring and by glazing. These flexural strength results are presented in table 3. Note that in each case the scored specimens are only slightly weaker than the com-

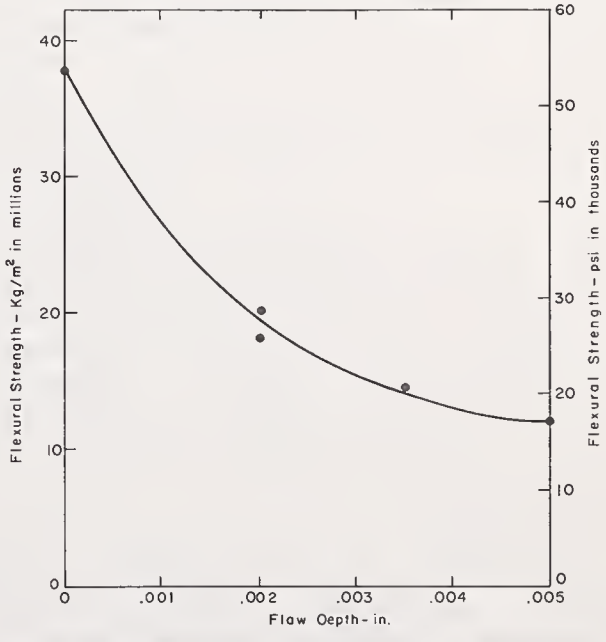

FIGURE 9. *Flexural strengths of 96 percent alumina rods scored to various depths.*

439-921 O - 72 - 24

TABLE 3. *Flexural strengths of scored [a] ALSIMAG #614 rods, refired or glazed (0.15 in diameter rods)*

Treatment	Treatment conditions			Average Flexural strength [b]	
	Temp. °C	Time hours	No. specimens		
				psi	kg/m^2-6 ×10
As received	----	--	5	46,800	32.9
Scored to 0.002 in	----	--	5	28,900	20.3
Refired, cooled with kiln	1500	1	5	51,400	36.1
Scored, refired, cooled with kiln	1500	1	5	46,900	32.9
Glazed, cooled with kiln	1500	1	5	62,400	43.8
Scored, glazed, cooled with kiln	1500	1	5	57,300	40.2

[a] Turned on lathe with diamond tip cutting tool to 0.002 in.
[b] Four point loading on a 2 in span.

parable unscored specimens indicating that the treatments are effective in either healing the cracks or preventing them from acting to cause failure.

2.4. Flaws Made by Thermal Shock Treatments

Flaws were also introduced by thermal shock treatments. In this case the specimens were quenched in room temperature water from a temperature 225 °C above room temperature. This treatment is sufficient to reduce the strength of the rods to about 25 percent of the "as received" value. The thermal shock treatment leads to very thin cracks that are observable by dye testing. They form as a result of tensile stresses induced in the surface layer by quenching.

Dye tested specimens, profilometer traces and optical and scanning electron micrographs were studied in an attempt to characterize these cracks. The area density of the cracks increases strongly with increasing quenching temperature. At the lowest quenching temperature at which cracks form, all of the cracks are circumferential. As the quenching temperature increases, some cracks bend to join neighboring cracks. At high quenching temperatures, a checkered pattern of cracks is formed. When the specimens were dye tested and then broken at the large cracks, the dye was observed to have penetrated to a depth of as much as one-third of the sample diameter (0.040 in for 0.125 in diameter samples). The depth and sharpness of these cracks accounts for the great loss in strength.

Photomicrographs of a quenched specimen are presented in figure 10. In this case the specimen was polished, thermally etched for five minutes at 1600 °C, and thermally shocked by quenching in water at 25 °C from an oven at 325 °C. Figure 10a, a scanning electron micrograph at 3000X shows a transgranular thermal shock crack about one micrometers wide running through alumina grains five to twelve micrometers in diameter. The crack seems to be filled with debris. The thermally etched grain boundaries are one-half to one micrometers wide. The grains have flat tops as a result of polishing.

Figure 10b, 1000×, shows a larger area of the specimen and provides an indication of the concentration of pores, pullouts, etc.

Figure 10c, an optical photomicrograph at 450× shows the thermal shock crack cutting across many grains. The microstructure of the body, including the variations in grain size and shape, porosity, and relationships of alumina grains to matrix material are evident.

The surface profiles of the thermally shocked 96 percent alumina were studied in an attempt to detect the cracks. The measurements were made at American Lava Corporation using a TALYSURF [2]. One specimen (fig. 11a) was polished, thermally etched, thermally shocked (ΔT = 300 °C) and repolished. Dye testing showed an average of a major thermal crack every 0.045 in across the surface. The trace in figure 11a shows a drop of more than 0.00001 in on the average of every 0.007 in across the surface. Assuming a hemispherical tip on the 0.0001 in diameter stylus, a crack or hole two micrometers in width is required to show this deflection. The thermal shock cracks are not wide enough and do not occur frequently enough to account for the large deflections shown in the figure. Since grain boundary relief formed by thermal etching is also quite narrow and occurs more frequently than the large deflections, these deflections cannot be ac-

[2] Measurements made under the direction of Mr. R. D. Dillender.

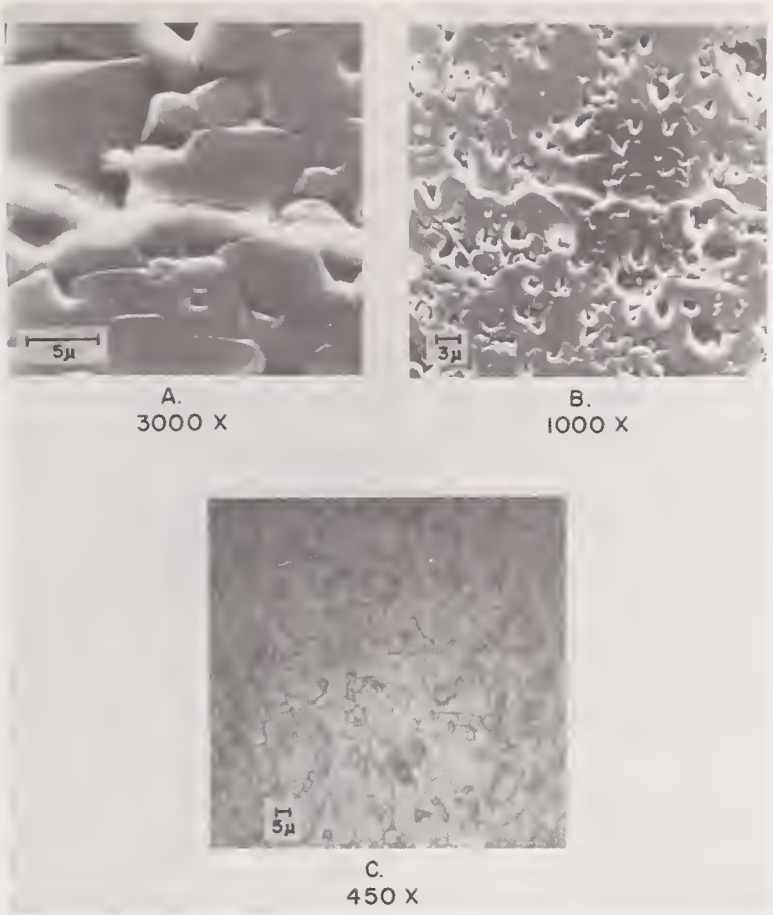

FIGURE 10. *Ninety six percent alumina polished, thermally etched and thermally shocked.*

counted for by grain boundaries. Therefore, it seems likely that these deflections represent rather wide, shallow voids caused by pores, pullouts, etc.

Figure 11b shows a trace on the same sample in the thermally etched condition before repolishing. The number of small peaks in this trace is consistent with the expected frequency of grain boundaries. In this case, major thermal shock cracks indicated by dye testing occurred every 0.080 in on the average across the surface. Again, the large deflections occur too frequently to be accounted for by the thermal shock cracks alone.

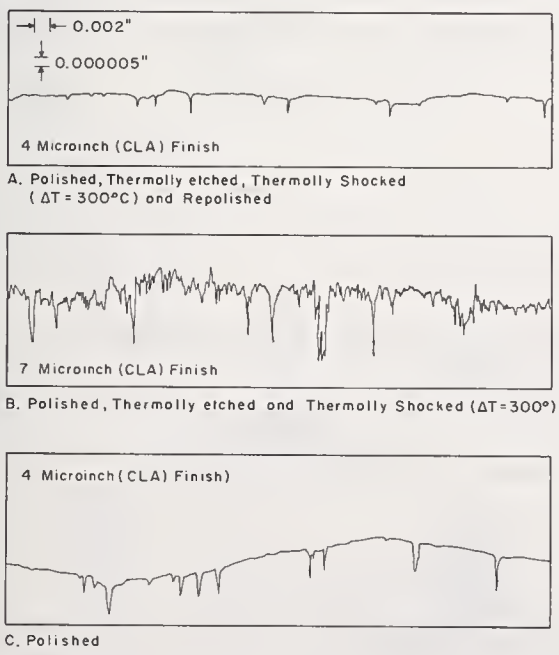

FIGURE 11. *Talysurf traces for thermally shocked ALSIMAG No. 614 96 percent alumina.*

Figure 11c shows the trace for a polished sample. After dye testing, this sample showed no flaws. The large deflections are slightly more frequent than they are in (a) but the traces are quite similar.

The thermal shock treatments are very effective in degrading the strength of alumina. This decrease in strength is the result of formation of very narrow, deep cracks. The surface profiles do not show evidence of these cracks. Measurements of surface roughness alone are not sufficient to evaluate the relationship between the quality of a surface and strength. The cracks are thought to lead to severe stress concentrations. Treatments with 76 percent H_2SO_4 + 12 percent HF or 85 percent orthophosphoric acid (H_3PO_4) were used in an attempt to round these cracks and thereby reduce their stress concentrating effect. These experiments were unsuccessful, although some im-

provement in strength of the "as received" specimens was observed as a result of chemical polishing. The flexural strength results are presented in table 4. Refiring of the thermally shocked specimens healed the cracks (although they remain visible at high temperatures because of increased emissivity) and the specimens became stronger than they were originally and comparable in strength to the "as received" specimens that were simply refired.

The flaws in the thermally shocked specimens can also be healed by gas-oxygen flame from a welding torch. The results are presented in table 5. This treatment might be useful for repairing small parts that are accidentally thermal shocked during use.

2.5. Abrasive Machining

The evidence presented in the previous sections shows that even though it is possible to

TABLE 4. *Flexural strengths of ALSIMAG #614 rods with flaws introduced by thermal shock treatments* (a) (*Rods 0.125 in diameter*)

Treatment	Treatment conditions		No. specimens	Average flexural strength (b)	
	Temp. °C	Time hours		*psi*	*kg/m²-6 ×10*
As received controls	----	--	5	41,800	29.4
Treatment in 76 per cent H_2SO_4 + 12 per cent HF, s.	----	--	5	42,200	29.6
Treated in H_3PO_4, 5 min.	----	--	5	43,800	30.8
Thermally shocked	----	--	5	10,400	7.3
Thermally shocked, treated in 76 per cent H_2SO_4, 12 per cent HF, 15 s. min.	----	--	4	11,800	8.3
Thermally shocked, treated in H_3PO_4 5 min.	----	--	5	11,800	6.0
Refired	1500	1	5	53,300	37.4
Refired, treated in 76 per cent H_2SO_4 + 12 per cent HF, 15 s.	1500	1	5	55,500	39.0
Refired, treated in H_3PO_4, 5 min.	1500	1	5	52,300	36.7
Thermally shocked, refired	1500	1	5	53,900	37.8
Thermally shocked, treated in 76 per cent H_2SO_4 + 12 per cent HF, 15 s., refired	1500	1	5	55,100	38.7
Thermally shocked, treated in H_3PO_4, 5 min, refired	1500	1	5	55,400	38.8

(a) Thermal shocked by quenching in water from 225 °C above room temperature
(b) Four point loading on a 2 in span.

TABLE 5. *Flexural strength of 96 per cent alumina rods, thermally shocked, cracks healed by gas torch* (*Rods 0.125 in diam.*)

Treatment	No. specimens	Average flexural strength (a)	
		psi	*kg/m²-6 ×10*
As received	5	41,800	29.4
Reheated with gas torch	5	41,000	28.8
Thermally shocked	5	10,400	7.3
Thermally shocked	4	10,900	7.7
Thermally shocked, reheated with gas torch to heal cracks	5	41,600 (b)	29.2

(a) Four point loading on a 2 in span.
(b) Some low values in group indicated partial rehealing

vary the strength of alumina ceramics by abrading, the resulting strength is not related primarily to the large scale surface roughness but depends mainly on some kind of microscopic damage. Although no comprehensive investigation of the effect of abrasive machining on the strength has been made at Ceramic Finishing Company, a limited amount of practical experience has supported the opinion that careful machining of 96 percent alumina has very little effect on the strength.

96 percent alumina rods were machined by two different methods. In one case tensile test specimens with a necked down diameter of about 0.125 in and 3 in long were machined from alumina rods 0.198 in in diameter by 7 in long. The strength of these tensile specimens was measured in flexure by four point loading on a 2 in span. In the other case, the diameter of rods 0.125 in in diameter was reduced in the center to about 0.110 in by forming an arc with a 4 in radius of curvature.

The principal precaution observed in machining these specimens was to rotate the wheel so that the scratches formed by the abrasive were parallel to the axis of the rods and parallel to the expected tensile stresses when the rods were tested in flexure. The machining was done with a Regular Rimlock Industrial Blade [3] 8 in in diameter by 0.040 in wide and rotated at 900 rpm. The alumina rod was rotated under the blade at 6 rpm. The coolant was a 40:1 solution of oil [4] in water.

The distributions of the flexural strengths of the machined specimens are compared with the distribution curve of the as received material in figure 12. The average flexural strengths and the distributions are very similar.

Machined specimens are also strengthened by refiring. The distribution for machined and refired samples is presented in figure 13. Except for the weakest specimens, the distribution is very similar to that of the specimens that are simply refired. At the low strength end of the distribution the machined and refired samples are stronger than the specimens that were simply refired. This observation may indicate that a larger fraction of the critical flaws in the machined samples are capable of being healed by refiring.

Machined specimens were stored in the laboratory for 300 days. The distribution of the flexural strengths of these samples is compared with the distribution before storage in figure 14. The distributions are very similar. Since the measurements after 300 days were made at substantially higher humidity than was present before storage one would expect the average strength to be lower than was observed. Possibly the machined specimens are less sensitive to changes in humidity, during testing, than the as received specimens.

Machined and refired rods were stored in the

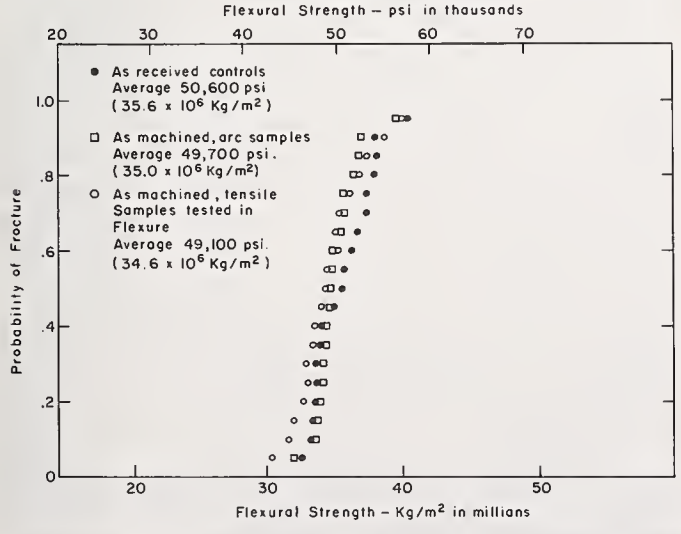

FIGURE 12. *Distribution of flexural strengths of 96 percent alumina before and after machining.*

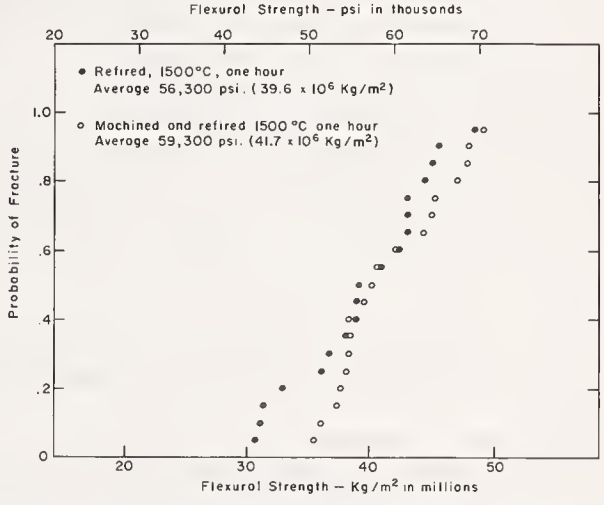

FIGURE 13. *Distribution of flexural strengths of 96 percent alumina machined and refired.*

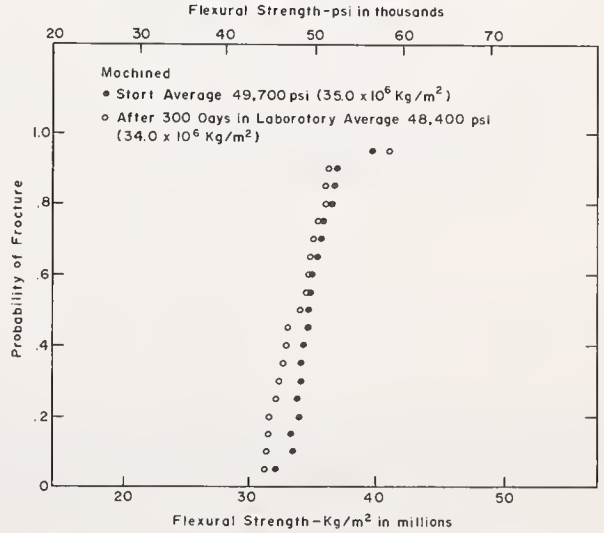

FIGURE 14. *Distribution of flexural strengths of machined alumina before and after storage for 300 days.*

[3] Felker Manufacturing Company.
[4] 0–214 U.S. Army.

laboratory for 300 days and then tested. The results are presented in figure 15. Again, the distribution of the strengths remained essentially unchanged.

3. Summary and Conclusions

Humidity variations in the test environment can cause variations of at least 14 percent in the measured flexural strength of 96 percent alumina. Therefore, comparative measurements should be made under controlled humidity or at the same relative humidity.

Refiring increases the average flexural strength of 96 percent alumina. The scatter of the individual strength values increases substantially. In a storage period of 300 days, the average strength and the distribution of strengths showed little or no tendency to revert back to the as received values.

Abrasion by loose grains can be used to decrease the scatter of the individual strengths. Abrasion by coated abrasives decreases the average flexural strength. This decrease is more than recovered on refiring even in the case of abrasion with 100 mesh SiC paper which causes substantial roughness.

Scratching and scoring with single point diamond tools decrease the average flexural strength. Axial scratches are less damaging than circumferential scratches. Refiring and glazing are effective in healing the critical flaws.

Thermal shock (quenching into water) has the most severe effect on the strength. Again, the loss of strength is more than recovered on refiring.

Although no extensive investigation of the effect of abrasive machining on the strength of 96 percent alumina has been made at Ceramic Finishing Company, the available evidence indicates that careful machining has little effect on either the average strength or the distribution of the individual strengths. Limited evidence from experiments not described in this paper indicates that fine grained, hot pressed alumina is somewhat more susceptible to loss of strength as a result of surface damage. Therefore, the flexural strength of the damaged material can be increased by careful polishing. This susceptibility may be grain size dependent so that this increase in strength may not be observed in coarse grained alumina.

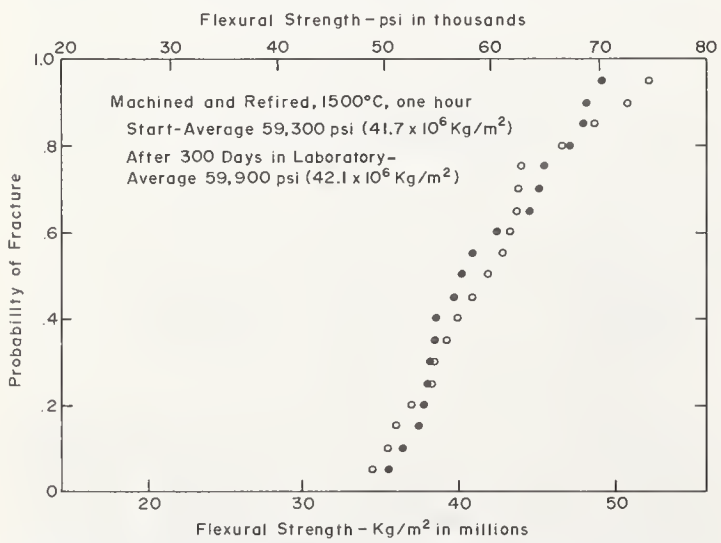

FIGURE 15. *Distribution of flexural strengths of machined and refired alumina before and after storage for 300 days.*

Present evidence indicates that there are several types of critical flaws that may act to cause failure. One class of these flaws, considered in very general terms, involves discontinuities in the elastic properties of the material which lead to stress concentrations. In some cases these flaws may involve missing material such as small cracks, pullouts or pores that open to the surface. The importance of these flaws was demonstrated by the weakening that occurred when the alumina was scratched, abraded or thermal shocked.

Another class of critical flaws are chemical flaws.[5] The importance of these flaws is indicated by the delayed fracture properties of alumina. These flaws are not the same as those above because, when delayed fracture tests on 96 percent alumina are interrupted and the short time strength is measured, the strength is the same as that of material that has not been subjected to the long time static stress. (In other words, it is not merely a matter of crack growth under the influence of stress corrosion.)

Still another class of flaws that may be important in some cases is the class consisting of the localized stresses caused by thermal expansion anisotropy. The critical nature of these stresses is evident in those materials that show increases in strength as these stresses are relieved by increasing the testing temperature.

In examining these types of flaws that are known to be of critical importance and considering other types of flaws that may be important, it is evident that only the first type of flaw is affected by the way material is removed in shaping a 96 percent alumina body. Even though considerable care is taken in grinding and polishing, and even assuming that subsurface pores do not become critical flaws when they come to the surface, the best that can be hoped for in strength improvement by grinding and polishing of 96 percent alumina is to shift the distribution of critical flaws so that other discontinuities in elastic properties, chemical flaws, and localized stresses account for the large majority of the fractures.

[5] Schmitz, G. K., Gulden, M. E., and Metcalfe, A. G., A Study of Stress Corrosion of Glass Fibers, Part II. Effect of Glass Composition, Solar Final Report Contract N00019-69-C-0145 (Feb. 1970).

This research was sponsored by the Naval Air Systems Command. The authors are pleased to acknowledge the contributions of their associates at Ceramic Finishing Company.

Discussion

HEUER: I would like to make one comment about your interpretation of interrupted tests. I think that one can take the view that stress corrosion or static fatigue can be the result of the growth of subcritical cracks. Clearly, if you have a population of "Griffith cracks" in the sample, fracture in a short term test will result from their propagation. If you impose a lower stress on the material, fracture is not observed until there is growth of the smaller cracks to the critical size. If this interpretation is correct, one would not expect to see any effect of "pre-fatiguing" on the subsequent short-time tests.

KIRCHNER: I don't regard this matter as being settled by any means, but I'm thinking mainly of the work that's being done at Solar where they have studied stress corrosion of fiber glass. They find flaws generated in fiber glass where apparently there was no inherent flaw to begin with. Furthermore, these flaws are very periodic rather than random.

WIEDERHORN: Regarding the experiment at Solar, I don't know if the information is transferable. What they showed was that the cracking in their fibers was a result of the ion exchange—hydrogen ions in the water with the sodium ions in the glass. You might not have this situation.

KIRCHNER: I think that's right, but I'm trying to make a point that perhaps the whole thing is a good deal more complicated than people thought.

NATIONAL BUREAU OF STANDARDS SPECIAL PUB. 348, THE SCIENCE OF CERAMIC MACHINING AND SURFACE FINISHING, Proceedings of a Symposium Sponsored by the American Ceramic Society, the Office of Naval Research, and the National Bureau of Standards, held at NBS Nov. 2–4, 1970, Gaithersburg, Md. (Issued May 1972).

The Effect of Grinding Direction on the Strength of Ceramics

R. W. Rice

Naval Research Laboratory, Washington, D.C. 20390

It is shown that grinding bars in a direction parallel with the tensile axis has limited effects on their strength, while grinding perpendicular to the tensile axis may have no effect or can reduce strengths as much as 50 percent. In single crystals, the reduction in strength generally increases with the hardness of the material, but can also depend on crystallographic orientation. In polycrystalline bodies, the reduction also depends a great deal on grain size, with the effect generally increasing with decreasing grain size. Also the effect tends to be greater in polycrystalline bodies that are weaker than normal. The effect of grinding direction on strength is attributed to stress concentrations due to grinding stria, whose continuity and depth generally increase with hardness. The severity of these stria tends to increase as the amount of plastic deformation in the machined surface decreases. The amount of plastic deformation is shown to vary approximately inversely with hardness. The effect of varying strength with grinding direction on the interpretation of various tests in discussed.

Key words: Carbides ceramics; fracture; grain size; grinding; hardness; mechanical testing; nitrides; oxides; strength.

1. Introduction

Grinding is the most widely used method of ceramic machining; almost always being the final finishing operation itself, or the step preceding final finishing. Some surfaces, e.g., flat ones, generally allow grinding in several, and often any, directions. Other surfaces, e.g., cylindrical ones, generally make it more difficult, or impossible, to grind in more than a few, or one, directions. Despite the fact that the option or constraint of grinding direction might affect the resultant strength under different stresses, grinding direction-strength relations have apparently not been studied. That such a study may be important is shown by Mould and Southwick's [1] [1] findings that hand abrasion of glass with emergy cloth (150 grit) perpendicular to the tensile axis results in strengths averaging about 50 percent lower than when abraded parallel with the axis of subsequent tensile stressing.

This paper examines some simple grinding direction-strength relations in a variety of ceramics, and shows that significant strength differences can occur, depending on the material and its microstructure.

2. Experimental Technique

The materials studied, shown in table 1, were diamond sawn into slabs (except for MgO crystals which were cleaved and the fine grain ZrO_2 which was received as fired bars).[2] The slabs were then ground in one direction on one side using a (Boyar Schultz) surface grinder with an 8 in dia. × 0.5 in wide (20.2 × 1.27 cm) 100-grit metal bonded diamond wheel operating at 1725 rpm. A water soluble oil-water mixture was used as a coolant. The depth of cut was 0.05± mm per pass with a feed rate of approximately 5 cm/min. The second side of the slab was then ground the same, except that the direction was 90° to the direction used on the first side. Polycrystalline and single crystal bodies of each type of material were generally ground together as a group. Some different single and polycrystalline materials were also ground together. The slabs were then diamond sawn (except MgO crystal slabs which were cleaved) into bars whose cross sections were nominally 3.8 × 1.8 mm, with the bar thickness being the slab thickness. The direction of sawing (or cleaving) was parallel with one of the grinding directions. The edges of all bars were then beveled by sequentially hand sanding (dry, and normal to the bar axis) on 120, 400, and 600 grit SiC papers.

For comparative purposes, some Al_2O_3 specimens were dry sanded with 150-grit SiC paper. Individual bars, or narrow slabs were sanded parallel to the tensile axis on one side and perpendicular on the other side. In order to assure that only the effect of sanding was observed, the polycrystalline bodies with previously as-fired surfaces and the single crystals were gas polished [2].

Ambient mechanical testing of bars was on an Instron machine in 3-point flexure on 1.27 cm span with a 1.27 mm/min head travel rate. The fracture surfaces, and some ground surfaces, were examined by standard optical and replica electron microscopy. Grain size was taken as the linear grain intercept on fracture surfaces.

[1] Figures in brackets indicate the literature references at the end of this paper.

[2] These bars were ground touching one another to approximate a plate.

TABLE 1. *Materials studied*

Material	Fabrication	Designation	Source
		(A) Glass	
Glassy carbon	Pyrolysis	Vitreous carbon	Beckwith Carbon Corp., VanNuys, California
Soda lime glass	Plate glass	Lustraglass double strength	American St. Gobain Corp., Kingsport, Tenn.
		(B) Single crystals	
Al_2O_3	Czochralski	Substrate material	Union Carbide Co., Union NJ
Al_2O_3	Verneuil	Split boule, Gem material	Walter E. Johnson, Morgan Hill, Calif.
TiO_2	Verneuil	Rutile, gem material	" " "
$MgAl_2O_4$	Verneuil	Gem material (approx. 3 MgO: 3.5 Al_2O_3)	DJEVA, Montrey, Switzerland
MgO	Shull melting	(N)*	Norton Co., Worcester, Mass.
MgO	Shull melting	High purity (H.P.)*	Semi-Elements, Saxonburg, Pa.
		(C) Polycrystalline bodies	
SiC	Sintering	KT	Carborundum Co., Niagara Falls, N.Y.
B_4C	Hot pressing		Norton Co., Worcester, Mass.
Si_3N_4	Hot pressing	(Plessey Co., England)	Courtesy of Dr. Lindley, Admiralty Materials Lab., England
$MgAl_2O_4$	Hot pressing		By author
$MgAl_2O_4$	Sintered	Transparent	Courtesy of D. Sellers of Coors Porcelain Co., Golden, Colo.
Al_2O_3	Sintering	Lucalox	General Electric Co., Cleveland, Ohio
Al_2O_3		ATD–998–A	Courtesy of J. Flobeck, Coor Porcelain Co., Golden, Colo.
Al_2O_3	Sintering	AD–94	Coor Porcelain Co., Golden, Colo.
Al_2O_3	Sintering	Alsimag 614	American Lava Co., Chattanooga, Tenn.
Al_2O_3	Hot pressing		By author
Al_2O_3	Sintering		Courtesy of J. Bailey, American Lava Co., Chattanooga, Tenn.
ZrO_2	Hot pressed, annealed	Zyttrite	Courtesy of K. Mazdiaysni, Air Force Materials Lab., Wright-Patterson AFB, Ohio
ZrO_2	Sintered		
ZrO_2	Sintered	Fine grain (Zircar)	Courtesy of A. Naumann, Union Carbide Corp., Tarrytown, N.Y.

*Author's designation

3. Results

The results for glass and oxide crystals are shown in table 2, which also indicates the general relationships between the tensile axis and crystal directions.[2] The orientations of the sapphire specimens from the split Verneuil boules is shown schematically in figure 1, along with summary strength data. The data on bars cut normal to the boule axis show more scatter because they are from three different boules. Comparison of individual specimens indicates that the strength difference due to the grinding effect may be 30 percent or more. The results for polycrystalline specimens are shown in table 3.

Fractures were examined to determine the fracture origins (where feasible), compare fracture features (e.g., mirrors on glass and

[2] Note the designation of the TiO_2 boule axis as the "c" axis is based on the suppliers information. The tensile direction is given as approximately the 110 direction since (a) the specimens were ground on a plane which was 90° ± 5° to the common cleavage plane and in a direction that was ± 10° to the intersection of this cleavage plane and the plane of grinding; and (b) reference 3 reports that the only plane of cleavage observed at room temperature is 110 cleavage.

TABLE 2. *The effect of grinding direction on the bend strength of glass and single crystals*

Material	Typical hardness vickers	Number of tests	Strengths, as-ground				Percent decrease
			Parallel to tensile axis		Perpendicular to tensile axis		
	kg/mm²		*10³ psi*	*10⁷ N/m²*	*10³ psi*	*10⁷ N/m²*	
Soda Lime Glass	550	7	14±1	9.7	10±1	6.9	27
Glassy Carbon	150–300	7	18±4	12	14±3	9.7	12
Sapphire 1 (Al_2O_3) [1]	2400	7	48±9	33	24±7	17	50
Sapphire 3 (Al_2O_3) [1]		9	48±9	33	26±6	18	47
Sapphire 1, 2, 3, (Al_2O_3)[2]		7	75±18	52	58±13	40	[8]22 (30)
Sapphire 0° [3]		4	50±6	35	38±3	26	24
Sapphire 30° [3]		4	55±5	38	52±11	36	5
Sapphire 60° [3]		4	61±2	42	59±6	40	3
Sapphire 90° [3]		4	48±3	33	46±5	32	6
Spinel [4]	1800	5	34±2	23	21±1	14	40
Spinel [5]		4	38±3	26	20±3	14	47
TiO_2[6]	1300	3	13±1	9	11±1	7.6	15
MgO (N)[7]	800	7	23±4	16	23±3	15	4
MgO[7] (H.P.)	600	4	20±3	14	20±3	14	0

[1] Sapphire from boules 1 and 3 were cut parallel to the boule axis as shown schematically in figure 1.
[2] Sapphire specimen from boules 1, 2 and 3 were cut perpendicular to the boule axis as sketched in figure 1.
[3] The number of degrees refers to the angle between the normal to the tensile surface and C axis. The tensile direction is <1010>.
[4] Al_2O_3-rich spinel, approx. 3 MgO to 3.5 Al_2O_3, tensile axis was parallel to the boule axis.
[5] The same Al_2O_3-rich spinel with the tensile axis perpendicular to the boule axis.
[6] Tensile axis perpendicular to the boule (c), approx. <110> direction.
[7] Tensile axis is <100> direction.
[8] See text.

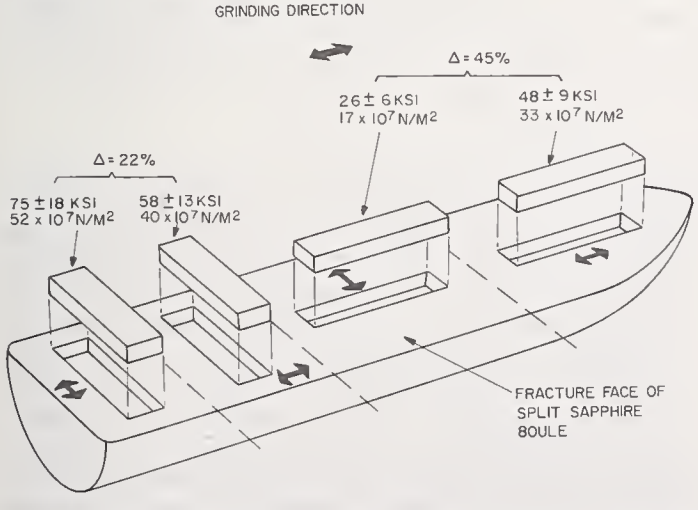

FIGURE 1. *Schematic representation of initial observations on the effect of grinding direction on strength of sapphire.* This sketch also indicates the orientations of bars from split boules. The tensile surfaces are {1010} and the tensile directions are within 20° of <1120> and <2423> for specimens cut with their tensile axes respectively parallel and perpendicular to the boule axis.

single crystals), and measure grain sizes on the polycrystalline specimens. As shown in table 4, many origins could be found and most were from the tensile surface. The greatest percentage of fractures originating from the edge were in specimens ground parallel to the tensile axis (i.e., the higher strength condition), especially in glass, which is known to be somewhat sensitive to edge effects. Also, three of the four 90° Czochralski sapphire bars ground parallel to the tensile axis failed from the corner. Fracture mirrors were measured on glass and single crystals of MgO, Al_2O_3, and TiO_2, and found to decrease with increasing strength in accordance with other testing (which will be covered in a later paper). While some of the edge fracture origins were in specimens failing at lower relative strengths, others were in specimens of at least medium or higher relative strengths.

The results of sanding trials are shown in table 5. Examination of the sanded sapphire fractures showed six of eight originated at the

TABLE 3. *The effect of grinding direction on the strength of polycrystalline bodies*

Materials	Fabrication [1] Designation [2]	Characterization		Number of tests	Strength As-ground				Percent change
		Approx. percent porosity	Approx. grain size μm [3]		Parallel to tensile axis		Perpendicular to tensile axis		
					10^3 psi	*10^7 N/m²*	*10^3 psi*	*10^7 N/m²*	
SiC	S	4	100	9	30±5	21	27±5	19	−10
B_4C	H.P.	0	30	6	56±8	39	49±5	34	−11
Si_3N_4	H.P.	0	1	3	95±9	66	52±2	36	−45
Al_2O_3	S (Lucalox)	0	60	7	37±2	26	39±3	27	+ 4
Al_2O_3		0	50	4	39±4	27	34±4	24	−13
Al_2O_3	S (AD–94)	7	20	3	51±2	35	48±3	33	− 6
Al_2O_3	S (A614)	6	12	4	60±6	41	54±4	37	−10
Al_2O_3	H.P.	0	9	5	66±5	46	59±5	41	−12
Al_2O_3	S	2	7	8	60±8	41	33±3	23	−45
Al_2O_3	H.P.	0	6	1	71	49	47	32	−34
$MgAl_2O_4$	S	0	100	5	31±4	21	30±4	21	− 3
$MgAl_2O_4$	H.P.	1	6	4	41±2	28	26±4	18	−37
ZrO_2	H.P.–A.	1	15	5	48±6	33	41±5	28	−15
ZrO_2	S	1	10	4	30±9	21	18±5	12	−40
ZrO_2	S	1	1	3	116±3	80	100±2	69	−14
MgO	H.P.–A.	0	100	3	18±2	12	20±2	14	+11
MgO	H.P.–A.	0	35	3	27±2	19	31±1	21	[4] +15(+1)
MgO	H.P. (LiF)–A	0	35	3	19±2	13	27±1	19	[4] +32(+7)
MgO	H.P.–A.	0	10	3	39±3	27	28±8	19	−28
MgO	H.P. (LiF)	0	3	3	35±2	24	20±5	14	−43

[1] S: Sintered; H.P. Hot pressed; (LiF) means hot pressed with LiF; –A means annealed in air after hot pressing (before grinding).
[2] Designation: Materials are listed in the same order as in table 1; however, some of the designations are repeated here for clarity.
[3] Note the grain sizes listed are the average of the larger grains, which control strength. The matrix grain size, which probably is more important in the grinding effect, is less (often half) of the value shown.
[4] Corrected per figure 6 as noted in the text.

tensile surface, and only two from the specimen edge.

While an exhaustive characterization of the surfaces was not feasible, some clear trends were evident. Grinding stria (fig. 2, 3) were readily visible with the unaided eye on sapphire and to a lesser extent on glass (least on the glassy carbon), but were generally visible on the spinel crystals only with the microscope, while such stria could not be seen optically on TiO_2 or MgO crystals. A similar trend was seen with the polycrystalline materials, but there was an important superimposed effect of grain size. Thus, grinding stria could be seen with the unaided eye on all the ZrO_2 bodies [3] and the finer grain Al_2O_3, $MgAl_2O_4$ and Si_3N_4 bodies, and to a lesser extent on B_4C, but not on the fine grain MgO. The stria were clearly defined under the optical microscope on the SiC and the medium grain Al_2O_3 bodies, but could not be clearly defined on the largest grain Al_2O_3. Only limited sporadic sections of stria were observed optically on the large grain spinel. On the MgO, stria were moderately clear optically on the fine grain body, and not defined on the largest grain body. The decreasing clarity of the stria appeared to result from both a decrease in the depth of the grooves of which they consist, and a decrease in the continuity due to surface spalling, grain pull-out, and related removal. Sample electron microscopy corroborated these results, and more clearly

[3] Note, in the case of the fine grain ZrO_2 bodies, the stria were not as pronounced, but were quite clear because of the very glossy nature of the ground surface.

TABLE 4. *Fracture origins of specimens ground*

Material	Parallel to the tensile axis				Perpendicular to the tensile axis			
	No. of tests	No. of origins located	No. from tensile surface	No. from specimen edges	No. of tests	No. of origins located	No. of origin from tensile surfaces	No. of origins specimen edges
A. Glass								
Soda lime	7	7	4	3	7	7	5	2
Glassy carbon	7	7	5	2	7	7	1	6
B. Single crystals								
Al_2O_3 (1)	8	8	6	2	7	7	6	1
Al_2O_3 (3)	9	6	3	3	9	6	6	0
Al_2O_3 (1, 2, 3)	7	6	3	3	8	5	4	1
Al_2O_3 (Czochralski)	16	16	11	5	16	16	14	2
$MgAl_2O_4$ (1)	5	5	3	2	5	5	5	0
$MgAl_2O_4$ (2)	5	5	3	2	5	5	5	0
TiO_2	3	3	3	0	3	3	2	1
MgO (N)	8	8	7	1	6	6	6	0
MgO (H.P.)	4	4	3	1	5	5	5	0
C. Polycrystals								
SiC	9	0			9	0		
B_4C	6	5	5	0	6	4	4	0
Si_3N_4	3	0			3	0		
$MgAl_2O_4$	5	5	3	2	5	5	3	2
$MgAl_2O_4$	4	2	2	0	4	3	3	0
Al_2O_3	32	0			32	0		
ZrO_2	11	8	5	3	11	9	5	4
MgO	15	5	4	1	15	8	7	1

[1] Tensile axis parallel to the boule axis.
[2] Tensile axis perpendicular to the boule axis.

TABLE 5. *The effect of standing direction on the bend strength of oxides*

Material	Grain size	No. of tests	Strength sanded parallel		Strength sanded perpendicular		Percent reduction
	(μm)[1]		*1000 psi*	*10^7 N/m²*	*1000 psi*	*10^7 N/m²*	
Al_2O_3	Single crystal	4	50±8	34	30±1	21	−38
Al_2O_3	20	5	53±	37	53±	37	0
Al_2O_3	7	4	56±3	39	52±3	36	−7

[1] Note the grain size is the average of the larger grains since they control strength. The matrix grain size, which probably is more important in this sanding effect, is less (often half) of the value shown.

showed the interruption of stria by spalling and related processes (fig. 3).

Optical examination of the sanded polycrystalline Al_2O_3 showed that striations were lower in density, continuity, and probably in height than on ground specimens. Sanded gas polished sapphire also showed substantially fewer striations, but their continuity and depth more closely approached that of their ground counterpart than did the polycrystals.

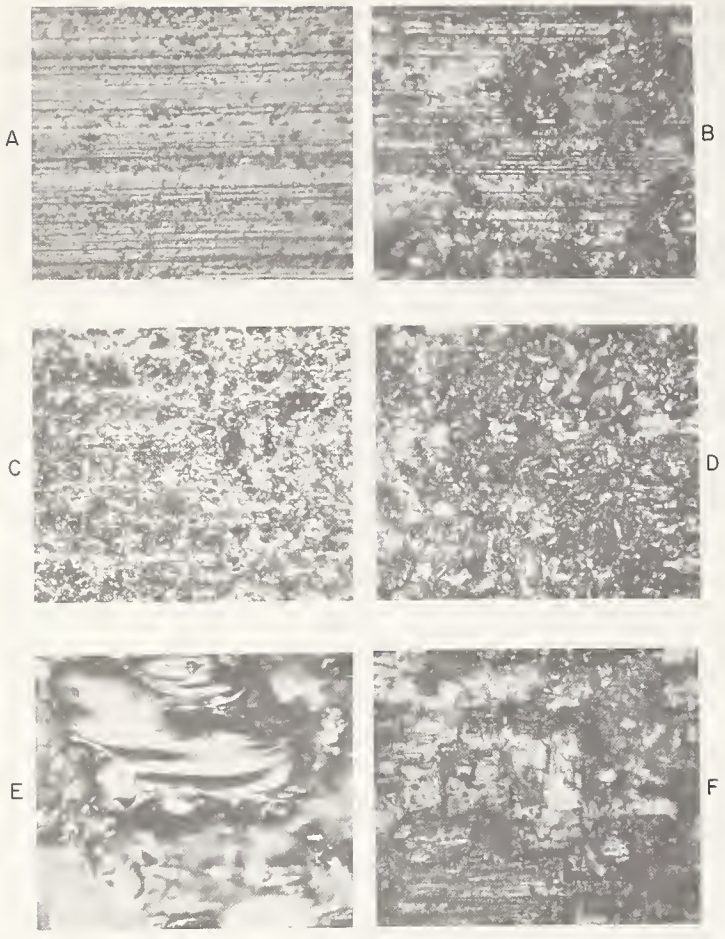

FIGURE 2. *Examples of grinding Striation.* Grinding was left to right. (A) Polycrystalline Si_3N_4; (B) Sapphire; (C) Polycrystalline B_4C; (D) Large grain polycrystalline $MgAl_2O_4$; (E) Rutile crystal; (F) MgO crystal.

4. Discussion

4.1. The Effect of Grinding Direction on the Strength of Glass and Oxide Crystals

Table 2 clearly shows that there can be a pronounced effect of grinding direction on the strength of soda lime glass and some oxide crystals. However, except for some sapphire orientations, it is clear that for the crystalline materials, the decrease in strength generally decreases with decreasing hardness, becoming zero for the softest MgO. This is consistent with other observations and with the trend of the grinding stria as follows. The author has shown that (a) the depth of slip from machining increases with decreasing yield stress [4], and (b), the yield stress (Y) of ceramics is generally one-third of the hardness as in metals [5]. Further, in NaCl [6] and MgO [7], it has been observed that the length of slip bands surrounding hardness indents are inversely proportional to the hardness (H). This is generally consistent with the above results, and suggests that the depth of slip from machining may be a function of $1/H$, and hence, $1/Y$. Brace [8] has shown that even mild sanding of fine grain NaCl results in a work-hardened layer of up to 1 mm in thickness. The author has shown that grinding of MgO normally introduces slip to two to three times the depth that sanding does [4], indicating that similar increases should occur in NaCl. Using this information and machining data for MgO, TiO_2 (see Appendix), and sapphire [9], a definite trend is seen in figure 4. Decreasing grain size decreases the depth of slip in machined MgO, so data for single crystal NaCl would be expected to be higher than that based on Brace's [8] fine grain NaCl, indicating even better agreement. The author has shown elsewhere [4] that data for CaO and for LiF indicate that these materials which are progressively softer than MgO develop greater depths of slip from machining than MgO. On the other hand, ZrO_2 and $MgAl_2O_4$, which are progressively harder than MgO, indicate less depth of

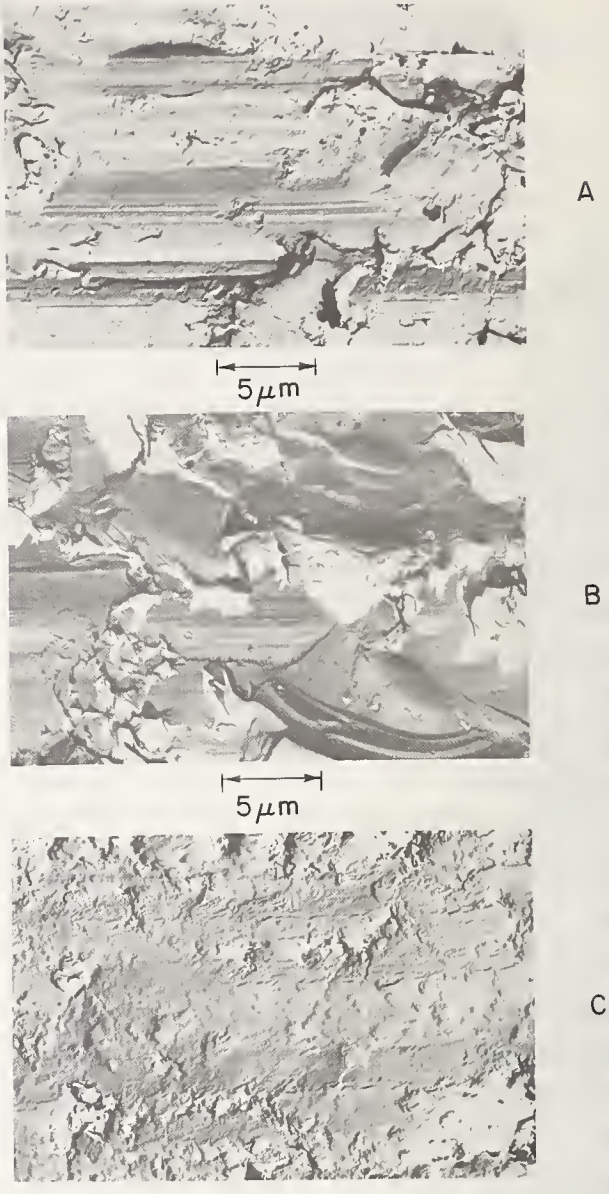

FIGURE 3. *Sample electron micrographs of samples ground left to right.* (A) Sapphire; (B) soda lime glass; (C) fine grain polycrystalline MgO.

machining effects than MgO. These observations corroborate the trend shown in figure 4.

The increasing clarity, and hence continuity and depth of grinding stria with increasing hardness, can be generally related to the above slip depth variations as follows. The impact and frictional energy of grinding can be dissipated by fracturing, deforming or heating of the surface material of the piece being machined (with heating aiding deformation). Increasing the amount of deformation in the material decreases the energy available for fracturing the surface heating. The energy absorbed in deformation is proportional to the volume of material deformed, and hence to the thickness of the layer of slip. As the layer of slip decreases, plastic deformation will be more localized around the individual grinding particles, due in part to more surface heating, resulting in more pronounced stria. The increasing stria clarity with increasing hardness is thus reasonable.

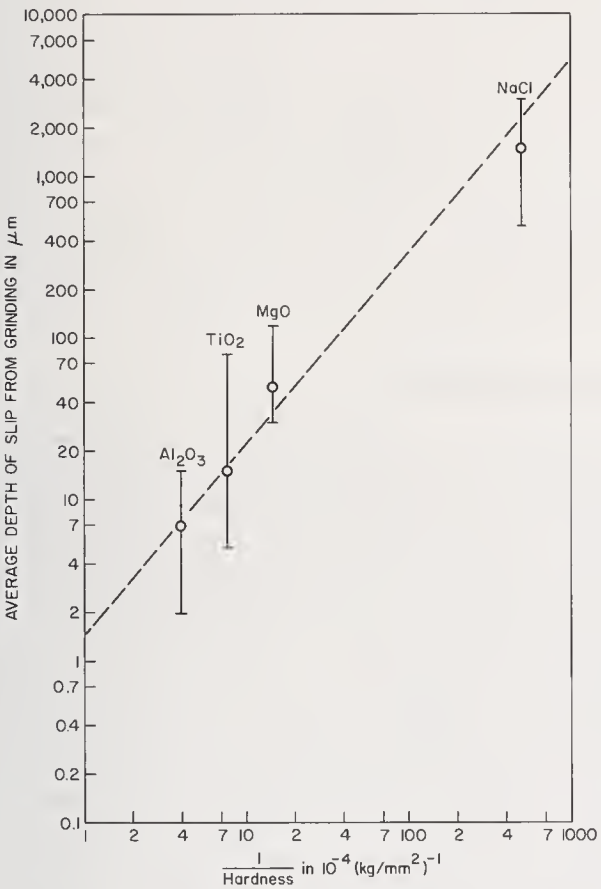

FIGURE 4. *The depth of slip from grinding as a function of hardness.*

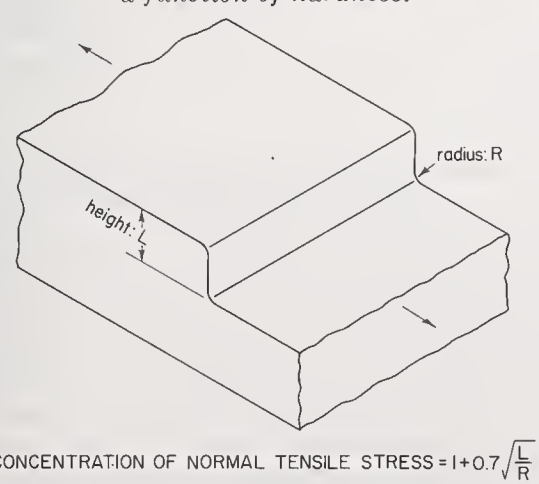

FIGURE 5. *Stress concentration due to a surface step after Marsh (10).*

The decrease in strength due to grinding perpendicular to tensile axis thus appears to be related to the orientation and extent of striation. These striations are essentially a series of surface steps. Marsh [10] has shown that such steps cause stress concentrations as shown in figure 5, which for larger step heights and smaller root radi results in stress concentrations as great as for Griffith flaws. It is also clear that reducing the continuity of the steps and their angle relative to the tensile axis will reduce the stress concentration as observed. The stria may be supplemented by fine (apparently discontinuous) cracks at or near the root of these steps (which would be one-half of each striation). The fact that almost all specimens ground perpendicular to the tensile axis failed away from the edge of the specimen indicates that such small cracks or variations of the step height occur to prevent failure from the edges.

The author [4] has observed that heavy grinding of MgO crystals increases their strengths 30–50 percent. However, moderate chemical polishing to give a smooth surface but leave most of the work hardened layer increased strengths still further (up to 50% more). Therefore minor, local steps due to spalling and related processes can also affect strengths. Other tests [11] showed that the strength of Al_2O_3 and spinel ground parallel with the tensile axis were essentially the same as mechanically polished specimens. Polishing of glass did improve strengths some (e.g., 14%). Trials indicated that perpendicular ground spinel had to be polished quite extensively to eliminate the effect of previous grinding direction on strength.

Thus, while the introduction of oriented Griffith flaws might have been expected to be the primary reason for the marked difference in strengths with grinding direction, stress concentrations due to surface steps appears to be the main cause. Further, flaws would be expected to often occur perpendicular to the stria and hence to give lower strengths for specimens ground parallel to the tensile axis. Also, an exclusive Griffith flaw-type failure would not be consistent with microplastic mechanisms of failure that are known to occur in MgO (and indicated in fig. 6), and might be factors in the strength of Al_2O_3 and TiO_2. However, some results, e.g., on polished spinel,

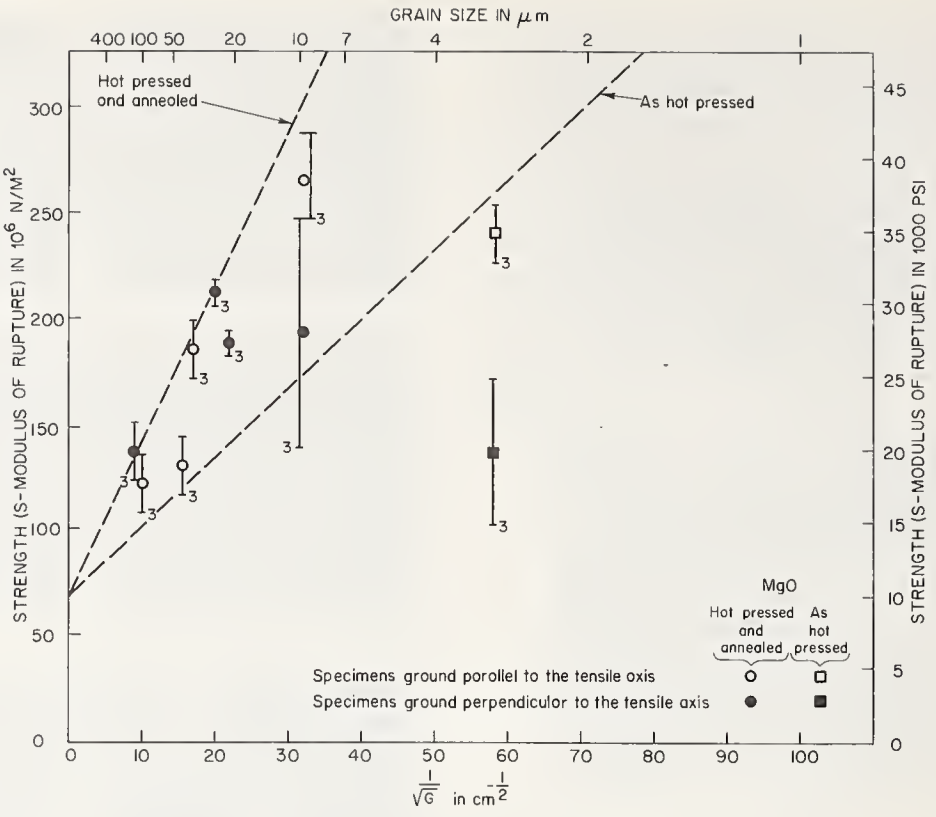

FIGURE 6. *Strength versus grain size of ground MgO.*

indicated that flaws were probably also generated in some cases.

The decrease in the strength of soda lime glass observed here is only about half that reported by Mould and Southwick [1]. However, their tests were run in a wet condition and for longer times to study stress corrosion, which probably accounts for the greater effect they observed. It is interesting to observe that application of Marsh's [12] theory of hardness and plastic flow in glass would approximately bring the soda lime glass result in line with the single crystal results. Marsh gives yield stress for glasses of about 450 kg/mm², which would correspond to a single crystal hardness of over 1000 kg/mm².

The smaller effect in the glassy carbon is generally consistent with its lower hardness. It is uncertain whether Marsh's theory applies to this material [5], thus the effect may be greater here relative to the other materials. This might arise from the low modulus allowing greater elastic strains which may reduce spalling and hence increase the continuity of the striations which are otherwise fairly moderate.

The one clear exception to the above trend of increasing stria clarity and strength difference with increasing hardness are some of the Czochralski sapphire specimens. The generally softer nature of Czochralski compared with Verneuil grown sapphire, and the variation of hardness with crystal orientation may explain part of the differences, e.g., the Czochralski-Verneuil differences. However, the differences for the 30°, 60°, and 90° specimens are much smaller than could be expected from the general hardness effect. Hockey's observation that both hardness indenting and grinding introduce many twins on non-basal planes (e.g., the rhmbohedral plane) but few, if any, on the basal (0°) plane (13), suggests a correlation. Twinning might alter either the nature of the stria or of possible associated flaws. However, since strength tends to increase (by nearly 2) as the tensile surface departs from the basal plane [14], the lower variation observed here in the parallel ground condition may be due to twinning limiting their strength. Twinning would normally be at an angle to the stria, and thus be effective in either orientation, and limit the rise in strength with departure from the basal plane observed in other (e.g., polished) specimens.

4.2. The Effect of Grinding Direction on the Strength of Polycrystals

The extent and clarity of the grinding stria on polycrystals shows general agreement with the concepts discussed for single crystals, but with an important superimposed effect of grain size. This grain size effect is due in part to effects discussed above. First, hardness of a material does generally increase with decreasing grain size, with the effect on microhardness being greatest at relatively fine grain sizes [5, 15].

Second, the author has shown that when the depth of slip exceeds the grain size, then further decreases in grain size result in some reduction of the depth of slip in MgO [4]. Similar effects would be expected in other materials. This grain size effect on slip depth is consistent with the increase in hardness (though it may be somewhat greater than expected from hardness increases). These both, in turn, corroborate the concept of reduction in the extent of slip increasing the extent of striation and resultant decreases in strength in specimens ground perpendicular to the tensile axis.

However, these effects do not appear to be sufficient to explain the substantial reduction of the directional effect in large grain bodies, especially in the harder materials. Spalling and grain pull-out appear to be the major factors since they interrupt the continuity and hence the stress concentration of the striations. Spalling probably occurs more in larger grain bodies because they are weaker. Since such spalls are normally limited by the grain size (due to grain boundary fracture), larger grains result in greater interruption of the striations.

The strengths of most parallel ground polycrystals were generally about the same [11] and sometimes possibly greater than specimens of the same materials with other finishes (annealling, chemical or mechanical polishing). This is illustrated, for example, by the agreement for MgO in figure 6, which was plotted since the intermediate grain sizes shown in table 3 were actually averages of a gradient across the specimens. Plotting the data for the average grain size of the different areas for the different tests shows that the increases in strengths for these specimens shown in table 3 are high. The general (but more uniform, as shown in figure 6) increase in strength of perpendicular ground MgO specimens is probably real. The narrower shape of these specimens resulted in incomplete contact with the full width of the wheel when ground parallel. This may have caused differences in these specimens.

The substantially greater effect of grinding direction on the intermediate grain size (sintered) ZrO_2 appears to be significant. This material is substantially weaker for its grain size than the similar material made by hot pressing and annealing the same raw material. Because of the purity and density, this must result from internal stresses or inhomogenities. (Since the fine grain ZrO_2 is made by a different process, detailed comparison of it with the above two ZrO_2 bodies is somewhat uncertain.) This effect of greater decrease in strength due to perpendicular grinding in weaker bodies is also indicated in the other oxides. The finest grain size bodies of MgO and $MgAl_2O_3$. and the three finest grain size bodies of Al_2O_3 were also somewhat weaker for their grain size relative to other bodies of these same materials. Thus, part of their greater effect may be due to this somewhat weaker character as well as their fine grain size.

The sanding trials clearly show that the extent of this directional effect is dependent on machining conditions, but is expected to be observed to varying degrees for a variety of conditions. The reductions from sanding polycrystals are probably low because only a few μm could be removed in a reasonable time. The resulting density of striations was thus low enough so that strengths may not have been reduced as much if the amount of material removed more closely approached that of grinding. On the other hand, slight uneveness of the gas polished sapphire resulted in initial contact only on a few areas, and a few small areas were not sanded at all. The resulting higher local pressure is probably partially responsible for the more severe striation and resulting strength reduction.

4.3. Application to Other Materials and Testing

The relation to hardness (i.e., yield stress) and grain size should make these results generally applicable to most other materials. For glassy materials, at least those which may exhibit phase segregation [5], it appears that Marsh's concepts of yield stress may be applicable. However, hardness will not necessarily be a good measure of yield stress in many materials containing pores or second phases, in which case, modification may be required.

The effect of grinding direction on strength can have important effects on different test techniques. Since the effect of grinding direction is a surface, and not an edge, effect, it should apply to tests that do not involve edges. For example, in biaxial testing of plates, there always will be a tensile component normal to the grinding stria. Thus, comparison to flexure testing, in which grinding will usually be parallel with the tensile axis will reflect in part these grinding differences. Failure to recognize possible resultant differences due to grinding can lead to false conclusions. Similarly, solid cylindrical rods used in uniaxial tension, and hollow cylinders used in hoop tension tests, will normally be ground circumferentially. The uniaxial tensile specimen will thus be ground perpendicular to the tensile axis, which can affect their strengths. Hoop tensile tests may also be affected, but further analysis is probably needed.

5. Summary and Conclusions

Soda lime glass, glassy carbon, and single crystals of MgO, TiO_2, $MgAl_2O_4$, and Al_2O_3 were tested with surfaces as-ground parallel

439-921 O - 72 - 25

or perpendicular to the tensile axis. No difference in strength was found for the softest MgO. The strengths of all other crystals ground perpendicular to the tensile axis decreased relative to the strengths of parallel ground specimens as the hardness (H) and therefore the yield stress increases. This is attributed to the reduction in the depth of slip from machining (which increases as a function of $1/H$), limiting deformation more to the local area around the individual grinding particles to generate the observed surface steps or stria. These cause maximum stress concentration when perpendicular to the tensile axis, and hence the difference in strengths, which can approach 50 percent in harder materials.

Polycrystalline bodies show a similar trend, but with an important grain size effect. Reduction of strength due to grinding perpendicular to the tensile axis, increases with decreasing grain size. The result is that large grain MgO shows little reduction, or possibly an increase in strength, as do single crystals. However, fine grain bodies are measurably weakened. On the other hand, while fine grain bodies of harder materials are weakened at comparable levels to that found in single crystals, large grain bodies are not. The effect also appears to be greater in bodies whose strengths are generally weaker than expected for their grain size.

Grinding of specimens by S. Slawson, and electron microscopy by J. Robinson, are gratefully acknowledged. Significant aid from Dr. P. Becher in orienting and testing some of the sapphire in the latter stages of the program is also gratefully acknowledged.

6. References

[1] Mould, R. E., and Southwick, R. D., Strength and static fatigue of abraded glass under controlled ambient conditions: II, Effect of various abrasions and the universal fatigue curve, J. Am. Ceram. Soc. 42, 582–92 (1959).

[2] Rice, R. W., Becher, P. F., and Schmidt, W. A., The strength of gas polished sapphire and rutile, this volume.

[3] Hirthe, W. M., and Brittain, J. O., Dislocations in rutile as revealed by the etch-pit technique, J. Am. Ceram. Soc. 45, 546–54, (1962).

[4] Rice, R. W., Machining and surface workhardening of MgO, submitted for publication.

[5] Rice, R. W., The compressive strengths of ceramics, to be presented at the conference on Ceramics in Severe Environments, Raleigh, N.C., Dec. 1970. Proceedings to be published.

[6] Matkin, D. I., and Caffyn, J. E., The surface hardness of sodium chloride containing divalent impurities, Trans. Brit. Ceram. Soc. 62, 753–61, (1963).

[7] Groves, G. W., and Fine, M. E., Solid solution and precipitation hardening in MgO-Fe-O alloys, J. Appe. Phys. 35, 3587–93, (1964).

[8] Brace, W. F., Behavior of rock salt, limestone, and anhydrite during indentation, J. Geophy. Res. 65, 1773–88, 1960.

[9] Hockey, B. J., Observations on mechanically abraded aluminum oxide crystals by transmission electron microscopy, this volume.

[10] Marsh, D. M., Stress concentrations at crystal surfaces and the embrittlement of sodium chloride, Phil. Mag. 5, 1197–99, (1960).

[11] Rice, R. W., The effect of sputtering on surface topography and strengths of ceramics, this volume.

[12] Marsh, D. M., Plastic flow in glass, Proc. Roy. Soc. A–269, 420–35, (1964).

[13] Hockey, B. J., private communication.

[14] Klassen-Nekludova, M. V., and Tomilovskii, G. E., Corundum crystal strength in bending and compression tests as a function of crystallographic orientation, Tr. In-ta Kyestallogr. An, SSSR, No. 8: 5–12 (1953).

[15] Brace, W. F., Dependence of fracture strength of rocks on grain size, Penn. State Univ. Mineral Expt. Sta. Bull. 76, 99–103, (1961).

7. Appendix. Surface Slip in Rutile during Grinding

TiO_2 crystal bars of the orientation described in the preceding paper were ground both as described there, and at somewhat lower removal rates. Fractures which were roughly normal to the ground surfaces were etched in boiling, concentrated H_2SO_4 for about 20 minutes after Hirthe and Brittain [3]. A variety of behavior was observed. Some specimens showed a thin layer (i.e. about 5 μm) of etch pits along parts of the surface, especially near depressions into the surface, which also frequently had short slip bands extending from some area, as shown in figure A1. Other specimens showed a much more uniform and thicker (e.g., to 80 μm) layer, as shown in figure A2. Annealing in air at temperatures of the order 1200 °C appeared to reduce the density of dislocations and result in limited polygonization, as shown in figure A3. The depth of this was in the range of slip observed between figs. 1 and 2. The average depth of slip in all specimens was of the order of 15 μm.

It is also interesting to note that there is a high density of dislocations which extend considerably

FIGURE A1. *TiO_2 crystal showing irregular depth of surface slip from grinding.* Etched fracture approximately normal to the ground (right-hand) surface.

deeper around the origin of fracture, figure 2. This was observed in several cases, and sometimes lines of pits suggesting slip bands were observed at such fracture origins. The depths of these and their association with fracture indicated that they were associated with the fracture process.

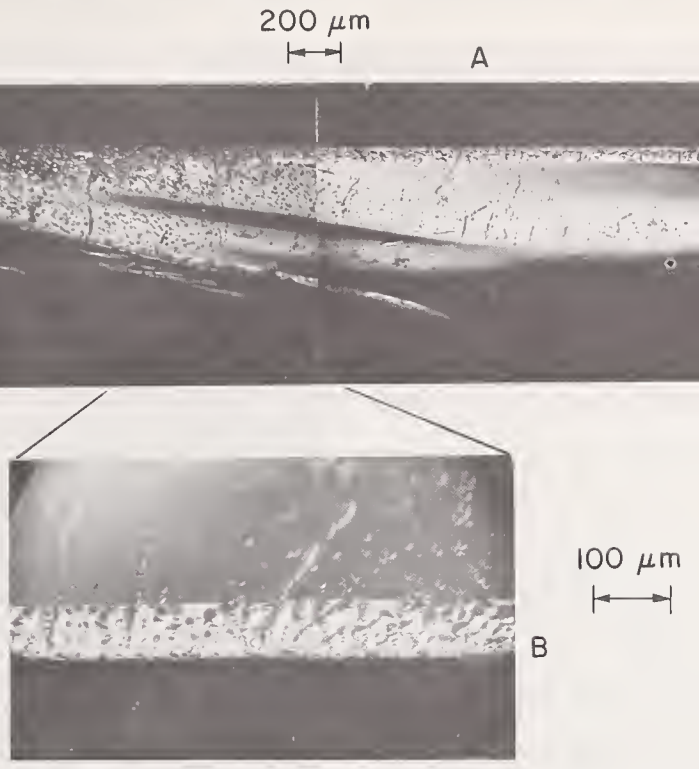

FIGURE A2. *TiO_2 crystal showing uniform depth of surface slip from grinding.* Etched fracture approximately normal to the ground (right-hand) surface.

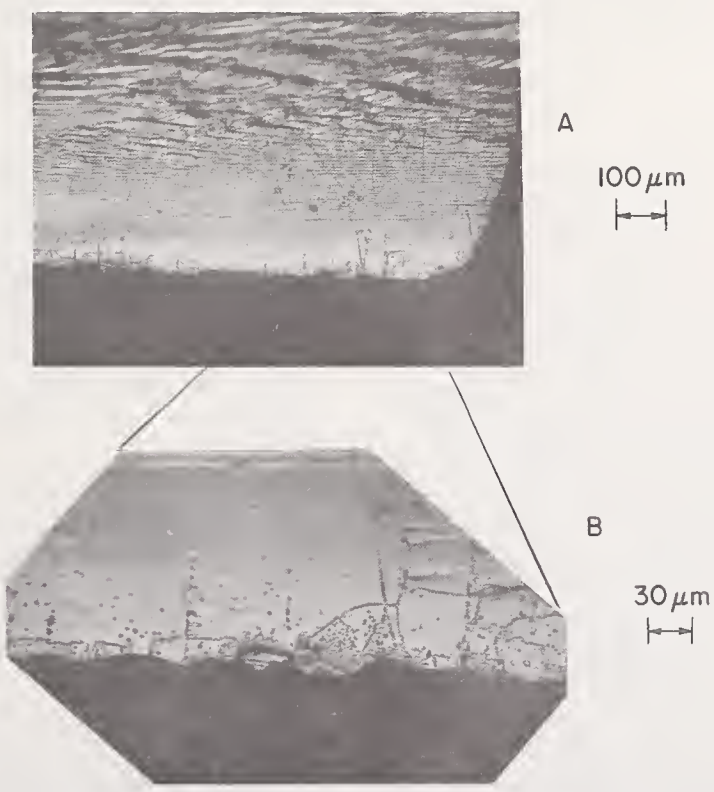

FIGURE A3. *Ground TiO_2 crystal after annealing in air at about 1200 °C.* Etched fracture approximately normal to the originally ground (right-hand) surface. Note sub-boundaries, some of which may have resulted from annealing the ground surface.

439-921 O - 72 - 26

DONOVAN: What were your units of hardness?

RICE: Kilograms per square millimeter.

DONOVAN: Well, how did you measure the hardness?

RICE: I took typical hardness values from the literature. I wasn't really concerned about making a differentiation between Knoop or Vickers hardness. Vickers hardness would normally be a little higher, say like 10 percent or so, but I was just taking average figures from the literature.

DONOVAN: I see, you didn't measure right on the specimen.

RICE: No, we haven't been able to do that yet.

GIELISSE: How much of this is due to the anisotropy in hardness as we know it to exist?

RICE: The anisotropy in hardness is much much less than the effect we saw here. I'd also like to mention that the effect of different orientations of sapphire seem to correspond very nicely to some work of Bernard Hockey in that all except for the 0° orientation we didn't see much of an effect. Bernard observes twinning in all those orientations except the 0° one. Therefore, it suggests that this mode of plastic deformation reduces the amount of difference in the strength between the two different grinding directions. However, when you don't have significant twinning on the basal plane you get a significant effect.

HEUER: I agree with the point that Peter Gielisse makes. The essential point is that defects due to grinding damage that can cause fracture can have stress concentration ratios greater than the hardness anisotropy ratios.

RICE: That may be true. My comment was that the difference in strength with different grinding direction was generally greater than the hardness anisotropy. We also see significant effects in glass, which should be isotropic. Thus, while hardness anisotropy may be a factor, it cannot explain the complete effect. The correlation is still poor if we narrow the consideration to only sapphire. The effect appears to be greater on the basal plane than the anisotropy of hardness. However, there is little or no effect on other planes where hardness anisotropy would be expected.

NATIONAL BUREAU OF STANDARDS SPECIAL PUB. 348, THE SCIENCE OF CERAMIC MACHINING AND SURFACE FINISHING, Proceedings of a Symposium Sponsored by the American Ceramic Society, the Office of Naval Research, and the National Bureau of Standards, held at NBS Nov. 2–4, 1970, Gaithersburg, Md. (Issued May 1972).

The Influences of Material Removal on the Strength and Surface of an Alumina

H. S. Starrett

Southern Research Institute, Birmingham, Alabama 35205

Southern Research is conducting a quantitative investigation of test methods used to evaluate brittle materials. The material for this study is a high purity, high density alumina manufactured by Coors Porcelain Company of Golden, Colorado. The primary scope of the total program is a study of test methods, scaling laws and surface finish effects. The scope has been broadened to include the effects of property interactions on strength and the relationships between micro and macro characterization and the mechanical properties.

Initial tensile and flexural data indicated that surface finish had no effect on the tensile strength of this particular alumina. Since this was contrary to generally accepted results, considerable effort has been expended in investigating this phenomenon. It has been postulated that the lack of an effect may have been due to subsurface damage that occurred during the grinding operations.

The investigations into surface/subsurface damage have focused into four principal areas. Microstructural characterization has been used to characterize the surfaces of interest, to look for evidence of damage and to look for microstructural events which may be normalizing the data. A study of fracture source distribution has been made in order to determine the depth of damage which would have a significant effect on the flexural data. Surfaces have been and are being subjected to different treatments such as refiring in modified environments and deep lapping in order to define the nature of the surface/subsurface damage, if it exists.

The microstructural work has not revealed any obvious damage; however, it was found that even by proceeding from a shop grind to a metallurgically lapped surface certain features such as exposed pores, interfaces between alumina matrix and second phase and evidence of the original ground surface did not totally disappear. The study of the fracture source distribution provided quantitative evidence that damage on the order of 0.005 in (approximately five maximum grain diameters) would have a significant effect on the flexural data. Results from the surface treatments, deep lapping and refiring show that these different preparations did not affect the flexural strength of the material. Other indirect evidence (statistical data) show this material to be insensitive to surface effects within the range of surface finishes investigated.

Key words: Alumina; surface finish; surface treatments; Weibull.

1. Introduction

Recent work on the effects of surface finish on the strength of a ceramic yielded results which were not consistent with the results normally presented in the literature. This study showed that the flexural strength of an alumina was insensitive to surface finish effects within the range of surface finishes and conditions studied.

The material under investigation was a high purity alumina manufactured by Coors Porcelain Company of Golden, Colorado. The material had the following microstructural characteristics.

1. Grain size — maximum grain diameter was 25 microns and the average grain intercept value was 3.6 microns.

2. Porosity — maximum pore diameter was 25 to 50 microns and the pore volume was 3–5 percent.

3. Secondary microconstituent—a second phase occurring as discrete grains and representing nominally 2 percent by volume was observed. In addition to aluminum, these grains contained the cations sodium, calcium, magnesium and silicon.

4. Fracture mode for tensile and flexural specimens—electron fractography indicated that approximately 90 percent of the fracture was intergranular. No intergranular phase was noted. The material was evaluated to determine whether or not it was uniform and reproducible with respect to mechanical strength and physical properties, and thereby suitable to be used for a comprehensive test methods study.

The outcome of preliminary tests for surface finish effects are shown in table 1. These results show that except for the as-fired surface, the surface finish did not affect the strength of the specimens. The ground surfaces, polished surfaces and metallurgically lapped surfaces gave essentially the same strength values in both flexure and tension. The nominal flexural strength was about 49,000 psi (337.8×10^6 N/m^2). The pressed and fired surface gave a 15 percent lower strength value of 40,820 psi (281.4×10^6 N/m^2). This lower value can be partially attributed to the fact that the flexural specimen could not be machined to the tol-

TABLE 1. *Results of surface finish study on macro specimens*

Surface condition	Remarks	Flexure psi (10^6 N/m^2)	Tension psi (10^6 N/m^2)
Pressed and fired (150–175 rms)	Blank 3A–10–088	40,820 (281.4)	
Pressed, green machined, and fired	No data		
Ground surface (15 rms) (shop ground)	Blank 3A–10–087	47,890 (330.1)	48,560 (334.8)
	Blank 3A–10–088	50,620 (349.0)	
Polished surface (3–4 rms) (shop polish)	Blank 3A–10–088	48,420 (333.8)	46,220 (318.6)
Polished surface (lapped) (metallurgically lapped)	Blank 3A–10–088 One-in (2.5 cm) specimens taken from two-in (5.0 cm) specimen. Alternate ends were evaluated as ground. MOR = 51,930 psi (358 × 10^6 N/m^2)	50,820 (350.4)	

erances used on the other specimens without machining the fired surfaces.

These observations can be rationalized in either of two general ways. The first would be to assume that the handling, machining or surface preparation did not affect the material at the surface or slightly below the surface. Then the results could be explained from one of several points of view. One would be that even though the "better" specimens were metallurgically lapped, sufficient material was not removed from the surface to do away with damage such as rough places and geometric discontinuities which create stress concentrations. Another interpretation might be that after a surface has become sufficiently "good", new flaws are exposed as material is removed, or as a third alternative, the fractures are initiating internally. The second approach would be to assume that during the course of handling, etc., the surface of the material and/or the subsurface regions were mechanically damaged. The presence of damage would then offset any changes resulting from surface preparation and normalize the data.

Since the initial results were somewhat unexpected and could bear directly on later analyses made regarding the material's behavior, a more complete understanding was sought. To this end an analytical study of the fracture source distribution was made to determine the depth of damage which would have a significant effect on the flexural data, surfaces were subjected to several secondary finishing techniques in an attempt to define the nature of any surface/subsurface damage, and microstructural characterization was used to characterize the surfaces of interest and to look for evidences of damage or microstructural events which could be normalizing the data.

In order to define the fracture source distribution the Weibull Distribution function was used in the following form:

$$S = \exp\left[-\int_V \left(\frac{\sigma}{\sigma_0}\right)^m dV \right]$$

where

S = survival probability
σ = tensile stress of arbitrary spatial distribution
σ_0 = constant
m = Weibull Modulus
V = volume subjected to tensile stress

which may be transformed to

$$S = \exp\left[-\beta^m \Gamma^m \right]$$

where

β = normalized stress, a reference ultimate stress divided by the average

Γ = Gamma Function, $\Gamma\left(1 + \frac{1}{m}\right)$

If the sample average $\bar{\sigma}$ is accepted ($\beta = \sigma/\bar{\sigma}$) the transformed form of the distribution shows that there is only one parameter left to define the distribution, the Weibull Modulus m. Intuitively it would be expected that the value of m based on a surface effect would be different from one based on a volume effect.

The question of probability of fracture with-

in some specified region of a test specimen relates the relative size of the region in question to the total specimen volume. For a simple example, the probability of fracture within a given region of a specimen subject to uniform tension is found by the ratio of the given region's volume to that of the whole specimen. This process may be generalized for any given stress distribution by finding the size of the specimen having the same probability of fracture but subject to uniform tension only. The ratios of such "equivalent" volumes represent the relative frequency of fracture expected to occur in the respective volumes.

Beginning with the Weibull Distribution

$$S = \exp\left[-\int_V \left(\frac{\sigma}{\sigma_0}\right)^m dV \right]$$

this can be altered by choosing normalized variables describing the stress distribution and the volume.

$$\sigma = \sigma_T \cdot f(\xi)$$
$$dV = CV_T\, g(\xi)\, d\xi$$

where

σ_T = reference stress, usually maximum tension
V_T = volume in tension
C = constant
ξ = normalized position variable

thus

$$S = \exp\left[-\left(\frac{\sigma_T}{\sigma_0}\right)^m V_T \int_{\xi_1}^{\xi_2} Cf(\xi)^m\, g(\xi)\, d\xi \right]$$

This integral is a function of the Weibull Modulus m and the limits of integration ξ_1 and ξ_2

$$\int_{\xi_1}^{\xi_2} Cf(\xi)^m\, g(\xi)\, d\xi = G(\xi_1, \xi_2, m)$$

so that

$$S = \exp\left[-\left(\frac{\sigma_T}{\sigma_0}\right)^m V_T \cdot G(\xi_1, \xi_2, m) \right]$$

This equation represents a portion of a specimen whose overall distribution integral G_T is given by the total limits as $G(u, v, m)$. Using σ_T as a convenient reference stress, the volume subject to a uniform tension σ_T having the same probability of failure as the whole specimen is given by

$$S = \exp\left[-\left(\frac{\sigma_T}{\sigma_0}\right)^m G_T V_T \right]$$

$$= \exp\left[-\left(\frac{\sigma_T}{\sigma_0}\right)^m V_{EQ_T} \right]$$

For a subsidiary portion within the limits (ξ_1, ξ_2) the same process yields

$$S_s = \exp\left[-\left(\frac{\sigma_T}{\sigma_0}\right)^m V_T G(u, \xi_2, \xi_1) \right]$$

$$= \exp\left[-\left(\frac{\sigma_T}{\sigma_0}\right)^m V_{EQ_S} \right]$$

The probability, F_s, that fracture will initiate in the subsidiary volume is simply the ratio of its "equivalent" volume V_{EQ_S} to the equivalent volume of the whole specimen V_{EQ_T} or

$$F_s = \frac{V_{EQ_S}}{V_{EQ_T}} = \frac{G(\xi_1, \xi_2, m)}{G(u, v, m)}$$

For a rectangular flexural specimen the dimensionless functions are

$$\sigma = \sigma_T \xi \quad , \quad f(\xi) = \xi$$

where ξ is the dimensionless transverse distance from the neutral plane and the volume under tension is

$$dV = V_T\, d\xi$$
$$G(\xi_1, \xi_2, m) = \int_{\xi_1}^{\xi_2} \xi^m\, d\xi$$

Putting in limits for the whole specimen $0 \leq \xi \leq 1$ gives

$$G_T(0, 1, m) = \int_0^1 \xi^m\, d\xi = \frac{1}{m+1}$$

and for a subsidiary portion $0 \leq \xi \leq \xi$

$$G_s = (0, \xi, m) = \int_0^{\xi} \xi^m\, d\xi = \frac{\xi^{m+1}}{m+1}$$

Now the probability of fracture initiating between the neutral axis and the fraction ξ of the beam half-height is

$$F = \frac{G_s}{G_T} \frac{\xi^{m+1}}{m+1} \frac{m+1}{1} = \xi^{m+1}$$

Figure 1 shows the fracture source distribution in a rectangular bar under pure bending for various values of m. Figure 2 shows the same curve for a round flexural specimen.

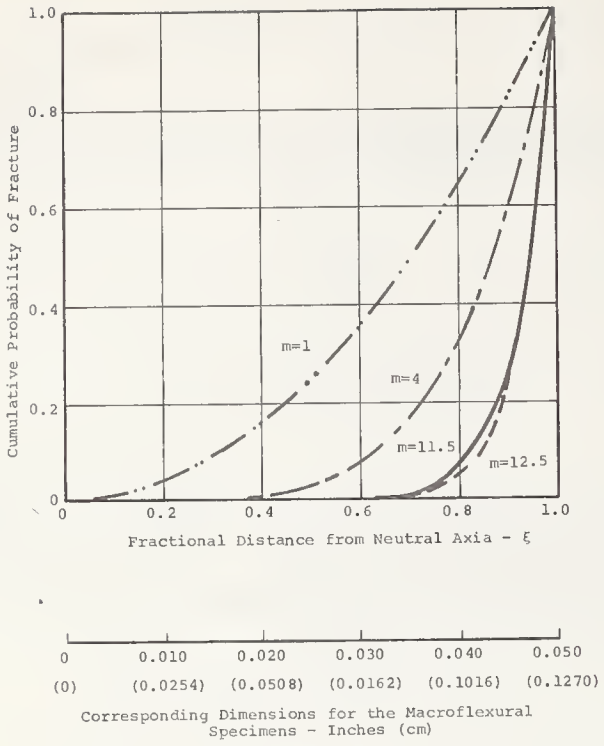

FIGURE 1. *Fracture-source distribution in pure bending for a rectangular specimen.*

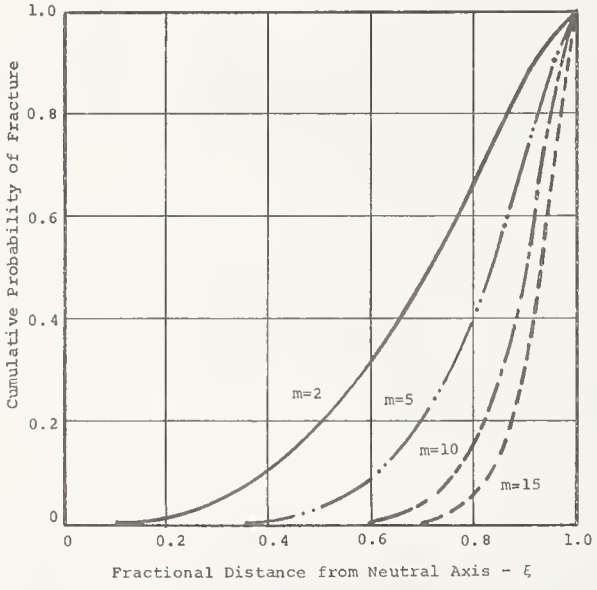

FIGURE 2. *Fracture-source distribution in pure bending (round specimen).*

For a specimen subjected to uniform tension

$$\sigma = \sigma_T, \; f(\xi) = 1$$
$$dV = 2V_T \; \xi d\xi$$

so that

$$G(\xi_1, \; \xi_2, \; m) = \int_{\xi_1}^{\xi_2} 2\xi \; d\xi$$

For the whole specimen

$$G_T \; (0, \; 1, \; m) = 2\int_0^1 \xi d\xi = 2\frac{\xi^2}{2}\Bigg|_0^1 = 1$$

and for a subsidiary portion

$$G_s \; (0, \; \xi, \; m) = 2\int_0^{\xi} \xi d\xi = \xi^2$$

and the probability of fracture is given by

$$F = \frac{G_s}{G_T} = \xi^2$$

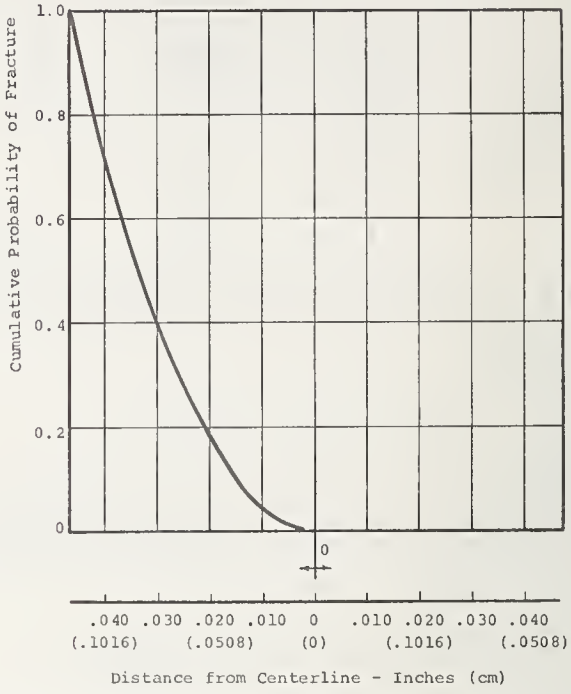

FIGURE 3. *Fracture-source distribution in pure tension for a round tensile specimen.*

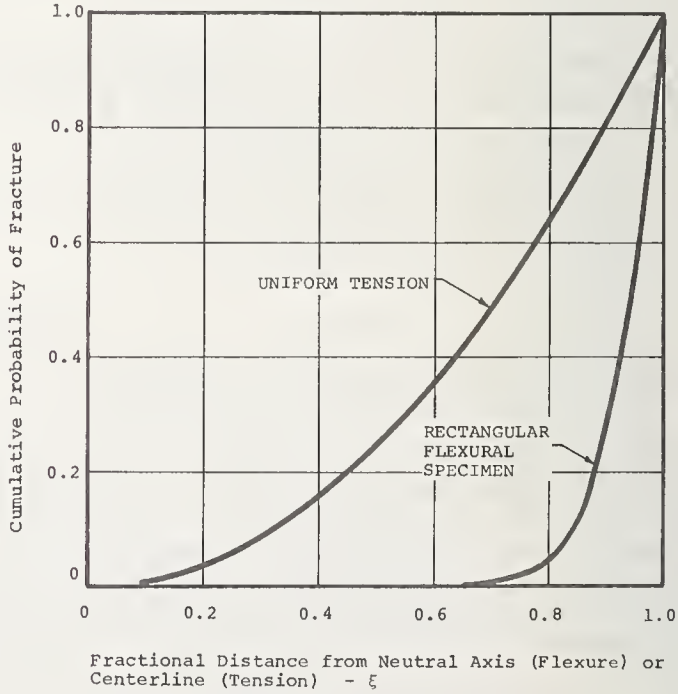

FIGURE 4. *Fracture-source distribution for a uniform tensile specimen and a rectangular flexural specimen (pure bending) for a material with a weibull modulus of 12.5.*

which is independent of m. Figure 3 shows the curve for a uniform tensile specimen. Figure 4 shows the fracture source distribution for the tensile and rectangular flexural specimen for a material where $m = 12.5$. From this plot it can be seen that over 70 percent of the fractures should initiate in 10 percent of the half-height and 95 percent should occur in 20 percent of the half-height. For the specimen used in this study, where the half-height $h = 0.050$ in, (0.1270 cm), 70 percent of the fractures should initiate within 0.005 in (0.0127 cm) of the tensile surface. This represents about 35 average grain diameters or 4–5 maximum grain diameters. Thus the existence of surface/subsurface damage or a change in the nature of the material within the first 0.005 in (0.0127 cm) of the surface should have a pronounced effect on the data.

With these results in mind, several secondary surface finishing techniques were employed on the flexural specimens (4 point loading) in order to gain insight into surface or subsurface damage. These techniques were not intended to change the nature of the material or to provide additional strength, but rather were for the purpose of determining whether or not surface/subsurface damage existed, and if so, to what extent. The main surfaces considered were:

1. Pressed, fired
2. Pressed, green machined, fired
3. Shop grind
4. Shop grind, shop polish
5. Shop grind, metallurgical polish (lap)
6. Shop grind, H_2 refire
7. Shop grind, lap, H_2 refire
8. Shop grind, air refire

Figures 5 through 12 are electron photomicrographs of these surfaces. Also evaluations were performed on chemically etched surfaces. These included specimens etched in hydrofluoric acid

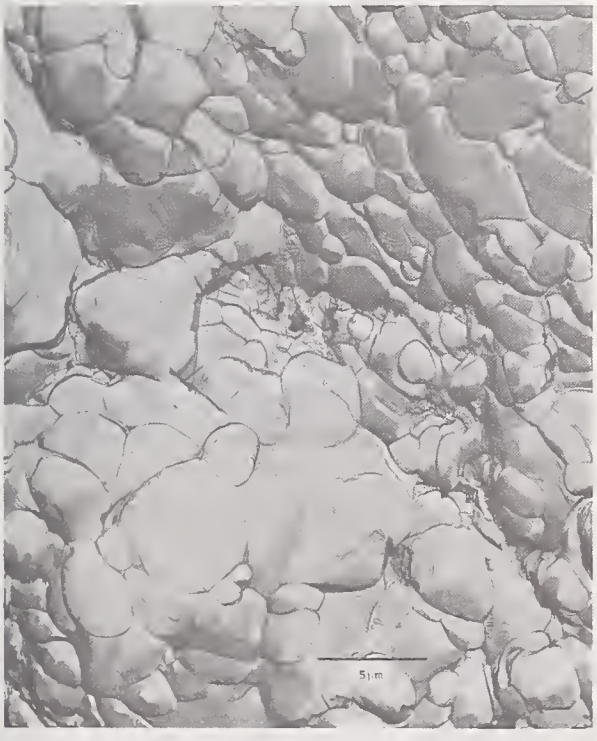

FIGURE 5. *Electron photomicrograph—as-received surface, pressed and fired.* Fiducial bar equals 5.0 microns.

FIGURE 6. *Electron photomicrograph—as-received surface, pressed, green machined and fired.* Fiducial bar equals 5.0 microns.

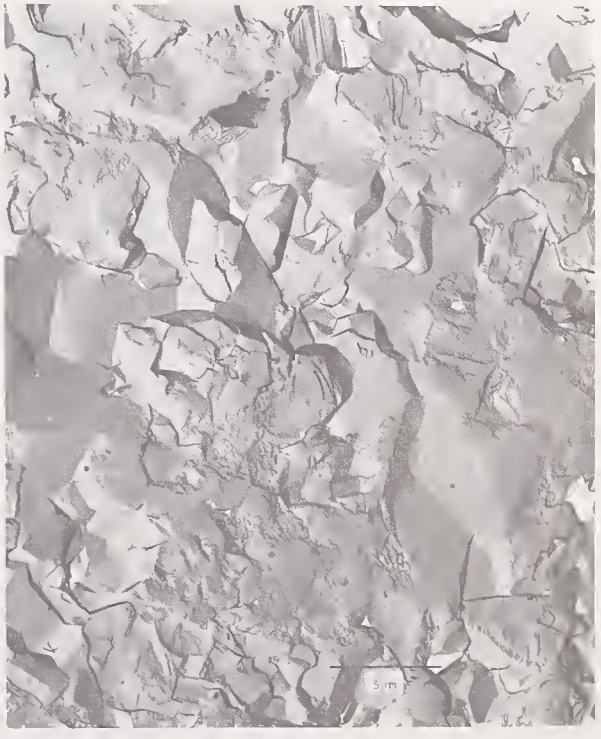

FIGURE 7. *Electron photomicrograph—15 rms surface created by standard shop surface grinding.* Fiducial bar equals 5.0 microns.

FIGURE 8. *Standard shop grind plus lapping with 15, 7, 1 and ¼ micron diamond.*

FIGURE 9. *Electron photomicrograph—<1 rms surface developed using metallurgical laboratory lapping techniques.* Fiducial bar equals 5.0 microns.

FIGURE 10. *Electron photomicrograph—Surface produced by refiring a 15 rms ground surface in hydrogen.* Fiducial bar equals 5.0 microns.

FIGURE 11. *Electron photomicrograph—Surface produced by refiring a 1 rms lapped surface in hydrogen.* Fiducial bar equals 5.0 microns.

and specimens immersed in Borax at 1500 °F (~840 °C).

The results of the flexural evaluations on the specimens which had undergone the several different surface treatments are shown in table 2. The standard shop ground surface was used as the baseline value. Normally, however, only from 3–10 specimens were employed to test a particular condition so that comparisons were made against as-ground specimens taken from the same blank of material as the treated specimens. The values used for comparison are separated in the table by the virgule. Also there was a problem in providing enough material for all the evaluations shown here plus other evaluations required by the continuing program.

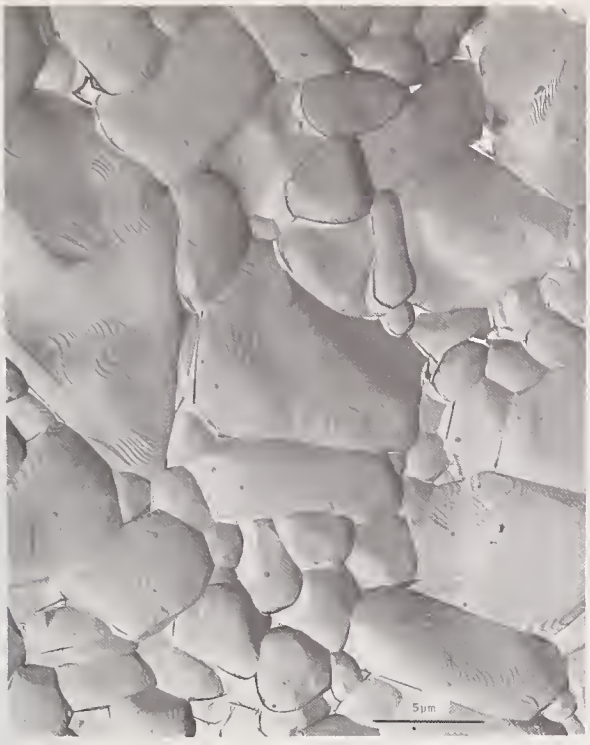

FIGURE 12. *Electron photomicrograph—Surface produced by refiring a 15 rms ground surface in air.* Fiducial bar equals 5.0 microns.

In order to have sufficient stock, material below the standards established by the majority of the blanks has been used for some of the tests. This material has been noted as A–11*. The average flexural strength of specimens taken from Blanks A–11* was 37,130 psi (256.0 × 10^6 N/m^2) compared to the overall average of 48,300 psi (333.0 × 10^6 N/m^2). Also specimens have been evaluated which have been precision ground, and some have been evaluated after only being sliced from the stock. These are also noted in the table.

From table 2 it can be seen there were no significant changes in the strength of the material as a result of the treatments. Basically the material remained unaffected.

The microstructural work has not revealed any obvious damage; however, it was found that even by proceeding from shop grind to a metallurgically lapped surface certain features such as exposed pores, interfaces between alumina matrix and second phase and evidence of the original ground surface did not disappear, see figure 9.

TABLE 2. *Effects of surface treatment on the flexural strength of an alumina*

Surface condition	Flexural strength psi (10^6N/m^2)	Remarks
1. Pressed, fired	40,820 (281.4)	Surface rough and pimpled
2. Pressed, green machined, fired	43,240 (298.1)	
3. Shop grind	48,300 333.0)	314 specimens
4. Shop grind, shop polish	48,420 (333.8)	3–4 runs
5. Shop grind, metallurgical polish (lap)	50,820/51,930 (350.4/358.0)	One-in (2.5 cm) specimens, matched pairs (3)
6. Shop grind, hydrogen refire	45,820/47,710 (315.9/328.9)	
7. Shop grind, lap, hydrogen refire	43,790/47,710 (301.9/328.9)	
8. Shop grind, air refire	44,450/47,710 (306.4/328.9)	
9. Sliced material/good grinding	43,980/50,680 (303.2/349.4)	For premium material
10. HF etch for 0.005 in (0.0127 cm), 0.004 in (0.0102 cm) removed by machining	39,800/37,130 (274.4/256.0)	Sliced material; A–11*
11. Immersed in Borax 2 minutes at 1550 °F (~840 °C)	45,300/50,680 (312.3/349.4)	Three specimens
12. Baked at 950 °C one hr, placed in vacuum, 20 hrs at 10^{-5} torr, 1 hr at 10^{-8} torr, broken at 10^{-8}	34,950/37,130 (240.9/256.0)	Sliced material; 3 specimens, A–11*

2. Discussion

Based on the surface finish effects data it appears that the alumina has not been affected adversely by the grinding or handling. Of course, it is possible that all of the treatments were ineffective in removing or repairing surface/subsurface damage that may have occurred. To date we have been unable to determine directly whether or not damage existed, consequently, we have been unable to determine whether or not we have been able to remove the damage. However, the indirect evidence indicates there was not a surface/subsurface damage effect. This judgment was based on the following observations:

1. The various surface treatments have not affected the flexural strength of the material.
2. The flexural (and tensile) data showed trends and effects caused by other factors.
3. The data (tensile and flexural) showed trends that were consistent with the Weibull calculations based on volume. Observation 1 was discussed earlier and will not be repeated here.

Recall that the analysis of the fracture source distribution revealed 70 percent of the fractures should initiate within 0.005 in (0.0127 cm) of the tensile surface. Therefore any significant damage which extended to this depth should have a pronounced effect on the flexural strength. In fact, it is reasonable to expect that such an effect would easily override other effects or trends in the data. Now consider figure 13 which is a plot of flexural strength versus minimum fired thickness (the minimum dimension of the fired part from which the flexural specimens were taken). Here it is easily seen that there is a definite correlation between the flexural strength and fired thickness. Figures 14 and 15 show other correlations that were obtained using flexural data. The existence of these trends as exhibited by the flexural data suggests that a material response was observed that had not been masked or normalized by some other dominant event.

Along these same lines consider the results shown in table 3. This is a table summarizing the results of statistical calculations which were performed to determine whether or not correlations existed between some of the more easily obtained material processing parameters and mechanical properties which can be measured in the laboratory. Both tensile and flexural data were employed. In this table there are nine

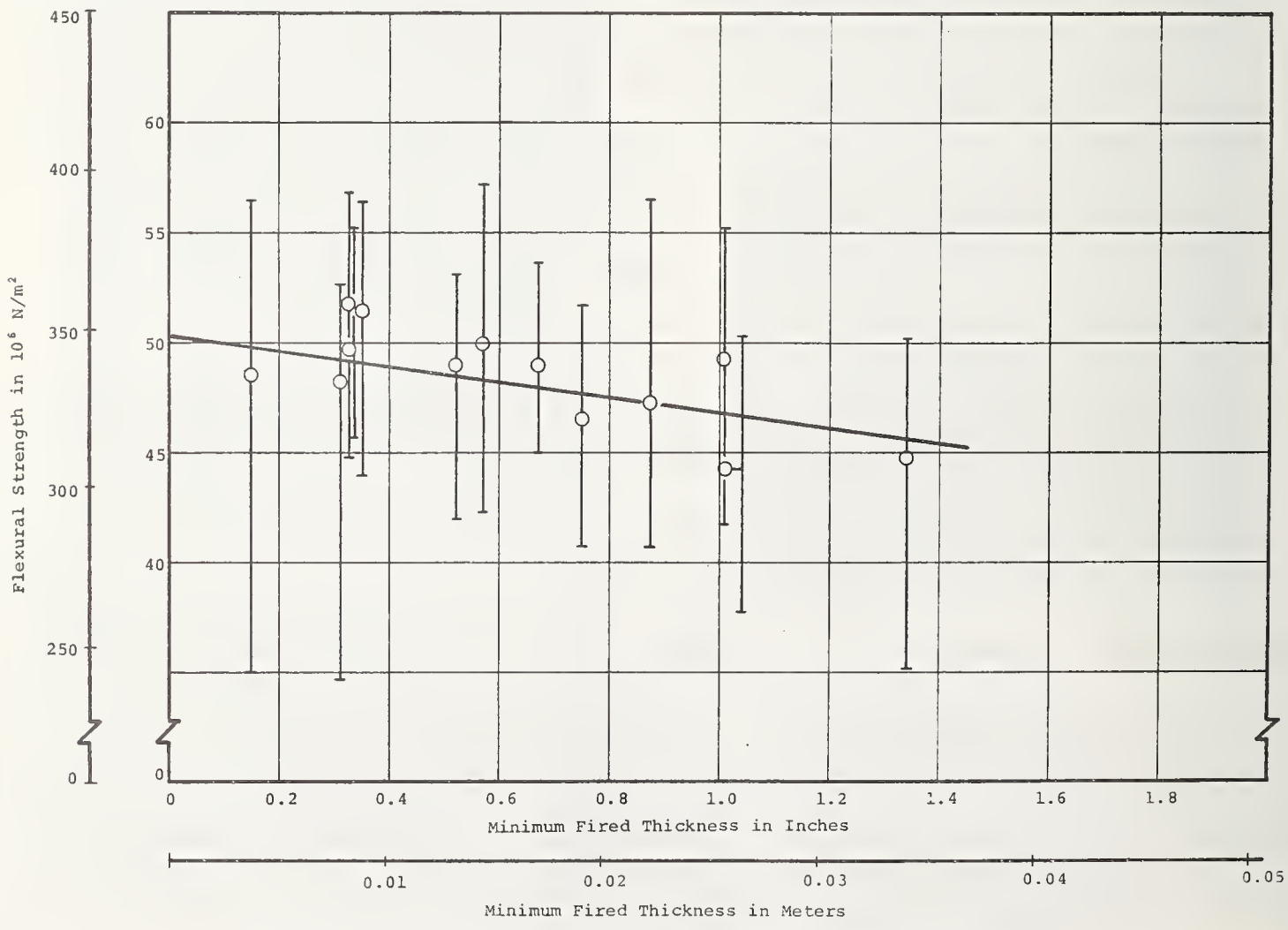

FIGURE 13. *Average flexural strengths versus minimum fired thickness.*

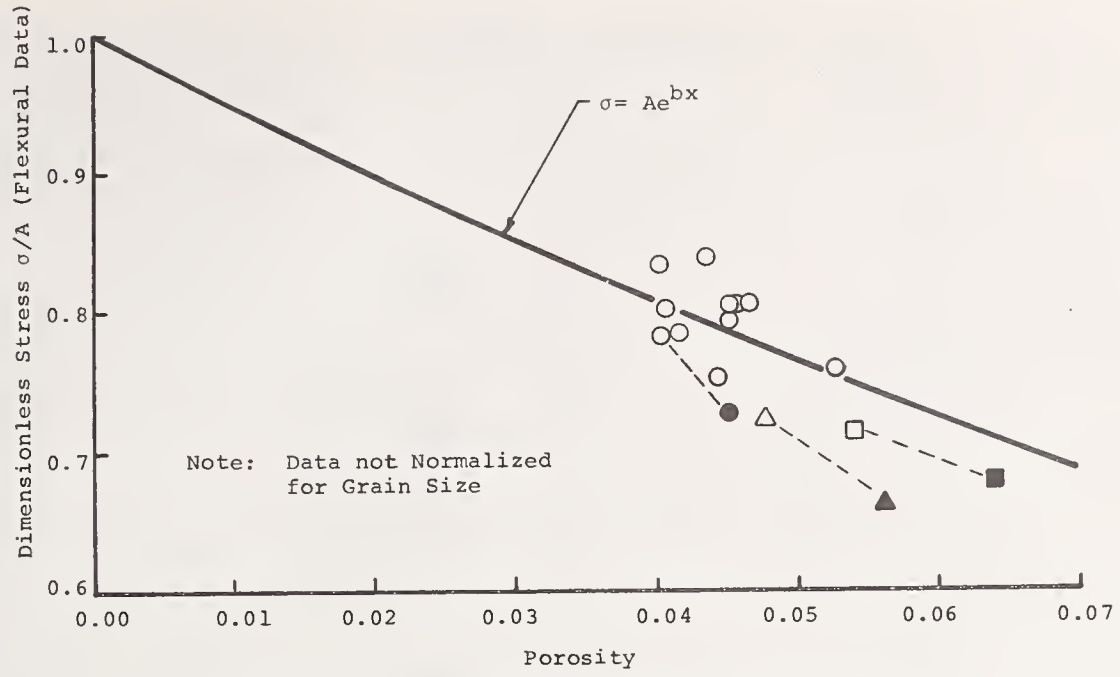

FIGURE 14. *Dimensionless stress versus porosity for alumina showing regressive curve.*

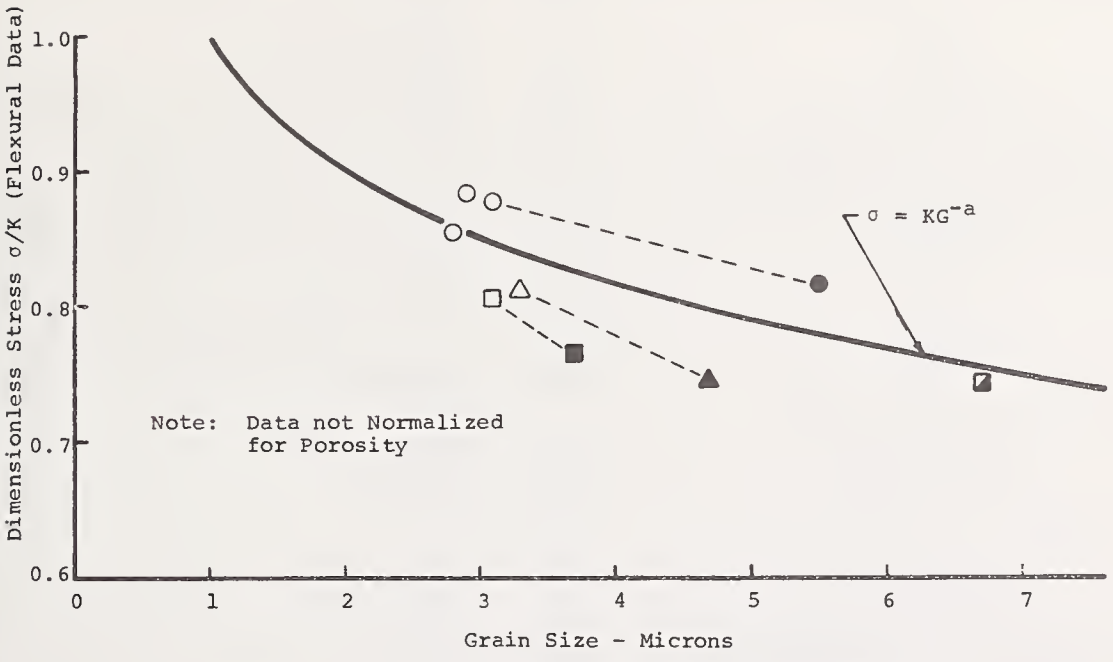

FIGURE 15. *Dimensionless stress versus grain size for alumina showing regression curve.*

direct comparisons between the tensile and flexural strength data. In seven of the nine comparisons the tensile and flexural data exhibited the same trends; in the other two cases, the data were inconclusive. Thus the flexural specimens, which are surface sensitive, are showing the same trends as the tensile specimens, which are less surface sensitive. This adds confidence to the earlier statement that the flexural data are revealing material responses and are not being normalized by surface effects or subsurface damage.

The third observation was based on calculations made by assuming the material responded in a manner consistent with Weibull's statistical theory of strength. Figures 16 and 17 show some probability of fracture curves for this material. Note that the value of the Weibull Modulus m was about 12.5 for both the tensile and flexural data. The average flexural strength for as-ground specimens was 48,300 psi (333.0×10^6 N/m^2). Using the equations developed earlier one could predict the tensile strength that should be obtained with the macrotensile specimens:

$$\sigma_T = \sigma_F \left[\frac{V_F}{V_T} \cdot \frac{1}{m+1} \right]^{1/m}$$

σ_T = tensile strength

TABLE 3. *Rank correlation tests*

Test no.	Items tested	Number of samples	Z	Correlation indicated: Positive	Negative	Indication too weak	Confidence level
RC 1	Green density vs sonic velocity						
(a)	Tensile	42	−1.801		X		92.82%
(b)	Flexural	158	−6.273		X		>99.99%
RC 2	Green density vs cone angle	45	−0.598			X	
RC 3	Green density vs tensile strength						
(a)	All blanks	98	3.089	X			99.8%
(b)	Less 11, 12, 13	55	0.354			X	
(c)	Blanks 11, 12, 13	43	3.271	X			99.9%
RC 4	Green density vs flexural strength						
(a)	All blanks	242	3.431	X			99.5%
(b)	Less 11, 12, 13	188	0.504			X	
(c)	Blanks 11, 12, 13	54	2.844	X			99.5%
RC 5	Green density vs fired density	37	−1.628			X	
RC 6	Cone angle vs sonic velocity						
(a)	Tensile	73	1.095			X	
(b)	Flexural	191	−0.520			X	
RC 7	Cone angle vs tensile strength	122	−4.219		X		>99.99%
RC 8	Cone angle vs flexural strength	293	−8.560		X		>99.99%
RC 9	Cone angle vs fired density						
(a)	Tensile	130	−0.290			X	
(b)	Flexural	293	18.691	X			>99.99%
RC 10	Sonic velocity vs tensile strength	71	0.355			X	
RC 11	Sonic velocity vs flexural strength	193	1.653	X			90.16
RC 12	Sonic velocity vs fired density						
(a)	Tensile	73	0.548			X	
(b)	Flexural	193	1.680	X			90.70
RC 13	Sonic velocity vs minimum thickness						
(a)	Tensile	73	1.043			X	
(b)	Flexural	182	1.416			X	
RC 14	Fired density vs tensile strength						
(a)	All blanks	141	4.085	X			>99.99%
(b)	Less 11, 12, 13	94	−0.017			X	
(c)	Blanks 11, 12, 13	47	−0.822			X	
RC 15	Fired density vs flexural strength						
(a)	All blanks	315	8.681	X			>99.99%
(b)	Less 11, 12, 13	236	2.421	X			98.4%
(c)	Blanks 11, 12, 13	79	0.907			X	
RC 16	Minimum thickness vs tensile strength	141	−6.748		X		>99.99%
RC 17	Minimum thickness vs flexural strength	304	−13.530		X		>99.99%
RC 18	Minimum thickness vs fired density	64	−3.727		X		>99.98%

σ_F = flexural strength
V_T = tensile volume in a tensile specimen
V_F = tensile volume in a flexural specimen
m = Weibull Modulus

For the macroflexural specimen, figure 18

σ_F = 48,300 psi (333.0 × 10^6 N/m²)
V_F = 0.0075 in³ (0.1229 cm³)

For the macrotensile specimen, figure 18

V_T = 0.0013 in³ (0.0213 cm³)

so that σ_T calculated to be 45,100 psi (310.9 × 10^6 N/m²). The measured value was 46,300 psi (319.2 × 10^6 N/m²). Figure 19 shows how the flexural and tensile data plots on a Weibull strength-volume curve. It can be seen here that the prediction based on volume is quite good. If the calculations were based on surface area the prediction would require that the tensile specimen be stronger since the flexural specimens had nominally 2–3 times the surface area of the tensile specimens. Thus, this reinforces

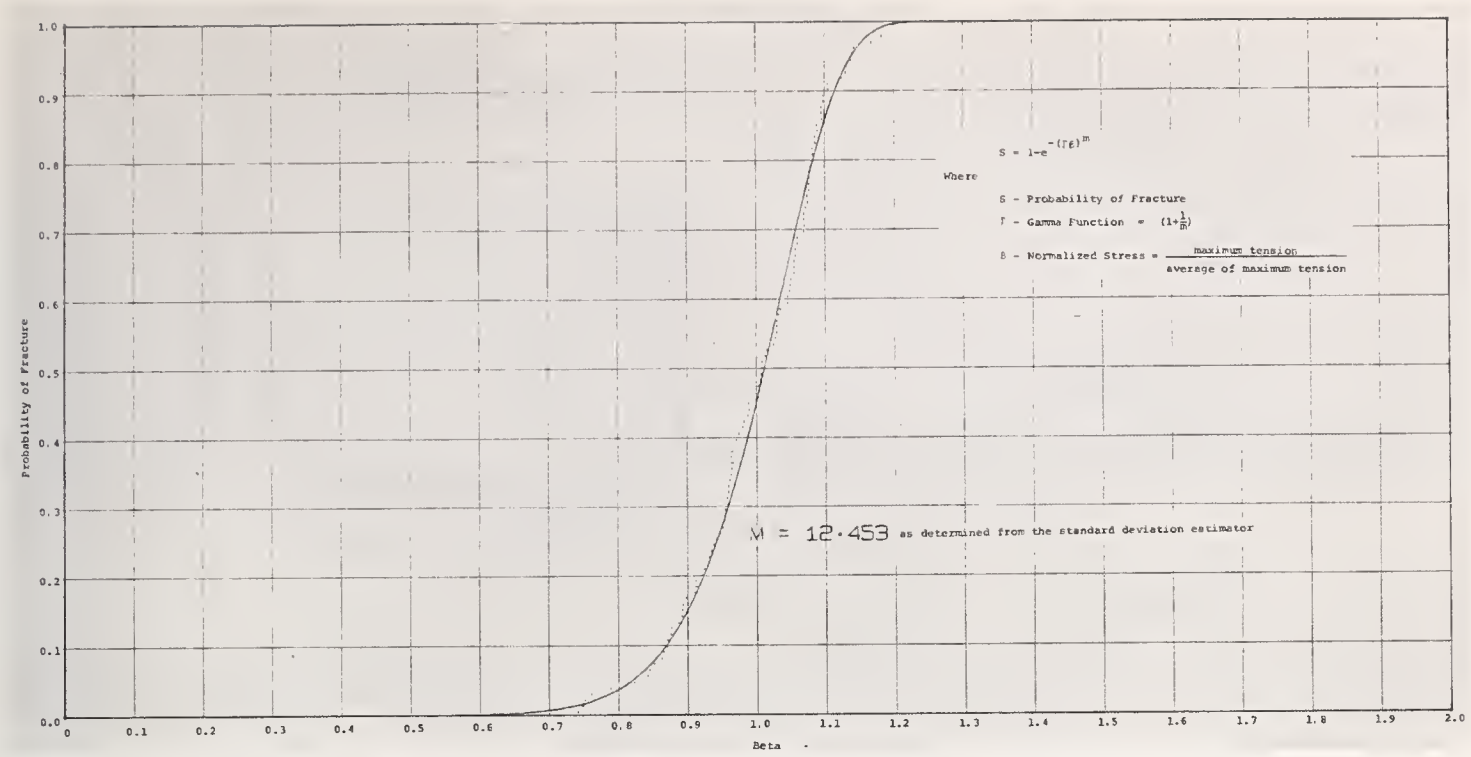

FIGURE 16. *Probability of fracture versus normalized stress β for the macrotensile specimens.*

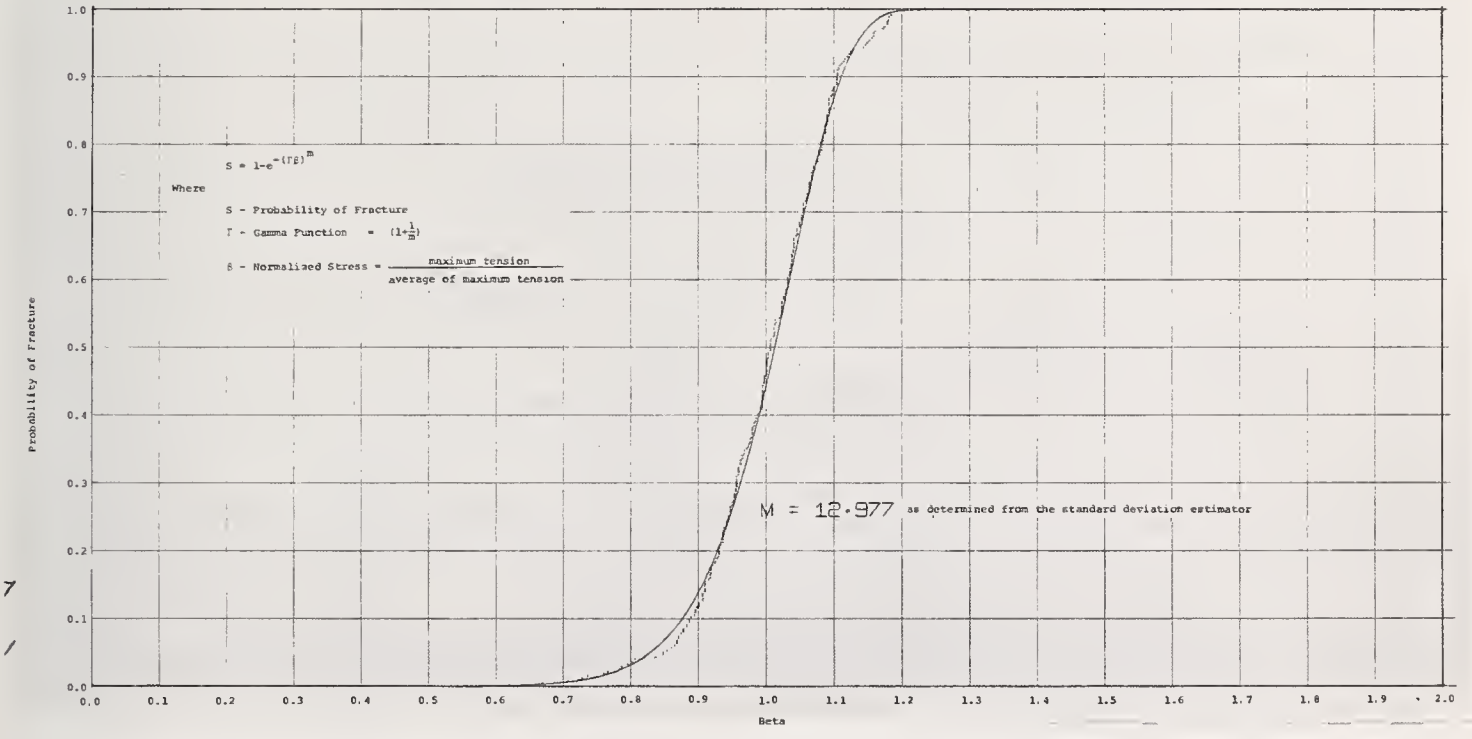

FIGURE 17. *Probability of fracture versus normalized stress β for the macroflexural specimens.*

the suggestions that surface/subsurface were not controlling the mechanical property data.

3. References

[1] Pears, C. D., Starrett, H. S., Bickelhaupt, R. E., et al., A Quantitative Evaluation of Test Methods for Brittle Materials, Technical Report AFML–TR–69–244, Part I, March, (1970).

[2] Pears, C. D., Starrett, H. S., Brown, J. R., et al., A Quantitative Evaluation of Test Methods for Brittle Materials, Technical Report AFML–TR–70–169.

[3] Robinson, E., Some Problems in the Estimation and Application of Weibull Statistics, Technical Report UCRL–70555, Sept. 1, 1967.

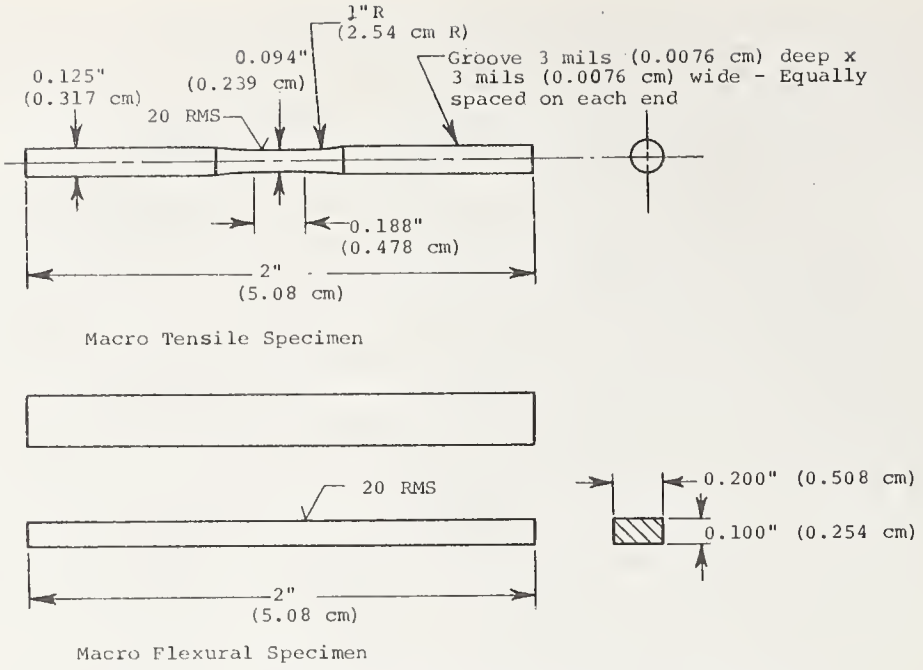

FIGURE 18. *Macrospecimens used for the evaluation of uniformity and reproducibility.*

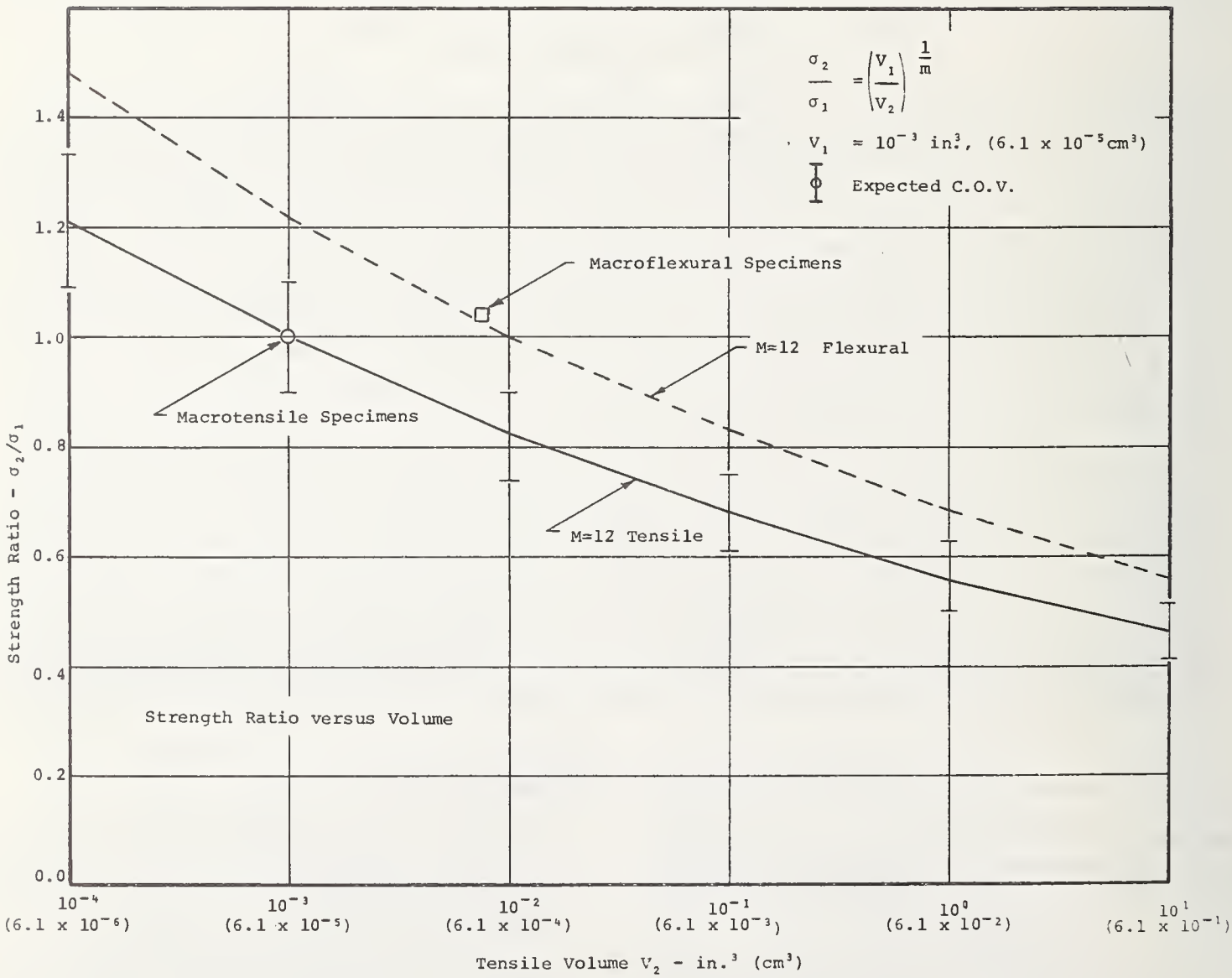

FIGURE 19. *Strength ratio versus tensile volume for tensile and flexural (4-Point) specimens.*

LANGE: Refiring can change the properties of a ceramic. Did you measure grain size both before and after refiring?

STARRETT: We measured grain size before firing. We have not completed the grain size measurements after firing. We think the slight decrease might be due to a slight increase in grain size, however, the refire temperature was selected so that grain growth would not occur. (Measurements made at a later date confirmed that grain growth did not occur during the refiring cycles.)

RICE: Comments—(1) The fact that you have a wide grain size distribution and in particular, have large grains scattered throughout a fine grain matrix would certainly indicate that there is a volume effect in fracture. This is because the large grains, regardless of whether it's a flaw or a microplastic mechanism of failure, would be the source of failure. This is one good explanation why you get a volumetric effect. (2) I've used some of your data as well as quite a bit of my own and analysis suggests that the strength controlling effect in alumina is microplasticity and quite probably twinning. This would go along with the fact that you don't see much effect of a wide variety of surface finishes.

NATIONAL BUREAU OF STANDARDS SPECIAL PUB. 348, THE SCIENCE OF CERAMIC MACHINING AND SURFACE FINISHING, Proceedings of a Symposium Sponsored by the American Ceramic Society, the Office of Naval Research, and the National Bureau of Standards, held at NBS Nov. 2–4, 1970, Gaithersburg, Md. (Issued May 1972).

The Effect of Grinding Variables on the Strength and Surface Finish of Alumina

Rudolf Sedlacek, F. A. Halden, and P. J. Jorgensen [1]

Stanford Research Institute
Menlo Park, California 94025

The tensile strength of alumina is used as a criterion for the evaluation of the effects of variables encountered in diamond grinding of ceramics. The variables studied include the grit size of diamond, rate of material removal, and sparkout. The difference in performance of natural and synthetic diamond is shown, and the feasibility of dry grinding is discussed. The ground surfaces were examined using profilometry, and transmission electron and scanning electron microscopy. The strengths of test specimens having ground or as-fired surfaces are compared.

Key words: Alumina; diamond grinding; surface finish; tensile strength.

1. Introduction

In recent years, oxide ceramics, which have certain favorable mechanical and physical properties, have been gaining wider acceptance in various applications. Some of the properties contributing to this acceptance are: superior strength retention at high temperatures, chemical inertness, dimensional stability, hardness, and dielectric properties. Unfortunately, ceramics are also brittle, which presents a serious deterrent to their use in structural applications. However, the requirements of modern technology are such that at times the designer can find no suitable alternative to ceramics. In these critical applications, the ceramic components are frequently machined to very close tolerances. The shaping of ceramics can take place in various steps of the manufacturing process, depending on the dimensional accuracy required. For instance, a piece can be either green-machined and then fired, or bisque-fired, machined, and then sintered to final density. However, in the vast majority of cases when high dimensional precision is required, the ceramic piece is first sintered to ultimate density and then finished to size. Because of the hardness of ceramics, the number of machining methods is limited, and grinding with bonded diamond constitutes the most widely used industrial method of material removal.

Like many other steps in ceramic manufacture, today's grinding process is the result of a highly pragmatic development and as such does not have a particularly solid theoretical foundation. As a matter of fact, very little is known about the physical principles of diamond grinding of ceramics, and most of the existing knowledge is considered proprietary by industry. One of the better known facts about grinding is that it controls the quality of the surface of the ceramic and thereby influences its mechanical properties, which are sensitive to surface conditions.

The method of material removal described in the present article was internal cylindrical grinding. This choice was dictated by the test method used for strength measurements, i.e., the SRI expanded ring test method. The full description of the test method is available in the open literature [1] [2] and will not be repeated here. Essentially the test specimen has the shape of a short thin-walled right cylinder in which a tangential tensile stress is generated by application of hydrostatic pressure to the inner wall. Since this is the locus of maximum tensile stress, it can be assumed that variations of grinding parameters in internal grinding will result in more pronounced changes in strength. Consequently, the method of grinding the outside walls and faces of the test specimens was not considered a variable and was kept constant throughout this study.

2. Experimental Procedure

The material used in the study was Wesgo Al-995 alumina. This is a nominally 99.5 percent pure alumina body, approximately 97 percent dense, having an average grain size of 18×10^{-6} m. The main reason for choosing Wesgo Al-995 alumina for this study was that this material has been studied extensively by various investigators. It is thus one of the most thoroughly documented ceramic bodies insofar as mechanical properties and the reproducibility of the manufacturing process are concerned. The test material was purchased in the form of ring-shaped blanks of such size that approximately 12.7×10^{-5} m (0.050 in) had to be removed from the internal and external diameters and the faces. The final dimensions of the test specimens were:

[1] Senior Research Ceramist, Associate Director Materials Laboratory, Manager Ceramics Group, respectively.

[2] Figures in brackets indicate the literature references at the end of this paper.

439-921 O - 72 - 27

Inside diameter: 5.080×10^{-2} m (2.000 in)
Outside diameter: 5.588×10^{-2} m (2.200 in)
Height: 0.762×10^{-2} m (0.300 in.)

All final dimensions were kept within $\pm 1.3 \times 10^{-5}$ m (0.0005 in) and were checked by means of air gages and micrometers.

2.1. Grinding Procedure

The machine used in this work was a precision universal cylindrical grinder (Tschudin, Model 300) equipped with a linear-position potentiometer for monitoring and reproducing table speeds, and several specialized holding fixtures were designed for the individual grinding steps. The basic grinding procedure consisted of the following steps:

(a) The blanks were ground on both ends so that their faces were parallel and properly spaced.

(b) Using a suitable mounting medium, the faced blanks were arranged in stacks each containing seven rings for cylindrical grinding. The details of the mounting procedure were rather complex and have been described elsewhere [2, 3]. The cylindrical grinding of the outside walls of the specimens always preceded the internal grinding.

The facing and external grinding of all specimens was identical in order to isolate and to better resolve the effect in strength of the variables studied in the internal grinding step. The wheel used in facing and in external grinding had a 0.305 m (12 in) diameter, a face width of 2.54×10^{-2} m (1 in), and was designated D320–N100M1/16. The following conditions were used in facing and external grinding:

Table speed: 5.08×10^{-3} m/s (1 ft/min)
Infeed: 6.4×10^{-6} m/pass (0.00025 in/pass)
Surface speed: 2.9×10 m/s (5,700 sfpm)
Sparkout: 180 s.

2.2. Grinding Variables

The variables in internal grinding whose effects on strength were evaluated were: grit size of diamond, rate of material removal, type of diamond (natural or synthetic), wet or dry grinding, and length of sparkout time. It became apparent that these variables could not be studied individually and that some compromise in the form of a combination of variables would be necessary. The diamond grit size offered the largest range of conditions to study the effect of the surface finish per se on strength and was varied from 36 to 1200.

All wheels were of the straight type (1A1), having an outside diameter of 2.54×10^{-2} m (1 in) and a face width of 1.27 or 0.63×10^{-2} m (1/2 in or 1/4 in). All wheels were metal bonded except the 36 grit wheel, which had a vitrified bond, and the 100 grit synthetic diamond wheel, which was resinoid bonded. For maximum perfection, all wheels were trued against a silicon carbide wheel mounted on the spindle of a brake-controlled trueing device, and rotated by contact friction. Subsequently, the wheels were dressed wet with silicon carbide sticks of proper grade to remove the glaze produced by the trueing operation.

The sparkout time was limited only by consideration of time, whereas other variables were less flexible. The study of the practicality of dry grinding, for instance, was limited to the resinoid-bonded wheel because it was soon discovered that metal-bonded wheels, although their matrix has a much better thermal conductivity than the plastic, wear fast, load up with grinding debris, and oxidize. The same is probably true of wheels having a vitrified bond, but this avenue has not been explored. In terms of effect on strength, the most difficult variable to assess in the grinding process was the rate of material removal. This variable can be resolved into two main components, i.e., the table travel speed and the depth of infeed. Both of these can be studied only over a limited range. One of the reasons for this is the nature of the grinding operation employed. Internal cylindrical grinding is undoubtedly the least suited machining operation for rapid stock removal. Unlike surface grinding in which the work piece is fixed rigidly to the table, in cylindrical grinding the work piece is supported on only one end and consequently is much less rigid. The grinding wheel in internal grinding is mounted on the end of an arbor whose length must be somewhat longer than the depth of the cavity being ground, and the arbor must be smaller in diameter than the grinding wheel itself. Consequently, this arbor is subjected to considerable bending forces which produce vibrations. However, in the work described the limits in the rate of stock removal were dictated primarily by the strength of the bond between individual rings of the stack.

The makeup of the grinding wheel, i.e., grit size, diamond concentration, and bond type, was found to be the most important and limiting factor in controlling the rate of stock removal. With the 60, 100, 120, and 320 grit wheels, the depth of cut presented no problem over the range investigated (2.5×10^{-6} m to 3.8×10^{-4} m — 0.0001 to 0.015 in). In taking heavier cuts (5×10^{-5} m to 12.7×10^{-4} m — 0.002 to 0.005 in) the fine grit wheels (600 and 1,200 grit) tended to slow down. The leading edges wore rapidly and the metal seemed to oxidize. The 36 grit vitrified bond wheel was used only for very light cuts to impart a coarse finish to stacks previously ground with another wheel within 2.5×10^{-5} m to 5×10^{-5} m (0.001 to 0.002 in) from the final dimensions. The

blocky diamond with large facets, few cutting edges, and low diamond concentration makes this type of wheel wholly unsuited for grinding of dense, hard ceramics. Furthermore, the vitrified bond lacks the toughness of the metal bond, and consequently the wheel was broken in an attempt to make a moderately deep cut, 12.5×10^{-5} m (0.005 in). The surface speed most commonly used in internal grinding on this program was 28.4 m/s (5,600 sfpm). The highest available speed (34.5 m/s—6,800 sfpm) was used with the 1,200 grit wheel in the finish grinding of a few stacks. This speed, however, exceeds the safety limits of both the wheel and the spindle. Since no noticeable improvement of surface finish or strength resulted, this procedure was discontinued.

There are many possible combinations of variables, and several of them were studied, i.e., effect on strength of a deep final cut, effect of a deep cut followed by several shallow cuts made with the fine grit-size wheel with or without sparkout, etc. These experiments did not clarify the picture; only heavy infeeds at low table speeds with coarse grit wheels showed conclusive evidence of damage.

3. Results and Discussion

In tabulating experimental strength data to show the effects on strength of individual machining variables, it became apparent that only a few of the variables employed could be used as valid criteria for evaluation. The effect of some variables is so small that it cannot be detected. The length of sparkout time is a prime example. Other variables, such as the rate of material removal, show a considerable effect, but in such a complicated manner, that it is not feasible to present the results in a unified logical way. Furthermore, in cases where several variables were changed simultaneously over a narrow range, it was impossible to decide which one caused the variations in strength, if any occurred.

The variable whose effect on strength can be shown most systematically is the grit size of the diamond used. Table 1 presents the average strength values of specimens finish ground with natural diamonds of the grit size indicated, regardless of the previous grinding history. Included are the strength values of specimens ground by the manufacturer, which can be considered indicative of results obtained in a routine production grinding process.

The relationship between the grit size and strength is very systematic, although greater strength differences were anticipated. In particular, lower strength values were expected from the specimens ground with the two coarsest wheels (36 and 60 grit).

A limited study of the practicality of dry grinding (without coolant) was made using a resinoid-bonded wheel containing 100 grit size synthetic diamond. The results are shown in table 2. This wheel was used without coolant to remove the last 5.1×10^{-5} m (0.002 in) in wall thickness in 2.58×10^{-6} m (0.0001 in) steps and at a table speed of 5.1×10^{-3} m/s (1 ft/min). (The initial grinding was done with the 320 grit wheel.) Five stacks were ground in this manner, five more stacks were ground under identical conditions except that coolant was used. The results presented in table 2 show that dry grinding under the experimental conditions employed does not improve strength. As a matter of fact, dry-ground specimens are considerably weaker than those ground in the conventional way, i.e., 21.0×10^{7} N/m^2 (30.5×10^{3} psi) versus 22.2×10^{7} N/m^2 (32.2×10^{3} psi).

It may be noted that the average tensile strength of specimens ground wet with the same wheel is practically identical to the strength of the specimens of the group D in table 1 ground with the 320 natural diamond.

TABLE 1. *Tensile strength of alumina as a function of the grit size of natural diamond in metal-bonded grinding wheels*

Group	Grit size	Number of specimens	Average tensile strength		Standard deviation		Coeff. of variation percent
			N/m^2 $\times 10^7$	psi $\times 10^3$	$\pm$N/m^2 $\times 10^6$	$\pm$psi $\times 10^3$	
	Unknown	12	20.5	29.8	8.1	1.2	4.0
A	36	29	21.3	30.9	11.7	1.7	5.5
B	60	37	21.4	31.1	12.4	1.8	5.8
C	120	48	21.9	31.7	8.2	1.2	3.8
D	320	33	22.3	32.3	7.6	1.1	3.4
E	600	45	22.5	32.6	10.3	1.5	4.6
F	1200	85	22.9	33.2	9.7	1.4	4.2

An indication of superior performance of synthetic diamond has also been observed by other workers [4] using various grades of synthetic and natural diamond in metal-bonded wheels. The lower strength of specimens of group A in table 2 indicates that dry grinding is not a recommendable procedure.

The effect of infeed on strength gave conclusive results only in the case of the heaviest cuts. For example, a group of specimens were ground with the 60 grit wheel using a table speed of 2.6×10^{-4} m/s (0.05 ft/min) and a depth of cut 3.8×10^{-4} m (0.015 in). The average strength of these specimens was 18.6×10^{7} N/m^2 (27.5×10^{3} psi). This is a significantly lower value than the strength of specimens of group B in table 1 which were finish ground with the 60 grit wheel under less severe infeed conditions. Similarly specimens of another stack were ground with the 100 grit resinoid-bonded wheel under identical conditions of infeed and table speed. Their average tensile strength was 20.5×10^{7} N/m^2 (29.8×10^{3} psi). Although this is lower than the average strength of specimens of group B in table 2, the difference is less pronounced (7.8%) than in the case of specimens ground with the metal-bonded 60 grit wheel (12.1%). Apparently the bond of the wheel makes a difference, but the nature of the difference is not well understood. It should also be pointed out that in these experiments in which a heavy infeed was used, the resinoid-bonded wheel lost approximately one-half of the diamond bearing layer, while the amount of wear of the metal-bonded wheel was not measurable with the micrometer. These two examples show clearly that heavy infeeds are detrimental to strength. However, this observation cannot be extended indiscriminately to the concept of the rate of material removal which represents the volume of material removed per unit time, and is equal to the product of infeed and table speed per unit time. In the aforementioned cases when a heavy infeed and slow table travel were used, this quantity equals 9.1×10^{-10} m^3/s (1.5×10^{-4} in^3/s. There were instances in which combinations of infeed and table speed resulted in considerably higher rates of material removal without any detrimental effect on strength. For instance, one stack in group C of table 1 was ground with an infeed of 12.5×10^{-5} m (0.005 in) at a table speed of 5.1×10^{-3} m/s (1 ft/min). In this case the rate of material removal was 6.1×10^{-9} m^3/s (1.0×10^{-3} in^3/s). This is 6.7 times higher than the previous value and yet this stack with an average strength of 22.5×10^{7} N/m^2 (32.7×10^{3} psi) was the strongest of all stacks of group C. Obviously, infeed and table speed do not have the same effect on strength, and this phenomenon probably depends on the rigidity and vibrational characteristics of both the work piece and the machine used.

4. Tensile Strength of Alumina having As-Fired or Ground Surfaces

No matter how gently done, grinding of ceramics is undoubtedly a harsh method of material removal. There will always be chipping, grooving of grains, pullouts, cracking of boundaries, etc. Therefore, it is not surprising that alternative means of material removal are being sought, for instance, chemical machining. To our knowledge, no practical solution to this problem is yet in sight. The question may then be raised whether or not any postfiring treatment is necessary, provided that the preceding manufacturing steps are carried out in such a way that no additional dimensional adjustments are required for the intended application of the ceramic product. This avenue was briefly explored.

For this study, a different lot of Al–995 alumina was used and the specimens were prepared in three different ways:

Group A—Specimens were green-machined to a size determined by the experimentally found shrinkage factor and then fired to final density.

Group B—Specimens were bisque-fired to 1450 °C, then machined to a size that would shrink in firing to the desired dimensions.

Group C—Specimens were oversized blanks which after firing were ground to final dimensions.

The two groups of specimens having the as-fired surfaces had a number of geometric imperfections caused by the manufacturing process. In the case of group A, the shrinkage factor was miscalculated so that all specimens turned out to be undersized on the inside diam-

TABLE 2. *Tensile strength of alumina ground with and without coolant*

Group	Number of specimens	Type of grinding	Average tensile strength		Standard deviation		Coeff. of variation percent
			$N/m^2 \times 10^7$	psi $\times 10^3$	$\pm N/m^2 \times 10^6$	$\pm$psi $\times 10^3$	
A	31	Dry	21.0	30.5	13.8	2.0	6.6
B	34	Wet	22.2	32.2	9.7	1.4	4.3

eter. Furthermore, the specimens had the general shape of slightly truncated cones rather than that of right cylinders. Specimens of group B did not appear to be tapered but were somewhat oversized. These specimens had another more serious defect, namely, crushed alumina grit fused firmly onto large areas of the surface, particularly on one end face. This grit adhered only loosely to specimens of group A, and was not found on the blanks of group C.

The wall thickness of all specimens of groups A and B was relatively uniform, but the outside diameters appeared to vary slightly in a completely random fashion, indicating a certain degree of out-of-roundness. Whether this is the result of improper machining or nonuniform shrinkage is not known at the present time. The comparison of tensile strength between the three groups of specimens is presented in table 3. The difference in strength between the two types of specimens is obvious, but we cannot simply state that the ground specimens are stronger (21.4×10^7 N/m^2—30.8×10^3 psi) than the as-fired ones (19.9×10^7 N/m^2—28.8×10^3 psi). The original intention was to make a comparison of strength based only on the difference between the surfaces and the means by which they were obtained. However, the real situation is complicated by factors stemming from the manufacturing process which obscured the original objective. In the case of group A, it is possible to say that the as-fired surface has an average roughness of 1.3 to 3.8 $\times 10^{-6}$ m (50 to 150 μin), but the observed strength and scatter cannot be only the results of surface conditions. They must also reflect the dimensional irregularities that upset the stress distribution in a way not amenable to analysis.

The observed average strength of specimens of group B is identical to that of group A, although the overall geometry of these specimens was considerably better than that of group A, and therefore a higher strength than in group A could be expected. Under the circumstances, we have no choice but to attribute the results to the surface conditions. This surface can only be described as a very rough interface between alumina and air evading any meaningful characterization. However, the macroscopic roughness of the surface should not be confused with the microscopic surface features controlling the strength because in that case lower strength values would have resulted.

The results do not show unambiguously whether a ground or as-fired surface is preferable to obtain higher strength, but they strongly indicate that in the present state of the art, grinding is necessary to make up for other shortcomings of the manufacturing process.

5. Evaluation of Ground Surfaces

In the case of glasses, it is well documented that in terms of strength, the surface conditions are of critical importance. It is not certain, however, to what degree this applies to polycrystalline materials, such as alumina. Generally, it is accepted that smoother surfaces are representative of higher strength. Whether this is a simple function of density and severity of surface imperfections, or a more complex relationship involving some stress-enhanced chemical reactivity dependent upon surface conditions, is not known. In either case, an interpretation and understanding of surface characteristics is most desirable.

In the work described, two basically different methods were employed for the identification and interpretation of surface features, i.e., microscopy and profilometry. Although transmission electron microscopy was also used, most of the work was done using a scanning electron microscope. The problems involved are best illustrated in figure 1. These are low power scanning electron micrographs of Al–995 surfaces produced by grinding wheels having different grit sizes of diamond. By using a little imagination, it may be possible to say that the surface produced by the 36 grit diamond appears to be somewhat more battered than the others and that the fewest pullouts were obtained with the 1,200 grit wheel. Beyond that, there is very little basic difference and it is virtually impossible to decide which grit size produced a particular finish.

To relate the appearance of the surface to strength would be almost pure guesswork. From a practical standpoint, it is nearly impossible to examine the entire specimen surface before

TABLE 3. *Tensile strength of alumina having as-fired or ground surfaces*

Group	Average tensile strength		Standard deviation		Coeff. of variation percent
	$N/m^2 \times 10^7$	psi $\times 10^3$	$\pm N/m^2 \times 10^6$	$\pm$psi $\times 10^3$	
A	19.9	28.8	20.0	3.0	10.4
B	19.9	28.8	13.1	1.9	6.4
C	21.2	30.8	6.9	1.0	3.2

FIGURE 1. *Scanning electron micrographs of Al–995 Alumina.*

testing to find the most damaged spot, e.g., the highest concentration of pullouts, and to see if it is the locus of failure. To examine fragments of broken specimens is a futile exercise in microscopy which may, at the best, lead only to a subjective interpretation of the studied surfaces.

Profilometric studies were made using a Clevite Corporation Surfanalyzer 150 System. The diamond stylus of this instrument has a 2.54×10^{-6} m (0.0001 in) tip radius and all measurements were made using a probe travel speed of 2.54×10^{-4} m/s (0.01 in/s) and a roughness width cutoff of 7.6×10^{-4} m (0.03 in).

Profilometry has certain advantages over visual evaluation of photographs. It gives a picture of a surface that is more tangible and easier to interpret, particularly in terms of depth and spacing of cracks and scratches. Furthermore, it is the most widely used method of graphic representation of surface conditions and it is quite suitable for comparison if equivalent profilometers are used.

The most obvious shortcomings of this method are the fact that the profilometer samples the surface only in one line and gives no indication of conditions of the surface on either side of this line. Also, the diameter of the stylus tip limits the depth to which the tip can penetrate.

Figure 2 shows profile traces of Al–995 alumina surfaces ground by different grits of diamond. Each vertical division represents 5.1×10^{-7} m (20 μin) and every horizontal division is 2.54×10^{-5} *m* (0.001 in). Subscripts indicate the arithmetic average roughness (AA) as generated by the profilometer on a different graph (not shown). It will be noticed that the AA roughness values are somewhat deceiving. For instance, the AA roughness value in the last graph is 5.1 to 7.6×10^{-8} m (2–3 μin). However, there is a 6.6×10^{-6} m (260 μin) deep crack, whose existence cannot be inferred from the AA roughness value. The disproportion between total roughness and AA roughness can be found in all of the graphs, and it is a characteristic of the averaging circuitry of the apparatus. Notwithstanding this shortcoming, we believe that profilometer traces convey better the qualitative differences between surfaces than micrographs. For instance, the AA roughness value for surfaces shown in figure 2 vary by a factor of 4 to 1 in order of decreasing diamond grit size. No such sharp distinction can be obtained from an inspection of the micrographs.

Whether or not these profilometer traces are typical of the surfaces studied is difficult to decide, because the recordings vary considerably from specimen to specimen, and also from place to place on the same piece. Furthermore, it is doubtful that the appearance of the most typical surface feature can lead to an understanding of the relationship between surface conditions and strength. What is really sought is some abnormal condition that leads to a decrease of strength, but so far this phenomenon has not been identified.

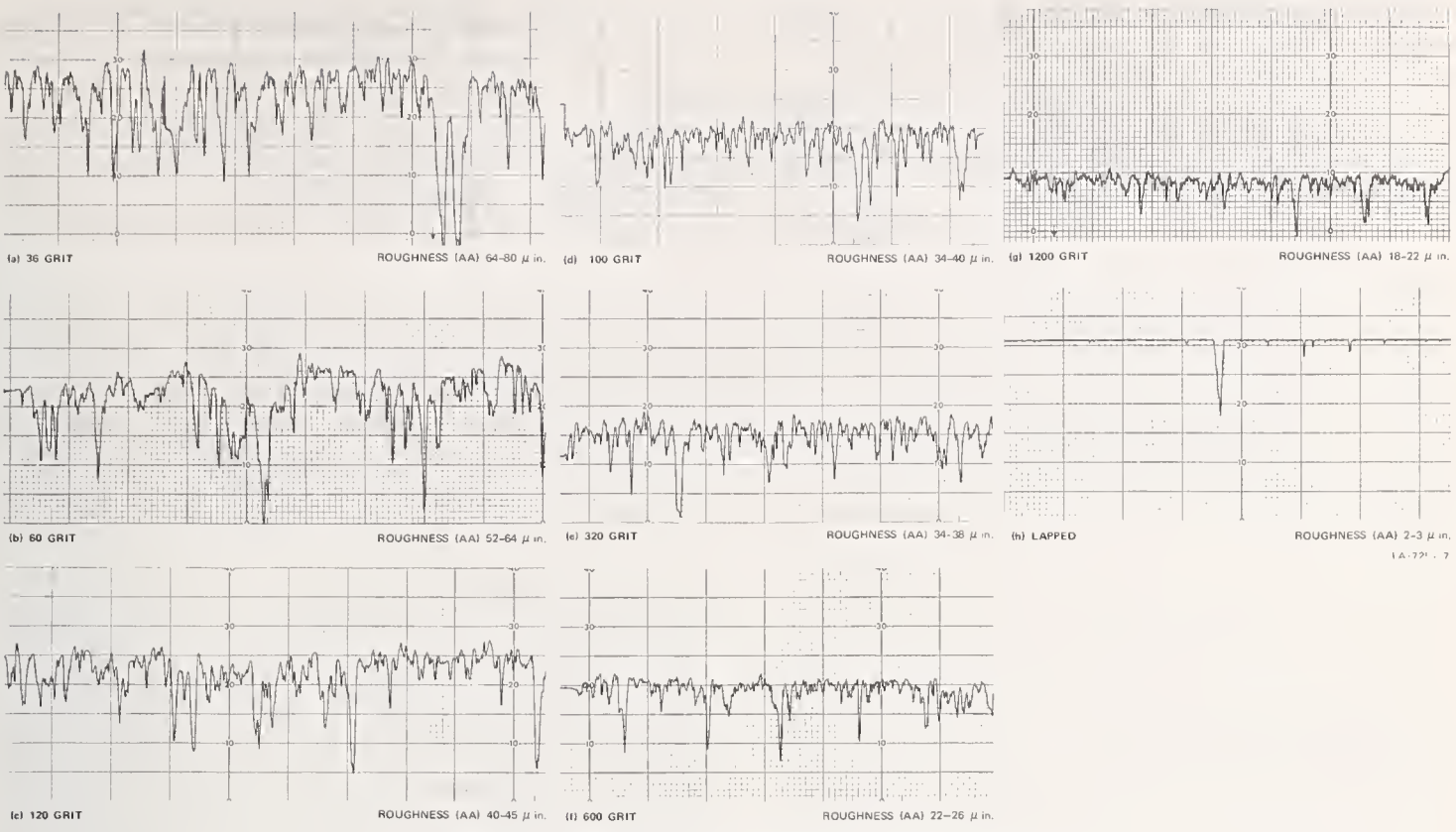

FIGURE 2. *Profile traces of alumina surfaces ground with different grit sizes of diamond.*

6. Conclusions

From the work described, the following conclusions can be drawn. Grinding of ceramics is a necessary operation because the ceramics manufacturing process is presently unable to produce an as-fired shape having a closely specified geometry. When reasonable care is exercised in grinding, the strength of ceramics is not markedly affected by changes in grinding variables over a wide range; however, excessive infeed (deep cut) is detrimental to strength. Surface features that we presently can observe and monitor are not a very sure indicator of strength.

The authors wish to acknowledge the support of the Naval Air Systems Command who sponsored this work under Contracts NOw–66–0383–d and NOOO19–67–C–0494.

7. References

[1] Sedlacek, R., and Halden, F. A., Method of tensile testing of brittle materials, Rev. Sci. Instr. 33, 298–300 March (1962).

[2] Sedlacek, R., and Farley, E. P., Processing of Ceramics—Surface Finishing Studies, Final Technical Report under Contract No. NOw 66–0383–d, Stanford Research Institute, May (1967).

[3] Sedlacek, R., Processing of Ceramic—Surface Finishing Studies, Final Technical Report under Contract No. NOOO19–67–c–0494, Stanford Research Institute, November (1968).

[4] Gielisse, P. J., et al., Ceramic Finishing with Diamond, Part I: The Workpiece, Ceramic Industry 80 February (1968), Part II: The Abrasive and the Bond System, *ibid.*, March (1968), Part III: External Influences and Cost Analysis, *ibid.*, April (1968).

Discussion

GIELISSE: Mr. Sedlacek, when you compared strengths of aluminas ground with the man-made 100 grit resinoid wheel versus 320 grit natural diamond metal bond wheel, did you intend to contrast bond type or did you intend to contrast the manufactured versus the natural? There are two possibilities there.

SEDLACEK: Well, I really did it simply out of curiosity. At that moment I had no reason to anticipate any difference.

UNIDENTIFIED: I wonder if some of those spikes as you called them could be due to strain. My second question is did you or did you not stress relieve after grinding?

SEDLACEK: I think that the spikes are due to pullouts rather than to anything else. We did not do any stress relieving after grinding.

LANGE: In your scanning electron microscopy work, did you look for and see any surface cracks? I think you would need higher magnification.

SEDLACEK: We have used higher magnifications and we do find cracks. We are always trying to look for some pertinent feature which we could correlate with the tendency to break, but so far it has eluded us.

DANIELS: Was there any attempt to try to correlate strength with either the frequency or magnitude of those pullouts?

SEDLACEK: No, we have not done that.

NATIONAL BUREAU OF STANDARDS SPECIAL PUB. 348, THE SCIENCE OF CERAMIC MACHINING AND SURFACE FINISHING, Proceedings of a Symposium Sponsored by the American Ceramic Society, the Office of Naval Research, and the National Bureau of Standards, held at NBS Nov. 2–4, 1970, Gaithersburg, Md. (Issued May 1972).

Edge Effect on the Modulus of Rupture of Ceramic Substrates

Wing C. Lo

Bell Telephone Laboratories, Inc.
555 Union Boulevard
Allentown, Pennsylvania 18103

Because of its simplicity, the modulus of rupture (or flexural strength) test is often used to evaluate the mechanical strength of ceramics. For large flat substrates, the natural tendency is to test specimens cut from the substrate.

Depending on the method of cutting and the resulting edge condition of the specimen, the flexural strength can be significantly different. This is illustrated by 3-point loading data on CO_2-laser-scribed and diamond-sawed specimens. The modulus of rupture of a laser-cut sample is about 70 percent of that of a diamond-sawed sample.

Key words: Alumina substrate; edge damage; flexural strength.

To evaluate the mechanical strength of ceramic substrate materials, there is a general tendency to use the bend test (3-point or 4-point loading) on cut specimens. Although there is awareness of the effect of the bearing surfaces, loading rate, the span length, size and surface condition of the test specimen [1] on the modulus of rupture calculated from bend test results, that of the edge condition of the specimen is often neglected. Since the damage to the surface at the cutting edge produced by different cutting methods can vary with different materials, the resulting modulus of rupture does not truly represent that property of the material tested. Of course, the test would be adequate as a use test for evaluating or monitoring the quality of piece parts from different sources if the method of cutting and preparing the test specimens is the same as those used for the piece parts.

This note presents some experimental data to show that the edge effect on the modulus of rupture can be highly significant.

Figure 1 shows the modulus of rupture of two samples of Alsimag 772 [2] substrates taken from the same lot. One sample is cut by laser scribing and the other by diamond sawing. The laser scribing method uses a pulsed beam from a CO_2 laser to effect a series of hairline cracks on the substrate which may then be snapped apart by hand. The CO_2 laser used is model 40A made by the Coherent Radiation Laboratories with an output wavelength of 10.6μm. The pulse rate is $\sim$ 333 pulses/s and the feeding rate is 150 in/min (64 mm/s). The diamond sawing is done with a 0.017 in (0.43 mm) thick 3 in (7.6 mm) diameter metal bonded diamond wheel (Norton's designation D220–N100M). It has a diamond imbedded section of 0.125 in (3.2 mm). The wheel rotates at 2,500 RPM. The feeding rate is approximately 1.3

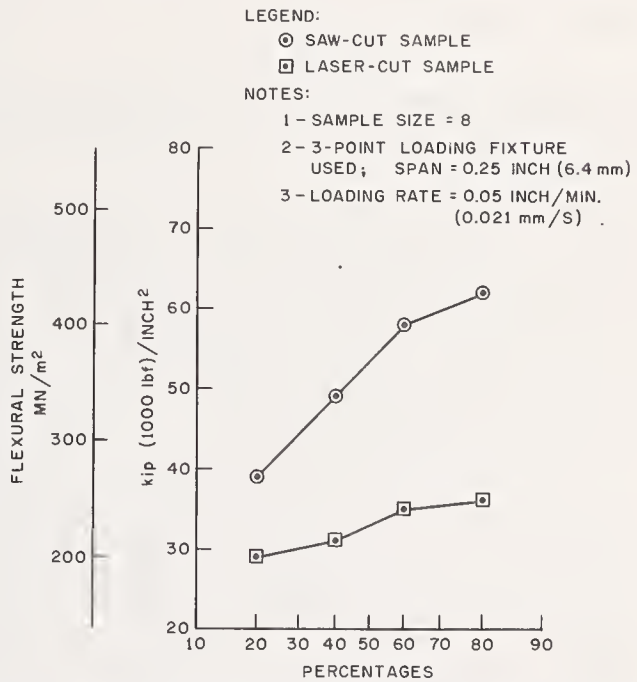

FIGURE 1. *Distribution of flexural strength of laser-cut and saw-cut ceramics (Alsimag 772 substrates).*

in/min (0.55 mm/s). The size of the test specimen is 0.350 in × 1.300 in (8.89 mm × 33.0mm with a thickness of approximately 0.025 in (0.63mm). In testing, the scribed side of the substrate is placed in tension.

The bend test was performed with a three point loading fixture using a 0.25 in span and a loading rate of 0.05 in/min. Eight specimens from each sample were tested.

The lower value of the laser-scribed sample (68% of that of the diamond-sawed sample) is attributed to the damage on the surface at the cut edge. This is made visible with the aid of a fluorescent penetrant (see fig. 2.) The damaged edge of the laser-cut ceramics adsorbs the penetrant and appears bright when viewed under ultraviolet light.

Examination under the microscope using the replica technique (fig. 3) shows quite clearly

[1] See for example ASTM F–103.
[2] Alsimag 772 is a 99.5 percent alumina body made by the American Lava Corporation, Chattanooga, Tenn., U.S.A.

FIGURE 2. *Zyglo test on laser-cut and saw-cut ceramic substrates.*

the presence of cracks in the amorphous or recrystallized material in the region where the laser strikes.

Similar results of edge effect on modulus of rupture were also reported by P. T. Morzenti.[3] Laser-scribed samples of Alsimag 772 and ADS 995 [4] gave modulus of rupture values about 72 percent and 73 percent respectively of those cut with a 15μm diamond wheel. However, with the ERC–105 substrate [5] which has a much finer grain structure [6] than the other two ceramics, the laser-scribed sample did not show any degradation in strength. This may be explained by the greater energy required to propagate cracks in a fine grain material which has more grain boundaries than in a coarser grain material (see figure 4).

These results are not to be construed to the use of laser-cutting as poor practice but are merely pointing out that when comparing modulus of rupture of ceramics one should be aware of the edge condition of the test specimens.

Thanks are due to Messrs. J. E. Clark, W. B. Grupen, F. L. Howland and P. I. Slick for their comments and to Mr. P. T. Morzenti for the use of his data.

[3] Private communication.
[4] ADS995 is a 99.5 percent alumina body made by Coors Porcelain Company, Golden Colorado, U.S.A.
[5] ERC–105 is a 99.5 percent alumina body developed by Western Electric Company Engineering Research Center, Princeton, New Jersey, U.S.A.
[6] The average grain size of the ERC–105 substrates is in the order of 1μm, while that of the other two samples is several microns.

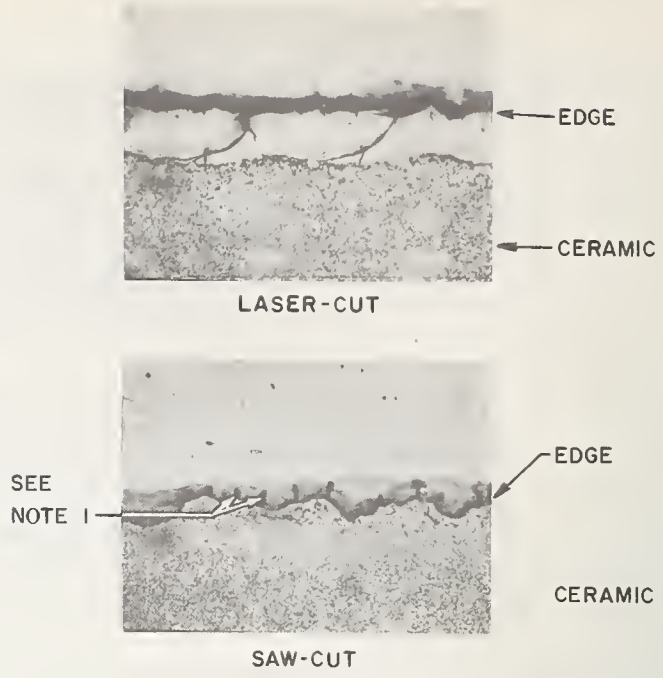

FIGURE 3. *Top view of edges of laser-cut and saw-cut ceramic substrates by transcopy replica technique.*

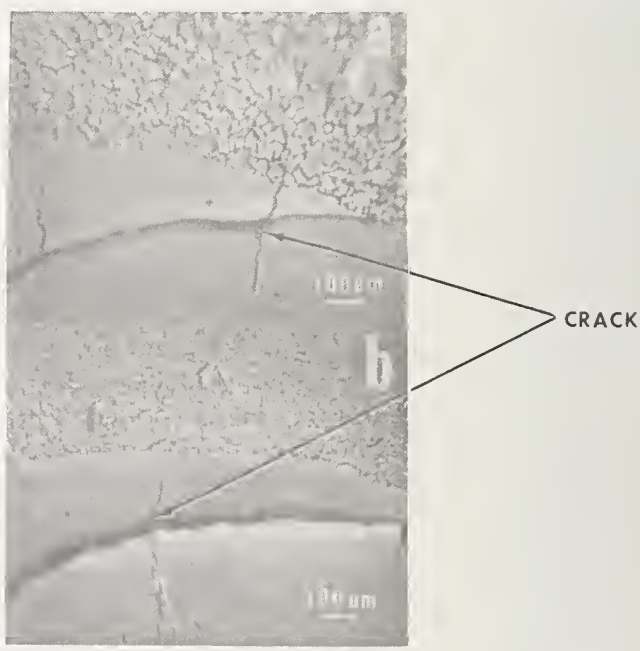

FIGURE 4. *Cracks generated by laser beam on 99.5 percent alumina substrates.*

Discussion

UNIDENTIFIED: The cracks in some of the laser-scribed substrates looked very much like grain boundary cracks. Is that true?

LO: Yes.

NATIONAL BUREAU OF STANDARDS SPECIAL PUB. 348, THE SCIENCE OF CERAMIC MACHINING AND SURFACE FINISHING, Proceedings of a Symposium Sponsored by the American Ceramic Society, the Office of Naval Research, and the National Bureau of Standards, held at NBS Nov. 2–4, 1970, Gaithersburg, Md. (Issued May 1972).

VI. PANEL DISCUSSION

J. B. Wachtman, Jr., Moderator

F. Ernsberger, P. J. Gielisse, A. H. Heuer, W. H. Rhodes, and R. W. Rice, Panel Members

J. B. WACHTMAN, JR., National Bureau of Standards, Gaithersburg, Md.—*Panel Moderator:*

Our intention here is to put the work presented at this conference into perspective. We have had a series of excellent invited and contributed papers addressed to various specific aspects of the sequence of machining, finishing, characterization, and physical properties. We now wish to look over this sequence from the point of view of several factors which are important throughout the sequence and which, accordingly, provide a basis for a unified point of view. Such a unified point of view depends upon an understanding of the processes occurring at the surface during machining and the consequences for characterization and for control of properties. Many of us are interested in physical properties and the factors controlling them, but we would like to focus the present discussion as much as possible on the processes occurring at the tool-workpiece interface, their interaction with the machining system, and their influence on the finished piece. Each of our panel members has chosen one or more themes around which to make his remarks. Each panel member's presentation will be followed by a short discussion period.

It is appropriate to begin with the question of the mechanism of machining. No one is better qualified to summarize present views and suggest areas needing further elucidation than Professor Peter Gielisse of Rhode Island University who has already presented a paper on his single point machining research and who needs no further introduction.

P. J. GIELISSE, University of Rhode Island, Kingston, R. I.—*Panel Member:*

I would like to discuss the knowledge we have on the mechanisms of ceramic finishing processes. It is of course understood that except for speciality applications, most of this falls in the area of the mechanical methods of stock removal or ceramic finishing. In reading over the various papers and from what I have heard during this conference I cannot get away from one particular thought. There remain, unfortunately, a large number of misconceptions, some of which, and only some of which, have possibly been done away with as a result of the actual presentations. We find, for instance, that reference is still made to the celebrated fact that grinding of ceramics is the same as the grinding of metals and that nothing new needs to be learned. A statement like that at a conference of this type certainly is extremely surprising and particularly surprising in the light of many of the presentations that were made today. A second claim which could be made is that all one apparently needs to do to evaluate grinding is to generate some sort of a grinding ratio or similar parameter and that physical characteristics and concepts can be replaced by an apparently more convenient shorthand notation, as seen on many of the slides on the screen here, which evaluates matters in terms of such (brand name) parameters as "XDY–MB3." The strength of materials is in effect claimed to be better expressed as a function of extrinsic parameters such as grit size rather than in terms of what is germane and intrinsic to the process and to the effective strength of materials. These are just a few observations and they are given merely by way of example here. What I am trying to indicate is what I believe to be the general futility in our efforts to understand the mechanical removal mechanism and the many observed experimental phenomena, in terms of what is only a part of the total systems analysis, namely the (important) economic aspects. It is, however, particularly noteworthy that even the economic analysis cannot really be fruitfully carried out unless we have an understanding of the full technical aspects. It is therefore important, I feel, that we continue to develop the science and technology of the grinding mechanism so as to generate and develop generally applicable ceramic finishing data. This information will provide a further understanding of the nature of the influence of the finishing cycle on the finished product, will guarantee that we have reproducibility in the finished ceramic part with regard to both the internal as well as external characteristics, and will generate new methods and approaches in ceramic finishing. I think it is not very well understood that the way we grind, the way we remove stock today, need not necessarily be the way we remove stock in the future. It is only when we try to understand the fundamentals involved in the materials removal process that

we will come closer to understanding the possibilities for improvement.

Attempts to further understand these matters should really be concentrated on essentially four areas. First of all, the recognition and study of the fundamental differences between the three basic methods of stock removal: Bonded Abrasive Machining (BAM), Contained Abrasive Machining (CAM), and Free Abrasive Machining (FAM). Secondly, the nature of the interaction between the tool and the workpiece from both a mechanical as well as a materials point of view. It is very important that we do not merely look at this from a mechanistic point of view or merely from a materials point of view. These two must come together. Thirdly, the function of each parameter in the tool as well as the workpiece which contributes positively or negatively to the stock removal process. Finally, the external or environmental effects which influence the system's performance advantageously or disadvantageously as part of the total system, not merely as an observation of the phenomenon. In other words, when we observe the phenomenon of the influence of the environment, it is not sufficient merely to make that particular observation, but it certainly ought to be tied to the parameters of the actual finishing system as a whole.

A. H. HEUER, Case Western Reserve University, Cleveland, Ohio:

It struck me while Bert Westwood was giving his talk yesterday that it would be important to find a "cutting fluid" for alumina. Probably more alumina is machined by diamond abrasives than any other single ceramic material and most of this machining is done wet. If a medium were found in which the cutting efficiency could be increased by two to twenty-fold, as Bert showed for some of his extreme examples, it should have considerable economic advantage.

K. M. SMITH, Applied Physics Laboratory, Johns Hopkins University, Scaggsville, Md.:

My experience is that high spots on a grinding wheel are particularly damaging when grinding is parallel to the face of the specimen as shown in Figure 1. Specimens ground in this way tend to crack upon refiring. High spots apparently do less damage when the specimen itself is also rotated during grinding as shown in Figure 2.

Commenting upon your statement concerning alumina, I found that morphaline is one of the safe coolant agents that I could add to water. Because it is an ammonia compound, it is very easily volatilized and it does not add any impurities like sodium or potassium that some coolants would do. So I use morphaline in mistic

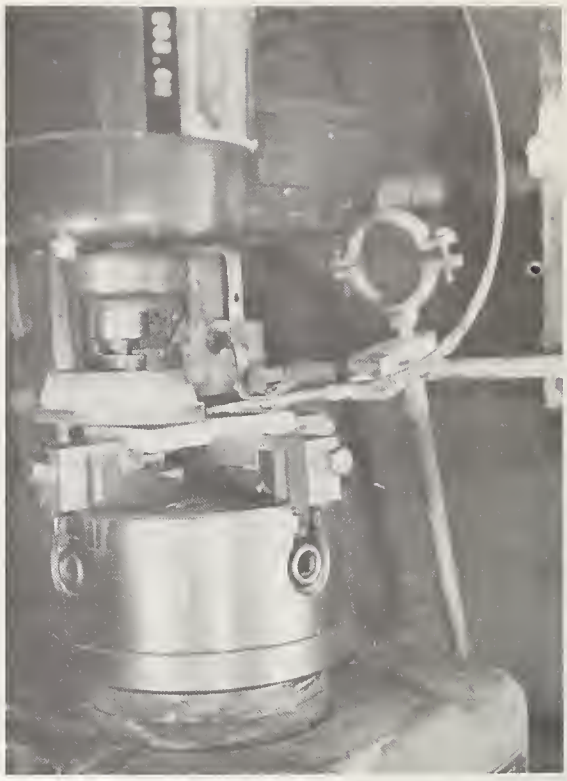

FIGURE 1. *Grinding parallel to specimen face.*

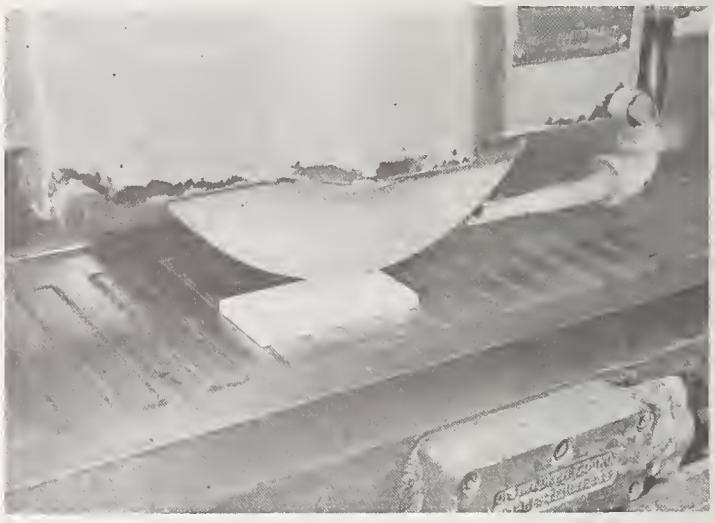

FIGURE 2. *Grinding with specimen rotating as well as grinding wheel.*

mist at about 125 lbs pressure. I must agree with your first statement, Dr. Gielisse, I don't think we can compare grinding metals and grinding ceramics. I think they are two separate materials. They must be handled differently.

P. J. GIELISSE, University of Rhode Island, Kingston, R. I.:

What you are stating is exactly the point I was trying to make. Some people want to take our knowledge of metal grinding (even there we know very little) and transfer it to the ceramic area. Now the only similarity I see is that in both we commonly use, in the majority of cases, a round wheel, and the label of the

manufacturers of the machines might or might not be identical. For the rest, there is absolutely no correlation.

H. A. PERRY, Naval Ordnance Laboratory, Silver Spring, Md.:

My horizons have widened at this meeting. I've been in the habit of thinking of grinding in terms of mechanical and chemical practices and also, possibly the actual phenomena used to explain the Rebinder effect. It comes to mind, however, that also in the environment are the occasional electric properties of the material which are involved in fracture and similar effects. Perhaps even optical and magnetic or electromagnetic effects are important. It seems to me that the picture is far more complicated in my mind than when I came.

P. J. GIELISSE, University of Rhode Island, Kingston, R. I.:

I think this is quite true. I believe that we made an observation on triboluminescence and, again in keeping with the idea of doing the fundamental studies, we have done studies in gases; we alluded to that in our paper. We very definitely see optical effects that are either the result of gaseous discharges or the result of triboluminescence. This could make for the so-called sparks in ceramic grinding. I believe that from all evidence we have right now, although it is still to an extent meager and possibly qualitative, it is certainly indicated that the so-called temperatures of grinding are considerably lower than most of us have felt them to be.

A. R. C. WESTWOOD, R.I.A.S., Martin Marietta Corporation, Baltimore, Md.:

Responding to one of Dr. Gielisse's points, I would like to propose one way in which an environment can influence the ease with which cracks are initiated in semibrittle solids. Once initiated, I would expect that the cracks would propagate and interact to form the chips which constitute the means of material removal. Consider the stress-strain curves shown in figure 3. Studies of the room temperature flow and fracture behavior on semibrittle solids, such as MgO monocrystals containing many surface sources, indicate that only limited work hardening occurs following yielding. Thus, the fracture stress is essentially determined by the stress at which dislocations first move and multiply, that is, the flow stress. In other words $F_1 \sim f_1$. If such a solid is placed in contact with an environment which facilitates dislocation mobility in the near surface regions, then the flow stress of the near surface region will be decreased, e.g., to f_2. It follows, of course, that the fracture stress of this region

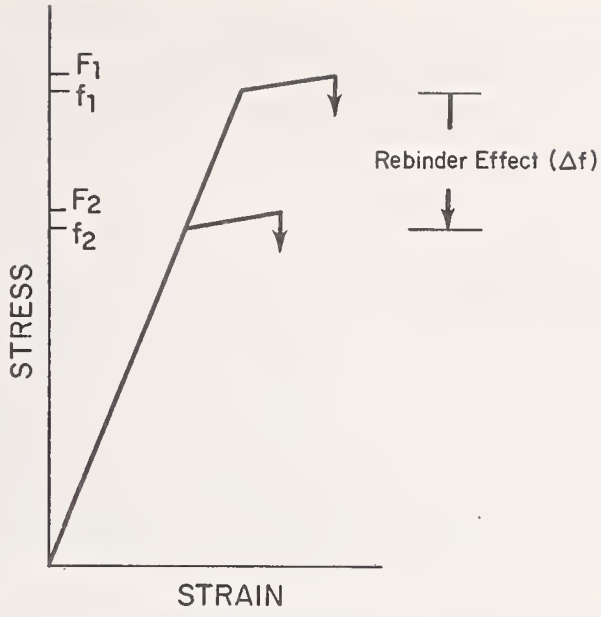

FIGURE 3. *Schematic illustration of manner in which the Rebinder effect (the adsorption-induced reduction in hardness) can facilitate fracture, and hence machinability, of a semibrittle solid such as MgO.*

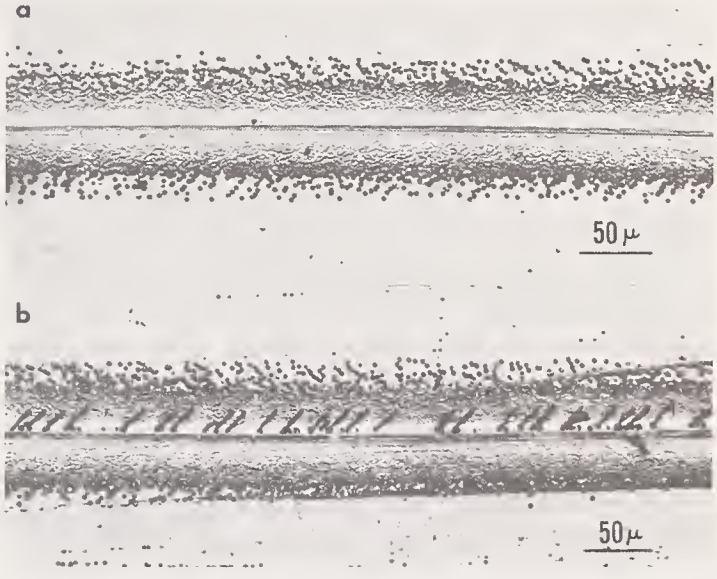

FIGURE 4. *Indenter tracks in freshly cleaved MgO surface produced (a) in air—a relatively inactive environment, and (b) surface-active n-hexadecane.* The load on the indenter was 20 g., and it was moved from left to right. Note prolific cracking at tracks produced under the active environment. (After Westwood and Goldheim, J. Am. Ceram. Soc. 53, 142–7 (1970)).

will also be lowered, e.g., to F_2. Thus, by reducing the flow stress, the fracture stress is also reduced, and material removal facilitated.

An example of environment-facilitated cracking in MgO is shown in figure 4. In this case, comparative scratch tests were performed on freshly cleaved {100} MgO surfaces. A 20 g load was applied to the diamond indenter, which was traversed at about 2 cm per min. The environments compared were air (that is, adsorbed water) and n– hexadecane. Under

these conditions, cracks were not formed in surfaces exposed to air (fig. 2a). Under hexadecane, however, cracking was prolific (fig. 2b), fracture occurring on both {110} planes intersecting the surface and {100} planes below the surface.

P. J. GIELISSE, University of Rhode Island, Kingston, R. I.:

Thank you Dr. Westwood. Just one observation. Might I put in a plea that most of our observations in the future be conducted under conditions that are typical of the grinding mode. I feel, namely, that in addition to the phenomena you describe there are unfortunately many processes that simply go unnoticed, that are the result of high impact-high velocity type of material deformation processes.

J. A. MUELLER, The Carborundum Company, Niagara Falls, N. Y.:

We've seen photomicrographs of a lot of samples which appeared to me to be badly damaged. Some of the parameters of grinding that were used to grind these samples would be considered to those skilled in the art as unsatisfactory. One example was the use of very heavy in-feeds with slow table speeds using an aluminum oxide vitrified wheel for grinding high purity, dense nonmetallics. This method could do nothing but produce a badly damaged surface. But my purpose in commenting now isn't to talk about that. My purpose is simply to point out that there is a wide lack of communication between those skilled in the art and the people who are doing this kind of work. Another thing, I think, that is quite well taken, concerns the debate about whether or not you can transfer knowledge of metallic grinding into the field of nonmetallic grinding. Now I don't know whether you can or cannot, but I know this—that there are many interesting phenomena that occur in metal grinding that also occur in ceramic grinding. For example, I think we saw one just a moment ago when the type II wheel was compared with the type I wheel. The gentleman indicated that the type I wheel grinds on one point. No question about it. We've got documentation in metal grinding to show that a wheel will grind on one point and that this point travels around the wheel face 360 degrees. There is documentation available and there are movies available that illustrate this phenomena.

Another example stated was grinding a large ceramic cylinder with a 3 in diameter grinding wheel running at a slow surface speed.

What happened was no doubt, that the use of a small wheel, grinding a large part, produced a badly damaged surface. The length of contact was too great for the wheel to operate efficiently. Again we have illustrated that, what happens in metal grinding, happens in nonmetallic grinding.

In metal grinding, when we grind hard brittle materials we use fine grit wheels. Some general rules are: hard materials—fine grit wheels, softer materials—coarse grit wheels, fine finish—fine grit wheels, coarse finish—coarse grit wheels.

In nonmetallic grinding we have found to date, that the same rules of grinding apply. There is a whole area in metallic grinding that compares to nonmetallic grinding. We are not certain that we can transfer it bodily. However, I feel that people interested in ceramic grinding should become acquainted with what knowledge is available in the metallic field and then attempt to transfer whatever is applicable. What I am saying is, I think there is a tremendous lack of communication between the gentlemen here and the gentlemen in the grinding operations and I think that they should get together. As a matter of fact, I would like to suggest that possibly when we grind samples there should be a standard method for grinding samples. Find the best way to grind a sample and then use that as a standard. In this way, better results will be produced and faster progress will be made.

P. J. GIELISSE, University of Rhode Island, Kingston, R. I.:

I'd like to make a comment on the first point. Some of the conditions used in some of the papers here were not necessarily representative of those in practice, but this is often a very important and necessary step in broadening our understanding. I think you often have to look at a much broader range of parameters than maybe the ideal ones for industrial practice in order to come to an understanding of the true mechanisms. If you can get a better picture of what goes on by using parameters which really aren't practical from the industrial standpoint, you may be able to transfer this knowledge to a better understanding of what will be happening under the conditions that are of practical interest. So I think there is some communication and appreciation of the point you make. Many of us may not know as much as we should about the practice and technology but I think you should recognize also that it is very often important to use "impractical" conditions in order to generate "practical" knowledge.

A. U. DANIELS, Metcut Research, Cincinnati, Ohio:

Whether or not there is a standard grinding test, I think it would be extremely appropriate to work out a standard method for presenting

the variables related to grinding or other cutting operations; that is, a systematic format for giving feeds, speeds, depths of cut, wheel types, coolants and so forth. If a standard format for machining data were used in papers and presentations, one could tell at a glance what the authors had done in general instead of having to ask about miscellaneous machining parameters afterward. I think that standardizing data presentations would improve communications whether or not standard tests are being used.

With regard to transfer of information from work done on machinability of metals—if I had a lot of wood to cut up and had my choice of hiring either someone who had never cut anything up or someone who had spent all of his life cutting up metal bars, I'd take the man with at least some cutting experience. In other words there is much useful machining theory and experience gained with metals which is transferable to ceramics. For one thing, metals aren't all like aluminum or soft steel. Metals run the full gamut of ductile and brittle properties. In fact, when aerospace alloys, hardened tool steels, and metal bonded tungsten carbides are considered, there is almost a continuous spectrum of materials from metallic lead to aluminum oxide ceramic which must be machined. Therefore, I think ceramic machining is only one aspect of a larger problem, and I have to ask why Dr. Gielisse would categorically state that everyone should ignore all of the metals machining background that has been developed.

P. J. GIELISSE, University of Rhode Island, Kingston, R. I.:

First of all, your statement which started this debate is only partially correct. If the picture really did lie the way you painted it then I too would say yes. If our objective were merely to cut ceramics or remove stock, fine, I would also hire the man who has this type of experience, but that is exactly the point; we want to move away from this, we want to understand what happens during this particular kind of cutting. The objective is not merely to cut, I mean not really with only that objective in mind. In that case, we could merely continue turning out grinding ratios and we would be able to make some sort of economic evaluation, but it would not give us the sort of data with which we could accurately go forward.

F. F. LANGE, Westinghouse Research and Development, Pittsburgh, Pa.:

Has anyone tried to cut ceramics at higher temperatures?

H. C. MILLER, Super-Cut, Inc., Chicago, Ill.:

We have done this with glass with which our company has had a lot of experience. We frequently get a glass combination that will crack when you drill it and there just seems to be nothing you can do. Yet if you will run it in water as hot as a man can possibly stand, you can drill beautiful holes without thermally shocking the glass. There are other ways to go to higher temperatures for grinding which have a first order effect.

S. D. BROWN, University of Illinois, Urbana, Ill.:

My son is an ichthyologist of sorts. He likes tropical fishes and every once in a while he will come home with a big bottle of some kind to cut. One time he came home with a carboy. The best way I found to cut it was to put a hot wire on it and it just pops right on through. Now I wonder if you couldn't do some cutting or machining by controlled heat input in low cross sections.

D. J. DONOVAN, Data Magnetics, Torrance, Calif.:

There are some possible industrial applications: changes in the magnetic properties of ferrites are induced by a hot wire at a given point. This may have application by locating the gap in a magnetic head core.

Note added in proof:

The normal way to create a gap in a head core is to make the core in two pieces and then bond them together. This hot wire method would not necessarily be a physical gap, but a disturbance in the magnetic path.

J. B. WACHTMAN, JR., National Bureau of Standards, Gaithersburg, Md. *Panel Moderator:*

We'll take our next two panel members in sequence and defer discussion until after the second presentation. We've had many references to plastic deformation. I believe both of the next two speakers intend to touch on that as one aspect of their talk. Our next panel member is Dr. Fred Ernsberger of PPG Industries. Dr. Ernsberger is well known for his own work on hardness and other properties of glass and he has general extensive knowledge of glass science and technology through the interests of his firm. The presence of a glassy phase in many, perhaps the majority of technical ceramics, makes it very appropriate to call on Dr. Ernsberger for his comments on this aspect of machining.

F. ERNSBERGER, PPG Industries, Pittsburgh, Pa.—*Panel Member:*

Thank you very much Jack. I am glad you made those introductory remarks because I

wouldn't want anyone to think that I am a specialist in machining of ceramics. My own area of expertise in glass is more in the area of strength; but that does give me some area of overlap with the material of this conference. I suppose that's why I was called to come and be an observer and to give my reactions.

As Jack has hinted, my principal reaction was to the number of times I have heard the concept of plastic flow in glasses and ceramics used very casually. I have some objections to that which I would like to raise. However, there are a few other things that I would like to mention before I get into that.

I feel very comfortable when I hear people talk about stress-corrosion and delayed-fracture effects and so on, because we see those, of course, in our work with glasses as well. We use about the same thinking in rationalizing them; the presence of water, stress corrosion, the Charles-Hillig theory, and so on. I gather that you are not entirely comfortable with this approach and this rationalization and I guess we're not either; though perhaps the chemistry is a little clearer and makes a little more sense in our case than in yours, so maybe we're a little more comfortable with it.

I'm also comfortable with the concept of surface flaws and their effect on properties, including strength. Naturally, volume flaws are also a matter of concern in your polycrystalline materials. What surprised me a little was Pollock's statement that with his thermally polished filaments of single crystal sapphire he was able to find internal origins for, I believe he said, every one of the cases of tensile fracture. He did this by potting is resin or something of the sort. This is something that no glass person has claimed ever to have done; either to find internal origins or, indeed, to find *any* origin in the fracture of a glass fiber or glass rod specimen under pristine glass conditions. There is too much fracturing and breakup. Possibly it is because of the higher modulus of alumina, so that alumina gives a higher stress without so much stored energy. At any rate, I wish he would come to a glass conference sometime and tell us how he did that.

The etching technique to reveal surface flaws is used, and a particularly pretty example was the paper we just heard a few minutes ago by Koepke on magnesium oxide. I think perhaps some of you are not using this enough. It is really a very powerful technique. I gather that it isn't quite as simple or as convenient to apply in the case of ceramics, particularly polycrystals, as it is in the case of glass. Dilute hydrofluoric acid is our all-purpose etching reagent, and it is easy to use at room temperature. It does give in many cases beautiful definitive results which you can hardly get any other way. You should use it more often, even if it does mean high temperatures and corrosive gases and things of that kind. I was sorry to see that in a case where etching could have been used readily to advantage (I'm speaking of Dr. Busch's movie), there was no sign that it had been considered. You remember the first sequence in that movie where he was dragging glass over a sphere; behind the point of contact there was what he described as stress waves or something. Any glass man would immediately guess that those were really crescent-shaped cracks which temporarily were held open by the stress behind the moving ball and then closed up and became invisible. One could easily check this hypothesis by simply etching the sample after the experiment was done. I hope this will be done sometime with that sort of experiment. I rather confidently predict that crescent cracking is what that effect will turn out to be.

The Rebinder effect was very prominently mentioned in Westwood's presentation and I have to report that among glass people the Rebinder effect has hardly made any waves at all. Perhaps we are missing something very important; and I, for one, am going to go back and study this paper and the data very carefully because I can see that at least one man is convinced that this is a very important effect. But among glass people, I suspect they mostly think as I do that the Rebinder effect is just one of those odd things that the Russians have come up with, like "polywater." These things are hard to disprove, but in the end will probably turn out to be nothing at all.

Now, if I have a little time left, I want to get to this question of plasticity and plastic flow. I consider it to be a hard thing to defend in most crystalline oxides and in all silicate glasses. I make one prominent exception: magnesium oxide. Magnesium oxide obviously shows very readily definable plastic effects at room temperature. One reason for this is the fact that it is a highly ionic material like sodium chloride, where you have similar effects; and another reason is that it has plenty of slip systems, inasmuch as it is face-centered cubic. Among the more covalent materials (of course, there is a spectrum with sodium chloride on one end and diamond on the other, and in this spectrum I certainly would place alumina among the more covalent materials) there is less justification for assuming that slip can happen at ordinary temperatures. The activation energy for movement of the existing dislocations is simply too great to be theoretically accountable at room temperature. So when you postulate this sort of thing, you have to be able either to explain theoretically how this can be, or else you have to point to a reasonable assumption that the temperature at least locally

and for a certain period of time was rather high. That is what I have to assume when I hear discussions of the burnishing of alumina, of dislocation concentrations near the surface, and things of that kind.

In glasses, you have what are called "microplastic effects." Until recently, these have been rather difficult to explain. Under the Vickers indenter you really can get a permanent identation which is crack free. This bothered me for a long time, but I published a paper [1] recently which rationalizes this, not in terms of plastic flow, but in terms of densification.

A few of you may find densification a novel concept so I'll just briefly explain what it is. Glasses having low coordination numbers for silicon (and for oxygen for that matter) have a lot of empty space in them. When compressed hydrostatically, or with various complex stresses that involve a substantial hydrostatic stress. they will condense in volume irreversibly. That is, when the stress is removed, you find that the specimen has actually diminished in volume. This is not plastic flow in the proper sense of the word, because plastic flow occurs by shear, it involves changes in atomic partners, and volume is conserved. Densification is clearly not that kind of a process. It is more of a displacive than a reconstructive process. I think Stokes put the thing rather clearly this morning when he talked about the "semibrittle" materials as opposed to the "absolutely brittle" materials. I would nominate alumina and our silicate glasses as being among the "absolutely brittle" materials at ordinary temperatures.

Thank you.

J. B. WACHTMAN, JR., National Bureau of Standards, Gaithersburg, Md. *Panel Moderator:*

Please hold all the comments that you have in mind as a result of Dr. Ernsberger's discussion until we have heard from Roy Rice of the Naval Research Laboratory. Mr. Rice has done extensive work on ceramic processing including high temperature pressure forming involving plastic deformation; he will also discuss the role of plastic deformation in machining.

R. W. RICE, Naval Research Laboratory, Washington, D. C.—*Panel Member:*

I would first like to briefly mention what are some of the factors in the occurrence of microplasticity in machining. Slip can occur in some softer materials (e.g., sodium chloride and magnesium oxide), and twinning may occur in some harder materials such as alumina at moderate stresses at room temperature. However, this does not explain the scope of materials in which such surface deformation occurs during conventional machining, nor the extent of such deformation as reported by many at this conference. The most important factor is probably the high compressive stresses that result from machining. These stresses will, I think, considerably enhance the opportunity for slip to occur first by inhibition of cracks due to their compressive nature, and second, by the high level of the stresses themselves. The rise in local temperatures in many machining operations may also measurably enhance the occurrence of microplasticity.

Next, I would like to look briefly at some of the possible roles of microplasticity in a typical machining operation. In a rough machining operation such as sawing, I would expect that fracture is most likely the predominant process. Here the role of microplasticity is probably one of aiding the amount, but limiting the depth of fracture, for example, by multiple crack nucleation. blunting cracks, and general energy absorption. In finer machining operations (e.g., most grinding) the propensity for cracking should diminish (in fact, I have observed this in MgO) and the extent (i.e., depth) of microplasticity to at least remain constant, if not increase. In polishing, microplasticity is probably the main mechanism of developing the fine surface topography and does not occur as deep as in grinding, as observed by Hockey in Al_2O_3 and myself in MgO. I think we should also note that, as has been pointed out previously, too much plasticity under certain machining conditions can be bad, e.g., certain machining conditions applied to soft materials, such as sodium chloride, would probably be rather difficult.

I would like to briefly mention, without infringing too much on Bill Rhodes' topic, some of the material parameters that may affect microplasticity during machining. First, is hardness. As I presented in one of my talks, we generally will expect the depth of microplasticity to decrease with increasing hardness. Second, is grain size. I have observed the depths of microplasticity to decrease with decreasing grain size in magnesium oxide, which is a rational trend. Third, is the effect of porosity. I think that one of the important things we have to recognize is that the location of pores (i.e., at grain boundaries, or within grains) is an important factor. This may be a key factor in the type and size of chips formed, and hence, important in both the machining operation and the topography of the resultant surface. There is also evidence that pores may be sources of dislocations; if so, this will also make the location of pores important (e.g., pores within grains should then enhance surface work hardening). Impurities are, of

[1] "Role of Densification in Deformation of Glasses Under Point Loading," J. Am. Ceramic Soc. 51, 545–547 (1968).

course, another important microstructural factor affecting microplasticity.

I would now like to discuss mechanical properties which have clearly been of considerable interest in the conference. Traditionally, the view would have been that the effect of machining was to introduce flaws that caused failure, thus determining strength. Both the growing evidence for microplastic processes associated with fracture and the evidence of plastic deformation during machining shown at this conference indicates that this is a rather shortsighted view. I find mechanical behavior much more understandable if I consider both microplasticity and flaws where flaws may be much more prevalent in certain materials, particularly the hard ones; while microplasticity would generally be more prevalent in softer materials. Twinning may also be important, possibly more at intermediate hardness, but it may not correlate as well with hardness as slip. I can see many situations in which microplasticity and Griffith flaws are competitive as to which may be the main cause of failure. I can also visualize situations in which these two mechanisms cooperate to lead to failure, as Bert Westwood also suggested (e.g., subcritical crack growth by microplasticity.)

I think many people tend to take a very skeptical attitude toward microplasticity since the Griffith concept has been around for a good deal of time and had a good deal of success in explaining glass behavior. Further, many people seem to seriously neglect the known or possible differences between microplasticity in ceramics and ductility in metals, and hence confuse them. No one duobts the importance that flaws can have on mechanical properties. However, if you look carefully at the evidence for mechanical failure in crystalline materials, I think you will find that the Griffith concept is no more firmly established than is the microplastic concept. For example, as Bob Stokes pointed out, there actually has been relatively little demonstration of Griffith flaws as a result of various machining or other operations in crystalline materials. In particular, there has been, to my knowledge, no specific fracture origins in single crystals demonstrated to be due to particular (i.e., known preexisting) flaws which clearly fit the Griffith criteria. There has been very limited observation of flaws in polycrystalline materials. One of the few cases that I can think of is rutile, and here, flaws were observed only in large grain bodies, did not go clear across the grain, and the behavior of these bodies was considerably different than the finer grain materials in which flaws were not observed.

A basic problem in applying the Griffith theory where it appears applicable is to explain the generally pronounced effect of grain size on strength of materials. It is commonly assumed that flaw size is related to grain size, which is certainly an appealing intuitive thought, but there is really no firm foundation that I know of to establish this. On the other hand, we have seen very good evidence at this conference that microplasticity does occur during machining of materials such as alumina and magnesia, and there is evidence in the literature for materials such as silica and tungsten carbide as well. Thus, since nucleation of cracks by microplasticity is related to grain size, microplasticity during machining may offer an explanation for the apparent relation of the size of at least some flaws to grain size. There also appears to be an important interaction between the microplastic deformation from machining and flaws. Hockey has observed that the deformed layer results in surface compressive stress. This is quite reasonable, and may be quite important.

Note added in proof:

While it is probably obvious, it is worth emphasizing two important effects of machining on microplastic mechanism of failure. First, while microplasticity during machining may nucleate cracks, it may in other cases inhibit or prevent crack nucleation as noted earlier. Thus, this can be an important factor in allowing microplastic mechanisms of failure to operate. Compressive surface stresses may also aid this. Second, fresh sources of dislocations (and probably twins) are often important to microplastic mechanisms of failure in ceramics. This conference clearly shows machining is a source of these.

Thus, in summary, while both machining and material parameters affect microplasticity during machining, it probably always occurs to some degree. This is important to both the machining process and the surface character of the body and thus resultant mechanical properties. Both flaw and microplastic mechanisms of failure are affected by the microplasticity in machining and each must be evaluated.

S. D. Brown, University of Illinois, Urbana, Ill.:

While it is altogether possible that very high temperatures are present locally under the tips of diamond indenters during indentation or scratching in which permanent deformation of glass is produced, it is not necessary that this be the case. Calculations show that even in the adiabatic approximation, the temperature rise for 15 percent densification of a typical soda lime-silica glass need not be more than ca. 10 °C.

I believe that the question of whether plastic flow is involved in the indentation of glass depends somewhat on how one defines plastic flow. If one is talking about so-called ideal plastic flow in which there is no volume change, then of course densification is involved in the case of glass, the volume changes, and the plastic flow (if that's what it is) is not ideal. In the case of glass indentation, the flow occurs under the influences of both hydrostatic pressure and shear. I would guess that free volume is removed from the glass by such a process, thus leading to densification. The activation energy of such a process would be expected to be small on account of the relatively large shear stresses present during the indentation. These large shear stresses are absent when the indenter is removed, so the free volume cannot return at any sensible rate; hence, the densification is permanent until the glass is heated to a temperature where thermal energy promotes the annealing reaction. The flow of the glass under pressure might be termed non-isometric plastic flow. The reason one does not see similar phenomena in crystals (e.g., Al_2O_3 is, I suppose, due to the fact that the crystals do not contain as much free volume as glasses do.

F. ERNSBERGER, PPG Industries, Pittsburgh, Pa.:

It is evident that Sherman Brown has thought very hard about this from several angles and I encourage you all to do the same thing. In fact, that is all I want to do today; I don't want to try to defend any particular concept that I have advanced. I just think it is something that you should think about, particularly before you write for publication. I'm glad he pointed out that the temperature rise question hardly enters into the case of indentations. It need not; you can certainly do them very slowly. Essentially, I stand pat on what I know about indentations because that is the only experiment in which I feel reasonably confident that I know where the temperature is at all times. In connection with what Roy Rice has said, let me remind you that I never said that magnesium oxide does not plastically deform or that sodium chloride does not and as a matter of fact, I don't say that alumina or even diamond does not deform if the temperature is high enough at the right time.

R. W. RICE, Naval Research Laboratory, Washington, D. C.:

I'd like to ask Fred Ernsberger what his interpretation would be of the curling chip removal we saw in the pointed diamond tool from the South African film. I think it certainly seems that one's first thought would be to think in terms of this as plastic flow. If he has a different interpretation I would be interested.

F. ERNSBERGER, PPG Industries, Pittsburgh, Pa.:

I simply fall back on the fact that I cannot think of any mechanism for plastic flow in glass at room temperature but I do know that it flows at elevated temperature by Newtonian mechanisms; so that is my answer.

A. H. HEUER, Case-Western Reserve University, Cleveland, Ohio:

I'd like to make a comment about this question of irreversible densification. My colleague, Al Cooper, has spent the last three or four years studying volume viscosity in B_2O_3 and has measured (with M. Mizouchi) the kinetics of the irreversible compaction that occurs under hydrostatic pressure. It is a very complicated process. For example, there is no equilibrium volume at an equilibrium pressure; the volume depends on the pressure history, and the concept of a "fictive pressure" (equivalent to a fictive temperature) is not sufficient. To my knowledge, there is no analogue in crystalline materials, which, when hydrostatically compressed, will deform elastically unless a phase transformation intervenes, which can usually not be quenched. I would tend to agree with Fred that this phenomena of irreversible compaction is really a different phenomena than anything occurring in crystals and it probably can occur only in glasses because of their open structure and lack of periodicity.

A. R. C. WESTWOOD, R.I.A.S., Martin Marietta Corporation, Baltimore, Md.:

I must rise to Fred Ernsberger's comment concerning the apparent elusiveness of the Rebinder effect. When this phenomenon was first reported in the British scientific literature in 1947 (Rebinder, P. A., Nature (London), 159, 866 (1947)), several Western scientists tried to reproduce Rebinder's results. They could not, and consequently some doubt arose concerning the existence of this effect—doubt which has persisted into the 60's and, apparently, even into the 70's. Yet the facts are that this is a real effect and, in nonmetallic solids, it can be a large effect. And, as I have said on many occasions, I believe that it is an effect whose technological potential make it well worth studying.

I am convinced that a "hard" look will not make this phenomenon disappear. The twenty-fold increase in drilling rate of soda lime glass in heptyl alcohol over that observed in water, demonstrated in our paper, is too large an effect to just go away. Moreover, the existence of this Rebinder effect in glass cannot be ex-

439-921 O - 72 - 28

plained on the basis of the two presently popular theories for interpreting environmental effects in this class of solids, nor can it be interpreted in terms of lubrication or coolant effects, etc. On the other hand, it does appear that a consistent explanation can be provided on the basis of the hypothesis that environment-sensitive flow can occur in glass at room temperature, and that the changes in hardness and machinability observed are related to adsorption-induced redistributions of the sodium and/or hydroxyl ions in the nearsurface layers of the glass.

Regarding the occurrence of environment-sensitive flow in glasses, let me mention briefly some experiments in progress at RIAS involving the slow propagation of stable, center-loaded cracks in soda lime glass. We are finding that the energy required to propagate such cracks is very sensitive to the chemistry of the test environment. Indeed, our preliminary results indicate that the fracture energy of this glass in the alkane environments varies in the same manner as the hardness of the glass. That is, the harder the glass, the greater the energy of fracture. Our present interpretation of this effect is that slow crack propagation in glass can be facilitated by localized, and environment-sensitive, flow processes in the vicinity of the crack tip, perhaps in an analogous manner to that in which dislocations emitted from the tips of cracks in semibrittle solids cause them to grow to critical size. You will appreciate that in this instance we are talking about glass specimens tested in tension, not in compression, where compaction may be a confusing variable.

Incidentally, regarding the possible mechanisms of flow in glass, Gilman (Gilman, J. J., in "Dislocation Dynamics", McGraw-Hill, New York, 3–25 (1968)) has suggested that if one will allow the possibility of a nonconstant Burgers vector, then it is possible to interpret the flow properties of amorphous solids in terms of the presence and movement of dislocations.

J. B. WACHTMAN, JR., National Bureau of Standards, Gaithersburg, Md. *Panel Moderator:*

Please hold your questions for a while so that we can go on to our next panel member, Dr. William Rhodes of AVCO. Dr. Rhodes has extensive experience with special ceramic processing techniques designed for control of microstructure and he will discuss the effect of microstructure on the machining process.

W. H. RHODES, AVCO Corporation, Lowell, Mass.—*Panel Member:*

A number of papers have touched on the effect of microstructure in polycrystalline ceramics on grinding and polishing behavior, but it is clear that we've really just begun to enter on to an era of a coupled analysis of machining and polishing behavior and physical ceramics. It is very difficult for me to try to pull a consensus of microstructure effects out of this meeting. We've talked about so many different materials and microstructural features were not systematically varied within a given set of tests. Therefore, the remarks on microstructural features will be quite general and some of them have already been stated, but I will state them again for emphasis. I'd like to touch briefly on grain size dependence, porosity dependence, second phase or chemical effects, and last, but not least, the problem that we all face everyday and that is the effect of nonhomogeneous defects in materials.

The lack of systematic studies of the effect of changing grain size within a given set of grinding tests without changing any other variables makes it impossible to state unequivocally what the effect of grain size will be, so I shall primarily talk about some very general conclusions. Roy Rice has mentioned one already and that is the effect of dislocation damage on grain size. With decreasing grain size you can expect a lower level of dislocation damage within the material under question. This would probably hold true to some degree in terms of crack damage as well because you can imagine that the cracks will certainly be blunted, twisted, and deflected at grain boundaries and therefore crack damage would probably decrease with decreasing grain size. There are many fine finishing (polishing) operations where we have this problem of grain pullouts and in many cases the surface finish is important. It is almost impossible to obtain a fine finish without some pullouts and obviously the depth of the final flaw will be dependent on grain size as well. In certain applications, such as the one that was mentioned this morning by Bob Stokes (the gyroscope application where very fine tolerances are required for very small spaces between mating surfaces), the grain size will be particularly important especially if there is a touchdown between mating surfaces and grains are, in fact, pulled out during use. So grain size will continue to be an important parameter in those applications. Now the tendency for pullout must be related to the chemistry of the system. Many of the commercial ceramics talked about in this conference are multiphase systems that certainly have what is normally called a grain boundary phase or a glass bond phase and we certainly can expect there to be quite different bond strengths between the matrix phase and the bond phase for the various materials under question. Of course, this would be quite different again if we went to a truly single phase material. I'd like to

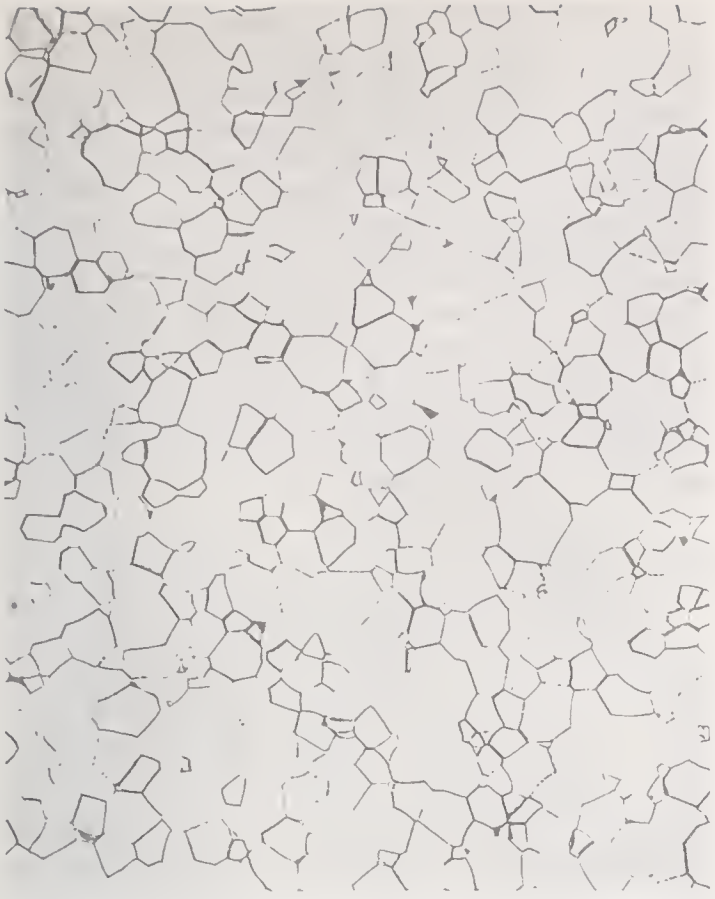

FIGURE 5. *Hot pressed MgO fabricated with additive. (250X)*

FIGURE 6. *Hot pressed MgO fabricated with LiF additive. (150X)*

illustrate this point with two slides. In figure 5 we have a material that really hasn't been talked about too much in terms of fine finishing and that is polycrystalline magnesium oxide. This is a material that was made without any deliberate additive in the hot pressing process. As you can see, a very good polish was obtained with very little grain pullout. Figure 6 will show magnesium oxide of similar grain size that was made by the lithium fluoride additive process. You can see a very large degree of pullout in this particular material. This illustrates that two materials that appear similar under an optical microscope can behave quite differently in the final polishing.

Porosity has not been studied with systematic changing of variables. Keeping chemistry and grain size the same while varying porosity is a very difficult study to make as a matter of fact. However, I think we can draw the general conclusion that surface roughness would increase with increasing porosity. Also, as you reach very high porosity, you can expect a lot of chip out around large pores, and the actual loss in pullout density will go up with decreasing porosity.

For the most part, we have talked about materials as if they were truly homogeneous. I was glad to see the papers today deal with the real world of nonhomogeneous materials. I think this is what we are all striving to eliminate, but a truly homogeneous material within a one or two cubic inch specimen is the exception rather than the rule in today's market, I'm afraid. Anyone who is connected with processing is daily trying to eliminate defects. We saw examples of defects this morning arising from agglomerates, from impurities, and I can go through a list of causes that we at AVCO have come up with. We've found defects from the above causes and incomplete mixing of a deliberate dopant. You can very often have inhomogeneities arising from this. You can have bits of a wrapper from your powder container that would actually get compressed in your material and during firing leave a void in your final piece—bristles from brushes that people use to clean screens—it goes on and on. Actually, towards the end of the week you might have to worry about dandruff. So it's a never ending battle, and something that all of us need to be aware of when we're describing surfaces and what we can expect as a final surface. We have to be realistic and acknowledge that there are these large defects that very well may be the limiting step in terms of obtaining an optimum fine surface.

In polycrystalline materials such as aluminum oxide, we also have anisotropy effects that certainly must come into play in the ability to maintain a surface finish. Anisotropic thermal expansion is a function of crystal habit that certainly must leave different retained strains in a body at different grain sizes under different processing conditions. So this well could be a variable that might be important in surface finishing. There are fabrication processes which will give anisotropic materials a preferred crystallographic orientation and these could have quite different finishing characteristics than randomly oriented material of the same grain size.

I would like to mention several summarizing guidelines for possible future research on the effect of microstructure on grinding and polishing. We do need a systematic study of grain size and porosity in grinding performance. Some sort of fundamental studies of chemistry on multiphase bodies and the bond strengths and how these relate to grinding and polishing behavior is also warranted. I'll mention again for emphasis that I think all of us need to eliminate the nonhomogeneous defects that are in real materials. Bob Stokes mentioned one research area that he wanted to see continued, and I would like to second the appeal for a systematic study of the depth of crack damage on surface finishing and polishing.

One area that doesn't really relate to microstructure but was extremely interesting to me was the fact that you can get quite different surface finishing effects by varying the type of diamond grit one uses, and I'd like to see and encourage our South African friends to continue that body of knowledge on all grades of commercial material.

L. BERRIN, Bell Telephone Laboratories, Allentown, Pa.:

There are two points, mentioned by Bill Rhodes, that we should certainly consider. First, for the most part, characterization of the material that we are investigating is not well defined. Many of us have heard this mentioned before, but it needs to be reemphasized until something is done. Also mentioned was the need of a systematic study of microstructural features, e.g., grain size and porosity, as a function of machining or polishing parameters. This, of course, is necessary, but in lieu of this it would at least be desirable to report the grain size and porosity of the material under investigation at the time we present our research. Other characteristics of the material that we're investigating, such as its chemistry or method of forming, would also be helpful. I think this criticism of data presentation has come up year after year, but I think it's something that cannot be overlooked.

J. B. WACHTMAN, JR., National Bureau of Standards, Gaithersburg, Md.:

That takes us back to some of the earlier comments by members of the audience who are familiar with the machining of metals and who have suggested a standard test or a standard method of presentation of data. Perhaps they would attempt to answer this question: If I come to you for advice on how to grind a given material, what information do you want from me? What do you want to be told about the material? Do you want to know its hardness, its porosity, or what are the factors you want to know before advising on the procedure for machining a given material?

H. C. MILLER, Super-Cut, Inc., Chicago, Ill.:

Just the things you'd expect. Metals are well categorized to ASTM and SAE standards. A description of chemical composition of the metal would be a necessity; equally important are hardness measurements and microstructures. There are standard descriptions available for microstructure and also, of course, for porosity. I haven't heard any mention of, for instance, use of the standard system for talking about things in terms of A–1 or A–2 porosity. Chemical composition can be described as 1040 steel or something of this sort; microstructure would be in terms of grain size measured by standard methods, porosity as measured by standard methods, and hardness by a standard method. In metals, hardness and tensile strength are usually very closely related so you don't always need both but can use one or the other. At least that much information is needed before anyone could tell you anything about or give you a recommendation on metal removal.

J. B. WACHTMAN, JR., National Bureau of Standards, Gaithersburg, Md.:

Is the gross chemical composition sufficient or do you need additional information such as the heat treatment and state of precipitation?

H. C. MILLER, Super-Cut, Inc., Chicago, Ill.:

Yes, usually the heat treatment information is desirable. Heat treatment is how you arrive at the condition of the final material and sometimes, that is of additional value. But if you have any other information for instance, microstructural data that will be helpful also. The heat treatment is especially important if it's the type of metal in which phase changes occur, something like titanium. You'd have to know heat treatment to know whether you had alpha or beta phases present.

J. A. MUELLER, Carborundum Company, Niagara Falls, N. Y.:

I would simply add to this that you should specify your objective; i.e., what you want to do with the material. Do you want to simply remove stock or do you want to generate a geometry or do you want to produce a finish or do you want to do all three? State your objective and then we can more logically and effectively select the grinding wheel to do the job.

R. J. CAVENY, Diamond Research Laboratory, Johannesburg, South Africa:

I think even with all these specifications and our present knowledge, it is going to be very difficult to get the grinding behavior. I'd like to quote just one example with tungsten carbide composites. We ground a certain grade of tungsten carbide from a certain manufacturer and we had some pretty good results. We changed batch and we got completely different results under the same conditions. We analyzed both with all the known techniques for cobalt bonded tungsten carbide and found no difference. We got a piece of it from a different manufacturer. Here again, we found the same physical properties but again found completely different grinding behavior. I think it boils down to the fact that at present we don't really know enough, and this is what Dr. Gielisse has said. We must investigate the fundamentals of grinding to elucidate techniques so that we can do these predictions. Otherwise we'll just have to do critical tests.

P. J. GIELISSE, University of Rhode Island, Kingston, R. I.:

I do agree. Every time the question is asked as to what you have to know in order to define the system for grinding, one gets at best some remarks with regard to materials being ground upon. One simply forgets the order of magnitude changes that you can cause in the actual operation by changing parameters which determine the performance of the wheel. There is sometimes the problem of pullout. The grinding system is being regarded as something that is fixed. I mean it is considered to be defined for us. You observe pullout, what can we do about it? We should really turn the question around and ask if the pullout can be prevented; it can, indeed, be entirely prevented if you simply tailor the grinding system to what you are trying to do. Another matter I wanted to comment on is this attempt to put things on a uniform basis by using the same grinding conditions. There can be no such situation as "the same grinding conditions." For each material, for each objective, there are different grinding conditions. That's why these bar charts which compare grinding on the basis of 3000 ft per min or for another particular boundary condition are essentially useless. We have to move beyond this.

R. J. CAVENY, Diamond Research Laboratory, Johannesburg, South Africa:

I'd like to make a comment on that. For instance, just consider our results that I quoted for grinding tungsten carbide—completely different behavior from three different ceramics. If one was optimizing the grinding conditions one wouldn't use the same conditions for the three different ceramics. A standard test is going to be very difficult.

H. C. MILLER, Super-Cut, Inc., Chicago, Ill.:

There is no such thing as a standard test and that's what I have against attempting to classify grinding conditions. I know this comes up because people want to compare things. It is very nice, particularly for engineers, to draw curves through points, but the thing is really that you can only standardize, for instance, with things such as the mode of grinding; shall we do it as surface grinding or not, what's the diameter of the wheel, and things like that. But each material very definitely is going to react very differently.

J. B. WACHTMAN, JR., National Bureau of Standards, Gaithersburg, Md. *Panel Moderator:*

Our final panel member is Professor Arthur Heuer of Case-Western Reserve University who has done extensive research on the mechanical properties of ceramics including surface effects and temperature effects. He will discuss the effect of heat treatment on ceramic surfaces and mechanical properties.

A. H. HEUER, Case-Western Reserve University, Cleveland, Ohio—Panel Member:

I must thank Peter Gielisse, because everything I have to say is going to sound mild, gentle and reasonable. I was asked to comment on the effect of heat treatment, which has been discussed by a number of conferees. One of the things that impressed me very much was the difference between single crystals and polycrystals. I'm thinking particularly of the work on alumina polycrystals by Sedlacek and by Kirchner on the one hand, and the work by Noone and Heuer on single crystals on the other. The strength increases that were achieved for polycrystals were, in general, very small, plus or minus 20 percent. (The only exception is very severe cracks introduced by thermal shock damage or by very deep and severe cracks, which are somewhat artificial because these can usually be avoided in practice.) In contrast, large strength increases have been obtained in alumina single crystals. The inter-

esting question is what is causing the difference. I think there is one factor which has been overlooked in the past, but was mentioned very briefly a few minutes ago by Bill Rhodes, viz. internal stresses in polycrystals due to thermal expansion anisotropy. I think that in the case of an anisotropic material like alumina, these probably play a more important role in determining the strength of polycrystals than is generally realized. Part of the difficulty is that at a zero order approximation, one concludes that the internal stresses should be independent of grain size and yet there is very clear evidence that there is something like a Griffith relation observed between the strength of polycrystalline alumina and its grain size. As a corollary question, why does the strength of polycrystalline alumina never exceed about 100,000 psi, even for fine-grained polycrystals? To understand the differences between single crystals and polycrystals, we have to understand (on a fundamental level) what are the factors controlling the strength, how these interact with the damage introduced during surface machining, and how they are affected by heat treatment. (The importance of machining damage in certain cases was illustrated very nicely in Bob Stokes' paper, where he showed that the body stresses introduced by machining can strongly influence electrical and magnetic properties.) Getting back to the effect of heat treatment, one of the significant new results was reported by Rice, Becher, and Schmidt, who showed how, using a helium-freon etching "heat treatment", one could dramatically improve the strength of single crystals of arbitrary shapes. As was pointed out, flame polishing of single crystals is rather restricted to simple shapes. The fact that it had no influence on the strength of polycrystals (or only a very limited effect) relates to the point discussed above.

Another very interesting observation was given by Sundahl and Berrin, who showed that impurity segregation to the surface during annealing had a very beneficial effect, in that the impurities enhanced metalizing. This is clearly a subtle effect, but one that obviously has very practical applications in many modern electronic uses of ceramic substrates.

There is one further point I want to mention, with respect to the environment during annealing, particularly the peculiar effect of hydrogen. Berrin told me in conversation that this is also a factor in his work; there are some funny things which happen when he heat-treats alumina in hydrogen. Again, this is an area where we need further understanding, particularly since furnaces for use above 1500 °C often operate in reducing atmospheres. If there are some poorly understood effects and interactions occurring in ceramic bodies in hydrogen or vacuum at elevated temperatcres, continued use of such environments may be questioned.

Finally, I was impressed by the Bell Labs paper this morning showing how well surfaces can be characterized using several new instrumental techniques—Auger electron spectroscopy, low energy electron diffraction, and reflection electron diffraction—as well as the better known scanning electron microscopy. I think these techniques can be used very well to understand changes occurring during heat treatment. For example, Schmidt and Davey demonstrated using reflection electron diffraction that the surface layer of mechanically polished sapphire crystals was amorphous. However, this layer could be recrystallized by heat treatment, and this represents a distinct improvement in our understanding of what happens when machined or polished surfaces are heat treated.

H. P. KIRCHNER: Carmic Finishing Company State College, Pa.:

I agree with Dr. Heuer about the importance of expansion anisotropy, and one thing that has been clear to me for sometime is that strong ceramics of phases with anisotropic crystals could not be made if what is important is the stress because the stresses are undoubtedly very high. But what is important is the residual deformation in an individual grain and if this is small as it is in a small grain size material then it is not possible for a crack to open up. The principal distinction is between the total deformation of the individual grain (inches per grain) and the strain (inches per inch).

A. H. HEUER, Case-Western Reserve University, Cleveland, Ohio:

I'm afraid I don't understand that point. It seems to me in a zero order approximation that the strain is independent of grain size; strain, and hence stress, result from change in length per unit length and this is independent of grain size. I think it's a problem a number of people have struggled with and it seems to be particularly important at this point in time.

R. C. SUNDAHL, Bell Telephone Laboratories, Inc., Allentown, Pa.:

Just another point on the effect of anisotropy; I briefly mentioned this morning some measurements of texture. It was found by Y. Nakada in our laboratory and P. L. Key, F. V. DiMarcello and J. C. Williams at the Murray Hill location of Bell Labs that there is wide variation in fiber texture in tape case substrates obtained from a variety of suppliers. If the anisotropy of the thermal expansion coefficient were important one might imagine there would be

wide variations in mechanical strengths of these same materials from batch to batch and from material to material. Another point is that although there seems to be some correlation between mechanical properties and grain size, it is dangerous to try to correlate one parameter solely with another, for example, mechanical properties with grain size, because there are a large number of parameters which have an influence both on microstructure and mechanical strength. One such parameter is the chemistry of the ceramic. It is not clear which of these various parameters dominate and how many of these observed effects are only indirect symptoms of the dominant effects.

A. H. HEUER, Case-Western Reserve University, Cleveland, Ohio:

I agree completely. I think it's a mistake to think of mechanical strength, say of alumina, as a function only of grain size. It depends on several factors and that is the point I was trying to make.

A. U. DANIELS, Metcut Research, Cincinnati, Ohio:

One comment I can't resist concerns this business or the use of standard methods of characterization or testing. I think there is fear that if people use standard methods they will stop thinking. I believe that's probably the fear concerning standard machining procedures; there's a feeling that maybe engineers do that; they just look at standard test results and then turn their minds off and treat the material as being fully described. I think instead that any kind of standard methods, if established, could serve to keep people thinking. Probably we have had an excellent example here at the conference. People are using profilometers and at the same time saying, "Look here, the profilometer says this, but when you look at the material under a scanning electron microscope you see that the materials can be very different with the same profilometer readings." I think that standard methods can do two things. They can serve as a bench mark or background from which people can extend their thinking. Standard tests are always inadequate, they always miss something, but they do serve as a bench mark or background against which you can begin to make a sensible comparison of materials. They also do another thing. There has been talk here about an information gap between applied and basic information and those standard test results can serve to bridge that gap. So that is the reason I make a strong point that standard tests, rather than restricting thinking, can serve as a background and a basis for which better description and better communication can take place.

P. J. GIELISSE, University of Rhode Island, Kingston, R. I.:

Just a brief comment on that. Being on the faculty of a college of engineering, I certainly do not support, of course, the idea that engineers stop thinking, and I believe we have to interpret that quite differently. Secondly, I have the greatest esteem for the efforts, of particularly your firm, in the area of standardization. You do mention something, the use of the profilometer and I entirely agree with your comments. People are not using the profilometer correctly now. They are taking roughness readings, but what can be done with profilometry is much more than is presently being practiced. I wish that this would be noticed and hopefully changed in the future.

A. H. HEUER, Case-Western Reserve University, Cleveland, Ohio:

I would like to make a rather philosophical comment, being also on the faculty of a school of engineering. In reading the ONR-London reports in the last couple of years, I've been struck by their reporting of the establishment of several departments of tribology in the United Kingdom. An entire academic discipline involved with machining and grinding of materials is being established, chairs are being created, and students are being graduated with sophisticated training in this particular discipline. To my knowledge, with perhaps the exception of Peter Gielisse's group at the University of Rhode Island, there is very little like that done in the United States. As an academic, I can assure you that what is required here is money—money from the Government, and also perhaps more importantly, money from industry (the users and producers of ceramics and ceramic machining wheels). My impression is that there is only meager support by industry for the academic disciplines with which they are most concerned. This communication gap that has been alluded to is perhaps a result of insufficient people being formally trained in the appropriate discipline, and I would hope that industrial firms could take the lead in effecting a change.

R. W. RICE, Naval Research Laboratory, Washington, D.C.:

I'd like to make two comments tying in with what both Art Heuer and Bill Rhodes said. First, concerning porosity, I wonder if it's possible to deposit (e.g., during grinding) sufficient swarf within existing pores in the material so that if you then anneal the material, you'll get one result; whereas under other grinding conditions, you may not deposit swarf in the pores, and hence your annealing results could be very different. Also, any cleaning process prior to

annealing could change the situation. Variables such as this should be kept in mind in looking at annealing effects. Second, I would very much agree with Art Heuer that mechanical properties do not depend entirely on grain size, but I think we must recognize that grain size is an extremely pervasive variable. We also have to recognize that the effects of grain size can be substantially changed. I think, for example, the data we showed on grinding direction shows this rather markedly: if you plot strength versus grain size for specimens ground in different directions, you'll get rather different curves. I would go along with the view that you have to be careful in describing strength as a function of grain size, but I think it has to be recognized that grain size is a very pervasive variable.

R. F. FIRESTONE, Case Western Reserve University, Cleveland, Ohio:

I'd like to try to put Professor Heuer's remarks in historic perspective. In 1880, Frederick Winslow Taylor, the Father of Scientific Management, began to study the art of cutting steel with single point tools at the Midvale Steel Company which later became part of the United States Steel Company of Andrew Carnegie. Taylor thought the study would take less than six months to complete.

Four years later he was still making experiments and had hired a graduate engineer to help with the mathematics. Twenty-six years later, after having reduced over 40 tons of steel to swarf, he had developed a formula to determine the optimum cutting conditions and he had developed the modern high speed tool steels. The results justified the effort.

The point I'm trying to make is that it took a great deal of time and money to discover the best way to machine low carbon steel, a homogeneous material, with a single point tool. Ceramics and the process of grinding are much more complex. I don't think there is any organization which is willing to put in the time and money required to solve the problem. This conference is certainly a step in the right direction but I am pessimistic about rapid progress being made.

P. J. GIELISSE, University of Rhode Island, Kingston, R. I.:

That's correct. I do think that the present concept of our university administrations certainly doesn't lend itself to continuing, long-term support of this nature, but I think the comments you make are in line with what Professor Heuer is saying. What we need is further interaction between the academic world, that can provide that sort of information, and the industrial users.

NATIONAL BUREAU OF STANDARDS SPECIAL PUB. 348, THE SCIENCE OF CERAMIC MACHINING AND SURFACE FINISHING, Proceedings of a Symposium Sponsored by the American Ceramic Society, the Office of Naval Research, and the National Bureau of Standards, held at NBS Nov. 2–4, 1970, Gaithersburg, Md. (Issued May 1972).

Author Index

Subject Index

FORM NBS-114A (1-71)

U.S. DEPT. OF COMM. BIBLIOGRAPHIC DATA SHEET	1. PUBLICATION OR REPORT NO. NBS SP-348	2. Gov't Accession No.	3. Recipient's Accession No.

4. TITLE AND SUBTITLE

Science of Ceramic Machining and Surface Finishing

5. Publication Date: May 1972

6. Performing Organization Code

7. AUTHOR(S)

S. J. Schneider, Jr. and R. W. Rice

8. Performing Organization

9. PERFORMING ORGANIZATION NAME AND ADDRESS

NATIONAL BUREAU OF STANDARDS
DEPARTMENT OF COMMERCE
WASHINGTON, D.C. 20234

10. Project/Task/Work Unit No.

11. Contract/Grant No.

12. Sponsoring Organization Name and Address

The American Ceramic Society, 4055 No. High Street, Columbus, Ohio 43214
Office of Naval Research, Arlington, Virginia 22203
National Bureau of Standards, Dept. of Commerce, Washington, D. C. 20234

13. Type of Report & Period Covered: Final

14. Sponsoring Agency Code

15. SUPPLEMENTARY NOTES

16. ABSTRACT (A 200-word or less factual summary of most significant information. If document includes a significant bibliography or literature survey, mention it here.)

This volume presents the proceedings of the Symposium on the Science of Ceramic Machining and Surface Finishing held at the National Bureau of Standards in Gaithersburg, Maryland on November 2-4, 1970. The symposium was jointly sponsored by the Baltimore-Washington Section of the American Ceramic Society, the Office of Naval Research, and the National Bureau of Standards. The purpose of the conference was to survey the developing science of ceramic machining and to stimulate further progress by discussion of current problems and research programs. In addition to a panel discussion, 37 review and original research papers were presented with attention focused on four main areas: (1) Techniques and Mechanisms of Removal and Shaping (2) Surface Treatment (3) Analysis and Characterization of Machining Effects and (4) Mechanical and Other Effects of Finishing. An edited version of the floor discussion following each paper is given.

17. KEY WORDS (Alphabetical order, separated by semicolons)

Ceramics; ceramic machining; mechanical effects of machining; removal and shaping of ceramics; surface treatment.

18. AVAILABILITY STATEMENT

[x] UNLIMITED.

[ ] FOR OFFICIAL DISTRIBUTION. DO NOT RELEASE TO NTIS.

19. SECURITY CLASS (THIS REPORT): UNCLASSIFIED

21. NO. OF PAGES: 431

20. SECURITY CLASS (THIS PAGE): UNCLASSIFIED

22. Price: $5.25

USCOMM-DC 66244-P71

U.S. GOVERNMENT PRINTING OFFICE: 1972 0—439-921